

H24/3616

MONASH UNIVERSITY
THESIS ACCEPTED IN SATISFACTION OF THE
REQUIREMENTS FOR THE DEGREE OF
DOCTOR OF PHILOSOPHY

ON..... 6 July 2004.....
.....

Sec. Research Graduate School Committee

Under the Copyright Act 1968, this thesis must be used only under the normal conditions of scholarly fair dealing for the purposes of research, criticism or review. In particular no results or conclusions should be extracted from it, nor should it be copied or closely paraphrased in whole or in part without the written consent of the author. Proper written acknowledgement should be made for any assistance obtained from this thesis.

p 9-19 para 2, 1st line: "slightly" for "*slightly*"

ADDENDUM

p 2-10 para 2, 3rd line, after "wave mechanics": insert "and measurements of force and velocity histories at a pile section near the pile head."

p 2-23 para 1, 6th line, after "e.g.": insert "Coyle and Gibson, 1970;"

p 2-23 para 1, 11th line: "*N* generally has..." for "*N* has..."

p 2-24 1st line: "series" for "parallel"

p 2-24 section 2.4.1, para 2, 2nd line, after "e.g.": insert "Coyle and Gibson, 1970;"

p 2-33 1st line, before "Litkouhi and Poskitt (1980)": insert "Coyle and Gibson (1970);"

p 3-14 para 1, 10th line: "an arbitrary" for "a convenient"

p 3-21 section 3.4.1.2, 6th line: "remained essentially" for "remained"

p 3-21 section 3.4.1.2, 7th line: "vary systematically" for "vary"

p 3-21 section 3.4.1.2, 8th line, after "velocity.": insert "However, based on the plot presented by Heerema (1979), it is possible that there were minute dynamic effects."

p 5-61 after para 3: add as new para: "Given that currently there is a lack of conclusive experimental evidence for supporting any of these hypotheses, no recommendation regarding the use of the damping factors for piles installed in sands can be proposed. Further research involving tests at higher shear rates is therefore required for any conclusion to be drawn."

p 6-11 para 1, 8th line: delete "lowest"

p 6-13 caption of Figure 6.6: add at the end of caption: "; scale indicated by 23mm-diameter coin."

p 8-32 last line, after "relationship": insert "and Equation (8.1)"

p 8-33 1st line to 8th line: delete and read "1. For a specimen that has been preconsolidated to a certain stress, the shear strength decreases with decreasing (current) applied stress and with increasing *OCR* value; therefore, the α value increases with decreasing applied stress and increasing *OCR* value. 2. For two specimens that are currently loaded at the same stress, the specimen with the lower preconsolidation stress and hence the lower *OCR* has a lower shear strength; therefore, the α value for this sample is higher."

p 9-13 para 2, 2nd sentence: delete and read "It is not known which one of the resistances (the ultimate or the instantaneous) is more appropriate; the use of either one of the resistances is discussed as follows."

p 9-19 para 3, last sentence: delete and read "The Shaft/Toe ratio computed by CAPWAP(expo) is slightly greater, and is generally about $\pm 30\%$ of the CAPWAP(linear) value."

p 9-31 para 4: delete last sentence

ERRATA

p 1-5 1st line: "Summary & Conclusion" for "Conclusion"

p 2-5 section 2.2.4, para 1, 5th line: "IM" for "R"

p 2-14 para 2, 12th line: "If no match can" for "If the no match can"

p 2-15 Figure 2.7, third box on left: "W↓" for "W"

p 2-19 section 2.3.1, 2nd line: delete "low"

p 2-24 section 2.4.1, para 1, 9th line: "inspiring" for "inspired"

p 3-2 1st line: "With" for "ith"

p 3-13 Table 3.1: "x" for "x"

p 3-50 Equation (3.6): "N" for "n"

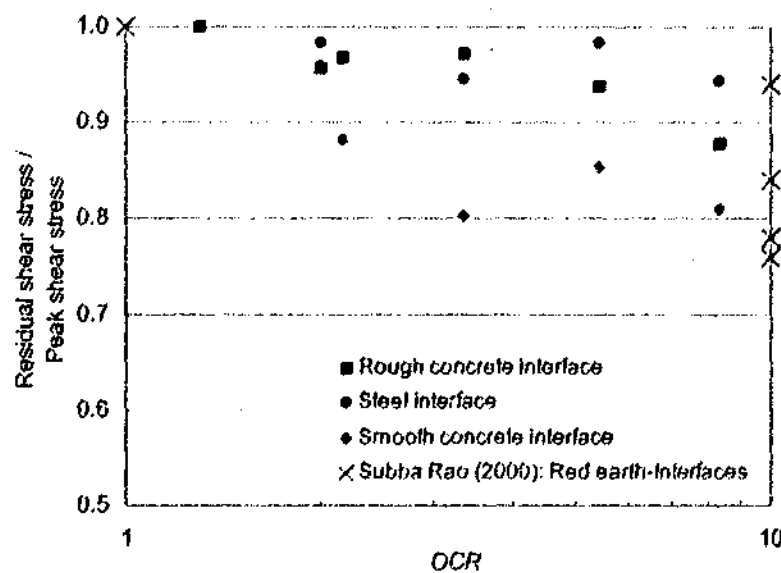
p 4-31 Equation (4.1): "interface" for "inteface"

p 5-2 section 5.2, para 2, 3rd line: delete "significantly"

p 6-31 para 2, 7th line: delete "that"

p 6-31 last sentence: "are" for "also"

p 6-32 Figure 6.22: symbols are as follows:



p 6-40 para 2, 2nd line, after "obtained": insert "by"

p 7-71 para 3, 6th line: "3.5s/m." for "3.5."

p 8-2 3rd line: delete "and"

p 8-7 para 2, 2nd line, after "(α)": insert "(for β fixed at 3.0s/m)"

p 8-12 Equation (8.1), "v" for "n"

**THE DYNAMIC RESPONSE OF
PILE-SOIL INTERFACES
DURING PILE DRIVING AND
DYNAMIC TESTING EVENTS**

BY

VICTOR B. L. CHIN, B.E.(Hons)

**A THESIS SUBMITTED FOR THE DEGREE OF
DOCTOR OF PHILOSOPHY IN THE DEPARTMENT
OF CIVIL ENGINEERING, MONASH UNIVERSITY**

DECEMBER, 2003

TO MY FAMILY & JADE

SYNOPSIS

The uncertainties inherent in the design and construction of piled foundations have necessitated the testing and verification of the capacity of installed piles. An economical testing method, known as dynamic testing, is increasingly replacing the traditional static load test. In addition, dynamic methods for forecasting the driveability of piles are being used increasingly. These dynamic methods are premised on accurate modeling of a dynamic phenomenon in the soil known as viscous damping, which enhances the soil resistance during the dynamic event. Whilst various models for modeling the viscous damping response have been proposed, these models are either not based on experimental data, or based on experimental studies which have significant limitations. Moreover, these models do not allow the values of the dynamic damping parameters to be determined rationally, and the damping parameters cannot be related to fundamental soil parameters. The uncertainties inherent in the use of such models reduce the reliability of both predictions of pile driveability and the interpretation of dynamic testing methods.

In order to improve the reliability of the dynamic testing methods, research is undertaken on the viscous damping response of the pile-soil interface during the dynamic event. The aim of the project was to develop an improved and physically based model of the dynamic pile-soil interface response. This was to be achieved by the conduct and analysis of laboratory simulations of the pile-driving event.

The project has involved testing of the pile-sand and pile-clay interfaces using the laboratory set-up, and observations of the post-test shear surfaces of the interfaces. The project has led to a hypothesis of the mechanism of viscous damping, and a simple method for estimating the value of the damping parameter based on conventional soil tests.

The proposed model for the characteristic damping response has been incorporated into a research version of a commercial signal-matching program known as CAPWAP. Analyses performed using the proposed model on field data have

demonstrated that the model can be applied with success to real pile behaviour outside the laboratory.

TABLE OF CONTENTS

SYNOPSIS	I
TABLE OF CONTENTS	III
STATEMENT	IX
ACKNOWLEDGMENTS	XI
NOTATION	XIII
1. INTRODUCTION	1-1
2. BACKGROUND	2-1
2.1 General	2-1
2.2 Pile Capacity Evaluation	2-2
2.2.1 Static design	2-2
2.2.2 Static pile testing	2-2
2.2.3 Dynamic formulae	2-4
2.2.4 Wave equation analysis	2-5
2.2.5 Pile dynamic testing	2-9
2.2.6 Statnamic testing	2-17
2.3 The Dynamic Response of the Pile Shaft-Soil System	2-18
2.3.1 Physical processes	2-19
2.3.2 Modelling of the dynamic response	2-21
2.4 Viscous Damping	2-24
2.4.1 Requirement for a correct viscous damping model	2-24
2.4.2 Mechanism behind viscous damping	2-25
2.4.3 Existing viscous damping models	2-30
2.5 Concluding Remarks	2-33
3. LITERATURE REVIEW	3-1
3.1 General	3-1
3.2 Previous Laboratory Simulations	3-1
3.2.1 Triaxial specimen impacted with falling weight	3-1
3.2.2 Penetrometer	3-6
3.2.3 Direct shear	3-9
3.2.4 Pile shaft encased in triaxial specimen	3-10
3.3 Presentation of Findings from Previous Studies	3-12
3.3.1 The use of strength ratio	3-12
3.3.2 A framework for presenting various data	3-14
3.4 Dynamic Effects in Sand – Previous Studies	3-18
3.4.1 Sand-pile interface shear tests	3-18
3.4.2 Shear tests in sand	3-22
3.4.3 Triaxial compression tests of sand	3-26

3.4.4	Concluding remarks – dynamic effects in sand – previous studies	3-36
3.5	Dynamic Effects in Clay – Previous Studies	3-37
3.5.1	Triaxial samples impacted with fallen weights	3-41
3.5.2	Penetrometer test	3-45
3.5.3	Direct shear test	3-56
3.5.4	Test involving pile shaft encased in triaxial specimen	3-61
3.5.5	Approach to obtaining the relationship between dynamic friction and velocity	3-63
3.5.6	Constant velocity tests	3-64
3.5.7	Pore pressure measurement	3-64
3.5.8	Effect of fundamental soil parameters on the viscous damping parameter	3-65
3.5.9	Concluding remarks – dynamic effects in clay - previous studies	3-79
3.6	Concluding Remarks	3-81
4.	DEVELOPMENT OF EXPERIMENTAL APPARATUS	4-1
4.1	Introduction	4-1
4.2	Key Requirements	4-1
4.2.1	Isolation of shaft from tip	4-2
4.2.2	Eliminating scale effects	4-2
4.2.3	Different pile characteristics	4-2
4.2.4	Transient velocity	4-2
4.2.5	Controlled and known normal stress	4-2
4.2.6	Limiting radiation damping	4-3
4.3	Alternative Schemes	4-3
4.4	The Quasi-Static & Dynamic Interface Shear Device	4-4
4.4.1	Development of the shear device	4-4
4.4.2	General description of the shear device	4-7
4.4.3	Components of the shear device	4-13
4.5	Data Acquisition	4-28
4.6	Validating Shear Device	4-31
4.7	Sample Test Output	4-32
4.8	Concluding Remarks	4-35
5.	QUASI-STATIC & DYNAMIC PILE-SAND INTERFACE BEHAVIOUR: TEST PROCEDURES, RESULTS & ANALYSIS	5-1
5.1	General	5-1
5.2	Quasi-Static & Dynamic Shear Rates	5-2
5.3	Test Programme – Static & Dynamic Tests	5-2
5.4	Test Procedures	5-7
5.4.1	Sample preparation	5-7
5.4.2	Soil-only tests	5-9
5.4.3	Interface tests	5-9
5.5	Quasi-Static Interface Tests	5-13
5.5.1	Results	5-13
5.5.2	Discussion	5-16
5.5.3	Concluding remarks – quasi-static tests	5-22

5.6	Dynamic Interface Tests	5-22
5.6.1	Post-test observations of interface	5-22
5.6.2	Typical test record	5-24
5.6.3	Procedures for analysis	5-28
5.6.4	Records of all tests	5-34
5.6.5	Discussion	5-56
5.7	Summary	5-61

6.	QUASI-STATIC PILE-CLAY INTERFACE BEHAVIOUR: TEST PROCEDURES, RESULTS & ANALYSIS	6-1
6.1	General	6-1
6.2	Test Programme	6-2
6.3	Test Procedures	6-5
6.3.1	Soil specimen fabrication	6-5
6.3.2	Soil-only tests	6-8
6.3.3	Quasi-static interface tests	6-8
6.3.4	Implications for the analyses	6-11
6.3.5	Post-test observation of shear surfaces	6-12
6.4	Interface Shear Failure: Observations & Discussion	6-13
6.4.1	Low & medium plasticity clay on smooth pile	6-13
6.4.2	Low & medium plasticity clay on rough pile	6-13
6.4.3	High plasticity clay on smooth pile	6-14
6.4.4	High plasticity clay on rough pile	6-15
6.5	Quasi-Static Interface & Soil Behaviour: Results	6-16
6.5.1	Soil-only tests	6-16
6.5.2	Interface tests	6-16
6.5.3	Summary table for soil-only & interface test results	6-17
6.6	Quasi-Static Soil-Only Behaviour: Discussion	6-20
6.6.1	Undrained strength analysis	6-20
6.6.2	Effective strength analysis	6-26
6.7	Quasi-Static Interface Strength Behaviour: Discussion	6-27
6.7.1	Undrained strength analysis	6-27
6.7.2	Effective Strength Analysis	6-33
6.8	Interface Strength/Soil Strength or Roughness Parameter	6-34
6.9	Summary	6-42

7.	DYNAMIC PILE-CLAY INTERFACE BEHAVIOUR: TEST PROCEDURES, RESULTS & ANALYSIS (PART I)	7-1
7.1	General	7-1
7.2	Test Programme	7-2
7.3	Test Procedure	7-3
7.3.1	Dynamic interface tests	7-3
7.3.2	Post-test observation of shear surfaces	7-4
7.4	A Sample Dynamic Record	7-4
7.5	Interface Shear Failure: Observations & Discussions	7-10
7.5.1	Mode 1 interface shear failure	7-10
7.5.2	Mode 2 interface shear failure	7-14

7.5.3	Mode 3 interface shear failure.....	7-17
7.5.4	Dynamic failure modes.....	7-19
7.5.5	Comparison with static failure modes.....	7-20
7.5.6	Implications for the interface friction.....	7-22
7.5.7	Implications for the normalisation of dynamic friction.....	7-24
7.6	Quasi-Static Interface Friction Associated with Dynamic Test.....	7-25
7.6.1	Procedure for obtaining quasi-static interface friction associated with dynamic test.....	7-25
7.6.2	Quasi-static interface friction associated with dynamic test vs. Quasi-static interface friction measured in quasi-static test.....	7-28
7.7	Analysing Data for Dynamic Effects.....	7-36
7.7.1	Selection of portion of record to be analysed.....	7-36
7.7.2	Velocity-dependence of dynamic friction.....	7-38
7.7.3	Strength Ratio-Velocity Responses.....	7-38
7.8	Fitting the Strength Ratio-Velocity Response.....	7-57
7.9	A Comparison of Data from This Study & Data from Previous Studies.....	7-65
7.9.1	Functional form.....	7-65
7.9.2	Magnitude of strength enhancement.....	7-68
7.10	Concluding Remarks.....	7-70

8. DYNAMIC PILE-CLAY INTERFACE BEHAVIOUR: ANALYSIS (PART II).....8-1

8.1	General.....	8-1
8.2	Proposed Mechanism of Viscous Damping.....	8-2
8.3	Shear Failure Modes.....	8-5
8.4	Shear Strength.....	8-6
8.5	Normal Stress.....	8-13
8.6	OCR.....	8-16
8.7	Clay Plasticity.....	8-20
8.8	Pile Roughness.....	8-21
8.9	Pile Surface Condition: Dry vs. Wet.....	8-25
8.10	Correlation & Estimation of a.....	8-27
8.11	Towards an Understanding of Viscous Damping.....	8-29
8.11.1	Occurrence of viscous damping in clay soils.....	8-29
8.11.2	Proposed mechanism of viscous damping.....	8-30
8.11.3	Implications of proposed hypothesis for pile-soil.....	8-30
8.11.4	Dependence on physical parameters.....	8-31
8.12	Summary.....	8-33

9. PERFORMANCE OF PROPOSED MODEL IN SIGNAL-MATCHING ANALYSES.....9-1

9.1	General.....	9-1
9.2	Methodology of the Study.....	9-2
9.2.1	Aims.....	9-4
9.2.2	Summary sheets.....	9-4
9.2.3	Cases selected for analyses.....	9-8
9.2.4	CAPWAP analysis.....	9-9

9.3	Shaft Damping Models in CAPWAP.....	9-11
9.4	CAPWAP-Computed Shaft Friction Distribution & Toe Bearing Capacity.....	9-14
9.5	Comparative Shaft, Toe and Total Capacities, and Shaft Capacity/Toe Capacity.....	9-18
9.6	Comparative Shaft Resistance Distributions.....	9-25
9.7	Comparative CAPWAP Parameters.....	9-29
9.8	Comparative Capacity Prediction Capability.....	9-37
9.9	Comparative Match Quality.....	9-40
9.10	Concluding Remarks – Comparative Studies.....	9-42
9.11	Relationship Between Damping Factor & Soil Type.....	9-44
9.12	Relationship Between Damping Factor & Shear Strength.....	9-47
9.12.1	Shear strength based on borelog data.....	9-47
9.12.2	Shear strength based on CAPWAP-computed friction.....	9-52
9.13	EOD Data vs. BOR Data.....	9-56
9.14	Concluding Remarks – Physical Meaning of Exponential Damping Factor.....	9-61
9.15	Summary.....	9-63

10. SUMMARY & CONCLUSION.....10-1

10.1	Summary & Conclusion.....	10-1
10.2	Future Research.....	10-6
10.2.1	Effects of pore pressure & remoulding of clay.....	10-6
10.2.2	Other cohesive soils.....	10-6
10.2.3	Dynamic pile-soil interface response in the high velocity regime.....	10-7
10.2.4	Further signal-matching analyses.....	10-7
10.2.5	Dynamic response of soil at pile base.....	10-7
10.2.6	Mechanism of viscous damping.....	10-7

APPENDIX A. STRESS-WAVE MECHANICS.....A-1

APPENDIX B. DEFINITIONS OF CAPWAP PARAMETERS.....B-1

B.1	Definition of CAPWAP Notation.....	B-1
B.2	Meaning of CAPWAP Parameters.....	B-3

APPENDIX C. OUTPUTS OF CAPWAP ANALYSES USING DIFFERENT DAMPING MODELS.....C-1

APPENDIX D. ESTIMATION OF SHAFT & TOE CAPACITIES BASED ON STATIC ANALYSES.....D-1

D.1	Shaft Capacity.....	D-1
D.2	Toe capacity.....	D-2

REFERENCES.....R-1

STATEMENT

This thesis contains no material which has been previously submitted for any degree or diploma in any university. To the best of my knowledge, the thesis contains no material published or written by others, except where due reference has been made in the text.



Victor B. L. Chin

ACKNOWLEDGMENTS

I would like to extend my gratitude to many who have contributed to this project.

I would like to thank my supervisor Dr. Julian Seidel for giving me the opportunity to work on this project and for his technical review of this thesis. I am also grateful to Assoc. Prof. Chris Haberfield and Assoc. Prof. Malek Bouazza for their assistance at various stages of this project.

The project has had a substantial experimental component, which has depended on the assistance of the staff of the Civil Engineering Laboratory. In this regard, I would like to acknowledge the assistance of Messrs Alan Taylor, Chris Powell, Graeme Rundle, Glenn Davis, Jeff Doddrell, Len Doddrell, Michael Leach, Roy Goswell and Tony Nixon.

This project was funded by the Australian Research Council, and my candidature was financially supported by MGS, MDS and MUPTRS of Monash University. I gratefully acknowledge the assistance of both these organizations.

I would like to thank Dr. Frank Rausche and Dr. Liqun Liang of Goble Rausche Likins, Inc. and Pile Dynamics, Inc., who supported the implementation of a new model into CAPWAP®.

I am grateful to Dr. Kuan Lee, Messrs Don McCarthy and Rob Alexander for their assistance in the preparation of some of the figures presented in this thesis.

Finally, thanks must go to my family and Jade, who encouraged me and who were patient with me, especially at difficult times during my candidature.

NOTATION

All notations and all symbols are defined where they first appear in the text. For convenience, they are also listed with their definitions subsequently. Metric units according to the S.I. system have been used unless otherwise noted.

CF	clay fraction
D_{10}	effective grain size; grain size corresponding to 10% percent passing
D_{50}	mean grain size; grain size corresponding to 50% percent passing
D_{60}	grain size corresponding to 60% percent passing
D_r	relative density of cohesionless soil
e	void ratio
e_{min}	void ratio in loosest state
e_{max}	void ratio in loosest state
F	force at a particular location along the pile
G_s	specific gravity of solid constituents
I_p	plasticity index
I_L	liquidity index
J	pile shaft-soil interface viscous damping constant for power law
$J(N=0.2)$	pile shaft-soil interface viscous damping constant for power law with exponent 0.2
J_c	Case damping factor defined for the Case Method which assumes that all dynamic resistance occurs only at the pile tip
J_{Smith}	pile shaft-soil interface viscous damping constant for Smith model
$J_{viscous}$	pile shaft-soil interface viscous damping constant for linear viscous damping model
$J_{tip}(N=0.2)$	pile tip or soil-only viscous damping constant for power law with exponent 0.2
k	stiffness at the pile-soil interface
k_1	pile shaft-soil interface damping constant defined by Dayal and Allen (1975)
k_2	pile shaft-soil interface damping constant defined by Benamar and co-workers (Lepert et al.; 1988a, 1988b; Benamar et al., 1991, 1992;

	Benamar, 1999)
k_3	pile shaft-soil interface damping exponent defined by Benamar and co-workers (Lepert et al.; 1988a, 1988b; Benamar et al., 1991, 1992; Benamar, 1999)
m	soil-only viscous damping parameter defined by Briaud and Garland (1985)
N	Exponent for the power law
n	soil-only viscous damping parameter defined by Graham et al. (1983)
OCR	ratio of the preconsolidation stress to applied normal or vertical stress
Q	quake; the maximum soil deformation that may occur elastically
R_d	dynamic pile-soil interface shear resistance due to viscous damping; the difference between the total shear resistance and the quasi-static shear resistance
R_s	quasi-static pile-soil interface shear resistance measured at a reference quasi-static shear rate
R_t	total pile-soil interface resistance; the sum of dynamic resistance and quasi-static resistance
R_{inst}	instantaneous pile-soil resistance
R_{ult}	ultimate pile-soil resistance
s	shear strength
s_u	undrained shear strength
v	relative pile-soil velocity; for the case where the soil is assumed to be stationary, the relative pile-soil velocity is equal to the pile velocity
v_s	reference quasi-static relative pile-soil velocity
$W\uparrow$	force of upward travelling wave
$W\downarrow$	force of downward travelling wave
w	water content in percent of dry weight
w_p	plastic limit
w_l	liquid limit
x	shear displacement
Z	pile impedance
α	average pile shaft-soil viscous damping constant for exponential model

α_0	original pile shaft-soil viscous damping constant for exponential model
β	average pile shaft-soil viscous damping exponent for exponential model
β_0	original pile shaft-soil viscous damping exponent for exponential model
δ	Angle of pile-soil interface friction
δ_p	Peak angle of pile-soil interface friction
δ_r	Residual angle of pile-soil interface friction
σ	normal applied stress
σ_n	normal applied stress
σ'_n	effective normal applied stress
σ_p	preconsolidation stress
σ'_p	effective preconsolidation stress
σ_v	vertical applied stress
σ'_v	effective vertical applied stress
τ_d	dynamic pile-soil interface shear stress due to viscous damping; the difference between the total shear stress and the quasi-static shear stress
τ_s	quasi-static pile-soil interface shear stress measured at a reference quasi-static shear rate
τ_t	total pile-soil interface stress; the sum of dynamic stress and quasi-static stress
τ_{inter}	shear strength of pile-soil interface
$\tau_{inter p}$	peak shear strength of pile-soil interface
$\tau_{inter r}$	residual shear strength of pile-soil interface
τ_{soil}	shear strength of soil
$\tau_{soil p}$	peak shear strength of soil
$\tau_{soil r}$	residual shear strength of soil
ϕ	Angle of soil friction
ϕ_p	Peak angle of soil friction
ϕ_r	Residual angle of soil friction

Chapter 1

1. Introduction

The design of piled foundations is fundamentally complex. The shear strength of the pile-soil interface is dependent on a knowledge of the frictional (and possibly cohesive) strength between the pile wall and the surrounding soil and the radial effective stresses regime at the interface. These in turn are dependent on soil type, pile type and wall roughness, construction effects, soil stress history and the effect of construction on soil stresses. It is not surprising, therefore, that the design of piles is subject to significant uncertainty. Engineers therefore generally resort to testing of constructed piles in order to verify that design capacities are achieved.

Traditionally, static load testing has been performed in order to provide a definitive measurement of pile capacity or pile-top load-deflection response. These tests continue to be performed, although with less frequency, because of their high cost and because of the availability of less expensive alternatives. They remain popular because they are a direct method which is apparently definitive and requires little or

no interpretation. It is not widely known that these tests are not always reliable, and may require significant analysis for correct interpretation.

Dynamic pile testing methods were developed in the mid to late 1970s, and were in commercial use from the early 1980s. This method has become popular and well accepted in many countries because of its cost, its speed, coupled with its technical capabilities both in determination of pile capacity, and more widely in project control. The fundamental difference between static and dynamic testing methods is that the dynamic methods are conducted during pile driving, when the pile is in significant motion. At this time, the pile is subjected not only to static soil resistance forces, but also dynamic or viscous damping forces that result from the relative pile-soil motion. Static pile capacity is therefore not a direct output of the test. The fundamental challenge for this method is to isolate the static and dynamic components of driving resistance so that reliable estimates of static capacity can be predicted. The success of this task is highly dependent on the reliability of the models of static resistance and of dynamic resistance used in the interpretation of the test measurements.

The dynamic behaviour of the pile-soil interface is not well understood, and various researchers have proposed viscous damping models based on a range of experimental studies. A review of the studies on which these models are based indicates a range of shortcomings and limitations. Furthermore, the models which have been proposed do not allow the critical parameters to be derived from or related to fundamental soil properties. These models therefore exist in the public domain, but have largely not been incorporated into commercial practice. Instead, the dynamic pile testing industry has continued to use the linear viscous damping model, despite the experimental research which has almost universally demonstrated that damping is not a linear phenomenon.

Given that a highly non-linear phenomenon is represented by a linear model, inaccuracies and errors of interpretation must result. A more reliable, physically-based dynamic model should allow more confident estimation of static capacity.

The primary aim of this research is therefore to improve the reliability of dynamic testing methods. The research program will concentrate on the dynamic responses of the pile-sand and pile-clay interfaces. The specific aims are to simulate the field response as accurately as practically possible in the laboratory under controlled conditions, and then, based on the experimental data, to develop an improved model of the dynamic response of the pile shaft-soil interface.

The progression toward the proposed dynamic friction model is presented in this dissertation in the following way:

Chapter 2 Background

The research conducted in this project is presented in the context of use of dynamic methods in the piled foundation industry, and in relation to pile-soil interaction during a dynamic event.

Chapter 3 Literature Review

This chapter discusses previous experimental studies into dynamic pile-soil interface behaviour, and the viscous damping responses for pile-sand and pile-clay interfaces that have been developed.

Chapter 4 Development of Experimental Apparatus

This chapter describes the substantial modifications to a large shear device to enable quasi-static and dynamic tests on pile-soil interfaces to be performed for this research.

Chapter 5 Quasi-Static & Dynamic Pile-Sand Interface Behaviour: Test Procedures, Results & Analysis

The testing program formulated for investigating the effects of various soil parameters and pile characteristics on the pile-sand interface response is described. The procedures adopted in preparing the interface and in performing the quasi-static and dynamic tests are discussed. The results of the quasi-static and dynamic pile-sand interface tests are presented and discussed.

Chapter 6 Quasi-Static Pile-Clay Interface Behaviour: Test Procedures, Results & Analysis

The testing program for the study of the viscous damping response of the pile-clay interface is described. The procedures used in preparing the interface and in performing the quasi-static tests are discussed. Post-test observations of the shear surfaces of the clay specimen and the pile surface subjected to quasi-static tests are described, and the quasi-static pile-clay interface behaviour is discussed.

Chapter 7 Dynamic Pile-Clay Interface Behaviour: Test Procedures, Results, & Analysis (Part I)

The procedures used in performing the dynamic tests are discussed. Post-test observations of the shear surfaces of the clay specimen and the pile surface involved in the dynamic tests are reported. The differences in the fabric of the shear surfaces from the quasi-static and dynamic tests, and the implications for the interface friction are discussed. A procedure for analysing the data from the dynamic test is developed so that the characteristic dynamic friction-velocity response can be obtained and modelled.

Chapter 8 Dynamic Pile-Clay Interface Behaviour: Analysis (Part II)

A mechanism for the viscous response is proposed based on experimental evidence. The effects of various soil parameters and pile characteristics on the viscous damping response of the pile-clay interfaces are discussed and interpreted using the proposed mechanism. A rational framework for understanding the viscous damping behaviour and predicting the dynamic friction due to viscous damping is proposed.

Chapter 9 Performance Of Proposed Model In Signal-Matching Analyses

The performance of the proposed damping model in the signal-matching analysis of dynamic pile testing records is discussed. The proposed damping model, which is based on laboratory tests, is verified with analyses of field-measured data, and the damping parameter is shown to be physically meaningful.

Chapter 10 Conclusion

The results of the research program are summarized, and conclusions drawn. Directions for future work relating to some of the unresolved issues raised in this research are suggested.

Chapter 2

2. Background

2.1 General

In order to establish the setting for the research undertaken in this study, it is necessary to consider the application of dynamic pile testing methods in practice, and also the dynamic interaction between pile and soil that occurs during a dynamic testing event. The former is discussed in the general context of available methods for determining the pile capacity and the pile driveability analysis. The latter is discussed with emphasis on a dynamic phenomenon at the pile-soil interface known as viscous damping which is the particular subject of this study.

2.2 Pile Capacity Evaluation

2.2.1 Static design

In the delivery of a piled foundation, there are essentially 4 phases involved: the site investigation for gathering soil data; the design of the pile for a required capacity; the construction of the pile; and the verification that the constructed pile has the required capacity, load-settlement performance and integrity. The design of the pile is primarily based on information obtained from site investigation. Whilst more theoretically rigorous design methods are available, approximate empirical methods are typically used because the inputs to the rigorous design methods (such as lateral ground stress) are often unknown or uncertain. The soil stratigraphy and soil properties across a site are typically highly variable but information is only available at limited and discrete borehole locations which may or may not allow adequate characterization. In addition, the construction process itself may alter the soil properties and stress conditions in the ground. These effects may have a profound effect on pile capacity. Because of all the inherent uncertainties in the design process and in the ground conditions, there will often be a low degree of confidence that the installed pile will have the required or designed capacity. As such, it is necessary to test the pile to ensure compliance to the required capacity. Pile testing, and in particular dynamic pile testing, is often undertaken on a statistically significant percentage of the installed piles (5 to 15%). Furthermore, physical testing overcomes the uncertainties of site variability and construction effects inherent in the design process. A higher degree of confidence ensues, and this allows lower factors of safety to be adopted, with consequential cost savings potential. Ideally, the verification of pile capacity should also be fed back to the design process to test the design assumptions and to optimize the current design and improve future design predictions (Poulos, 1998). Both traditional and more recent methods of determining the pile capacity are discussed in the following sections, with emphasis on the dynamic pile testing as it relates to the specific focus of the research undertaken.

2.2.2 Static pile testing

Traditionally, the pile capacity is mainly determined using the static load test. The static load test involves the application of vertical load to the pile head, in a

controlled sequence of load increments. The test may take a variety of forms, depending on how the reaction for the applied loading is supplied. Some of the reaction systems are kentledge, reaction piles or ground anchors, as shown in Figure 2.1 (Poulos, 1998). The applied load and settlement of the pile head are recorded; thus the pile capacity and deflection performance are directly obtained. It is worth noting that many or most static load tests are undertaken as proof tests to a contractually nominated test load. The value of such tests for design feedback is limited, as geotechnical pile failure is not achieved. The greatest benefit of static load testing is obtained when the test is instrumented with strain measurement devices along the pile axis. However, this sophistication is typically restricted these days to research applications.

Although static load testing may appear to provide an unequivocal evaluation of pile head load-settlement performance, considerable care needs to be taken with the execution, instrumentation and analysis to ensure that the test is valid. Fellenius (1988) reports large errors associated with the use of manometer measurements to indirectly determine pile-head load. Interaction between load and reaction must be minimized or appropriately considered, and the effect of residual stresses in the pile may lead to a misinterpretation of the relative contributions of shaft resistance and end bearing.

A static load test takes a significant amount of time to set up, execute and dismantle. Typically these tests take between two and seven days to complete. In addition, the need for significant reaction imposes a high cost. The high costs and time factors associated with static load testing have provided an incentive for the development of alternative “quick and cheap” methods. Once developed, static load testing has been less attractive, although it is still considered a reference test, and is performed albeit in smaller numbers for that reason. It should be noted that in some circumstances, particularly for piles constructed offshore, it may be difficult or impossible to undertake a static load test.

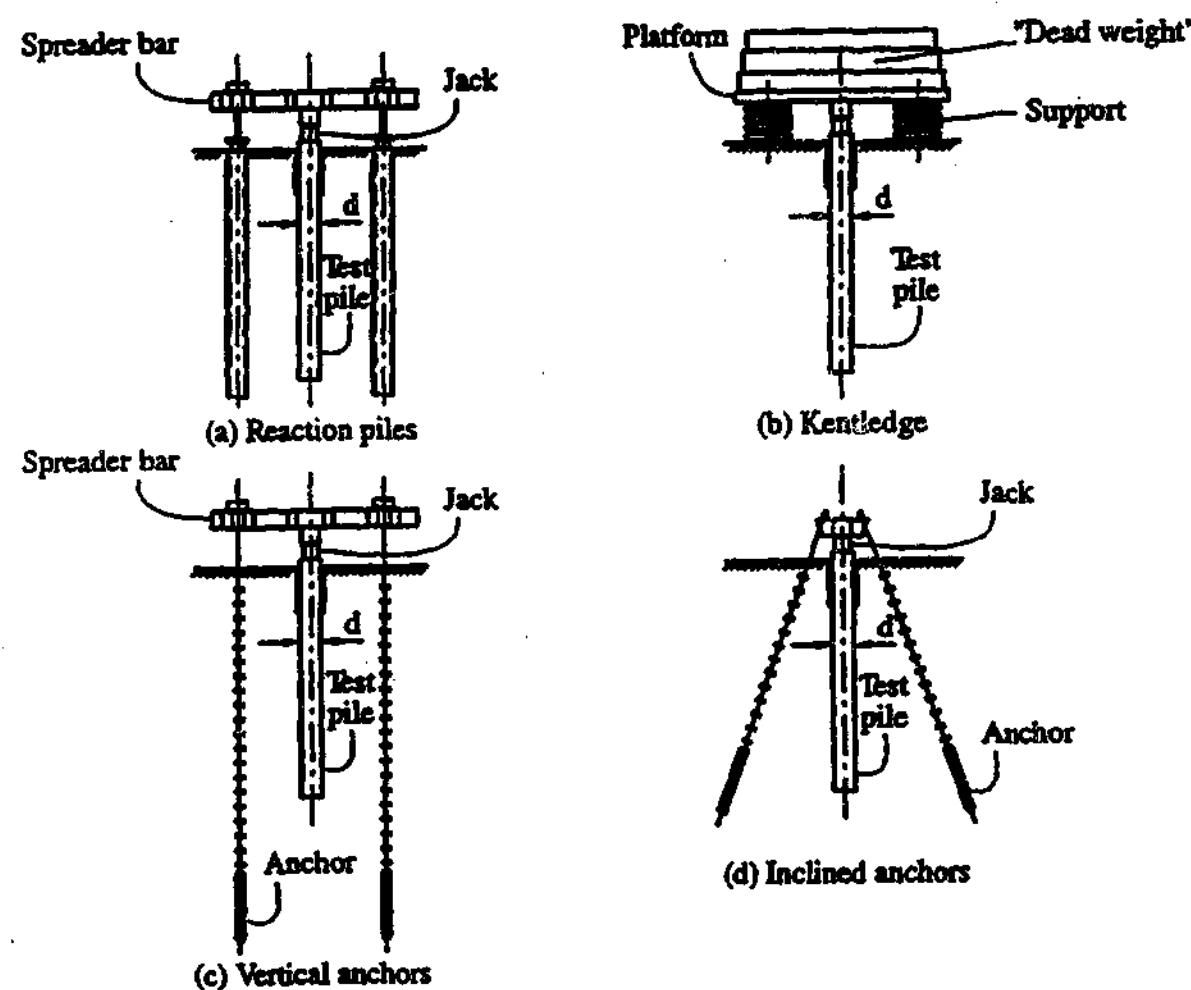


Figure 2.1 Some reaction systems for static load tests (Poulos, 1998)

2.2.3 Dynamic formulae

The other traditional method of determining the pile capacity applies only to driven piles. This method relies on so-called driving formulae which are based on equating the energy transmitted to the pile from the hammer to the elastic and plastic work done on the pile. There are a range of pile-driving formulae in use around the world, including the Hiley Formula, the Engineering News Formula, the Janbu Formula and the Danish Formula. Although there are specific differences between the methods, which arise from particular assumptions made in their derivation, it is possible to generalize that the capacities deduced using these methods are no more than approximate and are flawed given that:

- the methods are based on a representation of the hammer and pile as lumped rigid masses. The pile is a distributed mass which is dominated by stress-waves and does not respond as a rigid body (see also Table 2.1);

- the actual amount of useful energy being transmitted to the pile, i.e. the efficiency of the driving system, is unknown or must be estimated or assumed;
- the degree of elasticity or plasticity of the impact is represented in some methods by a 'coefficient of restitution' which is poorly known and understood;
- the pile driving resistance during an impact event is greater than the static component of resistance which is being estimated.

Table 2.1 Comparison of Newtonian collision theory and actual pile driving scenario

Newtonian collision	Pile driving
Force is propagated instantly through the pile.	Force is propagated through the pile as a wave.
The theory applies to stiff bodies which upon impact experience very small strains and large stresses.	The soil is very low in its stiffness, resulting in small stresses and large strains in the soil (Poskitt, 1991b).
The theory assumes the colliding bodies are not subject to an external restraint.	The pile is restrained by the soil mass into which it is driven.

Because of the oversimplifying assumptions, this method is understandably used with large safety factors – sometimes ranging as much as from 4 to 12. However, because of their simplicity, the formulae are still in common usage and are usually used to correlate the results of higher order testing (i.e. dynamic testing or static testing) at a particular site to the pile population at the same site.

2.2.4 Wave equation analysis

The many shortcomings of the dynamic formulae have been eliminated by the wave equation analysis which accurately simulates the hammer impacts and the pile penetration process. The approach was first developed by Smith (1960), and since then, several programs have been developed. The most widely used program in the industry for such an analysis is GRLWEAP[®]. The methodology involved in the GRLWEAP analysis is therefore discussed.

The pile, its helmet and the hammer used to strike the pile are modeled by a series of segments each consisting of a mass and a spring, as shown in Figure 2.2. The

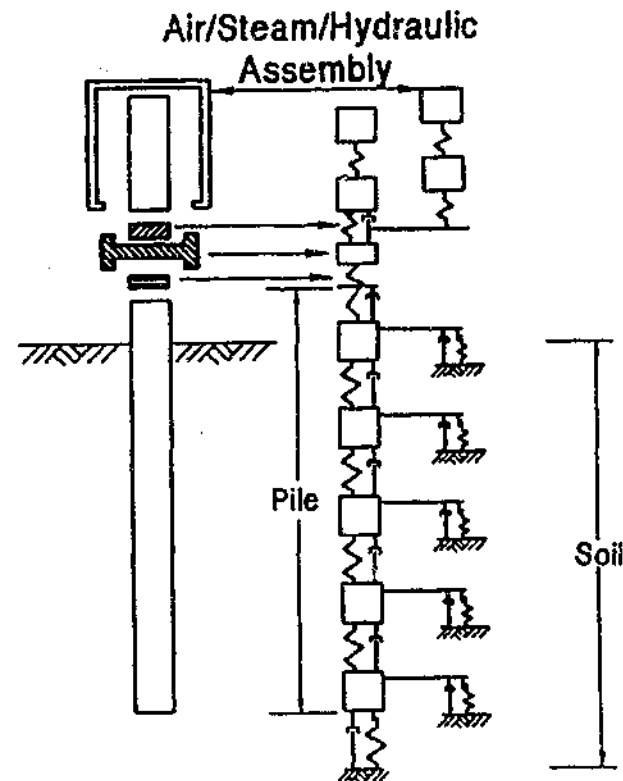


Figure 2.2 Pile model in GRLWEAP (after PDI, 1998)

stiffness of the spring is calculated from the cross sectional area and the relevant modulus of elasticity. To model the energy losses in cushion materials and in all segments which can separate from their adjacent segments by a certain distance, coefficients of restitution are specified.

The analysis commences by calculating a ram velocity using the input hammer efficient and stroke. The ram movement causes displacement of helmet and pile head springs, and therefore compressions (or extensions) and related forces acting at the top and bottom of the segments. Furthermore, the movement of a pile segment induces soil resistance forces. A summation of all forces acting on a segment divided by its mass yields the acceleration of the segment. The product of the acceleration and time step summed over time is the segment velocity. The velocity multiplied by the time step yields a change of segment displacement which then results in new spring forces. These forces divided by the pile cross sectional area at the corresponding section equal the stress at that point. Similar calculations are made for each segment until the accelerations, velocities and displacement of all segments have been calculated during the time step. The analysis repeats for the next time step using the updated motion of the segments from the previous time step. Thus, the

accelerations, velocities, displacements, forces and stresses for each segment are computed over time.

Essentially three forms of output known as the “bearing graph”, the “inspector’s chart” and driveability analysis can be generated from the analysis. The “bearing graph” which relates ultimate capacity to driving resistance, can be produced by performing the analysis over a wide range of ultimate capacities. The “inspector’s chart” relates the hammer energy or stroke to driving resistance for one particular user-specified ultimate capacity value and includes associated stress maxima of the pile. The driveability analysis computes the driving resistances and stresses based on user input shaft and toe resistance values at up to 100 user selected pile penetrations. The results are typically plotted together with the capacity values versus pile penetration. The plot allows the user to predict when refusal may be expected or where high driving stress levels may develop. In addition, the driving time, excluding interruptions, can be estimated.

In GRLWEAP, the *static* soil resistance is modeled conceptually with a linear elastic spring in series with a plastic slider. The plastic slider allows continued displacement with no increase of shear stress when the shear displacement exceeds the quake value. Thus, these two elements model the elasto-plastic behaviour of the soil resistance. The static soil resistance is shown schematically in Figure 2.3. The static resistance (R_s) is expressed mathematically as follows:

$$R_s = kx \quad (2.1)$$

where k is the soil stiffness at the pile-soil interface, and x is the shear displacement which is limited to the quake value (Q).

The *dynamic* force due to viscous damping is modeled with a viscous dashpot which acts in parallel to the elasto-plastic spring. GRLWEAP offers essentially a linear dynamic force model and a non-linear dynamic force model. The linear model, known as the linear viscous damping model, is based on but differs from the Smith damping model. The Smith model gives the dynamic force (R_d) in the form of:

$$R_d = J_{Smith} v R_{inst} \quad (2.2)$$

where J_{Smith} is the Smith damping factor, v is the relative velocity between the pile and the soil, and R_{inst} is the instantaneous resistance, whereas the linear viscous model gives the dynamic force (R_d) in the form of:

$$R_d = J_{viscous} v R_{ult} \quad (2.3)$$

where $J_{viscous}$ is the linear viscous damping factor, v is the relative pile-soil velocity, and R_{ult} is the ultimate resistance. The dynamic force modeled by the linear viscous damping model is shown schematically in Figure 2.3. The non-linear model is based on the work of Coyle and Gibson (1970), Heerema (1979), and Litkouhi and Poskitt (1980), and is in the form of:

$$R_d = J_{viscous} v^N R_{ult} \quad (2.4)$$

where N has a value of about 0.2 to model the non-linear response. Although the value of the damping factor has a significant influence on the predicted dynamic response, little guidance is available for the selection of an appropriate damping factor.

It is important to note that the GRLWEAP model assumes that the soil mass surrounding the pile does not move. Therefore, the relative pile-soil velocity is effectively the pile velocity. As will be discussed in more detail in Section 2.3.1, the assumption that the soil mass is stationary during a pile driving event is not strictly correct.

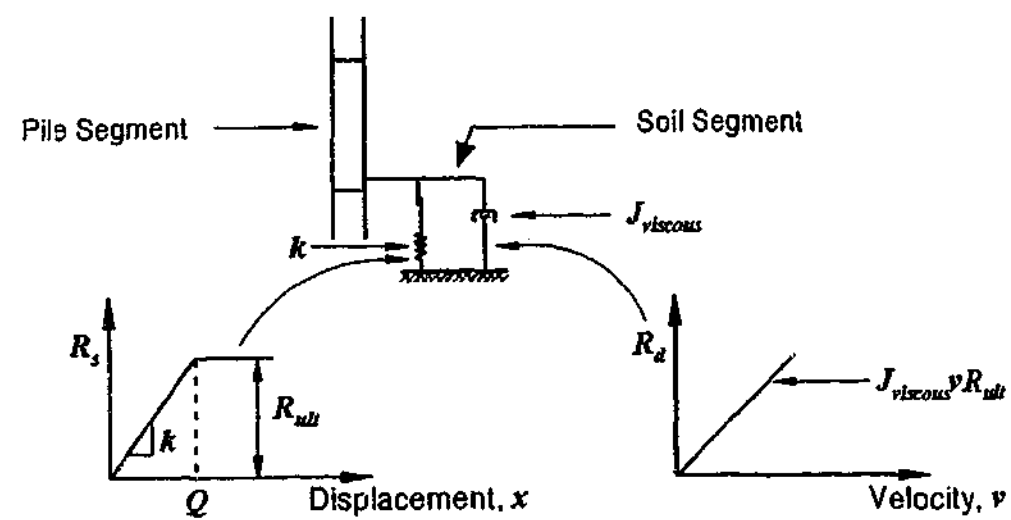


Figure 2.3 Static and dynamic soil models in GRLWEAP (after PDI, 2000)

2.2.5 Pile dynamic testing

A method of determining the pile capacity called dynamic testing was developed in the 1970's (Rausche et al., 1972). Today, dynamic pile testing is accepted as a valid technique of inferring the static capacity of piles and a standard quality assurance and construction control method for piled foundations. A typical set-up for carrying out a dynamic test involving a ram as well as strain gauges and accelerometers is shown in Figure 2.4, and the typical force and velocity records based on the strain and acceleration measurements on are shown in Figure 2.5. Probably the most widely used system for undertaking dynamic pile monitoring is the Pile Driving Analyser (PDA) shown in Figure 2.6.

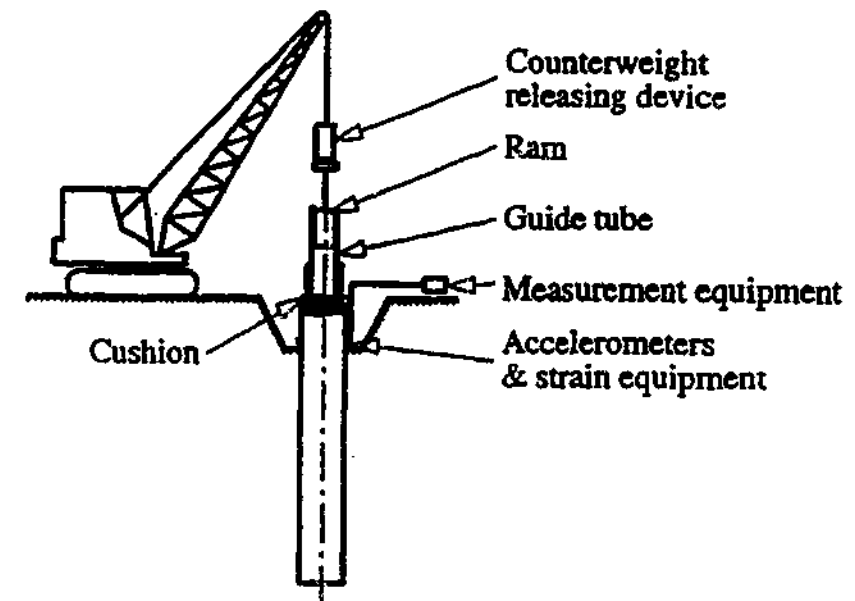


Figure 2.4 The dynamic load test (Poulos, 1998)

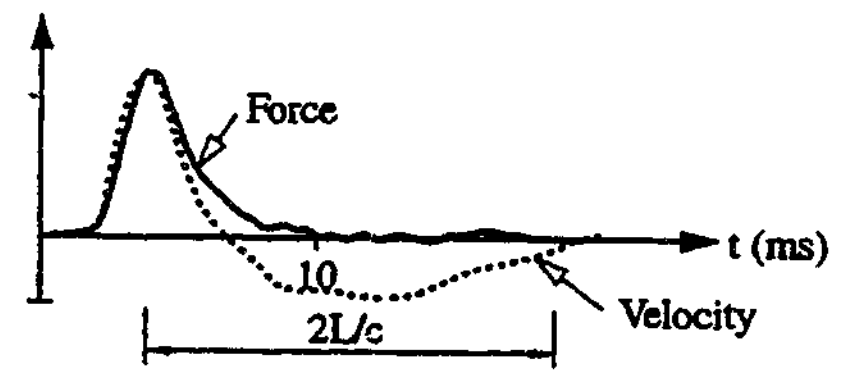


Figure 2.5 Typical force and velocity records (Poulos, 1998)

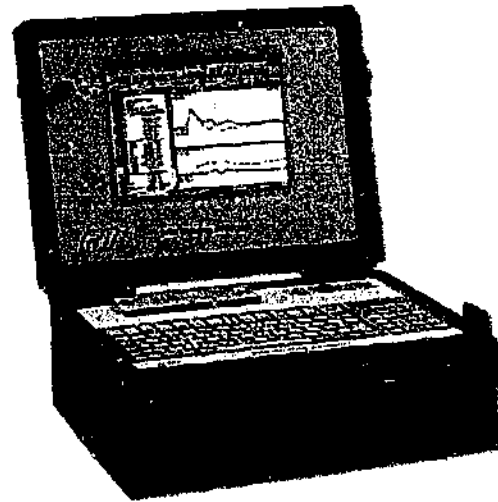


Figure 2.6 PDA unit (PDI and GRL, 2003)

The dynamic pile testing method is based on the analysis of stress-waves in the pile generated by the blow of the pile driving hammer, and reflected from soil resistance acting along and below the pile and from variations in the geometry and material properties of the pile. The theory of stress-wave propagation in the pile is well documented (e.g. Rausche et al., 1972; Goble et al., 1975; Rausche et al., 1985; Randolph, 1990; Fleming et al., 1992). An extract from Randolph (1990), which explains critical and relevant aspects of the theory, is included in Appendix A. Because dynamic (i.e. motion-related) effects occur when a pile is subjected to impact loading, the technique is based on the premise that the static resistance can be isolated from the dynamic effects. In order to correctly isolate the static and dynamic responses from the combined driving resistance, it is necessary to develop valid mathematical models of these components which reflect physical reality. If the model is flawed, the components of the driving resistance may be misinterpreted or misallocated, and the reliability of the deduced static capacity will be compromised. Developing a soundly-based physical model of the resistance components is a significant challenge for the researcher.

Compared to static load testing, dynamic pile testing is significantly more economical and is significantly faster to execute. Unlike dynamic formulae, the dynamic pile testing methods are founded on one-dimensional wave mechanics. As a more valid approximation of pile driving events, dynamic pile testing is more soundly based and is thus significantly more reliable, although the method can be further improved as will be discussed. The dynamic pile testing method was

originally developed specifically for driven piles. However, the method has general theoretical application, which allows successful application to bored piles (Seidel and Rausche, 1984) and barettes (Seidel et al., 1996). With trends toward screwed-in-place piling, the method has also been applied to such piles, although it should be noted that the use of dynamic testing methods in new situations should be carefully validated by reference static load testing. This is deemed particularly important when the resistance models adopted are empirically based. If the new testing situation lies outside the dataset on which the empirical parameters are based, caution must be exercised.

A special benefit of dynamic pile testing which is not available to static load testing is the ability to test the pile during the exact time of installation. It is well known that piles are installed in soils of all types, but particularly fine-grained soils below the water table experience time-dependent capacity changes. Capacity increases (known colloquially as set-up) are most common, but capacity reductions (known as relaxation) are also observed in relation to loss of toe capacity in particular formations. These capacity changes can be monitored by a sequence of dynamic tests commencing at the end of driving, and continuing for days, weeks or even years. Practical limitations make it impossible to statically load test a pile at the completion of installation, or to undertake sequential load tests, unless for a special research application. This feature of dynamic testing enables a direct relationship to be established between pile capacity and the field response (measured as set and temporary compression), and to develop a meaningful correlation between dynamic pile testing and dynamic formulae.

As previously mentioned, dynamic testing is used not only for estimating pile capacity, but also more generally for construction control, including stress control, damage assessment and pile driving hammer evaluation. These are important practical benefits of the technique; however, as they are independent of the static and dynamic soil resistance models adopted, they will not be discussed further.

However, the dynamic model on which the reliability of the method depends has yet to be established definitively. Whilst the linear model currently being used as the basis for analysis and interpretation usually yields reasonable results, experimental

studies conducted thus far show that the velocity-dependence of soil resistance is highly non-linear. This suggests that interpretations could be improved if an appropriate non-linear model could be introduced.

When a pile is dynamically tested during driving or after installation, the capacity of the pile can be approximated using a non-rigorous method called the Case Method and/or more accurately determined using a rigorous method involving signal-matching of the measured stress-wave record. These analyses are described subsequently.

2.2.5.1 The Case Method

The Case Method is an approximate closed-form solution for pile capacity based on the following assumptions:

- all the dynamic resistance is concentrated at the pile tip where soil is remoulded
- the cross-section or impedance of the pile is consistent along the pile length
- the static pile resistance is constant during the period $2L/c$ when the stress-wave travels to the pile tip and returns to the pile top.

Since these assumptions are an over-simplification, the method is only approximate.

The closed-form solution can be written as:

$$R_s = (1 - J_c) W\downarrow(t) + (1 + J_c) W\uparrow(t+2L/c) \quad (2.5)$$

where $W\downarrow(t)$ is the force of the downward traveling (incident) wave at an arbitrary time, t

$W\uparrow(t+2L/c)$ is the force of the upward traveling (reflected) wave at a time $2L/c$ after the arbitrary time, t

J_c is the Case damping parameter, which determines the relative contribution of static and dynamic resistances.

The value of the Case damping parameter (J_c) assumed for the modeling of the dynamic effect may have a large influence on the deduced static capacity, particularly in easy driving when velocities are highest, and especially at the pile toe. In general, a value of $J_c = 0$ implies no dynamic resistance. The value of J_c is not bounded, but typically does not exceed 1.0.

Where the value of the damping parameter can be calibrated against actual pile capacity obtained from a static load test or more rigorous dynamic analysis using signal matching, this method can be used to reasonably estimate the capacity of subsequently installed and monitored piles. It is noted that it may be difficult or impossible to correlate the Case Method to static load testing where there is a significant delay between the two tests.

2.2.5.2 CAPWAP signal-matching analysis

A more rigorous analysis known as signal-matching can be carried out to more accurately determine the pile capacity. The analysis can be considered as a “flipside” of the pile driveability analysis. The most commonly used commercially available software for signal-matching is CAPWAP[®] from Pile Dynamics Inc.. Therefore, the methodology involved in the CAPWAP analysis is described.

The CAPWAP analysis requires that the pile and the soil resistances acting on the pile are modeled. Unlike the spring-mass model used in GRLWEAP, the pile model in CAPWAP is known as a continuous model where the pile is divided into segments such that the wave travel time of all segments is equal. Each pile segment is subjected to a total soil resistance that comprises the static and dynamic components.

The adopted sign conventions are positive for compression waves and downward movement and negative for tension waves and upward movement. During the hammer blow, a compression (positive) wave travels downwards from the pile top. During downward loading of the pile shaft segment where the resistance acts upward against the pile segment, a compression wave (positive) equal to one half of the instantaneous (static and dynamic) resistance travels upwards from that location. Thus, the measured force and velocity at the pile top are the summed effect of the downward traveling wave from the hammer blow, and the upward traveling waves from the resistances of the pile segments and the pile toe.

In the analysis, the propagation of both upwards and downwards traveling waves is tracked. At any time, the forces of the downward ($W\downarrow$) and upwards ($W\uparrow$) traveling waves at a particular pile segment can be related to the force and the velocity of the pile segment using Equations (2.7) and (2.8).

$$W \uparrow = \frac{1}{2}(F - Zv) \quad (2.6)$$

$$W \downarrow = \frac{1}{2}(F + Zv) \quad (2.7)$$

Superposition of the two types of waves yields forces and velocities at the upper and/or lower boundary of a segment. The velocity of a particular segment at a particular time is integrated to obtain the displacement.

A chart showing the CAPWAP program flow has been included in Figure 2.7. Using the measured force and velocity as a starting point, the force, the velocity or the wave-up force ($W \uparrow$) signals at the pile top can be computed based on “guessed” resistance responses at the various pile segments. The resistance response at a pile segment is simulated with user-input soil static and dynamic resistances. By iteratively changing the soil static and dynamic distributions along the pile shaft and at the pile toe, the computed parameter (the force, the velocity, or the wave-up force ($W \uparrow$)) at the pile top can be adjusted until it most closely matches the equivalent measured signal at the pile top. The quality of the match is defined objectively by the match quality number or can be assessed subjectively. It is usually recommended that the matching be done based on the wave-up response as it isolates the soil resistance responses that are of primary interest in the CAPWAP analysis. If the no match can be achieved, the pile model and/or soil model will need to be refined. If reliable blowcount has been measured, it should be matched with the blowcount computed in the CAPWAP analysis. If the measured blowcount cannot be matched, then the measured record will need to be checked and may need to be adjusted. Having defined a “best match” of the curve (and of the blowcount for cases where the measured blowcount is reliable), the static pile capacity, the distribution of the static resistance, and the predicted load-movement response during loading and unloading are deemed to be determined.

It is accepted that signal matching does not result in a unique solution. Different values of viscous damping constants, elastic quakes and resistance distributions may be used for a particular match, resulting in different solutions. Because of the

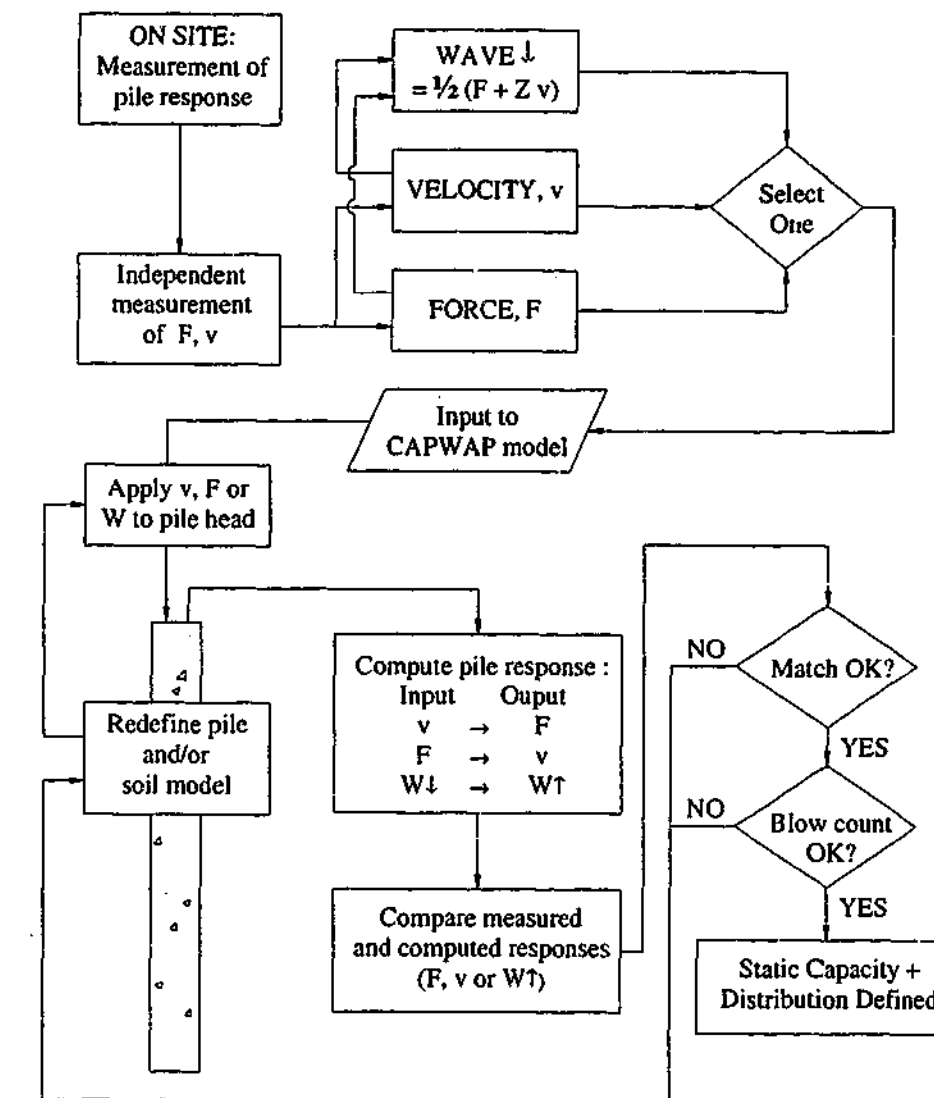


Figure 2.7 CAPWAP program flow (after Seidel et al., 1997)

different assessment of the amount of damping present, the predicted static capacity may vary from one operator to another (Fellenius, 1988). However, the computed total static resistance is generally thought to closely predict the actual field resistance, but the actual distribution of the resistance down the pile and the actual proportion of the resistance at the pile base may deviate from that predicted (Middendorp and van Weele, 1986).

The static resistance model is the same as that used in GRLWEAP. The dynamic resistance (due to viscous damping) for the shaft is the linear viscous damping model (which is also used in GRLWEAP) as it has been found that the linear damping model is more likely to match measured signals as compared to the Smith model (PDI, 1994). The dynamic resistance model for the toe can be the linear viscous

damping model used in GRLWEAP, the Smith damping model, or a combination of the two. Additional models for the toe are available for modeling a soil plug that exerts an external force against the toe, and a gap that might exist between the toe and the end bearing soil layer.

Unlike GRLWEAP, CAPWAP gives the user an option to model movement of soil surrounding the pile and thus allows an additional dynamic phenomenon known as radiation damping (which will be discussed in Section 2.3.1) to be modeled. It is noted that because of the soil movement, the velocity (v) used in the linear viscous damping model (which is defined as the relative pile-soil velocity) is no longer equal to the pile velocity.

The radiation damping models for the shaft and the toe are shown schematically in Figure 2.8, where the static and dynamic resistance (due to viscous damping) models as well as the soil plug and the gap models for the toe have also been included. The radiation damping model consists of a mass and an inertial dashpot (as opposed to a viscous dashpot) which is placed in series with the static resistance-viscous damping model. The radiation damping model adopted in CAPWAP is empirical, and the mass and dashpot constants for the shaft and the toe are not rationally determined from soil properties. Instead, the parameters are iteratively selected by the user until a good match is achieved. As such, the soil velocities and soil displacements thus calculated may not reflect physical reality.

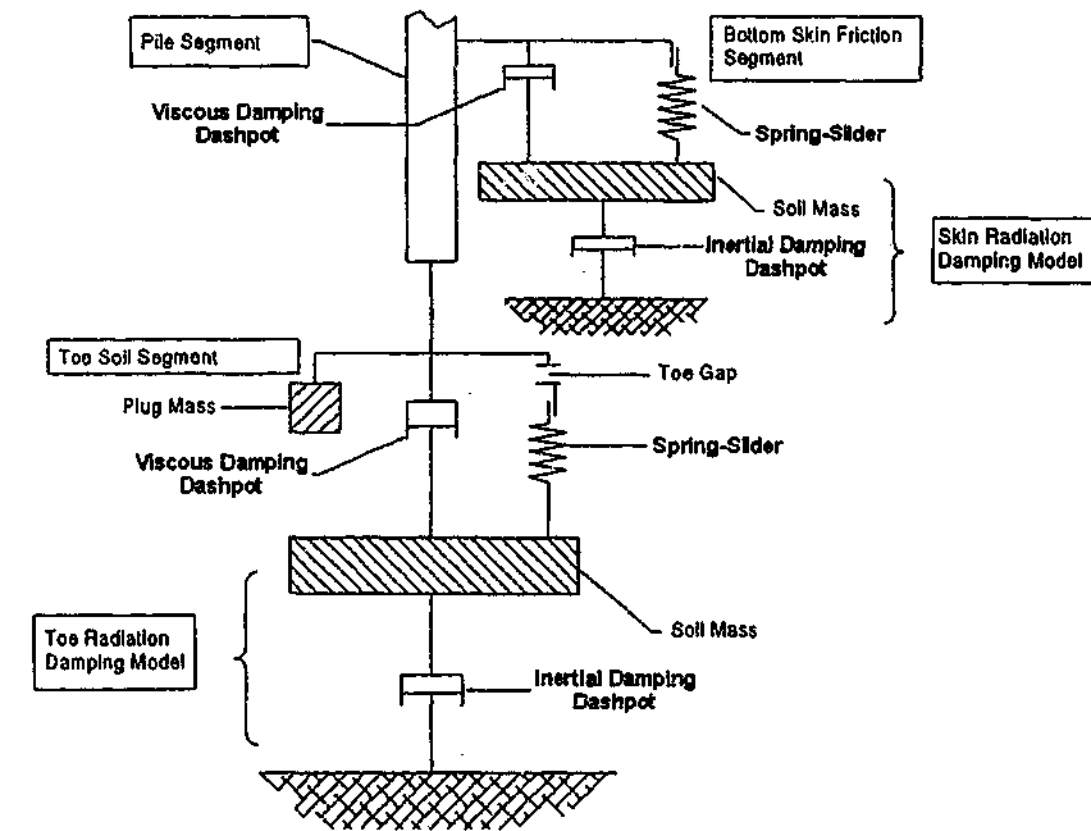


Figure 2.8 The radiation damping model (and static & dynamic soil resistance models, as well as soil plug and gap models for the toe) used in CAPWAP (after PDI, 2000)

2.2.6 Statnamic testing

The dynamic test involves applying a hammer blow to the pile head so that the pile is moved and the soil resistance mobilised. There is a variation of this method called Statnamic testing. The principles of Statnamic testing are shown in Figure 2.9. The impact force is applied to the pile head by the burning of fast-expanding fuel in a combustion chamber placed between the pile head and a mass, resulting in a pressure acting upwards on the reaction mass. The mass in turn produces an equal and opposite (inertial) force acting downward on the pile head. The peak pile velocities imparted using this method are generally lower than those delivered by the hammer blow, hence the term Statnamic (static-dynamic) testing. The velocity response during the impact event is recorded using accelerometers or a laser level. The force is determined directly by a load cell placed between the combustion chamber and the pile head.

Although the peak pile velocities generated during Statnamic testing are generally less than for dynamic pile testing, the velocities may be high if the charge of

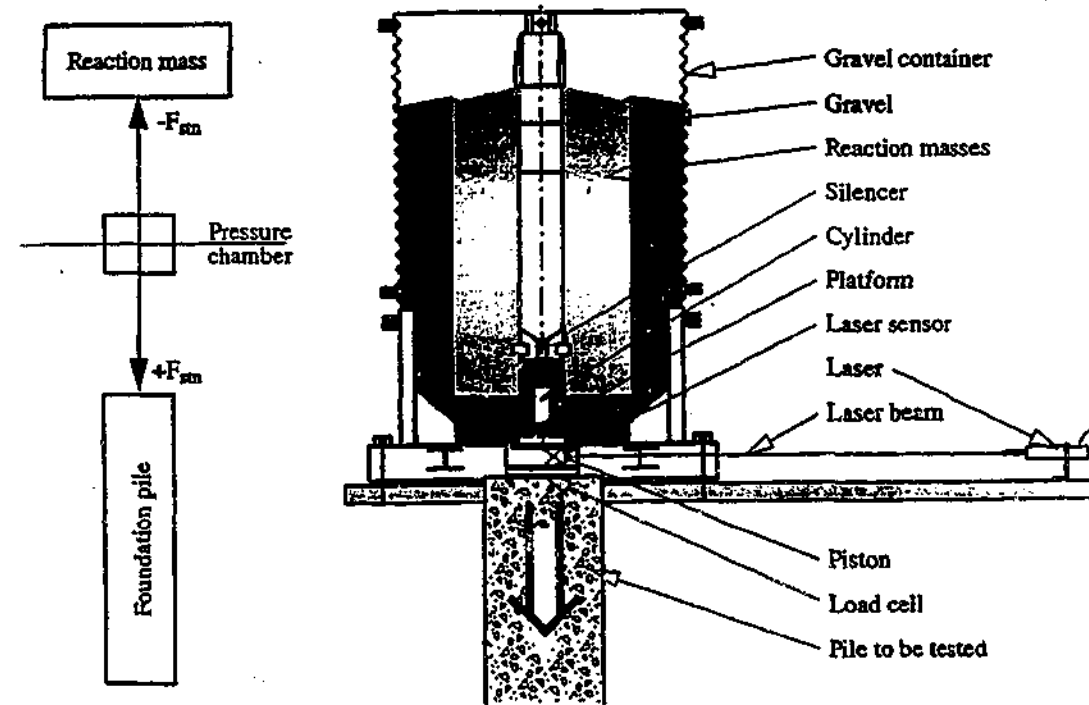


Figure 2.9 Schematic of the Statnamic test (Poulos, 1998)

combustible material used is excessive (which may be because the pile resistance has been overestimated). In such cases, velocities may be quite large. Under such circumstances, Statnamic testing may result in an overestimation of static capacity. It is suggested that this may result from the linear damping also used in the interpretation of these tests. Use of a non-linear model may improve prediction.

In addition, a critical review undertaken by Seidel et al. (1996) of the method of analysis of Statnamic tests indicates flaws in their interpretation, which are considered to be due in significant part to the linear damping law adopted (Seidel, 1998). Therefore, the linear viscous damping model, which has given reasonable results for the conventional dynamic testing method, cannot be assumed to be relevant to the Statnamic test (Seidel, 1998).

2.3 The Dynamic Response of the Pile Shaft-Soil System

From the discussion of the dynamic analyses in the previous section, it has become apparent that dynamic analyses (signal-matching and pile driveability analyses) rely on a correct model in order for the correct static resistance to be deduced. Such a model can only be formulated by taking into account the physical processes that occur during the dynamic event.

There are three differences between the static and dynamic response of piles. The first is the inertial effects of both the pile and the surrounding. The second is the velocity-dependence of the pile shaft-soil interface resistance and of the resistance of the soil mass at the pile tip. In the ensuing discussion, the two primary differences are discussed, with particular emphasis on the pile shaft component which is the focus of the present study. It is noted in passing that for driven open-ended piles for which soil plugging behavior is important, different modes of failure may occur under static and dynamic loading conditions (Smith et al., 1986).

2.3.1 Physical processes

As the pile head is loaded, the pile shaft is forced downward. In the initial stage, the strain in the soil adjacent to the pile wall is low very small, the shear stress is small, and the pile shaft and the soil move in concert. As the pile moves downward to a critical displacement, the plastic strength of the pile-soil interface is exceeded, resulting in a localized band of high shear strain in the soil at the interface and the pile shaft slips past the soil. At a subsequent stage of loading when shear stress reversal causes the shear stress at the interface to once again fall below the plastic strength, the pile and the soil movement is again linked. During the phase of relative movement between the pile and the soil, the pile-soil interface resistance, is found to be rate-dependent due to a phenomenon called viscous damping. The term "viscous damping" is used to describe the strength of a soil or a pile-soil interface being velocity-dependent. The word "viscous" is used to describe the increase in resistance with the increasing rate at which the force is applied. The word "damping" is used to describe the energy being dissipated during the process. It has been reported that the rate-dependent nature of soil strength was first recognized by a French engineer, A. Collin in 1846 (Schimming et al., 1966). This viscous damping phenomenon is the subject of investigation of the present study and will be discussed further in Section 2.4. Because viscous damping is localised at the interface, it is known as a *near-field* effect.

During the occurrence of the near-field effects, *far-field* effects also occur in the soil surrounding the pile. As the stress-wave travels down the pile, stress-waves from the pile-soil contact radiate outward from the pile to the surrounding soil (Gazetas and Dobry, 1984). It is well established that waves generated along the pile-soil interface

propagate mainly in horizontal directions and under essentially plane strain conditions (Gazetas and Dobry, 1984); this is shown schematically in Figure 2.10 and Figure 2.11. The radiation is also known to occur at the speed of the shear wave in the soil, which is a function of the shear strain modulus and the mass density of the soil. The shear waves cause vertical accelerations, velocities and displacements of the soil which, depending on the ease of driving, can sometimes be felt as the pile is driven. The radiation of the energy from the pile to the surrounding soil and the resulting absorption of the energy in the surrounding soil is known as either geometric, inertial or radiation damping. The radiation of the waves can be “visualised” by considering one wave front, as shown in Figure 2.11. As the wave front travels outward, it strains an annulus of the surrounding soil at any given time and internal strain energy is stored in that annulus of soil momentarily. As the wave encounters an increasingly larger volume of material as it travels outward, the energy density in each wave decreases with distance from the pile-soil contact; this implies that the internal strain energy imparted to the soil decreases as the distance away from the interface increases. In an ideal situation where soil hysteretic damping does not occur, this energy is transferred to an infinite distance from the pile. However, with the absorption due to soil hysteresis, the energy associated with the wave front eventually decreases to zero.

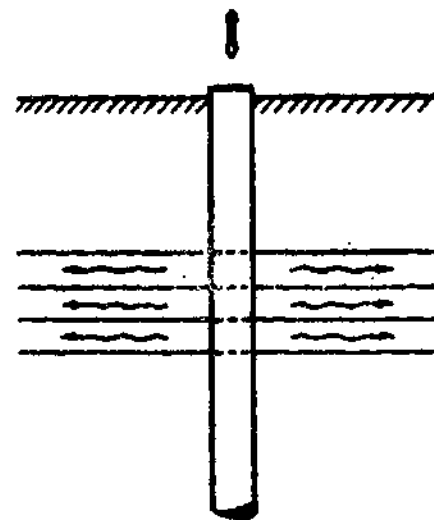


Figure 2.10 Illustration of stress-waves at the pile shaft propagating horizontally from the pile shaft (Gazetas and Dobry, 1984)

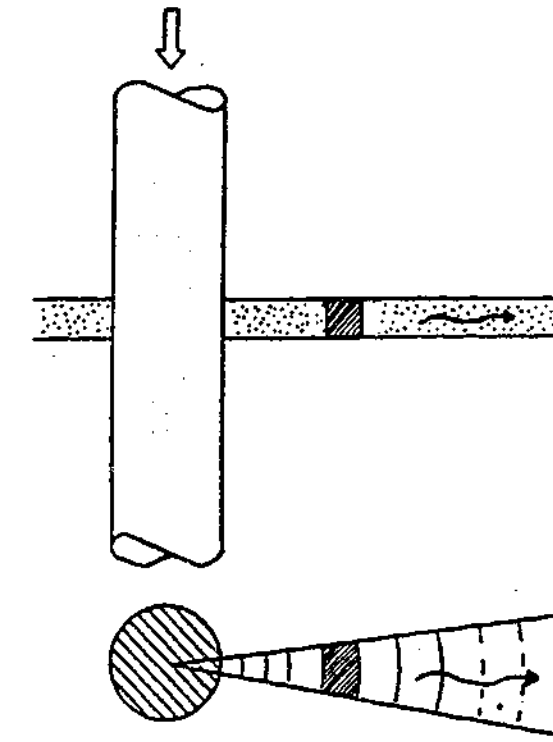


Figure 2.11 A soil element “experiencing” the stress-wave momentarily as the wave passes through it (Michaelides et al., 1997)

2.3.2 Modelling of the dynamic response

Various models with varying sophistication, empiricism and theoretical justification (some of which are used in the GRLWEAP and CAPWAP analyses) have been proposed for modeling the dynamic pile shaft-soil interaction.

The first ever model for this purpose is the semi-empirical model proposed by Smith (1960) which still dominates pile driving analysis in the industry today. This model is shown schematically in Figure 2.12.

The Smith static soil resistance model is the basis of the static soil resistance model of GRLWEAP and CAPWAP. As previously shown, the Smith static soil resistance model can be represented by the spring-slider system. The model has been discussed in Section 2.2.4 and expressed mathematically in Equation (2.1).

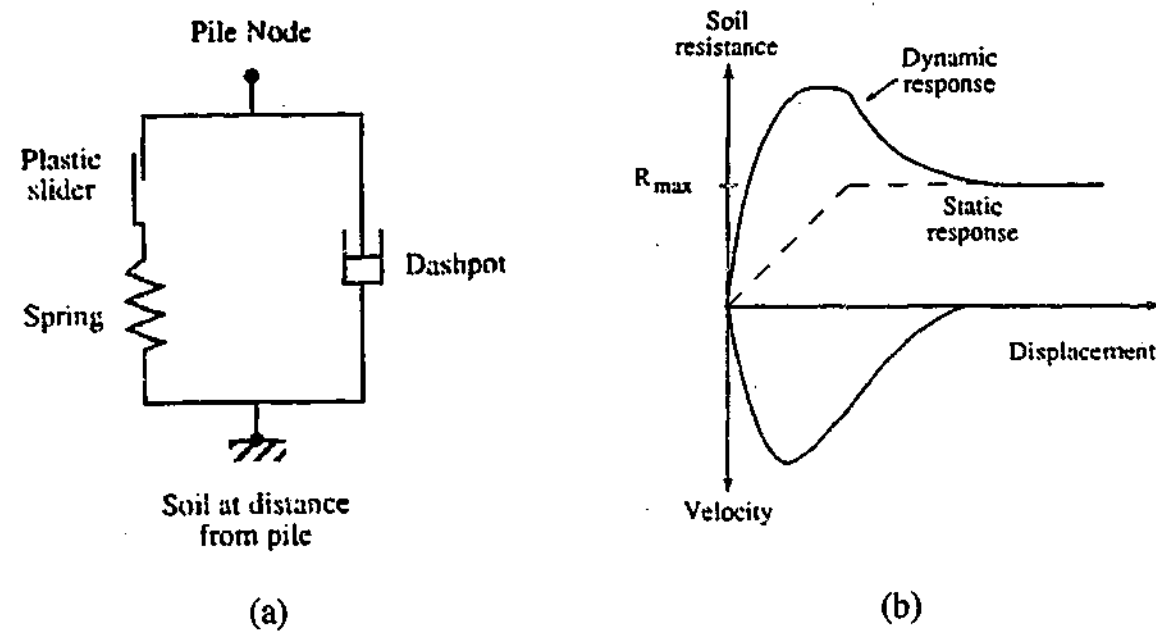


Figure 2.12 (a) The Smith shaft model (b) Typical shaft response (Randolph, 1990)

The Smith dynamic force can be represented by a dashpot which is placed in parallel to the spring-slider system. The dynamic force is in the form of:

$$R_d = J_{smith} v R_{inst} \quad (2.8)$$

where J_{smith} is the Smith damping factor, v is the relative pile-soil velocity, and R_{inst} is the instantaneous resistance. It is noted that the Smith model assumes that only the pile moves and the soil mass surrounding the pile does not move so that the relative pile-soil velocity is effectively the pile velocity. It is reiterated that the linear viscous damping model used in GRLWEAP and CAPWAP is a modified version of the Smith damping model, where the *instantaneous* resistance in Equation (2.8) has been replaced by the *ultimate* resistance.

It is significant that the Smith model assumes that the soil mass surrounding the pile does not move, and that inertial or radiation damping effects do not occur. The consequence is that, although the dashpot is originally intended to model viscous damping, it must in reality incorporate both viscous damping and radiation damping effects.

Arguably the most advanced model to date has been developed by Randolph and his co-workers (Randolph and Simons, 1986; Randolph, 1990; Randolph and Deeks, 1992; Randolph, 2000). It models the movement of the soil surrounding the pile in

addition to the movement of the pile, and thus distinguishes the near-field and the far-field responses. The various elements of the model are shown schematically in Figure 2.13. The near-field response is conceptually modeled with either the spring-in-series-with-slider or a slider for simplicity (as shown in Figure 2.13), in parallel with a *viscous* damping dashpot. The dynamic resistance modeled by the dashpot increases exponentially with velocity based on some experimental studies (e.g. Dayal and Allen, 1975; Heerema, 1979; Litkouhi and Poskitt, 1980). The dynamic resistance can be expressed as:

$$R_d = Jv^N R_{ult} \quad (2.9)$$

where R_{ult} is the ultimate resistance, v is the relative velocity between the pile and the soil, J is the damping factor for the power law and N has a value of about 0.2 to model the non-linear response. It is noted that because the soil surrounding the pile is allowed to move, the relative pile-soil velocity is not equal to the pile velocity.

The far-field response is conceptually modeled with a spring in parallel with the *inertial* damping dashpot based on the elastodynamic theory proposed by Novak et al. (1978), and the spring stiffness and dashpot constants are determined rationally from the elastic parameters of the soil. This is in contrast with the empirical radiation

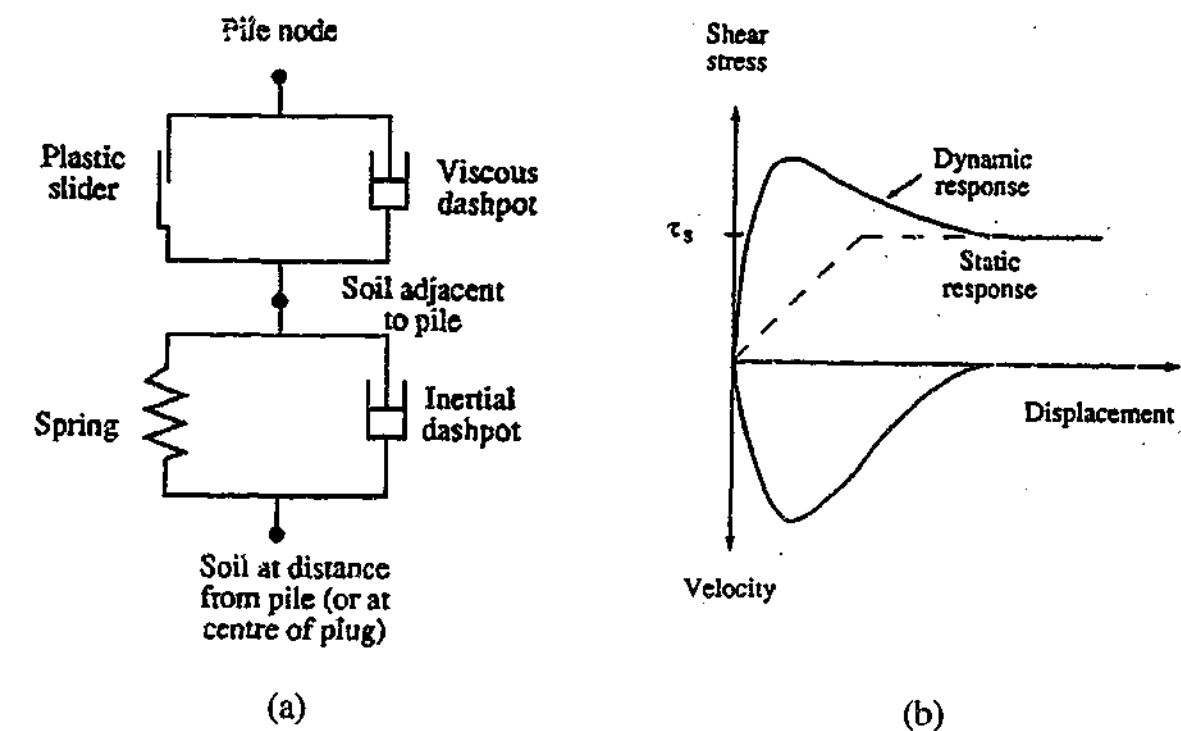


Figure 2.13 (a) Shaft model by Randolph and co-workers (b) Typical shaft response (after Randolph, 1990)

damping model in CAPWAP, which comprises a soil mass in parallel with a dashpot, and whose mass and dashpot constants are iteratively selected by the CAPWAP user until a good match is achieved. As shown in Figure 2.13, the near-field component and far-field component are coupled in series. To allow the soil surrounding the pile to move, an intermediate node between these components, which represents the soil immediately adjacent to the pile, is introduced. By tracing the motion of this node and the pile node, the displacements and velocities of the soil adjacent to the pile and the pile can be monitored simultaneously. Thus, the relative velocity between the pile and the soil (or the slip velocity) required in Equation (2.9) can be determined. When slip does not occur, the relative velocity will be equal to zero and the displacements will thus differ by a constant amount. During slip, the relative velocity will differ and the relative displacement will change.

2.4 Viscous Damping

2.4.1 Requirement for a correct viscous damping model

It has been discussed that dynamic methods for determining the pile capacity and for forecasting the driveability of piles are premised on accurate modeling of the dynamic processes that occur during the dynamic event. As has been mentioned, the far-field response is elastic/inertial and the influence of this response on the pile can be theoretically modeled with reasonable success. However, the near-field response of viscous damping has yet to be modeled with confidence. The damping model proposed by Smith had no theoretical basis and was proposed based solely on his intuition. Having said this, and given that it was developed in 1960 well in advance of any available measurements of pile behaviour, the model was inspired and has proved extraordinarily successful in a practical sense. Nevertheless, the assumed linear viscous damping response has been demonstrated to be invalid in many subsequent experimental studies.

Whilst experimental studies have shown the actual damping response at the pile-soil interface to be highly non-linear (e.g. Dayal and Allen, 1975; Heerema, 1979; Litkouhi and Poskitt, 1980; Benamar, 1999), these studies have themselves been limited or in some cases flawed, as will be discussed in detail in Chapter 3. As such, the functional form of the relationship between the dynamic friction and velocity,

and the magnitude of the strength increase due to the dynamic effect have not yet been established. Because of the uncertainties in the non-linear models, the dynamic testing industry has in the main adhered to the traditional Smith model or its modified version.

Given that the linear damping model deviates from the actual non-linear behaviour, the linear damping constant may not be physically meaningful and cannot be selected rationally. The linear damping constants have resisted all attempts to be related to common and fundamental soil properties or in-situ test methods. At most, it is observed that damping is higher for cohesive soils and lower for cohesionless soils.

Given that the use of the linear model in dynamic analyses results in uncertainties in the dynamic analyses, it is evident that a model is required, which is based on physical reality and that depends on fundamental soil properties (e.g. Goble and Rausche, 1980; Simons and Randolph, 1985; Lee et al., 1988). Such a model will improve the reliability of the predictions of pile driveability and of pile capacity.

2.4.2 Mechanism behind viscous damping

The mechanism behind viscous damping is to date unknown although various hypotheses have been proposed (Whitman and Healy, 1962; Briaud and Garland, 1985; Heerema, 1979; Mitchell, 1964). It would appear that the viscous damping phenomenon in soils stems from the interaction at a micro-level between the soil particles. The primary focus of this study is the modeling of the dynamic friction due to viscous damping, although a mechanism will be proposed to explain the viscous damping phenomenon in Chapter 8. Thus the treatment of viscous damping in this study is analogous to the treatment of gravity, where the phenomenon is accepted and modeled but cannot be fully explained.

It is noted that the increase in the shear strength of a soil with the rate of loading is not necessarily due to viscous damping. It has been shown experimentally that the increase in strength in sand and clay specimens tested at higher shear rates in triaxial compression tests is due to the rate-dependent volumetric response of the specimen rather than viscous effects. It has been observed that there is either an increase in dilation or a decrease in contraction, both of which cause a relatively lower pore

water pressure compared to that at slow shear rates. It has been hypothesized by Richardson and Whitman (1962), Whitman and Healy (1962) and Yamamuro and Lade (1993) that the volumetric behaviour is due to the soil particles tending to ride up over one another when sheared at higher shear rates. This volumetric behaviour results in a higher effective stress and hence higher resistance against the applied shear load. This is demonstrated for tests on sand specimens (Seed and Lundgren, 1954; Whitman and Healy, 1962; Yamamuro and Lade, 1993). Similar results are shown for clay specimens (Casagrande and Wilson, 1951; Bjerrum et al., 1958; Crawford, 1959; Richardson and Whitman, 1962; Crawford, 1965; Lefebvre and LeBoeuf, 1987).

Various hypotheses have been proposed to explain the mechanism of true viscous damping. Most of the hypotheses have been proposed in the context of soil-only shearing but the hypotheses can be equally applied to the pile-soil interface. It is however necessary to note that the shearing of the pile-soil interface is different from the shearing that occurs within a soil specimen. Apart from the obvious fact that the media forming the shear plane in the two scenarios are different, the soil at the pile-soil interface is highly remolded due to boring or driving, and the presence of a stiff surface at the interface may alter the shear behavior of the soil (Lupini et al., 1981; Lemos and Vaughan, 2000).

2.4.2.1 Whitman & Healy (1962)

The hypotheses proposed for viscous damping in sand are based on triaxial compression tests. Whitman and Healy (1962) proposed that the relative movement between two sand particles does not occur in a continuous manner. Rather, it occurs at opportune moments when the arrangement of the surrounding particles is allowed to occur with a minimum resistance. However, at high strain rates, the opportune moments occur less frequently for a given strain increment such that the grains have to rearrange with higher resistance.

2.4.2.2 Yamamuro (2002)

A fundamentally different mechanistic explanation has been proposed by Yamamuro (2002) based on sand specimens tested under full vacuum so that excess pore pressure, which has been found to be rate-dependent, cannot be generated. The

friction angle has been found to increase with strain rate but only at very high strain rates. Thus, it is proposed that the strength increase is caused by local inertial effects. According to this hypothesis, from a global and continuum perspective, the triaxial tests conducted at constant velocities should not cause any significant inertial effects. However, at the level of the sand grains, the specimen is not strictly a continuum. Whilst the specimen is strained globally at a constant velocity, some grains move in directions other than the specific global directions and are hence forced by the surrounding grains to move in the global directions. At high velocities, these grains have significant inertial forces which resist the global movement of the surrounding grains, thus creating an additional resistance.

2.4.2.3 Briaud & Garland (1985)

It has been hypothesized by Briaud and Garland (1985) that the rate effect is simply caused by the viscosity of the pore water in the clay. This hypothesis appears to be supported by tests conducted by Schimming et al. (1966), where fluids of different viscosities are used to replace water. It has been found that the strength ratio varies for each type of fluid used. However, since the variation in the strength increases are not in proportion with the respective fluid viscosities, it appears that the viscosity of the pore fluid is not solely responsible for viscous damping in clay soils.

It has been further hypothesized by Briaud and Garland (1985) and Litkouhi and Poskitt (1980), that the viscous behavior in clay is caused by the viscous contacts formed when adsorbed water layers of clay particles penetrate into each other. The viscosity of adsorbed water has been shown to have a higher viscosity than free water. Hence when the adsorbed layers are deeply penetrated such as in overconsolidated clays and when the clays have thick adsorbed layers such as in highly plastic clays, then such clays tend to have higher viscosities (Briaud and Garland, 1985).

It has been further hypothesized by Briaud and Garland (1985) that at low shear rates, soil particles deform in the shear plane with the least resistance. In contrast, at high shear rates, the particles do not have sufficient time to “find” the plane of least resistance or to move in the plane of least resistance, hence exhibiting a higher strength.

2.4.2.4 Heerema (1979)

Heerema (1979) is the only researcher who has attempted to explain the mechanism behind viscous damping specifically at the pile-clay interface. As shown schematically in Figure 2.14, under applied normal stress, the clay will adjust itself to fill the miniscule irregularities of the pile surface. When the surface displaces, tiny gaps are formed locally, thereby causing relative under-pressures. As a result of the pressure differentials, the clay will flow plastically to fit to the new shape. When the velocity of the pile is low, there is sufficient time for the clay to adjust itself. However, when the velocity increases, the adjustment of the clay becomes more difficult so that the interface friction increases. When the velocity becomes excessive, no further adjustment occurs so that any further increase in velocity does not alter the friction significantly; it is proposed that this is the reason for the flattening of the friction-velocity curve at high velocities. Following this hypothesis, hard clays adjust less to the roughness of the wall and hence demonstrate less velocity-dependence. For the pile-sand interface, it is explained that the sand does not adjust itself against the pile surface in such a way because sand particles do not flow plastically and the particles are relatively large compared to the irregularities of the pile wall. Thus viscous damping does not occur for the pile-sand interface.

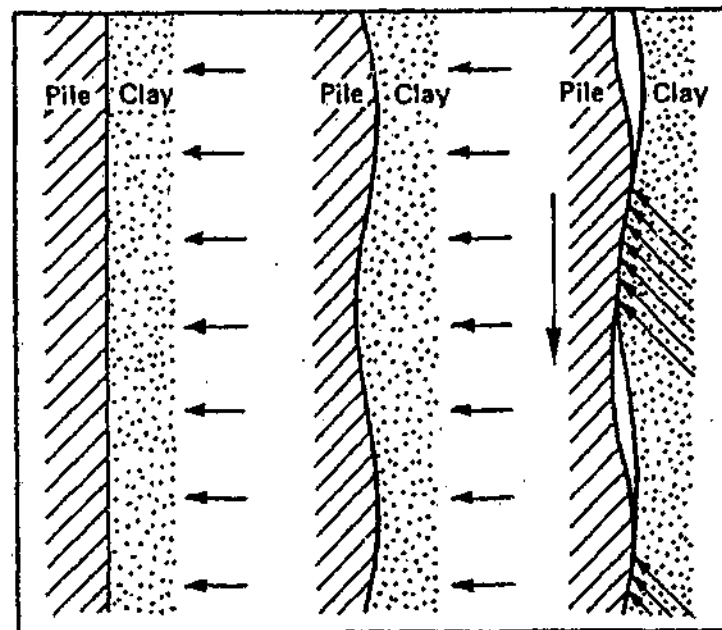


Figure 2.14 Pile wall-clay interaction proposed by Heerema (Heerema, 1979)

2.4.2.5 Mitchell (1964)

Another hypothesis is based on the rate process theory which has been adapted by Mitchell for the modeling of fundamental soil behaviour (Mitchell, 1964). Given that the theory has been found to correctly predict the relationship between strain rate and applied deviator stress as well as temperature, the theory must at least to some degree be capable of modeling the rate-dependent behaviour in soils. According to the theory, atoms, molecules and/or particles of a soil participate in the deformation process when the soil is sheared. In the state of equilibrium, these atoms, molecules and/or particles are prevented from movement relative to each other by energy barriers separating adjacent equilibrium positions. This results in a soil not undergoing deformation. In order for the soil to be deformed, these energy barriers must be overcome by an applied shear stress. The deformation proceeds at a rate dictated by the frequency with which particles can acquire sufficient energy to surmount or cross over the energy barriers between equilibrium positions.

More specifically, the amount of deformation in the soil per unit time is directly proportional to the number of energy barriers that can be successfully surmounted or crossed over. Based on statistical mechanics, Mitchell showed that the higher the external shear stress, the higher the number of successful crossings. In order to deform the soil by an amount necessary to incur soil failure per unit time, a certain number of barrier crossings corresponding to an applied stress needs to be overcome per unit time. Therefore, to achieve the same amount of soil deformation over a lesser period of time or at a higher deformation rate, a higher shear stress is required to achieve the same number of crossings. Thus the higher the strain rate, the higher the shear strength of the soil.

Although there does not seem to be any proof of the validity of the formulation of rate process theory, different parts of the equation adapted for soil mechanics have been tested separately and found to agree with experimental evidence (Mitchell, 1993). For instance, the theory correctly predicts the strain rate dependence of the shear resistance of soils, which is of direct relevance to this research.

2.4.3 Existing viscous damping models

The total friction measured during dynamic shearing can be defined as the sum of the viscous damping friction, τ_d , and the static friction, τ_s , and can be mathematically expressed as follows:

$$\tau_t = \tau_d + \tau_s \quad (2.10)$$

The static friction is the friction measured at a reference low shear rate and as such is really a quasi-static friction.

In order to normalize the total friction and to quantify the degree of the viscous damping effect, the total friction is divided by the static resistance as follows:

$$\frac{\tau_t}{\tau_s} = \frac{\tau_d + \tau_s}{\tau_s} = \frac{\tau_d}{\tau_s} + 1.0 \quad (2.11)$$

For the sake of convenience, the ratio of the total friction to the quasi-static static strength is referred to as the strength ratio from hereon. The numerical value of the strength ratio quantifies the proportion (or potentially the percentage) of the strength increase. It is noted that the magnitude of the strength ratio is significantly influenced by the magnitude of the quasi-static friction and hence the shear rate at which the quasi-static friction is defined. The higher the shear rate chosen to define the quasi-static friction, the higher the value of the quasi-static friction due to the viscous effects and the lower the value of the strength ratio. Thus, the use of non-standard shear rates to define the quasi-static friction by different researchers (as will be shown in the subsequent chapter) has made direct comparison of the magnitudes of the strength ratio obtained by the different researchers impossible.

All researchers who have measured the viscous effects have unanimously found that the total friction is dependent on the velocity of the pile. Theoretically, the strength increase due to viscous damping should be dependent on the relative velocity between the soil and the pile because viscous damping only occurs when the pile slips past the soil (e.g. Randolph and Deeks, 1992; Randolph, 1991). However, it is experimentally difficult to determine the relative velocity during the dynamic event as this will require measurement of the velocity of the soil at the interface. Apart from the short instance at the start of the event, the soil velocity is small compared to the pile velocity; thus it is reasonable to formulate the dynamic resistance in terms of

the pile velocity rather than the relative velocity. Also, in order to render the damping constant dimensionless, some researchers have proposed normalising the velocity by a reference velocity which for convenience is taken as 1.0m/s (e.g. Randolph, 1990).

The mathematical models that have been proposed thus by researchers are outlined in Equations (2.12) to(2.17). The equations of the Smith and modified Smith models that have been shown previously are rewritten in terms of the total friction.

It is noted that the model proposed by Smith (1960) and its modified version adopted in CAPWAP and GRLWEAP are not based on experimental studies but rather on Smith's experience. The other viscous damping models that have been proposed for the pile-soil interface are based on experimental studies.

Where the viscous damping response for the pile-sand interfaces has been investigated experimentally (Dayal and Allen, 1975; Heerema, 1979), it has been found that viscous damping is negligible. For pile-clay interfaces, it has been found that the strength ratio varies with shear velocity in a highly non-linear manner (Dayal and Allen, 1975; Heerema, 1979; Litkouhi and Poskitt, 1980; Lepert et al., 1988a, 1988b; Benamar et al., 1991, 1992; Benamar, 1999).

2.4.3.1 Smith (1960)

$$\tau_t = \tau_s(1 + J_{Smith}v) \quad (2.12)$$

where

τ_t = total friction [kPa]

τ_s = instantaneous static friction [kPa]

v = pile velocity [m/s]

J_{Smith} = damping parameter [s/m]

2.4.3.2 CAPWAP & GRLWEAP Model

$$\tau_t = \tau_s(1 + J_{viscous}v) \quad (2.13)$$

where

τ_t = total friction [kPa]

τ_s = ultimate static friction [kPa]

v = pile velocity [m/s]

$J_{viscous}$ = damping parameter [s/m]

2.4.3.3 Dayal & Allen (1975)

$$\tau_t = \tau_s \left(1 + k_1 \log_{10} \left(\frac{v}{v_s} \right) \right) \quad (2.14)$$

where

τ_t = total friction [kPa]

τ_s = ultimate static friction [kPa] at quasi-static velocity of 0.1mm/s

v = pile velocity [m/s]

v_s = reference quasi-static velocity of 0.1mm/s [m/s]

k_1 = damping constant [-]

2.4.3.4 Heerema (1979)

$$\tau_t = \sigma_n^{0.7} [(-0.0041s_u + 4.44)v^{0.2} + (0.0029s_u - 0.32)] \quad (2.15)$$

where

τ_t = total friction [kPa]

v = pile velocity [m/s]

s_u = undrained shear strength of clay [kPa]

σ_n = applied normal stress [kPa]

2.4.3.5 Litkouhi & Poskitt (1980)

$$\tau_t = \tau_s(1 + Jv^N) \quad (2.16)$$

where

τ_t = total friction [kPa]

τ_s = ultimate static friction [kPa] at quasi-static velocity of 0.3mm/s

v = pile velocity [m/s]

J = damping constant [(s/m)^N]

N = index [-] with a value of about 0.2

2.4.3.6 Lepert et al. (1988a, 1988b); Benamar et al. (1991, 1992); Benamar (1999)

$$R_t = k_2(1 - e^{-k_3v}) \quad (2.17)$$

where

R_t = total resistance [kN] (the static and dynamic components are not distinguished)

v = pile velocity [m/s]

k_2, k_3 = damping constant and damping exponent respectively [-]; dependent on soil type, soil density, duration of impact, confining pressure

e = natural exponential [-]

2.5 Concluding Remarks

This chapter has discussed the methods for determining the pile capacity, with emphasis on the dynamic methods. It has been argued that the reliability of the dynamic methods depends on accurate modeling of the dynamic response of the pile-soil system during the testing event. The dynamic response of the pile-soil system during the execution of the dynamic methods and the available models for modeling the response have been discussed. The importance of correct modeling of the viscous damping has been highlighted. The dynamic effect due to viscous damping, which is the subject of this dissertation, has been introduced. The various proposed mechanisms for explaining the phenomenon and the existing models for modeling the strength increase due to the phenomenon have been outlined.

From the discussion in this chapter, it is evident that a reliable viscous damping model has yet to be established and the main difficulty in dynamic analyses at present is the lack of confidence in the existing viscous damping model being used. It is evident that a model is required which is based on physical reality and that depends on fundamental soil properties. It is thus the aim of this study to develop a reliable experimental set-up for the study of the viscous damping phenomenon at the pile-soil interface so that reliable experimental data can be obtained. Based on the reliable data, the dynamic interface friction as a function of fundamental soil parameter(s) can be modeled. It is hoped that improved modeling of the viscous damping response of the pile-soil interface based on physical evidence will enable the reliability of the dynamic methods to be improved.

Chapter 3

3. Literature Review

3.1 General

This chapter contains three sections. This first section discusses the laboratory set-ups used by previous researchers to simulate the dynamic behavior of pile-soil interfaces. The second and third sections discuss the findings of previous researchers on the rate-dependency of sand and clay respectively based on the laboratory set-ups described in the first section. The laboratory set-ups and the findings based on investigations into *soil-only* dynamic behavior have also been reviewed in the chapter, as the outcome of these tests will be discussed in relation to the *interface* dynamic behavior.

3.2 Previous Laboratory Simulations

3.2.1 Triaxial specimen impacted with falling weight

Whitman and Healy (1962), Coyle and Gibson (1970), and Abrantes and Yamamuro (2002a, 2002b) as well as Yamamuro and Abrantes (2003) investigated the dynamic

response of triaxial soil specimens by dropping weights onto the specimens. With the exception of Coyle and Gibson, who tested both sand and clay samples, the other groups of researchers tested only sand samples. It is stated from the outset that the studies using this set-up were not concerned with the pile-soil interface behaviour. These studies are included in the discussion because they shed light onto the dynamic behaviour of pile-soil interfaces and may provide a useful point of reference. The relevance of these tests to the subject of investigation of this thesis will be discussed further in Section 3.4.3.6.

The apparatus used by each group of researchers was essentially the same with minor differences. Thus for brevity, only the apparatus used by Yamamuro and Abrantes is shown in Figure 3.1. The apparatus consisted essentially of a gravity drop-frame system and a custom-made triaxial cell. The gravity system consisted of the following:

- A guidance system for the drop weight
- A reaction frame to stop the falling weight
- A reaction frame and a pedestal for the triaxial cell

The gravity system dropped a weight onto the plunger of the tri-axial apparatus which loaded the specimen. By adjusting the drop height using a hand winch, different strain rates or loading velocities could be applied to the specimen. Damping pads were used at different locations as shown in Figure 3.1 to ensure that unwanted dynamic vibration produced by the falling weight was isolated from the various components listed previously.

In such a set-up, significant inertial forces can arise from the acceleration of the mass of the soil in the specimen which results in an additional resistance to the actual shear strength of the soil (Whitman and Healy, 1962; Abrantes and Yamamuro, 2002a). One source of the inertial forces is the inertial forces associated with waves travelling longitudinally through the specimen which directly oppose the applied force. The other would be the inertial forces associated with the radial expansion of the specimen which act as additional confining pressure and which indirectly oppose the applied force. However, in each of the studies involving this gravity system (Coyle and Gibson, 1970; Whitman and Healy, 1962; Abrantes and Yamamuro,

2002a, 2002b; Yamamuro and Abrantes, 2003), it was reported that the system achieved relatively constant loading velocities throughout the impact event and therefore minimised inertial effects. The deformation vs. time records from Abrantes and Yamamuro (2002a) for the test with the highest strain rate and from Coyle and Gibson (1970) are reproduced in Figure 3.2 and Figure 3.3 respectively. The records show that as the weight impacted on the specimen, the rate of deformation of the specimen was relatively constant, thus minimising inertial effects.

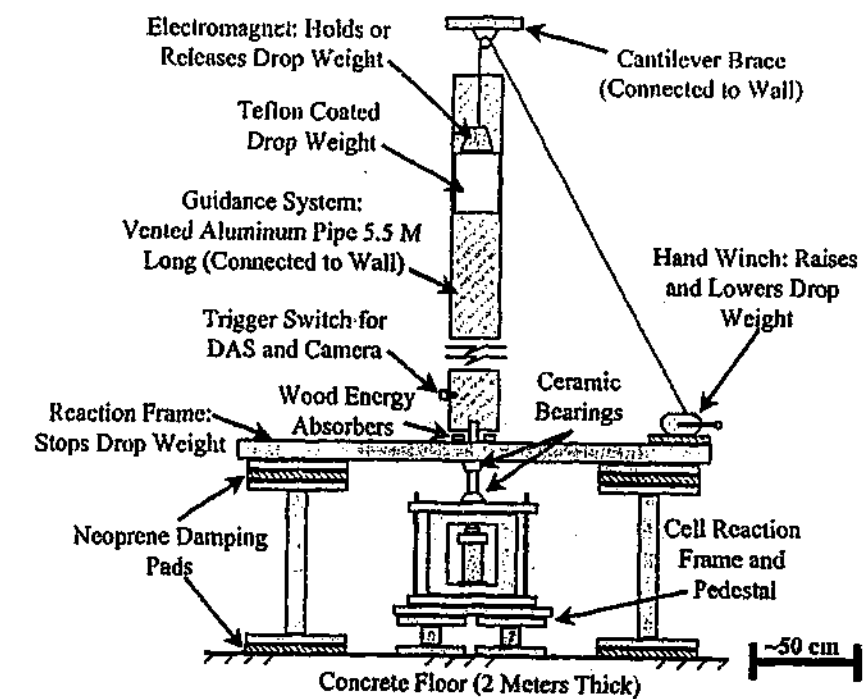


Figure 3.1 Schematic of experimental set-up by Abrantes and Yamamuro (Abrantes and Yamamuro, 2002a)

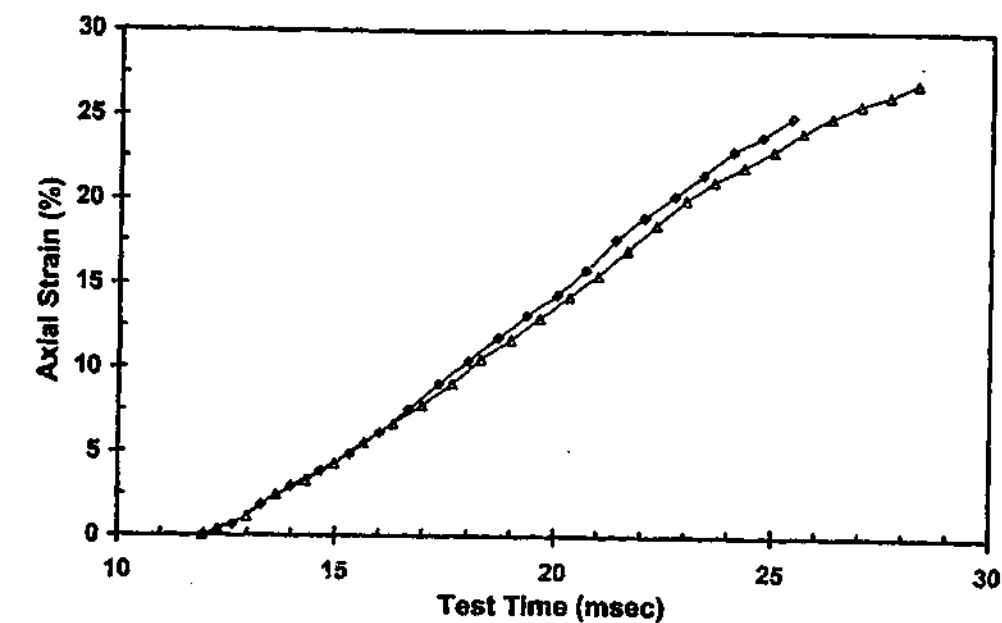


Figure 3.2 A deformation vs. time record from Abrantes and Yamamuro (Abrantes and Yamamuro, 2002a)

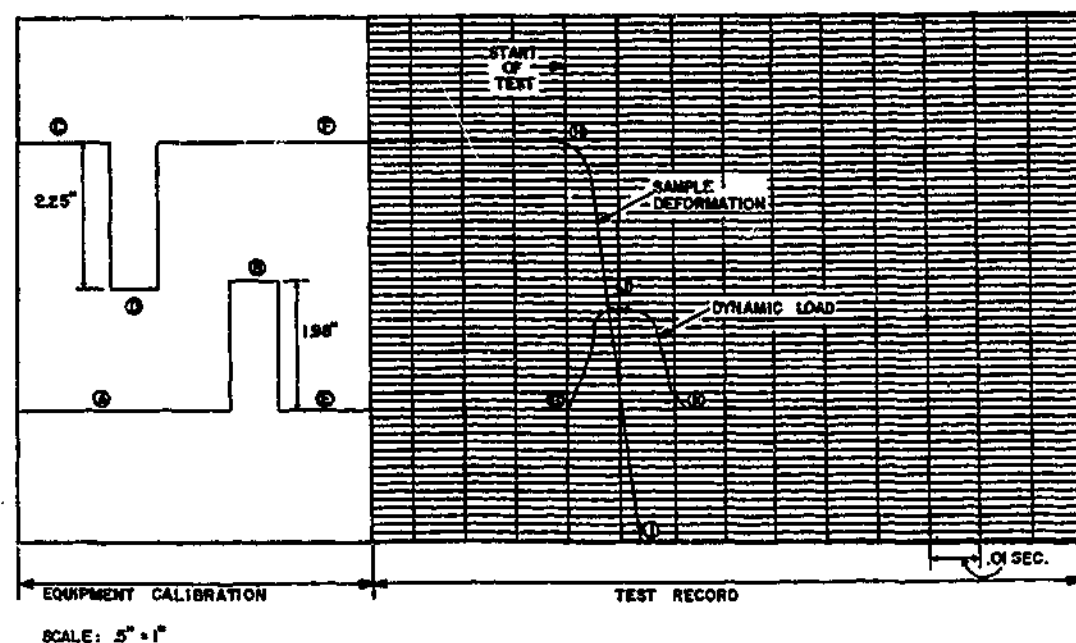


Figure 3.3 A deformation vs. time record from Coyle and Gibson (Coyle and Gibson, 1970)

As already stated, these tests were not intended for studying the pile-soil interface but because these tests could be relevant to the present study, they are reviewed. Indeed, there are 2 fundamental limitations in using these tests to infer the pile-soil interface behaviour:

- As previously stated, the set-up subjects the sample to compression rather than shear. This point will be discussed in more detail in Section 3.4.3.6.
- The shear failure in the triaxial samples involves a soil-only failure and is related to undisturbed soil (as opposed to remoulded soil).

The limitations inherent in the triaxial test are as follows:

- Non-uniform strains occur throughout most of a triaxial specimen where the deformation of the specimen is restrained at the cap-specimen interfaces (located at the 2 ends of the specimen), whilst the deformation of the specimen is unrestrained and uniform away from the restraints or at mid-height of the specimen (e.g. Abrantes and Yamamuro, 2002a, 2002b). Therefore, the triaxial specimen is subject to different volume change tendencies within different portions of the specimen (Whitman and Healy, 1962; Abrantes and Yamamuro, 2002a), as shown in Figure 3.4. Typically, the central portion of the specimen expands, whilst the end portions compress, which results in the pore water migrating from the ends toward the centre. Thus the shear failure that occurs in the central portion does not take

place at constant volume, which contrasts to that in a real soil mass that is sheared so rapidly that it remains at constant volume.

- According to Whitman and Healy (1962), when testing sand samples, the membrane can penetrate into the crevices between the particles especially when the sand particles are coarse, as shown in Figure 3.5. As the difference between the applied confining pressure and the pore pressure increases, the membrane is pushed further into the crevices. Because of the membrane action, it is possible to have a significant volume change in what would nominally be an undrained test.

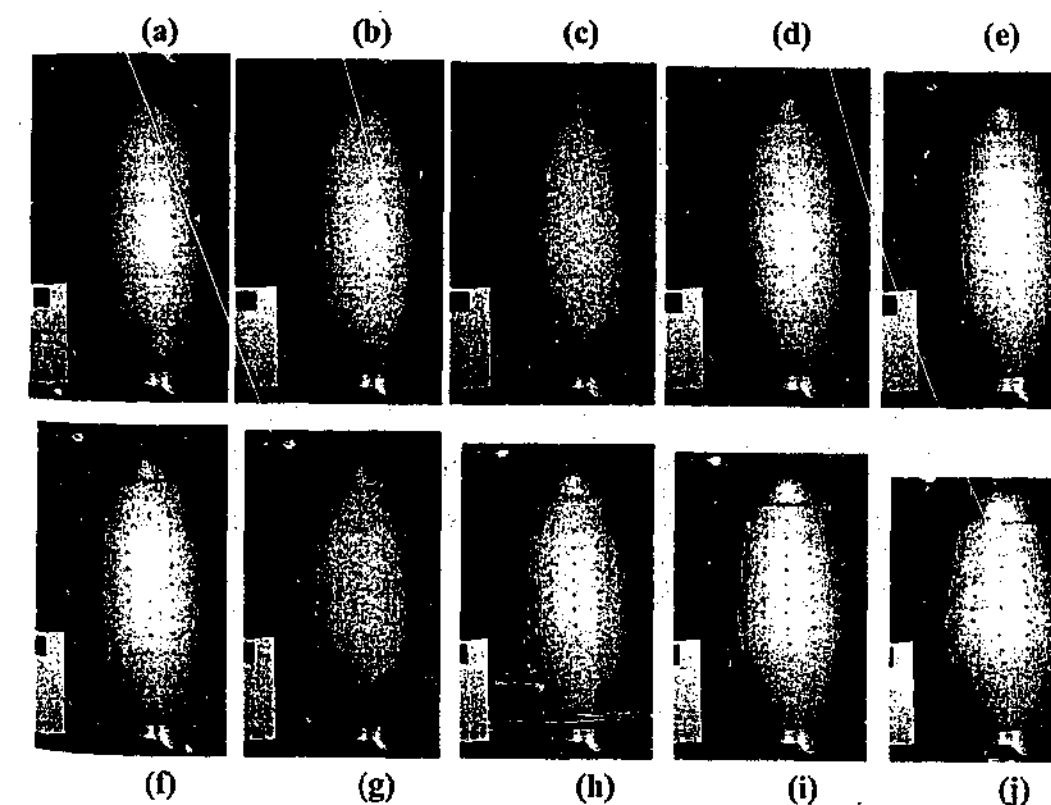


Figure 3.4 Non-uniform strains in specimen during loading (Abrantes and Yamamuro, 2002a)

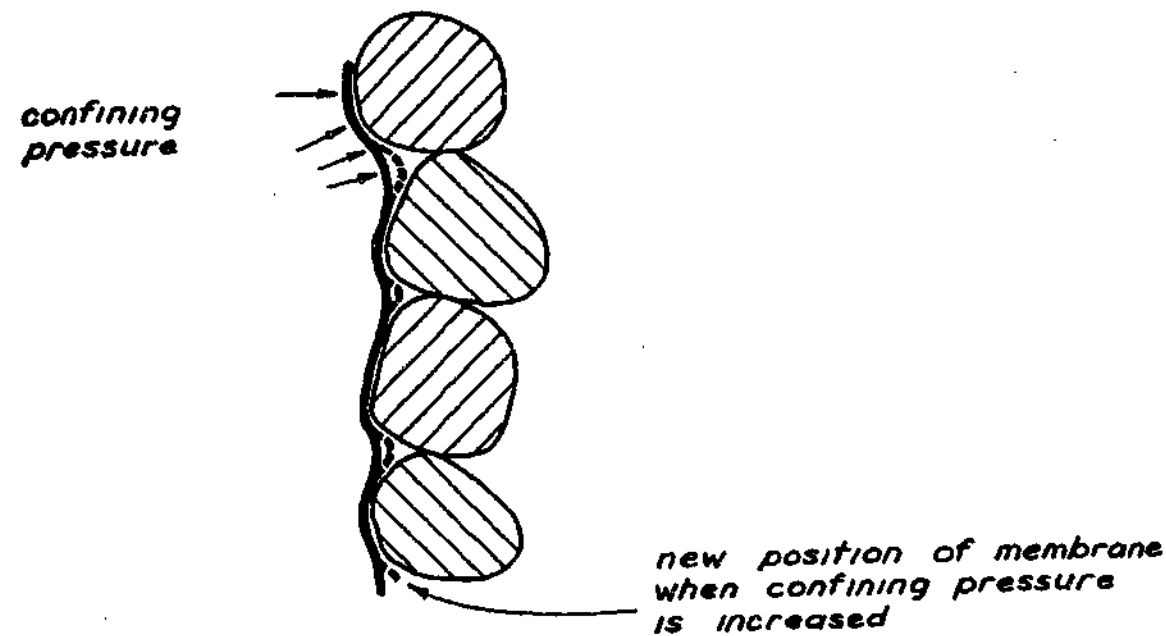


Figure 3.5 Membrane effect in laboratory tests

3.2.2 Penetrometer

Dayal and Allen (1975), Litkouhi and Poskitt (1980), and Poskitt and Leonard (1982) investigated the dynamic response of the pile-soil interface by performing constant velocity penetrometer tests. The first group of researchers performed the tests in both sand and clay samples, whilst the other two groups tested only clay samples. The test set-up was relatively simple as shown in Figure 3.6 and Figure 3.7. The test consisted of pushing the penetrometer into a soil specimen prepared in a container.

Dayal and Allen (1975) used a penetrometer which had a maximum stroke of 61cm and a cone tipped circular cylinder with the following geometry:

1. outer diameter of 3.56cm
2. cone angle of 60°
3. cone base area of 10cm²
4. friction sleeve area of 150cm²
5. length of 45.7cm

The penetrometer was instrumented with a friction sleeve load cell and a cone load cell for the measurements of the interface friction and the tip load respectively.

Litkouhi and Poskitt (1980) and Poskitt and Leonard (1982) used a slightly different penetrometer. The penetrometer had a stroke of 30cm and had the following geometry:

1. outer diameter of 1.0cm
2. length of 26.0cm
3. cone angle of 120°

The friction was deduced by subtracting the tip resistance from the total resistance. The total resistance was measured using a load cell mounted at the top of the penetrometer, whilst the tip resistance was measured using a cone load cell at the penetrometer tip.

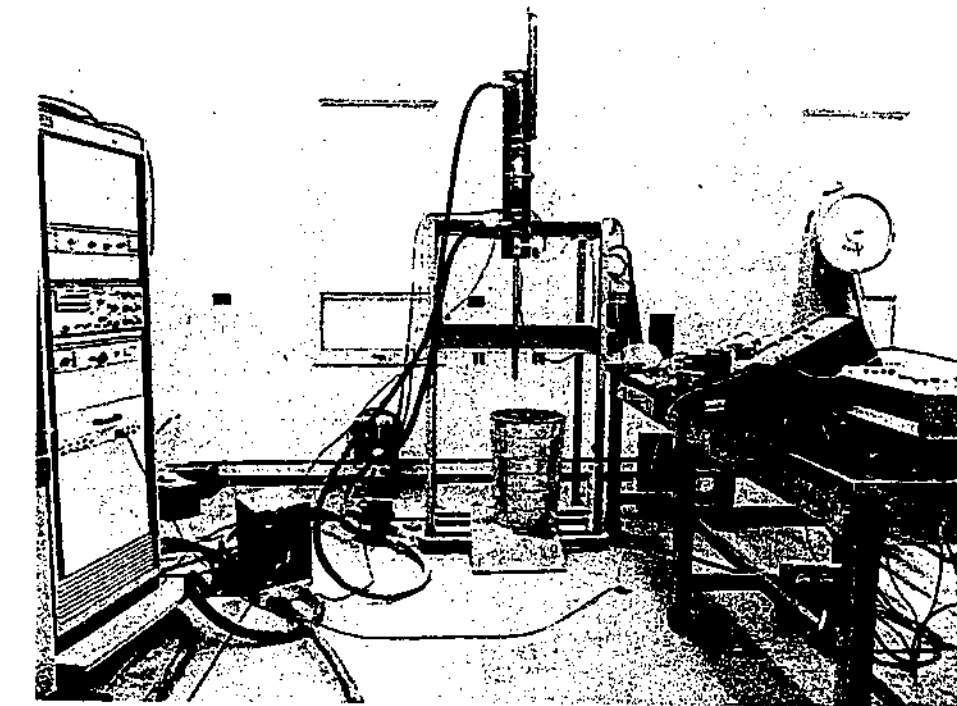


Figure 3.6 Penetrometer and soil container in experimental set-up (Dayal and Allen, 1975)

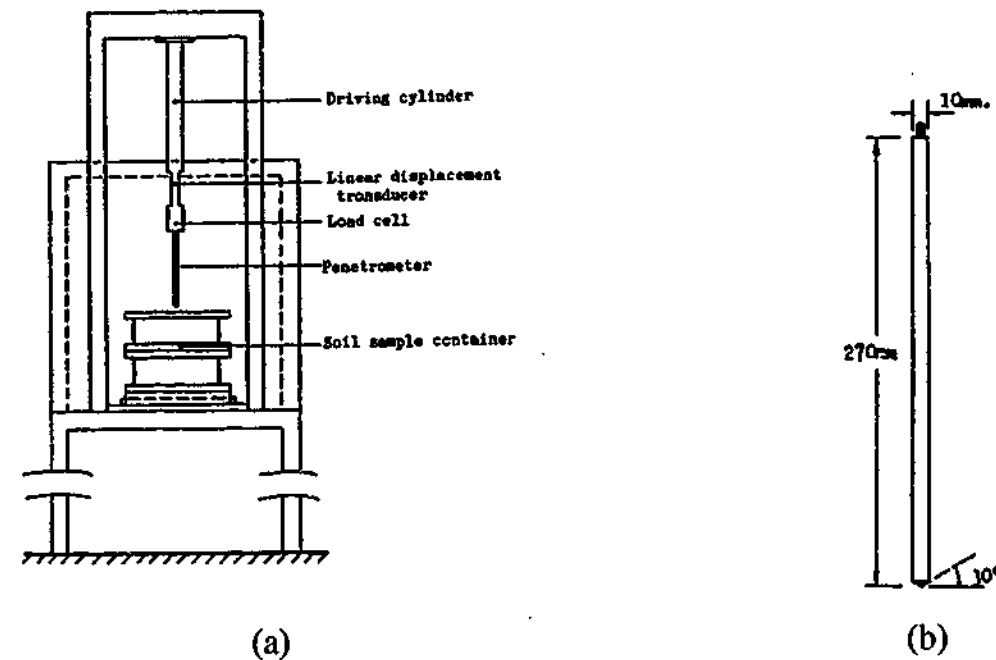


Figure 3.7 (a) Schematic of the test arrangement (b) geometry of penetrometer for side friction tests (Poskitt and Leonard, 1982)

There were several limitations in using the penetrometer to study the interface behaviour which are listed as follows:

- The friction behaviour was influenced by the preceding pile tip penetration as discussed in more detail in Section 3.5.2.4;
- although such a set-up enabled the combined pile tip and interface behaviour to be simulated, it might not be suitable for studying the interface behaviour in isolation;
- The penetrometer tests were performed at constant velocities which were significantly less than the transient velocities normally associated with pile driving;
- The magnitude of the normal stress at the pile-soil interface was unknown and could not be controlled or varied in order to investigate the effect of the normal stress;
- The use of penetrometers could have introduced significant scale effects arising from the relative magnitudes of the soil grains and the dimension of the model pile, especially for the penetrometer of 10mm diameter;
- The penetrometers have a machined steel surface which may be unrepresentative of normal pile materials.

3.2.3 Direct shear

Heerema (1979) simulated the response at the pile-sand interface by using the direct shear test arrangement shown in Figure 3.8. A flat and stiff steel plate was pressed against the face of the sample. The normal stress at the interface could be varied over a wide range (e.g. between 50kPa and 240kPa). During the tests, the steel plate was oscillated up and down against the face of the sample. The oscillation produced slightly varying but near-constant velocity throughout the stroke. The friction and velocity values at zero crossing was read when the stroke reached “zero crossing” which was the midpoint of the stroke. The velocities could be varied from near-zero to about 1.0m/s. The soil was sampled from the field using a steel tube measuring 50mm in diameter and 150mm in length. Before being tested, the sample in the tube was cut in half length-wise to minimize disturbance of the sample. During the tests, the sample was restrained at the top and bottom. The test arrangement allowed the dynamic friction, pile velocity and the normal stress at the pile-soil interface to be determined.

The test set-up was relatively simple and enabled different pile surfaces to be tested. However, there were also several limitations as follows:

- As the soil was subjected to the direct shear mode as opposed to the simple shear mode, stress concentrations would have existed at the two ends of the

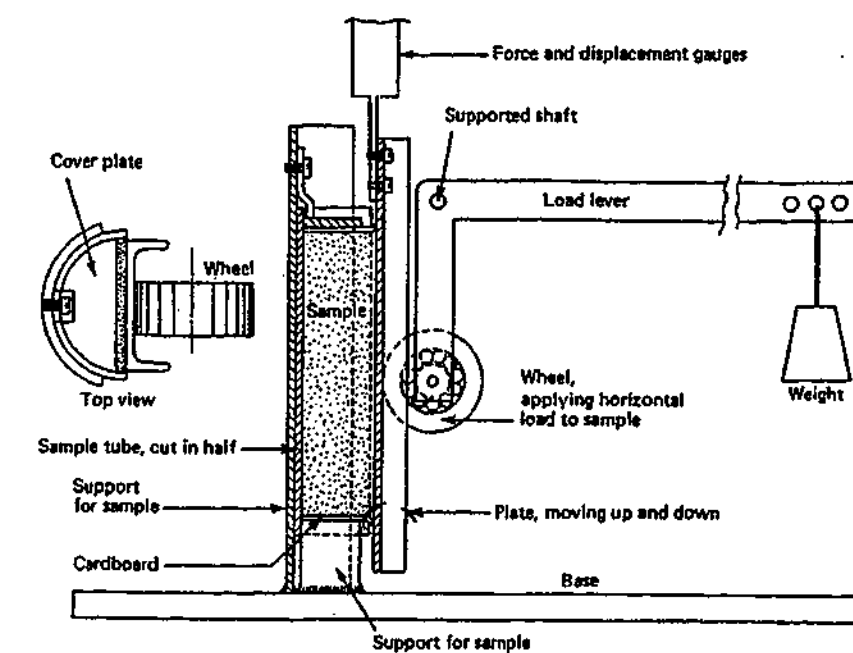


Figure 3.8 Half steel tube with semi-circular soil sample (after Heerema, 1979)

sample. The percentage error of the measured friction due to the stress concentrations might be significant given that the interface area was small.

- Cohesionless samples could not be tested in Heerema's apparatus because the steel plate was not designed to completely cover the shear surface of the specimen in order to avoid friction between the steel plate and the tube.

3.2.4 Pile shaft encased in triaxial specimen

Benamar et al. (1991, 1992) and Benamar (1999) used a sophisticated set-up for investigating the dynamic response of the pile-clay interface, shown in Figure 3.9 and Figure 3.10. A 20mm-diameter steel rod whose shaft was encased in a specimen was driven by a falling weight.

The specimen was kept in a custom-made triaxial cell where the confining pressure on the specimen could be controlled. The sample was prepared by consolidating a slurry around the rod in a special mold. Once it had finished consolidating, the sample was removed from the mold and placed into the triaxial cell. The transient velocity of the rod was measured by an opto-electronic sensor, whilst the forces at the rod above and below the soil sample were measured using strain gauges glued onto the rod. The interface friction was deduced by dynamic analyses using force and velocity records measured during the driving event. Details of the computations involved in deducing the friction can be found in Benamar et al. (1991) and Benamar (1996) but can be summarized as follows. In order to solve for the interface friction, the sample was modeled as many discrete thin layers, and stress equilibrium and velocity continuity equations were applied to each of the layers. However, it was claimed by the researchers that the procedure for deducing the interface friction could be simplified by treating the interface frictional force as a concentrated force located at the mid-height of the sample for "the usual range of the experimental conditions". Thus, the simplified procedure was adopted.

This experiment had a significant advantage over the other experiments because it enabled the instantaneous dynamic friction and the corresponding instantaneous pile velocity during one single driving event to be recorded and hence analysed. Furthermore, the friction-velocity relationship for a particular interface under a

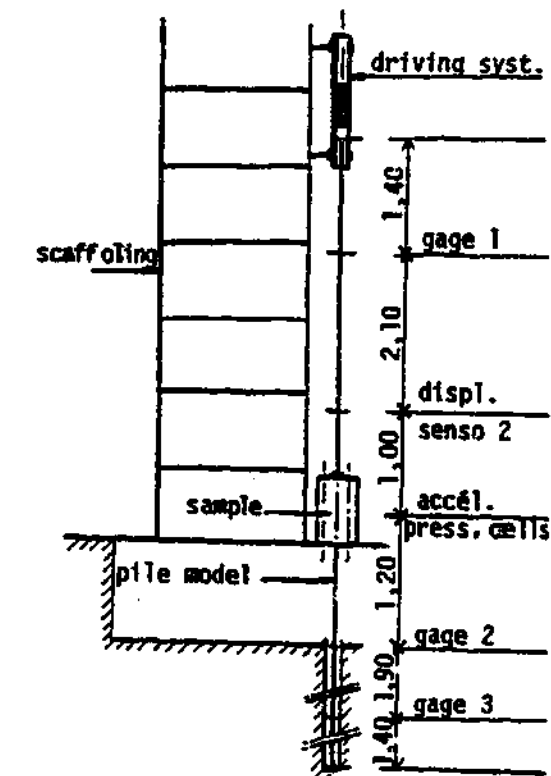


Figure 3.9 Steel rod passing through a triaxial cell (Lepert et al., 1988b)

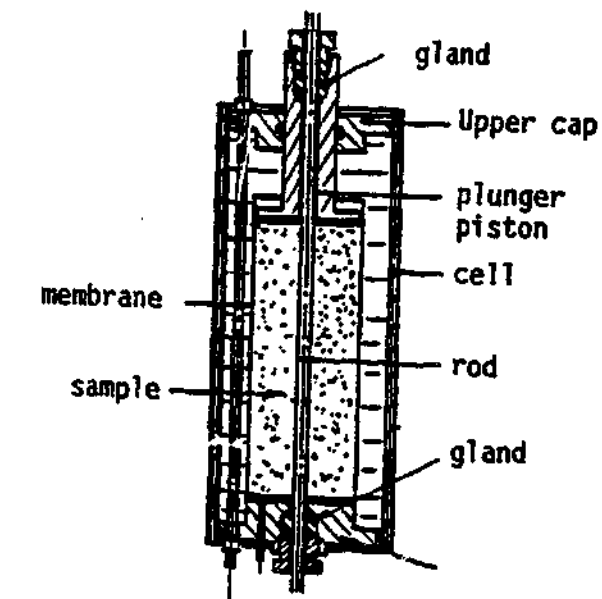


Figure 3.10 Sample in a triaxial cell (Lepert et al., 1988b)

particular set of test conditions could be established over the relevant velocity spectrum in the single test.

However, there were several limitations in using such a set-up:

- Owing to the nature of the set-up, the dynamic resistance could not be directly measured and had to be computed using stress wave analysis. This

analysis could potentially introduce significant error in the deduced interface friction. For example, the upward traveling wave generated by the interface friction would have been computed using $\frac{1}{2}(F-Zv)$ where F and v were the measured force and the velocity at the point of measurement and Z is the impedance of the pile. If F and Zv were of similar magnitude, then the absolute error from taking the difference of these two numbers might be a very large percentage of the difference.

- Given that the interfaces of the steel rod and the top and bottom sections of the triaxial cell had to be effectively sealed to prevent leakage of the confining pressure and to contain the water used in applying the pressure, these seals might be a source of unwanted friction;
- Because the soil was not allowed to deform in pure shear at the bottom of the cell, the stress concentrations in the soil might have caused significant error;
- The small diameter of the rod might have introduced significant scale effects arising from the relative magnitudes of the soil grains and the dimension of the model pile.

3.3 Presentation of Findings from Previous Studies

Before the findings of various researchers are discussed, it is necessary to define the way in which dynamic effect has been quantified by previous researchers and the way in which the diverse descriptions will be unified for purposes of comparison.

3.3.1 The use of strength ratio

As has been discussed in the previous chapter, the degree of the viscous damping effect is typically quantified using the strength ratio which is defined as the ratio of the total friction measured during dynamic shearing to the quasi-static friction. This is expressed mathematically as:

$$\frac{\tau_t}{\tau_s} = \frac{\tau_d + \tau_s}{\tau_s} = \frac{\tau_d}{\tau_s} + 1.0 \quad (3.1)$$

This strength ratio parameter enables the dynamic friction to be normalised. However, the magnitude of the strength ratio is significantly influenced by the magnitude of the quasi-static friction and hence the shear rate at which the quasi-static friction is defined. Therefore, ideally for the values of the strength ratio data from various groups of researchers to be compared on an equal basis, the quasi-static

friction should be defined as the resistance corresponding to a common and suitably low velocity. Since the shear rate at which the quasi-static friction is defined is unique to each of the previous studies as shown in Table 3.1, the values of the strength ratio from each study are not directly comparable.

Initially, an attempt was made to define a common quasi-static velocity for all these previous studies so that all the data could be “corrected” to the common velocity. However, this proved to be problematic. It was inappropriate to extrapolate *below* the shear rate at which quasi-static friction was measured because this would amount to creating data that did not exist. While it was possible to interpolate *above* the shear rate at which quasi-static friction was measured (i.e. to use a higher velocity as the reference quasi-static velocity, but one within the range of shear rates that were tested), the extrapolation might introduce significant error and thus misrepresent the experimental data. Also, in order to define a common velocity, obviously the highest reference velocity (i.e. 1.3×10^{-3} m/s of Dayal and Allen) had to be chosen, which however would cause significant data points from other groups of researchers to be ignored. Therefore, to avoid these problems, the strength ratio values as computed by the group of researchers (based on their unique definition of the quasi static friction) are presented.

Table 3.1 Quasi-static shear rates used by the researchers

Researchers	Quasi-static velocity (m/s)
Coyle and Gibson (1970)	2.1×10^{-5}
Dayal and Allen (1975)	1.3×10^{-3}
Heerema (1979) – sand	7.0×10^{-4}
Heerema (1979) – clay	7.8×10^{-7}
Litkouhi and Poskitt (1980)	3.0×10^{-4}
Poskitt and Leonard (1982)	2.0×10^{-4}

3.3.2 A framework for presenting various data

Where the strength of the soil was found to be dependent on rate, the strength ratio-velocity response has been modelled by most researchers (Heerema, 1979; Litkouhi and Poskitt, 1980; Coyle and Gibson, 1970) using a power law relationship of the following form:

$$\frac{\tau_t}{\tau_s} = 1 + Jv^N \quad (3.2)$$

where τ_s = quasi-static resistance measured at a very low velocity, τ_t = total resistance comprising dynamic resistance due to viscous damping and quasi-static resistance, at an arbitrary velocity in the range of interest, v = the relative velocity of pile and soil or the slip velocity [m/s]. τ_t is normalised with τ_s to obtain the strength ratio. In some cases, the velocity has been normalised by adopting a convenient reference velocity of 1.0m/s in order to make the parameter J dimensionless. However, this approach was not adopted in the present study. Therefore, in the present discussion, J has the unit $[s/m]^N$.

As noted in Section 2.4.3, Dayal and Allen (1975) modelled the friction-velocity response using a log function relationship. Given the exponential nature of both the log function and the power law, the data can also be modelled reasonably with the power law shown in Equation (3.2).

The response found by Benamar et al. (1991, 1992) and Benamar (1999) was modelled with an exponential function of the form:

$$R_t = k_2(1 - e^{-k_3v}) \quad (3.3)$$

where R_t = total force comprising dynamic resistance due to viscous damping and quasi-static resistance [N], v = the relative velocity of pile and soil or the slip velocity [m/s], and k_2 and k_3 = constants depending on soil properties and duration of impact [-] and [s/m]. In any case, the data presented by Benamar et al. (1991,1992) and Benamar (1999) could not be presented in the form of the strength ratio because the quasi-static friction was not measured and thus the degree of dynamic effect found in this study cannot be compared to that from another study.

Since the power law of Equation (3.2) can be used to model all the data presented by all the researchers except those by Benamar et al. (1991,1992) and Benamar (1999), it is used here as a common framework for presenting the data from various studies.

At this point, it is instructive to determine the effects of different values of J and N on the magnitude and shape of the function. The value of J is arbitrarily fixed at 1.00 to illustrate the effect of the value of N on the function in Figure 3.11. The value of N is fixed at an average of 0.2 to illustrate the effect of the value of J on the magnitude of the strength ratio in Figure 3.12.

Based on most of the studies (Litkouhi and Poskitt, 1980; Coyle and Gibson, 1970; Dayal and Allen, 1975), J falls between 0.6 and 2.7, and N ranges between 0.11 and 0.57. However, a value of N of 0.2 is recurrent in a number of the studies (Heerema, 1979; Litkouhi and Poskitt, 1980; Coyle and Gibson, 1970).

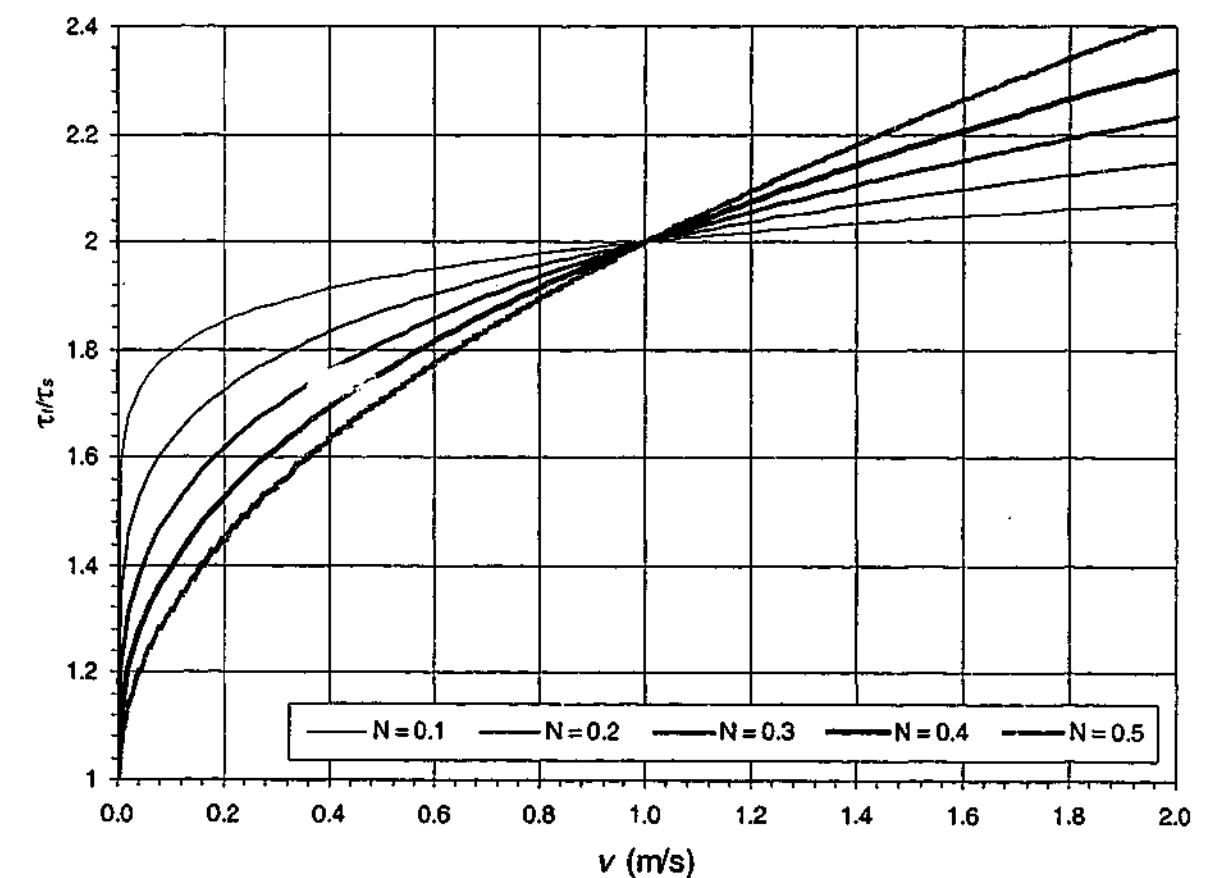


Figure 3.11 Variation of strength ratio with velocity for various values of N for $J = 1.0$ (normal scale)

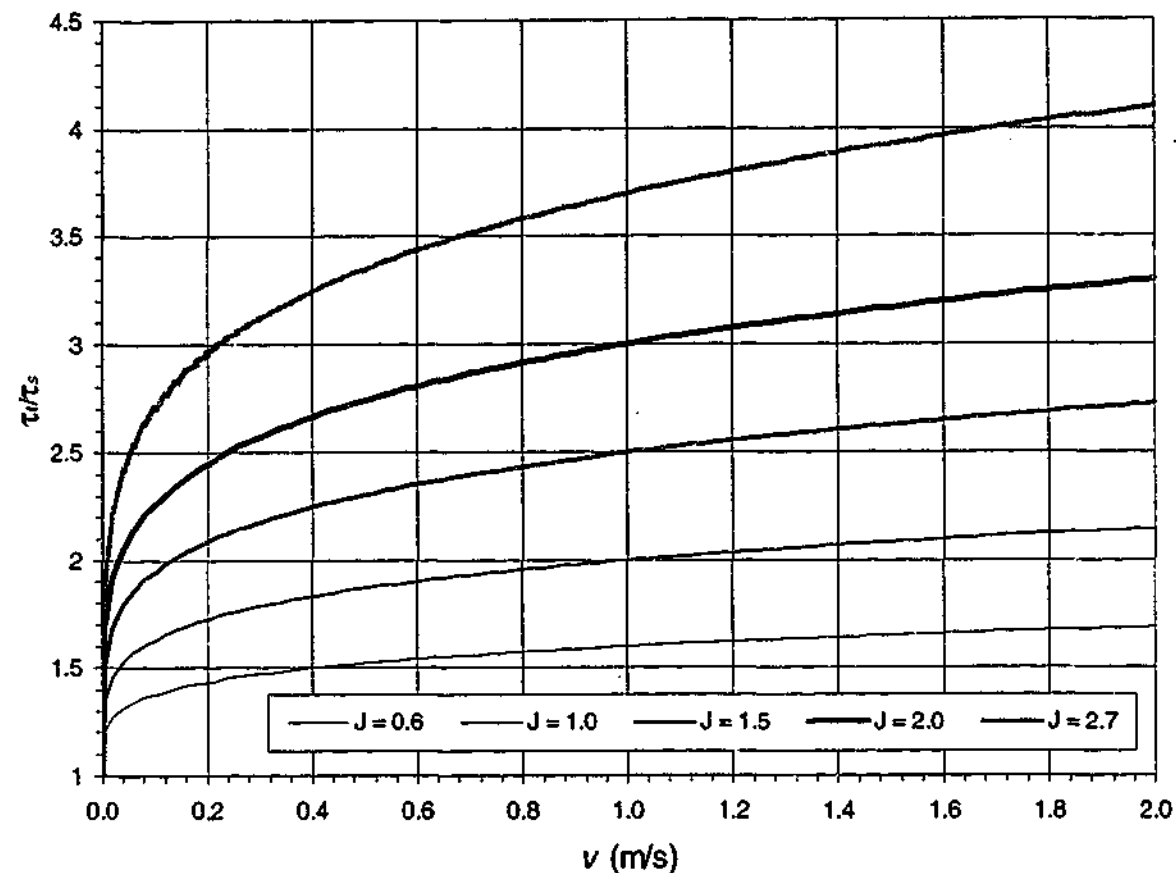


Figure 3.12 Variation of strength ratio with velocity, with various values of J for $N = 0.2$ (normal scale)

In the discussion of the data obtained by various researchers, the strength ratio-velocity plot originally presented by the researchers is reproduced. Since the strength ratio-velocity plot from each group of researchers was presented in various different formats, the strength ratio-velocity data are now replotted in a standard plot in order to standardise the presentation of the data and to facilitate comparison of the magnitudes of the strength ratio. The standard plot in the format is shown in Figure 3.13. The log plot for the x-axis is chosen so that a large range of velocity data can be presented and so that the variation of the velocity at near-zero velocity can be more clearly presented. Also, the log plot for the y-axis is chosen and is plotted as $\tau_s/\tau_d - 1$ rather than τ_s/τ_d , so that the variation of the strength ratio with velocity at near-zero velocity can be more clearly presented. The following features of the adopted standard plot should also be noted:

- Since the strength ratio from most of the studies could be modelled with the power law for N in the region of 0.2, reference lines based on the power law are included in each plot for various values of J for $N = 0.2$ for the purpose of referencing;

- For the work of Coyle and Gibson (1970) and Heerema (1979), Yamamuro and Abrantes (2003), the shear strength and the normal stress or confining stress of each sample are annotated in parenthesis in the plot. For the work of Dayal and Allen (1975), Litkouhi and Poskitt (1980) and Poskitt and Leonard (1982) involving penetrometer tests with unknown stress conditions, only the shear strength of each sample is indicated.
- The quasi-static rate, v_s , used to perform the quasi-static test is shown in the plot.

It is noted that the J values for N fixed at 0.2 suggested by the standard plot are different from the original J values for the optimal N which are reported. In order to make the distinction, the J parameter referring to the original J values is denoted J , whilst the J parameter corresponding to $N=0.2$ in the standard plot is denoted $J(N=0.20)$.

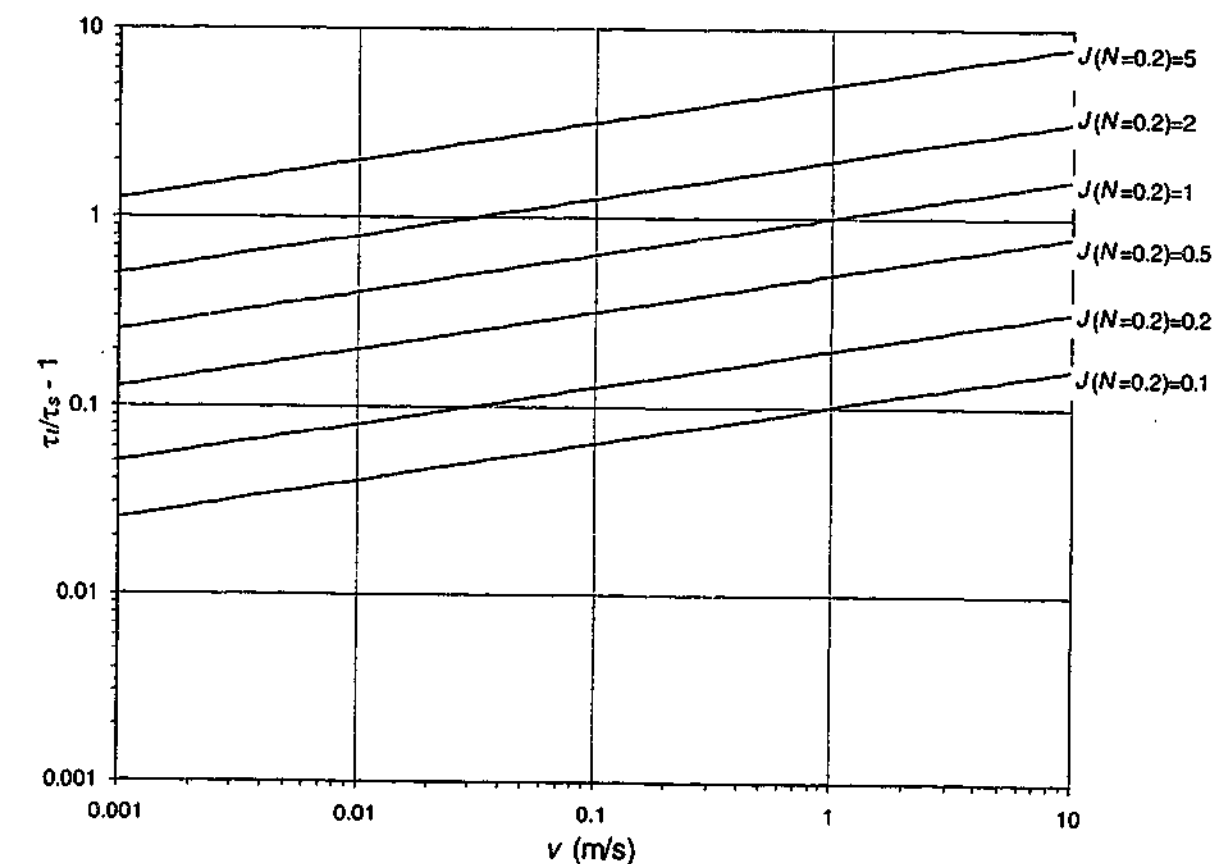


Figure 3.13 Strength ratio-velocity relationships for different values of J for $N = 0.2$, in log-log scale

3.4 Dynamic Effects in Sand – Previous Studies

Since the results from the various studies must be interpreted with regard to their respective experimental set-ups, it is best to discuss the results from the previous studies under the heading of the their respective experimental set-ups.

Previous studies have been conducted on the strain rate effects on strength behaviour of sand in sand-only shear tests and triaxial tests. These studies must in some way be relevant to the present study of the velocity-dependence of the pile-sand interface. As such, the findings of these studies are reported in addition to the findings of studies based on pile-sand interface tests.

The previous studies into the rate-dependent behaviour of sand are reviewed in the following order:

- sand-pile interface shear tests
- shear tests in sand
- triaxial compression tests of sand

3.4.1 Sand-pile interface shear tests

The details of the interface shear tests conducted by Dayal and Allen (1975) and Heerema (1979) are provided in Table 3.2.

Table 3.2 Details and findings of previous studies on the effects of strain rate on the pile-sand interface strength or friction angle

Researchers	Loading velocity or strain rates	Apparatus	Sample size	Interface	Normal stress (kPa)	Sand	D_{50} (mm)	D_{60}/D_{10}	State	Strength increase
Dayal and Allen (1975)	1.3×10^{-3} m/s - 0.81 m/s	Penetrometer	460mm diameter 610mm long	Smooth steel	Unknown	Medium to fine sand size $G_s = 2.67$	Unknown	NA (uniformly graded)	Dry loose sand dense	None
Heerema (1979)	0.7×10^{-3} m/s - 0.6 m/s	Direct shear	50mm width 150mm long	Steel	50 – 240	Fine and with a small silt content	NA	NA	Wetted but not saturated	None

3.4.1.1 Dayal & Allen (1975)

Using the experimental set-up described in Section 3.2.2, Dayal and Allen (1975) performed penetrometer tests on dry sand at 2 densities (i.e. at 1370kg/m^3 and 1450kg/m^3) and at constant velocities up to 0.8m/s . The interface friction associated with the shaft component of the penetrometer did not vary with shear rate for either the loose or the dense sand, as shown in Figure 3.14 and Figure 3.15 respectively. The tests were limited to only one type of sand, and the peak velocity was also relatively low compared to the peak velocities of pile driving and dynamic tests (ranging between 3.0 and 5.0m/s), and of Statnamic tests (ranging between 1.0 and 3.0m/s).

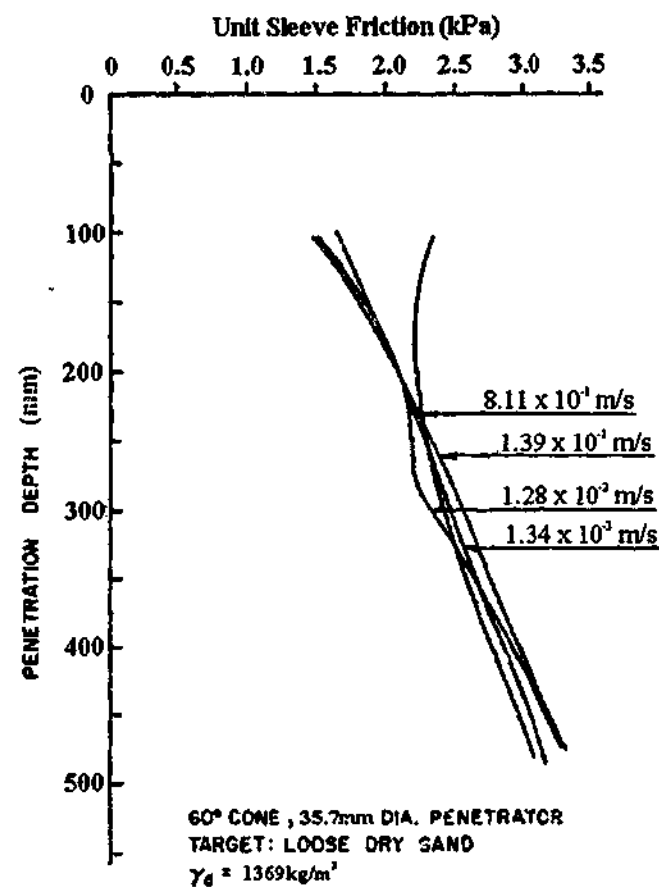


Figure 3.14 Penetration test results for loose sand (Dayal and Allen, 1975)

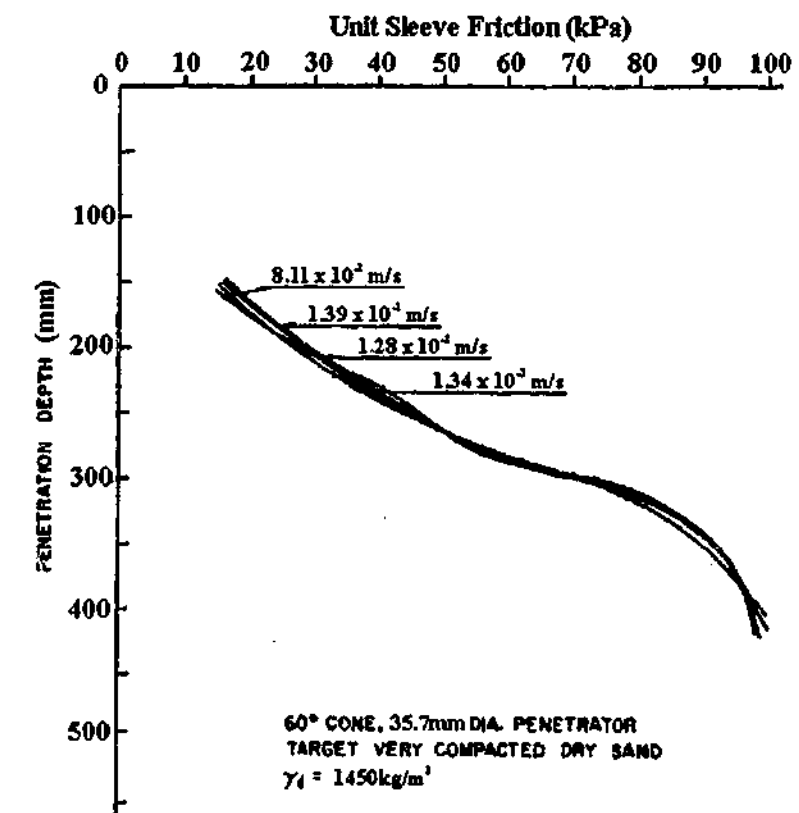


Figure 3.15 Penetration test results for denser sand (Dayal and Allen, 1975)

3.4.1.2 Heerema (1979)

Using the direct shear set-up described in Section 3.2.3, Heerema (1979) performed shear tests of a silty sand sample against a steel plate. The sample was wetted so that “it remained well collected” inside the test apparatus; thus it would appear that the sample was held together by the negative pore pressures in the silt. Velocities (at “zero crossings”) of up to 0.6m/s were tested. The interface friction for a normal stress of 85kPa remained constant at various shear velocities as shown in Figure 3.16. Thus the interface friction angle did not vary with the shear velocity. Like Dayal and Allen’s tests, Heerema’s tests were limited to only one type of sand, and the peak velocity was relatively low compared to the peak velocities of pile driving and dynamic testing events.

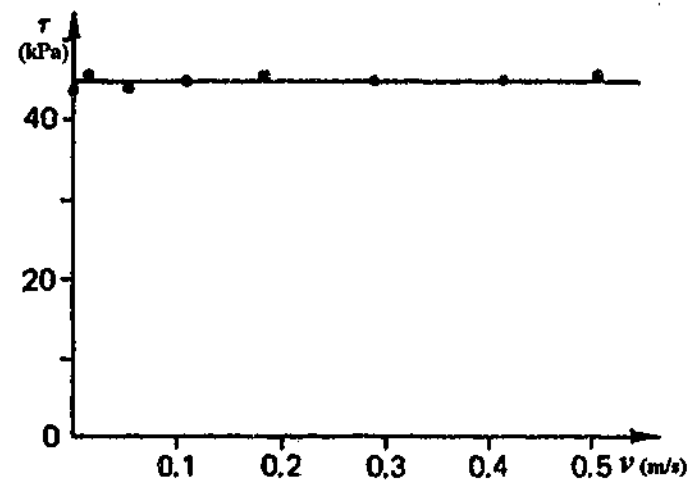


Figure 3.16 Friction-velocity relationship for sand at a normal stress of 85kPa (Heerema, 1979)

3.4.2 Shear tests in sand

Studies on the strain rate effect on sand specimens tested in sand-only shear tests are also reviewed for the following reasons:

- Since any velocity-dependency of the interface is a function of the sand itself, the velocity-dependency (or otherwise) for the sand-only shear test would indicate that for the pile-sand interface shear test.
- The viscous damping for the pile-soil interface is related to the slippage of the soil specimen against the pile surface. The shear tests that will be reviewed were performed in the direct shear device and the ring shear apparatus. In the direct shear test, the sand mass contained in the upper half of the shear box slips against the sand mass contained in the bottom half (at the plane designated by the shear device). In the ring shear test, the specimen is strained at small shear displacements, and slip occurs between the sand masses contained in the two halves of the device at higher shear displacements; since all the simple shear tests that will be reviewed were performed with large shear displacements, these tests involved slippage of the sand masses (at the plane designated by the shear device).

Thus, it would appear that the direct and ring shear tests that will be reviewed are relevant to the study of the pile-soil interface behaviour.

Many previous researchers performed shear tests on various granular materials including non-soil materials. The details and findings of the studies are provided in

Table 3.3. It is noted that each of the studies adopted a unique quasi-static shear rate and a unique maximum shear rate; as such, the magnitude of the variation in the friction angle from one study cannot be directly compared to that from another study on equal terms.

As shown in Table 3.3, the tests on the polystyrene beads showed that the friction angle was independent of the shear rate (Hung and Morgenstern, 1984a; Hung and Morgenstern, 1984b). However, findings on the effect of the shear rate on the friction angle of non-soil granular materials were mixed. Some shear tests on glass beads showed that the friction angle decreased significantly (by 8° relative to the quasi-static friction angle) with increasing shear rates (Novosad, 1964), whilst other shear tests on the same material showed that the friction angle was independent of the shear rate (Savage, 1982; Sassa, 1984, 1985).

As shown in Table 3.3, findings on the effect of the shear rate on the friction angle of sand were similarly mixed. Some tests showed that the friction angle was not velocity-dependent (Schimming et al., 1966; Hung and Morgenstern, 1984a, 1984b). Some tests showed that the friction angle decreased (by up to 3.5° relative to the quasi-static friction angle) with increasing shear rates (Hung and Morgenstern, 1984a for sand-flour mix; Lemos, 1986). Other tests showed that the friction angle increased (by 5° relative to the quasi-static friction angle) (Scarlett and Todd, 1969).

Based on the various studies, the friction angle of sand (and of other non-soil granular materials) was found to be either independent of the shear rates, or varied unsystematically (increased and decreased) with increasing shear rates. It is possible that the unsystematic variation was due to experimental error; for example, friction in the device might introduce some error in the measurements especially given the relatively small resistance corresponding to the small specimen sizes used in the direct shear and ring shear apparatus. Because of the conflicting findings, the velocity-dependence or otherwise of the friction angle cannot be concluded based on these findings.

Table 3.3 Details and findings of previous studies on the effects of strain rate on the strength of sands based on shear tests

Researchers	Loading velocity or strain rate	Apparatus	Effective normal stress (kPa)	Sand and other granular materials	State	D_{50}	D_{60}/D_{10}	Dynamic frictional angle relative to quasi-static friction angle*
Novosad (1964)	5.0×10^{-2} - 0.5m/s	Ring shear	0.5 - 2.0	Coarse sand	Dry	1.10	1.00	None
				Fine-medium sand	Dry	0.17	1.90	Increase of 1°
				Sugar	Dry	0.57	1.79	Decrease of 1°
				Glass spheres	Dry	2.50	1.00	Decrease of 8°
Schimming et al. (1966)	Unspecified (loading time between 10 to 30 milliseconds)	Direct shear	50 - 310	Sand	Dry loose & dense; saturated dense			None
Scarlett and Todd (1969)		Ring shear	2.2 - 6.5	Coarse sand	Dry	1.01	1.00	Increase by 1°
				Medium sand	Dry	0.36	1.00	Decrease by 3°
				Medium-fine sand	Dry	0.21		Increase by 5°
Savage (1982)	3.0×10^{-2} - 5.0m/s	Ring shear		Single-sized glass ballotini	Dry	0.5 - 2.0	1.00	None
				Single-sized polystyrene	Dry	0.5 - 2.0	1.00	None
				Binary mixture of glass ballotini	Dry			None
				Binary mixture of polystyrene	Dry			None
				Crushed walnut shells	Dry			None
Hungr and Morgenstern (1984a)	1.0×10^{-3} - 0.98m/s	Ring shear	20 - 200 (dry) 50-100 (saturated)	Coarse quartz sand with rounded grains	Dry & saturated	1.5 - 2.0	1.00	None

Table 3.3 (cont'd) Details and findings of previous studies on the effects of strain rate on the strength of sands based on shear tests

Researchers	Loading velocity or strain rate	Apparatus	Effective normal stress (kPa)	Sand and other granular materials	State	D_{50}	D_{60}/D_{10}	Dynamic frictional angle relative to static friction angle*
Cont'd	Cont'd	Cont'd	Cont'd	Coarse quartz sand with rounded grains	Dry & saturated	1.5 - 2.0	NA	None
				4:1 sand-rock flour mixture	Dry	NA	NA	Decrease by 2.0°
				2:1 sand-rock flour mixture	Dry	NA	NA	None
				Coarse rounded sand	Dry	2.0 - 3.0	NA	None
				Polystyrene beads	Dry	NA	NA	None
Hungr and Morgenstern (1984b)	Up to 6.0m/s	Flume	Low	Ottawa sand	Dry	NA	NA	None
				Polystyrene beads	Dry	NA	NA	None
Sassa (1984, 1985)	1.0×10^{-4} - 0.9076m/s	Ring shear	8- 20	Glass beads	Dry	1.0	1.0	None
Lemos (1986)	Up to 2.2×10^{-3} m/s	Ring shear	100	Coarse to medium sand	Saturated	0.63	1.06	Decrease by 3.5° & increase by 0.5°

* Quasi-static friction angle for a particular study is defined as the friction angle obtained from the test conducted at the lowest shear rate adopted in the particular

3.4.3 Triaxial compression tests of sand

The strain rate dependency of the sample loaded in the triaxial compression test might in some way be related to that of the sample sheared against a pile surface. Thus, the studies involving the triaxial test are included in the review. The details of the previous studies on the strain rate effect on the strength of sand specimens tested in the triaxial apparatus are tabulated in Table 3.4. It is noted that where the strain rate was reported, the equivalent loading velocity has been computed based on the initial length of the sample. Before discussing the findings from the previous studies, it is first necessary to understand some of the mechanics of the triaxial tests performed at high strain rates.

3.4.3.1 Mechanics of triaxial tests at high strain rates

All triaxial tests on dry and saturated sand specimens performed at relatively high strain rates are either partially undrained or fully undrained even in a nominally drained test (Seed and Lundgren, 1954; Whitman and Healy, 1962; Abrantes and Yamamuro, 2002b; Yamamuro and Abrantes, 2003). This is because the excess pore air and water pressure respectively do not have sufficient time to dissipate at the high strain rates. A threshold strain rate beyond which this effect occurs cannot be defined in absolute terms as it is dependent on the permeability of the specimen being tested.

Under undrained conditions, the pore water pressure in saturated sand can undergo changes that significantly affect the effective strength of the sample (e.g. Whitman and Healy, 1962; Abrantes and Yamamuro, 2002a). It has been found that as the applied strain rate increases, the specimen has an increased tendency to dilate. Thus, the excess pore pressures are lowered, leading to a higher strength. Under undrained conditions, even pore air pressure in a dry specimen can change the strength of the sample and can lead to a significant increase in the percentage of strength if the confining stress before shear is only moderately high (Whitman and Healy, 1962; Abrantes and Yamamuro, 2002a). Therefore, the strength increase in a sand specimen tested in the triaxial apparatus can originate from a decrease in the excess pore pressure generated or an increase in the friction angle or both. Thus, in the case of a triaxial test, it must be emphasised that “strength” and “friction angle” refer to

Table 3.4 Details of previous studies on the effects of strain rate on the strength of sand using the triaxial apparatus

Researchers	Strain rate or loading velocity	Test conditions	Confining pressure (kPa)	Sample size	Sand	D_{50}	D_{60}/D_{10}	State
Casagrande and Shannon (1949)	Up to 300%/s Up to 3.0×10^{-1} m/s	Partial vacuum	30 to 90	71mm diameter & 180mm high	Clean, medium grained with subangular quartz grains. $e_{max} = 0.51$; $e_{min} = 0.88$	NA	(Grain size: 0.21 - 0.42mm)	Dry dense ($e=0.62$)
Seed and Lundgren (1954)	Up to 1000%/s Up to 1.0m/s	Undrained and drained but drained tests effectively undrained	200	36mm diameter & 102mm high	Clean and fairly smooth subrounded fine sand Fairly smooth subrounded coarse sand	0.1 1.3	1.67 2.00	Saturated loose and dense Saturated loose and dense
Whitman and Healy (1962)	0.017 - 130 %/s Up to about 1.3×10^{-1} m/s	Partially undrained to drained (with partial to full vacuum) undrained	70 to 100	38mm diameter & from 76 to 102mm high	Coarse sand	0.6	1.43	Dry loose ($e=0.91$) and dense ($e=0.60$) Saturated loose ($e=0.64 - 0.68$) and dense ($e=0.49$)
Coyle and Gibson (1970)	2.1×10^{-5} m/s - 3.7m/s	Undrained	103	70mm diameter & 150mm high	Fine sand Medium sand with smooth grains Fine sand with sub-angular shaped grains Very fine sand with very angular grains	0.31 0.55 0.19 0.13	3.17 1.26 3.17 3.53	As above Saturated and majority at $e=0.55$ As above As above
Yamamuro and Lade (1993)	1.33×10^{-7} m/s - 2.2×10^{-5} m/s	Drained and undrained	34000	71mm diameter & 178mm high	Rounded grains	1.66	1.31	Saturated dense ($D_r=0.895$)
Abrantes and Yamamuro (2002a, 2002b); Yamamuro and Abrantes (2003)	0.00188%/sec to 1500%/sec 1.33×10^{-4} m/s to 2.7m/s	Drained condition achieved with full vacuum	98 (resulting from application of vacuum)	70mm diameter & 178mm high	Crushed coral sand with angular grains $e_{max}=1.20$; $e_{min}=0.74$	0.32	2.18	Loose ($e=1.03$) and medium ($e=0.94$)

different aspects of the shearing resistance of sand and that the strength of sand may vary with strain-rate even though the friction angle is independent of strain rate.

It is therefore important to be able to identify the source(s) of the increase in the resistance of a triaxial sand sample tested under high strain rates under undrained conditions. For a saturated sand specimen, the source(s) of the strength increase can be determined by measuring the transient pore pressure response; thus any increase apart from that caused by the pore pressure response must be due to an increase in the friction angle. However, accurate measurement is difficult because of the time delay required for the pore pressure wave to reach the transducer especially for short-duration events (Abrantes and Yamamuro, 2002a). For a dry sand specimen, excess pore air pressure can be minimised and a fully drained condition can be maintained if near complete vacuum is applied such that the induced pore pressure from even large volume changes in the sand during shear is negligible; this avoids the problematic measurement of transient pore pressure and yet enables the change (if any) in the friction angle with the strain rate to be determined (Abrantes and Yamamuro, 2002a).

3.4.3.2 Whitman & Healy (1962)

Whitman and Healy performed undrained triaxial tests with strain rates up to 130%/s or loading velocity of 0.13m/s (for the sample length of 100mm) on three types of sand in dry and saturated conditions, and loose and dense states. The transient pore water pressure response during shear was measured; however, it was acknowledged that there was some experimental error in the measurement due to the inherent difficulty in measuring transient pore pressures.

For the loose saturated sand specimen, the tendency of the specimen to dilate increased with increasing strain rates, resulting in a lower generated excess pore pressure at a given strain and hence higher strength. This tendency to dilate increased with decreasing confining pressure. It was found that tests under low confining pressure yielded lower excess pore pressure and contributed to an increase in total strength of up to 100%. However, because of the uncertainty in the pore water pressure measurement, it could not be ascertained whether the friction angle increased with strain rate.

In any case, Whitman and Healy (1962) proposed a mechanistic explanation for the motions of the sand particles (subjected to compressive triaxial loading) that would suggest that the friction angle of the sand is rate-dependent. It was hypothesised that the relative movement between two sand particles did not occur in a continuous manner. Rather, it occurred at opportune moments when the arrangement of the surrounding particles allowed the movement to occur with a minimum resistance and the particles settle into voids resulting from the particle rearrangement. However, at high strain rates, the opportune moments occurred less frequently for a given strain increment such that the grains had to rearrange with higher resistance and to move “up-and-over” the surrounding particles. Thus at high strain rates, the sand specimen would dilate more and the friction angle of the specimen would be higher, as compared to an instance when it was loaded at a slower strain rate.

3.4.3.3 Coyle & Gibson (1970)

The study by Coyle and Gibson is often referenced for the damping behaviour of sand. Coyle and Gibson conducted impact tests on triaxial sand samples with a set-up similar to that by Whitman and Healy but up to a loading velocity of 3.5m/s. All the sand samples were saturated. The dynamic tests were performed as unconsolidated-undrained tests at a void ratio of 0.55 and under a confining pressure of 103kPa; the undrained conditions were intended to simulate the pore pressure condition at the pile tip during driving. The quasi-static tests were performed as consolidated-drained tests at the same void ratio and confining pressure as the dynamic tests; the drained tests were intended to simulate the drained condition of zero pore water pressure at the pile tip during static loading.

The strength of each of the samples increased with the velocity of deformation. The strength ratio-velocity plot from Coyle and Gibson (1970) is reproduced in Figure 3.17 and replotted in Figure 3.18 in accordance with the plotting standard form adopted in this Chapter, with the shear strength followed by the confining stress indicated for each sample. In order to fit the experimental results, the power law was used. The value N ranged from 0.19 to 0.28 and the value J varied between 0.6 and 1.3. It is noted that the Ottawa sand behaved very differently compared with the Arkansas and Victoria sands. Without having access to the detail of the sands, this

would suggest that particle properties such as the surface texture, grading and particle size had a significant influence on the dynamic resistance.

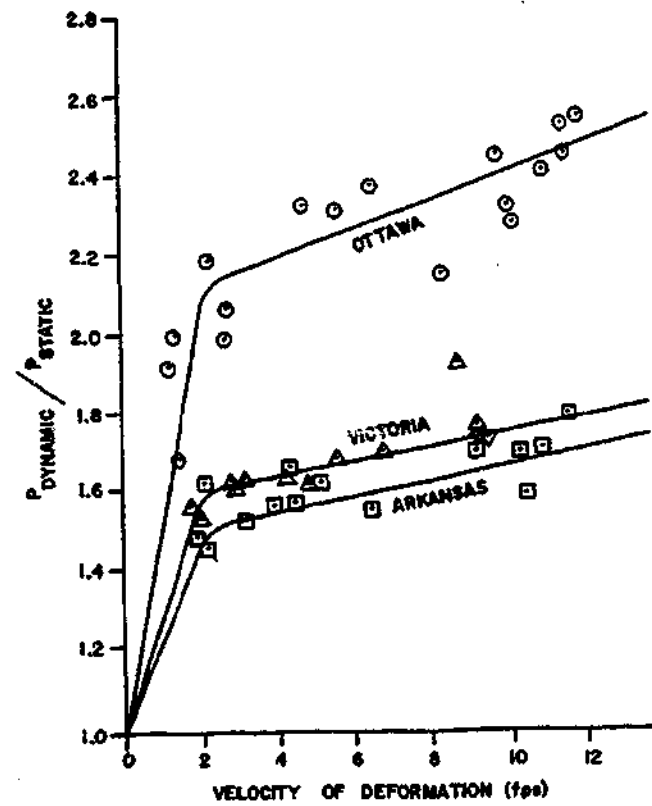


Figure 3.17 Strength ratio-velocity relationship (Coyle and Gibson, 1970)

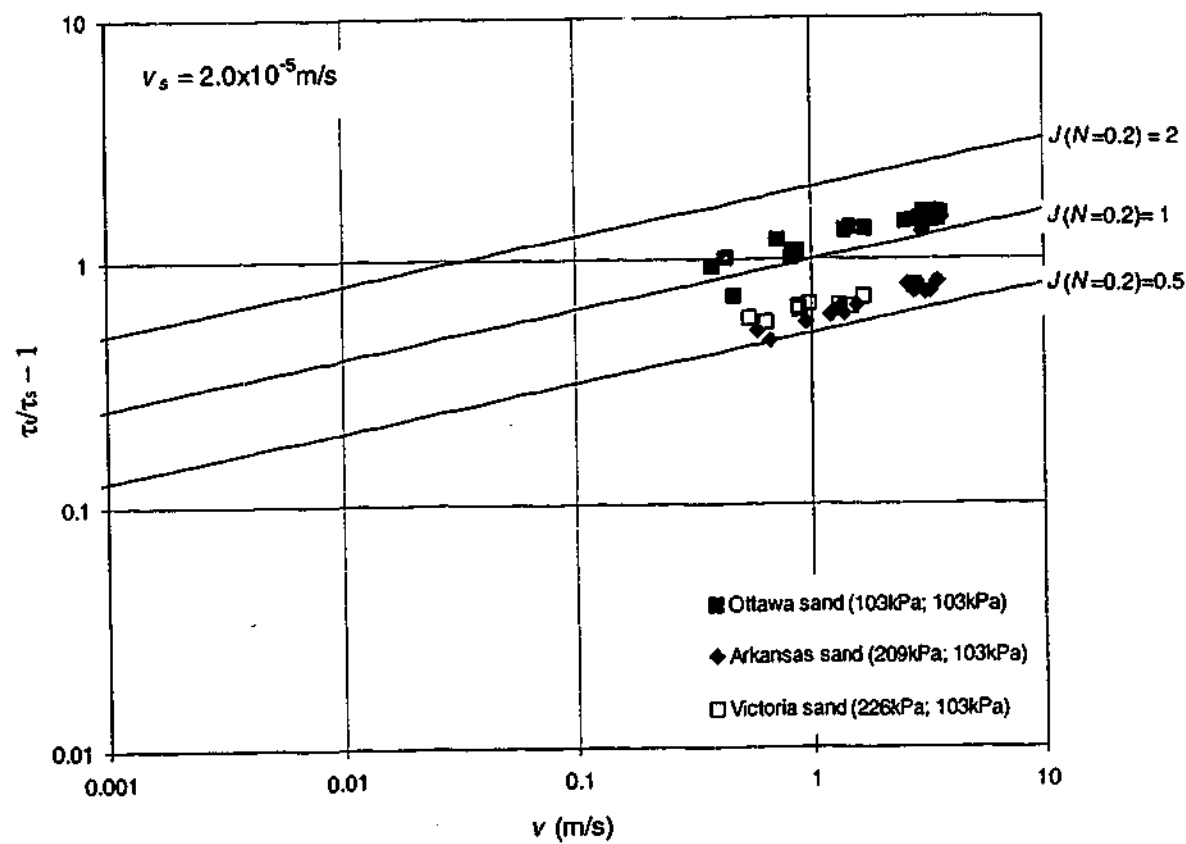


Figure 3.18 Strength ratio-velocity relationship based on data from Coyle and Gibson (1970), where the strength ratio was obtained for the quasi-static friction corresponding to 2.0×10^{-5} m/s

The damping factor J obtained by using $N=0.20$ was related to the effective friction angle (ϕ') as shown in Figure 3.19. The friction angle was obtained by conducting drained and undrained quasi-static tests with pore pressure measurements at a void ratio of 0.55. The damping constant J for Ottawa sand was also related to the void ratio for $N=0.20$ and for optimum values of N , as shown in Figure 3.20.

Since the pore pressure response was not measured, it was not possible to ascertain whether the source of the strength increase was a strain rate dependent friction angle, or a strain rate dependent, or both. However, given that the quasi-static and dynamic tests were performed under drained and undrained conditions respectively, it was most likely that the pore pressure response during the dynamic test had contributed to the strength increase.

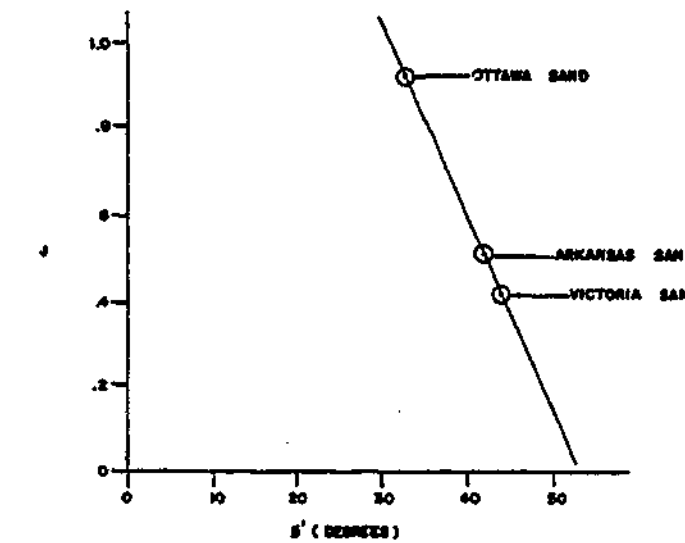


Figure 3.19 Relationship between internal angle of friction and damping factor (Coyle and Gibson, 1970)

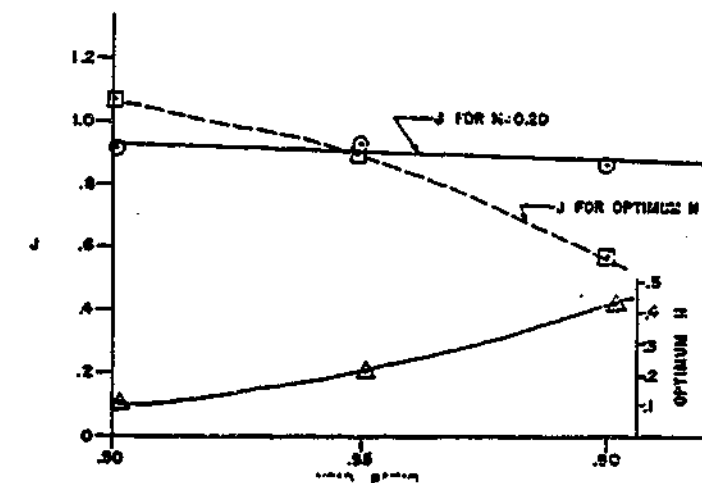


Figure 3.20 Relationship between void ratio and damping factor (Coyle and Gibson, 1970)

3.4.3.4 Yamamuro & Lade (1993)

The effects of strain rates on sands at high confining pressures were investigated by Yamamuro and Lade (1993) by performing both drained and undrained tests. The loading rates were chosen to be very low (as specified in Table 3.4) so that accurate pore pressure measurements could be made in undrained tests. It was found that for drained tests, the strength did not vary with strain rate. In undrained tests, the strength increased significantly with increasing strain rates due to lower generated excess pore pressures in the specimen (which is caused by the increased tendency of the specimen to dilate) rather than to an increase in the friction angle, as compared to when the specimen was strained at a lower rate.

It was hypothesised by the researchers that at higher strain rates, there was less time for particle crushing and grain rearrangement such that the sand appeared less compressive and more dilatant. This resulted in significantly higher strength due to more significant pore pressure differences. It was suggested that the same mechanism was likely to apply to tests at low confining pressures as well although no crushing would occur in such tests.

3.4.3.5 Abrantes & Yamamuro (2002b), & Yamamuro and Abrantes (2003)

Abrantes and Yamamuro (2002b) and Yamamuro and Abrantes (2003) in their recent studies were the first to show the variation of the friction angle of a sand specimen with strain rate for strain rates up to above 1100%/s or loading velocities up to 2.0m/s. Loose and medium dense sand specimens with relative densities of 36% and 58% respectively were tested. To avoid the effect of pore air pressure changes in the dry sand sample and maintain fully drained conditions, the researchers used near-complete vacuum to evacuate pore spaces so that the induced pore pressure for even large volume changes was negligible and so that the problem of measuring transient pore pressure could be circumvented. Therefore any increase in the compressive strength could be directly attributed to the increase in friction angle.

The increase in the maximum principle stress difference ratio (relative to the equivalent static value) has been plotted against the strain rate by the researchers as shown in Figure 3.21. For strain rates of between 0.0022%/s and approximately 1600%/s, the ratio increased by 35% for the loose sand specimen and 50% for the

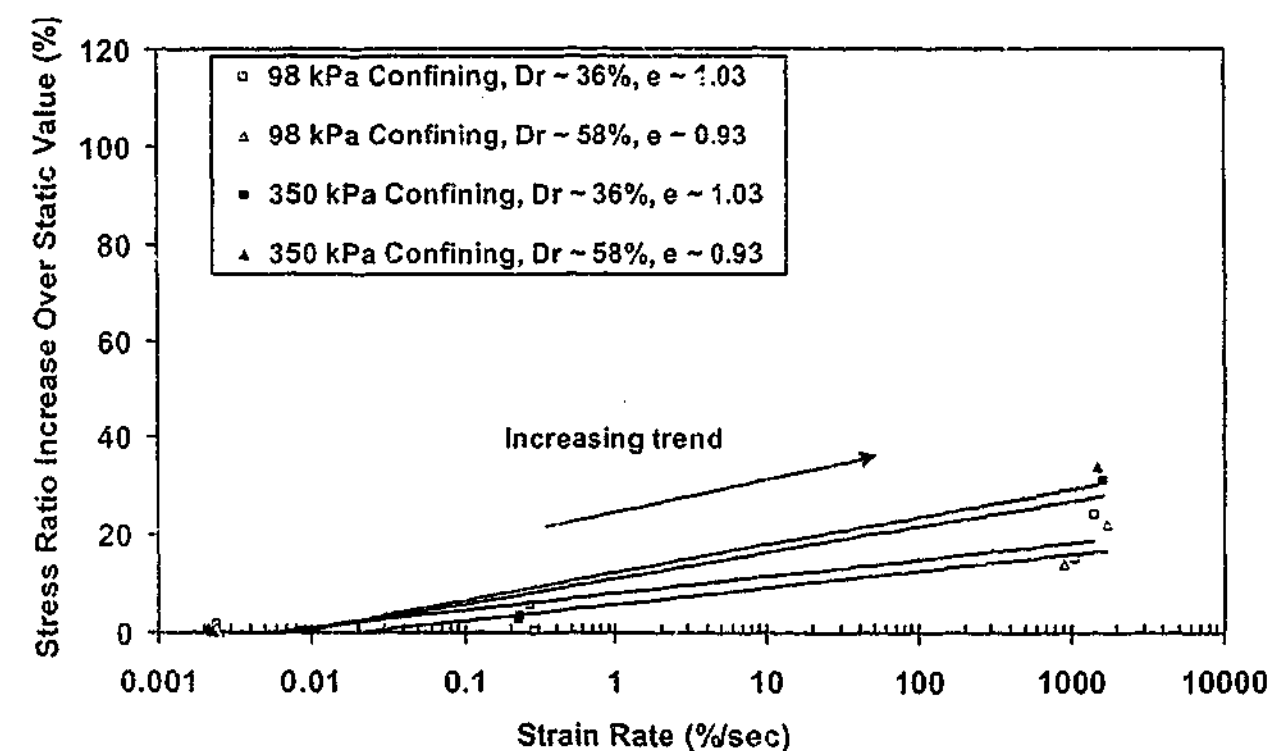


Figure 3.21 Increase in maximum principle stress ratio-strain rate relationship (Yamamuro and Abrantes, 2003)

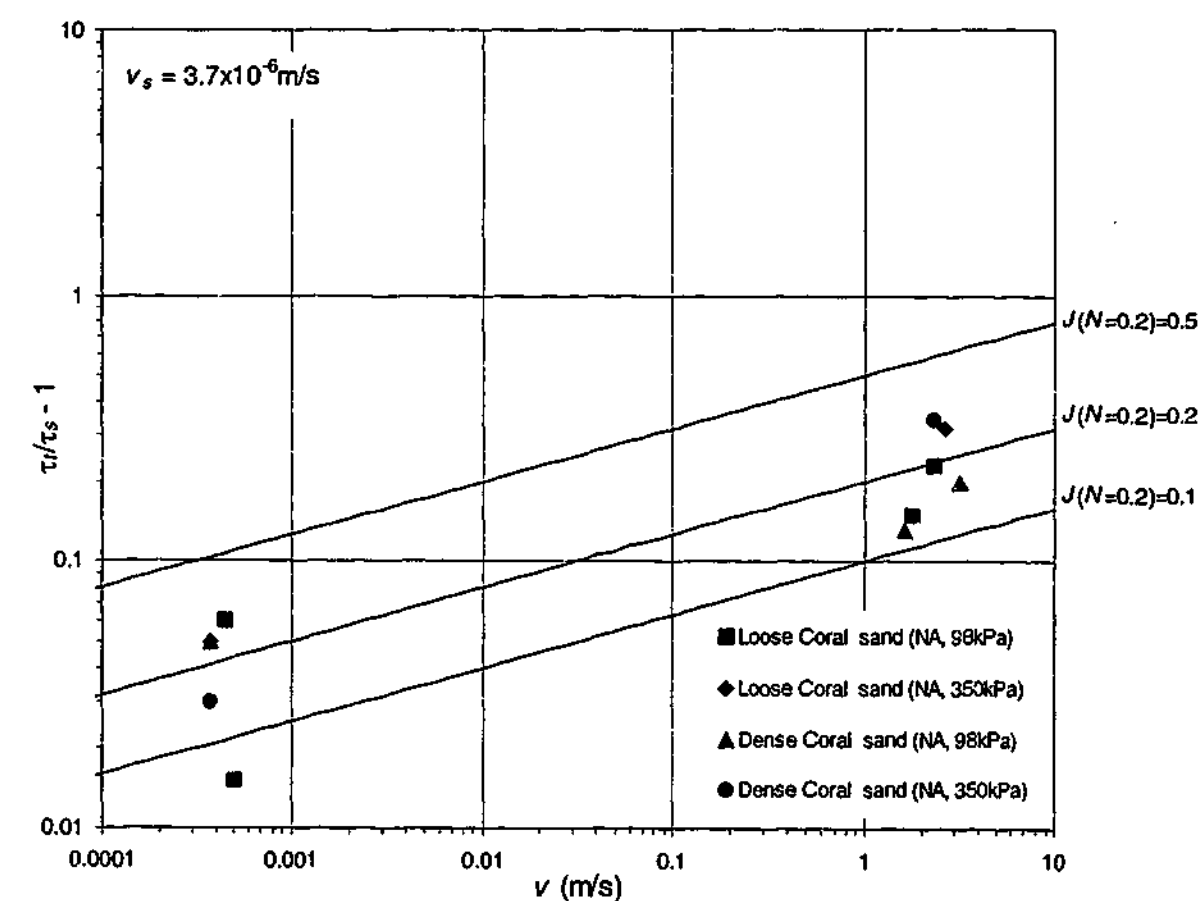


Figure 3.22 Strength ratio-strain rate relationship based on data from Yamamuro and Abrantes (2003), where the strength ratio was obtained for the quasi-static friction corresponding to 3.7×10^{-6} m/s

medium dense sand specimen; in terms of the friction angle, the increase was about 30% for both specimens. The data are replotted in the standard form in Figure 3.22. Given the lack of data points, it is difficult to quantify the value N . However, it is approximately equal to 0.2, and $J(N=0.2)$ varies between 0.1 and 0.3.

Yamamuro (2002) proposed that the strength increase was caused by local inertial effects. From a global and continuum perspective, their triaxial tests which were conducted at constant velocities would not have any significant inertia effects. However, at the level of the sand grains, the specimen was not strictly a continuum. Whilst the specimen was strained globally at a constant velocity, some grains moved in directions other than the specific global directions and hence were forced by the surrounding grains to move in the specific global directions. Since these grains had mass, they resisted this movement, thus creating an additional resistance. Thus at high strain rates, the friction angle would increase. Also, during loading, the grains might move “up-and-over” surrounding grains as opposed to falling into voids between grains because the grains were moving very quickly in different directions; this causes the specimen to have an increased tendency to dilate.

3.4.3.6 Relevance of triaxial tests

Based on both the findings by Coyle and Gibson (1970), Abrantes and Yamamuro (2002b), and Yamamuro and Abrantes (2003), it would appear that the (sand-only) friction angle increases with strain rate. However, it is noted that these findings based on the triaxial tests might not have direct relevance to the dynamic response of the pile-soil interface for reasons that are discussed as follows.

The mode of loading and of failure of a specimen tested in the compressive triaxial test is quite different from that of a specimen sheared against the pile surface. In a pile-soil interface shear test, the specimen shears against a pre-defined failure plane (i.e. that of the pile-soil interface). Only the particles of the specimen at the interface are involved in the shearing process. The failure condition is defined as the peak stress condition, where a shear band is formed at the interface and where relative movement between the pile and sand (slippage) occurs at the interface. Thus, the viscous damping phenomenon associated with the pile-soil interface is related to the

slippage between the soil and the pile, and thus to the slip velocity. On the other hand, in the triaxial test, the specimen is loaded in compression. Failure is typically defined as the point where peak principle stress difference occurs (e.g. Abrantes and Yamamuro, 2002a, 2002b). At this point, the specimen, which undergoes compressive deformation, fails by bulging. The bulging occurs as the deformation of the specimen at the cap-specimen interfaces is restrained, and as the deformation of the specimen at mid-height of the specimen is unrestrained (e.g. Abrantes and Yamamuro, 2002a, 2002b). Whilst the failure mode near the ends of the specimen is associated with non-uniform strains, the failure mode at its mid-height of the specimen is associated with a uniform state of strain (e.g. Yamamuro and Abrantes, 2003). Thus, slippage between two masses does not occur during failure. It is noted that if shear banding (which involves formation of a shear plane and thus slippage between two soil masses) occurs in the test, it would occur only as a post-peak failure phenomenon and would not be associated with the failure itself (e.g. Wroth and Houlsby, 1985; Wang and Lade, 2001, 2002). It would therefore appear that the modes of failure associated with the two types of test are fundamentally different.

Whilst it is intuitive that during failure slip must occur locally amongst the particles, this must occur at various slip velocities throughout the specimen. These velocities may be quite different from the global velocity of deformation of the entire specimen. Therefore, the strain rate or the loading velocity (deduced from the strain rate based on the original length of the sample) associated with the triaxial test may not have direct relevance to the slip velocity between the soil and the pile.

Furthermore, if Yamamuro's hypothesis that the rate-dependence of the strength of sand is due to local inertial forces generated by the grains is correct, then a significant volume of grains will be required for the strength increase to be apparent. Such volume is only available for a sample which is loaded in compression rather than sheared against an interface where only a thin zone of the specimen is involved.

Therefore, because of fundamental differences in the mode of loading of the sample tested in the triaxial test and of the sample sheared against the pile surface, the finding based on the triaxial tests should not be assumed to apply to the pile-soil interface.

3.4.4 Concluding remarks – dynamic effects in sand – previous studies

The studies of the dynamic response of the pile-sand interface have been limited to those by Heerema (1979) and Dayal and Allen (1975) who found that the interface friction angle was independent of the shear rate. It is noted that these studies were limited in that relatively low peak velocities (compared to the pile driving event) were tested; as such, any small increase in the friction angle, which will only be discernible at higher shear rates, would not have been detectable in these studies. Also, the possible effects of the sand characteristics (such as its particle size, particle shape and grading) on the dynamic friction angle were not investigated.

Based on sand-only direct and ring shear tests, findings of the rate-dependence of the friction angle on shear rate were mixed, with some tests showing that the friction angle was independent of the shear rate and other tests showing that the friction angle varied with shear rate. Where the friction angle was found to vary with shear rate, the variation of the friction angle appeared to be unsystematic.

Based on triaxial tests (Coyle and Gibson, 1970; Abrantes and Yamamuro, 2002b; Yamamuro and Abrantes, 2003), the friction angle of specimens increased with increasing strain rates. However, this finding which is based on the triaxial tests might not have direct relevance to the dynamic response of the pile-soil interface because the shearing mechanism occurring in a sample subjected to triaxial compression appears to be fundamentally different from that occurring in a sample subjected to shearing against a pile interface.

Given that little research has been conducted on the dynamic response of the pile-sand interface and available previous research shows mixed findings, further research is carried out in this study to ascertain the shear rate-dependence (or otherwise) of the pile-sand interface friction angle.

3.5 Dynamic Effects in Clay – Previous Studies

Previous studies into the dynamic strength of clay specimens tested in both soil-only and pile-clay interface tests are presented in Table 3.5, and the details and findings of each of the studies, including the values of the damping parameters, are tabulated in Table 3.6. It is noted that, as discussed in relation to the tests for sand, the values of the damping parameters quoted are specific to the particular shear rate at which the quasi-static friction was defined in each study.

Table 3.5 Details of previous studies on the effects of strain rate on the pile-clay interface strength

Researchers	Apparatus	Velocity	Interface	Normal stress or confining stress	Sample size
Coyle and Gibson (1970)	Unconsolidated undrained for both static and dynamic	$2.1 \times 10^{-5} \text{ m/s} - 3.7 \text{ m/s}$	NA	No confining stress	70mm diameter and 150mm high
Dayal (1974), Dayal and Allen (1975)	Penetrometer	Up to 5.5m/s, $1.34 \times 10^{-3} \text{ m/s} - 0.81 \text{ m/s}$	Steel	Unknown	NA (penetrometer inserted into specimen)
Heerema (1979)	Direct shear	$7.8 \times 10^{-7} \text{ m/s} - 1.04 \text{ m/s}$	Steel	10-490kPa	Semi-cylindrical: 50mm in diameter and 150mm long
Litkouhi and Poskitt (1980)	Penetrometer	$3.0 \times 10^{-4} \text{ m/s} - 1.7 \text{ m/s}$	Steel	Unknown	NA (penetrometer inserted into specimen)
Poskitt and Leonard (1982)	Penetrometer	$2.0 \times 10^{-4} \text{ m/s} - 2.0 \text{ m/s}$	Steel	Unknown	250mm in diameter and 300mm long
Benamar et al. (1991, 1992) Benamar (1999)	Shaft encased in triaxial specimen	Up to 2.1m/s	Steel	300-500kPa	200 diameter and 500mm high

3-38

Table 3.6 Details of previous studies on the effects of shear rate on the pile-clay interface strength

Researchers	Apparatus	Velocity	Interface	Normal stress (kPa)	Clay	Description	w _l (%)	w _p (%)	I _p (%)	s _v * (kPa)	N	J (s/m) ^N				
Coyle and Gibson (1970)	Unconsolidated undrained	$2.1 \times 10^{-5} \text{ m/s} - 3.7 \text{ m/s}$	NA	No confining stress	Organic31	Organic clay of high plasticity	53	23	30	59	0.18	0.93				
					Organic36								38	0.22	1.29	
					Easterw62	Inorganic clay of high plasticity	94	64	30	24	0.16	1.40				
					Easterw60								25	0.15	1.47	
					Easterw55								40	0.20	0.63	
					Easterw50	36	0.19	1.17								
Vettors55	Inorganic clay of high plasticity	80	53	27	17	0.25	1.11									
Vettors50								24	0.20	1.21						
Vettors46								32	0.14	1.10						
Hall Pit Clay	Inorganic clay of medium plasticity	48	25	23	31	0.11	0.88									
Dayal (1974), Dayal and Allen (1975)	Penetrometer	$1.34 \times 10^{-3} \text{ m/s} - 0.81 \text{ m/s}$	Steel	Unknown	Pottery	Clayey silt (MIT); Mainly of illite and chloride minerals with small quantity of quartz, feldspar and kaolinite; G _s = 2.61	37	21	16	3	0.16	2.7				
Heerema (1979)	Direct shear	$7.8 \times 10^{-7} \text{ m/s} - 1.04 \text{ m/s}$	Steel	31.5 87 104	Kontich	Undisturbed; Generally over-consolidated; Inorganic clays; plasticity from high to low; Most are silty or sandy; Depths of recovery from 2 to 70m.	NA	NA	NA	260	0.20	1.8				
					29								Claymore	55	0.20	3.6
					143								Heather	230	0.20	7.3
					750									390	0.20	3.0
					206									620	0.20	1.0
Litkouhi and Poskitt (1980)	Penetrometer	$3.0 \times 10^{-4} \text{ m/s} - 1.7 \text{ m/s}$	Steel	Unknown	London	NA	70	27	43	15	0.21	1.50				
					Forties					35			0.16	2.07		
										60					0.17	1.09
38	20	18	5	0.20	1.38											
Magnus (remoulded)	Very stiff silty clay with shell fragments and scattered gravel	31	17	20	5	0.45	1.83									
					40			0.36	2.68							

3-39

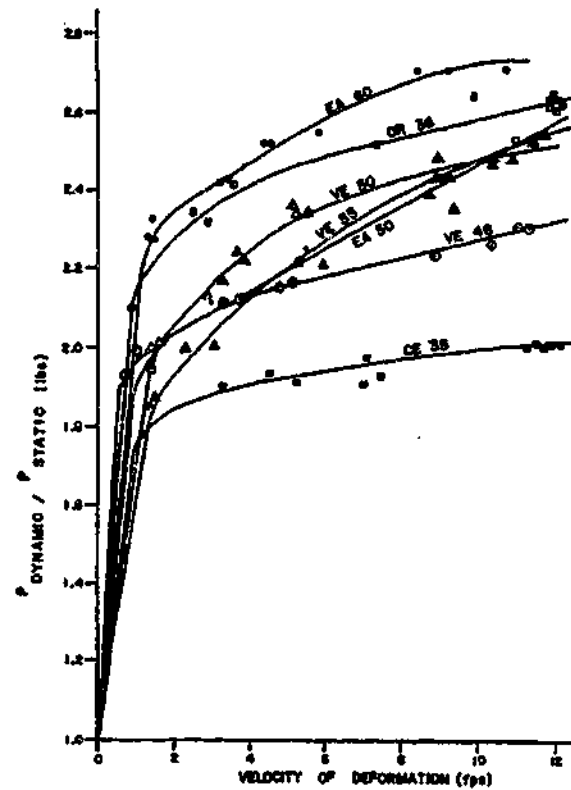


Figure 3.23 The strength ratio-velocity relationship, where the strength ratio was obtained for the quasi-static strength corresponding to a velocity of $2.0 \times 10^{-5} \text{ m/s}$ (Coyle and Gibson, 1970)

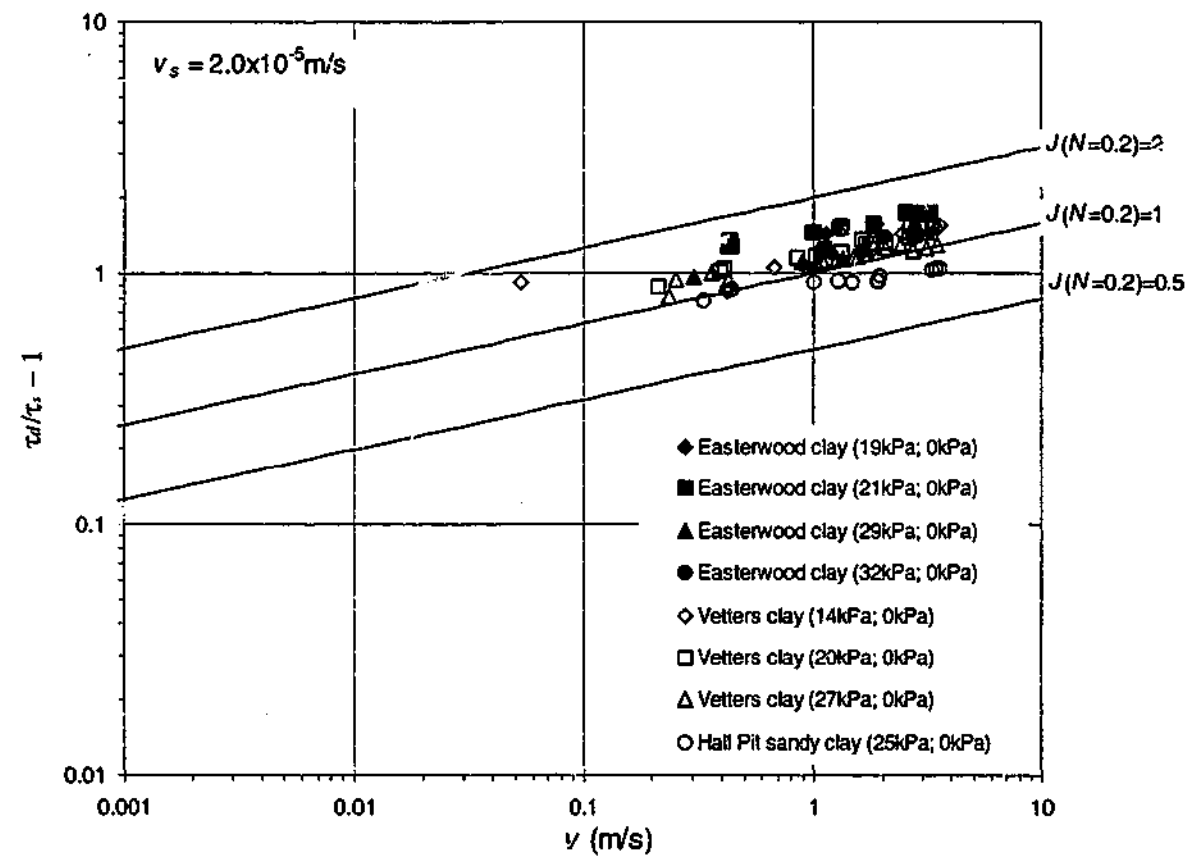


Figure 3.24 Strength ratio-velocity relationship based on data from Coyle and Gibson (1970), where the strength ratio was obtained for the quasi-static strength corresponding to $2.0 \times 10^{-5} \text{ m/s}$

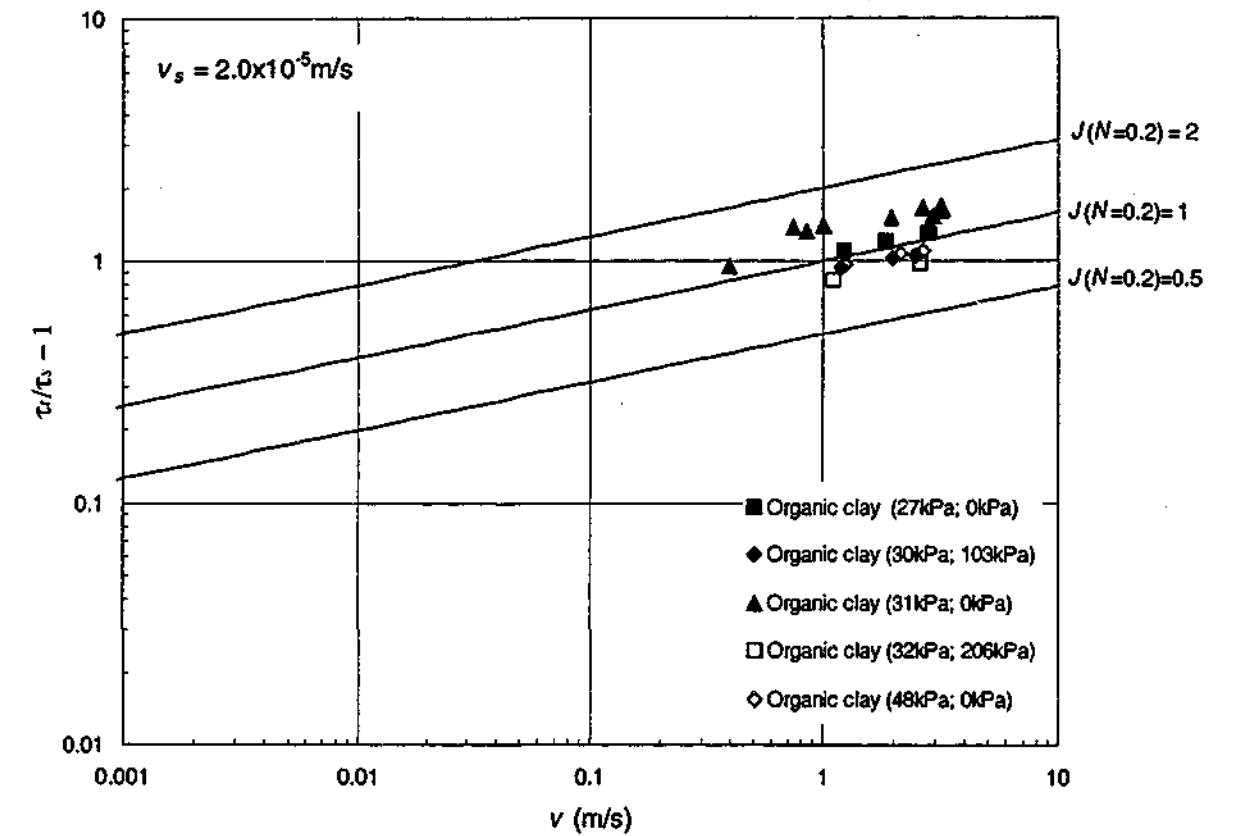


Figure 3.25 Strength ratio-velocity relationship, based on data from Coyle and Gibson (1970), where the strength ratio was obtained for the quasi-static strength corresponding to $2.0 \times 10^{-5} \text{ m/s}$

To enable correlations between the parameter J and soil properties to be made, N was fixed by the researchers at 0.18 such that J became a direct measure of the magnitude of the strength ratio. The value of J was found to be directly proportional to the moisture content; an example of this relationship for Vettiers Clay is shown in Figure 3.26. Also, the value of J was found to be directly proportional to the liquidity index as shown in Figure 3.27. It would appear that since the moisture content and the liquidity index of a sample were inversely proportional to strength of the sample, the degree of dynamic effect was inversely proportional to the shear strength of the sample.

As has been discussed in Section 3.4.3.6, there are fundamental differences in the mode of loading of the sample tested in the triaxial test and of the sample sheared against the pile surface. In addition to these differences, the shear failure of the tests is related to undisturbed soil rather than the highly remoulded soil that exists at the pile-soil interface of real piles. In addition, the strength increase in the triaxial specimens has been shown by many studies (e.g. Casagrande and Wilson, 1951;

Richardson and Whitman, 1962; Lefebvre and LeBoeuf, 1987) to be due in part to the tendency of the specimens to dilate. This tendency causes a decrease in the generated pore pressure during shear, and thus an increase in the effective stress and the strength. Thus the strength ratio-velocity response observed by Coyle and Gibson can be attributed to both viscous behaviour and the pore pressure response. Therefore, the strength ratio-velocity response obtained by Coyle and Gibson should not be assumed to apply to the dynamic response of the pile-soil interface.

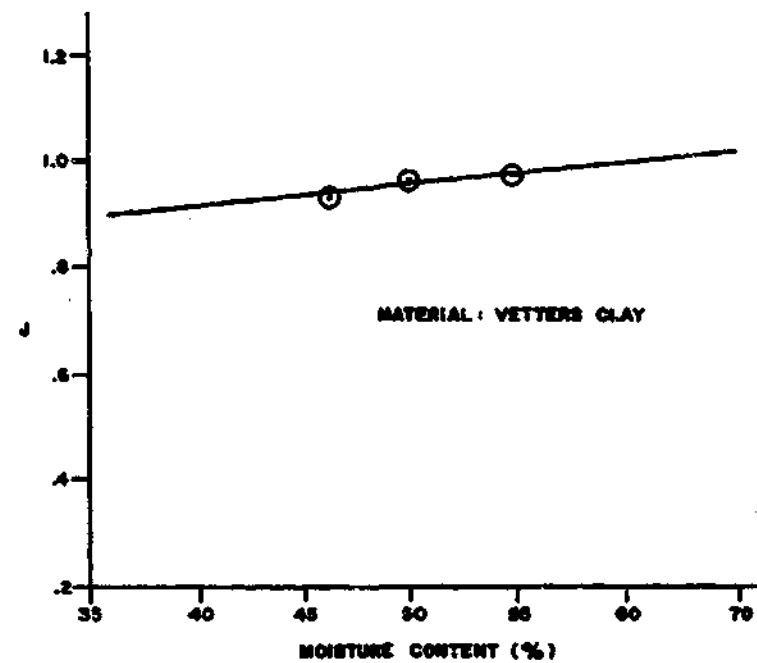


Figure 3.26 Correlation of J for $N=0.18$ with moisture content for Vettiers clay (Coyle and Gibson, 1970)

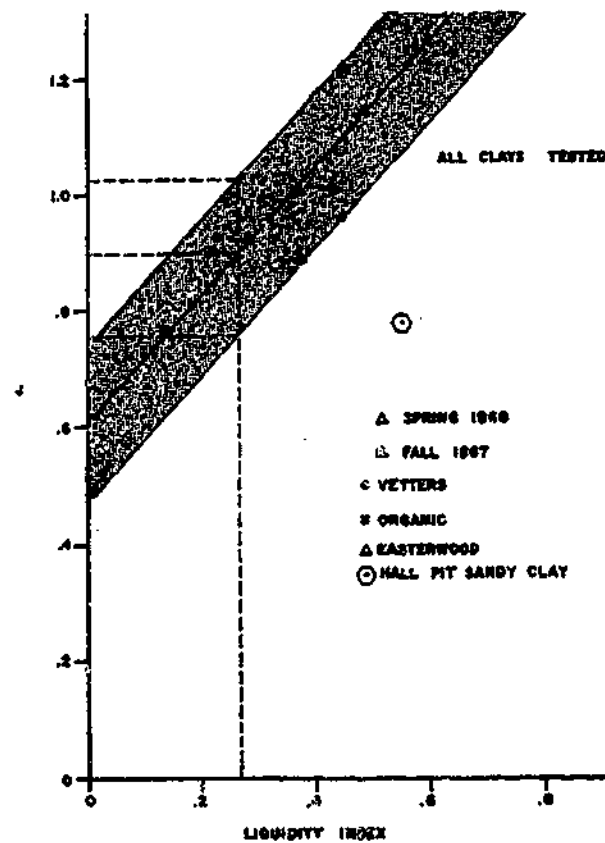


Figure 3.27 Correlation of J for $N=0.18$ with liquidity index (Coyle and Gibson, 1970)

3.5.2 Penetrometer test

Dayal and Allen (1975), Litkouhi and Poskitt (1980) and Poskitt and Leonard (1982) investigated the dynamic response of piles in clays by performing penetrometer tests.

3.5.2.1 Dayal & Allen (1975)

The penetrometer tests by Dayal and Allen (1975) were performed at constant velocities. Both remoulded and undisturbed samples were tested. The sample preparation for the remoulded samples was not described. The undisturbed samples were collected with thin-walled tubes which had a 254mm diameter and a length of 254mm. In general, the friction was found to increase to a depth of 4 times the diameter of the penetrometer, after which it remained almost constant. Thus for each test, the friction value used in the analysis corresponded to that obtained at a depth of greater than 4 times the diameter of the penetrometer.

In addition to the constant velocity data obtained in their study, Dayal and Allen (1975) also analysed data from impact penetrometer tests performed in another study

(Dayal, 1974). Based on both the constant velocity and impact tests, the strength ratio-velocity relationship was modeled using a log function as follows:

$$\frac{\tau_v}{\tau_s} = k_1 \log_{10} \left(\frac{v}{v_s} \right) \quad (3.5)$$

The parameter k_1 was defined as the soil viscosity coefficient. In this discussion, for the sake of standardisation, the raw data have been fitted with the closest equivalent power law in the form of Equation (3.2). Although, for a particular data set, the behaviour changed significantly at the so-called critical velocity, only one overall fit has been produced for the data set. An N value of about 0.16 has been found to be appropriate for all the data sets. The J values have been tabulated in Table 3.6.

The quasi-static friction, τ_s , was measured at $1.3 \times 10^{-3} \text{m/s}$. The researchers normalized the velocity, v , using the lowest velocity at which the quasi-static was obtained, v_s . The strength ratio-velocity ratio plots for the constant velocity tests (velocity up to 0.8m/s) and the impact tests (velocity up to 5.5m/s) are reproduced in Figure 3.28 and Figure 3.29 respectively.

As shown in Figure 3.28, the data set for "Test No. C.C.1" has significant scatter. For all data sets presented in Figure 3.28 and Figure 3.29, the rate of increase of the strength ratio is bilinear, with a consistent change in response in the log-log plot above and below a ratio of 108 corresponding to 0.14m/s. This sudden change in behaviour was attributed to the existence of a critical velocity by the researchers. Since the friction-velocity relationship for each interface was based on only a few data points, the apparent bi-linear relationship may be a function only of the limited data.

These data are re-plotted in standard form in Figure 3.30 in the standard strength ratio-velocity (with N fixed at 0.2), with the shear strength of the sample indicated for each sample). It could be seen that $J(N=0.2)$ ranged from 0.3 to 3.5.

It was also found that the strength ratio increased with decreasing shear strength of the clay. The effect of normal stress on the strength ratio could not be investigated because the normal stress at the interface was unknown.

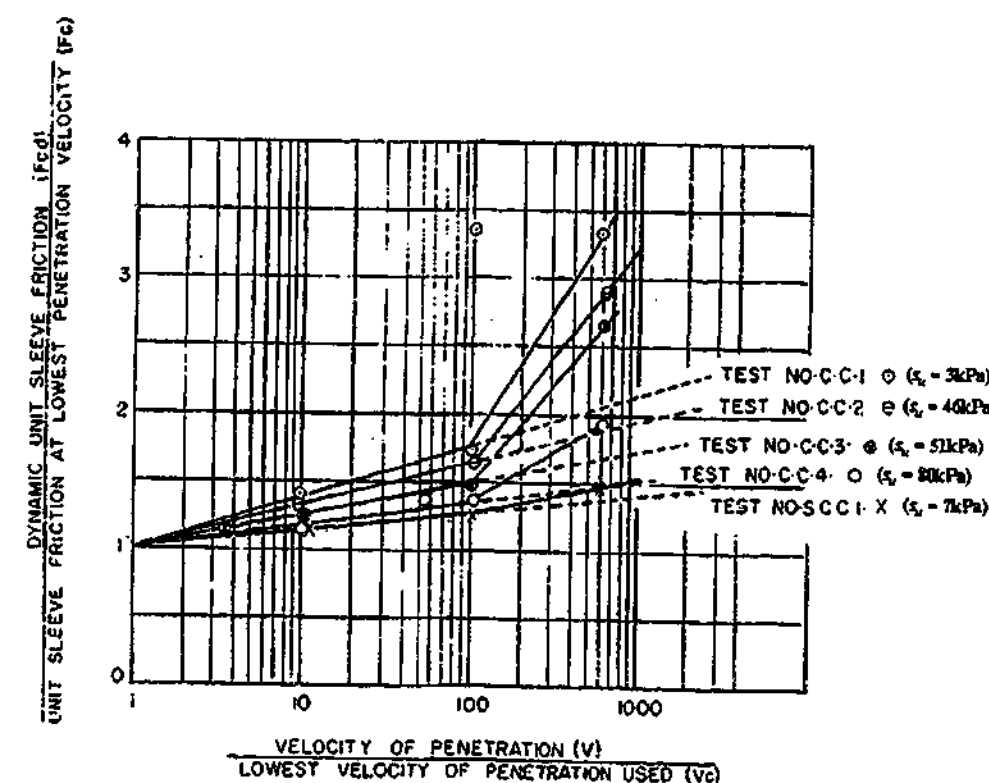


Figure 3.28 Constant velocity tests: Strength ratio-velocity ratio relationship, where the strength ratio was obtained for the quasi-static friction corresponding to $1.3 \times 10^{-3} \text{m/s}$ (after Dayal and Allen, 1975)

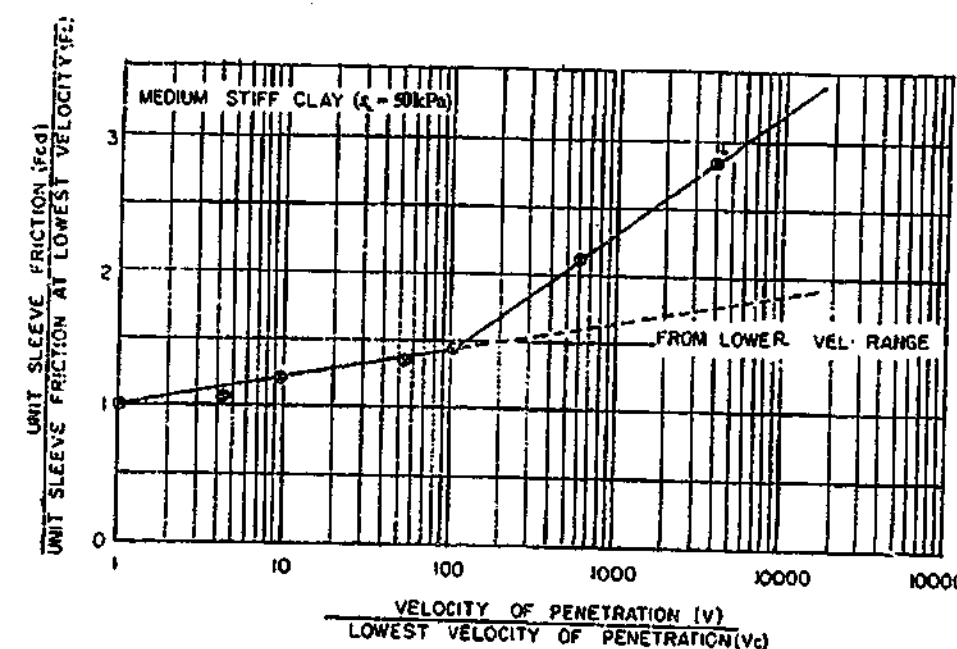


Figure 3.29 Impact tests: Strength ratio-velocity ratio relationship, where the strength ratio was obtained for the quasi-static friction corresponding to $1.3 \times 10^{-3} \text{m/s}$ (after Dayal and Allen, 1975)

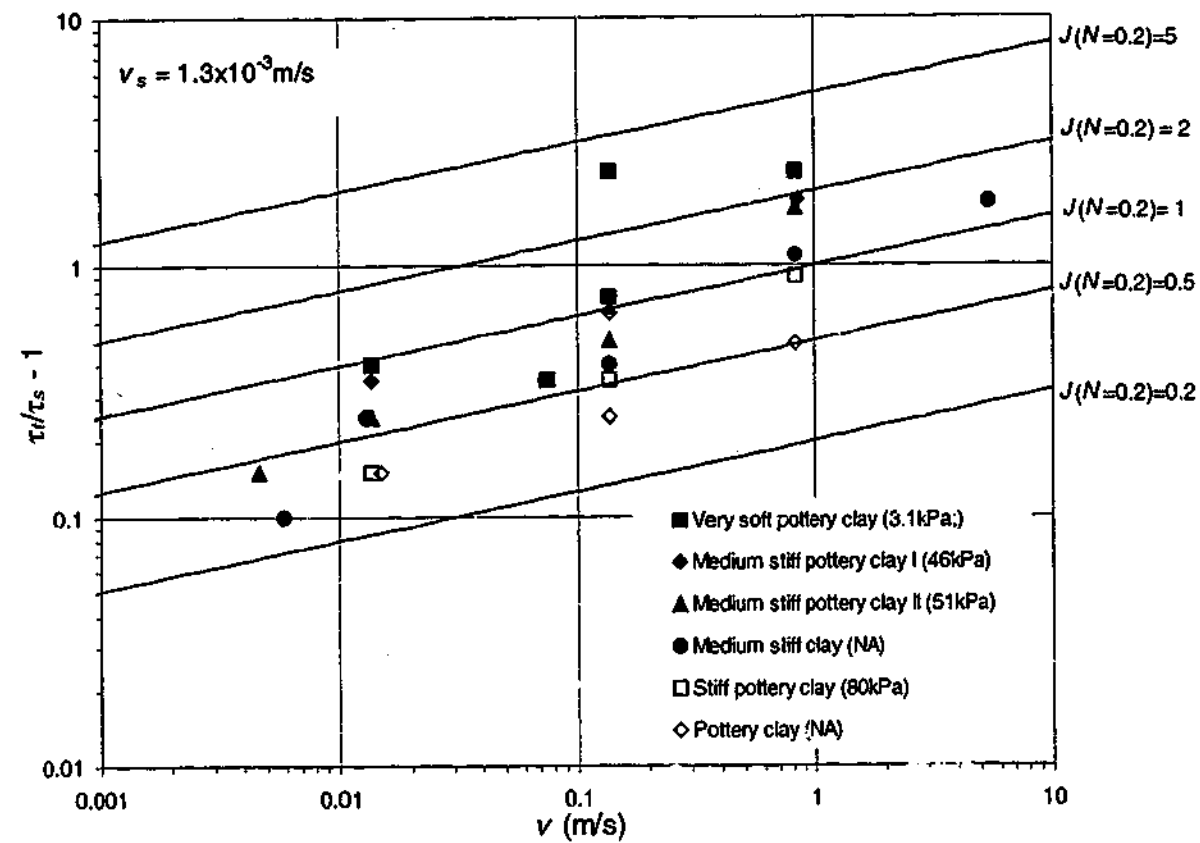


Figure 3.30 Strength ratio-velocity relationship based on data from Dayal and Allen (1975), where the strength ratio was obtained for the quasi-static friction corresponding to 1.3×10^{-3} m/s

A sample record of an impact test performed by Dayal (1974), which is reproduced in Figure 3.31, shows that the velocity decreased from its free-fall or initial impact velocity to zero as the penetrometer was decelerated to a stop, the dynamic friction was predominantly constant. This contradicted the finding that the friction was velocity-dependent; this anomaly is discussed in greater detail in Section 3.5.2.4. It would appear that, for these impact tests, Dayal and Allen associated the constant friction to an interpreted overall velocity rather than associating the instantaneous friction with the instantaneous velocity. If this was so, the friction-velocity relationship obtained in such a way might not give the real friction-velocity response of the interface.

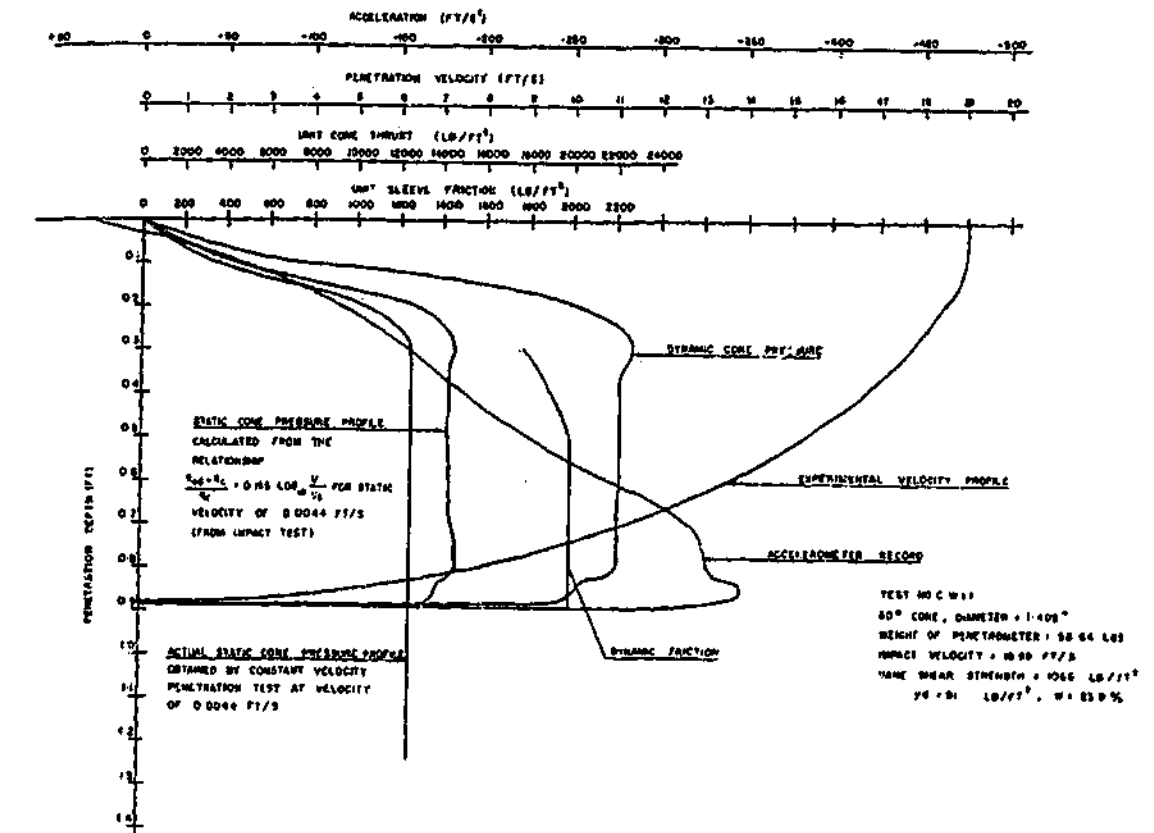


Figure 3.31 Record of an impact penetration test performed by Dayal (1974) (Dayal and Allen, 1975)

3.5.2.2 Litkouhi & Poskitt (1980)

Using a penetrometer that differed from that used by Dayal and Allen in geometry, Litkouhi and Poskitt found a different strength ratio-velocity response for the interface component of the penetrometer. To reduce the influence of disturbance, each test was performed at a minimum spacing of five times the penetrometer diameter and at least five penetrometer diameters away from the sampler wall. For most of the tests, the penetrometer penetrated to a depth of 150 to 200mm. It was found that over this range, the properties of the soil were reasonably constant. The interface friction increased almost uniformly with depth such that it was necessary to select a representative value of the interface friction for a particular test.

The strength ratio-velocity relationship was fitted with the power law in the following form:

$$\frac{\tau_t}{\tau_s} = 1 + Jv^N \quad (3.6)$$

The quasi-static friction, τ_s , was measured at 3.0×10^{-4} m/s. The values of J and N were found to vary between 1.10 and 2.68, and between 0.16 and 0.57 respectively.

Typical raw experimental results of some tests are reproduced in Figure 3.32; these tests were related to London clay specimens with shear strength of about 15kPa. It is noted that these values are highly variable even for tests performed with supposedly the same set of test conditions, and that the different values were averaged by the researchers to obtain a representative set of values for a particular set of test conditions. The raw data for tests other than for the London clay were not presented; instead, only the J and N values used to best-fit the data were reported, which are reproduced in Table 3.7.

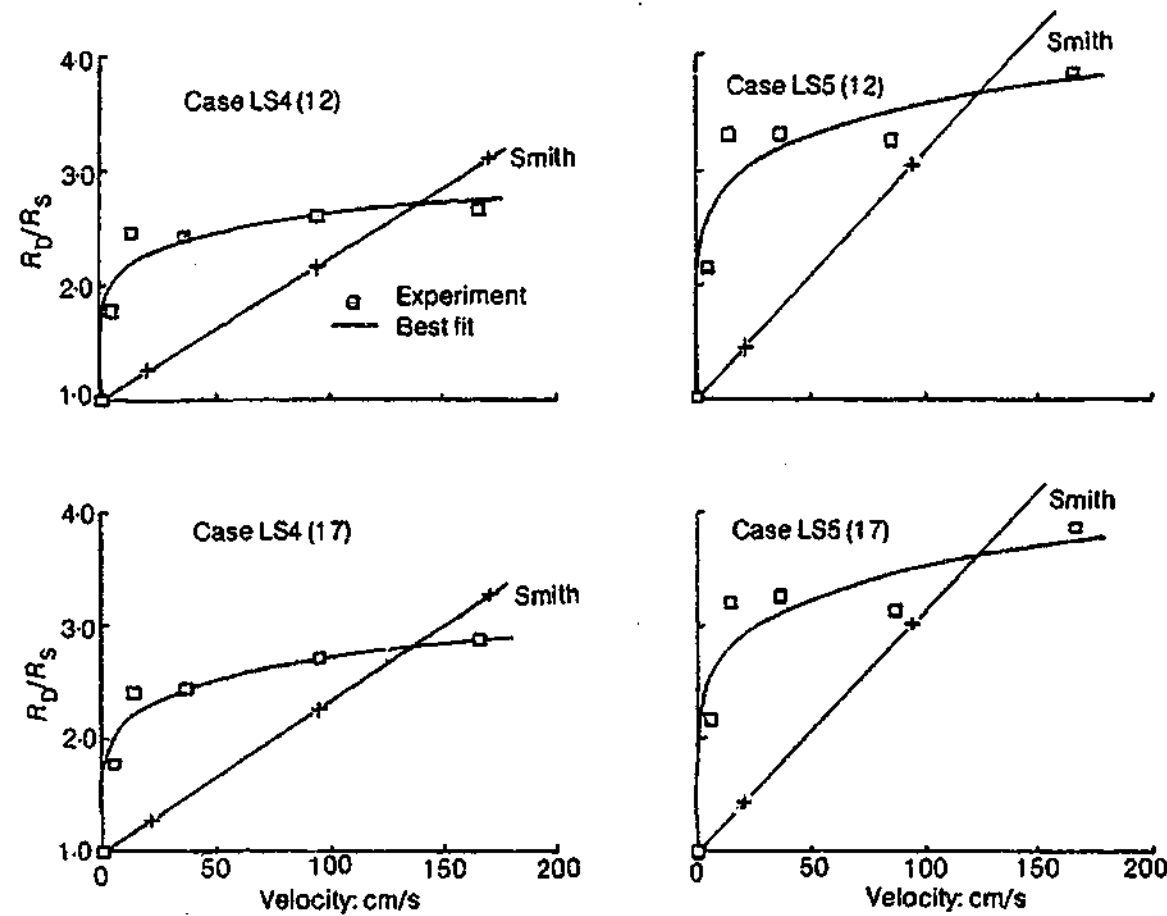


Figure 3.32 Strength ratio-velocity relationship in normal scale for London clay with shear strength of 35kPa (Litkouhi and Poskitt, 1980)

Table 3.7 the J and N values used to best-fit the raw data (a) London clay (b) Forties clay (c) Magnus clay (after Litkouhi and Poskitt, 1980)

Test No.	Best fit		Smith J' : s/cm	Average, C_u : kN/m ²	Rem. cons. pressure: kN/m ²
	J' : s/cm	N'			
LS1 (12)	0.69	0.23	0.017	15	70
LS1 (17)	0.64	0.21	0.014		
LS2 (12)	0.47	0.17	0.009		
LS2 (17)	0.48	0.21	0.011		
	0.57	0.21	0.013	Average	
LS3 (12)	0.77	0.24	0.018	35	210
LS3 (17)	0.89	0.19	0.017		
LS4 (12)	0.82	0.15	0.012		
LS4 (17)	0.72	0.19	0.013		
LS5 (12)	1.18	0.17	0.021		
LS5 (17)	1.13	0.18	0.021		
LS6 (12)	1.27	0.07	0.014	60	320
LS6 (17)	1.14	0.11	0.016		
	0.98	0.08	0.017	Average	
LS7 (12)	0.49	0.20	0.011	60	320
LS7 (17)	0.43	0.25	0.011		
LS8 (12)	0.53	0.13	0.008		
LS8 (17)	0.56	0.08	0.007		
	0.50	0.17	0.009	Average	

Test No.	Best fit		Smith J' : s/cm	Average, C_u : kN/m ²	Rem. cons. pressure: kN/m ²
	J' : s/cm	N'			
FS1 (12)	0.54	0.15	0.009	5	70
FS1 (17)	0.56	0.24	0.014		
	0.55	0.20	0.012		
				Average	
FS2 (12)	0.22	0.37	0.010	45	320
FS2 (17)	0.39	0.15	0.006		
	0.31	0.26	0.008	Average	

Test No.	Best fit		Smith J' : s/cm	Average, C_u : kN/m ²	Rem. cons. pressure: kN/m ²
	J' : s/cm	N'			
MS1 (8)	0.27	0.44	0.017	5	70
MS1 (13)	0.19	0.46	0.015		
	0.23	0.45	0.016		
				Average	
M2S (8)	0.47	0.35	0.020	40	320
MS2 (13)	0.56	0.38	0.028		
	0.51	0.36	0.024		
				Average	
MS3 (8)	0.09	0.45	0.006	80	Undis- turbed
MS3 (13)	0.06	0.69	0.012		
	0.08	0.57	0.009		
				Average	

Based on raw results for London clay and the best-fit J and N values, the data are re-plotted in Figure 3.33 in the standard plot format, with the shear strength of the sample indicated for each sample. For London and Forties clays (represented by solid symbols), the slope of a particular set of the data points is almost parallel to the reference lines drawn for $N=0.2$; thus N was approximately 0.2. The values of $J(N=0.2)$ varied from 0.8 to 2.3. For Magnus clay, the slope of a particular set of data points is steeper than the reference lines; thus N was greater than 0.2. The values of $J(N=0.2)$ varied from 0.4 to 3.0. All samples that were tested were remoulded except an undisturbed sample of Magnus clay which was sampled using a tube. This sample, which had a shear strength of 80kPa, is shown to have an N value that is greater than the other samples.

It is observed from data presented in Figure 3.32 and Table 3.7 that the data for tests performed on supposedly the same set of test conditions were not repeatable. Also, the trends of the data points were not clear because of the considerable scatter which was probably attributed to the tip-interface interaction (as will be discussed in Section 3.5.2.4), and there was considerable scatter about the inferred exponential relationships proposed by the researchers. It is also noted that since the measured friction had to be interpreted, these tests did not enable the real friction-velocity response of the interface to be obtained directly, and the interpreted friction-velocity relationship might be different from that of the real behaviour.

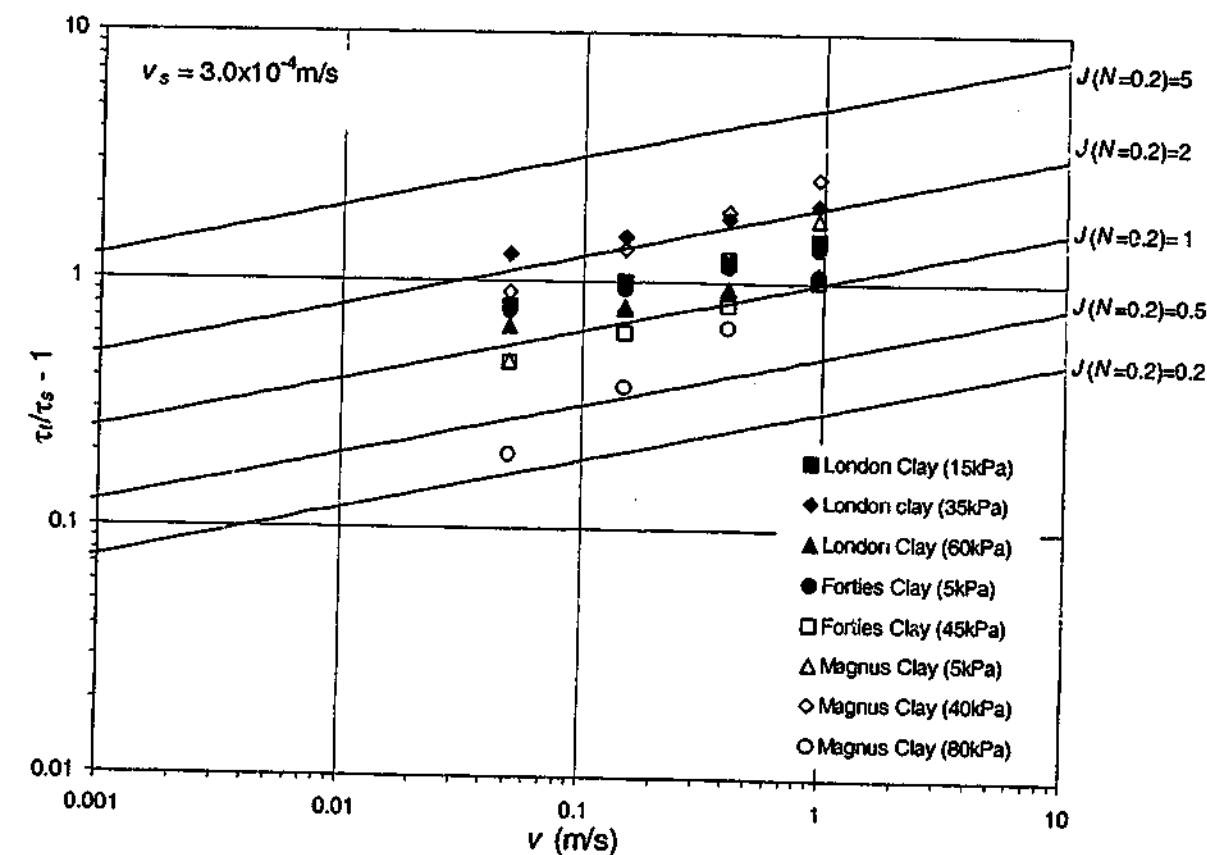


Figure 3.33 Strength ratio-velocity relationship based on data from Litkouhi and Poskitt, 1980, where the strength ratio was obtained for the quasi-static friction corresponding to 3.0×10^{-4} m/s

3.5.2.3 Poskitt & Leonard (1982)

Poskitt and Leonard (1982) extended the work of Litkouhi and Poskitt by testing another type of clay using the same apparatus as Litkouhi and Poskitt (1980). The data from the tests are reproduced in Figure 3.34. The strength ratio-velocity relationship was fitted with the power law where τ_s was defined at 2.0×10^{-4} m/s. The values of J and N were found to be 1.03 and 0.268 respectively. The data are re-plotted in Figure 3.35 in the standard plot (with the shear strength of the sample indicated for each sample), where N was 0.2 and $J(N=0.2)$ was approximately 1.0. It is noted that the data points form a steeper slope than the reference lines (that are plotted based on $N=0.2$) as N was greater than 0.2.

As with the data from Litkouhi and Poskitt (1980), there was considerable scatter in the data especially at velocities above 0.5 m/s. Possible reasons for this are discussed in Section 3.5.2.4.

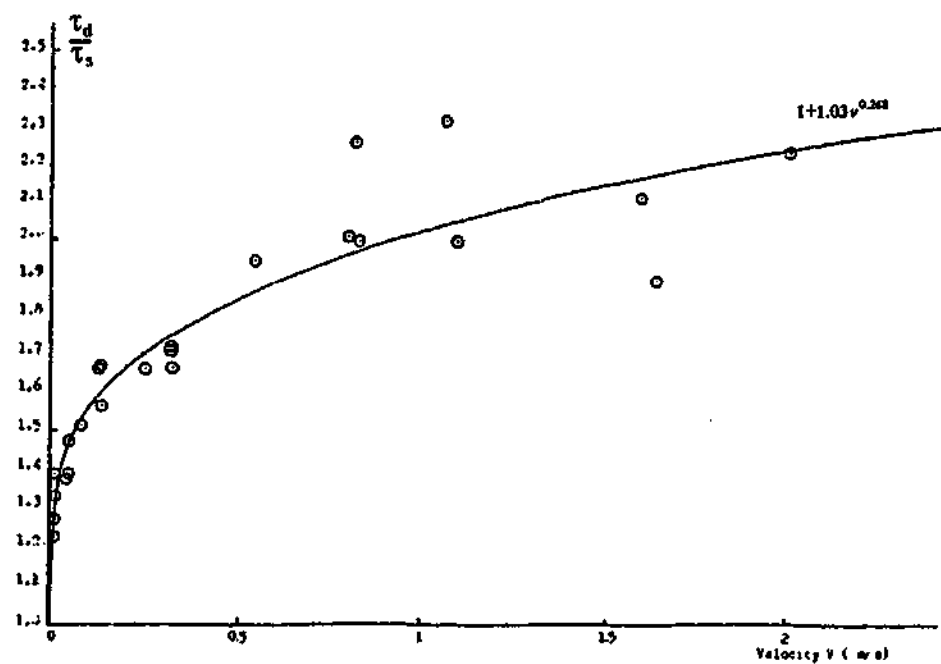


Figure 3.34 Dynamic friction-velocity relationships (after Poskitt and Leonard, 1982)

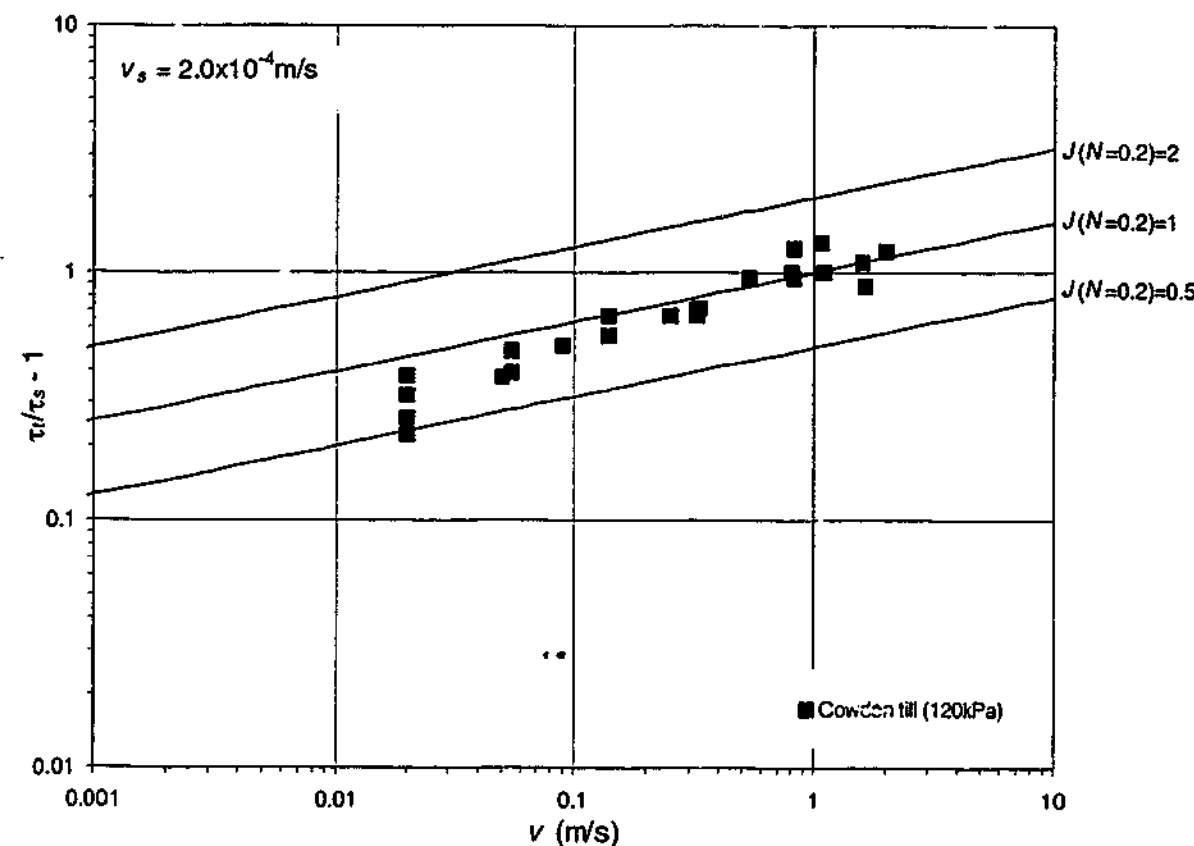


Figure 3.35 Strength ratio-velocity relationship, based on data from Poskitt and Leonard (1982), where the strength ratio was obtained for the quasi-static friction corresponding to 2.0×10^{-4} m/s

3.5.2.4 Discussion of penetrometer tests

There were several anomalies in the test results of the constant velocity penetrometer tests. The data from Litkouhi and Poskitt (1980) for tests performed under the same boundary condition were highly variable. Also, data from Dayal and Allen (1975) showed that a “critical velocity” existed below and above which the strength ratio increased at drastically different rates. For the impact tests from Dayal (1974) which were analysed by Dayal and Allen (1975), it was shown that the instantaneous dynamic friction did not vary significantly with instantaneous velocity, which was contradictory to the finding that the peak dynamic friction was dependent on the peak velocity. Therefore, it would appear that these anomalies were caused by the fact that the penetrometer test was not suitable for studying the interface-only behaviour.

The interface behaviour of the trailing pile shaft was apparently dependent on the way the leading tip deformed the soil. This was shown by the fact that the friction vs. depth responses found in Litkouhi and Poskitt, and Dayal and Allen, who used pile tips with different geometries, were different. More specifically, Litkouhi and Poskitt found the interface friction to increase “almost uniformly” throughout the tested depth of 15 to 20 times the diameter of the penetrometer and that the strength ratio changed gradually with velocity, whilst Dayal and Allen found it to be constant after a depth of penetration equal to 4 times the diameter of the penetrometer and that the strength ratio changed drastically at a certain velocity. Also, the penetration behaviour of the pile tip might have subjected the interface to different normal stresses depending on the rate of penetration, in which case, the strength ratio would be a function not only of rate, but also of consequent normal stress variations. Thus the interface component of the penetrometer test would appear to be unsuitable for studying the interface-only behaviour.

For the impact tests analysed by Dayal and Allen (1975), it was possible that the slow test and the impact test might not subject the soil to the same mode of deformation or failure. Some studies of very high speed penetration of projectiles into soil suggested that cavitation or a condition approaching cavitation might occur, where a cavity was formed by the action of the tip (Dayal and Allen, 1973). Also, studies of the shear front for very high speed impact, defined as the line bounding the

zone in which no shearing of the soil occurred, indicated that the failure mode for the dynamic case might not be the same as that of static (Dayal and Allen, 1973). Lastly, the slow and fast tests might differ due to inertial effects in the fast tests in addition to the rate effect. If any of these were true, then the dynamic friction from the penetrometer tests that was normalised by the static friction to give the strength ratio would give a misleading indication of the degree of rate effect.

3.5.3 Direct shear test

Using the direct shear set-up, Heerema (1979) performed shear tests of the steel-clay interface at constant velocities between 7.8×10^{-7} m/s and 1.04 m/s. The friction-velocity plots from Heerema are reproduced in Figure 3.36 and Figure 3.37.

Based on his experimental data, Heerema derived an empirical model based on the Smith model raised to the index N which is in the following form:

$$\tau_i = \tau_s + \tau_d J v^N \quad (3.7)$$

From his experiments, Heerema proposed the following equation for the total friction:

$$\tau_i = \sigma_n^{0.7} (0.0029 s_u - 0.32) + \sigma_n^{0.7} (-0.0041 s_u + 4.44) v^{0.2} \quad (3.8)$$

where σ_n is the normal stress acting at the interface [kPa] and s_u is the shear strength of the clay [kPa] based on an unspecified test method. This model was recommended for clays with shear strength between 55 and 620 kPa, normal stresses between 10 and 490 kPa, and pile velocities between 8×10^{-7} m/s and 1.0 m/s. The index was found to be consistently 0.2 for all the samples tested.

The first and second terms in Heerema's model in Equation (3.8) correspond to the static and dynamic components of Equation (3.7) respectively. The terms which are dependent on the shear strength and the normal stress applied at the interface are based on plots with very significant scatter, and are shown in Figure 3.38. Given that the value of the dynamic friction is highly sensitive to the two terms, using the best-fit line of the scattered data in the model can give misleading values of the dynamic friction. Also, it is noted in the two terms that the undrained shear strength, which should be stress independent, was combined with the normal stress; it can thus be

said that the empirical relationships determined do not marry well with fundamental soil mechanics principles. In any case, it is important to note that the static component is directly proportional to the shear strength of the soil, which is intuitive, and the dynamic component is inversely proportional to the shear strength of the soil.

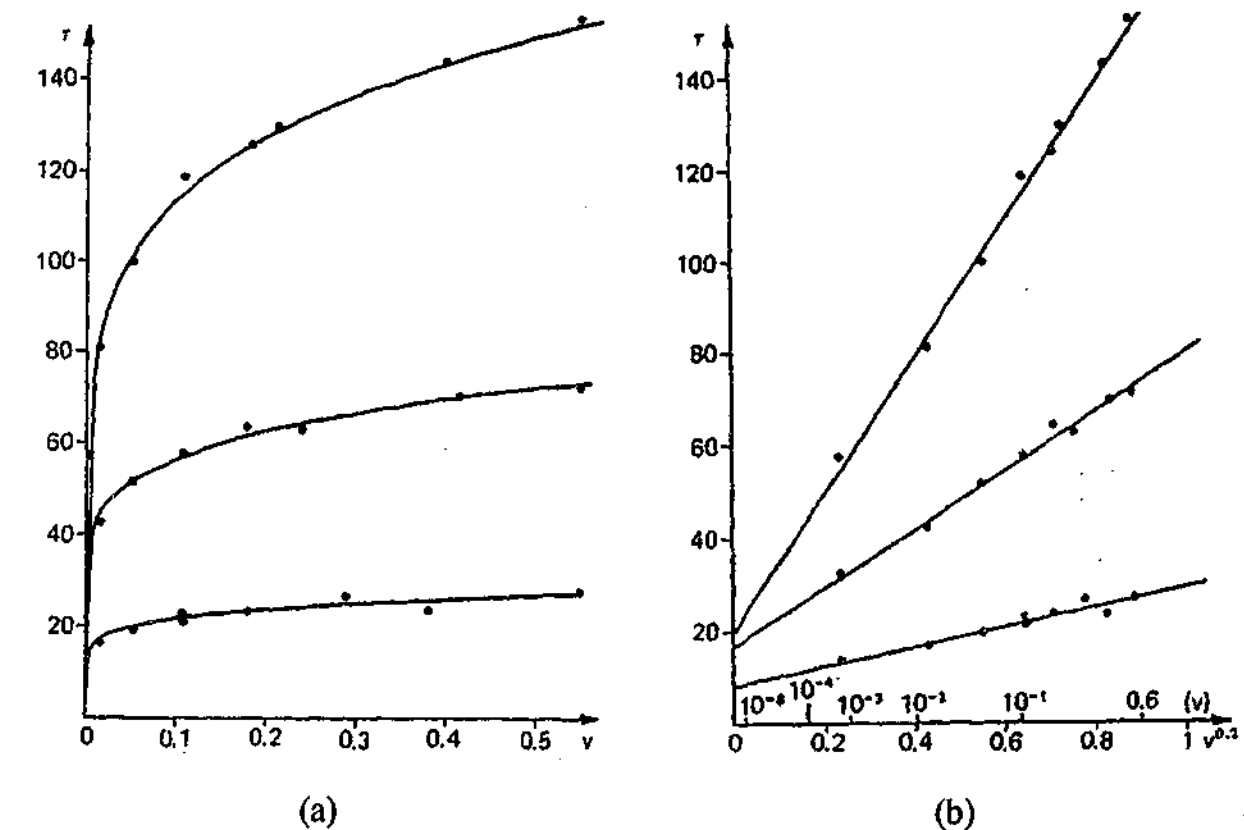


Figure 3.36 Friction-velocity relationships for Kontich clay with $s_u=260$ kPa for $\sigma_h=31.5, 87$ and 184 kPa respectively (Heerema, 1979)

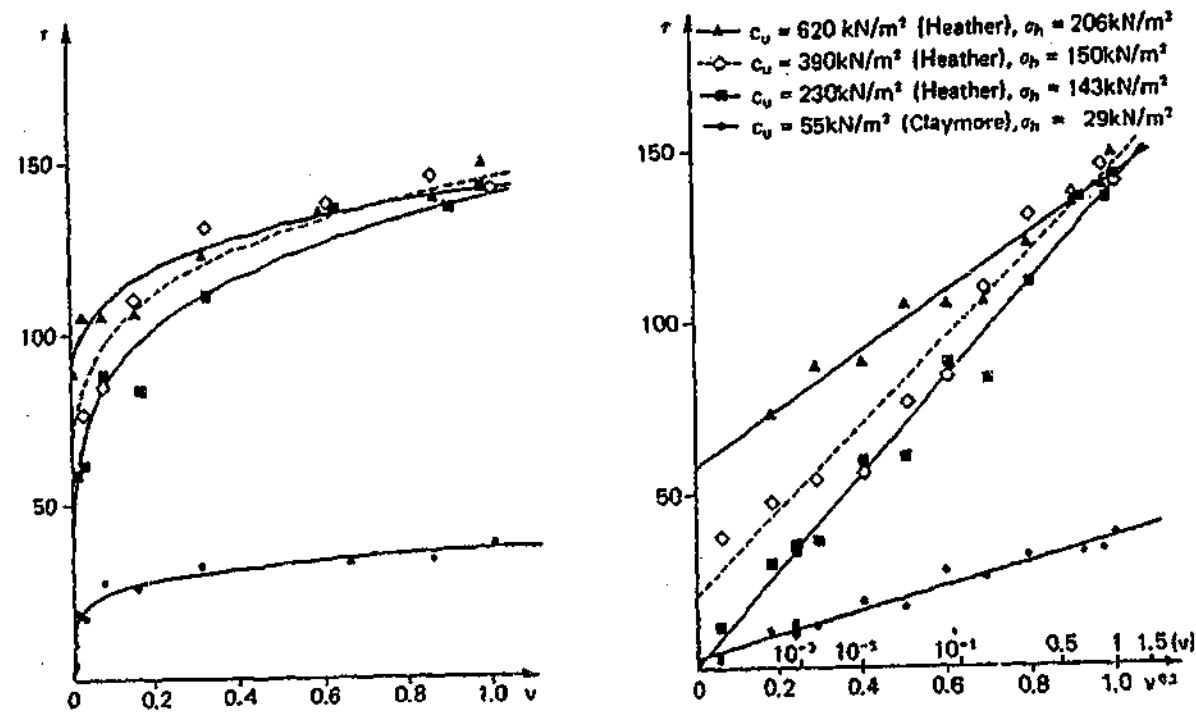


Figure 3.37 Friction-velocity relationships for Heather clay and Claymore clay with different s_u 's and different σ_h 's (Heerema, 1979)

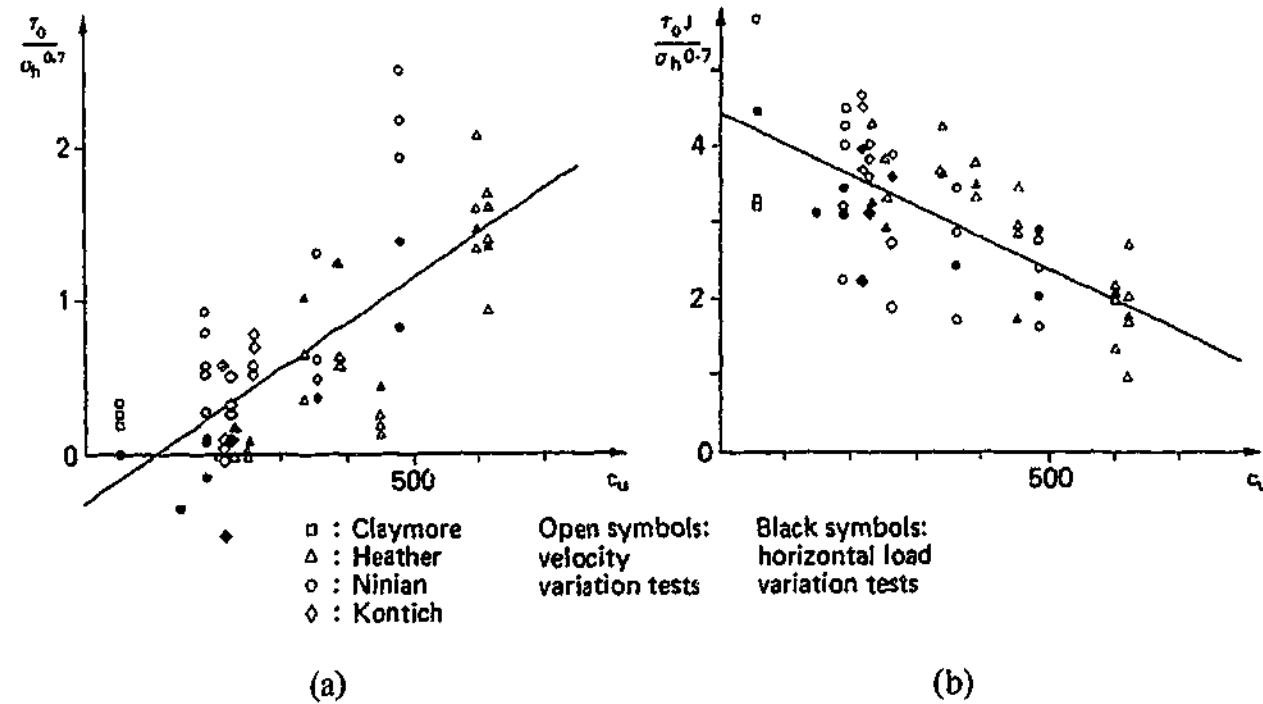


Figure 3.38 Correlations for (a) quasi-static static component (b) dynamic component (Heerema, 1979)

Since Heerema's dynamic friction model is not readily comparable to data from other studies, it is desirable to normalize the dynamic friction with the quasi-static friction to obtain the strength ratio. Two approaches can be taken to accomplish this.

In the first approach, Hereema's recommended dynamic friction model (Equation (3.8)) could be divided by the quasi-static friction algebraically to obtain the strength ratio, where the dynamic friction is given by the Hereema's model and the static friction is given by Heerema's model substituted for an arbitrary quasi-static velocity of say 1.0×10^{-5} m/s:

$$\frac{\tau_d}{\tau_s} = \frac{(0.0029s_u - 0.32) + (-0.0041s_u + 4.44)v^{0.2}}{(0.0029s_u - 0.32) + (-0.0041s_u + 4.44)(0.00001)^{0.2}} \quad (3.9)$$

However, since Equation (3.8) was based on highly scattered data, it would appear that this approach was unreliable; thus, this approach is not adopted.

In the second approach, the raw data from Heerema, shown in Figure 3.36 and Figure 3.37, are reanalysed to obtain the strength ratio. The quasi-static friction (τ_s) is arbitrarily defined as the resistance corresponding to a velocity of 1.0×10^{-5} m/s (which will be adopted as the quasi-static velocity in the test programme of the current dissertation) and is obtained from Figure 3.36 and Figure 3.37. The resulting strength ratio-velocity plot is presented in Figure 3.39, with the shear strength followed by the applied normal stress shown in parenthesis for each sample. Because Heerema's tests included the very low velocity range, the plot includes data for velocity less than the minimum of 0.001 m/s used in the standard plot. From Figure 3.39, the strength ratio of Kontich clay appears to increase with increasing normal stress, but the strength ratio of Heather clay appears to increase with decreasing normal stress. The value of N is 0.2 and $J(N=0.2)$ ranges between 0.5 and 8. However, as such high increases in the dynamic strength had not been encountered in practice, the validity of the data appears to be questionable.

In addition to the excessively high values of the strength ratio, the reliability of Heerema's test data is also questionable for the following reasons:

- It is observed from the schematic of a typical set of dynamic friction and displacement records from Heerema (reproduced in Figure 3.40) that the dynamic friction varied significantly even when the velocity had become nearly constant. This appears to be an anomaly in the experimental method which contradicts the finding that the friction was velocity-dependent.

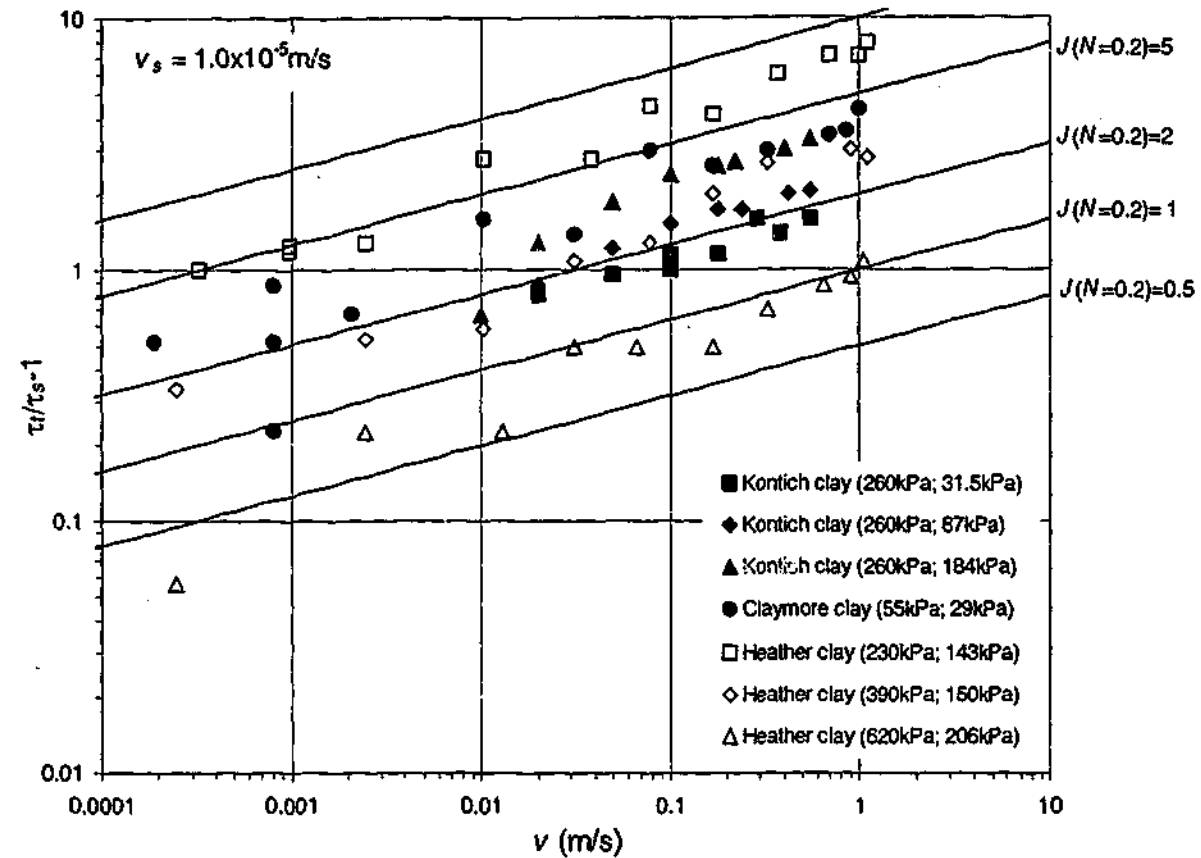


Figure 3.39 Raw data: Strength ratio-velocity relationship, based on data from Heerema (1979), where the strength ratio was obtained for the quasi-static friction corresponding to 1.0×10^{-5} m/s

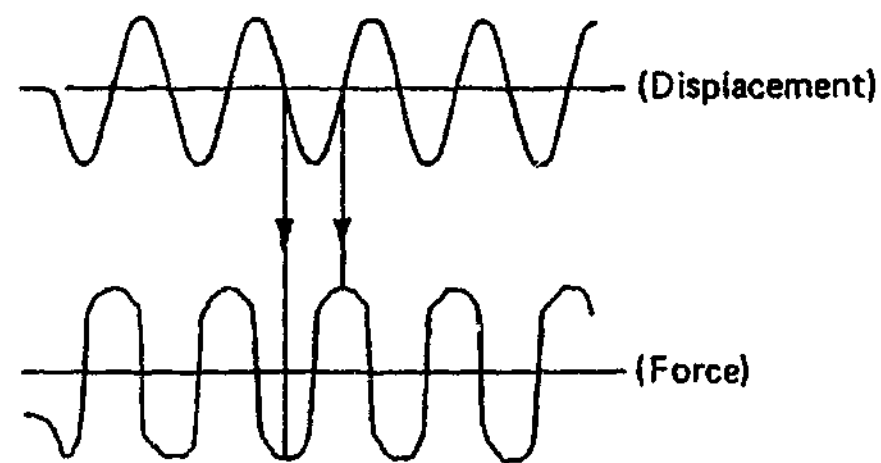


Figure 3.40 Schematic of typical test registration in Heerema's test (Heerema, 1979)

- Since the force varied significantly during the stroke, the value of the force corresponding to the near-constant velocity of a particular test was open to interpretation.
- As one sample was used in many tests, including the very slow quasi-static tests that took considerable time to complete, the sample could have lost

significant moisture as the tests were carried out. If so, this effect would have been additional to the rate effects and would have been reflected in the friction-velocity relationship.

3.5.4 Test involving pile shaft encased in triaxial specimen

Using the experimental set-up discussed previously, Benamar et al. (1991, 1992) and Benamar (1999) investigated the dynamic response of pile-clay interfaces by driving a miniature pile through the specimen contained in a triaxial cell.

This experiment was fundamentally different from the others because it enabled the instantaneous dynamic friction and the corresponding instantaneous pile velocity during one single driving event to be recorded, and the friction-velocity response for a single event to be directly obtained. In this respect, the experiment would be more appropriate for obtaining reliable data as compared to the tests performed by the other researchers, where the friction corresponding to a certain velocity had to be interpreted. The test which simulated the transient velocity of a driven pile also allowed the effect of acceleration on the dynamic response to be determined.

The dynamic friction was found to be dependent on the pile velocity. A plot of the dynamic friction-velocity behaviour by the researchers is reproduced in Figure 3.41. The friction-velocity relationship could be modelled by:

$$F_t = k_2(1 - e^{-k_3 v}) \quad (3.10)$$

where F_t is the friction in force [N], v is the pile velocity [m/s], and k_2 [-] and k_3 [s/m] are parameters that depended on the duration of impact, the confining pressure and soil properties. Typical values of k_2 and k_3 were found to be between 2800 and

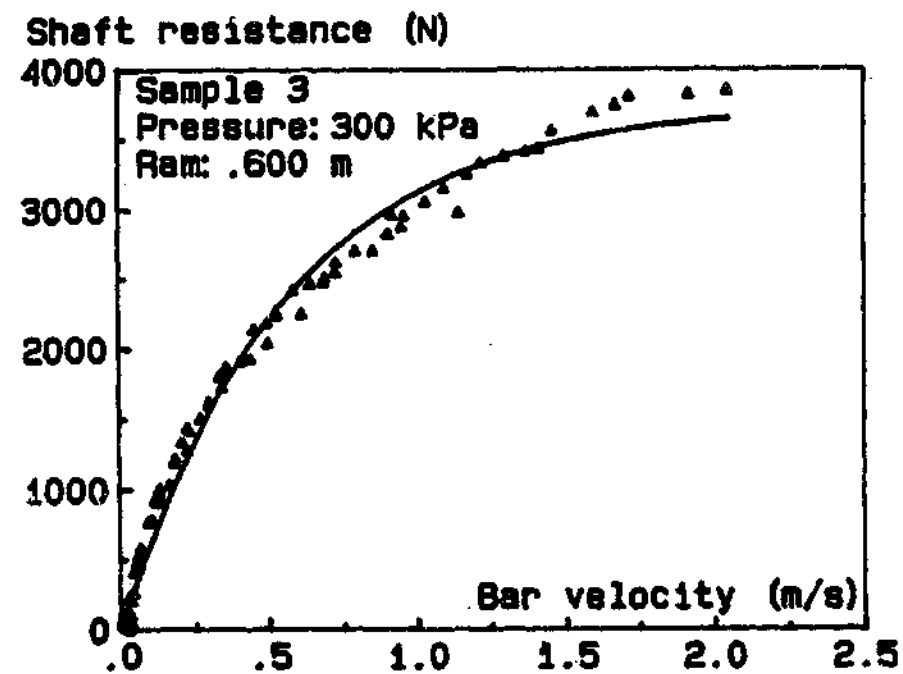


Figure 3.41 Dynamic resistance as a function of the rod velocity corresponding to different drop heights (Benamar et al., 1991)

4800, and between 1.0 and 2.8, respectively. It is noted that these values applied to the friction force rather than the strength ratio.

It is important to note that the friction-velocity plot is fundamentally different from the plots presented by other researchers. The data obtained by Benamar et al. (and hence the equation used to model the response) apply to the loading phase of a single driving event. At the beginning of the force-velocity curve, which is based on the initial loading stage of the event, two effects occur concurrently. The first effect is the dynamic or viscous effect. The second effect is the incomplete mobilization of the quasi-static resistance (that will only be fully mobilised after sufficient shear displacement known as the quake has been reached). Therefore, it is not possible to simultaneously determine the instantaneous static resistance and viscous damping resistance for the data at the beginning of the force-velocity curve. This has the implication that a quasi-static resistance cannot be computed by substituting an arbitrary reference quasi-static velocity into Equation (3.10) that models the partial mobilisation during the initial loading stage. This means that the dynamic friction cannot be normalised, and that the data from Benamar et al. cannot be compared to data obtained by other researchers.

As mentioned in Section 3.2.4, the interface resistance was assumed by the researchers to be a concentrated force but this assumption was not demonstrated to be reasonable by the researchers, and the computation of the interface resistance based on the measured parameters could potentially result in significant error. In these respects, the quality of the data obtained by the researchers might have been compromised.

3.5.5 Approach to obtaining the relationship between dynamic friction and velocity

Lepert et al. (1988a), Lepert et al. (1988a), Benamar et al. (1991, 1992) and Benamar (1999) attempted to obtain the friction-velocity relationship by continuously logging dynamic friction and velocity during a single driving event. It is the author's belief that this is the most reliable approach to obtaining the dynamic response of the interface in a driving event where the velocity of a particular segment of the pile increases to a maximum, then decreases to smaller values before becoming negative during rebound. The friction-velocity response obtained in this way would give the functional relationship between velocity and dynamic friction throughout the driving event. This approach also has the advantage of only needing to perform a single test to obtain multiple data points (that form the friction-velocity relationship) for a particular interface tested under a particular set of boundary conditions.

However, Dayal and Allen (1975), Heerema (1979), Litkouhi and Poskitt (1980) and Coyle and Gibson (1970) took a fundamentally different approach. In attempting to obtain the friction-velocity relationship, these researchers performed constant or near-constant velocity tests; it is noted that Coyle and Gibson's drop tests were practically constant velocity tests. For each constant or near-constant velocity test, the dynamic resistance that was interpreted to correspond to the constant or near-constant velocity was associated with that velocity such that one test yielded only one data point in the friction-velocity plot. Hence the data from a collection of these tests each performed at a different constant velocity form the friction-velocity plot.

Coyle and Gibson's triaxial tests related to the strength of an internal failure surface and thus the test data are not directly applicable to failure on a predefined pile-soil interface. Hence the friction-velocity plot based on their tests should not be assumed

to give the functional relationship between friction and velocity for the pile-soil interface. The tests by Litkouhi and Poskitt, Dayal and Allen and Heerema in theory should give the same friction-velocity plot as that found in the recent studies (e.g. Benamar, 1999) if and only if the instantaneous friction could be associated with its corresponding instantaneous velocity. However, there is indication that the interpretation of the dynamic friction in the work of Litkouhi and Poskitt, Dayal and Allen and Heerema was not unique and was questionable. Thus, the resulting friction-velocity response may not necessarily give the functional relationship between the instantaneous friction and the instantaneous velocity. The approach also has a significant disadvantage of having to perform many constant velocity tests in order to obtain the friction-velocity relationship for a particular interface. Furthermore, since the friction-velocity relationship was obtained by combining data points from individual constant velocity tests, there is typically significant scatter in the friction-velocity plot which makes the response difficult to discern.

In conclusion, the most reliable and direct approach to obtaining the functional dynamic friction-velocity relationship that applies to the interface behavior during a driving event is by measuring these parameters during a single test event.

3.5.6 Constant velocity tests

Most of the interface tests were performed with constant or near-constant velocity (Dayal and Allen, 1975; Heerema, 1979; Litkouhi and Poskitt, 1980; Poskitt and Leonard, 1982). There is merit in such a testing approach, as it simplifies analysis – a single dynamic response can be correlated against a discrete interface velocity, and by accumulation of data, a relationship can be inferred. In addition, constant velocity tests eliminate any possible effect due to accelerations. However, such tests do not simulate a typical pile driving event which involves transient velocities and varying acceleration during the event; as such, they did not allow any possible effect of acceleration on the dynamic friction to be investigated.

3.5.7 Pore pressure measurement

None of the researchers investigated the effect of the pore water pressure on the dynamic interface resistance and the velocity-dependent behaviour. Whilst the pore water pressure response will be very useful in the analysis of the dynamic behaviour

of the interface, it is well-known that transient pore pressures during fast shearing are very difficult to measure in practice for two reasons. The most fundamental requirement for the meaningful measurement of the pore pressure is for the sample and the pressure transducer to be fully saturated. Since interface shear tests do not have control over the saturation or the drainage of the sample, it is difficult to ensure or even achieve this requirement. Even in tests where drainage control is possible, namely in triaxial tests, accurate measurement of the transient pore pressures during a short event is difficult to achieve (e.g. Whitman and Healy, 1962; Lee et al., 1969; Yamamuro and Lade, 1993; Abrantes and Yamamuro, 2002a) because of the delays caused by the natural frequency of the transducer and by the pressure wave to reach the transducer (Abrantes and Yamamuro, 2002a). Measurement of pore pressures is therefore desirable for a comprehensive investigation of dynamic interface response, but is made impractical or impossible by physical constraints.

3.5.8 Effect of fundamental soil parameters on the viscous damping parameter

The effects of fundamental soil parameters on the viscous damping parameter for the pile-clay interface dynamic tests have not been investigated and as such there are generally insufficient data available for evaluating the dependence of the viscous damping parameter on these parameters.

Therefore, on the basis that the mechanism of viscous damping in the pile-soil interface shear is also operative in soil-only shear, data based on dynamic soil-only tests involving the tip of the penetrometer and triaxial tests are also used to evaluate the dependence of the viscous damping parameter on the soil parameters. However, it is important to note the differences between the shearing at pile-soil interfaces and shearing within a soil specimen which are discussed as follows:

- Apart from the obvious fact that the media being sheared in the two scenarios are different, soil-only tests may be performed on undisturbed soils whilst the pile-soil interface for a driven or bored pile only involves highly remoulded soil due to the pile installation process;
- The triaxial test involves the loading of the entire specimen whilst the interface test involves only a thin zone of the specimen.

Also, data for very low strain rates typical of the triaxial test may be relevant and have been included for want of any better information. These data are sourced from Briaud and Garland (1985), and Graham et al. (1983). The strain rates used in the tests were not specified by Briaud and Garland (1985). Strain rates of between 3.0×10^{-3} and 4.0%/hour, or 8.0×10^{-7} and 1.1×10^{-3} %/s were used by Graham et al. (1983). It is noted that these low strain rates differ from the high strain rates associated with pile driving.

3.5.8.1 Effect of shear strength

The viscous damping parameter has been suggested by Coyle and Gibson (1970), Dayal and Allen (1975) and Heerema (1979) to be dependent on the shear strength of the clay. In an attempt to determine whether the viscous damping strength ratio is dependent on the shear strength, the values of the damping parameter are plotted against the corresponding shear strengths for both interface and soil-only tests.

It is noted that the data sets from the various studies cannot be quantitatively compared to each other for several reasons:

- the experimental apparatus used in the various studies are fundamentally different;
- the different types of tests used in the various studies to determine the shear strengths (as shown in Table 3.8) resulted in alternative measures of the shear strength (e.g. Wroth, 1984);
- the rates at which the quasi-static tests were performed in the different studies varied, thus influencing the measure of the strength ratio.

Because of these differences, the relevant data from each of the studies is presented separately.

Table 3.8 Different types of tests used to measure the “undrained shear strength”

Researchers	Type of test for obtaining s_u
Litkouhi and Poskitt (1980)	Cone with cone tip angle of 120 degrees
Poskitt and Leonard (1982)	Cone with cone tip angle of 60 degrees
Dayal and Allen (1975)	Vane shear test

Pile-clay interface tests

Test data pertaining to the pile-soil interface are obtained from studies by Dayal and Allen (1975), Heerema (1979), Litkouhi and Poskitt (1980), and Poskitt and Leonard (1982). For the sake of consistency, data from Dayal and Allen (1975) have been fitted using the power law. For the purpose of plotting the data in the same format, the exponent for each of these studies is fixed at the generally recommended value of 0.2 so that the viscous damping parameter $J(N=0.2)$ can be used for all the studies. Although Heerema's model indicates excessively high strength ratios as noted earlier, they are of value in a qualitative sense. Data from Litkouhi and Poskitt (1980) are plotted together with data from Poskitt and Leonard (1982) as both sets of data were obtained using the same apparatus.

The shear strength- $J(N=0.2)$ plots for Dayal and Allen, Litkouhi and Poskitt as well as Poskitt and Leonard, and Heerema are plotted in Figure 3.42, Figure 3.43 and Figure 3.44 respectively. The data from Dayal and Allen (1975) and Heerema (1979) show that the strength ratio decreases with increasing shear strength. The data from Litkouhi and Poskitt together with Poskitt and Leonard show the same trend, but less strongly.

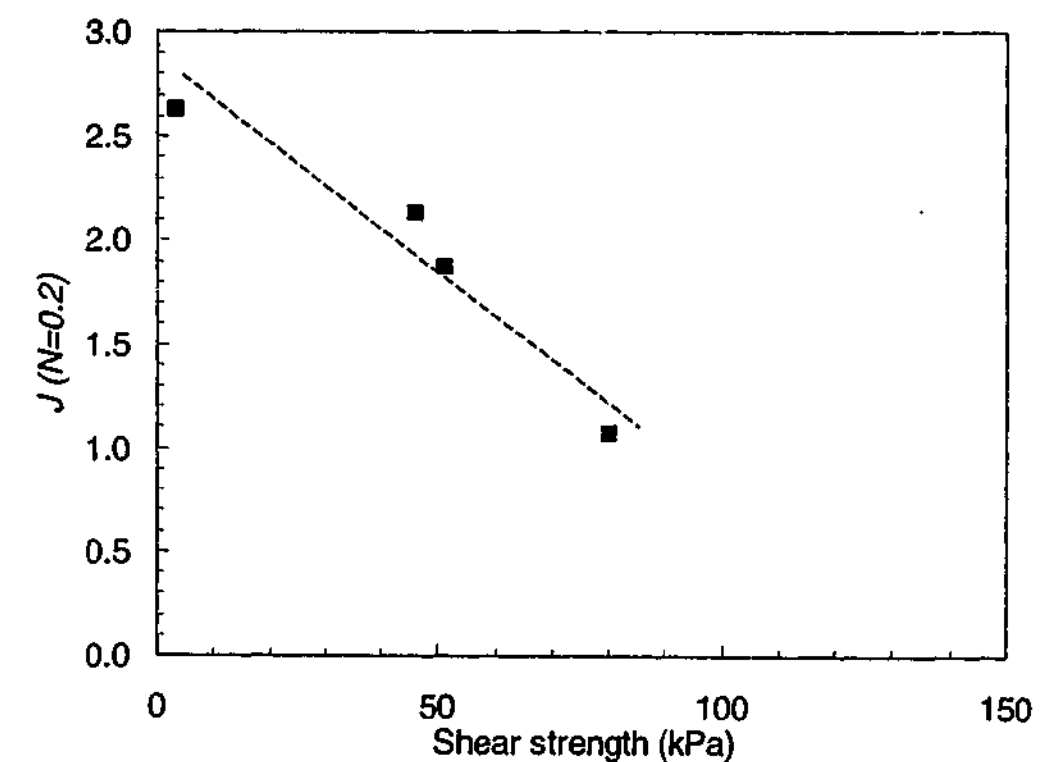


Figure 3.42 The effect of shear strength on the viscous damping parameter at the pile shaft-soil interface, $J(N=0.2)$, based on data from Dayal and Allen (1975)

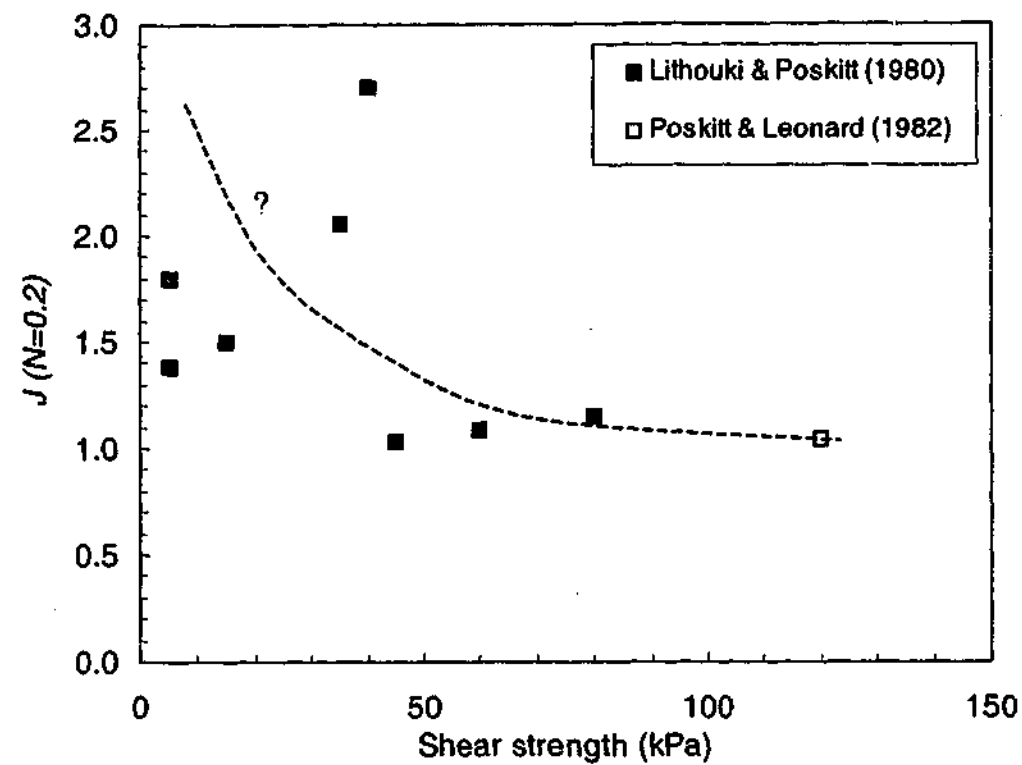


Figure 3.43 The effect of shear strength on the viscous damping parameter at the pile shaft-soil interface, $J(N=0.2)$, based on data from Litkouhi and Poskitt (1980) and Poskitt and Leonard (1982)

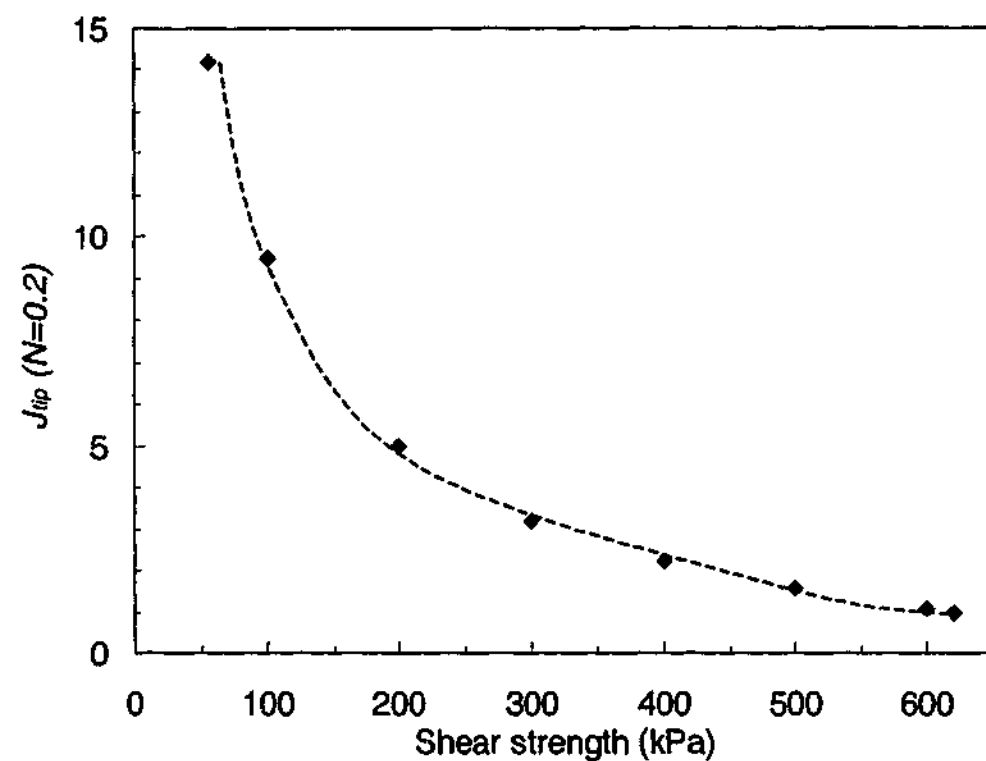


Figure 3.44 The effect of shear strength on the viscous damping parameter at the pile shaft-soil interface, $J(N=0.2)$, based on Heerema's proposed model (Heerema, 1979)

Soil-only tests

Experimental data from soil-only tests are used to investigate the proposed strength ratio-shear strength relationship. Test data are obtained from soil-only compression tests by Coyle and Gibson (1970), and from pile tip penetration tests (involving soil-only failure) conducted by Litkouhi and Poskitt (1980) as well as Poskitt and Leonard (1982), and Dayal and Allen (1975). Since the power law was adopted by all the researchers except Dayal and Allen, the power law damping parameter $J(N=0.2)$ is used here as a measure of the strength ratio. In any case, the data from Dayal and Allen can be fitted with the power law.

The plots of the parameter $J(N=0.2)$ against the shear strength for all the soil-only response based on Coyle and Gibson (1970), Litkouhi and Poskitt (1980) as well as Poskitt and Leonard (1982), and Dayal and Allen (1975) are shown in Figure 3.45, Figure 3.46 and Figure 3.47 respectively. The value of the damping parameter $J(N=0.2)$ has already been shown to increase with increasing liquidity index, I_l by Coyle and Gibson based on their experimental data. I_l is defined as follows:

$$I_l = \frac{w - w_p}{w_l - w_p} \quad (3.11)$$

As the water content of a cohesive soil approaches the lower limit of the plastic range, the stiffness and degree of compaction of the soil increase (Terzaghi et al., 1996). The inverse relationship between I_l and shear strength is shown in correlations for clays with various sensitivities (e.g. Wroth, 1979; Kulhawy and Mayne, 1990). Using a correlation by Wroth (1979) that is applicable to remoulded soils, the shear strengths for the samples are estimated from their reported I_l .

According to all researchers, the value of $J(N=0.2)$ increases with decreasing shear strength, although the specific relationship varies considerably.

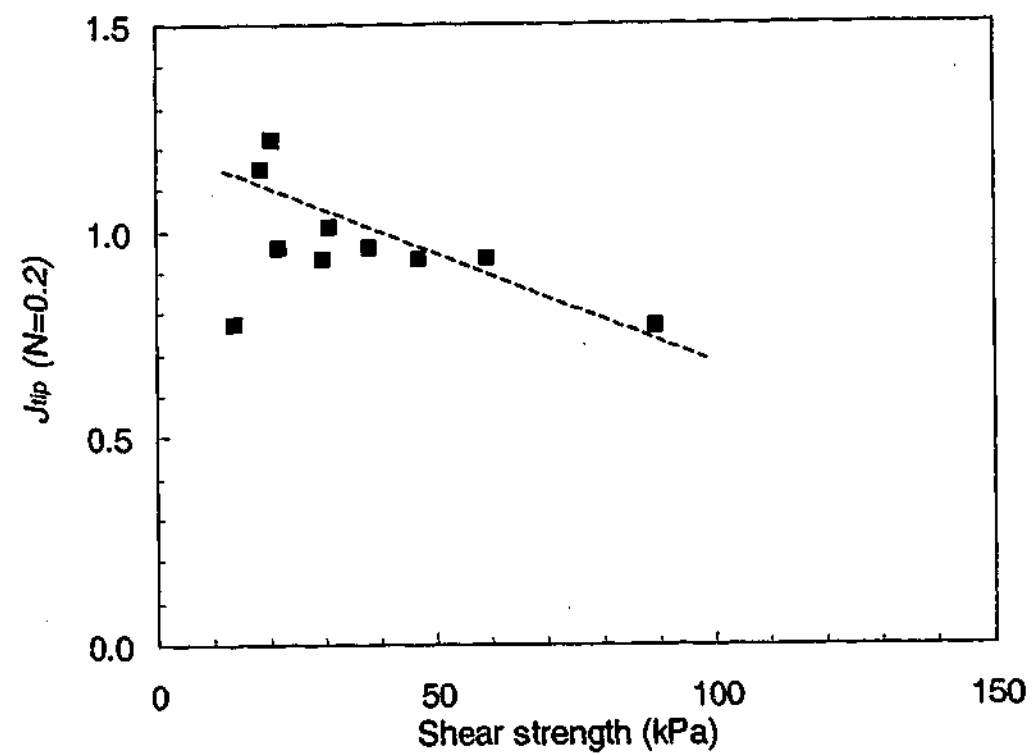


Figure 3.45 The effect of shear strength on the viscous damping parameter at the pile tip, $J_{tip}(N=0.2)$, based on data from Coyle and Gibson (1970)

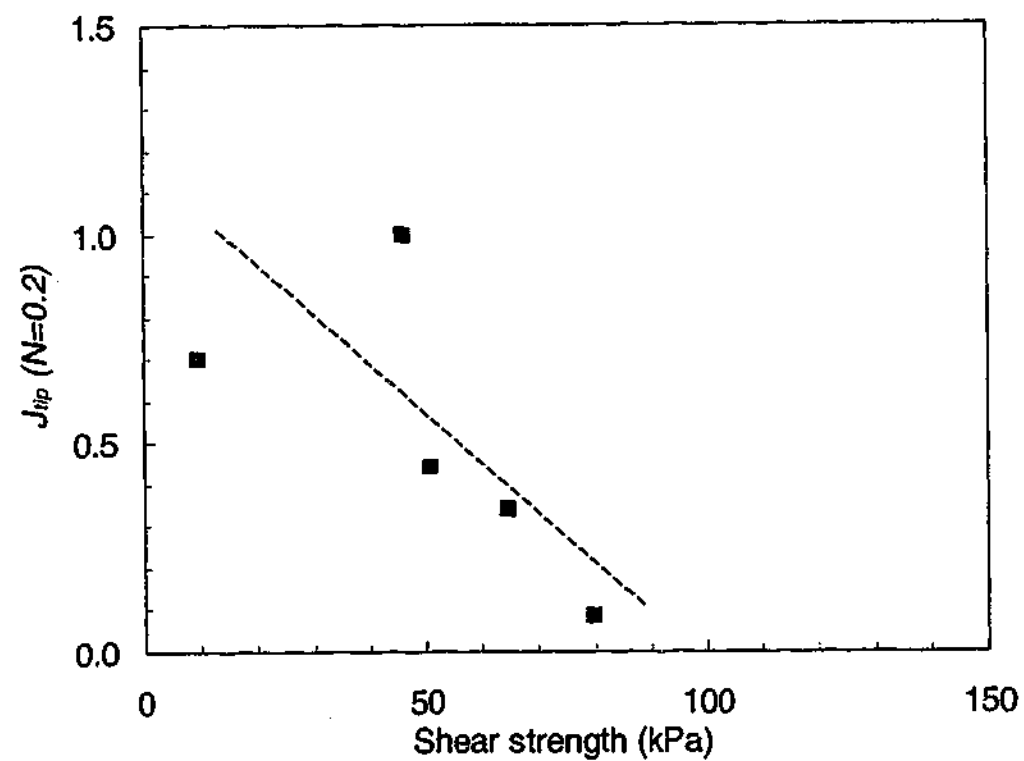


Figure 3.46 The effect of shear strength on the viscous damping parameter at the pile tip, $J_{tip}(N=0.2)$, based on data from Dayal and Allen (1975)

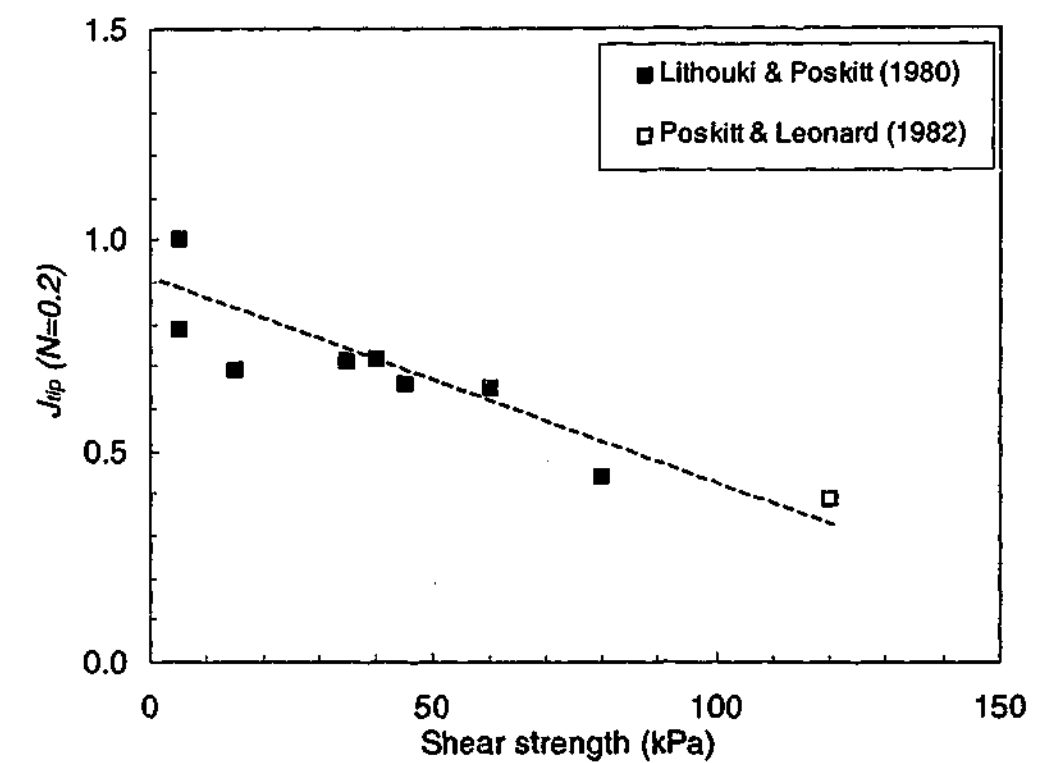


Figure 3.47 The effect of shear strength on the viscous damping parameter at the pile tip, $J_{tip}(N=0.2)$, based on data from Litkouhi and Poskitt (1980) & Poskitt and Leonard (1982)

Soil-only triaxial tests at relatively low strain rates

Data based on the triaxial compression tests (involving soil-only failure) performed at very slow strain rates have also been used to investigate the relationship (if any) between the viscous damping parameter and the shear strength.

Based on data from 150 undrained laboratory tests on clay samples compiled from the literature, Briaud and Garland (1985) correlated the values of the damping parameter against the corresponding shear strengths. In order to make use of Briaud and Garland's analysis, it is necessary to note that Briaud and Garland used a simple viscous damping model as follows:

$$\frac{s_2}{s_1} = \left(\frac{t_1}{t_2} \right)^m \quad (3.12)$$

where s_1 and s_2 are the undrained shear strengths with times to failure of t_1 and t_2 respectively. In this case, the viscous damping parameter is defined as a function of the time to failure rather than to the strain rate. The parameter m is defined by Briaud and Garland as the viscous damping parameter. To appreciate the significance of m , the percentage increase in strength due to viscous damping has been plotted against a

measure of the failure time in Figure 3.48 for m values ranging from the reported lower bound of near-zero to the reported upper bound of 0.18. According to this formulation, the higher the value of m , the higher the strength ratio.

The values of this damping parameter were correlated by Briaud and Garland with a reference shear strength as shown in Figure 3.49; the reference shear strength was defined based on a time to failure of 1 hour. It is noted that the best-fit lines included in all of Briaud and Garland's plots were after Briaud and Garland (1985). The plot shows that the value of the damping parameter increases with decreasing shear strength. This correlation is supported by two further correlations by Briaud and Garland (1985).

The values of m were also correlated to the corresponding moisture content by the researchers, as shown in Figure 3.50. The plot shows that m increases with increasing moisture content. Since the shear strength decreases with increasing moisture content for a particular clay type, this plot can be interpreted to suggest that m increases with decreasing shear strength.

Furthermore, the values of m were correlated with Liquidity Index (I_L) by the researchers as shown in Figure 3.51. The plot shows that m increases with increasing I_L , which is consistent with the data from Coyle and Gibson (1970). Since I_L is inversely proportional to the shear strength, m increases with decreasing shear strength.

Scatter in the data from triaxial compression tests performed at very low shear rates is very large, which reduces the reliability of the correlation. However, the data show some indication that the value of the damping parameter increases with decreasing shear strength.

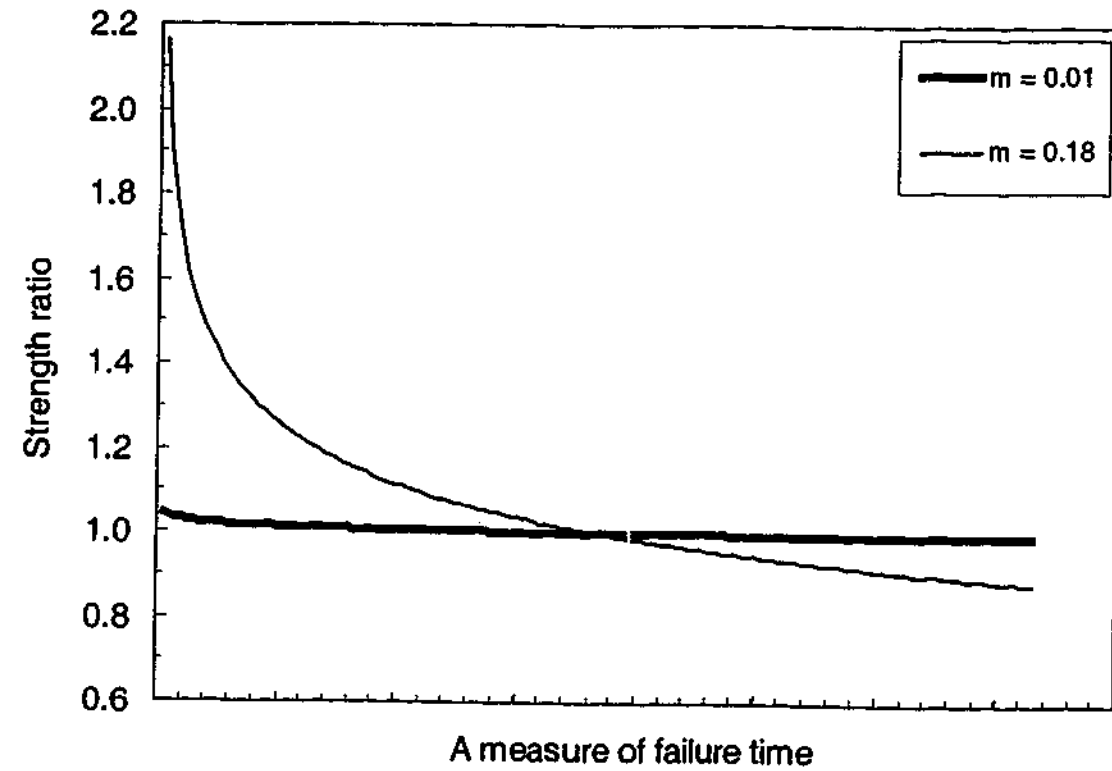


Figure 3.48 Significance of the Briaud and Garland viscous damping parameter, m , in relation to the strength ratio

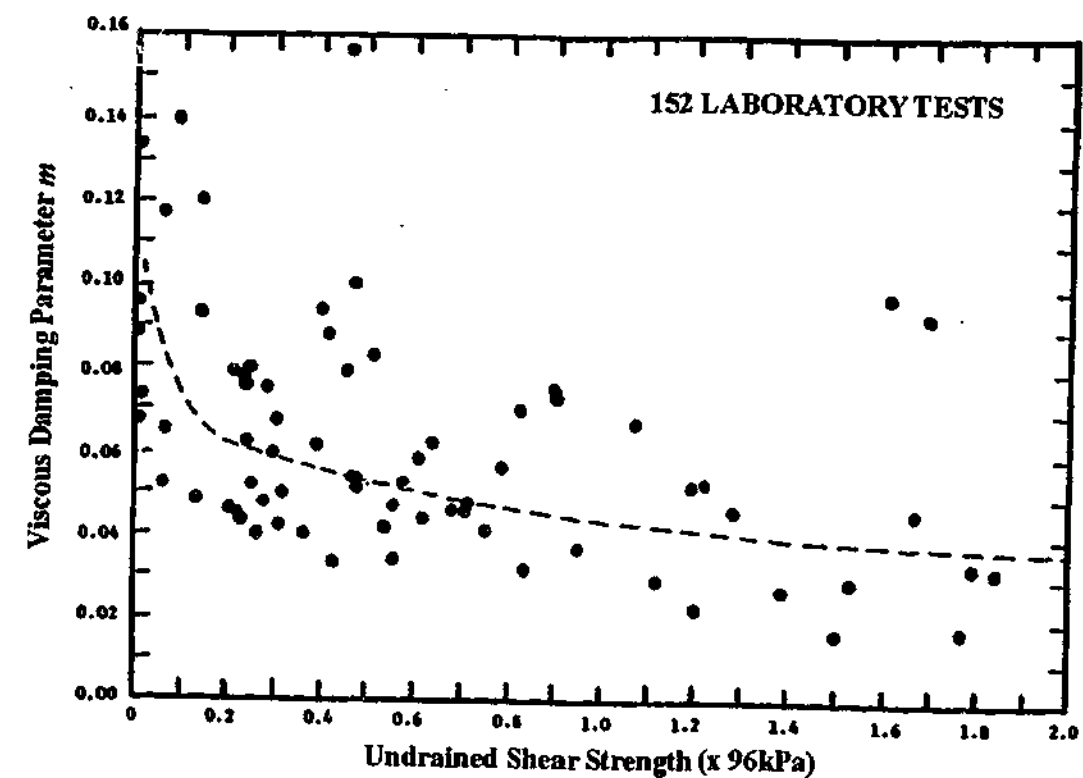


Figure 3.49 Effect of shear strength on the Briaud and Garland viscous damping parameter, m (after Briaud and Garland, 1985)

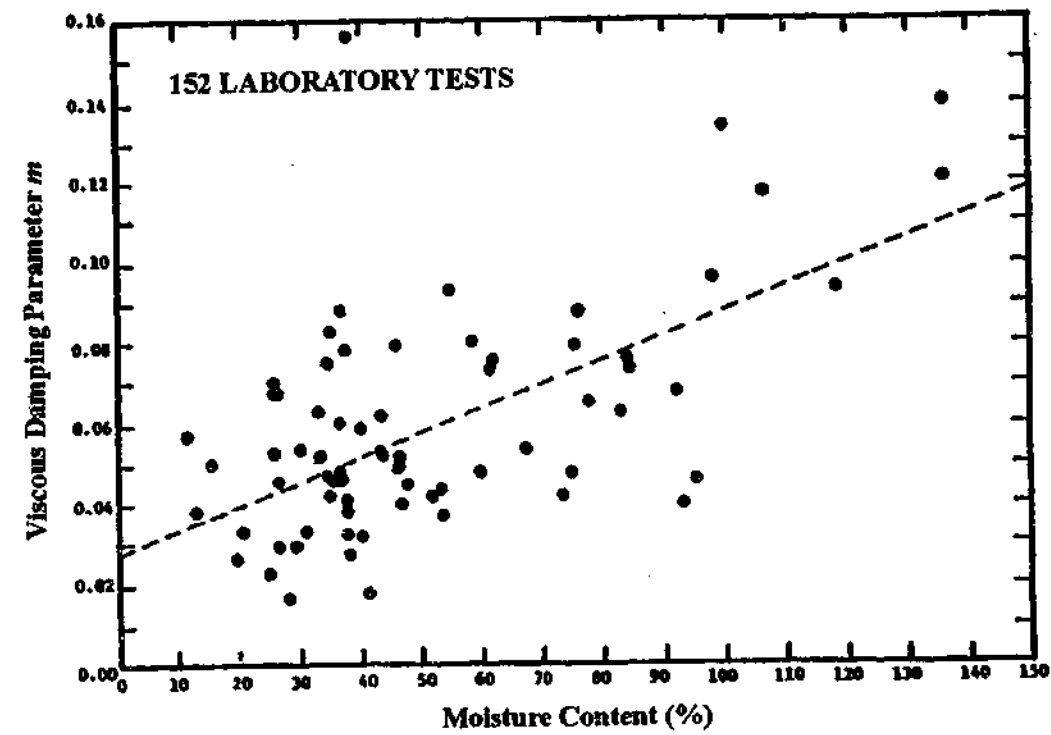


Figure 3.50 Effect of moisture content on the Briaud and Garland viscous damping parameter, m (after Briaud and Garland, 1985)

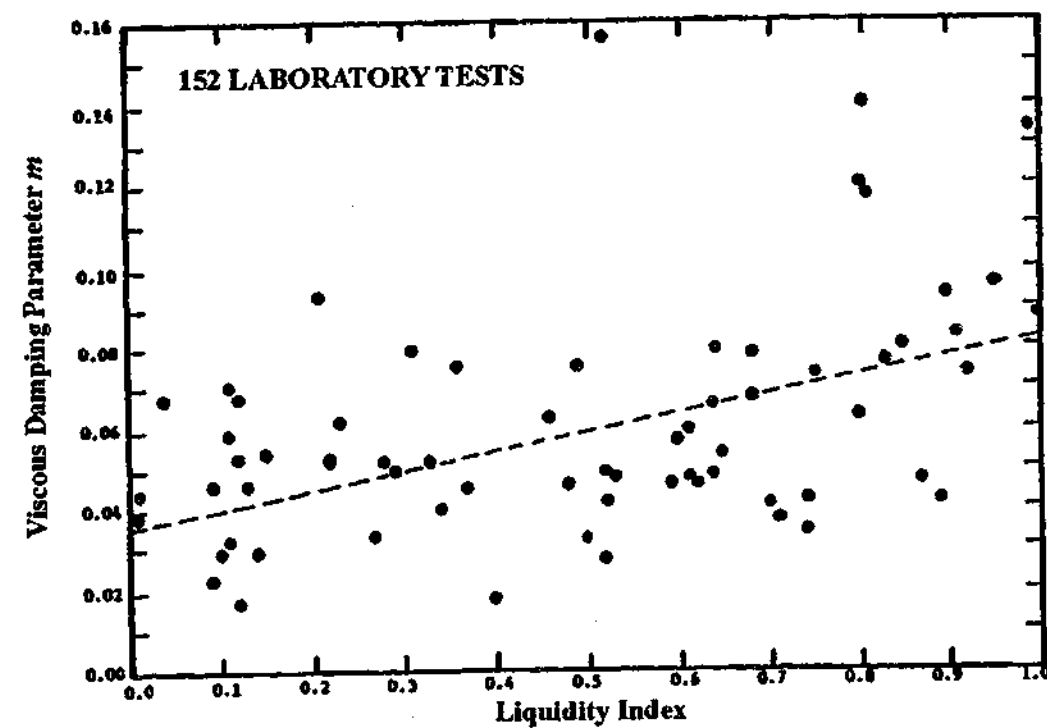


Figure 3.51 Effect of Liquidity Index on the Briaud and Garland viscous damping parameter, m (after Briaud and Garland, 1985)

3.5.8.2 Effect of OCR

Since none of the studies on the pile-clay interface investigated the effect of OCR on the viscous damping response, data based on triaxial compression tests performed within a range of very low strain rates is analysed. However, based on these data, there are conflicting indications of the effect of the OCR on the viscous damping parameter.

Triaxial tests on remoulded clays performed by Richardson and Whitman (1962) suggested that the strength ratio might increase with OCR , whilst triaxial tests on natural clays performed by Graham et al. (1983), Leroueil et al. (1983) and Lefebvre and LeBoeuf (1987) showed that the OCR had no apparent influence on the strength ratio.

The plot from Briaud and Garland (1985) is reproduced in Figure 3.52. Based on their compilation of a limited number of undrained tests on clay samples, the researchers suggested that m increases slightly with OCR over a broad range of OCR from 1 to 25. However, the lack of data between the extreme OCR values of 1 and 25 did not allow any significant conclusion to be drawn.

Perhaps the more conclusive amongst these studies is the study by Graham et al. (1983) which was based on a considerable number of tests. The plot from the researchers is reproduced in Figure 3.53. The strength increase was quantified by defining a viscous damping parameter as the change in shearing resistance caused by a tenfold change in strain rate, expressed as a percentage of the shearing resistance measured at 0.1% per hour. The plot of the value of the "Graham et al. viscous damping", n and OCR s from their study, differentiating isotropically and anisotropically consolidated undrained tests, is reproduced in Figure 3.53. Whilst the data points for a certain OCR value vary significantly due to the dependence of n on other parameters, any influence of the OCR on the strength ratio should be able to be discerned in the plot involving a large number of data. The OCR does not appear to have an influence on the viscous damping parameter.

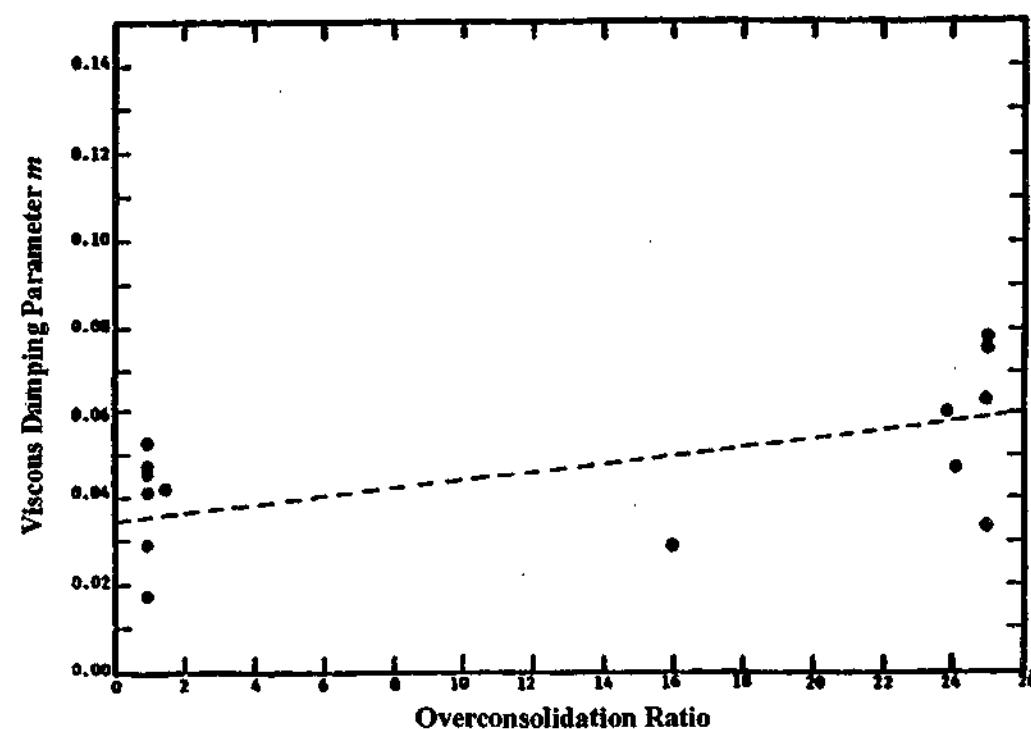


Figure 3.52 The effect of *OCR* on the "Briaud and Garland viscous damping parameter", *m* (after Briaud and Garland, 1985)

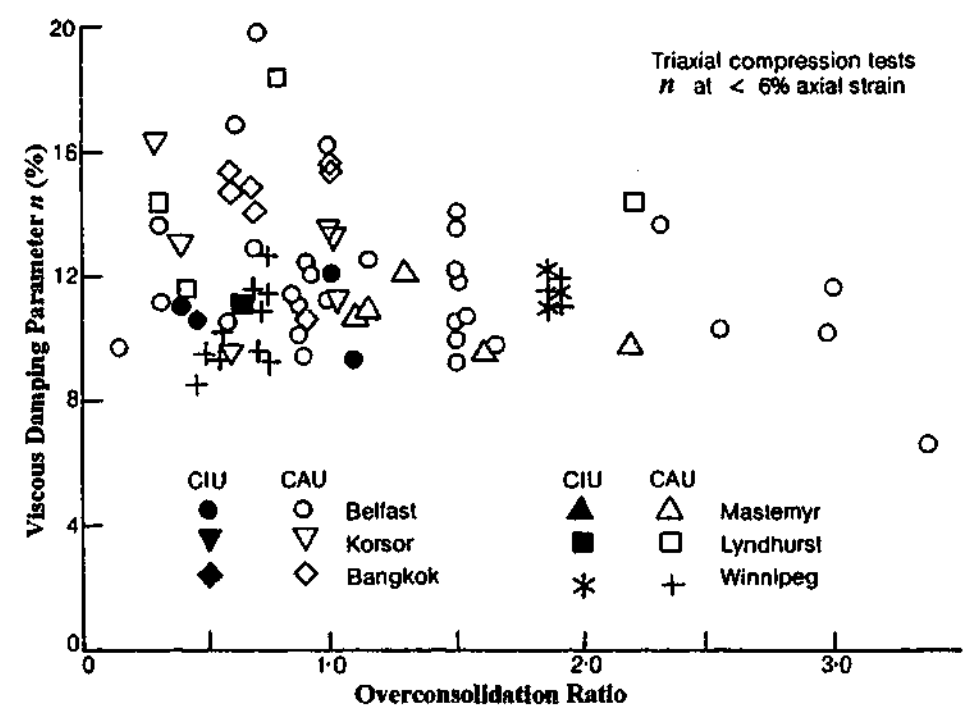


Figure 3.53 The effect of *OCR* on the "Graham et al. viscous damping parameter", *n* (after Graham et al., 1983)

3.5.8.3 Effect of normal stress

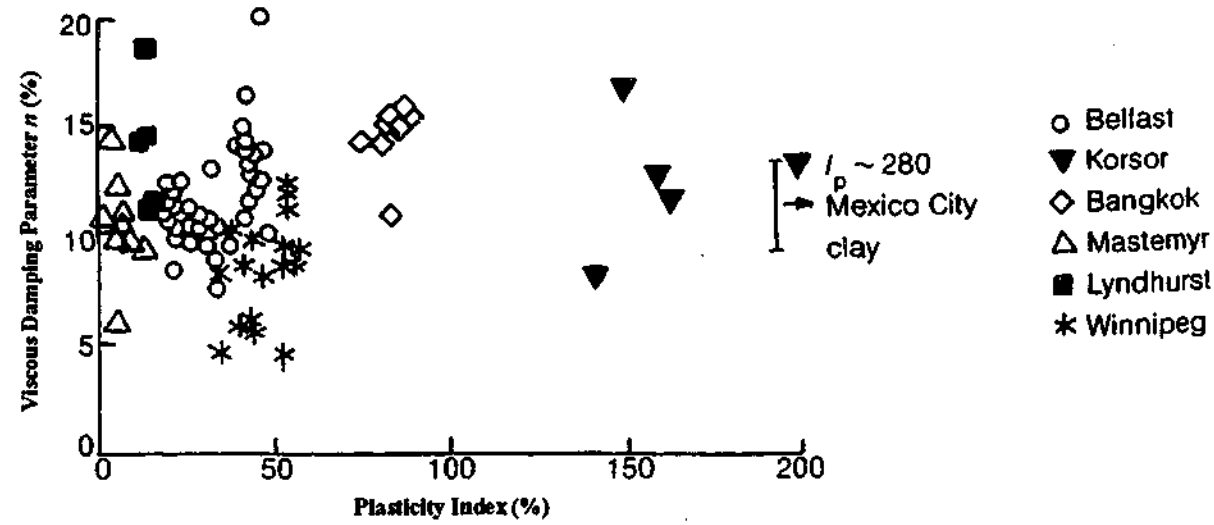
The effect of normal stress on the dynamic response was not investigated amongst the studies on the dynamic response of pile-soil interfaces with the exception of Heerema (1979). In any case, Heerema who tested undisturbed or natural samples, found that the normal stress did not have a consistent effect on the viscous damping parameter $J(N=0.2)$, with one type of clay showing the strength ratio increasing with decreasing normal stress and another type of clay showing the converse behaviour.

3.5.8.4 Effect of plasticity of clay

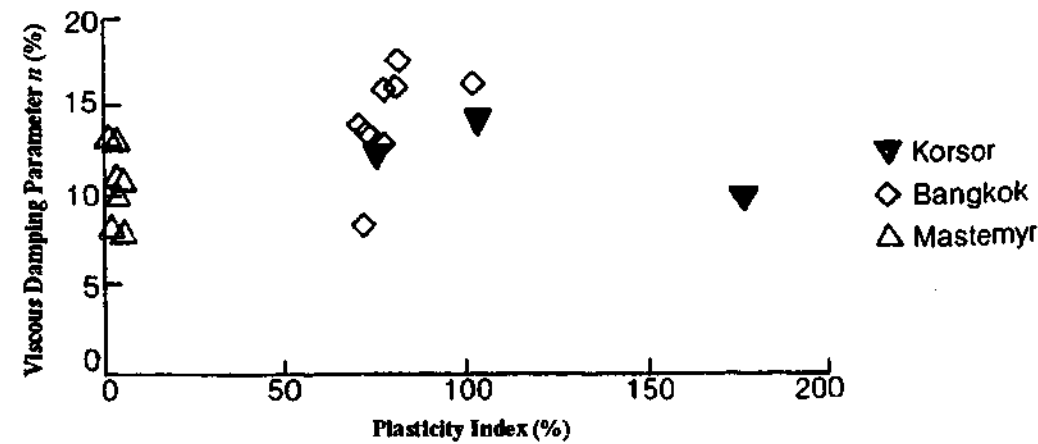
The effect of clay plasticity on the strength ratio or the viscous damping parameter has not been previously investigated for either pile-clay interface or the soil-only tests

performed at high shearing or loading rates. The only data available on the effect of plasticity index on the damping response are based on triaxial compression tests performed at low strain rates.

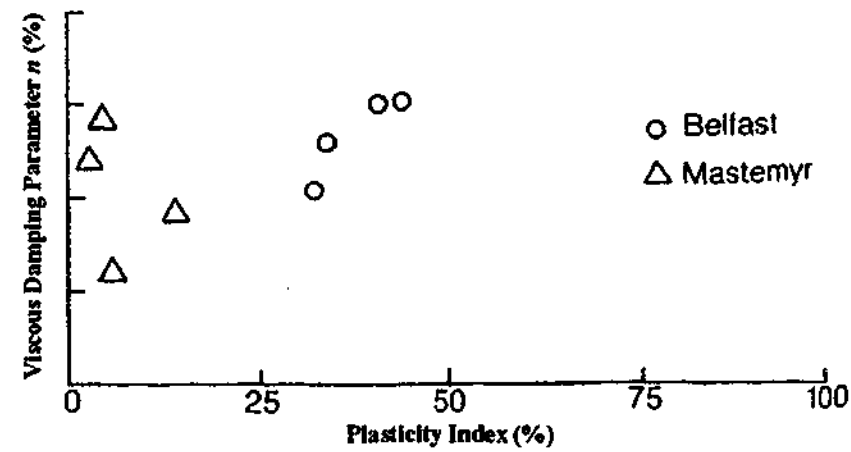
It is noted that any effect (or otherwise) of the plasticity of clay on the damping parameter can be only be discerned if numerous data points are included in the plot between the strength ratio and the plasticity index. Based on triaxial tests on many clay samples, Graham et al. (1983) and Briaud and Garland (1985) plotted their respective viscous damping parameters against the plasticity index (I_p) of the clays as shown in Figure 3.54 and Figure 3.55 respectively. Graham et al. (1983) found that the viscous damping parameter was independent of I_p . Whilst Briaud and Garland (1985) suggested that the viscous damping parameter was dependent on I_p , it can be noted that apart from 4 data points at high plasticity index which show m values of 0.12 or greater, there is little or no indication of a clear trend in the damping-plasticity relationship. Therefore, based on the data currently available in literature, the findings appear to be inconclusive.



(a)



(b)



(c)

Figure 3.54 The effect of plasticity index on the “Graham et al. viscous damping parameter”, n , based on (a) triaxial compression (b) direct simple shear (c) triaxial extension (after Graham et al., 1983)

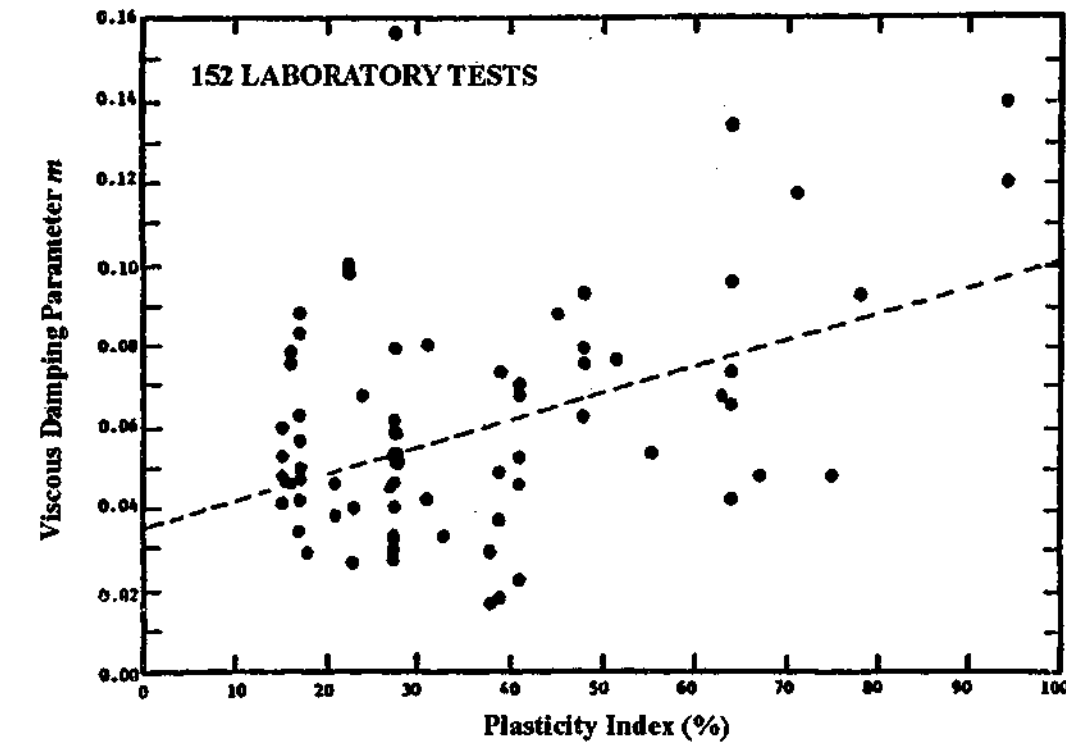


Figure 3.55 The effect of plasticity index on the “Briaud and Garland viscous damping parameter”, m (after Briaud and Garland, 1985)

3.5.9 Concluding remarks – dynamic effects in clay - previous studies

All previous researchers have consistently shown that the strength of both clay and pile-clay interfaces increase with increasing shear rate or strain rate. Based on the limited data from Coyle and Gibson (1970), Dayal and Allen (1975) and Heerema (1979) have suggested an inverse relationship between strength ratio and undrained shear strength. Apart from this correlation, the strength ratio has not been consistently correlated to any other fundamental soil parameter by any other researcher.

As discussed in detail, each of the studies has limitations, and it is readily accepted that due to the complexity of the matters under consideration, it is not possible to undertake a ‘perfect’ experimental program which is not limited in one or another aspect. Nevertheless, the most important limitations that might have prevented a reliable friction-velocity relationship for the interface to be obtained are summarised in the following.

The compression tests performed by Coyle and Gibson (1970) do not simulate the mode of failure at the pile-soil interface as they were associated with compression rather than shear, and were related to soil-only failure as well as unremoulded soil.

The penetrometer set-up used by Dayal and Allen (1975), Litkouhi and Poskitt (1980) and Poskitt and Leonard (1982) appears to be unsuitable for studying the interface-only behaviour because of the tip-shaft interaction. This interaction appears to be the predominant cause of significant data scatter for tests that were ostensibly performed under the same boundary condition (Litkouhi and Poskitt, 1980), for the existence of a "critical velocity" for constant velocity tests (Dayal and Allen, 1975), and the lack of velocity-dependence of friction during an impact test (Dayal and Allen, 1975).

The data obtained by Heerema (1979) suggested excessively high increases in the friction that has not been encountered in practice. The validity of the data is questioned on this basis. Heerema's experimental set-up was rather basic, and the interpretation of the data does not accord well with fundamental soil mechanics principles.

The friction-velocity relationship obtained by Benamar et al. (1991,1992) and Benamar (1999) was based on the loading phase of a driving event. Whilst the experiment appears to have simulated the dynamic response of the interface accurately, the friction-velocity plot presented by the researchers did not describe solely the dynamic effect due to viscous damping as the friction at the start of the event was not fully mobilised. Also, because the dynamic friction was not normalised with the quasi-static friction, the data cannot be compared to data from other researchers and cannot be used to model an actual pile driving event.

The pile-soil interface response with tests involving transient velocities and accelerations, which allowed the effect of acceleration to be investigated, was only simulated in the recent studies (Benamar et al., 1991, 1992, Benamar, 1999). Also, the test data pertaining to a single event, which would be most appropriate for modeling the interface response, was only obtained in these recent studies.

Given the limitations in each of the studies, there is scope for further investigation of the dynamic response of the pile-clay interface. Thus, a new experimental set-up which closely simulates the dynamic response of the pile-soil interface is developed in the present study and is used to obtain further information on the functional relationship between the interface friction and the pile velocity.

3.6 Concluding Remarks

The laboratory set-ups used to perform dynamic tests in the previous studies have been described in the first section of this chapter. In the second and third sections, findings from tests carried out using the laboratory set-ups have been reported, presented in a standard format and discussed.

The studies on the dynamic interface response of pile-sand interfaces have been limited to only two studies that in any case have been shown to have perceived deficiencies. Thus, studies involving soil-only shear tests and triaxial compression tests on sand specimens were also reviewed. The findings based on the studies involving the shear tests have been shown to be mixed and thus inconclusive. Whilst the findings based on the triaxial tests were consistent, it has been proposed that the triaxial test might not have direct relevance to the study of the pile-soil interface.

Various researchers consistently demonstrated that the interface strength of the pile-clay interface increased with shear rate. However, the studies were limited for reasons that have been discussed in detail in this chapter. Based on the data obtained from these studies, the apparent effects of fundamental soil parameters (shear strength, *OCR*, normal stress and clay plasticity) on the viscous damping parameter have been discussed; however, no definite trends could be established.

Thus, the dynamic responses of the pile-sand and pile-clay interfaces need to be investigated in detail. A laboratory set-up that overcomes the major limitations of the previous studies must be developed, and based on the data obtained using this set-up, a better understanding of the viscous damping response of the pile-sand and pile-clay interfaces must be obtained.

Chapter 4

4. Development of Experimental Apparatus

4.1 Introduction:

In the previous chapter, the previous laboratory studies for investigating the dynamic response of the pile-soil interfaces have been discussed in detail. The various characteristics of these experimental set-ups have been shown to limit the reliability and applicability of the results obtained. In an attempt to overcome some of the limitations of the previous laboratory set-ups, a new shear device has been developed for the present study. This chapter discusses the shear device and its capabilities.

4.2 Key Requirements

The requirements that were considered essential for the new shear device are briefly discussed with some reference to the previous laboratory set-ups.

4.2.1 Isolation of shaft from tip

The penetrometer tests performed by Dayal and Allen (1975), Litkouhi and Poskitt (1980), Poskitt and Leonard (1982) resulted in the shaft response being heavily influenced by the preceding penetration of the tip. In order for the pile-soil interface response to be studied, it was a priority that the pile tip response was isolated from the pile shaft-soil interface response.

4.2.2 Eliminating scale effects

Most previous experimental studies used relatively small pile specimens and soil specimens which may result in significant scale effects, especially in cases where soil grains are relatively large compared to the curvature and diameter of the pile specimen. It was therefore desirable to allow a one-to-one model of the interface to be tested.

4.2.3 Different pile characteristics

The penetrometer apparatus used by Litkouhi and Poskitt (1980), Dayal and Allen (1975) allowed only steel piles to be tested. The small-diameter pile used in driving the pile through the triaxial cell (e.g. Benamar, 2000) precluded testing of concrete piles. None of the previous studies investigated the effect of material (i.e. concrete and steel) and of pile roughness on the dynamic response of the pile-soil interface. The new experimental apparatus should therefore allow different pile materials and piles of different roughness to be modelled.

4.2.4 Transient velocity

In most of the studies (except studies by Benamar and his co-workers), the piles were sheared against the soil specimen at near-constant velocity. To more accurately simulate the pile driving event, one of the objectives for the development of the new apparatus was to deliver transient motions to the pile and thus enable the effect of acceleration (if any) on the dynamic resistance to be determined.

4.2.5 Controlled and known normal stress

In the experiments of Dayal and Allen (1975), Litkouhi and Poskitt (1980), Poskitt and Leonard (1982) the magnitude of the normal stress could not be controlled or varied and the normal stress at the sleeve-soil interface was not known. Given the

significance of normal stress on the interface behaviour, it was important that the new apparatus be able to allow the stress acting normal to the interface to be controlled and measured in order to replicate various stress conditions.

4.2.6 Limiting radiation damping

As discussed in Section 2.3.1, during a dynamic event, the pile-soil system has two markedly different responses that occur concurrently. Apart from energy being used at the interface due to viscous damping, some energy is lost in the soil specimen via the straining of the soil in radiation damping. In all the previous studies, there has been a lack of isolation of the near-field and the far-field. It was desirable therefore that the shear device would allow the occurrence of radiation damping (a far-field effect) to be minimised so that the measured response is dominated by viscous damping (a near-field effect). Practically, this means minimising the thickness of the soil specimen so that the energy imparted by the moving pile will not be used in straining the soil in radiation damping but rather be consumed by viscous damping.

4.3 Alternative Schemes

During conceptual stage of the development of the shear device, two schemes were considered. The first scheme was to have a set-up similar to that adopted by Benamar (2000) except at a larger scale. The soil specimen which encased the pile would be contained in a triaxial-like cell. Confining stress and backpressure would be applied to the specimen in the cell. Whilst this system satisfied all the essential requirements, it had two significant disadvantages. The annular holes through which the pile shaft penetrates at the top and bottom of the cell would need to be sealed; it would be difficult to ensure that significant friction between the seal and the pile surface at these two locations did not occur. Also, the pile-soil interface friction could not be measured directly and would have to be computed indirectly using stress-wave theory.

Such analysis would require that the pile-soil interface be modelled as many discrete sections, and that the stress equilibrium and velocity continuity relationships be applied to each of the sections in order to solve for the interface friction contributed by each of the sections. Given the significant length of the sample, significant amount of computation would be required.

The second scheme was a direct shear device, where the normal load would be applied to the soil specimen (and the interface) in the vertical direction and the shear load would be applied to the interface in the horizontal direction. Apart from satisfying the requirements, this system had the advantage of being able to measure the interface friction directly. Also, friction between the pile surface and the soil container could be avoided by slightly lifting the shear box above the pile surface as in a conventional direct shear test. The disadvantage was that because the contact between the soil and the pile surface was not sealed to avoid friction, sample may be lost through the gap.

The disadvantages associated with the first scheme might compromise the quality of the experimental results. Whilst the second scheme had the disadvantage of potential soil loss, it was appreciated that in any system where friction between the “container” of the soil specimen and the pile surface was to be avoided, the loss of soil was inevitable. It was thus decided that the second scheme would be more appropriate.

4.4 The Quasi-Static & Dynamic Interface Shear Device

4.4.1 Development of the shear device

The Civil Engineering Laboratory of Monash University houses a large shear device for the shearing of rock-concrete interfaces, which contains components that are very useful for interface tests. These components are as follows.

- A hydraulic actuator in the direction normal to the specimen and another hydraulic actuator in the shear direction of the specimen.
- A carriage travelling in the shear direction and a piston travelling in the normal direction. These components are guided by bearing systems that have been carefully designed with high rotational stiffness.

Thus this device was used as a basis for the development of the pile-soil interface shear device.

As the original device would still be used for the testing of rock-concrete interfaces, a design constraint was not to compromise its existing capabilities. Additional major components were designed and fabricated which together with the existing

components form the new shear device for dynamic shear testing of pile-soil interfaces. The major additional components include:

- a carriage that is lighter than the existing carriage and which accommodates the pile section (from hereon, the new carriage will be referred to as the “light carriage” whilst the existing carriage will be referred to as the “heavy carriage”)
- an actuator that is capable of delivering high velocities to the carriage
- a mechanism for stopping the carriage and the actuator
- a cushioning device for the stopping mechanism
- a connection between the actuator and the carriage
- a “box” for containing the soil specimen

Each of these components is described in detail in Section 4.4.3.

Schematics of the shear device in the side and the end elevations are shown in Figure 4.1 and a photograph of the shear device is shown in Figure 4.2.

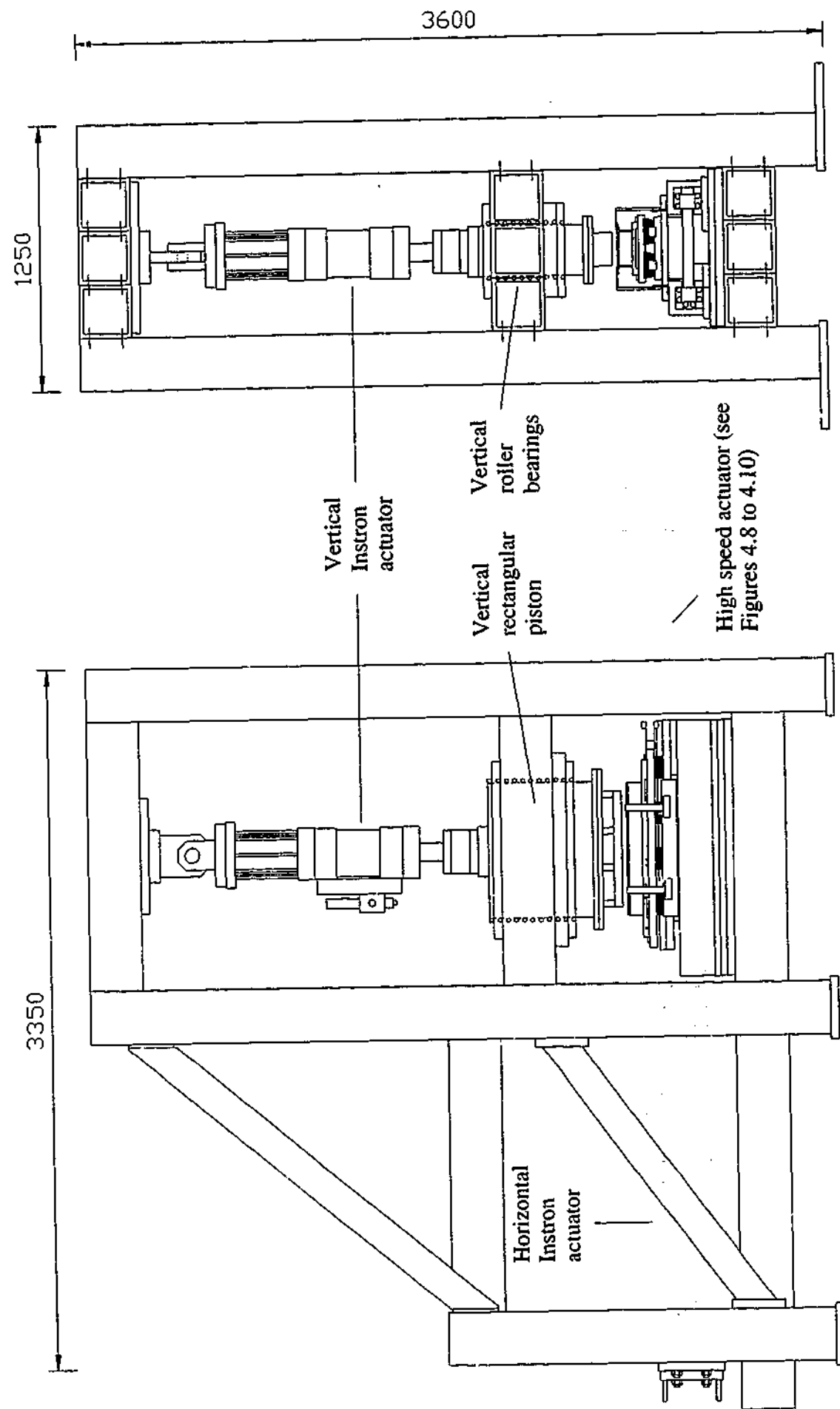


Figure 4.1 Side and end elevations of the shear device

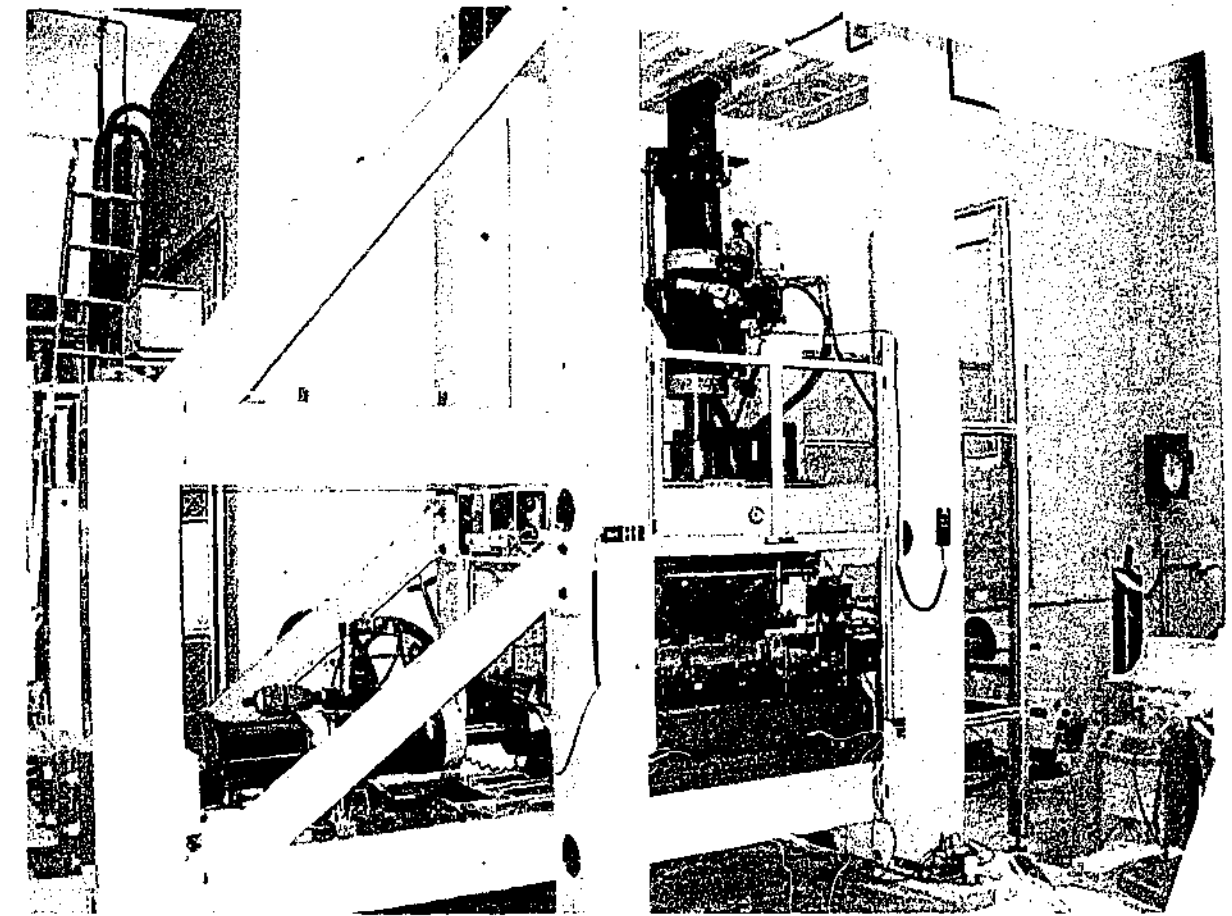


Figure 4.2 The shear device for the study of pile-soil interfaces

4.4.2 General description of the shear device

For both the quasi-static and dynamic tests, the soil specimen was loaded under constant normal load conditions by the existing vertical actuator via a loading platen. The loading platen was located inside the shear box as it applied a normal stress on the specimen so that the shear box and the specimen were prevented from moving whilst the pile section was moved. Shear keys were machined on the contact surface of loading platen in order to prevent failure along the plunger-soil interface.

The configuration of the shear device for the dynamic tests is shown in Figure 4.3 and Figure 4.4. The shear load is applied by a specially designed high-speed actuator as the existing Instron actuator was not capable of generating high-speed impacts. Since the heavy carriage had too small a plan area for accommodating the pile section and was too heavy to be accelerated effectively, a lighter carriage system was designed. The base of the light carriage system is bolted onto the stationary horizontal bed so that only the sliding steel plate can move.

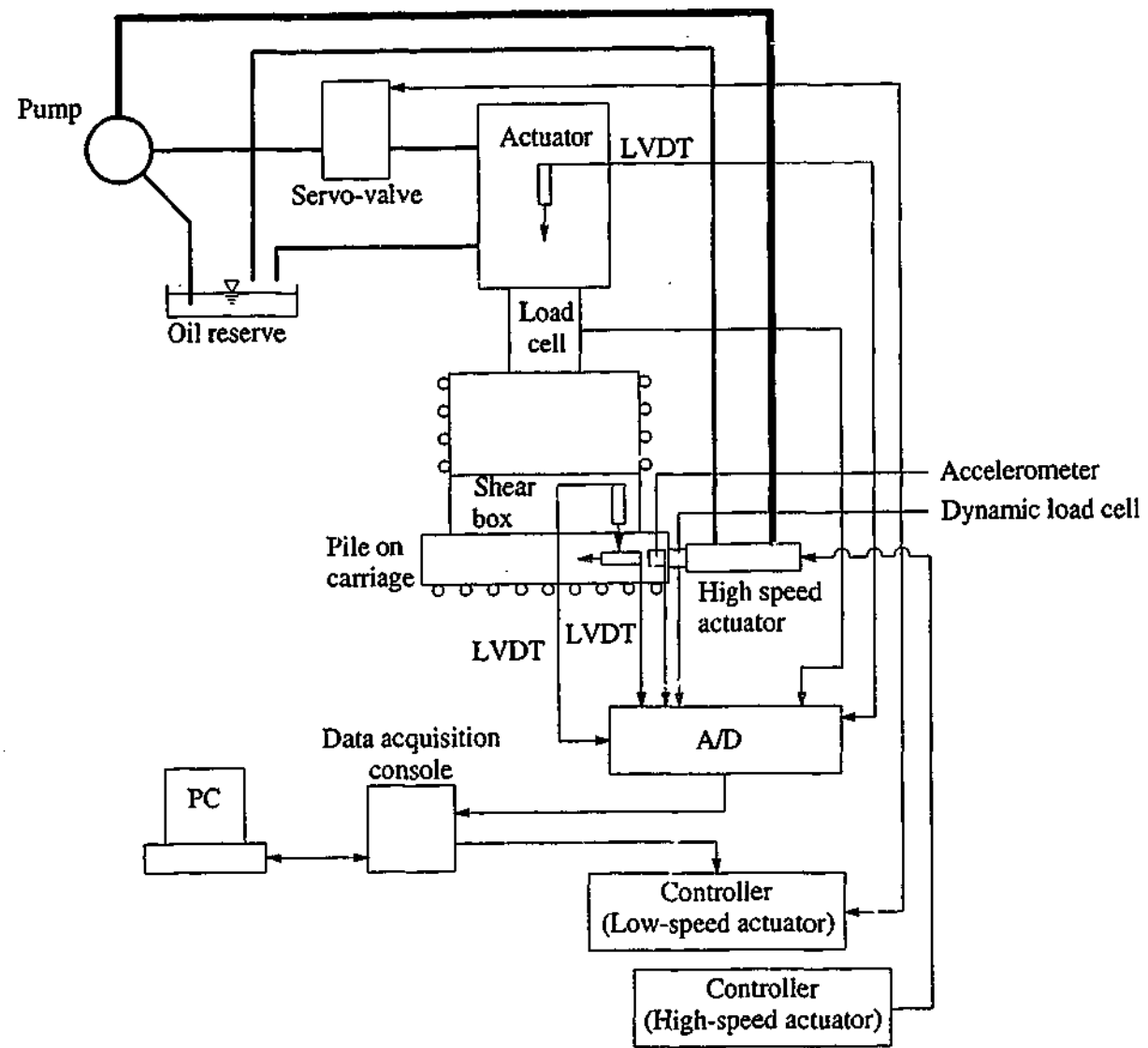


Figure 4.3 Flow diagram of the operation of the shear device and data acquisition under dynamic configuration

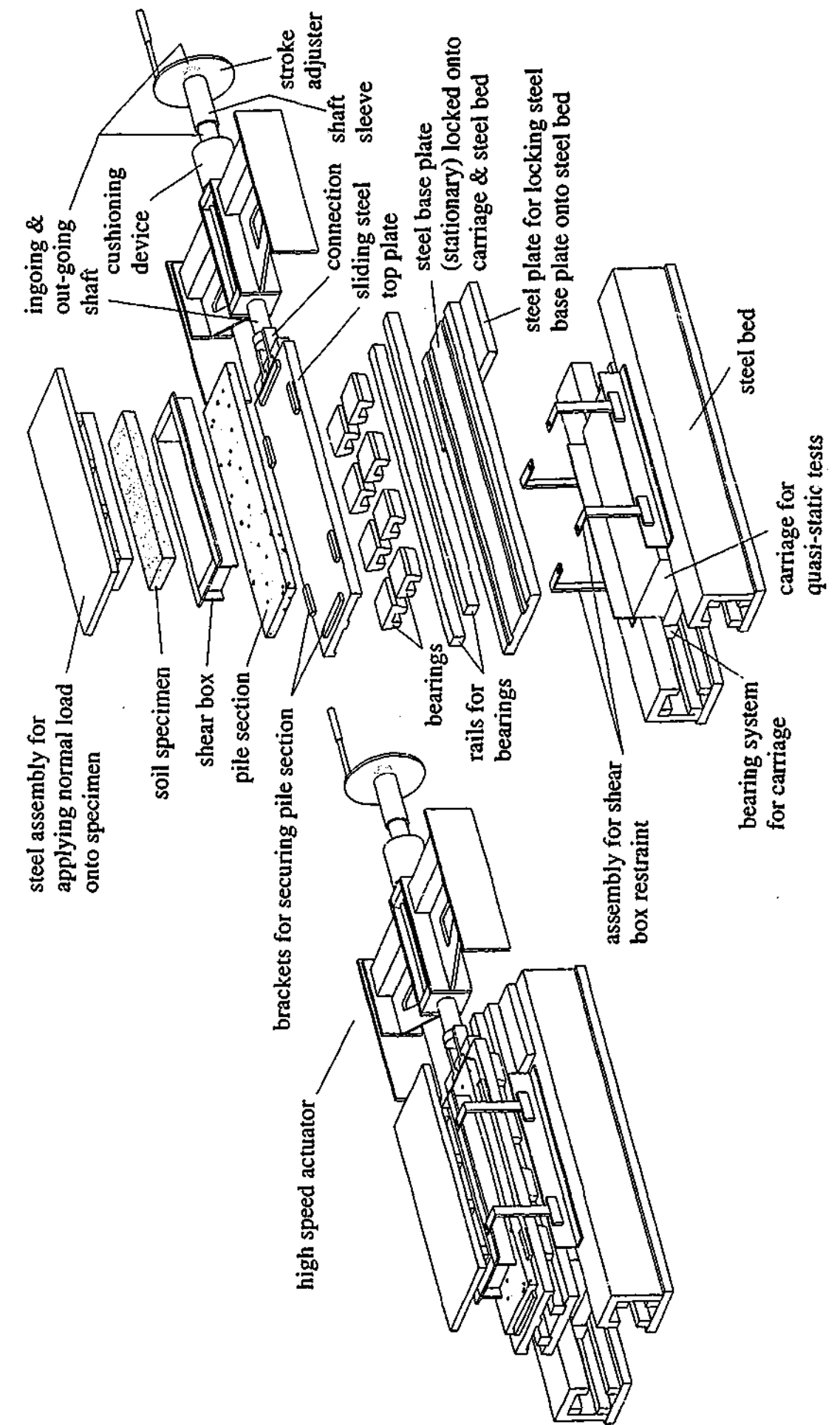


Figure 4.4 Configuration of the shear device for dynamic test

The light carriage is coupled to the high-speed actuator so that effectively it is pushed by the actuator rather than impacted. This avoids steel-to-steel impact, which may cause “ringing” in the force data and damage the dynamic load cell. The coupling also enables a single stopping mechanism to be used for the actuator and the carriage. The carriage and the actuator are stopped mechanically at the free end of the actuator with a “nut-and-bolt” system shown in Figure 4.4, which will be described in detail later.

The configuration of the shear device for the quasi-static tests is shown in Figure 4.5 and Figure 4.6. The shear load is delivered by the existing horizontal Instron actuator. As it is undesirable to uncouple the actuator from the old carriage (as this configuration is used for testing rock-concrete interfaces), the shear load is applied via the heavy carriage. This requires that the light sliding carriage be prevented from moving; this was achieved by engaging its two ends with steel brackets as illustrated in Figure 4.6.

The shear box is topless and bottomless so that the top of the sample can be engaged by the normal loading platen and the bottom of the sample can contact the pile surface. The depth of the shear box is greater than the thickness of the soil specimen so that the loading platen can be seated inside the shear box during testing. During preparation for testing sand specimens, the shear box was placed onto the pile, and sand was rained into the shear box and onto the pile surface. During preparation for testing clay specimens, the clay block was placed onto the pile surface and the shear box was placed around the clay specimen.

To record the test measurements, a high-speed data acquisition system was developed as detailed in Section 4.5.

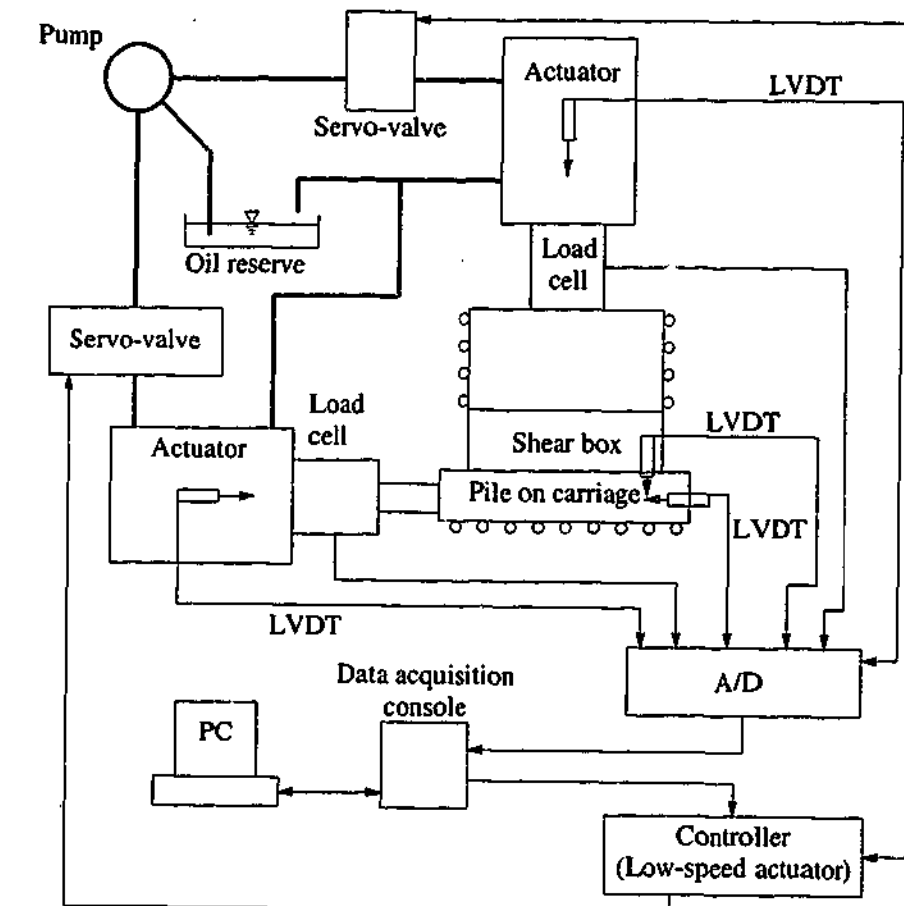


Figure 4.5 Flow diagram of the operation of the shear device and data acquisition under quasi-static configuration

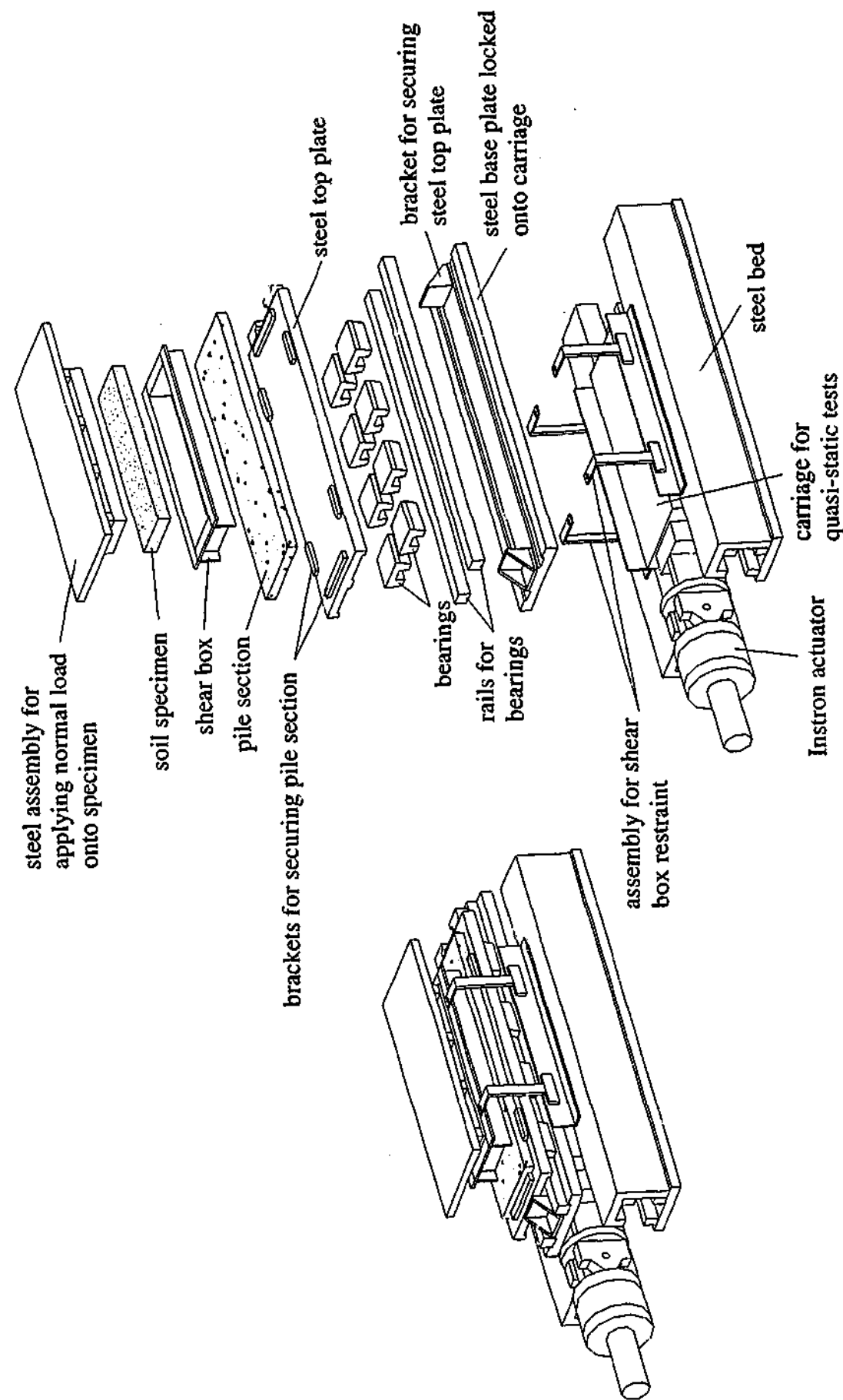


Figure 4.6 Configuration of the shear device for quasi-static test

4.4.3 Components of the shear device

4.1.1.1 Hydraulic actuators

The actuators for applying the normal load and the shear load are Intron series 3375 electro-hydraulic actuators. They have load capacities of $\pm 250\text{kN}$ static and $\pm 500\text{kN}$ dynamic, and a stroke of $\pm 125\text{mm}$. The actuators are capable of a maximum constant velocity of 50mm/s and a minimum constant velocity of 0.005mm/s . A reference quasi-static velocity selected for the testing programme was 0.01mm/s .

The actuators are fitted with Moog servo-valves which regulate the flow rate of the hydraulic oil as a function of the control current from the controller unit (IST, 1998). The actuators are controlled by the 8800 Servohydraulic Controller which allows the actuators to be operated under closed loop control.

The closed-loop system enables the applied load (measured by its load cell) to be fed back to the controller so that the controller can continuously adjust the actuator in order to match the user-specified load. For instance, the application of the normal load on the specimen relied on the closed-loop capability. The target normal load and the rate of load application were specified by the user via the controller and the control software. As the load on the specimen was increased at the specified rate, the actual applied normal load (as measured by the load cell) was fed back to the controller so that the controller could adjust the flow of oil such that the load continued to be incremented until the target load was reached.

4.1.1.2 Carriage & bearing systems for quasi-static test

The heavy carriage is coupled to the horizontal actuator and is moved in order to shear the pile-soil interface at low velocities. The carriage is guided by sets of vertically and horizontally constraining roller bearings that have been fabricated to tolerances of $\pm 0.01\text{mm}$ (Seidel, 1993). The bearing system has a large rotational stiffness which is important for preventing rotation of the two halves forming the interface during shearing. It has also been designed to have low friction. These characteristics of the bearing systems are critical to high quality experimental results.

4.1.1.3 Carriage & bearing system for dynamic tests

The light carriage was designed to accommodate a pile section, to allow displacement up to 110mm and to enable it to be accelerated to a high velocities over specified and selectable distances. The carriage system was designed to be removable so that the original set-up could be still used for the testing of rock-concrete interfaces.

The components of the carriage system are shown in Figure 4.4. The carriage measures 950mm by 320mm in plan. It consists of a 30mm-thick steel plate which accommodates the pile section measuring 60mm by 250mm in plan. Eight sets of bearings are bolted to the underside of this steel plate such that 4 sets are located at each of the two longitudinal edges of the steel plate. These bearings run on a pair of rails which are bolted onto the top of another steel plate. The bearings and the rails are INA[®] linear guidance system which again provide high rotational stiffness and low friction. The bottom steel plate is bolted to the heavy carriage and the stationary bed so that both the bottom steel plate and the heavy carriage are prevented from moving. The lighter carriage weighs approximately 100kg compared to 400kg of the old (heavy) carriage. Friction in the bearings was measured to be at less than an equivalent 0.3kPa for the specimen size of 160mm x 555mm.

The design of this carriage was based on a compromise between its weight and its robustness. The carriage was required to be sufficiently light so that it could be more effectively accelerated by the actuator and more easily decelerated by the stopping mechanism. However, it also had to be sufficiently robust to withstand the applied loads from the horizontal and vertical actuators, and to allow sufficient space for the detailing and construction of bearing systems and the connection to the actuator.

4.1.1.4 Vertical piston & bearing system for quasi-static & dynamic tests

As previously mentioned, the original set-up has a hollow rectangular section that travels in the direction normal to the shear plane. This section is coupled to the vertical actuator and the means whereby normal load is applied to the specimen. As with the heavy carriage, this section is guided by steel bearings and needle rollers providing high rotational stiffness and low friction.

4.1.1.5 High-speed hydraulic actuator for dynamic tests

Given that the existing actuator in the shear direction was only capable of a relatively low maximum velocity (of 50mm/s), a hydraulic actuator that was capable of delivering high velocities was developed. The hydraulic actuator was developed in collaboration with a firm of hydraulic specialists. Unlike the Instron actuator, the high-speed actuator is operated without feedback (open-loop system). The actuator was designed to achieve a peak velocity in excess of 5.0m/s. However, this maximum velocity was not used for the tests due to practical constraints which will be discussed further. The shaft of the actuator (and the carriage) could be extended and retracted in a "slow mode" at approximately 50mm/s so that the position of the carriage could be adjusted before a test was commenced, and so that the actuator could be retracted after a test was completed.

The shaft of the actuator and the supporting structural frame for the actuator have been shown in Figure 4.4. A photograph of the system is shown in Figure 4.7 to Figure 4.9. The major components of the actuator are labelled in Figure 4.9, and are as follows:

- An accumulator which stores the energy required for propelling the actuator shaft;
- Valves A and B which open or shut to allow or block the passage of oil;
- An orifice size adjuster located in Valve B which governs the rate at which the oil flows through Valve B;
- A differential cylinder which contains the shaft of the actuator. Because of the geometry of the shaft, which is shown schematically in Figure 4.10, there are two compartments within the cylinder. The compartment into which the oil flows has a relatively smaller diameter shaft and hence accommodates a larger volume of oil. Conversely, the compartment out of which the oil flows has a larger diameter shaft and hence accommodates a smaller volume of oil. A pressure differential is created across the two compartments, which helps in propelling the shaft.

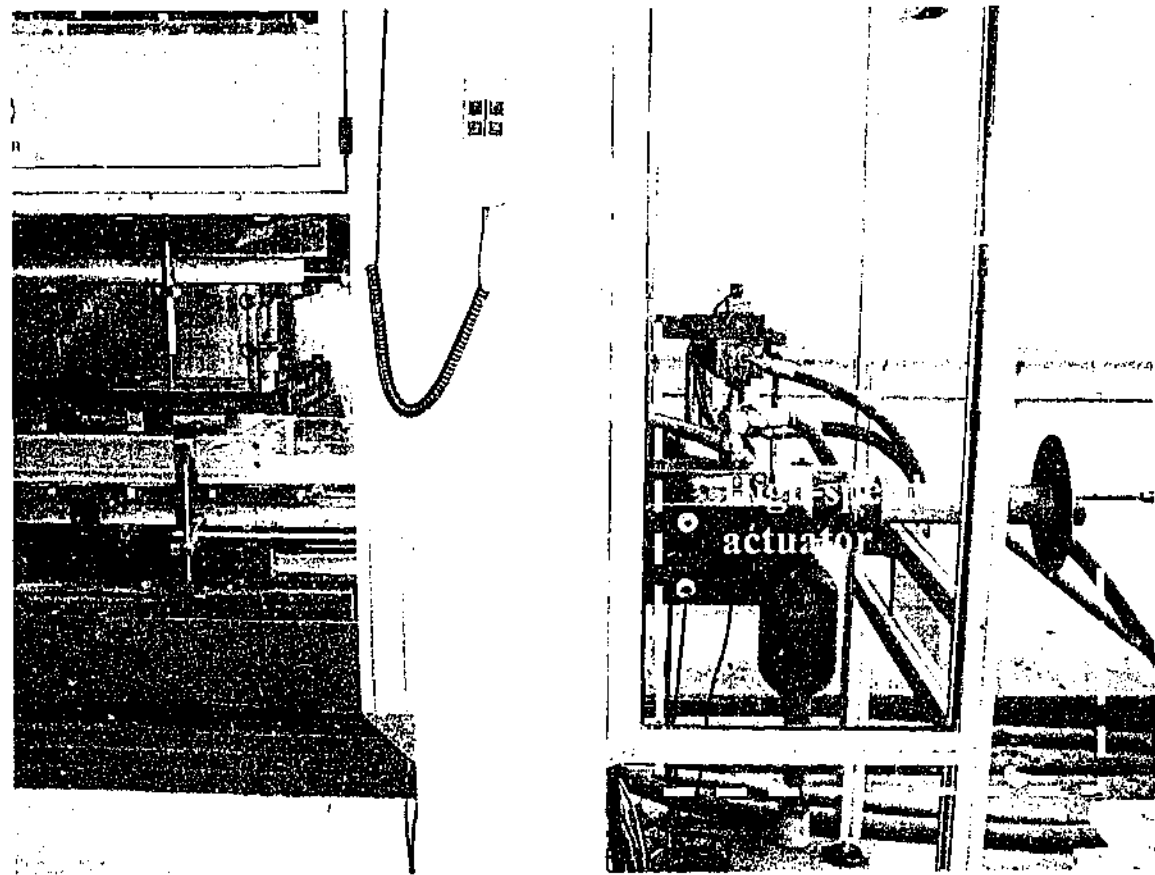


Figure 4.7 Side view of the high-speed actuator

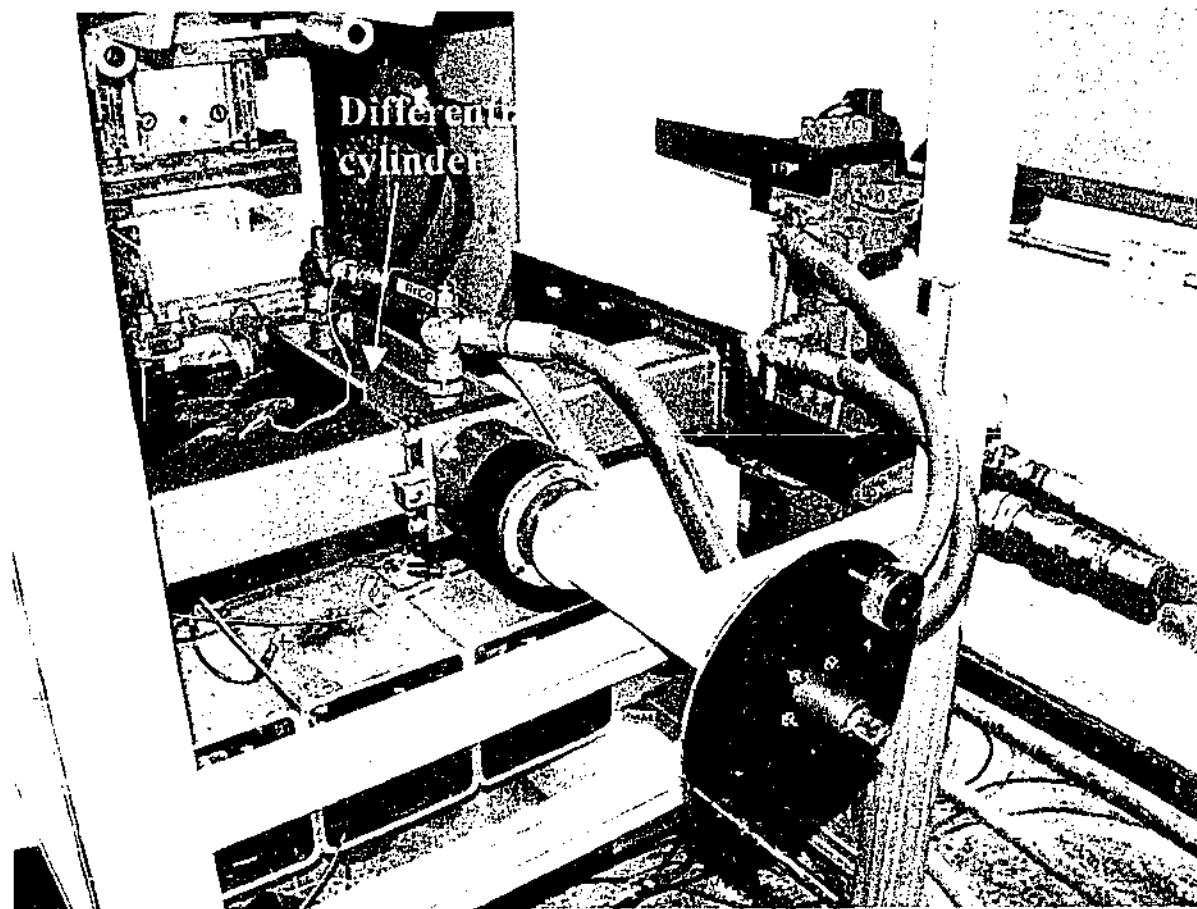


Figure 4.8 End view of high-speed actuator

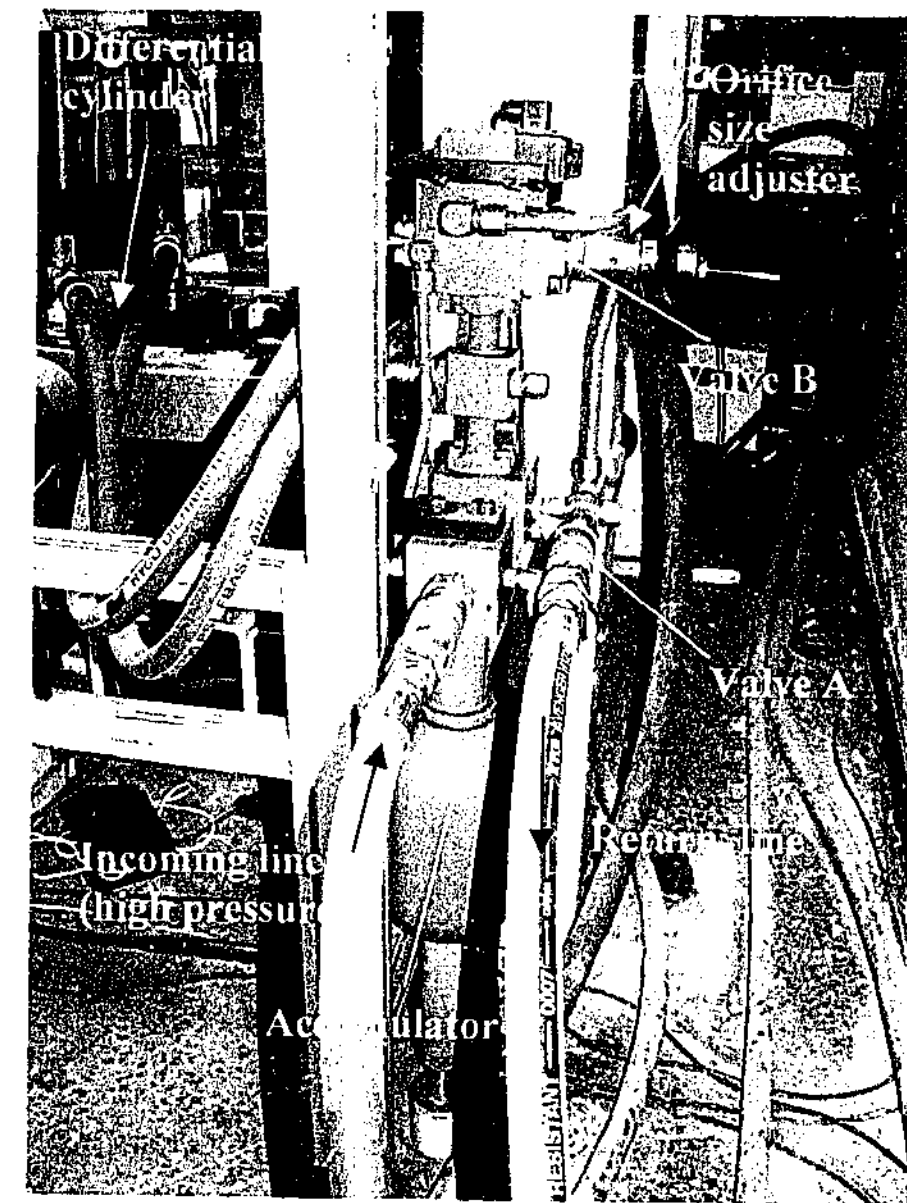


Figure 4.9 Major components of the high-speed actuator

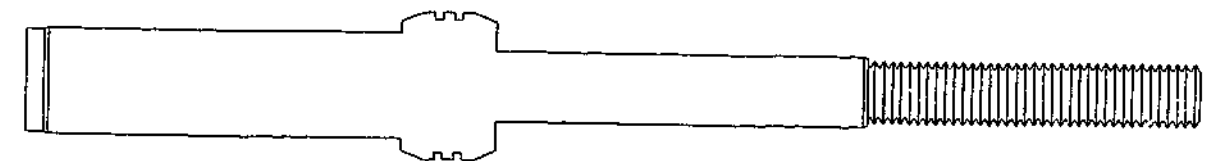


Figure 4.10 Schematic of a differential cylinder

The schematic in Figure 4.11 shows the major components of the actuator and the flow of the hydraulic oil in the system during a single stroke. The oil in the hydraulic system is sourced from an oil reserve and is pressurised by a pump located in the basement of the laboratory. Initially, Valves A and B are shut so that oil does not flow through the valves and the cylinder or the shaft is stationary. When the “run” button at the controller is activated, the two valves are opened simultaneously, and energy stored in the accumulator is released. Thus, oil flows through Valve A into the differential cylinder, thus propelling the shaft. The rate at which the shaft is moved or the rate at which the oil flows through the differential cylinder is dependent on the size of the orifice located in Valve B, which is adjustable.

The actuator is capable of 110mm of the stroke in the “fast mode”. The stroke of the actuator can be varied by adjusting the position at which the mechanical stop is engaged.

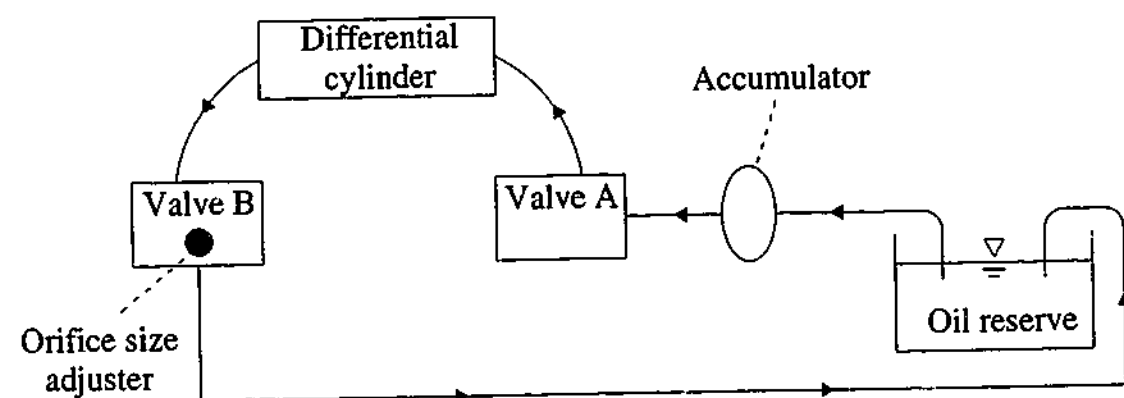


Figure 4.11 Major components of the high-speed actuator and the flow of oil during a single stroke

4.1.1.6 Stopping mechanism & Cushioning device

The moving carriage and high-speed actuator are stopped by a mechanical system located at one end of the shaft as shown in Figure 4.4 and Figure 4.12. The mechanical stop consists of a sleeve that with internal thread that is “screwed” onto a threaded section of the shaft. This system is analogous to a nut-and-bolt system.

During testing, a considerable amount of force resulted from high pressure hydraulic oil being exerted on the actuator and the inertial force of the moving carriage; thus the stopping of the actuator and the carriage could impart a severe shock load to the system. The shock load could fatigue the mechanical stop itself, the welds and structural frame supporting the actuator and the connection between the carriage and the actuator. It could also damage the data acquisition devices attached to the carriage such as the accelerometer. It was therefore imperative that this shock load was cushioned.

After experimentation with various materials including timber, synthetic materials and elastomeric laminate (layers of rubber stiffened by steel plates), it was found that a series of concave washers made out of spring steel was most effective in cushioning the impact. The series of concave washers form a “spring”, as shown in Figure 4.13. The washers allow significant (elastic) deformation to occur which cause a significant amount of energy to be absorbed during the compression of the washers and are reusable.

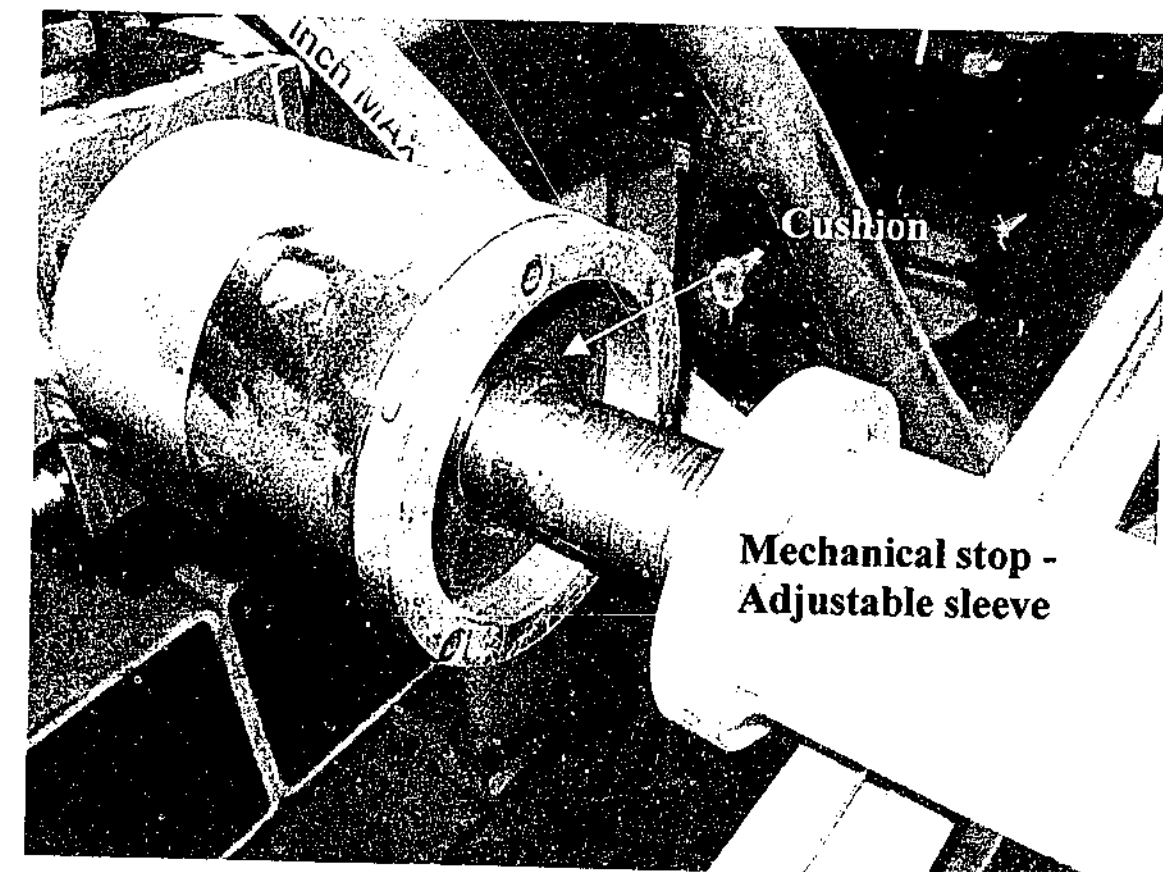


Figure 4.12 Stopping mechanism

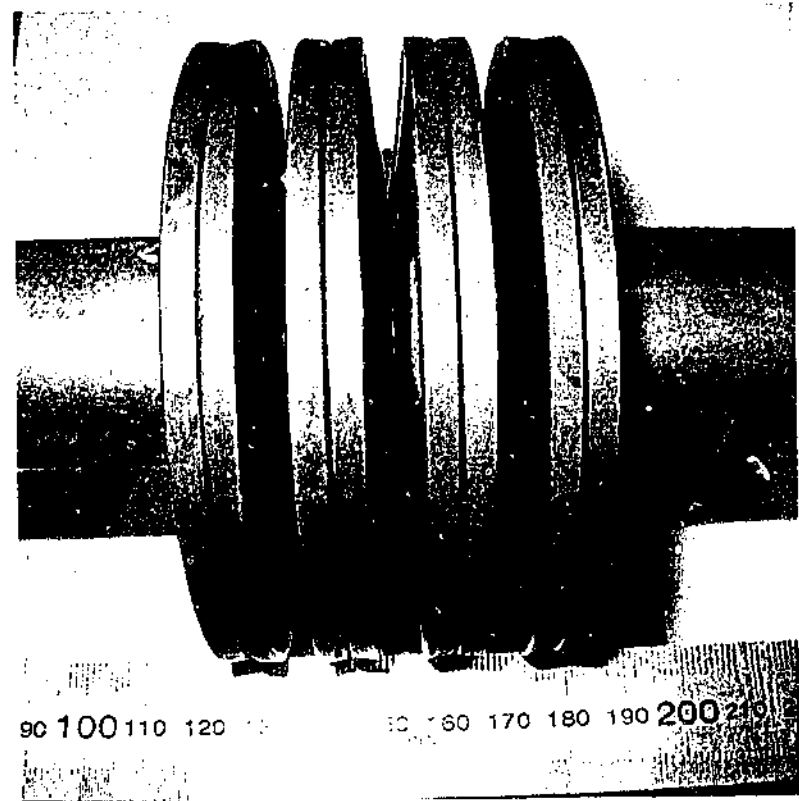


Figure 4.13 Four out of the eight pairs of washers used for cushioning

4.1.1.7 Connection

A dynamic load cell works on the basis of the compression of the active pressure-sensitive quartz crystal element and is thus primarily designed to measure compressive forces. Although some tension force measurement capability can be obtained by pre-loading the quartz crystal, the maximum tension force that can be measured is typically small. The dynamic load cell used had internal threads at its two ends to allow fixture to the interfacing components. Since the load cell has relatively low-tension measurement capacity, the tensile capacity of the thread is correspondingly low and cannot withstand the high shock load (in tension) of the carriage-ram system.

The dynamic load cell was interfaced between the actuator and the carriage in order to measure the dynamic load imparted from the actuator to the carriage. In order to avoid loading the load cell in tension, the dynamic load cell had to be fixed onto the actuator shaft at one end whilst the other end was free. The result was that the tensile force during the test event could not be measured. This was accepted as a necessary limitation of the set-up.

For cases where the interface resistance was high, the load cell did not ever lose contact with the carriage during the test event. Such cases included pile-sand interfaces tested at moderate normal stresses (150kPa) or above, and pile-clay interfaces tested at high normal stresses (250kPa) or above. This limitation did not prevent the dynamic friction for the full range of the pile velocities and the pile accelerations of the test event to be obtained. During acceleration of the actuator shaft, the load cell was compressed throughout this time, whilst during the deceleration of the actuator, the load cell lost contact with the carriage for a short period of time before rejoining with the carriage again. The combined dynamic force data during the acceleration and deceleration phases were found to be sufficient for obtaining the dynamic friction for the full range of the pile velocities and the pile accelerations.

In order to couple the carriage to the shaft of the actuator, a connection was designed to carry any tension force while still allowing the full load to pass through the load cell in compression. The schematic of the connection has been included in Figure 4.4 and its two working modes are shown in Figure 4.14 and Figure 4.15. Before the actuator was activated, the free end of the load cell was 0.5mm away from the carriage so that no load was imposed on the dynamic load, as shown in Figure 4.14. When the actuator pushed against the carriage, the free end of the load cell was compressed against the carriage as shown in Figure 4.15. During the compression, the connection did not come in contact with the carriage. When the carriage started to separate away from the load cell, the carriage was restrained by the connection from travelling further than the 0.5mm.

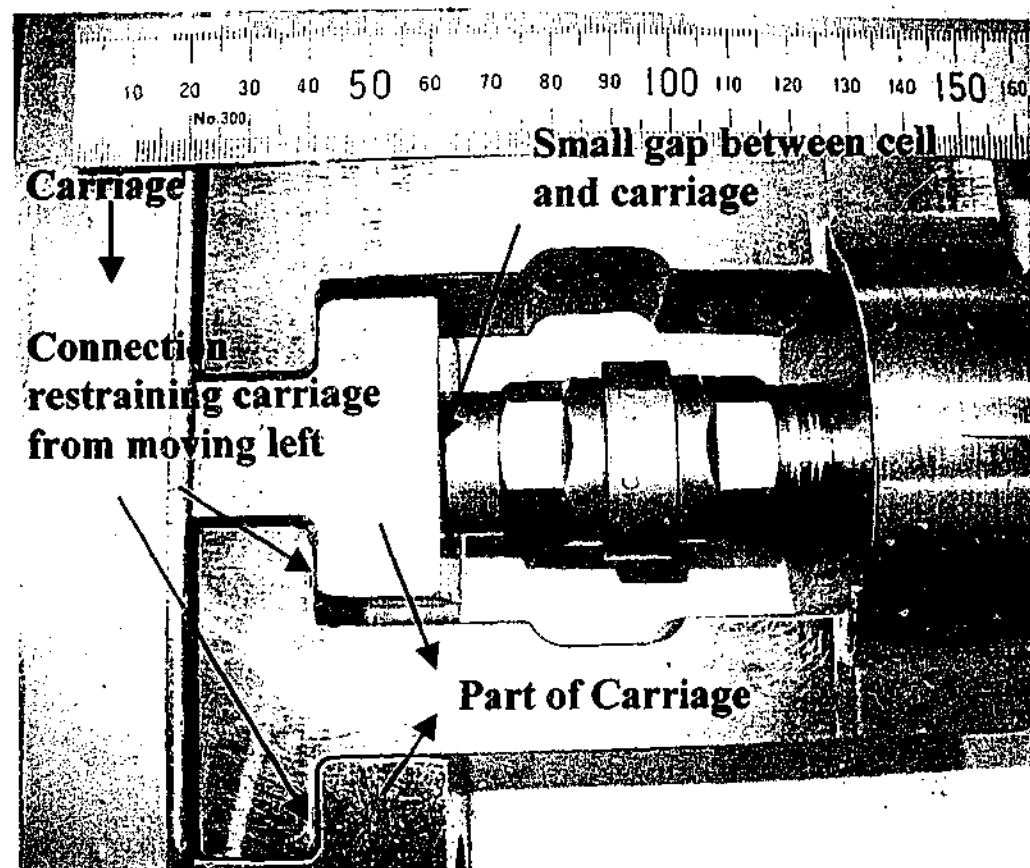


Figure 4.14 Connection between the carriage and actuator when the load cell loses contact with the carriage

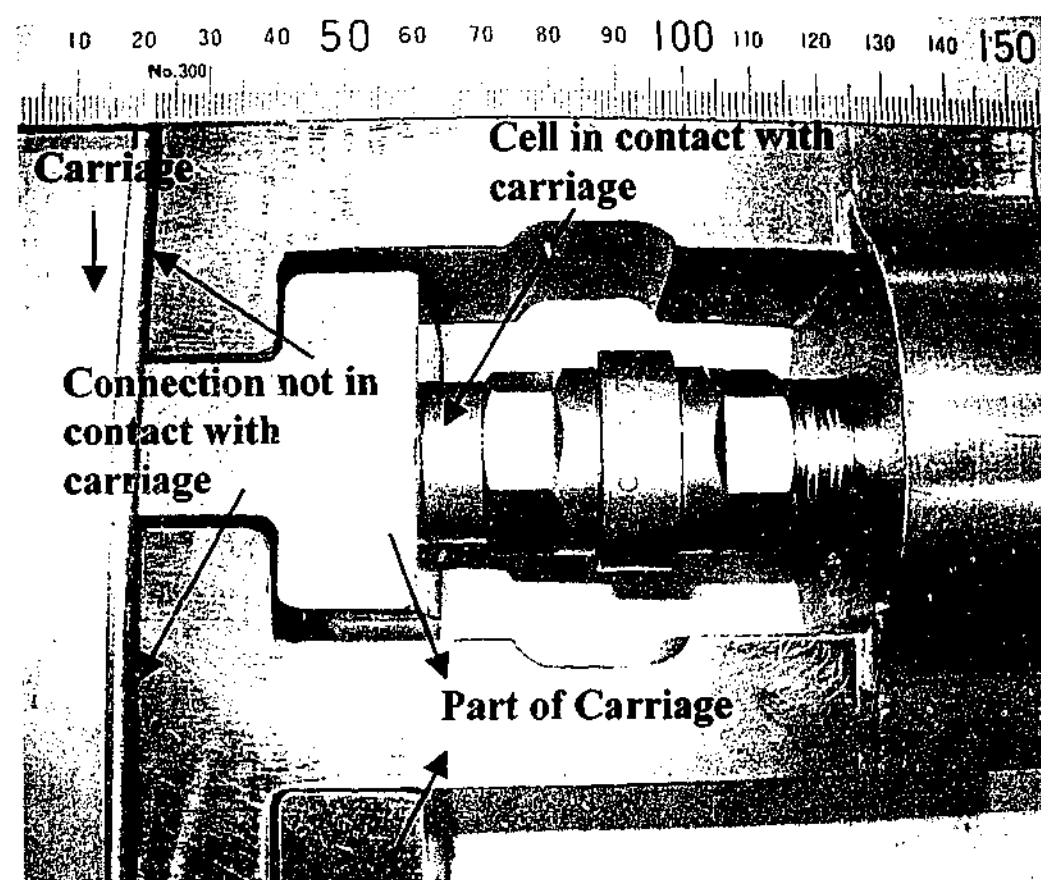


Figure 4.15 Connection between the carriage and actuator when the load cell is compressed against the carriage

4.1.1.8 Shear box

When a pile is loaded in the field, the soil around a pile is subjected to pure shear as shown in Figure 4.16 (Randolph and Wroth, 1981). Pure shear is defined as the state where the horizontal stress σ'_x and the vertical stress σ'_y on the sample remain constant whilst shear stress on the sample τ_{yx} increases gradually throughout the shearing process (Randolph and Wroth, 1981); the stresses are shown to act on the sample in Figure 4.17. It is therefore desirable in laboratory tests to allow the soil specimen to undergo the same mode of shear so that the magnitude of the shear stress and the shear stress-shear displacement behaviour in the field can be simulated.

In the laboratory, the shear mode of the soil specimen is dictated by the type of shear apparatus being used. Whilst many types of interface shear apparatuses have been used in previous interface studies (e.g. Paikowsky et al., 1995), they can be generally classified into the direct shear apparatus and the simple shear apparatus.

The direct shear device has been used in many studies to study the interface behaviour because of its simplicity and its ease of operation (e.g. Fedá, 1976; Potyondy, 1961). However the direct shear test has some inherent weaknesses in simulating pure shear (e.g. Yin et al., 1995; Yoshimi and Kishida, 1981; Yoshimi and Kishida, 1982; Tsubakihara and Kishida, 1993; Tsubakihara et al., 1993). During shearing, the front and rear non-deformable ends of the shear box prevent the soil specimen from undergoing pure shear. As a result, shear strains and the shear stresses in the specimen are unevenly distributed over the contact surface. The shear strengths at the two ends of the soil specimen are mobilized first, and sliding started from these locations. As the average shear stress and the overall relative displacement of the pile and the soil increase, the progressive failure spreads towards the centre until the entire interface is failed.

The simple shear devices used for shearing of interfaces typically consisted of a stack of thin plates that form a rectangular hollow section (Uesugi and Kishida, 1986a, and 1986b; Tsubakihara and Kishida, 1993; Tsubakihara et al., 1993; Paikowsky et al., 1995; Fakharian and Evgin, 1997). The plates slide across each other and sway in the

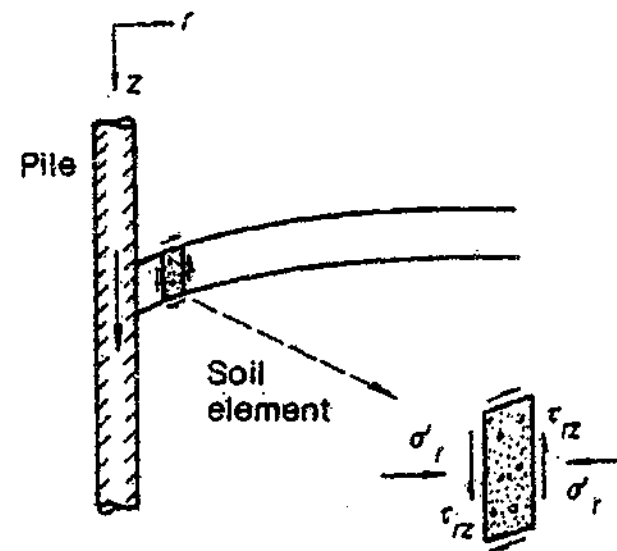


Figure 4.16 Soil deformation in simple shear test and during pile-loading and driving (after Randolph and Wroth, 1981)

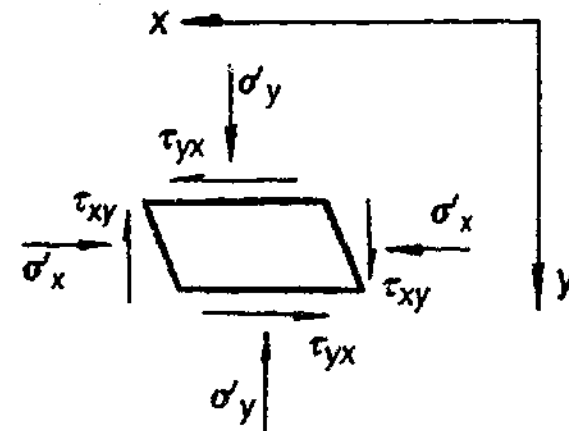


Figure 4.17 Annotations (Randolph and Wroth, 1981)

direction of shear as the soil specimen deforms in shear as shown in Figure 4.18. The bottom-most plate slips on the pile surface as the soil slips against the pile surface.

In the early stage of the shearing, the stress conditions are the same as those of pure shear; however, as plastic deformation starts occurring in the soil, the stress changes in the specimen no longer correspond to pure shear (Randolph and Wroth, 1981). However, the departure from the pure shear mode is to a much lesser degree compared to that of the direct shear device (Paikowsky et al., 1995). Thus the simple shear test is much more capable than the direct shear test in simulating the shear mode of the soil (around a pile) in the field.

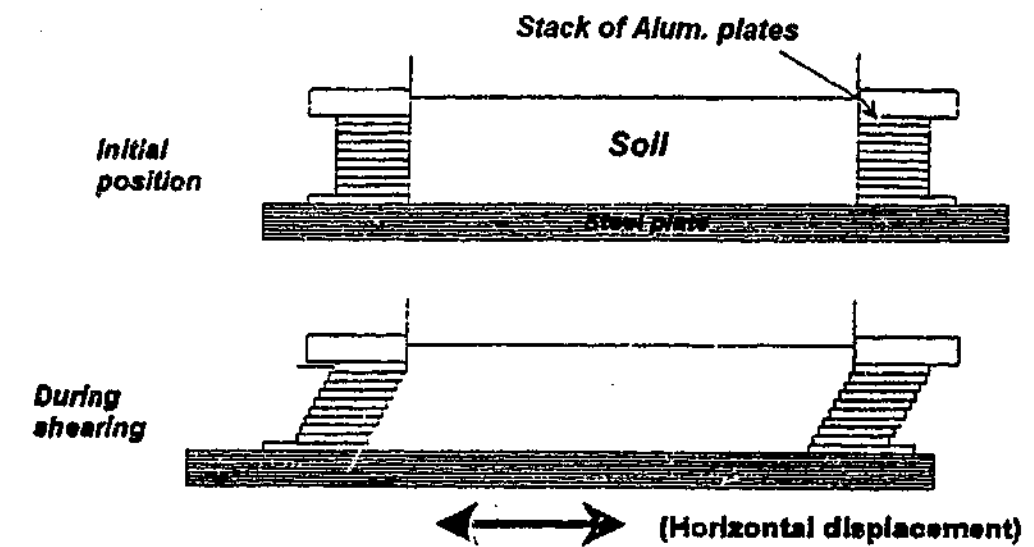


Figure 4.18 Swaying of plates during shear (after Evgin and Fakharian, 1996)

Because of the merit of the simple shear test, a simple shear box similar to those previously used in previous interface studies was developed. The shear box is shown in Figure 4.19. The plates were made out of aluminium. Thirty plates were used to form the "box". Each plate was 3mm thick and was coated with Teflon in order to minimise the friction between adjacent plates and between the bottom-most plate and the pile surface. During specimen placement, the plates were aligned using two pins that were inserted into two holes located at two diagonal corners. Before shearing commences, the pins were removed to allow simple shear to occur in the specimen. The aluminium plates were 30mm wide and were designed to be sufficiently stiff in the horizontal plane in order to withstand the lateral stresses in the specimen caused by the applied normal stress.

Whilst similar simple shear boxes have been used successfully in quasi-static interface tests, preliminary testing using the simple shear box showed that it was unsuitable for dynamic interface tests. Trial tests showed that the inertia of the plates imparted to the plates by the moving pile caused the plates to be displaced in a disorderly manner. Also, it was found that the bottom-most plate jammed against the pile surface especially when a rougher pile surface was tested. Furthermore, as the specimen had already deformed with the movement of the shear plates, it could not be sheared in the other direction. Thus the use of the simple shear device did not allow a series of tests to be performed on any given clay specimen. As the clay

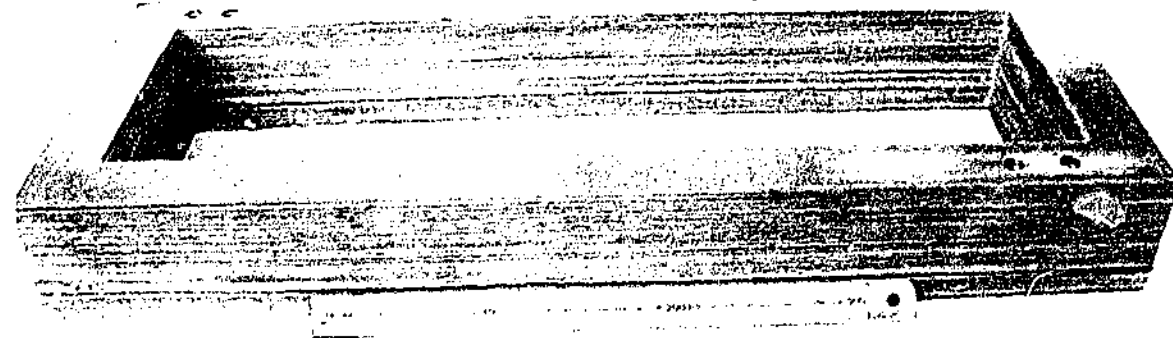


Figure 4.19 Simple shear box: stack of aluminium plates

specimens took a considerable amount of time to fabricate (as described in a later chapter), this became an issue of efficiency of the test program.

Because of these practical limitations, the direct shear box was adopted instead to perform the interface tests. The shear box is shown in Figure 4.20. The direct shear box allows the soil specimen to be tested in both directions and hence allows a maximum number of tests to be performed on a single specimen. It can also be lifted slightly above the pile surface to avoid friction between the pile surface and the shear box. It is acknowledged that the specimen subjected to the direct shear mode cannot simulate the pure shear mode. However, the error associated with the shear mode probably has little effect on the *ratio* of the dynamic strength to the static strength, which is the parameter that is of primary interest to the current study.

During testing, the shear box was lifted above the pile surface in order to prevent friction between the shear box and the pile surface. The small gap caused a small amount of soil to be lost during testing. As mentioned previously, in any system where friction between the “container” of the soil specimen and the pile surface is to be avoided, the loss of soil is inevitable.

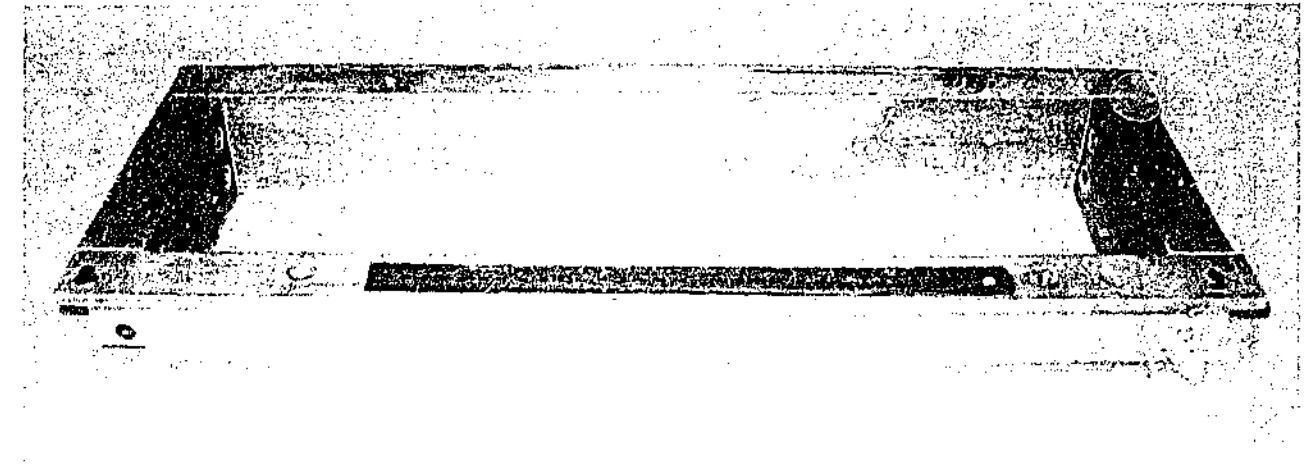


Figure 4.20 Direct shear box

4.1.1.9 Shear box restraint

Preliminary testing showed that just as in the conventional direct shear test, the shear box tended to rotate during shearing such that one end of the box lifted up significantly, causing a loss of sample, whilst the other end came in contact with the pile surface, causing friction. Therefore the shear box was fixed in its initial position and lifted up to maintain a small clearance above the pile surface using four restraints – a pair on each side of the shear box. Schematics of the restraints have been shown in Figure 4.4 and Figure 4.6, and a photograph of the restraints is shown in Figure 4.21.

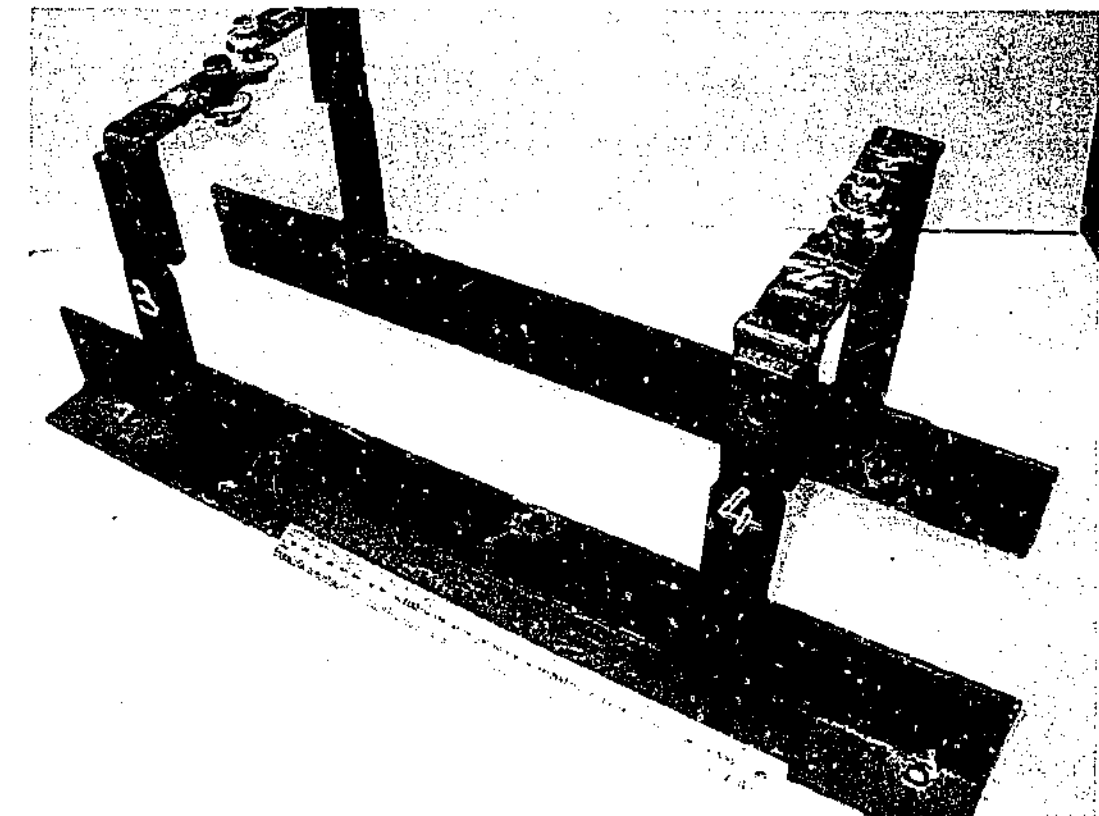


Figure 4.21 Shear box restraints

4.5 Data Acquisition

The data acquisition system was based on the following:

- A Pentium II 400MHz PC with a 32-bit analog
- A signal-conditioner with modules for the dynamic load cell, the accelerometer, the LVDTs
- A digital input/output data acquisition card. The card allows at a maximum of 40kHz sampling rate for each of the channels.
- A software specially written based on HP-VEE[®] data acquisition language.

For the dynamic tests, a sampling rate of 10kHz was found to be sufficient. The high-speed data acquisition system was activated using a physical trigger. The trigger was activated when the control button of the high-speed actuator was depressed. The data were displayed on the screen in the form of graphs in real time for quasi-static tests and immediately after the test was conducted for each dynamic test.

Table 4.1 summarises the data acquisition devices used, their locations, the measured parameters, and the calculated parameters based on the measurements. Photographs of the data acquisition devices are shown in Figure 4.22 and Figure 4.23.

The Instron[®] load cell for measuring the normal load was not a truly dynamic load cell with limited capabilities in measuring very transient forces. It will be discussed in Chapters 5 and 7 that the fluctuation in the normal load for the tests involving the sand specimens could be severe and the fluctuation for the tests involving the clay specimens was minimal. (This is because the physically stiffer sand specimen has a stiffer vertical displacement response.) Whilst the load cell was sufficiently adequate for the measurement of the reasonably constant normal load in the tests involving the pile-clay interface, the limitation of the load cell caused a complication in the analyses of the pile-sand interface test results, which will be discussed and addressed in Chapter 5.

The velocity of the carriage and the pile was obtained by integrating the acceleration record with respect to time. It was usually necessary to apply controlled corrections to the acceleration record (by a constant value) so that the computed velocities were zero at the start and the end of each event.

Table 4.1 Data acquisition devices, their locations, measured parameters and parameters computed based on the measured parameter

Device	Location	Measured Parameter	Deduced Parameter
M224C ICP PCB [®] dynamic load cell (112kN compression, 36kN tension)	Located between new carriage and high-speed actuator. One end of the load cell is fixed to the ram, and the other end is free	Dynamic load (for dynamic test)	Subtracting product of acceleration and the sum of masses of pile and moving steel plate from the dynamic force to obtain dynamic interface force
Instron [®] load cell (+/-250kN)	Fixed between old carriage and horizontal (slow-speed) actuator	Shear load (for quasi-static test)	NA
Instron [®] load cell (+/-250kN)	Fixed between vertical piston and vertical actuator	Normal load	NA
ICS [®] accelerometer (+/-50g)	Attached to carriage	Pile acceleration	<ul style="list-style-type: none"> • Integrating pile acceleration to obtain pile velocity • Subtracting product of acceleration and the sum of masses of pile and moving steel plate from the dynamic force to obtain dynamic interface force
Lucas Shaevitz [®] LVDT (+/- 125mm)	Rod attached to carriage	Pile displacement	<ul style="list-style-type: none"> • Differentiating pile displacement to obtain pile velocity • Differentiating pile displacement twice to obtain pile acceleration
Lucas Shaevitz [®] LVDT (+/- 7.5mm)	Fixed on loading platen, with rod against surface of carriage	Vertical displacement of sample	NA

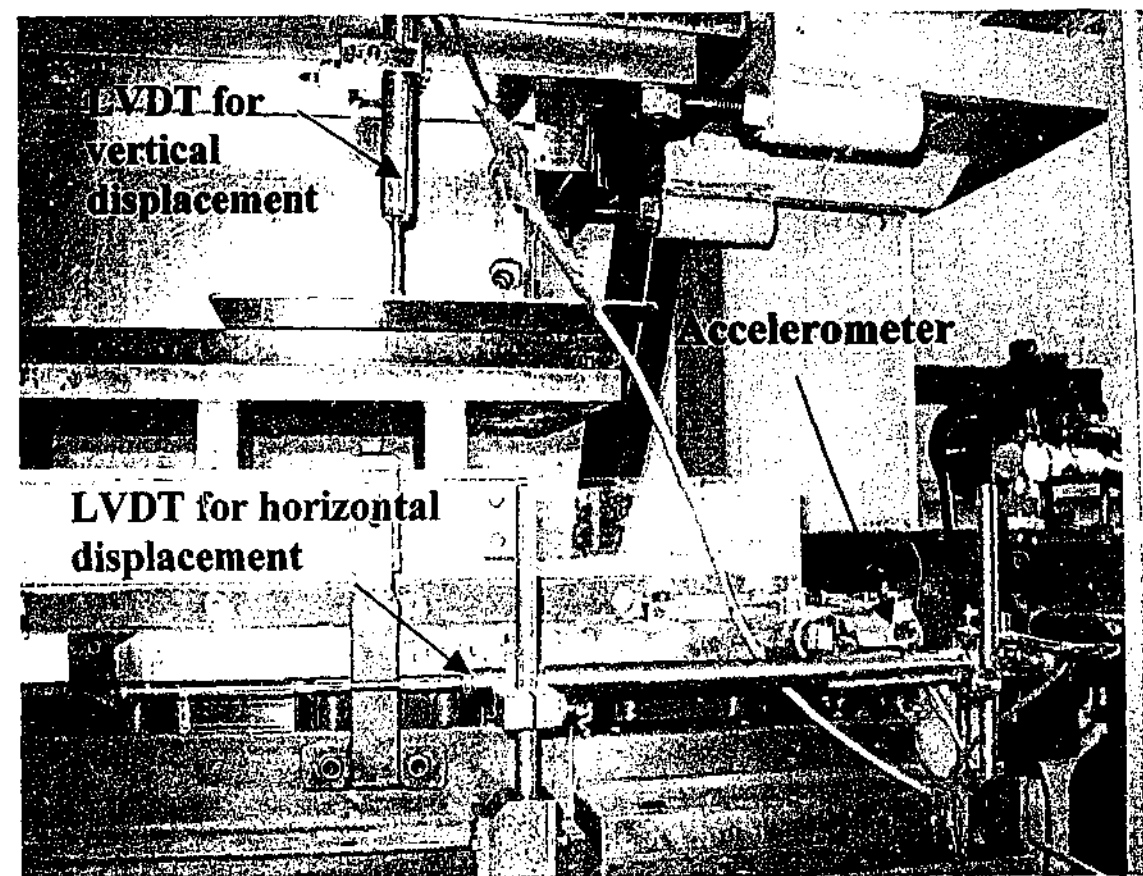


Figure 4.22 Some data acquisition devices

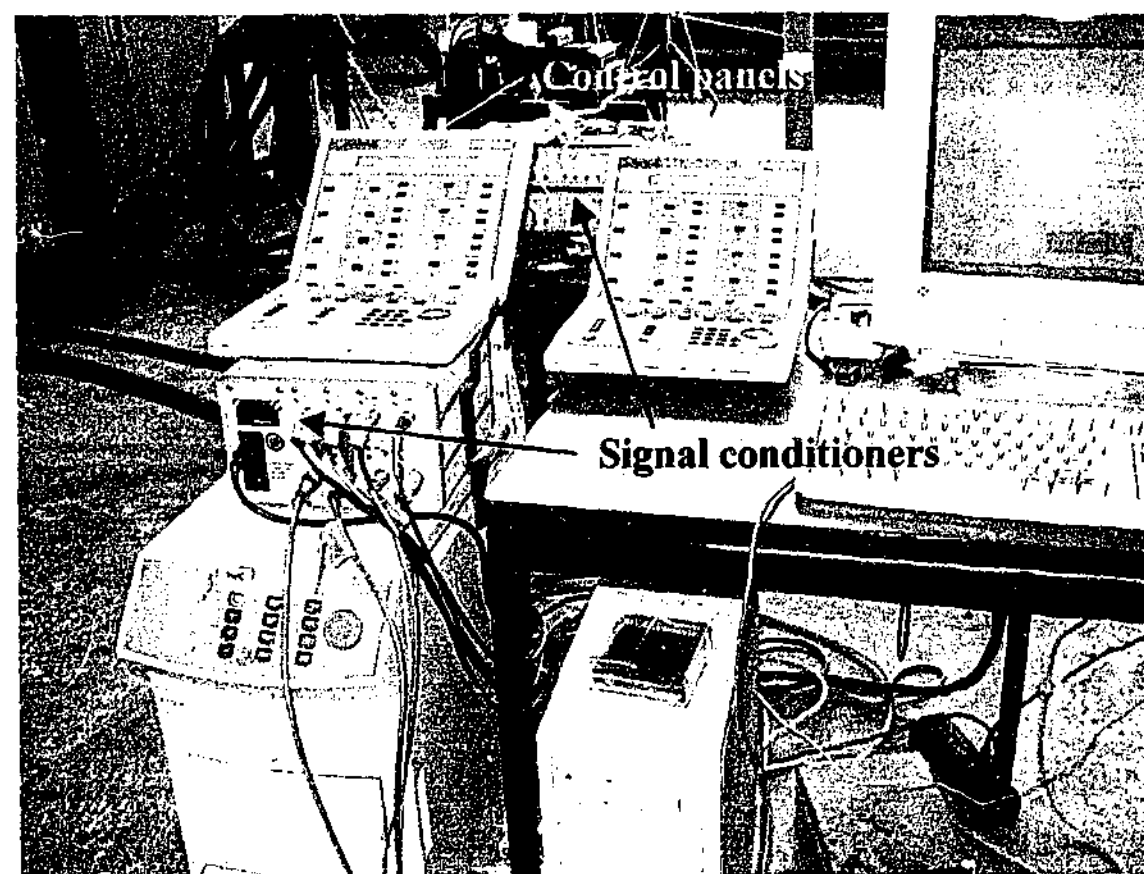


Figure 4.23 Control and data acquisition systems

An accelerometer with a high shock capacity typically has a high measuring range and thus (relatively) low resolution. Thus, the choice of a suitable accelerometer was based on a compromise of the shock capacity and the resolution of the data. Whilst a high shock capacity was required to withstand the shock load, an accelerometer with a relatively small capacity was required to give high-resolution data. After experimenting with different several piezoresistive accelerometers, a Model 3058-50 ICS[®] piezoresistive silicon accelerometer was chosen for its 50g capacity and high shock capacity of 1000g. High shock resistance and built-in damping were achieved in the silicon accelerometer by adding silicon caps to the top and bottom of the piezoresistors (MSI, 2000).

4.6 Validating Shear Device

The reliability of the accelerometer was verified by integrating the measured pile acceleration with respect to time in order to obtain velocity and comparing the velocity to that obtained by differentiating the displacement obtained with the LVDT.

The reliability of the dynamic load cell was checked by conducting a special series of tests. Tests were performed without any interface resistance during which the dynamic force imparted by the actuator to the carriage and the acceleration of the carriage were measured. The imparted dynamic load was found to be equal to the inertial force of the carriage throughout the event except of course when the load cell lost contact with the carriage. This test not only served to confirm that the dynamic load cell was obtaining reliable measurements but also that the friction in the bearings of the light carriage system was sufficiently low.

As noted in Table 4.1, the dynamic interface friction was deduced based on:

$$F_{actuator} - R_{interface} = m_{carriage} a_{carriage} \quad (4.1)$$

where $F_{actuator}$ is the force imparted by the actuator to the carriage, $R_{interface}$ is the interface resistance, $m_{carriage}$ and $a_{carriage}$ are the mass and acceleration of the carriage and the pile which was attached to the carriage. This relationship was verified by the previous test where it was shown that the inertial force was equal to the measured

dynamic force between the actuator and the carriage when there was no interface friction. The relationship was further verified by two additional tests.

- Quasi-static and dynamic tests were performed on a timber-steel interface. Given that no viscous damping is expected for this interface, the deduced “dynamic” friction should be equal to the measured friction measured at a low shear rate.
- Quasi-static and dynamic tests were performed on a clay-pile interface. Given that clay had been reported to exhibit viscous damping behaviour, it was expected that the pile-clay interface friction would increase at high rates; indeed, the computed dynamic interface friction was found to be proportional to the shear rate. In addition, the computed dynamic friction decreased to the quasi-static friction as the instantaneous shear rate reduced to near-zero.

4.7 Sample Test Output

A sample of the processed data from a dynamic pile-clay test obtained using the data acquisition system is shown in Figure 4.24. The record consists of 3 plots that are labelled alphabetically.

Graph A shows:

- the dynamic force which is measured by the dynamic load cell interfaced between the ram and the carriage (labelled F_{ram})
- the inertial force of the carriage and the pile section (labelled $F_{inertial}$)
- the normal force at the interface (labelled F_{normal})

Graph B shows:

- the acceleration of the pile section (labelled Pile acceleration)
- the velocity of the pile section (labelled Pile velocity)

Graph C shows:

- the displacement of the pile (labelled Pile displacement)
- the vertical displacement of sample (labelled Vertical displacement)

FILENAME BALLR.SC 250 INITIAL NORMAL STRESS 250 kPa
PILE Smooth concrete
CLAY BallR

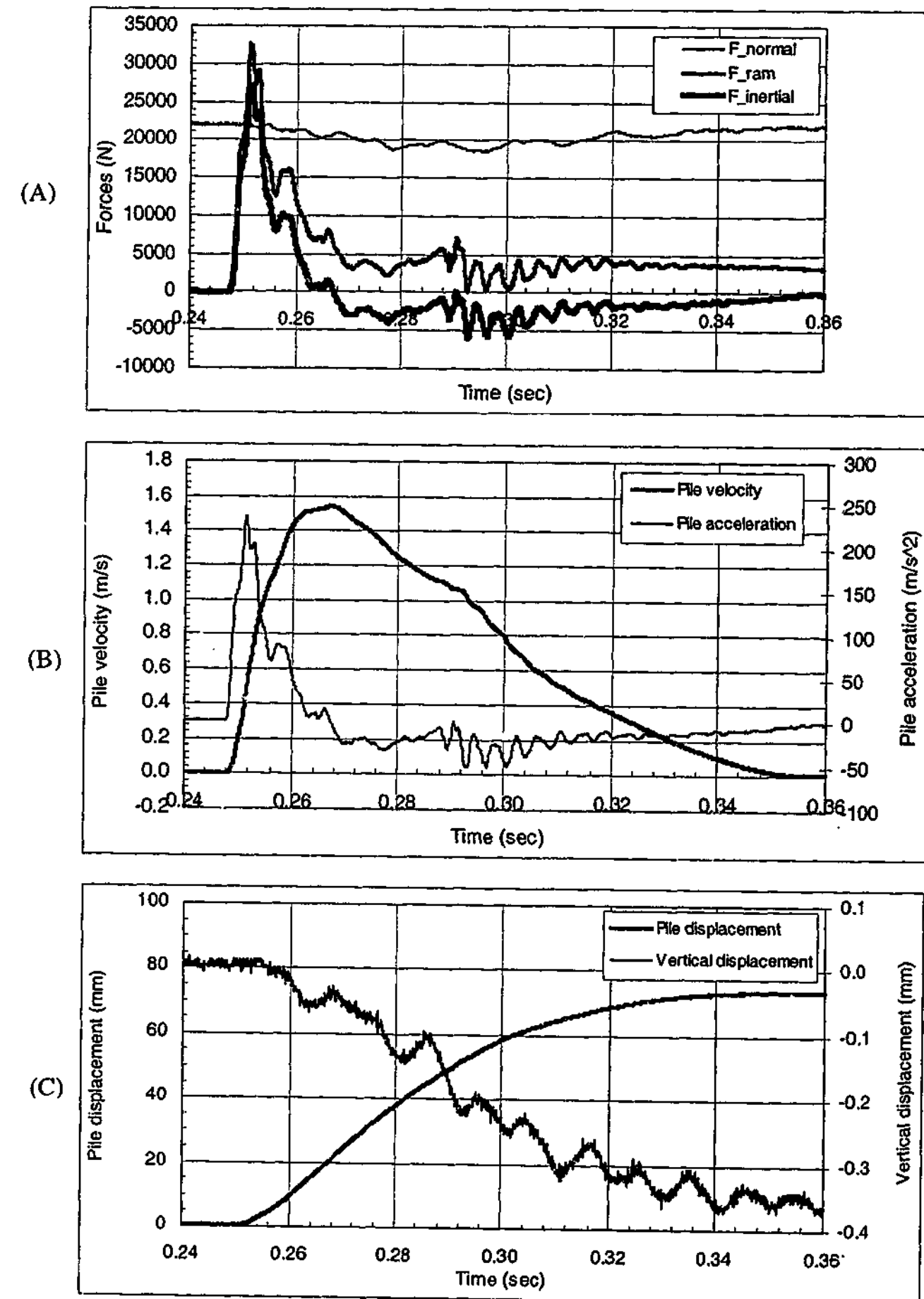


Figure 4.24 A sample record showing measured parameters for a dynamic test

As mentioned earlier, the specimen was loaded under constant normal load using the vertical actuator which was operated under a closed loop system. As shown in Graph A, the applied normal load varied and fluctuated slightly during the event. In general, based on numerous tests performed in the test programme, it was found that the fluctuation in the normal load was most severe when the vertical movement of the sample was most drastic such as that for a sand specimen sheared against a rough concrete pile (where the sample rode up and down the large asperities of the surface). It was also found that the fluctuation in the normal load for the tests involving the sand specimens was significantly more severe than those involving the clay specimens because of the stiffer vertical displacement response of the physically stiffer sand specimens.

The fluctuation could be due to either the closed-loop system not being able to maintain the designated constant normal load during the dynamic event, or to the transient inertia of the steel assembly that was the means by which normal load was applied on the sample, or both. The transient inertial force of the assembly was caused by the vertical movement of sample during the dynamic event and was additional to the normal load applied by the closed-loop system. To determine the source of the observed fluctuation in the normal load, a series of dynamic tests was performed whereby the normal load on the sample was applied using dead weight rather than the closed-loop system. It was found that the normal load in these tests fluctuated in a similar manner to that in the tests performed using the closed-loop system, and therefore, it was concluded that the fluctuation in the normal load was caused primarily by the inertia of the assembly rather than poor control of the closed-loop system.

As expected, it is observed in Graph A that the dynamic force (measured by the load cell) and the inertial force (given by the product of the acceleration measured by the accelerometer and the mass of the carriage) were in phase with each other.

As previously discussed, due to practical constraints, the tension force could not be measured by the dynamic load cell. For the particular case of the presented sample record, the load cell did not lose contact with the carriage. In cases where the interface resistance was relatively low, the load cell tended to lose contact with the

carriage momentarily before coming in contact again. As mentioned earlier, this limitation did not prevent sufficient dynamic force data to be obtained from a test event.

It can be observed in Graph A that the deduced interface resistance record had unexpected peaks which corresponded to the drastic changes in acceleration which occurred when the carriage was accelerated from zero velocity to peak velocity. These peaks were due to the lack of exact correspondence between the dynamic force (as measured by the dynamic load cell) and the acceleration (measured by the accelerometer). Although the devices were synchronised electronically, it was difficult in practice to achieve perfect synchronisation. The poor resolution was also due to the error resulting from subtracting the relatively large inertial force (the product of mass and acceleration) from the comparably large dynamic force. In theory, this error could be minimised by having a carriage with low mass; however, as explained previously, it was not possible to have a lighter carriage because of the over-riding requirement for robustness.

Because of the loss of sample (which decreased the thickness of the sample), the measurement of the vertical displacement of the specimen could not reveal whether the specimen was contracting or dilating. Thus this measurement was not considered to be significant. In any case, it is noted in Graph C that the LVDT measurement of the vertical displacement of the specimen did not have a high resolution; this is because the LVDT did not have a high frequency response and had a high effective stroke of 50mm relative to the measured quantity.

4.8 Concluding Remarks

This chapter has discussed the development of a purpose-built interface shear device for performing quasi-static and dynamic shear tests on pile-soil interfaces. The capabilities and the components of the shear device have been described. The steps that have been taken to verify that the device is effective and that reliable data can be obtained have been presented.

The design, development, fabrication, implementation, progressive modification and validation of the dynamic shear testing apparatus was a major undertaking, and consumed approximately 20 months of effort before experimental results could be obtained. This therefore represented a significant component of the doctoral works.

The results of the quasi-static and dynamic tests will be presented in the following chapters.

Chapter 5

5. Quasi-Static & Dynamic Pile-Sand Interface Behaviour: Test Procedures, Results & Analysis

5.1 General

Using the experimental apparatus described in the previous chapter, dynamic and quasi-static shear tests were performed on pile-sand interfaces. This chapter describes the experimental programme and the test procedures adopted in conducting the quasi-static and dynamic tests, and reports and discusses the results of the quasi-static and dynamic pile-sand interface tests.

The quasi-static behaviour of the pile-sand interface has been well-established in previous studies. However, as discussed in Section 3.4, there has been little research conducted on the dynamic response of the pile-sand interface. Thus, the test programme was designed to investigate the effect of shear rate on the pile-sand

interface angle of friction for interfaces involving various soil properties, pile surface characteristics and applied normal stresses. Quasi-static interface tests were also performed to obtain the interface static friction angle with which to normalise the interface dynamic friction angle.

It is important to note that the dynamic interface friction angle is associated with large-displacement, residual or the critical state where shearing occurs with no volume change. Therefore, only the residual (rather than the peak) soil and interface friction angles are of practical significance in this study.

5.2 Quasi-Static & Dynamic Shear Rates

In order to investigate the effect of shear rate on the interface friction angle, tests were conducted at slow and fast rates. The quasi-static tests were conducted at 0.01mm/s which was the lowest speed the electro-hydraulic actuator was capable of delivering.

As discussed in Section 4.1.1.5, although the dynamic actuator was designed to achieve peak velocities in excess of 5.0m/s, the requirement to minimise the shock load from stopping the actuator meant that only significantly peak velocities of up to 2.0m/s were used.

5.3 Test Programme – Static & Dynamic Tests

50WS, 8/16, Mix4 and Yea sands of various gradings, particle shapes and particle sizes were tested. The Mix4 sand was obtained by mixing poorly graded 50WS, 8/16, 16/30 and 30/60 sands. The 50WS, 8/16, 16/30 and 30/60 sands were obtained from a specialist supplier and were quality-controlled, whilst the Yea sand was obtained from a quarry. The soil properties of the sands are tabulated in Table 5.1. The particle shape description of the sands was based on SAA HB.21. – 1998 (Standards Australia, 1998). The grading curves for the various sands are shown in Figure 5.1.

In order to investigate the effect of grain size on the dynamic interface response, sand samples with a wide range of particle sizes (shown in Table 5.1) were tested. To determine the effect of grading on the dynamic interface response, well-graded Mix4

Table 5.1 Soil properties of sands

Sand type	Particle shape	Effective size D_{50} (mm)	Uniformity coefficient D_{60}/D_{10}
50WS	Rounded to sub-rounded	0.26	1.88
8/16	Rounded to sub-rounded	1.55	1.45
Mix4	Rounded to sub-rounded	0.54	2.96
Yea	Angular	0.60	5.53

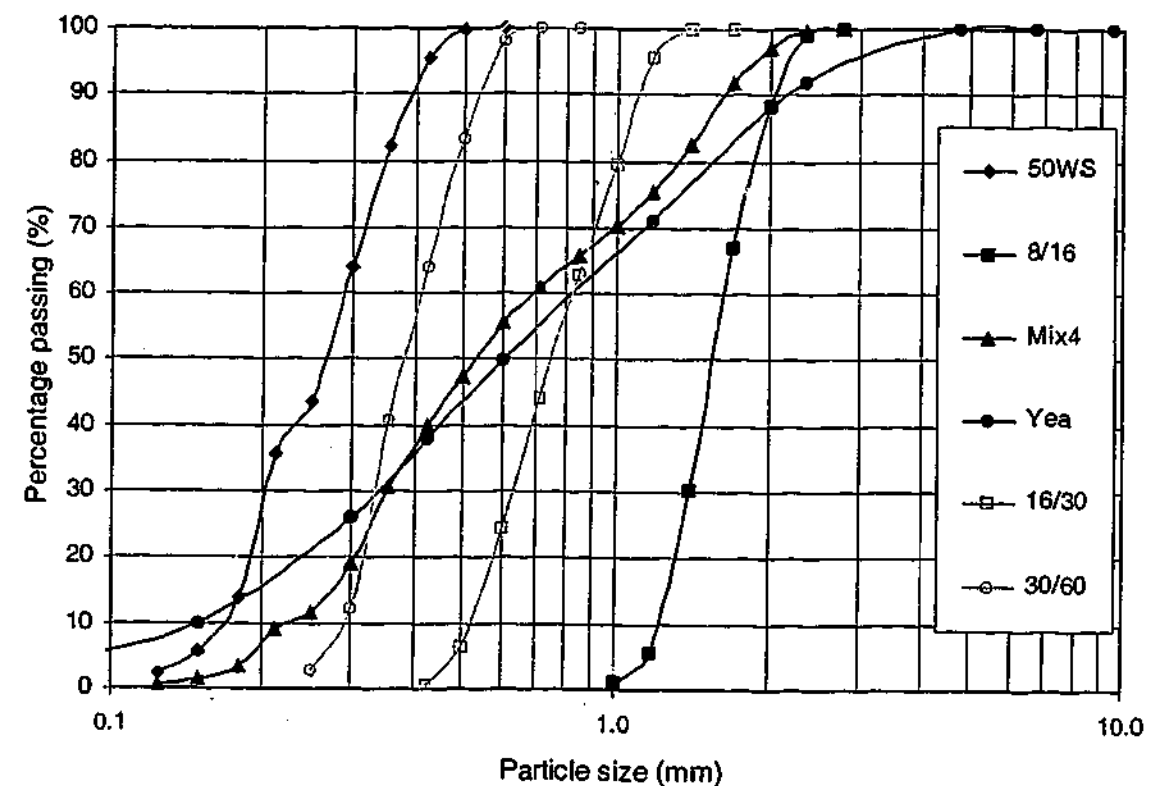


Figure 5.1 Gradings of sands tested in the experimental programme

and Yea sands and poorly graded 50WS and 8/16 sands were tested. The effect of particle shape on the dynamic interface response was also investigated by testing round-subrounded and angular sands. The effect of saturation was investigated by testing a saturated 50WS sample on a pile surface immersed in a bath of water.

A smooth concrete surface and a rough concrete surface were tested to investigate the effect of roughness on the dynamic response at the interface. These surfaces are shown in Figure 5.2 and Figure 5.3. The descriptions of the material and surface roughness of the pile surfaces are given in Table 5.2. The smooth concrete surface was achieved by casting the concrete against smooth wood panels, with no grain, and the rough concrete surface was obtained by trowelling the concrete surface

immediately after the concrete was poured. The effect of a wet pile surface was also investigated where the pile surface was immersed in a bath.

Table 5.2 Description of piles used in the tests

Pile type	Description	Surface Roughness
Smooth concrete	Surface obtained by casting on smooth timber form (no grain)	Very smooth
Rough concrete	Surface obtained by trowelling after concrete was poured	Rough

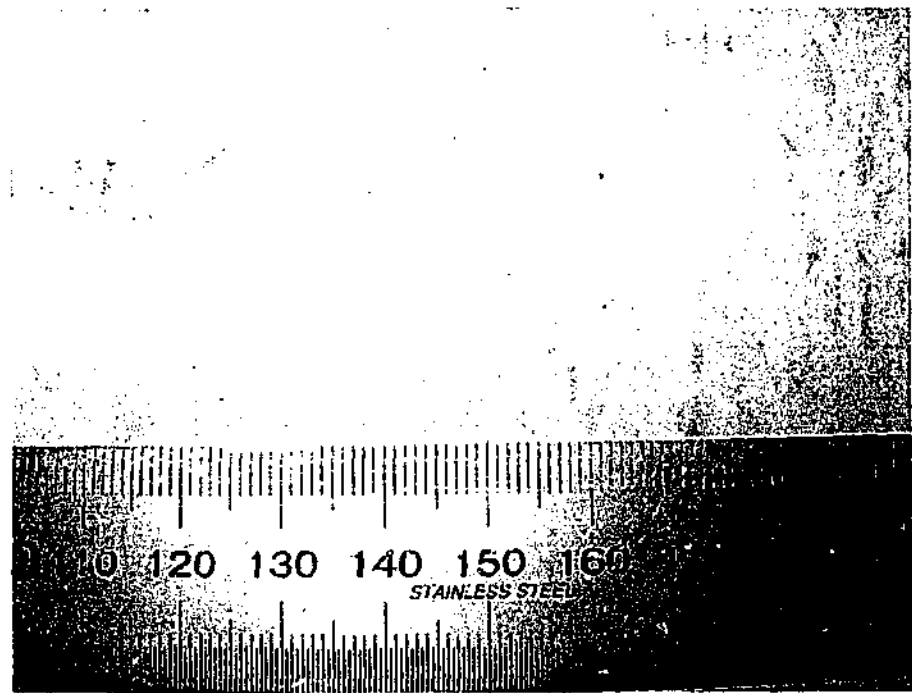


Figure 5.2 Plan view: Surface of smooth concrete pile

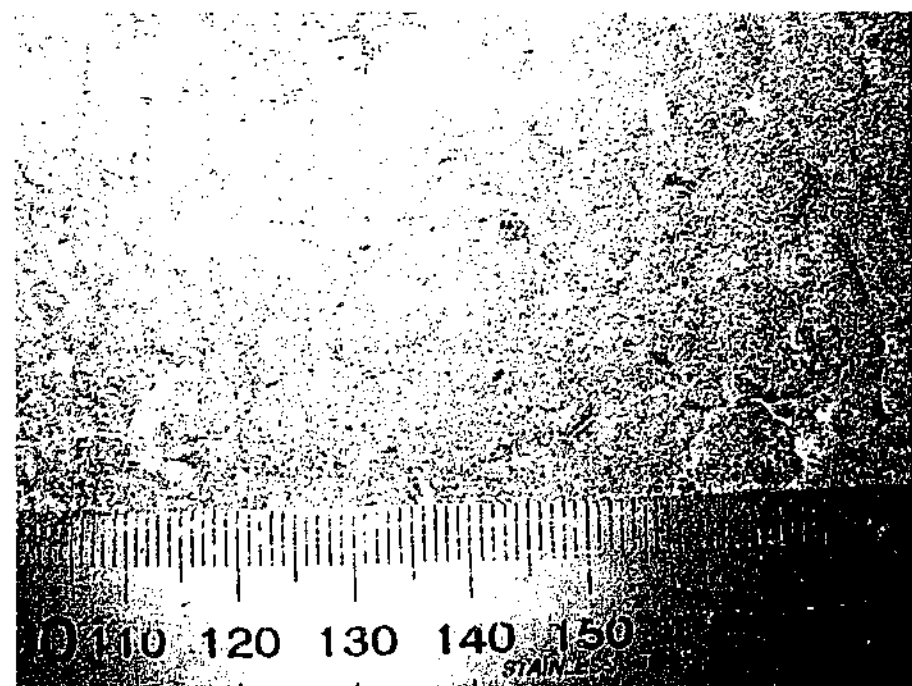


Figure 5.3 Plan view: Surface of rough concrete pile

The interface tests were carried out at normal stresses of 50kPa, 150kPa and 250kPa to replicate stresses acting on a field pile.

In the test programme, each type of sand needed only to be prepared at one density, as discussed subsequently. For samples prepared at the critical void ratio or above the critical void ratio (which hence have low density), the soil-only and pile-sand interface strengths reach residual state immediately so that it is not meaningful to distinguish between the peak friction angle and the residual friction angle. On the other hand, for samples prepared at void ratios lower than the critical value (and hence compacted and have greater density), the soil-only and pile-sand interface strengths peak before decreasing to the residual values. It has been well-established that whilst the peak soil and interface friction angles are dependent on the initial density of the sample, the residual soil and interface friction angles are independent of the initial density (e.g. Head, 1994; Al-Douri and Poulos, 1991). This is because the void ratio changes to the critical value as the sample is sheared from the peak strength to the residual strength. As a consequence, for any given sample prepared at different initial densities and subjected to either soil-only or interface testing, the same residual soil friction angle (ϕ_r) or residual interface friction angle (δ_r) will result (Turner and Kulhawy, 1990; Lehane et al., 1993; Jardine and Chow, 1996). Dynamic testing and pile driving event, involve large shear displacements such that only the residual soil friction angle (ϕ_r) and the residual interface friction angle (δ_r) are of practical significance. Thus for the purpose of investigating the dynamic response of pile-sand interfaces involving large displacements, each type of sand need only be prepared at one density. The poorly graded 50WS and 8/16 sands, which in any case could not be significantly densified, were therefore tested at the critical void ratio or at void ratios above critical state. The well-graded Mix4 and Yea sands were also tested at the critical void ratio or at void ratios above critical state, even though it would have been possible to subject them to greater compaction.

The testing programme for the quasi-static and dynamic pile-sand interface tests, which incorporates the various parameters to be tested, is summarised in Table 5.3.

Table 5.3 Test programme for quasi-static and dynamic pile-sand interface tests

Sand type	Pile surface	Normal stress (kPa)
50WS	Smooth concrete	250
		150
		50
	Rough concrete	250
		150
		50
Saturated 50WS	Smooth concrete	250
		150
		50
8/16	Smooth concrete	250
		150
		50
	Rough concrete	250
		150
		50
Mix4	Smooth concrete	250
		150
		50
	Rough concrete	250
		150
		50
Yea	Smooth concrete	250
		150
		50
	Rough concrete	250
		150
		50

5.4 Test Procedures

5.4.1 Sample preparation

Sand was rained into the shear box from a constant height using a raining device shown in Figure 5.4. The rainer had the same plan dimensions as the shear box, measuring 555mm x 160mm, and was built up at its four sides to contain the sand sample. It consisted of two perforated plates; the top plate was fixed whilst the bottom part could slide in and out. Sand was dropped into the shear box when the holes of the plates coincided as the bottom part was slid out. The rainer was extended downward by plastic sheets into the shear box to prevent fine particles from escaping when the sample was dropped. The height at which the sand was dropped could be adjusted by moving the rainer vertically along the four support rods. However, since the initial density of the sample does not affect either the residual soil friction angle or the residual interface friction angle, the drop height was fixed at 50mm for convenience. In any case, trial tests revealed that the density of the sand prepared using the pluviation device and vibration was repeatable as shown by the small variations of the densities of the samples, which are tabulated in Table 5.5. Once the sand sample was prepared, its top surface was levelled off using a template shown in Figure 5.5, and the density of the sample was measured.

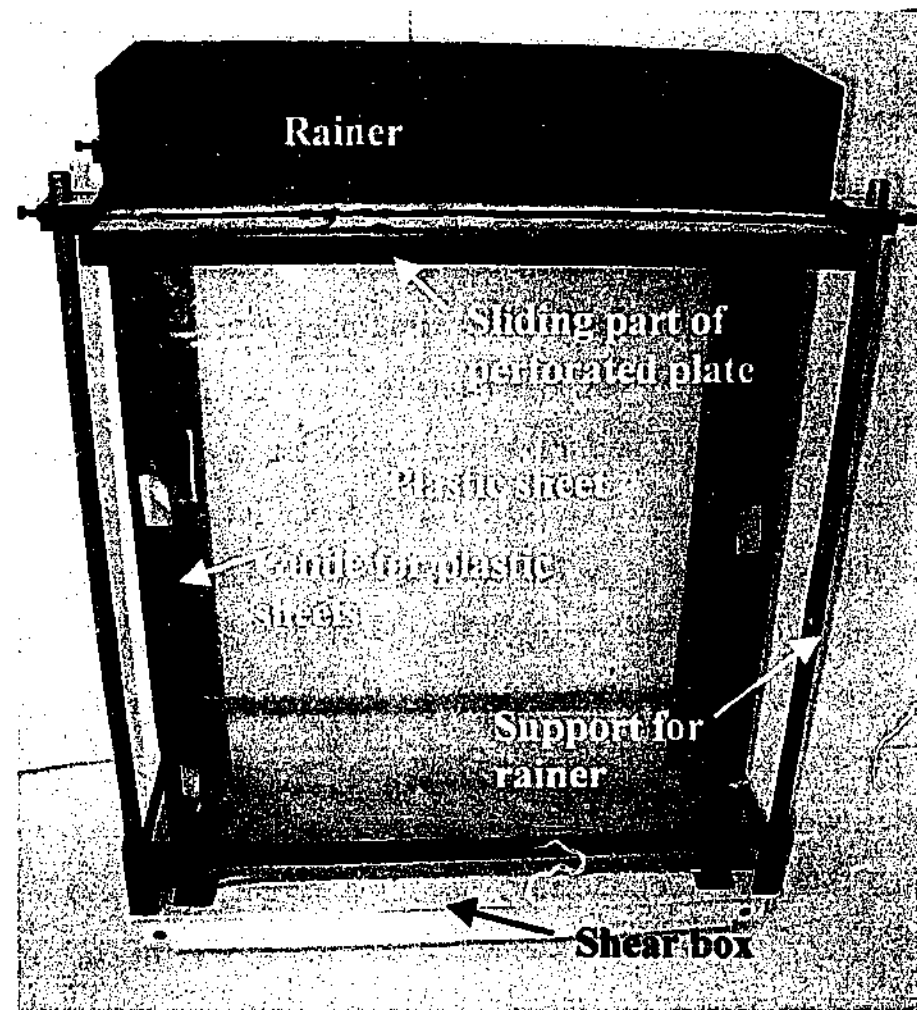


Figure 5.4 Rainer device used for pluviating the sand

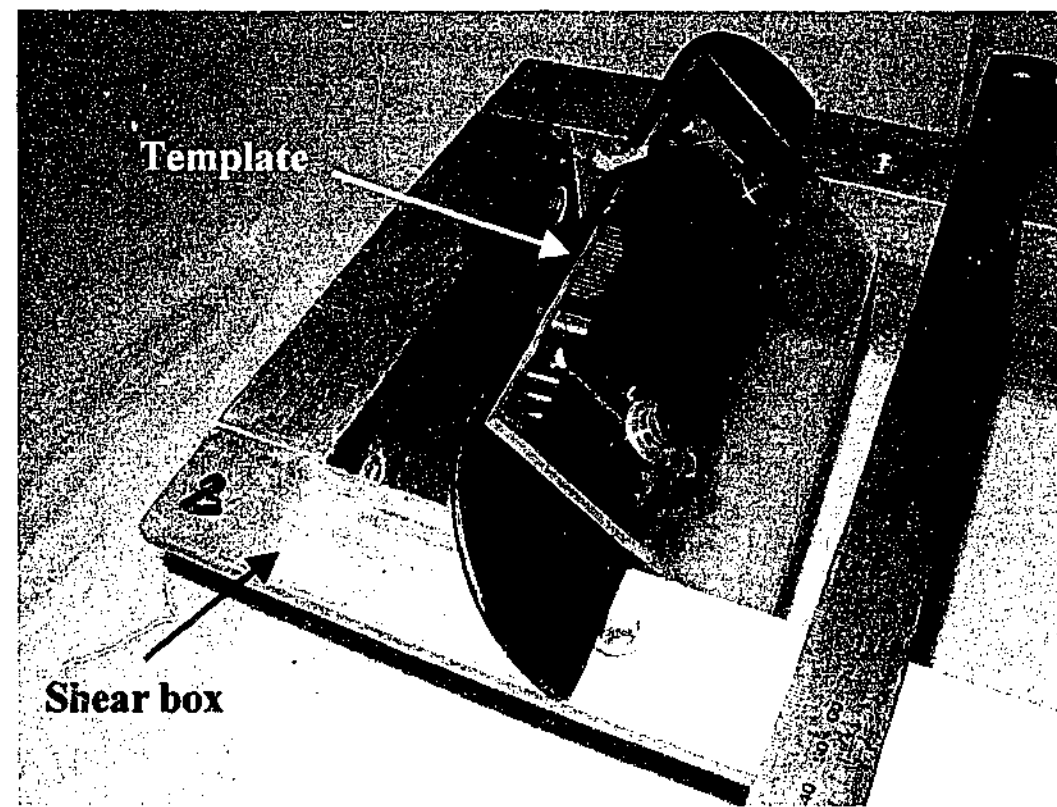


Figure 5.5 Leveller

The preparation of the saturated 50WS sand and the pile surface was different from the rest of the tests. For the former, water was poured onto the pile surface, which was contained in a bath formed by the Perspex sheets built up on four sides of the pile. The 50WS sample was saturated in a container of water and placed into the shear box and onto the pile, and levelled. Being saturated, the sample was dense and had a relatively consistent density with an average of 1950kg/m^3 .

5.4.2 Soil-only tests

Sand-only shear tests were conducted using the standard direct shear device in order to characterise the strengths of the sand samples subjected to the interface tests. It is thus noted that the soil-only tests and the interface tests were conducted with different devices. Since all the samples tested do not exhibit peak strength behaviour (because they were prepared at the critical void ratio or above the critical void ratio), it was not necessary to test a newly prepared sample in each test for the peak strength. Thus, the multi-stage testing procedure outlined in Head (1994) was adopted, where the same sample was subjected to different tests. Normal stresses of 50kPa, 150kPa and 250kPa applied during the direct shear box tests were the same as those applied in the interface tests in order to replicate the strengths of the samples tested in the interface tests. The shear rate of the direct shear box test was selected at 0.01mm/s to correspond to the shear rate adopted for the quasi-static interface test.

5.4.3 Interface tests

The shear box was placed in a central position on the pile section. The sand was rained into the shear box and onto the pile. The pile-shear box assembly was then transferred to the rig and bolted onto the carriage. Four 1.0mm thick packers were slid in between the shear box and the pile surface at the four corners of the box to lift the shear box clear of the pile surface. The four restraints described in Section 4.1.1.9 were used to fix the position of the shear box, a pair on each side of the shear box, after which the packers were removed. These restraints were used to prevent the rotation of the shear box during testing, and to maintain a small clearance above the pile surface so that friction between the shear box and the pile surface was eliminated.

The vertical loading platen was lowered slowly into the shear box, after which it was allowed to settle under its own self-weight (which for the sample size was the equivalent of about 40kPa). The normal stress was incremented at a rate of 1.1kPa/sec from the current stress imposed by the self-weight until the target stress was achieved. Once the target normal stress was attained, the target stress was held for 1 minute. Under the applied normal stress, the pile-sand interface was sheared by moving the carriage using the actuator.

5.4.3.1 Quasi-static tests

The static tests were performed in the “static configuration” of the shear rig, which has been described in detail in Section 4.4.2. Under a certain applied normal stress, the pile-sand interface was sheared by moving the carriage using the actuator at a slow rate of 0.01mm/s monotonically.

The preparation of the sample and the assembling of the pile-soil sample onto the purpose-built shear device were time-consuming. Therefore, as with the soil-only tests, multi-stage testing was performed, based on the principles of the multi-stage standard (soil-only) direct shear testing outlined in Head (1994). In the first stage, a normal stress of 250kPa was applied and the interface was sheared until the residual value was reached (which required a shear displacement of less than 5mm). When the test was completed, the normal stress was removed. In the second stage, the same procedure was carried out but a normal stress of 150kPa was applied instead. In the third stage, a normal stress of 50kPa was applied. The sample was tested with normal stresses in the order of 250kPa, 150kPa and 50kPa in an attempt to keep the densities during the 3 stages as identical as practically possible. The same sample was used for the tests conducted at the three different normal stresses. The sample was only replaced when tests were to be performed on a different pile interface. Typical shear stress-shear displacement behaviour of the pile-sand interface and a summary of the results of all the pile-sand interface tests undertaken will be presented in Section 5.5.1.

5.4.3.2 Dynamic tests

The dynamic tests were performed in the “dynamic configuration” of the shear rig, which has been described in detail in Section 4.4.2. Under a certain applied normal stress, the pile-sand interface was sheared by pushing the carriage using the high-speed actuator at shear rates up to 2.0m/s and over a typical designated stroke of 90mm.

As with the quasi-static tests, the same sample was used for the tests conducted at different normal stresses and the sample was only replaced when tests were to be performed on a different pile interface. Tests were carried out with normal stresses in the order of 250kPa, 150kPa and 50kPa. At the end of each test, the actuator (and the carriage) was reversed to its original starting position at a slow rate of approximately 50mm/s while maintaining the normal stress on the interface, in order to perform the subsequent test on the same sample. The reversal of the pile to its starting position, which was a practical necessity for the interface to be tested repetitively, may be justified on the basis that piles rebound during driving. A sample record of the dynamic pile-sand interface test will be presented and discussed in Section 5.6.2.

For dynamic tests involving a saturated sand sample and the smooth concrete pile immersed in a bath of water, a foam material was used to cover the opening above the pile surface to prevent splashing of water during testing.

5.4.3.3 Observations of specimens

Since the surface roughness has a significant influence on the interface friction angle, the smooth concrete surface was constantly monitored during testing so that the concrete could be replaced with a new specimen when there was noticeable abrasion. After all the tests on a particular interface were completed, the sand grains at the interface were observed for signs of particle crushing.

5.4.3.4 Discussion

As discussed in Section 4.1.1.8, there was an inherent difficulty in the testing of an interface between a solid material and soil. If the shear box containing the soil was clamped onto the pile surface to prevent loss of sample, significant friction between

the shear box and the pile surface would lead to erroneous measurement of the interface friction. On the other hand, if the shear box was lifted above the pile section to prevent friction, sample would be lost through the clearance. In the tests performed in this study, the latter option was chosen. Sand grains were inevitably lost through the gap during shearing of the interface, at the two ends of the shear box. The amount of sample lost depended on the size of the sand grains and the clearance between the bottom edge of the shear box and the pile section. When testing smooth piles (i.e. the smooth concrete and steel), the clearance was minimised to less than 1mm, whilst when testing rough piles (very rough concrete pile), lifting up the shear box slightly to clear the top edge of the asperities of the pile left significant clearance. The loss could be quantified as the percentage of the mass of the lost sample to the mass of the initial sample. For the quasi-static test, the amount of sample loss was negligible as the test involved shear displacements of less than 5mm. For the dynamic test involving a shear displacement of up to 90mm, the percentages for the various scenarios are summarised in Table 5.4. The percentages show that the amounts of sample loss were insignificant. It is noted that the area associated with the ends of the shear box where the sample loss occurred was relatively small compared to the total area of the sample. Hence the sample loss was not expected to cause a significant percentage of error.

As discussed in Section 4.1.1.8, the direct shear box is known to introduce stress concentrations and non-uniform strain distributions in the sample. Since a simple shear box was found to be unsuitable for dynamic tests, this limitation was inevitable.

Table 5.4 Mass of lost sample as a percentage of mass of total sample

Pile-sand interface	Mass of initial sample (g)	Mass of lost sample (g)	Percentage loss (%)
Smooth pile-small particle sand (50WS)	6500	8	0.1
Smooth pile-big particle sand (8/16)	6500	Negligible	Negligible
Rough pile-small particle sand (50WS)	6500	27	0.4
Rough pile-big particle sand (8/16)	6500	15	0.2

5.5 Quasi-Static Interface Tests

5.5.1 Results

The shear stress-shear displacement behaviour of the Yea sand tested at normal stresses of 250, 150 and 50kPa is shown in Figure 5.6. The shear stress-shear displacement behaviour of the Yea sand sheared against the smooth concrete and rough concrete at normal stresses of 250, 150 and 50kPa are shown in Figure 5.7 and Figure 5.8. The results of all the quasi-static tests performed in the test programme are summarised in Table 5.5. Since the shear stress reaches residual state immediately as the shear stress peaks, no distinction is made between the peak and the residual values. The soil friction angle will simply be referred to as ϕ , and the interface friction angle as δ .

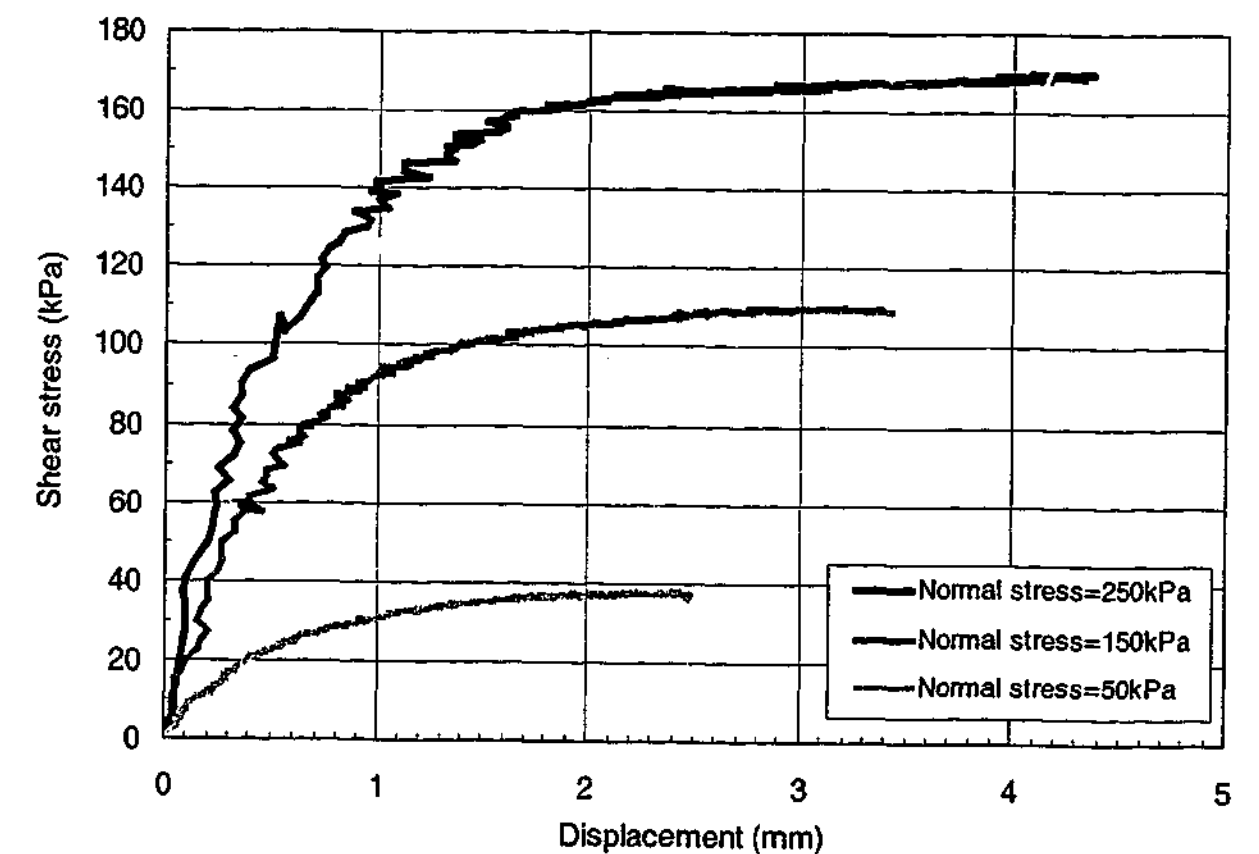


Figure 5.6 Shear stress-shear displacement responses of Yea sand tested at 3 normal stresses

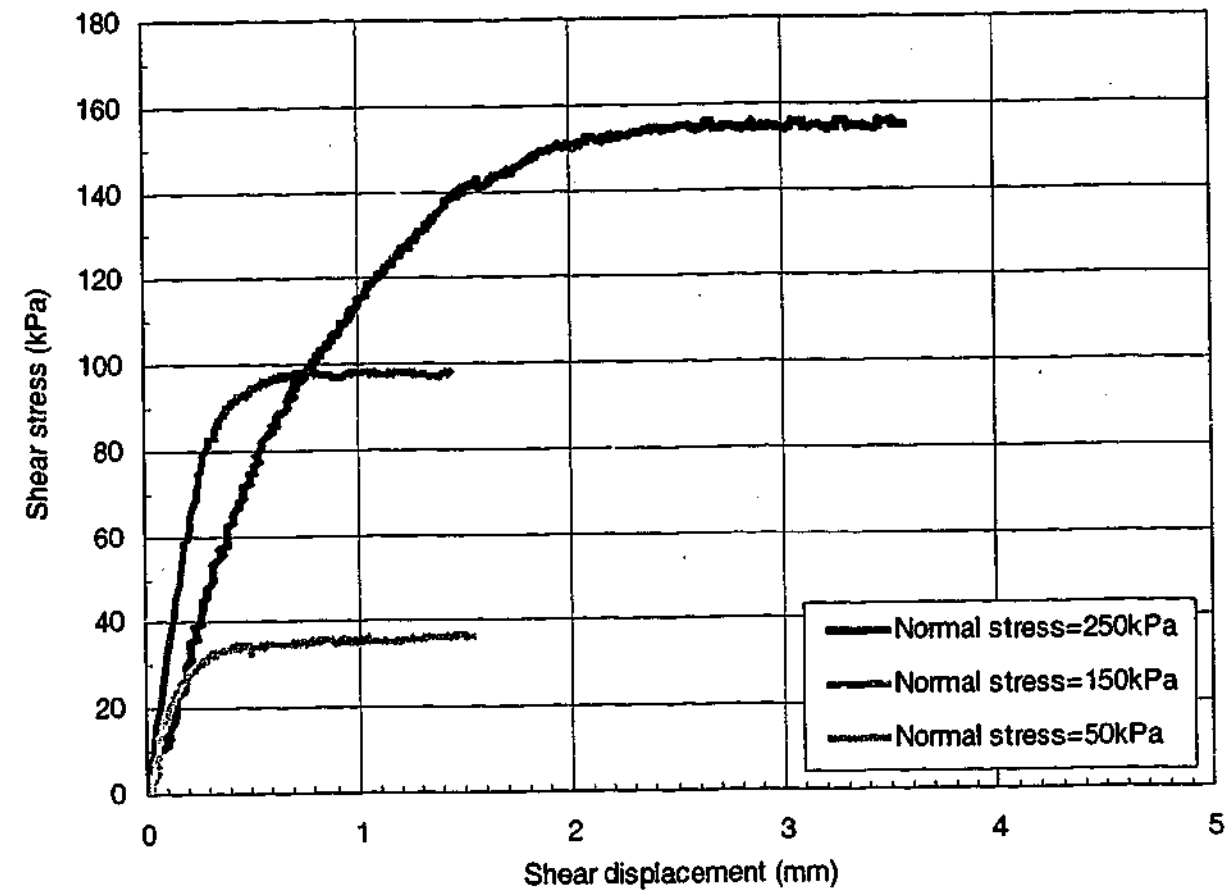


Figure 5.7 Shear stress-shear displacement responses of Yea sand sheared against smooth concrete at 3 normal stresses

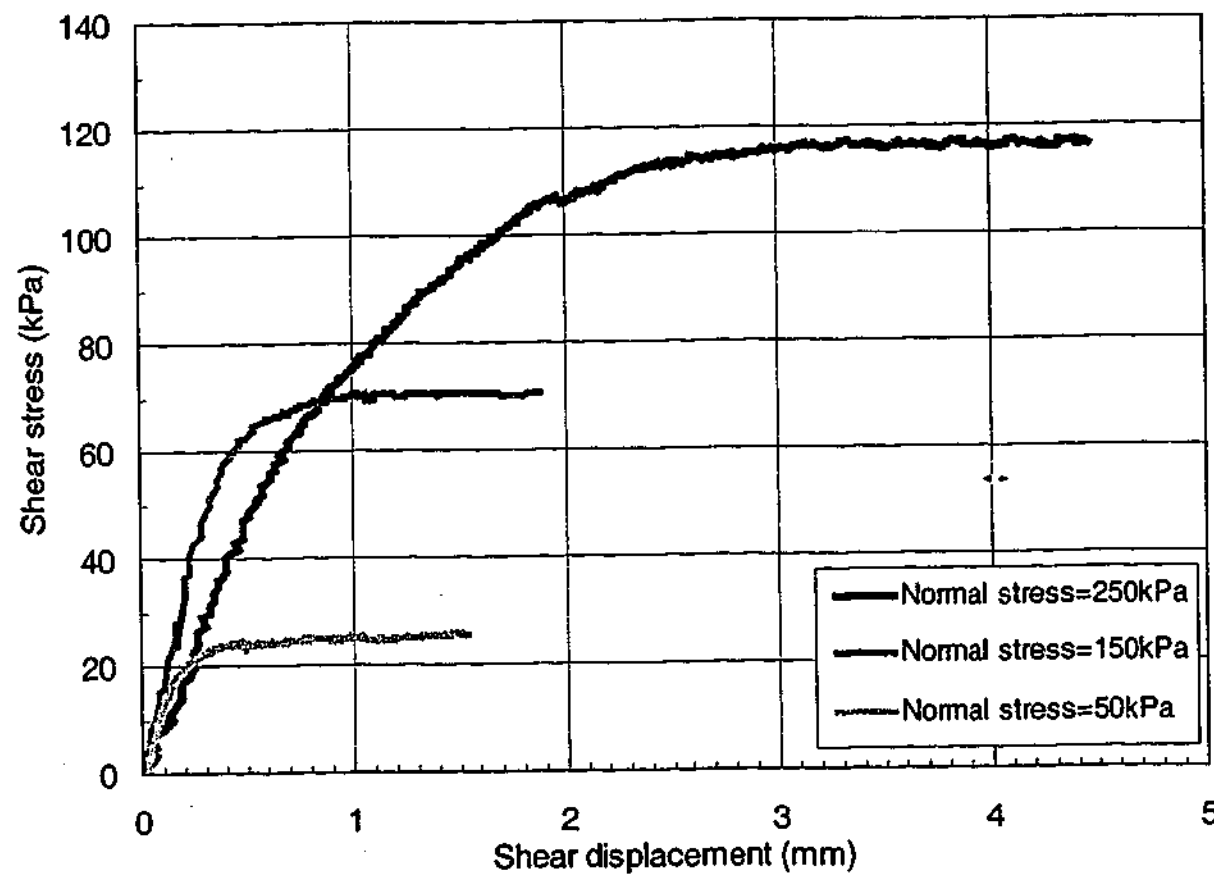


Figure 5.8 Shear stress-shear displacement responses of sand sheared against rough concrete at 3 normal stresses

Table 5.5 Values of ϕ and δ for all quasi-static soil and interface tests

Sand	Density (kg/m ³)	Normal stress k(Pa)	Friction angle (degree)		
			Soil-only	Soil-Smooth concrete	Soil-Rough concrete
50WS	1520-1560	250	31.0	29.0	30.3
		150	31.7	29.2	31.0
		50	33.3	30.0	32.3
Saturated 50WS	1930-1970	250	34.3	29.1	NA
		150	35.4	29.3	NA
		50	37.0	30.5	NA
8/16	1450-1490	250	39.5	30.0	34.5
		150	40.2	30.5	35.4
		50	42.4	31.9	37.6
Yea	1640-1690	250	34.1	25.0	31.8
		150	36.0	25.5	33.2
		50	37.2	26.6	34.0
Mix4	1560-1600	250	31.9	27.0	30.9
		150	33.0	27.2	32.7
		50	34.0	27.5	33.5

5.5.2 Discussion

The values of ϕ and δ are plotted against normal stress in Figure 5.9 to Figure 5.13, with trend lines indicated. It can be observed that the values of ϕ and δ decrease with increasing normal stress (Potyondy, 1961; Acar et al., 1982; Al-Douri and Poulos, 1992). It can also be noted that the value of δ increases with increasing roughness (Kulhawy and Peterson, 1979; Acar et al., 1982; Subba Rao et al., 1998) but δ is less than ϕ . In fact, previous research has shown that the limiting value of δ is ϕ where the interface strength is higher than the soil-only strength so that failure occurred within the sand itself (Acar et al., 1982; Levacher and Sieffert, 1984; Desai et al., 1985; O'Rourke et al., 1990; Uesugi et al., 1990; Lehane et al., 1993).

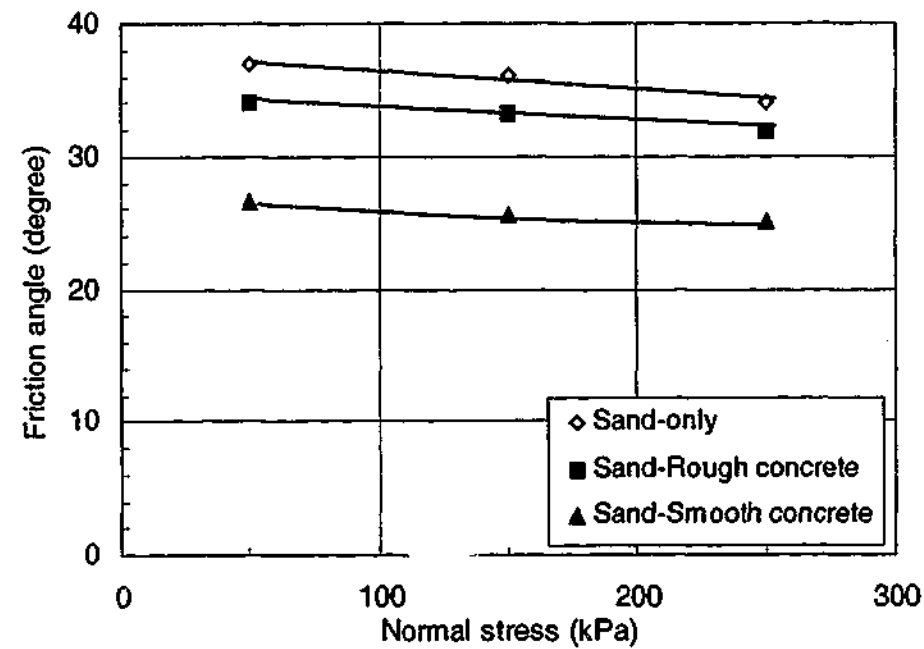


Figure 5.9 Yea: Variation of ϕ and δ with normal stress and pile roughness

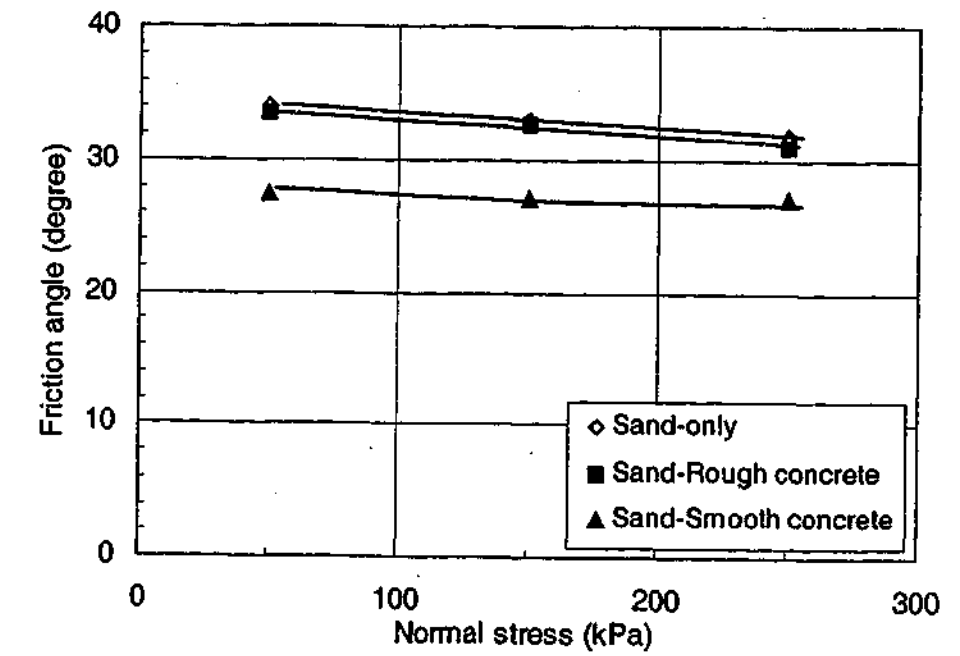


Figure 5.10 Mix4: Variation of ϕ and δ with normal stress and pile roughness

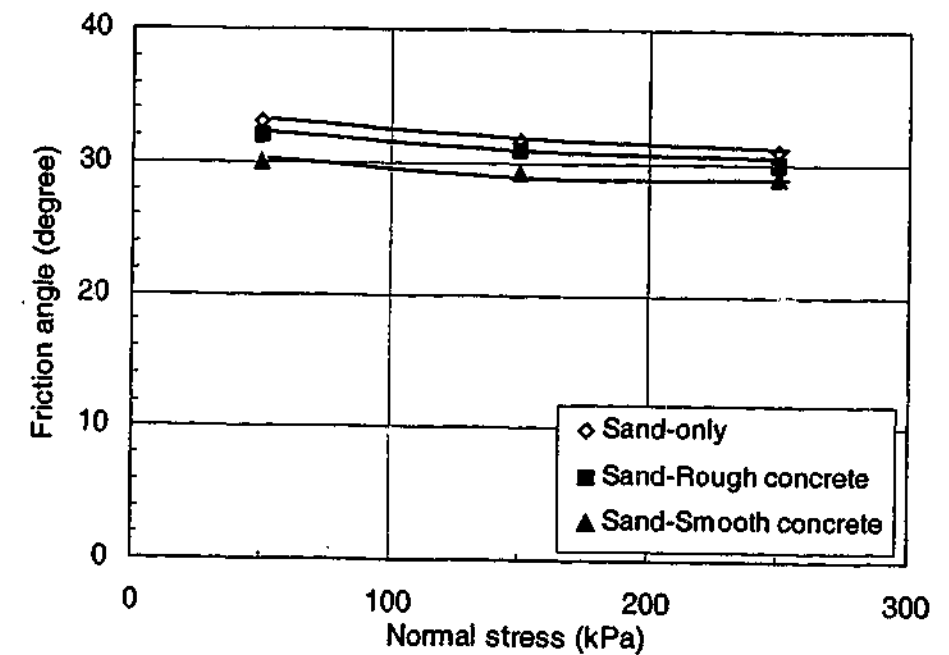


Figure 5.11 50WS: Variation of ϕ and δ with normal stress and pile roughness

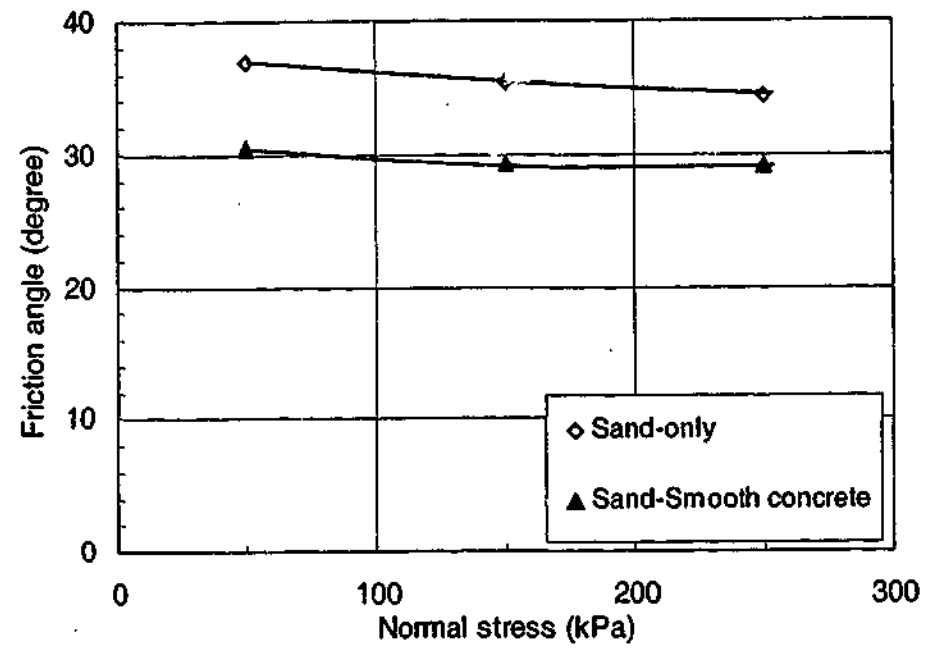


Figure 5.12 Saturated 50WS: Variation of ϕ and δ with normal stress and pile roughness

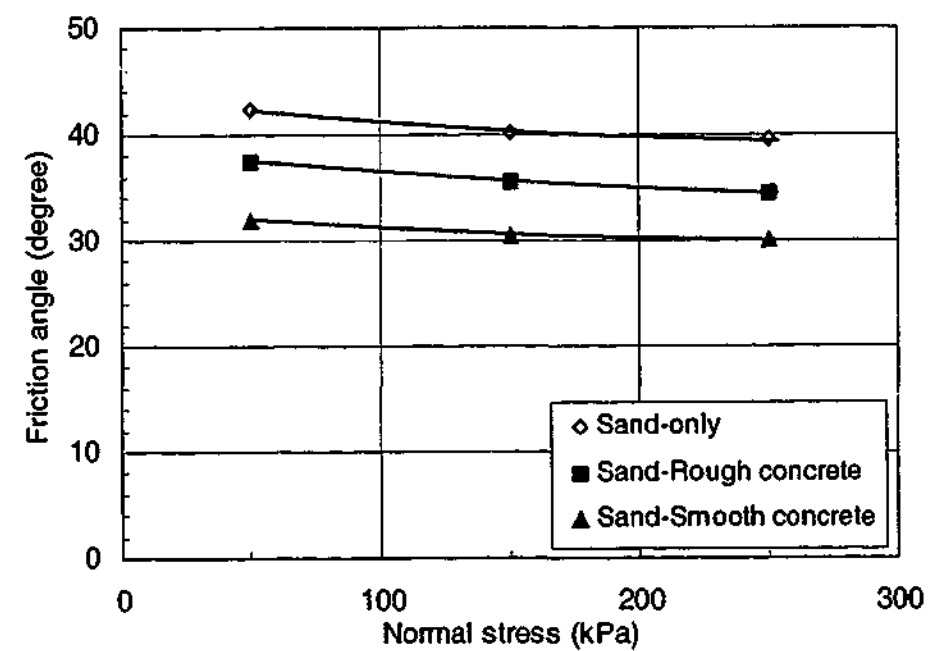


Figure 5.13 8/16: Variation of ϕ and δ with normal stress and pile roughness

The ratio of the interface friction angle to the soil friction angle (δ/ϕ) is a useful parameter for the analysis of the interface behaviour because it enables the interface friction angle to be normalised and also because it is a measure of the roughness of the interface. Thus, the values of δ/ϕ are plotted against the normal stresses in Figure 5.14 and Figure 5.15. It is noted that the values of the ratio are essentially constant at different normal stresses (O'Rourke et al., 1990; Acar et al., 1982). As expected, for a

particular sand, the value of δ/ϕ is higher for the sand sheared against the rougher interface as compared to that for the sand sheared against the smoother interface (e.g. Potyondy, 1961; Acar et al., 1982; Subba Rao et al., 1998).

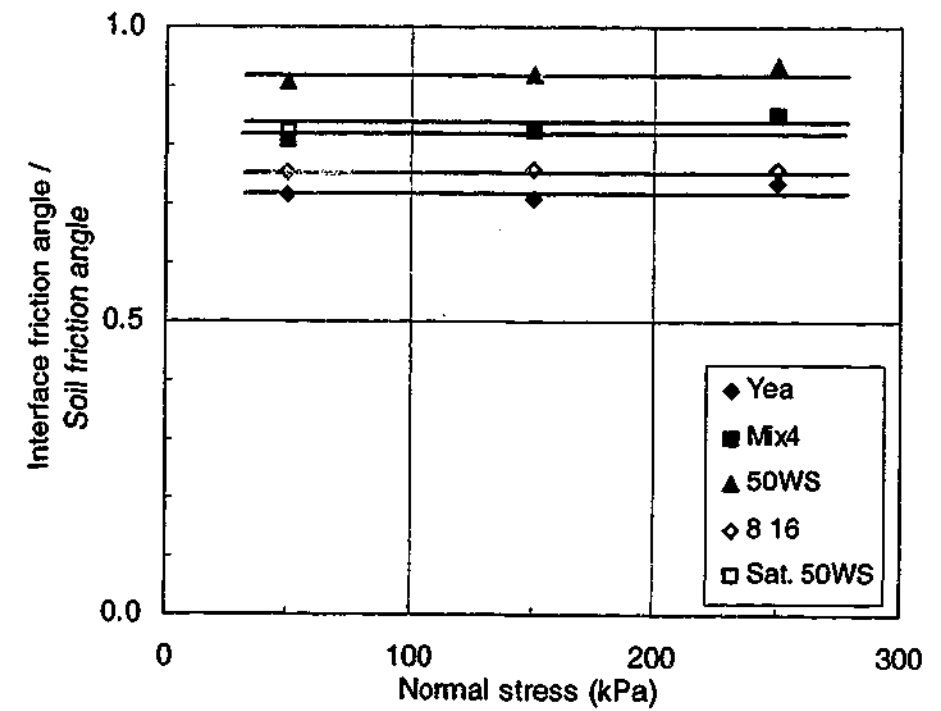


Figure 5.14 Yea, Mix4, 50WS, saturated 50WS, 8/16 sheared against smooth concrete: Variation of δ/ϕ with normal stress

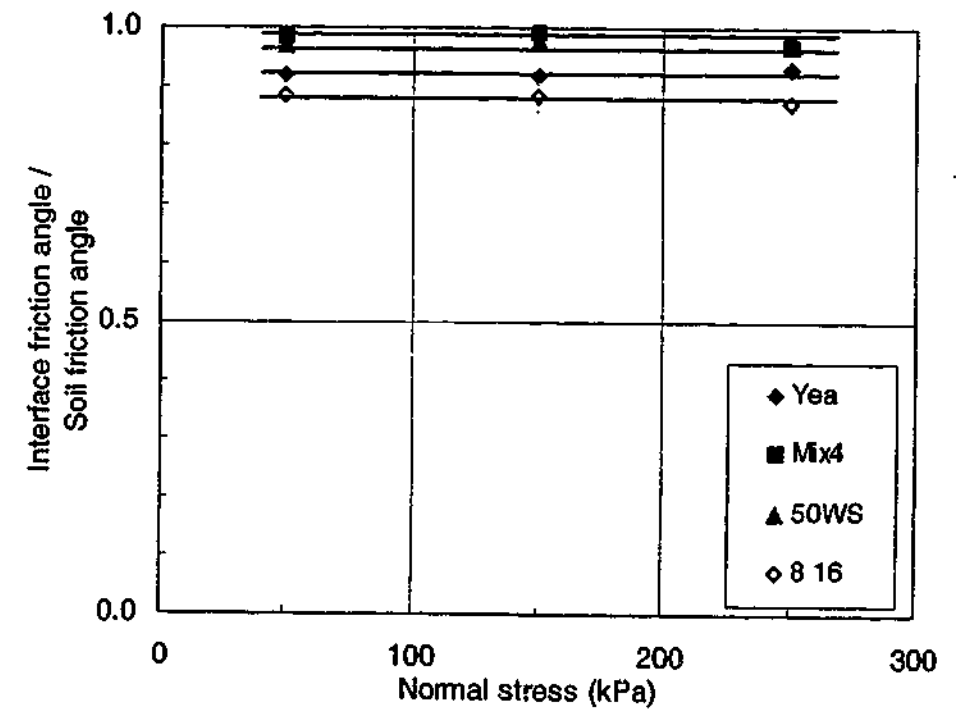


Figure 5.15 Yea, Mix4, 50WS, saturated 50WS and 8/16 sheared against rough concrete: Variation of δ/ϕ with normal stress

The values of δ/ϕ obtained from this study involving the smooth concrete and rough concrete are compared to data obtained by previous researchers in Figure 5.16 and Figure 5.17. It can be noted from these plots that the δ/ϕ value obtained by the previous researchers is independent of the normal stress, as found in this study.

Different types of sand sheared against the same interface from this study yield significantly different values of δ/ϕ - the value ranges between 0.7 and 0.9 for the smooth interface, and between 0.85 and 0.98 for the rough interface. This suggests that, in addition to the interface roughness, the sand type has a significant influence on the value of the ratio. Since different types of sand were tested in the current study and the previous studies, the comparison cannot take into account the influence of the type of the sand on the ratio. Therefore, it is noted that the one value of δ/ϕ presented in each of the studies by Acar et al. (1982) and Potyondy (1961) (shown in Figure 5.16 and Figure 5.17) is not intended to suggest a universal value for all types of sand; instead, for each of these two studies, only one type of sand was tested.

Comparison of the δ/ϕ values from Potyondy (1961) and Kulhawy and Peterson (1979) for smooth and rough concrete in Figure 5.16 and Figure 5.17 shows that the δ/ϕ value for the rougher interface is higher, according with expectation. It is noted that the δ/ϕ value for the rough concrete from Kulhawy and Peterson (1979) is equal to one, indicating that the interface strength is higher than the soil-only strength so that failure occurred in the sand itself.

It can be noted in Figure 5.16 that for the smooth concrete interface, the values of δ/ϕ from this study are comparable to those obtained by Potyondy (1961), Kulhawy and Peterson (1979), and Acar et al. (1982). It could be noted in Figure 5.17 that for the rough concrete interface, the values of δ/ϕ obtained from this study are lower than but comparable to those obtained by Potyondy (1961) and Kulhawy and Peterson (1979). In the present study, the concrete was trowelled immediately after the concrete was poured. In the study by Kulhawy and Peterson, the concrete was cast and at a later stage before the concrete set, the surface was brushed to expose the aggregates, whilst in the study by Potyondy, the concrete was cast on the ground. It

would appear that the surfaces prepared in both these previous studies were comparatively rougher, and hence would account for the higher value obtained.

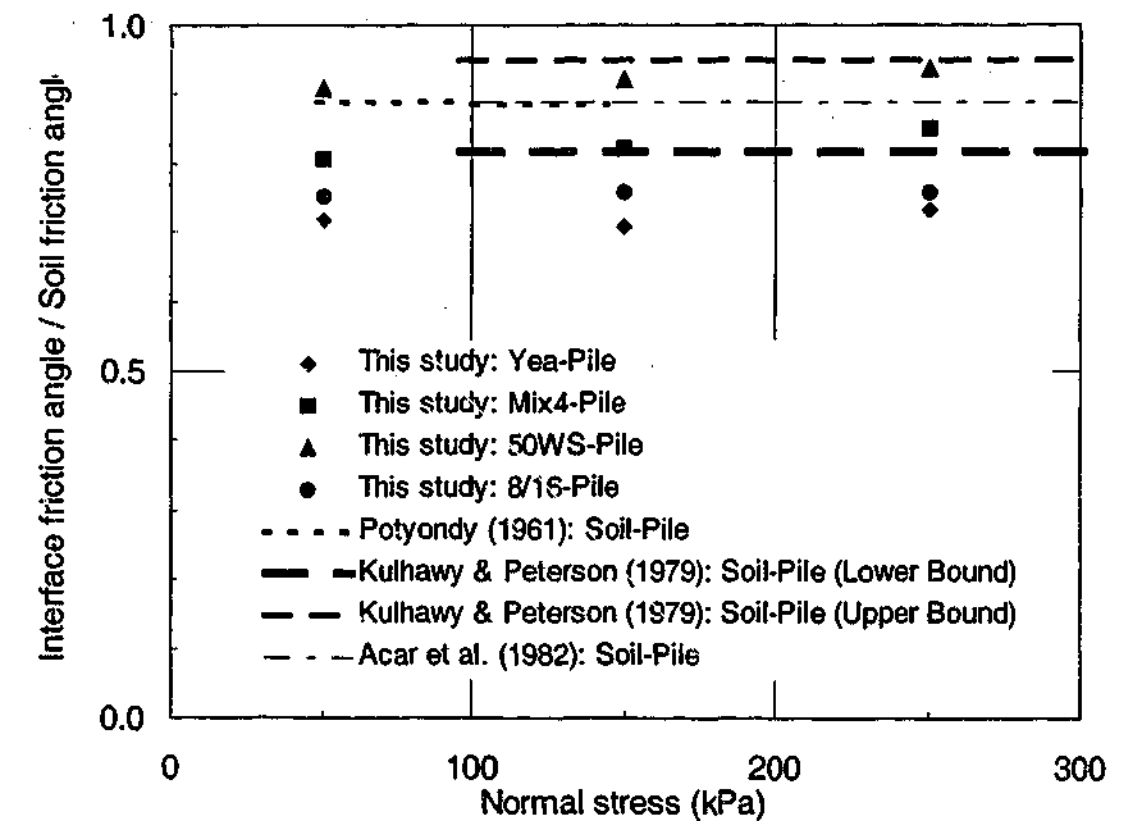


Figure 5.16 Values of δ/ϕ for smooth concrete: data from this study vs. data from previous studies

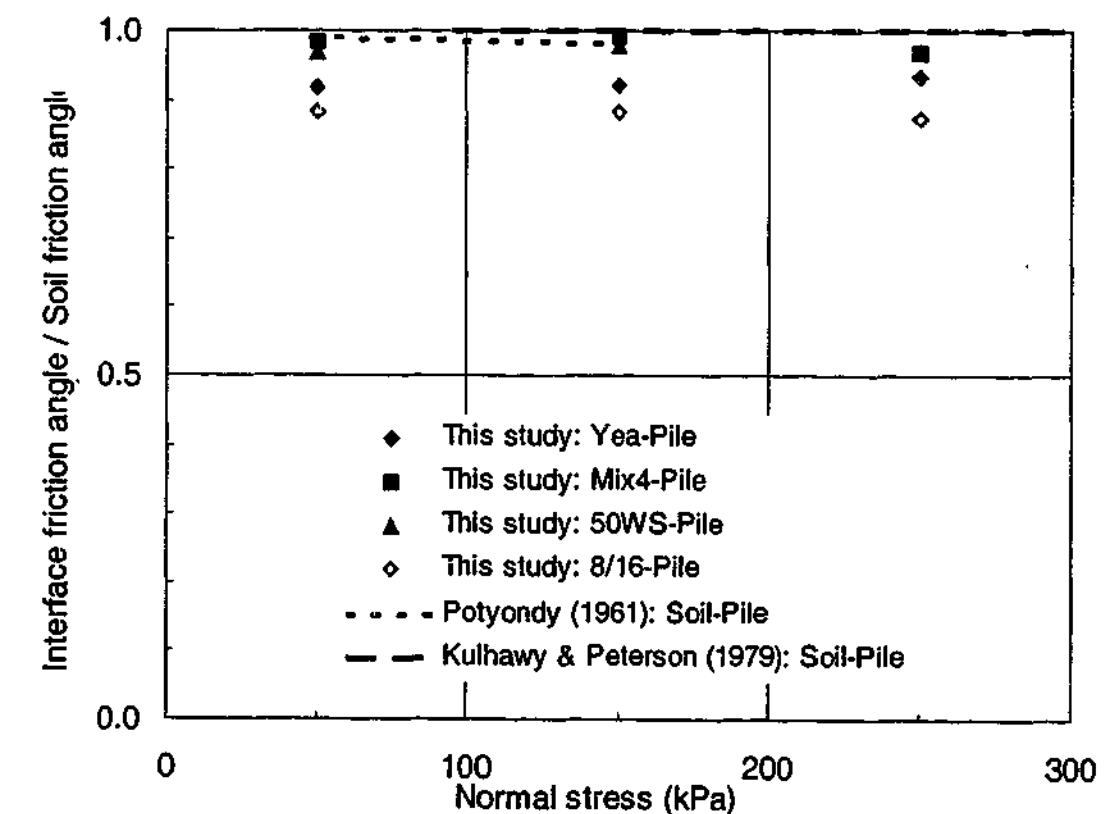


Figure 5.17 Values of δ/ϕ for rough concrete: data from this study vs. data from previous studies

5.5.3 Concluding remarks – quasi-static tests

Based on the quasi-static tests performed, the soil and interface strength behaviour has been shown to be consistent with expectation and the work of others. Thus, it has been demonstrated that the soil and interface strength behaviour is credible, and that the interface large-displacement or residual friction angles obtained are valid reference values for comparing against the dynamic friction angles.

5.6 Dynamic Interface Tests

5.6.1 Post-test observations of interface

During the trial run of the experimental apparatus, the 50WS sand-smooth concrete interface was tested at various settings of the high-speed actuator, giving various velocity and acceleration profiles. Because the same sand sample and pile surface were tested many times during the trial run, a noticeable amount of particle crushing occurred at the interface and the pile surface was slightly abraded. A photograph of the sample with particle crushing is shown in Figure 5.18 where the crushed particles are of a lighter colour as compared to the whole particles. A photograph of the abraded pile surface is shown in Figure 5.19 where the abraded surface has a darker colour compared to the original surface. However, when the test programme was carried out, the pile surface was replaced as soon there were signs of abrasion, as has been mentioned in Section 5.4.3.3. Post-test observations of the sand grains at the interface showed no signs of particle crushing; this is to be expected as the sample was only subjected to a limited number of tests.

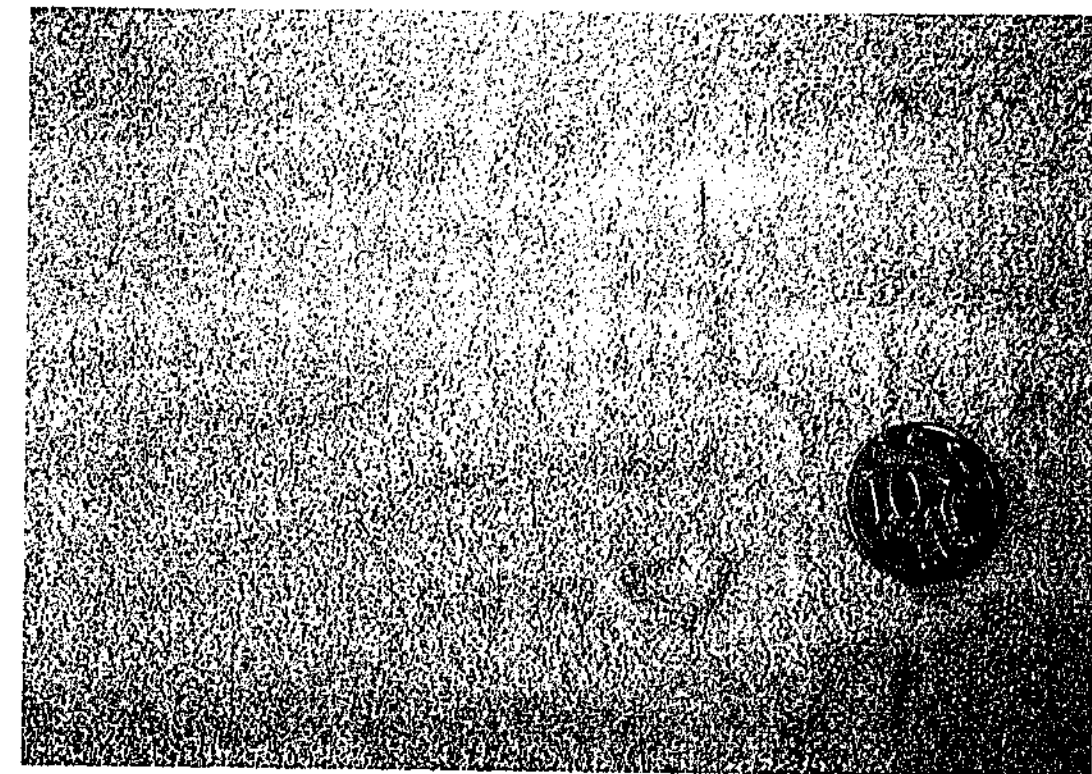


Figure 5.18 Crushed particles (with lighter colour) of 50WS at the interface

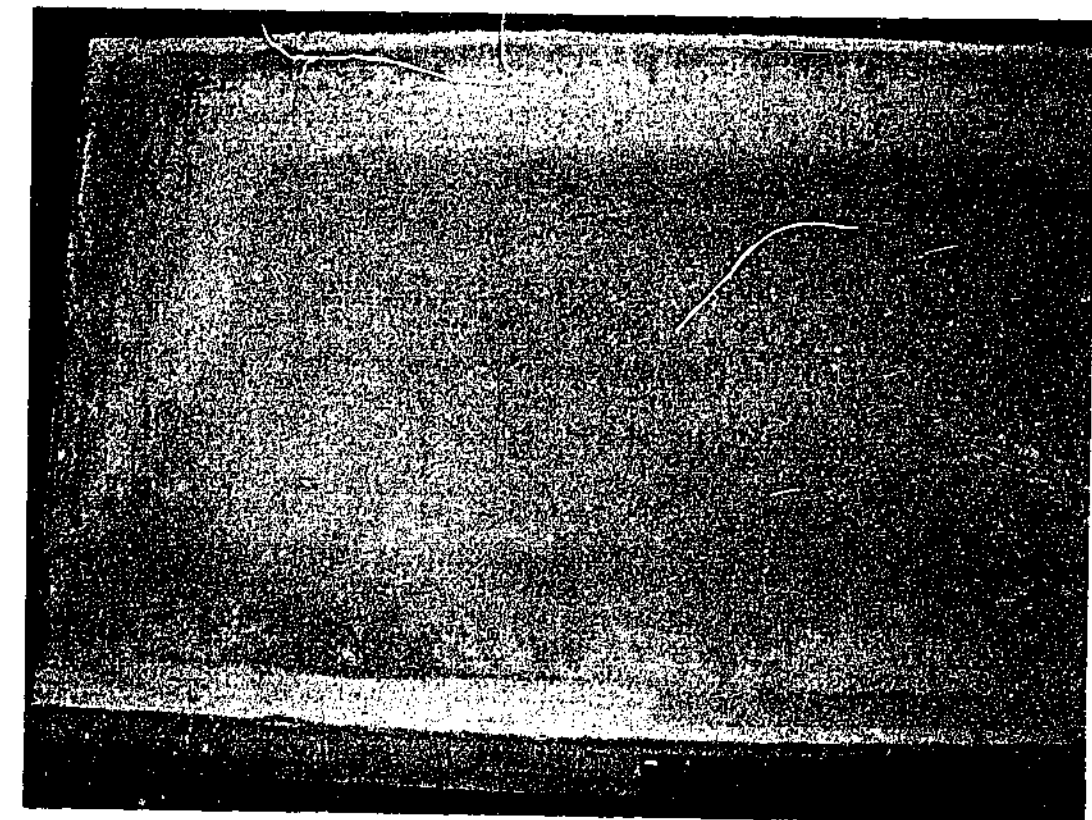


Figure 5.19 Abrasion of smooth concrete surface (shown by the darker colour) where the sample was sheared against surface

5.6.2 Typical test record

A sample test record from a typical dynamic pile-sand interface test is presented in Figure 5.20. The record comprises 6 graphs which have been labelled Graphs A to F. Graphs A, B and C relate to the data obtained during the event, whilst Graphs D, E and F show derived analyses of the data. The contents of each of the graphs are explained subsequently.

Graph A shows:

- the dynamic force which is measured by the dynamic load cell interfaced between the ram and the carriage (labelled F_{ram})
- the inertial force of the carriage and the pile section (labelled $F_{inertial}$), which is the product of the mass of the carriage and the pile section, and the acceleration of the carriage and the pile
- the normal force at the interface (labelled F_{normal})

Graph B shows:

- the acceleration of the pile section (labelled Pile acceleration)
- the velocity of the pile section (labelled Pile velocity), which is obtained by integrating the acceleration

Graph C shows:

- the displacement of the pile (labelled Pile displacement)
- the vertical displacement of sample (labelled Vertical displacement)

It has been explained in Section 5.4.3.4 that sample was lost in the shearing process; this is confirmed by the reduction in the thickness of the sample during the test shown in Graph C. Therefore, it cannot be assumed that the reduction was due to the contractile response of the sample during shearing.

Graph D shows:

- the dynamic interface frictional force (labelled F_d) which is obtained by taking the difference between F_{ram} and $F_{inertial}$

- the quasi-static interface frictional force (labelled F_s) which is computed using the Mohr-Coulomb law – i.e. by taking the product of the instantaneous F_{normal} and the tangent of the instantaneous quasi-static interface friction angle. The quasi-static tests yielded three sets of data (the three interface friction angles values corresponding the three applied normal loads) for one particular interface. The three data points, plotted in the interface friction angle vs. normal force plot (presented in Section 5.5.2), are fitted with an equation of best-fit, where the interface friction angle is expressed as a function of the applied normal force. Using this equation, the instantaneous quasi-static friction angle during the dynamic event can be computed from the instantaneous applied normal force.

As will be observed in Section 5.6.4 where the test records are presented in their entirety, the amplitude of fluctuation of the F_d curve for a particular sand sheared against rough concrete is greater than that for the sand sheared against smooth concrete. This is to be expected during shearing as the sand particles ride on and over the pile asperities of the rougher surface, causing fluctuations in the normal load and hence in the F_d curve.

Graph E shows:

- the ratio of F_d to F_s (labelled F_d/F_s)
- the pile acceleration

Graph F shows:

- F_d/F_s
- the pile velocity

In Graphs E and F, the F_d/F_s curve has been plotted against the pile acceleration and the velocity in order to determine if there is any systematic variation of the strength ratio value with either or both of these two parameters.

FILENAME 816.RC 250 INITIAL NORMAL STRESS 250 kPa
 PILE Rough concrete INITIAL DENSITY 1450 kg/m³
 SAND 8/16

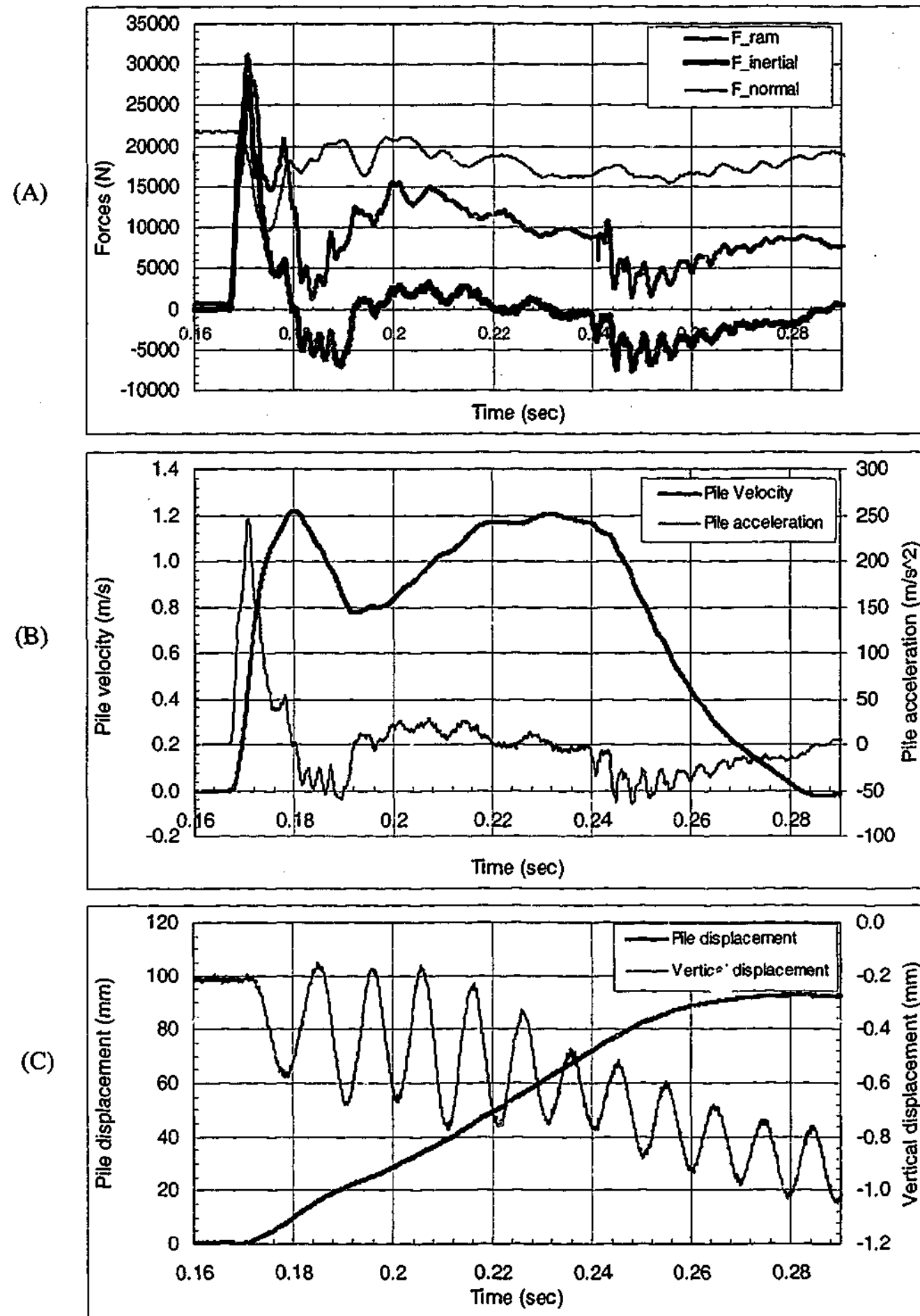


Figure 5.20 Sample record of a smooth pile-sand interface dynamic shear test

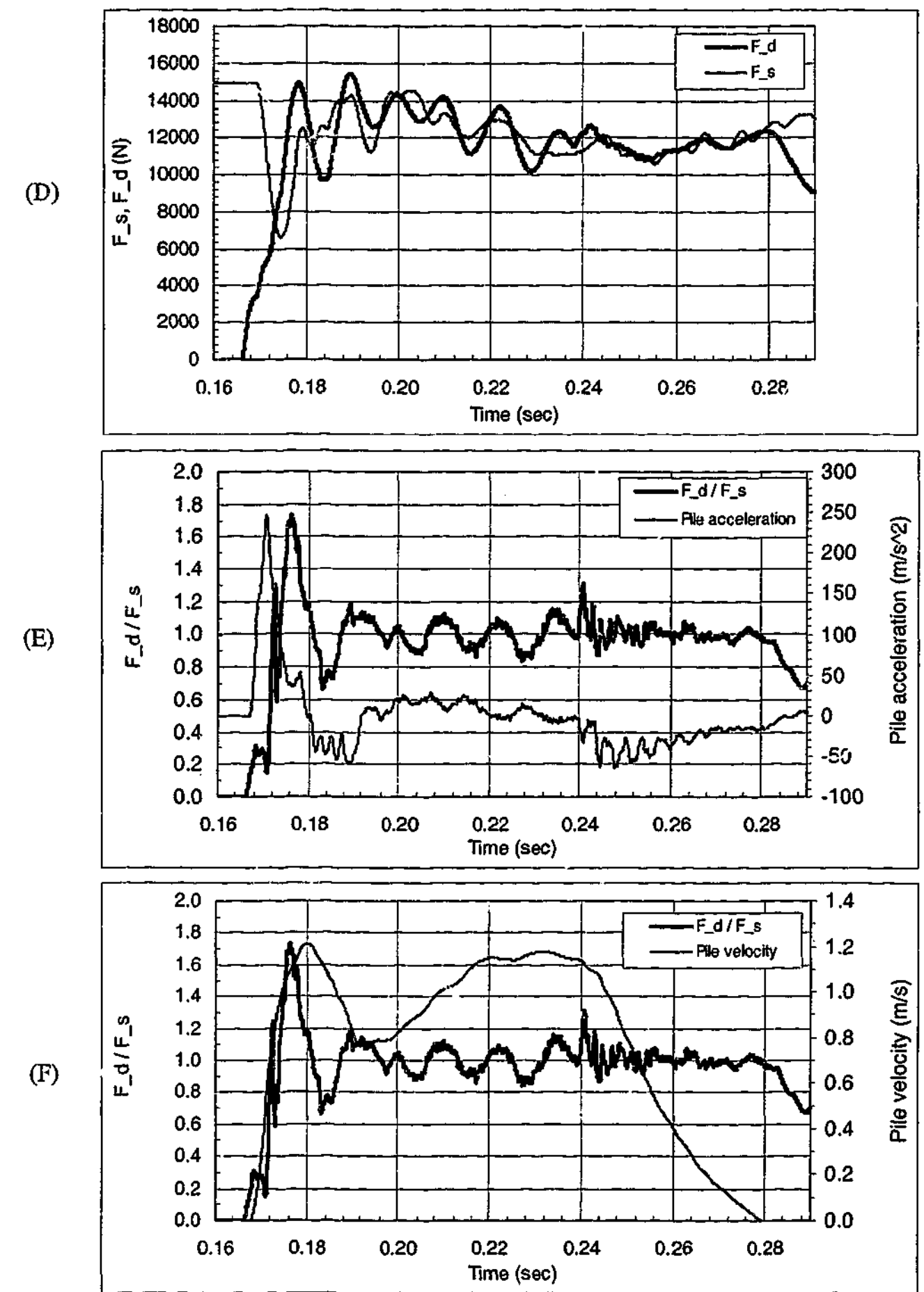


Figure 5.20(cont'd) Sample record of a smooth pile-sand interface dynamic shear test

5.6.2.1 Error in measurement of F_{normal}

As shown in Graph A of Figure 5.20, the fluctuations in the F_{normal} curve are highly transient. It has been discussed in Section 4.5 that the fluctuation in the F_{normal} curve was primarily due to the fluctuating inertial forces in the loading platen caused by the stiff vertical displacement response of the sand sample. Since the load cell used to measure the normal load is not a dynamic load cell (as has been discussed in Section 4.5), it cannot be expected to register the correct magnitude of the applied normal load, and the correct response of the applied normal load (for example, the response might be delayed such that the measured normal load lagged the actual response).

As a consequence, the F_s curve (shown in Graph D) which is computed from the erroneous F_{normal} curve is also erroneous. The F_d curve, shown in Graph D, is deduced from F_{ram} (measured using a dynamic load cell) and the pile acceleration (measured using an accelerometer), and can be expected to be reliable. It is known that the fluctuation of the F_d curve must be in synchronisation with that of the F_s curve throughout the event. However, as shown in Graph D, this is not the case because of the error in the F_s curve.

As noted in Graphs E and F, the F_d/F_s curve fluctuates about the ' $F_d/F_s = 1.0$ reference line'. Any variation of the interface friction due to any real soil rate effect must vary systematically with any test parameter (either velocity or acceleration). Therefore, the unsystematic deviation of the F_d/F_s value from 1.0 is due to the error in F_s , which results in the fluctuations in the F_s curve and the F_d curve being out of synchronisation.

5.6.3 Procedures for analysis

Given the reliability of the F_d measurement, the F_d curve can be used as a benchmark for determining the accuracy or otherwise of the F_s curve throughout the event. As noted in Graph D, the fluctuation of the F_s curve differs from that of the F_d curve to varying degrees through the course of the dynamic event. Alternatively, it can be noted in Graphs E and F that the degree of fluctuation in the F_d/F_s curve varies through the course of the dynamic event. It can thus be

concluded that the reliability of the F_s curve varies throughout the event. It is important that the analyses to be undertaken are based on the part of the record with the reliable data. Analyses of all the test records show that the reliability of the F_s curve is markedly different in three sections of the record. These sections are labelled Section 1, Section 2 and Section 3, and are indicated in Figure 5.21 for Graphs D, E and F of the sample record presented previously.

Section 1 of the record can be conveniently defined as the time when the pile accelerates from zero velocity to the peak velocity. This section of the record is indicated in Figure 5.21. As shown in Section 1 of either Graph E or Graph F, the fluctuation in F_s varies most significantly from that of F_d at the very start of the event, indicating that the error in F_s and hence in F_{normal} is greatest in this part of the record. The significant error at the very start of the event is likely to be caused by the highly transient changes in the applied normal load as the closed-loop system becomes instantaneously unstable (as shearing of the interface causes the user-assigned constant load to be altered drastically).

Section 2 of the record can generally be defined as that part of the record between Section 1 and the time when the pile decelerates. As shown in Section 2 of Graph D, the fluctuation of the F_s curve remains unsynchronised with that of F_d but the average about which F_s fluctuates appears to agree closely with the average of F_d .

Section 3 of the record can be defined as that part of the record between the end of Section 2 and the point where the pile has decelerated to zero velocity, as indicated in Graph F. It can be noted in Section 3 of either Graph D or Graph E that the fluctuation of the F_s curve is synchronised with that of F_d , indicating that the F_s curve in this region is reliable. The measurement of the F_s curve (which is based on the F_{normal} curve) is reliable in this section of the record as the applied normal load becomes more stable. The reliability of the F_s curve in this part of the record can be validated by the fact that the F_s is equal to F_d at near-zero velocity, thus giving a F_d/F_s value of 1.0 at near-zero velocities.

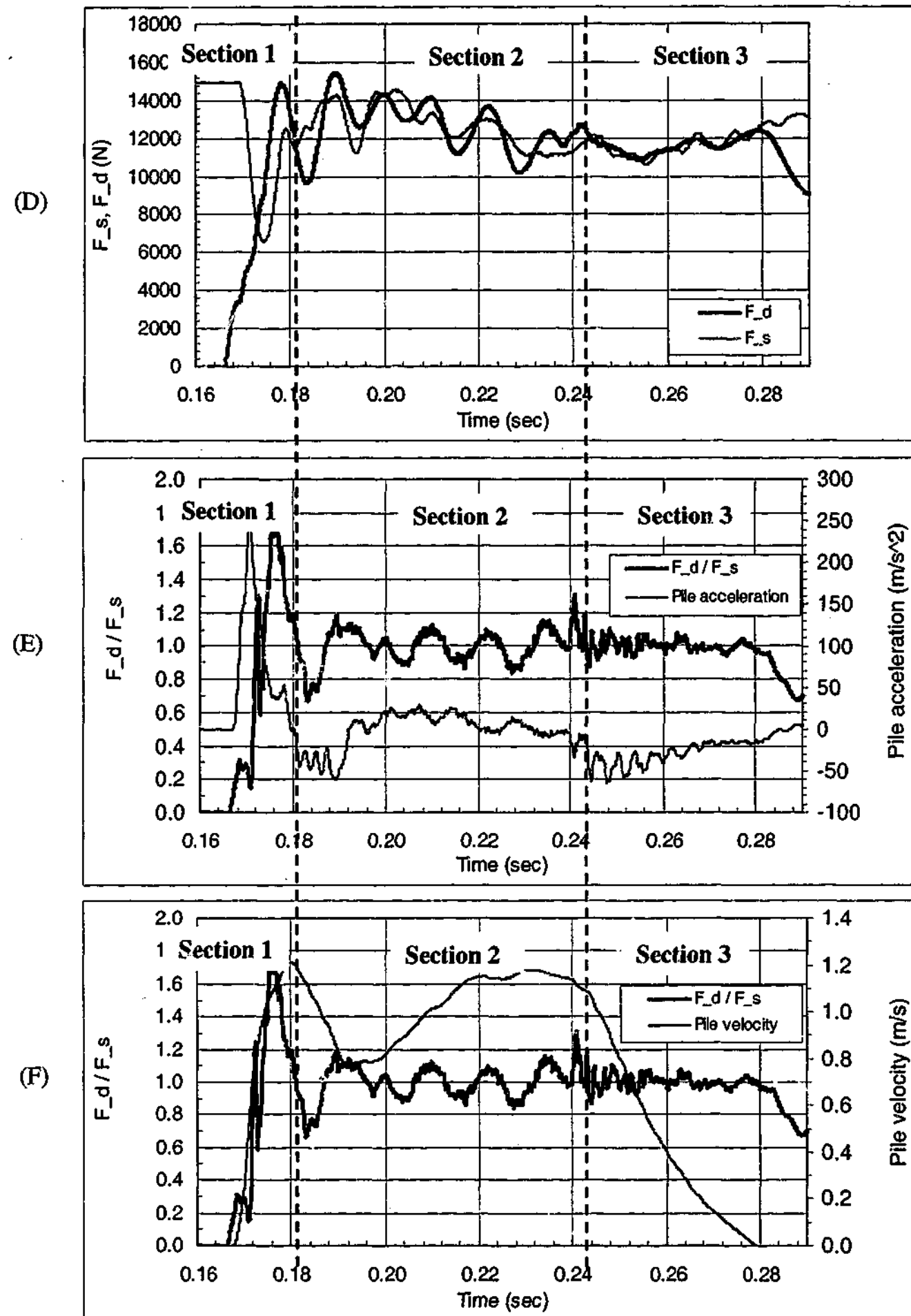


Figure 5.21 Sections 1, 2 and 3 of record

Since the data in Section 3 of the record is reliable, it is suitable for analysis. As pointed out previously, the value of F_d/F_s fluctuates in Sections 1 and 2 of the record due to the error in the measurement of the F_{normal} . Since the data in Section 1 is unreliable, it should be ignored. However, the data in Section 2 can be processed such that the error is minimised.

It can be noted from Section 2 in Graph D of Figure 5.21 that the average of the fluctuating F_s curve coincides with that of the F_d curve (which is known to be reliable). This indicates that, whilst the load cell for measuring F_{normal} could not accurately measure the highly transient changes in the applied normal load, the load cell was able to correctly register the average force. Thus, the data points of F_{normal} can be averaged in order to minimise (if not eliminate) the error in the F_s curve in Section 2. Although the fluctuations in the F_d curve must be real, data points for F_d can also be averaged in order to minimise the fluctuations in the F_d/F_s curve. In order to make the data in Section 2 amenable to analyses, the data points for F_s and F_d for all the test records are averaged.

It is necessary to note several features of the curves based on the averaged data points, which are best illustrated using a sample of a processed record in Figure 5.22. The curve based on averaged data points of F_s (labelled F_{s_avg}) and the curve based on the averaged data points of F_d (labelled F_{d_avg}) are shown in Graph I of Figure 5.22. The F_{d_avg}/F_{s_avg} curve is shown in Graphs II and III. The Sections 1, 2 and 3 of the record are also indicated.

It can be noted in Graph I that both F_s and F_d increase from 0.17 to 0.19 seconds, decrease from 0.19 to 0.23 seconds, and remain almost constant from 0.23 to 0.28 seconds. In averaging the data points of F_s and F_d (in order to minimise the fluctuations in the F_d/F_s curve), it is important that such salient features of F_s and F_d curves are not "lost". Thus, the degree of averaging of the data points of F_s and F_d is a compromise between minimising the fluctuations in the F_d/F_s curve and retaining the salient features of the F_s and F_d curves. Therefore, as can be noted in Graphs II and III of Figure 5.22, the F_{s_avg} and F_{d_avg} curves and hence the F_{d_avg}/F_{s_avg} curve contain slight fluctuations.

FILENAME	816.RC 250	INITIAL NORMAL STRESS	250 KPa
PILE	Rough concrete	INITIAL DENSITY	1450 kg/m ³
SAND	8/16		

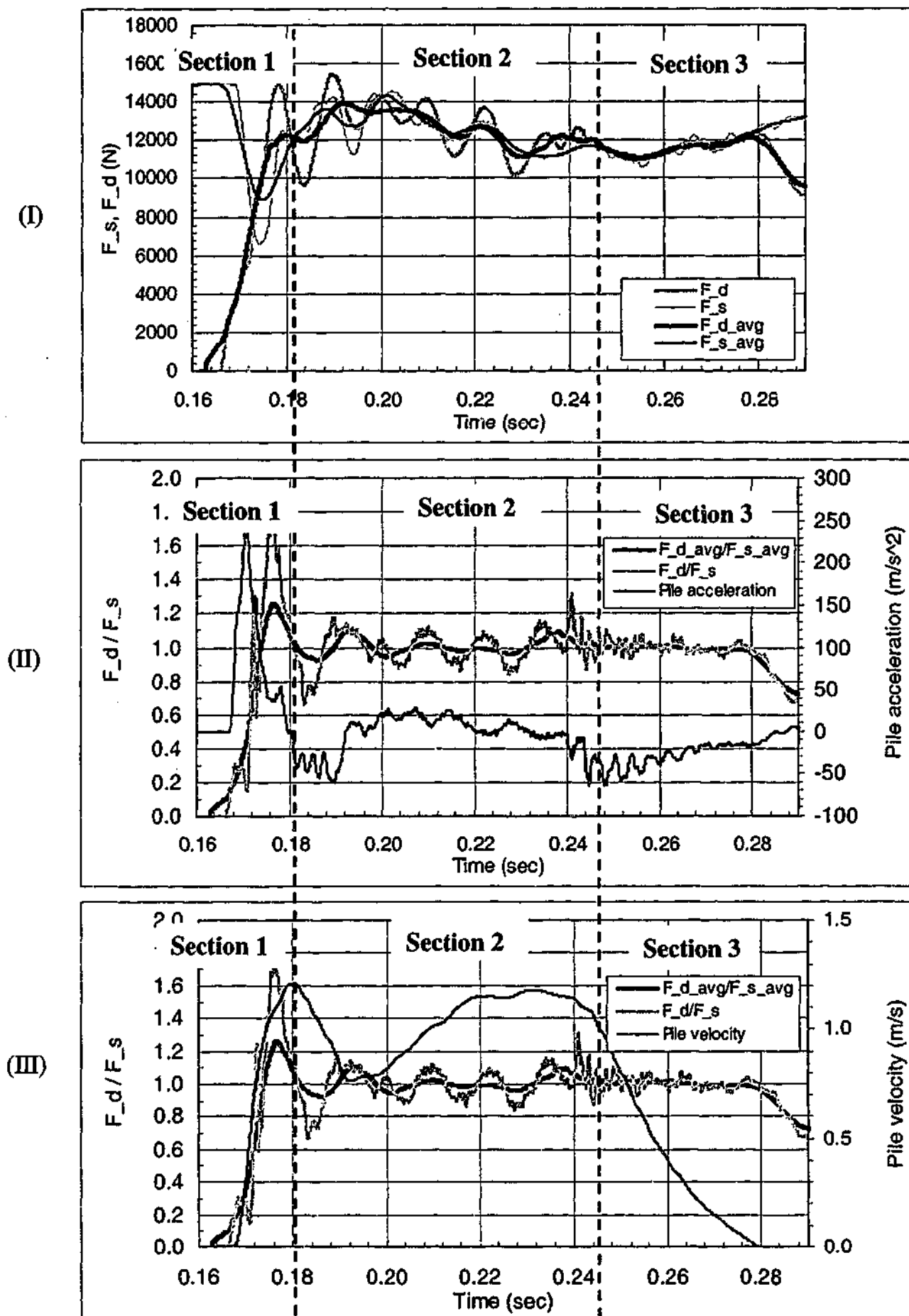


Figure 5.22 A sample of processed record

It is also noted that the number of points averaged varies from one test record to another because of the different degrees of fluctuation in each test. For example, a sand sample tested against the smooth concrete surface involves a lesser degree of fluctuation in the F_s and F_d curves and hence a lesser number of points is averaged, as compared to the same sand sample tested against the rough concrete surface.

Because the averaging of the F_d curve at the end of the event is based in part on data points involving rapidly decreasing F_d values (as the dynamic load cell discharges its voltages), F_{d_avg}/F_{s_avg} decreases sooner than F_d/F_s , as shown in Figure 5.22. This results in the F_{d_avg}/F_{s_avg} value corresponding to near-zero velocities not being equal to 1.0 as expected. As the value is a significant reference point for assessing the presence of any dynamic effect, the F_{d_avg} curve towards the end of the event is replaced with the (unaveraged) F_d curve.

Since the F_s data in Section 1 are known to be unreliable, the F_{s_avg} and hence the F_{d_avg}/F_{s_avg} data in Section 1 are ignored.

It can be noted in Graph I that the fluctuations in the F_s curve in Section 2 of the record has been significantly reduced by the averaging procedure. The F_{s_avg} curve contains all the salient features of the F_d curve and thus agrees closely with the F_{d_avg} , indicating that the error in the F_s data has been minimised, if not eliminated, by the averaging procedure. As shown in Graph II or Graph III, the fluctuation in the F_d/F_s curve has been significantly reduced so that the data is now amenable to analysis.

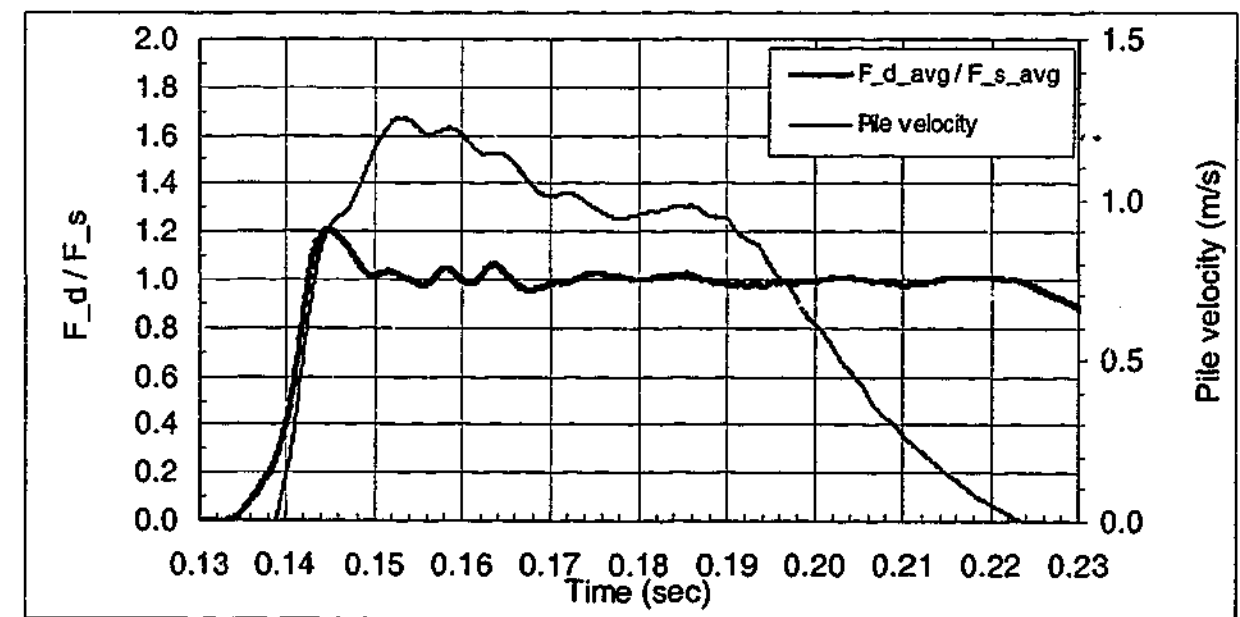
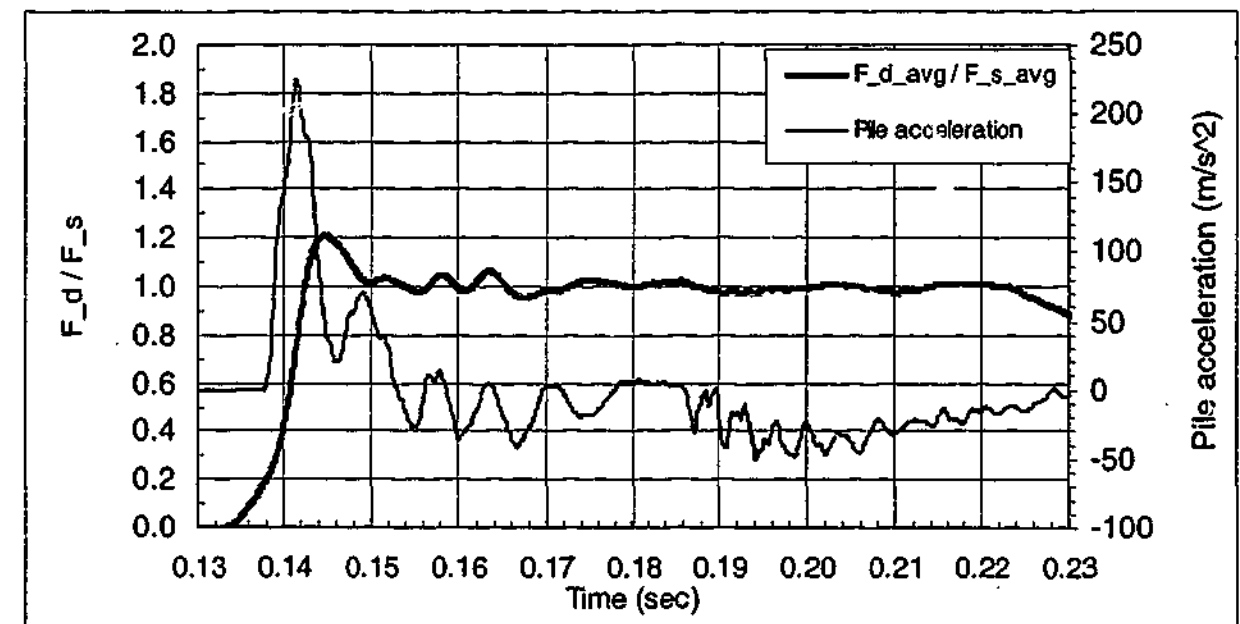
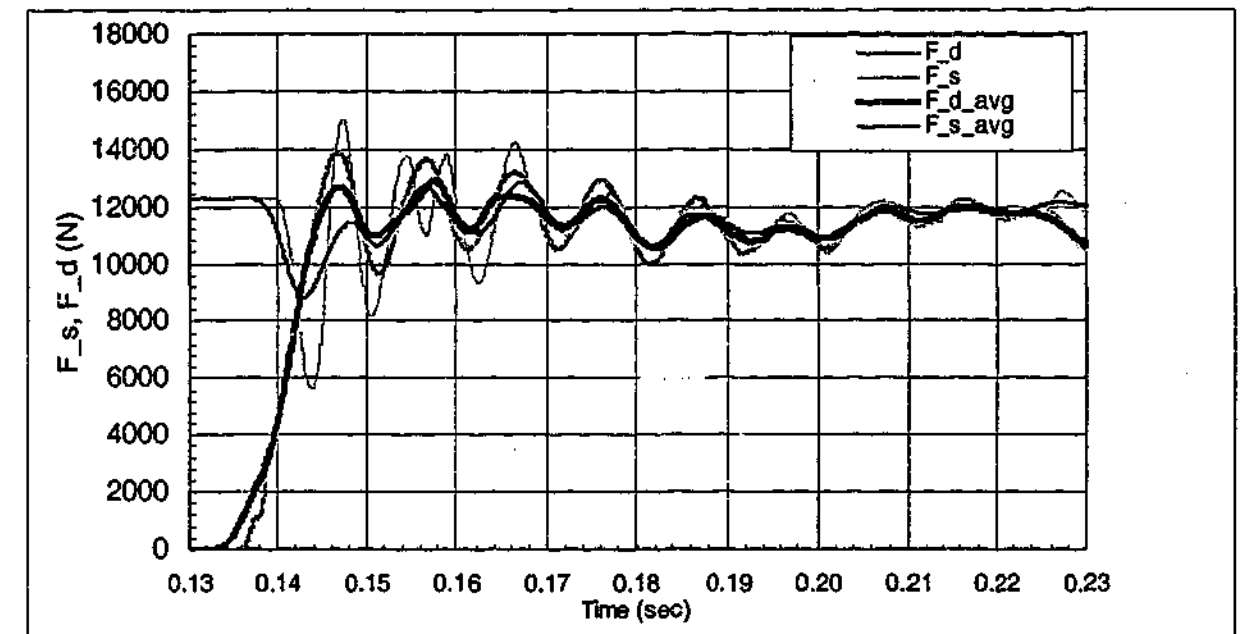
It can be noted in Section 3 in either Graph II or Graph III (where F_s data are known to be accurate) that F_{d_avg}/F_{s_avg} is equal to 1.0 or F_{s_avg} is equal to F_{d_avg} at near-zero velocity, as expected.

Therefore, it would appear that with the averaging procedure, data in Sections 2 and 3 of the record are now suitable for the analysis of any dynamic effect.

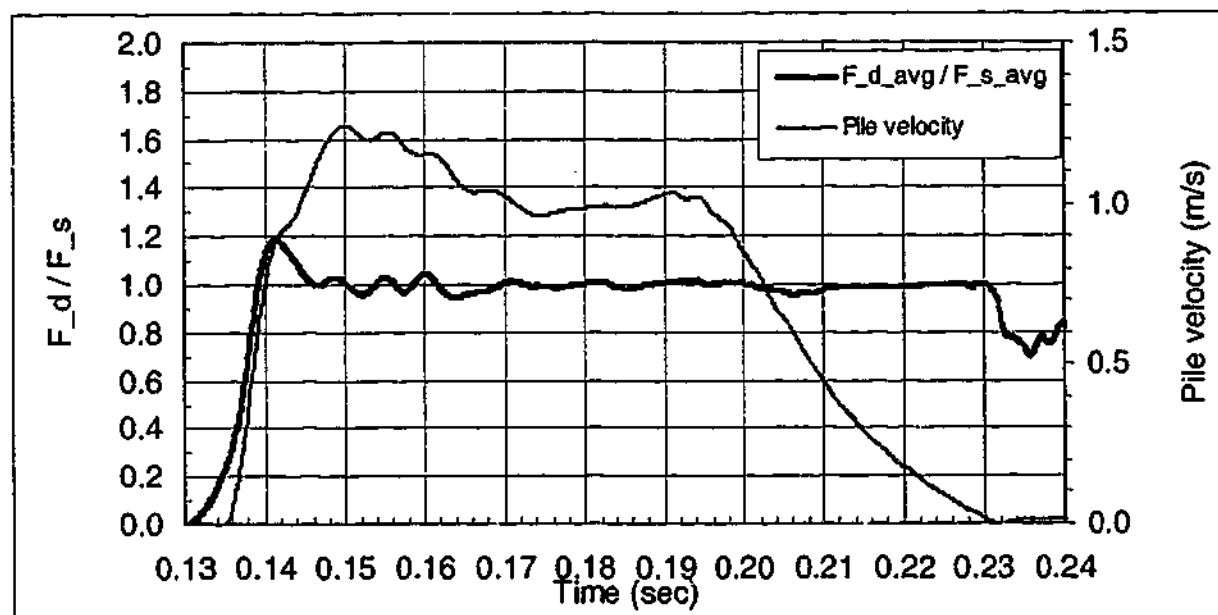
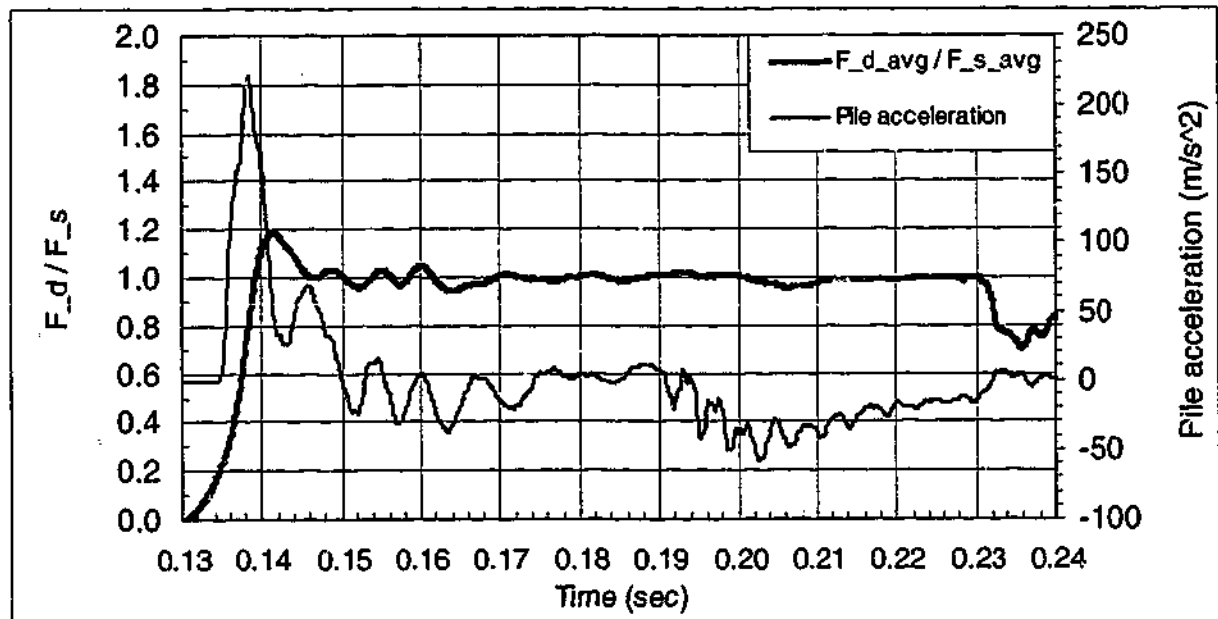
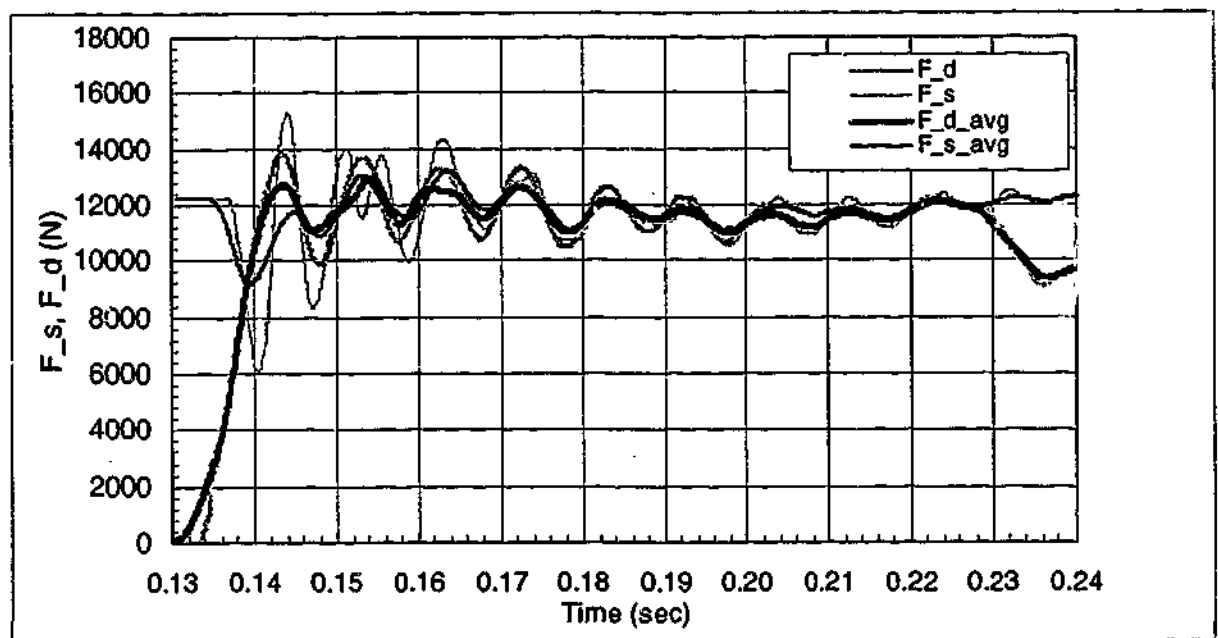
5.6.4 Records of all tests

The test records of all dynamic tests conducted at the normal stress of 50kPa have significantly high fluctuations in the F_{normal} curve and are deemed to be unsuitable for analysis; thus these records are not presented. The processed records of all the dynamic pile-sand interface tests conducted at normal stresses of 150kPa and 250kPa are presented in this section. The details of each test are shown at the top of each of the records. For brevity only the plots pertaining to the derived analyses in the form of Graphs D to F are presented for each of the tests. Each record shows the original F_s and F_d curves, and the processed F_{s_avg} and F_{d_avg} curves. However, since the F_d/F_s curve comprises very severe fluctuation to be meaningful or useful, only the F_{d_avg}/F_{s_avg} curve is shown.

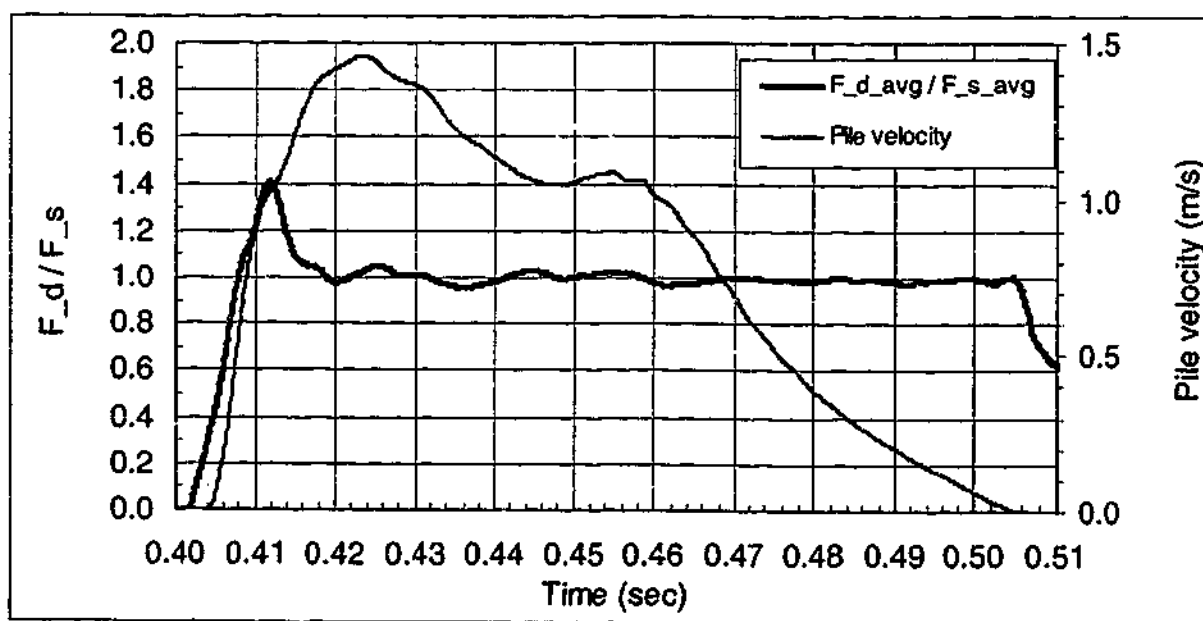
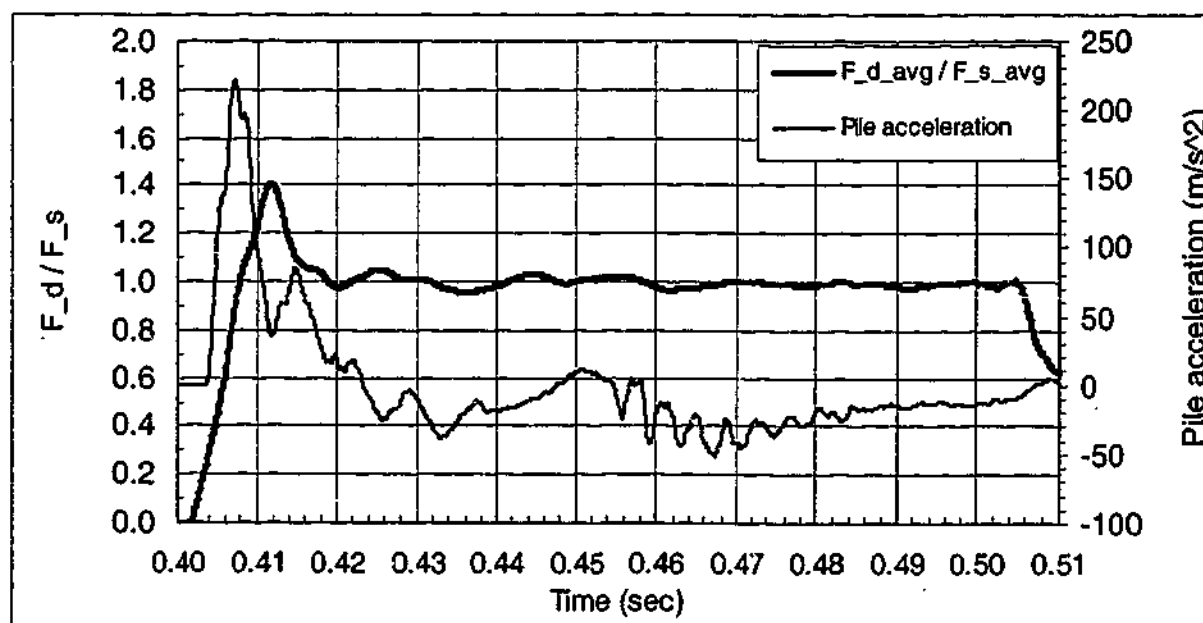
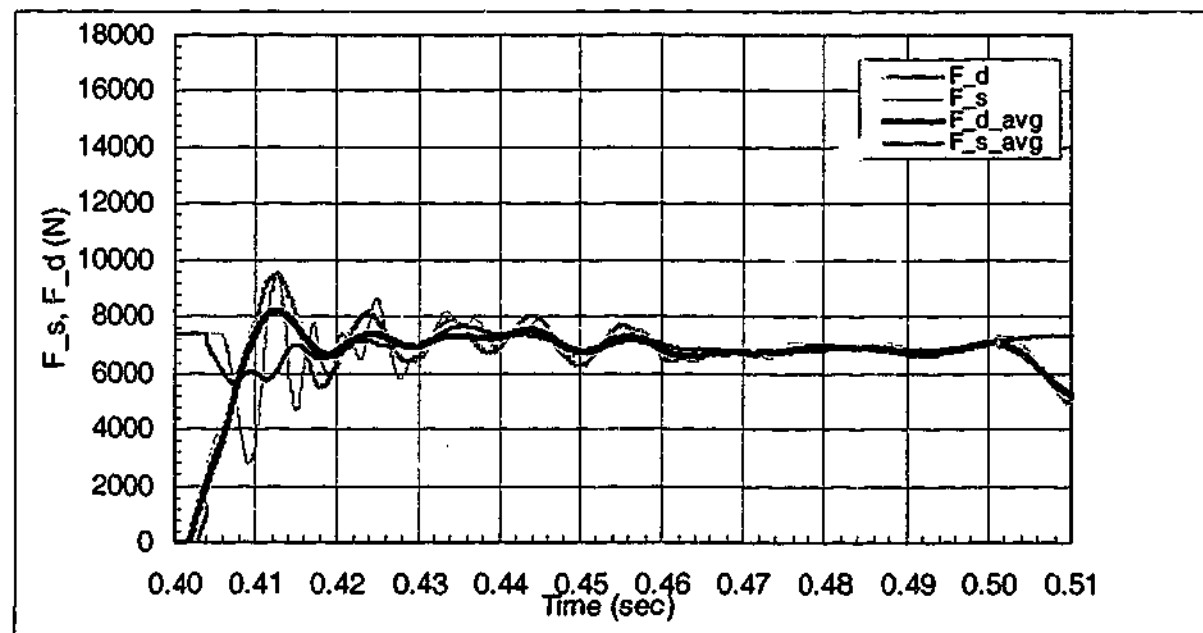
FILENAME	50WS.SC 250	INITIAL NORMAL STRESS	250 kPa
PILE	Smooth concrete	INITIAL DENSITY	1550 kg/m ³
SAND	50WS		



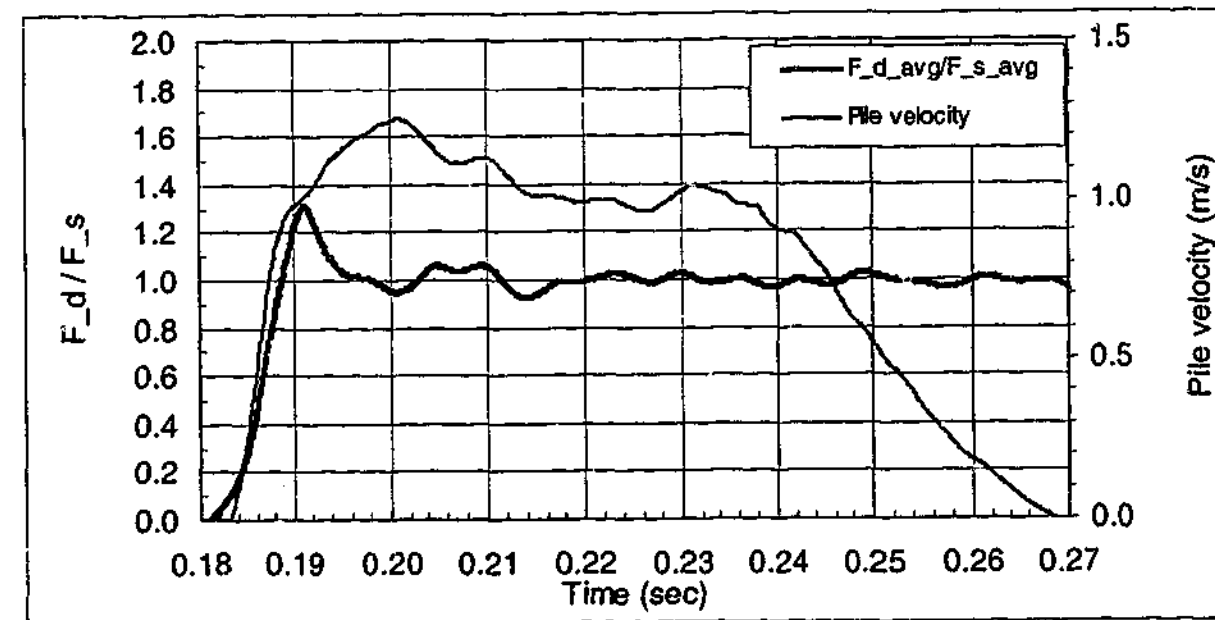
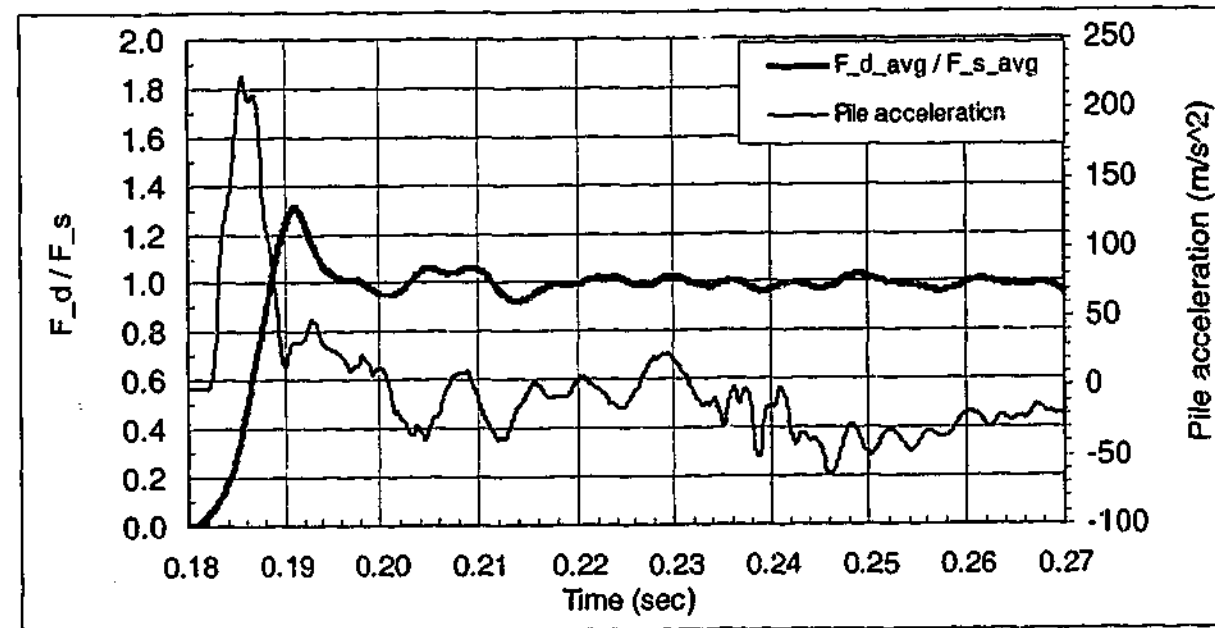
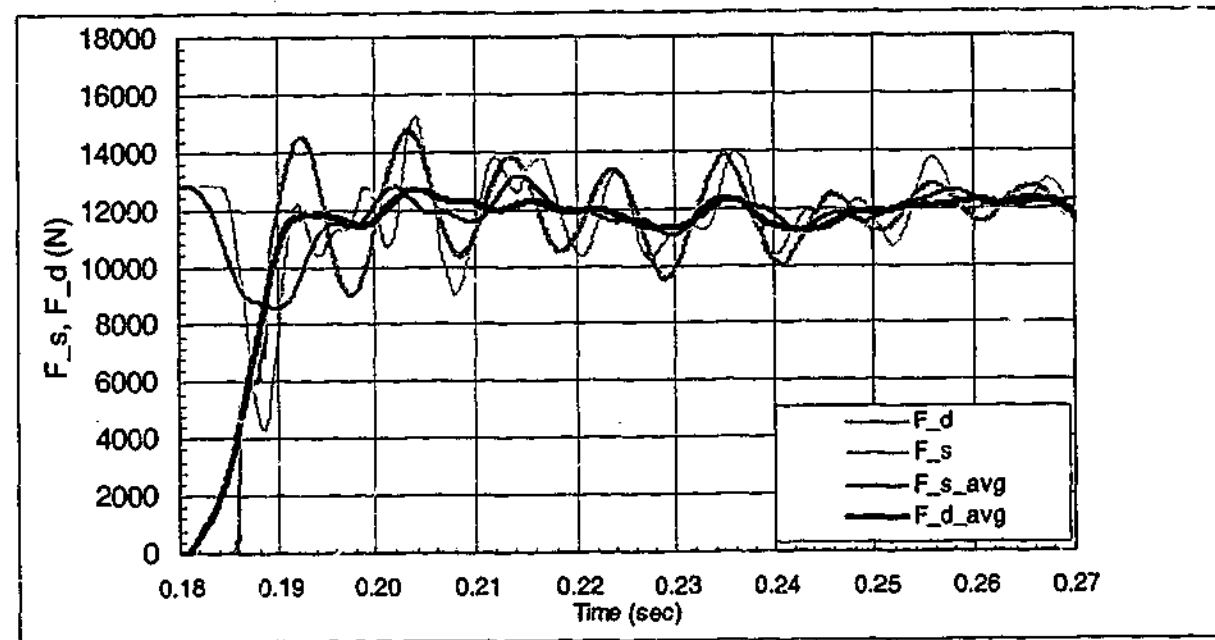
FILENAME 50WS.SC 250(repeat) INITIAL NORMAL STRESS 250 kPa
 PILE Smooth concrete INITIAL DENSITY 1520 kg/m³
 SAND 50WS



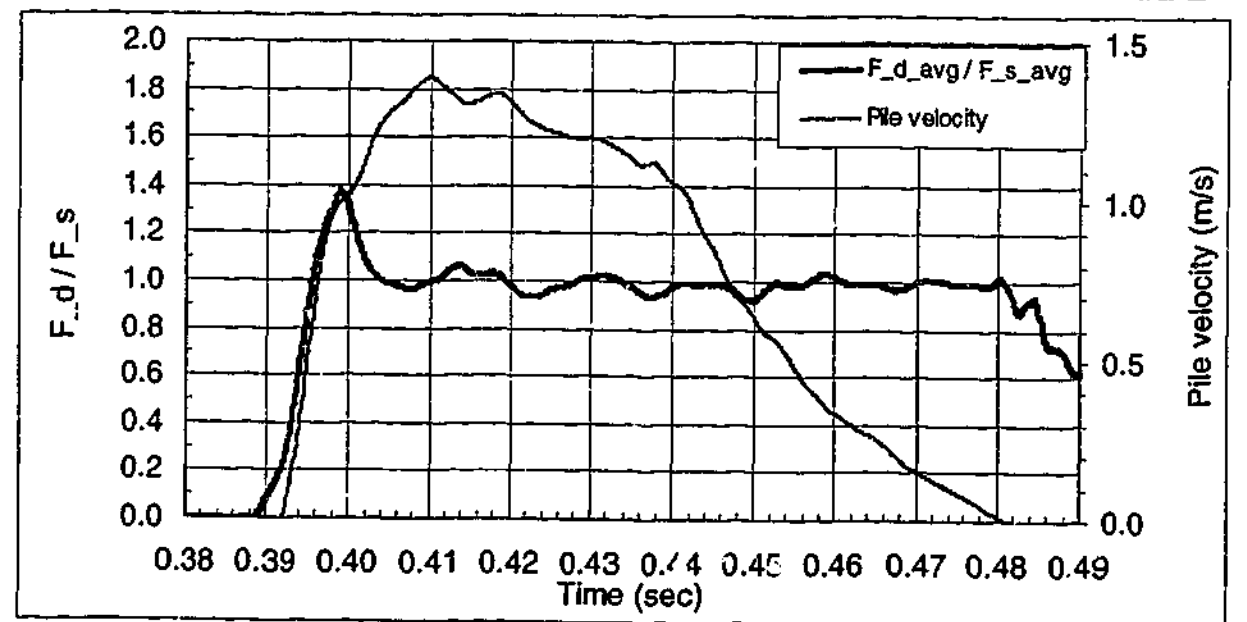
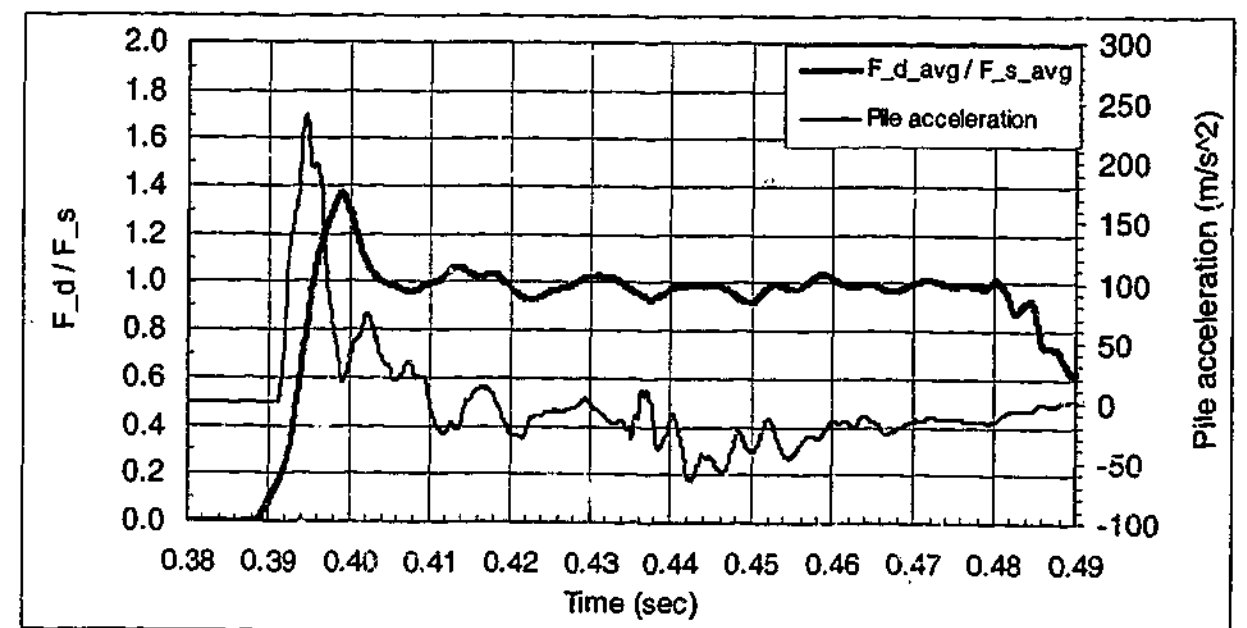
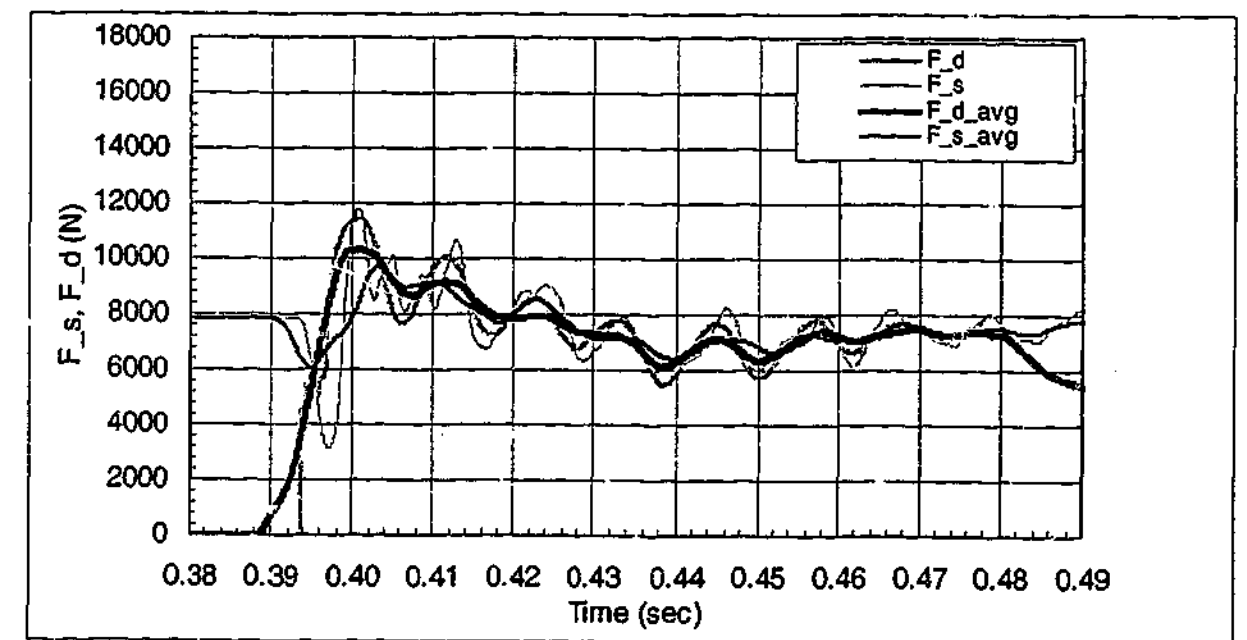
FILENAME 50WS.SC 150 INITIAL NORMAL STRESS 150 kPa
 PILE Smooth concrete INITIAL DENSITY 1540 kg/m³
 SAND 50WS



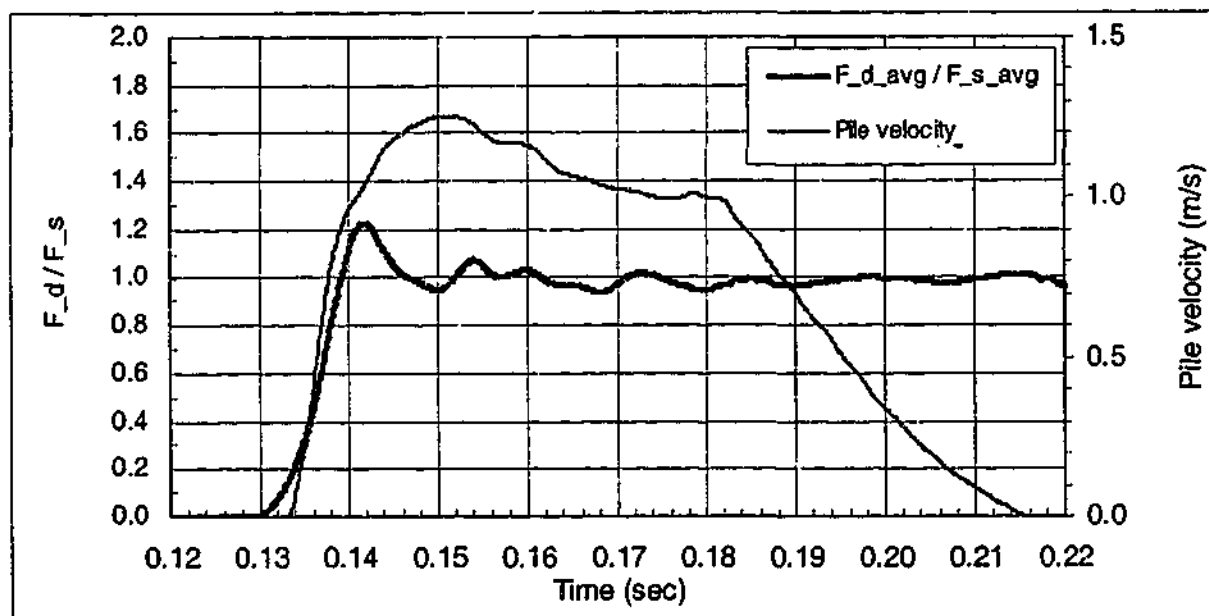
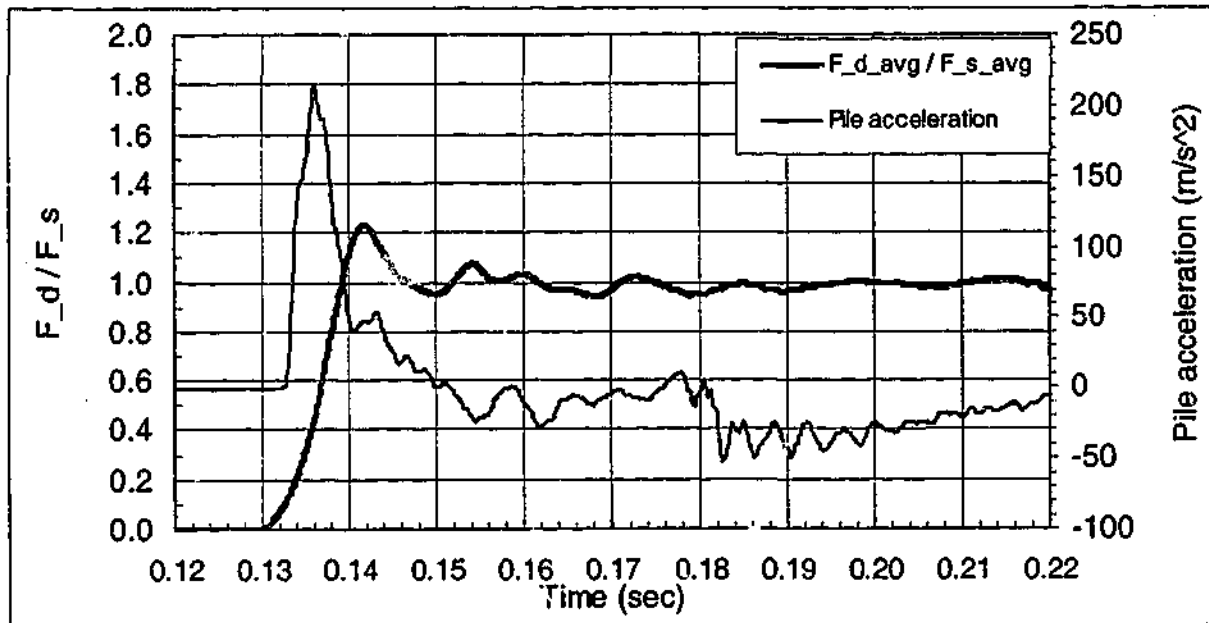
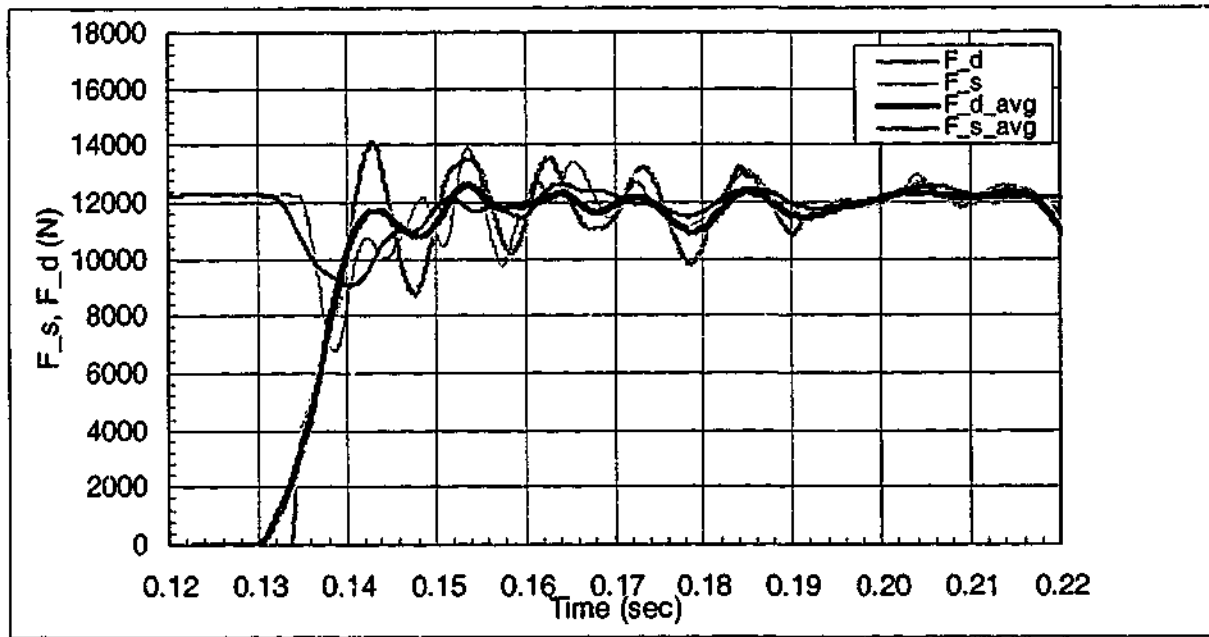
FILENAME 50WS.RC 250 INITIAL NORMAL STRESS 250 KPa.
 PILE Rough concrete INITIAL DENSITY 1540 kg/m³
 SAND 50WS



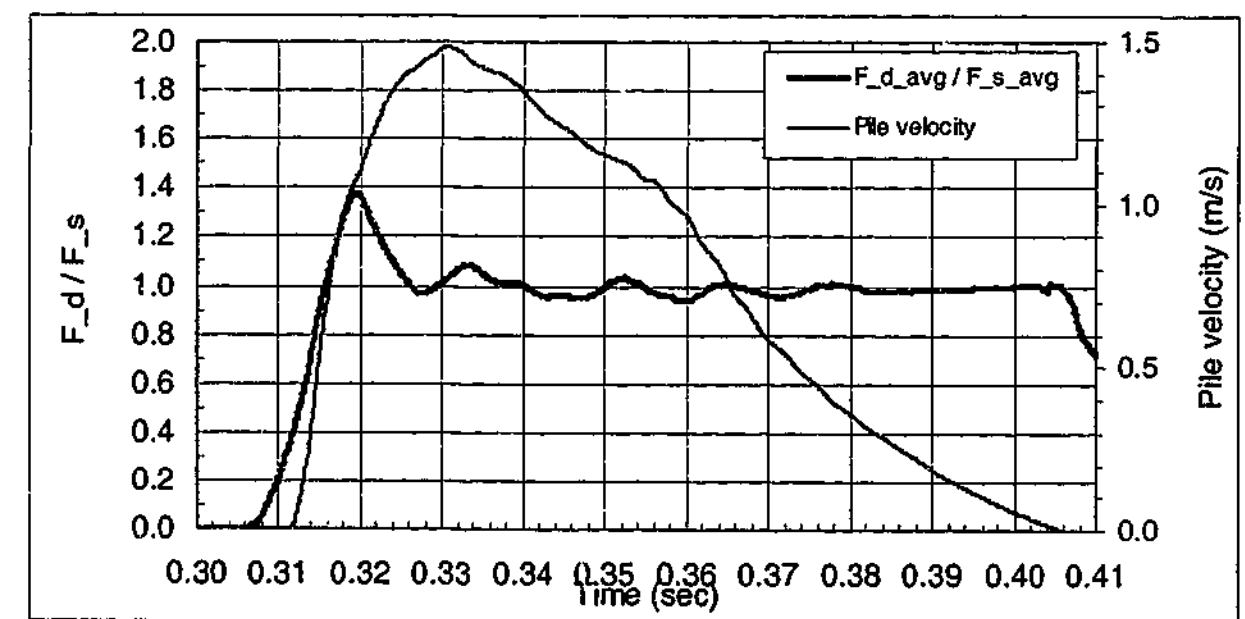
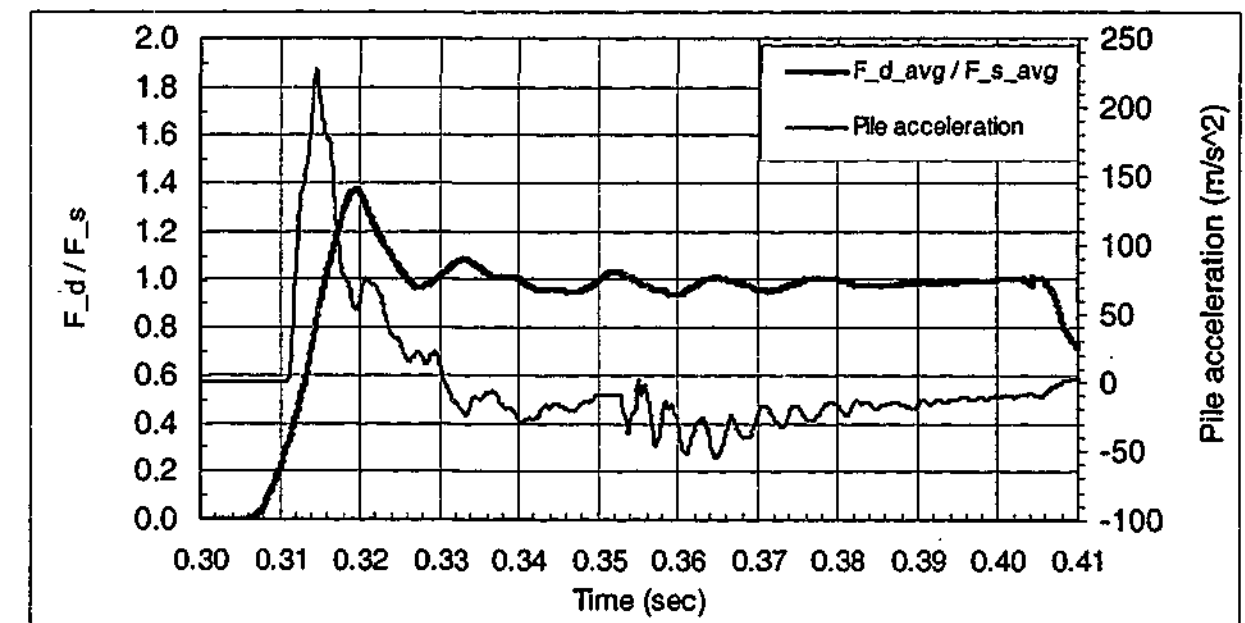
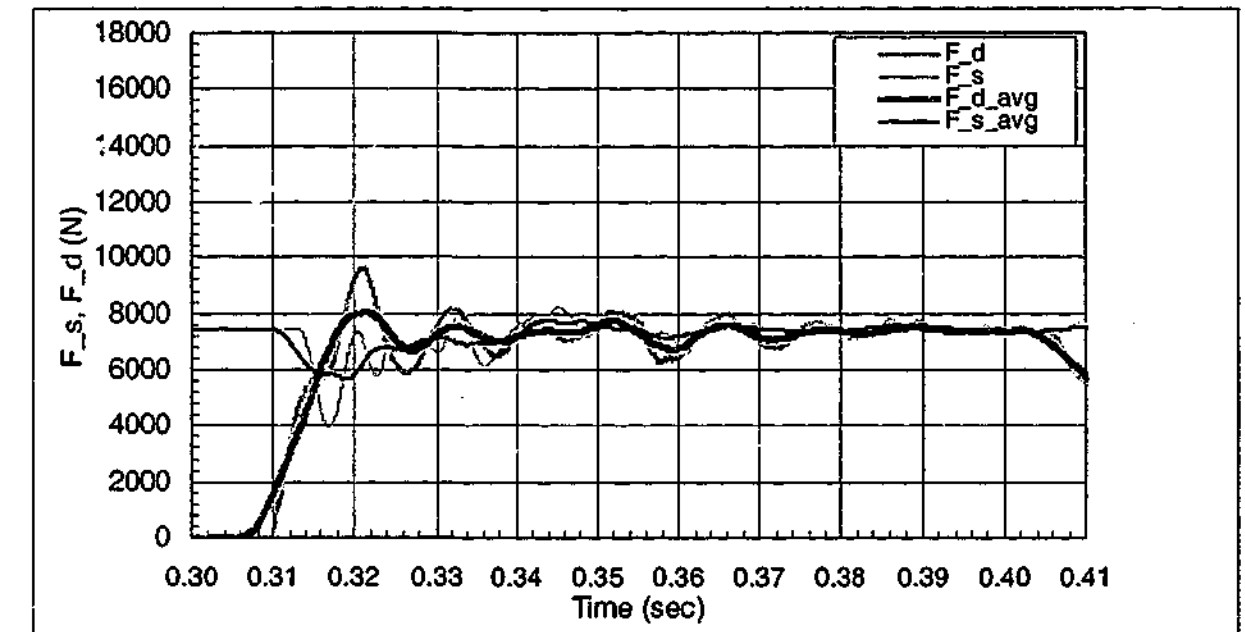
FILENAME 50WS.RC 150 INITIAL NORMAL STRESS 150 kPa
 PILE Rough concrete INITIAL DENSITY 1540 kg/m³
 SAND 50WS



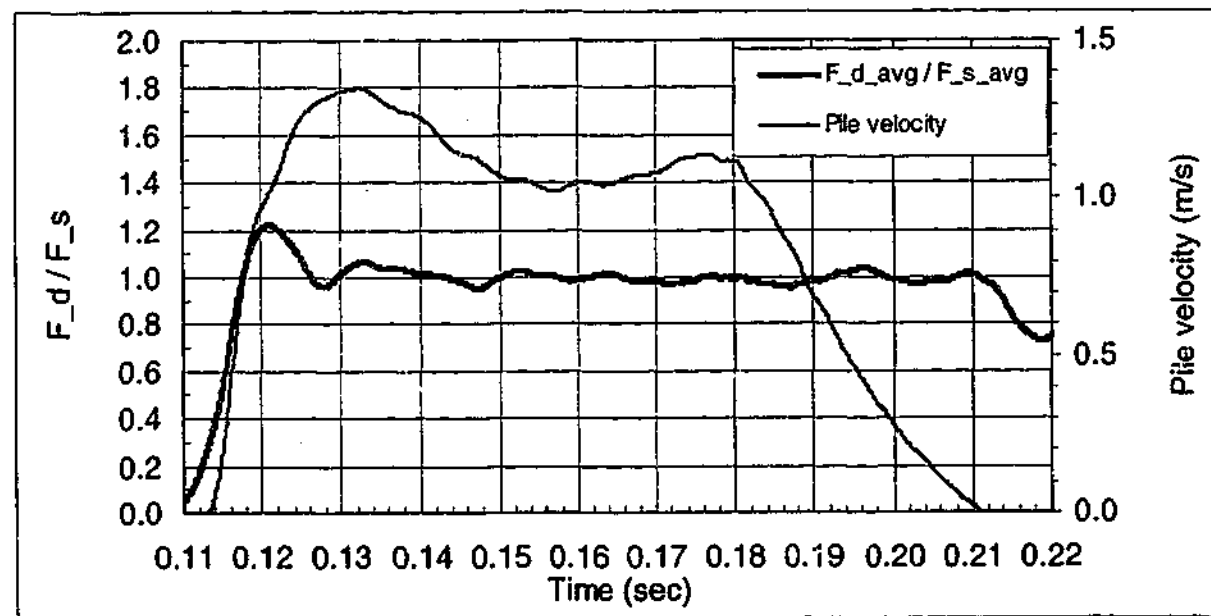
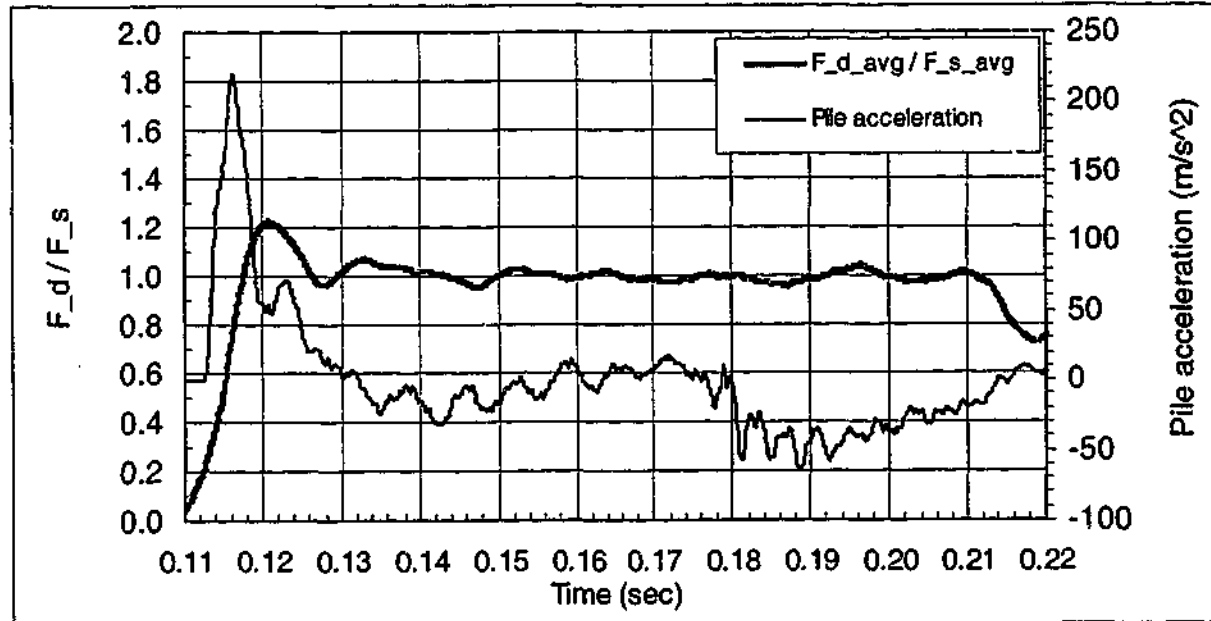
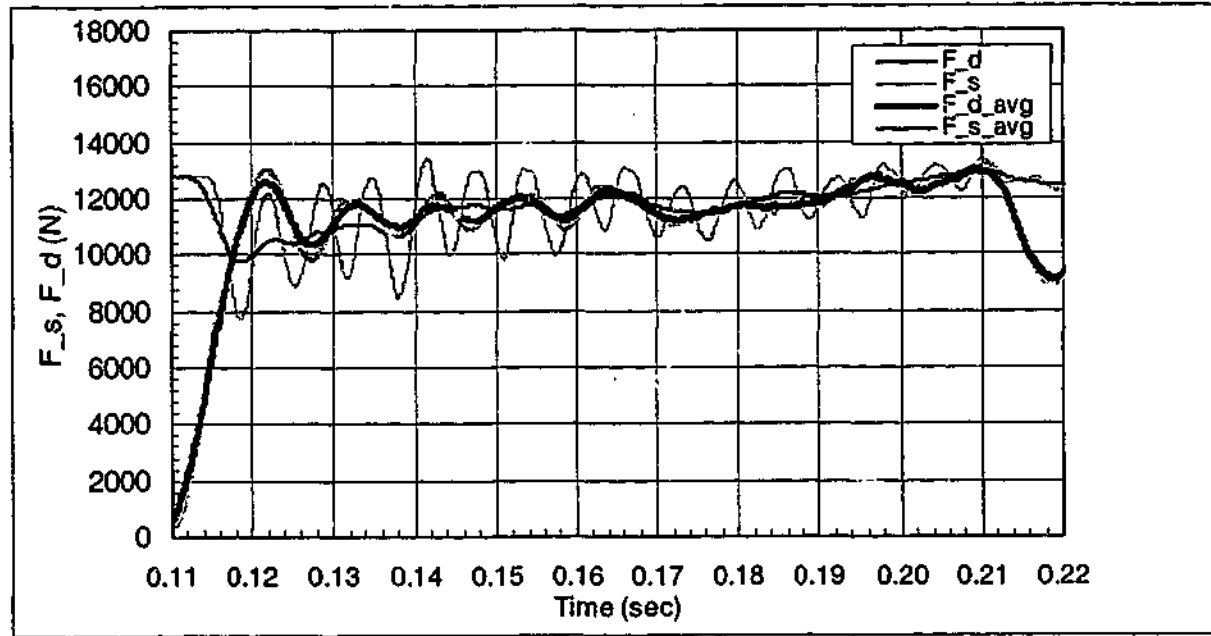
FILENAME Sat50WS.SC 250 INITIAL NORMAL STRESS 250 kPa
 PILE Smooth concrete INITIAL DENSITY kg/m³
 SAND Saturated 50WS



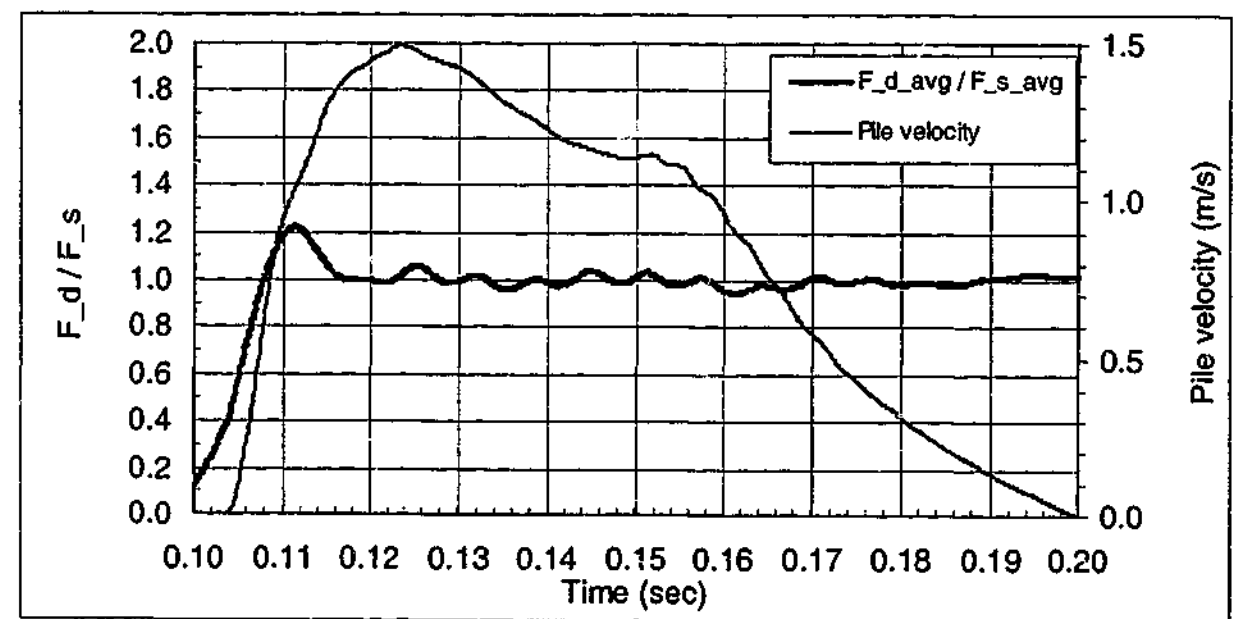
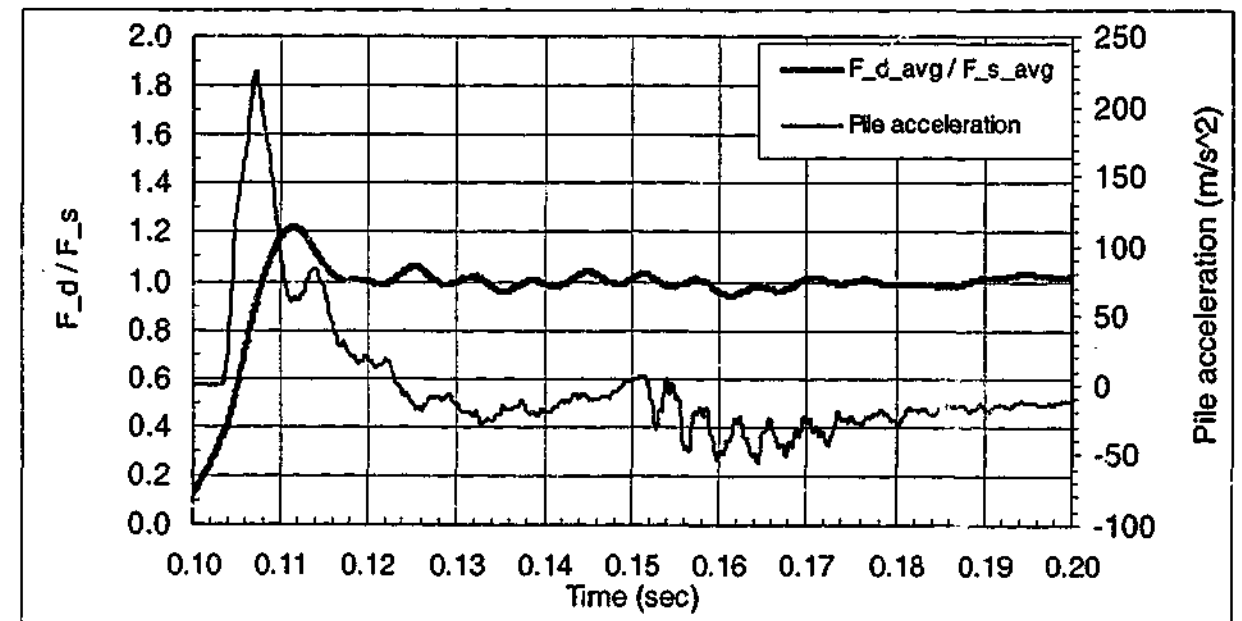
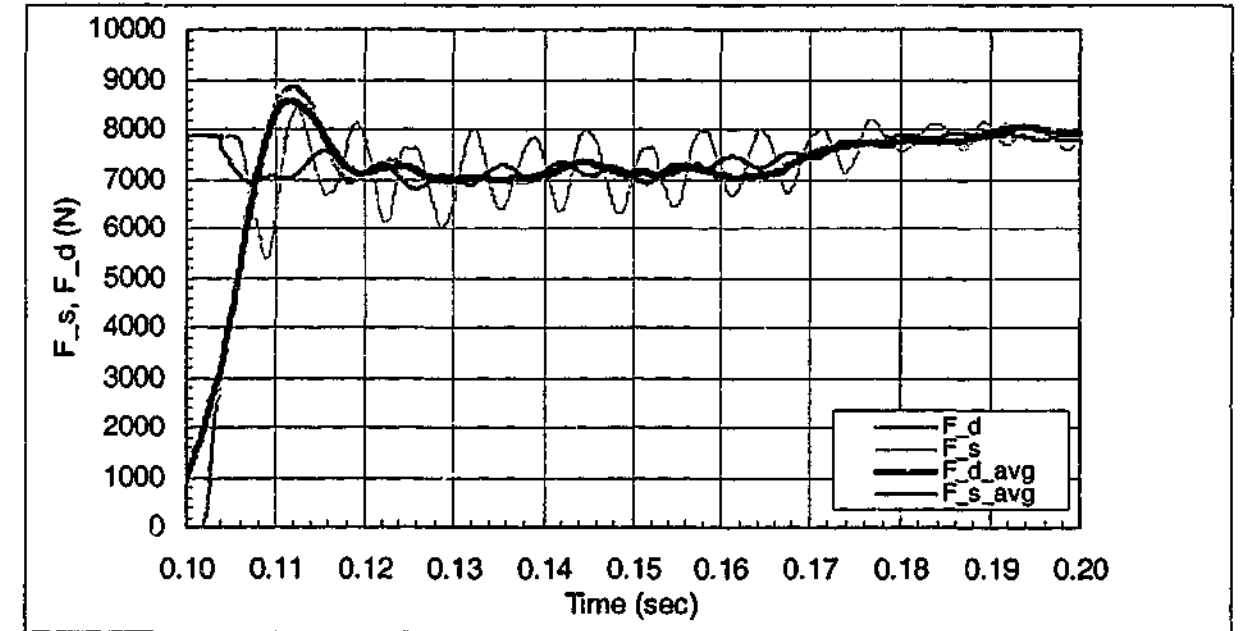
FILENAME Sat50WS.SC 150 INITIAL NORMAL STRESS 150 kPa
 PILE Smooth concrete INITIAL DENSITY kg/m³
 SAND Saturated 50WS



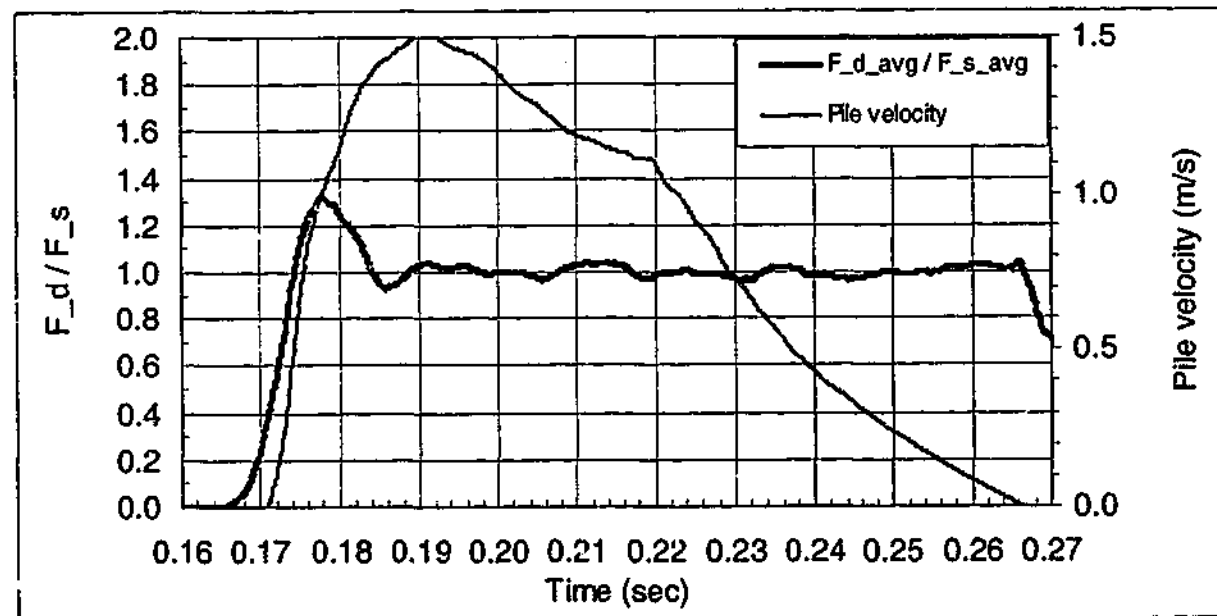
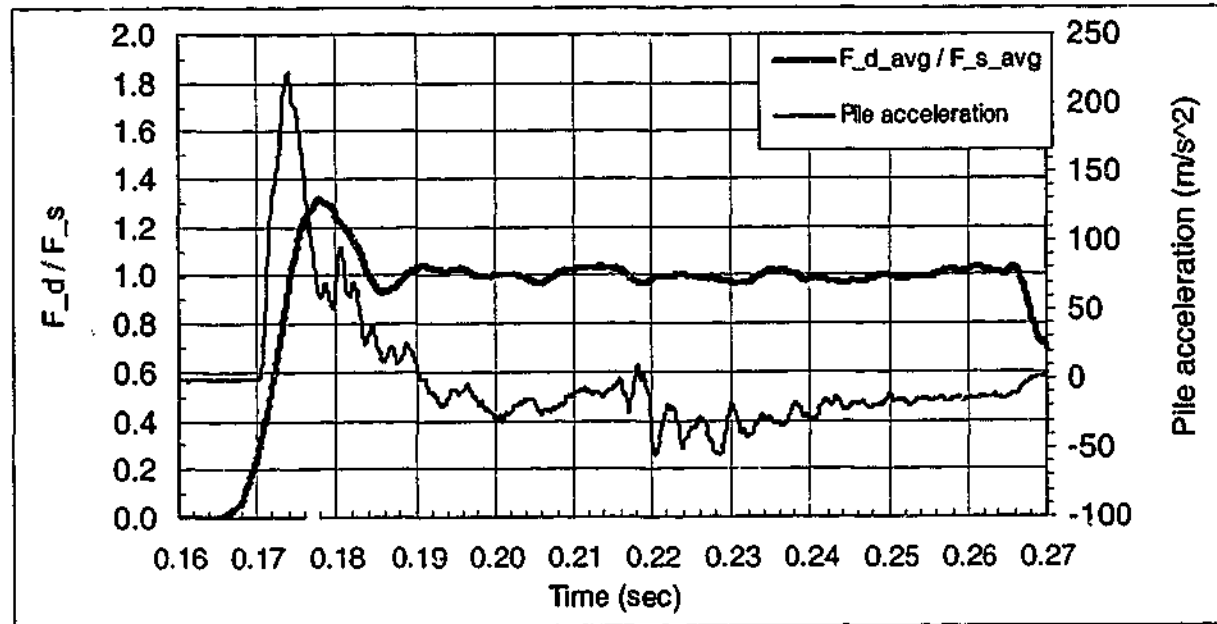
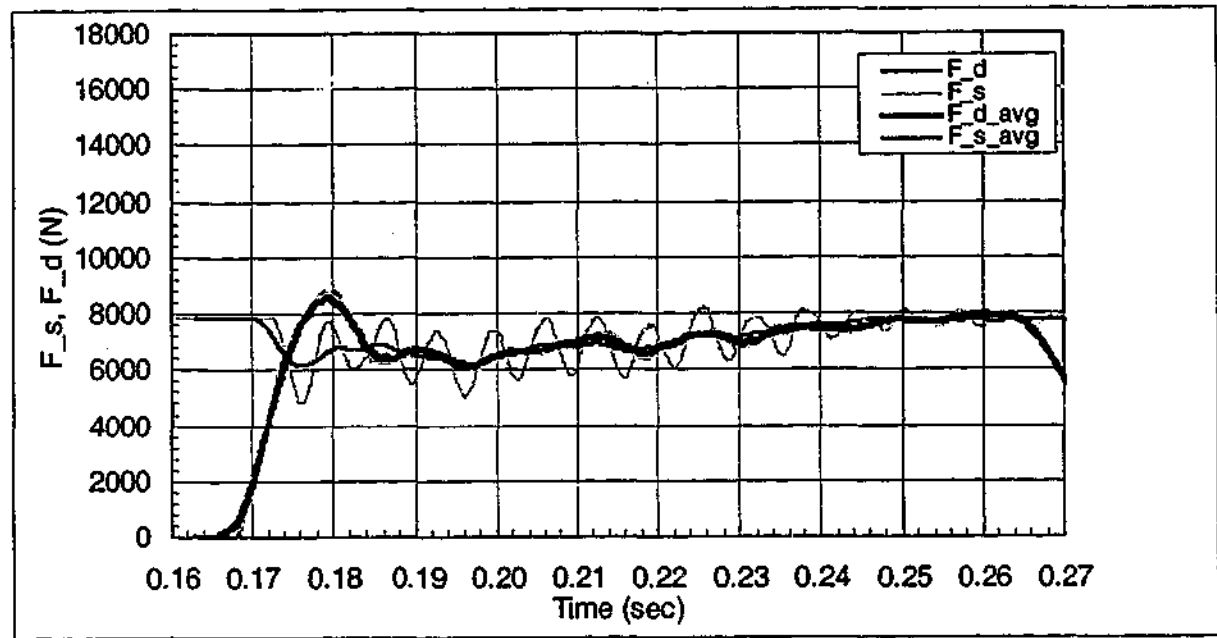
FILENAME 816.SC 250 INITIAL NORMAL STRESS 250 kPa
 PILE Smooth concrete INITIAL DENSITY 1460 kg/m³
 SAND 8/16



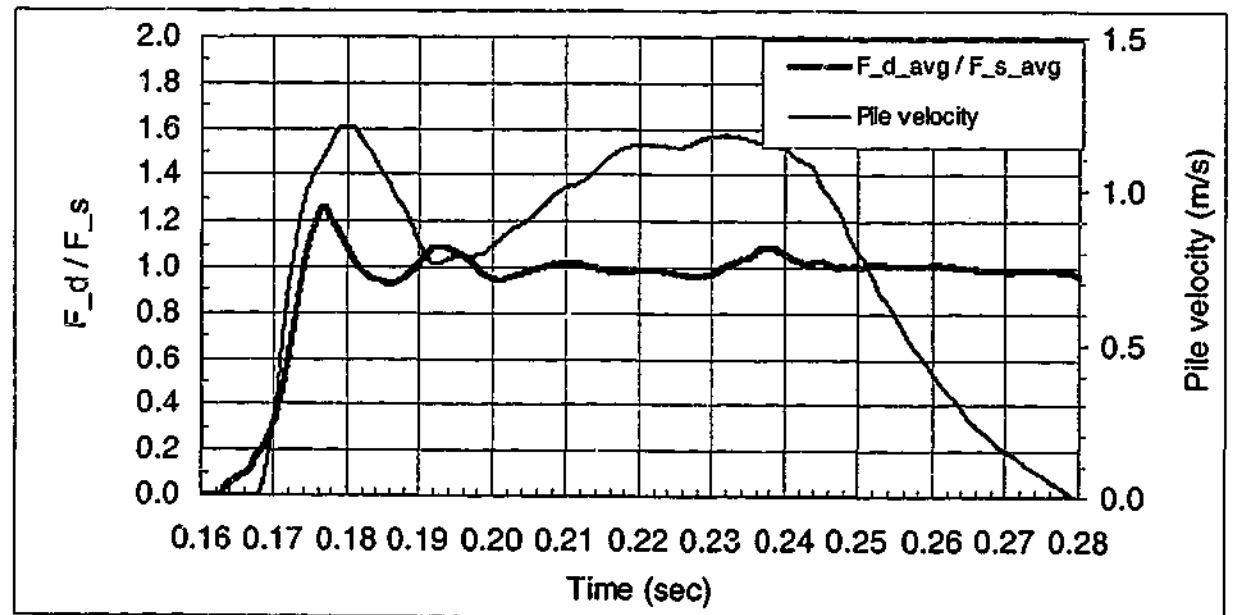
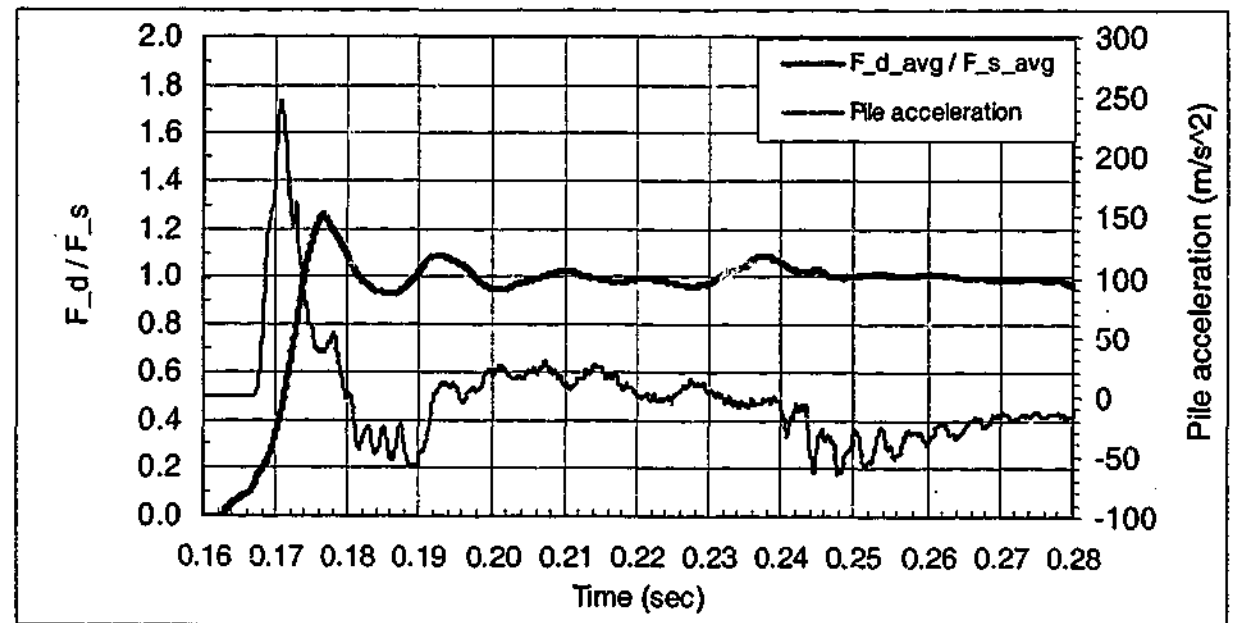
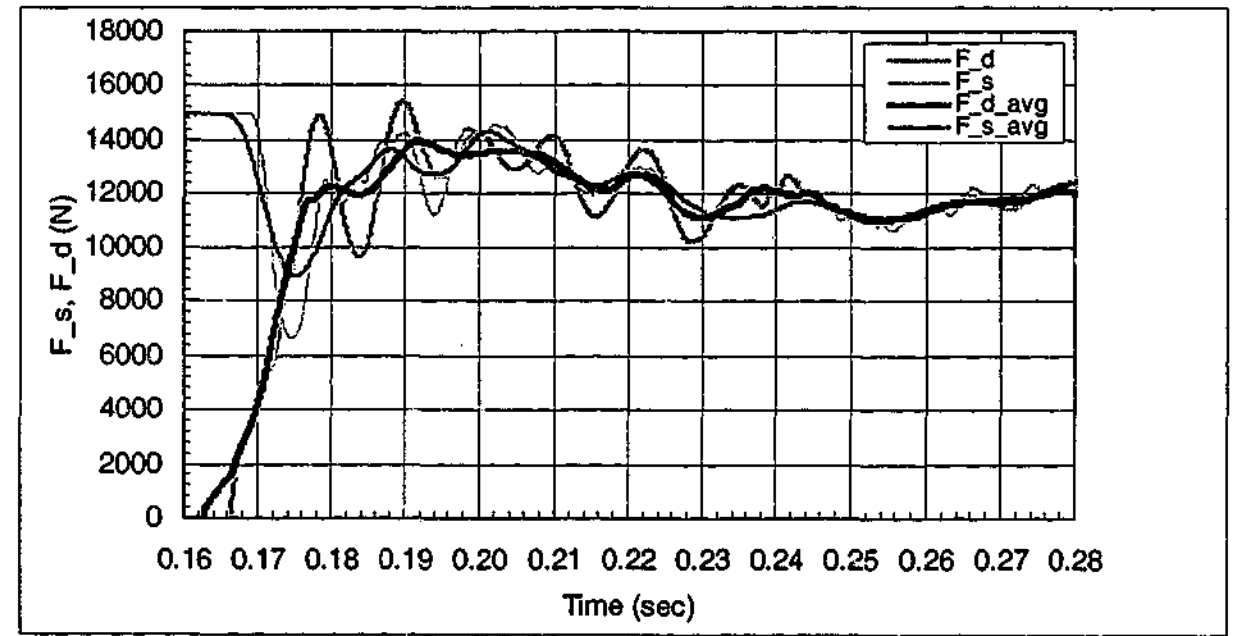
FILENAME 816.SC 150 INITIAL NORMAL STRESS 150 kPa
 PILE Smooth concrete INITIAL DENSITY 1460 kg/m³
 SAND 8/16



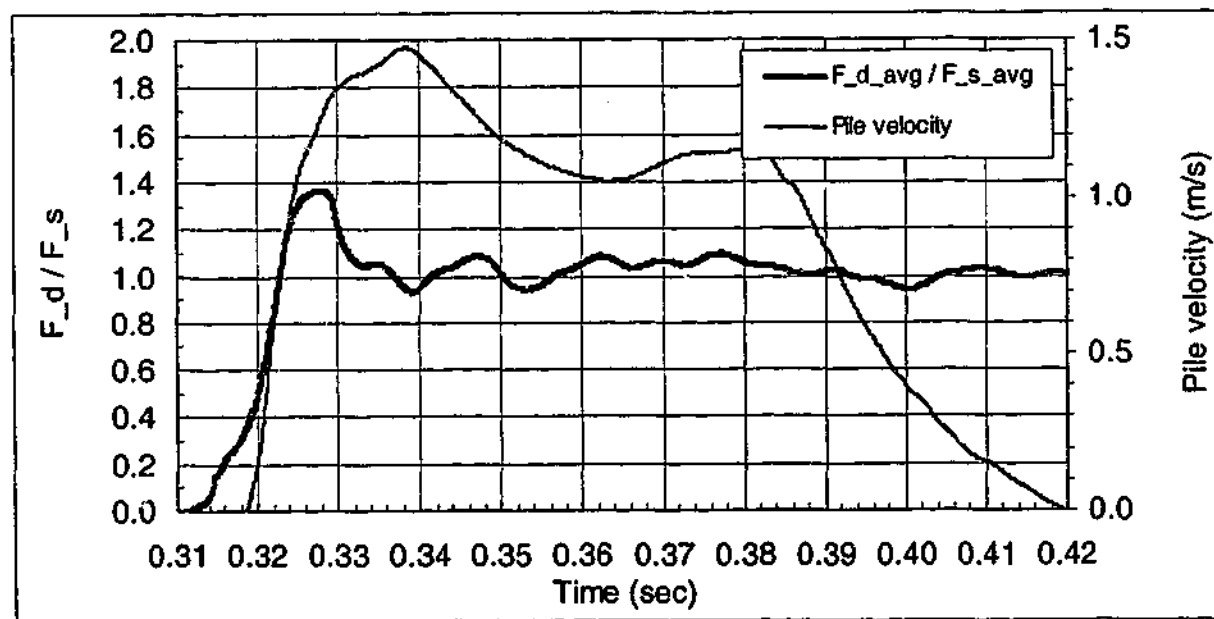
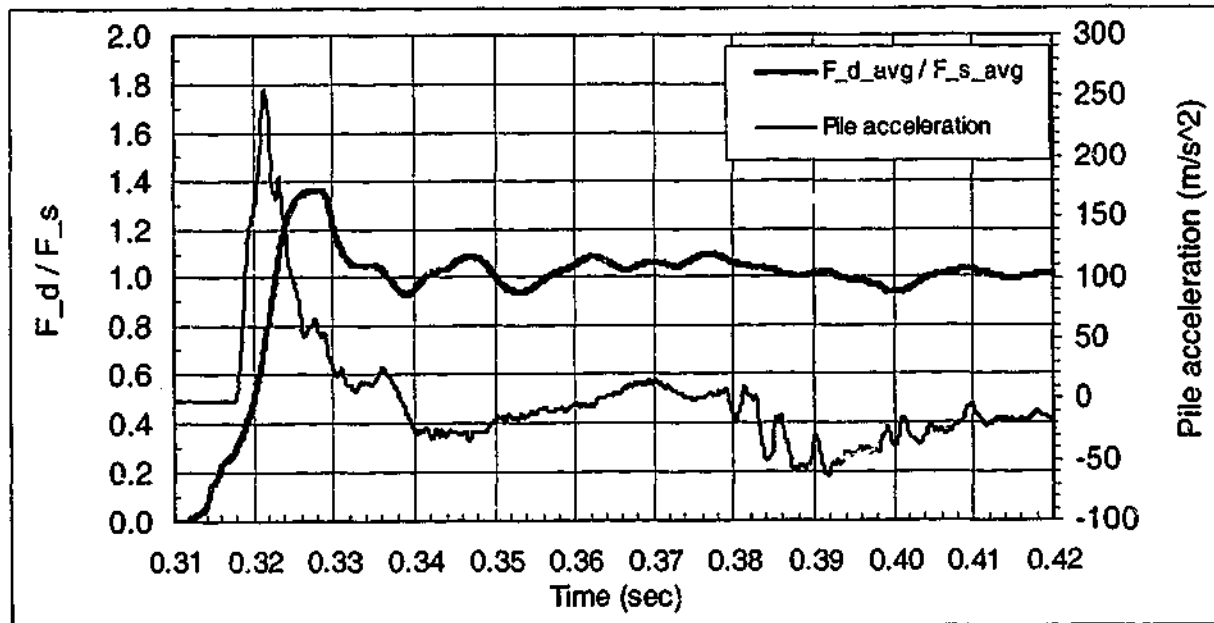
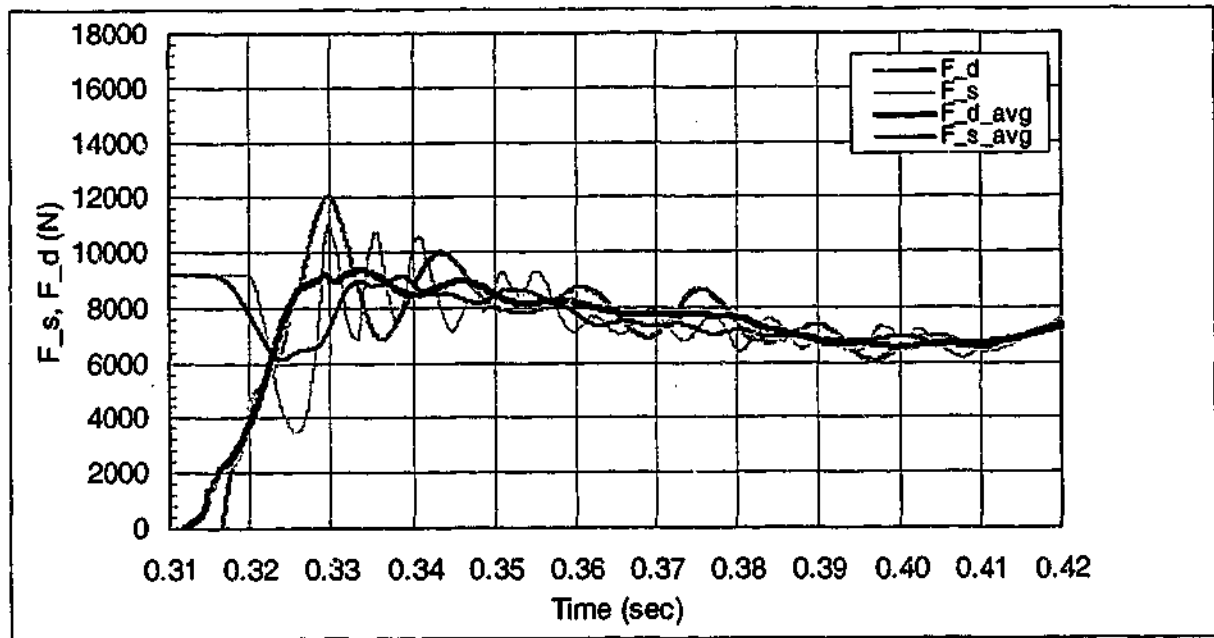
FILENAME 816.SC 150(repeat) INITIAL NORMAL STRESS 150 kPa
 PILE Smooth concrete INITIAL DENSITY 1450 kg/m³
 SAND 8/16



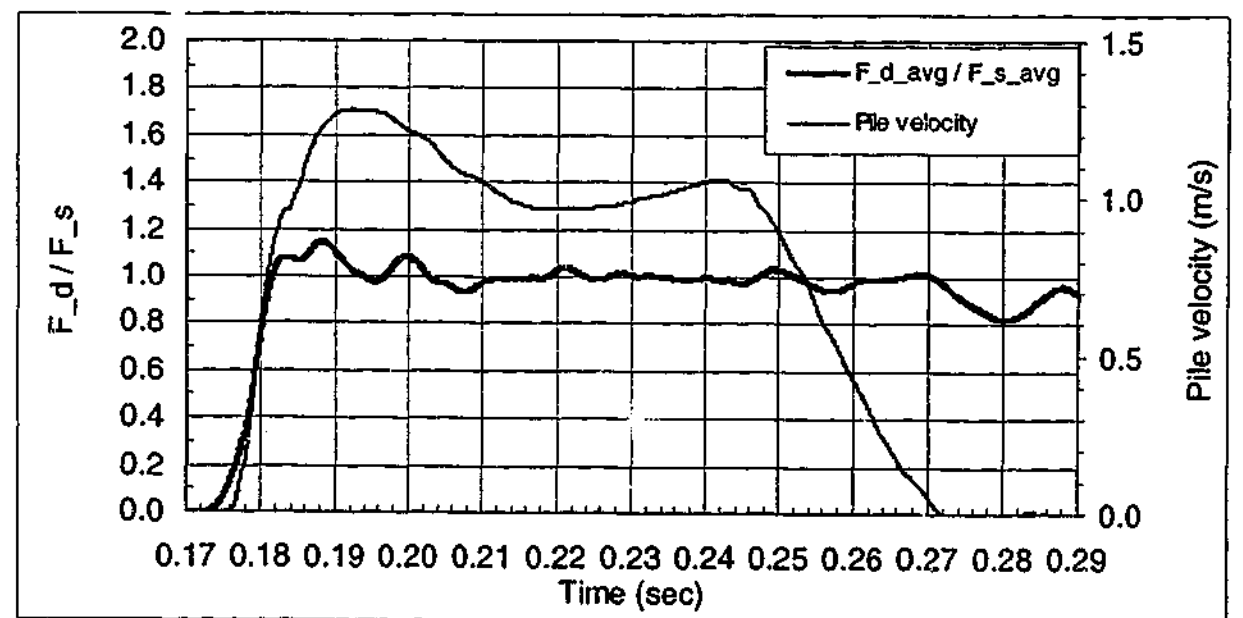
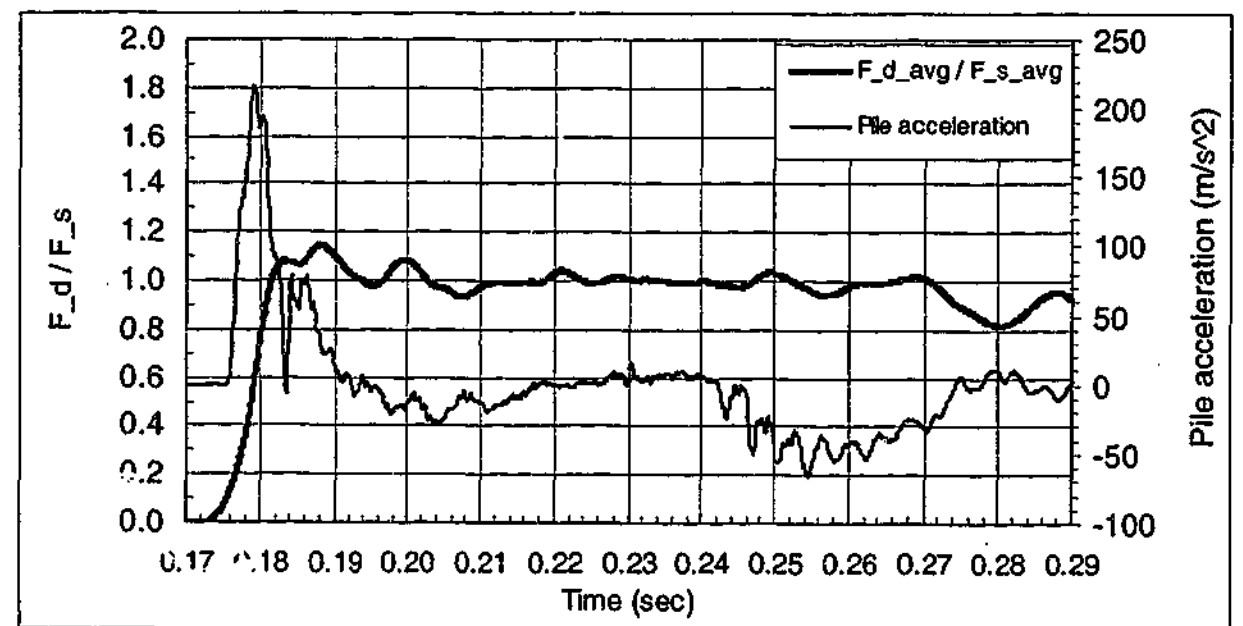
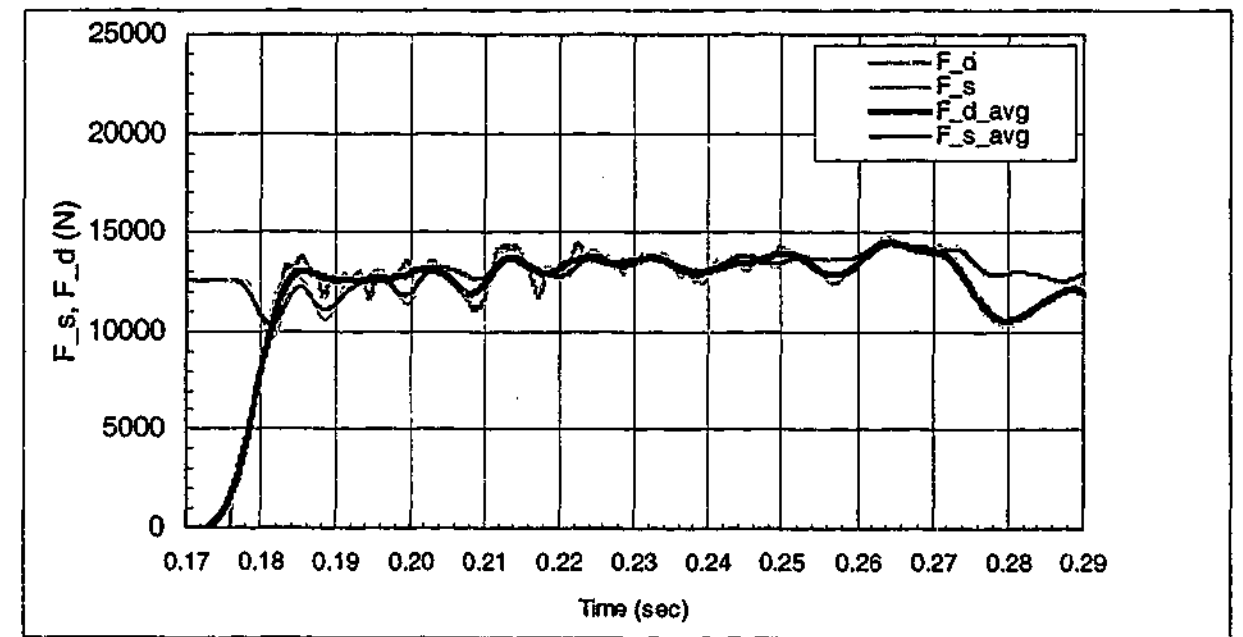
FILENAME 816.RC 250 INITIAL NORMAL STRESS 250 kPa
 PILE Rough concrete INITIAL DENSITY 1450 kg/m³
 SAND 8/16



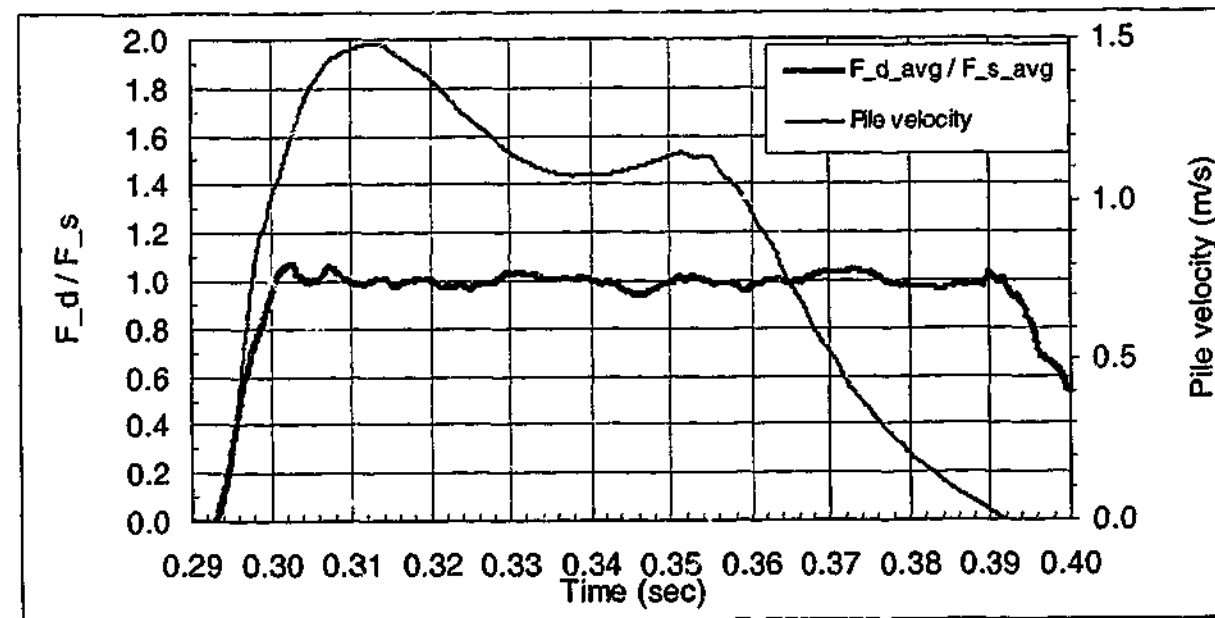
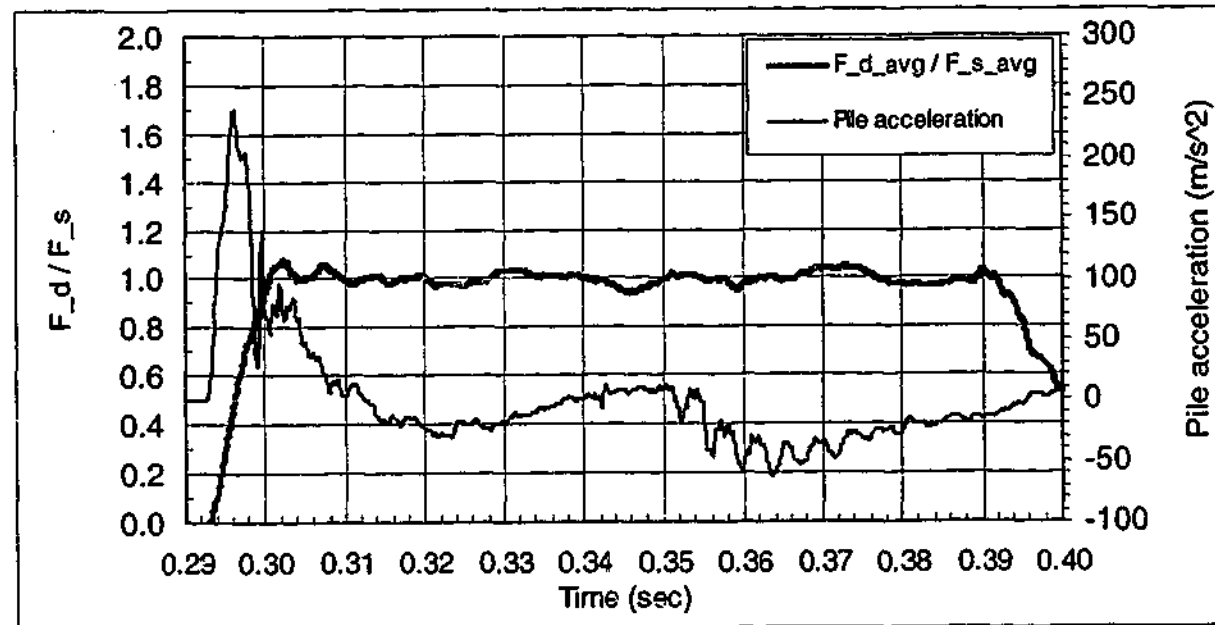
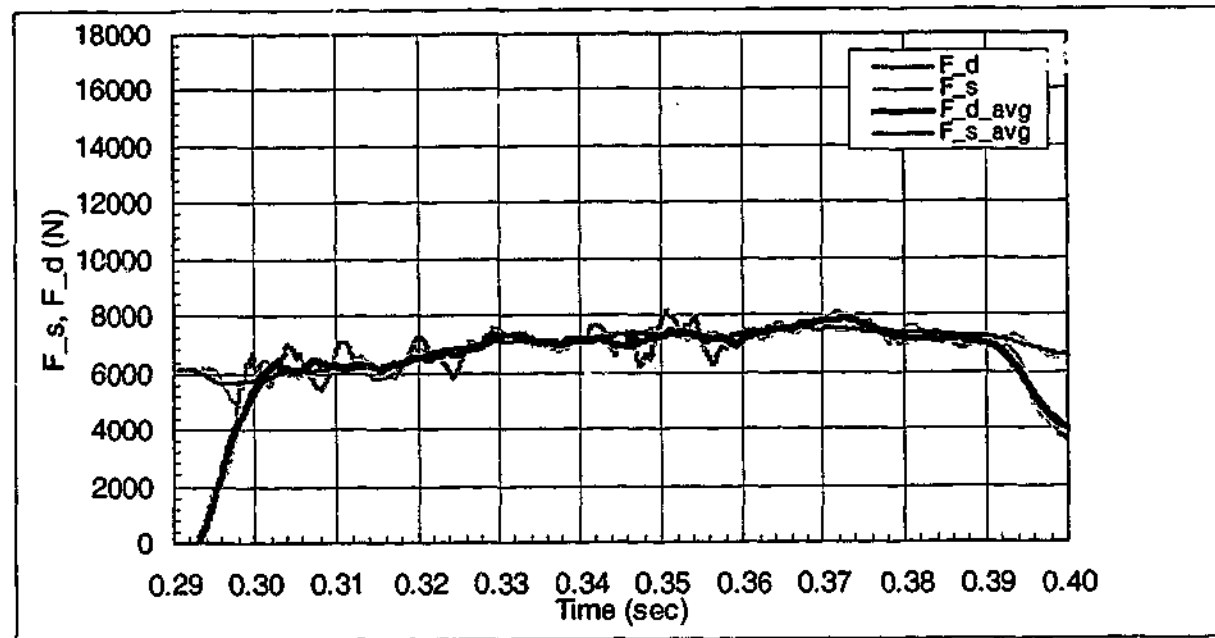
FILENAME 816.RC 150 INITIAL NORMAL STRESS 150 kPa
 PILE Rough concrete INITIAL DENSITY 1480 kg/m³
 SAND 8/16



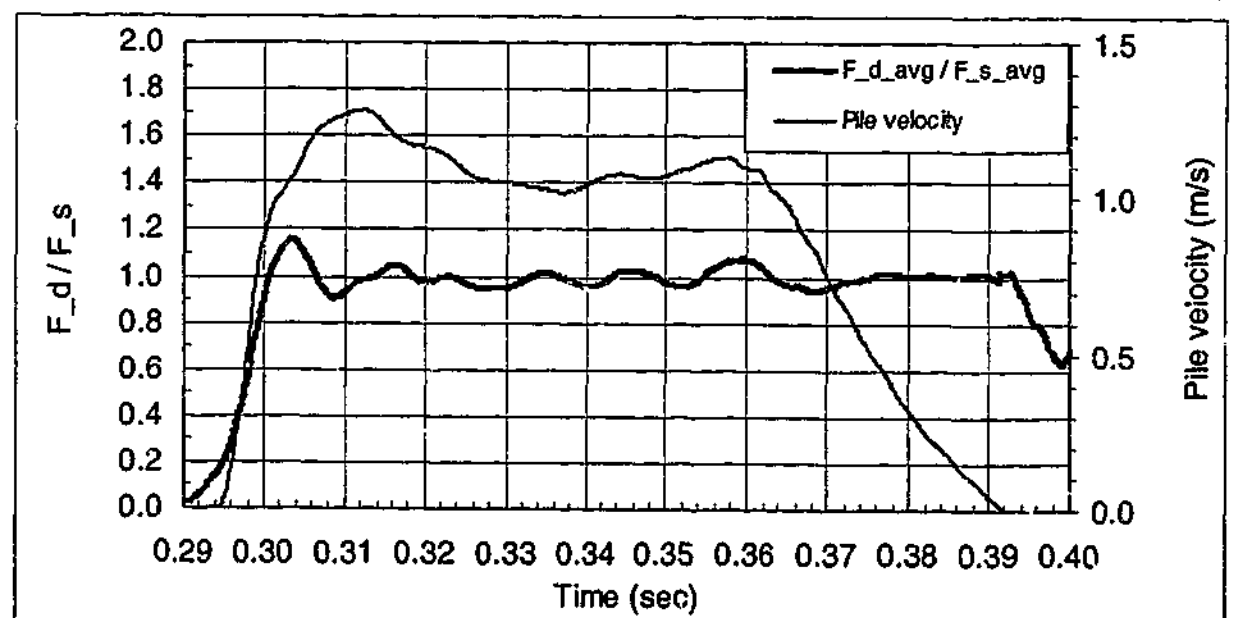
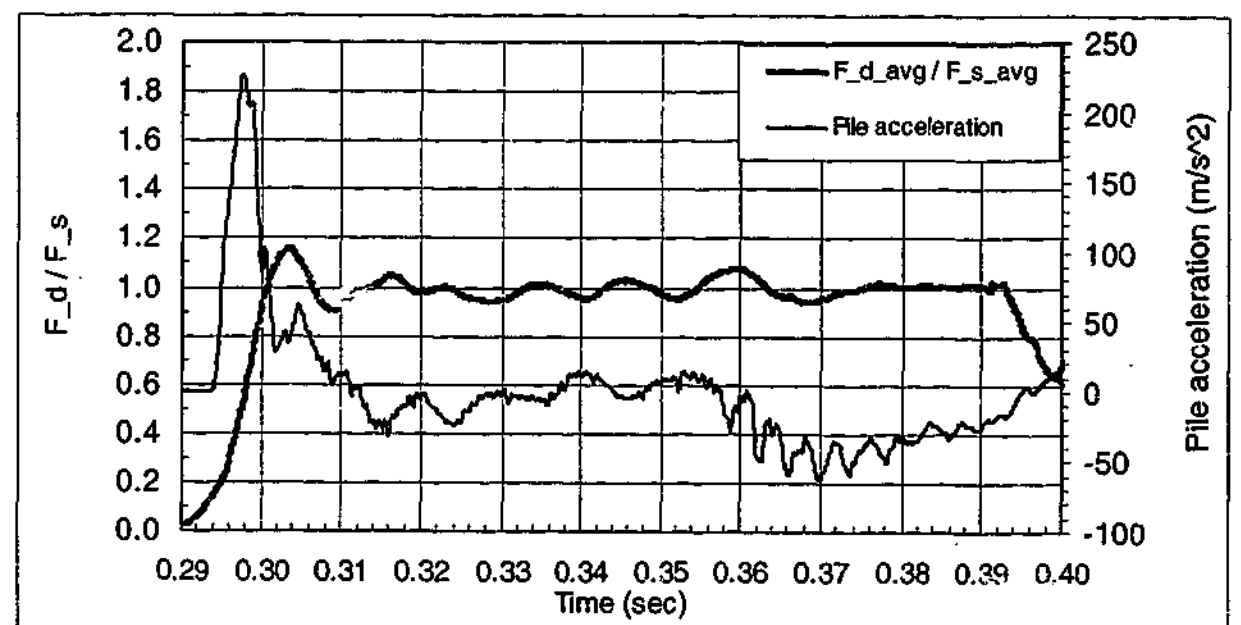
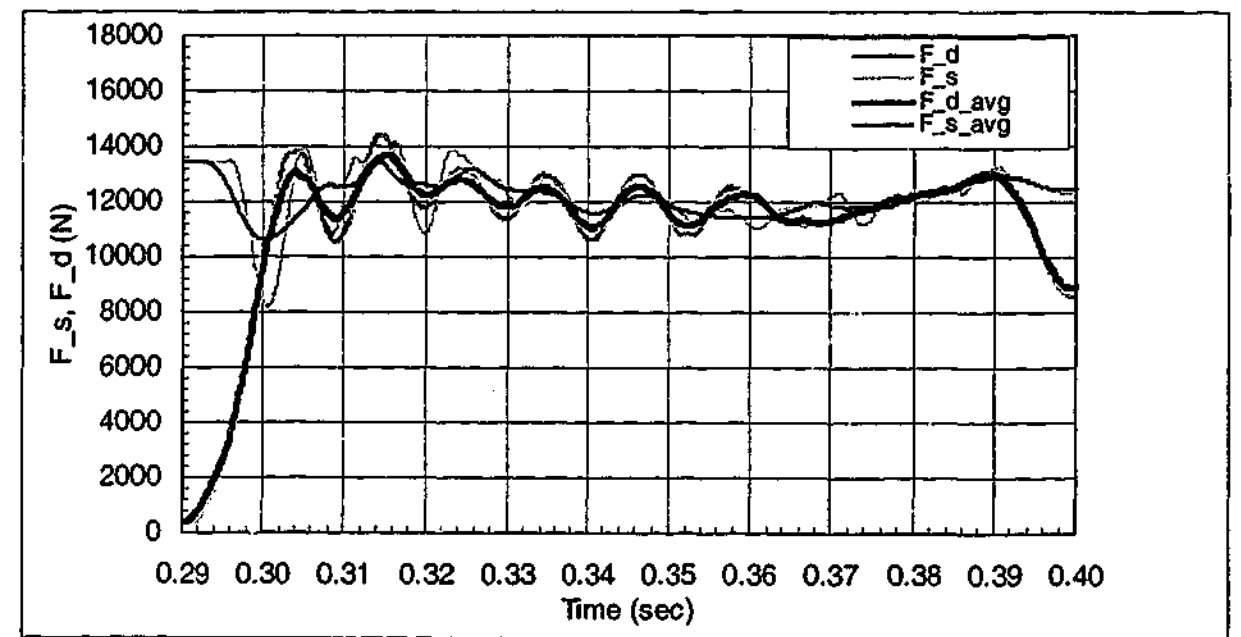
FILENAME Y.SC 250 INITIAL NORMAL STRESS 250 kPa
 PILE Smooth concrete INITIAL DENSITY 1650 kg/m³
 SAND Yea



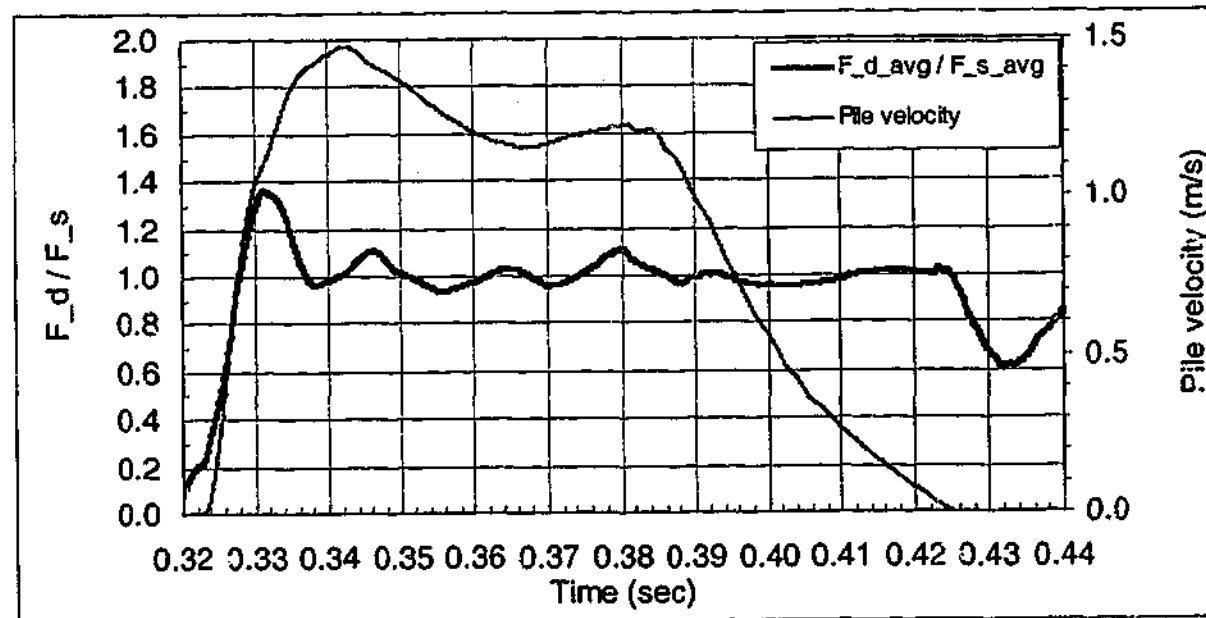
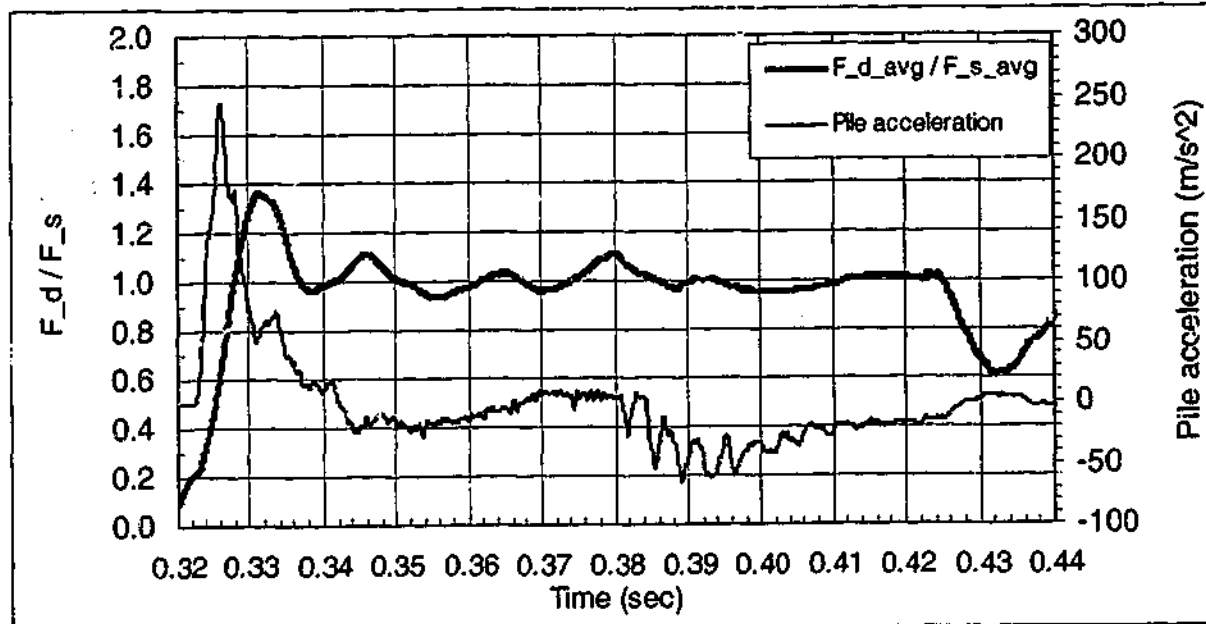
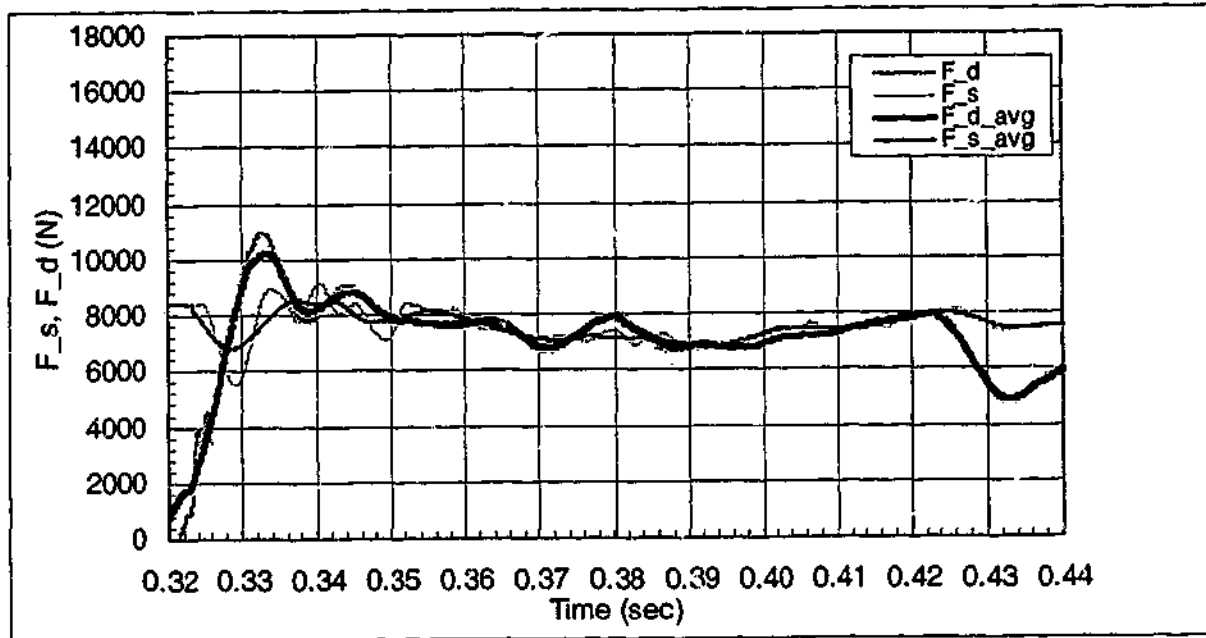
FILENAME Y.SC 150 INITIAL NORMAL STRESS 150 kPa
 PILE Smooth concrete INITIAL DENSITY 1650 kg/m³
 SAND Yea



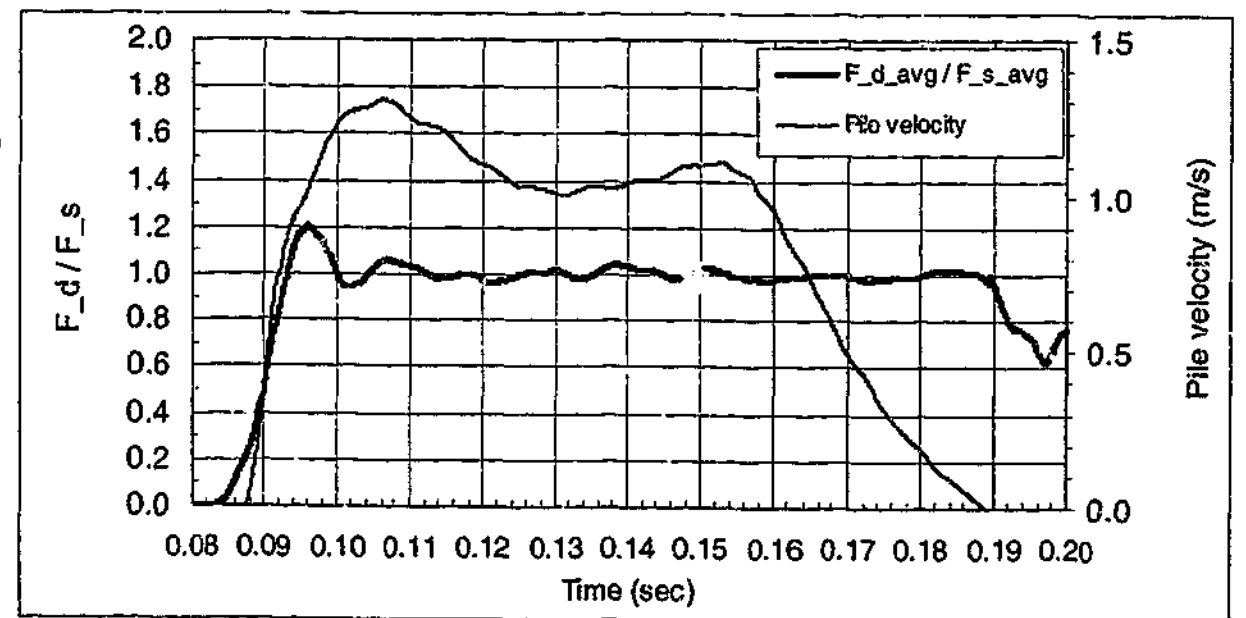
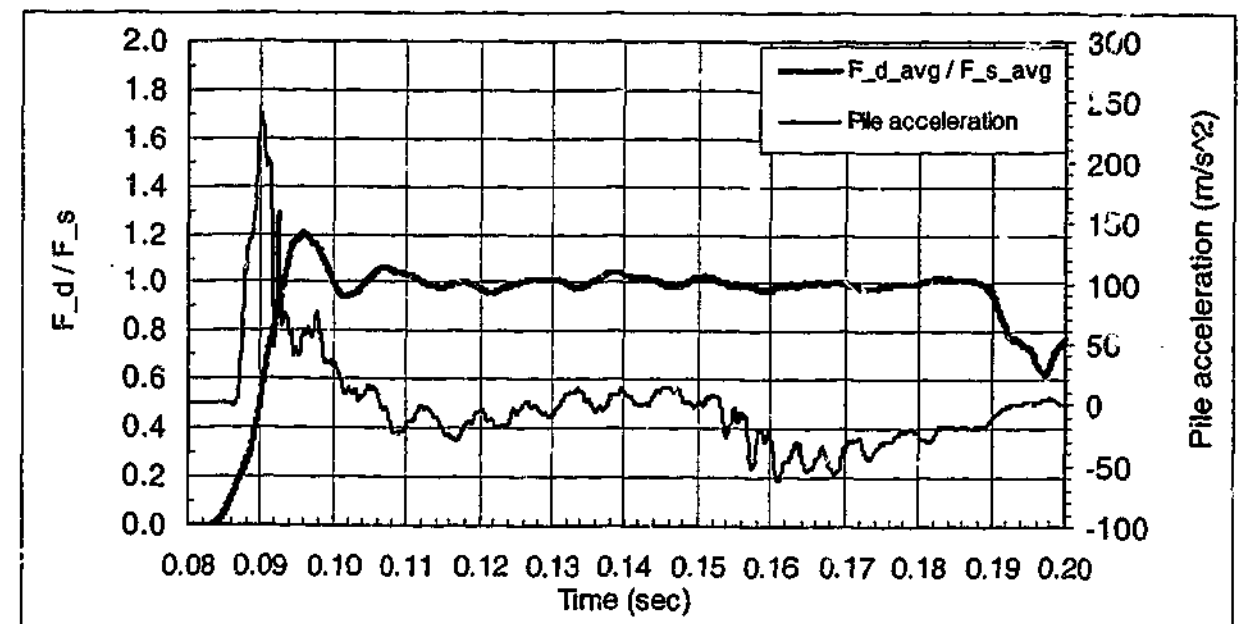
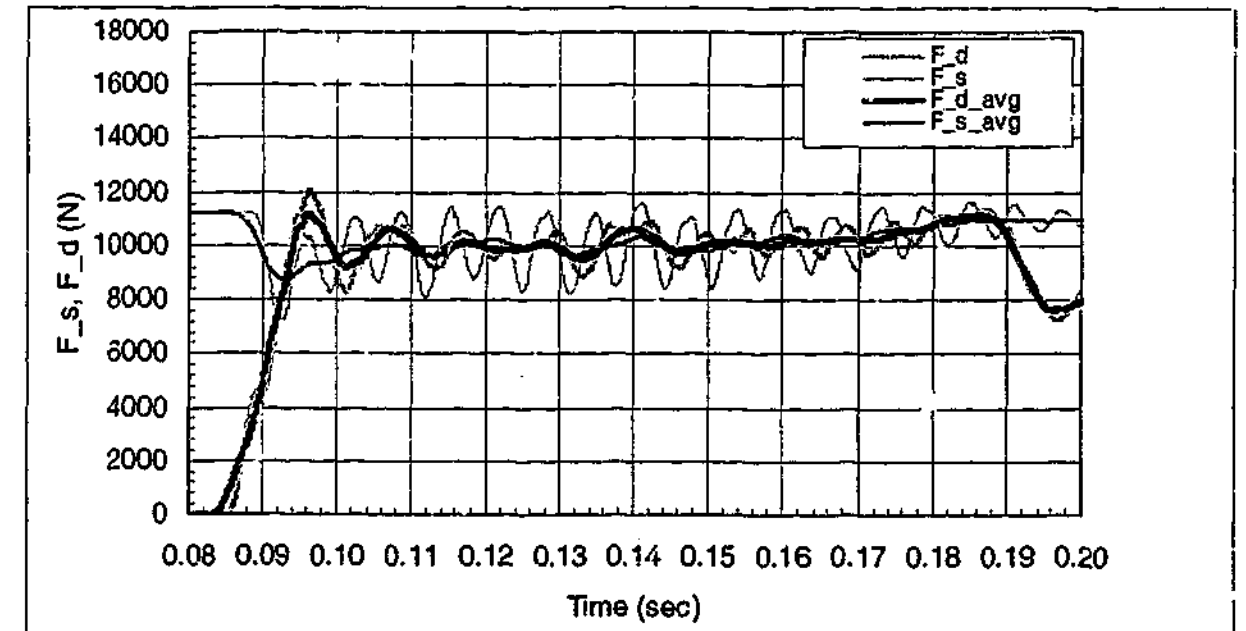
FILENAME Y.RC 250 INITIAL NORMAL STRESS 250 kPa
 PILE Rough concrete INITIAL DENSITY 1670 kg/m³
 SAND Yea



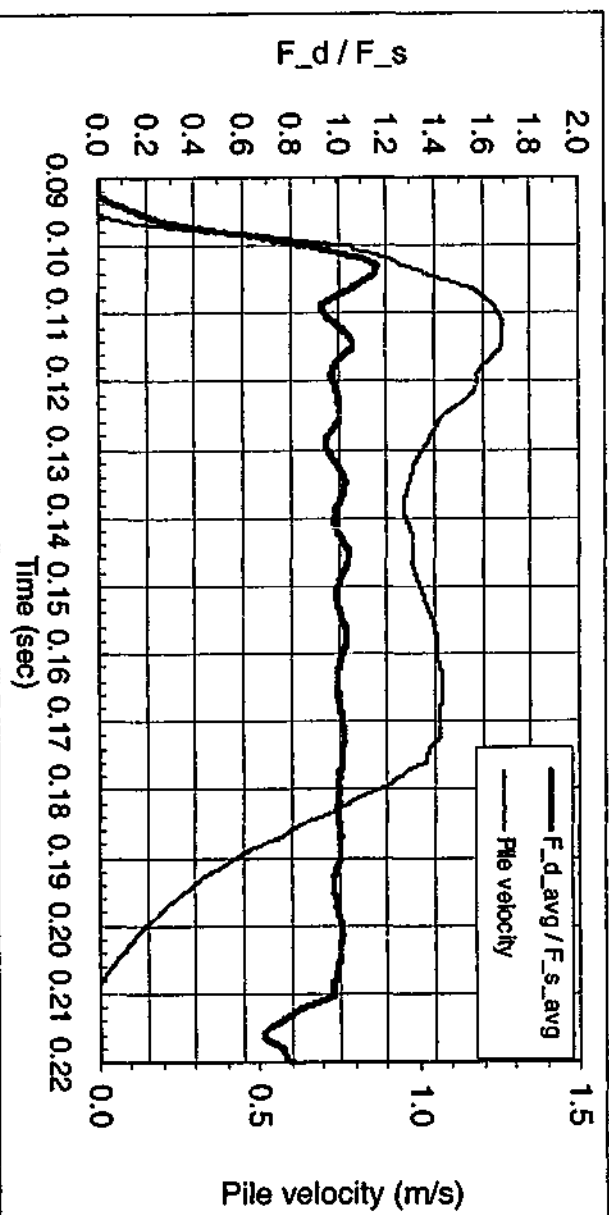
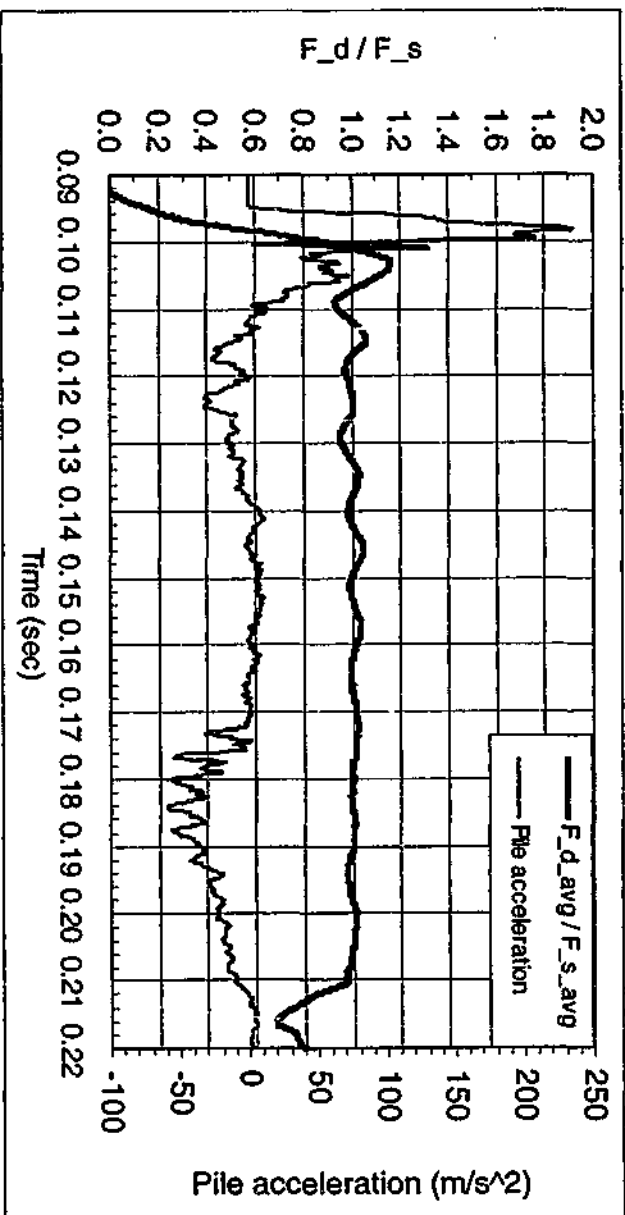
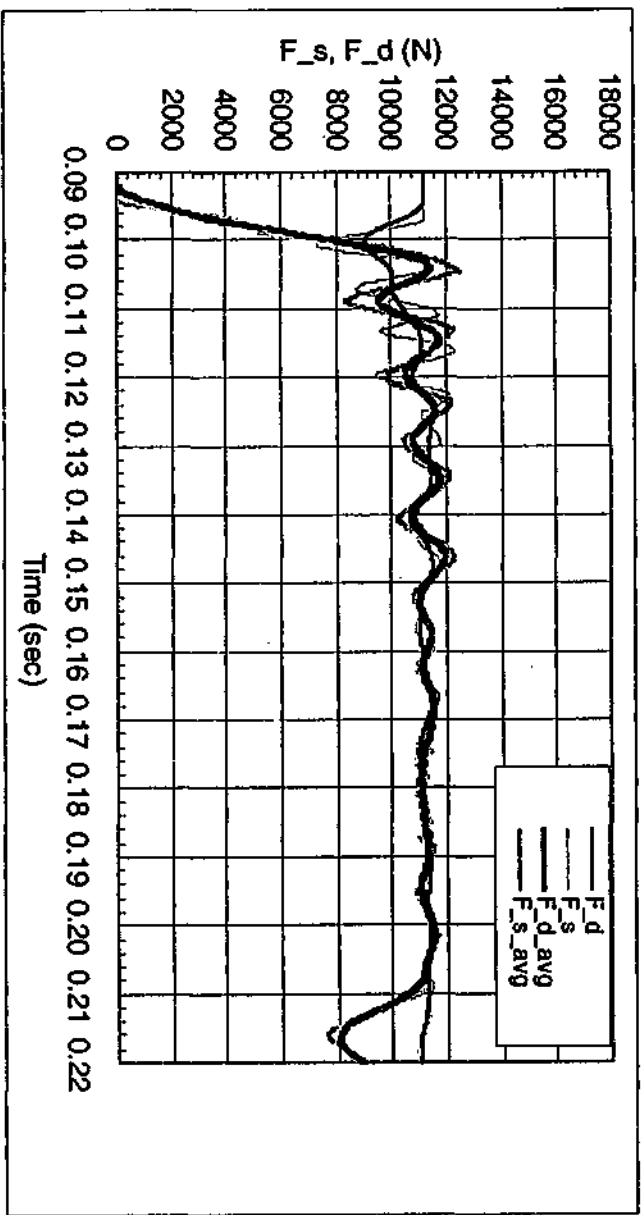
FILENAME Y.RC 150 INITIAL NORMAL STRESS 150 kPa
 PILE Rough concrete INITIAL DENSITY 1670 kg/m³
 SAND Yea



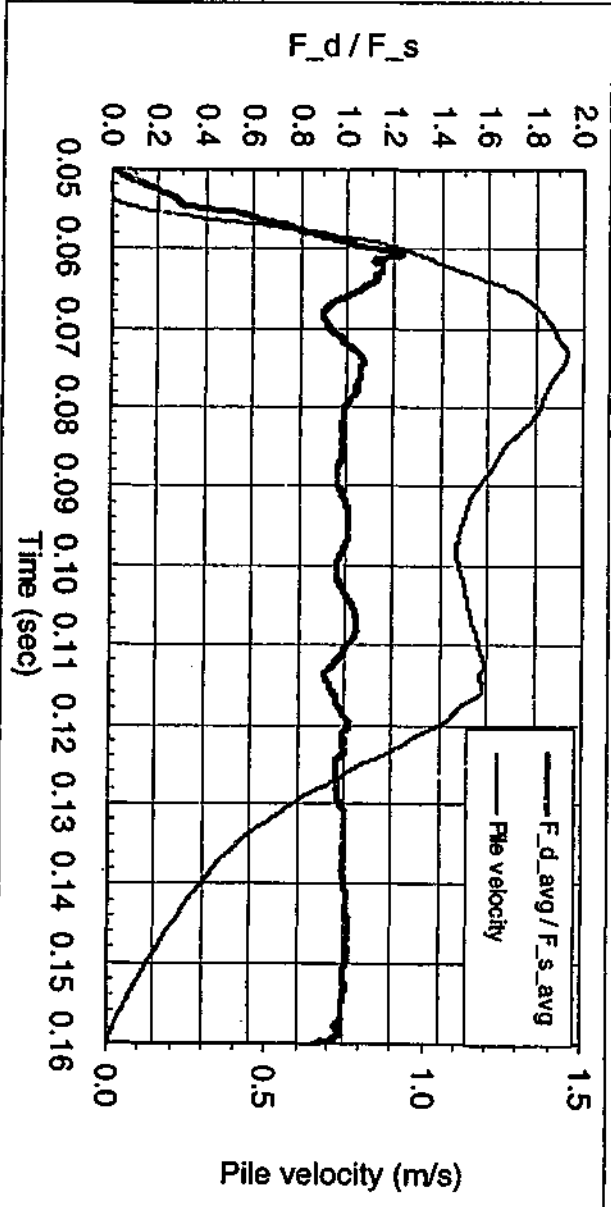
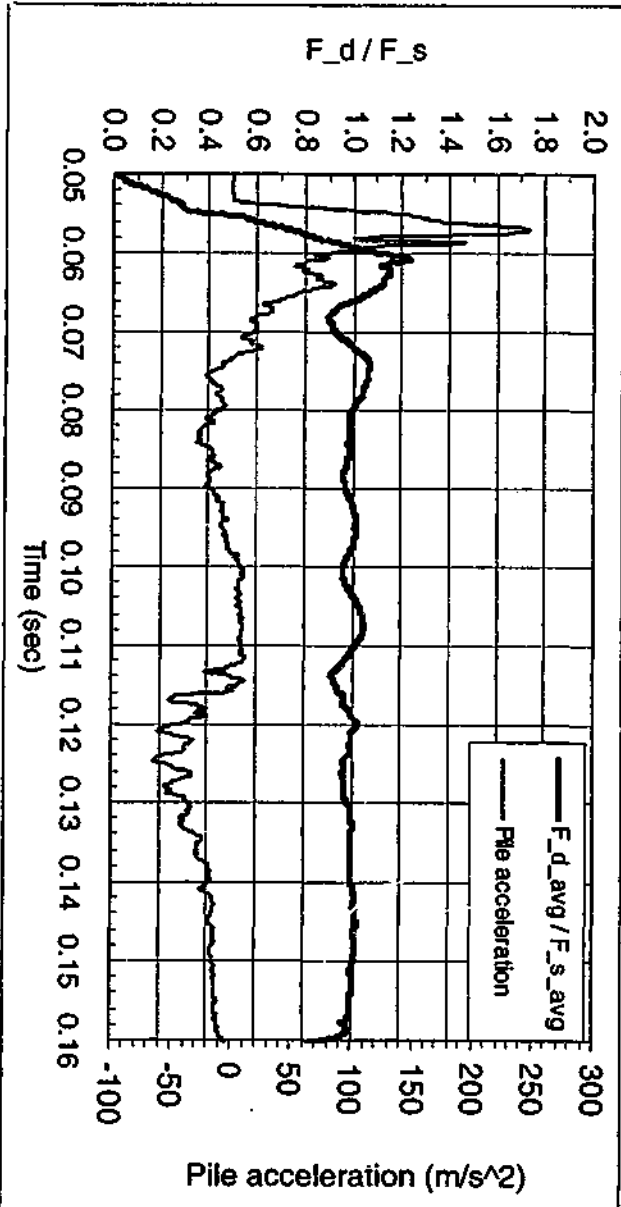
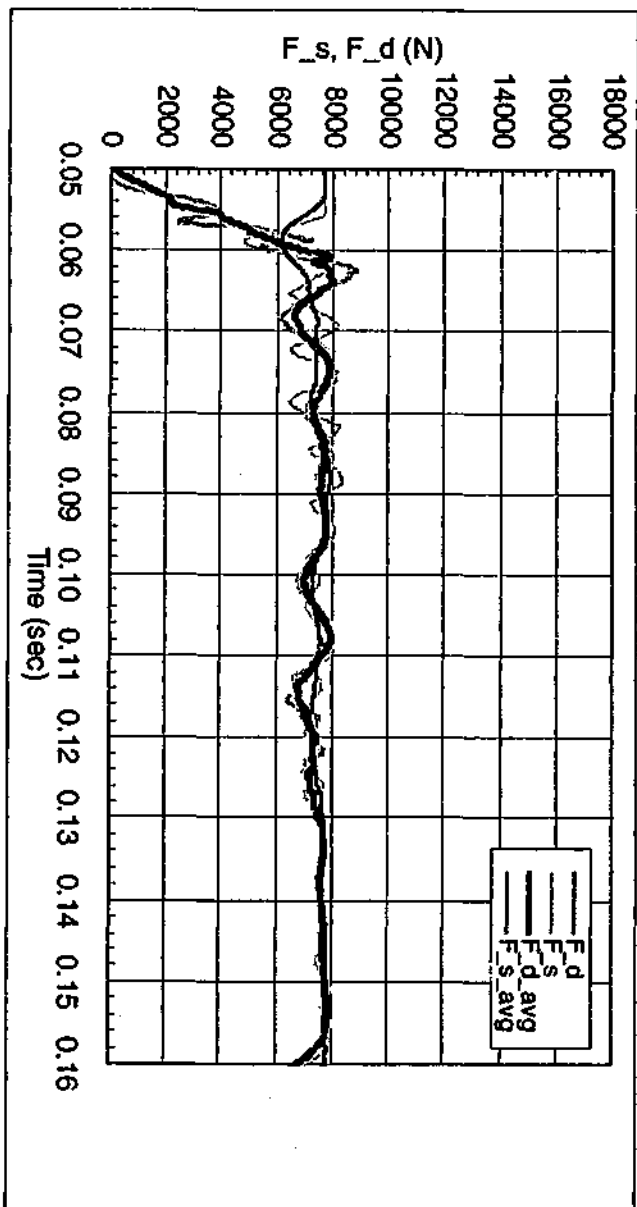
FILENAME M4.SC 250 INITIAL NORMAL STRESS 250 kPa
 PILE Smooth concrete INITIAL DENSITY 1580 kg/m³
 SAND Mix4



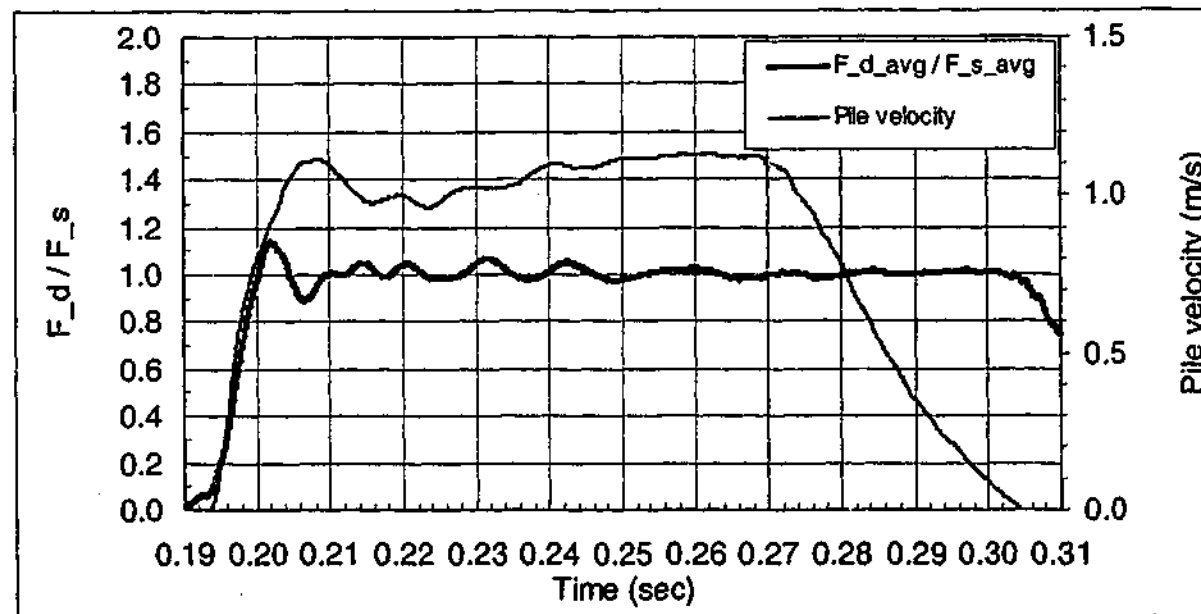
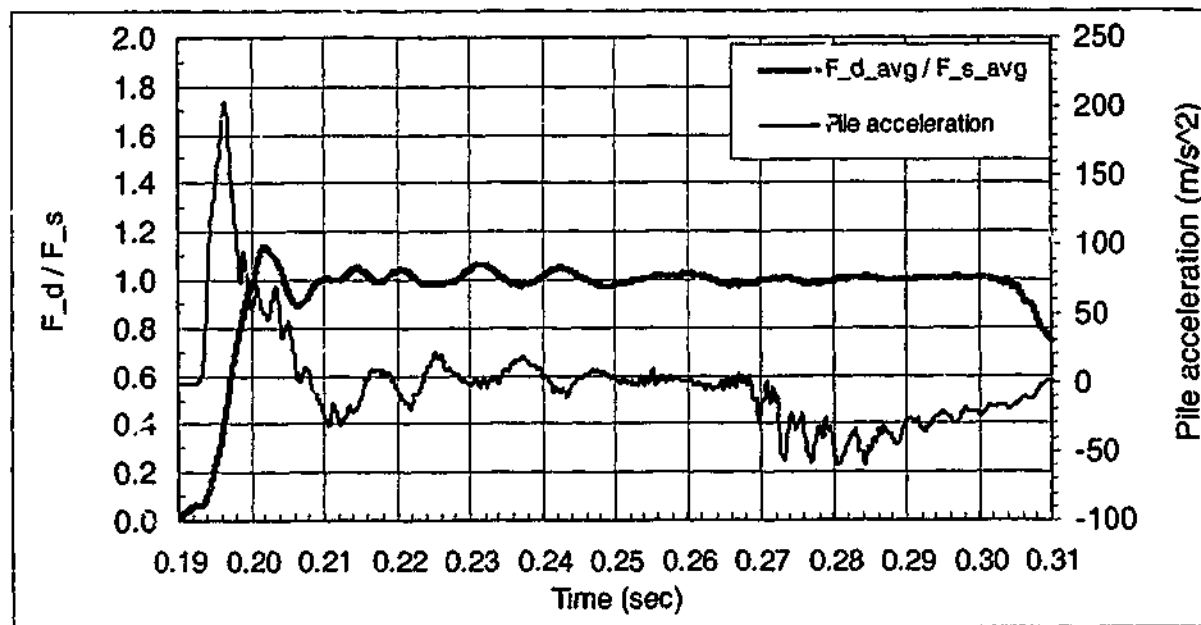
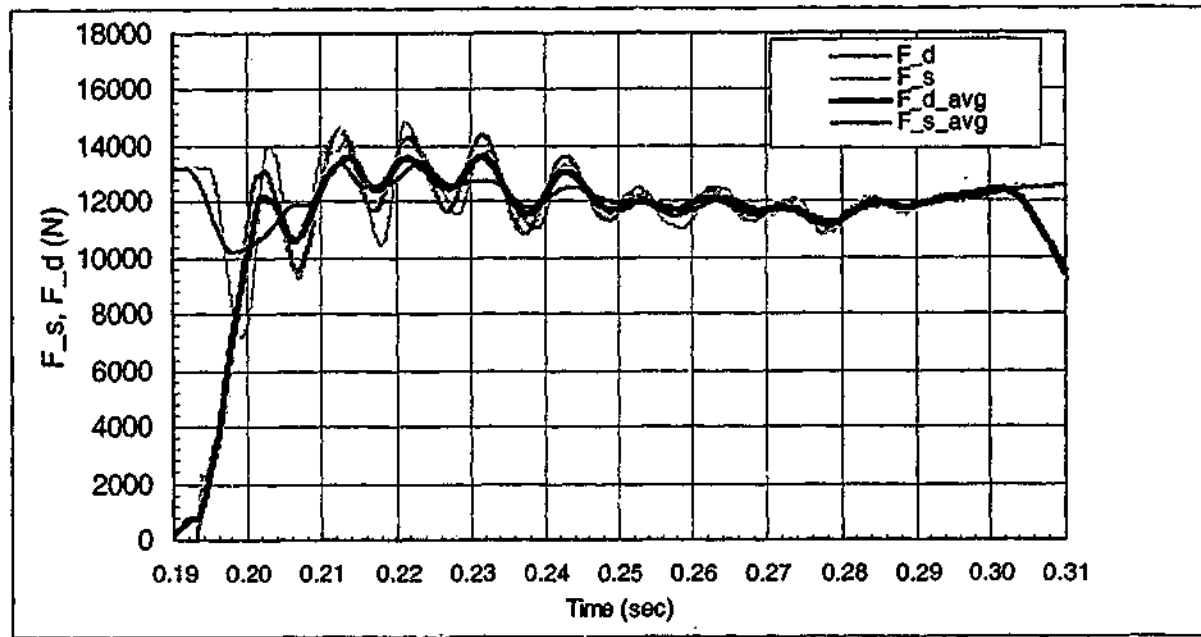
FILENAME M4.SC 250(repeat) INITIAL NORMAL STRESS 250 kPa
 PILE Smooth concrete INITIAL DENSITY 1580 kg/m³
 SAND Mix4



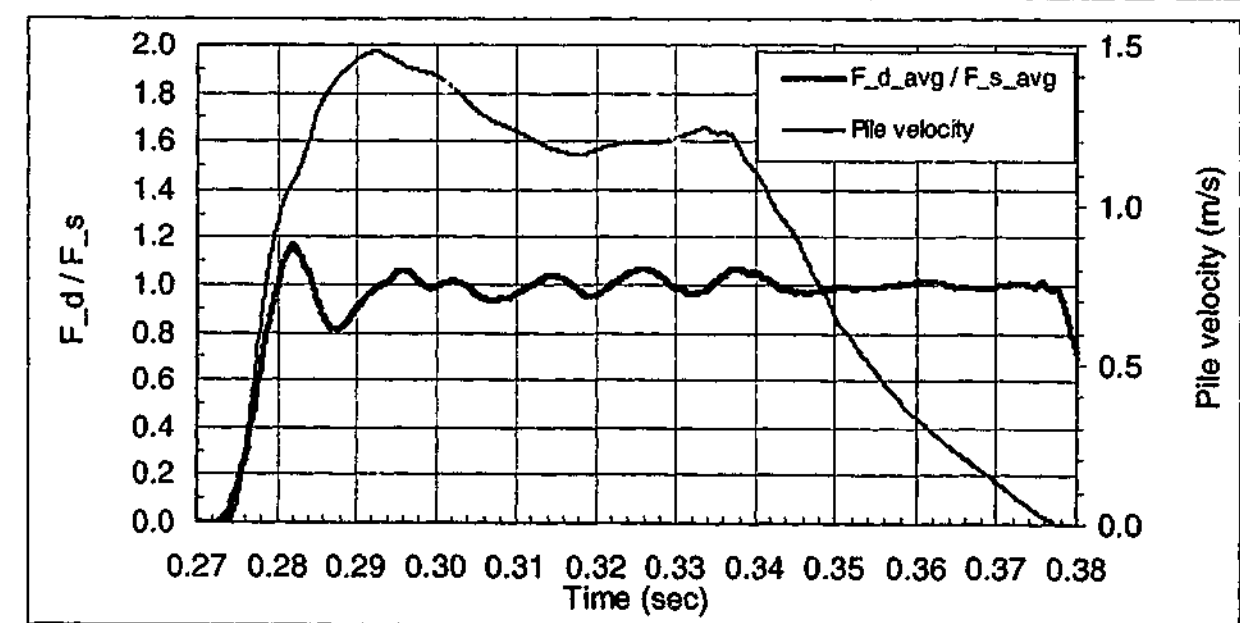
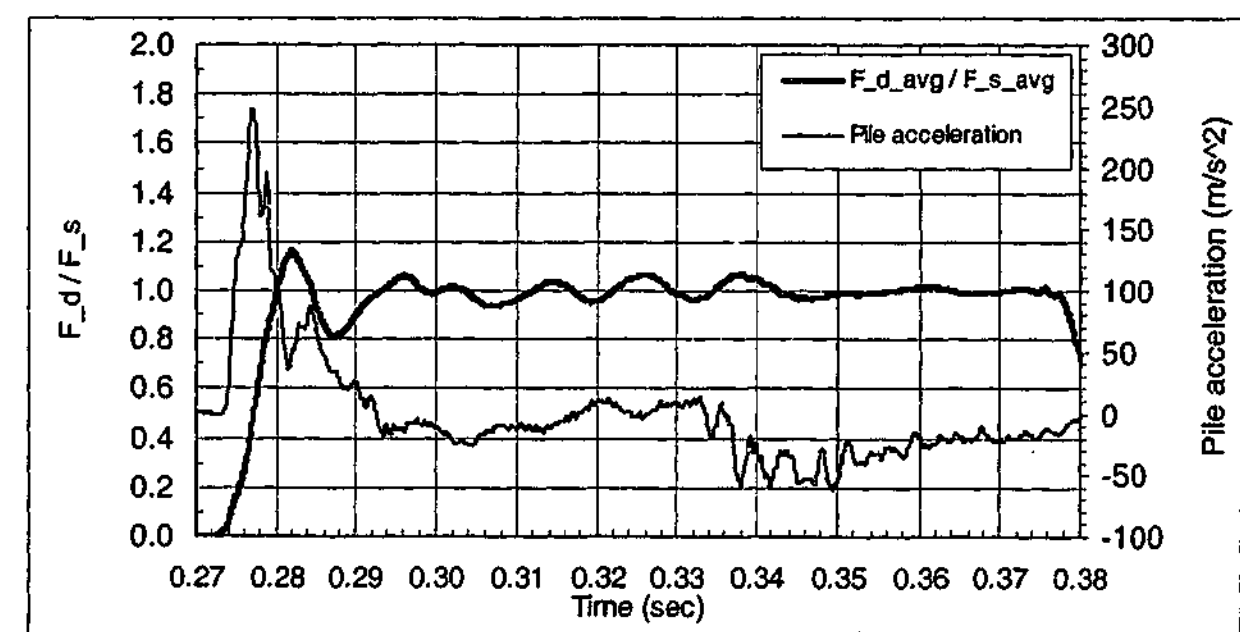
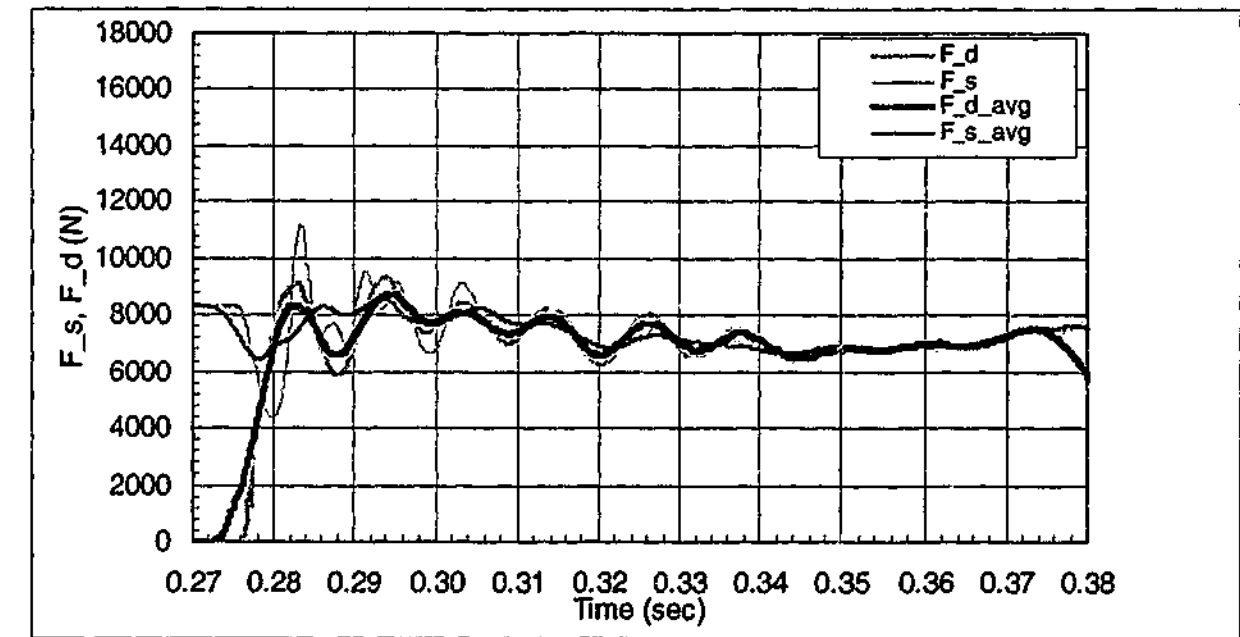
FILENAME M4.SC 150 INITIAL NORMAL STRESS 150 kPa
 PILE Smooth concrete INITIAL DENSITY 1580 kg/m³
 SAND Mix4



FILENAME M4.RC 250 INITIAL NORMAL STRESS 150 kPa
 PILE Rough concrete INITIAL DENSITY 1570 kg/m³
 SAND Mix4



FILENAME M4.RC 150 INITIAL NORMAL STRESS 150 kPa
 PILE Rough concrete INITIAL DENSITY 1570 kg/m³
 SAND Mix4



5.6.5 Discussion

5.6.5.1 Test results

The results of all the tests have been summarised in Table 5.6. Each record has been divided into 3 Sections by reference to the time of the event, as shown in Table 5.6. The minimum and maximum velocities in Sections 2 and 3 of the test event have also been tabulated.

As has been discussed, the data in Section 3 are reliable. It could also be noted that the variation in the velocity is most significant in Section 3 (apart from Section 1 of the record where the data have been concluded to be unreliable). Thus, the data in Section 3 are most suitable for determining the presence of any dynamic effect. The existence of rate effects is also evaluated based on the data in Section 2 where the averaging procedure has enabled the error in F_s to be minimised. The results of the evaluation based on Sections 2 and 3 data are shown in Table 5.6.

Table 5.6 (a) Results of dynamic pile-sand interface tests based on Sections 1 and 2 of records

Filename	Sand	Density kg/m ³	Pile*	Normal stress kPa	Peak vel m/s	Section 1		Section 2		Rate effect**
						Time (sec) between	Time(sec) between	Vel. (m/s) between	Vel. (m/s) between	
50WS.SC.250	50WS	1550	SC	250	1.25	0.138 & 0.153	0.153 & 0.178	1.00 & 1.25	1.00 & 1.25	NE
50WS.SC	50WS	1550	SC	250	1.25	0.135 & 0.150	0.150 & 0.170	1.05 & 1.25	1.05 & 1.25	NE
50WS.SC.150	50WS	1550	SC	150	1.45	0.405 & 0.423	0.423 & 0.446	1.10 & 1.45	1.10 & 1.45	NE
50WS.RC.250	50WS	1540	RC	250	1.30	0.183 & 0.200	0.200 & 0.245	0.80 & 1.30	0.80 & 1.30	NE
50WS.RC.150	Sat.50WS	1970	RC	150	1.35	0.392 & 0.410	0.410 & 0.450	0.70 & 1.35	0.70 & 1.35	NE
Sat.50WS.SC.250	Sat.50WS	1970	SC	250	1.30	0.134 & 0.150	0.150 & 0.183	1.00 & 1.30	1.00 & 1.30	NE
Sat.50WS.SC.150	50WS	1460	SC	150	1.50	0.312 & 0.330	0.330 & 0.358	1.00 & 1.50	1.00 & 1.50	NE
816.SC.250	8/16	1460	SC	250	1.35	0.113 & 0.130	0.130 & 0.174	1.15 & 1.35	1.15 & 1.35	NE
816.SC.150	8/16	1460	SC	150	1.50	0.104 & 0.124	0.124 & 0.170	0.55 & 1.50	0.55 & 1.50	NE
816.SC.150(repeat)	8/16	1460	SC	150	1.50	0.171 & 0.190	0.190 & 0.220	1.15 & 1.50	1.15 & 1.50	NE
816.RC.250	8/16	1480	RC	250	1.20	0.168 & 0.180	0.180 & 0.244	1.05 & 1.60	1.05 & 1.60	NE
816.RC.150	8/16	1480	RC	150	1.45	0.318 & 0.380	0.380 & 0.400	0.35 & 1.45	0.35 & 1.45	NE
Y.SC.250	Yea	1650	SC	250	1.30	0.176 & 0.190	0.190 & 0.224	1.05 & 1.30	1.05 & 1.30	NE
Y.SC.150	Yea	1650	SC	150	1.45	0.293 & 0.310	0.310 & 0.327	1.15 & 1.50	1.15 & 1.50	NE
Y.RC.250	Yea	1670	RC	250	1.30	0.294 & 0.310	0.310 & 0.332	1.15 & 1.30	1.15 & 1.30	NE
Y.RC.150	Yea	1670	RC	150	1.45	0.324 & 0.342	0.342 & 0.385	1.15 & 1.45	1.15 & 1.45	NE
M4.SC.250	Mix4	1580	SC	250	1.30	0.088 & 0.106	0.106 & 0.150	1.10 & 1.30	1.10 & 1.30	NE
M4.SC.250(repeat)	Mix4	1580	SC	250	1.30	0.095 & 0.110	0.110 & 0.146	1.05 & 1.30	1.05 & 1.30	NE
M4.SC.150	Mix4	1580	SC	150	1.45	0.054 & 0.073	0.073 & 0.118	1.15 & 1.45	1.15 & 1.45	NE
M4.RC.250	Mix4	1570	SC	250	1.15	0.194 & 0.210	0.210 & 0.242	1.15 & 1.15	1.15 & 1.15	NE
M4.RC.150	Mix4	1570	SC	150	1.50	0.274 & 0.293	0.293 & 0.340	1.15 & 1.50	1.15 & 1.50	NE

*SC = Smooth Concrete; RC = Rough Concrete;
**NE=Not Evident

Table 5.6 (b) Results of dynamic pile-sand interface tests based on Section 3 of records

Filename	Sand	Density kg/m ³	Pile*	Normal stress kPa	Peak vel m/s	Section 3		Rate effect**
						Time(sec) between	Vel. (m/s) between	
50WS.SC.250	50WS	1550	SC	250	1.25	0.178 & 0.223	0.00 & 1.00	NE
50WS.SC.250(repeat)	50WS	1550	SC	250	1.25	0.170 & 0.230	0.00 & 1.05	NE
50WS.SC.150	50WS	1550	SC	150	1.45	0.446 & 0.505	0.00 & 1.10	NE
50WS.RC.250	50WS	1540	RC	250	1.30	0.245 & 0.268	0.00 & 0.80	NE
50WS.RC.150	Sat.50WS	1970	RC	150	1.35	0.450 & 0.480	0.00 & 0.70	NE
Sat.50WS.SC.250	Sat.50WS	1970	SC	250	1.30	0.183 & 0.215	0.00 & 1.00	NE
Sat.50WS.SC.150	50WS	1460	SC	150	1.50	0.358 & 0.405	0.00 & 1.00	NE
816.SC.250	8/16	1460	SC	250	1.35	0.174 & 0.211	0.00 & 1.15	NE
816.SC.150	8/16	1460	SC	150	1.50	0.170 & 0.200	0.00 & 0.55	NE
816.SC.150(repeat)	8/16	1460	SC	150	1.50	0.220 & 0.266	0.00 & 1.15	NE
816.RC.250	8/16	1480	RC	250	1.20	0.244 & 0.280	0.00 & 1.05	NE
816.RC.150	8/16	1480	RC	150	1.45	0.400 & 0.420	0.00 & 0.35	NE
Y.SC.250	Yea	1650	SC	250	1.30	0.224 & 0.272	0.00 & 1.05	NE
Y.SC.150	Yea	1650	SCC	150	1.45	0.327 & 0.392	0.00 & 1.15	NE
Y.RC.250	Yea	1670	RC	250	1.30	0.332 & 0.392	0.00 & 1.15	NE
Y.RC.150	Yea	1670	RC	150	1.45	0.385 & 0.425	0.00 & 1.15	NE
M4.SC.250	Mix4	1580	SC	250	1.30	0.150 & 0.188	0.00 & 1.10	NE
M4.SC.250(repeat)	Mix4	1580	SC	250	1.30	0.146 & 0.208	0.00 & 1.05	NE
M4.SC.150	Mix4	1580	SC	150	1.45	0.118 & 0.160	0.00 & 1.15	NE
M4.RC.250	Mix4	1570	SC	250	1.15	0.242 & 0.304	0.00 & 1.15	NE
M4.RC.150	Mix4	1570	SC	150	1.50	0.340 & 0.377	0.00 & 1.15	NE

*SC = Smooth Concrete; RC = Rough Concrete;
**NE=Not Evident

As shown in Table 5.6, for all the test records, the value of F_{d_avg}/F_{s_avg} in Section 2 of the record does not vary with velocity, suggesting either no rate effects or negligible rate effects for velocities up to 1.5m/s which is the maximum velocity associated with Section 2 of the record. Also, for all tests, the value of F_{d_avg}/F_{s_avg} in Section 3 of the record does not vary with velocity, indicating either no rate effects or negligible rate effects for velocities up to 1.15m/s which is the maximum velocity associated with Section 3 of the record. It is noted that the interface strength data pertaining to velocities higher than 1.5m/s are part of the data in Section 1; as such, no conclusion can be drawn about the dynamic response for velocities higher than 1.5m/s. In addition, data from Sections 2 and 3 of the records show that the value of F_{d_avg}/F_{s_avg} is independent of the pile acceleration.

Therefore, it is concluded that dynamic effects are negligible for velocities of at least up to 1.5m/s. However, it is acknowledged that the averaging procedure may have slightly compromised the accuracy of the value of F_{d_avg}/F_{s_avg} and that the small fluctuations in the F_{d_avg}/F_{s_avg} curve may have caused any minute variation in the value of the F_{d}/F_{s} throughout the event to be less evident. The implication is that any small degree of rate-dependence of the interface strength would not be evident. It is estimated that an increase in dynamic strength over the static strength of up to about 5% (or an increase of the strength ratio of up to 1.05) will not be discernible in the F_{d_avg}/F_{s_avg} vs. time plots presented in Section 5.6.4.

Whilst it is not possible to conclude that there is absolutely no dynamic effect for the pile-sand interface, it can be concluded based on this study that dynamic effects are negligible for velocities of at least up to 1.5m/s. It is emphasised that the finding that dynamic effects are negligible for velocities up to 1.5m/s cannot be taken to imply that there is also negligible strength increase in the interface at higher velocities. If there is indeed a rate-dependent strength increase of up to 5% for a peak velocity of about 1.5m/s, this small strength increase will translate to a much more significant (and hence more measurable) strength increase in the higher peak velocity range associated with pile driving (which is typically between 3.0 and 7.5m/s (Seidel, 1998)). Assuming that the Smith damping law applies, an increase of 5% relative to the quasi-static strength for a velocity of 1.0m/s equates to a damping factor of

0.033s/m. For a peak velocity of 2m/s, this damping amounts to a 7% increase in strength over the quasi-static strength and for a peak velocity of 4m/s, a 13% increase. It is therefore recommended that tests be performed at shear rates higher than 1.5m/s in order to establish any rate-dependence of the interface strength in the high velocity regime.

The finding that the interface friction angle is essentially independent of velocity for velocities up to 1.5m/s is consistent with the previous finding based on interface shear tests by Dayal and Allen (1975) and Heerema (1979) who similarly found no discernible strength increase for velocities up to 0.6m/s and 0.8m/s respectively.

It has been shown in Section 3.4.2 that the findings based on soil-only shear tests involving low (between 1.0×10^{-4} m/s to 5×10^{-2} m/s) and high (up to 6.0m/s) velocity regimes were mixed. The finding from this study is supported by the studies by Schimming et al. (1966), Hungr and Morgenstern (1984a) and Hungr and Morgenstern (1984b), which showed that the friction angle was independent of the shear rate. However, the current study did not find any decrease in the interface friction angle as reported by Lemos (1986) and Scarlett and Todd (1969), or any increase as reported by Scarlett and Todd (1969).

5.6.5.2 Concluding remarks - dynamic effects for the pile-sand interface

It is noted that in the current practice of signal-matching analyses using CAPWAP, low damping factors which nevertheless model higher than negligible damping found in this study have been used. Similarly, signal-matching of dynamic data for piles installed in cohesionless soils using a signal-matching package IMPACT (Randolph, 1992), which theoretically models radiation damping, similarly requires the use of low damping factors (Randolph, 2003). Ostensibly, the damping factors are used to model viscous damping at the pile-sand interface. Several hypotheses can be offered to explain the seeming contradiction of the use of damping factors in signal-matching and the experimental finding from this study and other studies.

As previously discussed, it is possible that there is a small increase in strength corresponding to the low peak velocity tested in this study and in other studies, which cannot be detected. It has been demonstrated that this small increase could

translate to much more significant increases in the higher velocity range associated with pile-driving.

It is noted that in this study, only clean sands were tested and the finding that viscous damping is negligible for the interface between clean sand and pile (for velocities up to 1.5m/s) should not be presumed to apply to sandy soils with a significant fines content. It is possible that the damping factors used in signal-matching are required to model the strength increase due to the fines component in the sandy soil especially since real soils rarely consist exclusively of sand particles (Wroth and Houlsby, 1985) and only a relatively small fraction, say 10 to 15%, of clay, is required to make the behaviour of a sandy soil like that of clay (Wroth and Houlsby, 1985).

It is possible that the strength increase apparently attributed to viscous damping is in actual fact due to the rate-dependent volumetric and pore pressure responses (rather than viscous damping). According to Randolph (2003), the damping factors for the pile-sand interface used in signal-matching with IMPACT are primarily required to model the pore pressure-induced strength increase. As discussed in Section 3.4.3, the high strain rate associated with pile driving is likely to cause an increased tendency in the sand to dilate (Whitman and Healy, 1962; Yamamuro and Lade, 1993; Yamamuro and Abrantes, 2003). In cases where undrained loading occurs, the increased dilation will cause the generated excess pore pressure to be relatively lower compared to that associated with a low strain rate, thus leading to a higher strength in the sand and the interface.

5.7 Summary

This chapter has described the test programme for investigating the dynamic behaviour of the pile-sand interface, and the test procedures for performing the tests. The results of both the quasi-static and dynamic tests have been presented and discussed.

Based on the quasi-static tests, the quasi-static behaviour of the interface has been shown to be consistent with expectation and the work of others; thus the quasi-static

interface strengths can be used as valid points for normalising the dynamic interface strength.

Due to the limitation of the test device, it can only be concluded that the interface strength increase for the pile-sand interface is negligible for up to a peak velocity of 1.5m/s. This finding is consistent with the findings of previous studies that any interface strength increase with increasing shear rates was negligible. Given that the use of damping factors for the interface in signal-matching of piles installed in sands apparently indicates the presence of viscous damping, several hypotheses have been proposed to explain the seemingly contradictory experimental evidence and the experience in signal-matching analyses.

Chapter 6

6. Quasi-Static Pile-Clay Interface Behaviour: Test Procedures, Results & Analysis

6.1 General

Using the device described in Chapter 4, quasi-static pile-clay interface tests were performed for two primary reasons. In order to understand the dynamic behaviour of the pile-clay interface which is the subject of investigation in this project, it is first required that the static or quasi-static behaviour of pile-clay interfaces be characterised and the fundamental parameters that influence it be identified. This is especially important given that relatively little controlled experimental research has been performed on pile-soil interface behaviour and even less so for over-consolidated clays, as will be discussed in this chapter. Also, in order to quantify the strength increase due to the dynamic effect, the quasi-static interface strength for a particular interface must be known so that the dynamic strength of the equivalent

interface can be normalised, whose behaviour is the focus of this project. It is noted that the dynamic interface strength associated with the pile-driving event relates to the high-displacement or the residual strength. As such, the quasi-static interface strength for normalising the dynamic strength should correspondingly be the large-displacement or residual strength. Nevertheless, both the residual and peak strength data are discussed.

This chapter describes the programme for the quasi-static tests and the test procedures for performing these tests. It also discusses the observed post-test shear failure mode of the interface and the quasi-static strength behaviour of the interface.

6.2 Test Programme

In the test programme, BallR, HR1F and BallR/Talc clays were tested. The general description and the geotechnical properties of these clays are tabulated in Table 6.1, and their chemical constituents are tabulated in Table 6.2. According to the plasticity chart, the clays could be categorised as low, medium and high plasticity clays.

Table 6.1 Geotechnical properties of the 3 types of clay tested

Clay type	General description	Geotechnical properties	
		I_p	% $<2\mu m$
BallR Clay	Kaolin Dry-milled; typically used in ceramics, bricks, rubber compounds; from Port Melbourne White and floury when dry "CL" – inorganic clay of medium plasticity	w_p	20%
		w_l	18%
		G	38%
		G	2.71
HR1F Clay	Kaolin Dry-milled; from Gulgong, New South Wales White and floury when dry "CH" - inorganic clay of high plasticity	w_p	53%
		w_l	37%
		G	30%
		G	67%
Ball R Clay-Talc	Mixed from Ball Clay R and Talc White and floury when dry "CL" – inorganic clay of low plasticity	w_p	2.65
		w_l	60%
		G	8%
		G	22%

Table 6.2 Chemical constituents of BallR, HR1F and Talc

Clay type	Constituent	%	Constituent	%
BallR Clay	SiO ₂	64.7	CaO	0.06
	MgO	0.6	K ₂ O	2.5
	Al ₂ O ₃	22.2	Na ₂ O	0.3
	Fe ₂ O ₃	1.1	TiO ₂	1.5
HR1F Clay	SiO ₂	49.3	CaO	0.1
	MgO	0.3	K ₂ O	0.2
	Al ₂ O ₃	35.0	Na ₂ O	0.2
	Fe ₂ O ₃	1.1	TiO ₂	1.0
Talc	SiO ₂	56.0	CaO	0.9
	MgO	3.3	K ₂ O	0.4
	Al ₂ O ₃	16.0	Na ₂ O	2.9
	Fe ₂ O ₃	4.6	LOI	5.7

In order to determine the effect of the roughness of the pile surface on the interface behaviour, the tests were conducted on a smooth concrete pile, a rough concrete pile, and a smooth steel pile. The first two piles have been described in Section 5.3. The steel pile was a commercial mild steel that was slightly rougher than the smooth concrete pile; a photograph of its surface in plan view is shown in Figure 6.1.

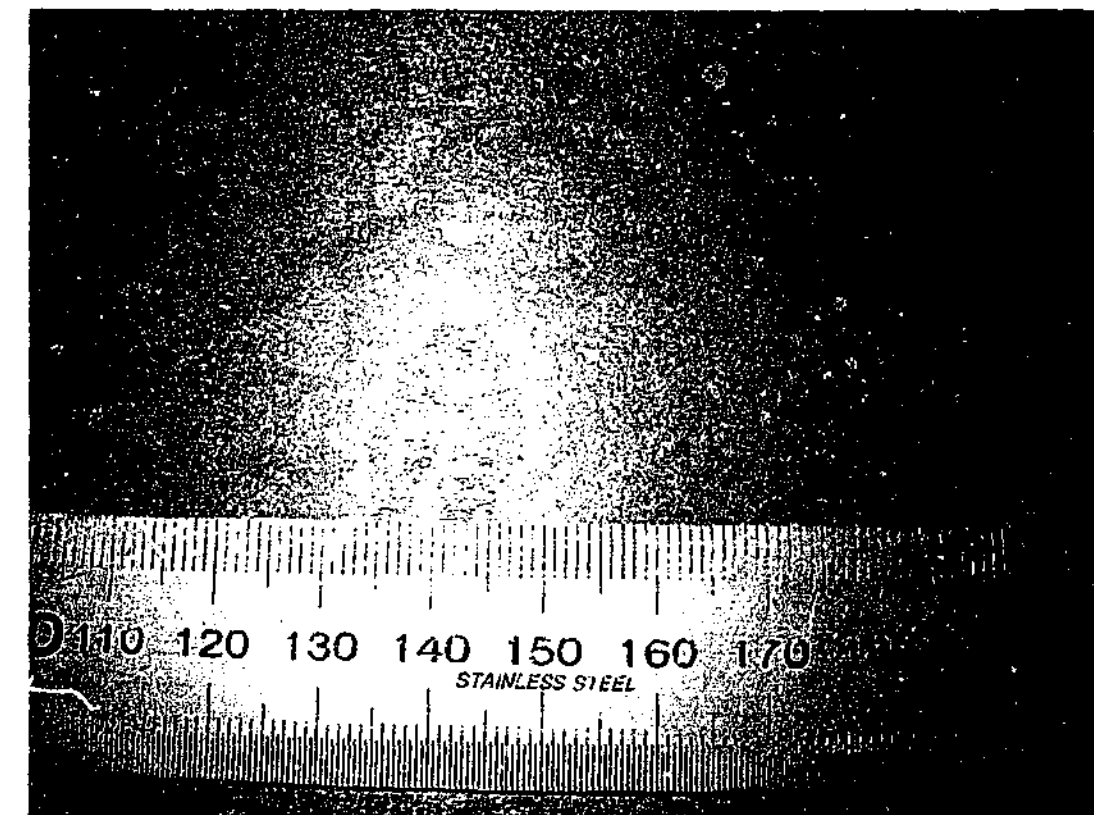


Figure 6.1 Plan view: surface of steel pile

Since the quasi-static interface residual strength of a particular interface is required for normalising the dynamic interface strength of the equivalent interface, the test programmes for the quasi-static tests and the dynamic tests were identical. The test programme for the quasi-static (and the dynamic) pile-clay interface tests is outlined in Table 6.3. The quasi-static tests were performed at a shear rate of 0.01mm/s, which was the lowest reliable shear rate that the electro-hydraulic actuator was capable of delivering. In order to investigate the effects of the preconsolidation stress, normal stress, *OCR* and shear strength on the interface behaviour, these parameters were varied. For a particular type of clay, samples with two preconsolidation stresses at 325kPa and 500kPa were fabricated, and for a particular preconsolidated sample, normal stresses ranging from 60 to 250kPa were applied to the sample during the tests. Thus, the effective *OCR* of the sample and the shear strength of the sample (which depended on the normal stress and the *OCR*) were varied.

Table 6.3 Test programme for quasi-static (and dynamic) pile-clay interface tests

Clay type	Pile surface	Preconsolidation stress (kPa)	Normal stress (kPa)	<i>OCR</i>
BallR (medium plasticity)	For each of steel, smooth concrete and rough concrete.	325	250	1.3
			150	2.2
			60	5.4
		500	250	2.0
			150	3.3
			60	8.3
	For each of wetted steel, wetted smooth concrete and wetted rough concrete.	325	250	1.3
			150	2.2
			60	5.4
		500	250	2.0
			150	3.3
			60	8.3
BallR/Talc (low plasticity)	Steel	325	250	1.3
			150	2.2
			60	5.4
		500	250	2.0
			150	3.3
			60	8.3
HR1F (high plasticity)	Steel	325	250	1.3
			150	2.2
			60	5.4
		500	250	2.0
			150	3.3
			60	8.3

6.3 Test Procedures

6.3.1 Soil specimen fabrication

The clay was supplied in the form of dry powder. The powder was mixed with water in a mixer to form a slurry at a water content 1.1 times the liquid limit in order to avoid trapped air and to ensure full saturation. To ensure the slurry was uniformly and thoroughly mixed, the slurry was stirred for half an hour in a large mixer. The slurry was left to equilibrate overnight in the mixer bowl. To minimise loss of moisture, the mixer bowl was covered with a wet cloth over its opening and wrapped with a plastic bag.

A purpose-built apparatus was used to consolidate slurry. The apparatus consisted of a four-sided mould, a base plate, a plunger for loading the sample and porous plates for drainage of water, as shown in Figure 6.2 and Figure 6.3. The mould was designed to produce clay blocks that would fit into the plan area of the shear box. In order to maximise the rate of drainage and hence the consolidation of the sample, a highly porous medium was required to facilitate drainage at the top and the bottom of the sample. Sandstone for housing construction was used for this purpose. The sandstone was specially cut to the required dimensions using a bandsaw. Two sections of sandstone were necessary to form a porous plate for each of the top and the bottom of the sample, as shown in Figure 6.3. The sections were found to be extremely fragile when saturated and very often broke when removed from the sample.

The steps in preparing a clay sample were as follows. The mold was bolted to the base plate to form a box. The porous plate was placed inside the mold at its base. The gaps between the inner walls of the mold and the porous plate was filled with wetted paper towel to prevent excessive loss of slurry during consolidation. The clay mix was placed into the mold onto the porous plate. The mix was placed by 30mm-layers using a scraper and pressed in to avoid trapped air, until a thickness of about 100mm was formed. Once the top of the sample was levelled, another porous plate was placed onto the top of the sample, and the gaps between the mold and the plate were filled with wetted paper towel. The loading platen was placed onto the porous stone and the "box" with the sample within it was transferred to a loading machine.

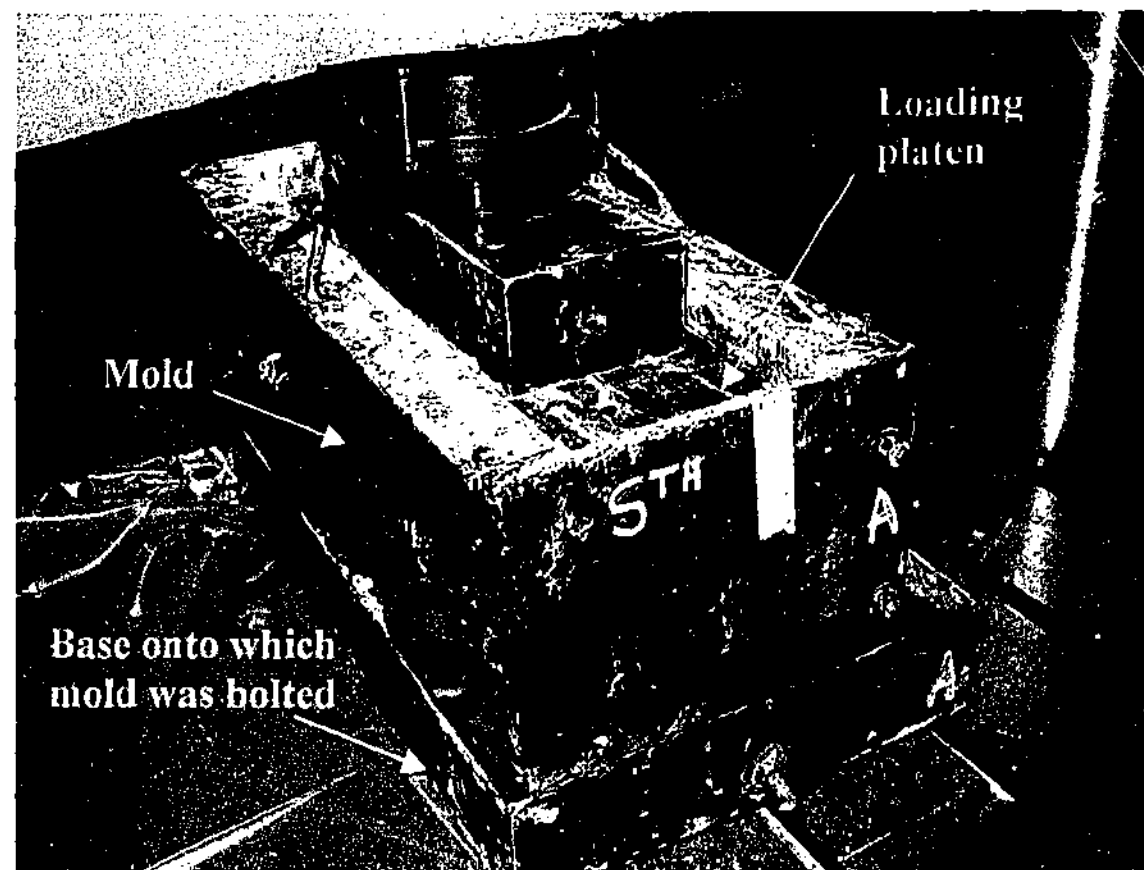


Figure 6.2 The mold, its base and the loading platen

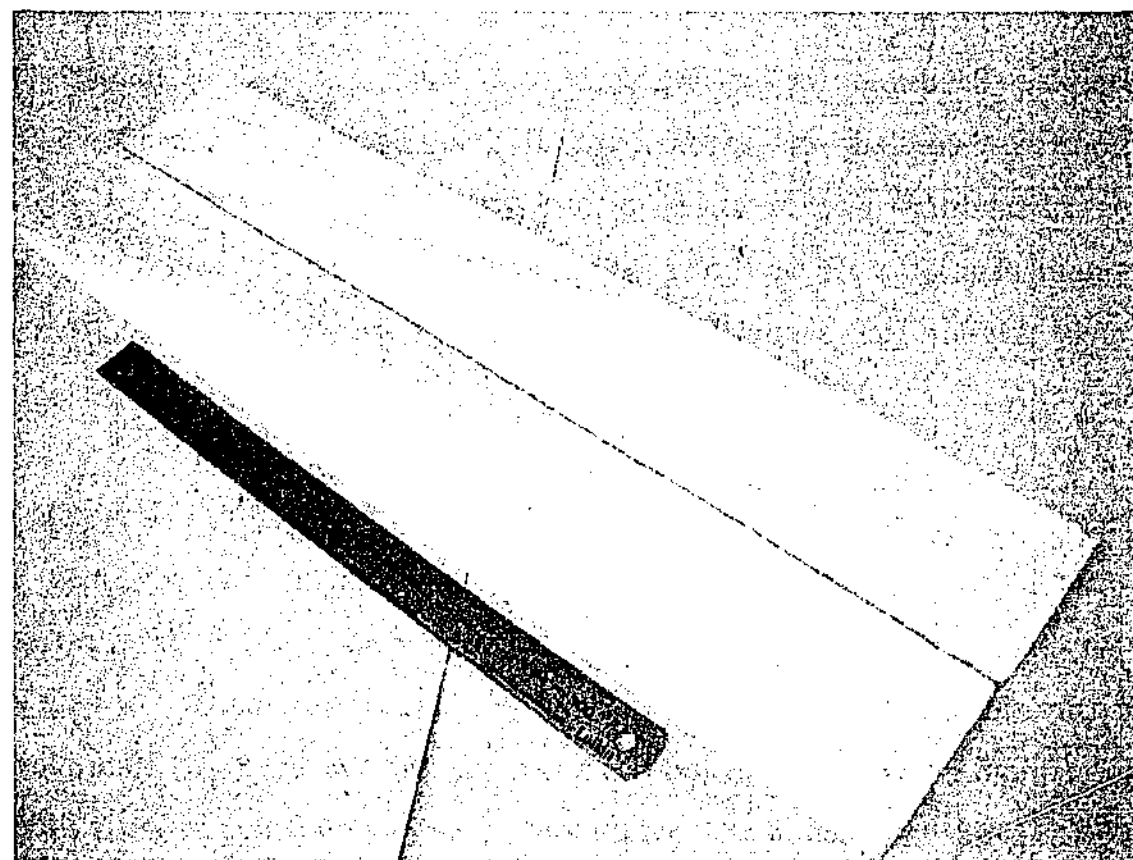


Figure 6.3 A set of porous "plate", measuring 554mm x 159mm x 10mm, which was formed out of 2 pieces of sandstone

The mix was consolidated in stages until the target preconsolidation load was achieved. The first applied load was 5kN, after which the existing load was doubled after each hour to approach the target load. The load increments were small to ensure that the mix would not extrude through the gaps between the inner walls of the mold and the loading plate. At each increment of load, water was expelled from the slurry through the top and bottom porous plates. During each stage of consolidation, the settlement of the sample was continuously logged.

It was necessary for the sample to complete its primary consolidation (defined using the square root of time method by Taylor cited in Holtz and Kovacs (1981)) under the designated preconsolidation stress overnight for over 15 hours. On the next day, the sample was unloaded, the loading platen was removed from the mold, and the mold was separated from its base. The mold with the clay sample contained within it was supported on two pieces of timber on its two edges so that the clay sample could be extruded as a block. A 100mm-thick slurry would typically produce an 80mm-thick clay block, shown in Figure 6.4, after consolidation and loss of sample. This block of clay was cut across the horizontal plane using a wire-cutter to form two 40mm-thick samples. Each sample was wrapped with Gladwrap® and transferred to the shear rig to be tested.

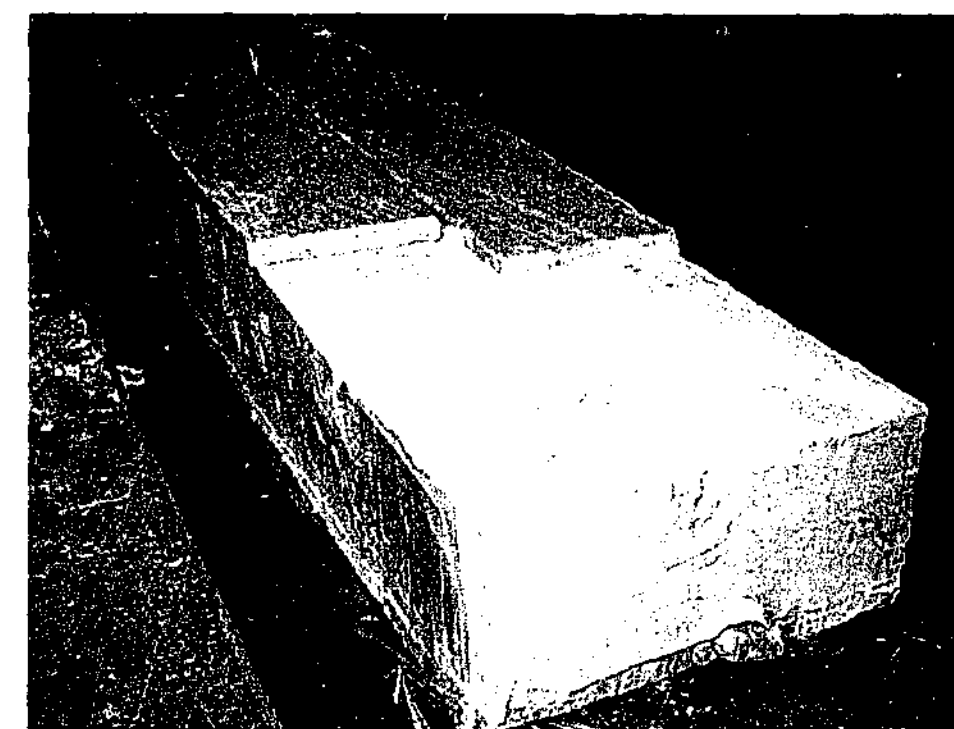


Figure 6.4 The extruded sample, with porous sandstones at the top and bottom of the sample; the saturated sandstones were broken upon removal

6.3.2 Soil-only tests

In addition to the interface tests, soil-only tests were performed under the same normal stresses and at the same shear rate as the interface tests to replicate the shear strengths of the samples tested in the interface tests. This was so that the soil-only shear strength could be compared with the interface shear strength.

Because the purpose-built interface shear device did not have the facility for testing soil specimens for soil-only strength, the soil-only tests were performed using the standard shear device using the procedures outlined in Head (1994). Furthermore, the use of the standard shear device allows standard soil strength parameters to be obtained (which will be used for correlation with the damping factor in Chapter 8).

The fabricated sample was cut across the horizontal plane to form a 20mm-thick layer. From this layer, 60mm x 60mm samples were cut using the standard cutter (for the direct shear box test) and wrapped with Gladwrap® to prevent them from drying out. The sample was incrementally loaded in the normal direction and sheared to the full allowable shear displacement of about 15mm (Head, 1994) to obtain the peak and residual response. Each sample was tested at one normal stress in “one-off” tests so that for a particular clay, 3 “once-off” tests at the 3 normal stresses were performed.

6.3.3 Quasi-static interface tests

The quasi-static interface tests were performed in the “static configuration” of the shear rig, at a shear rate of 0.01mm/s. The clay sample was placed centrally on the pile section and aligned with the loading platen. The shear box was then placed around the sample. The pile section was then transferred to the rig and bolted onto the carriage. Four 1.0mm thick packers were slid in between the shear box and the pile surface at the 4 corners of the box to lift up the shear box by the thickness of the packers. Clamps were used to fix the position of the shear box after which the packers were removed.

As the clay specimens took a considerable amount of time to fabricate, three-staged testing was performed on the same interface sample for the sake of efficiency. The

multi-stage testing was based on the principle of multi-stage testing of soil in the standard direct shear device as outlined in Head (1994) but with slight variations.

For the first stage, the target normal stress was 250kPa. The vertical loading platen was lowered into the shear box after and allowed to settle under its own weight. The normal load was incremented at a rate of 1.1kPa/sec until the target load was achieved. Water was poured onto the pile section and around the sample to prevent moisture loss at the interface. The water was contained in a bath formed by Perspex strips glued to the four sides of the pile section. The target load was held for 10 minutes to ensure the sample had sufficient time to fill the space between the sample and the inner walls of the shear box and to be in intimate contact with the pile surface. Under the applied normal stress, the pile-clay interface was sheared by moving the carriage using the actuator until the residual strength was reached. Thus, the first test was completed and the normal stress was removed. For the second stage of testing, the normal stress was incremented to a target of 150kPa, held for 10 minutes, before the sample was tested in the same shear direction as before and unloaded. For the last stage of testing, the sample was tested at a normal stress of 60kPa, using the same. The sample was replaced only when tests were to be performed on a different pile interface.

The following were recorded during a quasi-static test: the normal stress on the sample, the shear force imparted to the carriage by the actuator, the pile displacement and the vertical movement of the sample.

As discussed for the pile-sand interface tests, a small clearance between the bottom of the shear box and the pile surface was necessary to avoid friction between the two elements. During testing, the edge of the shear box that was located slightly above the pile surface could shear across the clay block at one end of the shear box, causing some loss of sample at one end of the shear box indicated schematically in Figure 6.5. The amount of lost sample depended on the clearance between the bottom edge of the shear box and the pile section. When testing smooth piles (i.e. the smooth concrete and steel), the clearance was minimised to less than 1mm, and when testing rough piles (very rough concrete pile), lifting up the shear box slightly to clear the top edge of the asperities of the pile left significant clearances between the shear box

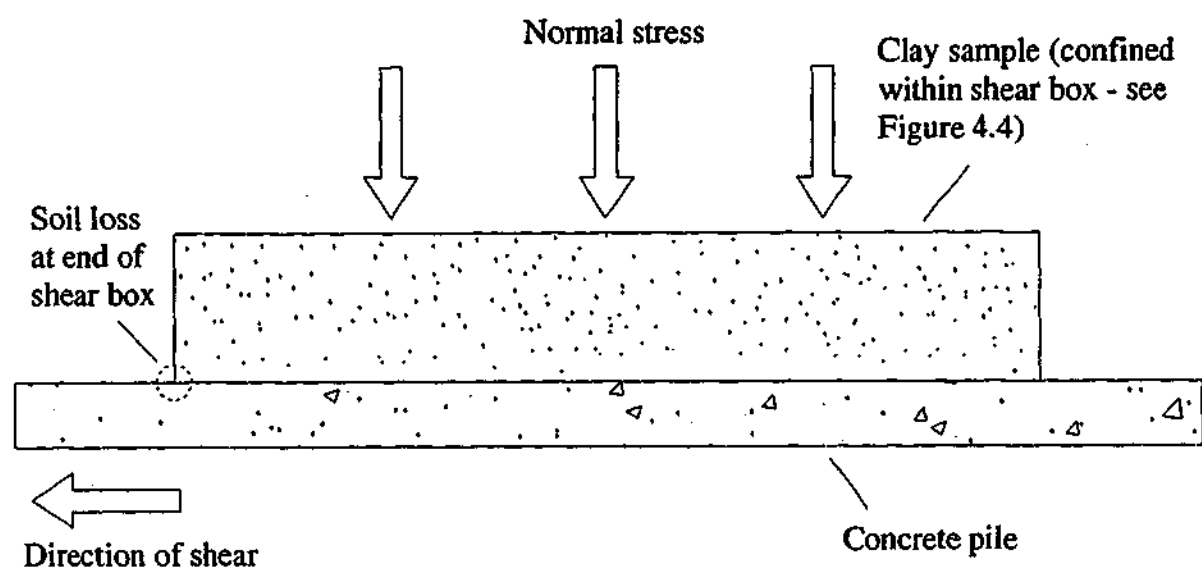


Figure 6.5 Schematic showing loss of sample during shearing at one end of the shear box

and the pile surface. The amount of sample lost could be quantified as the mass of the lost sample as a percentage of the mass of the total sample. For a typical quasi-static test involving a shear displacement, the typical percentages are tabulated in Table 6.4. Thus, the amounts of sample loss were insignificant. Also, the area of the sample affected by the soil loss was relatively small compared to the total area of the sample, so the loss of sample was not expected to cause significant error.

As has been discussed for the pile-sand interface, the direct shear box was known to introduce stress concentrations and non-uniform strain distributions in the sample but this limitation was inevitable since the simple shear was found to be unsuitable for dynamic tests. However, this limitation probably has little effect on the ratio of the dynamic strength to the static strength, which is the parameter of primary interest in this study.

Table 6.4 Mass of the lost sample as a percentage of the mass of the total sample

Interface	Percentage loss of sample (%)
Smooth pile-Clay	0.1
Rough pile-Clay	0.2

6.3.4 Implications for the analyses

The shear rate which allows drained shearing of the soil can be arbitrarily defined as the rate which ensures 90% consolidation of the soil specimen after a shear displacement of 1mm, after Lupini et al. (1981), Tika et al. (1996) and Lemos and Vaughan (2000). Thus, the rates of consolidation of the 3 clays selected in the test programme at an applied vertical stress of 60kPa based on oedometer tests were computed using the Casagrande method (Holtz and Kovacs, 1981). The stress level of 60kPa, which was the lowest of the 3 applied stresses used in the programme, was selected in order to estimate the lowest rate of consolidation applicable to the tests. The “drained” rate was estimated from the lowest of the 3 rates of consolidation, and found to be 0.0015mm/s. However, due to the long duration required to perform the drained tests and as the lowest speed the electro-hydraulic actuator was capable of delivering was 0.01mm/s, this was the rate selected for performing the quasi-static tests.

Since the shear box configured for simple shear was found to be unsuitable for the dynamic tests (as discussed in Section 4.1.1.8), the specimen had to be tested in direct shear mode for the dynamic test, and for the sake of consistency, for the quasi-static test as well. At the high shear rates of the dynamic test, the volume of the specimen is assumed to be constant so that the test is effectively undrained. However, at the low shear rates of the quasi-static test, the direct shear test allows volume changes in the specimen (namely contraction or dilation of the sample) to occur, implying that the test is not strictly undrained. It is noted that for this reason, researchers (e.g. Ladd et al., 1977; Andresen et al., 1979) used simple shear devices, which do not allow volumetric changes in the specimen, to measure the undrained strength.

Given the uncertainties in the nature of the shear strength obtained due to both the limitation of practical shear rate imposed by the equipment, and to the type of shear test mode applied, the shear strengths obtained from the quasi-static shear tests are simply designated ‘shear strength’ with no particular implication of drainage condition. The shear strengths obtained in the experimental program have been evaluated both in terms of undrained and drained strength criteria. In terms of

undrained conditions, the strength ratio (shear stress normalised by the normal stress) has been used, which can be mathematically expressed as follows:

$$\tau_{inter}/\sigma = \sigma \tan(\phi)/\sigma = \tan(\phi)$$

In terms of drained conditions, the (equivalent) friction angle has been computed and analysed. The friction angle for the soil is denoted ϕ and that for the interface denoted δ . To differentiate between the peak strength and the residual strength, the subscripts “p” and “r” respectively are used, and to differentiate between the soil-only strength and the interface strength, the subscripts “soil” and “inter” are used.

6.3.5 Post-test observation of shear surfaces

Once a series of tests with the particular pile section was complete, the clay sample was separated from the pile surface so that the shear surface of the clay and the pile surface could be observed. The observation of the interface was important for identification of the failure mode of the interface subjected to quasi-static shearing. The observations of the interfaces subjected to quasi-static shearing will be compared to those of the equivalent interfaces subjected to dynamic shearing in Chapter 7.

6.4 Interface Shear Failure: Observations & Discussion

After each interface test, the sample was separated from the pile surface so that the shear surface of the sample and the pile surface could be observed. This observation helps in identifying the actual shear plane location.

6.4.1 Low & medium plasticity clay on smooth pile

For interface tests involving BallR and BallR/Talc (medium and low plasticity clays) and smooth materials (steel and smooth concrete), the clay texture after testing was smooth and polished in appearance, with minute striations orientated in the direction of shear, as shown in Figure 6.6(a). There was no sign of remoulding having occurred. The pile surface corresponding to the shear surface was clean as shown in Figure 6.6(b). It is evident that shear failure occurred at the interface boundary during shearing.

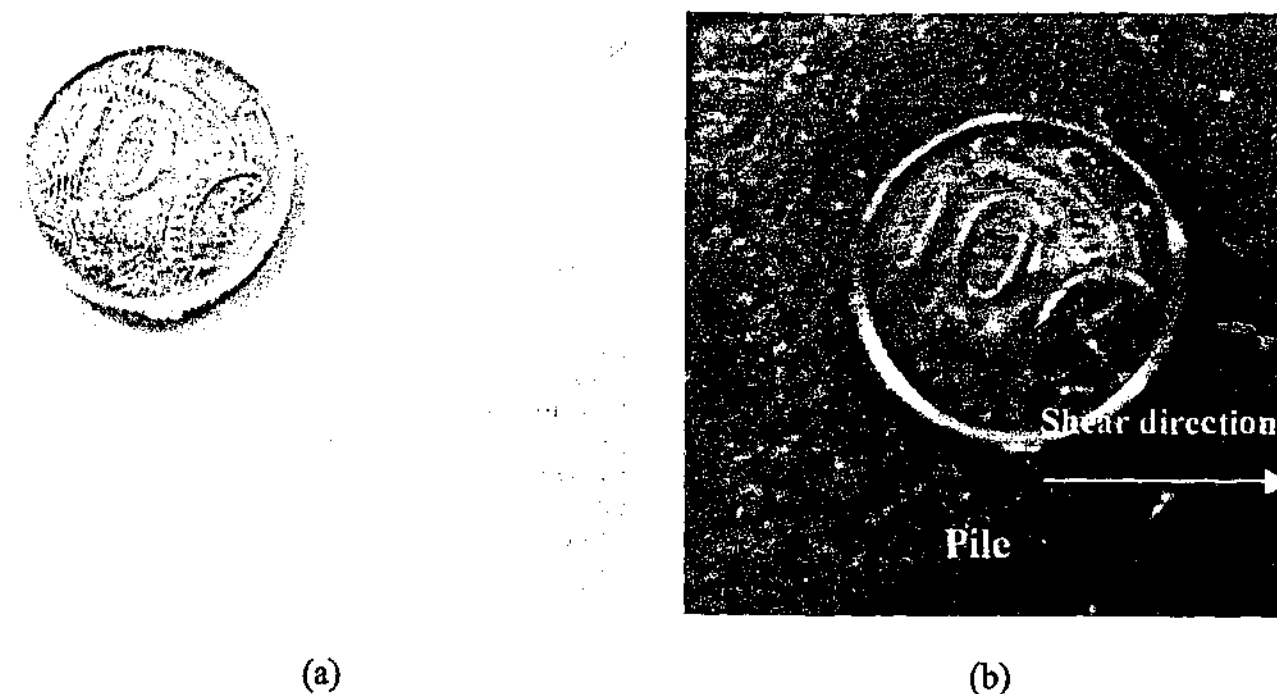


Figure 6.6 (a) Post-test BallR/Talc texture with smooth and polished appearance (b) Clean pile surface

6.4.2 Low & medium plasticity clay on rough pile

When pried apart, the specimen and the pile surface separated at the interface, indicating that shear failure again occurred at the interface. As shown in

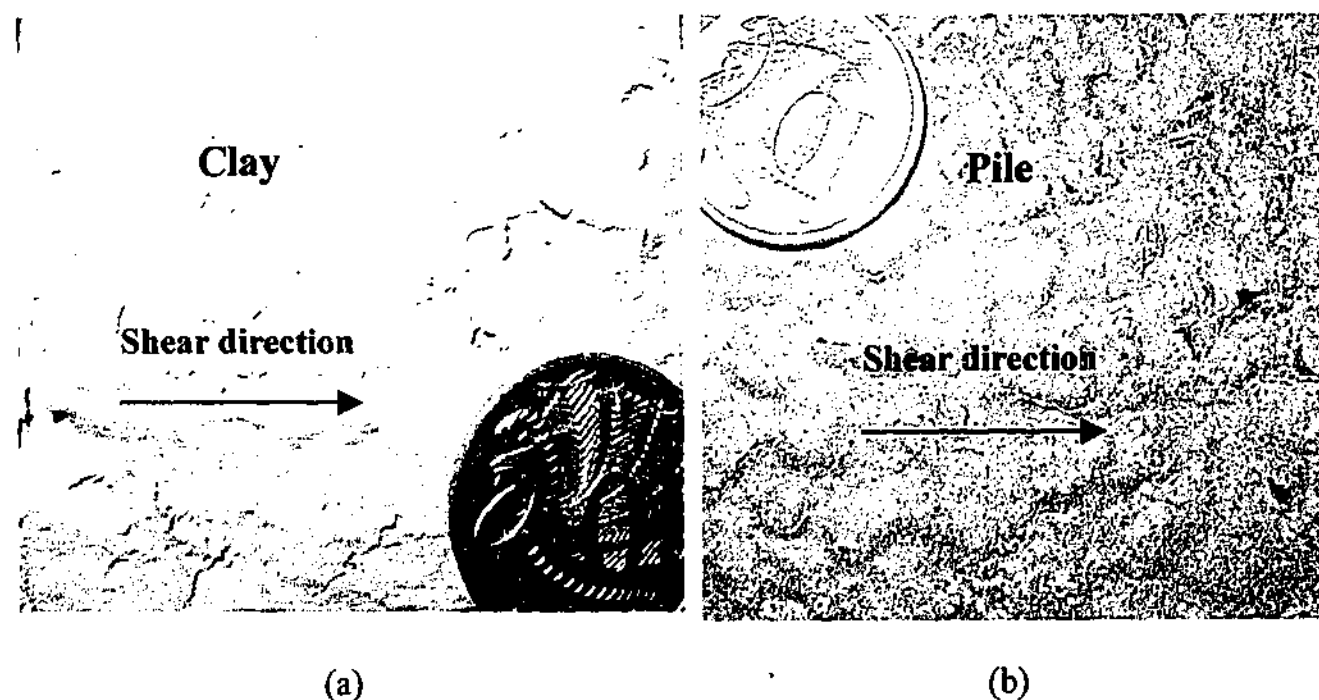


Figure 6.7 (a) Post-test BallR texture showing imprints made by asperities of the pile
(b) Clean pile surface

Figure 6.7(a), the shear surface of the specimen was rough as it has been imprinted by the large asperities of the rough surface. Apparently, during shearing, the clay deformed according to the shapes of the asperities. As in Figure 6.7(b), the rough surface was clean which indicates that the shear plane occurred at the pile-soil interface.

6.4.3 High plasticity clay on smooth pile

For interfaces involving HR1F (a high plasticity clay) and smooth materials, the clay sample adhered strongly to the pile after shearing. When the sample was forced to separate from the interface, a layer of clay was observed on the pile surface, as shown in Figure 6.8(b). The tendency for such high plasticity to adhere to the pile surface has been similarly observed in the laboratory and field tests involving the high plasticity London clay, by Tika-Vassilikos (1991) and Bond and Jardine (1991) respectively.

Examination of the shear zone of the specimen showed varying fabric as shown in Figure 6.8(a). In some sections, the clay fabric was rough due to tearing of the clay as some clay adhered to the pile surface. In other sections, the clay fabric showed some signs of the clay having flowed in the direction of shear. In the remaining sections, the surface was smooth and polished.

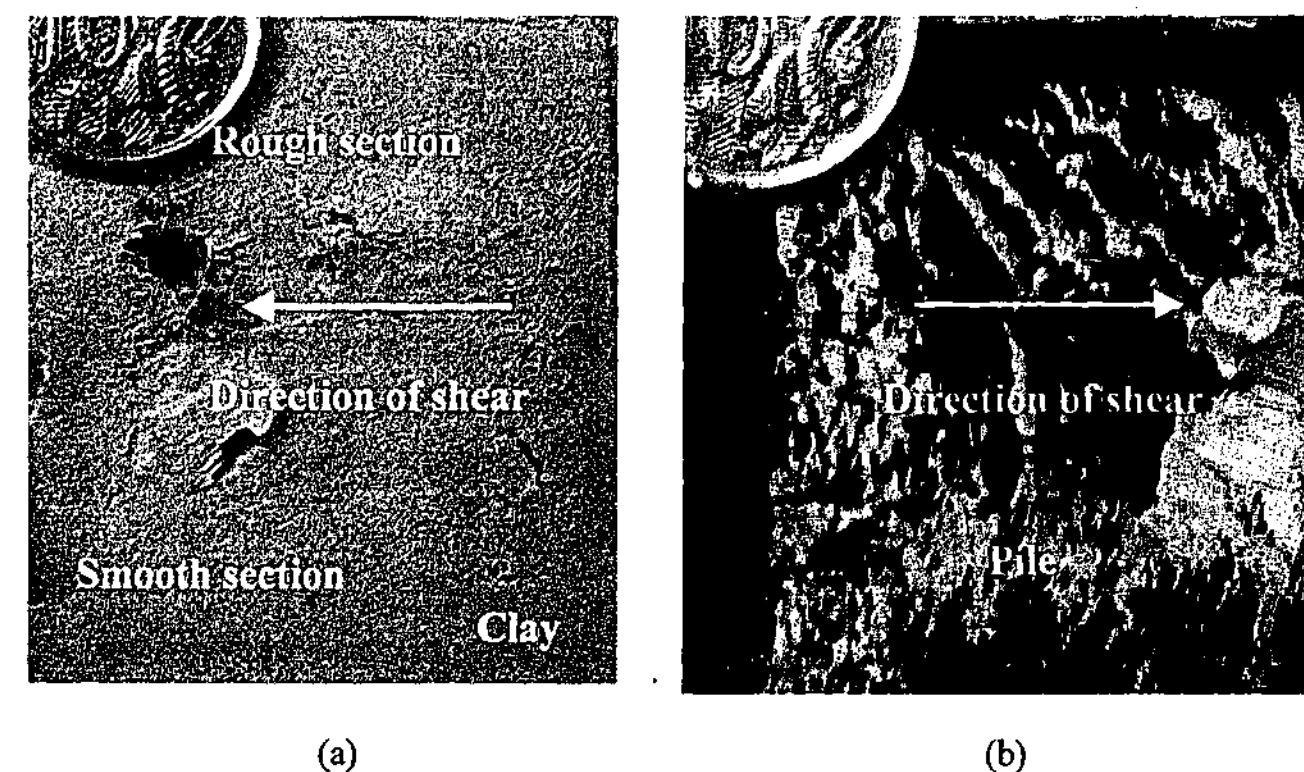


Figure 6.8 (a) Post-test HR1F clay texture showing signs of clay having flowed in the direction of shearing (b) Pile surface covered with an uneven layer of HR1F clay, showing even more clearly that the clay has flowed

Because the interface friction angle was less than the equivalent soil friction angle, it was inferred that shearing did not occur fully within the soil. It would appear that where the clay fabric showed signs of the clay having flowed, shearing occurred partially within the clay and partially by sliding on the pile surface, whilst where the clay fabric was smooth, shearing occurred by sliding on the interface. The partial failure within the clay would be consistent with the fact that some clay had adhered to the pile surface. Thus, the overall failure was likely to be a combination of the two mechanisms as has been similarly observed in interface tests by Littleton (1976) and Tsubakihara et al. (1993).

6.4.4 High plasticity clay on rough pile

The high plasticity clay was not tested against the rough pile due to the time constraints in this project. The original intention of testing the high plasticity was to ascertain the effect of the clay plasticity on the smooth steel surface and to compare the result of the high plasticity clay-smooth surface interface to the results of the low plasticity clay-smooth surface interface and the medium plasticity-smooth surface interface.

6.5 Quasi-Static Interface & Soil Behaviour: Results

6.5.1 Soil-only tests

Typical shear stress-shear displacement responses of BallR samples which were preconsolidated to 325kPa and then tested at normal stresses of 250, 150 and 60kPa are shown in Figure 6.9. For the lightly overconsolidated soil sample with *OCR* of 1.3, the shear stress does not peak but reaches the residual strength. For the overconsolidated sample with *OCR* of 5.4, the shear stress increases to a peak and then decreases to a residual value. This difference in behaviour is well-established (Head, 1994). Overall, the ratio of the interface residual strength to interface peak strength ranges from 0.8 to 1.0, as is shown graphically in Figure 6.13 in Section 6.6.1.

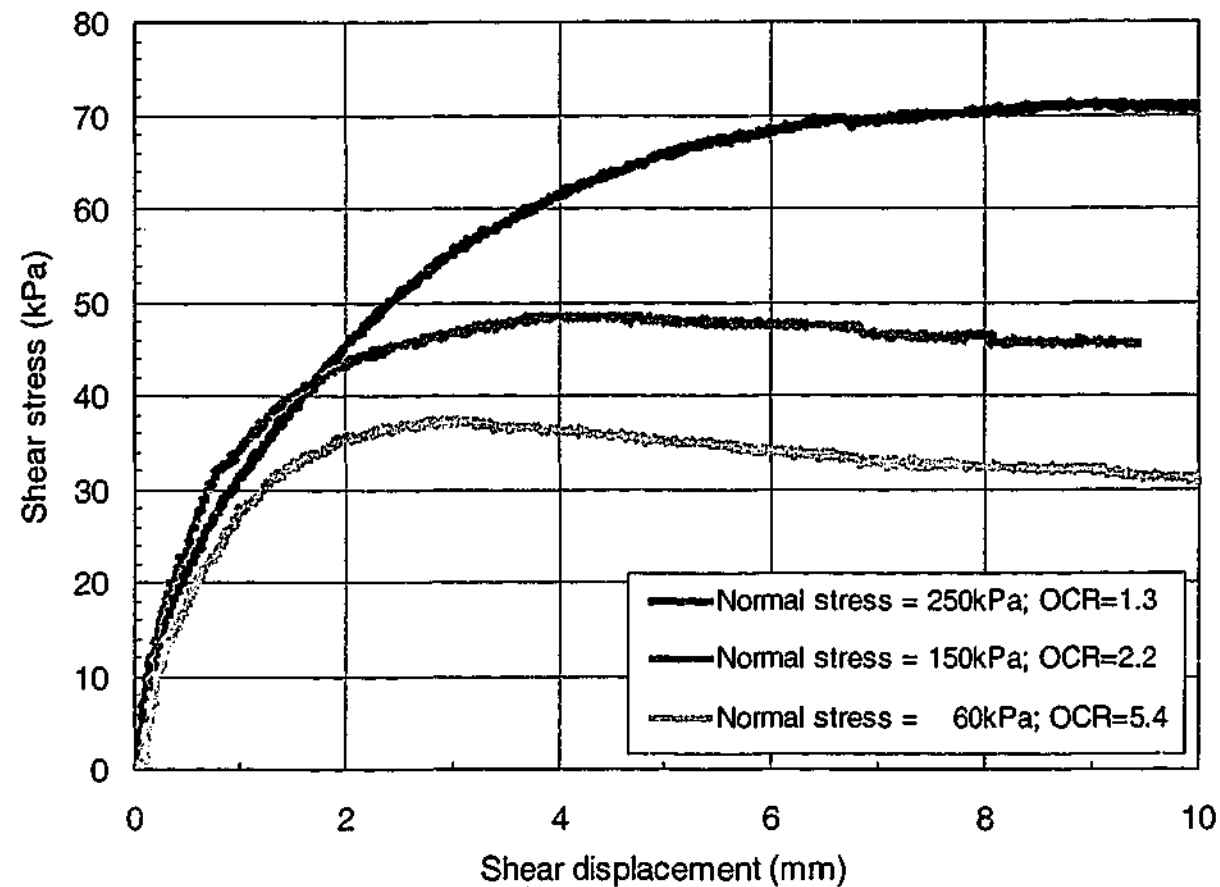


Figure 6.9 Shear stress-shear displacement responses of BallR (preconsolidated at 325kPa) tested at 3 normal stresses and *OCR*s

6.5.2 Interface tests

The shear stress-shear displacement responses of BallR samples (preconsolidated to 325kPa) sheared against the rough concrete at normal stresses of 250, 150 and 60kPa are shown in Figure 6.10. Qualitatively, the sample sheared against concrete behaves

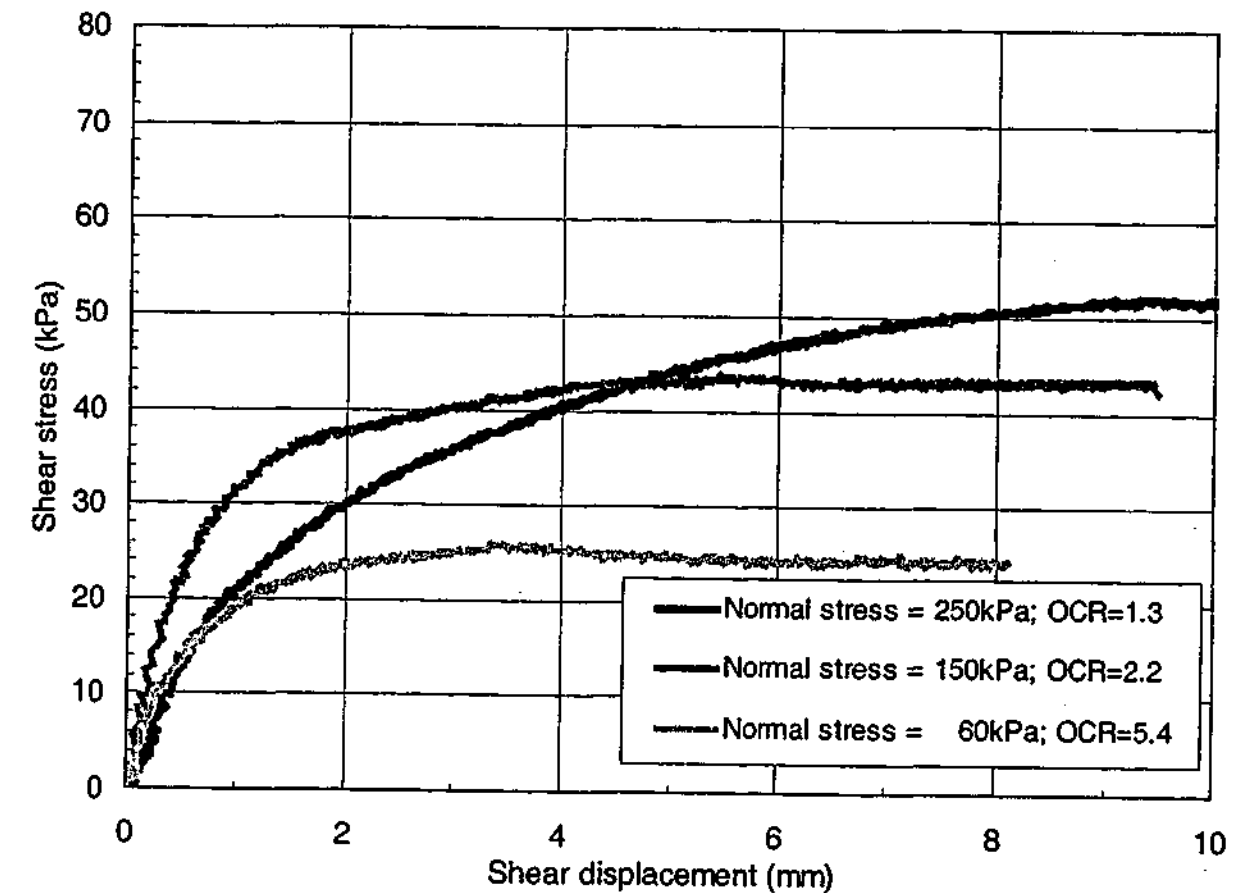


Figure 6.10 Shear stress-shear displacement responses of BallR (preconsolidated at 325kPa) sheared against rough concrete at 3 normal stresses and *OCR*s

in a similar manner to the sample sheared in the soil-only test. That is, for the lightly over-consolidated sample, the shear stress reaches residual strength without first peaking, and for the over-consolidated sample, the shear stress peaks first before reaching the residual strength. Overall, the ratio of the interface residual strength to interface peak strength ranges from 0.8 to 1.0, as will be shown graphically in Figure 6.22, Figure 6.23 and Figure 6.24 in Section 6.7.1.

6.5.3 Summary table for soil-only & interface test results

The peak values of the soil friction angle (ϕ_p), the interface friction angle (δ_p), the soil strength ratio ($\sigma \tan(\phi_p)/\sigma$), the interface strength ratio ($\sigma \tan(\delta_p)/\sigma$), and the ratio of the interface strength to the soil strength ($\tau_{inter p}/\tau_{soil p} = \sigma \tan(\delta_p)/\sigma / (\sigma \tan(\phi_p)/\sigma) = \tan(\delta_p)/\tan(\phi_p)$) are shown in Table 6.5. The values of the corresponding residual values are shown in Table 6.6.

Table 6.5 Soil & interface peak friction angles, peak strength ratios & interface peak strength/soil peak strength

Clay	Preconsol. stress (kPa)	Normal stress (kPa)	OCR	Friction angle = ϕ or δ (degree)				Strength Ratio = $\tau / \sigma = \tan(\phi$ or $\delta)$				$\tau_{inter} / \tau_{soil} = \tan(\delta) / \tan(\phi)$		
				Soil-Only	Soil-Steel	Soil-Smooth Con.	Soil-Rough Con.	Soil-Only	Soil-Steel	Soil-Smooth Con.	Soil-Rough Con.	Soil-Steel	Soil-Smooth Con.	Soil-Rough Con.
BallR/Talc	500	250	2.0	20.5	12.0	-	-	0.37	0.21	-	-	0.57	-	-
BallR/Talc	500	150	3.3	25.4	14.4	-	-	0.47	0.26	-	-	0.54	-	-
BallR/Talc	500	60	8.3	42.5	25.0	-	-	0.92	0.47	-	-	0.51	-	-
BallR/Talc	325	250	1.3	18.0	10.0	-	-	0.32	0.18	-	-	0.54	-	-
BallR/Talc	325	150	2.2	22.3	13.0	-	-	0.41	0.23	-	-	0.56	-	-
BallR/Talc	325	60	5.4	34.0	19.3	-	-	0.67	0.35	-	-	0.52	-	-
HR1F	500	250	2.0	13.1	7.0	-	-	0.23	0.12	-	-	0.53	-	-
HR1F	500	150	3.3	18.0	10.0	-	-	0.32	0.18	-	-	0.54	-	-
HR1F	500	60	8.3	35.0	19.8	-	-	0.70	0.36	-	-	0.52	-	-
HR1F	325	250	1.3	11.0	6.0	-	-	0.19	0.11	-	-	0.54	-	-
HR1F	325	150	2.2	12.5	7.7	-	-	0.22	0.14	-	-	0.61	-	-
HR1F	325	60	5.4	24.5	13.5	-	-	0.46	0.24	-	-	0.53	-	-
BallIR	500	250	2.0	20.0	12.6	10.0	14.7	0.36	0.22	0.18	0.26	0.61	0.48	0.72
BallIR	500	150	3.3	25.0	15.3	13.0	18.5	0.47	0.27	0.23	0.33	0.59	0.50	0.72
BallIR	500	60	8.3	38.0	24.0	19.5	28.0	0.78	0.45	0.35	0.53	0.57	0.45	0.68
BallIR	325	250	1.3	16.0	9.5	7.5	11.7	0.29	0.17	0.13	0.21	0.58	0.46	0.72
BallIR	325	150	2.2	21.0	12.4	11.3	16.0	0.38	0.22	0.20	0.29	0.57	0.52	0.75
BallIR	325	60	5.4	32.1	18.7	15.7	23.0	0.62	0.34	0.28	0.42	0.54	0.45	0.68

6-18

Table 6.6 Soil & interface residual friction angles, residual strength ratios & interface residual strength/soil residual strength

Clay	Preconsol. stress (kPa)	Normal stress (kPa)	OCR	Friction angle = ϕ or δ (degree)				Strength Ratio = $\tau / \sigma_r = \tan(\phi$ or $\delta)$				$\tau_{inter} / \tau_{soil} = \tan(\delta) / \tan(\phi)$		
				Soil-Only	Soil-Steel	Soil-Smooth Con.	Soil-Rough Con.	Soil-Only	Soil-Steel	Soil-Smooth Con.	Soil-Rough Con.	Soil-Steel	Soil-Smooth Con.	Soil-Rough Con.
BallR/Talc	500	250	2.0	20.5	12.0	-	-	0.38	0.21	-	-	0.55	-	-
BallR/Talc	500	150	3.3	22.8	13.3	-	-	0.42	0.24	-	-	0.56	-	-
BallR/Talc	500	60	8.3	36.0	20.5	-	-	0.73	0.37	-	-	0.51	-	-
BallR/Talc	325	250	1.3	19.5	10.0	-	-	0.35	0.18	-	-	0.50	-	-
BallR/Talc	325	150	2.2	21.7	12.6	-	-	0.40	0.23	-	-	0.58	-	-
BallR/Talc	325	60	5.4	29.5	18.0	-	-	0.57	0.35	-	-	0.62	-	-
HR1F	500	250	2.0	11.0	7.0	-	-	0.19	0.12	-	-	0.63	-	-
HR1F	500	150	3.3	14.0	9.5	-	-	0.25	0.17	-	-	0.67	-	-
HR1F	500	60	8.3	28.5	18.5	-	-	0.54	0.33	-	-	0.62	-	-
HR1F	325	250	1.3	10.4	6.0	-	-	0.19	0.11	-	-	0.57	-	-
HR1F	325	150	2.2	10.5	7.7	-	-	0.19	0.14	-	-	0.73	-	-
HR1F	325	60	5.4	20.0	12.0	-	-	0.36	0.24	-	-	0.58	-	-
BallIR	500	250	2.0	19.4	12.4	9.6	14.1	0.35	0.22	0.17	0.25	0.62	0.48	0.71
BallIR	500	150	3.3	22.4	14.5	10.5	18.0	0.41	0.26	0.29	0.32	0.63	0.45	0.79
BallIR	500	60	8.3	33.0	22.8	16.0	25.0	0.65	0.42	0.29	0.47	0.65	0.44	0.72
BallIR	325	250	1.3	16.0	9.5	7.5	11.7	0.29	0.17	0.13	0.21	0.58	0.46	0.72
BallIR	325	150	2.2	20.0	12.0	10.0	15.5	0.36	0.21	0.18	0.28	0.58	0.48	0.76
BallIR	325	60	5.4	27.0	18.4	13.5	21.7	0.51	0.33	0.24	0.40	0.65	0.47	0.78

6-19

6.6 Quasi-Static Soil-Only Behaviour: Discussion

Although the subject of the current study is the interface strength behaviour, the soil-only behaviour has also been analysed for the following reasons:

- Abundant soil-only test data from previous studies are available which can be used to establish that the quasi-static tests performed in this study, for which the drainage conditions are uncertain, yield strength behaviour that is consistent with that reported in previous research.
- There is a lack of published data available on the interface strength behaviour so that the interface strength behaviour observed in this study cannot be directly validated by comparison with data from previous research. However, since the interface strength behaviour follows closely after the soil-only strength behaviour as will be demonstrated in Section 6.6, the validity of the interface strength behaviour observed in the present study can be indirectly validated by validating the soil-only strength behaviour.
- It is important that the soil-only data are shown to be credible, as the soil strength parameters obtained from the quasi-static tests will be used for correlation with the damping factor in Chapter 8.

6.6.1 Undrained strength analysis

In the analyses of the undrained soil strength behaviour, the undrained shear strength is typically normalised by the vertical effective overburden to obtain what is termed the shear strength ratio (e.g. Ladd et al. (1977); Wroth, 1984; Terzaghi et al., 1996; Jardine and Chow, 1996). It is implicit that the term “strength ratio” relates to the peak strength ratio; however, in order to differentiate the peak and residual values, the terms “peak strength ratio” ($\tau_{soil p}/\sigma$) and “residual strength ratio” ($\tau_{soil r}/\sigma$) will be used in the subsequent discussion to refer to the respective strength values.

For a particular clay type that is tested at different *OCR*s, the peak strength ratio ($\tau_{soil p}/\sigma$) can be correlated with *OCR* for samples tested in simple shear for samples that are consolidated one-dimensionally and triaxial compression for samples consolidated under either isotropic or anisotropic conditions (e.g. Wroth, 1984; Terzaghi et al., 1996). The peak strength ratio-*OCR* relationship can be described by the relationship given by:

$$\frac{S_u}{\sigma'_v} = \left[\frac{S_u}{\sigma'_n} \right]_{\sigma'_p=1} \left(\frac{\sigma'_p}{\sigma'_v} \right)^m \quad (6.1)$$

where σ'_p is the preconsolidation stress and σ'_v is the vertical effective overburden.

$\left[\frac{S_u}{\sigma'_n} \right]_{\sigma'_p=1}$ is the shear strength ratio for the normally consolidated sample for the

particular type of clay, and $\left(\frac{\sigma'_p}{\sigma'_v} \right)$ is the over-consolidation ratio, *OCR*. For

undrained tests, the normalised shear strength ratio varies as *OCR* to the power *m* where *m* lies in the range 0.68 to 0.86 and is related physically to the compression index (Wroth, 1984).

In order to analyse the peak strength behaviour observed in this study, the values of the peak strength ratios were obtained by assuming that the shear-induced pore pressure generated to be small in the quasi-static direct shear test, so that the vertical effective stress in the case of the direct shear test can be taken as being approximately equal to the applied vertical stress. It is noted that the peak strength ratios for a sample that is consolidated one-dimensionally are different from those for a sample that is consolidated isotropically, and that the peak strength ratios in the context of the present discussion relate to the direct shear test where the sample is consolidated one-dimensionally.

The peak strength ratios ($\tau_{soil p}/\sigma$) are plotted against the *OCR* in Figure 6.11. The residual strength ratios ($\tau_{soil r}/\sigma$) are also plotted against the *OCR*, as shown in Figure 6.12. The graphs were plotted as a linear-log plot in the same format used by Ladd et al. (1977) (whose study was based on simple shear tests), although these ratios were plotted as a log-log plot by Jardine and Chow (1996) and Terzaghi et al. (1996). Trend lines are included in the plots.

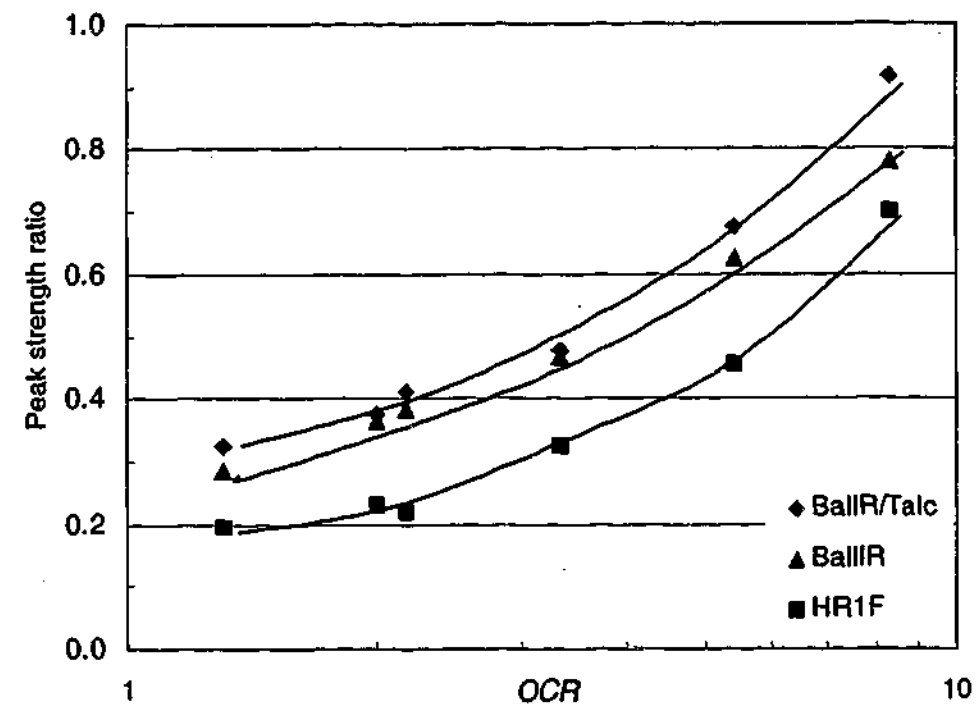


Figure 6.11 BallR, BallR/Talc and HR1F: Soil peak strength ratio-OCR relationships

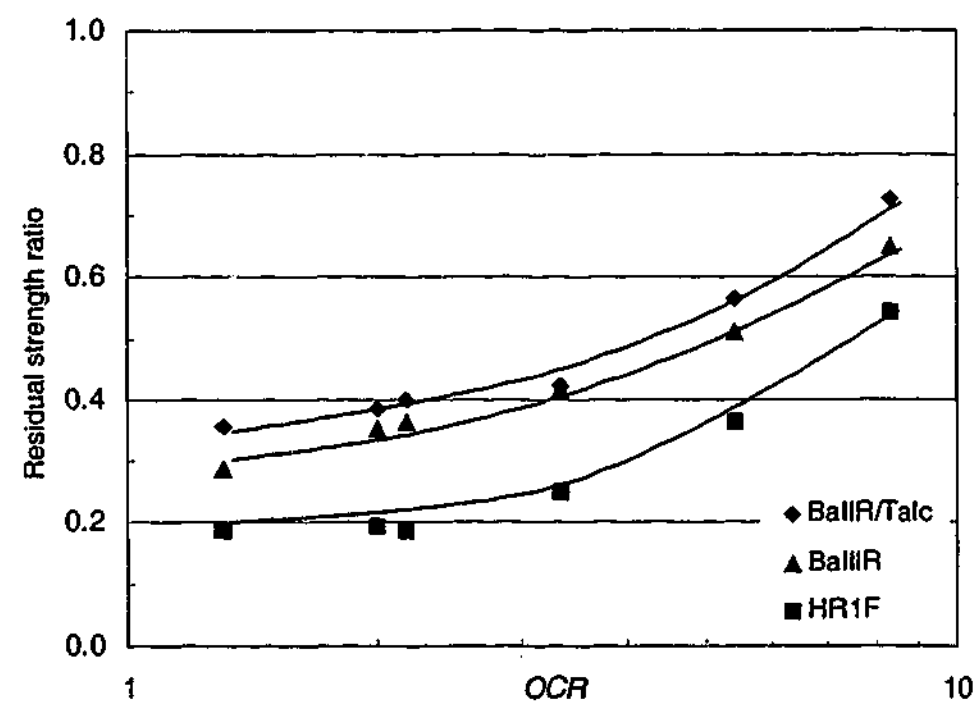


Figure 6.12 Soil residual strength ratio-OCR relationships for BallR, BallR/Talc and HR1F

As can be noted, the values of $\tau_{soil p}/\sigma$ and $\tau_{soil r}/\sigma$ increase with OCR exponentially as found in previous research and consistent with Equation 7.1 which is based on undrained data. It can also be noted in Figure 6.11 that the peak strength envelopes

for the three clays are almost parallel to each other. The same applies to the residual strength envelopes as can be seen in Figure 6.12.

In order to quantify the variation of the residual strength relative to the peak strength or the reduction in the strength from the peak strength to residual strength, the values of $\tau_{soil r}/\tau_{soil p}$ have been plotted against the OCR for each of the 3 soils in Figure 6.13. Data obtained by Subba Rao et al. (2000) for one clay tested at a normally consolidated state ($OCR=1.0$) and an over-consolidated state ($OCR=10$) have been included for comparison.

It is noted that the data points are slightly scattered. The specimens of a particular clay tested in the direct shear box might not have identical moisture contents as uneven drainage might have occurred during consolidation of the large fabricated clay block. However, the general trend is evident. As has been discussed in Section 6.5.1, when the sample was normally consolidated (or was close to the normally consolidated state), the shear stress increased to a peak value and maintained this value even with further displacement to the residual state (i.e. there was no peak-then-residual behaviour) and the residual strength was equal to the peak strength ($\tau_{soil r}/\tau_{soil p} = 1.0$), and when the sample was over-consolidated, the sample exhibited peak-then-residual behaviour so that the residual strength was lower than the peak strength ($\tau_{soil r}/\tau_{soil p}$ less than 1.0) (e.g. Head, 1994; Subba Rao et al., 2000). Thus, as can be noted in Figure 6.13, $\tau_{soil r}/\tau_{soil p}$ is equal to almost equal to 1.0 for low OCR s, and decreases with increasing OCR . It can also be noted that the test data from this study compare well with the data from Subba Rao et al.

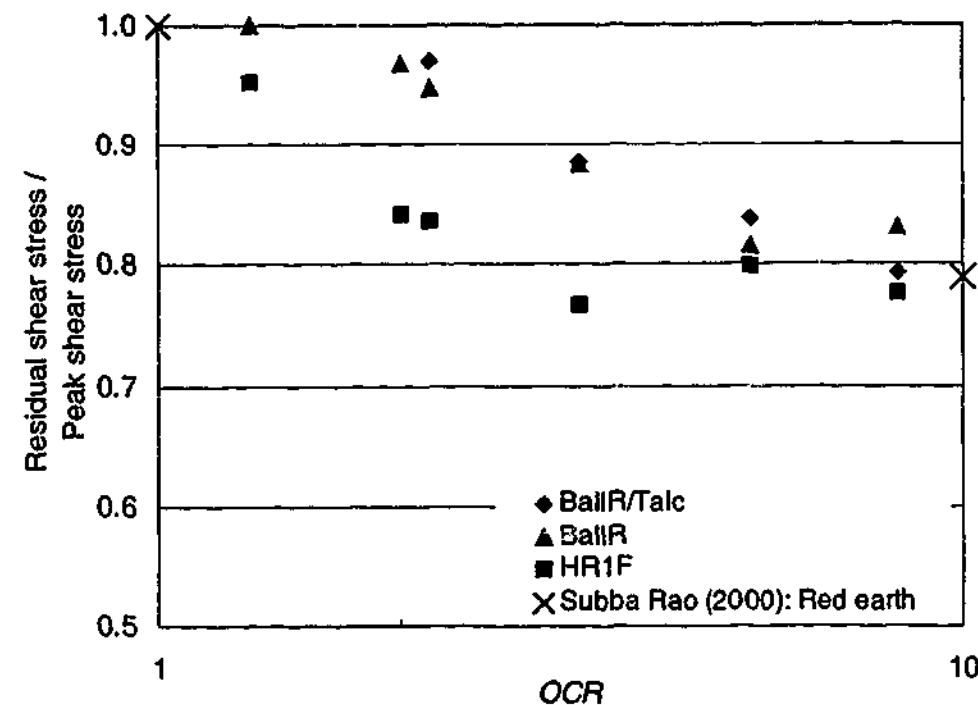


Figure 6.13 BallR, BallR/Talc, HR1F: Soil residual shear stress/Soil peak shear stress vs. *OCR*

In order to check the validity of the tests performed in this study and the data obtained from these tests, the data from this study are compared to those from previous studies. To the best of the knowledge of the author, no data of the residual strength ratio in relation to the *OCR* are available so that comparison can only be made for the peak strength data.

The peak strength data from this study are compared to undrained shear test peak data from Ladd et al. (1977) and from Jardine (1985), in Figure 6.14. The data from Ladd et al. (1977) are based on one-dimensionally consolidated specimens tested in the simple shear test, and the range of values within the upper and lower bounds are based for seven clays with medium and high plasticity. Qualitatively, the relationships between the strength ratio and the *OCR* from this study and Ladd et al are similar. In fact, as mentioned earlier, the relationship between the peak strength ratio and the *OCR* for undrained tests is well supported by various sets of data (e.g. Ladd and Edgers, 1972 cited in Wroth, 1984; Jardine, 1985 cited in Jardine and Chow, 1996; Andresen et al., 1979; Terzaghi et al., 1996). Although the tests conducted in this study were not strictly undrained tests (as has been discussed in Section 6.3.4), the shear strength-*OCR* relationship based on these tests is similar to

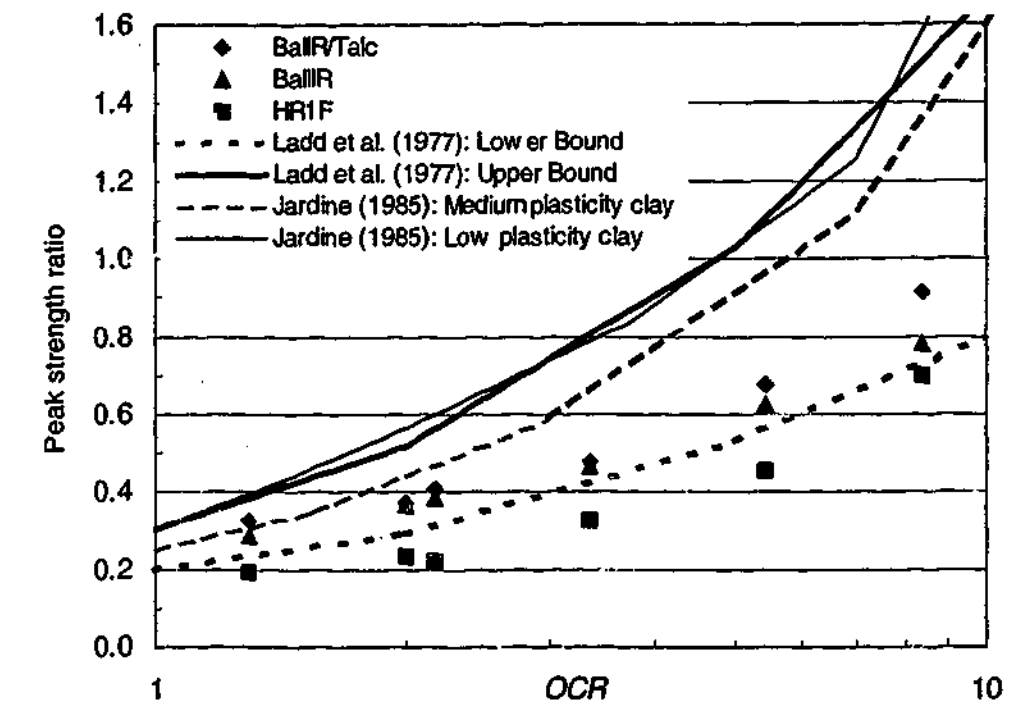


Figure 6.14 Comparison of soil peak strength ratios: Data from this study vs. Data from Ladd et al. (1977) for 7 clays and from Jardine (1985)

that for truly undrained tests. Quantitatively, the data from the current study compare well with the lower bound of the data from Ladd et al. (1977). The peak strength ratios in the present study show values below and above the lower bound determined by Ladd et al. (1977). Since the specimens in this study and in the study of Ladd et al. (1977) were both consolidated one-dimensionally, this difference must be due to the shear mode and the volumetric or the pore pressure response, and the different types of clay that were tested.

The data from Jardine (1985) cited in Jardine and Chow (1996) are based on specimens consolidated in the K_0 condition and tested in triaxial compression. The K_0 constant relates the horizontal stress on a soil element to the vertical stress on the soil element in the field. Thus, the K_0 consolidation involves increasing the vertical consolidation stress and the confining stress on the specimen at the same rate so that a constant value of K_0 is maintained. It is noted that the data plotted are for a low plasticity clay and a medium plasticity clay. Qualitatively, the data show the same trend as do the data reported by Ladd et al and in this study. Quantitatively, the values of strength ratio data almost coincide with the upper bound values obtained by Ladd et al. and are thus higher than those obtained in this study.

Based on the data obtained from this study, the peak strength ratio decreases with increasing plasticity of the clay. This is consistent with the data from Jardine (1985). However, based on the data from Ladd et al. (1977), no such relationship between the strength ratio and the clay plasticity can be observed. The reason for the lack of agreement between the data obtained from this study and Jardine's study and the data obtained from Ladd et al. (1977) is unclear.

Thus, the comparison establishes that the quasi-static strength behaviour obtained from this study is credible and consistent with expectation and the work of others.

6.6.2 Effective strength analysis

It is emphasised that the results of the total stress and effective stress analyses based on the same data are not fundamentally different. Thus, it is of no further value to present the data in terms of the effective stress parameter (or the friction angle, ϕ). The previous total stress analyses using the total stress parameters have implied that the peak (ϕ_p) and residual (ϕ_r) friction angles will similarly increase with OCR , and the value of ϕ_r/ϕ_p will similarly decrease from 1.0 to less than 1.0 as the sample goes from being normally consolidated to being over-consolidated. However, for comparison against the data from Subba Rao et al. (2000) which are based on drained tests, the data obtained in this study are presented in terms of the friction angle as well.

Subba Rao et al. (2000) who performed drained tests showed that the drained soil strength behaviour could be analysed by plotting the values of ϕ_p against the OCR . Following Subba Rao et al. (2000), the values of ϕ_p based on the data from this study have been plotted against the OCR in Figure 6.15. The data from Subba Rao et al. have also been included in the plot. It is noted that the data from Subba Rao et al. are based on one-dimensionally consolidated specimens, and that because the samples were tested at only 3 different OCR s, the data points have been joined with linear lines. As can be noted, ϕ_p increases with OCR for each clay type but the values of ϕ_p from this study at low OCR s are significantly lower than those from Subba Rao et al. (2000). This confirms that the tests conducted in this study were closer to the undrained tests as has been demonstrated previously, and thus lower friction angles

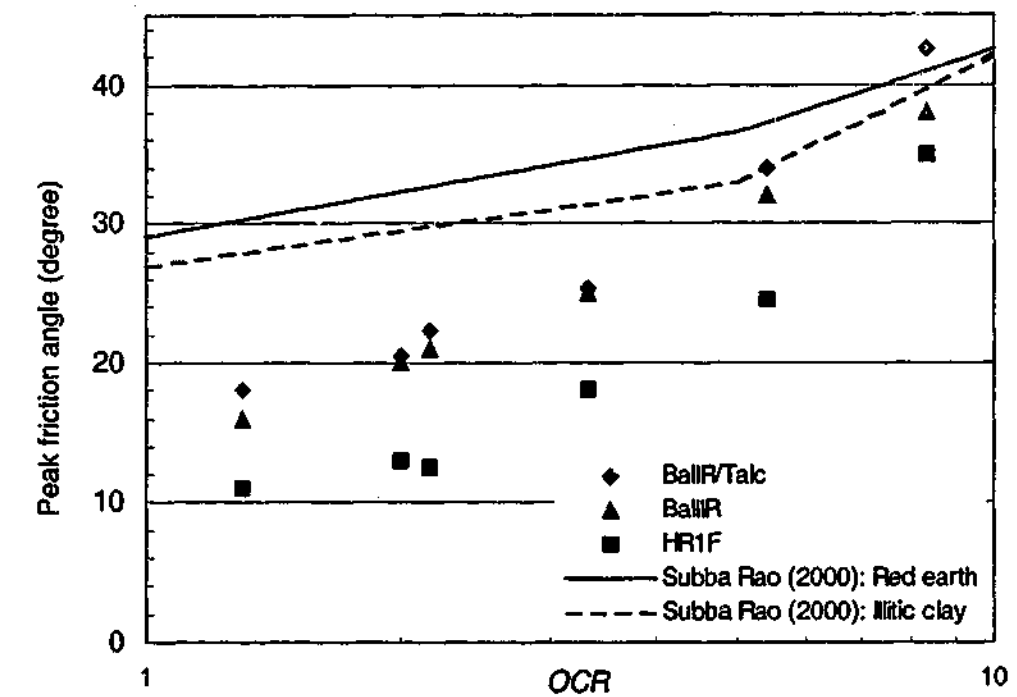


Figure 6.15 Comparison of soil peak friction angles: Data from this study vs. Data from Subba Rao et al. (2000) based on drained tests

were obtained. In any case, irrespective of whether the strength behaviour is drained or undrained, it has been established that the quasi-static strength behaviour observed in this study is credible.

6.7 Quasi-Static Interface Strength Behaviour: Discussion

6.7.1 Undrained strength analysis

Following the analysis of the soil data, the interface peak strength ratio ($\tau_{inter p}/\sigma$) data for the three clays have been plotted against the OCR in Figure 6.16, Figure 6.18 and Figure 6.20, and the interface residual strength ratio ($\tau_{inter r}/\sigma$) data have been plotted against the OCR in Figure 6.17, Figure 6.19 and Figure 6.21. The interface strength data points have been fitted with full lines, and the soil strength data points, which have also been included for comparison, have been fitted with a dashed line. It is noted that the soil strength has been obtained using the standard direct shear test whilst the interface strength has been obtained using the purpose-built device so that scale effects might need to be considered when comparing the two sets of data.

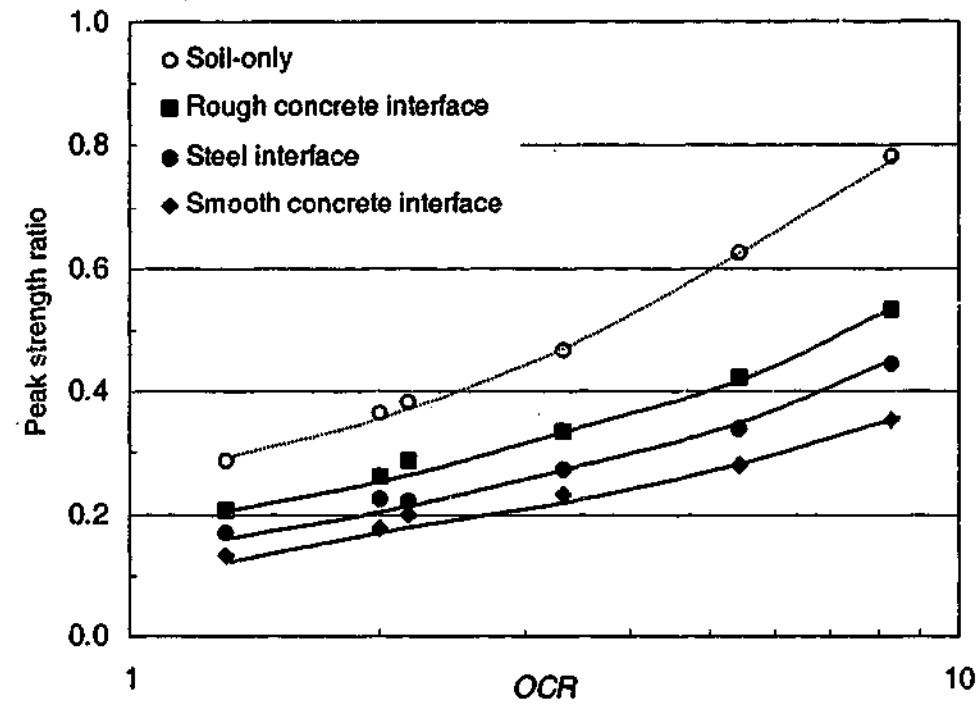


Figure 6.16 BallR: Interface (and soil) peak strength ratios-OCR relationships

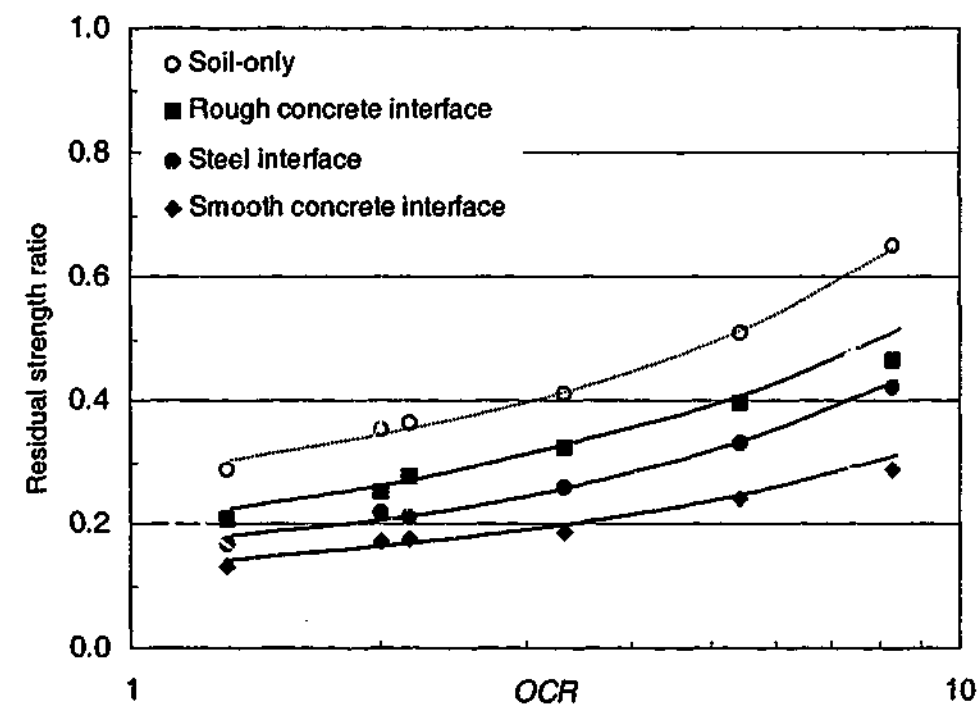


Figure 6.17 BallR: Interface (and soil) residual strength ratios-OCR relationships

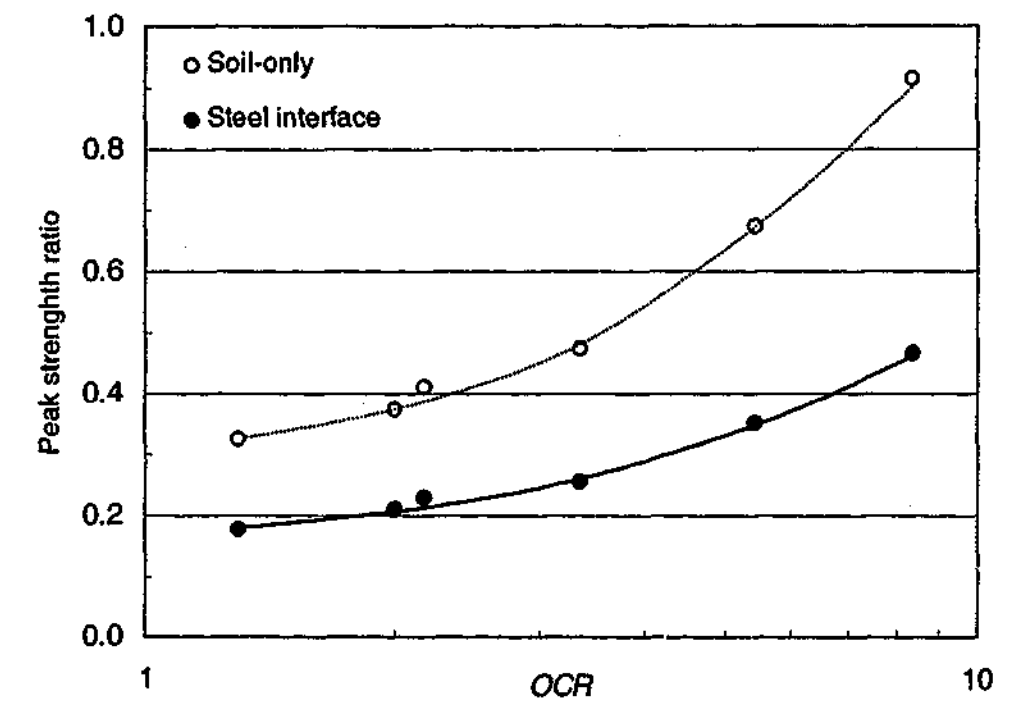


Figure 6.18 BallR/Talc: Interface (and soil) peak strength ratio-OCR relationships

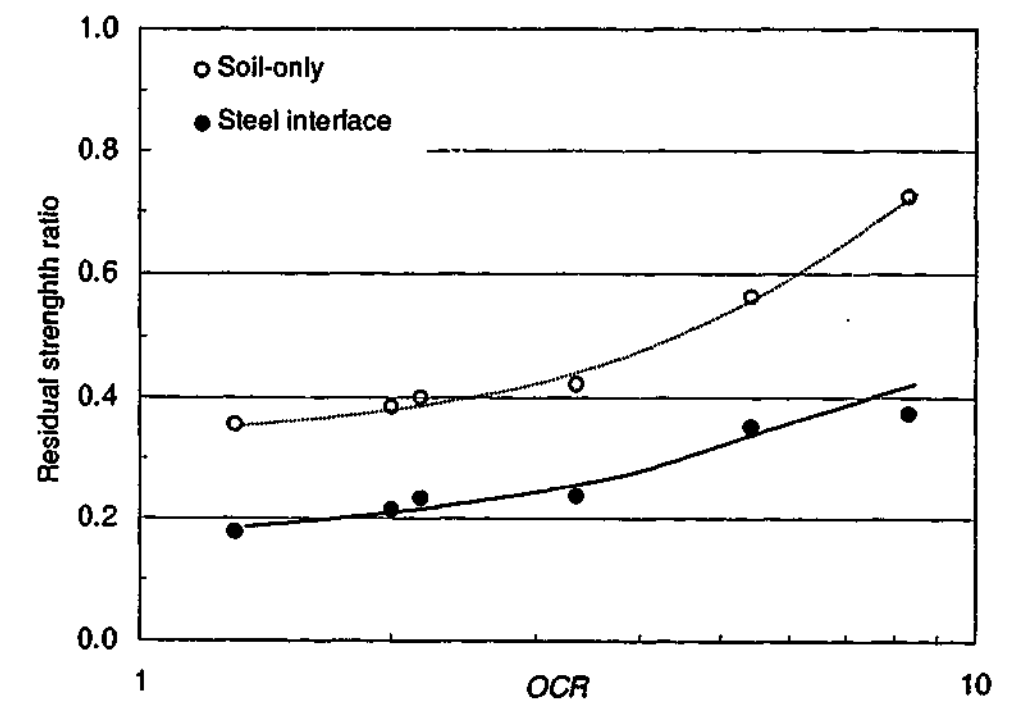


Figure 6.19 BallR/Talc: Interface (and soil) residual strength ratio-OCR relationships

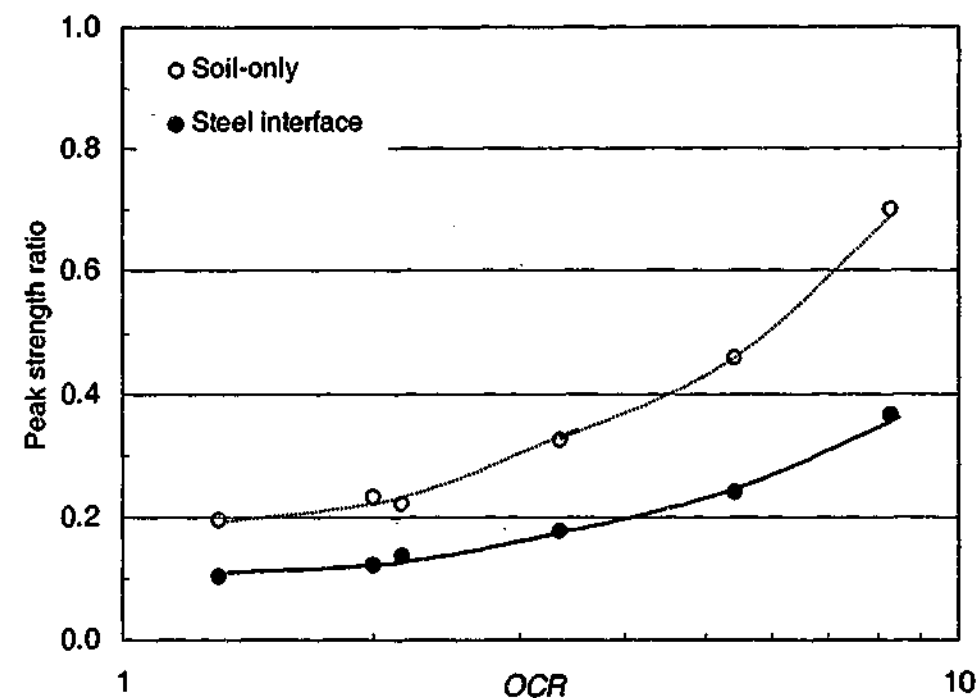


Figure 6.20 HR1F: Interface (and soil) peak strength ratio-OCR relationships

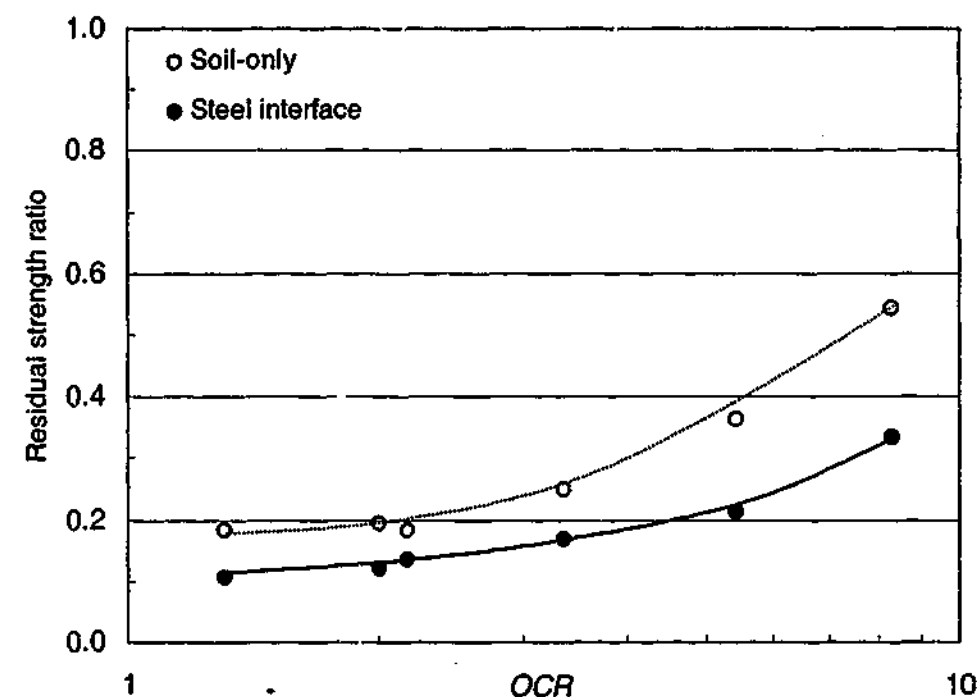


Figure 6.21 HR1F: Interface (and soil) residual strength ratio-OCR relationships

It can be observed in Figure 6.16, Figure 6.18 and Figure 6.20 that, for each interface, the *interface* peak friction angle increases with the *OCR* at practically the same rate as the *soil* peak friction angle, giving parallel “envelopes”. It can also be observed in Figure 6.17, Figure 6.19 and Figure 6.21 that the same applies to the residual strength parameter. It would appear that the two sets of data obtained using

the two devices were not significantly affected by different scales of the two devices. Thus, the interface behaviour for the pile-soil interface tests closely follows the behaviour for the soil-only tests.

Figure 6.16 to Figure 6.21 show that, for each type of clay, the interface peak and residual strengths are less than the soil-only peak and residual strengths respectively, as expected. Also, the interface peak and residual strengths increase with increasing surface roughness as is intuitive and as has been well established in previous studies (e.g. Meyerhof and Murdock, 1953; Potyondy, 1961; Clark and Meyerhof, 1972; Kanji, 1974; Littleton, 1976; Kraft et al., 1981). In fact, it has been shown by Subba Rao et al. (2000) that the limiting value of the peak interface strength is the soil strength.

To the best knowledge of the author, no undrained interface test data have been published so that direct verification of the data obtained in this study by comparison with previous data is not possible. However, the validity of the interface data can be demonstrated indirectly via the soil data. It has been verified in Section 6.6 that the soil strength data obtained in this study are consistent with the data from other studies. As it has just been demonstrated that the interface behaviour closely follows the soil behaviour (since interface and soil have parallel envelopes), it would appear that the interface strength data obtained from this study are also credible.

In order to quantify the variation of the residual strength relative to the peak strength or the reduction in the strength from the peak to residual strengths, the ratios of the interface residual shear strength to the interface peak shear strength ($\tau_{inter r}/\tau_{inter p}$) have been plotted against the *OCR* for BallR, BallR/Talc and HR1F in Figure 6.22, Figure 6.23 and Figure 6.24 respectively. The interface strength data from Subba Rao et al. (2000) have also been included in each of the plots.

Consistent with the equivalent soil parameter, the value of $\tau_{inter r}/\tau_{inter p}$ is equal to 1.0 for *OCR* of about 1.0 and it decreases with increasing *OCR*. It can also be noted that the values of the ratio also comparable to the values obtained by Subba Rao et al..

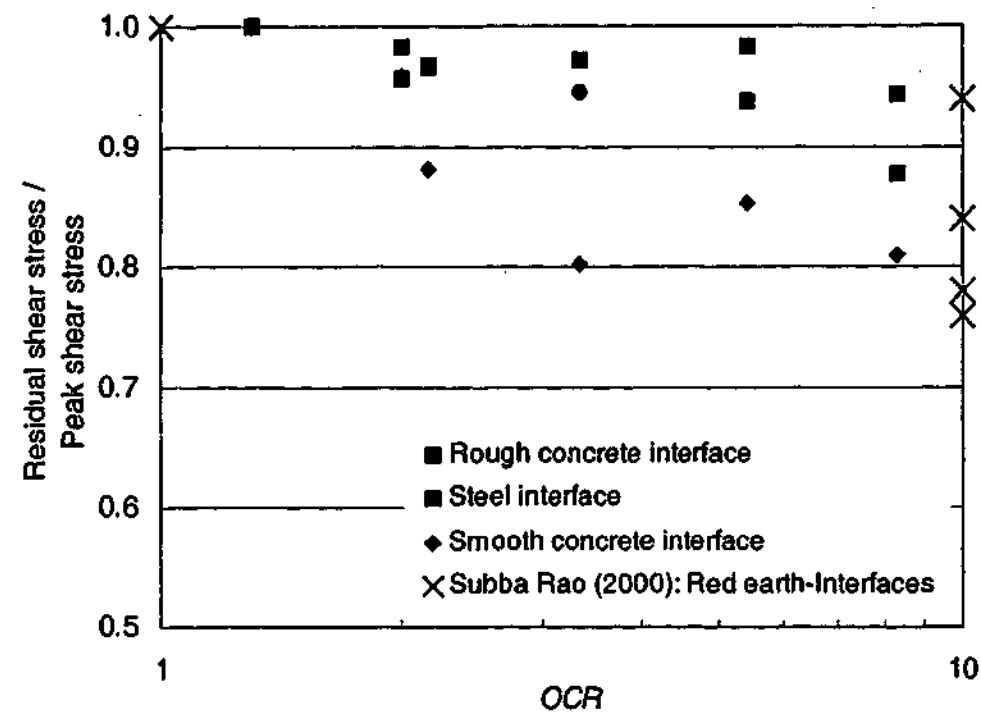


Figure 6.22 BallR: Interface residual strength/Interface peak strength vs. *OCR*

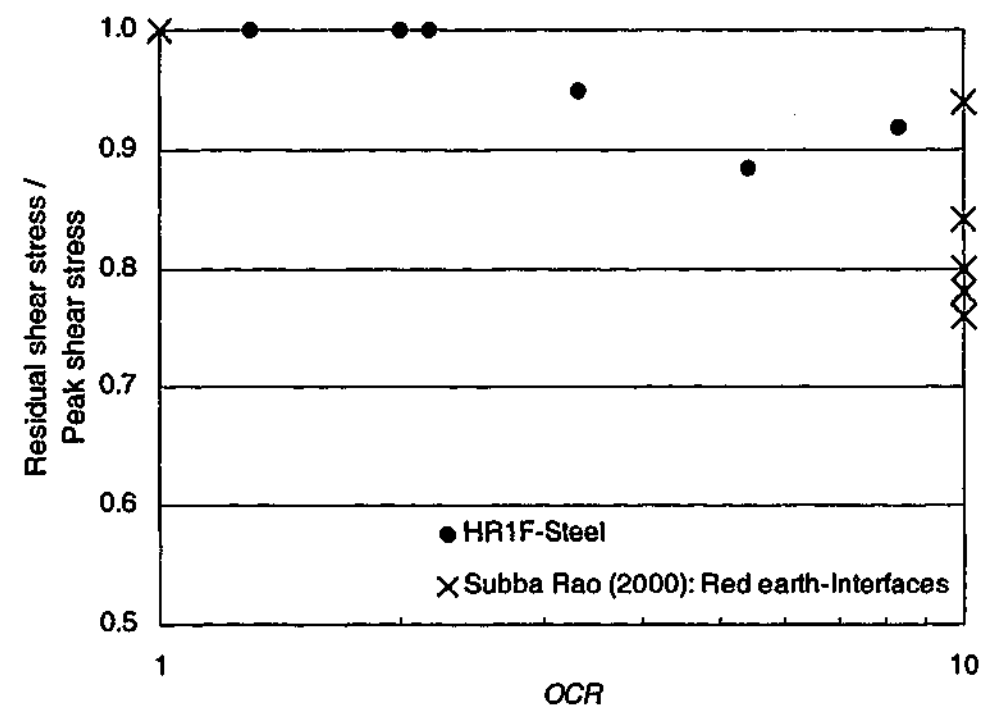


Figure 6.23 BallR/Talc: Interface residual strength/Interface peak strength vs. *OCR*

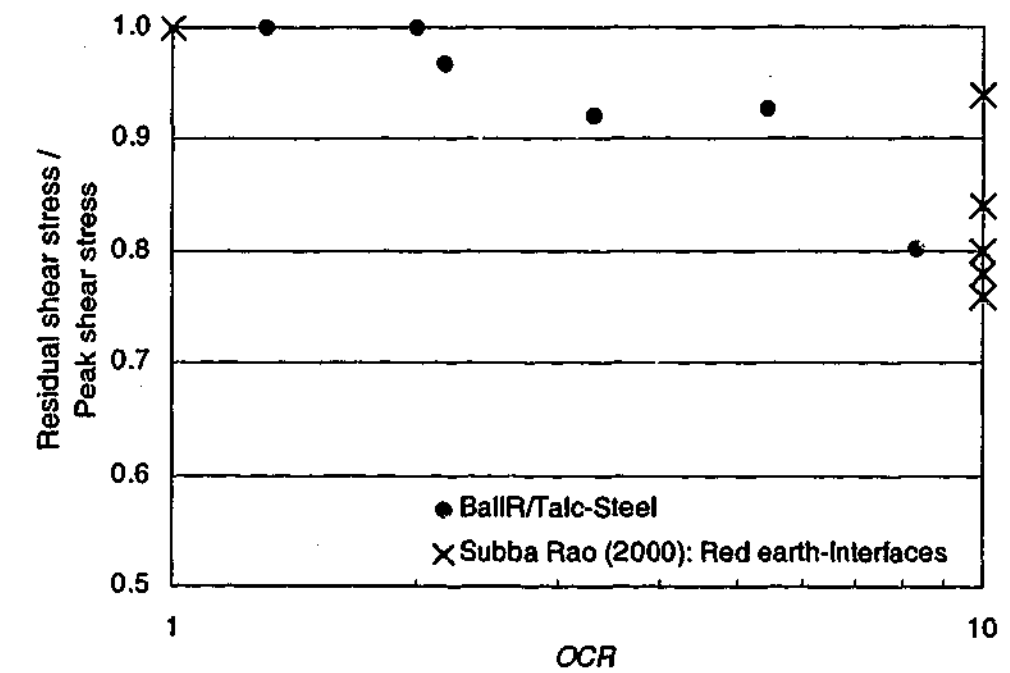


Figure 6.24 HR1F: Interface residual strength/Interface peak strength vs. *OCR*

6.7.2 Effective Strength Analysis

Since the data presented in terms of the effective parameter will also show the same trend of the strength parameter increasing with *OCR* (as has been discussed in Section 6.6), it is of no further value to present friction angle-*OCR* plots.

However, the interface peak friction angles (δ_p) have been collectively plotted against *OCR* in Figure 6.25 in order to be compared to data from Subba Rao et al. (2000) which are based on drained tests. The interface strength data obtained in this study show that the strength behaviour is significantly different from the drained strength behaviour, confirming that the behaviour observed in this study agrees more closely with the undrained behaviour.

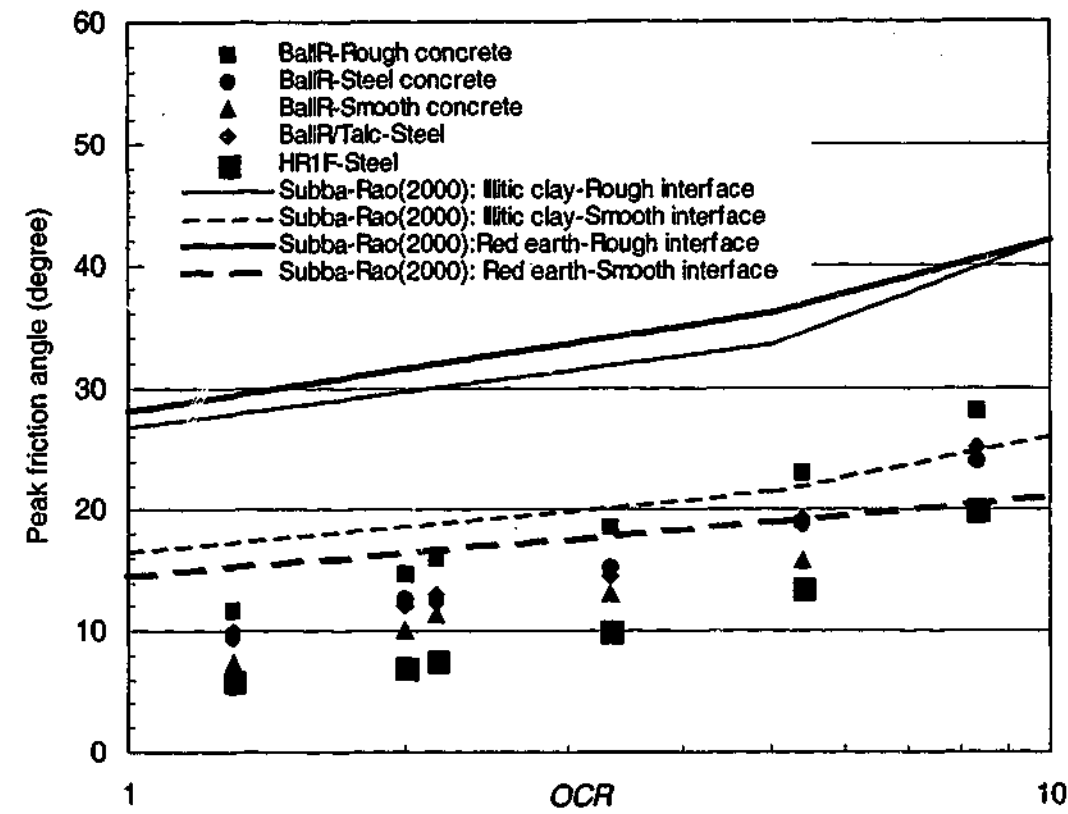


Figure 6.25 Comparison of interface peak friction angles: Data from this study vs. Data from Subba Rao et al. (2000) based on drained tests

6.8 Interface Strength/Soil Strength or Roughness Parameter

The ratio of the interface peak friction angle to soil peak friction angle (δ_p/ϕ_p) has been proposed as a measure of the roughness of the interface material for the pile-clay interface by Subba Rao et al. (2000). They showed that the values of δ_p/ϕ_p for a particular interface are constant regardless of the *OCR* of the soil, based on drained tests. It would appear that the roughness parameter is not dependent on the drainage conditions so that the parameter can be presented in terms of either the ratio of the interface friction angle to the soil friction angle (δ/ϕ) or the ratio of the interface strength ratio to the soil strength ratio ($(\tau_{inter}/\sigma)/(\tau_{soil}/\sigma) = \tau_{inter}/\tau_{soil}$). However, in order to facilitate comparison with the data from Subba Rao et al. (which are in terms of the friction angle), the data from this study are plotted in terms of δ/ϕ . Because the undrained and drained strength analyses on the same set of data yield essentially the same information, the data from this study are not plotted in terms of $(\tau_{inter}/\sigma)/(\tau_{soil}/\sigma) = \tau_{inter}/\tau_{soil}$.

The ratio of the interface peak friction angle to the soil peak friction angle (δ_p/ϕ_p) have been plotted against the *OCR* for BallR, BallR/Talc and HR1F in Figure 6.26, Figure 6.28 and Figure 6.30 respectively. Given the importance of the residual or large-displacement parameter in the current study, the values of δ_r/ϕ_r are also plotted against the *OCR* in Figure 6.27, Figure 6.29 and Figure 6.31.

For a particular interface, the values of δ_p/ϕ_p are almost constant regardless of the *OCR*, as suggested by the parallel envelopes of the soil data and the interface data shown previously. However, for a particular interface, the values of δ_r/ϕ_r vary slightly from each other, with the exception of the values for the BallR-Smooth concrete interface which are almost constant. Despite the variations, the values of δ_r/ϕ_r are almost constant. The suggested approximate values are indicated by the dashed lines, whilst the almost constant values for the BallR-Smooth concrete interface are indicated by the full line.

Based on the plots in Figure 6.26 to Figure 6.31, it can also be concluded that the values of δ_p/ϕ_p and δ_r/ϕ_r increase with the pile roughness, as found by Subba Rao et al. (2000). In fact, it has been shown in previous studies (e.g. Tsubakihara and Kishida, 1993; Tsubakihara et al., 1993) that the limiting value of δ_p/ϕ_p is 1.0, where the interface material is so rough that failure occurs within the soil rather than at the interface.

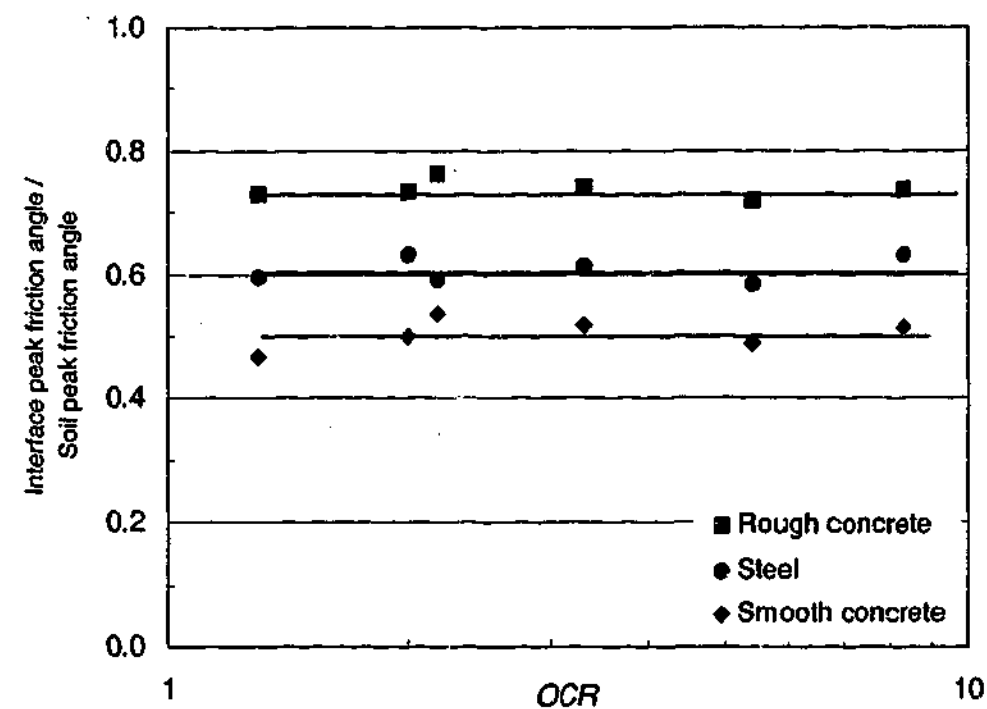


Figure 6.26 BallR: Ratios of interface peak friction angle to soil peak friction angle (δ_p/ϕ_p) for various OCRs

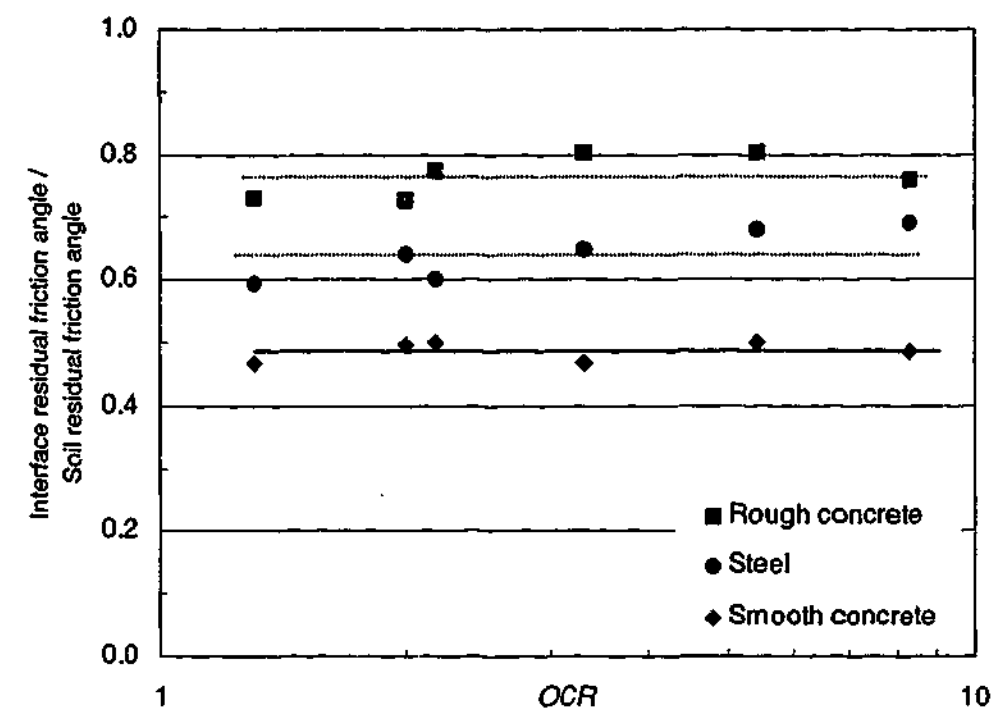


Figure 6.27 BallR: Ratios of interface residual friction angle to soil residual friction angle (δ_r/ϕ_r) for various OCRs

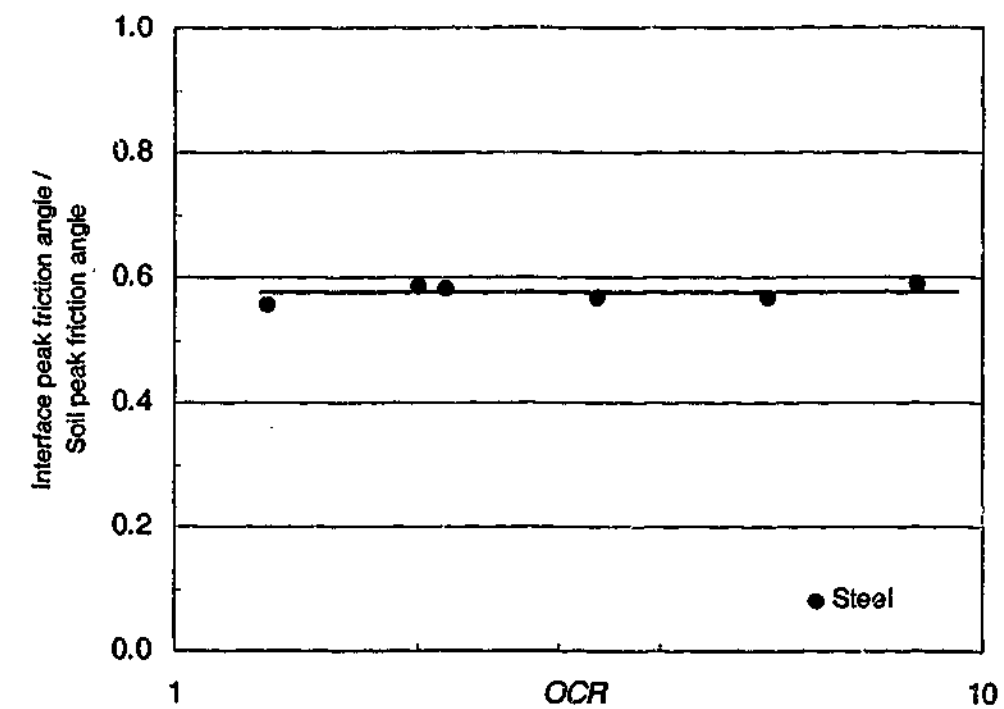


Figure 6.28 BallR/Talc: Ratio of interface peak friction angle to soil peak friction angle (δ_p/ϕ_p) for various OCRs

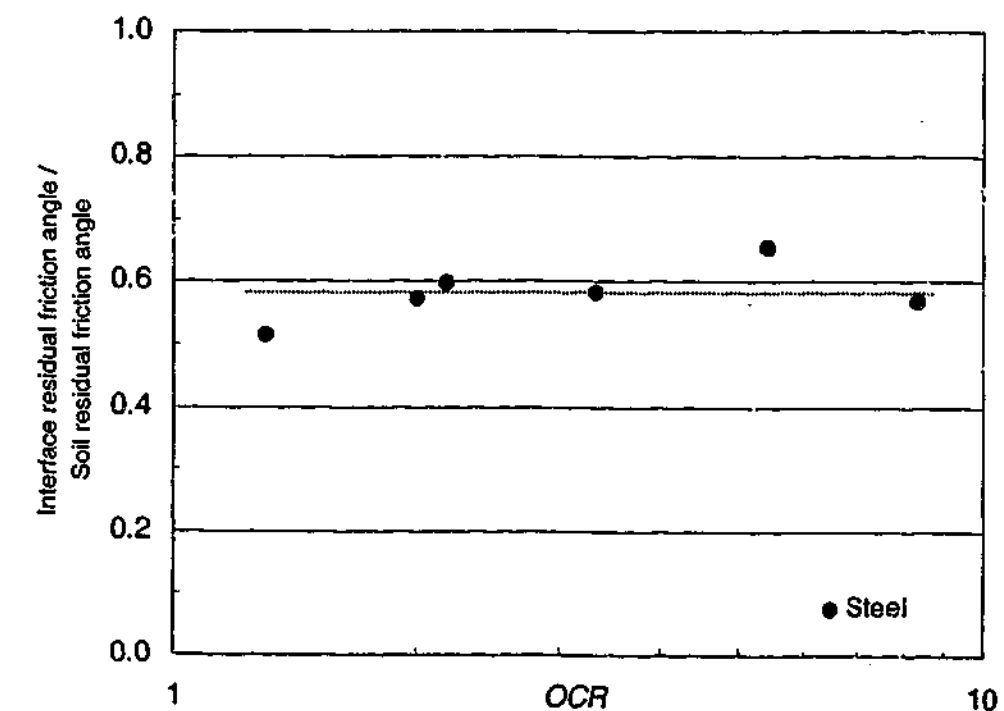


Figure 6.29 BallR/Talc: Ratio of interface residual friction angle to soil residual friction angle (δ_r/ϕ_r) for various OCRs

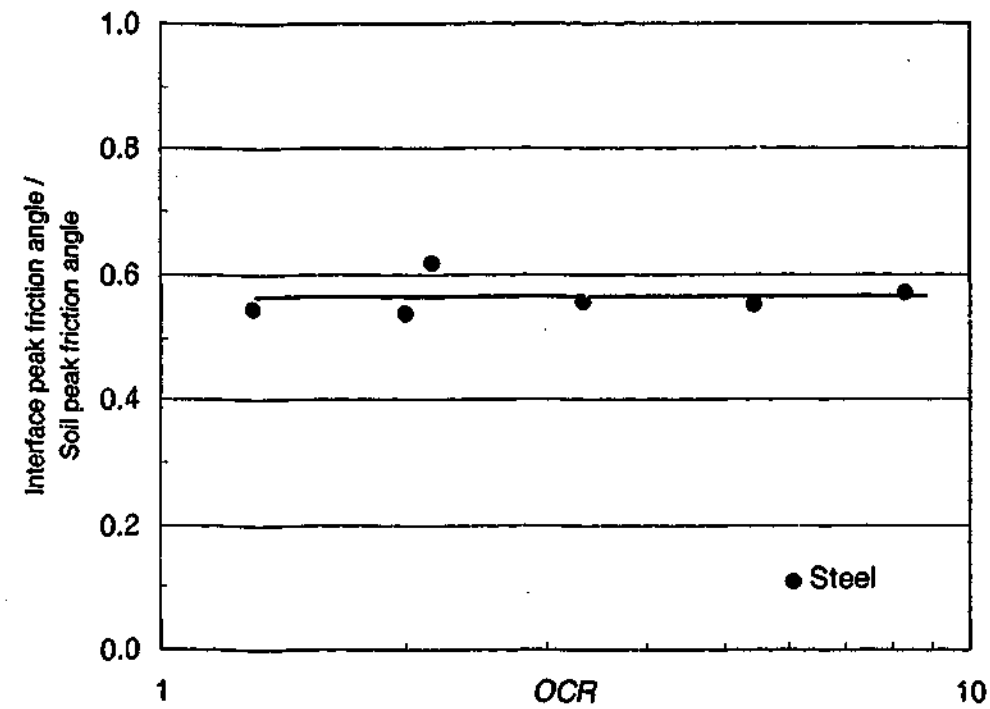


Figure 6.30 HR1F: Ratio of interface peak friction angle to soil peak friction angle (δ_p/ϕ_p) for various OCRs

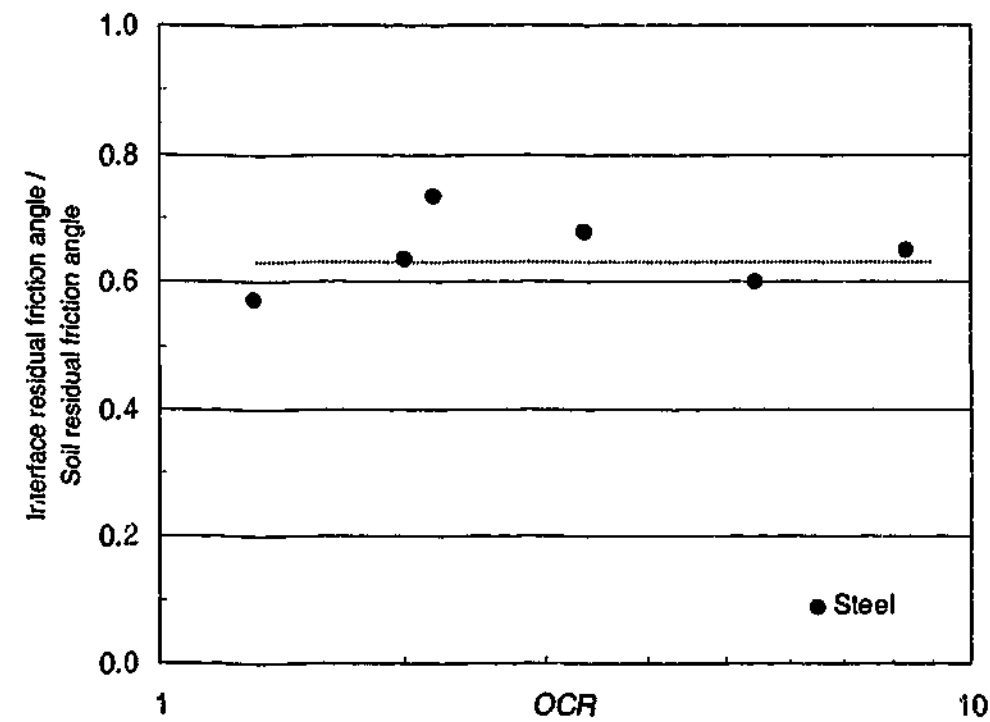


Figure 6.31 HR1F: Ratio of interface residual friction angle to soil residual friction angle (δ_r/ϕ_r) for various OCRs

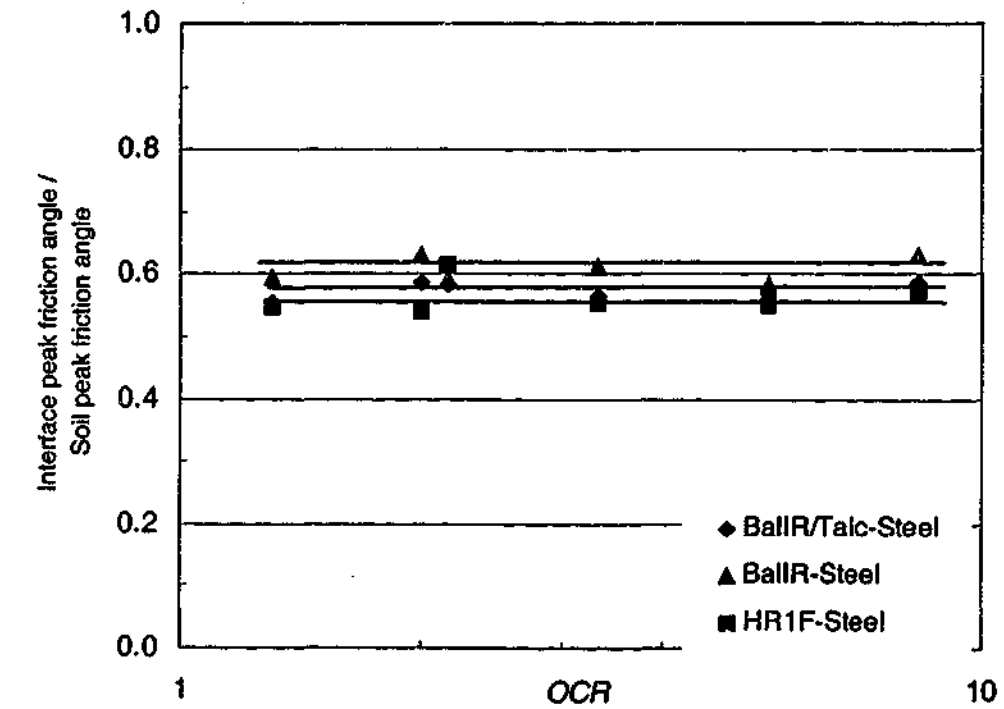


Figure 6.32 BallR, BallR/Talc and HR1F-Steel Interface: Ratios of interface peak friction angle to soil peak friction angle (δ_p/ϕ_p) for various OCRs

To the best of the author's knowledge, only data based on drained tests from Subba Rao et al. (2000) are available in the literature for comparison with the data from this study. As has been discussed, the roughness parameter by definition should not be dependent on the drainage conditions so that direct comparison between the data obtained from this study and the data from Subba Rao et al. is justifiable. The data from the various clays sheared against steel interfaces have been plotted collectively and compared to the data from Subba Rao et al. in Figure 6.33. It can be noted that, for the three types of clays tested against the same interface in this study, the value of δ_p/ϕ_p is remarkably constant, indicating that the plasticity of the clay has little influence on the values of δ_p/ϕ_p . It is noted that the data from Subba Rao et al. are based on 2 clays (with OCRs of 1, 5 and 10) tested against a rough mild steel and a stainless steel, where the upper limit and the lower limit of their data are indicated. It must be noted that the values of the ratio from the different studies are dependent on both the interface roughness and the type of clay. Since different types of clay were tested in the various studies, the comparison cannot take into the account the influence of the type or nature of the clay on the value of the ratio.

It can be observed that the plotted data from this study, which are based on a smooth structural steel, fall within the upper and lower limits. Since the value of the ratio

increases with the roughness of the interface, it would appear that the smooth structural steel is smoother than the rough mild steel but rougher than the stainless steel.

The values of δ_p/ϕ_p obtained from this study for the interface involving the concrete interface are compared to data obtained Subba Rao et al. (2000) in Figure 6.34. The data from Subba Rao et al. were based on two clays (with OCRs of 1, 5 and 10) tested on a smoother cement mortar and a rougher cement mortar. The data from Subba Rao et al. involving smooth and rough concrete show that the ratio increases with the surface roughness, as found in the current study. Thus, the importance of surface roughness is therefore further demonstrated. It is noted that the values for cement mortar from Subba Rao et al. are higher than the values for concrete determined in this study (between 1.0 and slightly lower) where the value of 1.0 indicates that the interface strength was higher than that of the soil so that shearing occurred within the soil rather than at the interface. The higher values of δ_p/ϕ_p from Subba Rao et al. would indicate that the cement mortar was rougher than both the rough concrete and smooth concrete used in this study.

In conclusion, the analyses based on the roughness parameter have further demonstrated that the data obtained in this study are consistent with the findings from previous research.

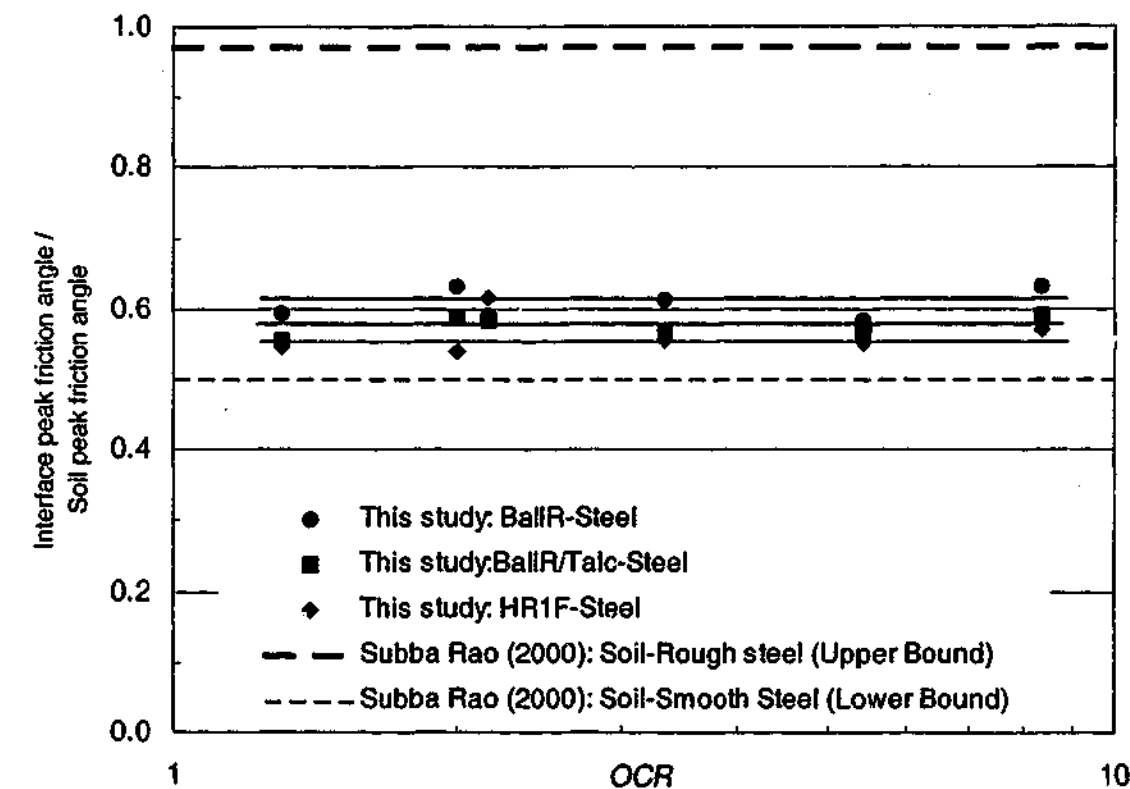


Figure 6.33 Comparison of ratios of peak *steel* interface friction angle to soil peak friction angle (δ_p/ϕ_p): Data from this study vs. data from Subba Rao et al. (2000)

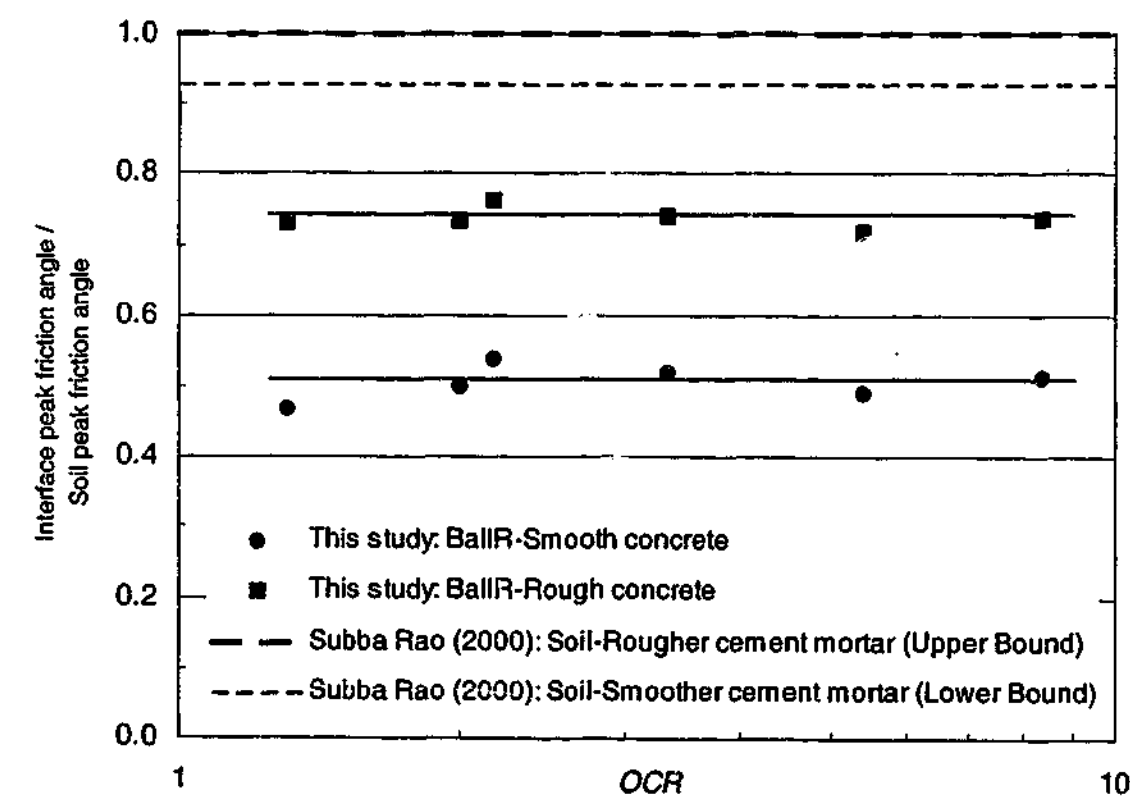


Figure 6.34 Comparison of ratios of peak *concrete* interface friction angle to soil peak friction angle (δ_p/ϕ_p): Data from this study vs. data from Subba Rao et al. (2000)

6.9 Summary

This chapter has described the laboratory soil and pile specimens used for performing quasi-static tests. The test procedures for performing these tests and the test programme have been discussed. The results of the tests have also been presented and discussed.

It has been demonstrated that the soil and interface strength behaviour is credible and consistent with expectation and the findings from previous research. More specifically, it has been shown that the soil and interface peak strengths increase with increasing *OCR*; that the strength behaviour is closer to the undrained behaviour; the residual strength (soil and interface) to peak strength (soil and interface) is equal to 1.0 for normally consolidated samples; that the value of the roughness parameter (δ/ϕ) is constant regardless of the *OCR* of the soil. These analyses have therefore verified that the data obtained based on the quasi-static tests performed in this study are credible, so that the soil strength values obtained in these tests can be used for correlation with the damping factor and so that the interface residual strength values obtained from these tests can be used as valid reference points for the dynamic interface (large-displacement or residual) strength values.

Chapter 7

7. Dynamic Pile-Clay Interface Behaviour: Test Procedures, Results & Analysis (Part I)

7.1 General

Based on the test programme outlined in the previous chapter for the quasi-static tests, dynamic tests on the pile-clay interfaces were performed for the following reasons:

- To investigate the effect of shear rate on the pile-clay interface resistance
- To establish the strength ratio-velocity relationship for the dynamic response of the pile-clay interface
- To investigate the effects of certain soil properties and pile characteristics on the dynamic response of pile-clay interfaces.

In this chapter, the test procedures associated with conducting the dynamic tests will be described, and the post-test observations of the interface and the results of the dynamic tests will be reported and discussed. This chapter and the following chapter (Chapter 8) are complimentary chapters that discuss the analyses of the test data obtained from the dynamic tests. This chapter discusses the first part (Part I) of the analyses – the dynamic response of the pile-clay interface. Chapter 8 discusses the second part (Part II) of the analyses – the effects of certain soil parameters and pile characteristics on the dynamic response.

In this chapter, it will be shown, based on post-test observations, that the pile-clay interfaces subjected to dynamic shearing are markedly different from those subjected to quasi-static shearing. This difference implies that the quasi-static friction measured in the quasi-static tests (presented in the previous chapter) is different from the quasi-static friction applicable to the dynamic tests, and thus cannot be used for normalising the dynamic friction. Therefore, a procedure for obtaining the appropriate quasi-static interface friction is developed and this friction value determined. Using this friction value, the dynamic friction is normalised. The normalised dynamic friction or the strength ratio is then analysed for dynamic effects. The dynamic responses of the interface are modelled, and their functional form is compared to that reported in previous research.

7.2 Test Programme

The types and properties of the clay specimens, and the piles and their surface characteristics that were tested in the dynamic tests have been described in Section 6.2. Based on the test programme outlined in Section 6.2 for the quasi-static tests, dynamic tests were performed on the equivalent pile-clay interfaces and at the equivalent normal stresses. Additional tests were performed on the wetted surfaces of the three piles in order to investigate the influence of the presence of lubricant at the pile surfaces and to gain insight into the mechanism causing viscous behaviour.

7.3 Test Procedure

The process of fabricating the clay specimens has been explained in Section 6.3.1.

7.3.1 Dynamic interface tests

The dynamic tests were performed in the “dynamic configuration” of the shear apparatus at transient velocities up to 1.6m/s. The test commenced with the pile being pushed by the ram over the maximum stroke of 100mm. After the first test, two more tests were performed on the interface under the same normal stress in order to investigate the effects of repetitive shearing (such as soil remoulding) on the interface strength behaviour. In order to perform the subsequent test on the same sample, the ram was reversed to its original starting position at a slow rate of approximately 50mm/s (which was not adjustable) while maintaining the normal stress on the sample.

The repetitive testing of the interface simulated the repetitive driving in the field which causes remoulding of the clay at the interface. The reversal of the pile to the original starting position (which was a practical necessity in performing the tests) could be justified as simulating pile rebound, although it must be stated that pile rebound is partial rather than complete. The reversal in the direction of shearing (in either the test or the field) could be significant in reversing the orientation of the clay fabric on the shear surface of the clay.

It is noted that when the pile was moved in the opposite direction of shearing, residual stresses might be locked in at the interface, as will be discussed in more detail in Section 7.7.1.

The following were recorded during a dynamic test: the normal stress on the sample, the dynamic force imparted to the carriage by the ram, the acceleration of the carriage and the pile, the pile displacement and the vertical movement of the sample. The pile velocity and the dynamic interface friction were derived from some of these measurements, as will be explained in more detail in Section 7.4.

The discussion on the loss of sample and the limitation of the direct shear test for the quasi-static shear tests in Section 6.3.3 also apply here. However, because the dynamic tests involved larger displacements of between 50 to 60mm, the sample loss was more significant as tabulated in Table 7.1. The amount of sample lost could be quantified as the mass of the lost sample as a percentage of the mass of the total sample. For a dynamic test involving a shear displacement of between 70 and 80mm, the typical percentages are tabulated in Table 7.1. The percentages show that the amounts of sample loss were insignificant. Also, the area associated with the ends of the shear box where the sample loss occurred was relatively small compared to the total area of the sample. Hence the sample loss was not expected to cause a significant percentage of error.

Table 7.1 Mass of the lost sample as a percentage of the mass of the total sample

Pile-Clay Interface	Percentage loss of sample (%)
Smooth pile-Clay	0.5
Rough pile-Clay	0.7

7.3.2 Post-test observation of shear surfaces

The physical characteristics of the shear surface at the pile-soil interface can give significant insights into the shear behaviour of the interface. As such, these characteristics have been studied by many researchers in an attempt to gain insight into the shear mechanism and shear failure mode (e.g. Coop and Wroth, 1989; Bond and Jardine, 1991; Tika-Vassilikos, 1991; Tika et al., 1996).

Given the significance of these physical characteristics, the clay sample was separated from the pile after each series of dynamic tests in order to observe the shear failure mode, the location of the shear failure plane, the shear surface and the fabric of the clay, and the surface condition of the pile (i.e. whether it was clean or covered with clay).

7.4 A Sample Dynamic Record

A sample test record from a typical dynamic pile-clay interface is presented in Figure 7.1. This record is presented in the same format as that for the pile-sand interface test where Graphs A, B and C relate to the data obtained during the event,

whilst Graphs D, E and F show derived analyses of the data. The various analysed quantities, except for the quasi-static interface frictional force (labelled F_{static}), were obtained using the same methods as those described for the pile-sand test records. The contents of each of the graphs are discussed here.

Graph A shows:

- the dynamic force measured by the dynamic load cell located between the ram and the carriage (labelled F_{ram})
- the inertial force of the carriage and the pile section (labelled $F_{inertial}$)
- the normal force at the interface (labelled F_{normal}).

As explained in Section 5.6.2.1, the stiff response from the vertical movement of the sand sample caused fluctuating inertial forces in the loading assembly (for applying normal stress), which in turn caused the applied normal stress to fluctuate. However, for the tests involving clay, the response from the vertical movement of the clay sample was less stiff as clay was a softer material. The response is shown in Graph A and it can be seen that F_{normal} fluctuates only slightly and remains reasonably constant throughout the event. Given that the applied normal load was not highly transient, it can be expected that the load cell (which is not a dynamic load cell) was able to measure the applied force adequately.

Graph B shows:

- the acceleration of the pile section (labelled Pile acceleration)
- the velocity of the pile section (labelled Pile velocity), which is obtained by integrating the acceleration.

Graph C shows:

- the displacement of the pile (labelled Pile displacement)
- the vertical displacement of the sample (labelled Vertical displacement).

The pile was typically displaced by the ram by up to 75mm.

As shown in Graph C, the measured vertical displacement fluctuates significantly throughout the event. As noted in Section 5.6.2, given that the LVDT used for the measurement of the vertical displacement had a relatively low resolution (due to its

relatively high effective stroke) and frequency response, the measured displacement and the fluctuation might not necessarily reflect the actual response. However, the measured values at the start and the end of the record can be expected to be reliable. Based on these values, the thickness of the sample reduced by less than 0.5mm during shearing; this small displacement is an insignificant 1% of the initial sample thickness of about 40mm. The reduction in the sample thickness was due to sample loss through the shear box-pile surface gap during shearing (the amount of which has been quantified in Section 7.3.1) and the subsequent consolidation of the sample. Thus the contractile response of the sample cannot be assumed to be due to the response of the sample to dynamic shearing.

Graph D shows:

- the dynamic interface frictional force (labelled F_d) which is computed by taking the difference between F_{ram} and $F_{inertial}$.
- the instantaneous quasi-static interface resistance (labelled F_s). The quasi-static tests yielded three sets of data (the three residual frictional resistance values corresponding the three applied normal force values) for one particular interface. The three data points, plotted in a quasi-static interface resistance vs. normal force plot, are fitted with an equation of best-fit, where the quasi-static interface resistance is expressed as a function of the applied normal force. Using this equation, the instantaneous quasi-static interface resistance during the dynamic event can be computed from the instantaneous applied normal force.

It can be noted in Graph D that F_s does not vary significantly during the event because of the relatively small fluctuations in the normal load. It can also be observed that there is some scatter in the dynamic interface resistance data at the start of the event. The scatter is likely to be due to:

- the lack of perfect synchronisation between the measured acceleration and the measured dynamic force (which was imparted to the carriage by the ram) because of the transient nature and the short duration of the shock loading
- the absolute error from the taking the difference between the two relatively large numbers.

Graph E shows

- the ratio of F_d to F_s (labelled F_d/F_s)
- the pile acceleration

Graph F shows:

- F_d/F_s
- the pile velocity

In Graphs E and F, the F_d/F_s curve is plotted against the pile acceleration and the velocity in order to determine if there is any systematic variation of the strength ratio value with either or both of these two parameters.

FILENAME BALLR.SC 250 INITIAL NORMAL STRESS 250 kPa
 PILE Smooth concrete
 CLAY BallR

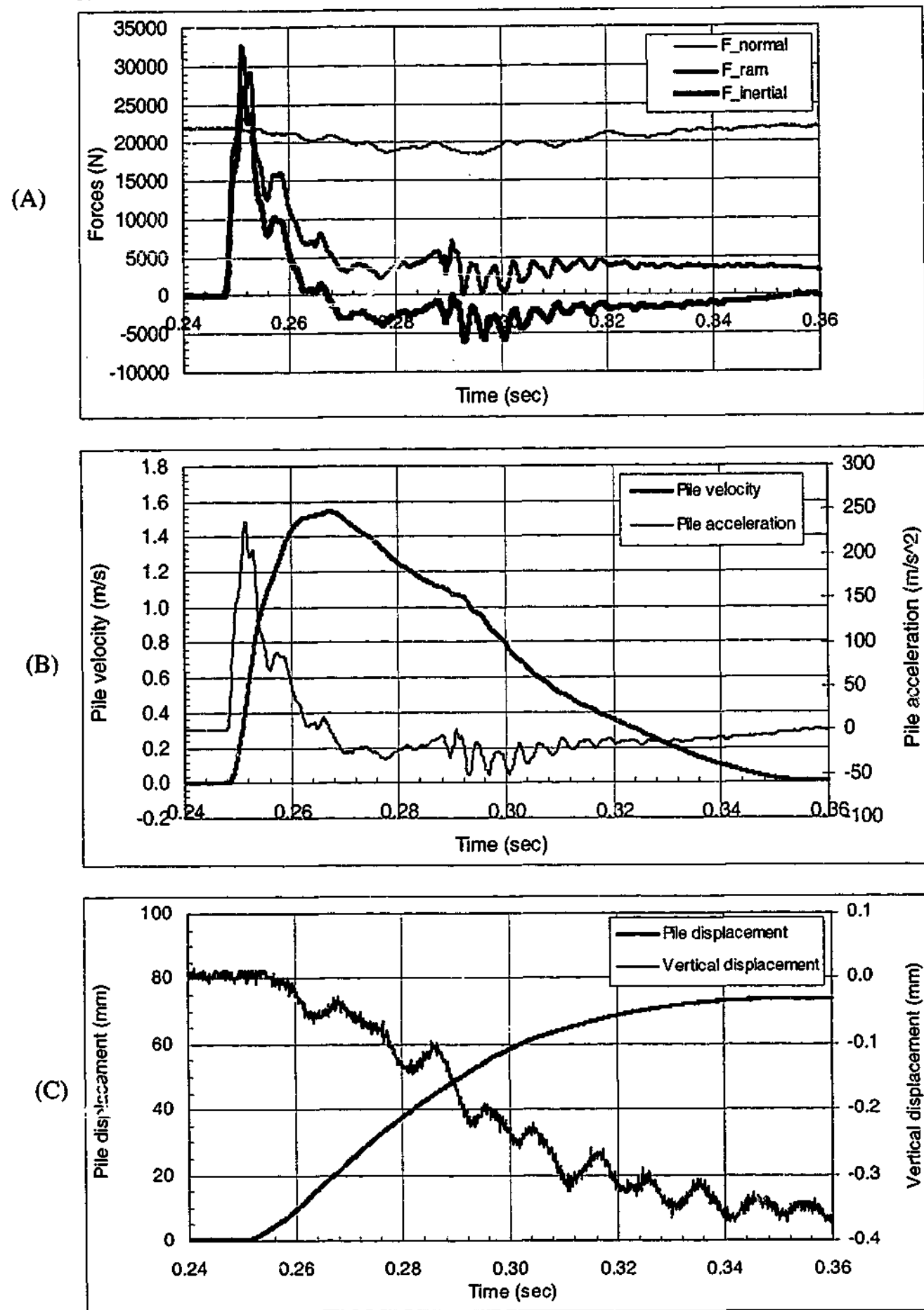


Figure 7.1 Sample record of a dynamic interface pile-clay test

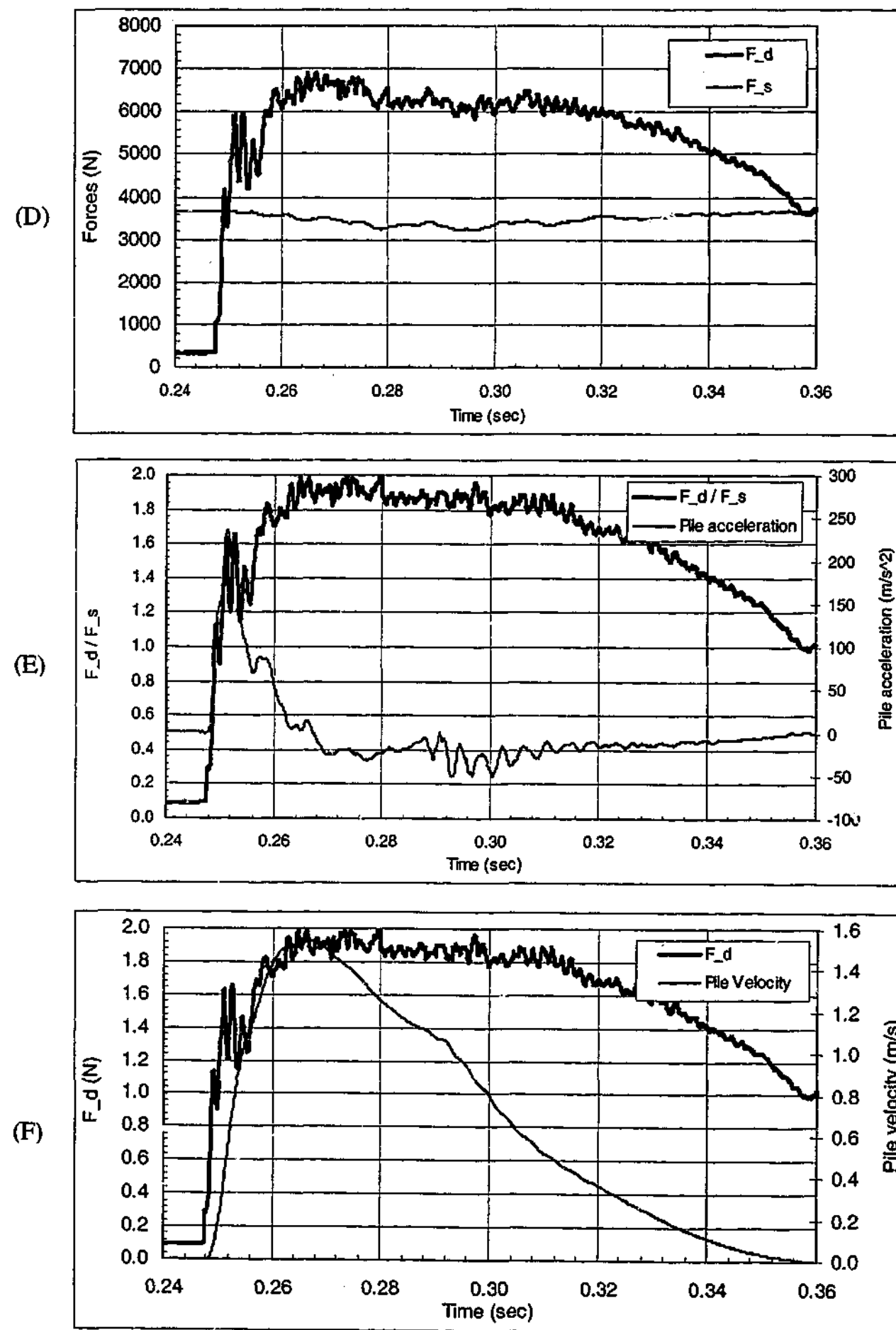


Figure 7.1(cont'd) Sample record of a dynamic interface pile-clay test

7.5 Interface Shear Failure: Observations & Discussions

Based on the post-test observations, the failure mode of the interface subjected to dynamic shearing was identified. Three modes of interface failure, which are designated as Modes 1, 2 and 3 shear failure, were identified and are discussed subsequently.

7.5.1 Mode 1 interface shear failure

The post-test observations of interfaces of low and medium plasticity clays (i.e. BallR and BallR/Talc) and smooth piles (i.e. smooth concrete and steel) are presented and discussed in this section. The interface shear failure for such interfaces has been designated Mode 1 interface shear.

When pried apart, the clay block and the pile surface separated at the interface boundary. There were fragmented pieces of clay that adhered lightly to the pile surface from shear surfaces on the specimen. The failure had clearly occurred at the interface. Tests with this type of shear plane have been designated Mode 1.

The shear surfaces subjected to dynamic tests involving BallR (medium plasticity) are shown for in Figure 7.2 and Figure 7.3, whilst those involving BallR/Talc (low plasticity) are shown in Figure 7.4, Figure 7.5 and Figure 7.6. Whilst the fabric of clay associated with quasi-static shearing for the equivalent interface was very smooth and the shear surface was homogenous with very light continuous striations oriented in the direction of shear (as has been reported in Section 6.4.1), the fabric of clay associated with fast shearing consisted of discontinuous residual shear surfaces located randomly throughout the clay surface (Figure 7.3 and Figure 7.5). These surfaces, which were also rough in appearance, were heavily destructured such that small patches of clay were left on the pile surface when the clay was separated from the pile (Figure 7.2 and Figure 7.4).

Areas between these shear surfaces were smoother in texture (but comparatively rougher than the surface subjected to quasi-static shearing). There were however slight differences in the fabric of the BallR and BallR/Talc clays. For BallR, the smoother surface had non-uniform striations, and was disrupted by very small shear surfaces (Figure 7.3). For BallR/Talc, striations were less visible (Figure 7.5), and

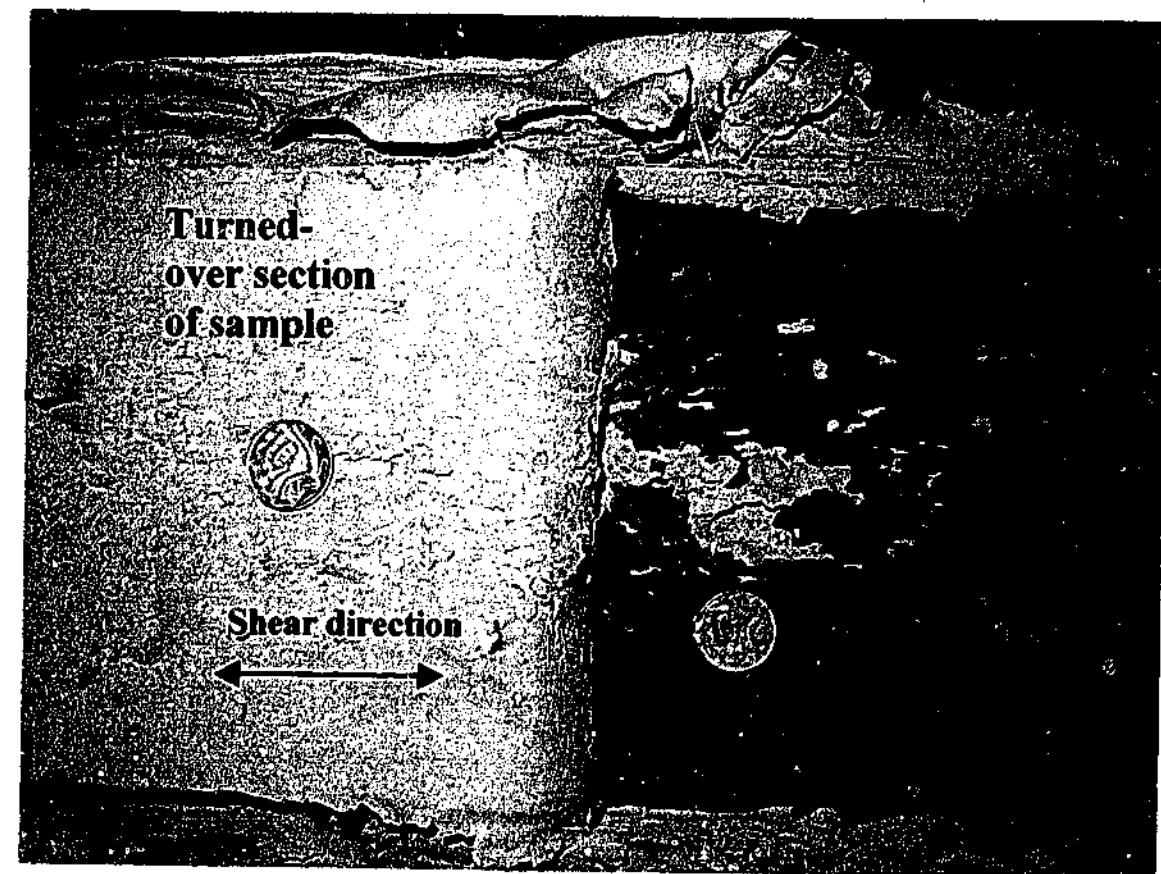


Figure 7.2 Mode 1: Steel pile and BallR clay fabric after BallR sample was separated from pile

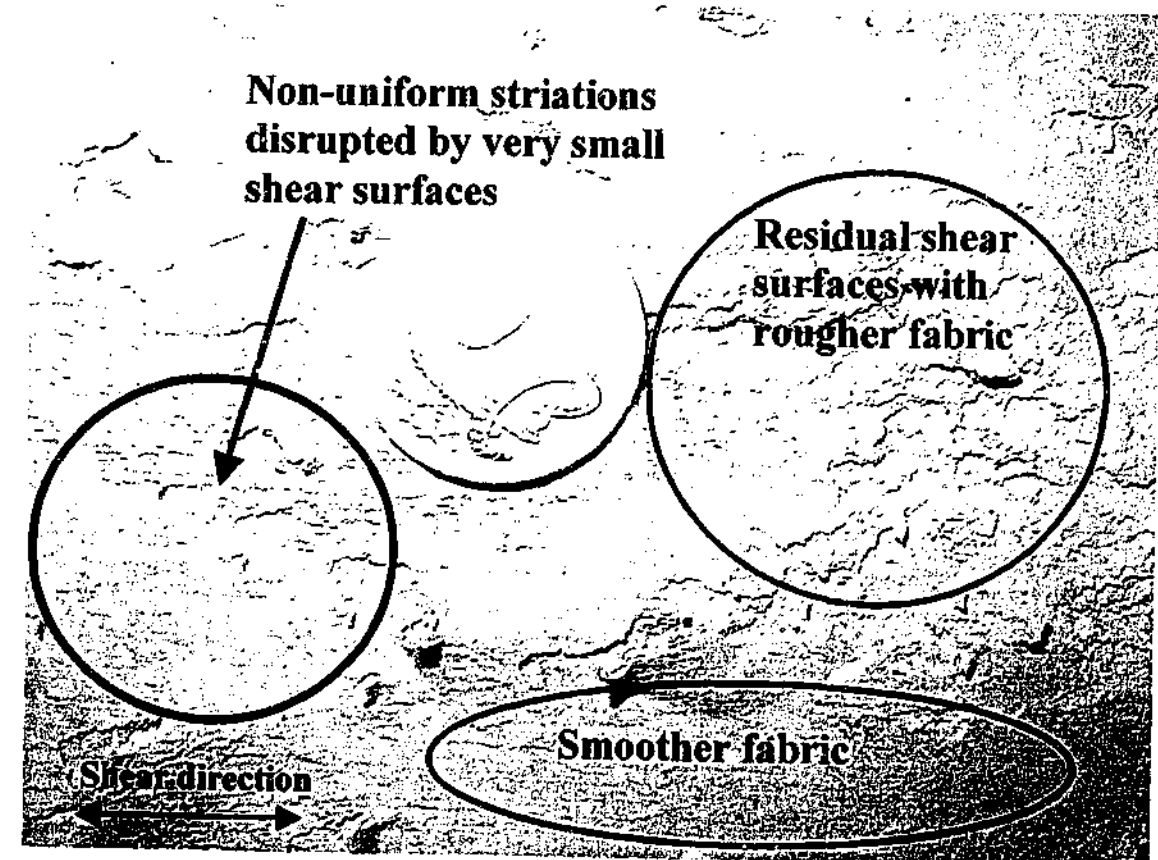


Figure 7.3 Mode 1: Close-up of BallR clay surface showing rough fabric, smooth fabric and striations; scale indicated by 23mm-diameter coin

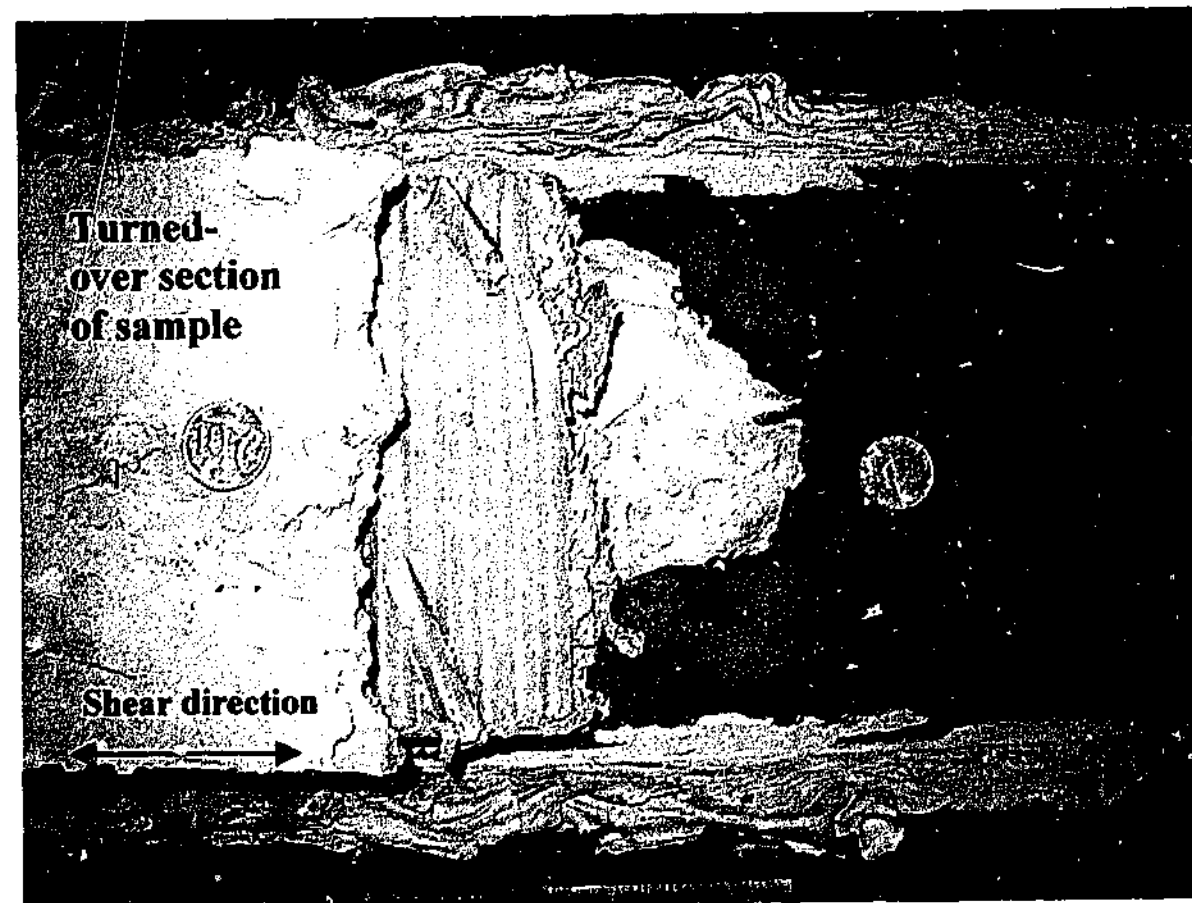


Figure 7.4 Mode 1: Steel pile and BallR/Talc clay fabric after the sample was separated from pile

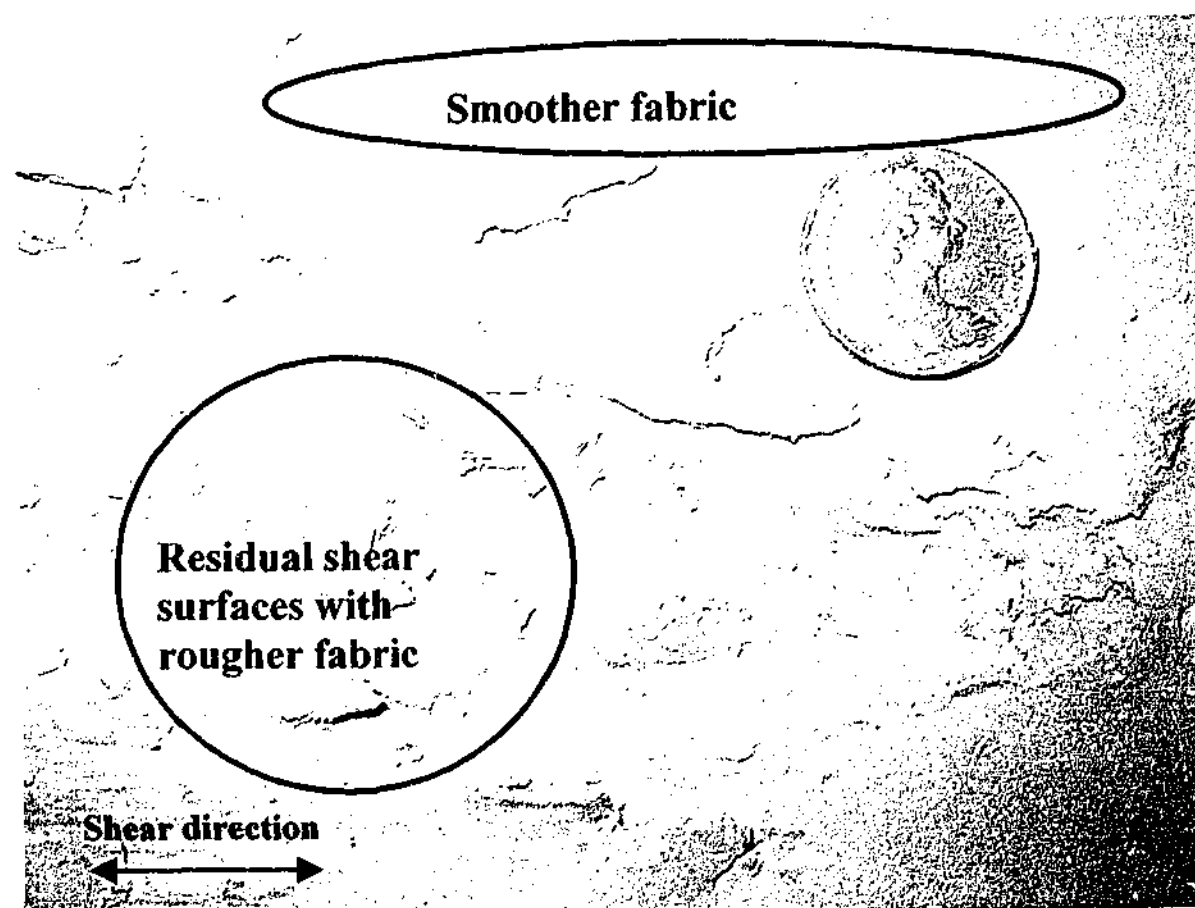


Figure 7.5 Mode 1: Close-up of BallR/Talc clay surface showing rough fabric and smooth fabric

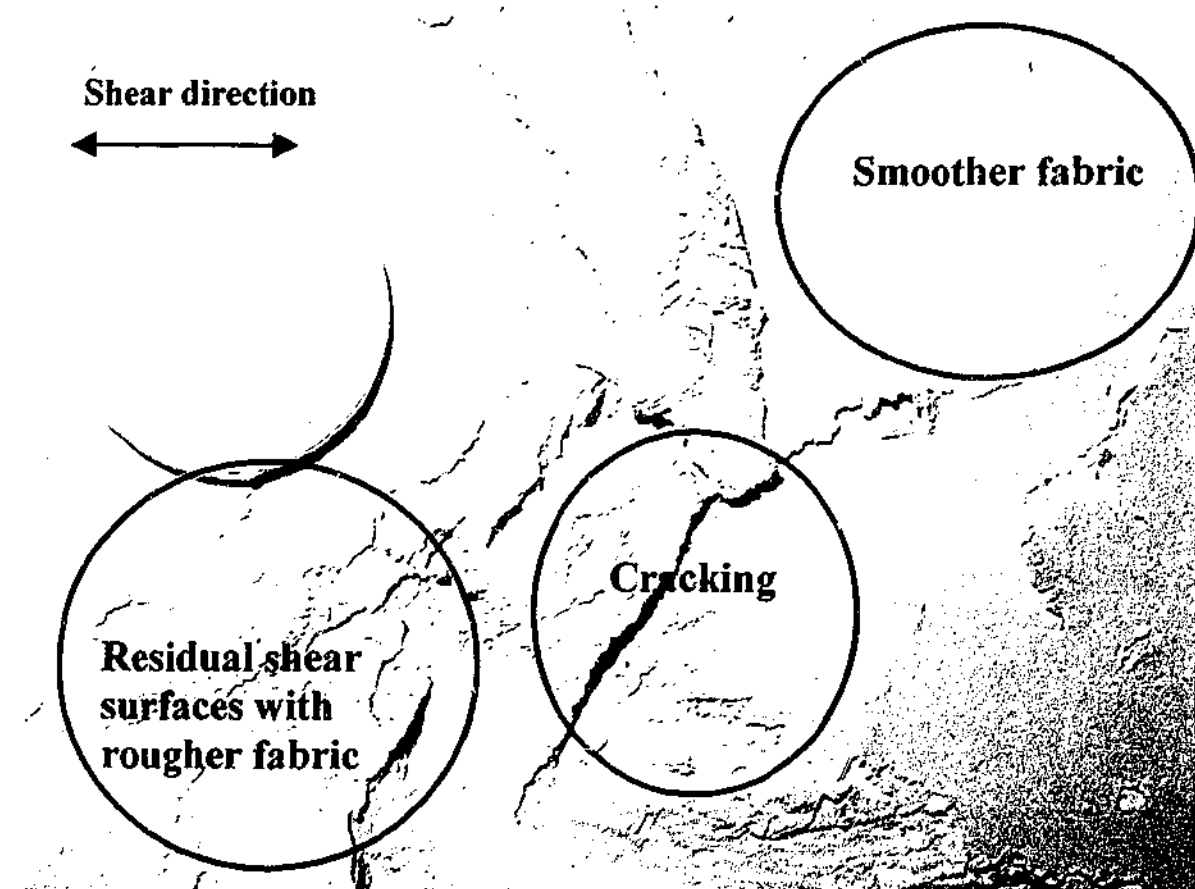


Figure 7.6 Mode 1: Close-up of BallR/Talc clay surface showing sections of rough and smooth fabric, and cracking due to low plasticity of the clay

cracking of the clay was observed because of the low plasticity of the clay (Figure 7.6).

For the rougher fabric and the smoother fabric of both clays, the shear zone was observed to be thicker than that involved in the quasi-shearing. Given that failure occurred at the interface and the clay fabric encountered in the interfaces involving BallR and BallR/Talc was essentially the same, the shear failure of both clays is considered to be Mode 1 interface shear failure.

The non-uniform striations, the small shear surfaces amongst the striations and the discontinuous shear surfaces (as opposed to a smooth and homogenous surface with very light and uniform striations) and the thicker shear zone indicate that the clay particles were disordered by the fast shearing. Bond and Jardine (1991), Tika-Vassilikos et al. (1992) and Tika et al. (1996), who also observed the rough appearance of the surface, the discontinuous shear surfaces and the thicker shear zone, also concluded that the clay particles were disordered by the fast shearing. The

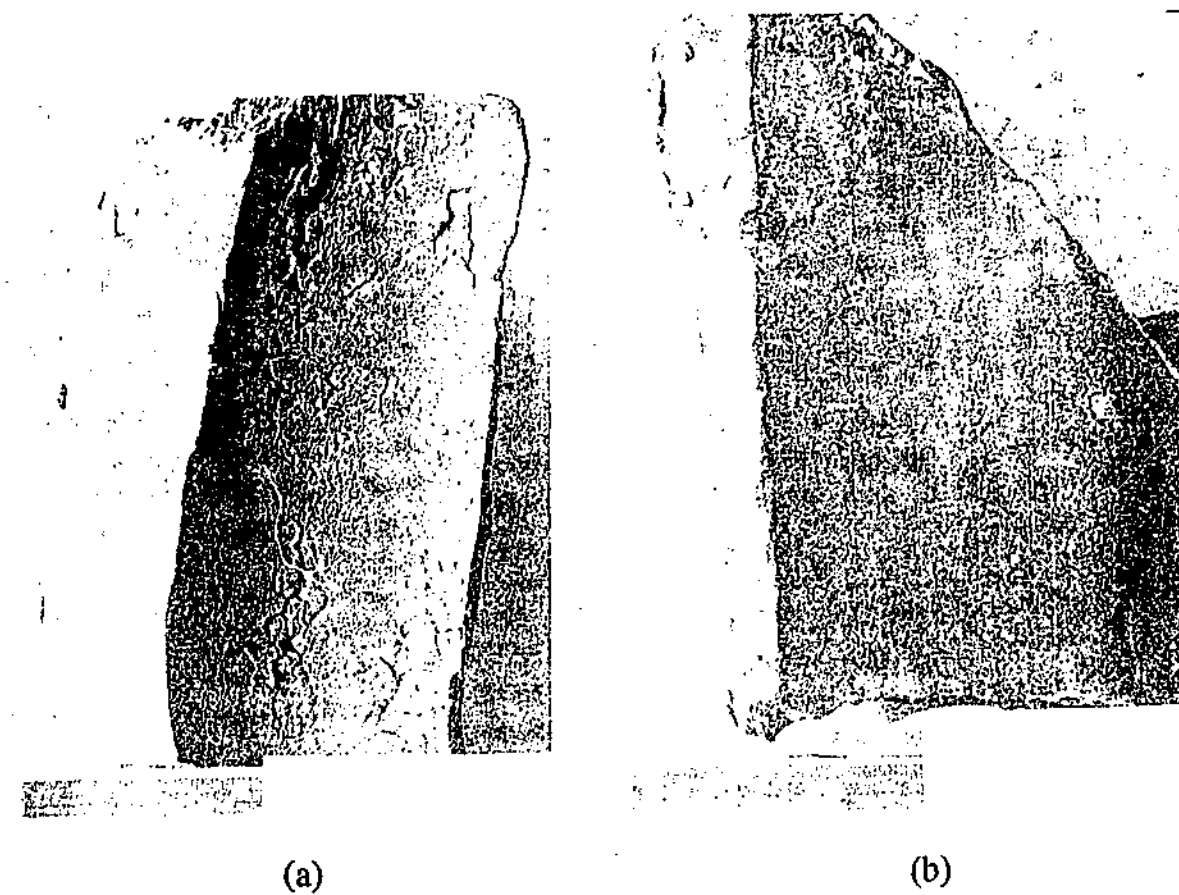


Figure 7.7 Clay fabric associated with (a) pile driving and (b) slow pile jacking as found by Bond and Jardine in field tests (Bond and Jardine, 1991)

photographs by Bond and Jardine (1991) showing the difference between the clay fabric associated with driving (or fast shearing) and that associated with slow jacking (or quasi-static shearing) have been reproduced in Figure 7.7.

7.5.2 Mode 2 interface shear failure

In this section, the post-test observations of interfaces of involving low and medium plasticity clays (i.e. BallR and BallR/Talc) and a rough pile (i.e. rough concrete) are presented and discussed.

The clay separated easily from the pile surface at the pile-soil interface boundary, indicating that shearing had occurred at the boundary of the interface. The clay surface was imprinted with the large asperities of the rough concrete and had deep striations created by the ploughing action of the asperities, as shown in Figure 7.8 and Figure 7.9. Unlike the Mode 1 interface shear failure, no discontinuous residual shear surfaces were present on the shear surface probably because any such surface would have been destroyed by the ploughing action of the asperities. Because of the

ploughing of the clay, the pile surface was smeared with the destructured clay, as shown in Figure 7.10. Tests with this type of shear plane have been designated Mode 2.

The characteristics of the shear surface associated with these dynamic tests were very different from those of the shear surface associated with the quasi-static test.

The shear surface subjected to slow shearing was imprinted with the large asperities but not ploughed by the asperities as the clay had sufficient time to conform to the asperities; thus the shear surface showed no sign of the deep striations observed for the shear surface subjected to fast shearing.

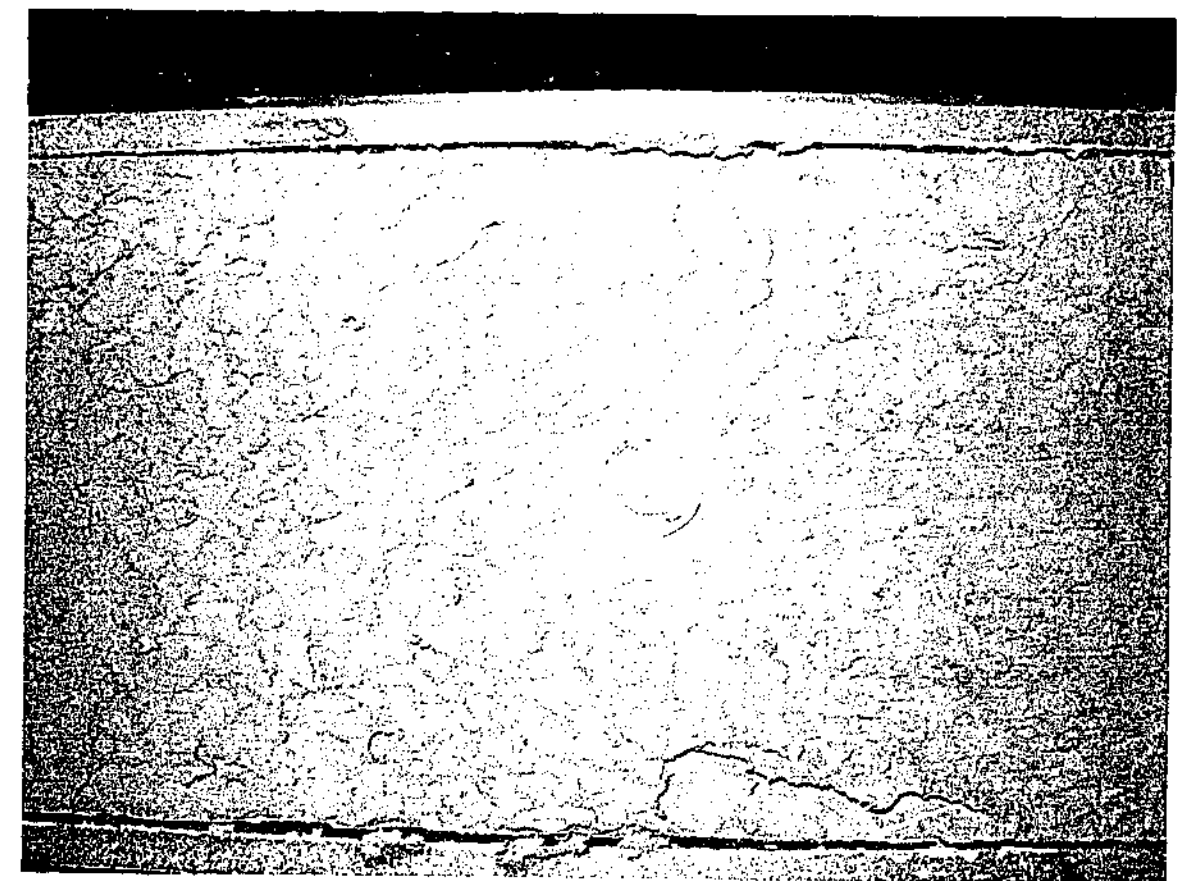


Figure 7.8 Mode 2: BallR clay fabric after tests

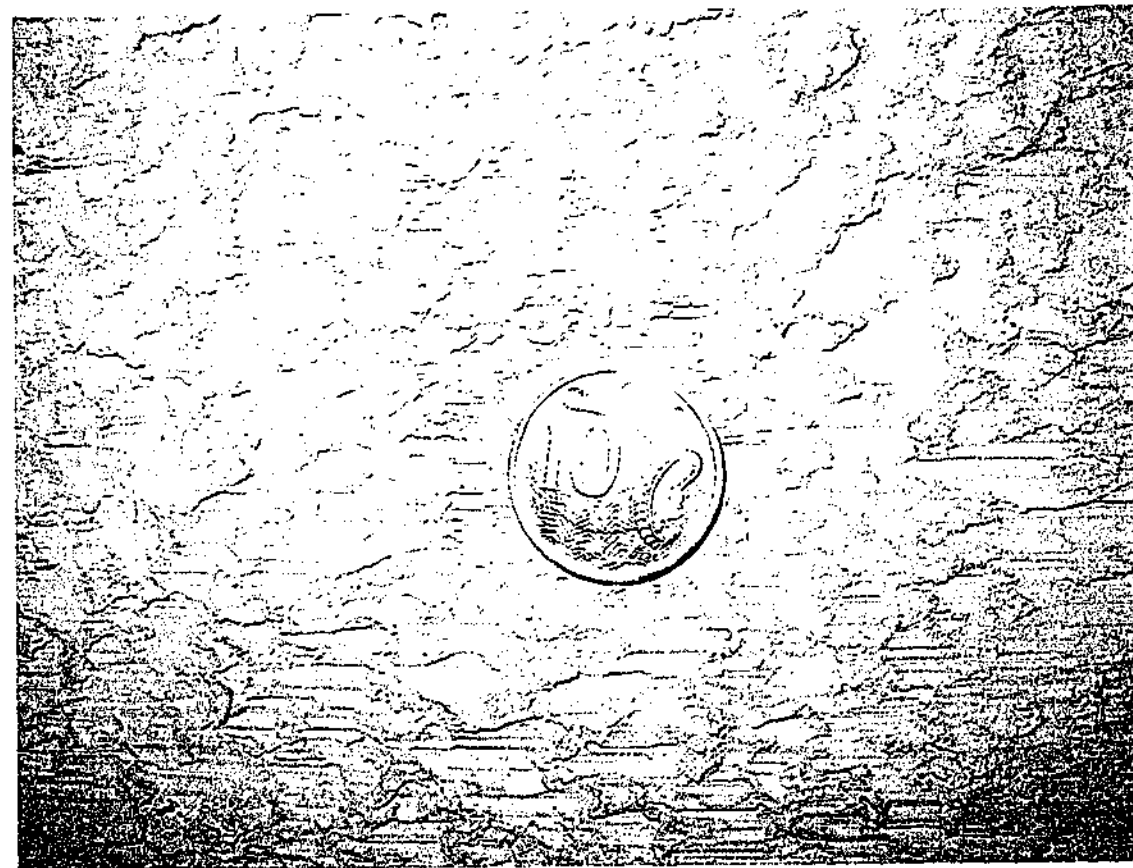


Figure 7.9 Mode 2: Close-up of BallR clay fabric

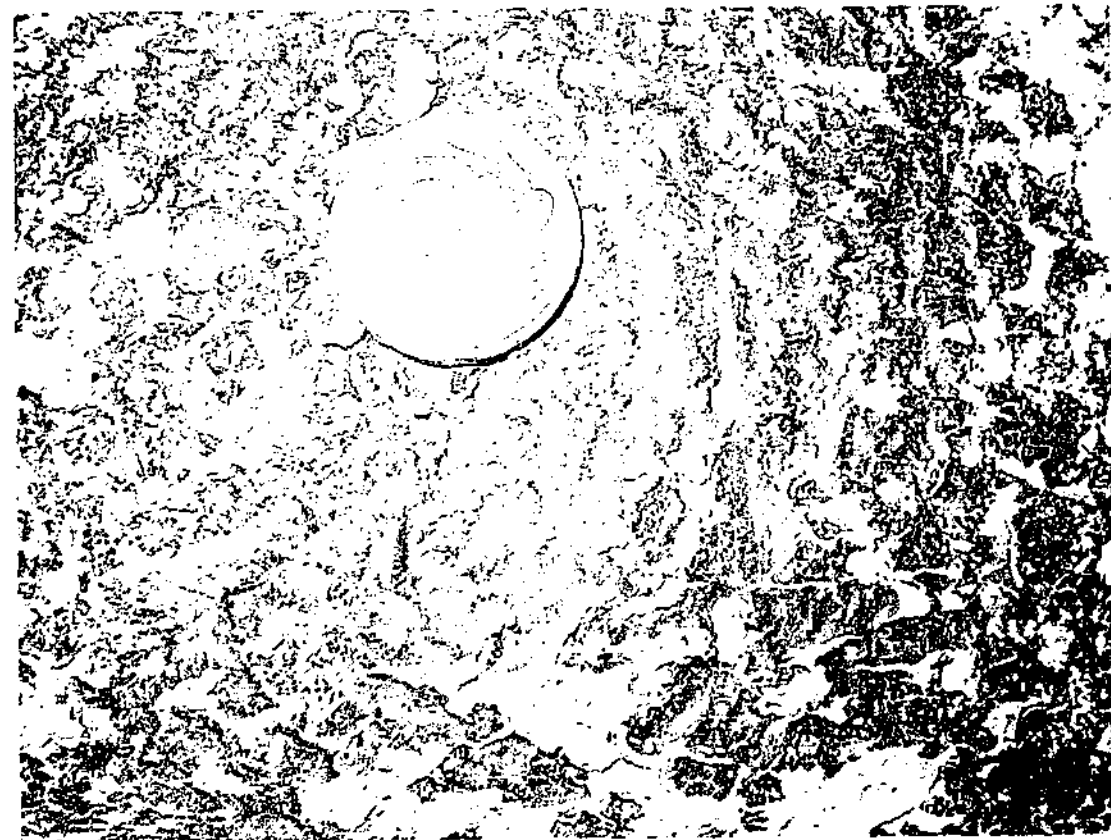


Figure 7.10 Mode 2: Smearied pile surface

7.5.3 Mode 3 interface shear failure

When the HR1F clay sample was pried away from the pile, the highly plastic HR1F clay was found to have adhered strongly to the pile surface. The sample at certain sections tore along a clay-clay plane leaving a thick layer of clay approximately 5mm on the pile surface, and the sample at other sections separated intact from the pile surface, leaving a very thin layer of clay on the pile surface. This is shown in Figure 7.11.

In this instance, it was more difficult to identify where the shearing plane occurred in the tests. It was certain that the actual shear plane during the test did not occur between the intact clay and the thick clay layer observed when separating the sample from the pile because there was no sign of shearing having occurred at the two surfaces. In the discussion of the results of the quasi-static test of the equivalent interface in Section 6.4.3, it was discussed how shearing was likely to have involved sliding of the clay specimen on the pile surface, and also within the specimen itself which was manifested in some clay adhering to the pile surface. It was likely that the same mixed mechanism occurred in at least the first few cycles of dynamic loading on the one sample.

However, as the amount of clay on the surface increased, it was likely to occur by sliding of the intact clay block on the layer of clay that adhered to the pile surface and within the specimen itself.

At the section where the clay separated intact from the clay-covered pile surface, the shear surfaces of the specimen and the layer of clay were observed to be much rougher than the shear surface of the specimen tested in the quasi-static test, as shown in Figure 7.12. The dynamic tests with this type of shear plane have been designated Mode 3.

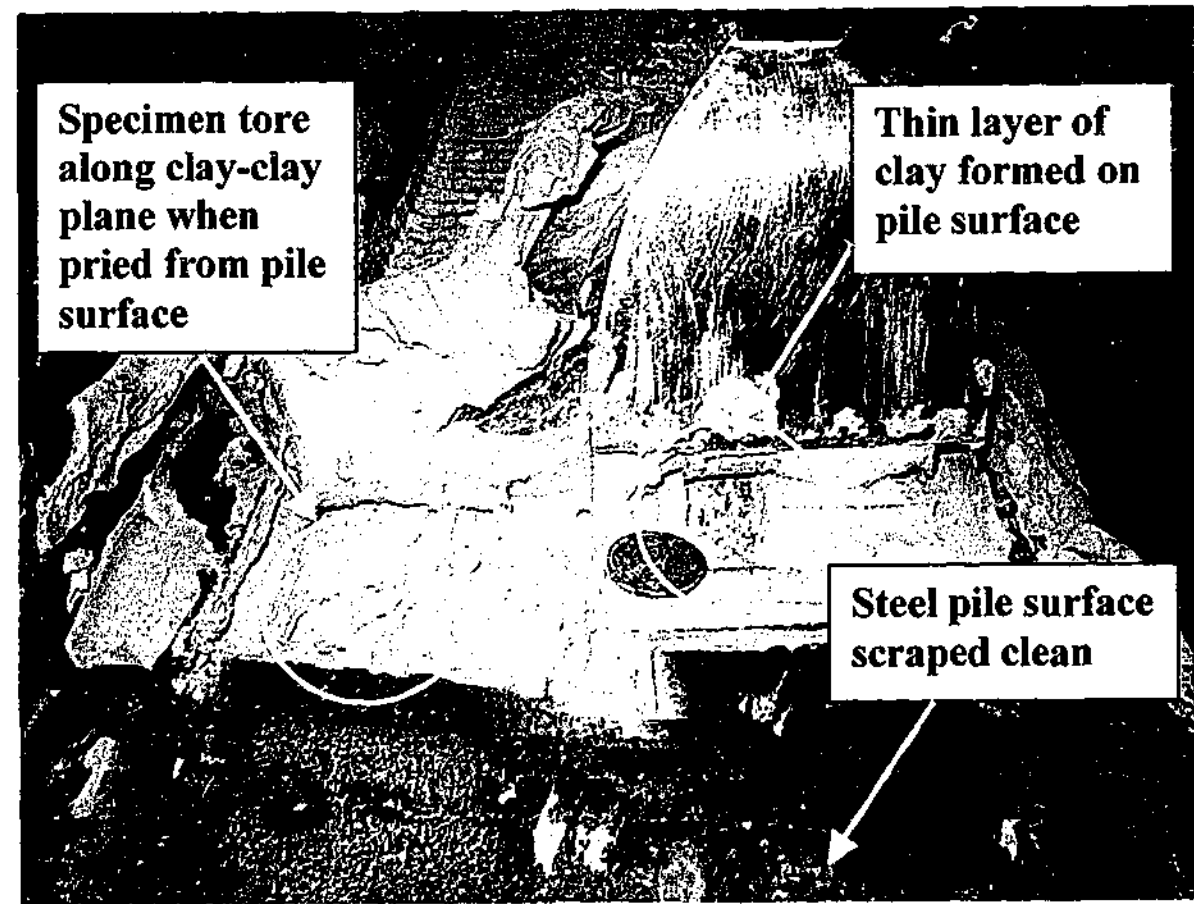


Figure 7.11 Mode 3: HR1F clay adhering to pile surface, and the thin layer formed on pile

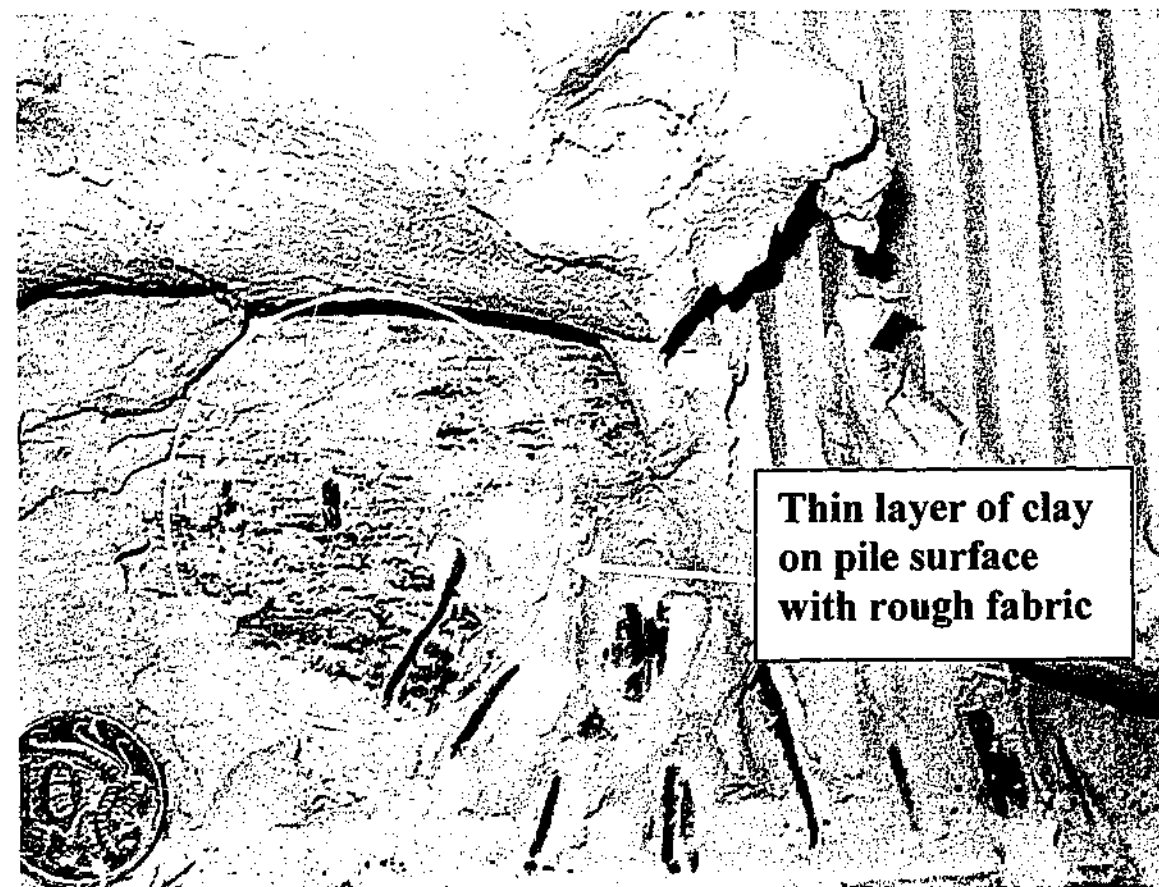


Figure 7.12 Mode 3: The thin layer of HR1F formed on the pile

7.5.4 Dynamic failure modes

Based on the dynamic tests conducted in the experimental programme, essentially three modes of shear failure occurred. Mode 1 occurred when the interface involved a smooth pile surface and a low or medium plasticity clay. Mode 2 occurred when the interface involved a rough pile surface and medium plasticity clay. Mode 3 shear occurred when the interface involved a smooth surface and high plasticity clay. It is possible that for a clay with plasticity intermediate between the “medium” ($I_p=20\%$) and the “high” ($I_p=37\%$) sheared against a smooth pile, mixed mode of Modes 1 and 3 would result.

Due to the time constraints in the project, the high and low plasticity clays were not tested on the rough surface. Tests involving high and low plasticity clays were performed against only the smooth pile surface in order to investigate the effect of clay plasticity on the smooth pile for comparison with the tests performed on the low and medium plasticity clays on the smooth pile. However, it is intuitive that a high plasticity clay sheared against the rough concrete will result in a layer of clay being formed on the rough pile surface and thus result in Mode 3 failure, and a low plasticity clay sheared against a rough concrete will similarly result in ploughing of the clay surface and hence smearing of the pile, and thus result in Mode 2 failure.

The dependence of the mode of failure on the pile roughness and the plasticity of the clay is summarised in Figure 7.13, where dotted lines indicate the hypothesised and likely effect of the pile roughness and the clay plasticity on the failure mode.

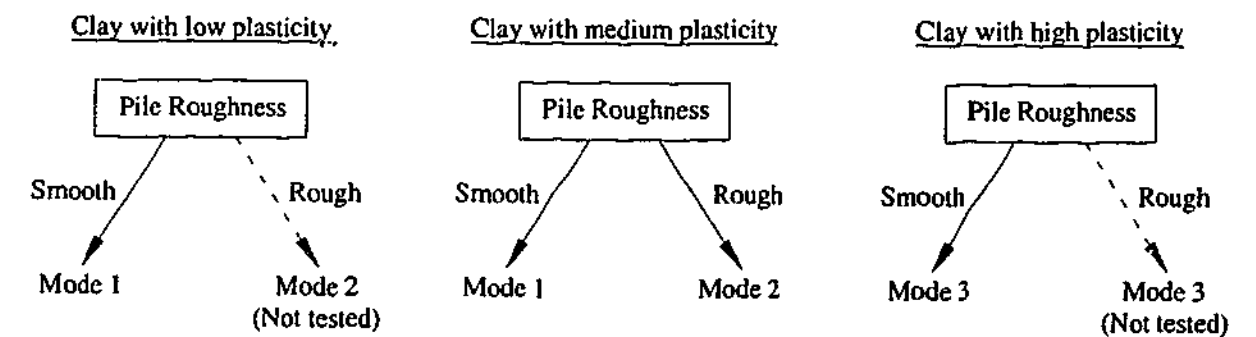


Figure 7.13 The dependence of failure mode of an interface on the pile roughness and the plasticity of the clay

7.5.5 Comparison with static failure modes

Based on the post-test observations of the shear surfaces, it has been established that the shear mode and the physical characteristics of an interface subjected to the dynamic test were different from those of the equivalent interface subjected to the quasi-static test. The different shear modes and physical characteristics of the interface for these two types of tests are compared in Table 7.2.

It is evident that the different characteristics of the interface subjected to the dynamic and quasi-static tests must be due to the different features of the quasi-static test and the dynamic test. The features of the two types of tests can be summarised in Table 7.3.

For all the interfaces subjected to dynamic shearing, the clay surface showed signs of destructuring or remoulding. For the equivalent interfaces tested in the quasi-static tests, no sign of remoulding could be observed. The remoulding in the samples subjected to dynamic shearing would appear to have been caused by the high shearing displacement and repetitive shearing of the interface associated with the dynamic test. These two features of the dynamic test also occur in pile-driving where the phenomenon of remoulding is well-known (e.g. Fleming et al., 1992) and is well-reported (e.g. Roy et al., 1981; Hunt et al., 2002). For interfaces involving Mode 3 failure where the pile surface was covered with a layer of clay, the zone of remoulding in the clay specimen is likely to have been less extensive as compared to that for interfaces involving Modes 1 and 2.

It is also evident that for all interfaces subjected to dynamic shearing, excess pore pressures induced by the shearing process must have occurred in the shear zone of the clay. Whilst excess pore pressures would also have developed in the samples tested in the quasi-static tests (as the tests were not fully drained tests), the pressures generated in the dynamic tests would have been greater. They would have been caused by the high shearing displacement and repetitive shearing of the interface associated with the dynamic test.

Table 7.2 Comparison of dynamic & static shear failure modes

Interface	Description of dynamic shear surface		Description of quasi-static shear surface
BallR-Steel BallR-Smooth concrete BallR/Talc- Steel	Failure mode 1	<ul style="list-style-type: none"> • Shearing occurred between the pile surface and the clay specimen • Clay fabric was inhomogenous: <ol style="list-style-type: none"> 1. Some sections with discontinuous residual shear surfaces with rough appearance 2. Some sections with striations disrupted by very small shear surfaces 3. Some sections were smooth in appearance 	<ul style="list-style-type: none"> • Shearing occurred between the pile surface and the clay specimen • Clay fabric was homogenous - smooth and polished in appearance, with minute striations orientated in the direction of shear and without sign of remoulding
BallR-Rough concrete	Failure mode 2	<ul style="list-style-type: none"> • Shearing occurred between the smeared rough pile and the clay specimen • Clay shear surface was imprinted by the large asperities and had deep striations created by the ploughing action of the asperities 	<ul style="list-style-type: none"> • Shearing failure occurred between the pile surface and the clay specimen • Clay shear surface was rough and imprinted by the large asperities of the rough surface - clay surface deformed according to the shapes of the asperities
HRIF-steel	Failure mode 3	<ul style="list-style-type: none"> • Shearing occurred between the intact clay specimen and a thin layer of clay that adhered to the pile and • Clay fabric inhomogeneous: <ol style="list-style-type: none"> 1. Some sections where clay adhered to the pile surface 2. Some sections where shear surface of intact clay (after separation from pile surface) was rough 	<ul style="list-style-type: none"> • Shearing occurred partially within the clay and partially between the pile and the clay specimen • Clay fabric was inhomogeneous: <ol style="list-style-type: none"> 1. Some sections where clay adhered to the pile surface 2. Some sections where clay flowed in the direction of shear 3. Some sections where the surface was smooth and polished

Table 7.3 Features of quasi-static and dynamic tests

Features	Quasi-static tests	Dynamic tests
Shear displacement	Small (typically < 20mm)	Large (typically 70 to 80mm)
Number of times the sample is sheared	3 times, each for a normal stress of 250kPa, 150kPa and 60kPa	Repetitive
Shearing direction	Monotonic	Cyclic
Rate of shear	Slow	Fast

For the interfaces involving Mode 2 failure (medium plasticity clay and rough surface) and interfaces involving Mode 3 failure (high plasticity clay and smooth surface), effects additional to remoulding and development of excess pore pressures were likely to have occurred in the dynamic test. For interfaces involving Mode 2 failure, ploughing of the clay by the pile asperities appears to have been caused by the fast shearing; the ploughing phenomenon did not occur in the quasi-static test as the clay had sufficient time to conform to the asperities. For interface involving Mode 3 failure, a layer of clay was formed on the pile surface. As this feature was not evident for the equivalent interface tested in the quasi-static test, it would appear to have been caused by the cyclic and repetitive shearing.

Based on this study, it is not obvious which of the four features of the dynamic test had caused the rougher fabric of the shear surface observed for interfaces failing in Modes 1 and 3 and discontinuous shear surfaces for interfaces failing in Mode 1. (For Mode 2 failure, any effect due to fast shearing on the fabric of the shear surface could not be observed because any such fabric would have been destroyed by the ploughing action of the asperities.) However, previous interface studies involving interface tests (Bond and Jardine, 1991; Tika-Vassilikos, 1991; Lemos and Vaughan, 2000) and soil-only tests (Tika et al., 1996), which similarly reported the formation of the rougher fabric in the shear surface, concluded that the rougher fabric was due to the fast shearing.

7.5.6 Implications for the interface friction

Since the physical states of the pile surface and the clay sample for an interface subjected to the dynamic test are different to those for the equivalent interface subjected to the quasi-static test, it is evident that the quasi-static interface friction

associated with the dynamic test can be significantly different from the quasi-static interface friction measured in the quasi-static test.

It is known qualitatively that the effect of remoulding, of development of significant excess pore water pressures (for the all failure modes) and of pile-smearing (due to ploughing of the clay surface for Mode 2 and spreading of the sample onto the pile surface for Mode 3) is to decrease the interface friction.

The effect of the rougher fabric (for Mode 1) on the interface friction is however less obvious. Insight can be gained from studies which reported similar changes in the fabric of the clay subjected to fast shearing. In soil-only tests performed by Tika et al. (1996) and interface tests performed by Tika-Vassilikos (1991) and Lemos and Vaughan (2000), the effect of the rougher fabric of the shear surface subjected to fast shearing was established by performing a series of tests in the order of a slow test, a fast test and a slow test, where the sample was reconsolidated after each of the first two tests. The rougher fabric was found to have caused an increase in the peak friction in the second slow test, but had no influence on the large-displacement residual friction. The latter observation is consistent with the demonstration by Bishop et al. (1971) that the residual friction angle was unaffected by the initial structure of the soil. However, in the context of the dynamic test performed in this study, since the sample was not left to consolidate and since the interface friction relates to the residual or large-displacement value, the rougher fabric would appear not to cause the quasi-static friction associated with the dynamic test to differ from the quasi-static friction measured in the quasi-static test. There is further evidence in Section 7.6.1 to suggest that this is the case.

In order to quantify the difference between the quasi-static interface friction associated with the dynamic test and that measured in the quasi-static test due to the aforementioned dynamic effects, a procedure is required which allows the quasi-static friction associated with the dynamic friction to be estimated. Such a procedure will be developed in Section 7.6.1 and the difference in the quasi-static friction will be quantified in Section 7.6.2.

7.5.7 Implications for the normalisation of dynamic friction

As discussed in Section 3.3.1, the quasi-static friction is required to normalise the dynamic friction to obtain the strength ratio, which is used as a measure of the degree of strength increase due to viscous damping. However, because of the physical differences in the clay and the pile surfaces during the quasi-static test and the dynamic test, the quasi-static friction measured from the quasi-static test could not be used to normalise the dynamic friction measured from the dynamic test.

The possible exception is for the very first cycle of each dynamic test sequence because the physical characteristics of the interface at this stage might be closest to the characteristics of the interface during the quasi-static test, as the pore water pressure, remoulding, pile-smearing would be expected to be least at the end of the first dynamic test cycle, and the change in fabric of the shear surface of the clay is not likely to increase the interface friction.

Ideally, the quasi-static friction for normalising the dynamic friction could be obtained by performing a quasi-static test immediately after a dynamic test to obtain the quasi-static friction operative at that time. However, this was not possible from a practical point of view because the high-speed actuator used for the dynamic tests was not capable of delivering quasi-static shear rates, and also, because it was considered important that the dynamic tests were performed repetitively within short time intervals to simulate pile driving.

Therefore, it was necessary to develop a reasonable and independent method of estimating the quasi-static friction associated with the dynamic friction for all the dynamic tests at various test cycles and various applied normal stresses.

It is noted that the quasi-static tests performed in this study for obtaining the quasi-static friction values have nevertheless been necessary for the following reasons:

- As has been explained in Section 6.1, one of the aims of the quasi-static tests was to establish the quasi-static behaviour of the pile-clay interface as little research had been performed on this subject.

- As demonstrated in Section 7.5.5, a knowledge of the post-test characteristics of the interface subjected to quasi-static shearing is required to enable a comparison with the characteristics of the equivalent interface subjected to dynamic shearing.
- As discussed previously, since the physical characteristics of the interface during the first cycle of the dynamic test can be expected to be closest to the characteristics of the interface tested the quasi-static test, the measured quasi-static friction can be expected to be comparable to the quasi-static friction associated with the dynamic test. A procedure will be developed for deducing the quasi-static friction in Section 7.6.1; the effectiveness of the procedure in deducing the friction value (for the dynamic test involving the first cycle) can be evaluated by using the measured quasi-static friction value as a benchmark.
- The measured quasi-static friction values will also be compared with the deduced quasi-static friction values for quantifying the net effect of remoulding, development of excess pore pressures and pile-smearing, in Section 7.6.2.

7.6 Quasi-Static Interface Friction Associated with Dynamic Test

7.6.1 Procedure for obtaining quasi-static interface friction associated with dynamic test

Based on the dynamic test record (a sample of which has been shown in Figure 7.1), the quasi-static friction can be defined as the friction corresponding to near-zero pile velocity towards the end of the dynamic event; this definition of the quasi-static friction is illustrated in Figure 7.14. The appropriate point to be selected on the interface dynamic friction curve is the point immediately before the pile became stationary (namely when the interface shear force was still mobilised). Since the dynamic load cell works on the basis that voltage is only registered when there is an applied differential force, the load cell starts to discharge voltage when the carriage is stationary. In all cases, the occurrence of zero carriage velocity coincides with a characteristic plateau followed by erratic oscillation in the dynamic load response, as

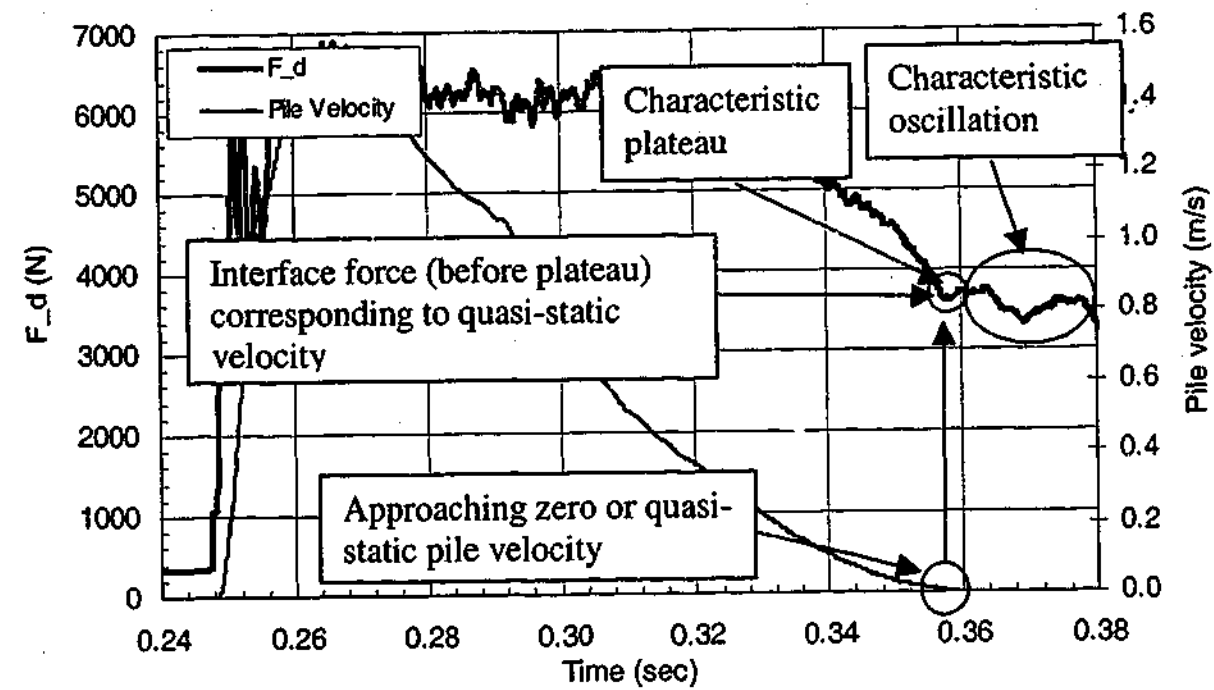


Figure 7.14 The definition of the quasi-static friction from a dynamic test

shown in Figure 7.14. This characteristic of the dynamic load cell helps in identifying the aforementioned point.

Given the consistent characteristic of the dynamic load cell response, a procedure can be developed to determine the quasi-static friction. The start of the characteristic plateau (which is followed by the characteristic oscillation) in the dynamic force curve (labelled F_d) can be identified and the quasi-static friction corresponding to the time immediately before the pile became stationary can be defined. Whilst it would be desirable to compare the velocity corresponding to the quasi-static friction obtained using the procedure with the quasi-static shear rate, the velocity could not be reliably determined because of its minute value and the limited accuracy of the velocity (based on the measured acceleration).

Previous research (e.g. Litkouhi and Poskitt, 1980; Heerema, 1979) indicated that the strength ratio increased dramatically at near-zero velocities. Therefore, the importance of correctly defining the correct quasi-static friction is fundamental and the procedure for calculating it is validated in the following.

It has been discussed in Section 7.5.7 that the development of shear-induced pore pressures, the remoulding, and for Modes 2 and 3, the pile-smearing after the first test cycle in the dynamic test sequence are likely to be insignificant. Therefore, it could be expected that the deduced quasi-static friction associated with the first test cycle in the dynamic test sequence is comparable to that measured in the quasi-static test. The two values for the various interfaces tested are tabulated in Table 7.4. Because the first test in a series of dynamic tests was always performed at a normal stress of 250kPa, the comparison could only be made for tests at the normal stress of 250kPa. Comparison of the values measured in the quasi-static tests and the values inferred from the initial cycles of the dynamic tests are not only comparable but agree closely. As shown in the table, the maximum percentage difference in the strength ratio is 7%. The comparison indicates that the procedure for deducing the quasi-static friction is effective.

Table 7.4 Comparison of the deduced and measured quasi-static friction based on the first dynamic tests

Interface tests at normal stress = 250kPa	Measured from quasi-static test (N)	Deduced from dynamic record (N)	Difference (N)	Percentage difference (%)
BallR ($\sigma_p=500\text{kPa}$)-Steel	4960	4750	-130	-3
BallR ($\sigma_p=325\text{kPa}$)-Steel	3720	3540	-180	-5
BallR ($\sigma_p=500\text{kPa}$)-Smooth concrete	3760	3750	-10	0
BallR ($\sigma_p=325\text{kPa}$)-Smooth concrete	2920	3130	+210	+7
BallR ($\sigma_p=500\text{kPa}$)-Rough concrete	5580	5700	+120	+2
BallR ($\sigma_p=325\text{kPa}$)-Rough concrete	4600	4500	-100	-2
BallR/Talc ($\sigma_p=500\text{kPa}$)-Steel	4720	4650	-70	-1
BallR/Talc ($\sigma_p=325\text{kPa}$)-Steel	3910	3790	-120	-3
HR1F ($\sigma_p=500\text{kPa}$)-Steel	2730	2670	-60	-2
HR1F ($\sigma_p=325\text{kPa}$)-Steel	2330	2290	-40	-2

The reasonableness of the estimated quasi-static value was further evaluated by observing the strength ratio (which was based on the estimated quasi-static value) vs. pile velocity plot. Since it had been established that the dynamic friction increased with increasing velocity, the strength ratio must increase from a value of 1.0 to a higher value as the velocity increases. Indeed, this was found to be the case for all the strength ratio vs. velocity plots which will be later presented in Section 7.7.3.

Given the reasonableness of the procedure, the quasi-static friction associated with each dynamic test cycles was estimated.

7.6.2 Quasi-static interface friction associated with dynamic test vs. Quasi-static interface friction measured in quasi-static test

As has been discussed in Section 7.5.6, the clay was subjected to remoulding, development of excess pore pressures in the 3 modes of failure, and the pile surface was smeared in the Mode 2 failure and was adhered to in the Mode 3 failure. These various effects are categorised under each of the three dynamic failure modes for convenience in the subsequent discussion, as follows:

Whilst it was not possible in the present study to quantify for a particular interface the effect of each the four factors (as the pore pressure response was not measured, and the degree of smearing of the pile surface as well as the degree of remoulding of the sample could not be quantified), the net effect of these effects on the interface friction can be quantified by comparing the quasi-static value associated with the dynamic test and the quasi-static values measured in the quasi-static test.

Table 7.5 Phenomena occurring at the shear surfaces of the clay specimen and the pile specimen for each of the 3 dynamic failure modes

Phenomena	Mode 1	Mode 2	Mode 3
Remoulding in clay	✓	✓	✓
Development of excess pore water pressure in clay	✓	✓	✓
Smearing of pile surface	×	✓	×
Spreading of sample onto pile surface	×	×	✓

The comparison of these values with those measured from the quasi-static test for various interfaces is shown graphically in Figure 7.15 to Figure 7.24. In each figure, the interface resistances (in N) measured in the quasi-static tests performed at normal stresses of 250kPa, 150kPa and 60kPa are each labelled "Measured" followed by the pertinent normal stress, whilst the resistances (in N) deduced from the dynamic tests performed at the three normal stresses are each labelled "Deduced" followed by the normal stress.

As has been previously noted in Section 7.6.1 and in these comparative plots, for all interfaces, the deduced quasi-static value associated with the first test cycle in the dynamic test sequence is in general only slightly different from the value measured in the quasi-static test. As noted previously in Section 7.6.1, this would suggest remoulding, development of pore water pressure and pile-smearing after the first test cycle are not yet significant.

For all the interfaces, the deduced quasi-static value is generally lower than the measured for the cycles subsequent to the first test cycle. This will be discussed in detail in the following sub-sections.

7.6.2.1 Mode 1 interface shear failure

As shown in Table 7.4, Mode 1 interface shear (involving BallR-Steel, BallR-Smooth concrete and BallR/Talc-Steel interfaces) was susceptible to the effects of remoulding and development of excess pore pressures. As can be noted in Figure 7.15 to Figure 7.20, the deduced quasi-static interface friction associated with the tests subsequent to the first test was generally lower than the measured quasi-static friction. The reduction must have been due either to remoulding in the sample, or excess pore pressures, or a combination of both. It can also be noted that in general as repeated load cycles were carried out, the interface friction reduced progressively. The progressive reduction is a well-known phenomenon in pile driving in clays, and is largely responsible for the phenomenon of 'set-up'.

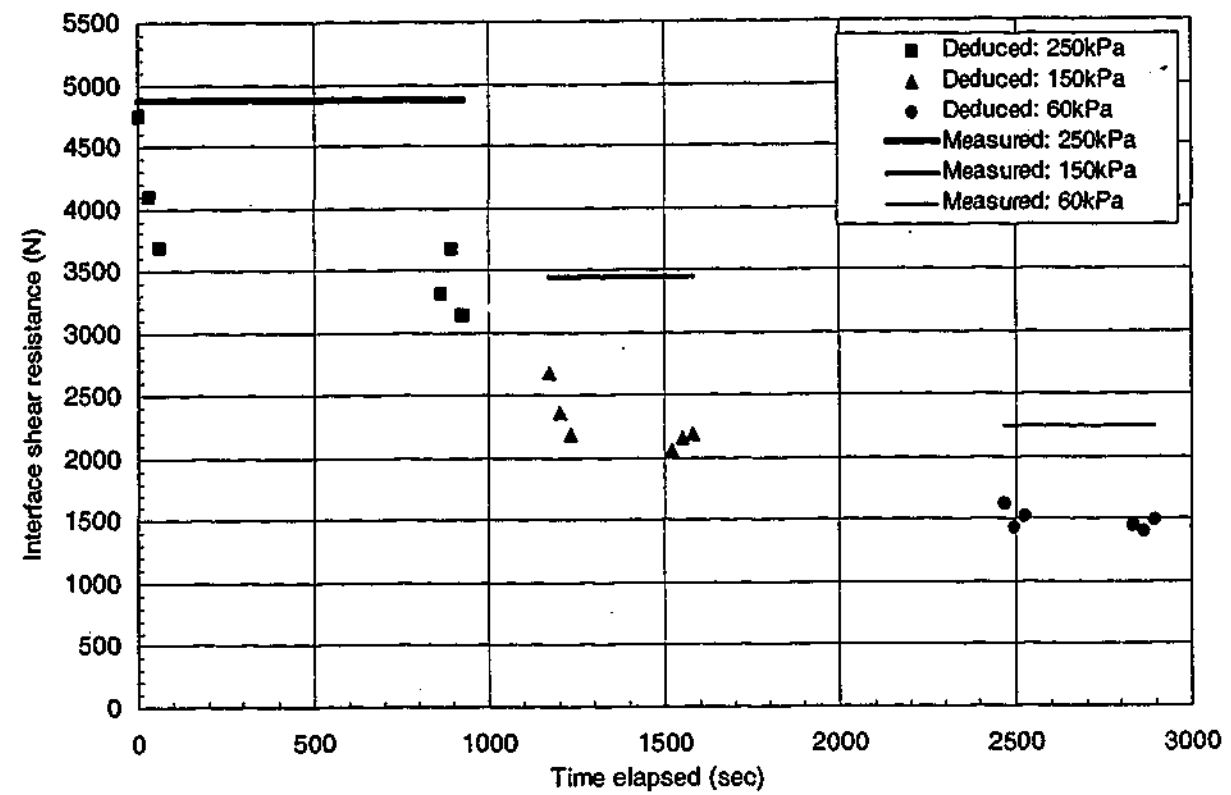


Figure 7.15 Mode 1: Comparison of the deduced static friction and measured static friction (from quasi-static test) over time elapsed for BallR($\sigma'_p=500\text{kPa}$)-Steel interface

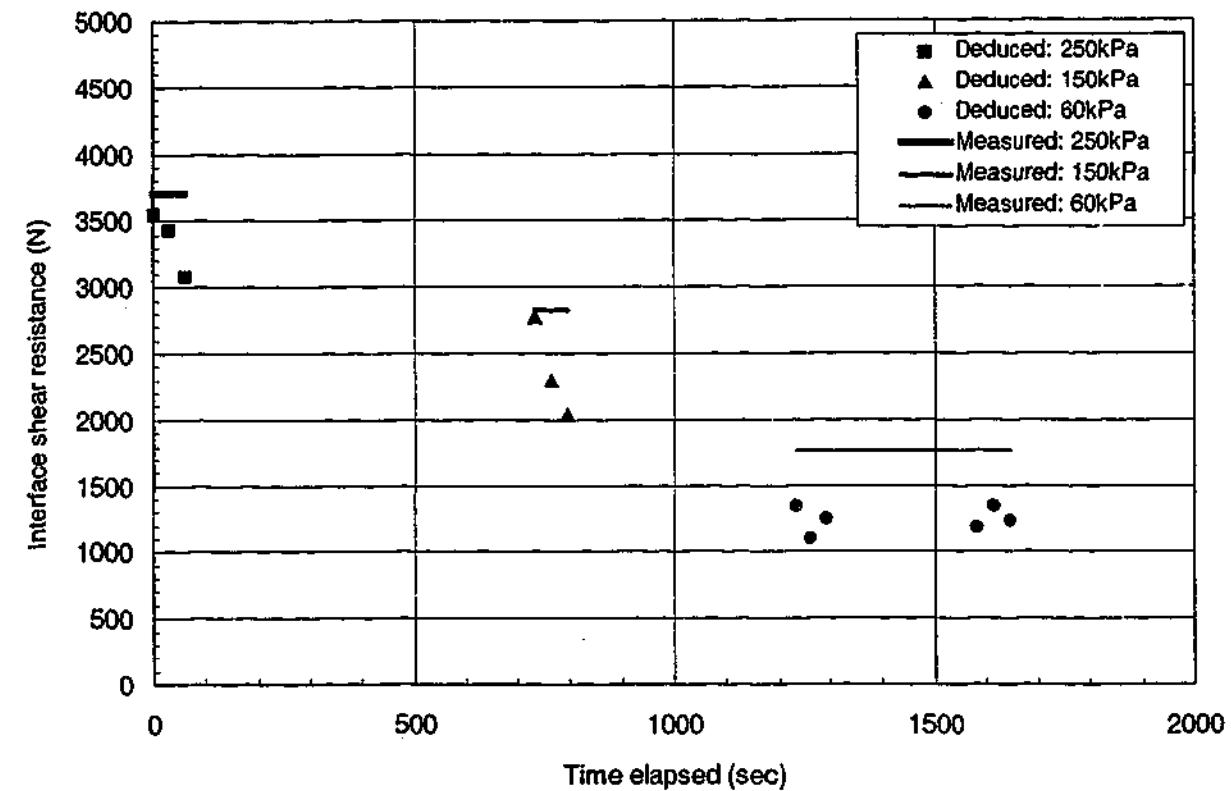


Figure 7.16 Mode 1: Comparison of the deduced static friction and measured static friction (from quasi-static test) over time elapsed for BallR($\sigma'_p=325\text{kPa}$)-Steel interface

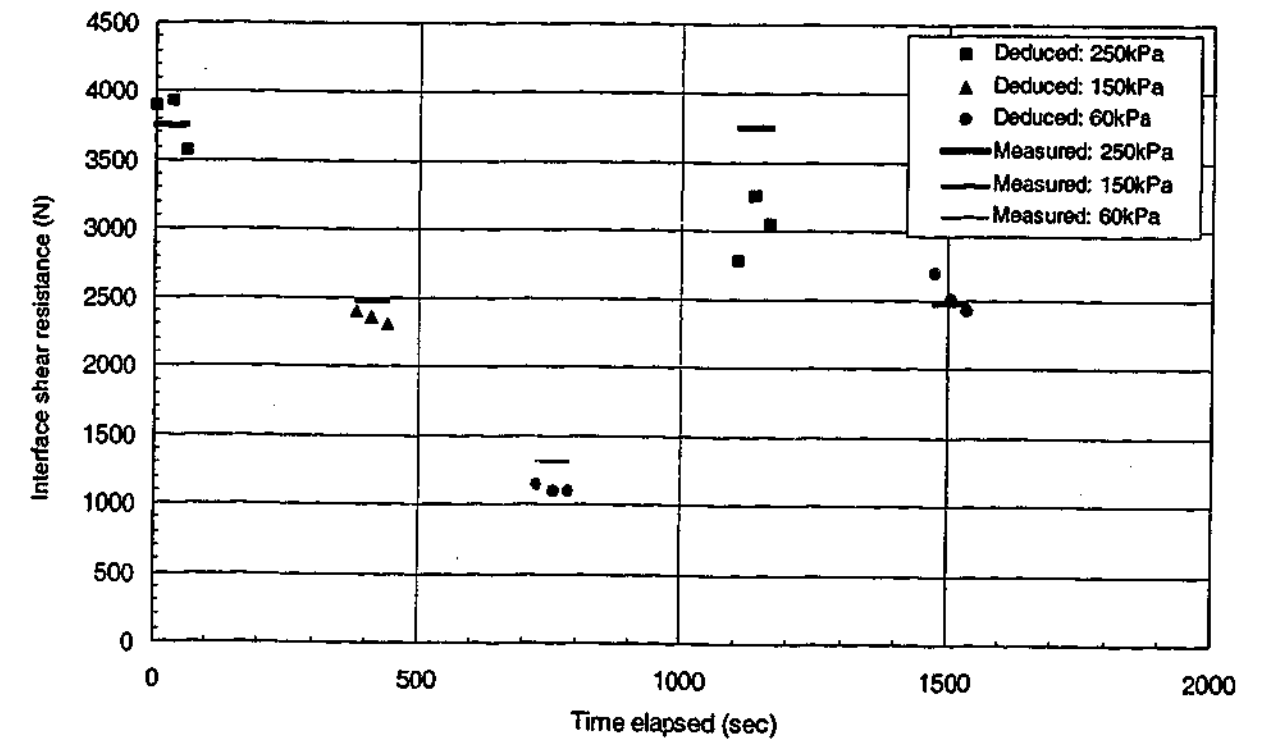


Figure 7.17 Mode 1: Comparison of the deduced static friction and measured static friction (from quasi-static test) over time elapsed for BallR($\sigma'_p=500\text{kPa}$)-Smooth concrete interface

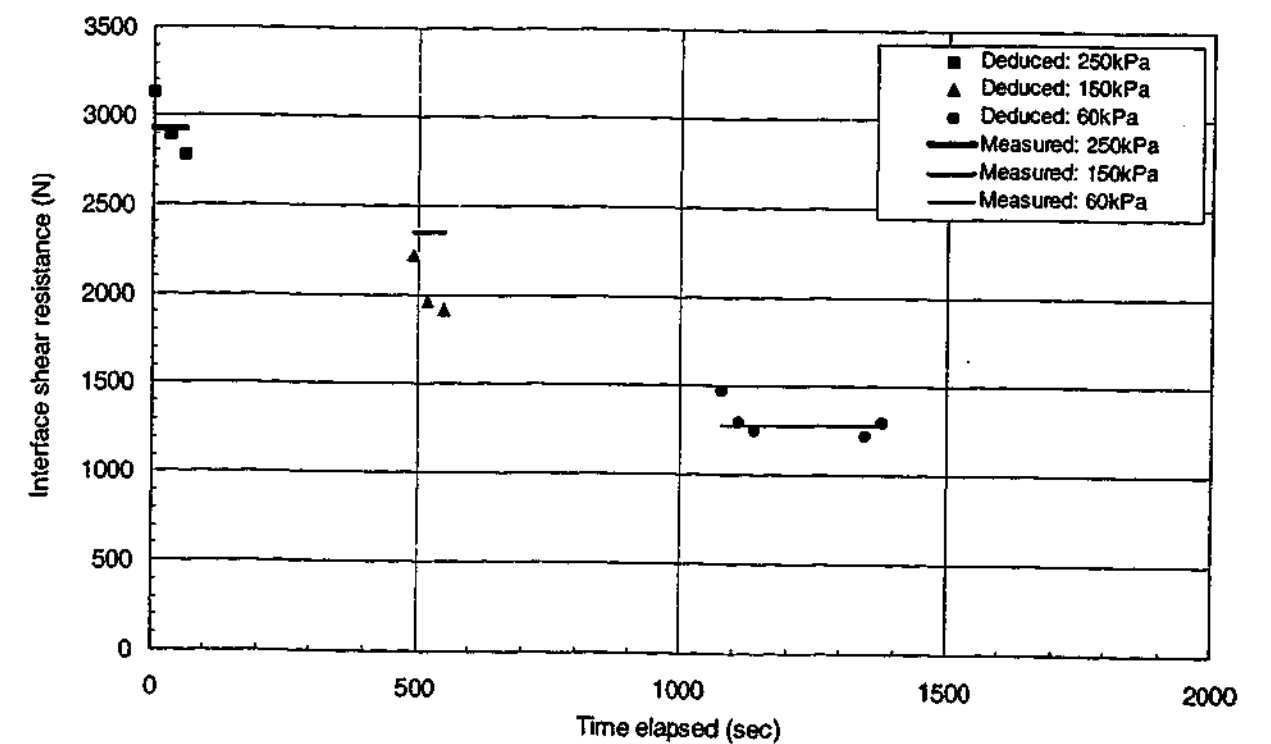


Figure 7.18 Mode 1: Comparison of the deduced static friction and measured static friction (from quasi-static test) over time elapsed for BallR($\sigma'_p=325\text{kPa}$)-Smooth concrete interface

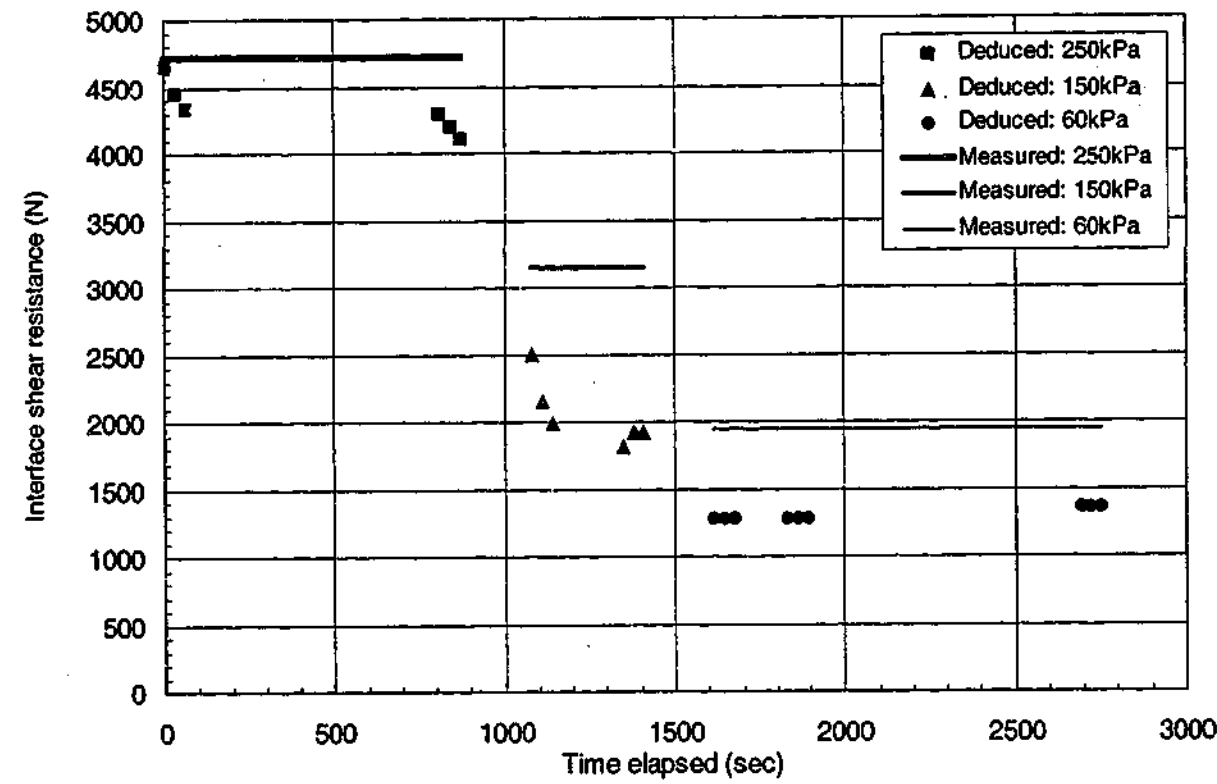


Figure 7.19 Mode 1: Comparison of the deduced static friction and measured static friction (from quasi-static test) over time elapsed for BallR/Talc($\sigma'_p=500\text{kPa}$)-Steel interface

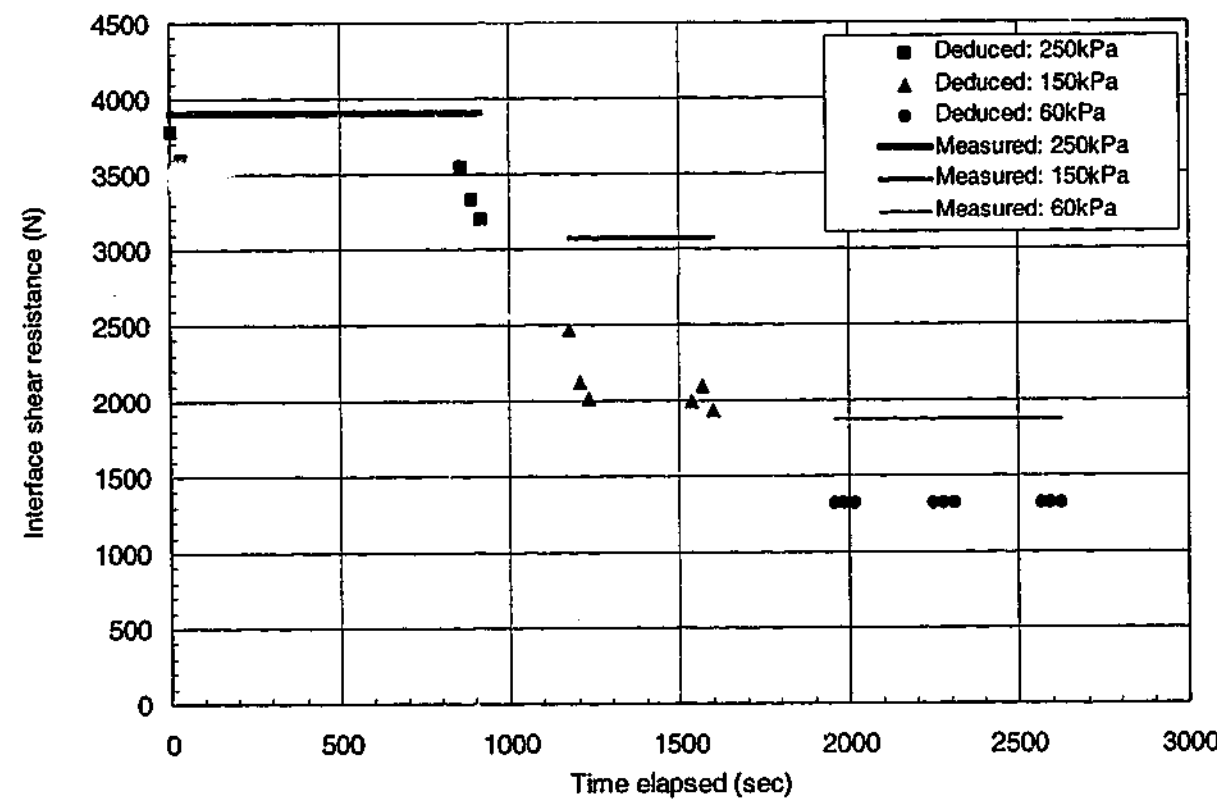


Figure 7.20 Mode 1: Comparison of the deduced static friction and measured static friction (from quasi-static test) over time elapsed for BallR/Talc($\sigma'_p=325\text{kPa}$)-Steel interface

7.6.2.2 Mode 2 interface shear failure

As shown in Table 7.4, the BallR-Rough concrete interfaces which sheared in Mode 2 failure were susceptible to remoulding, pore pressure effects and smearing of the pile surface. As can be noted in Figure 7.21 and Figure 7.22, the deduced quasi-static friction reduced very dramatically with cycles subsequent to first cycle. Given that the BallR clay tested against the smooth concrete did not exhibit such rapid reduction in the friction, the rapid reduction must be due to the smearing of the pile surface.

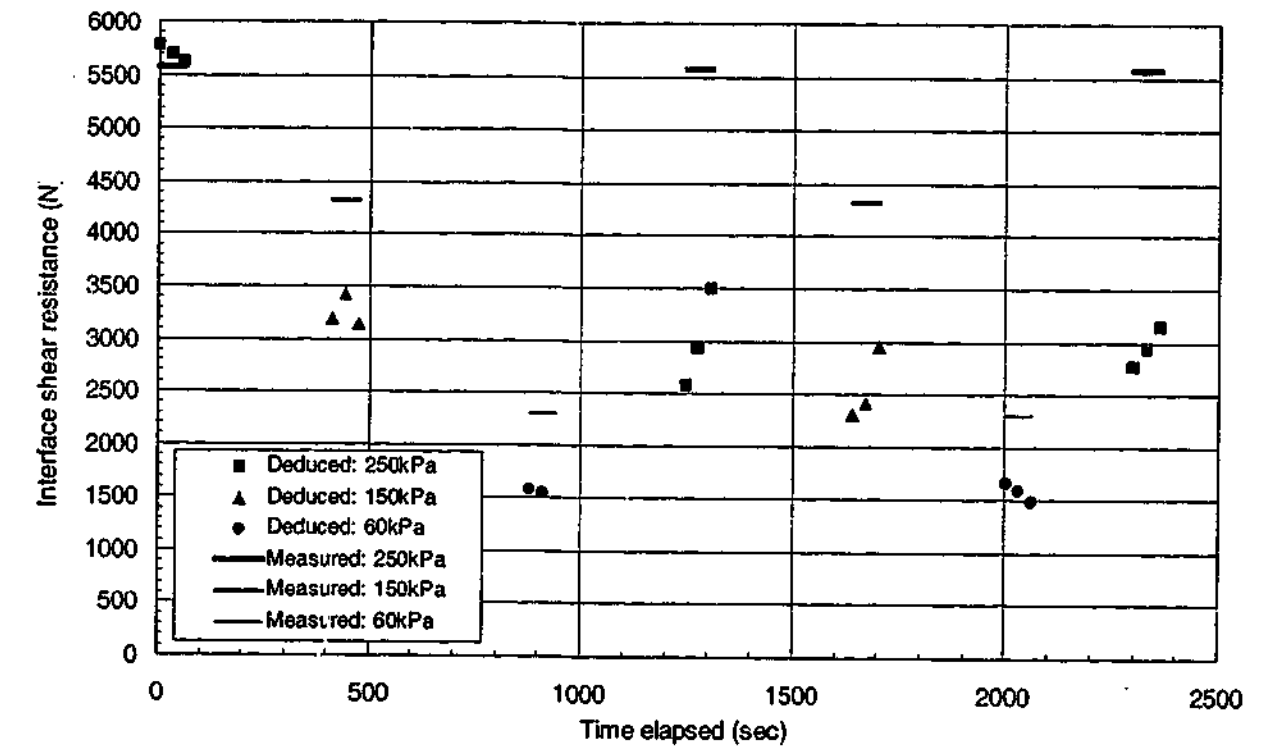


Figure 7.21 Mode 2: Comparison of the deduced static friction and measured static friction (from quasi-static test) over time elapsed for BallR($\sigma'_p=500\text{kPa}$)-Rough concrete interface

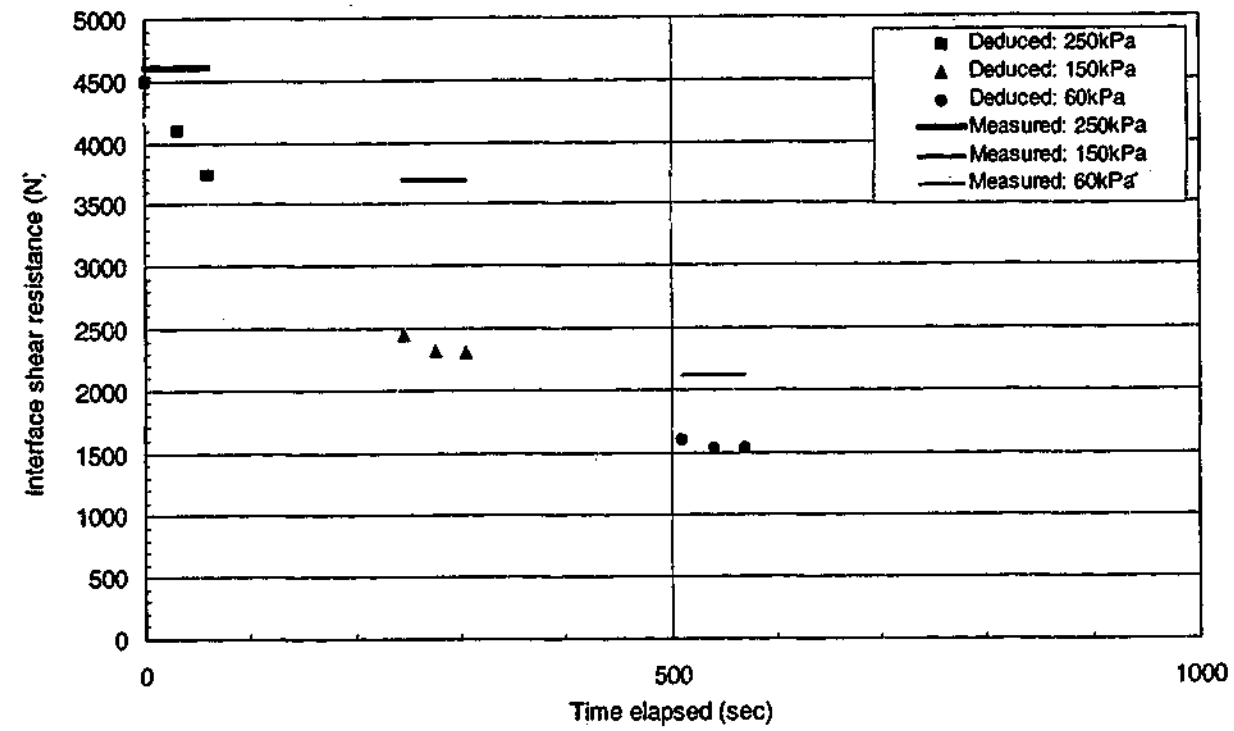


Figure 7.22 Mode 2: Comparison of the deduced static friction and measured static friction (from quasi-static test) over time elapsed for BallR($\sigma'_p=325\text{kPa}$)-Rough concrete interface

7.6.2.3 Mode 3 interface shear failure

As shown in Table 7.4, the HR1F-Smooth steel interface which sheared in Mode 3 failure is susceptible to remoulding, pore pressure effects, and the effect of the “spreading” of the high plasticity clay sample on the pile surface. However as shown in Figure 7.23 and Figure 7.24, the measured and deduced quasi-static friction values were in significantly closer agreement compared to those in Mode 1 and Mode 2 failure for the complete test sequence. It is significant that the failure plane was observed to be apparently within the soil and not at the interface as for the other tests. It would appear that the shearing which took place between the intact clay block and the layer of clay that had adhered to the pile surface resulted in minimal remoulding and pore pressure effects, and hence significantly less reduction in the quasi-static friction as compared to that in Mode 1 and Mode 2 failure.

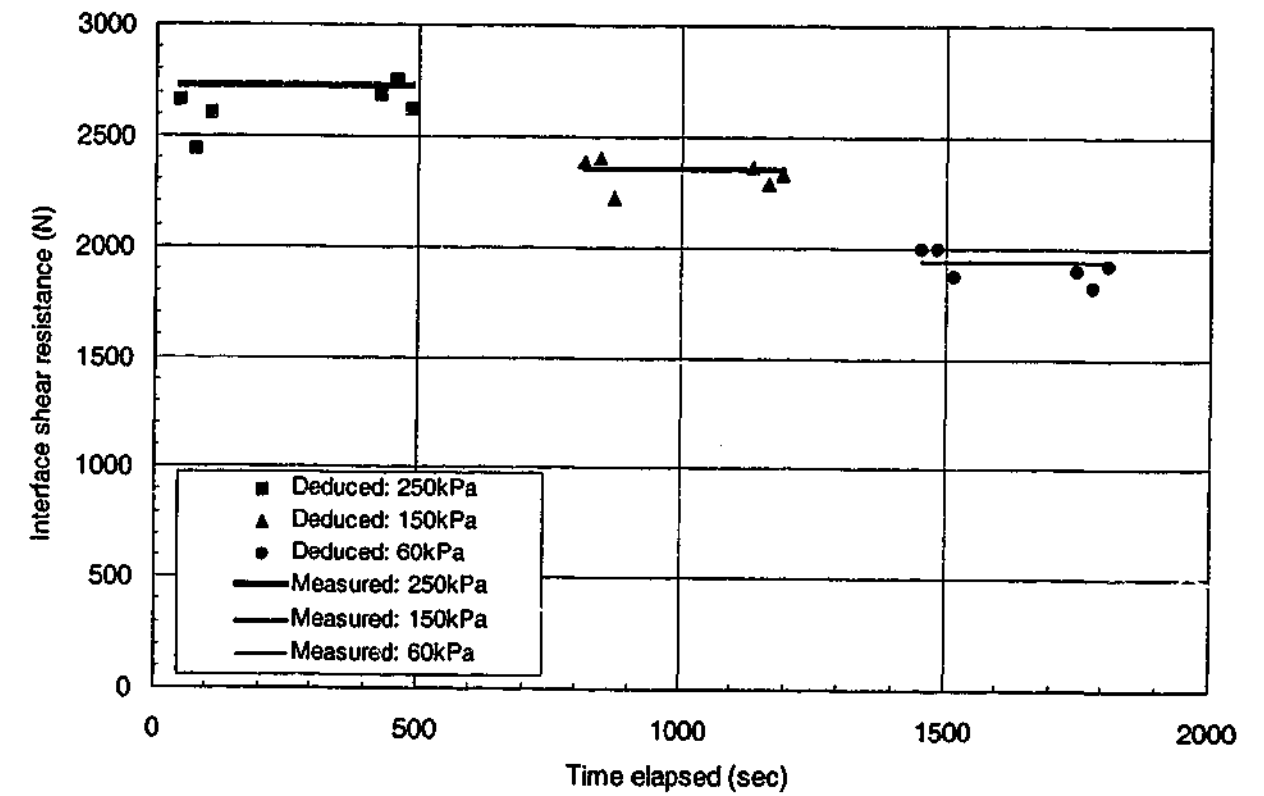


Figure 7.23 Mode 3: Comparison of the deduced static friction and measured static friction (from quasi-static test) over time elapsed for HR1F($\sigma'_p=500\text{kPa}$)-Steel interface

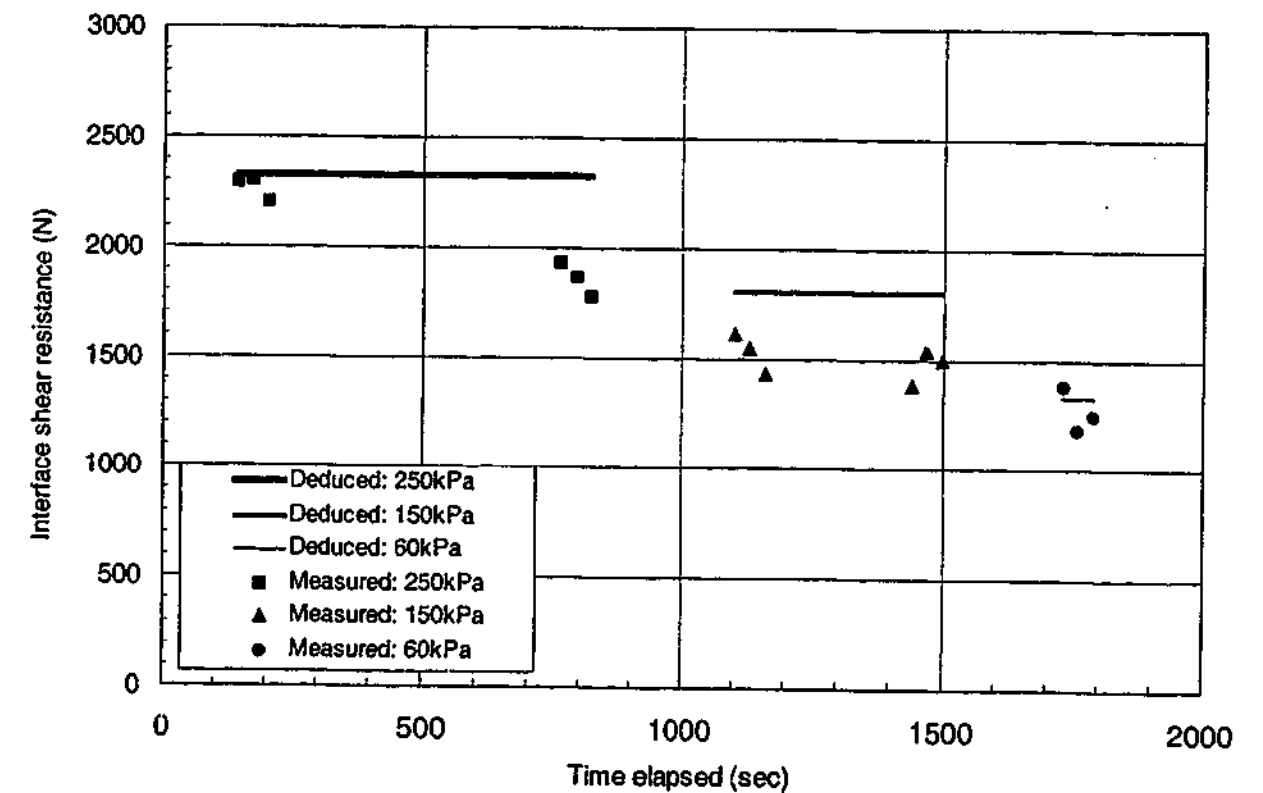


Figure 7.24 Mode 3: Comparison of the deduced static friction and measured static friction (from quasi-static test) over time elapsed for HR1F($\sigma'_p=325\text{kPa}$)-Steel interface

7.7 Analysing Data for Dynamic Effects

7.7.1 Selection of portion of record to be analysed

In order to determine the dynamic response of the pile-clay interface, the dynamic records (a sample of which has been presented in Section 7.4) are analysed for dynamic effects.

However, in the initial loading stage, two effects occurred which make the data in this portion of the record difficult to analyse. Firstly, there was incomplete mobilization of the quasi-static resistance in the initial loading stage. The limiting friction of the interface was only fully mobilised after the quake was reached; this concept is shown schematically in Figure 7.25. Adopting a reference quake of 2.5mm based on historical convention (Smith, 1960), the limiting friction is estimated to only have been reached after the pile velocity reached between 0.9 and 1.1m/s. Therefore it is not possible to simultaneously determine the instantaneous static and dynamic resistance during this initial mobilization.

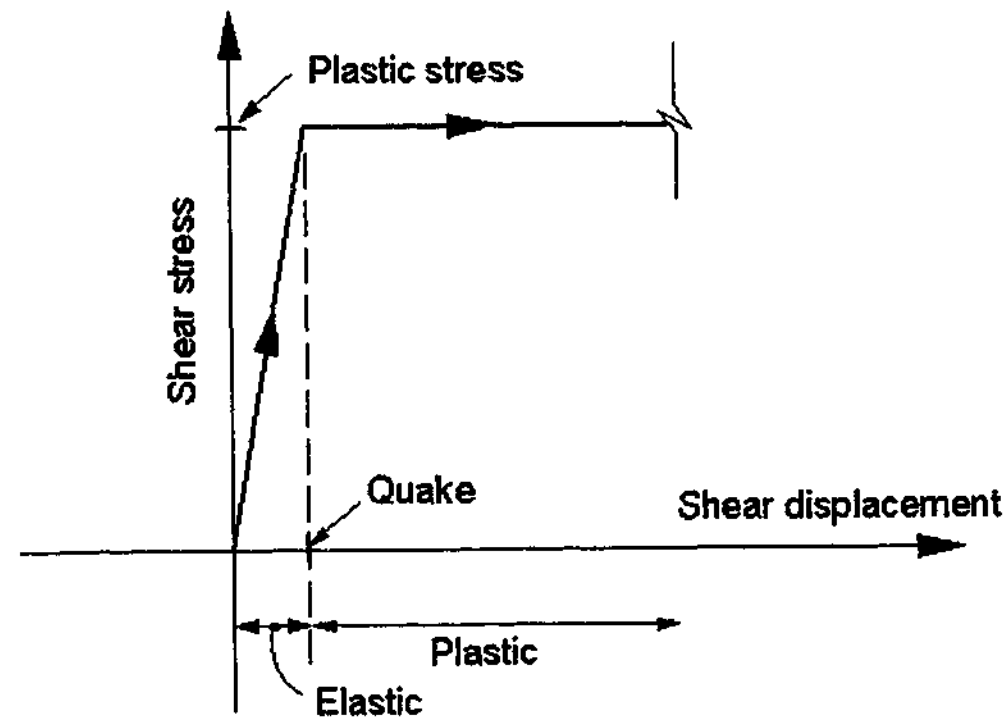


Figure 7.25 Schematic showing idealised load-displacement response before and after the plastic friction is reached

Also, residual stresses due to previous stresses generated by the reverse stroke were present at the interface in the initial loading stage. When the carriage was reversed to its starting position (for a subsequent test), residual stresses were locked at the pile-soil interface in the negative direction, which opposed the next positive shearing event. In order to mobilise the interface friction in the designated direction in the subsequent test, the residual stress had to be overcome first, as can be best illustrated schematically in Figure 7.26.

Hence, to analyse the dynamic effect, the only data which is readily amenable is that portion of the record after the quasi-static shear resistance has been fully mobilized and where the effect of residual stresses is not present. The value of the quake is not known especially given the additional effect of the residual stresses; however, it is safe to assume that the resistance has been fully mobilised by the time the peak velocity is reached. Thus, the portion of the record which is amenable to analysis is defined as that after the peak velocity has been reached to the time of zero velocity. Beyond the point of zero pile velocity, the velocity becomes negative as the carriage rebounds and the shear direction changes, and the interface resistance begins to unload and is no longer fully mobilised. In any case, the data beyond the zero velocity point should be excluded because after the point of zero velocity or when the carriage rebounds, the dynamic load cell loses contact with the carriage and is thus no longer giving reliable reading.

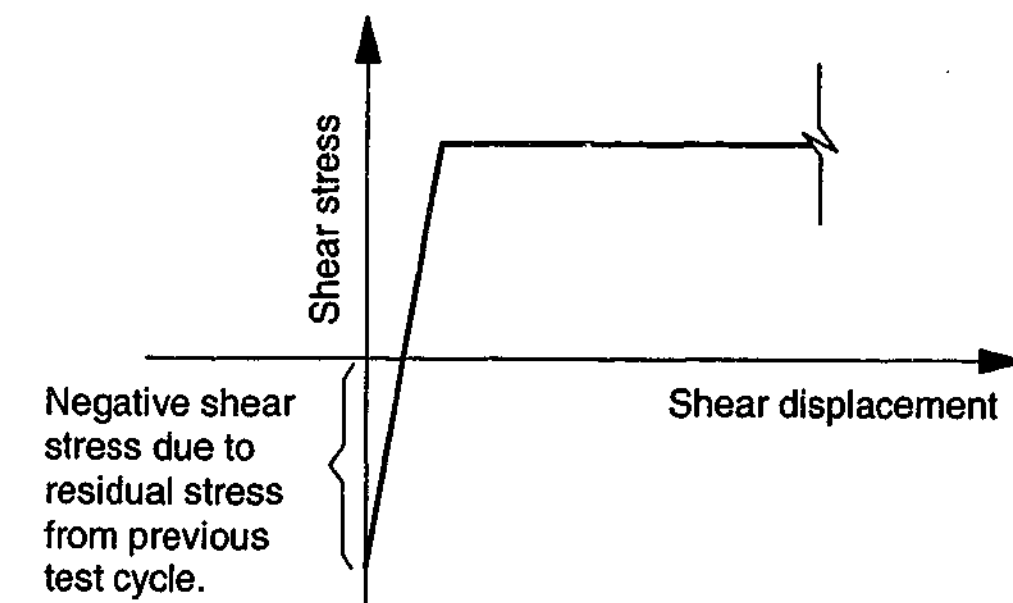


Figure 7.26 Schematic showing the effect of residual stress on the load-displacement response

It is noted that in addition to these reasons, the selection of the later portion of the record also has the advantage of excluding the initial portion of the event where the data during ramping up from zero to peak velocity is less reliable (due to the shock loading applied, the lack of perfect synchronisation between the measurements, and the absolute error from the taking the difference between the two relatively large numbers).

7.7.2 Velocity-dependence of dynamic friction

It can be observed in the typical record presented in Figure 7.1 that the dynamic friction was greater than the quasi-static friction, and that the dynamic friction consistently decreased with decreasing velocity. Analyses of the other records similarly showed that the dynamic friction for the pile-clay interface is velocity-dependent. This is consistent with the findings from previous studies (e.g. Dayal and Allen, 1975; Heerema, 1979; Litkouhi and Poskitt, 1980; Benamar, 1999).

7.7.3 Strength Ratio-Velocity Responses

Given that the dynamic interface friction is dependent on the pile velocity or the rate at which the interface is sheared, the dynamic response is best presented using a plot of the normalised dynamic friction or the strength ratio vs. the pile velocity.

The strength ratio-velocity plots for all the dynamic tests were produced. The strength ratio-velocity plots for the various interfaces are shown in their entirety in this section, under the headings of the dynamic failure modes. The plots are presented in the following order:

Mode 1 interface shear failure

- Figure 7.27 BallR($\sigma'_p=325\text{kPa}$)-Steel
- Figure 7.28 BallR($\sigma'_p=500\text{kPa}$)-Steel
- Figure 7.29 BallR($\sigma'_p=325\text{kPa}$)-Smooth Concrete
- Figure 7.30 BallR($\sigma'_p=500\text{kPa}$)-Smooth Concrete
- Figure 7.31 BallR($\sigma'_p=325\text{kPa}$)-Wetted Steel
- Figure 7.32 BallR($\sigma'_p=500\text{kPa}$)-Wetted Steel
- Figure 7.33 BallR($\sigma'_p=325\text{kPa}$)-Wetted Smooth Concrete
- Figure 7.34 BallR($\sigma'_p=500\text{kPa}$)-Wetted Smooth Concrete

Figure 7.35 BallR/Talc($\sigma'_p=325\text{kPa}$)-Steel

Figure 7.36 BallR/Talc($\sigma'_p=500\text{kPa}$)-Steel

Mode 2 interface shear failure

Figure 7.37 BallR($\sigma'_p=325\text{kPa}$)-Rough Concrete

Figure 7.38 BallR($\sigma'_p=500\text{kPa}$)-Rough Concrete

Figure 7.39 BallR($\sigma'_p=325\text{kPa}$)-Wetted Rough Concrete

Figure 7.40 BallR($\sigma'_p=500\text{kPa}$)-Wetted Rough Concrete

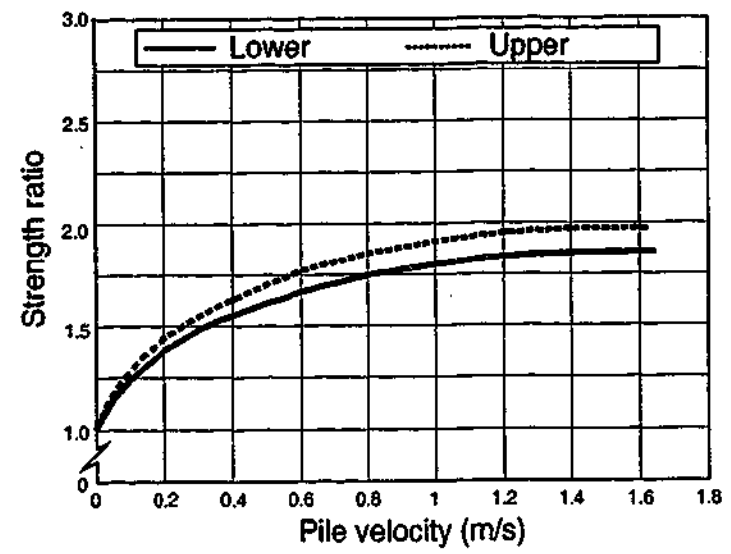
Mode 3 interface shear failure

Figure 7.41 HR1F($\sigma'_p=325\text{kPa}$)-Steel

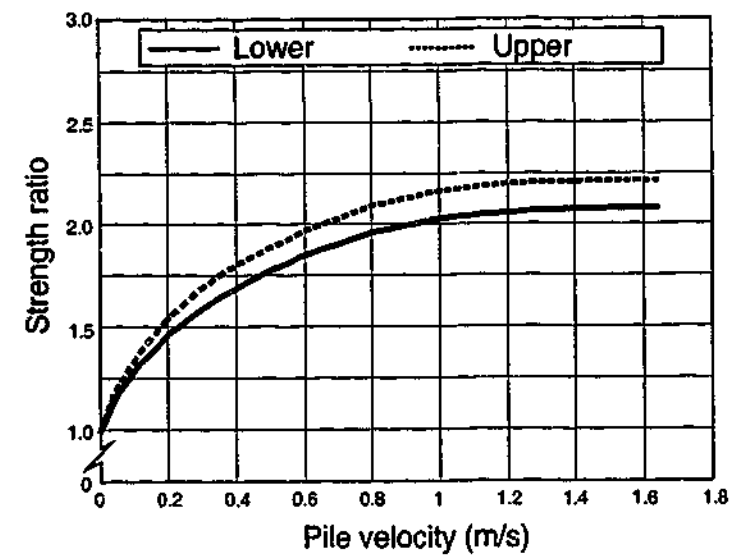
Figure 7.42 HR1F($\sigma'_p=500\text{kPa}$)-Steel

The plots, which contain experimental scatter, have been drafted for the sake of presentation. For each interface, three plots have been presented, for tests performed at normal stresses of 250kPa, 150kPa and 60kPa respectively. As mentioned in Section 7.3.1, three consecutive tests were performed for a particular boundary condition; the “lower” and “upper” labels relate to the lower bound and the upper bound of the responses for the consecutive tests. It has been acknowledged that the estimated quasi-static friction introduces some error in the strength ratio but the error in the calculated strength ratio is estimated to be not more than 10%. It is noted that the strength ratio-velocity relationships are limited to a velocity of 1.6m/s which was the peak velocity achieved for the pile-clay tests.

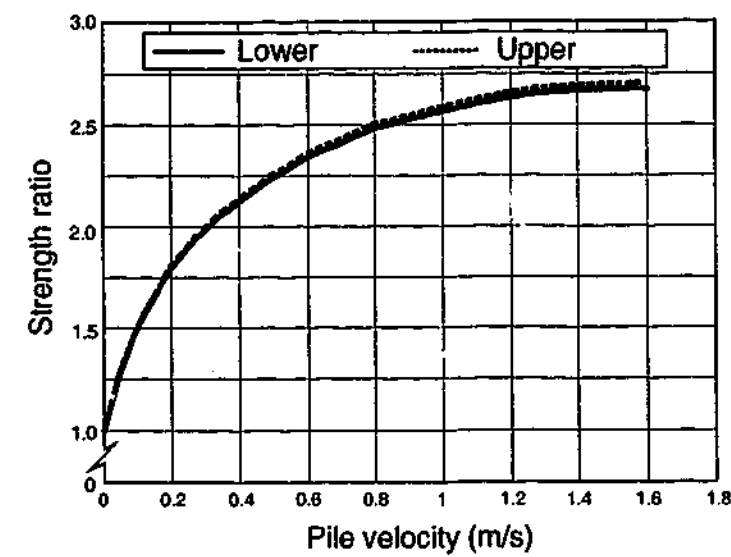
7.7.3.1 Mode 1 interface shear failure



(a)

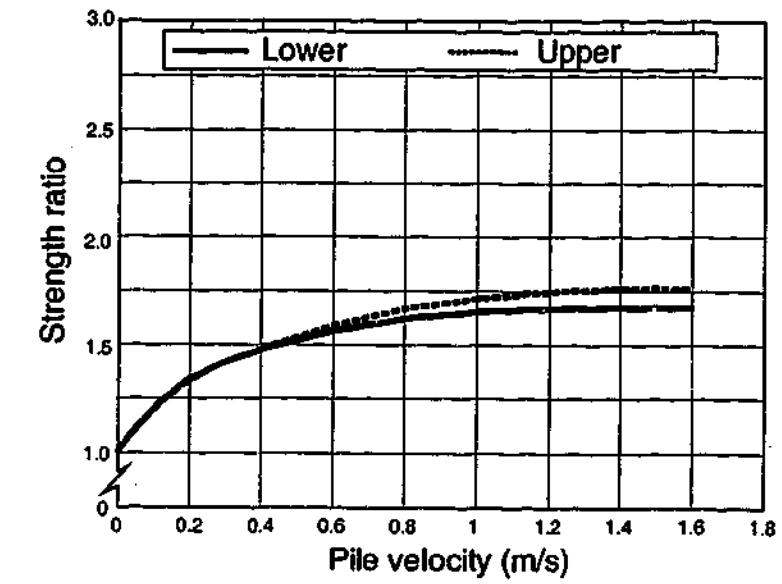


(b)

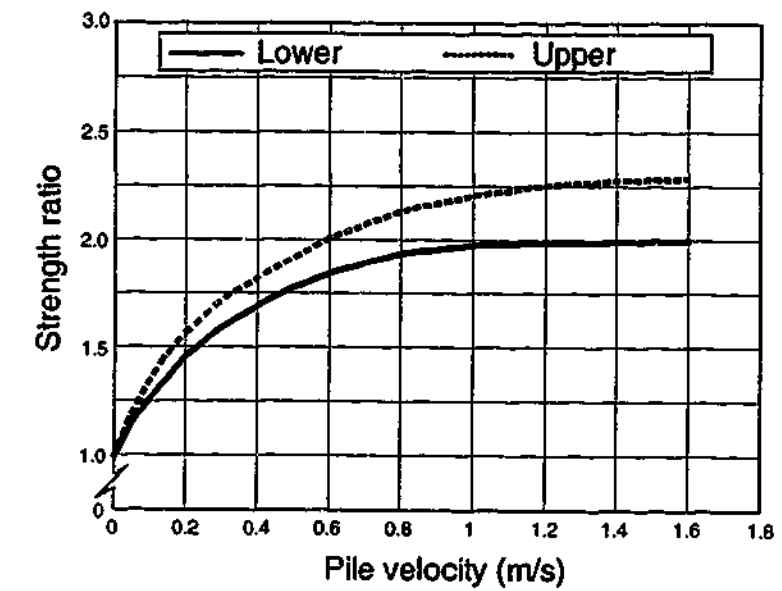


(c)

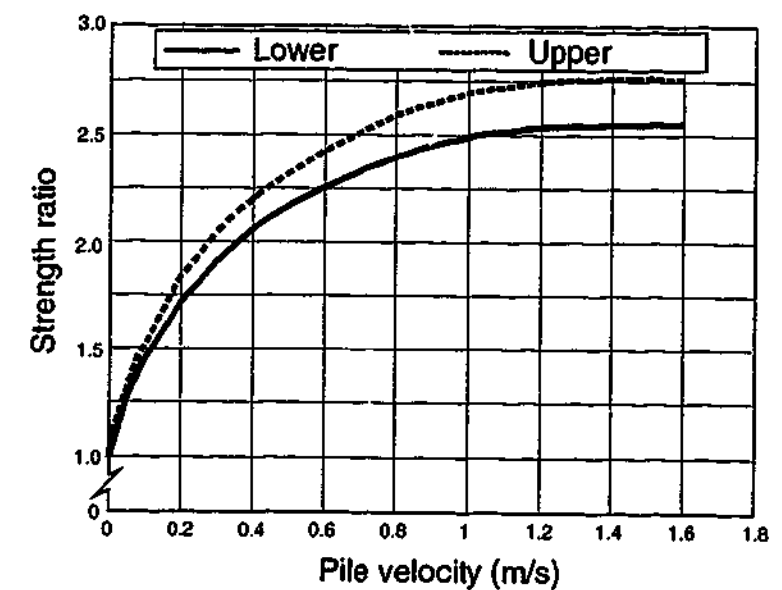
Figure 7.27 BallR($\sigma'_p=325\text{kPa}$)-Steel: Strength ratio-velocity responses at normal stresses of (a) 250kPa (b) 150kPa (c) 60kPa



(a)

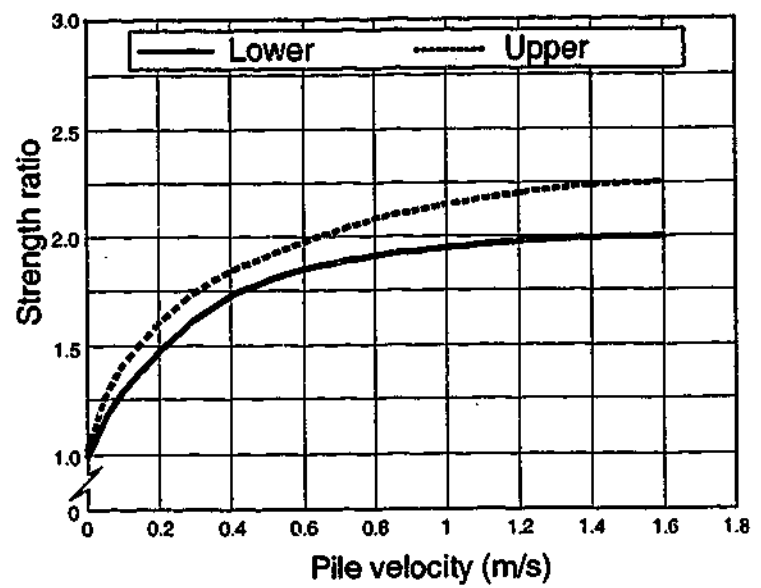


(b)

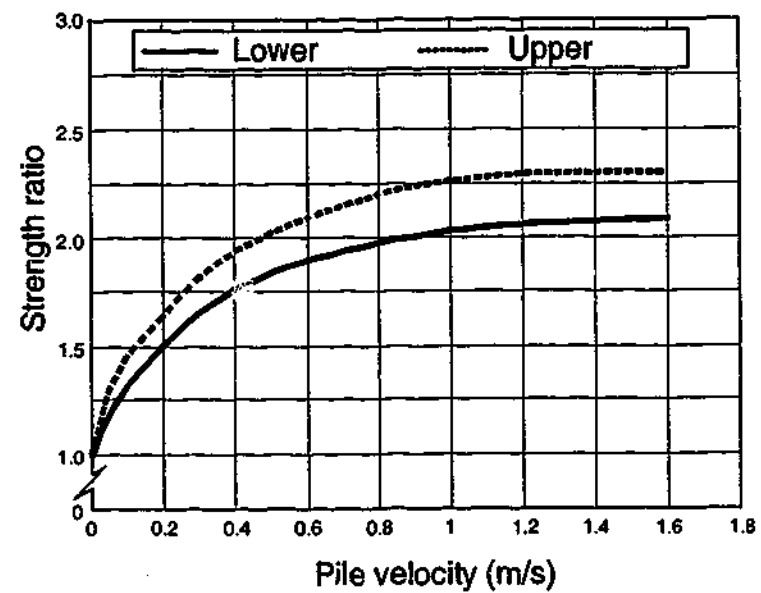


(c)

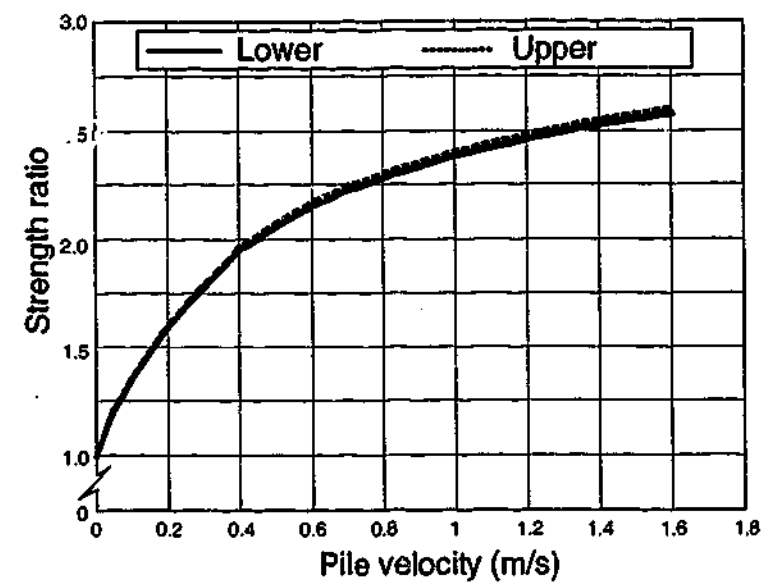
Figure 7.28 BallR($\sigma'_p=500\text{kPa}$)-Steel: Strength ratio-velocity responses at normal stresses of (a) 250kPa (b) 150kPa (c) 60kPa



(a)

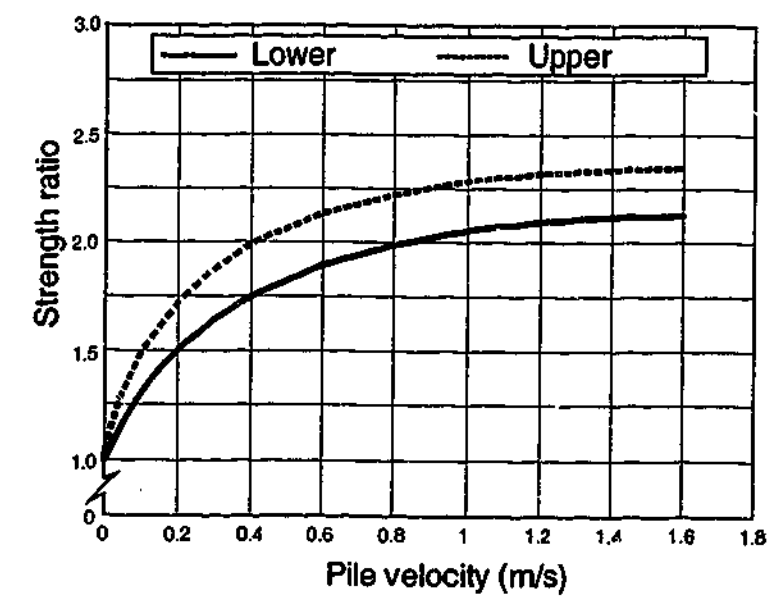


(b)

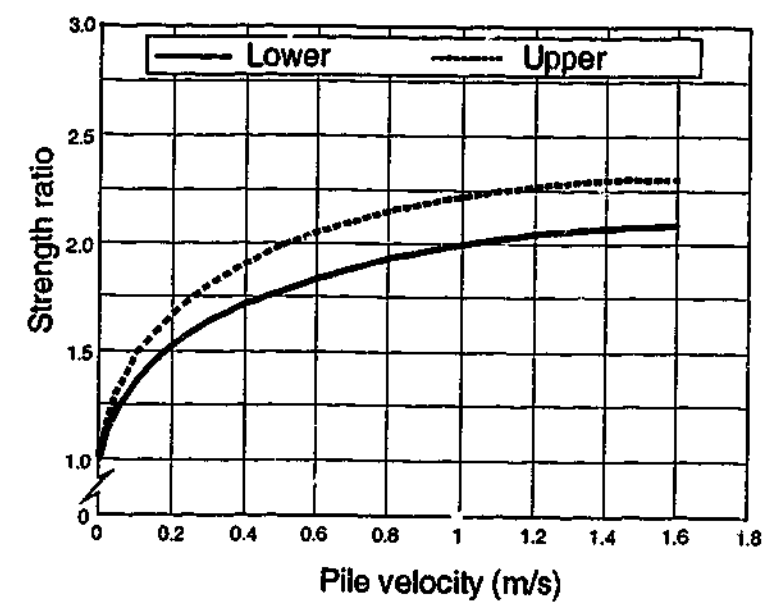


(c)

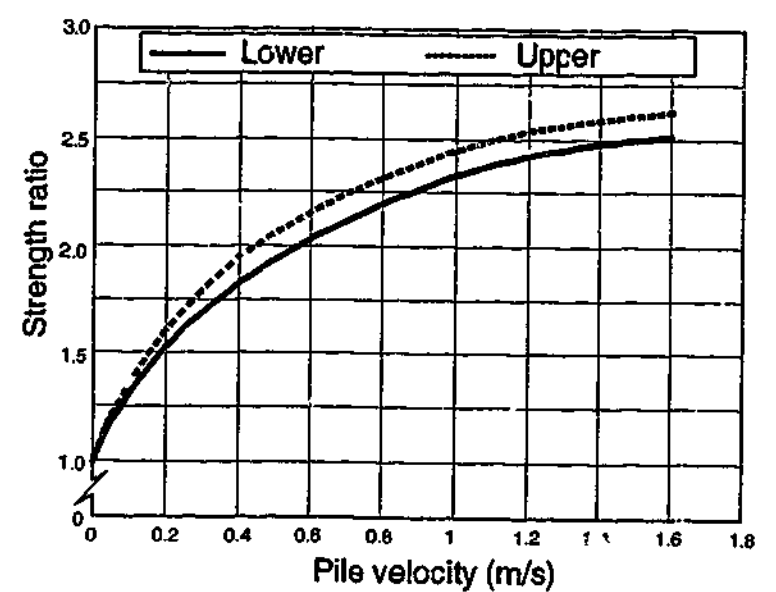
Figure 7.29 BallR($\sigma'_p=325\text{kPa}$)-Smooth Concrete: Strength ratio-velocity responses at normal stresses of (a) 250kPa (b) 150kPa (c) 60kPa



(a)

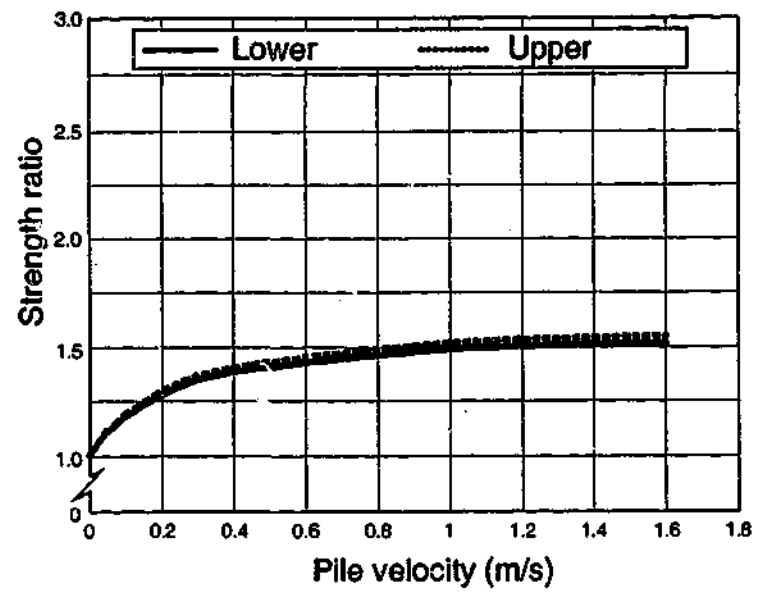


(b)

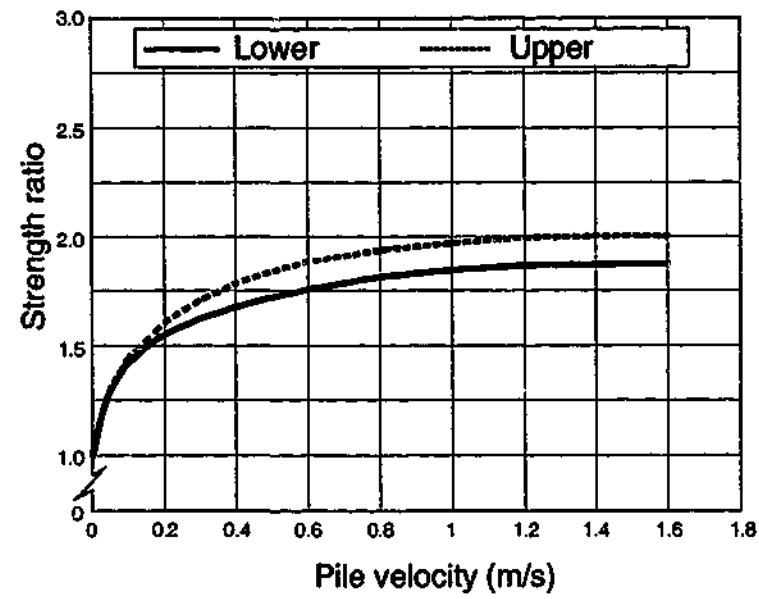


(c)

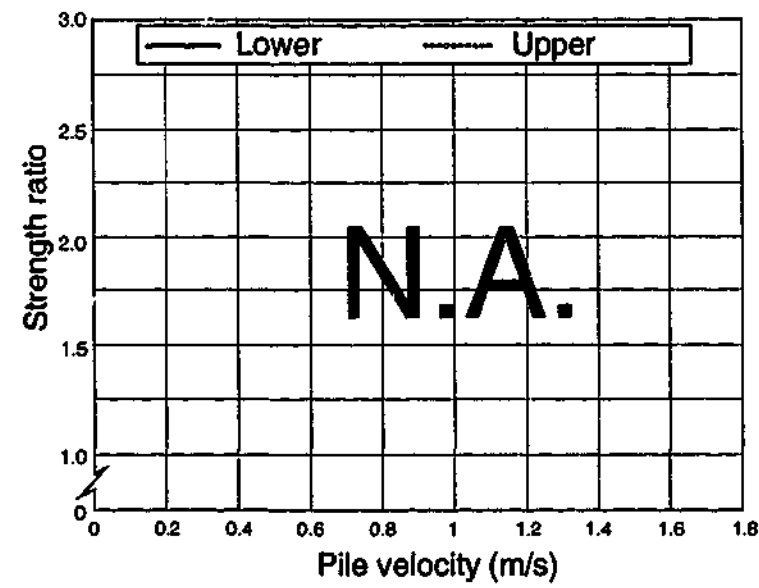
Figure 7.30 BallR($\sigma'_p=500\text{kPa}$)-Smooth Concrete: Strength ratio-velocity responses at normal stresses of (a) 250kPa (b) 150kPa (c) 60kPa



(a)

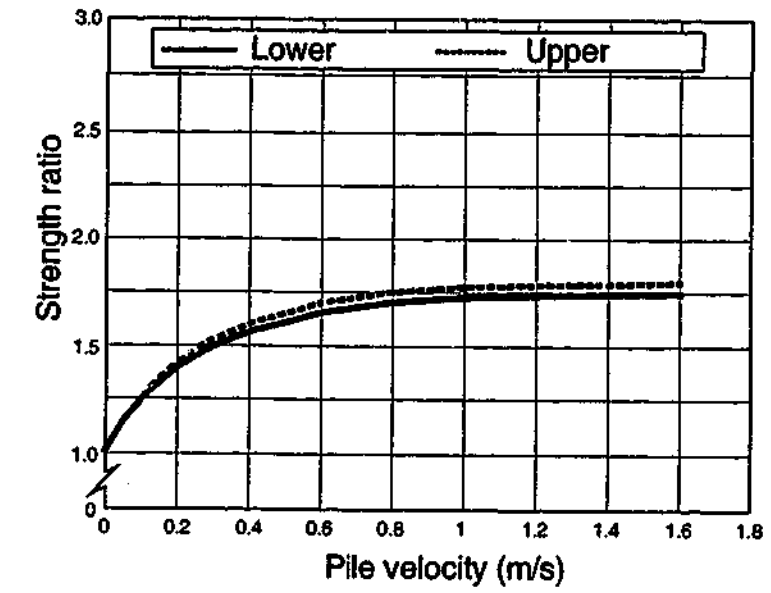


(b)

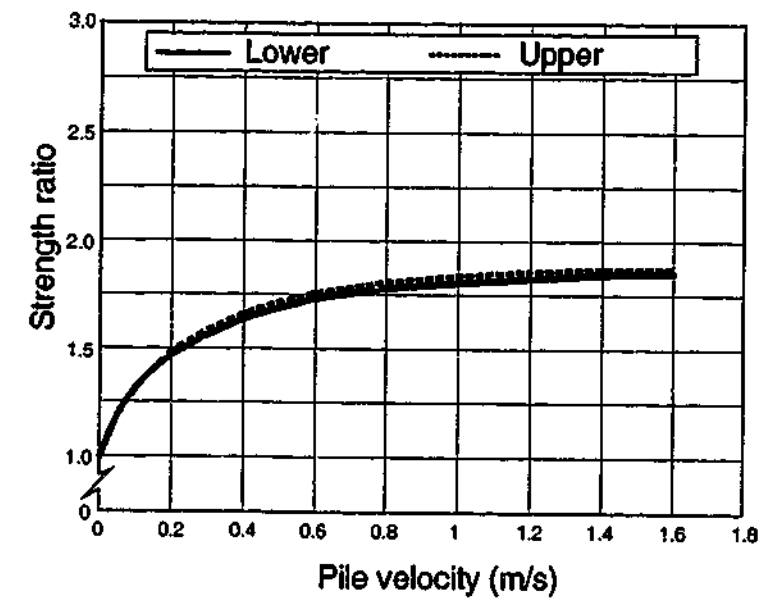


(c)

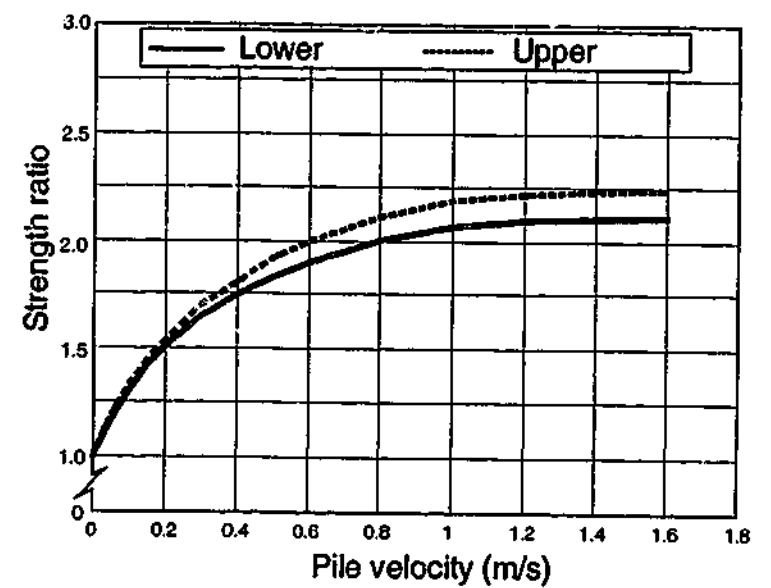
Figure 7.31 BallR($\sigma'_p=325\text{kPa}$)-Wetted Steel: Strength ratio-velocity responses at normal stresses of (a) 250kPa (b) 150kPa (c) 60kPa



(a)

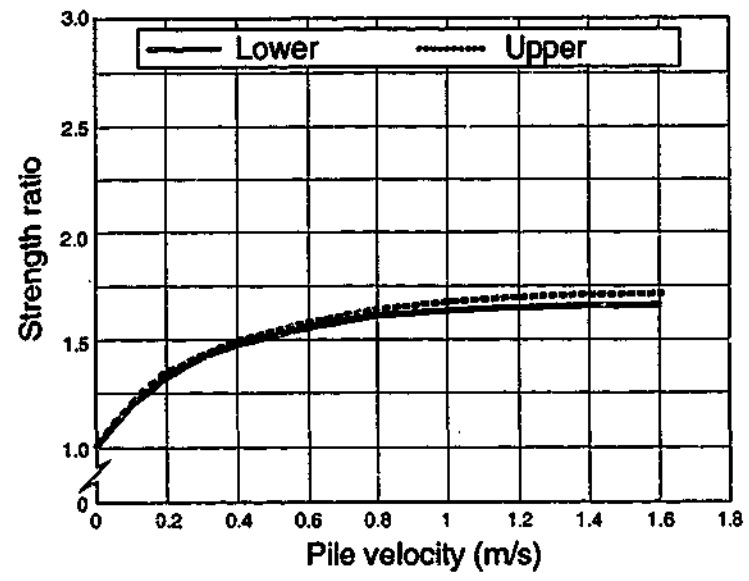


(b)

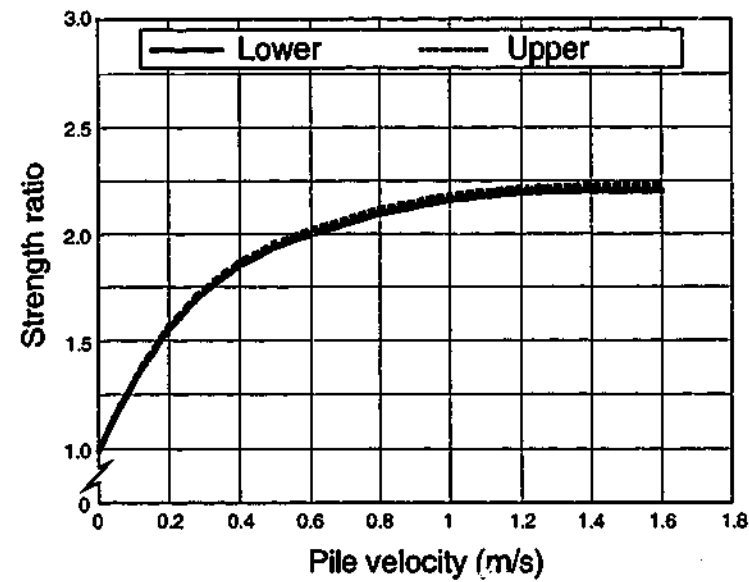


(c)

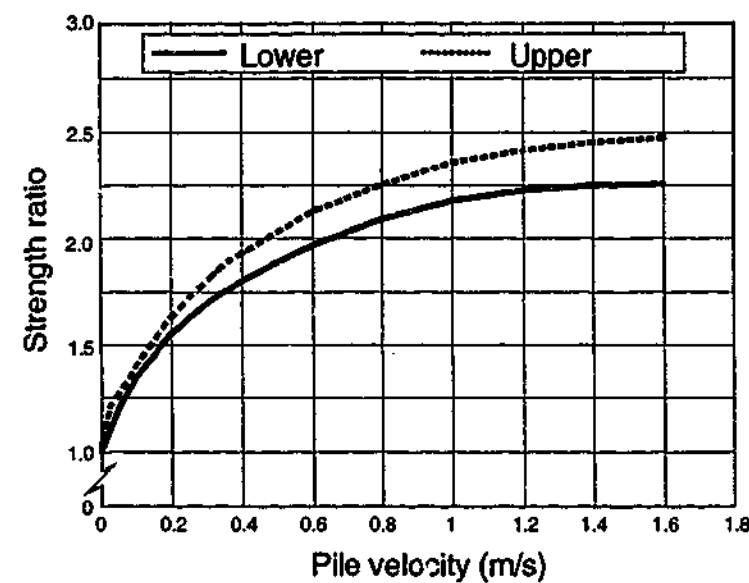
Figure 7.32 BallR($\sigma'_p=500\text{kPa}$)-Wetted Steel: Strength ratio-velocity responses at normal stresses of (a) 250kPa (b) 150kPa (c) 60kPa



(a)

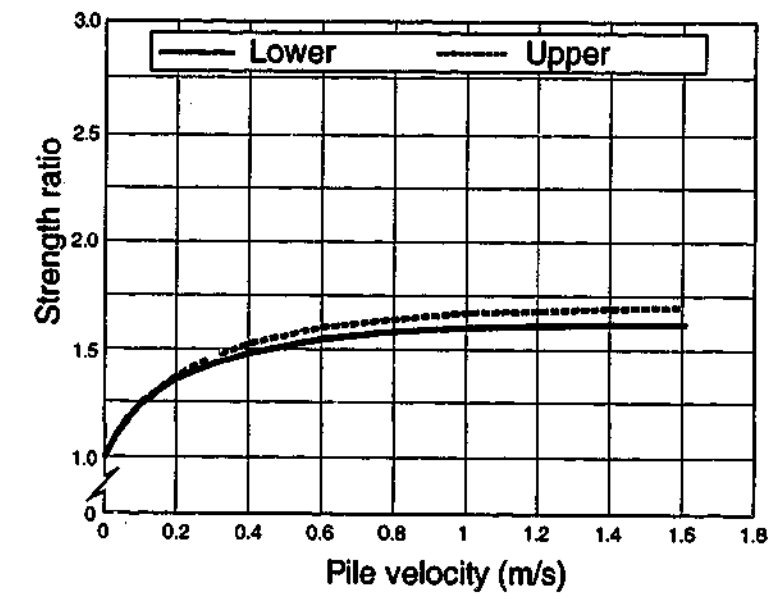


(b)

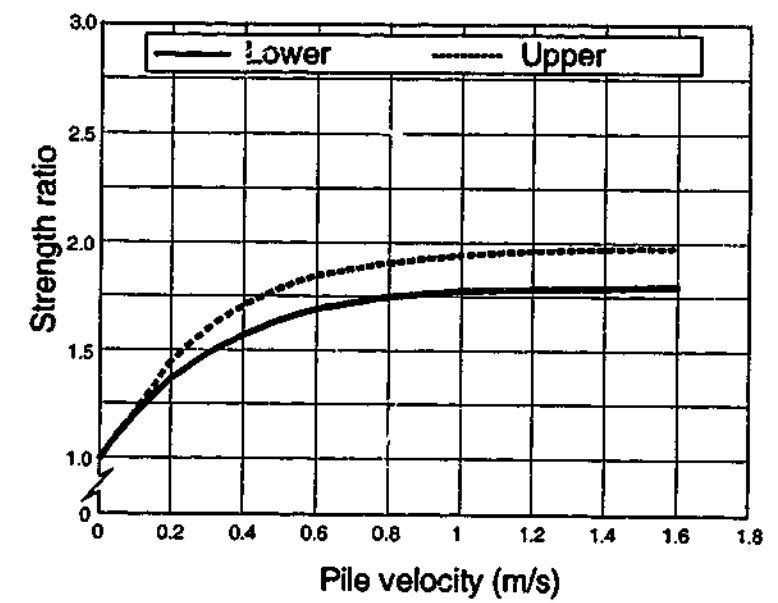


(c)

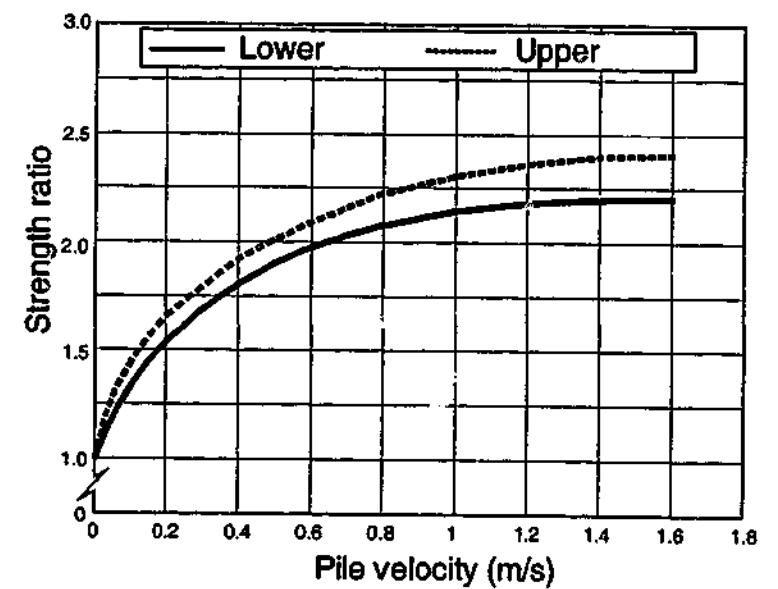
Figure 7.33 BallR($\sigma'_p=325\text{kPa}$)-Wetted Smooth Concrete: Strength ratio-velocity responses at normal stresses of (a) 250kPa (b) 150kPa (c) 60kPa



(a)

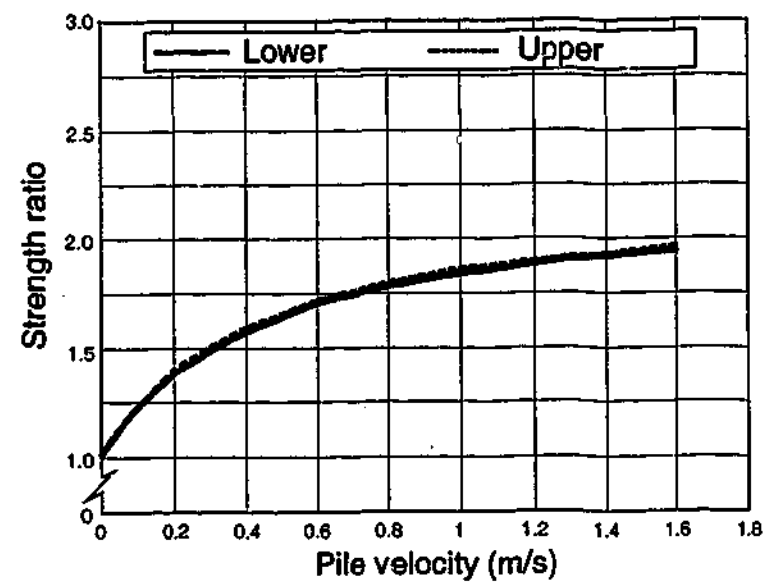


(b)

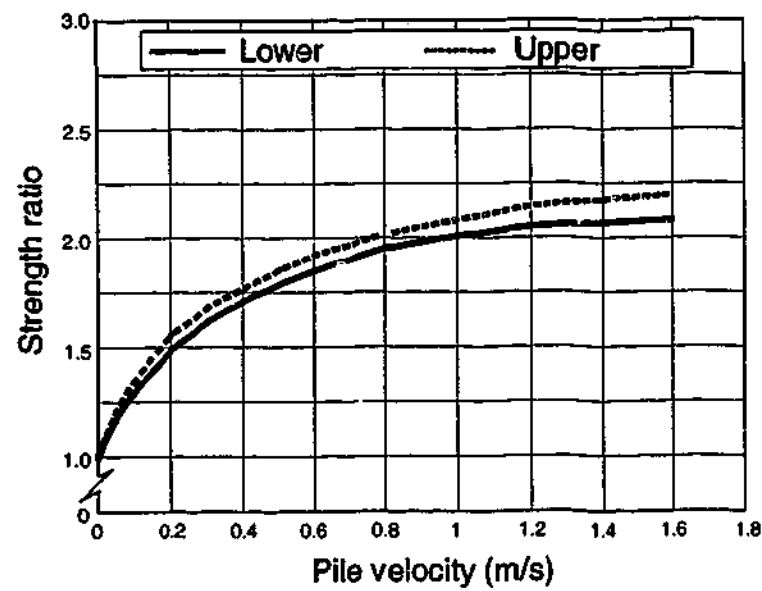


(c)

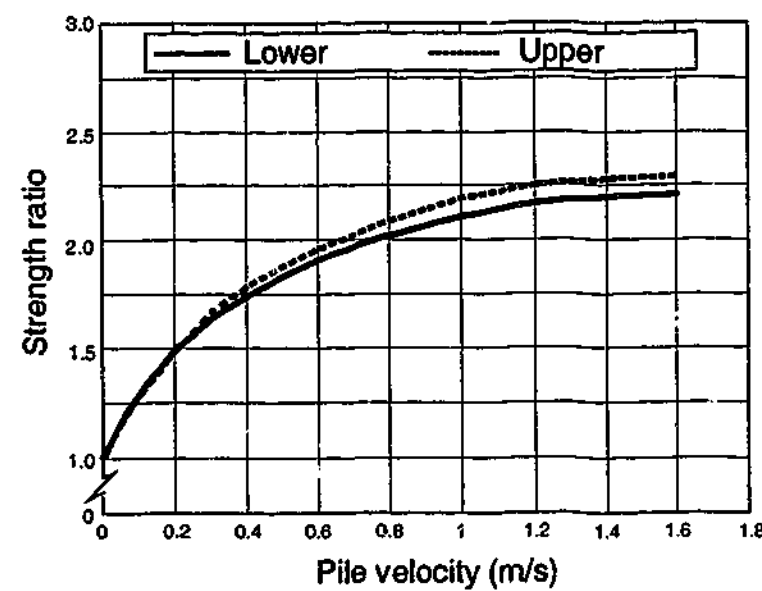
Figure 7.34 BallR($\sigma'_p=500\text{kPa}$)-Wetted Smooth Concrete: Strength ratio-velocity responses at normal stresses of (a) 250kPa (b) 150kPa (c) 60kPa



(a)

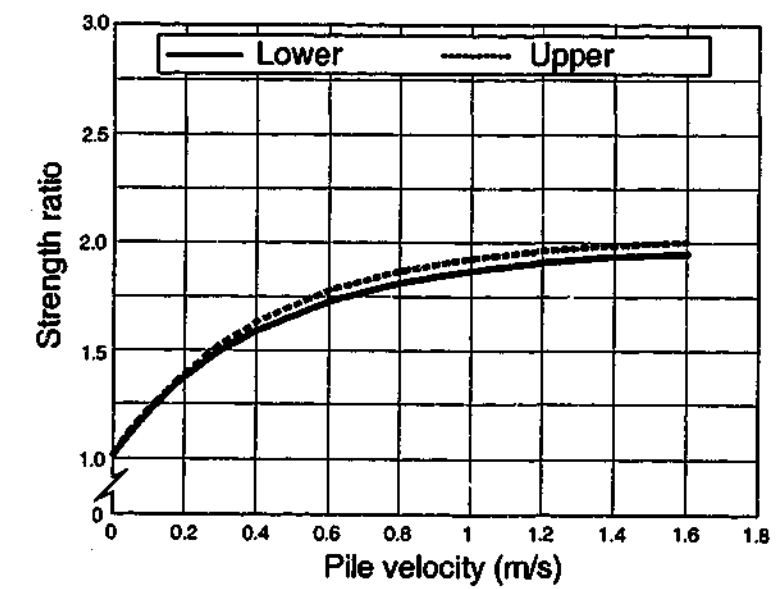


(b)

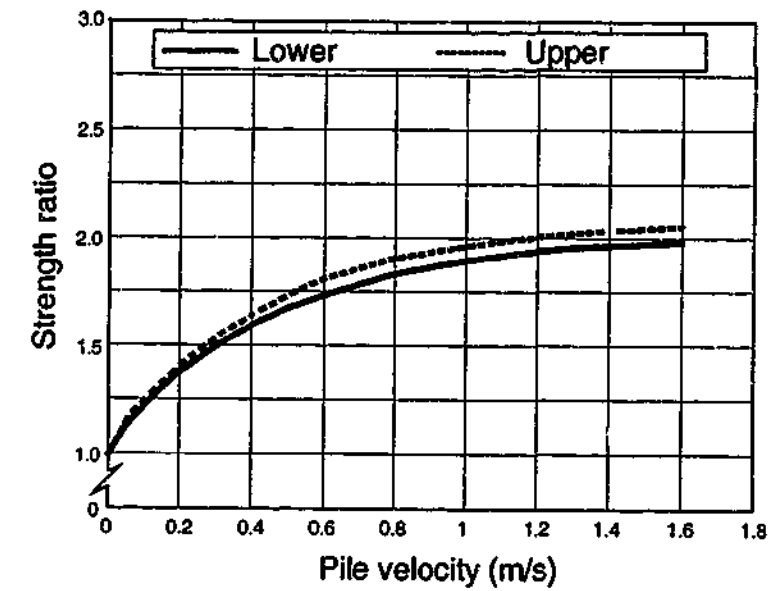


(c)

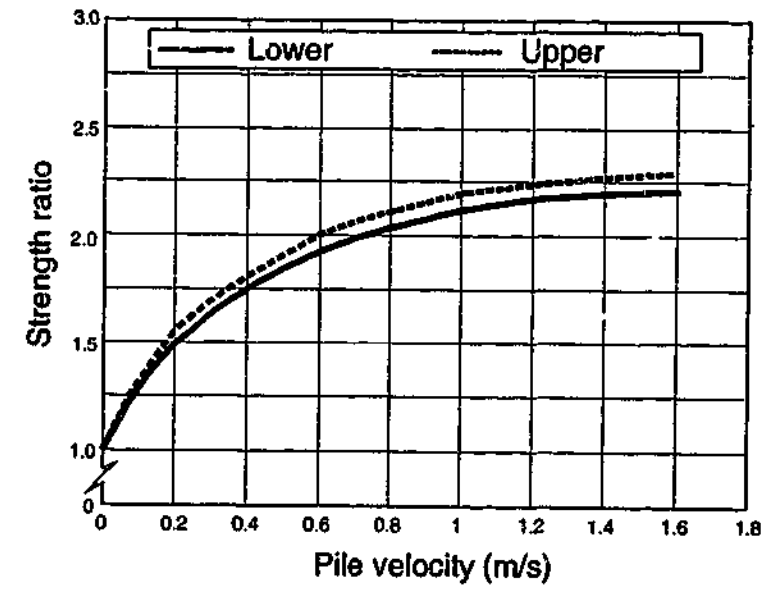
Figure 7.35 BallR/Talc($\sigma'_p=325\text{kPa}$)-Steel: Strength ratio-velocity responses at normal stresses of (a) 250kPa (b) 150kPa (c) 60kPa



(a)



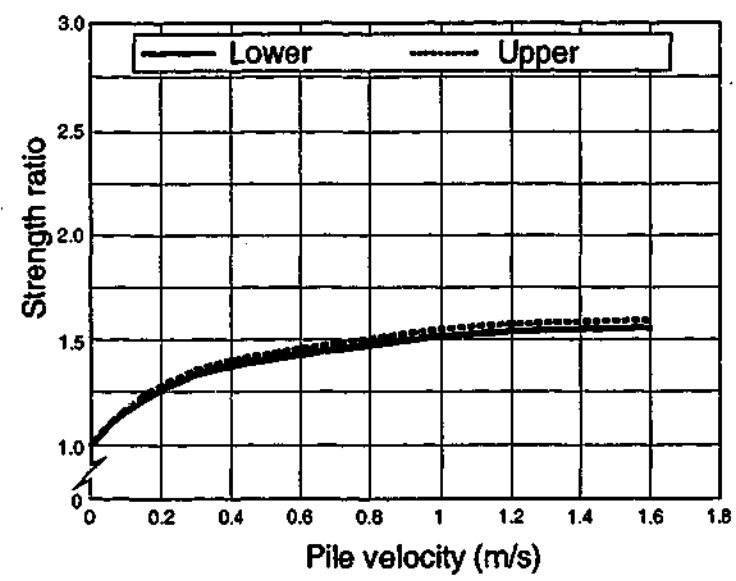
(b)



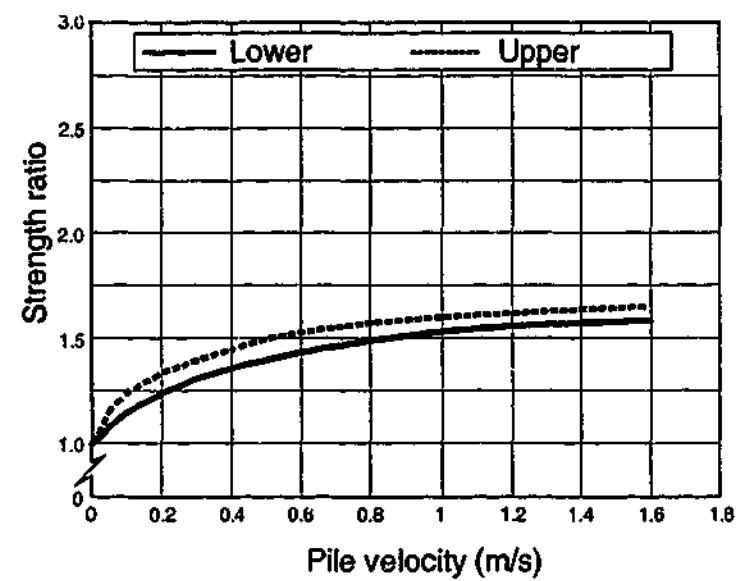
(c)

Figure 7.36 BallR/Talc($\sigma'_p=500\text{kPa}$)-Steel: Strength ratio-velocity responses at normal stresses of (a) 250kPa (b) 150kPa (c) 60kPa

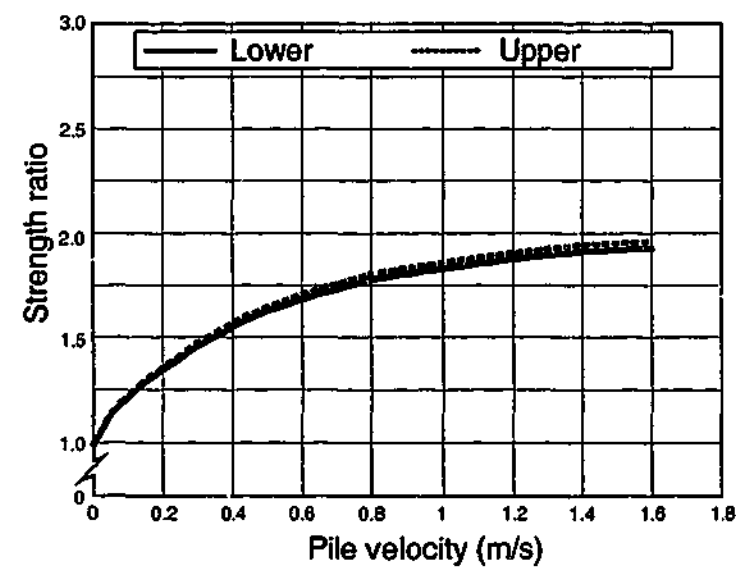
7.7.3.2 Mode 2 interface shear failure



(a)

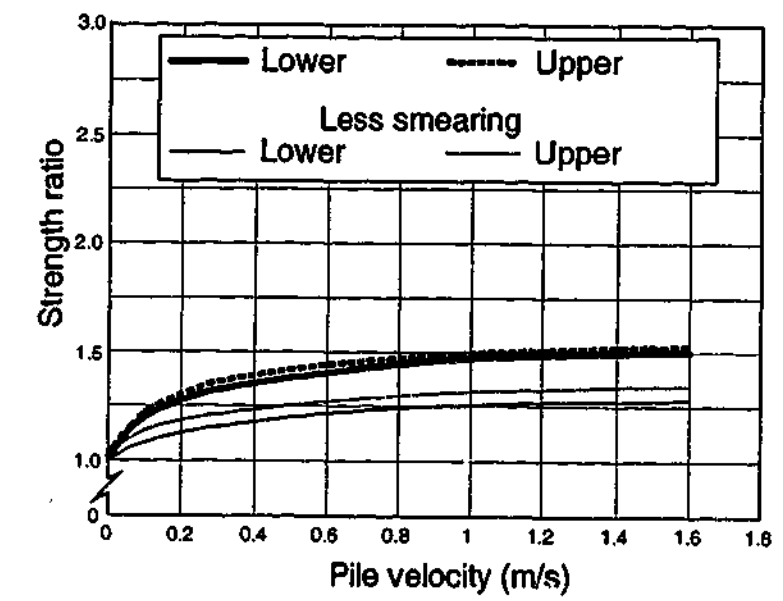


(b)

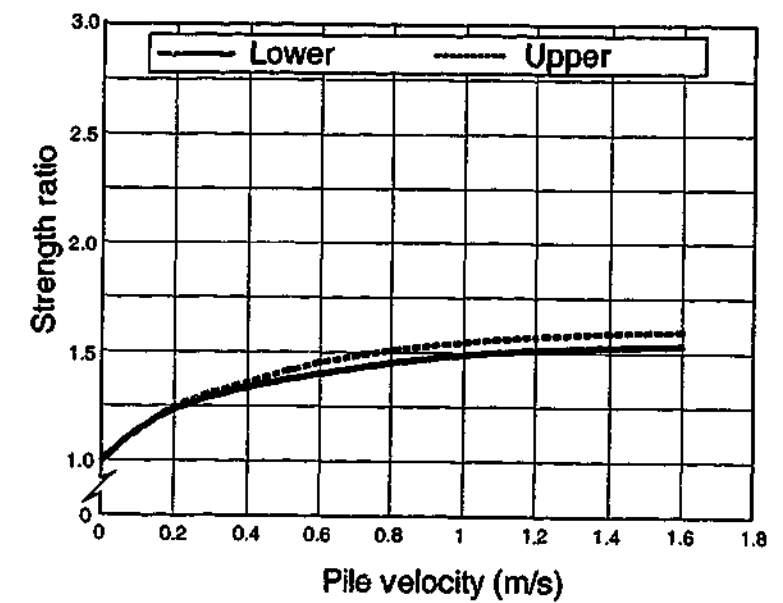


(c)

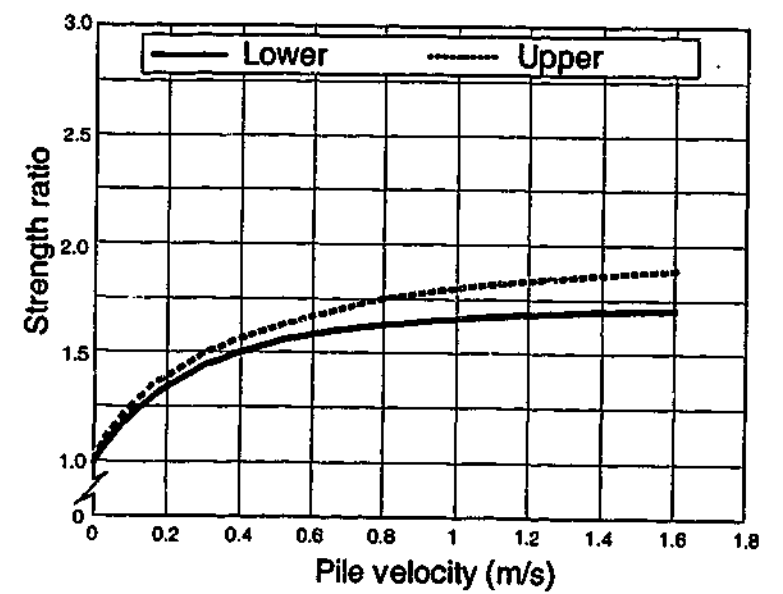
Figure 7.37 BallR($\sigma'_p=325\text{kPa}$)-Rough concrete: Strength ratio-velocity responses at normal stresses of (a) 250kPa (b) 150kPa (c) 60kPa



(a)

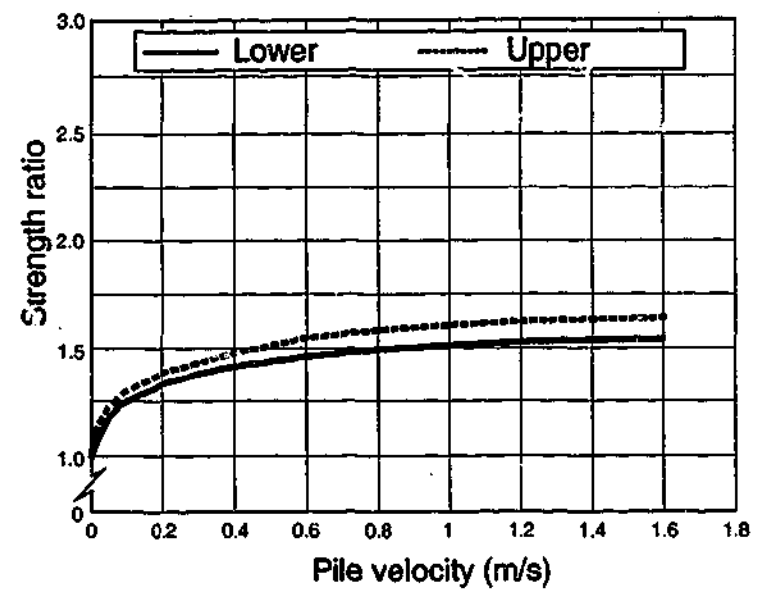


(b)

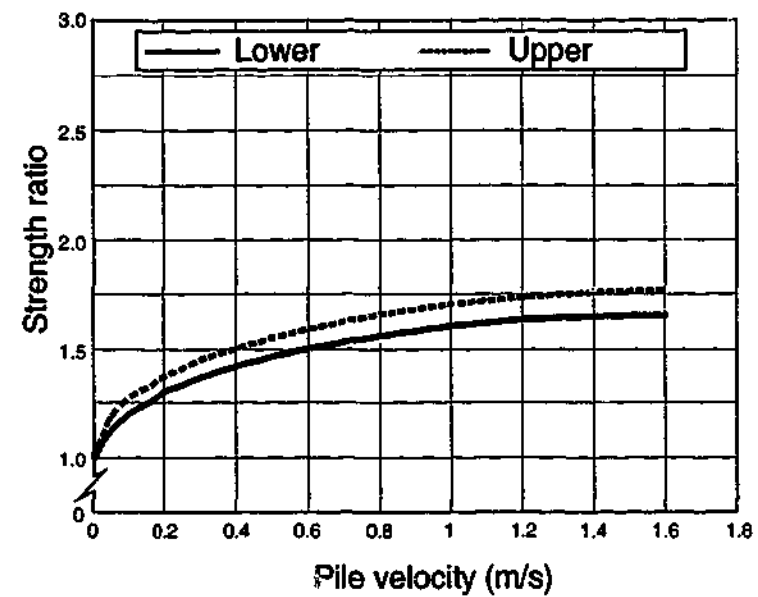


(c)

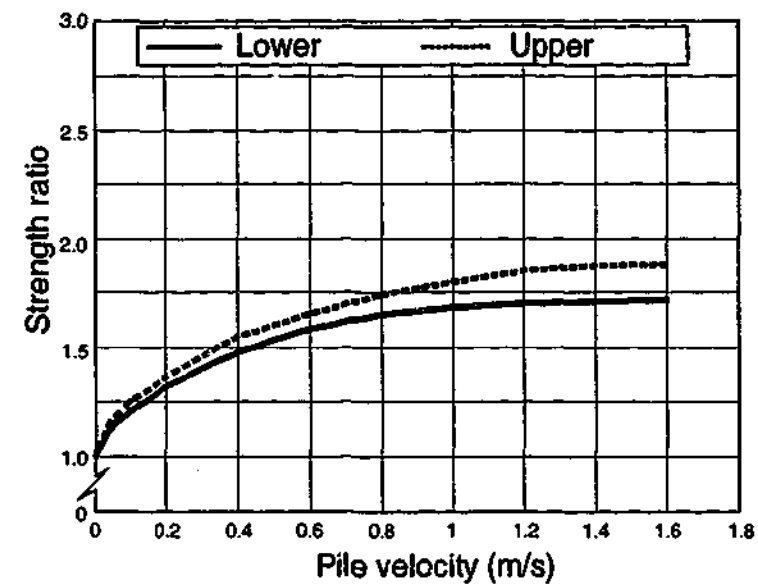
Figure 7.38 BallR($\sigma'_p=500\text{kPa}$)-Rough concrete: Strength ratio-velocity responses at normal stresses of (a) 250kPa (b) 150kPa (c) 60kPa



(a)

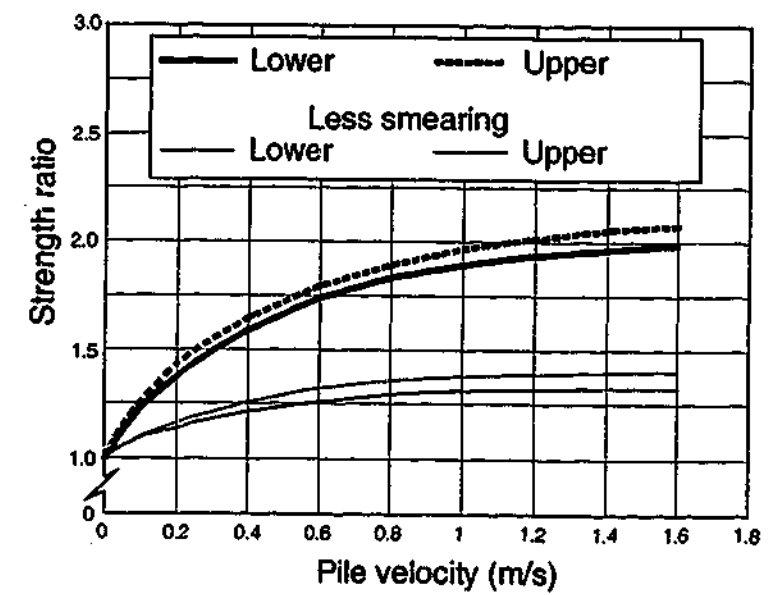


(b)

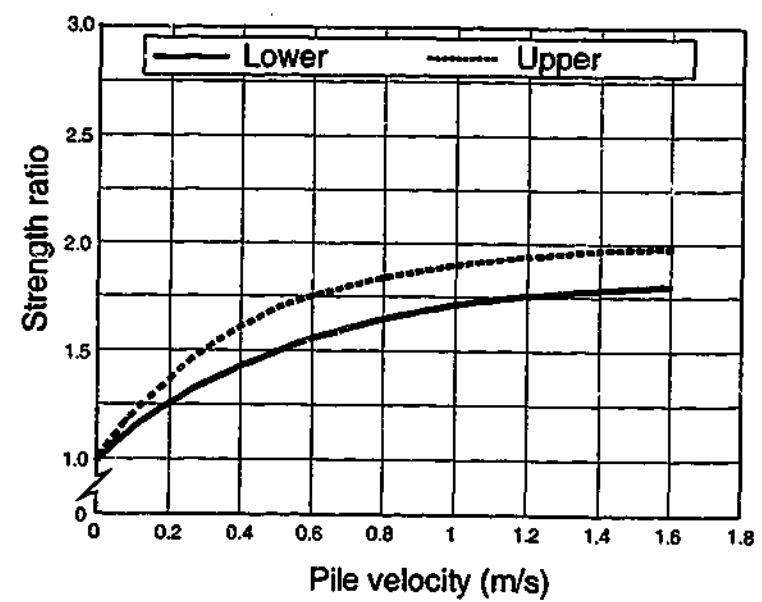


(c)

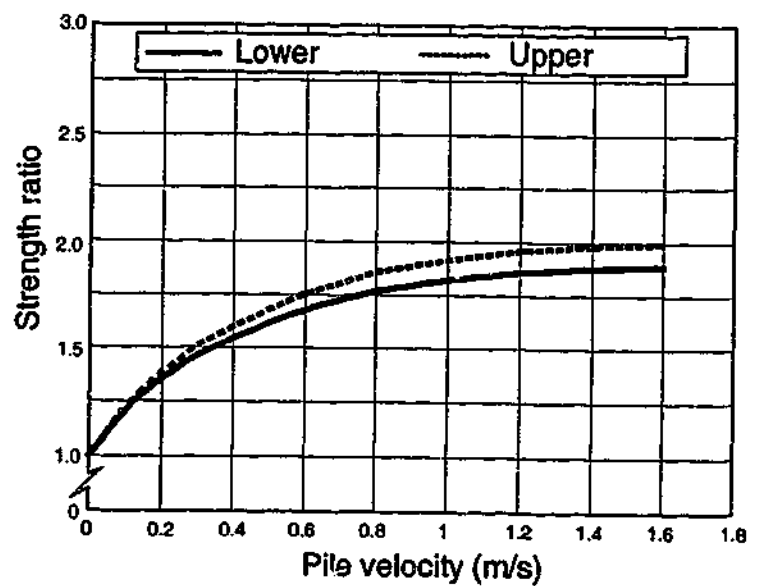
Figure 7.39 BallR($\sigma'_p=325\text{kPa}$)-Wetted Rough concrete: Strength ratio-velocity responses at normal stresses of (a) 250kPa (b) 150kPa (c) 60kPa



(a)



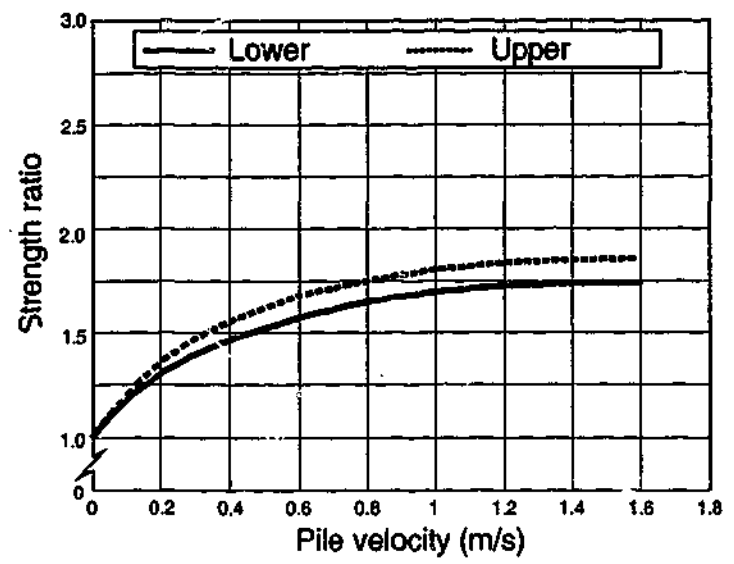
(b)



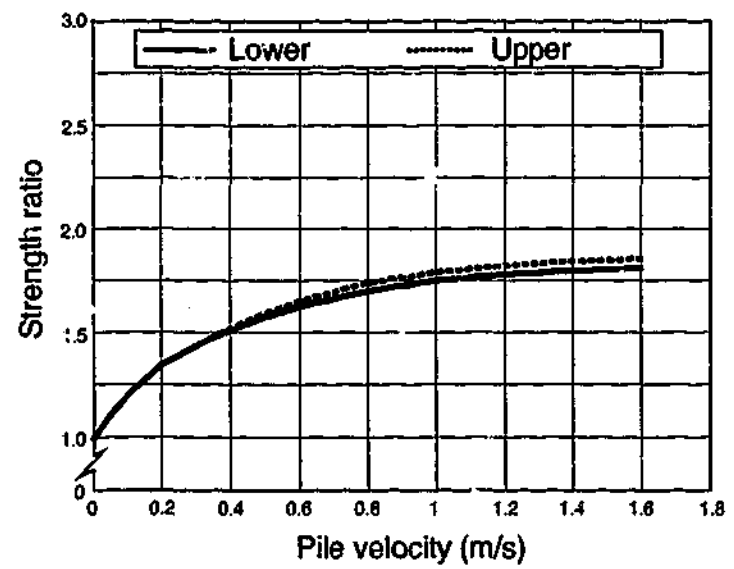
(c)

Figure 7.40 BallR($\sigma'_p=500\text{kPa}$)-Wetted Rough concrete: Strength ratio-velocity responses at normal stresses of (a) 250kPa (b) 150kPa (c) 60kPa

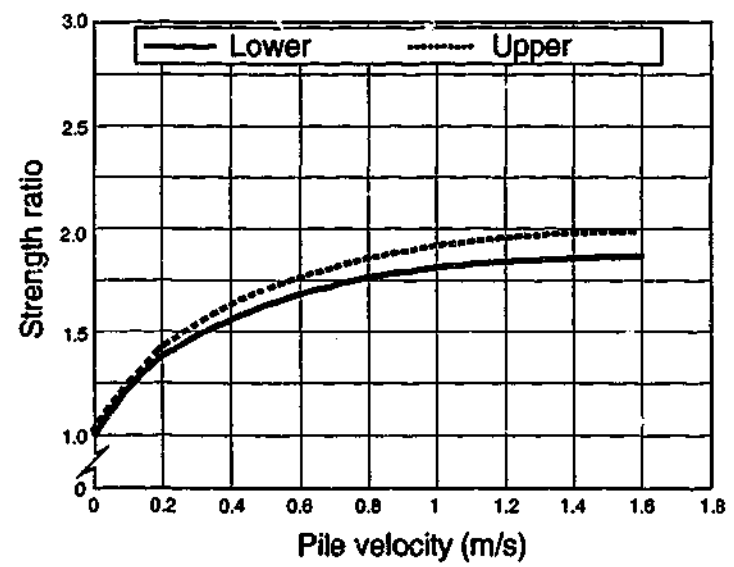
7.7.3.3 Mode 3 interface shear failure



(a)

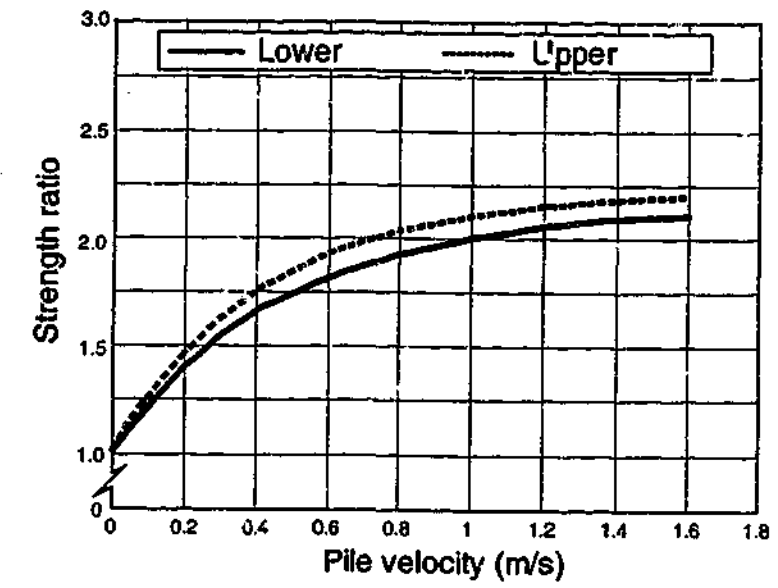


(b)

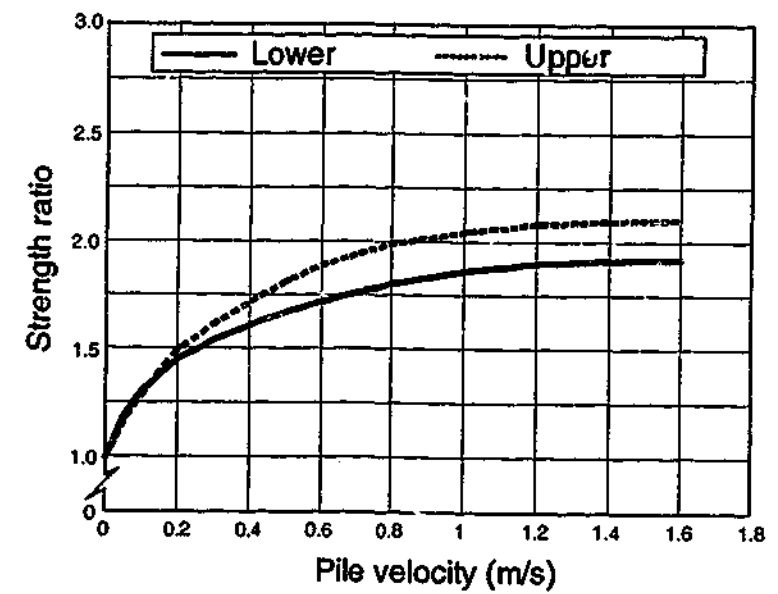


(c)

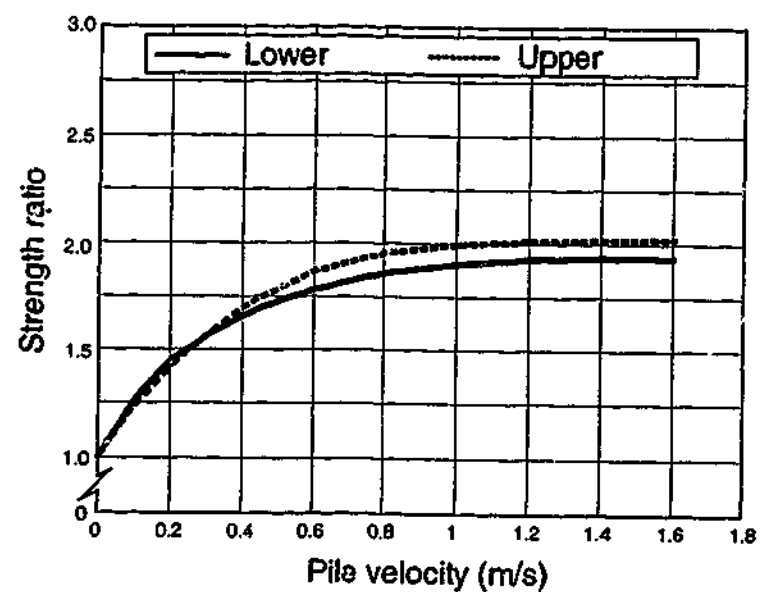
Figure 7.41 HR1F($\sigma'_p=325\text{kPa}$)-Steel: Strength ratio-velocity responses at normal stresses of (a) 250kPa (b) 150kPa (c) 60kPa



(a)



(b)



(c)

Figure 7.42 HR1F($\sigma'_p=500\text{kPa}$)-Steel: Strength ratio-velocity responses at normal stresses of (a) 250kPa (b) 150kPa (c) 60kPa

7.7.3.4 Discussion

As indicated by the upper and lower bounds, the strength ratio-velocity responses associated with the three consecutive tests have been found in most tests to vary from each other in the magnitude of the strength ratio. However, all the responses have the same functional form.

It should be noted that the variation in the three responses is in general not significant for all the interfaces regardless of the failure mode with the exception of the first few tests conducted for the interface failing in Mode 2. The slight variation in the magnitude of the strength ratio for the same boundary condition is understandable given the changes in the sample and hence in the quasi-static friction due to remoulding of the sample and shear-induced excess pore pressures in the shear zone of the sample. However, analyses of the strength ratio-velocity responses could not establish the effects of increased remoulding as well as increased excess pore pressures on the dynamic response. Possible reasons for this are as follows:

- The increased remoulding of the sample and the increased excess pore pressure may have conflicting effects on the strength ratio-velocity responses. Since these effects occur concurrently, the sum of the effects may be inconsistent.
- The effect of increased remoulding of the sample and increased excess pore pressure may be small on the strength ratio-velocity responses. Since the computation of quasi-static friction introduces a percentage of error, the small effect due to the remoulding and excess pore pressure on the strength ratio-velocity responses may not be discernible.

As mentioned earlier, for the interface with Mode 2 shear failure, the strength ratio-velocity responses vary significantly during the first few test cycles of the interface. The strength ratio associated with the response was found to decrease substantially as further tests were performed (whose exact responses will be presented in the next chapter). The variation is due, in addition to the remoulding and pore pressure effects, to the drastic changes in the physical characteristics of the interface during the first few tests. During the first few tests, the rough pile surface was observed to change from being lightly smeared in the first test to being more heavily smeared in

the third test. In order to investigate the effect of smearing, two out of the four series of tests involving Mode 2 were tested more extensively. For these two series of tests, shear tests at 250kPa normal stress were repetitively performed until the amount of smearing was visually observed to stabilise. Analyses of the friction-velocity response showed that as more tests were performed, the response became more consistent, indicating that the variation is due to the amount of smearing. The effect of the smearing of the pile surface on the strength ratio-velocity response will be discussed in more detail in the next chapter.

It is sufficient at this stage to note that:

- the strength ratio-velocity responses have a similar form such that they can be described by a common mathematical function
- the particular value of the viscous damping parameter α is highly dependent on the type of interface being tested, namely the specimen and the pile surface, and the applied normal stress.

The effects of various parameters on the strength ratio-velocity relationship or the value of the viscous damping parameter α of a particular interface will be discussed in the next chapter.

7.8 Fitting the Strength Ratio-Velocity Response

In attempting to find a suitable function for modelling the strength ratio-velocity data obtained in this study, various mathematical functions were used to fit the data. The suitability of the various functions in modelling the salient features of the strength ratio-velocity relationship is discussed in this section.

The power law with exponent 0.45 and the *inverse sinh* were used to fit a set of typical experimental data as shown in Figure 7.43. The power law with $N=0.45$ and the *inverse sinh* both model the salient features of the data up to 0.8m/s. However both functions give excessively high strength ratios for velocities greater than 0.8m/s.

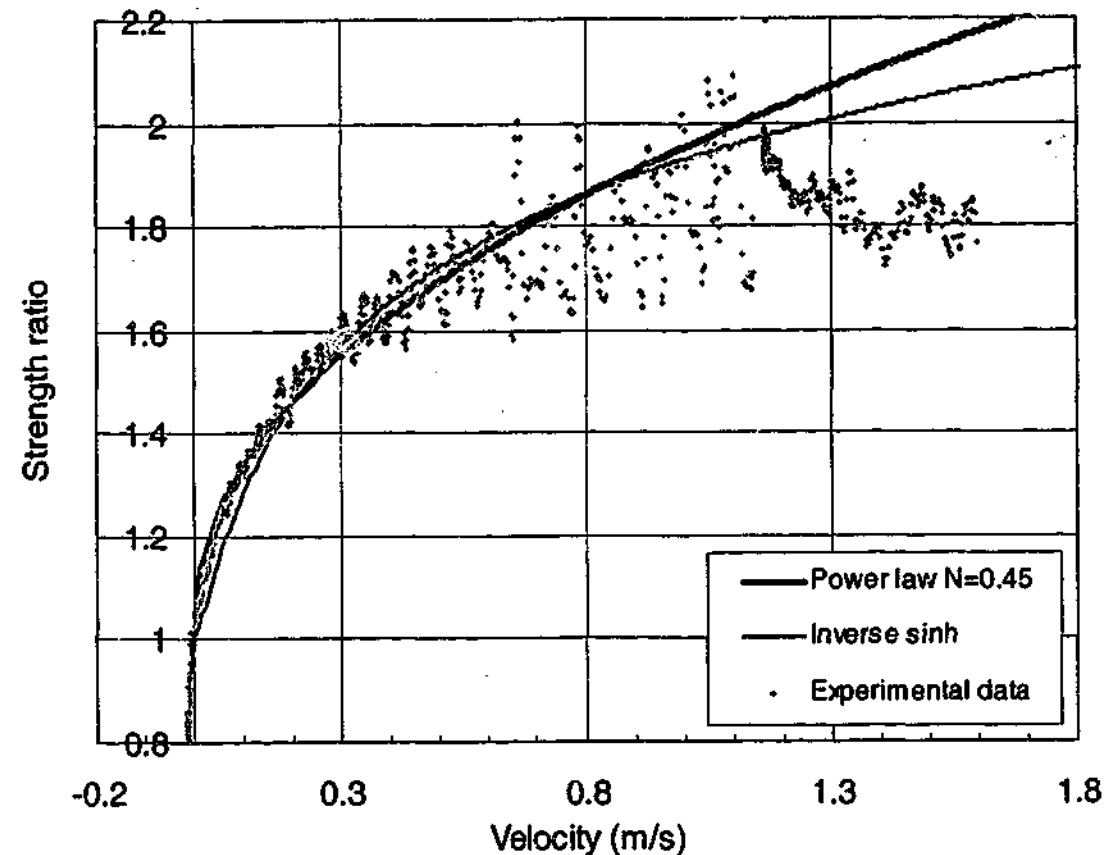


Figure 7.43 Fitting of strength ratio-velocity relationship data with *inverse sinh* function and power law with exponent 0.45

The *tanh* function and exponential function of the form, $\alpha(1-e^{-\beta v})$ were used to fit a set of typical experimental data as shown in Figure 7.44. Overall, both functions fit the data over the relevant range of velocities reasonably well. However, compared to the power law with $N=0.45$, the exponential function does not fit the data up to 0.3m/s as well and the *tanh* function does not fit the data between 0.3m/s and 0.8m/s as well. It is also noted that the *tanh* function models an almost constant strength ratio beyond a velocity of 1.6m/s, whilst the exponential function models a slightly increasing strength ratio in the same velocity range.

Although the numerical difference between the strength ratio values modelled by the two functions is probably not of practical significance, it is important to ascertain the characteristics of the curve beyond 1.6m/s for the sake of theoretical correctness especially given that the peak velocities associated with pile-driving events are higher than the 1.6m/s available from the test data. Benamar and his co-workers' test data (Benamar et al., 1991, 1992; Benamar, 1999) presented in Section 3.5.4, which

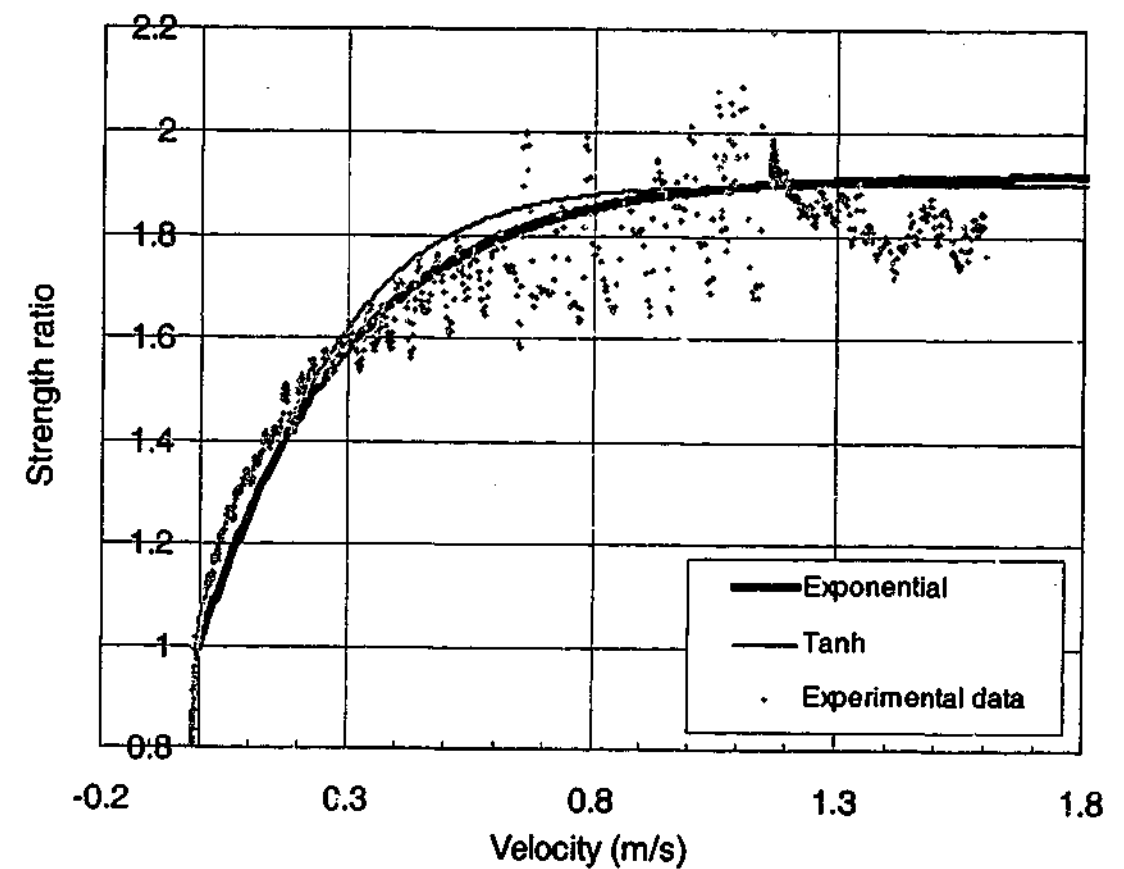


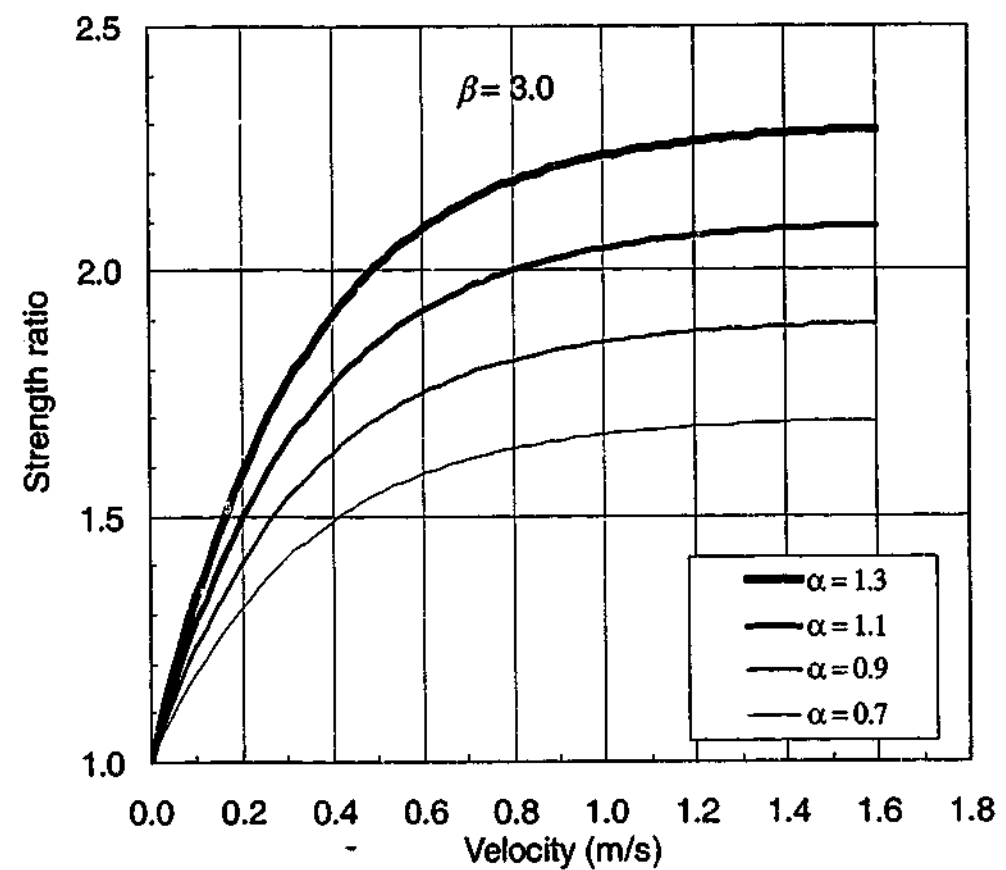
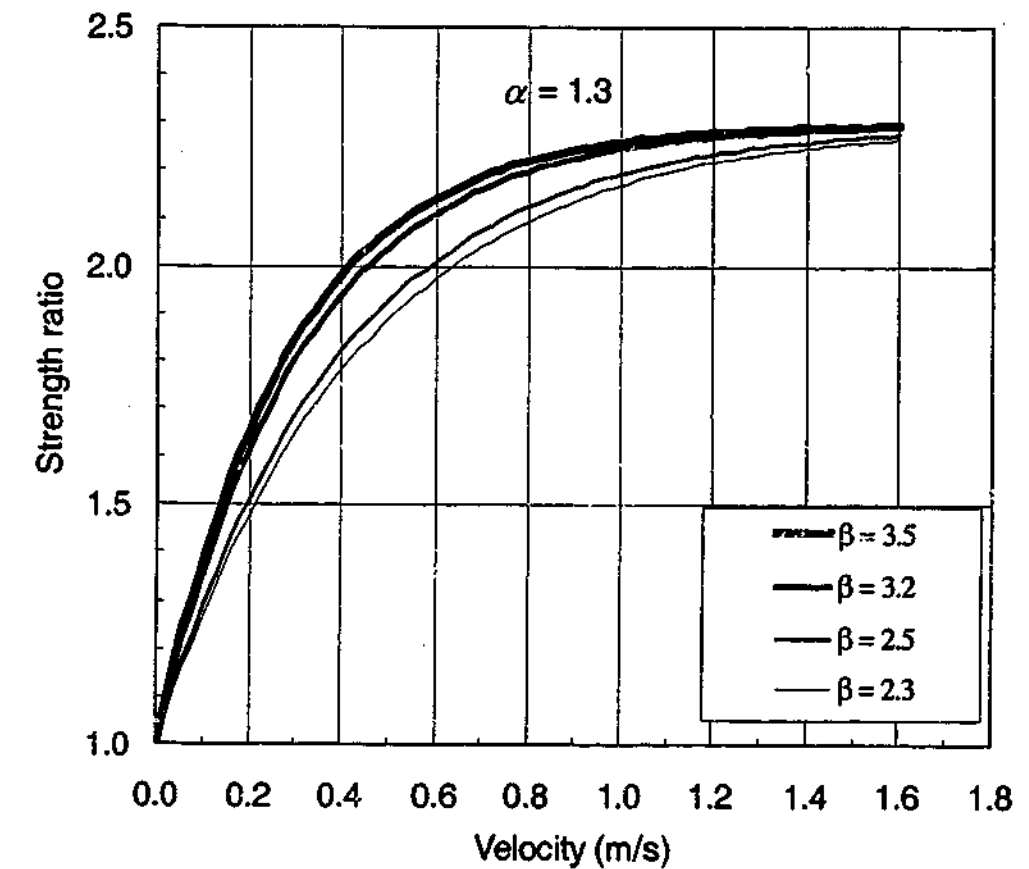
Figure 7.44 Fitting of strength ratio-velocity relationship data with hyperbolic tangent and exponential functions

involved pile velocities up to 2.0m/s, give an indication of the response beyond the 1.6m/s. Their experimental set-up appears to be suitable for studying the pile-soil interface, as has been discussed in Section 3.5.4. The data from Benamar and his co-workers indicate that there is a very small increase in the rate of increase of the friction with velocity which can be modelled using the same exponential function under consideration. Thus, the exponential function appears to be more suitable than the *tanh* function for fitting the experimental data.

The exponential function is a simpler function compared to the *tanh* function in that the effects of the variation in the values of its parameters (i.e. α and β) on the response are more obvious.

Based on these considerations, the exponential function was selected for fitting the experimental data obtained in this study.

It is noted that for the selected exponential function of the form $\alpha(1-e^{-\beta v})$, the parameter α is unitless whilst β has the unit [s/m]. To appreciate the influence of α and β values on the characteristics of the curve, curves are plotted based on the range of α and β values used to fit the experimental data. The magnitude of α for a fixed β value controls the magnitude of the ratio, as shown in Figure 7.45. Hence for a fixed β , the parameter α is a quantitative measure of the magnitude of the strength ratio. For a fixed α , the magnitude of β value dictates the gradient of the strength ratio at the near-zero velocity and at higher velocities (1.0m/s to 1.6m/s), as shown in Figure 7.46. The higher the value of β , the steeper the gradient at near-zero velocity and the flatter the gradient at higher velocities.

Figure 7.45 Influence of α on the magnitude of the ratioFigure 7.46 Influence of β on the shape of the curve

As mentioned previously, there were lower bound and upper bound responses for a particular interface tested at a certain normal stress. Given that the band of responses is relatively small, the average response has been fitted with the exponential function. The α and β parameters used to fit the response of the various interfaces are denoted by the subscript "o" (i.e. α_o and β_o), and are summarised for each of the interfaces in Table 7.6. It has been found that the value of β_o for a particular interface varies slightly depending on the boundary conditions imposed on the interface; therefore, for practicality, the value of β_o is fixed at an average representative value for the particular interface.

As can be noted in Table 7.6, the value of β_o varies more significantly across different interfaces; however, it can be noted, within the experimental accuracy of the tests, there is not any obvious relationship between β_o and any of the pile-soil parameters (i.e. type of clay, pile roughness, preconsolidation stress, normal stress).

Table 7.6 Values of the original α_o and β_o values for various interfaces

Clay	Pile surface	Normal stress (kPa)	Original	
			α_o [-]	β_o [s/m]
BallR ($\sigma_p=500$ kPa)	Steel	250	0.73	3.0
		150	1.20	
		60	1.70	
BallR ($\sigma_p=325$ kPa)	Steel	250	0.91	3.0
		150	1.15	
		60	1.70	
BallR ($\sigma_p=500$ kPa)	Smooth concrete	250	1.20	3.0
		150	1.20	
		60	1.58	
BallR ($\sigma_p=325$ kPa)	Smooth concrete	250	1.16	3.0
		150	1.22	
		60	1.60	
BallR ($\sigma_p=500$ kPa)	Rough concrete	250	0.51	3.0
		150	0.57	
		60	0.79	
BallR ($\sigma_p=325$ kPa)	Rough concrete	250	0.58	3.0
		150	0.60	
		60	0.95	
BallR ($\sigma_p=500$ kPa)	Wet steel	250	0.78	3.5
		150	0.87	
		60	1.17	
BallR ($\sigma_p=325$ kPa)	Wet steel	250	0.55	3.5
		150	0.93	
		60	-	
BallR ($\sigma_p=500$ kPa)	Wet smooth concrete	250	0.67	3.5
		150	0.89	
		60	1.30	
BallR ($\sigma_p=325$ kPa)	Wet smooth concrete	250	0.69	3.5
		150	1.20	
		60	1.35	
BallR ($\sigma_p=500$ kPa)	Wet rough concrete	250	0.90	2.5
		150	0.93	
		60	0.95	
BallR ($\sigma_p=325$ kPa)	Wet rough concrete	250	0.65	2.5
		150	0.75	
		60	0.88	
BallR/Talc ($\sigma_p=500$ kPa)	Steel	250	1.01	2.3
		150	1.05	
		60	1.29	
BallR/Talc ($\sigma_p=325$ kPa)	Steel	250	0.97	2.3
		150	1.14	
		60	1.28	
HR1F ($\sigma_p=500$ kPa)	Steel	250	0.84	2.5
		150	0.84	
		60	0.94	
HR1F ($\sigma_p=325$ kPa)	Steel	250	1.15	2.5
		150	1.04	
		60	1.00	

In order to compare the dynamic responses of different interfaces (with different β_o values), it was desirable to fix the value of β_o with an average representative value of 3.0 so that only the α parameter was used in the analyses of the effects of various parameters on the dynamic response. In order to differentiate the two sets of parameters, these newly defined parameters were simply represented by α and β . The parameter α is henceforth termed the viscous damping parameter or the exponential damping factor. For practical purposes, the values of α_o and α are the same for the range of β_o values encountered. The values of α and β for each interface are summarised in Table 7.7.

Table 7.7 Values of the averaged α and β values for various interfaces

Clay	Pile surface	Normal stress (kPa)	Averaged	
			α [-]	β [s/m]
BallR ($\sigma_p=500$ kPa)	Steel	250	0.73	3.0
		150	1.20	
		60	1.70	
BallR ($\sigma_p=325$ kPa)	Steel	250	0.91	3.0
		150	1.15	
		60	1.70	
BallR ($\sigma_p=500$ kPa)	Smooth concrete	250	1.20	3.0
		150	1.20	
		60	1.58	
BallR ($\sigma_p=325$ kPa)	Smooth concrete	250	1.16	3.0
		150	1.22	
		60	1.60	
BallR ($\sigma_p=500$ kPa)	Rough concrete	250	0.51	3.0
		150	0.57	
		60	0.79	
BallR ($\sigma_p=325$ kPa)	Rough concrete	250	0.58	3.0
		150	0.60	
		60	0.95	
BallR ($\sigma_p=500$ kPa)	Wet steel	250	0.78	3.0
		150	0.87	
		60	1.17	
BallR ($\sigma_p=325$ kPa)	Wet steel	250	0.55	3.0
		150	0.93	
		60	-	
BallR ($\sigma_p=500$ kPa)	Wet smooth concrete	250	0.67	3.0
		150	0.89	
		60	1.30	
BallR ($\sigma_p=325$ kPa)	Wet smooth concrete	250	0.69	3.0
		150	1.20	
		60	1.35	
BallR ($\sigma_p=500$ kPa)	Wet rough concrete	250	0.90	3.0
		150	0.93	
		60	0.95	
BallR ($\sigma_p=325$ kPa)	Wet rough concrete	250	0.65	3.0
		150	0.75	
		60	0.88	
BallR/Talc ($\sigma_p=500$ kPa)	Steel	250	1.01	3.0
		150	1.05	
		60	1.29	
BallR/Talc ($\sigma_p=325$ kPa)	Steel	250	0.97	3.0
		150	1.14	
		60	1.28	
HR1F ($\sigma_p=500$ kPa)	Steel	250	0.84	3.0
		150	0.84	
		60	0.94	
HR1F ($\sigma_p=325$ kPa)	Steel	250	1.15	3.0
		150	1.04	
		60	1.00	

7.9 A Comparison of Data from This Study & Data from Previous Studies

7.9.1 Functional form

In contrast to the exponential function proposed in this study, Heerema (1979), and Litkouhi and Poskitt (1980) (for two out of the three clays tested) found that the strength ratio-velocity relationship could be described using the power law with exponent 0.2. However, a gradually increasing strength ratio at near-zero velocities similar to that found in this study has been reported by a number of other researchers. Coyle et al. (1972), who conducted extensive field tests on 11 sites using a 60mm-diameter pile, concluded that the proposed power law with exponent 0.2 suggested by Coyle and Gibson (1970) could not model the pile tip data and that N was equal to 0.35, indicating a more gradual response comparable to that found in this study. Dayal and Allen (1975) for all the four types of clay tested and Litkouhi and Poskitt (1980) for one out of the three types of clay tested found that the dynamic friction at near-zero velocity increased much more gradually than the power law with exponent 0.2.

Despite the different clays tested by Dayal and Allen (1975) and Litkouhi and Poskitt (1980), in all likelihood, the functional form of the dynamic friction-velocity relationship should be similar. It is logical to conclude that the different responses found by Dayal and Allen and Litkouhi and Poskitt, and by the author are due to the fundamental differences in the experimental techniques used by the two groups of researchers, as discussed in the following.

- The present study isolated the shaft response from the tip response such that no interaction between the shaft and the tip was allowed. In contrast, Litkouhi and Poskitt (1980) and Dayal and Allen (1975) performed penetrometer tests which by their nature did not allow the shaft-only response to be studied in isolation. Litkouhi and Poskitt (1980) found that the strength ratio increased dramatically at near-zero velocities whilst Dayal and Allen (1975) found that strength ratio increased only moderately at the same velocities but increased suddenly at a critical velocity such that responses before and after the critical velocity were completely different. The fact that the responses obtained by

Litkouhi and Poskitt (1980) and Dayal and Allen (1975) were significantly different suggests that the shaft response was strongly influenced by the tip responses.

- As has been discussed in Sections 3.5.2 and 3.5.3, data presented by Lithouki and Poskitt showed that the shaft friction continued to increase with depth and data presented by Heerema showed that the dynamic friction varied significantly even when the velocity was almost constant. Therefore, interpretation of the value of the dynamic friction (associated to the relevant velocity) is necessary. Since the strength ratio-velocity response presented by Heerema (1979), Litkouhi and Poskitt (1980) and Dayal and Allen (1975) was obtained from series of discrete constant velocity tests (each of which provided a single data point at the pertinent velocity), the relationship might have been affected by inaccurate interpretation of the value of the dynamic friction. In contrast, the strength ratio-velocity response proposed in the present study was obtained from continuous monitoring of a single shear event, which required no interpretation of the appropriate interface friction, and which enabled the direct association of interface friction with the corresponding velocity.
- The present study involved repetitive shearing of the pile-soil interface and hence involved remoulded clay as would be the case for both driven and drilled piles. In contrast, the studies by Litkouhi and Poskitt (1980) and Dayal and Allen (1975) involved once-off shearing of the pile-soil interface.

For the above reasons, it is believed that this study provides a more reliable indicator of the interface response of piles installed under field conditions.

In order to compare the functional form of the model (i.e. exponential function) found in this study with previous models (i.e. power law and linear model), the latter functions are used to fit a common set of data from the current study, as shown in Figure 7.47. Furthermore, to appreciate the quantitative difference of the power law and linear model relative to the exponential model for a particular velocity, the strength ratio given by the power law and strength ratio given by the linear model is divided by the strength ratio given by the exponential function. If the value of the

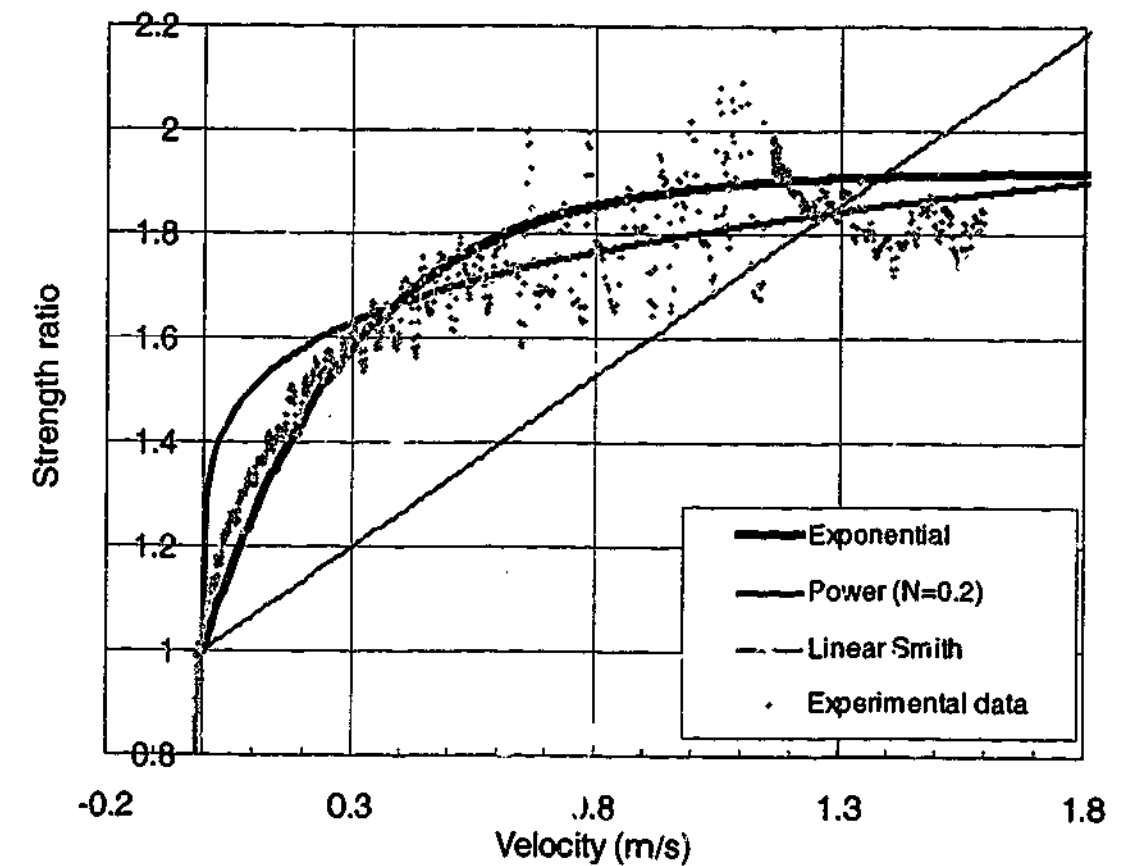


Figure 7.47 Power law with exponents 0.2 and exponential function used to fit a strength ratio-velocity response

resulting ratio is less than 1.0, the strength ratio given by the particular model is less than the strength ratio given by the exponential model, and if the value of the resulting ratio is greater than 1.0, the converse is true.

Clearly, the rate of increase of the strength ratio with velocity as modelled by the linear model and the power law is significantly different from that modelled by the exponential function. In the following section, the magnitude of the rate of increase of the strength ratio and the magnitude of the strength ratio of the power law and the linear model are discussed relative to those of the exponential model. As shown in Figure 7.48, the power law with exponent 0.2 gives a dramatic increase in the rate of increase of the strength ratio at near-zero velocities and thus severely overestimates the strength ratio at velocities less than 0.5m/s. It models a similar rate of increase of the strength ratio at velocities greater than 0.5m/s and thus models a comparable strength ratio. The linear model models a slower rate of increase of the strength ratio and thus severely underestimates the actual strength ratio at velocities less than about

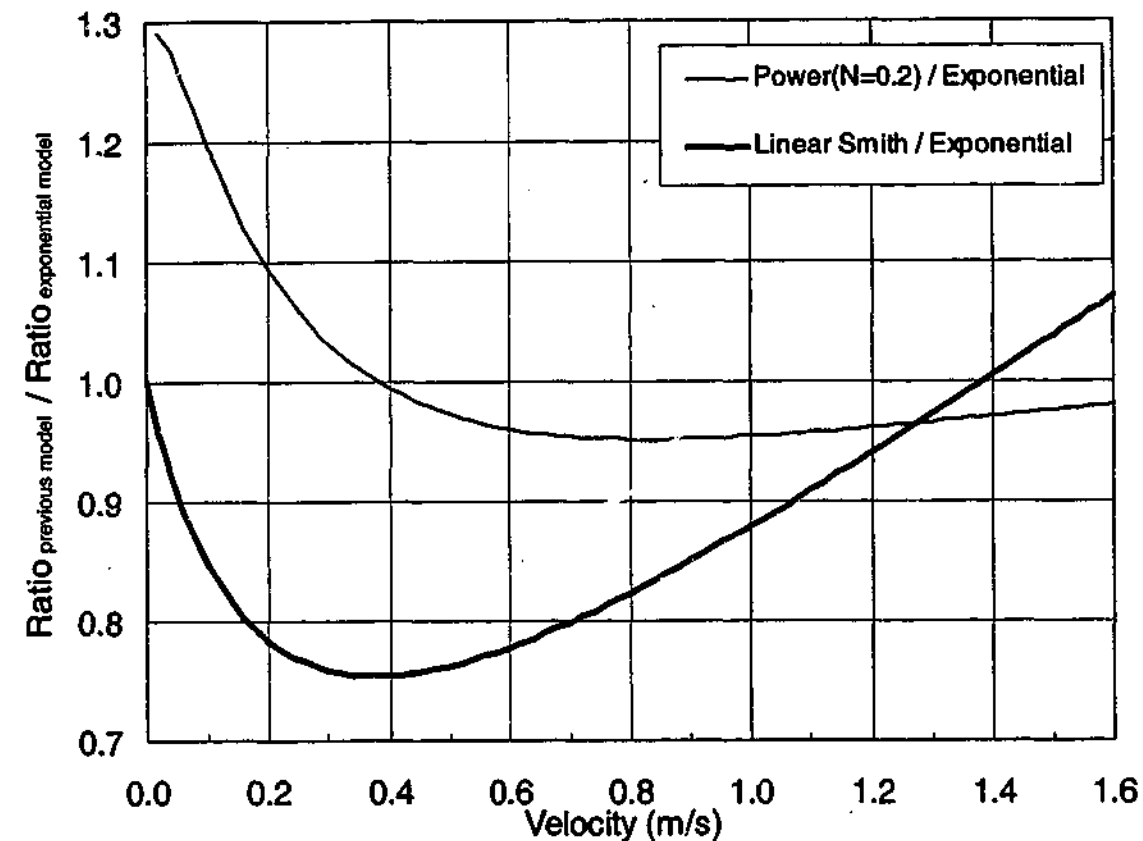


Figure 7.48 Comparison of functional form of strength ratio-velocity relationship given by the linear model and the power law model with exponent 0.2, relative to the exponential model

1.0m/s. It models a faster rate of increase of the strength ratio and thus significantly overestimates the actual strength ratio at velocities greater than 1.3m/s.

7.9.2 Magnitude of strength enhancement

The values of the strength ratio from the current study cannot be directly compared to those from previous studies because of significant differences in the following:

- The rate at which the quasi-static tests were performed;
- The normal stress at the interface;
- The type of clay tested (its mineralogy, plasticity) and the shear strength of the samples;
- The experimental methods and set-ups. The data obtained from penetrometer tests (Dayal and Allen, 1975; Litkouhi and Poskitt, 1980; Poskitt and Leonard, 1982) were influenced by the preceding tip penetration and perhaps scale effects; and

- The state of the clay specimen. The interface tested in this study involved remoulded clay whilst the interfaces tested in other studies involved undisturbed clay.

However, the reasonableness of the values of the strength ratios suggested by each of the studies can be assessed by comparing them to those back-calculated from typical monitoring and conventional analysis of dynamic pile testing events. Thus, the upper and lower bounds of the strength ratio-velocity relationships from signal-matching experience, from the current study and from a number of previous studies are plotted in Figure 7.49. The upper bound value of the linear damping factor recommended in CAPWAP for piles installed in clay is 1.3s/m. Since the lower bound value recommended in CAPWAP is intended for piles installed in sand, a lower bound value of 0.5s/m based on experience in signal-matching analyses is adopted in this exercise. For convenience, data from Dayal and Allen (1975) have been modelled using the power law with exponent 0.2 although they were originally modelled with two logarithm functions by the researchers. The data from Heerema (1979) were not included because of the excessively high strength ratio for a quasi-static rate based on the lowest shear rate tested in the study.

The values of the strength ratio of Litkouhi and Poskitt (1980) and Dayal and Allen (1975) are generally higher than appears to be encountered in practice. As noted in Section 3.5.3, the values of strength ratio found by Heerema (1979) are excessively high compared with those encountered in practice. It is encouraging to note, however, that the values of the strength ratio found in the present study are comparable to those encountered in practice based on the linear model.

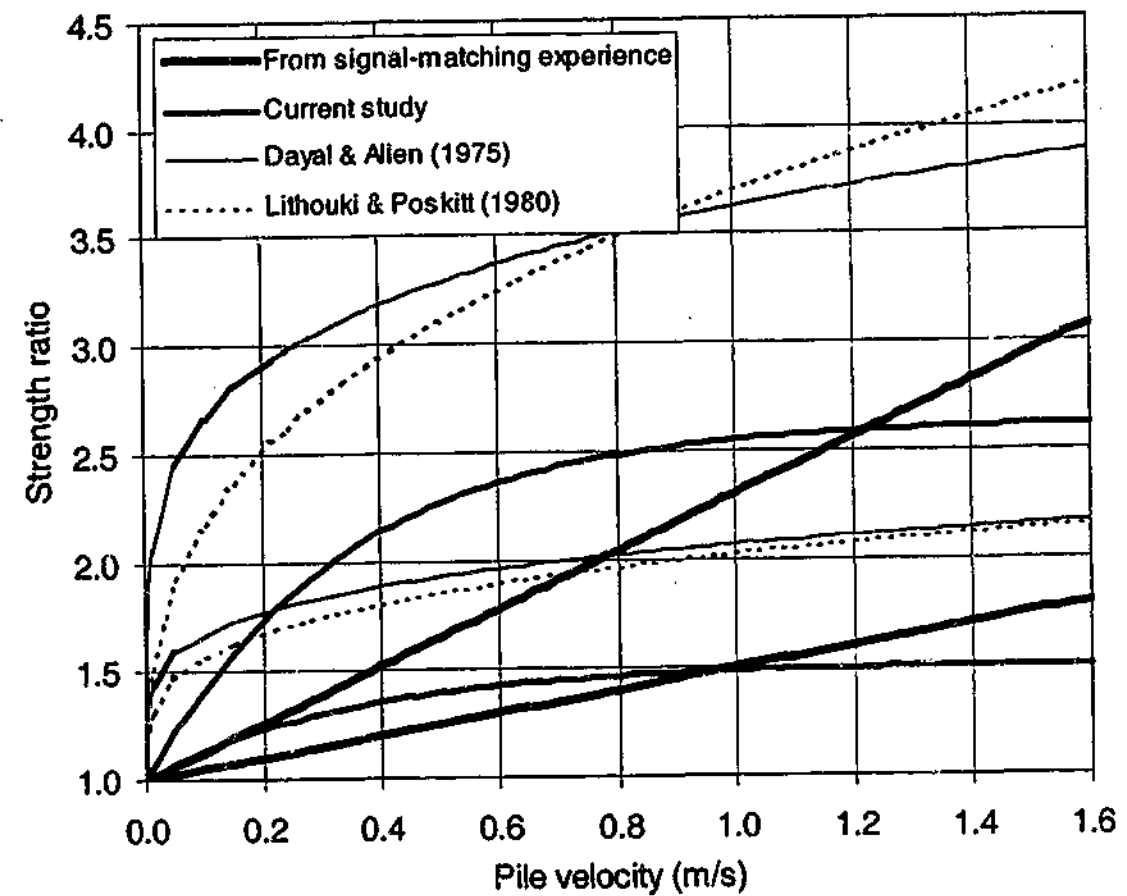


Figure 7.49 Upper and lower bounds of strength ratio-velocity relationships from current and past research

7.10 Concluding Remarks

This chapter has outlined the test procedures used in conducting the dynamic pile-clay interface tests.

The clay specimens and the pile surfaces subjected to dynamic shearing were significantly different from those subjected to quasi-static shearing because of significant remoulding of the clay specimen, significant development of shear-induced excess pore pressures in the shear zone of the specimen and smearing of the pile surface in the dynamic tests. This meant that the quasi-static friction measured in the quasi-static test could not be used to normalise dynamic friction.

In order to normalise the dynamic friction and also to quantify the difference in the interface friction, a procedure was developed to determine the quasi-static friction associated with a dynamic test. Using this procedure, the quasi-static friction

associated with the dynamic test was computed. It was found that the quasi-static friction associated with the first test cycle in dynamic test sequence was comparable to that measured in the quasi-static test, indicating that the remoulding, development of excess pore pressures and the pile-smearing were not significant after the first test cycle. However, the quasi-static friction associated with the dynamic test in the subsequent test cycles was significantly less than that measured in the quasi-static test.

At the start of the event, the interface friction was not yet fully mobilised and the effect of residual friction (caused by the previous test cycle) was present. Therefore, in the investigation of the damping response, the data at the start of the event were not amenable to analysis. Thus, only the dynamic data pertaining to the deceleration of the pile from the peak velocity to zero velocity were analysed.

The dynamic friction was normalised with the deduced quasi-static friction, and the strength ratio was found to be dependent on the pile velocity or the interface shear rate. To characterise the damping response, the strength ratio was plotted against the pile velocity for each of the dynamic tests. The response was best modelled with a function in the form of $\alpha(1-e^{-\beta v})$ where the α values were between 0.51 and 1.70, whilst the β values ranged between 2.5 and 3.5.

The functional form of the response obtained in this study was different to that found by Heerema (1979), Dayal and Allen (1975), and Litkouhi and Poskitt (1980). It was suggested that significant limitations in the work of the latter groups of researchers resulted in the different findings. The values of the strength ratio found in this study were shown to be comparable to those used in signal-matching (based on the linear damping model), whilst the values proposed by the three groups of researchers were found to be apparently higher than those encountered in signal-matching. It would thus appear that the experimental finding was consistent with the actual pile-soil interface damping response.

Chapter 8

8. Dynamic Pile-Clay Interface Behaviour: Analysis (Part II)

8.1 General

As discussed in Section 3.5.8, the effects of certain fundamental parameters on the viscous damping parameter have been investigated in previous studies. Coyle and Gibson (1970), who investigated the dynamic response of triaxial samples, were able to correlate the viscous damping parameter to the liquidity index of the specimen. Dayal and Allen (1975) found some correlation between the viscous damping parameter and the shear strength, whilst Litkouhi and Poskitt (1980) did not find such a correlation, although both groups of researchers made use of the same experimental set-up using the penetrometer as a model pile. Heerema (1979) who performed the plate-soil shear tests correlated the viscous damping parameter with the shear strength of the soil.

Using the improved experimental set-up developed for this study, post-test observations of the shear surface of the soil have been possible and reliable data of the pile-soil interface response have been obtained and. In this chapter, which forms Part II of the analyses of the dynamic response of the pile-clay interface, a hypothesis for the mechanism of the viscous response is proposed based on the experimental observations of the shear surface of the soil that have been reported in the previous chapter. Also, based on the experimental data, the effects of various parameters on the viscous damping parameter (α) are discussed and interpreted in the context of the proposed hypothesis. These parameters can be classified into the soil parameters and the pile parameters. The soil parameters are the shear strength, the applied normal stress, the overconsolidation ratio (*OCR*) and the clay plasticity, and the pile parameters are the surface roughness and the surface condition of the pile, that is whether it is wet or dry.

In order to improve the reliability of the pile driveability analyses and analyses of pile testing events, a reliable correlation between dynamic behaviour and standard soil parameters is required. Thus, the experimental data collected for this research is evaluated in this chapter with a view to providing more reliable correlations than have previously been possible. It will be shown that when α values (for β fixed at 3.0 which has been shown in Section 7.8 to be the average for all the pile-clay interfaces tested in this study) are plotted against shear strength, meaningful α -shear strength relationships for the three dynamic shear modes could be observed. However, when α values are plotted against normal stress and *OCR*, general but less consistent trends could be observed. Thus, based on the α -shear strength correlation, a simple procedure is proposed for estimating the α value.

8.2 Proposed Mechanism of Viscous Damping

In order to interpret the effects of the aforementioned parameters on the viscous damping phenomenon, it is necessary to have an understanding of the mechanism of viscous damping. However, the mechanism of the viscous damping phenomenon has yet to be established primarily because it is inherently difficult to study the interaction at the micro level between the soil particles. In order to discuss the effects

of the various soil and pile parameters on the viscous damping parameter, it is thus necessary to propose a hypothesis for the mechanism of viscous damping.

As discussed in Section 2.4.2, it has been hypothesised that the strength increase associated with fast shearing can be caused by volumetric or pore pressure changes (Richardson and Whitman, 1962; Lefebvre and LeBoeuf, 1987; Briaud and Garland, 1985). Whilst the volumetric change may in part be responsible for the strength increase in the samples tested under triaxial compression and the strength increase associated with relatively minute strain rates, it does not explain in isolation the strength increase observed in this study. The experimental data show that the strength ratio-velocity relationships based on consecutive shear tests on an interface are reasonably consistent. If viscous damping is caused purely by the volume changes and hence pore pressure changes in the soil, a subsequent test carried out should show a drastically different degree of velocity-dependence since the pore pressure will not have dissipated within the short time between consecutive tests.

Another hypothesis that has been proposed is that the viscous behaviour is simply due to the inherent viscosity of pore water in a cohesive specimen (Richardson and Whitman, 1962; Briaud and Garland, 1985; Lefebvre and LeBoeuf, 1987; Schimming et al., 1966) and the adsorbed water layers on clay particles (Briaud and Garland, 1985; Dayal and Allen, 1975). This hypothesis is also consistent with a perception that increased viscosity is associated with higher moisture contents. However, as will be shown in the experimental results obtained in this study, the values of the viscous damping parameter can vary greatly for a sample with a given moisture content that is tested at different normal stresses.

Based on experimental observations from this and some other studies, a new hypothesis is proposed. It is proposed that the strength increase due to viscous damping is caused by constant disordering of the particles at the shear surface.

The shear surfaces of soil specimens that have been sheared in interface tests and soil-only tests have been observed in this study and the studies by Tika-Vassilikos (1991), Bond and Jardine (1991), Tika et al. (1996), and Lemos and Vaughan (2000). After a shear test at a low rate, it has been observed in this study and in those by

Bond and Jardine (1991), Tika-Vassilikos (1991) and Tika-Vassilikos et al. (1992) that the shear surface is smooth, single and continuous along its length, and with striations aligned with the direction of shear. In contrast, after a shear test at a high rate, it has been observed in this study and in the studies by Bond and Jardine (1991) and Tika et al. (1996) that the shear zone consists of discontinuous shear surfaces that are not aligned to the direction of shearing, and is rougher in texture and thicker. Thus, it has been concluded in this study as well as in those of Tika et al. (1996) and Lemos and Vaughan (2000), that these characteristics indicate that the clay particles at the shear surface have been disordered and the alignment of the particles to direction of shearing has been disrupted (Tika et al., 1996; Lemos and Vaughan, 2000).

Since these characteristics were observed after fast shearing, it can be concluded that fast shearing causes disordering of the clay particles. The mechanistic explanation proposed by Richardson and Whitman (1962) and Whitman and Healy (1962) appears to be able to explain the disordering effect. It was hypothesised that at a low shear rate, the clay particles at the shear surface have the opportunity to move relative to each other in the path of minimal resistance. At a high shear rate, however, the clay particles are not given the opportunity to move in such a way, and under an externally applied shear force, move in a disorderly manner, and ride on and over each other. The “riding on and over” behaviour appears to be supported by two observations made in previous studies involving tests at high shear rates. The first observation is that the shear zone is thicker (Tika et al., 1996). The second observation is that dilation is increased or the contraction is decreased, which results in less positive excess pore water pressures or more negative excess pore water pressures respectively (Casagrande and Wilson, 1951; Bjerrum et al., 1958; Crawford, 1959; Richardson and Whitman, 1962; Crawford, 1965; Lefebvre and LeBoeuf, 1987; Sheahan et al., 1996).

Furthermore, it has been shown by Tika-Vassilikos (1991), Tika-Vassilikos et al. (1992) and Lemos and Vaughan (2000) that the disordering of the clay particles at a shear surface results in a higher resistance compared to ordered particles. This has been demonstrated by performing a series of shear tests in the order of a slow test, a fast test and a slow test. Such tests have been performed for both interface and soil-

only tests. The peak strength of the second slow test has been found to be higher than the residual strength obtained in the first slow test and to drop with further displacement to the residual strength of the first slow test. These laboratory tests have been validated with field tests (Jardine and Bond, 1989; Tika-Vassilikos et al., 1992). It has also been found that the peak strength of the second slow test (after fast shearing) increased with the rate at which the fast test is performed, indicating that the disordering becomes increasingly severe with increasing rates (Tika et al., 1996).

Based on the premise that fast shearing causes disordering of the particles at the shear surface and that the disordering causes an increase in the resistance, it is hypothesised that the strength increase due to viscous damping observed in a fast test is likely to be due to the disordering of the particles at the shear surface. Based on this hypothesis, the degree of disordering increases with increasing shear rate so that the value of viscous damping parameter increases with increasing shear rate.

This hypothesis is used as a framework for interpreting the effects of the various parameters on the viscous damping parameter based on the experimental data.

8.3 Shear Failure Modes

As discussed in the previous chapter, essentially 3 dynamic failure modes for the interface, designated as Modes 1, 2 and 3, have been identified. For low and medium plasticity clays sheared against a smooth pile, Mode 1 failure occurs, whilst for low and medium plasticity clays sheared against a rough pile, Mode 2 failure occurs. For high plasticity clays sheared against a smooth pile surface, the Mode 3 interface failure occurs. Thus, the mode of failure is dependent on the pile roughness and the plasticity of the clay. The likely modes of failure for the interfaces which were not tested in this study have also been discussed in the previous chapter. The dependence of the dynamic shear failure mode on the pile roughness and the plasticity of the clay has been illustrated in Figure 7.13 of the previous chapter which is reproduced in Figure 8.1.

Since the different failure modes result in changes in the physical characteristics of the shear surface of the clay specimen and the condition of the pile surface, it is

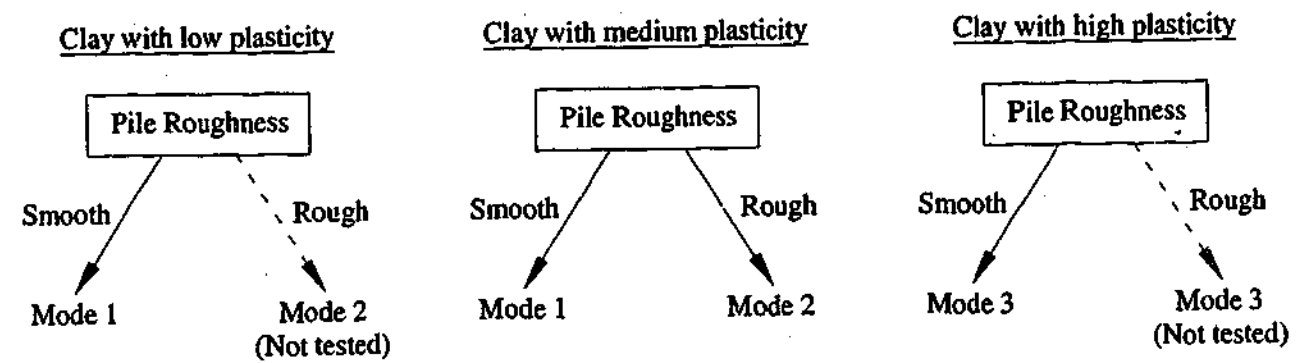


Figure 8.1 Failure mode of an interface being dependent on the pile roughness and the plasticity of the clay

logical that different failure modes result in fundamentally different dynamic responses. Therefore, the effect of a certain parameter on the dynamic response is described under the separate headings of Modes 1, 2 and 3.

8.4 Shear Strength

As noted in Section 3.5.8, dynamic pile-clay interface tests by Dayal and Allen (1975) and Heerema (1979) indicate that the viscous damping parameter α can be correlated with shear strength. Furthermore, data based on dynamic tests involving soil-only failure (Litkouhi and Poskitt, 1980; Poskitt and Leonard, 1982; Coyle and Gibson, 1970) and data based on triaxial compression tests (involving soil-only failure) performed at low strain rates (Briaud and Garland, 1985) suggests the same.

To determine the effect of the shear strength on the dynamic response, the exponential viscous damping parameter α has been plotted against the shear strength of the clay for each of the Modes 1, 2 and 3 interfaces, distinguishing the clay and the pile surface involved, in Figure 8.2, Figure 8.3 and Figure 8.4 respectively. The scattering of the data might be due to variations in the shear strength resulting from shear-induced excess pore water pressure and remoulding of the clay. The data for the BallR-Wet steel interface are even more scattered compared to those for the BallR-Dry steel due perhaps to the interaction of the film of water with the clay particles at the interface, whose effect is additional to the pore pressure and remoulding effects.

It is noted that the shear strength of the soil has been measured using the direct shear test (as described in Section 6.3.2) where the soil has been subjected to the stress condition corresponding to that during a dynamic interface test. As discussed in Section 7.5.6, the “instantaneous” value is lower than the “initial” value because of the remoulding of the soil and shear-induced excess pore pressures as reflected in the decrease in the interface friction. However, the damping factor has been correlated to the normally measured initial shear strength of the specimen rather than the “instantaneous” shear strength of the soil at the shear zone at the time of shearing.

As shown in Figure 8.2, for interfaces with Mode 1 failure, the value of the damping parameter (α) consistently decreases with increasing shear strength.

It can be observed that the BallR-dry steel interface has α values within a wider range of between 0.7 and 1.7, whilst the BallR-dry smooth concrete interface has α values within a narrower range of between 1.2 and 1.5. Given that the dry steel was rougher than the dry smooth concrete, it would appear that the interfaces involving rougher surfaces are more sensitive to changes in the shear strength compared to the interfaces involving smoother surfaces.

It can also be noted that the BallR-dry steel interface has α values within a wider range of between 0.7 and 1.7, whilst the BallR/Talc-dry steel interface has α values within a narrower range of between 1.2 and 0.9. It would thus appear that the interfaces involving a higher plasticity clay are more sensitive to changes in the shear strength compared to the interfaces involving a lower plasticity clay.

It is important to note from Figure 8.2 that, for the same shear strength, the α values for interfaces involving the wet pile surface are lower than those for interfaces involving the dry pile surface.

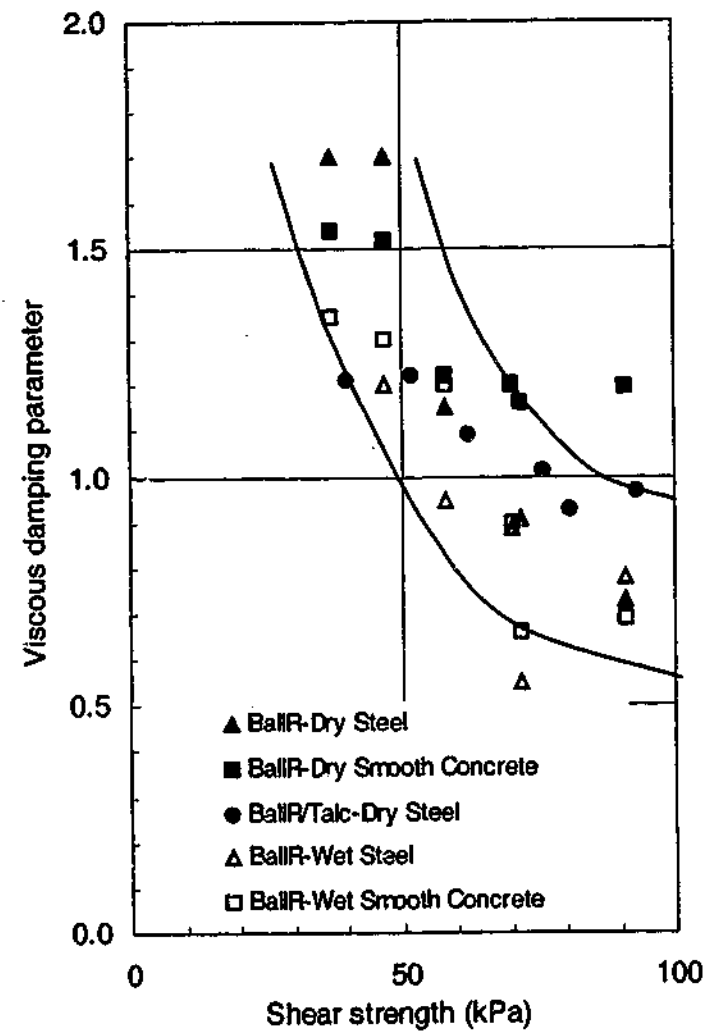


Figure 8.2 Mode 1: The effect of shear strength on the viscous damping parameter, α

For interfaces with Mode 2 failure, the value of α also decreases with increasing shear strength, as shown in Figure 8.3. At a particular shear strength, the α values of these interfaces are lower than those for interfaces with Mode 1 failure.

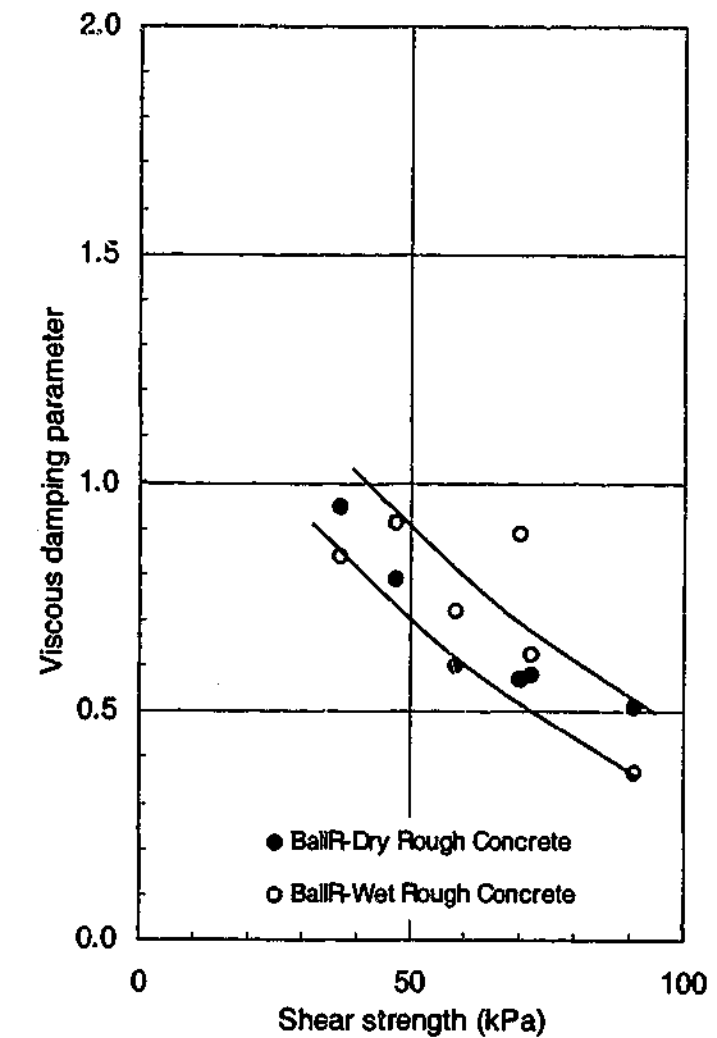


Figure 8.3 Mode 2: The effect of shear strength on the viscous damping parameter, α

As for the Modes 1 and 2 interfaces, the value of α for the interfaces with Mode 3 failure decreases with increasing shear strength of the clay. For particular shear strength, the α values of these interfaces are similar to those for interfaces with Mode 2 failure and lower than those for interfaces with Mode 1 failure.

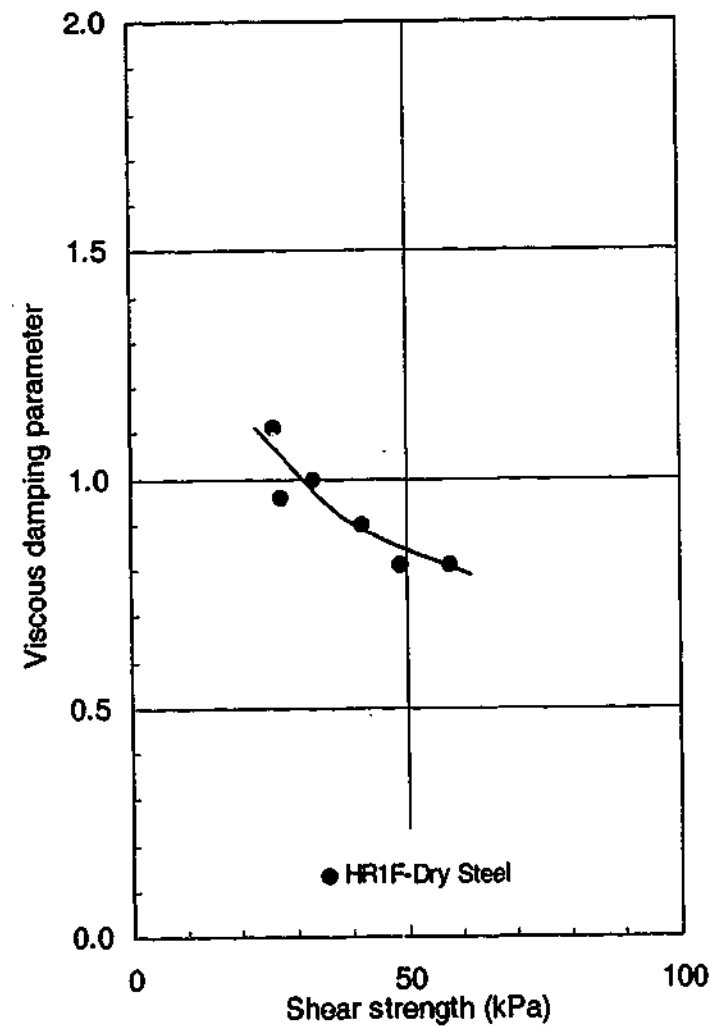


Figure 8.4 Mode 3: The effect of shear strength on the viscous damping parameter, α

When the data points from the two failure modes are plotted together as in Figure 8.5, there are essentially two bands of data, with the upper band associated with Mode 1 and the lower band associated with Modes 2 and 3. As previously mentioned, the α values for interfaces with failure in Modes 2 and 3 are lower than those for interfaces with Mode 1. It can thus be inferred that the viscous damping parameter for a clay specimen sheared against a clean pile surface (Mode 1) is higher compared to that for a clay specimen sheared against a layer of clay (adhering to the pile surface) (Mode 3) or a pile surface smeared with clay (Mode 2). It is interesting to note that the α values for the soil-only tests from the previous studies are lower than those of the pile-soil interface tests. Thus, it appears that the Modes 2 and 3 failures, which involve shearing between a clay-smeared pile and the clay specimen, and shearing between a layer of clay and the clay specimen respectively, more closely resemble soil-only shearing.

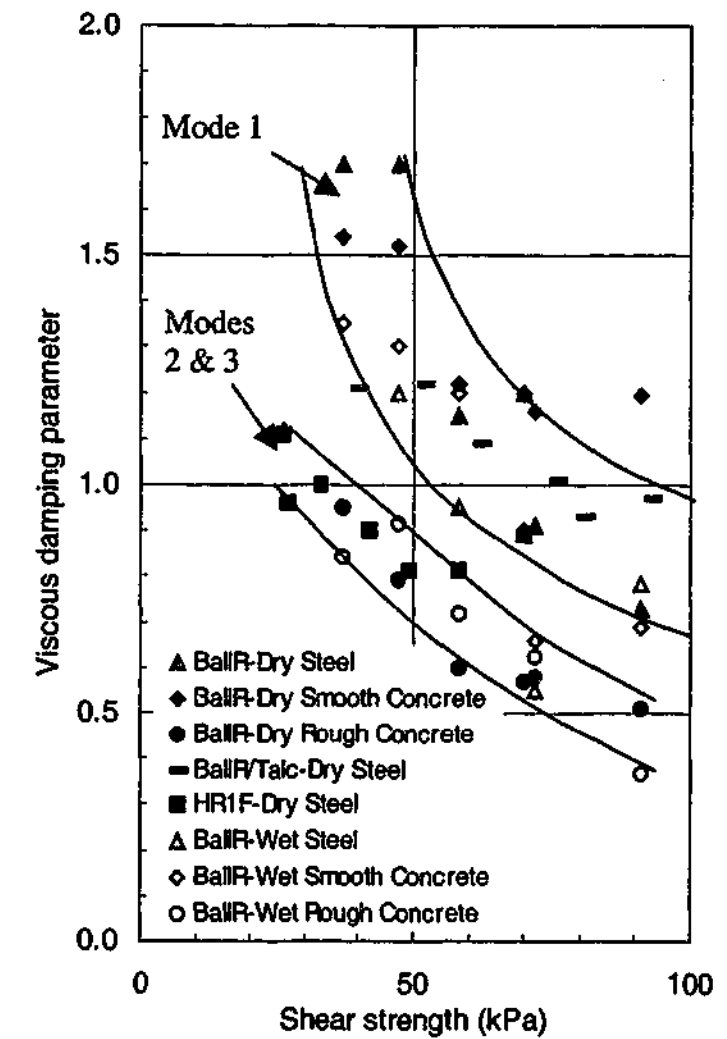


Figure 8.5 The effect of shear strength on the viscous damping parameter, α , for all interface failure modes

The significantly different magnitudes of α for the two bands of data can perhaps be explained using the proposed mechanism of particle disordering. Intuitively, the clay particles of the specimen at the shear surface would be more highly disordered by the “hard” pile surface (Mode 1) as compared to the “soft” surface formed by the layer of clay adhering to the pile surface (Mode 3) or by the clay-smeared pile surface (Mode 2).

The dependence of the value of the damping parameter, α on shear strength is consistent with the hypothesis that has been proposed for the mechanism of viscous damping. For a particular type of clay, the shear strength is physically related to the normal and preconsolidation stresses, and can be expressed as follows:

$$\frac{S_u}{\sigma'_v} = \left[\frac{S_u}{\sigma'_n} \right]_{\frac{\sigma'_p}{\sigma'_v}=1} \left(\frac{\sigma'_p}{\sigma'_v} \right)^m \quad (8.1)$$

where, as previously explained in Section 6.6.1, σ'_p is the preconsolidation stress and σ'_v is the vertical effective overburden. $\left[\frac{S_u}{\sigma'_n} \right]_{\frac{\sigma'_p}{\sigma'_v}=1}$ is the shear strength ratio for the

normally consolidated sample for the particular type of clay, and $\left(\frac{\sigma'_p}{\sigma'_v} \right)$ is the over-consolidation ratio, *OCR*. For undrained tests, the normalised shear strength ratio varies as *OCR* to the power *m* where *m* lies in the range 0.68 to 0.86 and is related physically to the compression index (Wroth, 1984).

This relationship has been explained by Terzaghi et al. (1996) and Mitchell (1993) as follows. The normal compressive force establishes contact between one clay particle to another across an area that increases or decreases as the force increases or decreases. Bonds are formed across the contact areas, the number of which increases with increasing interparticle contact area or the transmitted compressive force transmitted at the contact. These bonds resist tangential or sliding movements, thus giving the soil its shear resistance. The macroscopic strength is therefore directly proportional to the number of bonds. Therefore, it is intuitive that the higher the number of interparticle bonds in the clay specimen, the more difficult it is to disorder the clay particles. Thus, a specimen with a higher shear strength is less susceptible to its clay particles being disordered by the pile surface (at high shear rates) and will have a lower viscous damping parameter as compared to a specimen with a lower shear strength. Interestingly enough, it has been shown in Mitchell (1964) and Mitchell (1993), using the rate process theory, that the dynamic force component due to viscous damping for any fixed range of shear rates is directly proportional to the number of bonds or the shear strength of the soil.

8.5 Normal Stress

As noted in Section 3.5.8.3, the effect of normal stress on the dynamic response of the pile-soil interface has not been investigated in the previous studies with the exception of Heerema (1979). The data from Heerema suggested that normal stress did not have a consistent effect on the viscous damping parameter.

Based on the data from the current study, the viscous damping parameter α has been plotted against the applied normal stress for interfaces with Modes 1, 2 and 3 failures in Figure 8.6, Figure 8.7 and Figure 8.8 respectively, where the specimens preconsolidated to 325kPa and 500kPa are distinguished by the notation "(325)" and "(500)" in the legends.

As shown in Figure 8.6, for all interfaces with Mode 1 failure, increasing the applied normal stress on a specimen with a certain preconsolidation stress has the effect of decreasing the value of α significantly. This applies to both dry and wetted pile surfaces. As the normal stress is directly proportional to the shear strength for a specimen with a certain preconsolidation stress, this finding is consistent with the previous finding that the value of α decreases with increasing shear strength.

It can also be noted that the value of α for the BallR/Talc clay with lower plasticity is less sensitive to variation in the normal stress as compared to the BallR with higher plasticity.

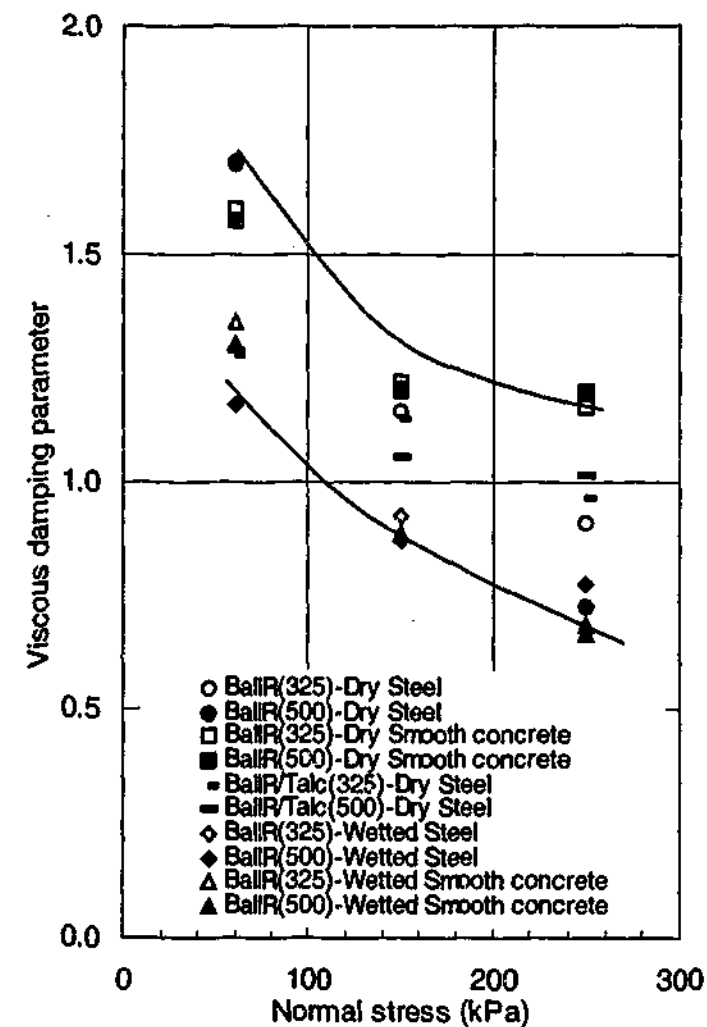


Figure 8.6 Mode 1: The effect of normal stress on the viscous damping parameter, α

As shown in Figure 8.7, for the interface with Mode 2 failure, the normal stress has a similar influence on the value of α . However the value of α for the interface involving the dry pile surface is more sensitive to variation in the normal stress as compared to the interface involving the wetted pile surface.

The inverse relationship between the value of α and the applied normal stress for interfaces with Modes 1 and 2 failures could be explained in the context of the proposed mechanism behind viscous damping. It is hypothesised that at higher applied normal stresses, the clay particles at the interface are relatively less disordered during shear because the clay particles are more densely packed, and are restrained from riding on and over other surrounding particles.

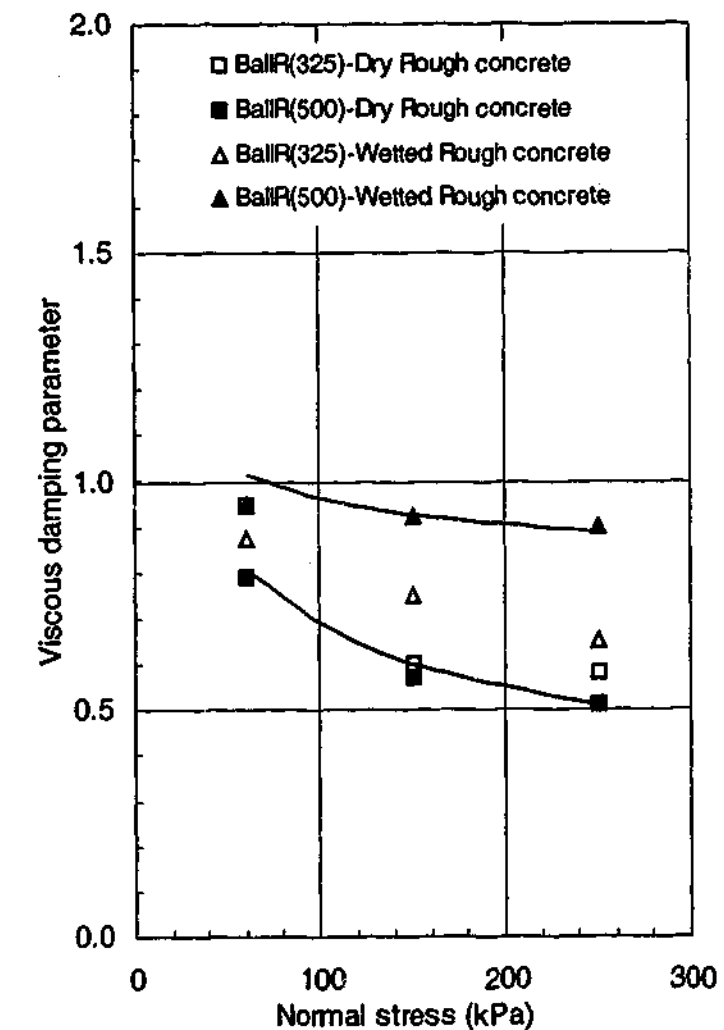


Figure 8.7 Mode 2: The effect of normal stress on the viscous damping parameter, α

As demonstrated in Figure 8.8, in contrast with interfaces with Modes 1 and 2 failure, the value of α for interfaces with Mode 3 failure appears to be almost independent of the normal stress; in fact, the α values for the specimen preconsolidated to 325kPa show a slight increase with increasing normal stress. Based on the proposed mechanism, it would appear that for interfaces with Mode 3 failure where an intact clay block is sheared against a layer of clay (that had adhered to the pile surface), the normal stress has little effect in restraining the clay particles of the specimen from being disordered. This is probably because the clay particles of the specimen are "locked onto" the clay particles of the clay layer such that disordering of the particles occurs regardless of the level of applied normal stress.

Overall, for all modes of failure, it is concluded that there is generally a decrease in the viscous damping parameter with increased normal stress for any given soil strength; however, the relationship is not clear, consistent or easily quantifiable.

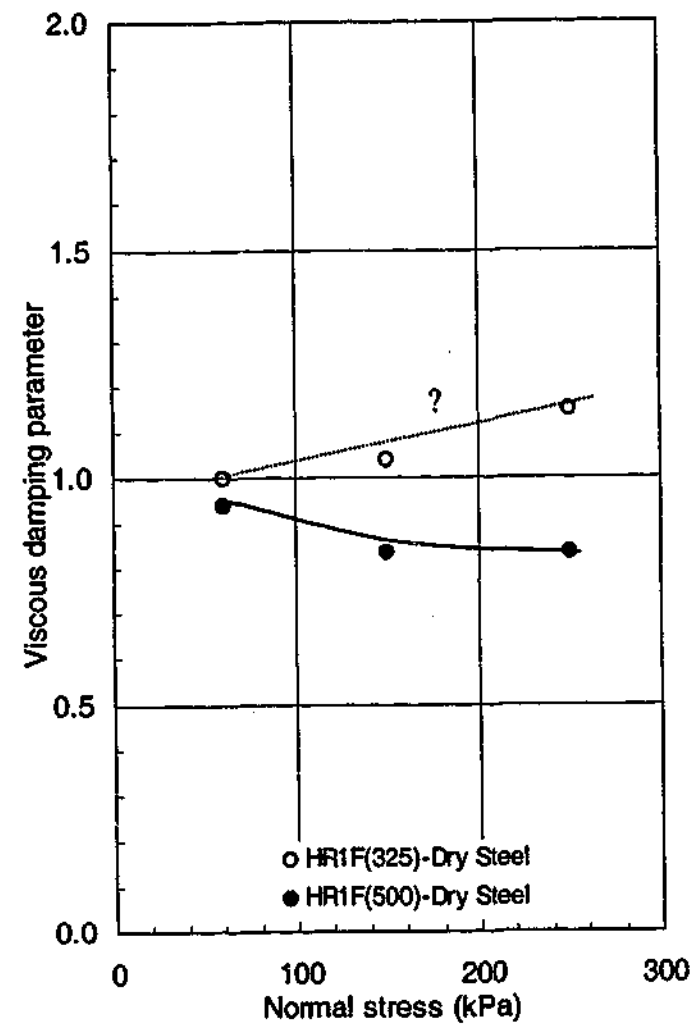


Figure 8.8 Mode 3: The effect of normal stress on the viscous damping parameter, α

8.6 OCR

The overconsolidation ratio (*OCR*) is defined as the ratio of the preconsolidation pressure to the current applied pressure and is an indirect measure of the clay deformation characteristics of the specimen to the current applied pressure. For example, a specimen with an *OCR* less than 1.0 (applied pressure is equal to the preconsolidation pressure) is highly deformable in response to increased applied pressure, whilst a specimen with a high *OCR* value (applied pressure is less than the preconsolidation pressure) is less deformable under the same applied increase in pressure.

As noted in Section 3.5.8.2, none of the studies involving pile-clay interface tests investigated the effect of *OCR* on the viscous damping parameter. However, it has

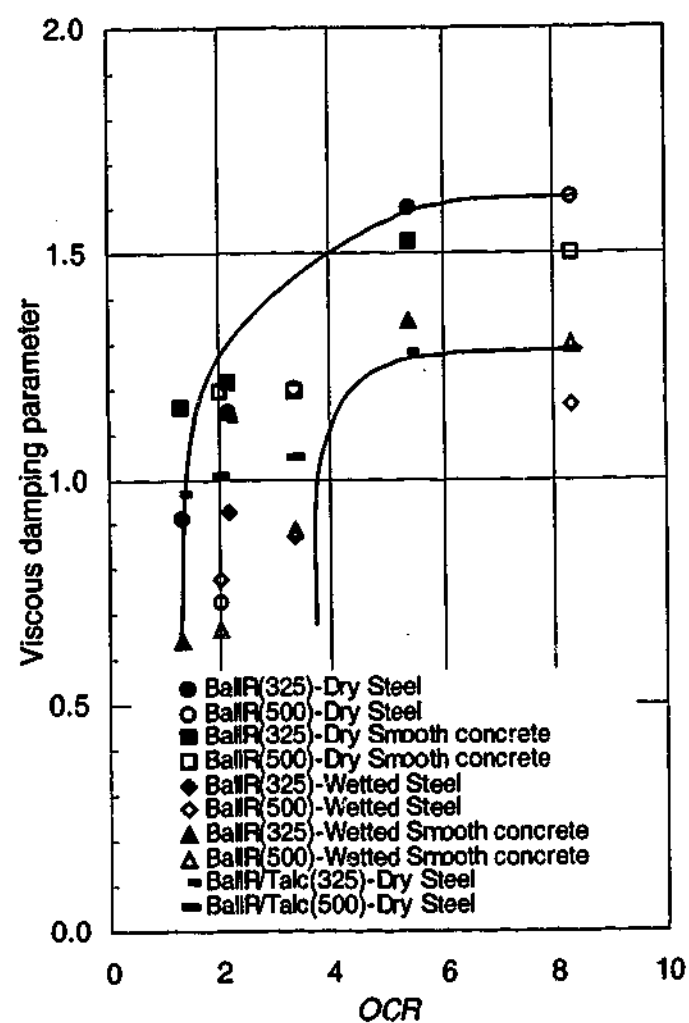
been shown that for (soil-only) triaxial tests, the *OCR* had no apparent influence on the viscous damping parameter (Graham et al., 1983).

In this study, the *OCR* is varied by testing a specimen with a particular preconsolidation stress at three normal stresses. Since specimens were preconsolidated to two stresses, six different *OCR*s result. The preconsolidation stresses, the normal stresses, and the resulting *OCR*s for each of the 3 types of clay are shown in Table 8.1.

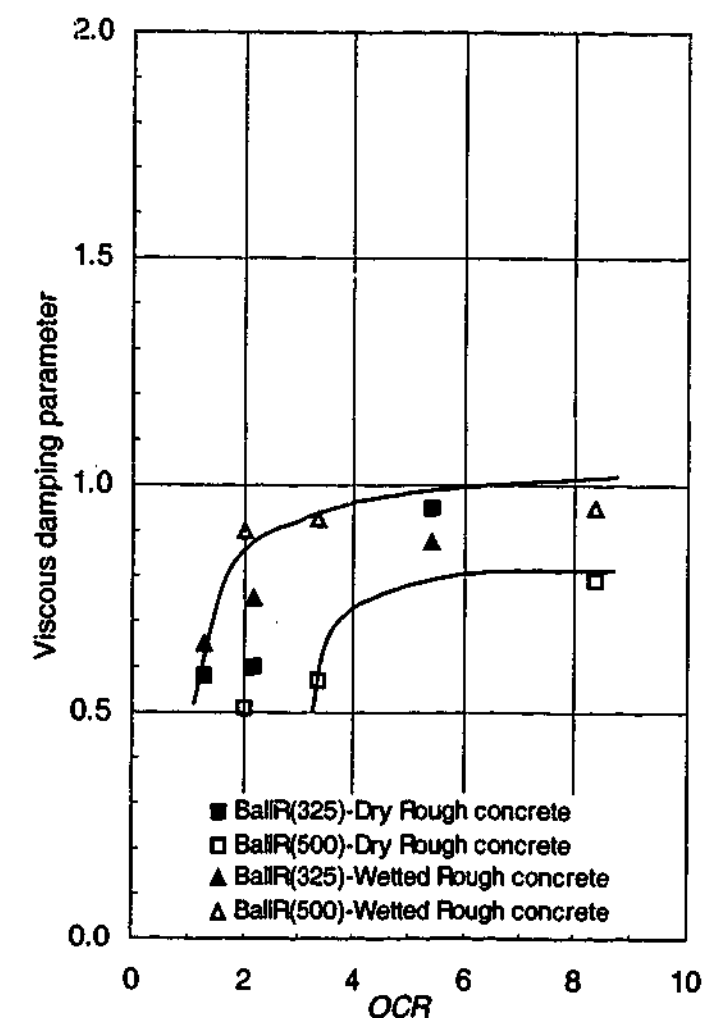
For interfaces with Mode 1 failure, the α values have been plotted against the relevant *OCR*s, distinguishing the two different preconsolidation stresses of the specimens and the pile, in Figure 8.9. It can be observed that the α -*OCR* curves for the two preconsolidation stresses are distinctly different. It would thus appear that the variation in the value of α with *OCR* is the indirect result of the variation in the value of α with shear strength, which can be explained as follows. For a specimen with a given preconsolidation stress, α increases with increasing *OCR* due to the inverse relationships between α and shear strength and between *OCR* and normal stress. For a given preconsolidation stress, a higher *OCR* implies that the current normal stress is lower, so that the strength is also correspondingly lower (since there is an approximately square root relationship between *OCR* and strength shown in Equation (8.1). Given that α reduces with an increase in strength, α can be expected to increase with *OCR*.

Table 8.1 Preconsolidation and normal stresses and their resulting *OCR*s

Preconsolidation stress (kPa)	Normal stress (kPa)	<i>OCR</i>
500	250	2.0
	150	3.3
	60	8.3
325	250	1.3
	150	2.2
	60	5.4

Figure 8.9 Mode 1: The effect of *OCR* on the viscous damping parameter, α

For interfaces with Mode 2 and Mode 3 failure, the α values have been plotted against the relevant *OCR*s in Figure 8.10 and Figure 8.11 respectively. The suggestion that the variation in the value of α with *OCR* is the indirect result of the variation in the value of α with shear strength also applies to the interfaces with Mode 2 and Mode 3 failure. However, for the Mode 2 failure, since the damping parameter α is less sensitive to the shear strength as shown in Section 8.4, the apparent variation of the parameter with *OCR* is less significant, as shown in Figure 8.10. For the Mode 3 failure, since the damping parameter is almost independent of the shear strength as shown in Section 8.4, the parameter does not vary with *OCR* in any definite trend.

Figure 8.10 Mode 2: The effect of *OCR* on the viscous damping parameter, α

In relation to the proposed hypothesis for the mechanism of viscous damping, it is tempting to reason that a more deformable specimen is more susceptible to disordering. However, the tendency of the specimen to disordering should be dependent on the number of bonds holding the particles, which is measured by the shear strength of the specimen rather than the deformation characteristics of the specimen. Therefore, the viscous damping parameter cannot be expected to vary directly with *OCR*, and as has been proposed, any variation in the value of α with *OCR* is the indirect result of the variation in the value of α with shear strength.

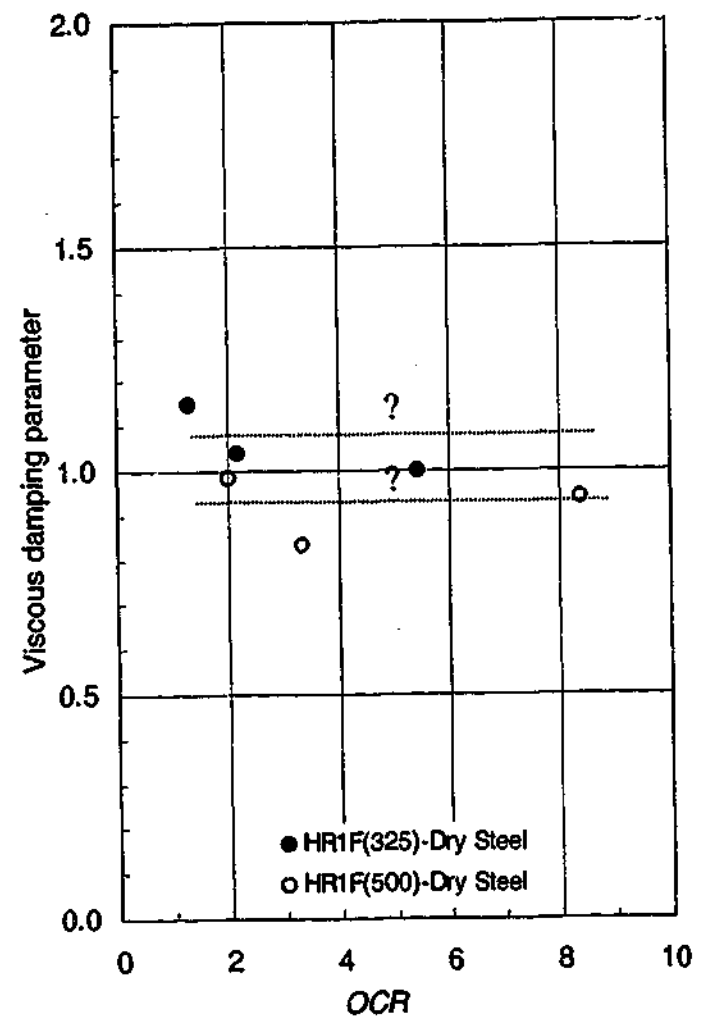


Figure 8.11 Mode 3: The effect of *OCR* on the viscous damping parameter, α .

8.7 Clay Plasticity

A common parameter for differentiating different types of clay is the plasticity index. The plasticity of a clay is directly proportional to the percentage of the clay size fraction (where the clay size fraction is defined as grains smaller than 2 microns), and can be classified into low, medium and high according to the plasticity chart using the liquid limit, the plastic limit and the plasticity index of the clay.

Since no data of the effect of the clay plasticity on the viscous damping parameter, α is available based on pile-soil interface tests, data from (soil-only) triaxial compression tests performed at relatively much lower rates may be pertinent. Data from Graham et al. (1983) indicate that the viscous damping parameter is independent of the plasticity index (I_p), whilst data from Briaud and Garland (1985) indicate otherwise.

As mentioned from the outset, the plasticity of the clay has been found to have a significant influence on the shear failure mode of the interface. Keeping the stress conditions (preconsolidation and applied normal stresses) exactly the same, interface tests involving clays of medium and low plasticity (BallR and BallR/Talc respectively) result in Mode 1 failure, whilst interface tests involving a clay of high plasticity (HR1F) result in Mode 3 failure. Since the failure mode has been shown experimentally to affect the viscous damping parameter α , the clay plasticity has an indirect influence on the value of α .

Given that the failure mode influences the dynamic response of an interface, the effect of plasticity index on the dynamic response can only be ascertained for interfaces subjected to a particular failure mode. Therefore, since the effect of the plasticity index on the value of α can only be ascertained from the very limited data based on the two interfaces Mode 1 failure (namely BallR clay-Steel and BallR/Talc clay-Steel) in this particular study, the effect of clay plasticity on the damping parameter cannot be ascertained. For any trend between the clay plasticity and the damping factor (for a particular shear failure mode) to be discerned, many data points are required because the viscous damping parameter is a function of other parameters as well.

8.8 Pile Roughness

The effect of pile roughness on the dynamic response of the pile-clay interfaces has not been investigated in previous studies. The present study has shown for the Mode 3 failure (high plasticity clay-smooth surface) that shearing occurs between the clay block and the clay-covered surface; therefore, the pile roughness is not expected to have any influence on the dynamic response of the interface with Mode 3 failure. For the Modes 1 and 2 failure however, it has been shown that the pile roughness can dictate the failure mode at the interface that in turn significantly affects the dynamic response of the interface.

It was observed that before testing of the clay-rough pile surface interface (Mode 2) commenced, the surface of the rough concrete was clean and that as the first shear test cycle took place, the pile surface became smeared with remoulded clay. As

subsequent tests were carried out on the same interface, the smearing was observed to increase to a point where the amount of smearing appeared to stabilise. In order to determine the effect of pile-smearing on the dynamic response, the dynamic responses of the first test cycle and of a latter test cycle (where the amount of smearing has stabilised) are plotted in Figure 8.12(a) and Figure 8.12(b) for the dry and wet pile cases respectively. It can be noted that the dynamic response of the interface changed significantly as the amount of smearing increased. More specifically, the viscous damping parameter for the less smeared surface is significantly lower than that for the more smeared surface. A possible explanation is that as the amount of smearing increased, the pile surface became lubricated such that the slippery surface was less capable of disordering the clay particles.

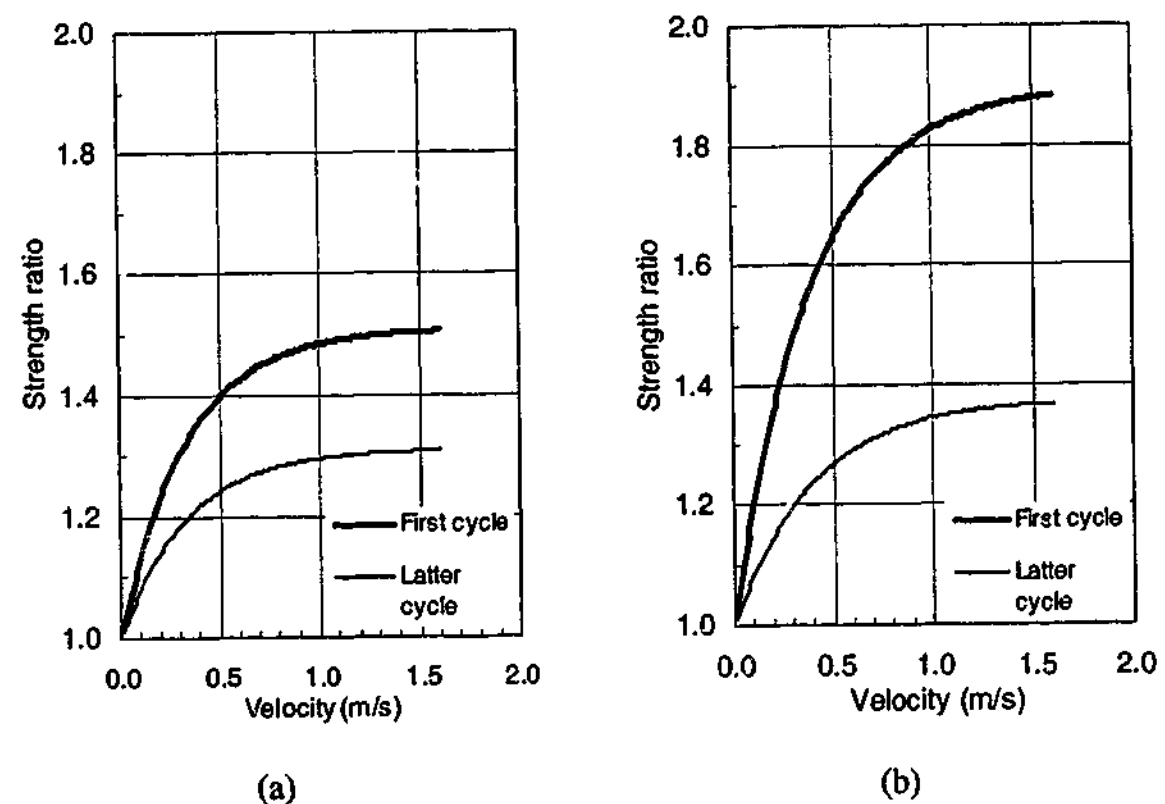


Figure 8.12 Mode 2: The effect of the amount of smearing on the dynamic response of interfaces between BallR and (a) dry rough concrete (b) wet rough concrete; at the normal stress of 250kPa

It has been established that a low or medium plasticity clay sheared against the smooth steel and concrete interfaces results in Mode 1 failure, whilst the same clay sheared against the rough concrete interface results in Mode 2 failure. The dynamic responses of these two modes of failure are compared in Figure 8.13 and Figure 8.14, where the plotted dynamic responses for Mode 2 relate to the latter test cycles (i.e. where the pile-smearing occurs), and where the dynamic responses of the interfaces with Mode 3 failure have been included for reference.

Before comparing the responses of the Modes 1 and 2 failure, it can be noted that the BallR-steel and the BallR-smooth concrete interfaces with Mode 1 failure yield very similar dynamic responses at normal stresses of 150kPa and 60kPa; this is to be expected because the steel and the smooth concrete are of similar roughness. However, the responses are notably different at a normal stress of 250kPa, where the smooth concrete surface, which is slightly smoother than the steel surface, yields a higher value of α than the steel surface. It is not apparent why this is the case.

It can be observed in Figure 8.13 and Figure 8.14 that the viscous damping parameter for Mode 2 failure is consistently significantly lower than that for Mode 1 failure. If the proposed hypothesis for the mechanism of viscous damping is correct, this would indicate that the degree of disordering of the clay particles is less for the interface with Mode 2 failure. It is hypothesised that for this interface, the asperities of the rough surface plough the clay at the shear surface, as can be illustrated schematically in Figure 8.15. At any one time during shearing, the clay particles at the tip of the asperities are disordered by the asperities, whilst the clay particles at the grooves between the asperities are ploughed by the asperities. Thus less particles across the interface are disordered at any one time, thus resulting in a lower value of the damping parameter. The occurrence of ploughing of the clay appears to be verified by the presence of deep striations on the shear surface of the clay and of destructured clay (which had been ploughed by the pile asperities) on the rough pile surface, observed during post-test observations of the shear surface. (The post-observations have been discussed in detail in Section 7.5).

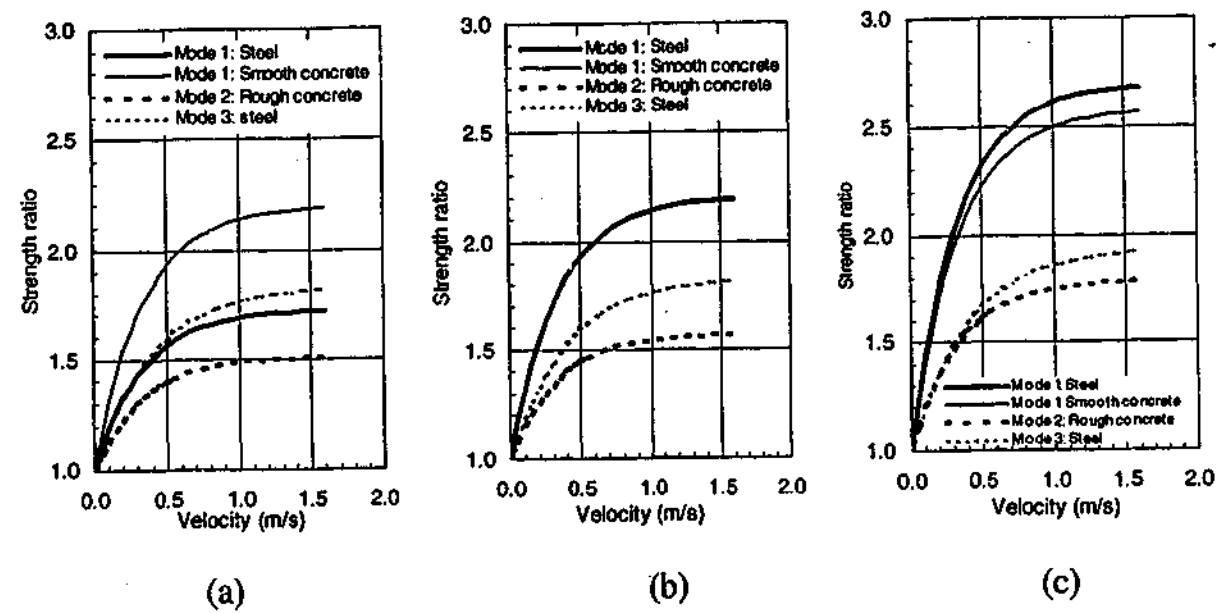


Figure 8.13 Modes 1 & 2: The effect of pile roughness on the dynamic response of interfaces between BallR ($\sigma_p' = 500\text{kPa}$) and different pile surfaces at normal stresses of (a) 250kPa (b) 150kPa (c) 60kPa

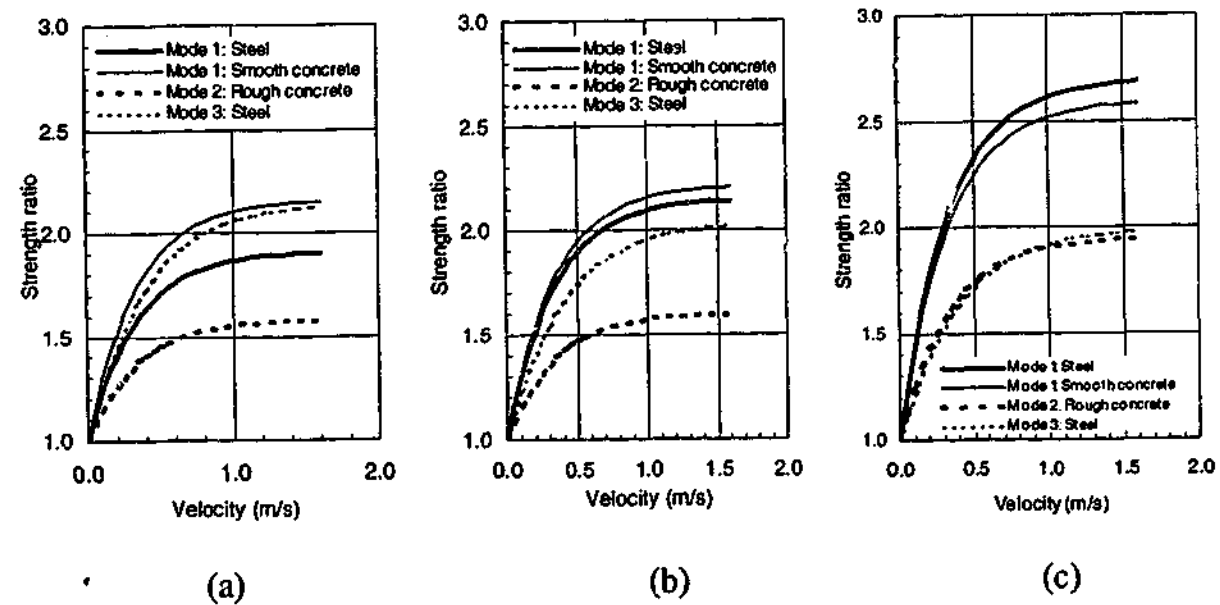


Figure 8.14 Modes 1 & 2: The effect of pile roughness on the dynamic response of interfaces between BallR ($\sigma_p' = 325\text{kPa}$) and different pile surfaces at normal stresses of (a) 250kPa (b) 150kPa (c) 60kPa

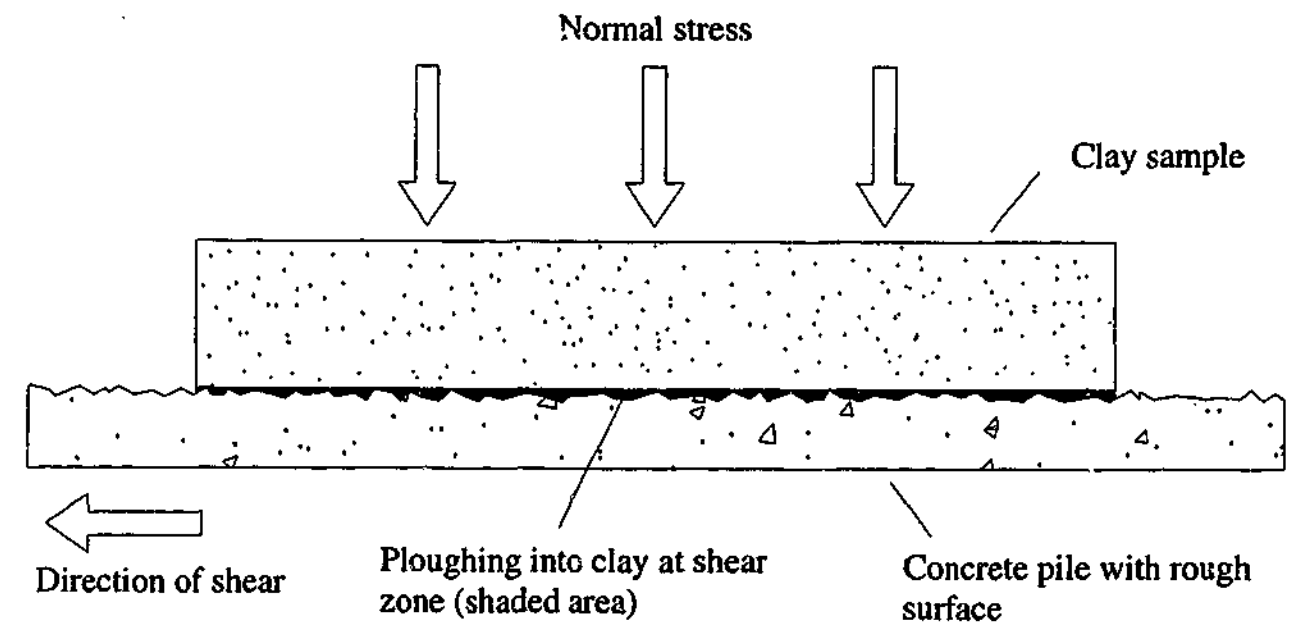


Figure 8.15 Ploughing action of the pile asperities

8.9 Pile Surface Condition: Dry vs. Wet

To determine the effect of a lubricating medium such as water at the interface on the dynamic response of the interface, the clay specimen was sheared against wetted pile surfaces. Although the wetted pile surface may be an unrealistic situation since it is unlikely that free water will find access to the pile-soil interface, this series of tests can give insights into the mechanism of the viscous behaviour. Furthermore, the presence of other lubricants such as bitumen, which are used to coat pile shafts in order to reduce potential down-drag, can be inferred from these tests.

For the interfaces with Mode 1 failure, the α values for dry and wetted pile surfaces are shown in Figure 8.16. It can be observed that for a particular specimen tested at a certain normal stress, the viscous damping parameter associated with the wetted pile is generally lower than that for the dry pile. It would appear that the presence of water on the pile surface decreases the amount of disordering of the clay particles at the interface.

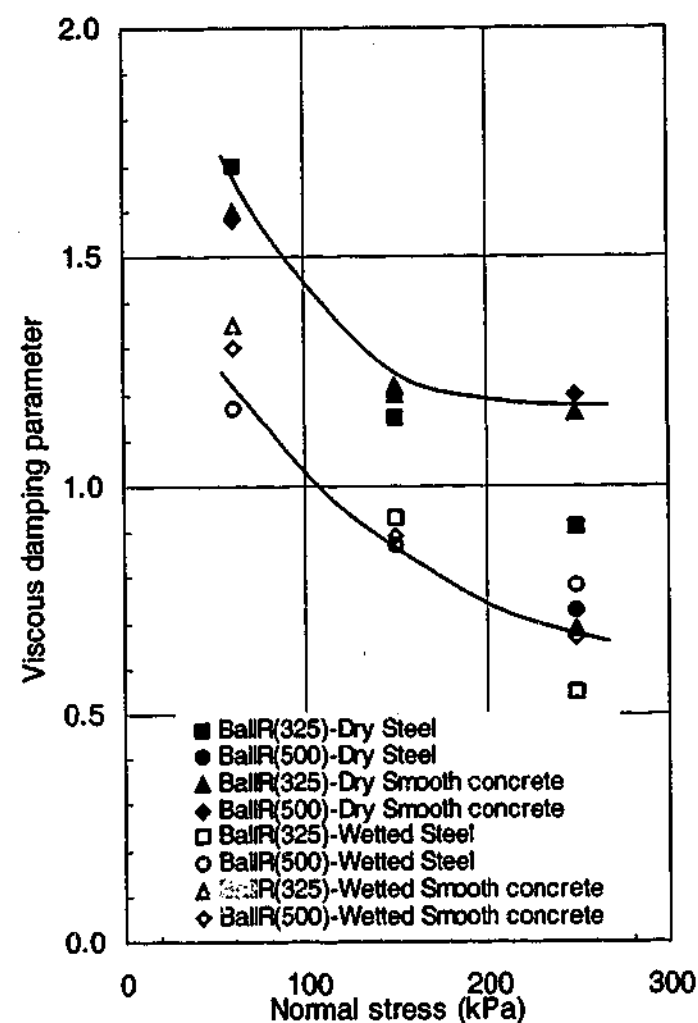


Figure 8.16 Mode 1: The effect of wetted pile surface on the viscous damping parameter

For the interfaces with Mode 2 failure, the dynamic responses of the BallR clay tested on dry and wetted pile surfaces are compared in Figure 8.17. The viscous damping parameter for the wetted pile does not vary in a consistent manner relative to the dry pile; this can perhaps be attributed to the complex interaction between the water on the pile surface, the smeared pile surface and the applied normal stress.

Since it has been established for Mode 3 failure that shearing occurred between the intact clay block and the layer of clay that had adhered to the pile surface, the pile condition is not expected to affect the dynamic response of the interface with Mode 3 failure.

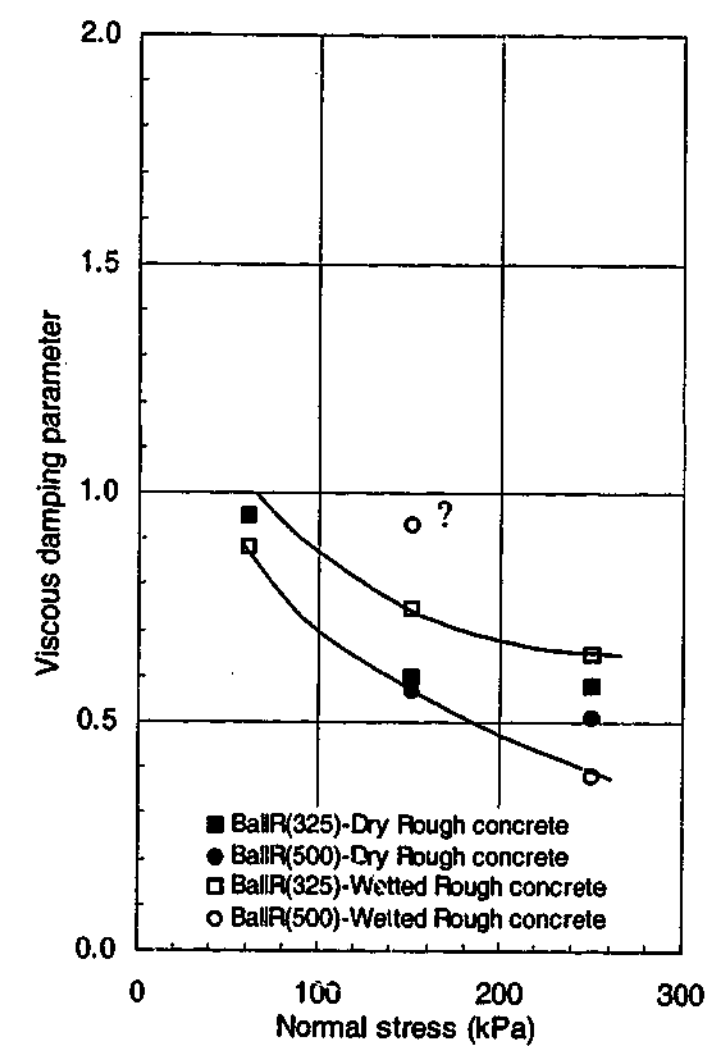


Figure 8.17 Mode 2: The effect of wetted pile surface on the viscous damping parameter, α of the interface

8.10 Correlation & Estimation of α

It has been shown that when α values are plotted against shear strength, consistent α -shear strength relationships for the three dynamic shear modes could be observed. However, when α values are plotted against normal stress and OCR , general but less consistent trends could be observed.

As shown in Equation (8.1), the shear strength is dependent on the preconsolidation stress and the applied stress, and the properties of the clay (as the shear strength ratio

for the normally consolidated sample $\left[\frac{S_u}{\sigma'_v} \right]_{\sigma'_p=1}$ and the power m depend on the

properties of the particular type of clay). Therefore, the shear strength is a fundamental soil parameter that encapsulates the stress conditions imposed on the

soil and the intrinsic properties of the clay (plasticity and mineralogy). It is thus a suitable and meaningful parameter against which to correlate the damping parameter. The α -shear strength correlations, differentiating the failure mode, have been presented in a more general form in Figure 8.18. The plot shows essentially two bands of data, with the upper band associated with Mode 1 and the lower band associated with Modes 2 and 3. The data interfaces involving wetted surfaces have been excluded as free water is not expected to gain access to the interface. It is noted that further research will be required to obtain data for low plasticity clay-rough surface and high plasticity rough surface interfaces.

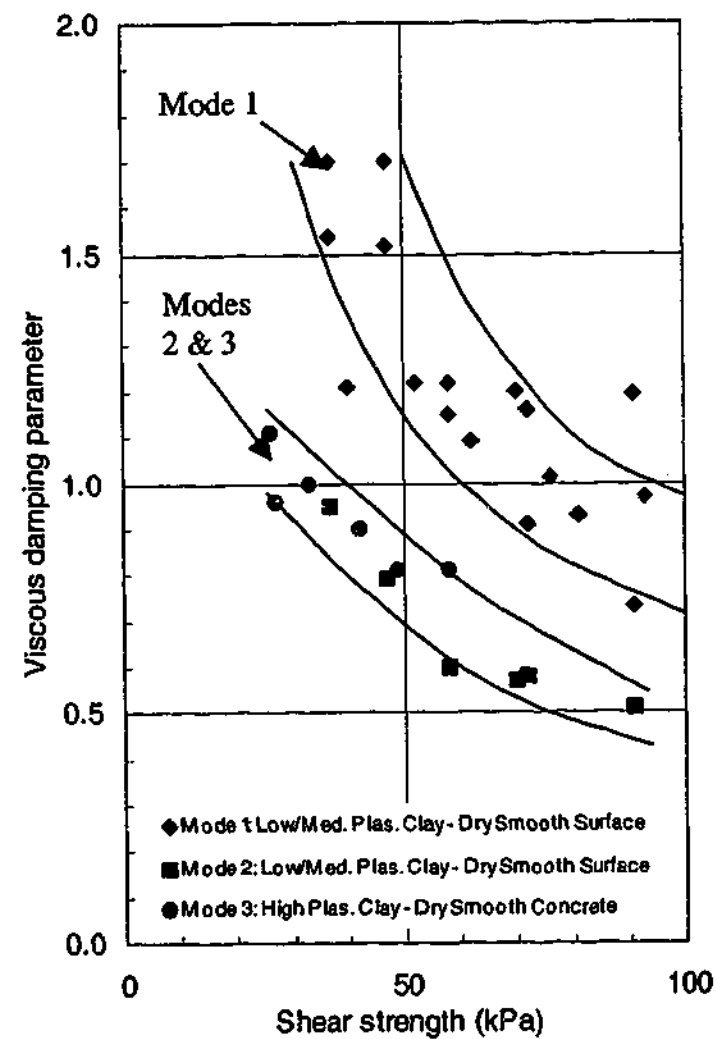


Figure 8.18 Guideline for selecting the value of α for Modes 1, 2 and 3 interface failure

It is noted once again that the initial (rather than the instantaneous) shear strength of the specimen has been used in the correlation. Such a correlation is of more practical value because in practice, the initial shear strength of the soil at a site (obtained from a site investigation) will be used to estimate the damping factor. It is also noted that this correlation is limited to three clays that are essentially kaolinite clays, three different plasticities (one low, one medium and one high) and with shear strengths ranging from soft to stiff clay. Despite the limited scope, it is proposed that until more data are available, the damping parameter-shear strength correlation may be used as a guide for estimating the interface dynamic friction. In the subsequent chapter, it will be shown that α values for piles installed in clays with various shear strengths back-calculated based on signal-matching analyses are consistent with the proposed correlation.

Based on the α -shear strength correlation, a simple procedure is proposed for estimating the α value (for a fixed value of $\beta = 3.0$) for a field pile installed in clay. Using Figure 8.1, the plasticity of the clay and the roughness of the pile are used to assess the failure mode. The smooth steel and smooth concrete surfaces have been classified as "smooth surface". For driven steel and concrete piles, the pile roughness should be approximately equivalent to this "smooth surface". Using the deduced failure mode and shear strength obtained from the site investigation, the value of α can be estimated from the correlation presented in Figure 8.18.

8.11 Towards an Understanding of Viscous Damping

The outcome of the analyses of the experimental data collected in this study provides a starting point in understanding and predicting the dynamic friction due to viscous damping.

8.11.1 Occurrence of viscous damping in clay soils

It has been found that the friction at the pile-clay interface increases with increasing shear rate, whilst the friction at the pile-sand interface is essentially independent of the shear rate. The different viscous damping responses of the pile-sand interface and the pile-clay interface would suggest that significant viscous damping at the interface only occurs when the soil contains at least some clay fraction. It is noted that real

soils rarely consist exclusively of sand, and that only a relatively small fraction (say 10 to 15%) of clay is required to make the behaviour of a sandy soil like that of clay (Wroth and Houlsby, 1985).

The significantly different damping responses for the pile-sand and the pile-clay interfaces are clearly due to fundamental differences in the clay and the sand. Some of the main differences can be summarised as follows:

- The mineralogy of sand is very different from that of clay (Mitchell, 1993);
- Sand particles are relatively rotund as compared to the plate-like forms of clay particles (Wroth and Houlsby, 1985);
- The interaction between the sand particles can be understood in terms of purely mechanical interaction, whereas the interaction between clay particles is a more complex process involving electro-chemical forces (Wroth and Houlsby, 1985) where bonds between the clay particles are present even in the absence of an externally applied force on the specimen.

Further fundamental studies of the viscous damping phenomenon will be required to identify the exact source(s) of the significantly different damping responses of the two materials.

8.11.2 Proposed mechanism of viscous damping

Based on experimental observations of the shear surface, it has been hypothesised that the increase in the pile-clay interface resistance at high shear rates is due to the disordering of the clay particles at the interface. According to this hypothesis, the higher the shear rate, the higher the degree of disordering and the corresponding the value of the damping parameter. This hypothesis has been used as a framework for interpreting the effects of the shear failure mode, the shear strength, normal stress, *OCR*, pile surface condition (wet or dry) and pile roughness on the viscous damping parameter, and the hypothesis appears to be able to give meaningful interpretations of the effects of these parameters on the value of the viscous damping parameter.

8.11.3 Implications of proposed hypothesis for pile-soil

If the proposed hypothesis is correct, then the fundamental differences in the soil-only and interface shear tests may result in different mechanisms of disordering of the clay particles. The first difference is that bonds are formed between the soil

particles within a soil specimen whilst bonds are formed between the clay particles at the interface and the pile surface such that the particle disordering in the latter depends on the characteristics of the pile surface in addition to the properties of the soil. Secondly, it has been postulated by Lupini et al. (1981) and later confirmed experimentally by Lemos and Vaughan (2000) that the movement of the clay particles for a clay being sheared in a soil-only test can be different from that for the same clay being sheared against an interface. Finally, if the hypothesis that has been proposed for the mechanism behind viscous damping is true, then the disordering of the clay particles at the shear plane is likely to be more drastic for a clay being sheared against an interface. This is because intuitively the hard surface (as opposed to the surrounding clay particles) is more effective in causing the disordering. This reasoning is consistent with:

- the finding based on penetrometer tests by Dayal and Allen (1975) and Litkouhi and Poskitt (1980) that the viscous damping parameter for the interface response is higher than that for the soil-only pile tip response;
- general recommendations that favour the use of lower damping values at the pile base than along the shaft (Randolph, 1990); and
- the finding from this study that the viscous damping parameter of the interface subjected to the Mode 3 failure (which involves shearing between the clay specimen and a layer of clay) is lower than that of the interface subjected to the Mode 1 failure.

8.11.4 Dependence on physical parameters

Based on the pile-clay interface tests conducted in this study, the effects of the physical parameters, which are classified into soil parameters and pile parameters, on the viscous damping parameter can be illustrated in Figure 8.19. The preconsolidation stress of the specimen, the applied normal stress on the specimen and the clay type determine the shear strength of the specimen, as mathematically expressed in Equation (8.1). The plasticity of the clay and the pile roughness dictate the failure mode of the interface, as has been illustrated earlier in Figure 8.1. In turn, the shear strength of the specimen, the failure mode of the interface, the pile roughness and the surface condition of the pile surface (wetted or dry) determine the strength ratio and hence the value of the damping parameter (α).

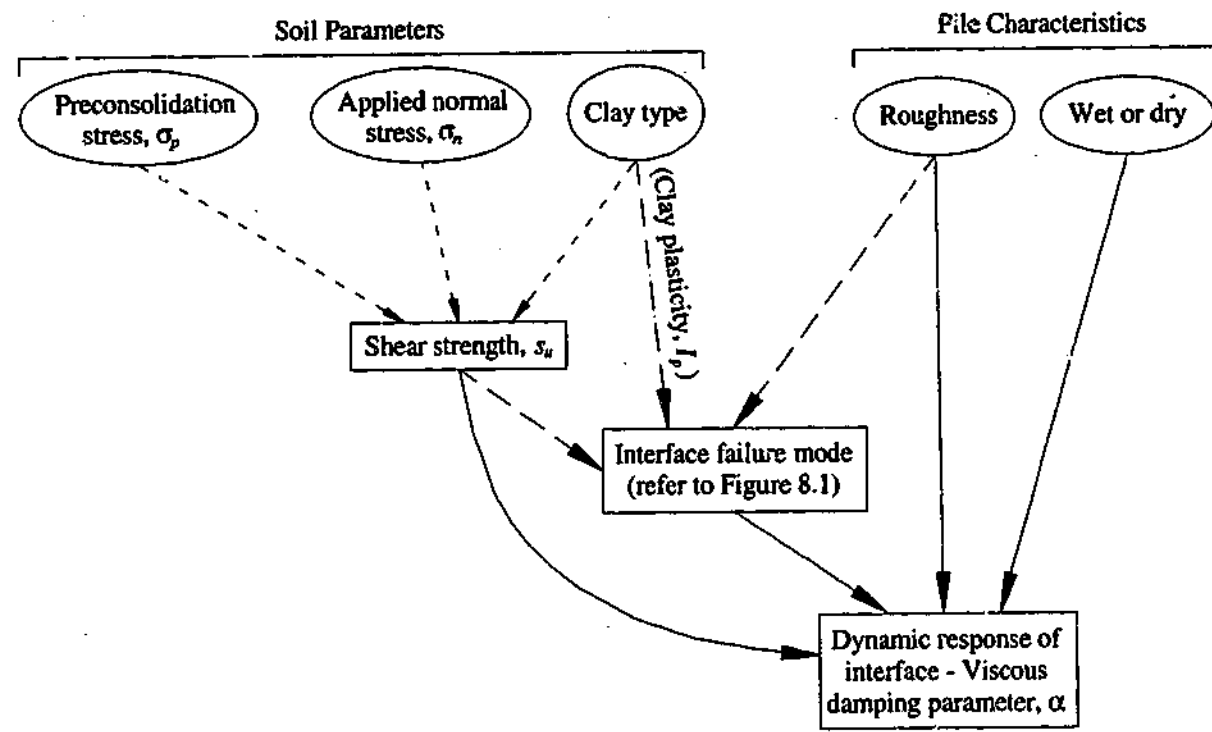


Figure 8.19 Influences of pile characteristics and soil properties on the viscous damping parameter

More specifically, the dependence of the value of the damping parameter, α on the parameters is summarised as follows:

Dependence on interface shear failure mode

- The value of α for an interface failing in Mode 1 is higher than that of an interface failing in either Mode 2 or 3.

Dependence on pile characteristics

- A clay being sheared against a wetted pile surface has a lower value of α than a clay being sheared against a dry pile surface.
- A low or medium plasticity clay being sheared against a smooth pile surface results in Mode 1.
- A low or medium plasticity clay being sheared against a smooth pile surface results in Mode 2.

Dependence on soil parameters

- For a particular failure mode (and hence a particular clay and pile surface), the value of α increases with decreasing shear strength. This relationship is supported by experimental data from previous studies (Dayal and Allen, 1975; Heerema, 1979). As a result of this relationship, the following is true:

1. For a specimen that has been preconsolidated to a certain stress, the value of α increases with decreasing normal stress;
 2. For two specimens that are loaded at the same normal stress, the specimen with the higher preconsolidation stress has a lower value of α ; and
 3. For a specimen that has been preconsolidated to a certain stress, the value of α increases with increasing *OCR* (or decreasing normal stress).
- A low or medium plasticity clay being sheared against a smooth pile surface results in either Mode 1 or 2 failure, depending on the pile roughness.
 - A high plasticity clay being sheared against a pile surface of any roughness results in Mode 3 failure.

8.12 Summary

In this chapter, a hypothesis for the mechanism of viscous damping has been proposed based on the experimental observations of shear surfaces on the clay specimen that have been subjected to fast shearing. This hypothesis has been used as a framework for interpreting the effects of soil and pile parameters on the value of the damping parameter, α and has been found to be consistent with the experimental data.

The value of the damping parameter for a particular pile-clay interface has been found to be dependent on the soil and pile parameters, and the failure mode resulting from the interaction between the plasticity of the clay and the surface roughness of the pile. It has been found for each of the dynamic failure modes that the viscous damping parameter α is inversely proportional to the shear strength of the clay. Also, it has been found that, when α values are plotted against normal stress and *OCR*, general but less consistent trends could be observed.

The correlation between α and the shear strength is convenient as the shear strength encapsulates the effects of the stress conditions of the soil and the intrinsic properties of the clay. Since the clay plasticity and the surface roughness dictate the dynamic failure mode, these two parameters will therefore serve as inputs to the α -shear

strength plot for determining the appropriate α value for a particular interface. Thus, the correlation coupled with the exponential function (formulated in Section 7.8) have been proposed as a new viscous damping model.

Chapter 9

9. Performance of Proposed Model in Signal-Matching Analyses

9.1 General

In Section 2.2.5.2, the principles of the CAPWAP[®] signal-matching analysis, which makes use of a damping model for modelling the dynamic resistance, have been discussed. In collaboration with Pile Dynamics, Inc., and GRL Engineers, Inc., the exponential damping model proposed in this study has been incorporated into a research version of CAPWAP[®]. In this chapter, the performance of the proposed exponential damping model in signal-matching is evaluated using the linear viscous damping model as a benchmark, for over 40 sets of dynamic data.

9.2 Methodology of the Study

In order to assess the performance of the proposed exponential model in signal-matching, the model has been implemented, through the collaboration and the support of Pile Dynamics, Inc. and GRL Engineers, Inc., into a research version of CAPWAP[®] known as CAPWAP[®] 2003-1.Research.BETA. (It is noted that CAPWAP is a registered software; however for the sake of convenience the trademark symbol [®] is excluded from hereon). It is noted that the proposed exponential damping model is implemented only to the damping model for the pile shaft as the proposed model applies only to the pile-soil interface.

CAPWAP has been chosen as a platform for the implementation of the model and the signal-matching analyses because it is the most commonly used signal-matching package in the industry and a vast experience of signal-matching analysis based on this package is available. Furthermore, the implementation of the new proposed model into the research version of CAPWAP will hopefully pave the way for the use of the proposed model in practice.

Using the research version of CAPWAP, the dynamic data are signal-matched using both the exponential model and the original linear model. The CAPWAP analysis performed using the exponential model is simply referred to as “CAPWAP(expo)” and the CAPWAP analysis performed using the original linear model is referred to as “CAPWAP(linear)”. Furthermore, the values of the CAPWAP parameters obtained from the CAPWAP(expo) analysis are denoted with “(expo)” and those obtained from the CAPWAP(linear) analysis are denoted with “(linear)”.

Although CAPWAP allows different amounts of damping to be modelled at different segments along the pile, in practice a single damping factor is typically applied to the entire length of the pile for several reasons:

- the appropriate amounts of damping for different soil materials are not known;

- the natural soil strata usually consist of many layers of different soils for the modelling (in terms of the damping) of each of the individual layers to be practical; and
- modelling different amounts of damping for different soil layers is usually not justifiable as it is not likely to improve the match and the accuracy of the computed pile capacity.

The use of a single damping factor results in an “average” damping factor being computed for a pile in the signal-matching process. As such, the static resistance for the soil layer exhibiting less damping is underpredicted and the static resistance for the soil layer exhibiting more damping is overpredicted (PDI, 1994). However, it is also noted that since the error resulting from the use of a single damping factor is “absorbed” by the static resistance, the use of the single damping factor does not compromise the quality of the match or the capability of the analysis in predicting the pile capacity.

To ensure that the shaft and toe resistance values computed with CAPWAP are credible, static analyses are performed based on geotechnical data (when available) to estimate the resistance values and it was ensured that the CAPWAP-computed values are not drastically different from the estimated values. However, this can only be done for cases where geotechnical data are available.

For each of the two CAPWAP analyses, the match quality is optimised, and when the match has been optimised, the values of the resistances and the CAPWAP parameters are deemed to be determined.

It is noted that the CAPWAP analysis does not yield a unique solution, as discussed in Section 2.2.5. Thus, the values of the resistances and the CAPWAP parameters obtained from the two analyses are not unique.

9.2.1 Aims

The aims of the CAPWAP analyses are:

1. To confirm that the exponential damping model derived from the laboratory tests can be used to successfully match pile-soil responses measured in dynamic tests;
2. To determine the effect of the exponential damping model on the shaft, toe and total capacities, the shaft friction distribution, the loading and unloading soil parameters used in CAPWAP, and the quality of the match;
3. To determine the effect of the model on the capacity prediction capability in cases for which static load test data are available;
4. To determine the relationship (if any) between the exponential damping factor and the soil type;
5. To confirm that a relationship between the shear strength of clay and the exponential damping factor does exist as indicated by the experimental data obtained from this study;
6. To determine whether the exponential model (which models the actual damping response) will enable more consistent damping factors for EOD blows (performed at the end of pile installation) and for BOR (restrike blows performed sometime afterwards) to be computed; and
7. Based on the outcomes of points 5, 6 and 7, to determine whether the exponential damping factor is physically meaningful and dependent on standard soil properties.

9.2.2 Summary sheets

Aims 2, 3 and 4 are achieved using the original linear damping model as a benchmark. In order to facilitate comparison of the outcomes of the two analyses, the outputs from the two analyses for each case are summarised in the form of a 2-page summary. A sample of the summary is included in Figure 9.1. On the first page, the output of the CAPWAP(linear) analysis is shown on the left-hand side, whilst the output of the CAPWAP(expo) analysis is shown on the right-hand side. The summary on this page contains:

- details of the pile model
- shaft, tip and total capacity

- resistance distribution in numerical and graphical forms
- CAPWAP parameters
- match quality number
- measured and computed wave-up curve
- measured and computed set (in mm) and equivalent blowcount (in blows/metre (b/m)).

The meaning and significance of the CAPWAP parameters are explained in detail in the CAPWAP manual (PDI, 2000); for the convenience of the reader, the relevant sections have been reproduced in Appendix B.

On the second page, the following are included:

- A summary of available stratigraphic information;
- The measured force and velocity at the pile top;
- The computed static, dynamic and total resistances of the system (rather than of any individual element) during the testing event, for both the linear and exponential models;
- The measured velocity at the pile top and the CAPWAP-computed velocities of the middle and bottom segments of the pile during the testing event. This allows the relevant velocity regime in the strength ratio vs. velocity relationship to be identified; and
- The strength ratio vs. velocity relationships obtained based on the two models for a single element and for the velocity regime relevant to the particular case. It is important to note that the strength ratio vs. velocity relationship does not indicate the total amount of damping modelled for the entire system.

The summary sheets for all the cases analysed can be found in Appendix C in the following order:

- ID1 to ID26 sourced from Pile Dynamics Inc.
- ID27 to ID38 sourced from PDA-W example files provided by Pile Dynamics Inc.
- ID39 to ID44 sourced from local foundation companies based in Melbourne, Australia

ID 1
817720 L310K300-320;uCL11;CL-TLL; H pile

Filename: 1.daf
Smith Linear Viscous Damping using RuR for Shaft

(A) Pile Model

Depth (m)	Area (cm ²)	E-Mod (MPa)	Spec Wt (kN/m ³)	Circum (m)	Top Impedance (322.79 kN/m ²)	Added Impedance (None)	Wave Speed (5119.8 m/s)
0	80	206579	77.287	1.016			
21.95	80	206579	77.287	1.016			

(B) Resistance Distribution

Depth (m)	Ru (kN)	Unit (kPa)	Total capacity (kN)	Shaft capacity (kN)	Toe capacity (kN)
2.1	5.1	4.84	1815.4	1502	313.0
3.1	5.1	4.84			
4.2	5.4	5.13			
5.2	14.4	13.58			
6.3	14.3	13.49			
7.3	14.1	13.3			
8.4	21.8	20.52			
9.4	31.5	29.84			
10.5	30.6	28.78			
11.5	33.1	31.15			
12.5	51.1	48.16			
13.6	142.2	133.94			
14.6	208.9	198.73			
15.7	208.9	198.73			
16.7	104.4	98.32			
17.8	104.1	98.03			
18.8	107.8	101.55			
19.9	107.8	101.55			
20.9	145.6	137.17			
21.9	145.6	137.17			

Avg Skin: 75.1 kN/m
Toe: 313.4 kN

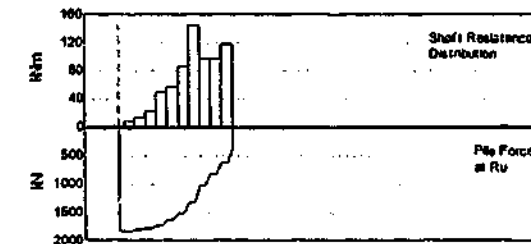
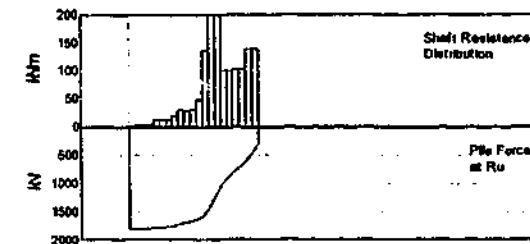
Filename: 1.rinat.m
Exponential Viscous Damping using Rinat for shaft

(A) Pile Model
As per Smith Linear Viscous Damping

(B) Resistance Distribution

Depth (m)	Ru (kN)	Unit (kPa)	Total capacity (kN)	Shaft capacity (kN)	Toe capacity (kN)
3.1	18.9	8.98	1834.4	1450	384.5
5.2	28.4	13.39			
7.3	47.6	22.42			
9.4	102.7	48.35			
11.5	119.3	58.18			
13.6	180.1	84.83			
15.7	302.6	142.49			
17.8	201.7	95			
19.9	201.7	95			
21.9	247.1	116.37			

Avg Skin: 145 kN/m
Toe: 384.3 kN



(C) CAPWAP Parameters

JS	SS	QS	UN	CS	LS	PI	OP
2.261	0.48	2.4	0	1	0	0.01	0
JT	ST	QT	TG	CT	LT	PL	
0.851	0.676	4.8	0	1	0	2.8	

(C) CAPWAP Parameters

JS	SS	QS	UN	CS	LS	PI	OP
2.138	0.48	2	0.025	1	0	0.01	0
JT	ST	QT	TG	CT	LT	PL	
0.413	0.33	1	3.5	1	0	0	

(D) Match
CAPWAP match quality: 2.26 (Wave Up Match)
Observed: final set = 1.693 mm; blow count = 591 b/m
Computed: final set = 0.836 mm; blow count = 1204 b/m

(D) Match
CAPWAP match quality: 1.94 (Wave Up Match)
Observed: final set = 1.693 mm; blow count = 591 b/m
Computed: final set = 0.914 mm; blow count = 1094 b/m

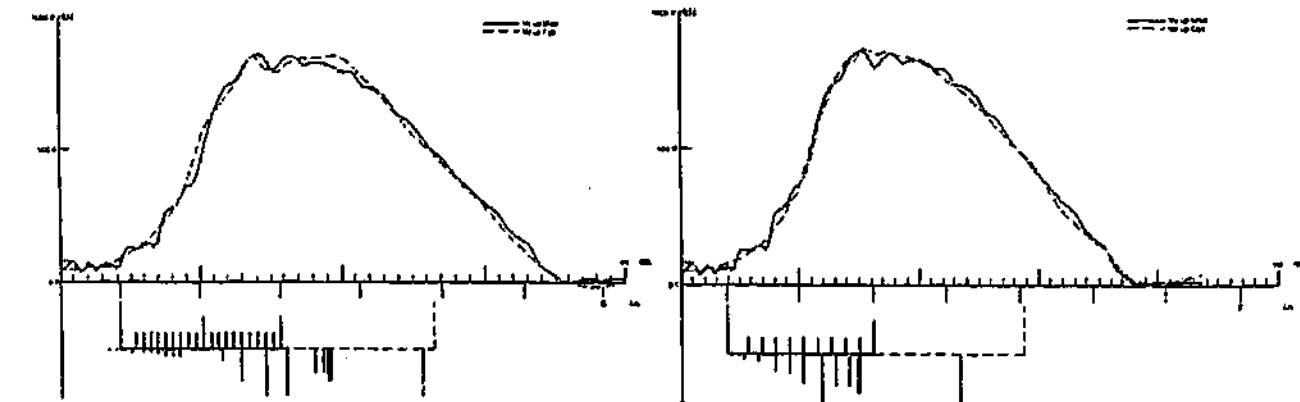


Figure 9.1 A sample of the 2-page summary for one case

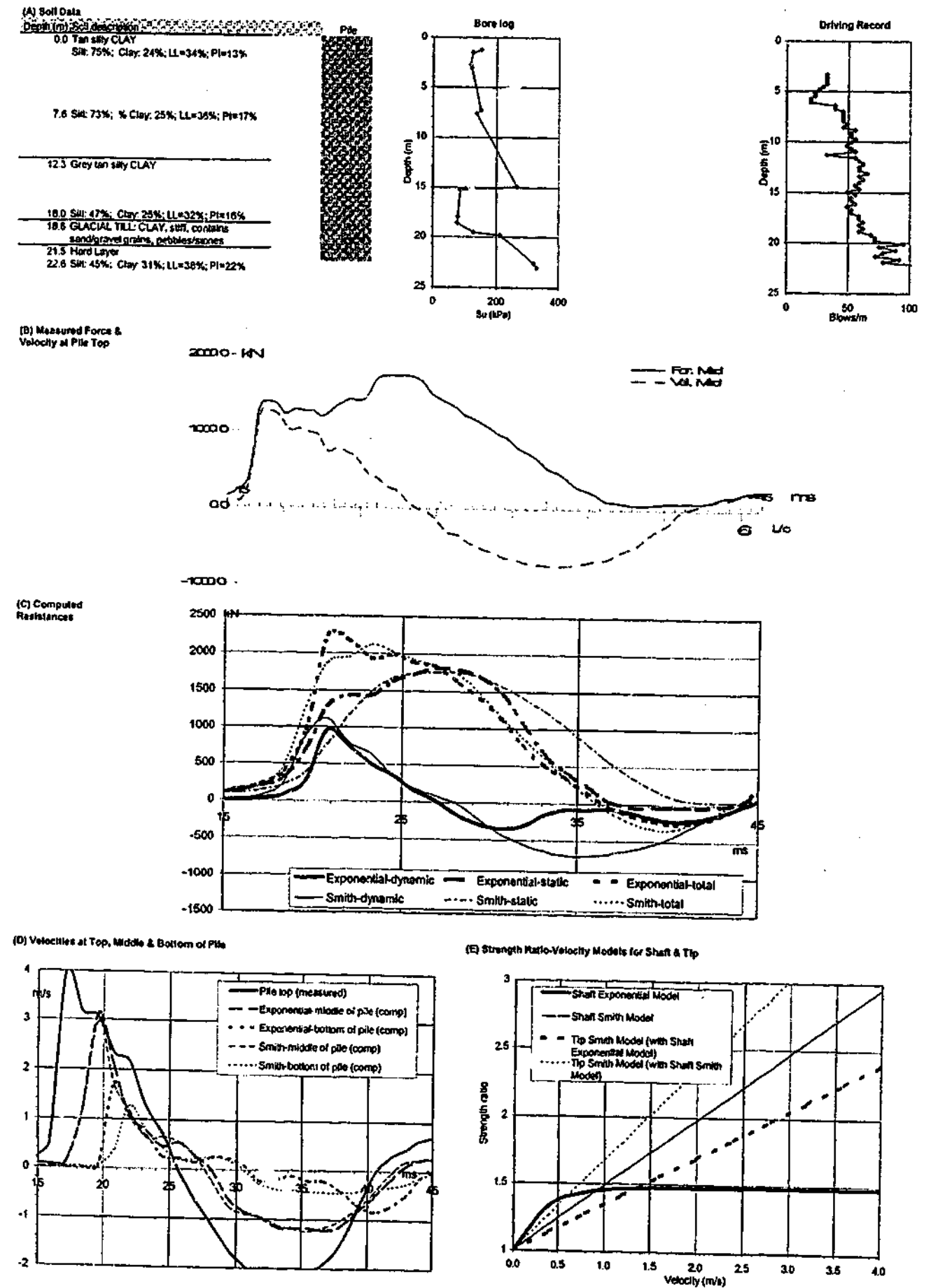


Figure 9.1(cont'd) A sample of the 2-page summary for one case

9.2.3 Cases selected for analyses

Since viscous damping at the pile-sand interface has been found to be negligible, only cases involving pile shafts installed in cohesive soils are analysed. These cohesive soils vary from pure clays to sands with significant fines content. Some of the cases involve piles with their tips founded on sands.

Most of the cases selected involve moderate to high pile sets as it is believed that the difference between the two damping models will be most evident in such cases.

Altogether 44 cases have been selected for analysis and have been named ID1 to ID44. The 44 cases involve driven steel (closed-ended tube, open-ended tube, H sections) and concrete piles (prestressed, simply reinforced), but not drilled shafts or bored piles.

Nine of the cases are end-of-drive (EOD) records whilst the other 35 are beginning-of-restrike (BOR) cases. An EOD record pertains to a hammer blow at the end of the pile installation, whilst a BOR record pertains to a hammer blow applied some time after the pile has been installed. It is noted that between the time of installation and the time afterwards, the pile capacity may increase due to 'set-up', particularly for piles in cohesive soils. The set-up effect is primarily associated with the dissipation of positive excess pore pressure built up in the soil surrounding the pile during driving installation. Therefore to assess the long-term capacity of the pile, the static load test and the dynamic test are usually performed some time after the pile installation. During a restrike dynamic test, it is desirable that the full pile capacity is mobilised within the first few blows in order not to destroy the set-up effect, thus the *beginning* of restrike is preferred for analysis.

The selected cases can be classified into two broad categories, namely, cases with and without static load test data. The cases without static load test data have been sourced from local foundation companies and the collection of PDA-W example files provided by Pile Dynamics Inc. The cases with static load test have been sourced from the database developed by Pile Dynamics Inc. The cases in the database contain the following as outlined by Likins et al. (1996):

- Static load test data where the test was carried to the Davisson failure or beyond to the ultimate failure load;
- Dynamic test record for BOR;
- Dates of the static load test and the dynamic test for ensuring that the dynamic test has been performed at a time comparable with the static load test;
- The details of the pile including the length, the embedment length, type and shape, and the details of hammer used including the rated energy and the type;
- Soil information including soil description and soil strength information, based on a soil boring in the vicinity of the pile; and
- Pile driving record with blowcounts from EOD and BOR, and pile embedment lengths corresponding to the EOD and BOR blows.

All the cases sourced from the Pile Dynamics Inc. database have soil information. Most of the cases sourced from the local companies have detailed soil information based on a soil boring in the vicinity of the pile (including the SPT and soil description along the depth of the boring), whilst all the cases from PDA-W example files contain only a general description of the soil.

9.2.4 CAPWAP analysis

9.2.4.1 General

It is emphasised that CAPWAP analyses do not yield unique solutions and thus the CAPWAP-computed values presented in this study should not be assumed to be unique.

Out of the 44 cases analysed, 14 cases contained geotechnical data. For these cases, the tip capacity and shaft capacity are estimated based on static analyses to ensure that the computed shaft friction and toe capacity values are comparable to the estimated values and are hence credible. However, the credibility of the computed resistance values can only be checked as much as is practically possible because the static analysis and the data upon which the static analysis is performed involved some uncertainties (which will be discussed in detail in Section 9.4) – which is why

dynamic tests and analyses are necessary in the first place. Therefore, during CAPWAP analyses, the estimated shaft resistance distribution is not strictly adhered to at the expense of the match quality.

The observed blowcount is prone to being inaccurately measured and/or recorded in the field. Therefore, it is stated in the CAPWAP manual that it is desirable to match the set or the blowcount only if the blowcount has been accurately measured and recorded. Given that the reliability of the recorded blowcount is not known for the 44 cases, no attempt is made to match the measured set.

9.2.4.2 Radiation damping

As noted in Section 2.3.1, when a hammer blow is delivered to the pile head, the pile and to some degree, the soil surrounding the pile moves. Energy from the pile is used up in the shearing of the pile-soil interface in viscous damping and radiated away from the pile in radiation damping. The effect of viscous damping is more important than the effect of radiation damping when plastic displacement or true shearing occurs at the pile-soil interface (Danziger et al., 1999). Whilst at least some degree of radiation damping occurs during an impact event, its effect is most significant when the pile movements are low (hard driving) such that true shear does not occur at the pile-soil interface and the displacements are essentially elastic (Danziger et al., 1999; PDI, 2000). Two examples of such cases are a pile founded on hard rock and a drilled shaft installed in a cohesionless soil. In both cases, the pile does not slip past the soil but engages the soil in its small movement.

Since this is a study of the viscous damping behaviour, it is logical to select cases involving significant plastic displacements of the pile or cases with relatively high sets. Furthermore, these “high-set cases” have high velocities for which the differences in the exponential damping response and the linear damping response will be most pronounced, enabling the effects of the two viscous damping models on the analyses to be most clearly evaluated. Thus cases with relatively high sets were selected, with the exception of a few hard driving cases that were selected to evaluate the influence of the different damping models on hard driving. Consistent with the findings of the other researchers, almost all of the selected cases (i.e. with high sets) can be matched using CAPWAP without using its radiation damping model.

As discussed in Section 2.3.2, radiation damping along the pile shaft (and the pile tip) has been modelled theoretically by Randolph and his co-workers based on Novak’s elastodynamic theory. Apart from the geometry of the pile, the radiation damping parameters are dependent on the elastic parameters of the soil. The displacement and velocity of the soil are computed theoretically based on these parameters. However, in CAPWAP, radiation damping is modelled empirically. The radiation damping parameters are selected by the user in order to produce an ‘optimal’ match and are not necessarily dependent on the physical properties of the soil (although good practice would suggest that relating to ‘geotechnical truth’ is recommended). Nevertheless as a process, the soil velocity and displacement are calculated based on user-selected parameters (for producing a good match) and as such may not be representative of physical reality.

Given that the user-selected radiation damping parameters in CAPWAP are not necessarily based on a theoretically based model and that almost all the cases that have been encountered can be satisfactorily matched without the need for invoking the radiation damping model, it was decided that the analyses would be performed exclusive of any consideration of radiation damping. For the sake of consistency, the few cases which require the radiation damping model to produce satisfactory matches were excluded from this study.

9.3 Shaft Damping Models in CAPWAP

In Chapter 2, various damping models have been described in the general context of the dynamic methods. In this section, the damping models specific to CAPWAP, including the model proposed in this study, are discussed.

The original Smith model for a segment of the pile shaft is defined as:

$$R_{di} = J_{Smith} v R_{insti} \quad (9.1)$$

where i denotes the segment number, R_{insti} [kN] is the instantaneous static resistance at the interface between the pile segment and the surrounding soil, and the J_{Smith} [s/m] is the Smith damping factor. It is noted that the Smith formulation does not allow for soil movement so that the velocity used is the pile velocity rather than the relative pile-soil velocity.

It has been found that the linear viscous model, which is a modified version of the Smith damping model, is more likely to match measured records (PDI, 1994) and has since been adopted in CAPWAP. It is defined as:

$$R_{di} = J_{viscous} v R_{ulti} \quad (9.2)$$

where R_{ulti} [kN] is the ultimate static resistance mobilised at the interface and $J_{viscous}$ [s/m] is the linear viscous damping factor for the interface. It is noted that CAPWAP allows for the soil surrounding the pile to move if the empirical radiation damping model is invoked. In cases where the soil movement is modelled, the velocity used to compute damping is the relative pile-soil velocity. However, since radiation damping has not been considered for the cases analysed in this study, the velocity of the soil is zero and the viscous damping is effectively computed based on the pile velocity only. When there is a need, different damping factors can be applied to different pile segments by using damping multipliers and/or added damping. However, in the current study, a single 'average' damping factor is applied for the entire length of the shaft.

It is noted that the damping factor can be non-dimensionalised as follows:

$$J_c = \frac{\sum J_{viscous} R_{ulti}}{Z} \quad (9.3)$$

where Z [kN.s/m] is the pile impedance, computed as EA/c where E is the elastic modulus, A the cross-sectional area of the pile and c is the wave speed. This damping factor is known as the Case damping factor and is typically used in the context of the Case Method (PDI, 2000).

The alternative exponential model developed can be implemented in the research version of CAPWAP in either of the following forms:

$$R_{di} = \alpha(1 - e^{-\beta v}) R_{insti} \quad (9.4)$$

$$R_{di} = \alpha(1 - e^{-\beta v}) R_{ulti} \quad (9.5)$$

The velocity is the relative pile-soil velocity but since soil movement is not modelled for the selected cases, this velocity is effectively the pile velocity. It is noted that β has units [s/m] whilst α is dimensionless.

The exponential damping model has been implemented into CAPWAP in such a way that either the *instantaneous* static resistance or the *ultimate* static resistance can be used, depending on which produces a better match of the dynamic record. The use of either the ultimate or the instantaneous resistance can be justified as follows. When a dynamic interface test is performed, the total interface resistance (comprising the static and dynamic components) is measured and the total resistance can only be "isolated" into the static and dynamic components by dividing it with the *ultimate* static resistance obtained from a quasi-static test. Thus, the viscous damping model proposed based on the tests is formulated as a function of the *ultimate* static resistance rather than the *instantaneous* resistance. However, it can be argued that the total resistance during the elastic range at a particular time depends on the *instantaneous* static resistance (rather than the *ultimate* resistance) at the particular time.

The damping models for the pile toe in CAPWAP remain unchanged. The toe damping models can be the linear viscous model which is the most commonly used to produce a good match, the Smith model, or a combination of the Smith and linear viscous models (PDI, 2000).

In the subsequent discussion, the shaft damping factor based on the linear viscous damping model and computed from CAPWAP will simply be referred to as "the linear damping factor", and the shaft damping factor based on the proposed exponential model and computed from CAPWAP will simply be referred to as "the exponential damping factor".

9.4 CAPWAP-Computed Shaft Friction Distribution & Toe Bearing Capacity

As noted in Section 9.2.4.1, the tip capacity and the shaft resistance distribution have been estimated based on static analyses for the 14 cases for which soil data are available. The static analyses for all the cases (which involved piles installed in clay) were performed based on conventional total stress approach as detailed in Appendix D. It is reiterated that the credibility of the computed resistance values can only be checked as much as is practically possible due to various factors that might cause the estimated values (based on borelog data) to differ from the actual values at the time the dynamic test is carried out. These factors include the following.

- The dynamic test might not have mobilised the full tip capacity or/and shaft capacity of the pile;
- Whilst the borelog might be located in the vicinity of the pile concerned, the borelog might not be fully representative of the soil condition at the pile;
- There is a range of possible bearing capacity factors for stiff clays. A lower bound value of 9 is selected which is a conservative value widely used in practice based on the work of Skempton (1951). An upper bound value of 15 is selected after considering the study by Butterfield and Ghosh (1978) who reported a value of 15, and the study by Steele et al. (1990) who reported values in excess of 20 for stiff clay;
- The shaft capacity and toe capacity at the time of dynamic testing may differ from those computed based on the borelog because of the increase in the lateral stress (due to the introduction of the pile volume into the soil). Also, during the installation process, excess pore water pressure develops and remoulding occurs in the soil. After the pile installation, the excess pressure dissipates so that the strength of the soil (and the pile capacity) increases gradually with time. Therefore, the pile capacity estimated based on the borelog will be different from that at the time of the test; and
- For cases where only SPT data are available, the SPT number has been converted into shear strength. The correlation between the SPT number and shear strength is known to vary widely as shown by the comprehensive compilation of various correlations by Kulhawy and Mayne (1990). Based on

the overall average of the various compilations presented in Kulhawy and Mayne (1990), the shear strength is assumed to be 9 times the SPT number in the computation. Thus, the shear strength values used in these cases are only approximate.

Given the inherent uncertainties in the estimation of the shaft and tip capacities, the CAPWAP-computed values (necessary to produce a good match) may deviate from the estimated values; this is why dynamic tests and analyses are necessary in the first place. Therefore, as has been noted in Section 9.2.4.1, the estimated shaft resistance distribution is not strictly adhered to at the expense of the quality of the match.

The estimated and computed values from the two CAPWAP analyses of the shaft capacities are presented graphically in Figure 9.2. The details of the static analysis computation can be found in Appendix D. As shown in Figure 9.2, the two CAPWAP-computed shaft friction distributions are comparable and are not drastically different to the estimated distribution, indicating that CAPWAP-computed distributions are credible.

The estimated and computed values from the two CAPWAP analyses of the toe capacities are presented graphically in Figure 9.3. The details of the static analysis computation can be found in Appendix D. It is noted that a few of the cases involve piles with their tips founded on sand, and that for cases where the pile is founded on stiff clay, upper and lower bounds have been computed because of the range of possible toe bearing capacity factors. As shown in Figure 9.3, the CAPWAP-computed toe capacity generally falls between the lower and the upper bound values and/or is generally comparable to either of the lower bound or the upper bound values, indicating that CAPWAP-computed values are credible.

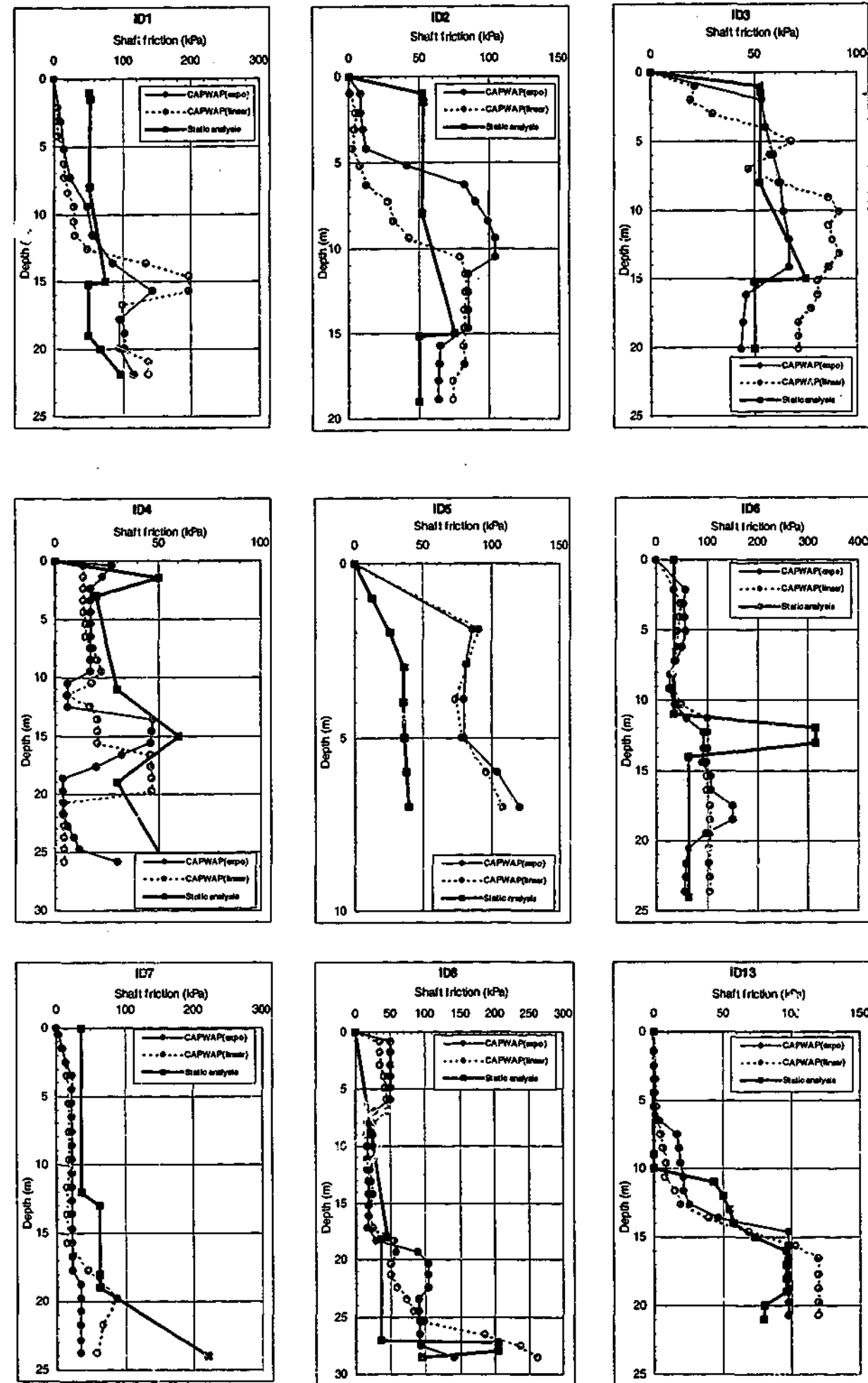


Figure 9.2 Estimated and CAPWAP-computed shaft friction values for the 14 cases

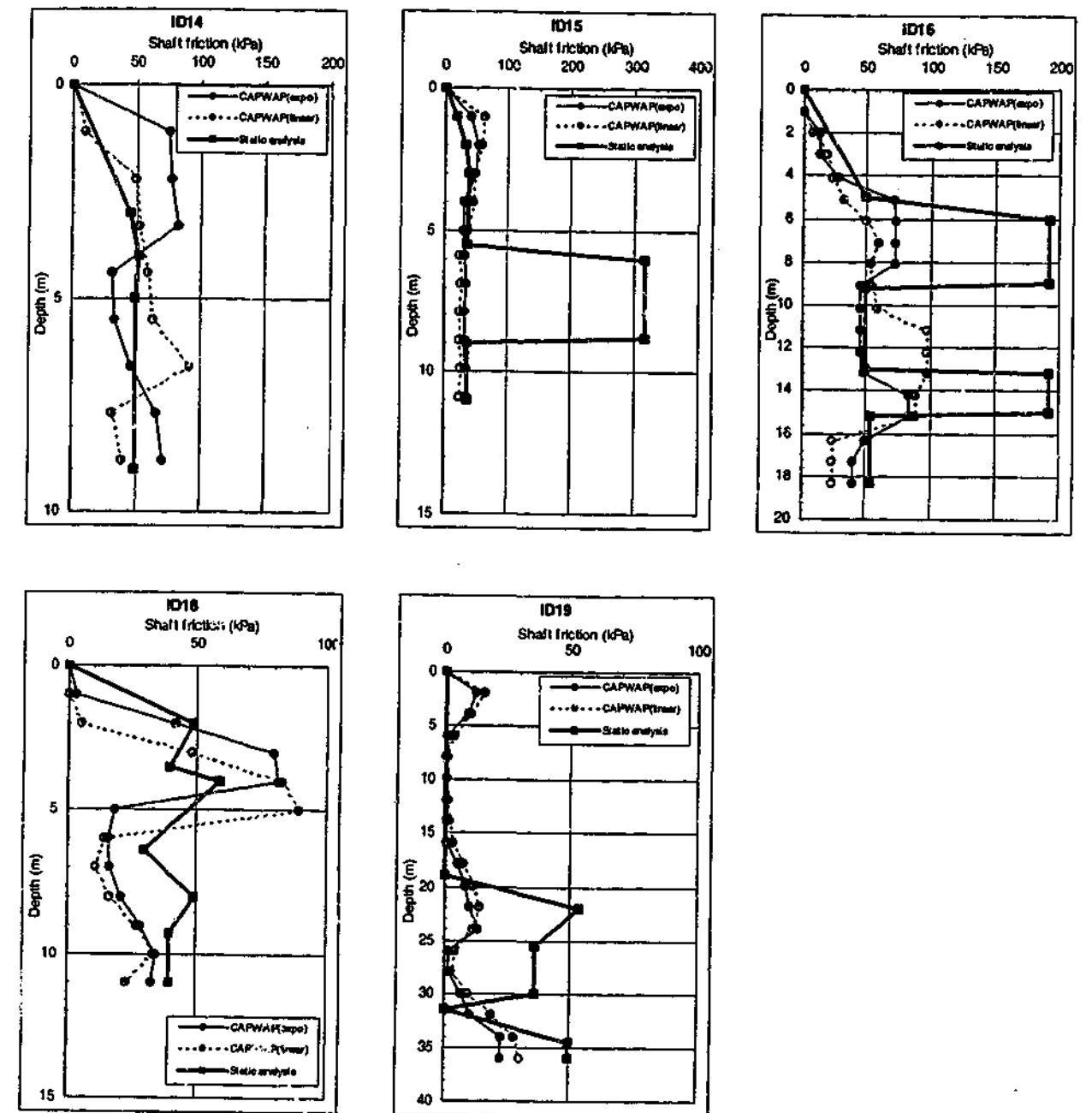


Figure 9.2(cont'd) Estimated and CAPWAP-computed shaft friction values for the 14 cases

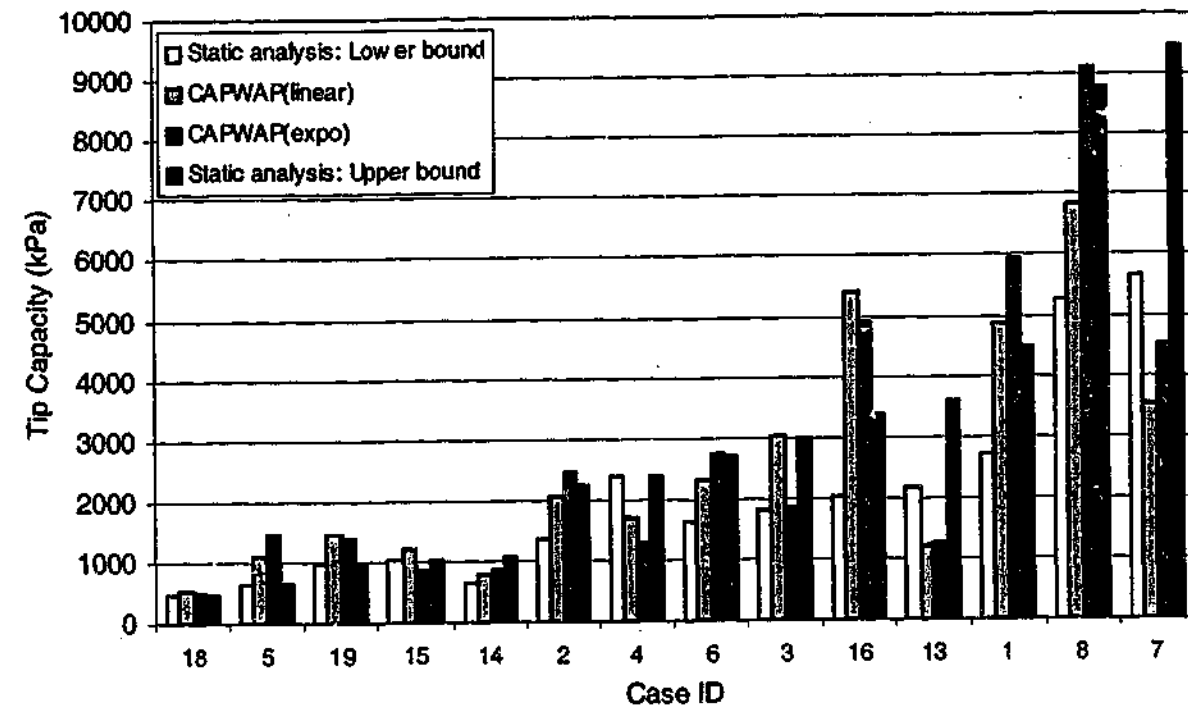


Figure 9.3 Estimated and CAPWAP-computed toe capacity values for the 14 cases

9.5 Comparative Shaft, Toe and Total Capacities, and Shaft Capacity/Toe Capacity

In order to determine the effect of the exponential damping model on the shaft, toe and total capacities, as well as on shaft capacity/toe capacity ratio, comparisons are made between the values obtained using the two analyses. The values of the four parameters obtained with the two shaft damping models are compared using bar charts in Figure 9.4, Figure 9.5, Figure 9.6 and Figure 9.7 respectively. The comparative values are also plotted in the x:y plot in Figure 9.8, Figure 9.9, Figure 9.10 and Figure 9.11 respectively, where the full line is the $y=x$ line and the dashed lines are reference lines indicating the range within which the CAPWAP(expo) value is $\pm 25\%$ of the CAPWAP(linear) value. As shown in these figures, for each of the four parameters, most of the CAPWAP(expo) values are within $\pm 25\%$ of the CAPWAP(linear) values.

The relative values of each of the four parameters computed with CAPWAP(expo) relative to the equivalent values computed with CAPWAP(linear) can be quantitatively assessed by obtaining the ratio of the CAPWAP(expo)-computed value to the CAPWAP(linear)-computed value. This is so that the values of the ratio

greater than 1.0, equal to 1.0 and less than 1.0 indicate that the value computed by CAPWAP(expo) is greater than, equal to and less than the equivalent value computed by CAPWAP(linear) respectively. For brevity, the ratios are denoted by Shaft(expo)/Shaft(linear), Toe(expo)/Toe(linear), Total(expo)/Total(linear) and (Shaft/Toe)(expo)/(Shaft/Toe)(linear). Statistical analyses are then performed on the respective ratios as shown in Table 9.1.

Table 9.1 Statistical analysis of Shaft(expo)/Shaft(linear), Toe(expo)/Toe(linear), Total(expo)/Total(linear) and (Shaft/Toe)(expo)/(Shaft/Toe)(linear), for all 44 cases

	Shaft(expo)/ Shaft(linear)	Toe(expo)/ Toe(linear)	Total (expo)/ Total(linear)	(Shaft/Toe)(expo)/ (Shaft/Toe)(linear)
Mean	1.02	1.05	1.02	1.03
Standard deviation	± 0.18	± 0.23	± 0.11	± 0.32

The mean values indicate that CAPWAP(expo) tends to predict a *slightly* (but not significantly) higher shaft, toe and hence total resistances. Thus, it follows that CAPWAP(expo) tends to compute an amount of total damping that is slightly less than or practically the same as CAPWAP(linear). It is noted the capacity prediction capability of CAPWAP(expo) (and CAPWAP(linear)) can only be ascertained where static load test data are available as in Section 9.8.

The toe and shaft capacities computed by CAPWAP(expo) are generally about $\pm 20\%$ of the equivalent CAPWAP(linear) values, whilst the total capacity computed by CAPWAP(expo) is generally only about $\pm 10\%$ of the CAPWAP(linear) value. The Shaft/Toe ratio computed by CAPWAP(expo) is greater because of the greater numerical values of the ratio.

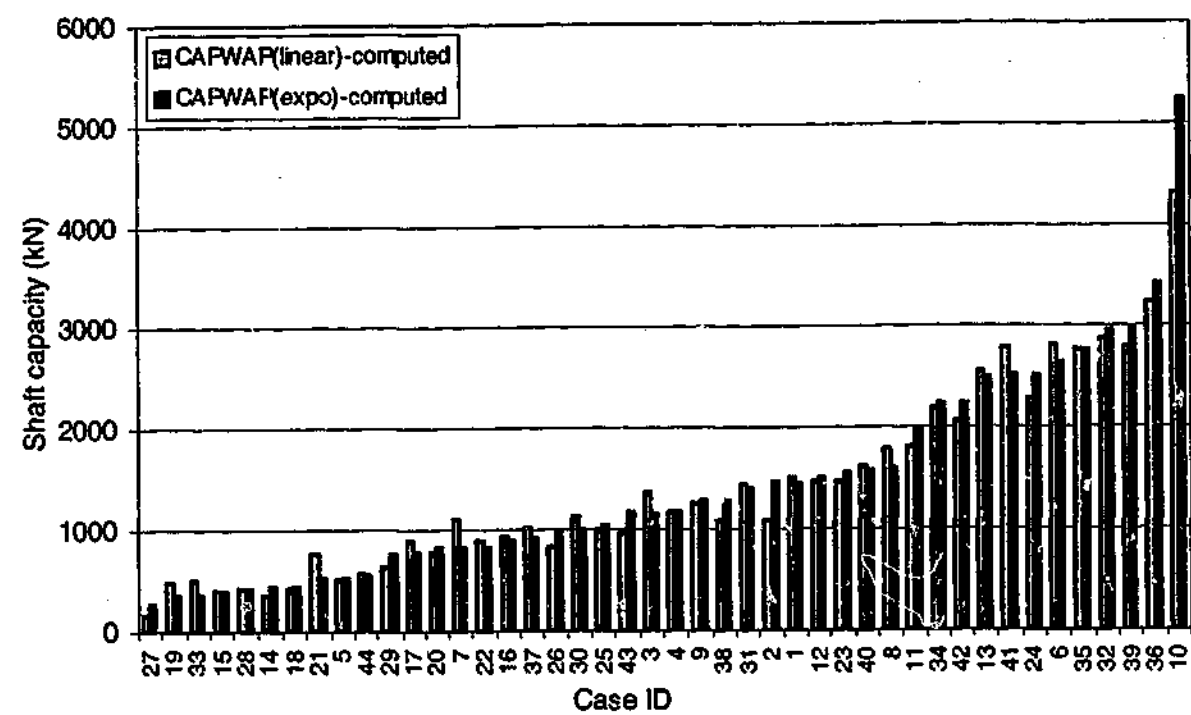


Figure 9.4 Comparative shaft capacity values computed using CAPWAP(linear) and CAPWAP(expo)

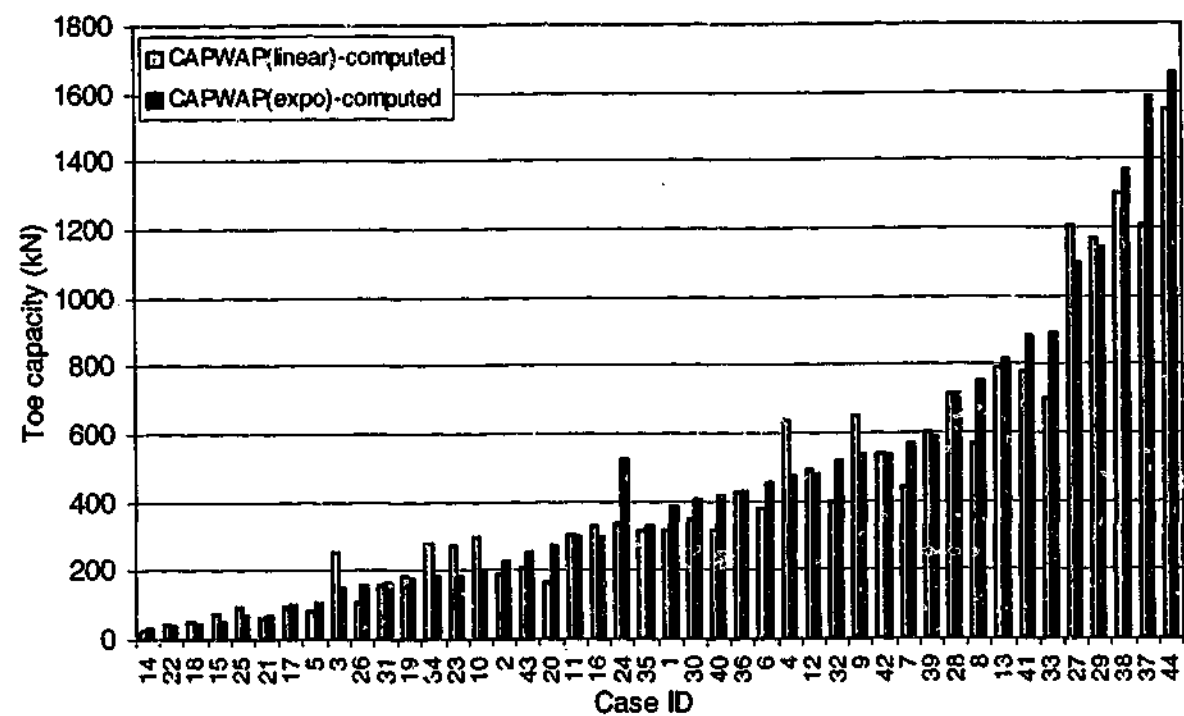


Figure 9.5 Comparative toe capacity values computed using CAPWAP(linear) and CAPWAP(expo)

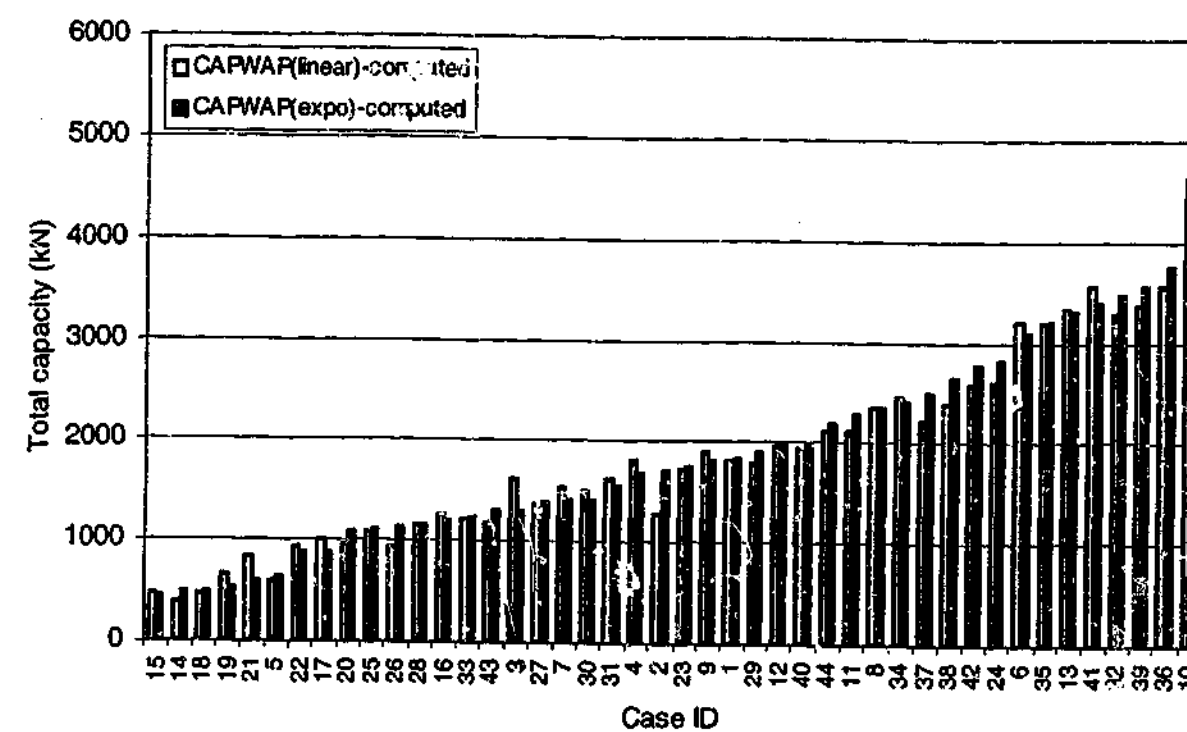


Figure 9.6 Comparative total capacity values computed using CAPWAP(linear) and CAPWAP(expo)

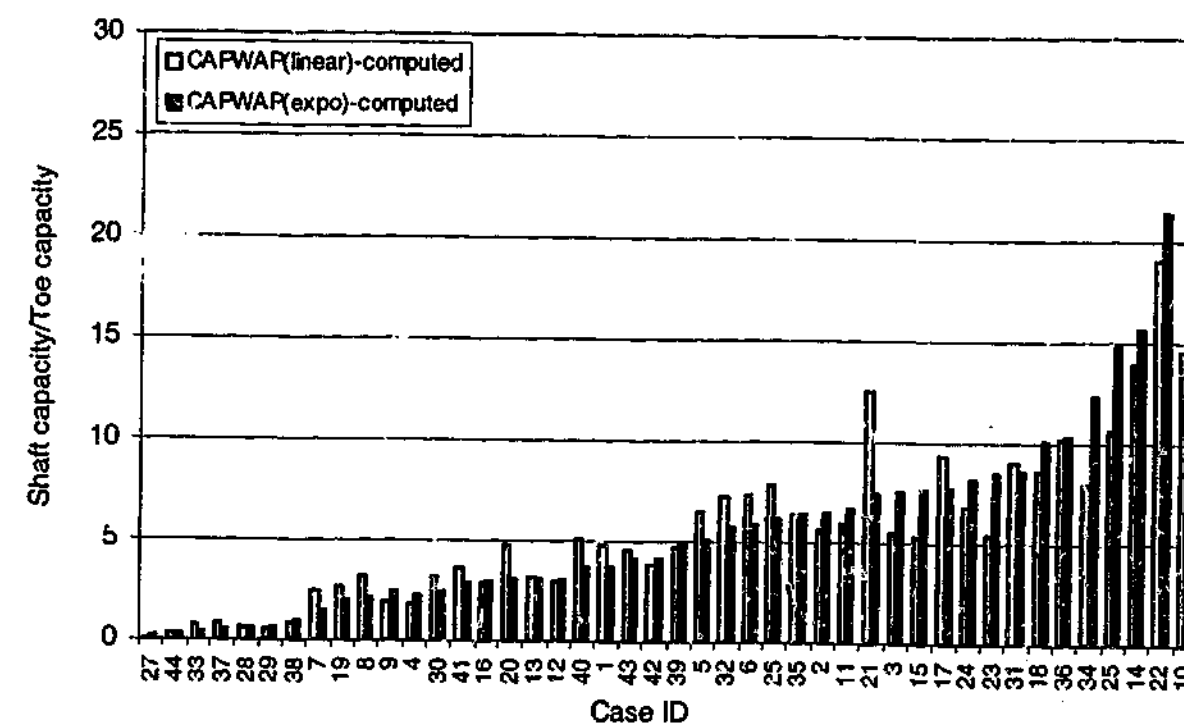


Figure 9.7 Comparative shaft capacity/toe capacity values computed using CAPWAP(linear) and CAPWAP(expo)

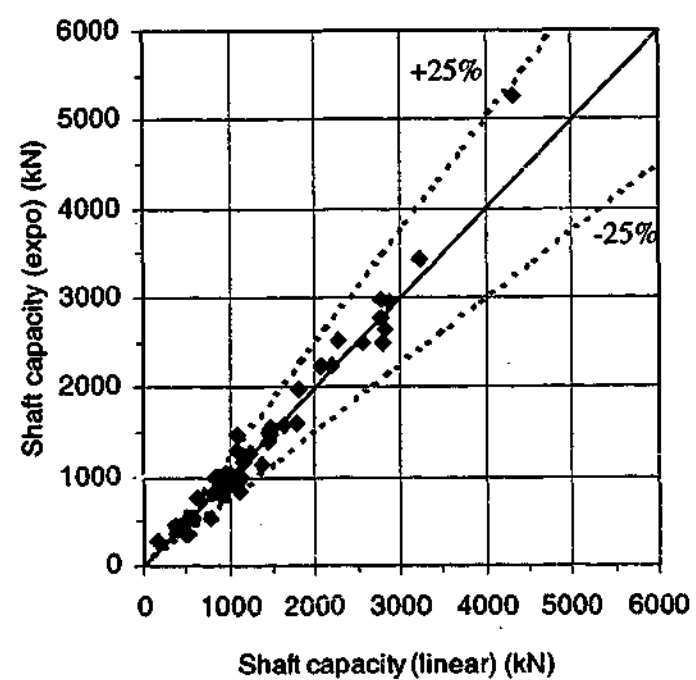


Figure 9.8 Shaft capacity values computed using CAPWAP(linear) and CAPWAP(expo)

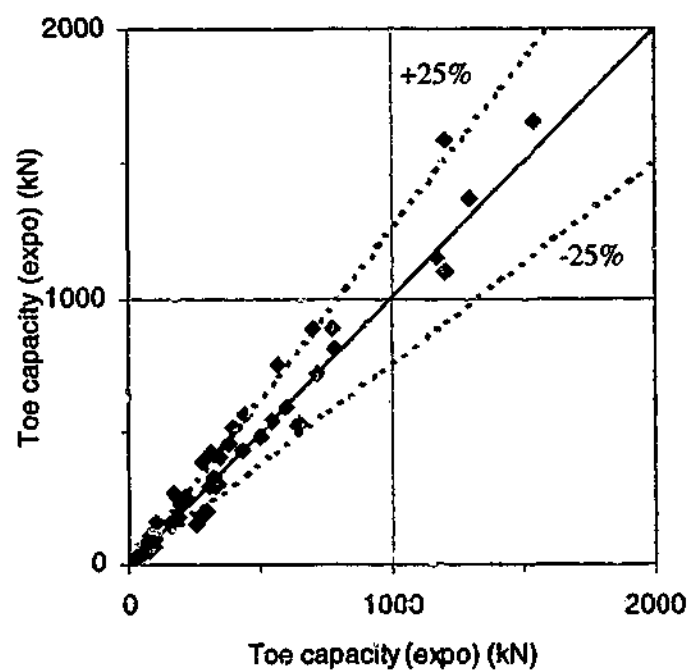


Figure 9.9 Toe capacity values computed using CAPWAP(linear) and CAPWAP(expo)

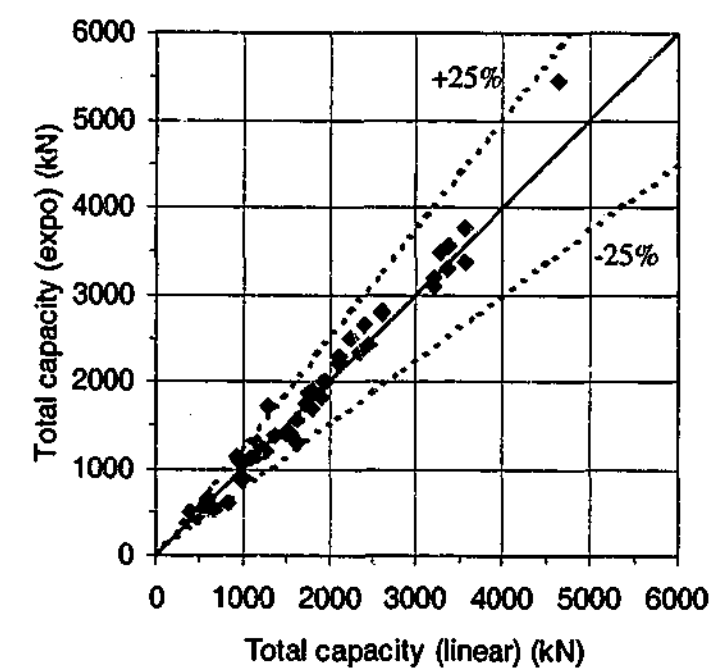


Figure 9.10 Total capacity values computed using CAPWAP(linear) and CAPWAP(expo)

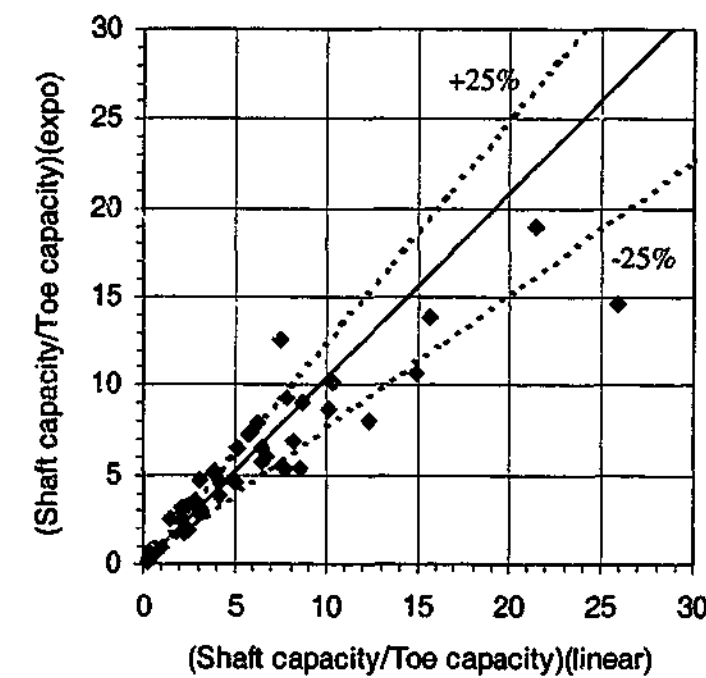


Figure 9.11 Shaft capacity/Toe capacity values computed using CAPWAP(linear) and CAPWAP(expo)

The 44 cases can be categorised according to their driving condition. The driving conditions can be classified as hard, moderate and easy driving using the definition in Table 9.2. In order to determine if there is any relationship between the value of the ratio of each of the four parameters and the driving condition, statistical analyses were performed on the cases for each of the three driving categories, as shown in Table 9.3, where the number of cases falling into each category is also indicated.

As has been previously demonstrated, the mean values for each of the four parameters show that CAPWAP(expo) tends to compute a slightly higher value than that computed by CAPWAP(linear). However the variation of the CAPWAP(expo) value relative to the CAPWAP(linear) value does not appear to vary with the driving condition.

Table 9.2 Definitions of hard, moderate and easy driving

Category	Definition
Hard driving	Set \leq 0.5mm
Moderate driving	0.5mm < Set < 5.0mm
Easy driving	Set \geq 5.0mm

Table 9.3 Statistical analysis of the values of Shaft(expo)/Shaft(linear), Toe(expo)/Toe(linear), Total(expo)/Total(linear) and (Shaft/Toe)(expo)/(Shaft/Toe)(linear) for each driving condition

Category	Statistical measures	Shaft(expo)/Shaft(linear)	Toe(expo)/Toe(linear)	Total (expo)/Total(linear)	(Shaft/Toe)(expo)/(Shaft/Toe)(linear)
Hard (4 cases)	Mean	1.01	1.03	1.03	1.00
	Standard deviation	± 0.09	± 0.10	± 0.06	± 0.19
Moderate (21 cases)	Mean	1.03	1.02	1.00	1.07
	Standard deviation	± 0.20	± 0.22	± 0.08	± 0.38
Easy (19 cases)	Mean	1.01	1.08	1.04	0.99
	Standard deviation	± 0.16	± 0.27	± 0.15	± 0.27

9.6 Comparative Shaft Resistance Distributions

In order to ascertain the effect of the new damping model on the computed shaft distribution along the pile length, the distributions computed using CAPWAP(linear) and CAPWAP(expo) are compared.

For the 30 cases without borelog data, the distributions are plotted in Figure 9.12. For 24 of these cases, the two computed distributions are similar. Of the remaining six cases (IDs 20, 30, 32, 37, 41, 42), the two computed distributions are significantly different. Given the lack of borelog data, it is not possible to ascertain which of the two analyses gives a more accurate prediction.

For the 14 cases equipped with borelog data, the CAPWAP(linear) and CAPWAP(expo)-computed shaft resistance distributions as well as the estimated distribution based on static analyses of the borelog data is shown in Section 9.4. It can be noted in Figure 9.2 that the two computed distributions are comparable in 9 cases, and are significantly different in the remaining 5 cases (IDs 2, 3, 4, 14, 16). For IDs 2 and 14, CAPWAP(linear) appears to have computed distributions that are more consistent with the estimated distribution, whilst for IDs 3, 4 and 16, CAPWAP(expo) appears to have computed distributions that are more agreeable with the estimate distribution. Because of the limited cases with significantly different computed distributions and the fact that the CAPWAP solution is not unique, no definite conclusion can be drawn about which one of the two analyses produces a more accurate shaft resistance distribution. It can only be stated that given that CAPWAP(expo) and CAPWAP(linear) yield similar distributions in the majority of the cases, it would appear that the use of the exponential damping model in CAPWAP tends to have little effect on the shaft friction distribution.

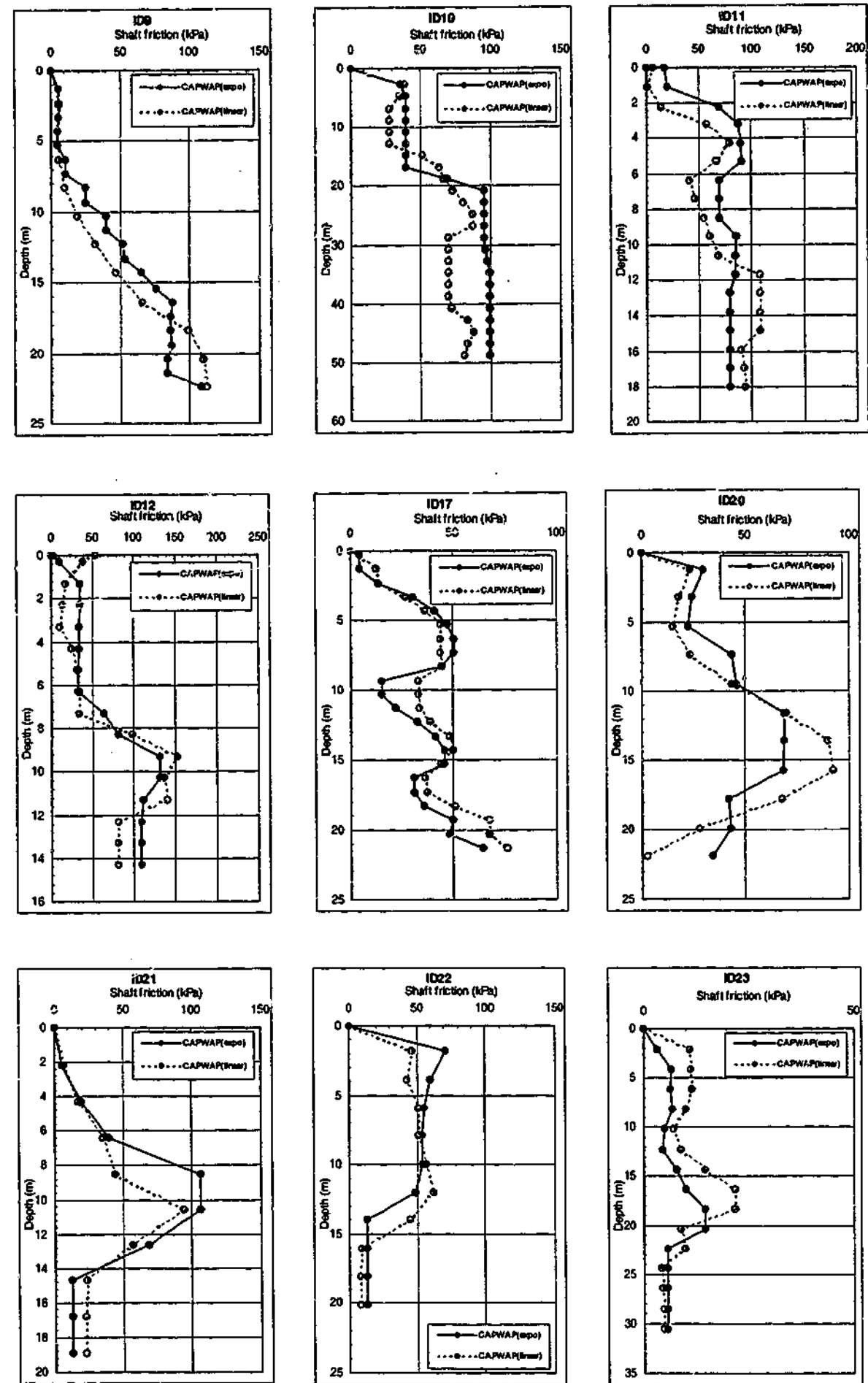


Figure 9.12 Shaft friction distributions computed using CAPWAP(linear) and CAPWAP(expo) values for the 30 cases

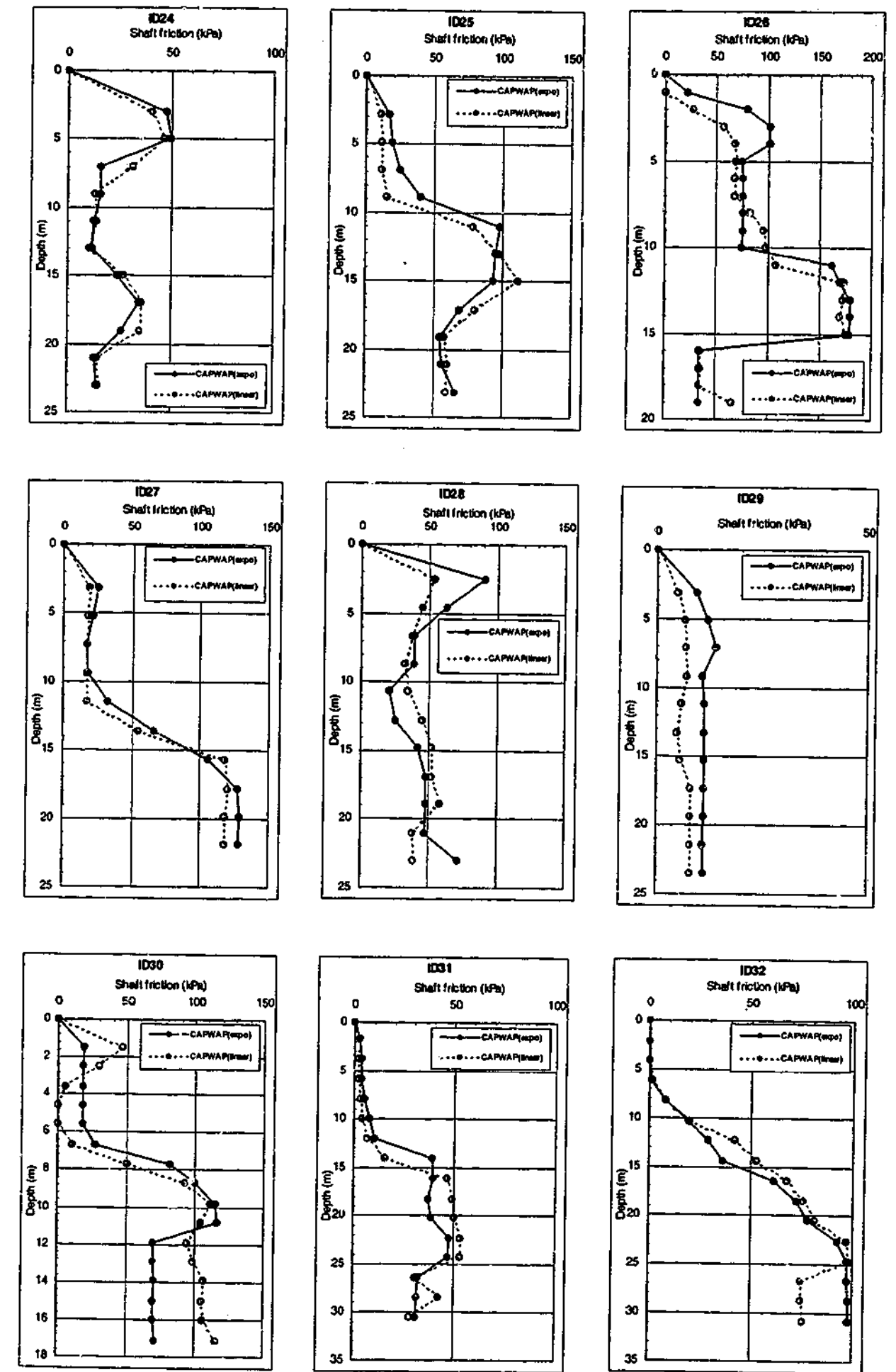


Figure 9.12(cont'd) Shaft friction distributions computed using CAPWAP(linear) and CAPWAP(expo) values for the 30 cases

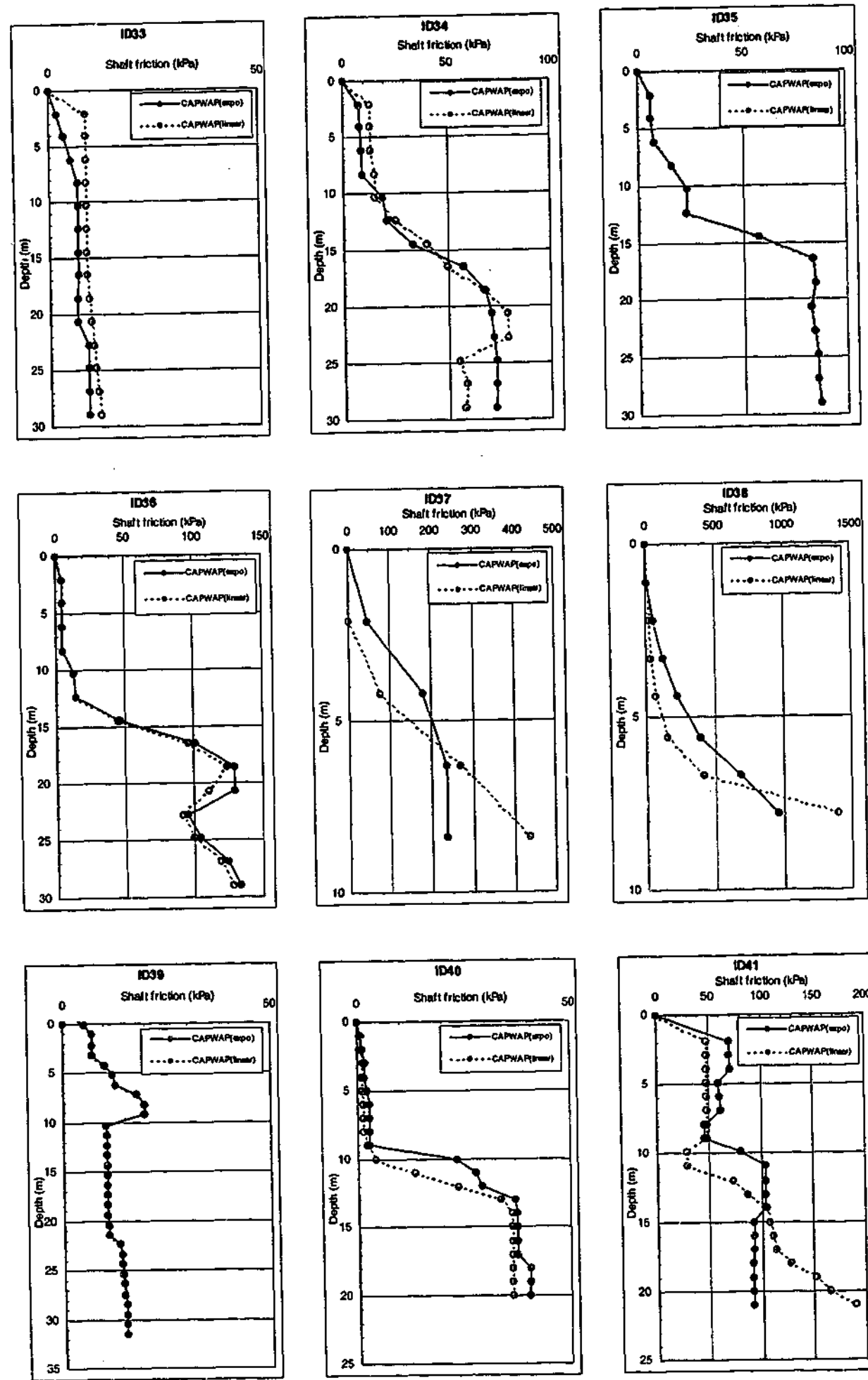


Figure 9.12(cont'd) Shaft friction distributions computed using CAPWAP(linear) and CAPWAP(expo) values for the 30 cases

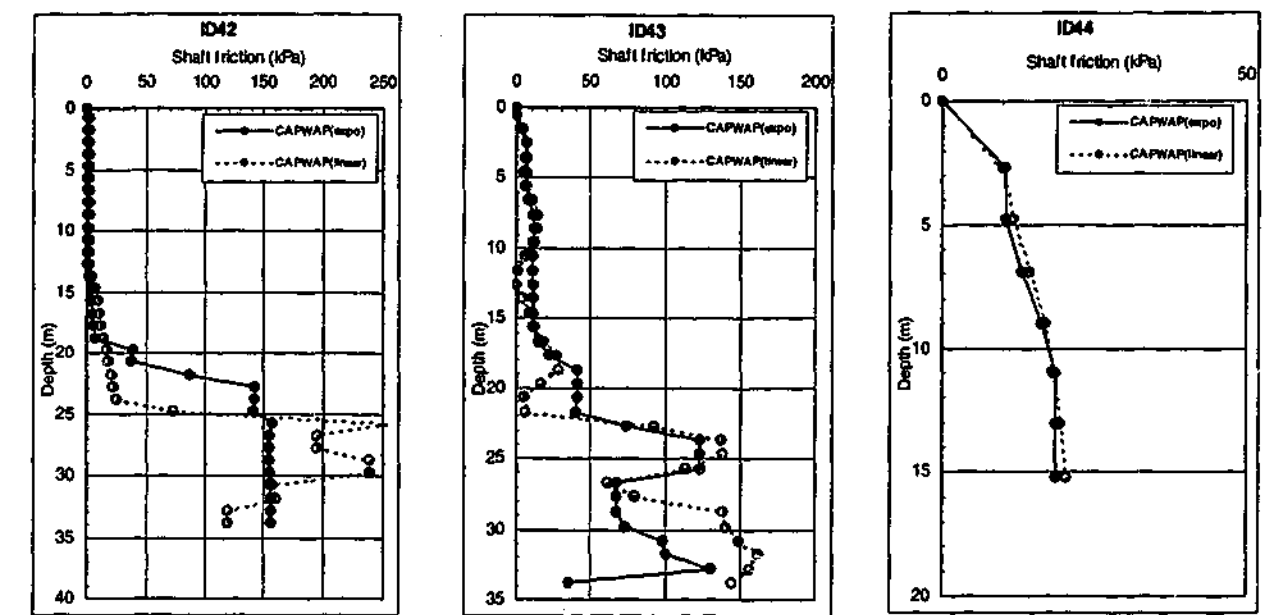


Figure 9.12(cont'd) Shaft friction distributions computed using CAPWAP(linear) and CAPWAP(expo) values for the 30 cases

9.7 Comparative CAPWAP Parameters

The CAPWAP parameters have been defined and their significance explained in Appendix B. Since the exponential shaft damping model is significantly different from the linear pile shaft damping model, the use of the exponential damping model must directly affect the pile shaft parameters and indirectly influence the pile toe parameters.

In order to determine the effect of the new damping model on the CAPWAP parameters, values of the parameters computed with CAPWAP(expo) are compared to the equivalent values computed with CAPWAP(linear), for all 44 cases. The CAPWAP parameters that affect the loading phase (the shaft damping factor, shaft quake, toe damping factor, toe quake and toe gap, and toe plug) are first presented followed by the CAPWAP parameters that affect the unloading phase (the unloading shaft quake and the unloading toe quake, and the negative shaft resistance unloading limit).

The values of the CAPWAP parameters obtained from the two analyses have been plotted in x:y plots. The parameters computed with CAPWAP(expo) and CAPWAP(linear) are distinguished with the notations “(expo)” and “(linear)”

respectively. The comparative plots for each of the parameters can be found as follows:

- the shaft damping factor in Figure 9.13
- the shaft quake in Figure 9.14
- the toe damping factor in Figure 9.15
- the toe quake in Figure 9.16
- the toe gap in Figure 9.17
- the sum of the toe gap and the toe quake in Figure 9.18
- the toe plug in Figure 9.19
- the unloading shaft quake in Figure 9.20
- the unloading toe quake in Figure 9.21
- the shaft unloading limit in Figure 9.22

As shown in all the plots, the values of the various parameters computed from the 2 analyses do not vary from each other in any consistent manner. However, the following points should be noted.

Since the exponential and linear damping factors are based on different functions, their numerical values in Figure 9.13 cannot be used to infer the relative amounts of damping that have been modelled. As such, the plot only shows that the exponential shaft damping factor is generally numerically greater than the linear viscous damping factor for a particular case. It is noted that the range of back-calculated exponential damping factors of between 0.3 and 2.35 is comparable to the laboratory values of between 0.35 and 1.7.

In Figure 9.17, the toe gap values obtained from the 2 analyses are distinguished by their relative toe quake values. It can be noted that for cases where the CAPWAP(expo)-computed toe quake value is relatively higher than the CAPWAP(linear)-computed value, the CAPWAP(expo)-computed toe gap value tends to be lower than the CAPWAP(linear)-computed value. In other words, the sum of the toe gap and the toe quake value of CAPWAP(expo) tends to be similar to that of CAPWAP(linear), despite significant differences in the toe gap and toe quake values, as shown in Figure 9.18. Thus, it appears that higher toe gap values are

compensated by lower toe quake values, and conversely, lower toe gap values are compensated by higher toe quake values.

Figure 9.20 shows the comparative plot for the unloading shaft quake, distinguishing the relative values of the (loading) shaft toe quake obtained from the two analyses, whilst Figure 9.21 shows the comparative plot for the unloading toe quake, distinguishing the relative values of the (loading) toe quake obtained from the two analyses. The plots show that the unloading quake values are generally carried over from the loading quake values.

In addition to the plots presented previously, the CAPWAP parameters computed with the two analyses have also been plotted in the same format but with distinction of the driving conditions: hard driving (sets less than 0.5mm), moderate driving condition (sets between 0.5 to 5mm inclusive), and easy driving (sets greater than 5mm). It has been found that the values of the CAPWAP(expo) and CAPWAP(linear) parameters do not vary relative to each other in a way that is dependent on the driving condition or the set. As these plots are of no further value, they are not presented.

In conclusion, the use of a more realistic damping model (i.e. exponential model) has not only affected the shaft damping factor but the other CAPWAP parameters as well. Given that the exponential model reflects the actual damping response, it is reasonable to state that the back-calculated parameters should more accurately reflect reality. It is thus cautioned that whilst the use of the CAPWAP(linear) is able to predict the pile capacity and match measured signals reasonably, it might give back-calculated parameters that do not reflect the actual values.

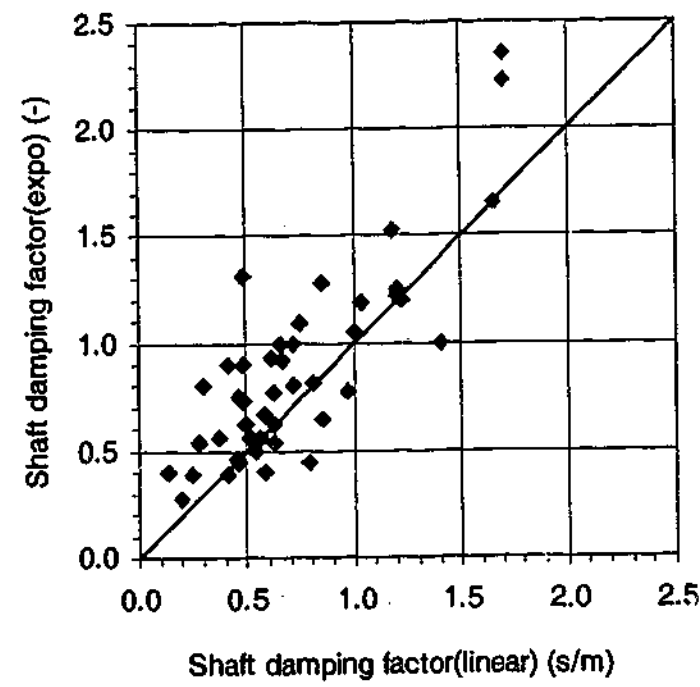


Figure 9.13 Comparison of the shaft damping factor values based on the analyses using CAPWAP(expo) and CAPWAP(linear)

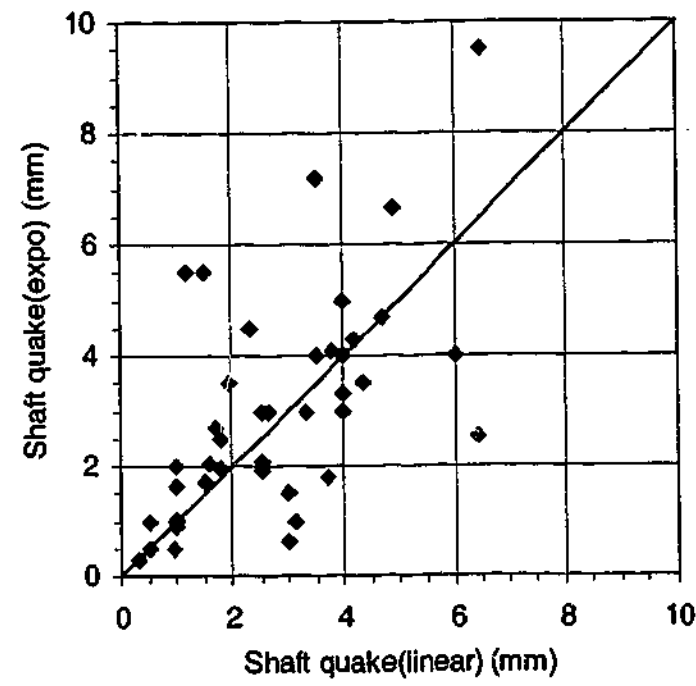


Figure 9.14 Comparison of the shaft quake values based on the analyses using CAPWAP(expo) and CAPWAP(linear)

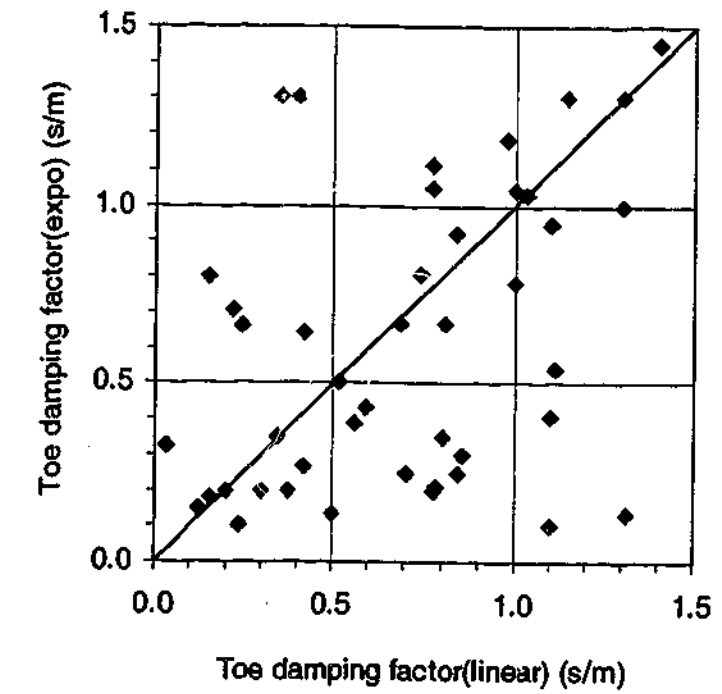


Figure 9.15 Comparison of the toe damping factor values based on the analyses using CAPWAP(expo) and CAPWAP(linear)

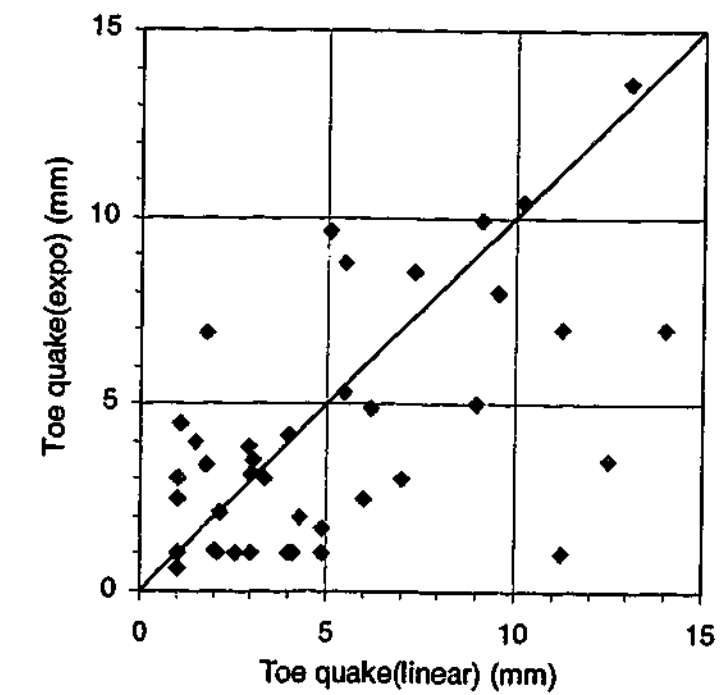


Figure 9.16 Comparison of the toe quake values based on the analyses using CAPWAP(expo) and CAPWAP(linear)

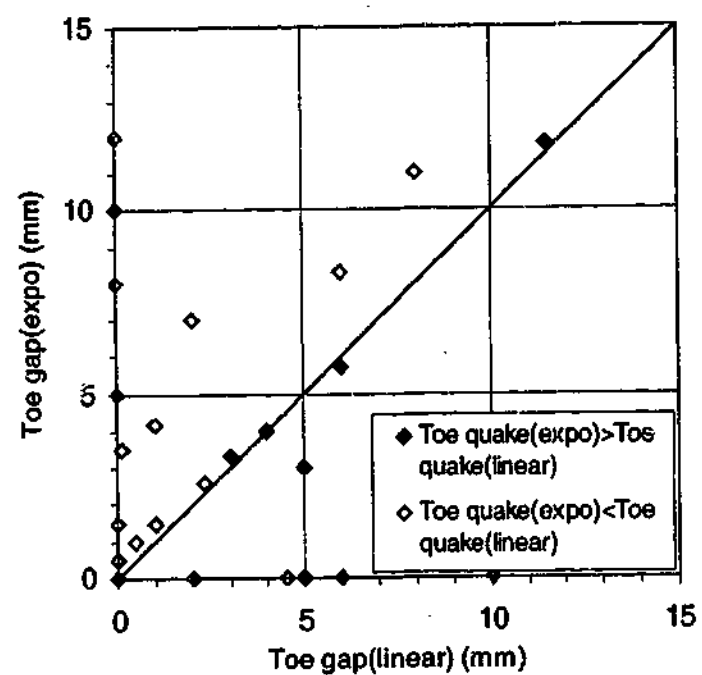


Figure 9.17 Comparison of the toe gap values based on the analyses using CAPWAP(expo) and CAPWAP(linear)

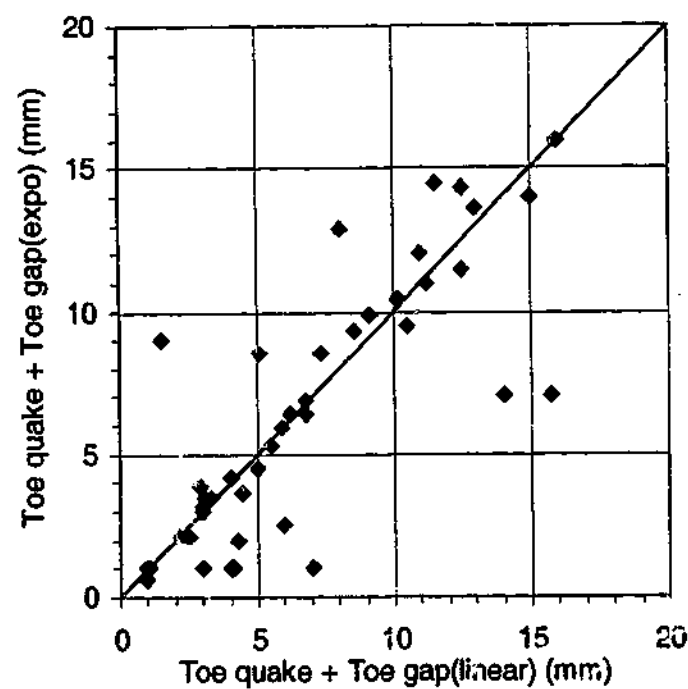


Figure 9.18 Comparison of the sum of toe quake and toe gap values based on the analyses using CAPWAP(expo) and CAPWAP(linear)

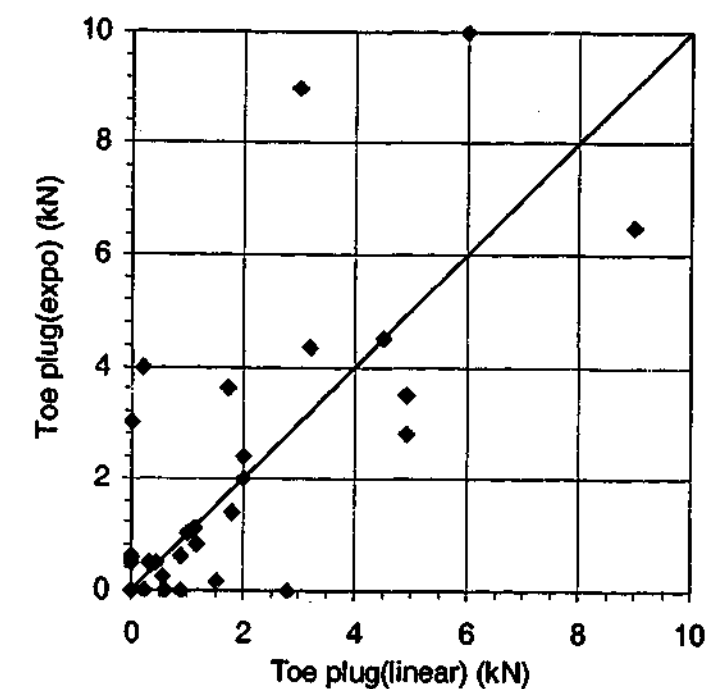


Figure 9.19 Comparison of the toe plug values based on the analyses using CAPWAP(expo) and CAPWAP(linear)

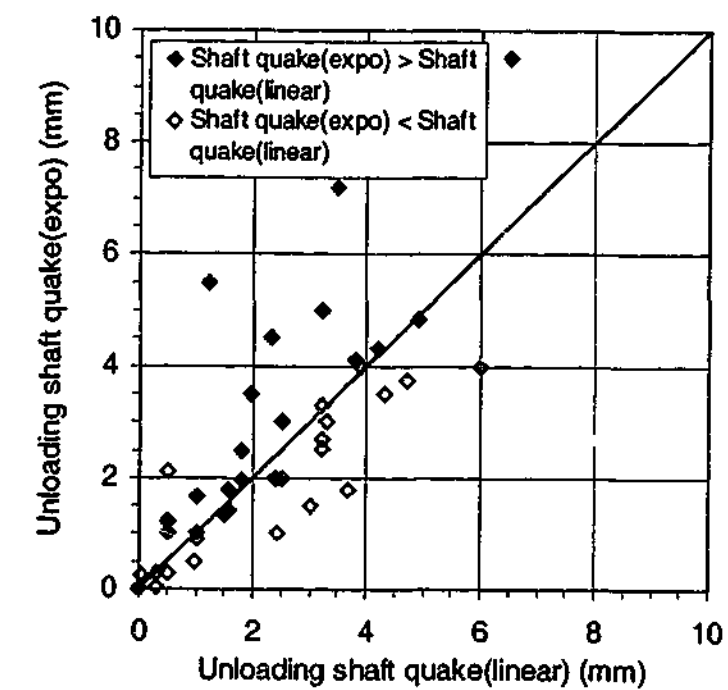


Figure 9.20 Comparison of the unloading shaft quake values based on the analyses using CAPWAP(expo) and CAPWAP(linear)

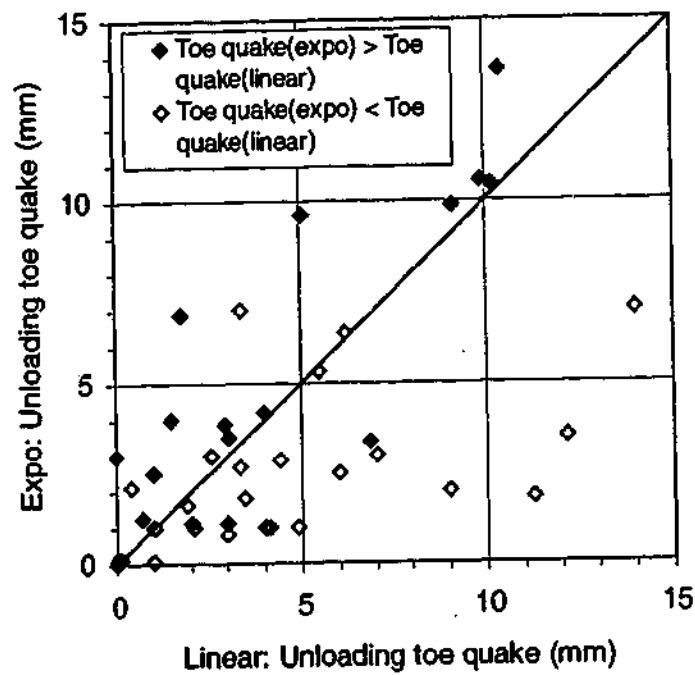


Figure 9.21 Comparison of the unloading toe quake values based on the analyses using CAPWAP(expo) and CAPWAP(linear), distinguishing relative toe quake values

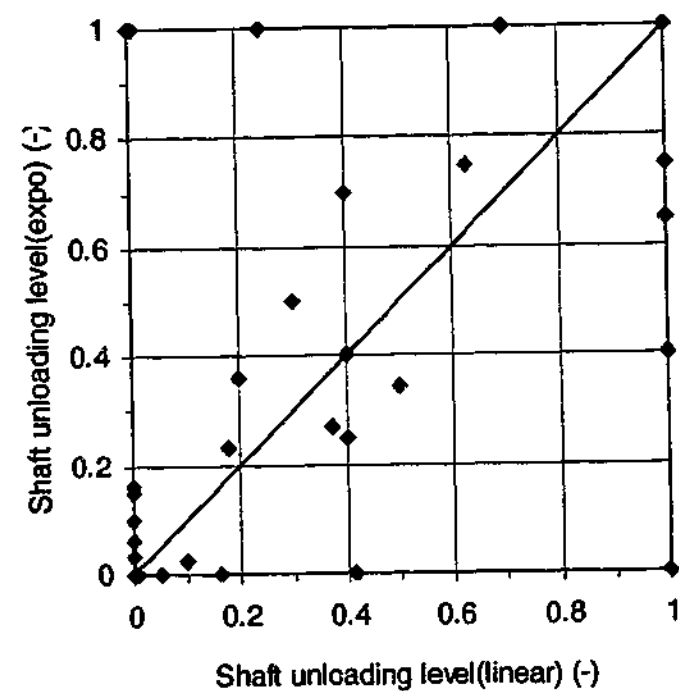


Figure 9.22 Comparison of shaft unloading level values based on the analyses using CAPWAP(expo) and CAPWAP(linear)

9.8 Comparative Capacity Prediction Capability

In order to determine the capacity prediction capability of CAPWAP(expo) in its own right and relative to that of CAPWAP(linear), the capacities computed using CAPWAP(expo) and CAPWAP(linear) are compared to that of the measured capacity. Since the capacity computed in CAPWAP is the ultimate capacity, the measured capacity must similarly be the ultimate capacity (rather than an arbitrary capacity based on a failure criterion such as the Davisson criterion). Thus, only cases where the pile has been statically loaded to failure can be included in the comparison. Out of the 44 cases, 19 cases are equipped with the ultimate capacity data.

However, it is important to note that there are uncertainties inherent in such a comparison of the statically measured capacity and the capacity deduced from dynamic analysis. These uncertainties are discussed as follows:

- For a dynamic test to mobilise the full capacity of a pile (which is the measured quantity in static load test carried to failure), sufficient driving energy is required. In some cases, insufficient energy is applied during a dynamic test so that the full capacity of the pile is not mobilised. The implication is that when the CAPWAP computed capacity is less than that measured in the static load test, it is difficult to ascertain whether the discrepancy is caused by the pile capacity not having been fully mobilised or by the CAPWAP analysis having under-predicted the pile capacity;
- During the installation phase, excess pore water pressure is developed in the soil around the pile and remoulding of the soil occurs. With time, the excess pore water pressure begins to dissipate and the soil begins to consolidate such that the strength of the soil increases with time (a phenomenon known as 'set-up'). Therefore, for the statically measured capacity to be compared to the CAPWAP-computed capacity on equal terms, both the static and dynamic tests must be performed at about the same time. However, because of construction schedules, this is not always the case;
- In certain cases, some effect of 'set-up' is destroyed before the actual dynamic test is performed because of early blows on the pile required for warming up the hammer. Also, some soil exhibits "strain softening" behaviour where an early restrike blow yields a higher capacity than that

which can be sustained under static loading conditions. In such cases, the static load test will not be comparable to the dynamic test; and

- It is possible that the measurement of the load in the static load test is inaccurate due for example to an inaccurate recalibration factor being used for the load measurement device.

These uncertainties should therefore be borne in mind when comparing the CAPWAP-computed capacity and the capacity measured in the static load test.

The capacities computed using CAPWAP(expo) and CAPWAP(linear), and the measured capacity are presented in a series of bar charts in Figure 9.23. The capacities computed using CAPWAP(expo) and CAPWAP(linear) are also plotted against the measured capacity in Figure 9.24. The plot shows that most of the CAPWAP-computed values fall within $\pm 30\%$ of the measured capacity value. It is noted that since the selection of the cases for analysis in this chapter has been biased towards cases of high sets, the plot is not intended to show the proportion of occurrences when CAPWAP accurately predicts, overpredicts and underpredicts the measured capacity.

In order to quantify the relative values of the measured capacity and the computed capacity, the ratios of the predicted capacity to the measured capacity (denoted $\text{Capacity(expo)/Capacity(measured)}$ and $\text{Capacity(linear)/Capacity(measured)}$) are computed and are statistically analysed. The results of the statistical analysis on the 19 cases are shown in Table 9.4.

Table 9.4 Statistical analysis of the CAPWAP-computed capacity relative to the measured capacity, for the 19 cases

CAPWAP(expo)/ Measured	Capacity(linear)/ Capacity(measured)	Capacity(expo)/ Capacity(measured)
Mean	1.00	0.99
Standard deviation	0.25	0.22

The mean values of $\text{Capacity(expo)/Capacity(measured)}$ and $\text{Capacity(linear)/Capacity(measured)}$ are equal to or close to 1.0, indicating that CAPWAP(expo) and CAPWAP(linear) tend to predict the actual capacity accurately. The similar mean values suggest that CAPWAP(expo) analyses give predicted capacities that are

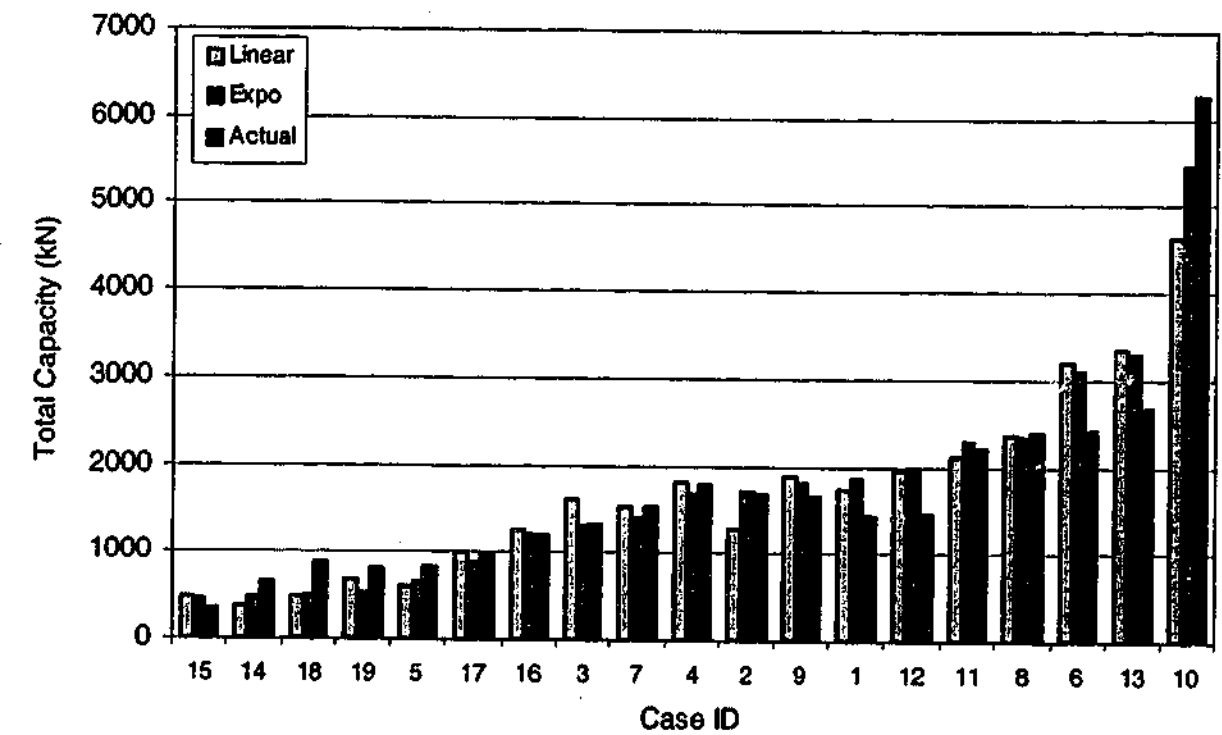


Figure 9.23 Capacities computed using CAPWAP(linear) and CAPWAP(expo) vs. Measured capacity

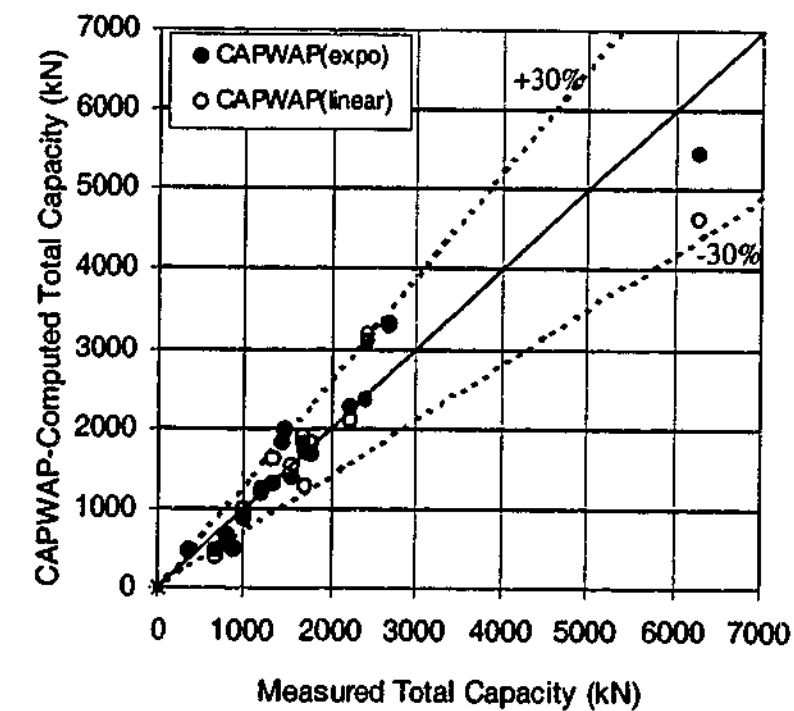


Figure 9.24 Capacities computed using CAPWAP(linear) and CAPWAP(expo) vs. measured capacity

comparable to the CAPWAP(linear) analyses. Therefore, the finding that the CAPWAP(expo)-computed capacity is generally slightly higher than the CAPWAP(linear)-computed capacity in Section 9.5 based on all the 44 cases does

not appear to have resulted in any significant improvement or worsening of the capacity prediction capability of CAPWAP(expo). However, the CAPWAP(expo)-computed capacity is closer to the measured capacity in 12 out of the 19 cases, indicating a slightly better capacity prediction capability.

The relatively high standard deviation values of both the analyses are likely to be attributed to the uncertainties that have been discussed. It should be noted that CAPWAP(expo) predicts between a slightly narrower range of 78% to 122% of the actual capacity as compared to CAPWAP(linear) which predicts between 75% and 125% of the actual capacity. This suggests that CAPWAP(expo) tends to be able to predict the actual capacity slightly more accurately, as has been previously observed.

Since the extensive experience with CAPWAP (linear) has shown that CAPWAP(linear) is able to predict the capacity satisfactorily, the fact that Capacity(expo)/Capacity(measured) yields mean and standard deviation values that are comparable to those of Capacity(linear)/Capacity(measured) can be taken as a positive indication that CAPWAP(expo) is able to effectively predict the capacity. It is thus concluded that the capacity prediction capability of CAPWAP(expo) is as good if not slightly better than that of CAPWAP(linear).

9.9 Comparative Match Quality

The quality of the match obtained using CAPWAP(expo) is compared to that of CAPWAP(linear) in order to determine the effect of the new damping model on the quality of the match. The match quality is quantified in CAPWAP by the use of the Match Quality Number (MQ No.). The MQ No. is a quantitative measure of the quality of the match based on the numerical difference between the measured and the computed responses, so that a lower MQ No. indicates a better match. The comparative MQ values obtained with CAPWAP(linear) and CAPWAP(expo) are presented by means of a series of bar charts in Figure 9.25, and of an x:y plot in Figure 9.26 where the reference lines showing the range within which the CAPWAP(expo) value is $\pm 25\%$ of the CAPWAP(linear) value. The latter plot shows that in most cases, the CAPWAP(expo) value is within $\pm 25\%$ of the CAPWAP(linear) value.

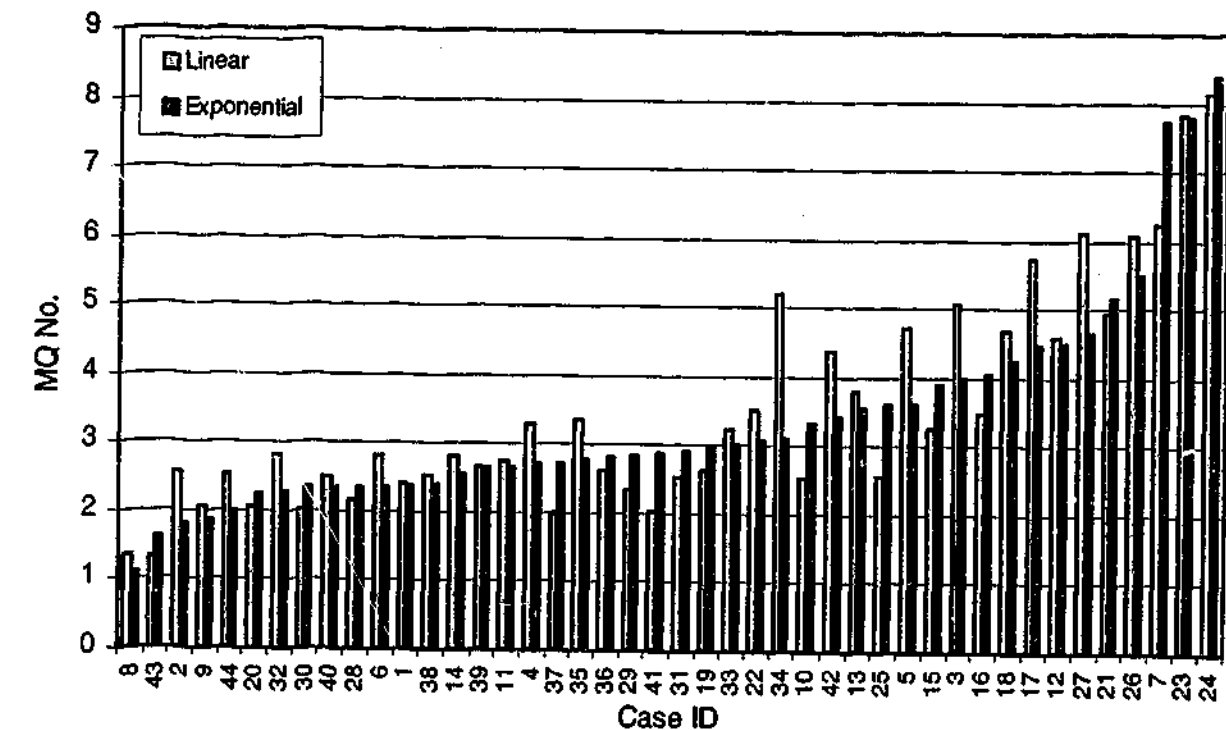


Figure 9.25 Comparative values of MQ No. obtained using CAPWAP(linear) and CAPWAP(expo)

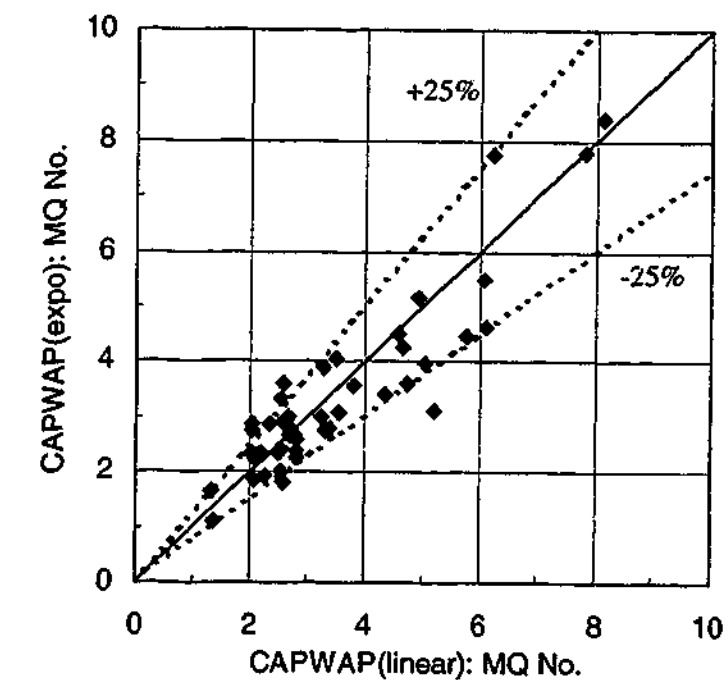


Figure 9.26 Comparative values of MQ No. obtained using CAPWAP(linear) and CAPWAP(expo)

The results of the statistical analyses on the MQ No.'s of CAPWAP(expo) and CAPWAP(linear) (denoted MQ No.(expo) and MQ No.(linear)) for all the 44 cases are shown in Table 9.5. The mean values indicate that CAPWAP(expo) tends to produce slightly better match quality than CAPWAP(linear). Consistent with the mean values, CAPWAP(expo) yields a superior match to CAPWAP(linear) in 27 out of the 44 cases.

Table 9.5 Statistical analysis on the MQ No. for all 44 cases

	MQ No.(linear)	MQ No.(expo)
Mean	3.51	3.38
Standard deviation	1.628	1.564

At times, a match with a higher MQ No. can be more satisfactory if it can better match a certain salient feature of the measured response. Thus, the quality of the match should not be based solely on the MQ number but together with a visual comparison of the measured and the computed curves. Based on the subjective comparison, CAPWAP(expo) yields a better match in 15 cases, a worse match in 10 cases and similar match quality in 19 cases.

Overall, it is concluded that CAPWAP (expo) is able to achieve as good if not superior match quality to CAPWAP(linear).

As has been discussed in Section 9.3, the exponential damping model can be implemented as either a function of the ultimate static resistance or the instantaneous static resistance. It has been found that the use of the instantaneous resistance is necessary to achieve a match in 32 out of the 44 cases analysed.

9.10 Concluding Remarks – Comparative Studies

The preceding comparative studies have shown that the loading and unloading CAPWAP parameters (toe damping factor, shaft quake, toe quake, toe gap, toe plug, unloading shaft quake, unloading toe quake and unloading limit for negative shaft resistance) computed by CAPWAP(expo) do not vary in any consistent trend relative to the equivalent values computed by CAPWAP(linear). Also, the total, shaft and toe capacities computed using CAPWAP(expo) on average tend to be only slightly greater than or practically similar to those computed using CAPWAP(linear). In

addition, the shaft friction distribution computed using CAPWAP(expo) tends to be similar to that computed using CAPWAP(linear). The findings that the implementation of the exponential model (to the linear model) has not resulted in any significant variation of the aforementioned parameters, and especially that the capacity predicted by CAPWAP(expo) is similar to that by CAPWAP(linear), would suggest that the total amounts of damping applied in the two models are similar. This would explain why the linear damping model has been able to satisfactorily match measured dynamic data despite the deviation of the linear behaviour from the non-linear behaviour established based on laboratory testing. If the linear model does indeed model a similar amount of damping to the exponential model, the linear damping factor must be appropriately chosen during signal-matching such that the linear model applies the same amount of damping as the non-linear model. This would imply that the linear model must model more dynamic resistance at low velocities and less dynamic resistance at high velocities.

As has been noted, the values of a particular CAPWAP parameter obtained using CAPWAP(linear) and CAPWAP(expo) can vary significantly. Given that the exponential model reflects the actual damping response, it is reasonable to state that the back-calculated parameters should more accurately reflect reality. It is thus cautioned that the CAPWAP(linear) may give values that are not representative of the true values.

The comparative studies have also shown that CAPWAP(expo) has signal-matching and capacity prediction capabilities that are as good as if not slightly better than CAPWAP(linear). Therefore, as it can be argued that the exponential damping model more realistically models the damping behaviour at the pile-soil interface using a physically-based parameter and is easy to implement, the implementation of the new shaft damping model is recommended for signal-matching analyses. It is noted that the current investigation involves more accurate modelling of the damping at the pile shaft. Given that the tip damping has been established in previous research (Coyle and Gibson, 1970; Dayal and Allen, 1975; Litkouhi and Poskitt, 1980) to also increase exponentially with velocity, more realistic modelling of the damping response at the pile tip is also recommended.

9.11 Relationship Between Damping Factor & Soil Type

As explained in Section 2.2.5.1, the Case Method is premised on the assumption that the damping resistance is concentrated at the toe. The resulting Case damping factor has been correlated with soil type by Rausche et al. (1985) as shown in Figure 9.27. The correlation shows that the Case damping factor generally increases with decreasing soil grain size. Despite the somewhat promising correlation, it has since been found that the linear damping factor resulting from the signal-matching analysis using CAPWAP shows little correlation between the factor and soil type (Zhang et al., 2001; Rausche et al., 1996; Abou-matar et al., 1996; Thendean et al., 1996; Liang and Zhou, 1997). It would thus appear that the linear damping factor cannot be correlated with soil type in all cases.

In order to investigate any relationship between the damping factor and the soil type, the back-calculated linear viscous factors have been plotted against the soil type for the 44 cases analysed in this study, as shown in Figure 9.28. In this instance, there is a trend between the maximum value of the damping factor and the soil type.

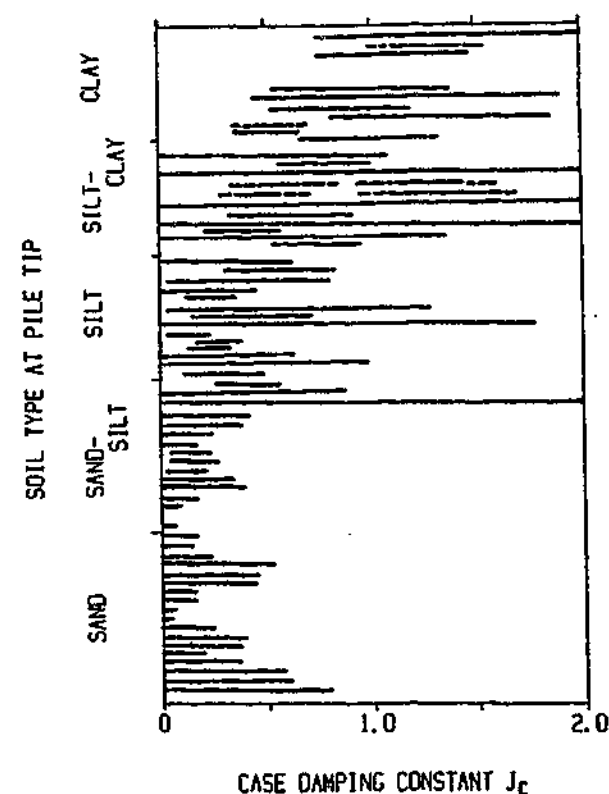


Figure 9.27 Correlation of Case damping factor and soil type (Rausche et al., 1985)

The back-calculated exponential damping factors have also been plotted against soil type in Figure 9.29. The plot similarly shows that the maximum value of the damping parameter decreases as the soil type "approaches" sandy soils. This trend is consistent with the laboratory finding that clay exhibits significant damping whilst sand exhibits less damping. Based on this trend, one can thus interpret that the amount of viscous damping increases with increasing clay content of the soil.

The plot also shows that there is a range of damping factor values for a particular soil type. For the pile-clay interface, the values of the viscous damping parameter for clay has been shown based on laboratory data to be dependent on the shear strength of the clay. This will also be confirmed in the subsequent section for some cases involving clayey soils that have been analysed. It can be hypothesised that, by extension, the variation of the damping values for the other soil types shown in Figure 9.29 is also due to the dependence on the shear strength.

The scattering of the shaft damping factor values for a particular soil type can also be explained by the different compositions of the soils classified under the same category. For example, a particular case of "clay-sand" soil may have a large percentage of sand relative to clay, which would result (based on experimental data) in a lower damping factor. Another case with the same classification may have a significantly higher proportion of clay and thus have a high damping factor. Despite this simplistic classification of soils, the correlation shows that the maximum value of the exponential damping factor can be correlated with the soil type, and given the limited experience with CAPWAP(expo), the correlation can be used as a guide to the range of exponential damping factor values that can be expected for a certain soil.

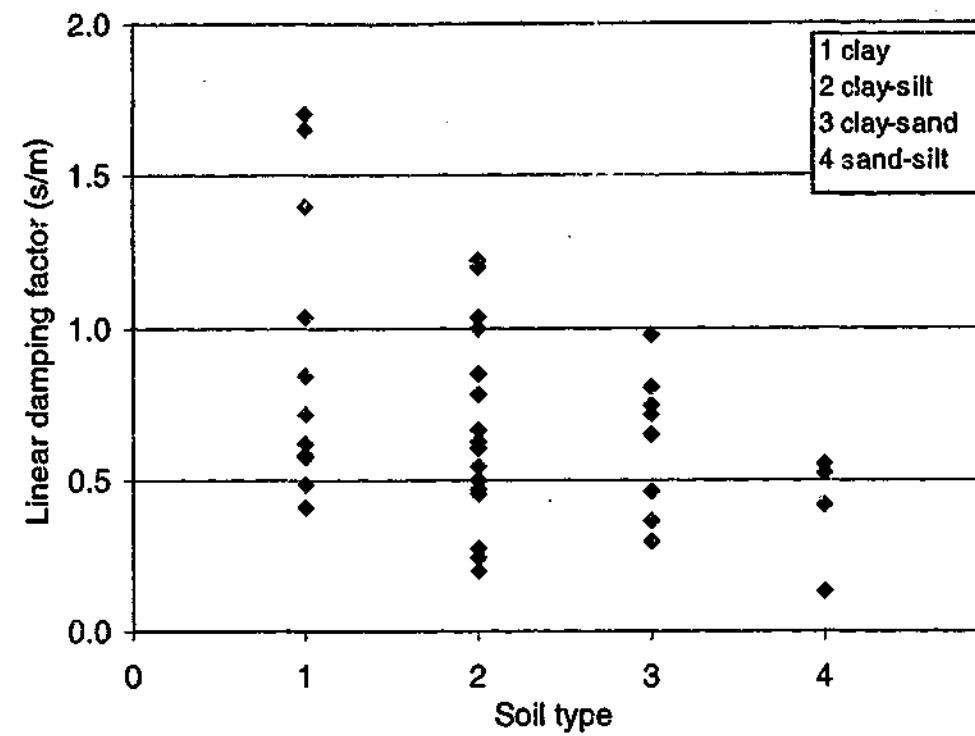


Figure 9.28 Correlation of linear viscous damping factor and soil type based on this study

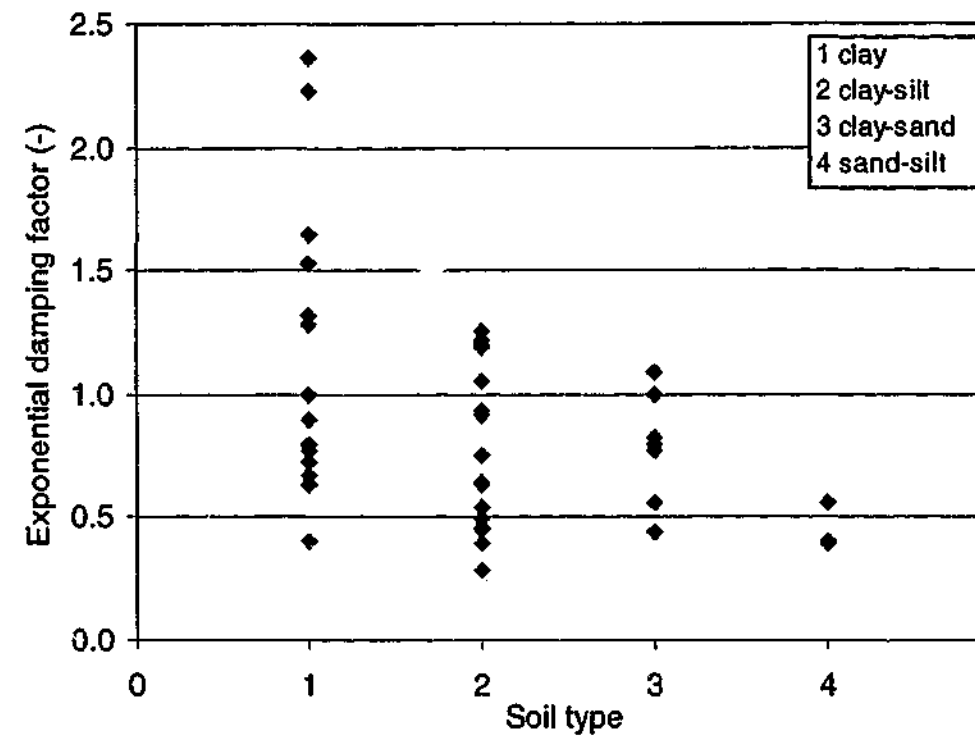


Figure 9.29 Correlation of exponential damping factor and soil type based on this study

9.12 Relationship Between Damping Factor & Shear Strength

The experimental data from the present study have shown that, for a pile-clay interface, the damping factor increases with decreasing shear strength of the clay. This finding has also been shown in Section 8.4 to be consistent with the hypothesis that has been proposed to explain the mechanism of viscous damping. Also, there have been observations that a lower damping factor is used for a pile installed in hard clay and conversely a higher damping factor is used for a pile installed in soft clay (Rausche et al., 1996). Furthermore, it is intuitive that the degree of viscous damping should increase with higher moisture content in the soil and thus with lower shear strength.

9.12.1 Shear strength based on borelog data

In order to validate the relationship between the damping factor and shear strength based on the laboratory data, damping factors computed from the CAPWAP analyses are plotted against their corresponding shear strengths. These cases are selected based on the criteria that the pile must be installed in a predominantly clay soil and that the available shear strength profile must not vary too drastically to the point where a representative shear strength cannot be ascertained.

Such cases are shown together with the available types of shear strength data in Table 9.6. The cases that relate to a particular site have been grouped together. It is noted that the details of the shear strength data vary for each of the cases analysed:

- Cases ID5 and ID19 contain only SPT values which have been converted to shear strength. Since the correlation between SPT and shear strength can vary widely, the converted values are obtained by averaging the lower and upper bound values given by Terzaghi and Peck (1967) cited in Kulhawy and Mayne (1990) and a soil sampling manual by the US Army Corps of Engineers (USACE, 1996) respectively. The averaged value results in the shear strength being equal to about 9 times the SPT number of blows which is consistent with the overall average based on various correlations presented in Kulhawy and Mayne (1990).
- Cases ID10 to ID12, which pertain to piles at the same site, contain no quantitative measure of the soil strength. Driving records indicate that the

strength increased with depth at a relatively constant rate up to a depth of 40m, and at a relatively constant but higher rate down to 50m. This indicates that the soil strength is fairly constant or increases slightly with depth down to 40m, and then increases significantly at 40m. The borelog down to a depth of 35m described the soil as a stiff and fissured Boom clay. According to the sampling manual by USACE (1996), a stiff soil has a shear strength between 100 and 190kPa. This means the shear strength in cases ID10 to ID12 (which are not equipped with quantitative shear strength data) is comparable to that in cases ID1 to ID3, if not greater. Based on the qualitative description in the borelog, it is reasonable to group these cases together with ID1 to ID3 which have an average shear strength of 130kPa.

The shear strength vs. depth plot for all the selected cases except ID10 to ID120 is shown in Figure 9.30; it is noted that the cases that relate to a particular site have been grouped together, and that the information is truncated at the location of the pile tip so that only the soil strength surrounding the pile shaft is considered.

For each of the cases outlined in Table 9.6, a crude average shear strength is estimated based on the shear strength-depth plot in Figure 9.30. The estimated average shear strength, as shown in Table 9.7, allows the back-calculated linear and exponential damping factors to be plotted against the averaged shear strength.

Table 9.6 Type of information available on shear strength of clay

Case	Information on shear strength of clay
ID1, ID2, ID3	Qualitative description; SPT; laboratory-measured
ID4	Qualitative description; laboratory-measured
ID5	Qualitative description, SPT
ID10, ID11, ID12	Qualitative description
ID14	Qualitative description; SPT; laboratory-measured
ID18	Qualitative description; ; laboratory-measured
ID19	Qualitative description, SPT

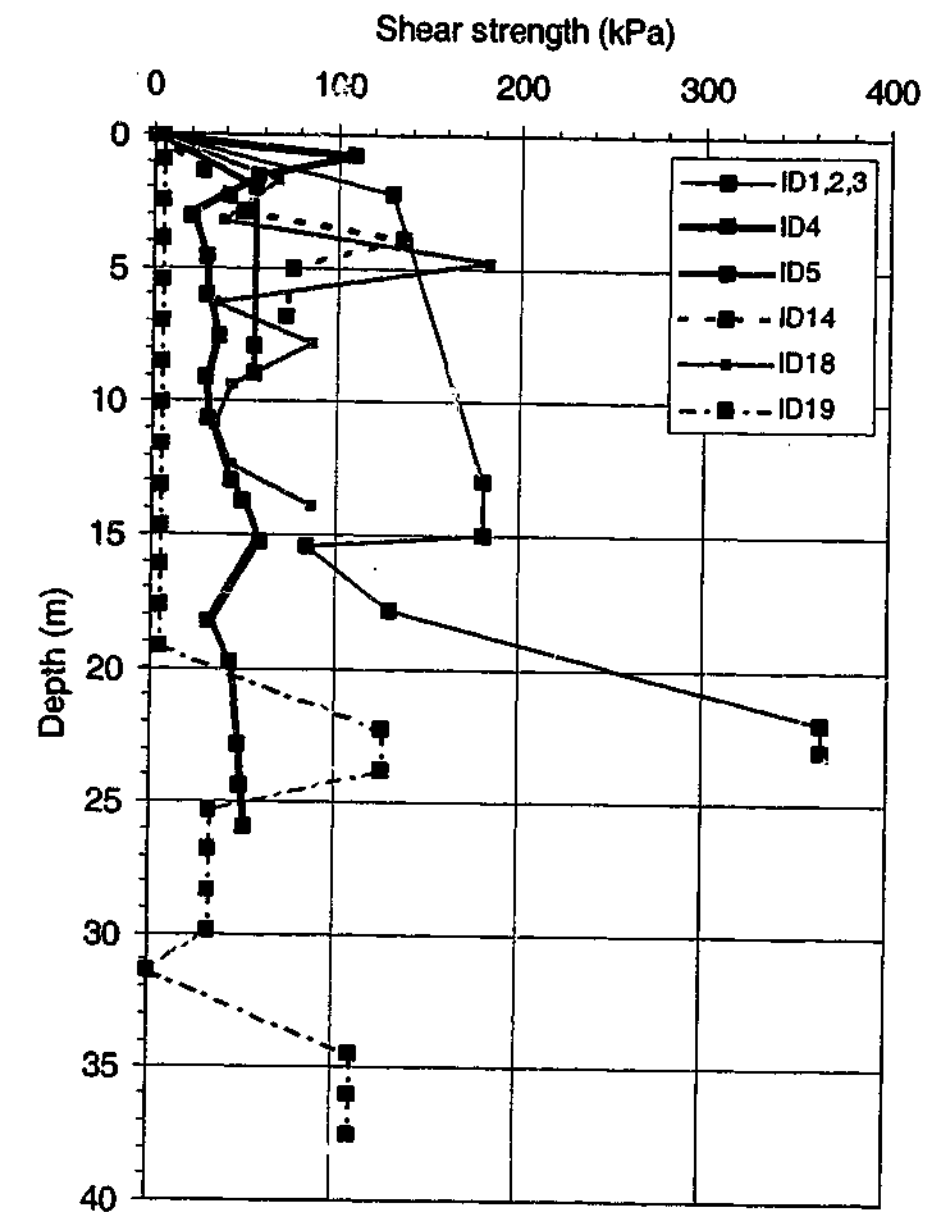


Figure 9.30 Shear strength based on bore log data vs. depth

Table 9.7 Average shear strength based on bore log

Case	Average shear strength (kPa)
ID 1	130
ID 2	130
ID 3	130
ID 4	40
ID 5	60
ID 10	130
ID 11	130
ID 12	130
ID 14	60
ID 18	60
ID 19	20

The back-calculated linear damping factors are plotted against the averaged shear strength in Figure 9.31. It can be noted that there is no consistent relationship between the linear damping factor and the shear strength. However, in general, higher factors apply to soft clays and conversely lower factors apply to hard clays as has sometimes been observed in the CAPWAP experience (PDI, 1994; Rausche et al., 1996).

The back-calculated exponential damping factors are plotted against the averaged shear strength in Figure 9.32. The range of damping factors for the three failure modes obtained from the laboratory have also been included in the plot for comparison. It can be noted that the values of the damping factors back-calculated in CAPWAP and from laboratory data compare remarkably well with regard to both the numerical values and trends.

The exponential damping factors back-calculated in CAPWAP analyses ranged from 0.4 to 2.6 for shear strengths with average values between approximately 20kPa and 200kPa. These values are comparable to the values obtained from the experiments, which ranged from 0.35 to 1.7 for shear strengths between 25kPa and 100kPa. Whilst no laboratory data are available regarding the magnitude of the damping factor for shear strengths less than 40kPa and greater than 100kPa, the correlation based on the back-calculated values suggests a damping factor of up to 2.5 for shear strengths less than 40kPa and of approximately 0.35 for shear strengths greater than 100kPa. The extrapolated trend lines are shown in Figure 9.32.

All but one of the data points from the CAPWAP analyses compare well with the range of laboratory data for the interfaces with Mode 1 failure. One data point falls in the range of laboratory data for interface with Modes 2 and 3 failure. As observed in the laboratory, Mode 2 relates to low or medium plasticity clay sheared against a rough surface; since the CAPWAP cases involve conventional steel and concrete piles which would have been of comparative smoothness to the smooth pile rather than the rough pile tested in the laboratory, the failure mode of the CAPWAP case in the Modes 2 and 3 range is likely to be Mode 3. However, since no data are available regarding the plasticity of the clay in the CAPWAP cases, it is not possible to validate the occurrence of either Mode 1 or Mode 3 failure in each of the cases.

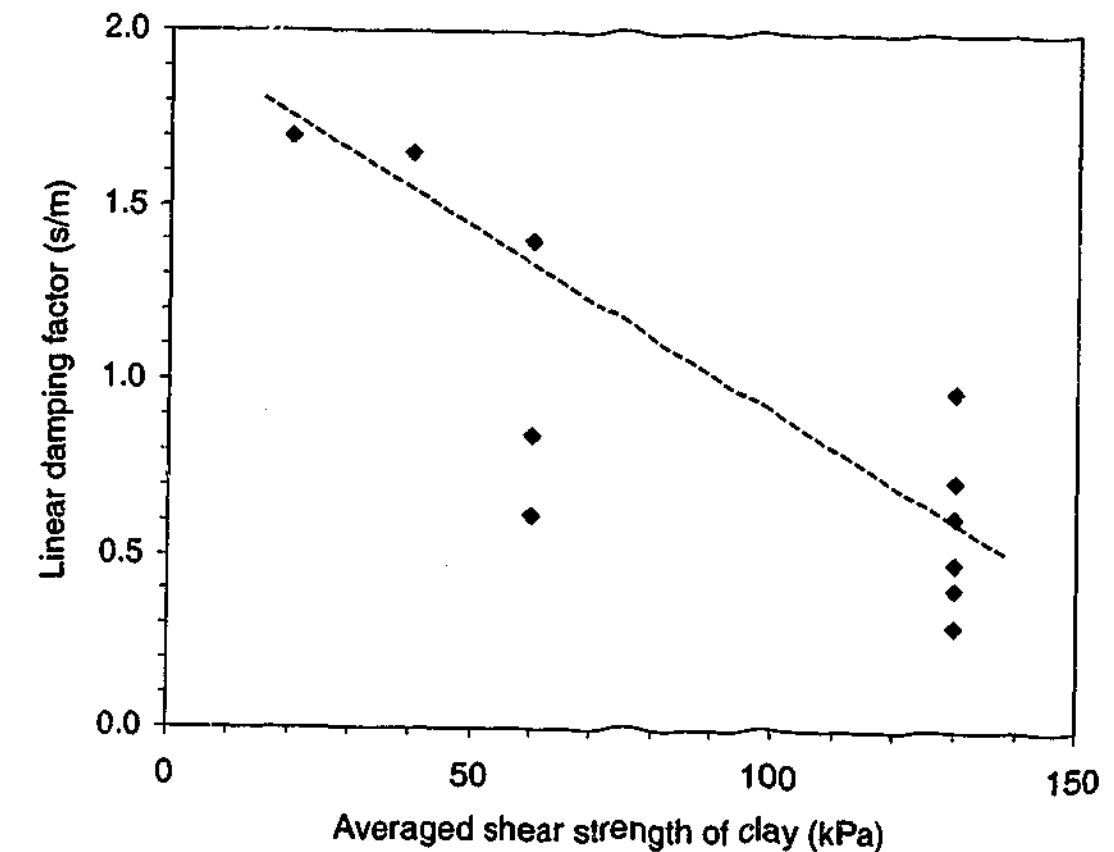


Figure 9.31 Relationship between linear damping factor & averaged shear strength

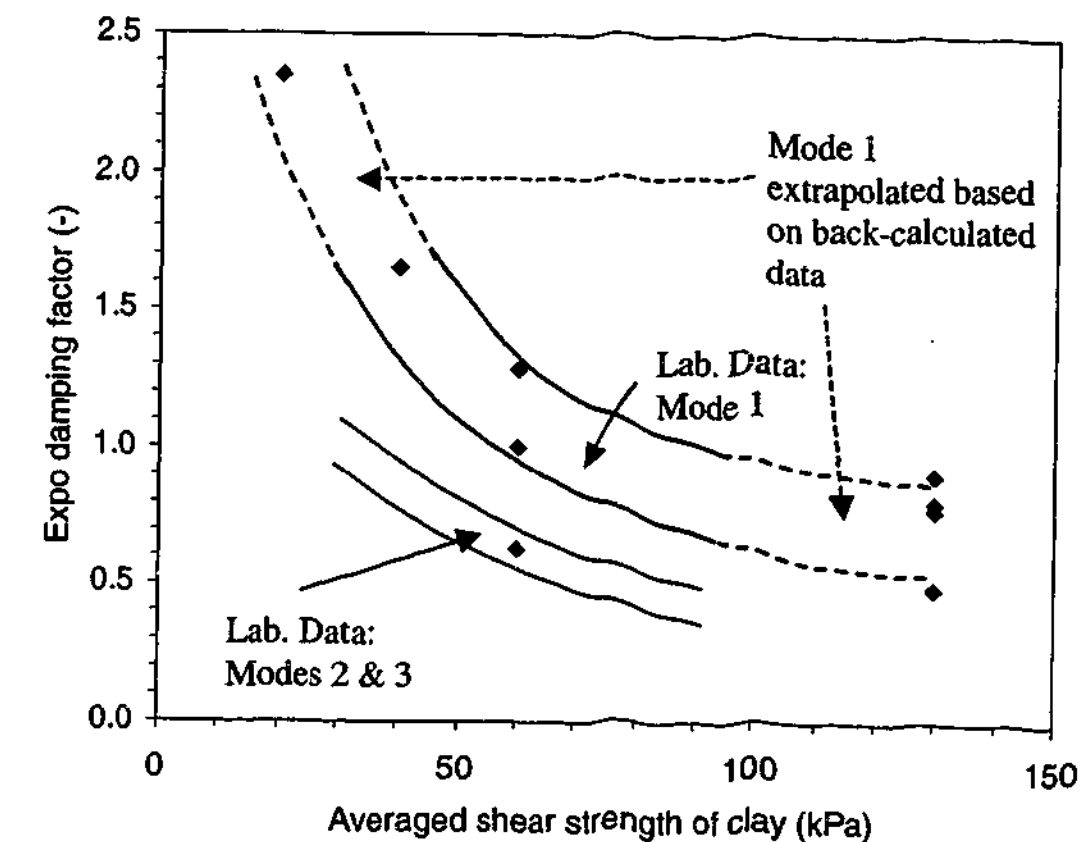


Figure 9.32 Relationship between exponential damping factor & averaged shear strength

It has been shown that the use of the physically or experimentally-based exponential damping model has allowed the damping factor to be correlated with the fundamental soil property. Furthermore, it has been shown that the linear damping factor, being based on a model that does not model the true damping response, has obscured the relationship between the amount of viscous damping and shear strength.

It is noted that the damping factor-shear strength relationship is based on pile-clay interfaces and piles installed in clays. Although it would appear that, by extension, the factor would also vary with the shear strength for other soils, this will of course require validation by further laboratory testing.

Although the damping factor has been correlated to a shear strength that is only approximate to the shear strength of the soil at the time of the shearing, this correlation can still be a useful guide for the selection of an appropriate damping factor for a soil with a particular shear strength. In fact, in practice, only the initial shear strength of the soil from the site investigation bore log is available for the estimation of the damping factor, and the “instantaneous shear strength” of the clay adjacent to the pile shaft is unknown.

9.12.2 Shear strength based on CAPWAP-computed friction

In the previous section, the damping factor values have been related to the soil shear strength values obtained from the borelog data. However, the shear strength of the soil given by the bore log is different from the shear strength of the soil at the time the dynamic was conducted because of the changes in the soil strength brought about by the pile installation process. The installation process results in the following:

- an increase in the lateral stress due to the introduction of the pile volume, which increases in the soil strength;
- remoulding of the soil which decreases the soil strength;
- development of excess pore water pressures in the soil which decreases the soil strength; and
- subsequent dissipation of the excess pressures and consolidation of the soil, which increase the soil strength.

Therefore, it is desirable to plot the damping factor against the shear strength of the soil at the time the dynamic test was carried out. This will also serve to validate the relationship between the exponential damping factor and the shear strength of the soil obtained in the previous section.

Since the shear strength of the soil at the time of the dynamic test is not immediately available, the shear strengths can be deduced from the CAPWAP-computed interface friction profile. It is acknowledged that the interface friction is a function of not only the shear strength but also the pile roughness. However, since all the cases involve driven steel and concrete piles, these piles can be assumed to have similar surface roughness, and therefore, an assessment of the shear strength of the soil based on the interface friction is reasonable. Rather than deducing the shear strength quantitatively by assuming a factor to account for the pile roughness, the relative magnitudes of the shear strength of the various cases are ranked (based on the interface friction values) using a qualitative measure of the shear strength, where a smaller number indicates a lower shear strength.

The CAPWAP(expo)-computed friction vs. depth for the various cases is shown in Figure 9.33. Based on Figure 9.33, the shear strengths corresponding to the various cases are ranked based on the CAPWAP(expo)-computed shaft friction, as shown in Table 9.8. Each number used in the qualitative measure applies to a range of average friction values, as annotated in Table 9.8 and Figure 9.33. The exponential damping factor is plotted against the qualitative measure of the shear strength in Figure 9.35. The relationship shows a definite trend of the factors decreasing with increasing shear strengths. Thus, the damping factor-shear strength relationship observed in the previous section and the laboratory data has been validated.

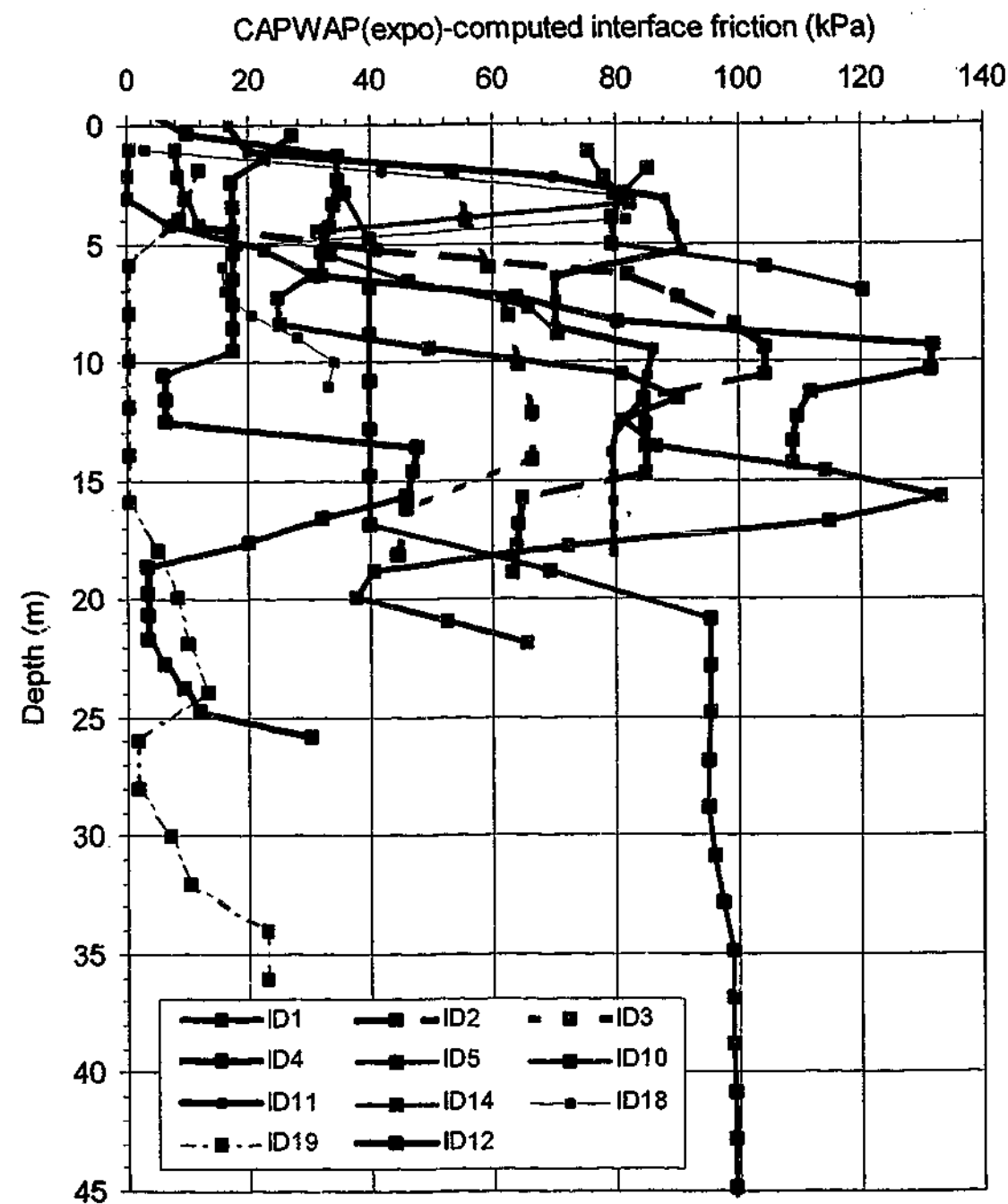


Figure 9.33 CAPWAP(expo)-computed shaft friction vs. depth

Table 9.8 Qualitative ranking of shear strengths based on CAPWAP(expo)-computed interface friction

Case ID	Ranking based on CAPWAP(expo)-computed interface friction*
ID1	3
ID2	3
ID3	3
ID4	2
ID5	4
ID10	3
ID11	4
ID12	3
ID14	3
ID18	2
ID19	1

* 1 - <10kPa; 2 - 10kPa; 3 - 50-80kPa; 4 - 80-100kPa

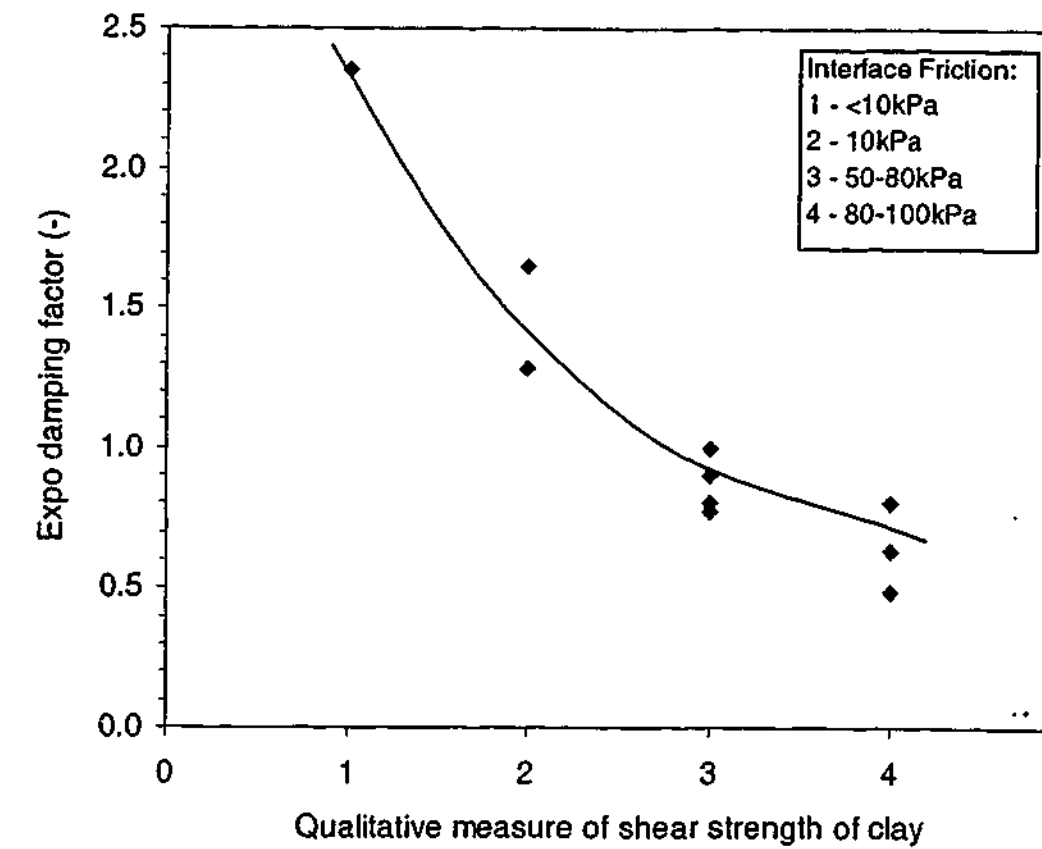


Figure 9.34 Relationship between exponential damping factor and the relative shear strengths based on CAPWAP(expo)-computed interface friction

9.13 EOD Data vs. BOR Data

It is known from the CAPWAP experience that for piles installed in soils susceptible to set-up, the back-calculated linear viscous damping factors for beginning of restrike (BOR) blows are usually significantly different from those for end of drive (EOD) blows. In fact, the BOR values have been found to be generally higher than the EOD values (e.g. Rausche et al., 1996; Liang and Zhou, 1997; Svinkin and Teferra, 1994). As an example, a plot by Svinkin and Teferra (1994) in Figure 9.35 shows that the damping factor increases with time for a pile that was restruck at three different times after its installation (note the units shown are s/ft). Two hypotheses have been proposed to explain the variation of the linear viscous damping factors for the same pile tested at the time of installation and at restrike.

The first hypothesis is that the linear viscous damping factor itself is velocity-dependent. The highly non-linear damping response has been established experimentally in the current study and many other previous studies (e.g. Heerema, 1979; Litkouhi and Poskitt, 1980; Dayal and Allen, 1975), and is also consistent with

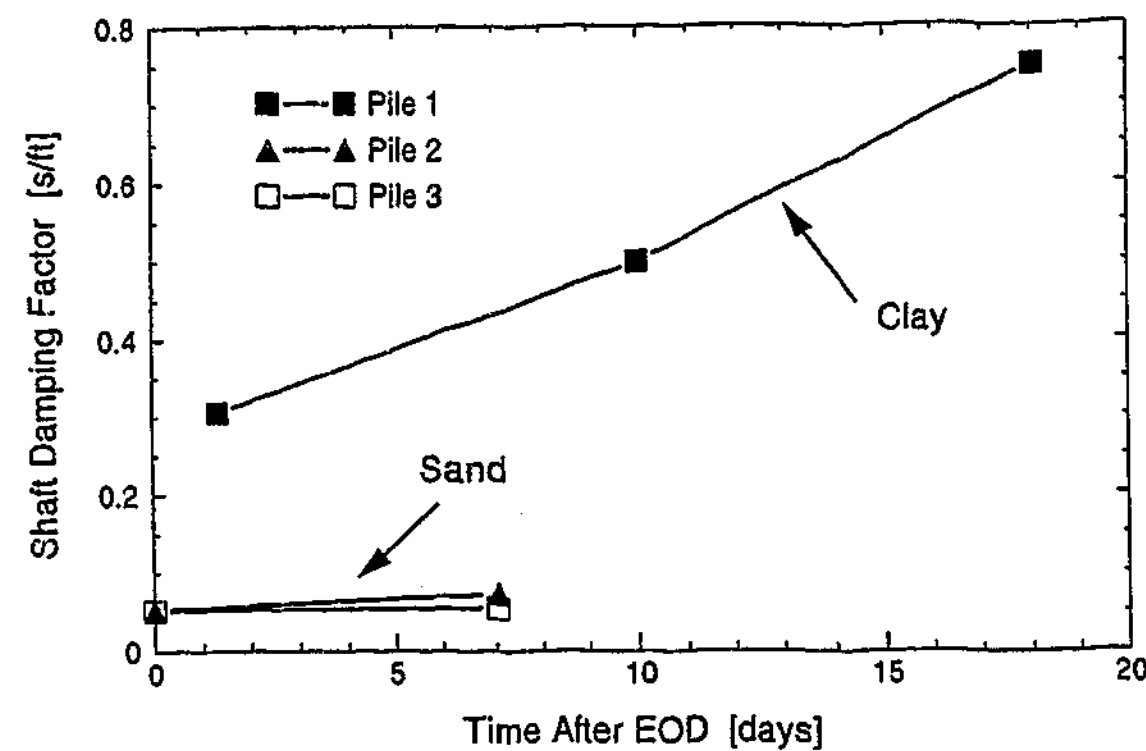


Figure 9.35 Variation of the linear viscous damping factor with time (after Svinkin and Teferra, 1994)

the experience in signal-matching which indicated that the damping maxima appears to be only marginally related to the pile velocity at high velocities (Rausche et al., 1996). It can be illustrated that when the linear model is used to model a particular non-linear response, a higher linear damping factor is required if the non-linear response involves a high peak velocity, and conversely, a lower linear damping factor is required if the non-linear response involves a low peak velocity. For a hypothetical exponential damping response of $\alpha=1.1$ and $\beta=3.0$, the linear model to best-fit the non-linear response involving (a) a high peak velocity and (b) a low peak velocity are shown in Figure 9.36(a) and Figure 9.36(b) respectively. The linear damping factor ($J_{viscous}$) in Figure 9.36(a) is lower than that in Figure 9.36(b). The various values of $J_{viscous}$ required to best-fit a non-linear curve with various peak velocities are plotted against the various peak velocities in Figure 9.37. Thus, $J_{viscous}$ decreases with increasing peak velocities of the exponential curve.

If set-up occurs after the installation of the pile was executed, which causes the pile capacity at BOR to be higher than that at EOD, the average pile velocity at the BOR will tend to be lower than that at the EOD because the same hammer is typically used at the BOR and the EOD. Therefore, it is hypothesised that a higher value of the linear damping factor will be required for the BOR test.

The second hypothesis is that the variation in the linear viscous damping factor is due to changes in the soil properties related to set-up between the time of driving and restrike. During set-up, the remoulded soil at the interface regains its strength as the radial effective stress increases with the dissipation of excess pore pressure induced during driving.

Whilst the second hypothesis is theoretically possible, it contradicts the experimental evidence obtained in this study. Based on the experimental results from this study, an increase in soil strength should result in a decrease rather than an increase in the damping factor. It would thus appear that the first hypothesis is the reason for the highly variable linear damping factors for the EOD and the BOR blows. The hypothesis is validated by showing that for a particular pile, the *exponential* damping factors corresponding to the EOD and the BOR blows are more consistent as

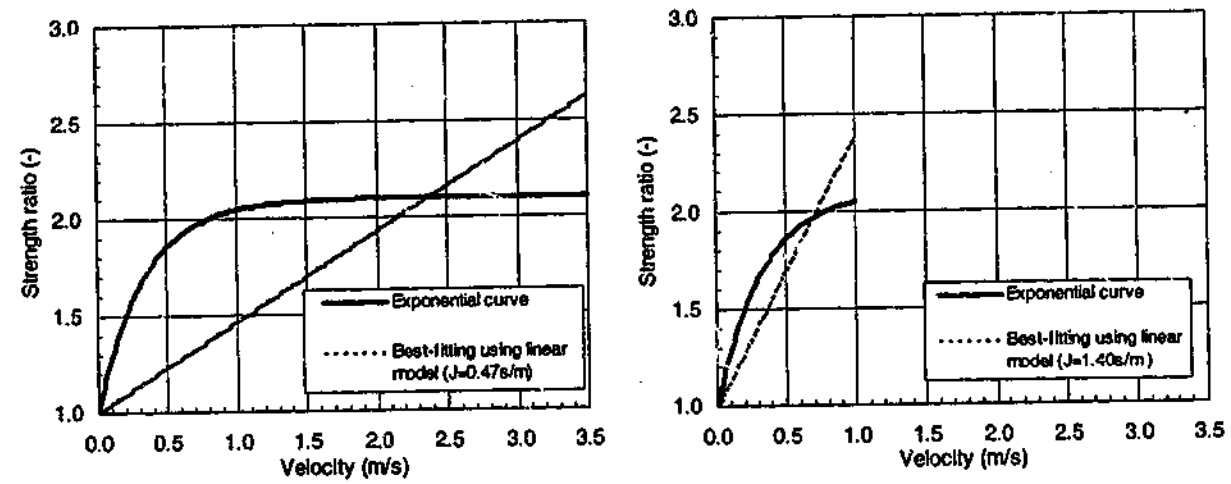


Figure 9.36 Using a linear model to approximate the non-linear response for (a) low velocities (b) high velocities

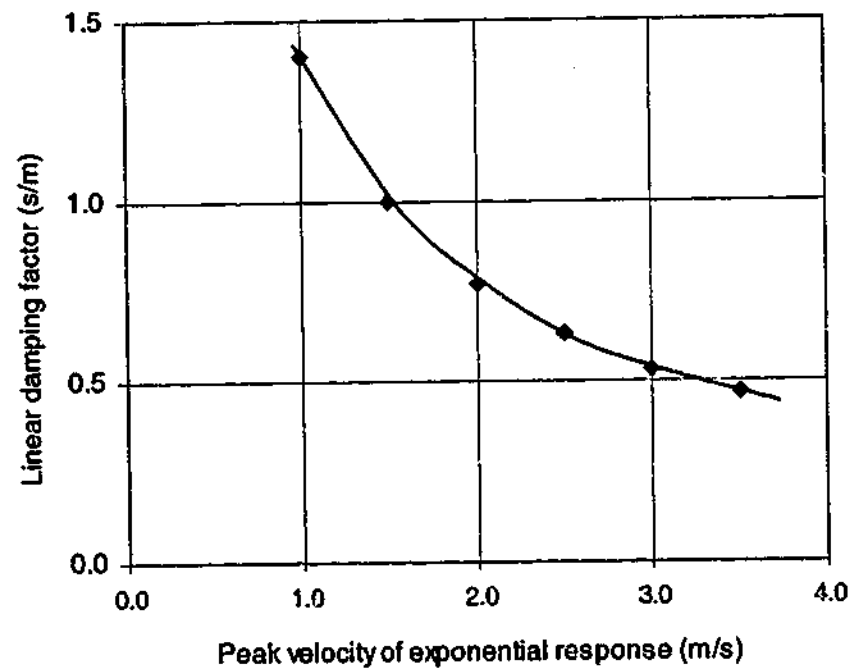


Figure 9.37 Relationship between linear damping factor and peak velocity of the exponential response ($\alpha=1.1$, $\beta=3.0$)

compared to the equivalent *linear* damping factors corresponding to the EOD and the BOR blows.

Dynamic data sets for nine piles comprising both EOD and BOR records were analysed using the linear viscous model and the exponential model. Figure 9.38 and Figure 9.39 show comparisons of the EOD and BOR values for the linear factor and exponential factor respectively, where reference lines for $\pm 25\%$ of the BOR value are indicated. The variation of the values of the factors pertaining to EOD and BOR can

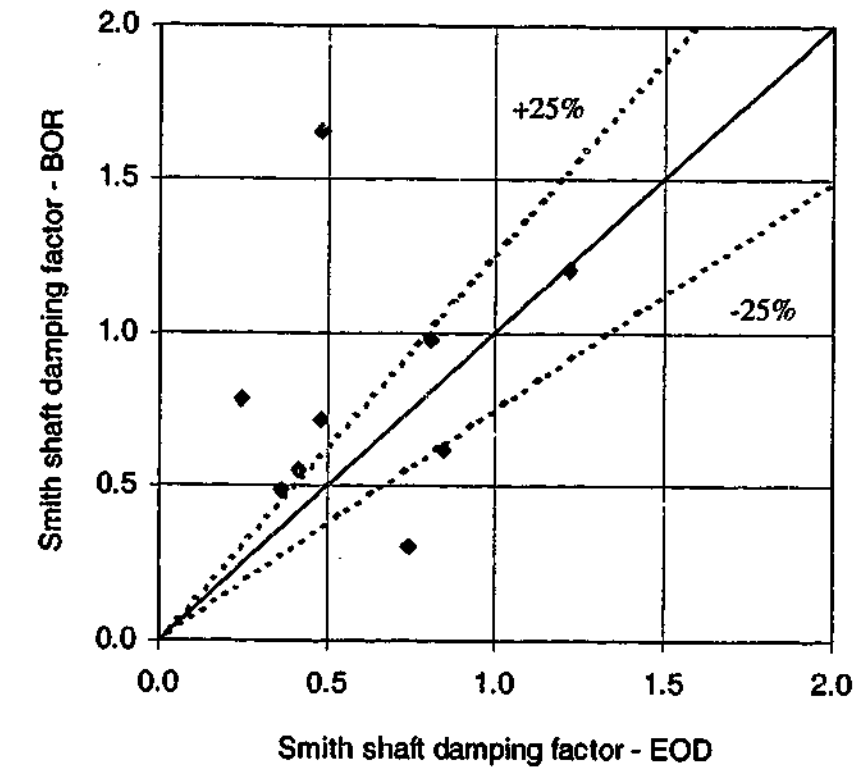


Figure 9.38 Comparison of the linear viscous damping factors for EOD and BOR

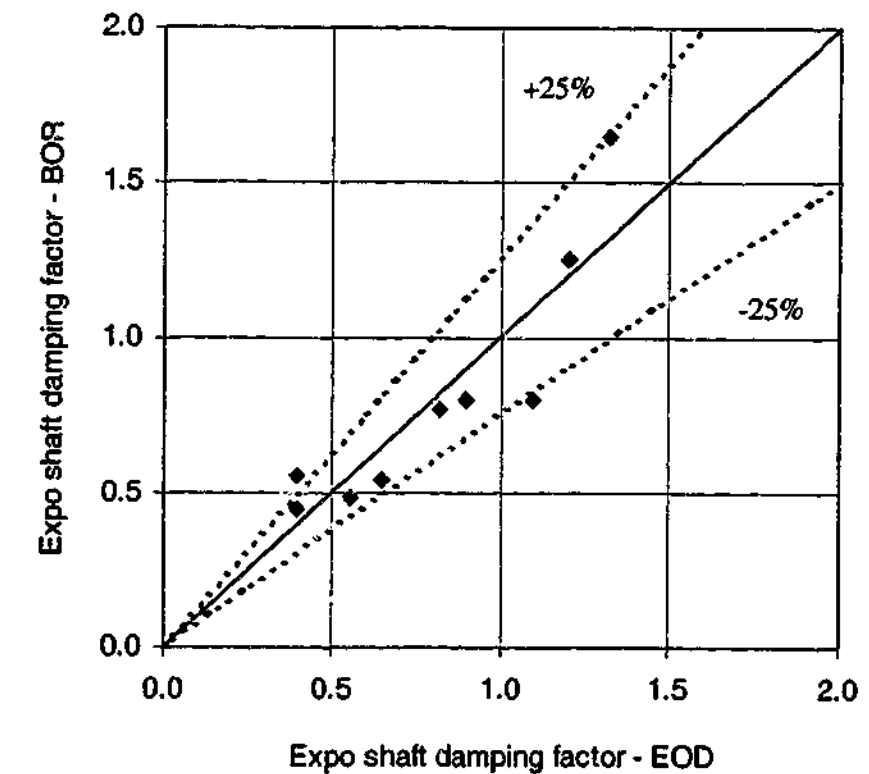


Figure 9.39 Comparison of the exponential damping factors for EOD and BOR

be quantified by defining the ratio of the BOR factor to the EOD factor (denoted linear factor(BOR)/linear factor(EOD) and exponential factor(BOR)/exponential factor(EOD)) and statistical analyses are performed on the values of the ratio, with the results shown in Table 9.9.

Table 9.9 Statistical analysis on linear damping factor(BOR)/linear damping factor(EOD) and linear damping factor(BOR)/linear damping factor(EOD) for the 9 cases

	Linear factor(BOR)/ Linear factor(EOD)	Exponential factor(BOR)/ Exponential factor(EOD)
Mean	1.56	1.01
Standard deviation	1.04	0.22

The results clearly show that the *exponential* factors for BOR and EOD are relatively consistent, with the average BOR value being equal to the EOD value and with the BOR values being $\pm 22\%$ of the EOD values. The *linear* factors for BOR values tend to be significantly higher than those for EOD, with the average BOR value being 1.56 times the EOD value and with the BOR values varying between 0.52 to 2.6 ($=1.56 \pm 1.04$) times the EOD value. It would thus appear that the first hypothesis that the BOR values are higher than the EOD values because of the velocity-dependence of the linear factor is correct. It is thus proposed that the use of a model that is capable of modelling the actual damping response has allowed the back-calculated damping factors for the same pile to be more consistent, and that the exponential factor (unlike the linear factor) is dependent only on the physical characteristics of the interface.

Experimental results presented in Section 8.4 have shown that the amount of viscous damping decreases with an increase in the soil strength. This is also consistent with the suggestion that higher damping factors are required for soft clays (PDI, 1994; Rausche et al., 1996) and the intuition that the viscosity of the soil increases as the moisture content increases. However, the factors for the BOR associated with relatively higher soil strength due to set-up are not consistently lower than those for the EOD - with 5 cases with BOR lower than EOD, and the remaining 4 cases with the BOR value either about equal to or higher than the EOD value.

It is proposed that in addition to the increase in the soil strength, there are other changes taking place in the soil between the times of driving and of restrike, which may counter the effect of the strength increase on the damping value. These other changes may include the following:

- For sensitive clays, the soil structure is destroyed by repeated shearing during installation or at the EOD (e.g. PDI, 1994). The structure is regained during set-up or by the time the BOR is performed;
- It has been reported that for overconsolidated clays, the fabric of the clay may be smoothed by repeated shearing during installation (or at the EOD) (e.g. PDI, 1994). As the soil consolidates against the pile surface during set-up (or at the time the BOR is performed), the fabric of the soil at the interface is altered; and
- During driving, the soil may not be in intimate contact with the pile shaft at some sections of the pile shaft. This is caused by horizontal pile motions due to pile whipping and the Poisson's effect, and where applicable, due to voids created by plugs formed in "open" section piles (H pile and open ended tube), oversize pile shoes and oversize closure plates for tubes (PDI, 1994). During set-up, the soil gradually establishes contact with the pile shaft as the soil deforms radially towards the pile during the dissipation of the excess pore pressure generated during installation, as has been established in field studies (e.g. Pestana et al., 2002).

9.14 Concluding Remarks – Physical Meaning of Exponential Damping Factor

It has been discussed in Section 2.4.1 that the Smith model and the modified Smith model or the linear damping model are based on Smith's intuition rather than experimental evidence, and that in fact, the actual damping response at the pile-soil interface has been shown in experimental studies to be highly non-linear. It is therefore not surprising that extensive experience in signal-matching analyses using the linear viscous damping model indicates that linear damping factors cannot be related to common and fundamental soil properties. Also, the linear damping factor appears to be dependent not only on the physical characteristics of the interface but also on the velocity as well as. In these regards, it would appear that the linear

damping factor is not physically meaningful, as has been suggested by some previous researchers as well (Lai et al., 1996; Liang and Zhou, 1996, 1997).

It has been shown that the maximum value of the CAPWAP-computed exponential damping factor increases with the increasing cohesive content of the soil, and that the factor varies within a range for each soil type. Also, based on the laboratory data obtained from this study and the CAPWAP analyses of dynamic data sets involving piles installed in clay, it has been demonstrated that, for the pile-clay interface, the exponential damping factor is dependent on the shear strength of the clay. Furthermore, it has been shown that the exponential damping factor, unlike the linear damping factor, is apparently dependent only on the physical characteristics of the interface. Based on these findings, it would appear that the use of the exponential damping model, which more accurately models the actual damping response, has enabled a physically meaningful damping factor to be defined.

It is hoped that the use of a physically meaningful damping factor in dynamic signal-matching and pile driveability analyses will result in improved reliability of the analyses for piles installed in clays, in the following aspects:

- As the exponential factor is apparently dependent only on the physical properties of the pile-soil interface (soil type, and for the pile-clay interface, the soil strength). The use of the physically-based model and damping factor in signal-matching analyses will enable analyses to be carried out with more confidence;
- In pile driveability analyses where the damping factor is required for a particular soil as an input, the more determinable factor will enable a more accurate amount of damping to be modelled and hence a more reliable prediction of the dynamic response of the pile;
- The physically dependent exponential damping factor will enable it to be more confidently applied to piles installed at a particular site and in similar soils at other sites, in either signal-matching analysis or pile driveability analysis; and

- The use of the realistic damping model will enable more confident back-calculation of actual CAPWAP soil parameters in the signal-matching analysis.

9.15 Summary

In this chapter, the methodology adopted for evaluating the performance of the proposed exponential damping model has been outlined.

Based on 44 selected data sets, comparative studies of various parameters (the shaft, toe and total capacities, the shaft resistance distribution, as well as the loading and unloading CAPWAP parameters) computed using CAPWAP(expo) and CAPWAP(linear) have been conducted. A comparative study of the signal-matching capabilities of CAPWAP(expo) and CAPWAP(linear) has also been carried out. Based on these studies, it has been proposed that two analyses compute similar amounts of total damping.

Based on the relationship of the exponential damping factor with physical soil parameters and the apparent dependence on only the physical characteristics of the interface, it has been proposed that the exponential damping factor is physically meaningful.

Chapter 10

10. Summary & Conclusion

10.1 Summary & Conclusion

The dynamic methods for determining the pile capacity and for forecasting the driveability of piles are premised on accurate modelling of the physical processes that occur during the pile driving process. However, the linear model currently used in practice for modelling the viscous damping response does not appear to be supported by experimental evidence, and in fact, experimental studies have shown that the actual damping response is highly non-linear. Other models have been proposed based on experimental studies which have various perceived deficiencies and have generally not modelled well the physical characteristics and boundary conditions of the pile-soil interface. It is to be expected that if the dynamic model does not realistically model the viscous component of pile-soil behaviour, then the reliability of the pile driveability and signal-matching analyses will be compromised.

In order to improve the reliability of the dynamic methods, research has been undertaken to better model and characterize the dynamic response of the pile-soil interface during pile-driving events. The approach adopted in this research program has been to simulate the field response as accurately as practically possible in the laboratory under controlled conditions, and in a way which overcomes the deficiencies perceived in previous research programs. The experience of developing the experimental equipment and testing has highlighted to the author the many difficulties in developing a novel experimental equipment and executing a valid test program without too many compromises. The response of the pile-soil interface thus attained has captured the essential characteristics of the dynamic response and enabled the development of an improved alternative model of viscous damping.

In the testing program, both pile-sand and pile-clay interfaces have been evaluated. For each type of interface, quasi-static and dynamic tests have been performed. The quasi-static tests have been conducted primarily for obtaining the quasi-static resistance required for normalising the dynamic resistance. The quasi-static behaviour of both types of interface has been shown to be consistent with expectation and with previous research.

Based on the data obtained from the dynamic tests, it has been possible to characterise the viscous damping responses of the pile-sand interface and the pile-clay interface. For the pile-sand interface, viscous damping has been found to be insignificant for shear rates up to 1.5m/s. It has been proposed that any small degree of rate-dependence of the interface strength (estimated to be up to 5% increase over the static strength) could not be reliably determined because of the limitations of the test device, and that the finding that dynamic effects are negligible for velocities up to 1.5m/s cannot therefore be taken to imply that there is also negligible strength increase in the interface at higher velocities. It has thus been recommended that tests be performed at higher shear rates in order to establish any rate-dependence of the pile-sand interface strength in the high velocity regime.

For the pile-clay interface, the dynamic friction due to viscous damping has been demonstrated to be dependent on the shear rate, and it has been found that the functional form of the characteristic strength ratio-velocity response can be described

by an exponential function. A damping parameter based on this new model has been defined and referred to as the exponential damping factor or the viscous damping parameter.

For the pile-clay interface, the post-test shear surfaces of the interfaces subjected to both low and high shear rates have been observed. The clay specimens and the pile surfaces subjected to dynamic shearing have been found to be significantly different from those subjected to quasi-static shearing because of significant remoulding of the clay specimen, significant development of shear-induced excess pore pressures in the shear zone of the specimen and smearing of the pile surface in the dynamic tests. This implies that the quasi-static friction measured in the quasi-static test cannot be used to normalise dynamic friction. In order to normalise the dynamic friction and also to quantify the difference in the interface friction values, a procedure for determining the quasi-static friction associated with a dynamic test has been developed and verified. It has been noted that the data at the start of the dynamic test event were not amenable to the analysis because at that time, the interface friction was not yet fully mobilised and the effect of residual friction (caused by the previous test cycle) was present; therefore, only the data pertaining to the deceleration of the pile from the peak velocity to zero velocity have been analysed.

Based on the post-test observations, essentially three dynamic modes of interface shear failure were observed for various pile-clay interfaces, with the dynamic shear mode being dependent on the clay plasticity and the pile roughness. Thus, from the clay plasticity and the pile roughness pertaining to a particular interface, the dynamic shear failure mode can be determined. Also, based on these observations, a mechanism of viscous damping for the pile-clay interface has been proposed.

The experimental testing has attempted to investigate the effects of the following parameters on the viscous damping response: the normal stress, the *OCR*, the shear strength of the clay, the clay type, the pile roughness as well as the dry and wet conditions of the pile surface. The effects of the various parameters on the interface response have been discussed and interpreted using the proposed hypothesis. The value of the damping parameter based on the model has been shown to be dependent on the physical characteristics of both the interface and the soil. For each dynamic

shear mode, the viscous damping parameter can be related to the shear strength of the clay to give a relationship whereby the value of the parameter increases with decreasing shear strengths. However, when the values of viscous damping parameter are plotted against the normal stress and the *OCR*, general but less consistent trends have been observed.

Therefore, based on knowledge of the clay plasticity and the pile roughness and the damping parameter-shear strength relationship, a simple method of estimating the value of the damping parameter has been proposed. The dynamic failure mode is determined from the clay plasticity and the pile roughness, and the value of the damping parameter is estimated from the damping parameter-shear strength relationship for the particular dynamic failure mode.

The proposed function for describing the characteristics of the dynamic friction-velocity response has been incorporated into the most widely used signal-matching package known as CAPWAP, and used for signal-matching of 44 sets of dynamic data obtained from the field. Specific results of the CAPWAP analyses are as follows:

- CAPWAP equipped with the new pile shaft-soil model (denoted CAPWAP(expo)) has a matching capability that is as good as if not slightly better than the original CAPWAP (denoted CAPWAP(linear));
- The values of the back-calculated CAPWAP parameters that affect the loading phase (namely the toe damping factor, the shaft quake, the toe quake, the toe gap and the toe plug) and the unloading phase (namely the unloading shaft quake, the unloading toe quake and the negative shaft resistance limit) can vary significantly compared to those back-calculated with the linear model being used in the industry. Given that the physically based exponential model should enable more realistic values of the parameters to be computed, it is thus cautioned that the analysis performed using the linear model may give values that are not representative of the true values.
- The toe, shaft and total resistances and the shaft resistance distribution computed using CAPWAP(expo) are generally comparable to those computed using CAPWAP(linear).

It has been a somewhat unexpected conclusion that, although the linear response departs from the actual non-linear response, the signal-matching analysis performed using the non-linear model does not appear to result in an interpreted pile capacity that is significantly different to that obtained from the analysis performed using the linear model. It has been proposed that the total amounts of damping applied when the linear and exponential models are used are similar. This would also explain why the linear damping model has been able to satisfactorily match measured dynamic data.

The results of the signal-matching analyses suggest that the proposed exponential damping parameter is physically meaningful in the following regards:

- The range of values of the back-calculated viscous damping parameter from the dynamic analyses of field piles is comparable to that obtained from the laboratory data;
- The maximum value of the damping parameter can be correlated with the soil type, where the value increases with the cohesion of the sample, as indicated by the laboratory data obtained from this study;
- For the pile-clay interface, the CAPWAP-computed exponential damping factor increases with decreasing shear strength. This relationship is consistent with that found based on the laboratory data;
- The CAPWAP-computed exponential damping factors for the end-of-drive (EOD) and beginning-of-restrike (BOR) have been shown to be more consistent than would have been the case if the linear damping is employed. This has been taken to imply that, unlike the linear damping factor, the exponential damping factor is dependent only on the physical characteristics of the interface.

As it can be argued that the exponential damping model more realistically models the damping behaviour at the pile-soil interface using a physically-based parameter and is easy to implement, the implementation of the new shaft damping model is recommended for signal-matching. It is hoped that the use of a physically meaningful damping parameter based on the actual characteristic damping response will enable the dynamic response of piles to be predicted more accurately in pile drivability

analyses, and will increase the level of confidence in the pile capacity and the CAPWAP soil parameters computed in the signal-matching analysis.

10.2 Future Research

In its limited scope, this study has by no means investigated the effects of all parameters that may influence on the interface dynamic friction. Therefore, further research is recommended to establish the effects of certain significant parameters on the dynamic response of the interface, as outlined subsequently.

The study has opened up areas of research that are worthy of investigation; these topics of research are suggested subsequently.

10.2.1 Effects of pore pressure & remoulding of clay

It is suggested that tests with measurement of the excess pore pressure in the soil at the interface be carried out. For an interface whose pile surface condition remains the same (i.e. the pile surface is not smeared) throughout a series of cyclic tests, measurement of the pore pressure will also enable the magnitude of the interface strength reduction caused by the remoulding of the clay to be quantified. Having quantified the excess pore pressures and the degree of remoulding of the clay, it would then be possible to determine the effects of these two parameters on the dynamic response of the interface. It is however noted that the measurement of the pore pressure in the clay poses a significant challenge to the future researcher, as an interface shear test cannot ensure full saturation of the specimen at the interface, which is necessary for meaningful measurements of the pore water pressure.

10.2.2 Other cohesive soils

The research in this project on clay has been limited to three types of kaolinitic clay. Whilst back-calculated values for piles installed in other types of clay and natural clays fall in the range of the experimental values, it is recommended that further research is carried out on interfaces involving clays of different mineralogy, other cohesive soils such as silts, and combinations of cohesive and cohesionless soils.

10.2.3 Dynamic pile-soil interface response in the high velocity regime

The pile-sand and the pile-clay interface tests performed in this research are limited, due to practical constraints, to peak velocities of 1.5m/s and 1.6m/s respectively. These velocities are low compared to peak velocities ranging from 3.0 to 7.5m/s that are often associated with pile driving. For the pile-clay interface, experimental data obtained in this study indicate that the strength ratio increases with velocity at a low or an almost constant rate beyond 1.6m/s. For the pile-sand interface, whilst the experimental data show negligible strength increase up to 1.5m/s, significant and thus measurable strength increase may occur at higher shear rates. Tests involving higher shear rates would thus be required to establish the dynamic responses of the pile-sand and pile-clay interfaces in the high velocity regime.

10.2.4 Further signal-matching analyses

The signal-matching analyses performed in this study has suggested that, statistically, analyses performed using CAPWAP(expo) has not resulted in significantly different interpreted pile capacities, as compared to those computed using CAPWAP(linear). However, the effect of the analyses have been performed on only 19 cases where static load test data have been available. Further analyses on a larger number of cases will therefore be required to validate the finding.

10.2.5 Dynamic response of soil at pile base

The work described in this dissertation has focussed entirely on the interface between the pile shaft and the surrounding soil. Previous research has shown that strength increase due to the viscous damping phenomenon also occurs in clay and sand specimens tested in compressive triaxial tests which closely simulate the loading of the soil at the pile tip. Thus, the dynamic response of sand and clay at the pile base should be a fruitful area for research.

10.2.6 Mechanism of viscous damping

In this study, the mechanism of viscous damping has been proposed based on post-test observations of the shear surfaces that have been subjected to fast shearing. A study devoted to understanding the mechanism of viscous damping is recommended for evaluating the validity of this hypothesis. It is likely that the mechanism of

viscous damping for the pile-clay interface will be relevant to if not the same as the mechanism for soil-only failure.

Appendix A

A. Stress-Wave Mechanics

The following is an excerpt from Fleming et al. (1992), which explains the theory of stress-wave mechanics relevant to dynamically loaded piles.

9.3.1 Wave equation analysis

The propagation of driving energy along a pile, allowing for interaction with the surrounding soil, may be analysed with sufficient accuracy using a 'one-dimensional' idealization. In this idealization, only vertical (strictly speaking 'axial'), displacement of the pile is considered, and the governing differential equation is

$$(AE)_p \frac{\partial^2 w}{\partial z^2} = (A\rho)_p \frac{\partial^2 w}{\partial t^2} - f \quad (9.1)$$

or

$$\frac{\partial^2 w}{\partial z^2} = \frac{1}{c^2} \frac{\partial^2 w}{\partial t^2} - \frac{f}{(AE)_p} \quad (9.2)$$

where $(AE)_p$ is the cross-sectional stiffness of the pile,

$(A\rho)_p$ is the mass per unit length of the pile,

c is the wave propagation speed in the pile ($=\sqrt{EI/\rho}$),

w is the vertical displacement of the pile,

z is the distance down the pile,
 t is the time variable, and
 f is the mobilized soil resistance per unit length of pile.

Historically, this equation has been implemented using finite difference or finite element techniques, with the pile being modeled as a discrete assembly of mass points interconnected by springs. This model, originating in the work of Smith (1960), forms the basis of a range of computer programs for studying pile drivability.

More recently, equation (9.2) has been solved numerically by using the characteristic solutions, which are of the form

$$w = g(z - ct) + h(x + ct) \quad (9.3)$$

where g and h are unspecified functions which represent downward (increasing z) and upward traveling waves respectively. Taking downward displacement and compressive strain and stress as positive, the force, F , and particle velocity, c , in the pile are given by

$$F = -(AE)_p \frac{\partial w}{\partial z} = -(AE)_p (g' + h') \quad (9.4)$$

and

$$v = \frac{\partial w}{\partial t} = -c(g' - h') \quad (9.5)$$

where the prime denotes the derivative of the function with respect to its argument.

The velocity and force can each be considered as made up of two components, one due to the downward traveling wave (represented by the function g) and one due to the upward traveling wave (represented by the function h). Using subscripts d and u for these two components, the velocity is

$$v = v_d + v_u = -cg' + ch' \quad (9.6)$$

The force F is similarly expressed as:

$$F = F_d + F_u = -(AE)_p g' - (AE)_p h' = Z(v_d - v_u) \quad (9.7)$$

where $Z = (AE)_p/c$ is referred to as the pile impedance. [Note, some authors have referred to the pile impedance as $Z = E/c$, relating axial stress and velocity rather than force and velocity. The more common definition of pile impedance as $Z = (AE)_p/c$ will be adopted here.]

The relationships given above may be used to model the passage of waves down and up piles of varying cross-section, allowing for interaction with the surrounding soil. It is helpful to consider the pile as made up of a number of elements, each of length Δz , with the soil resistance acting at nodes at the mid-point of each element (see Figure 9.28). Numerical implementation of the characteristic solutions involves tracing the passage of the downward and upward traveling waves from one element interface to the next. The time increment, Δt , is chosen such that each wave travels across one element in the time increment (giving $\Delta t = \Delta z/c$).

Between nodes i and $i + 1$, the soil resistance may be taken as T_i , the value of which will depend on the local soil displacement and velocity (see later). Taking T_i as positive when acting upwards on the pile (that is, with the soil resisting downward motion of the pile), the soil resistance will lead to upward and downward waves of magnitude

$$\Delta F_u = -\Delta F_d = T_i/2 \quad (9.8)$$

These waves will lead to modification of the waves propagating up and down the pile.

The procedure for calculating new values of wave velocities at each node is shown schematically in Figure 9.29. Thus, consider the downward and upward waves at nodes $i - 1$ and $i + 1$, at time t . The new downward traveling wave at node i at time $t + \Delta t$ is given by

$$(v_d)_i[t + \Delta t] = (v_d)_{i-1}[t] - T_{i-1}[t + \Delta t]/(2Z) \quad (9.9)$$

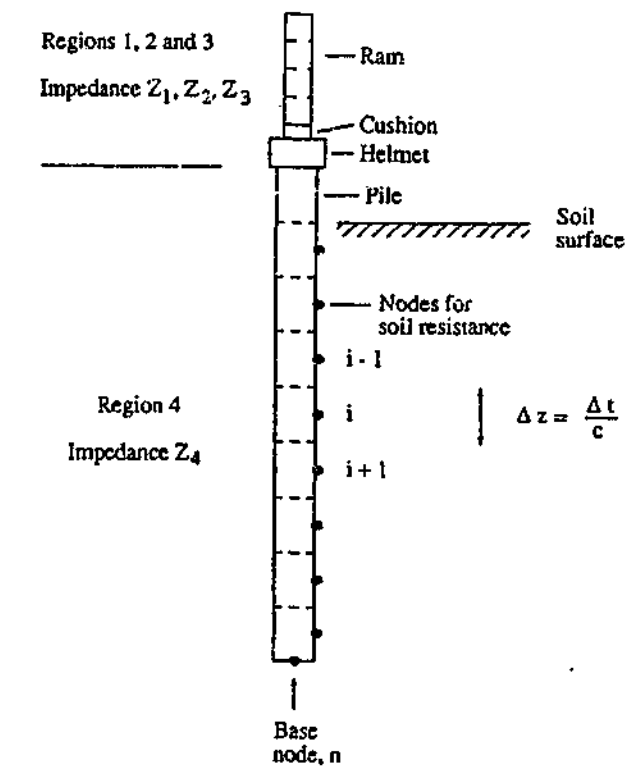


Figure 9.28 Idealization of pile as elastic rod with soil interaction at discrete nodes

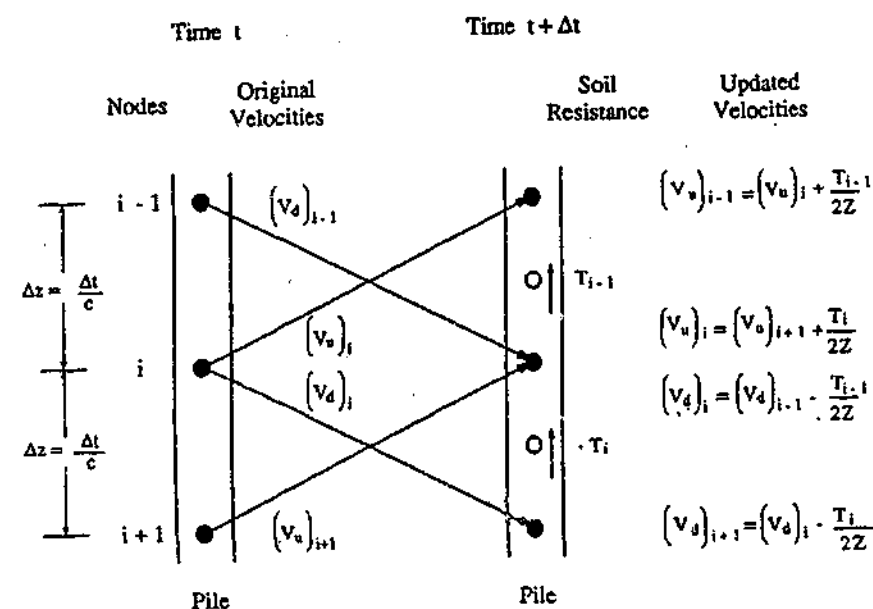


Figure 9.29 Modification of downward and upward waves due to soil interaction. After Middendorp and van Weele (1986)

while the new upward traveling wave fractionally above node i is

$$(v_u)_i[t + \Delta t] = (v_u)_{i+1}[t] + T_i[t + \Delta t]/(2Z) \quad (9.10)$$

At the base of the pile, the downward traveling wave will be reflected, with the magnitude of the reflected wave dependent on the base resistance, Q_b , offered by the soil. The axial force in the pile must balance the base resistance, which leads to an expression for the reflected (upward traveling) wave velocity of

$$(v_u)_n[t + \Delta t] = (v_d)_n[t + \Delta t] - Q_b[t + \Delta t]/Z \quad (9.11)$$

The base velocity (the n^{th} node) is

$$v_n = 2v_u + Q_b/Z = 2v_d - Q_b/Z \quad (9.12)$$

where all quantities refer to time $t + \Delta t$.

For a force F_d arriving at the pile tip, equation (9.11) implies a reflected force of

$$F_u = -Zv_u = Q_b - F_d \quad (9.13)$$

The magnitude of the reflected wave thus varies from $-F_d$, where the tip resistance is zero, to F_d , where the base velocity is zero and the base resistance is twice the magnitude of the incident force (see equation (9.12)).

It should be noted that the characteristic solutions of the wave equation may be used to model the pile hammer assembly as well as the pile, in order to perform drivability studies. The geometry and mass density of each component (ram, cushion, helmet) is matched, and the ram is given an initial velocity to model the impact. As discussed by Middendorp and van Weele (1986), a relatively crude model of the hammer will generally suffice to give adequate results.

Appendix B

B. Definition & Meaning of CAPWAP Parameters

B.1 Definition of CAPWAP Notation

The notation of the CAPWAP parameters is defined in the CAPWAP for Windows Manual 2000 (PDI, 2000). The relevant section has been reproduced.

JS is the Case damping factor, J for the Skin (dimensionless). This damping will be distributed proportionately to the static resistance such that the individual soil damping factor (at segment i) becomes

$$SJ_i = JS(Z) R_i / RS$$

where Z is the pile impedance, RS is the shaft resistance and R_i is the resistance at segment i .

Note:

- These damping factors may be individually modified in the **Damping-Add Display Mode** by "added" damping or in **Display Mode Damping-Multiplies** by non-proportional distribution of the damping factors.
- SJ_i multiplied with the pile segment velocity yields the damping force at segment i .

- JT** is the Case J-value for the Toe (dimensionless). JT times the pile impedance yields the viscous toe damping factor which multiplied by the toe velocity yields the toe damping force.
- SS** is the Smith damping value for the Skin in s/m (s/ft); it is linked to the viscous damping factor.
- $$SS = S_j / R_i$$
- ST** is the Smith damping value for the Toe s/m (s/ft); it is linked to JT.
- $$ST = JT (Z) / RT.$$
- Note:**
- As long as no static resistance values have been assigned, Smith to Case damping conversions (and vice-versa) are not possible.
 - Either Smith or Case damping factors may be entered; however, Smith factors change when static resistance values are modified.
- QS** is the Quake at the Shaft or skin in mm (in). The value displayed is the quake for soil segment number one. Upon entering a new QS each skin quake value will be multiplied by the ratio of the new to old pile top quake.
- QT** is the Quake at the pile Toe (Segment number $N_{soil} + 1$) in mm (in).
- UN** is the negative skin friction unloading limit, i.e., a "1.0" means that the skin friction can unload to negative values that are equal (but with opposite sign) to the positive ultimate skin friction values. A "0.0" would mean that there can be no negative shaft resistance during pile rebound (as it is always the case at the pile toe).
- Note 1:**
- If the residual stress analysis is to be performed then meaningful results are only possible with an $UN > 0$.
- Note 2:**
- If the **Auto** option is set (near the **MBA** option in Window 1), **UN** may be automatically adjusted depending on the match.)
- TG** may be thought of as being a small distance between the pile toe and the soil. Thus, as long as the pile toe has not moved more than this gap the static toe resistance is zero. **TG** should be entered in mm (in).
- CS** is something like a Coefficient of restitution of Skin resistance or the skin unloading quake divided by the skin loading quake.
- Note 1:**
- CS** and **CT** values (see below) normally start at 1.0. One should not use values less than 0.05 (better 0.2) or greater than 1.0 (it appears, however, that exceptions to this rule may be made when the radiation damping model or other unusual soil model parameters are used; then **CS** and **CT** > 1 occasionally yield the only reasonable matches).
- Note 2:**
- If the **Auto** option is set (near the **MBA** option in Window 1), **CS** may be automatically adjusted depending on the match.)
- CT** is something like a Coefficient of restitution of Toe resistance or unloading quake divided by the loading toe quake (see also **CS**).
- See also Note 1 and Note 2 for CS.**
- LS** is the reloading Level for the Skin. Any skin resistance values which are loading a second time below the reloading level will load at a stiffness given by the unloading quake. The reloading level is normalized by division with **FI** (the ultimate resistance value at soil segment i) and may be entered with values between -1 and 1 inclusive.
- LT** is the reloading Level for the Toe (see also **LSkn**).
- PI** is not a soil resistance parameter. It is given here for convenience sake and because its effect is similar to **PL**. **PI** is the pile damping factor; values less than 0.01 for steel, 0.02 for concrete and 0.03 for timber may be reasonable.
- PL** is a soil mass in FU which produces a resistance proportional to acceleration

- at the pile toe segment.
- SK** is the **SK** soil support dashpot in pile impedance (EA/c) units. For further comments see **BT**. Use the recommendation in the help line.
- BT** is the soil support dashpot at the pile **Bottom** in impedance units. A zero value is equivalent to an infinitely rigid toe soil support. A "1" would give a significant unloading effect and non-zero values less than 1 should be used with great caution. A large value, i.e. 100, will usually not change the results significantly from the rigid assumption. In contrast to **SK**, **BT** recommendations have not been checked by comparison analysis.
- MS** is the weight of soil Mass between Skin resistance and skin soil support dashpot in FU. Use the recommendation given in the help line.
- MT** is the weight of soil Mass between Toe resistance and toe soil support dashpot in FU. Use the recommendation given in the help line.
- OP** Toe damping option: 0-Viscous, 1-Smith, 2-Smith to full resistance activation then Viscous (see Background of CAPWAP). Option 1 or 2 may be advantageous in the presence of a toe gap ($TG > 0$).

B.2 Meaning of CAPWAP Parameters

The definitions of the CAPWAP parameters can be found in the CAPWAP for Windows Manual 2000 (PDI, 2000). The relevant section has been reproduced.

2.2 The Soil Model

2.2.1 Basic Relationships

The displacement and velocity of each pile segment relative to the soil (Note: in the Smith approach, the soil is considered fixed) is the basis for computing the soil resistance forces. The soil model consists of an elasto-plastic spring and a linear dashpot (Figure 2.2.1) described by three parameters: ultimate resistance R_{uk} , quake q_k , and viscous damping factor J_k . The total static bearing capacity R_{st} is the sum of all R_{uk} . The total (static plus dynamic) resistance force R_i at segment i is computed from

$$R_i = R_{si} + R_{di} \quad (2.3)$$

where $R_{si} = R_{di}$ are the time varying static and dynamic soil resistance forces at segment i.

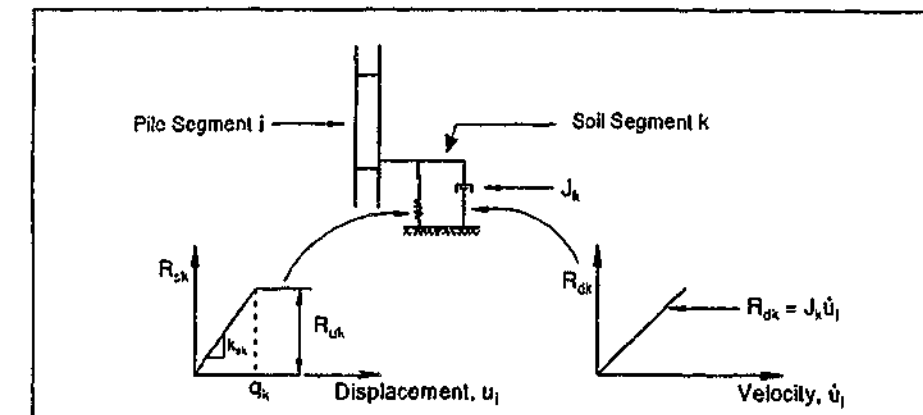


Figure 2.2.1: The Smith soil resistance model
(Viscous damping model instead of a strict Smith damping is shown)

Soil resistances may act at each pile segment. However, since the pile segments are usually rather short, it may be sufficient to have one soil resistance element at the bottom pile segment for end bearing and one shaft resistance element at every second pile segment for the portion of pile embedded in the soil. Thus, the number of pile segments N_p may be greater than or equal to the number of shaft resistance elements

N_s . Consider a soil element k at pile segment i . Knowing pile segment velocity \dot{u}_i , and displacement u_i , and a viscous damping factor J_k , the k -th resistance force becomes

$$R_k = R_{sk} + J_k(\dot{u}_i) \quad (2.4)$$

with the static resistance represented by

$$R_{sk} = k_{sk} u_i \quad (2.5)$$

and

$$R_{nk} \leq R_{sk} \leq R_{uk} \quad (2.6)$$

R_{uk} and R_{nk} are ultimate soil resistance at segment k when the pile is moving downwards (positively) and upwards (negatively), respectively.

2.2.2 Unloading and Reloading

The lower static resistance bound (or negative uplift capacity¹) in Eq. 2.6 is

$$R_{nk} = -U_n R_{uk} \quad (2.7)$$

with

$$0 \leq U_n \leq 1 \quad (2.8)$$

Note that U_n is always zero for **end bearing** (no tensile end bearing). Smith's static shaft resistance wave equation model assumes that during rebound the uplift capacity is of the same magnitude as the ultimate compressive shaft resistance. Extensive experience in CAPWAP signal matching has shown this hypothesis to be usually not true.

The shaft unloading level multiplier U_n (called "UN" in CAPWAP) varies between 0 and 1, inclusively (see Figure 2.2.2). $U_n = 1$ corresponds to the original Smith approach while $U_n = 0$ allows no downward directed shaft resistance during pile rebound. U_n is assumed to be constant along the shaft. In easy driving, U_n has no effect (no rebound). In hard driving, U_n may be chosen as low as zero. The effect of U_n is most easily observed in the later portion of the record. Lower values raise the later portion of the computed curve.

The quantity, k_{sk} , in Eq. 2.5 is the soil stiffness of the k -th resistance. For positive (downward) velocities

$$k_{sk} = R_{uk} / q_k \quad (2.9)$$

with q_k being the actual **loading** quake (**QS** for shaft and **QT** for toe in CAPWAP). Quakes physically and numerically cannot be zero. Under extreme circumstances their maxima may be 1 inch (25 mm) or more on the toe and .3 inches (10 mm) on the shaft. However, most commonly they are in the neighborhood of .1 to .2 inches (2.5 to 5 mm) for the shaft.

¹ Although R_{nk} is mobilized during pile rebound, it may not be equal to the uplift capacity during static loading. Also, R_{nk} has nothing to do with the geotechnical term "negative skin friction" which occurs when the soil through consolidation moves downwards relative to the pile.

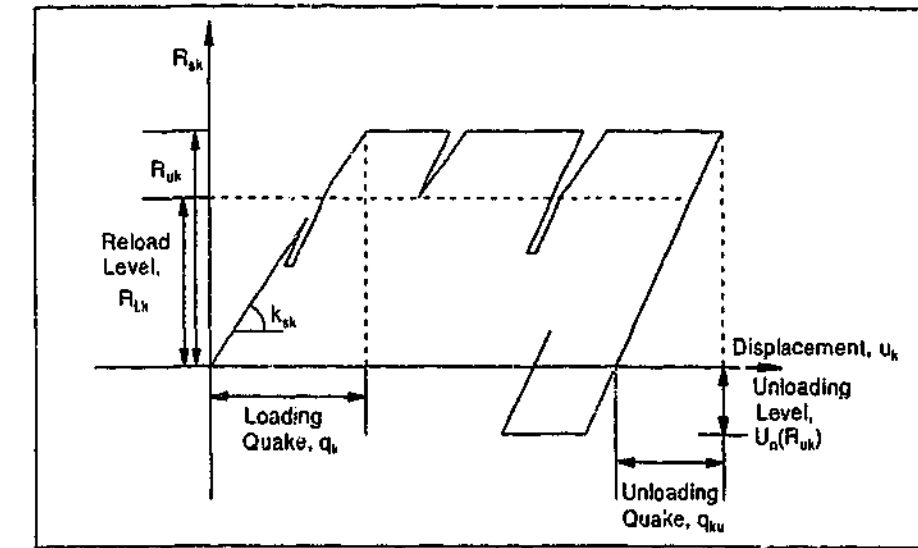


Figure 2.2.2: Static shaft resistance

For negative (upward, rebound) pile velocities, a modified or unloading quake is calculated.

$$Q_{km} = q_k C_k \quad (2.10)$$

and the stiffness is then

$$k_{sk} = R_{uk} / Q_{km} \quad (2.11)$$

The **Skin or Toe Unloading Quake Multipliers (CS or CT)** are used to assign unloading quakes lower than the loading quakes. The multiplier default is 1.0 which makes loading and unloading quakes equal. The same value **CS** is applied to all skin quakes. A low unloading quake causes a quick shedding of load during rebound and therefore lowers the computed force record at the end of the blow. To avoid zero unloading quakes, which are a numerical impossibility, **CS** and **CT** cannot be zero, in fact they are rarely less than 0.1.

The reloading option specifies the **loading level (LS or LT)** in a second or later loading cycle: "Below the reloading level, R_{uk} , the soil stiffness equals the soil's unloading stiffness in a second or later loading cycle within the same blow." Figure 2.2.2 (2.2.3) illustrates the shaft (toe) static resistance versus pile displacement model.

2.1 Toe Model Extensions Gap and Plug

For piles on a very hard end bearing layer, a gap, g_t (**TG** in the CAPWAP program) beneath the pile toe sometimes exists. As the pile toe moves through the gap distance, the static toe resistance remains zero and increases only after the toe displacement exceeds the gap. For full resistance activation, the sum of the toe gap plus toe quake must be less than the maximum pile toe displacement of the blow. The static soil resistance, subject to the gap g_t , is therefore

$$R_{sk} = k_{sk} (u_i - g_t) \quad (2.12)$$

for

$$g_t < u_i \quad (2.13)$$

where k is equal to $N_k + 1$ (pile toe) and i equals N_p . R_{sk} is zero for displacements less than the gap and equal to R_{uk} for displacements greater than the sum of gap and toe quake. During unloading, the toe resistance follows the unloading quake (Figure 2.2.3). In general wave equation works and therefore also in the CAPWAP output, the gap is added to the toe quake.

Another match parameter is the soil mass, m_p , (**PL** in CAPWAP) which might exert an external resistance force (R_{Nj}) at time j , acting against the pile bottom,

$$R_{Nj} = m_p (\dot{u}_{bj} - \dot{u}_{bj-1}) / \Delta t \quad (2.14)$$

where \dot{u}_b is the pile bottom velocity and Δt is the computational time increment. Figure 2.2.3 illustrates the static toe resistance versus pile bottom displacement.

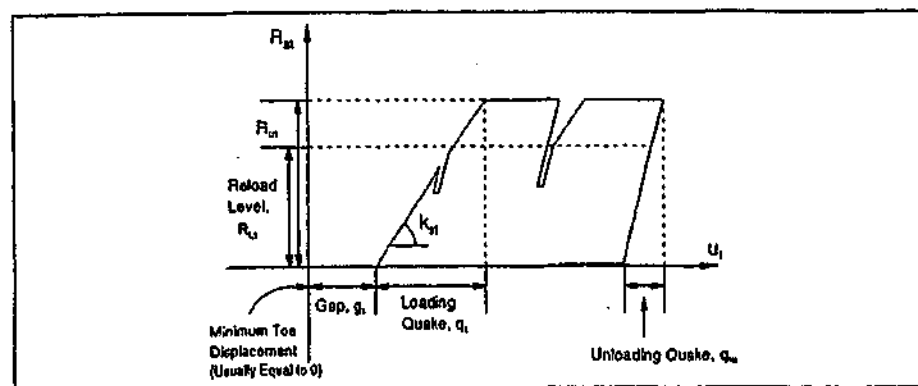


Figure 2.2.3: Static toe resistance

2.2.4 Damping

Viscous forces (which are a function of velocity) also resist pile penetration. The traditional Smith wave equation definition is

$$R_{dk} = J_{sk} \dot{u}_i R_{sk} \quad (2.15)$$

which makes the dynamic resistance, R_{dk} , dependent upon both segment velocity, \dot{u}_i , and temporary static segment resistance, R_{sk} , by a dimensional damping Smith factor J_{sk} for soil element k . However, for signal matching it is more convenient to use linear viscous coefficients:

$$R_{dk} = J_{vk} u_i \quad (2.16)$$

rather than the Smith values since they can then be assigned independently of the static resistance. Smith damping factors can be approximately computed from viscous factors J_{vk} (by setting $R_{sk} = R_{dk}$) using the so-called Smith-viscous approach:

$$J_{sk} = J_{vk}/R_{sk} \quad (2.17)$$

In order to avoid referring to individual viscous skin damping parameters, the Case shaft damping factor J_c is defined as the nondimensionalized (Case Method type) sum of the viscous damping factors.

$$J_c = E(J_{vk})/Z \quad (2.18)$$

where Z is the pile impedance. In CAPWAP, skin damping can be specified by the nondimensional Case factor J_c (**JS**) or with the Smith-viscous damping factor, J_{sk} (**SS**). However, any change of static resistance will modify J_{sk} while J_c remains unaffected. Similarly, for the pile toe, one obtains the Case toe damping factor

$$J_{tc} = J_{vk}/Z \quad (2.19)$$

where $k = N_s+1$ refers to the toe soil element. In CAPWAP toe damping can be specified either with the Case damping factor (**JT**) or with the Smith-viscous (**ST**) factor.

In CAPWAP shaft damping forces are calculated according to Eq. 2.16. However, for the pile toe, occasionally the original Smith calculation of Eq. 2.15 is better suited. The toe damping type option (**OP**) can be selected as either linearly viscous (**OP** = 0), Smith (1), or a combination (2) of viscous before and Smith after the ultimate toe resistance has been first fully activated. **OP** options 1 and 2 often improve results when the toe quake is relatively high and/or a toe gap is present.

Appendix C

C. Outputs of CAPWAP Analyses Using Different Damping Models

This appendix presents the CAPWAP analyses performed on 44 sets of field-measured dynamic data, using the linear viscous damping model being used in the industry and the proposed exponential damping model. The 44 sets of data or cases have been presented in the following order:

- ID1 to ID26 sourced from the database of Pile Dynamic Inc.
- ID27 to ID38 sourced from the collection of PDA-W example files provided by Pile Dynamic Inc.
- ID39 to ID 44 sourced from local foundation companies

ID 1
S17712D L310K300-320;siCL11;CL-TILL; H pile

Filename 1 def
Smith Linear Viscous Damping using Rult for Shaft

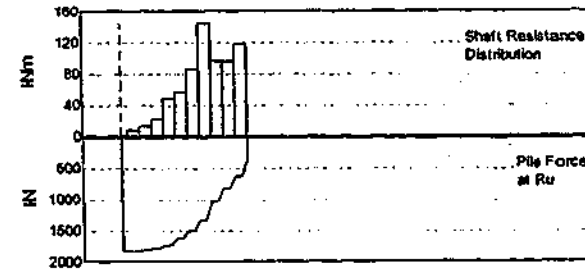
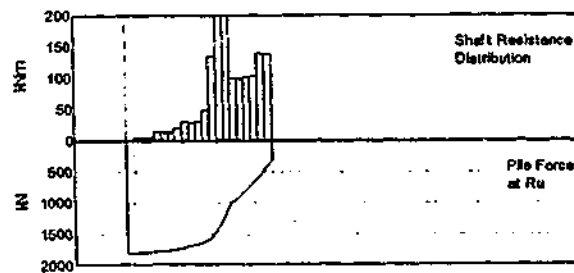
Depth	Area	E-Mod	Spec Wei	Cicum	Top Impedance
m	cm ²	MPa	kN/m ³	m	kN/m/s
0	80	206579	77.287	1.016	None
21.95	80	206579	77.287	1.016	5119.8 m/s

Depth	Ru	Unit	Total capacity
m	kN	kPa	kN
2.1	5.1	4.84	1815.4
3.1	5.1	4.84	1502
4.2	5.4	5.13	313.8
5.2	14.4	13.58	
6.3	14.3	13.49	
7.3	14.1	13.3	
8.4	21.8	20.52	
9.4	31.5	29.84	
10.5	30.6	28.78	
11.5	33.1	31.18	
12.5	51.1	48.16	
13.6	142.2	133.84	
14.6	208.9	196.73	
15.7	208.9	196.73	
16.7	104.4	98.32	
17.8	104.1	98.03	
18.8	107.8	101.55	
19.9	107.8	101.55	
20.9	145.6	137.17	
21.9	145.6	137.17	
Avg Skin	75.1	70.73	
Toe	313.4	4857.57	

Filename 1 rinst nm
Exponential Viscous Damping using Rinst for shaft

(A) Pile Model
As per Smith Linear Viscous Damping

Depth	Ru	Unit	Total capacity
Below Grade	Ru	(Area)	kN
3.1	18.8	8.86	1834.4
5.2	28.4	13.99	1450
7.3	47.6	22.42	384.5
9.4	102.7	48.35	
11.5	119.3	56.19	
13.6	180.1	84.83	
15.7	302.6	142.48	
17.8	201.7	95	
19.9	201.7	95	
21.9	247.1	116.37	
Avg Skin	145	68.29	
Toe	384.3	5957.7	



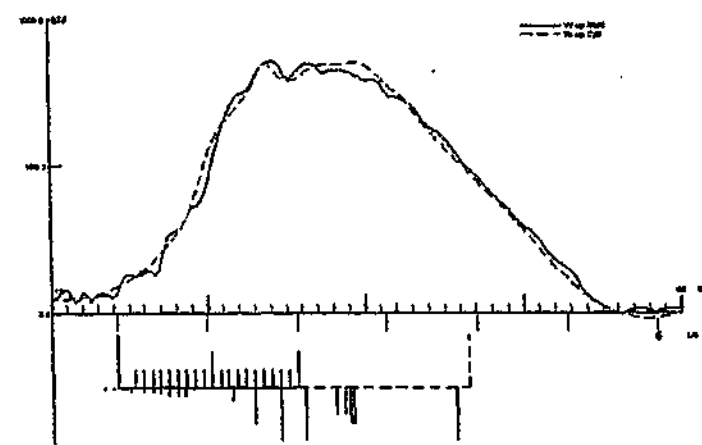
(C) CAPWAP Parameters

JS	SS	QS	UN	CS	LS	PI	OP
2.281	0.49	2.4	0	1	0	0.01	0
JT	ST	QT	TG	CT	LT	PL	
0.651	0.678	4.8	0	1	0	2.8	

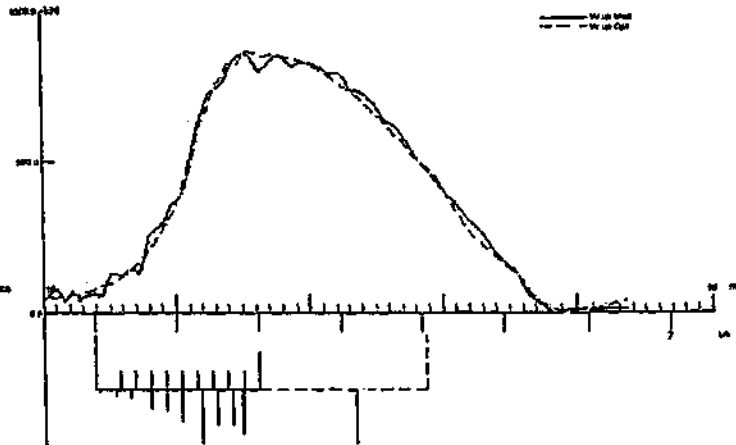
(C) CAPWAP Parameters

JS	SS	QS	UN	CS	LS	PI	OP
2.138	0.48	2	0.025	1	0	0.01	0
JT	ST	QT	TG	CT	LT	PL	
0.413	0.35	1	3.5	1	0	0	

(D) Match
CAPWAP match quality: 2.26 (Wave Up Match)
Observed: final set = 1.693 mm; blow count = 591 b/m
Computed: final set = 0.830 mm; blow count = 1204 b/m



(D) Match
CAPWAP match quality: 1.94 (Wave Up Match)
Observed: final set = 1.693 mm; blow count = 591 b/m
Computed: final set = 0.914 mm; blow count = 1094 b/m



(A) Soil Data
Depth (m) Soil description
0.0 Tan silty CLAY
Silt: 75%; Clay: 24%; LL=34%; PI=13%

7.6 Silt: 73%; % Clay: 25%; LL=33%; PI=17%

12.3 Grey tan silty CLAY

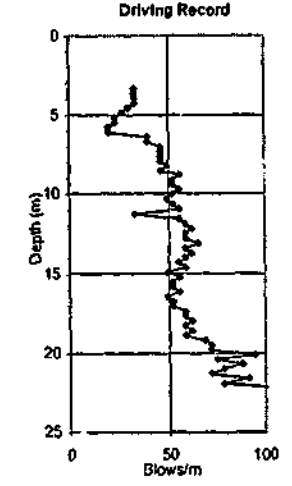
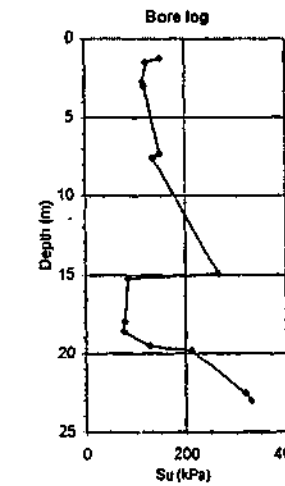
18.0 Silt: 47%; Clay: 25%; LL=32%; PI=16%

18.6 GLACIAL TILL: CLAY, stiff, contains

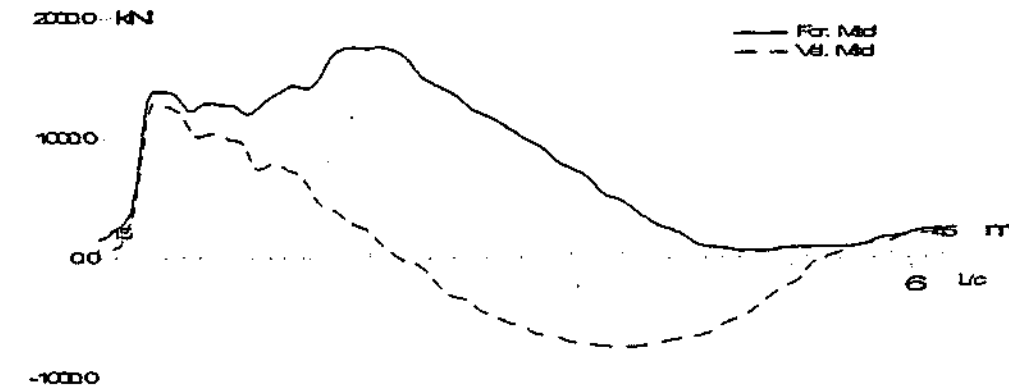
sand/gravel grains, pebbles/stones

21.5 Hard Layer

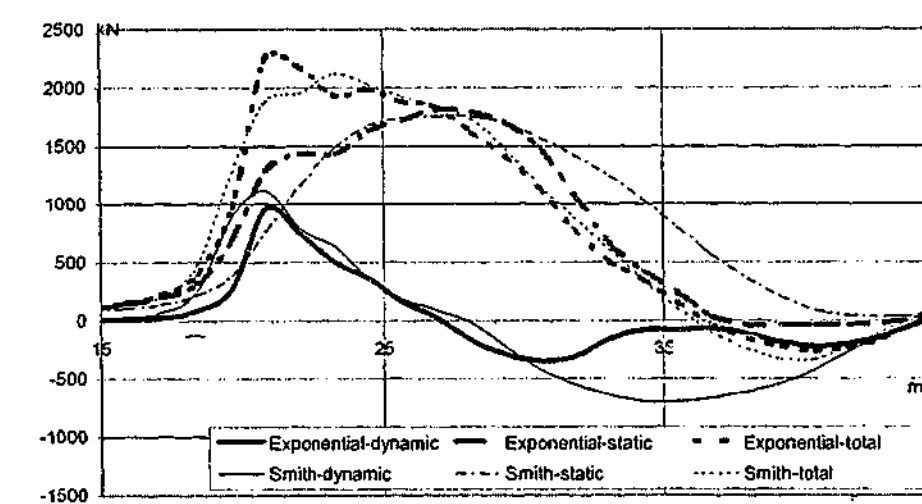
22.6 Silt: 45%; Clay: 31%; LL=36%; PI=22%



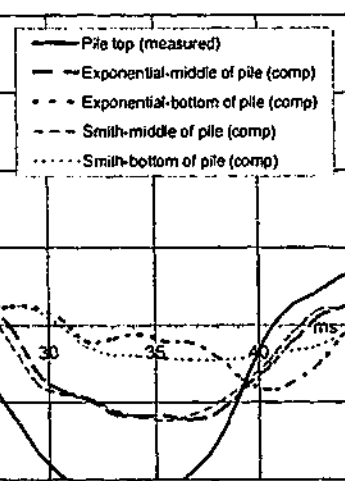
(B) Measured Force & Velocity at Pile Top



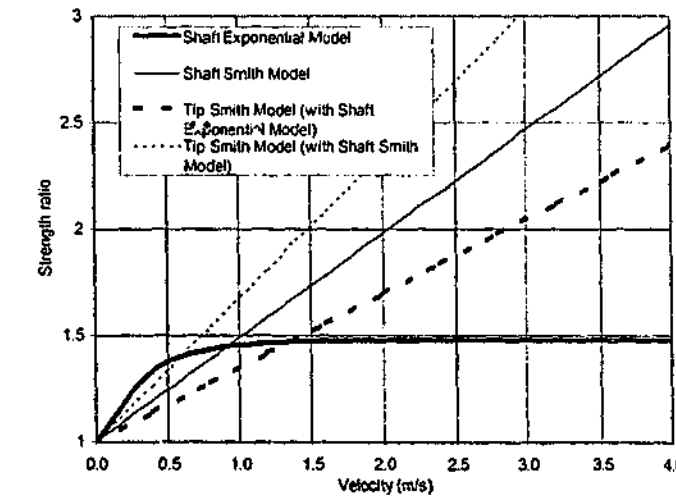
(C) Computed Resistances



(D) Velocities at Top, Middle & Bottom of Pile



(E) Strength Ratio-Velocity Models for Shaft & Tip



ID2
 S1810D L380K/380-380; sICL10; CL-TILL; 305mm PSC

Filename 2 def
 Smith Linear Viscous Damping using Rult for Shaft

(A) Pile Model

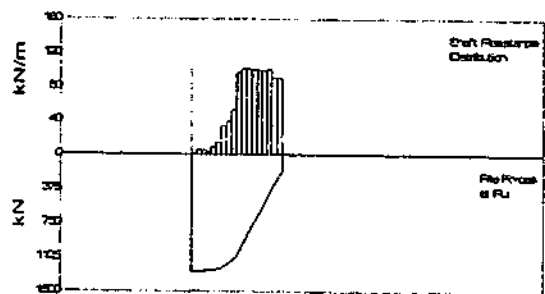
Depth (m)	Area (cm ²)	E-Mod (MPa)	Spec Wei (kN/m ³)	Circum (m)	Impedance (kN/m/s)
0	929.03	37590.2	23.563	1.218	882.82
18.9	929.03	37590.2	23.563	1.218	None

Wave Speed 3955.3 m/s

(B) Resistance Distribution

Depth (m)	Ru (kN)	Unit (kPa)	Total capacity (kN)	Shaft capacity (kN)	Toe capacity (kN)
1	1.3	1.02	1263.1	1090.8	192.4
2.1	5.3	4.15			
3.1	5.2	4.07			
4.2	3	2.35			
5.2	9.8	7.52			
6.3	14.8	11.59			
7.3	35.1	27.41			
8.4	40	31.25			
9.4	54.7	42.78			
10.5	101	78.95			
11.5	106.1	82.88			
12.6	106	82.79			
13.6	105.4	82.32			
14.7	104.7	81.85			
15.7	103.9	81.22			
16.8	104.9	82			
17.8	94.8	74.09			
18.9	94.8	74.09			

Avg Skin 60.6 47.35
 Toe 192.4 2070.51



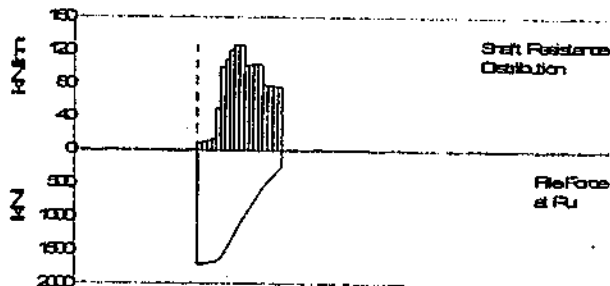
Filename 2 rinst nm
 Exponential Viscous Damping using Rinst for shaft

(A) Pile Model
 As per Smith Linear Viscous Damping

(B) Resistance Distribution

Depth (m)	Ru (kN)	Unit (kPa)	Total capacity (kN)	Shaft capacity (kN)	Toe capacity (kN)
1	10.2	7.98	1704.3	1477.3	227.2
2.1	10.4	8.14			
3.1	12.2	9.55			
4.2	15.1	11.82			
5.2	52.5	41.02			
6.3	105.1	82.11			
7.3	115.4	90.17			
8.4	127.3	99.49			
9.4	133.4	104.26			
10.5	133.4	104.26			
11.5	108.6	84.85			
12.6	108.9	85.09			
13.6	108.7	84.93			
14.7	108.7	84.93			
15.7	82.7	64.68			
16.8	82.1	64.19			
17.8	81.5	63.72			
18.9	80.8	63.17			

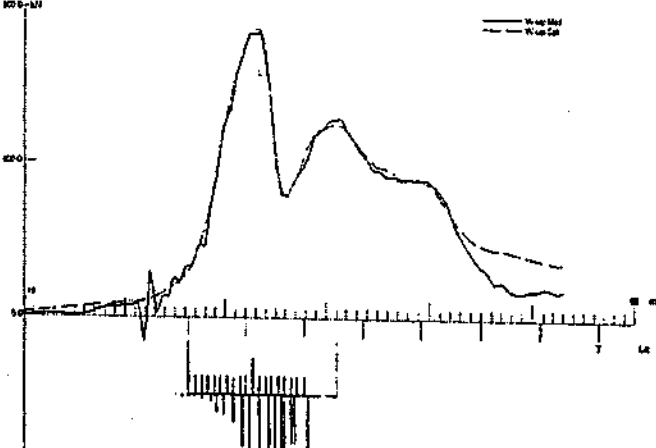
Avg Skin 82.1 64.13
 Toe 227 2443.47



(C) CAPWAP Parameters

JS	SS	QS	UN	CS	LS	PI	OP
1.202	0.975	4.9	0	1	0	0.02	0
JT	ST	QT	TG	CT	LT	PL	
0.167	0.77	6	0	1	0	1.7	

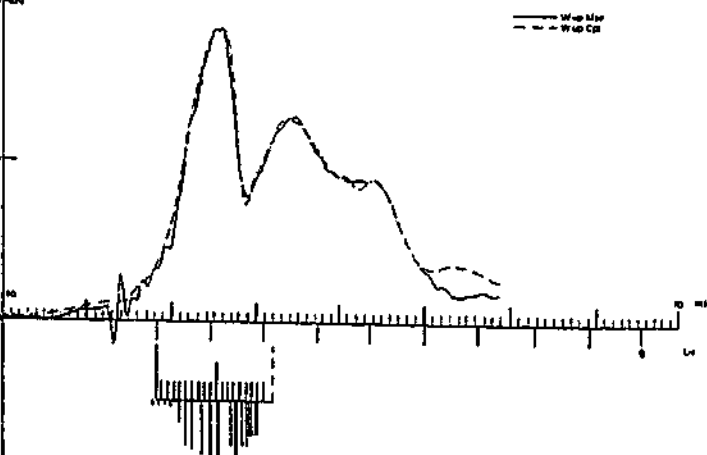
(D) Match
 CAPWAP match quality: 2.57 (Wave Up Match)
 Observed: final set = 5.623 mm; blow count = 197 b/m
 Computed: final set = 3.683 mm; blow count = 272 b/m



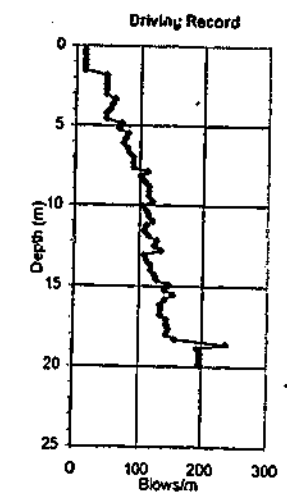
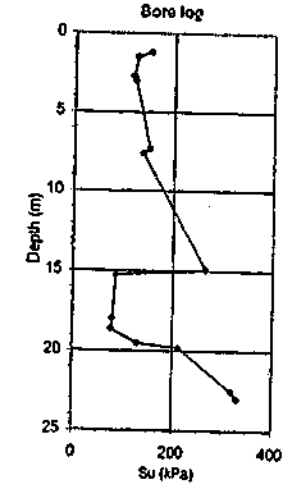
(C) CAPWAP Parameters

JS	SS	QS	UN	CS	LS	PI	OP
1.286	0.77	6.65	0	0.73	0	0.02	1
JT	ST	QT	TG	CT	LT	PL	
0.27	1.05	2.5	0	1	0	3.6	

(D) Match
 CAPWAP match quality: 1.82 (Wave Up Match)
 Observed: final set = 5.080 mm; blow count = 197 b/m
 Computed: final set = 4.080 mm; blow count = 245 b/m



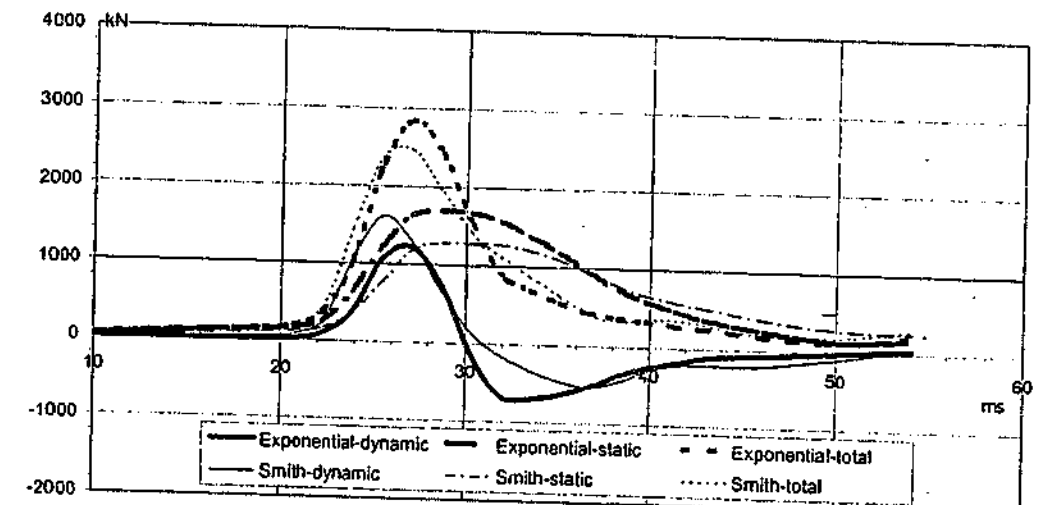
(A) Soil Data
 Depth (m) Soil description
 0.0 Tan silty CLAY
 Silt: 75%; Clay: 24%; LL=34%; PI=13%
 7.6 Silt: 73%; Clay: 25%; LL=36%; PI=17%
 12.3 Grey tan silty CLAY
 18.0 Silt: 47%; Clay: 25%; LL=32%; PI=16%
 18.6 GLACIAL TILL: CLAY, silt, contains sand/gravel grains, pebbles/stones
 21.5 Hard Layer
 22.6 Silt: 45%; Clay: 31%; LL=38%; PI=22%



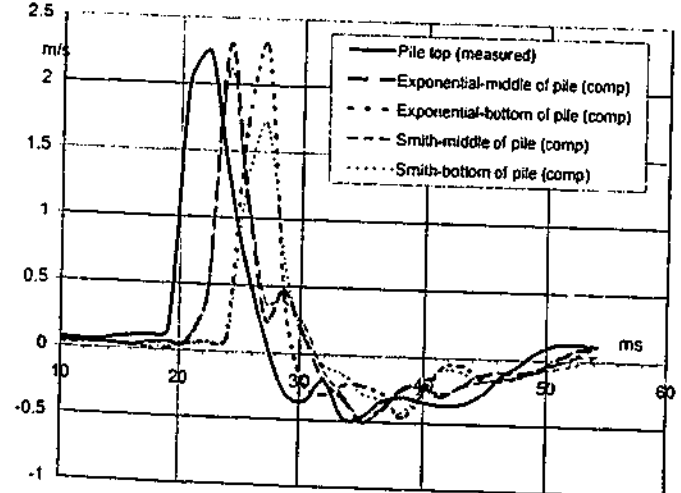
(B) Measured Force & Velocity at Pile Top



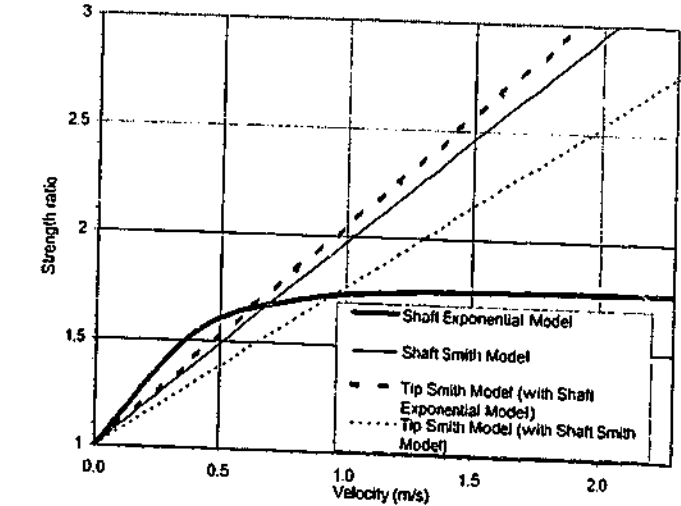
(C) Computed Resistances



(D) Velocities at Top, Middle & Bottom of Pile



(E) Strength Ratio-Velocity Models for Shaft & Tip



ID3
S17/12D L310K/300-320;eICL11;CL-TILL; H pile

Filename 3 def
Smith Linear Viscous Damping using Rull for Shaft

(A) Pile Model

Depth (m)	Area (cm ²)	E-Mod (MPa)	Spec Wel (kN/m ³)	Circum (m)	Top Impedance (499.81 kN/m/s)	Added Impedance (None)	Wave Speed (5119.6 m/s)
0	123.87	206579.3	77.287	1.018			
20.12	123.87	206579.3	77.287	1.018			

(B) Resistance Distribution

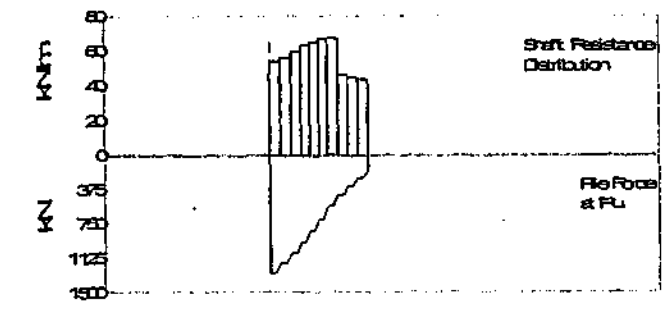
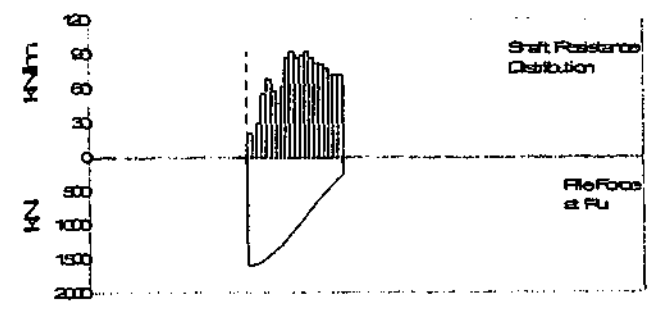
Depth (m)	Ru (kN)	Unit (kPa)	Total capacity (kN)
1	21.7	21.19	1622.6
2	19.6	18.11	1372.1
3	30.5	29.8	250.4
4	56.5	55.15	
5	69.5	67.92	
6	58.7	57.33	
7	47.9	46.73	
8	63.1	61.58	
9.1	68.1	66.04	
10.1	93.8	91.39	
11.1	88.1	86.04	
12.1	90.2	88.12	
13.1	93.6	91.39	
14.1	88.1	86.04	
15.1	82.8	80.69	
16.1	82.8	80.69	
17.1	78.4	77.53	
18.1	72.8	71.09	
19.1	72.8	71.09	
20.1	72.8	71.09	
Avg skin	66.6	67	
Toe	250.4	3028.65	

Filename 3 rull am
Exponential Viscous Damping using Rull for shaft

(A) Pile Model
As per Smith Linear Viscous Damping

(B) Resistance Distribution

Depth (m)	Ru (kN)	Unit (kPa)	Total capacity (kN)
2	108.2	53.3	1302.5
4	113.7	55.54	1149.9
6	121	58.06	152.6
8	128.3	62.84	
10.1	131.5	64.23	
12.1	136.1	66.46	
14.1	136.1	66.46	
16.1	93.7	45.75	
18.1	91	44.46	
20.1	89.2	43.56	
Avg skin	115	56.15	
Toe	152.6	1845.54	



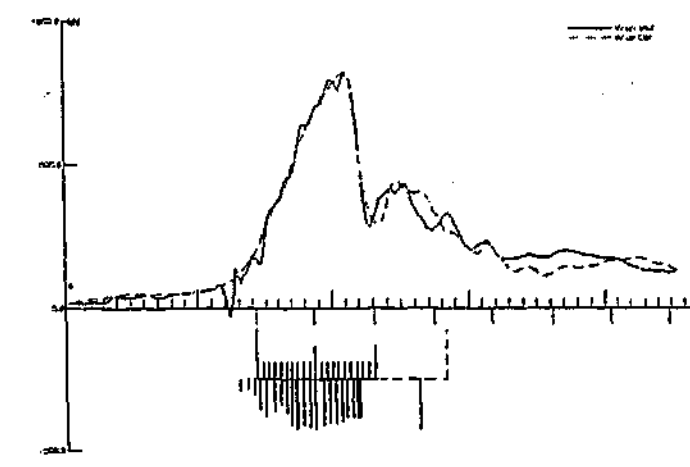
(C) CAPWAP Parameters

JS	SS	QS	UN	CS	LS	PI	OP
0.813	0.3	1.2	0	1	0	0.01	2
JT	ST	QT	TG	CT	LT	PL	
0.074	0.15	9.1	0	1	0	1.797	

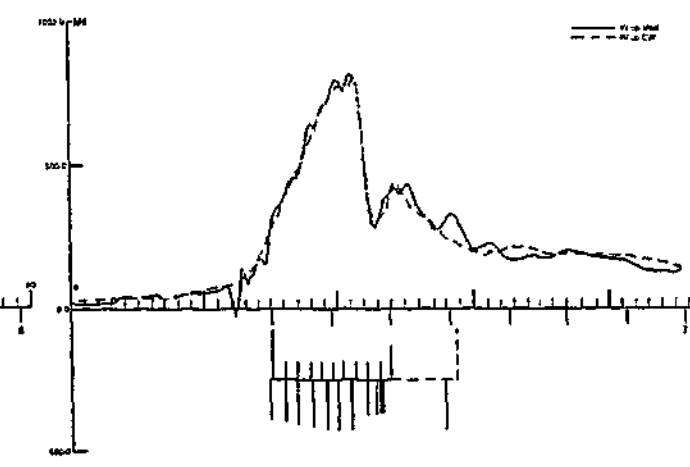
(C) CAPWAP Parameters

JS	SS	QS	UN	CS	LS	PI	OP
1.81	0.8	5.5	1	1	0	0.01	0
JT	ST	QT	TG	CT	LT	PL	
0.24	0.2	9.9	0	1	0	1.373	

(D) Match
CAPWAP match quality: 5.07 (Wave Up Match)
Observed: final set = 5.080 mm; blow count = 197 b/m
Computed: final set = 8.198 mm; blow count = 122 b/m



(D) Match
CAPWAP match quality: 3.98 (Wave Up Match)
Observed: final set = 5.060 mm; blow count = 197 b/m
Computed: final set = 7.824 mm; blow count = 128 b/m

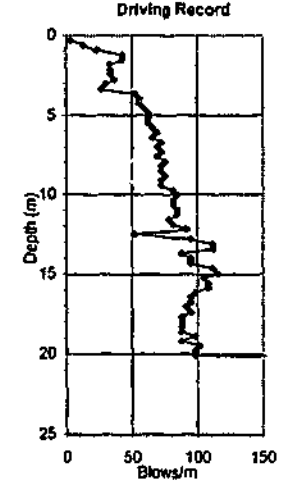
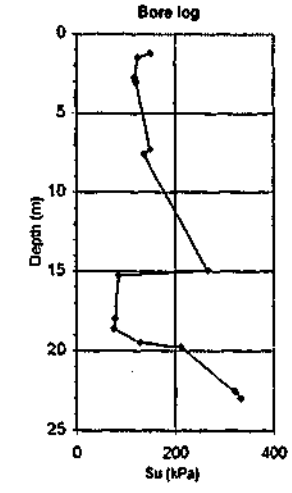


(A) Soil Data
Depth (m) Soil description:
0.0 Tan silty CLAY
Silt: 75%; Clay: 24%; LL=34%; PI=13%

7.6 Silt: 73%; % Clay: 25%; LL=36%; PI=17%

12.3 Grey tan silty CLAY

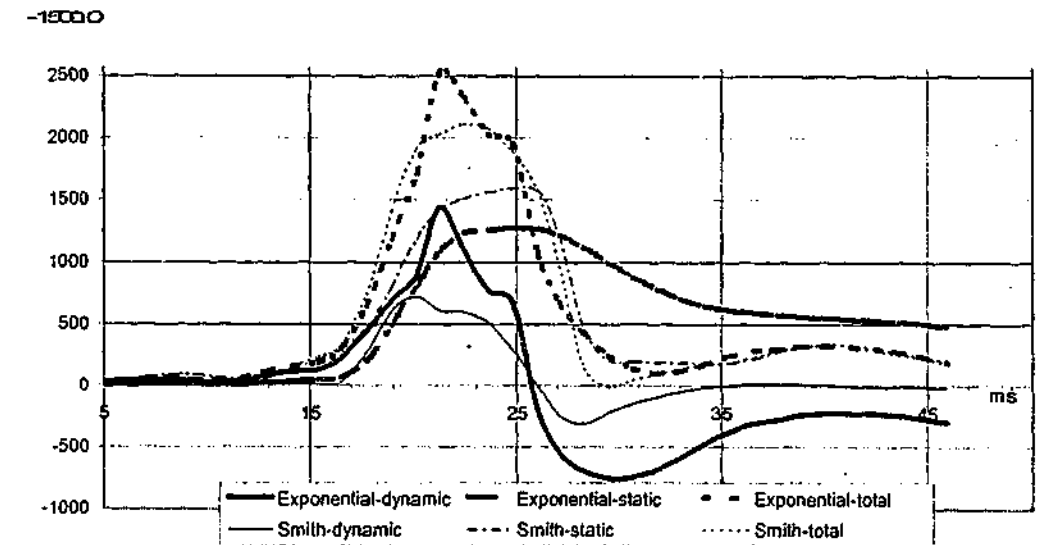
18.0 Silt: 47%; Clay: 25%; LL=32%; PI=16%
18.6 GLACIAL TILL: CLAY, stiff, contains sand/gravel grains, pebbles/stones
21.5 Hard Layer
22.6 Silt: 45%; Clay: 31%; LL=38%; PI=22%



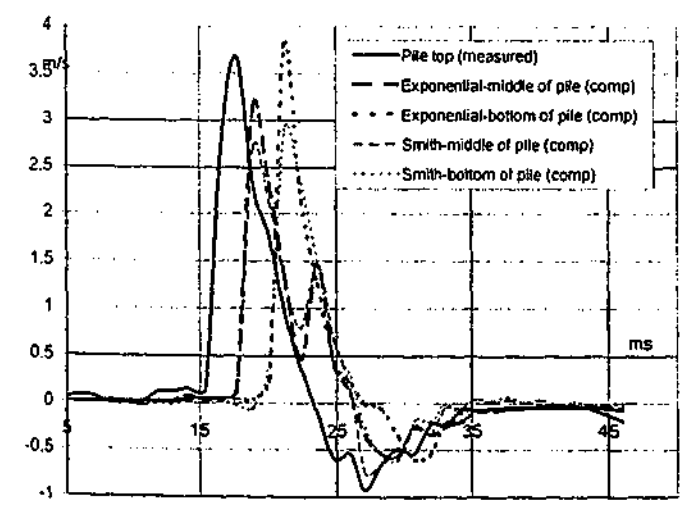
(B) Measured Force & Velocity at Pile Top



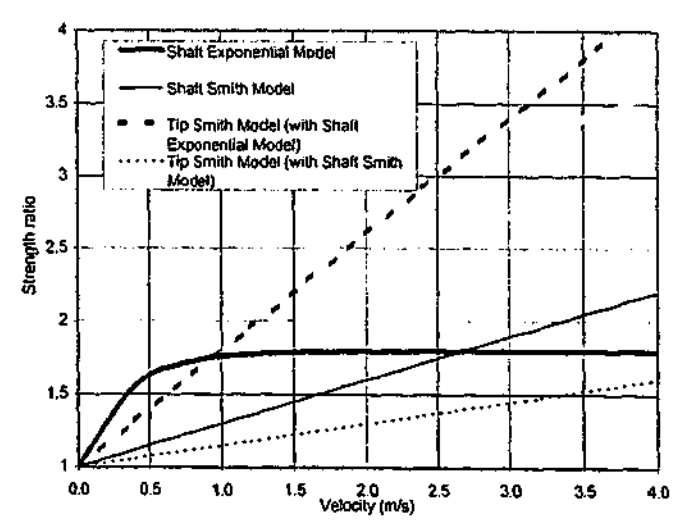
(C) Computed Resistances



(D) Velocities at Top, Middle & Bottom of Pile



(E) Strength Ratio-Velocity Models for Shaft & Tip



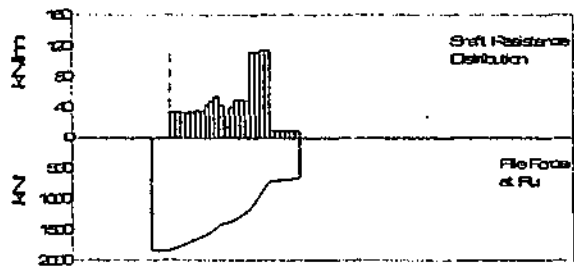
Filename 4 def
Smith Linear Viscous Damping using Rint for Shaft

(A) Pile Model

Depth	Area	E-Mod	Spec Wet	Circum	Impedance
m	cm ²	MPa	kN/m ³	m	
0-29.26	2987.09	41273.5	23.583	2.438	0-1.02 2974.87kN/m ²
29.26-30.4	3716.12	41273.5	23.583	2.438	1.02-29.46 3120.44kN/m ²
					29.46-30.4 3700.67kN/m ²
					Wave Speed 4144.6 m/s

(B) Resistance Distribution

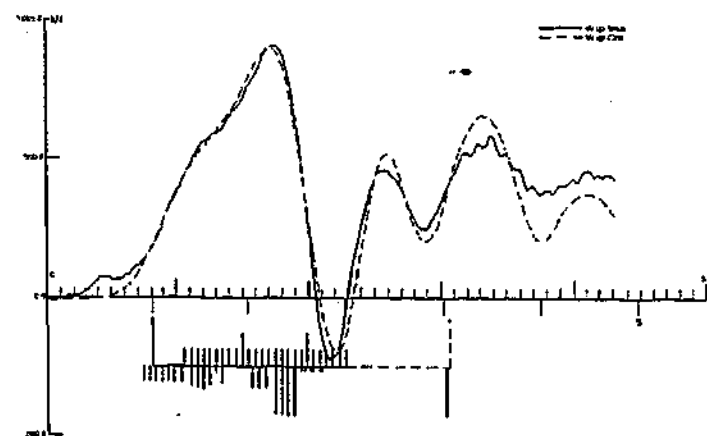
Depth	Ru	Unit	Total capacity	1808.7	kN
Below	Ru		Shaft capacity	1168.7	kN
Grade	(Area)		Toe capacity	640	kN
m	kN	kPa			
0.4	34.2	13.8			
1.4	34.2	13.8			
2.4	34.2	13.8			
3.4	34.2	13.8			
4.4	34.2	13.8			
5.4	36.8	14.84			
6.5	36.8	14.84			
7.5	45.5	18.38			
8.5	50.1	20.24			
9.5	55.1	22.25			
10.5	44.4	17.92			
11.5	14.3	5.76			
12.5	41.3	16.68			
13.6	50.7	20.48			
14.6	50.7	20.48			
15.6	50.1	20.24			
16.6	114.3	46.13			
17.6	114.3	46.13			
18.6	116	46.05			
19.7	116	46.05			
20.7	10.2	4.12			
21.7	10.2	4.12			
22.7	10.2	4.12			
23.7	10.2	4.12			
24.7	10.2	4.12			
25.8	10.2	4.12			
Avg Skin	45	18.15			
Toe	640	1722.25			



(C) CAPWAP Parameters

JS	SS	QS	UN	CS	LS	PI	OP
0.718	1.811	1	0	1	0	0.02	0
JT	ST	QT	TG	CT	LT	PL	
0.212	0.975	1.8	5	3.8	0	6	

(D) Match
CAPWAP match quality: 3.30 (Wave Up Match)
Observed: final set = 2.309 mm; blow count = 433 b/m
Computed: final set = 3.819 mm; blow count = 262 b/m

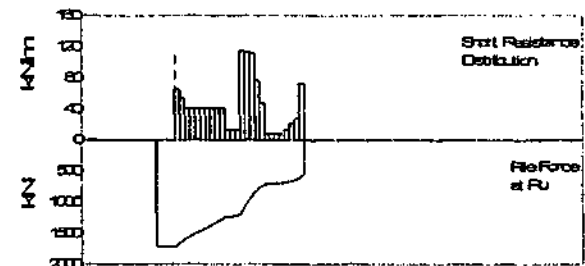


Filename 4 rin1
Exponential Viscous Damping using Rint for shaft

(A) Pile Model
As per Smith Linear Viscous Damping

(B) Resistance Distribution

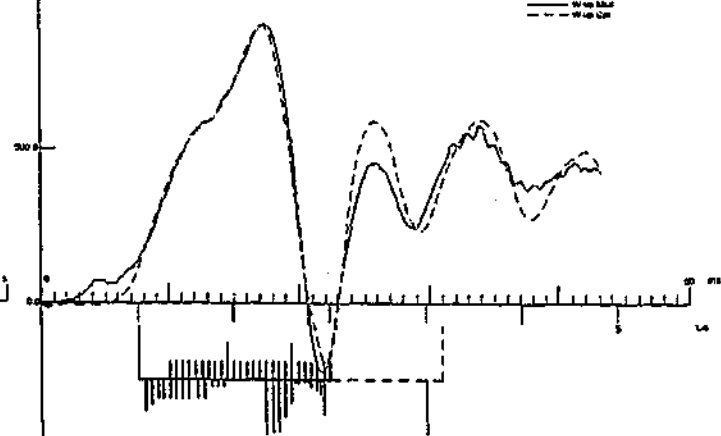
Depth	Ru	Unit	Total capacity	1687.3	kN
Below	Ru		Shaft capacity	1160.2	kN
Grade	(Area)		Toe capacity	527.3	kN
m	kN	kPa			
0.4	67.3	27.19			
1.4	56	22.59			
2.4	42.4	17.11			
3.4	42.8	17.27			
4.4	42.8	17.27			
5.4	42.7	17.23			
6.5	42.7	17.23			
7.5	42.7	17.23			
8.5	42.7	17.23			
9.5	42.7	17.23			
10.5	14.8	5.96			
11.5	15.1	6.08			
12.5	15.1	6.08			
13.6	117.6	47.48			
14.6	115.8	46.66			
15.6	113.8	45.94			
16.6	79.2	31.99			
17.6	49.5	19.99			
18.6	8.4	3.4			
19.7	8.4	3.4			
20.7	8.4	3.4			
21.7	8.4	3.4			
22.7	14.5	5.84			
23.7	23.1	9.32			
24.7	29.1	11.76			
25.8	74.7	30.15			
Avg Skin	44.8	18.02			
Toe	527.1	1418.38			



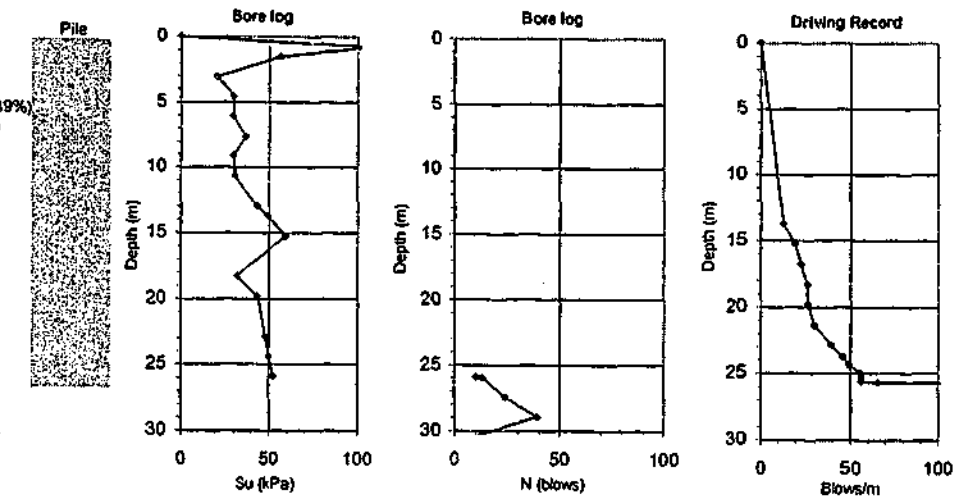
(C) CAPWAP Parameters

JS	SS	QS	UN	CS	LS	PI	OP
0.85	1.85	1.85	0	1	0	0.02	0
JT	ST	QT	TG	CT	LT	PL	
0.211	1.18	3.4	3	1	0	10	

(D) Match
CAPWAP match quality: 2.73 (Wave Up Match)
Observed: final set = 2.309 mm; blow count = 433 b/m
Computed: final set = 1.604 mm; blow count = 285 b/m

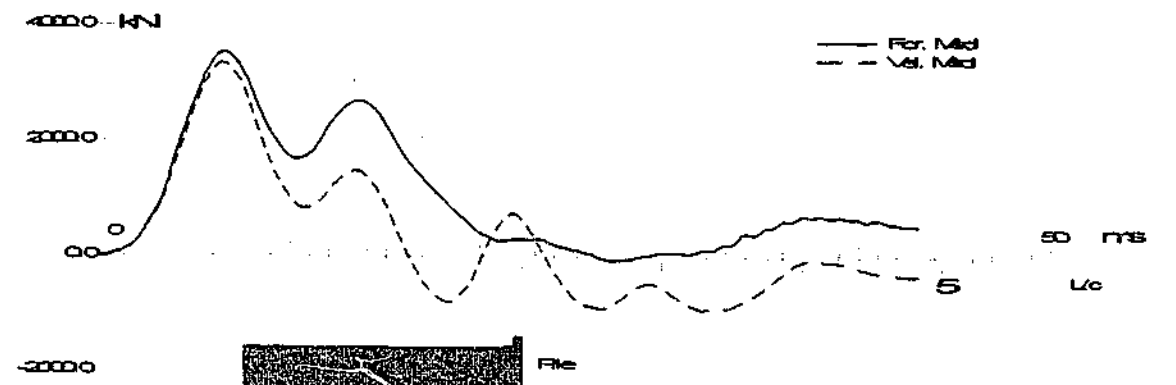


(A) Soil Data
Depth (m) Soil description
0.782 Brown silty CLAY w/ trace gravel (mc=25%)
1.524 Gray silty CLAY w/ lenses silt
3.048 Organic silty clay w/ trace rotting wood (mc=35%)
4.572 Gray silty CLAY w/ trace rotting wood, organic (mc=49%)
6.096 Gray CLAY w/ trace rotting wood, organic (mc=56%)

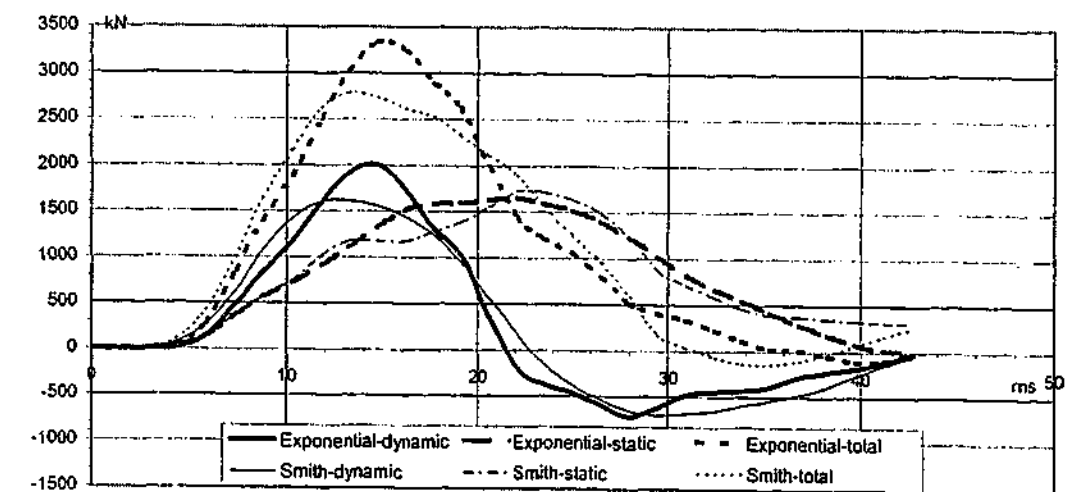


12.192 Gray clay with rotting wood (mc=86%)
12.654 Gray clay (mc=40%)
13.716 Gray silty clay w/ trace rotting wood (mc=37%)
15.24 Gray clay w/ trace rotting wood (mc=48%)
18.288 Gray CLAY w/ trace shell (mc=49%)
19.812 Gray CLAY (mc=54%)
22.86 Gray CLAY w/ trace shell (mc=42%)
24.384 (mc=47%)
25.908 Gray silty CLAY w/ trace organics (mc=25%)
27.432 Gray fine silty SAND
28.956 Gray fine SAND

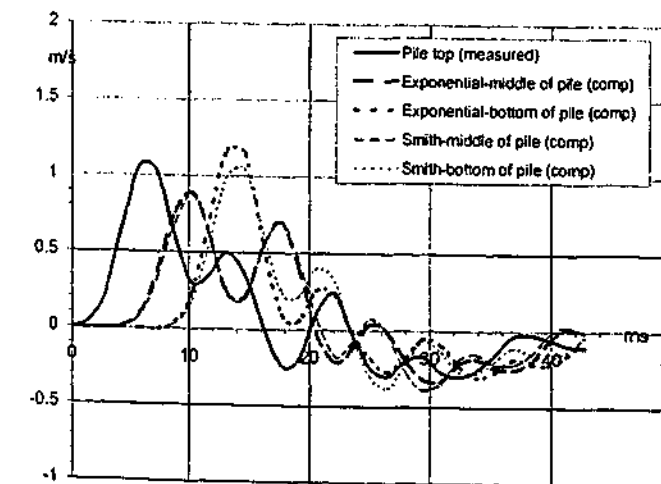
(B) Measured Force & Velocity at Pile Top



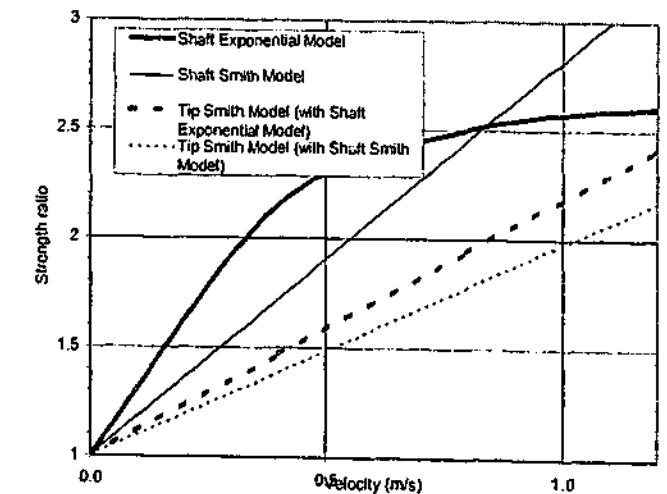
(C) Computed Resistances



(D) Velocities at Top, Middle & Bottom of Pile



(E) Strength Ratio-Velocity Models for Shaft & Tip



ID5
S44 CEP L162180MX;ciCL&ciST; ci-SI42

Filename 5 def
Smith Linear Viscous Damping using Rult for Shaft

(A) Pile Model

Depth	Area	E-Mod	Spec Wei	Circum	Impedance
m	cm ²	MPa	kN/m ³	m	kN/m/s
0	44.97	206579	77.287	0.957	181.45
12.34	44.97	206579	77.287	0.957	None

Wave Speed 5119.8 m/s

(B) Resistance Distribution

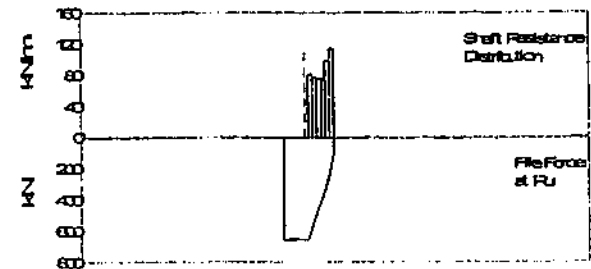
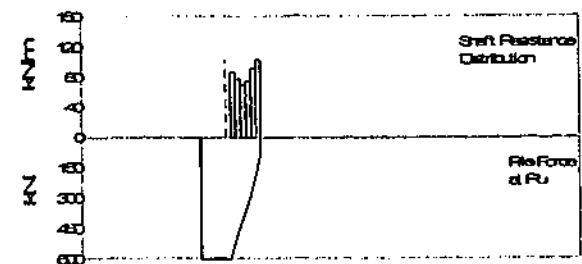
Depth	Ru	Unit	Total capacity	599	kN
Below Grade	Ru (Area)		Shaft capacity	519.4	kN
m	kN	kPa	Toe capacity	79.8	kN
1.9	86.2	90.58			
2.9	80.4	81.65			
3.9	72.3	73.43			
5	77.1	78.3			
6	94.1	95.55			
7	106.4	108.12			
Avg Skin	86.8	87.84			
Toe	79.8	1098.19			

Filename 5 nm rinst
Exponential Viscous Damping using Rinst for shaft

(A) Pile Model
As per Smith Linear Viscous Damping

(B) Resistance Distribution

Depth	Ru	Unit	Total capacity	649	kN
Below Grade	Ru (Area)		Shaft capacity	542.3	kN
m	kN	kPa	Toe capacity	106.7	kN
1.9	84.1	85.41			
2.9	80.2	81.46			
3.9	78.4	79.83			
5	78.4	79.83			
6	102.8	104.38			
7	118.5	120.41			
Avg Skin	90.4	91.82			
Toe	106.7	1471.78			



(C) CAPWAP Parameters

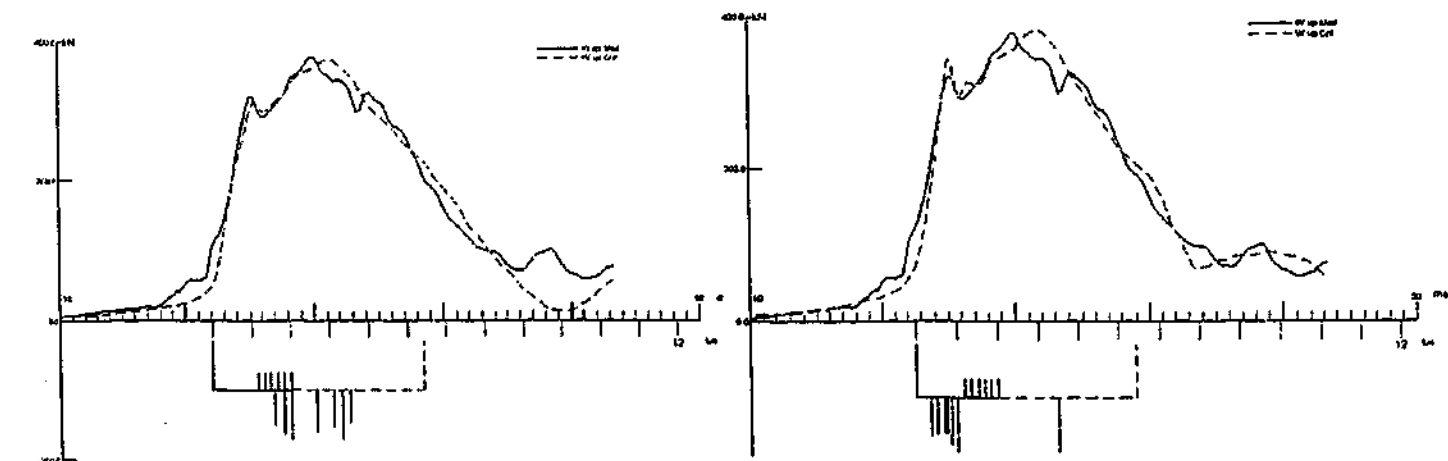
JS	SS	QS	UN	CS	LS	PI	OP
1.778	0.62	10.5	0	1	0	0.01	0
JT	ST	QT	TG	CT	LT	PL	
0.483	1.1	4	4	2	0	0.55	

(C) CAPWAP Parameters

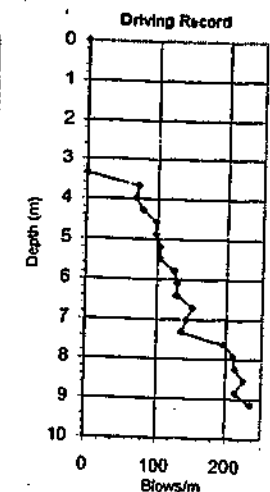
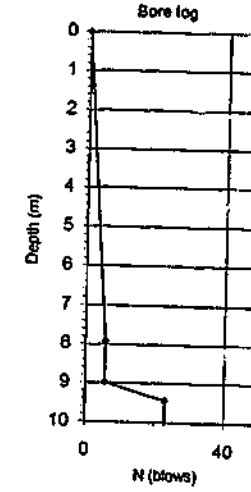
JS	SS	QS	UN	CS	LS	PI	OP
1.880	0.63	2.3	0	1	0	0.01	1
JT	ST	QT	TG	CT	LT	PL	
0.059	0.1	4.5	4	4	0	0.24	

(D) Match
CAPWAP match quality: 4.73 (Wave Up Match)
Observed: final set = 5.080 mm; blow count = 197 b/m
Computed: final set = 6.122 mm; blow count = 163 b/m

(D) Match
CAPWAP match quality: 3.61 (Wave Up Match)
Observed: final set = 5.080 mm; blow count = 197 b/m
Computed: final set = 4.333 mm; blow count = 231 b/m



(A) Soil Data
Depth Description
0 Gray and brown silty CLAY, very moist-soft



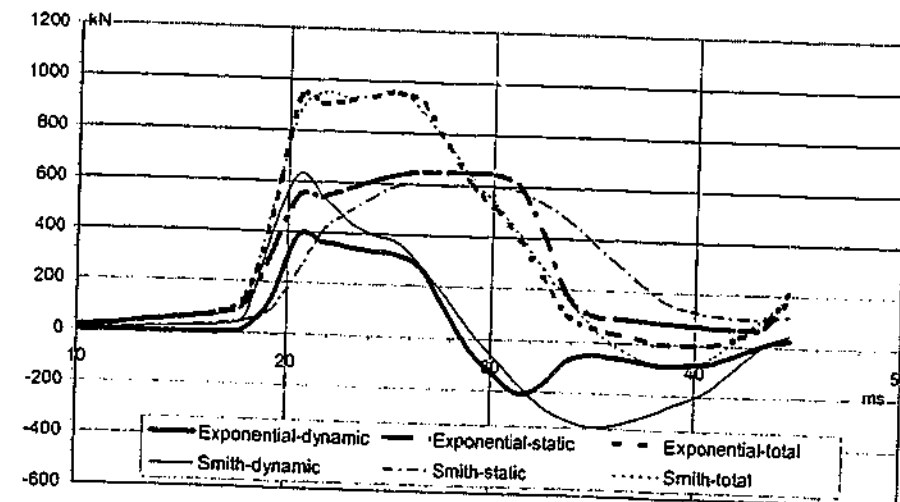
8.9916 Grey and brown silty clayey SAND, gravel/rock fragments, w/organic, 9.4468 wet, medium density (FILL)

10.5156 Gray sandy silty CLAY, trace of rock fragments and fine gravel, very moist- medium stiff

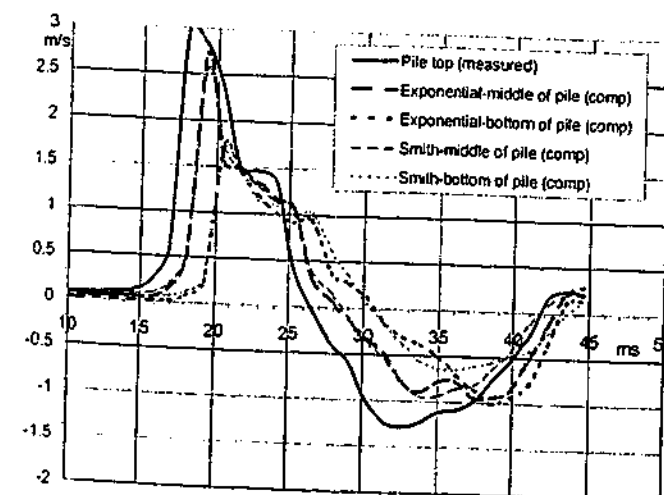
(B) Measured Force & Velocity at Pile Top



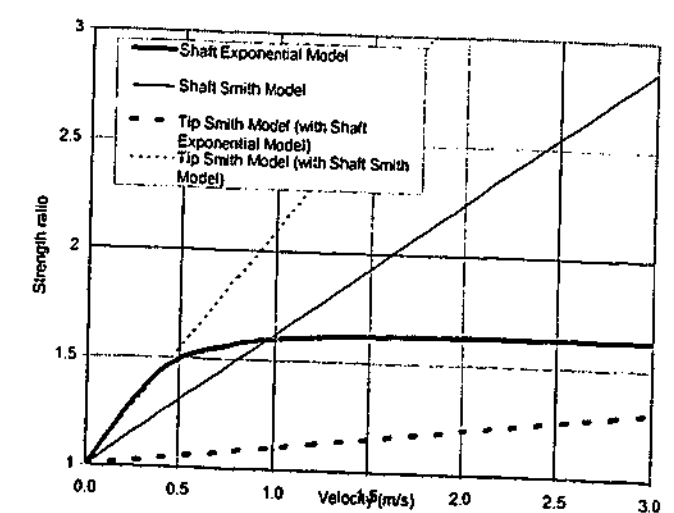
(C) Computed Resistances



(D) Velocities at Top, Middle & Bottom of Pile



(E) Strength Ratio-Velocity Models for Shaft & Tip



ID6
S69/15D 16PSC 13dL590;SISA;siCL:siCL:

Filename 6 def
Smith Linear Viscous Damping using Rult for Shaft

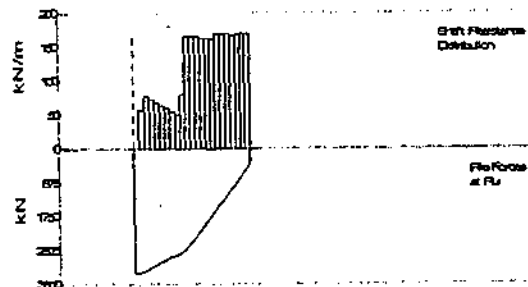
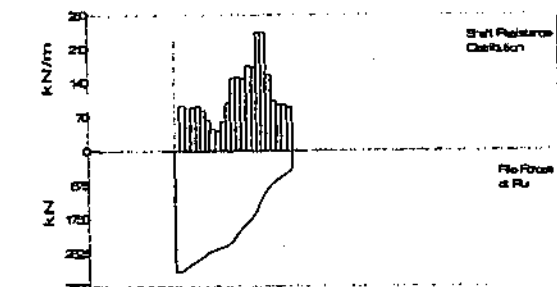
Depth m	Area cm ²	E-Mod MPa	Spec Weir kN/m ³	Circum m	Impedance 1434.85 kN/m/s
0	1567.74	34868.9	23.563	1.625	Added impedance None Wave Speed 3809.4 m/s
23.62	1567.74	34868.9	23.563	1.625	

Depth Below Grade m	Ru kN	Unit kPa	Total capacity kN
2.1	57.8	34.63	3200.2
3.1	79.3	47.52	2816.7
4.1	74.7	44.76	361.5
5.1	70.1	42	
6.2	65.2	39.07	
7.2	60.6	36.31	
8.2	55.8	33.43	
9.2	51.1	30.62	
10.3	46.4	27.81	
11.3	41.7	25.00	
12.3	37.0	22.19	
13.4	32.3	19.38	
14.4	27.6	16.57	
15.4	22.9	13.76	
16.4	18.2	10.95	
17.5	13.5	8.14	
18.5	8.8	5.33	
19.5	4.1	2.52	
20.5	-0.6	-0.29	
21.6	-1.3	-0.58	
22.6	-2.0	-0.87	
23.6	-2.7	-1.16	
Avg Skin	128.1	76.77	
Toe	381.5	2309.97	

Filename 6 final nm
Exponential Viscous Damping using Rinst for shaft

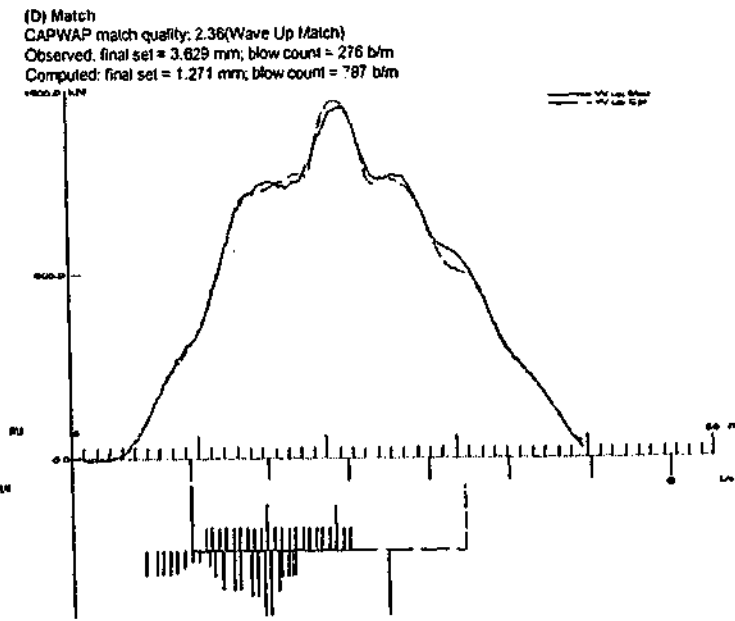
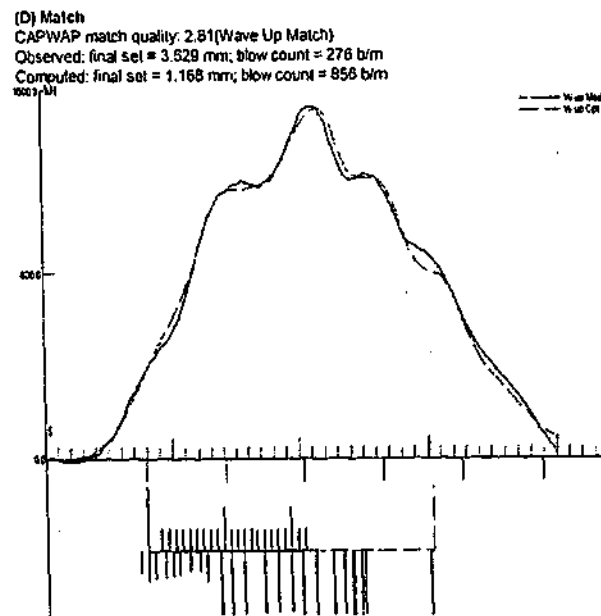
(A) Pile Model
As per Smith Linear Viscous Damping

Depth Below Grade m	Ru kN	Unit kPa	Total capacity kN
2.1	94.7	56.74	3099.6
3.1	89.9	53.87	2645.5
4.1	82.2	55.24	454.3
5.1	94.9	56.86	
6.2	88.1	51.59	
7.2	65.4	38.19	
8.2	48.2	27.68	
9.2	42.5	25.47	
10.3	37.0	22.19	
11.3	31.5	18.91	
12.3	26.0	15.63	
13.4	20.5	12.35	
14.4	15.0	9.07	
15.4	9.5	5.79	
16.4	4.0	2.50	
17.5	-1.5	-0.91	
18.5	-4.0	-2.50	
19.5	-6.5	-4.09	
20.5	-9.0	-5.68	
21.6	-11.5	-7.27	
22.6	-14.0	-8.86	
23.6	-16.5	-10.45	
Avg Skin	120.3	72.05	
Toe	454.3	2750.77	



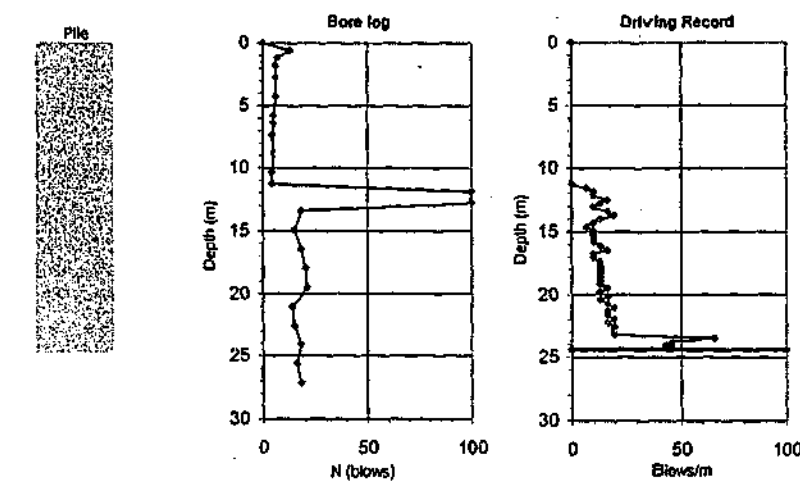
JS	SS	QS	UN	CS	LS	PI	OP
1.532	0.78	3.7	0	1	0	0.02	0
JT	ST	QT	TG	CT	LT	PL	
0.090	0.35	2.1	2.3	1	0	0	

JS	SS	QS	UN	CS	LS	PI	OP
0.83	0.45	1.8	0.033	1	0	0.02	2
JT	ST	QT	TG	CT	LT	PL	
0.412	1.3	1	2.6		0	0	



(A) Soil Data

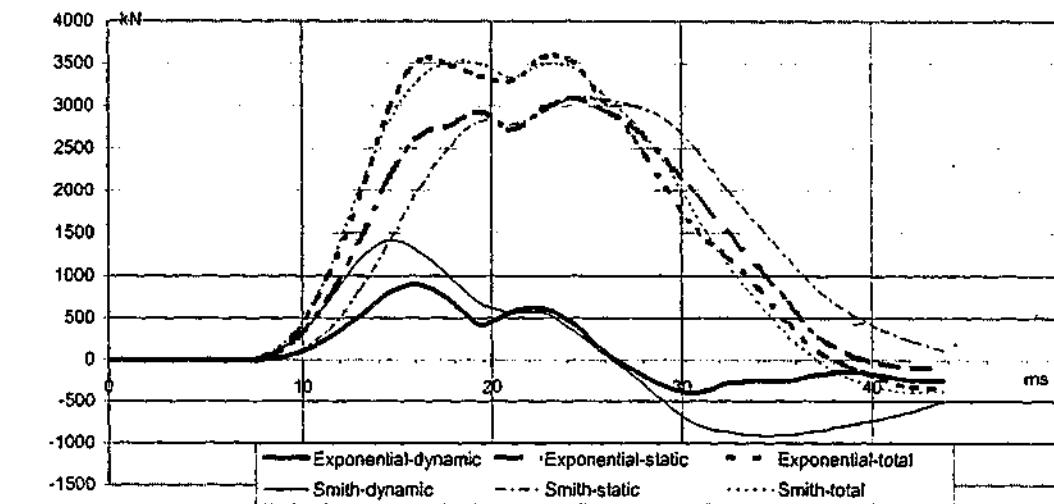
Depth	Soil description
0.0	FILL: medium dense-loose tan grey slightly silty fine SAND
6.4	Soft to firm dark black grey organic silty CLAY w/marsh roots
11.3	Very dense dark grey medium to coarse SAND
12.6	Very stiff to stiff olive green silty CLAY (Marl)



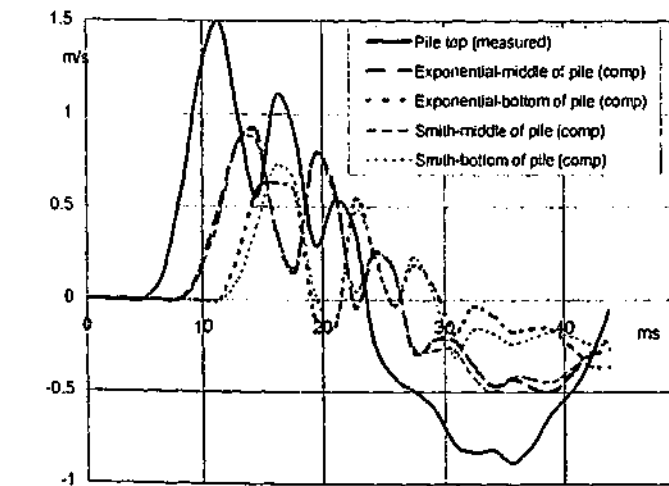
(B) Measured Force & Velocity at Pile Top



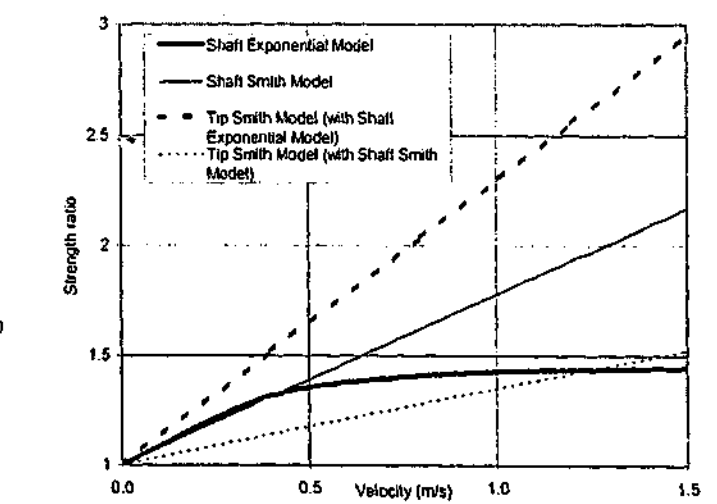
(C) Computed Resistances



(D) Velocities at Top, Middle & Bottom of Pile



(E) Strength Ratio-Velocity Models for Shaft & Tip



ID7
S7110D H/ch 9dL320/345MX;fSA&CL;fSA;cCL; Blow: 539

Filename 7 def
Smith Linear Viscous Damping using Rnt for Shaft

(A) Pile Model

Depth	Area	E-Mod	Spec Wei	Circum	Impedance
m	cm ²	MPa	kN/m ³	m	kN/m/s
0	157.42	206825	77.287	1.422	365.4
24.32	157.42	206825	77.287	1.422	1200

Added impedance 1200kN/m/s last 2 metres
Wave Speed 5123.7 m/s

(B) Resistance Distribution

Depth	Ru	Unit	Total capacity
Below	Ru	(Area)	Shaft capacity
Grade			Toe capacity
m	kN	kPa	kN
1.5	21.7	7.53	1543
3.5	43.5	15.09	1099.9
5.5	53.1	18.44	443.3
7.6	53.1	18.44	
9.6	53.1	18.44	
11.6	44.3	15.37	
13.6	44.3	15.37	
15.7	44.3	15.37	
17.7	130.8	45.38	
18.7	250.6	86.93	
21.7	193.8	67.23	
23.8	187	57.91	
Avg skin	91.7	31.78	
Toe	443.1	3506.59	

Filename 7 rinst nm
Exponential Viscous Damping using Rnt for shaft

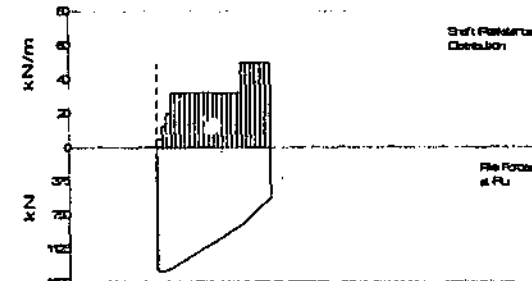
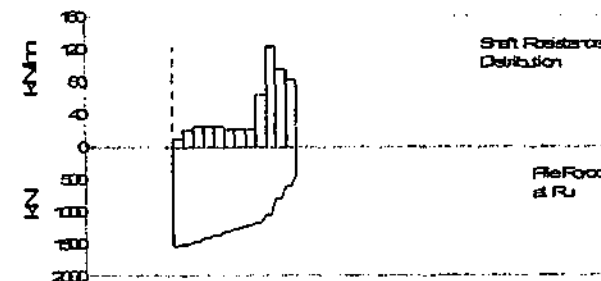
(A) Pile Model

Depth	Area	E-Mod	Spec Wei	Circum	Impedance
m	cm ²	MPa	kN/m ³	m	kN/m/s
0	157.42	206825	77.287	1.422	365.4
24.32	157.42	206825	77.287	1.422	1200

As per Smith Linear Viscous Damping

(B) Resistance Distribution

Depth	Ru	Unit	Total capacity
Below	Ru	(Area)	Shaft capacity
Grade			Toe capacity
m	kN	kPa	kN
0.5	5.1	3.52	1399.6
1.5	12.7	8.81	838.4
2.5	20.3	14.1	569.2
3.5	32.5	22.56	
4.5	32.5	22.56	
5.5	32.5	22.56	
6.5	32.5	22.56	
7.6	32.5	22.56	
8.6	32.5	22.56	
9.6	32.5	22.56	
10.6	32.5	22.56	
11.6	32.5	22.56	
12.6	32.5	22.56	
13.6	32.5	22.56	
14.7	32.5	22.56	
15.7	32.5	22.56	
16.7	32.5	22.56	
17.7	32.5	22.56	
18.7	50.8	35.24	
19.7	50.8	35.24	
20.7	50.8	35.24	
21.7	50.8	35.24	
22.8	50.8	35.24	
23.8	50.8	35.24	
Avg skin	34.6	24.01	
Toe	569.2	4504.64	



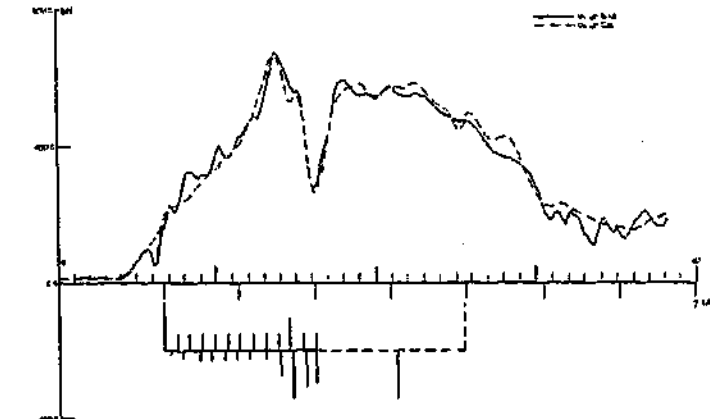
(C) CAPWAP Parameters

JS	SS	QS	UN	CS	LS	FI	OP
0.914	0.47	4	0	0.8	0	0.01	0
JT	ST	QT	TG	CT	LT	FL	
0.171	0.218	9	2	1	0	0.6	

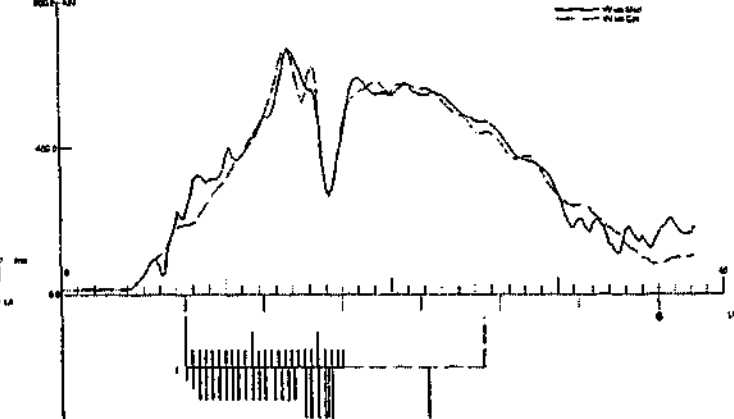
(C) CAPWAP Parameters

JS	SS	QS	UN	CS	LS	FI	OP
1.1	0.75	5	0	1	0	0.01	0
JT	ST	QT	TG	CT	LT	FL	
0.712	0.708	5	7	0.4	0	0	

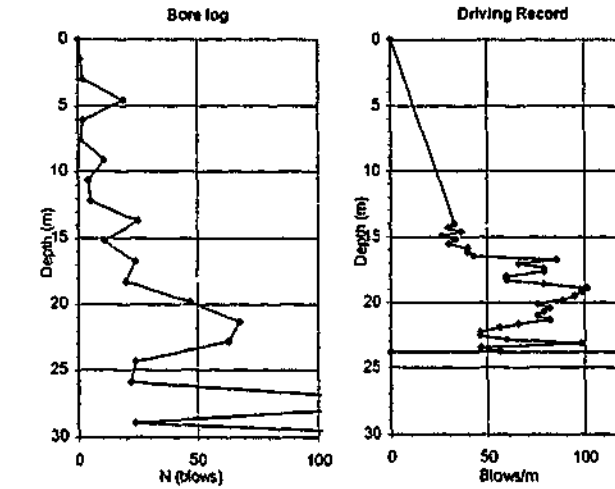
(D) Match
CAPWAP match quality: 6.24 (Wave Up Match)
Observed: final set = 3.175 mm; blow count = 315 b/m
Computed: final set = 6.317 mm; blow count = 120 b/m



(D) Match
CAPWAP match quality: 7.74 (Wave Up Match)
Observed: final set = 3.175 mm; blow count = 315 b/m
Computed: final set = 9.755 mm; blow count = 103 b/m



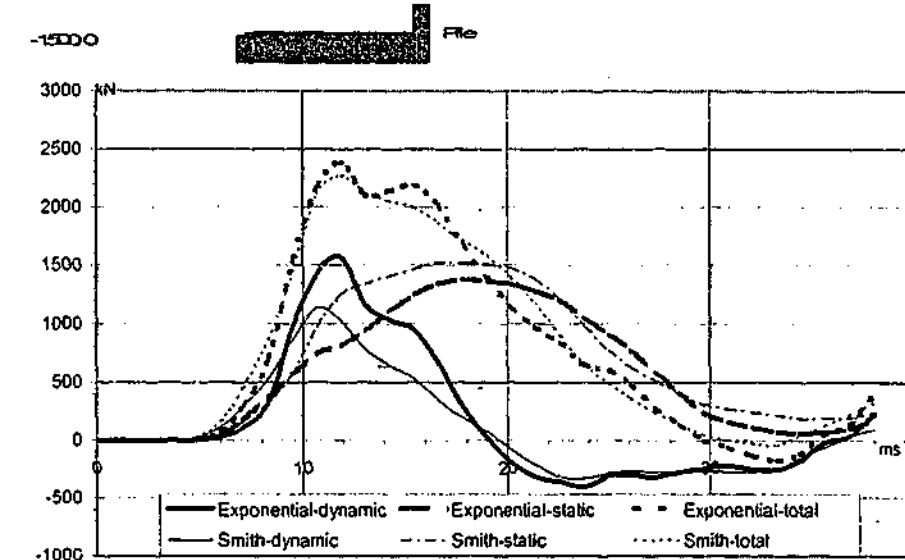
(A) Soil Data
Depth (m) Soil description
0.0 CLAY, med. plasticity, brown
1.5 PEAT and WOOD, highly organic dark brown, very soft
3.0 SANDY CLAY, med plasticity, dark brown very soft
4.6 SAND, fine to med grained, light grey, med dense
6.1 CLAY, highly plastic, dark grey-grey w/mica very soft
9.1 SAND fine to med grained grey med dense
10.7 CLAY highly plastic, grey to greenish grey soft to firm
12.2 SAND, fine to med grained grey loose to med dense
15.2 CLAY, highly plastic dark grey w/silty sand partings stiff
18.8 SAND, fine to med grained grey med dense to v. dense
22.9 SANDY CLAY, medium plasticity, dark grey, hard with
24.4 cemented layers, calcareous



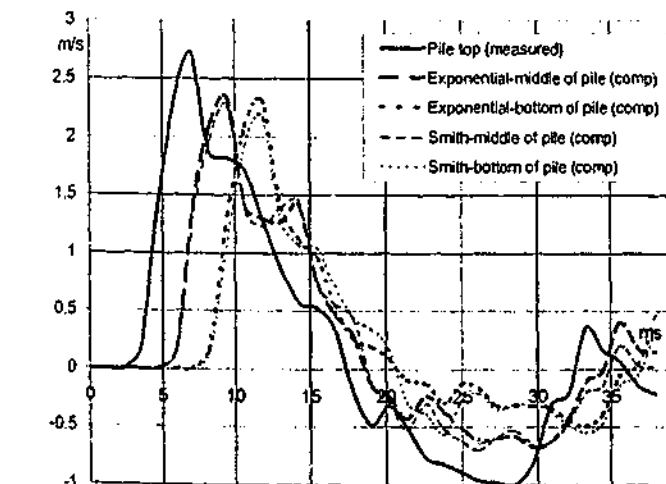
(B) Measured Force & Velocity at Pile Top



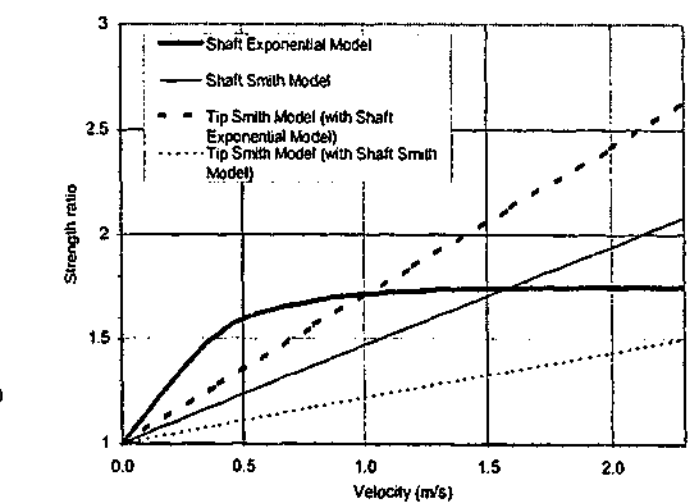
(C) Computed Resistances



(D) Velocities at Top, Middle & Bottom of Pile



(E) Strength Ratio-Velocity Models for Shaft & Tip



IDB
588/39D PIC 150460/540X;siCL;siCL32; Blow: 538

Filename 8 del
Smith Linear Viscous Damping using Rult for Shaft

(A) Pile Model

Depth	Area	E-Mod	Spec Wei	Circum	Impedance
m	cm ²	MPa	kN/m ³	m	1045.58 kN/m/s
0	823.87	54351.4	29.061	1.018	Added impedance None
28.78	823.87	54351.4	29.061	1.018	Wave Speed 4282.6 m/s

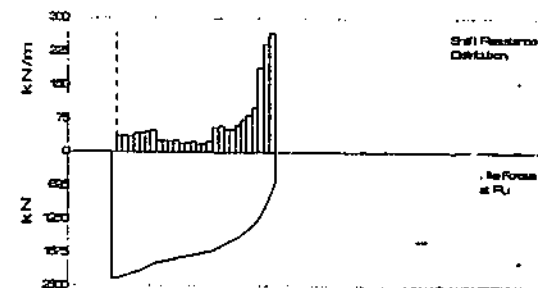
(B) Resistance Distribution

Depth	Ru	Unit	Total capacity
Below Grade	Ru (Area)	Unit	Shaft capacity
m	kN	kPa	Toe capacity
0.8	36.2	34.8	2355.8 kN
1.8	38.4	34.79	1789.4 kN
2.9	35.5	33.93	568.3 kN
3.9	42.4	40.52	
4.9	44.8	42.81	
5.9	47.2	45.11	
7	49.6	47.4	
8	25.8	24.86	
9	25.9	24.75	
10	25.9	24.75	
11.1	27.5	26.28	
12.1	21.1	20.18	
13.1	21.5	20.55	
14.2	25.3	24.18	
15.2	19.2	18.35	
16.2	19.2	18.35	
17.2	25.1	23.89	
18.3	58.1	53.71	
19.3	60.4	57.82	
20.3	52.2	49.88	
21.3	51.9	49.7	
22.4	62.1	59.44	
23.4	75.1	71.87	
24.4	85.9	82.19	
25.4	102.4	97.86	
26.5	193.7	185.31	
27.5	247.9	237.1	
28.5	273.4	261.57	

(C) CAPWAP Parameters

JS	SS	QS	UN	CS	LS	PI	OP
1.038	0.605	2.5	0.1	1	0	0.01	0
JT	ST	QT	TG	CT	LT	PL	
0.37	0.682	4.9	1	0.9	0	0	

(D) Match
CAPWAP match quality: 1.38 (Wave Up Match)
Observed: final set = 1.814 mm; blow count = 551 b/m
Computed: final set = 1.822 mm; blow count = 549 b/m



Filename 8 rinst nm
Exponential Viscous Damping using Rinst for shaft

(A) Pile Model

Depth	Area	E-Mod	Spec Wei	Circum	Impedance
m	cm ²	MPa	kN/m ³	m	1045.58 kN/m/s
0	823.87	54351.4	29.061	1.018	Added impedance None
28.78	823.87	54351.4	29.061	1.018	Wave Speed 4282.6 m/s

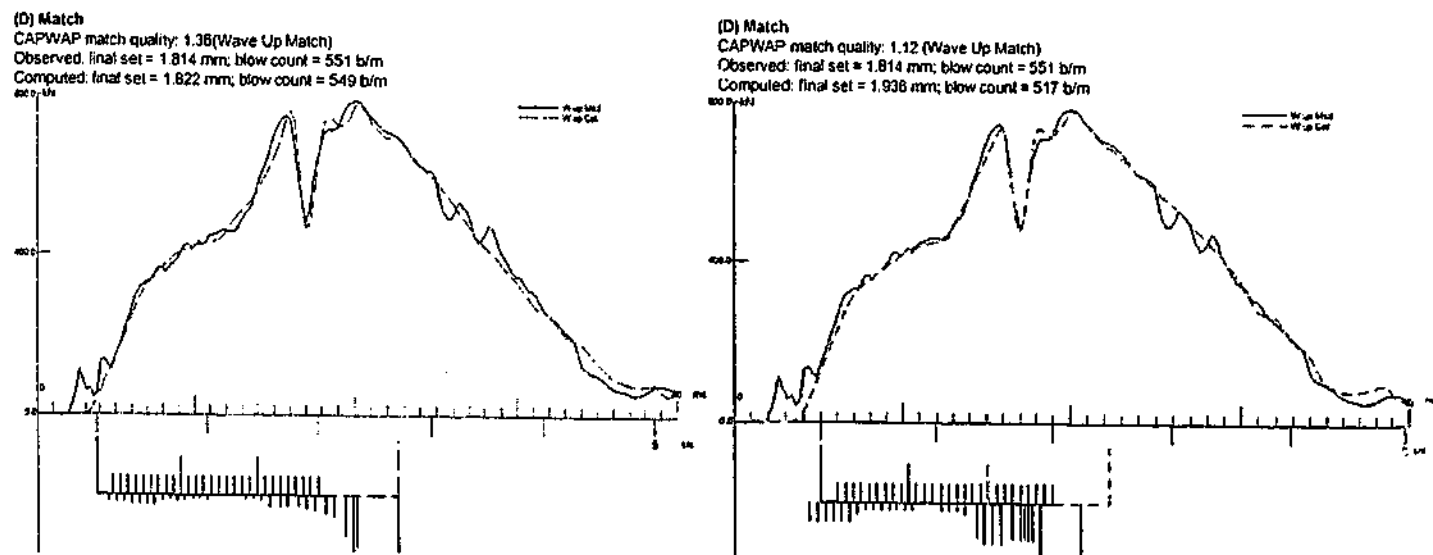
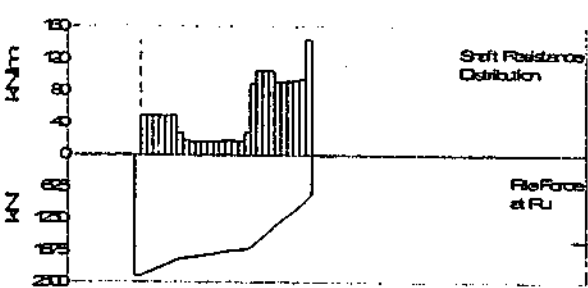
(B) Resistance Distribution

Depth	Ru	Unit	Total capacity
Below Grade	Ru (Area)	Unit	Shaft capacity
m	kN	kPa	Toe capacity
0.8	51.5	49.31	2347.7 kN
1.8	51.5	49.31	1585.3 kN
2.9	51.5	49.31	752.4 kN
3.9	51.5	49.31	
4.9	51.5	49.31	
5.9	51.5	49.31	
7	28.5	27.24	
8	19.1	18.25	
9	17.5	16.72	
10	17.7	16.92	
11.1	18	17.2	
12.1	18.1	17.3	
13.1	18.4	17.58	
14.2	18.6	17.78	
15.2	18.6	17.78	
16.2	18.6	17.78	
17.2	18	17.2	
18.3	29.7	28.38	
19.3	92.7	88.89	
20.3	108.5	103.79	
21.3	108.3	103.6	
22.4	108.3	103.6	
23.4	94.2	90.12	
24.4	95	90.88	
25.4	95.5	91.36	
26.5	98.9	92.7	
27.5	98.3	94.04	
28.5	147.8	141.34	

(C) CAPWAP Parameters

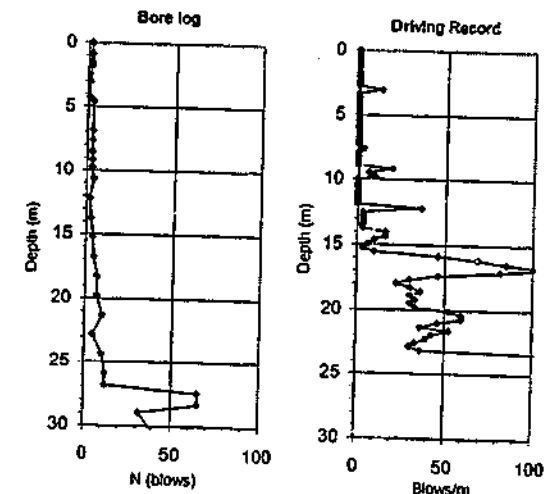
JS	SS	QS	UN	CS	LS	PI	OP
1.421	0.93	2	0.025	1	0	0.01	0
JT	ST	QT	TG	CT	LT	PL	
0.481	0.668	1.7	4.2	1.7	0	0	

(D) Match
CAPWAP match quality: 1.12 (Wave Up Match)
Observed: final set = 1.814 mm; blow count = 551 b/m
Computed: final set = 1.936 mm; blow count = 517 b/m



(A) Soil Data

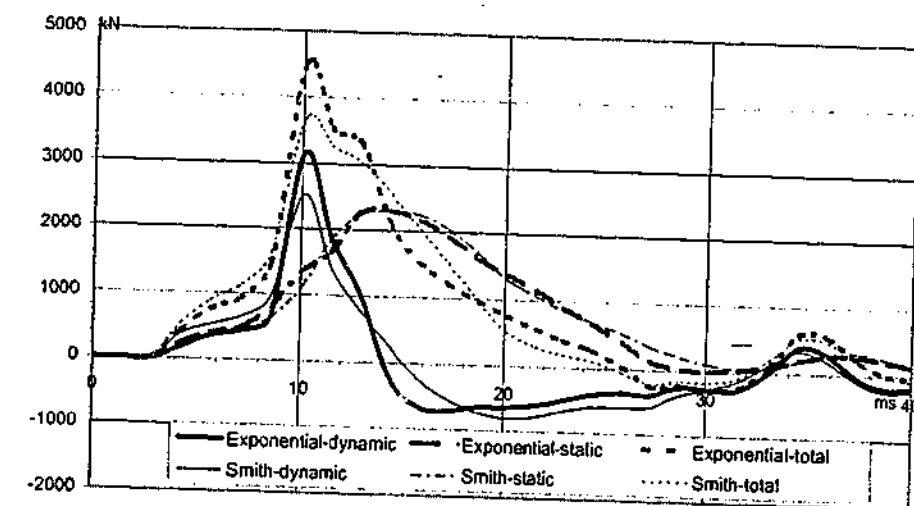
Depth (m)	Soil description	Pile (m)
0.0	Very soft dark brown organic sandy SILT, dry (FILL)	
0.9	Very loose grey silty SAND, trace organics/shells, moist (FILL)	
1.8	Very soft to soft grey silty CLAY, trace organics, moist (FILL)	
4.3	Very loose grey silty SAND, trace shells layer soft silty clay, wet	
6.9	Very soft grey silty CLAY, trace organics/shells, moist	
8.5	Very loose grey silty SAND, trace organics/shells, wet	
9.8	Soft grey organic clayey SILT, trace shells, moist	
15.2	Very soft grey silty CLAY, wet	
18.3	Very soft grey org clayey SILT, some shells layer sand, moist	
24.4	Loose grey silty SAND w/organics, moist to wet	
25.9	Soft grey clayey SILT, trace sand, moist	
26.8	Very dense fine and grey SAND, some silty clay, trace gravel, wet	
28.3	Medium stiff to very stiff brownish grey silty CLAY, wet	



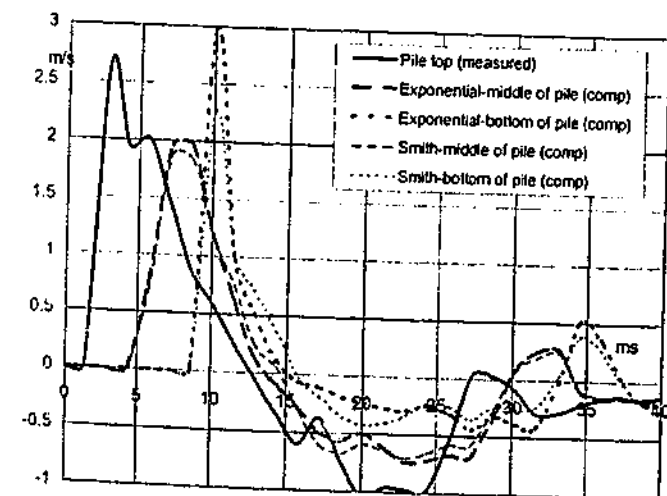
(B) Measured Force & Velocity at Pile Top



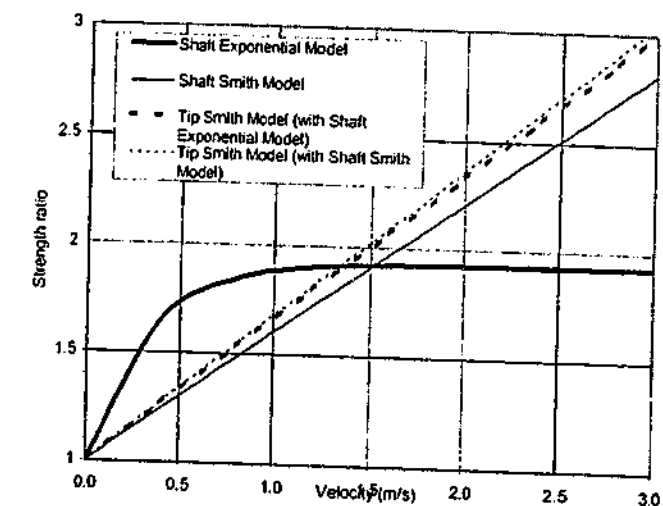
(C) Computed Resistances



(D) Velocities at Top, Middle & Bottom of Pile



(E) Strength Ratio-Velocity Models for Shaft & Tip



ID9
R102/SH H 3d7396K;S+SA;SAs1125

Filename 9 def
Smith Linear Viscous Damping using Rult for Shaft

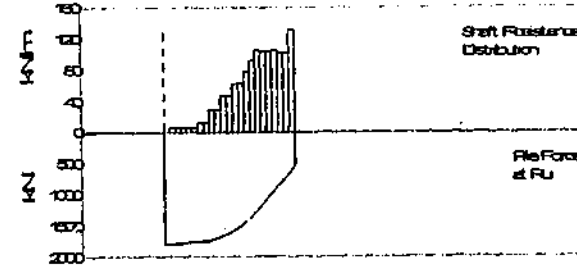
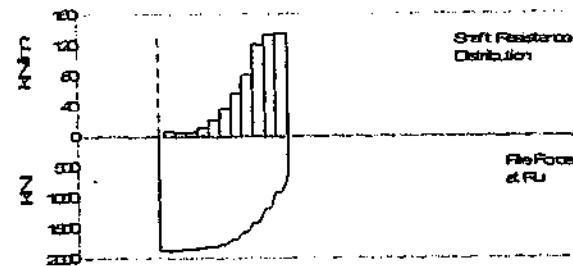
Depth	Area	E-Mod	Spec Wei	Circum	Impedance
m	cm ²	MPa	kN/m ³	m	403.42kN/m/s
0	100	206579	77.287	1.219	Added Impedance None
23.16	100	206579	77.287	1.219	Wave Speed 5120.6 m/s

(B) Resistance Distribution			Total capacity	1897.9 kN
Depth	Ru	Unit	Shaft capacity	1249.3 kN
Below Grade	(Area)		Toe capacity	648.6 kN
m	kN	kPa		
2.3	15.4	6.27		
4.3	11.8	4.82		
6.3	12.3	5.03		
8.3	23.5	9.55		
10.3	45.4	18.48		
12.3	78.5	31.15		
14.3	115.1	46.86		
16.4	162.6	66.21		
18.4	243.3	98.07		
20.4	359.4	142.7		
22.4	518.9	206.58		
Avg skin	113.6	46.24		
Toe	648.6	256.96		

Filename 9 nm rult
Exponential Viscous Damping using Rult for shaft

(A) Pile Model
As per Smith Linear Viscous Damping

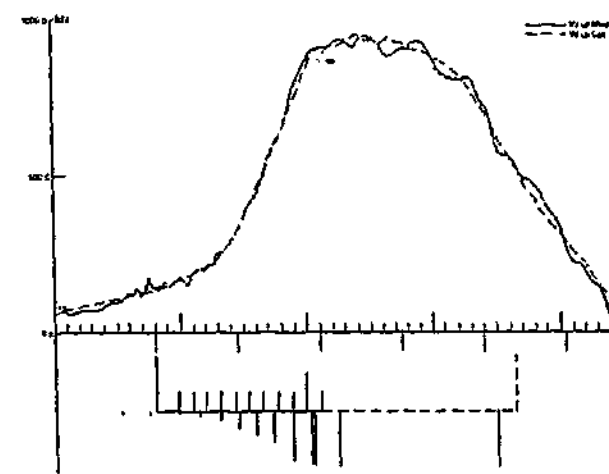
(B) Resistance Distribution			Total capacity	1817.4 kN
Depth	Ru	Unit	Shaft capacity	1282.6 kN
Below Grade	(Area)		Toe capacity	534.7 kN
m	kN	kPa		
1.3	6.3	5.16		
2.3	6.3	5.16		
3.3	8.3	5.16		
4.3	5.8	4.74		
5.3	5.8	4.74		
6.3	13.2	10.73		
7.3	13.2	10.73		
8.3	30.5	24.87		
9.3	30.3	24.7		
10.3	48.4	39.42		
11.3	48.4	39.42		
12.3	83.8	51.98		
13.3	65	52.98		
14.3	79.7	64.55		
15.4	93.4	76.1		
16.4	107.3	87.41		
17.4	106.1	86.41		
18.4	106.1	86.41		
19.4	107	87.16		
20.4	103.3	84.18		
21.4	103.3	84.18		
22.4	132.8	108.2		
Avg skin	58.3	47.49		
Toe	534.7	213.88		



(C) CAPWAP Parameters

JS	SS	QS	UN	CS	LS	PI	OP
1.679	6.553	1.5	0.4	0.8	0	0.01	0
JT	ST	QT	TG	CT	LT	PL	
1.734	1.1	4	0	1	0	0.853	

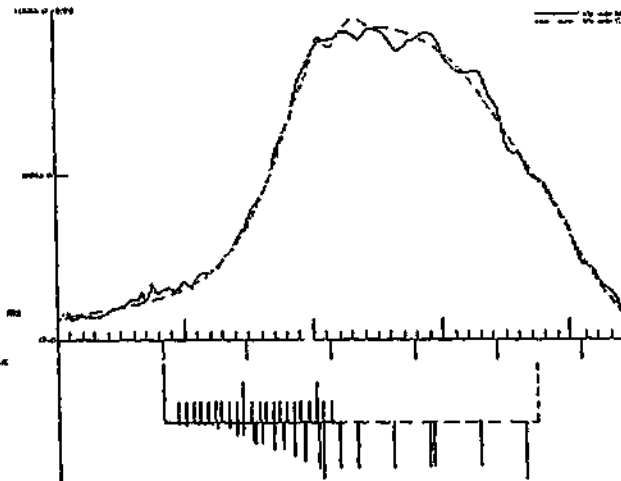
(D) Match
CAPWAP match quality: 2.05 (Wave Up Match)
Observed: final set = 1.587 mm; blow count = 630 b/m
Computed: final set = 1.574 mm; blow count = 636 b/m



(C) CAPWAP Parameters

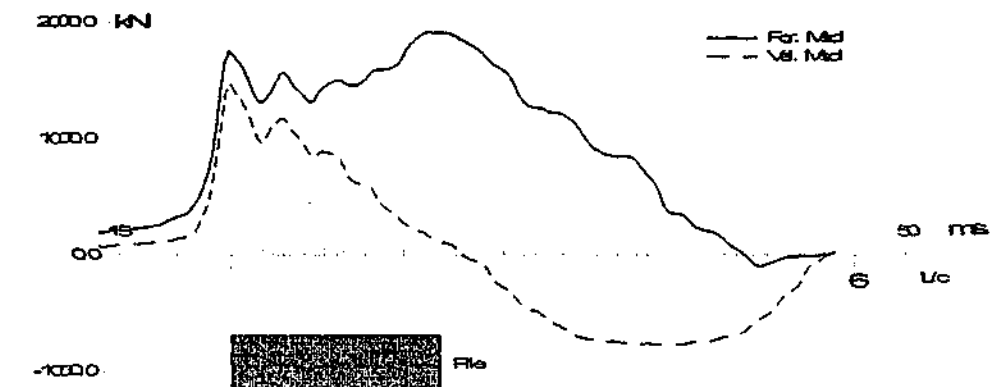
JS	SS	QS	UN	CS	LS	PI	OP
1.744	6.56	5.5	0.25	1	0	0.01	0
JT	ST	QT	TG	CT	LT	PL	
0.524	0.494	1	0	1	0	0.8	

(D) Match
CAPWAP match quality: 1.86 (Wave Up Match)
Observed: final set = 1.587 mm; blow count = 630 b/m
Computed: final set = 2.059 mm; blow count = 483 b/m

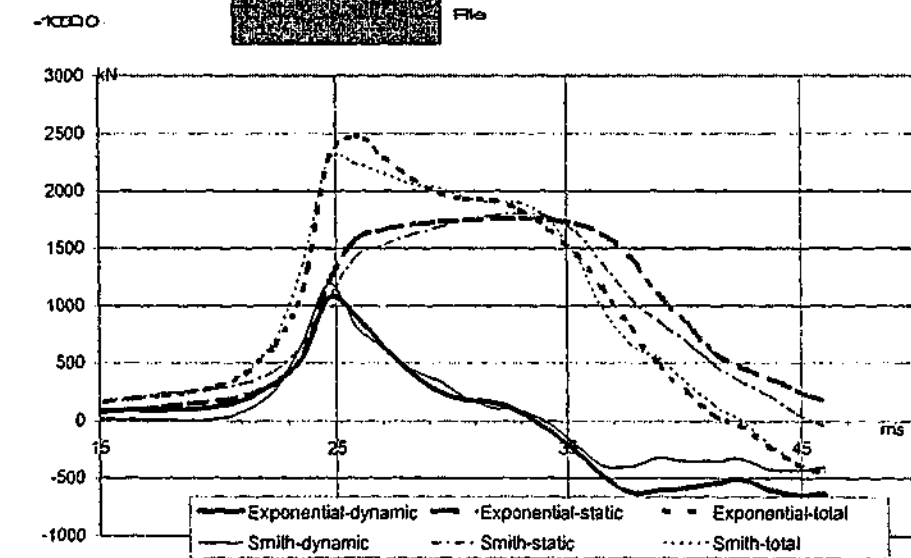


(A) Soil Data
Depth (m) Soil description

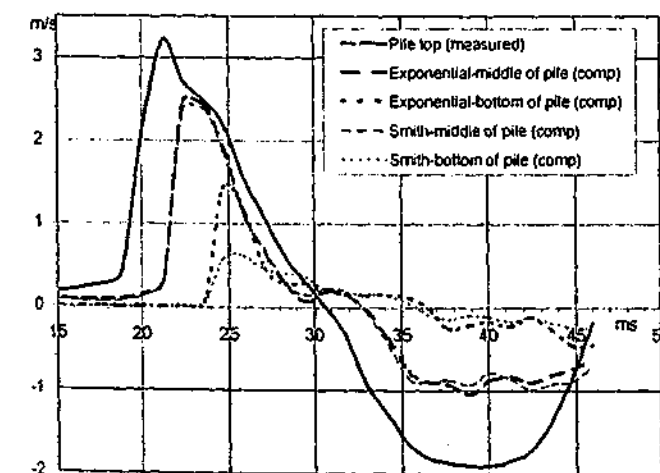
(B) Measured Force & Velocity at Pile Top



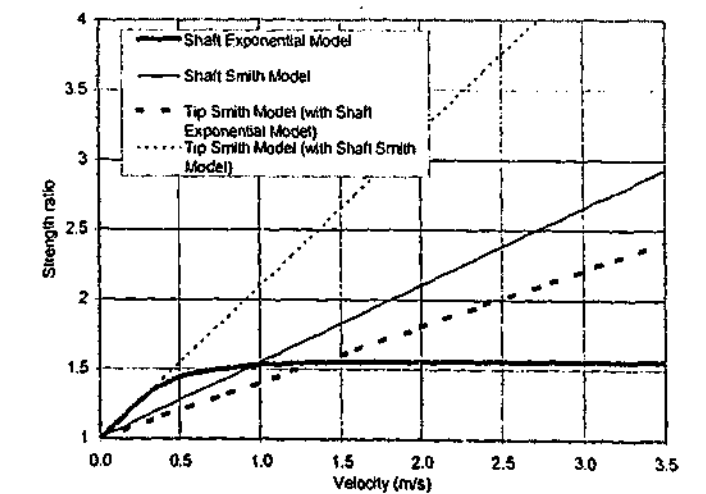
(C) Computed Resistances



(D) Velocities at Top, Middle & Bottom of Pile



(E) Strength Ratio-Velocity Models for Shaft & Tip



ID10

R1178D H 358mm 1369/1320-1408X;CL;CL

Filename 10 def
Smith Linear Viscous Damping using Rult for Shaft

Filename 10 rinst nm
Exponential Viscous Damping using Rinst for shaft

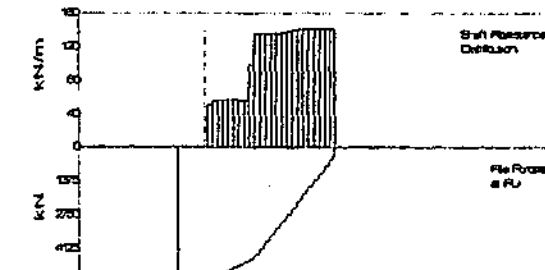
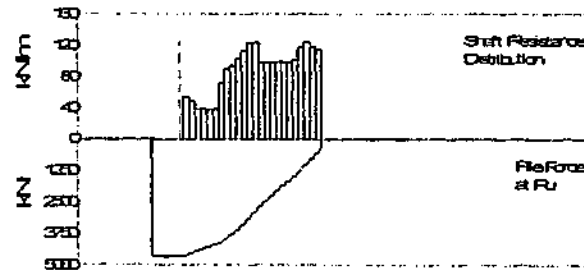
(A) Pile Model					(A) Pile Model				
Depth	Area	E-Mod	Spec Wei	Circum	Impedance	1090.5kN/m/s	As per Smith Linear Viscous Damping	Impedance	1090.5kN/m/s
m	cm ²	MPa	kN/m ³	m	Added Impedance	1400kN/m/s bet 40 to 42m depth	Wave Speed	1300kN/m/s bet 39 to 43m depth	
0	270.32	206579	77.287	1.422					
59.01	270.32	206579	77.287	1.422					

(B) Resistance Distribution

Depth	Ru	Unit	Total capacity	4625.5 kN
Below	Ru	Unit	Shaft capacity	4329.2 kN
Grade	(Area)	Unit	Toe capacity	296.5 kN
m	kN	kPa		
2.8	109.4	38.44		
4.8	99.4	34.95		
6.8	79.4	27.92		
8.8	79.4	27.92		
10.8	79.4	27.92		
12.8	79.4	27.92		
14.8	145.6	51.18		
16.8	181	63.81		
18.8	189.3	66.54		
20.8	207.6	72.06		
22.8	228.3	80.24		
24.8	248.6	87.37		
26.8	248.6	87.37		
28.8	198.9	69.89		
30.8	198.9	69.89		
32.8	198.9	69.89		
34.8	198.9	69.89		
36.8	198.9	69.89		
38.8	198.9	69.89		
40.8	205	72.05		
42.8	238.8	83.24		
44.8	250.3	87.97		
46.8	237.9	83.62		
48.8	230.5	81.01		
Avg Skin	180.4	63.4		
Toe	296.3	2343.22		

(B) Resistance Distribution

Depth	Ru	Unit	Total capacity	5462.4 kN
Below	Ru	Unit	Shaft capacity	5259 kN
Grade	(Area)	Unit	Toe capacity	203.3 kN
m	kN	kPa		
2.8	101.8	35.77		
4.8	113.3	39.83		
6.8	113.3	39.83		
8.8	113.3	39.83		
10.8	113.3	39.83		
12.8	113.3	39.83		
14.8	113.3	39.83		
16.8	113.3	39.83		
18.8	197.6	69.46		
20.8	271.7	95.49		
22.8	271.6	95.46		
24.8	271.6	95.46		
26.8	271.1	95.28		
28.8	271.1	95.28		
30.8	273.2	96.02		
32.8	277.3	97.47		
34.8	281.5	96.95		
36.8	282.4	99.27		
38.8	281.7	99.02		
40.8	282.6	99.34		
42.8	282.6	99.34		
44.8	282.6	99.34		
46.8	282.6	99.34		
48.8	282.6	99.34		
Avg Skin	219.1	77.02		
Toe	203.3	1608.21		



(C) CAPWAP Parameters

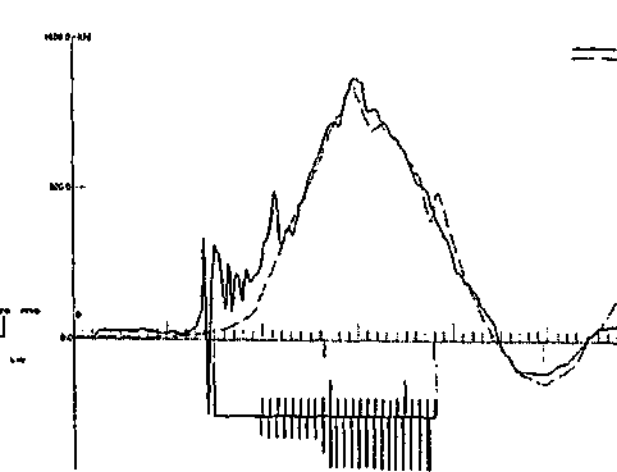
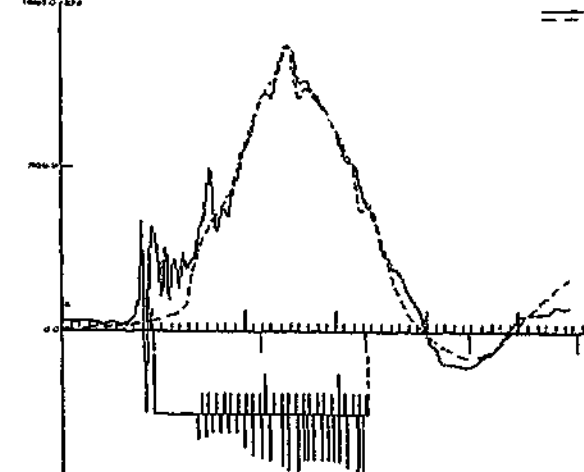
JS	SS	QS	UN	CS	LS	PI	OP
2.451	0.62	4.33	0.179	1	0	0.01	0
JT	ST	QT	TG	CT	LT	PL	
0.311	1.148	1.03	0	1	0	0.954	

(C) CAPWAP Parameters

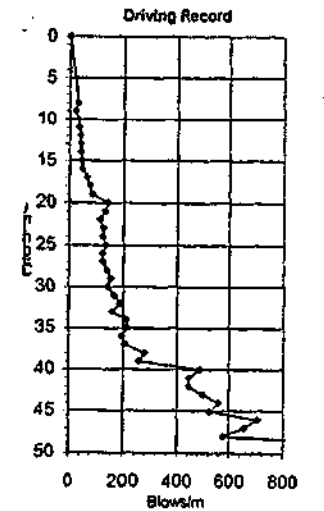
JS	SS	QS	UN	CS	LS	PI	OP
3.7	0.77	3.5	0.23	1	0	0.01	0
JT	ST	QT	TG	CT	LT	PL	
0.241	1.3	1	0	1	0	0	

(D) Match
CAPWAP match quality: 2.52 (Wave Up Match)
Observed: final set = 0.863 mm; blow count = 1158 b/m
Computed: final set = 0.909 mm; blow count = 1100 b/m

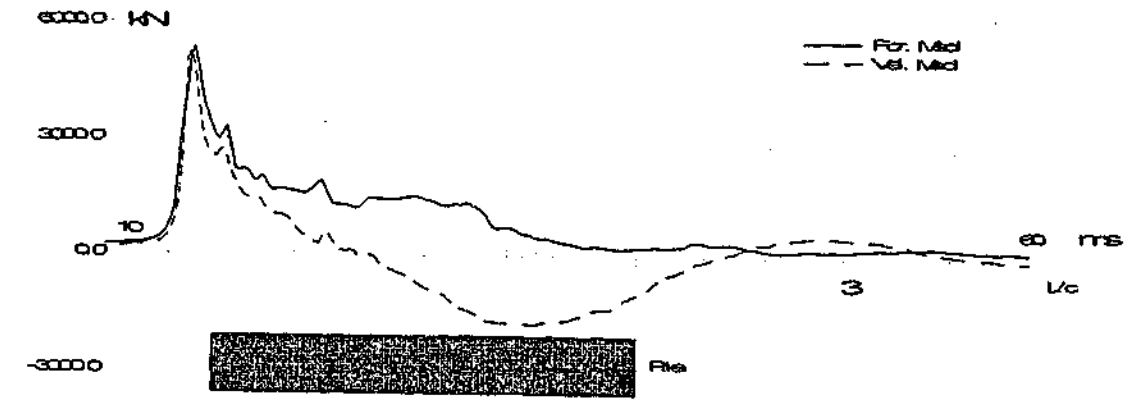
(D) Match
CAPWAP match quality: 3.34 (Wave Up Match)
Observed: final set = 0.863 mm; blow count = 1158 b/m
Computed: final set = 1.109 mm; blow count = 901 b/m



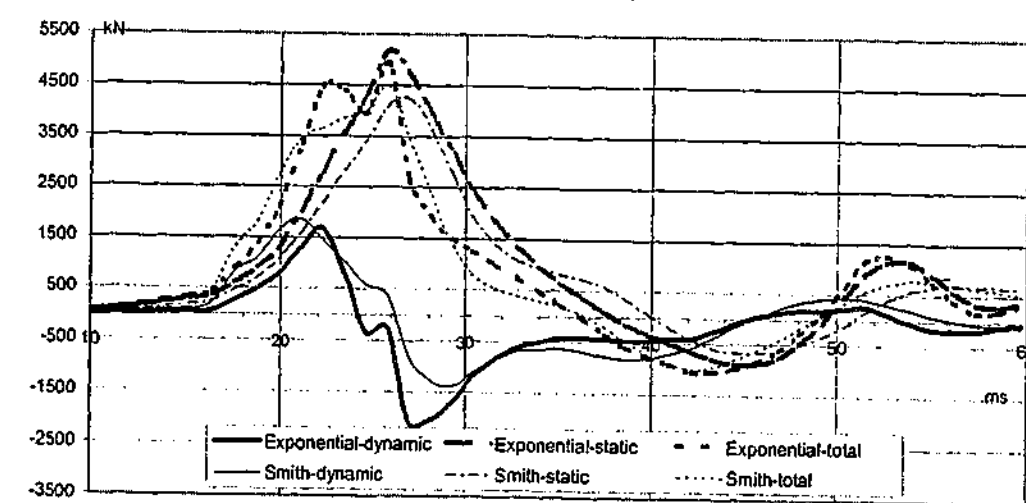
(A) Soil Data
Depth (m) Soil description
0.0 Sandy LOAM or clayey fine SAND (FILL)
3.0 Soil, fissured and stratified Boom CLAY



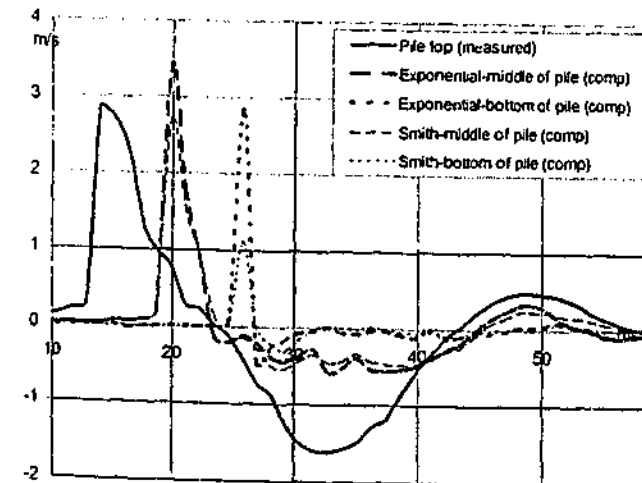
(B) Measured Force & Velocity at Pile Top



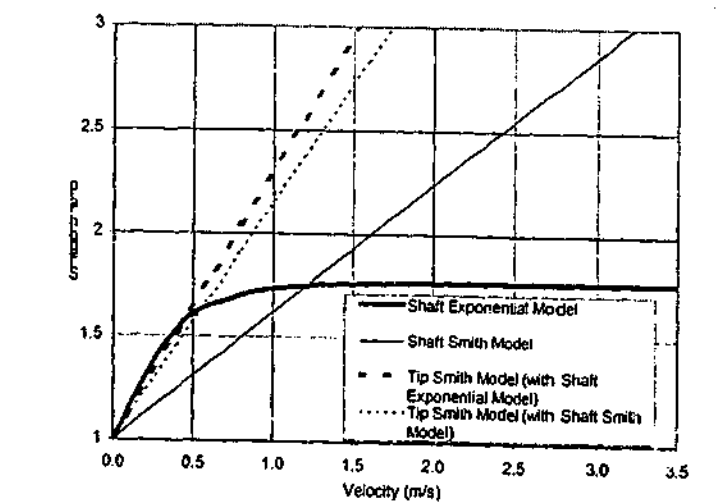
(C) Computed Resistances



(D) Velocities at Top, Middle & Bottom of Pile



(E) Strength Ratio-Velocity Models for Shaft & Tip



ID11
R11613D H 7497462-502X;CL;CL; Blow: 538

Filename 11 def
Smith Linear Viscous Damping using Rult for Shaft

(A) Pile Model

Depth	Area	E-Mod	Spec Wei	Circum	Impedance
m	cm ²	MPa	kN/m ³	m	1090.72 kN/m ⁵
0	270.32	206579	77.287	1.422	Added impedance None
18.99	270.32	206579	77.287	1.422	Wave Speed 5119.8 m/s

(B) Resistance Distribution

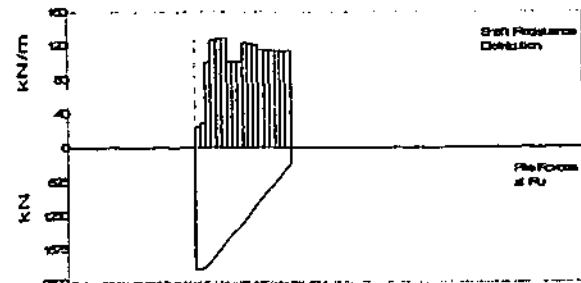
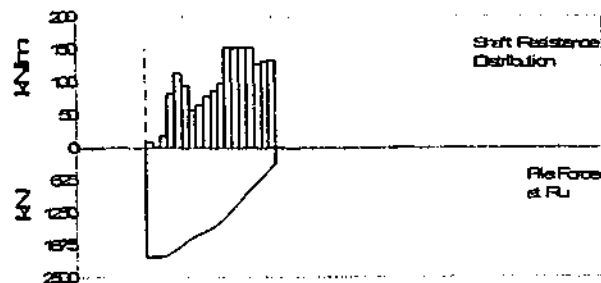
Depth	Ru	Unit	Total capacity
Below	Ru		Shaft capacity
Grade	(Area)		Toe capacity
m	kN	kPa	kN
0	9.4	8.29	2109.4
1.1	1.8	1.21	1807.6
2.2	20.5	13.65	301.5
3.2	87.1	59.05	
4.3	120.2	80.15	
5.3	101	67.38	
6.4	60.9	40.58	
7.4	68.3	45.53	
8.5	82.3	54.84	
9.5	92.2	61.47	
10.6	103.7	69.1	
11.7	161.3	107.53	
12.7	161.3	107.53	
13.8	161.3	107.53	
14.8	161.3	107.53	
15.9	134.4	89.59	
16.9	139.8	93.2	
18	141	94.01	
Avg Skin	100.4	66.95	
Toe	301.5	2384.76	

Filename 11 nm rinst
Exponential Viscous Damping using Rinst for shaft

(A) Pile Model
As per Smith Linear Viscous Damping

(B) Resistance Distribution

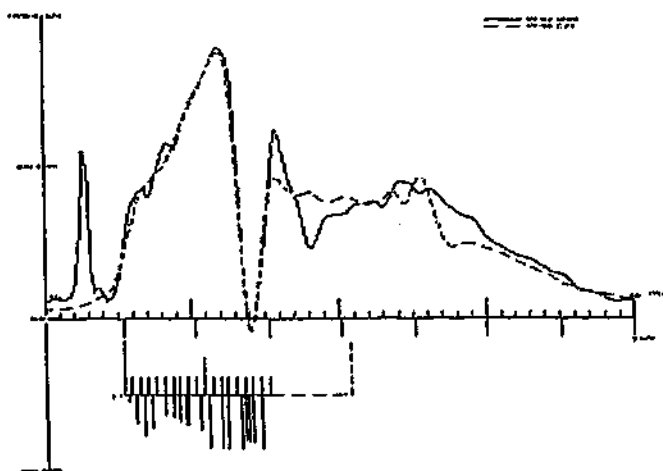
Depth	Ru	Unit	Total capacity
Below	Ru		Shaft capacity
Grade	(Area)		Toe capacity
m	kN	kPa	kN
0	25.2	16.8	2280
1.1	29.7	19.81	1964.8
2.2	105	70.01	295.2
3.2	132.6	88.42	
4.3	134.3	89.56	
5.3	136.4	90.9	
6.4	105.7	70.48	
7.4	105.7	70.48	
8.5	105.7	70.48	
9.5	128.6	86.41	
10.6	128.2	85.48	
11.7	125.8	84.54	
12.7	120.7	80.48	
13.8	119.4	79.59	
14.8	119.9	79.92	
15.9	119.9	79.92	
16.9	119.9	79.92	
18	119.9	79.92	
Avg Skin	110.3	73.51	
Toe	295.2	2334.74	



(C) CAPWAP Parameters

JS	SS	QS	UN	CS	LS	PI	OP
1.182	0.716	4.2	1	1	0	0.01	1
JT	ST	QT	TG	CT	LT	PL	
0.11	6.4	1	4.5	0.3	0	1.997	

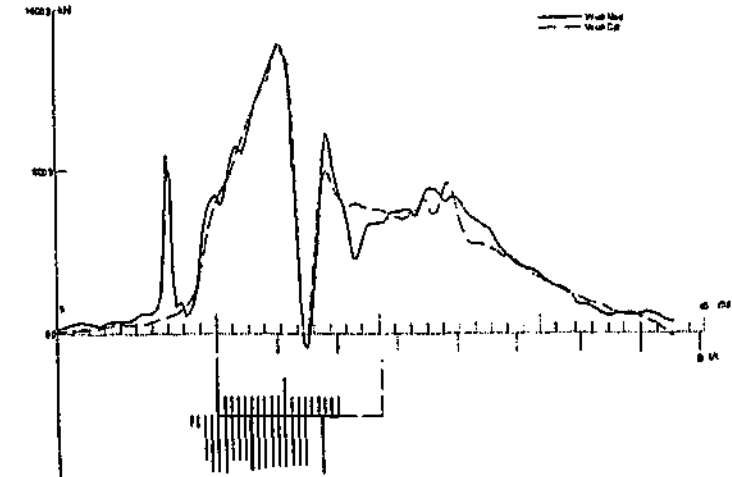
(D) Match
CAPWAP match quality: 2.77 (Wave Up Match)
Observed: final set = 5.155 mm; blow count = 194 b/m
Computed: final set = 5.902 mm; blow count = 169 b/m



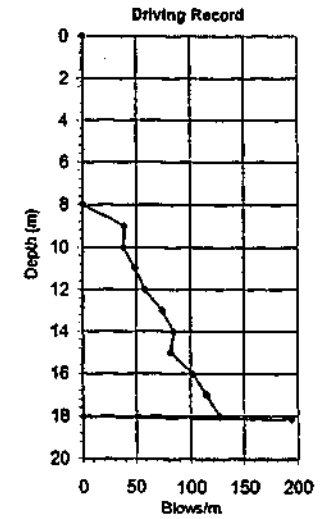
(C) CAPWAP Parameters

JS	SS	QS	UN	CS	LS	PI	OP
1.45	0.8	4.3	0.16	1	0	0.01	0
JT	ST	QT	TG	CT	LT	PL	
0.35	1.3	7	0	1	0	2.4	

(D) Match
CAPWAP match quality: 2.67 (Wave Up Match)
Observed: final set = 5.169 mm; blow count = 194 b/m
Computed: final set = 5.664 mm; blow count = 177 b/m



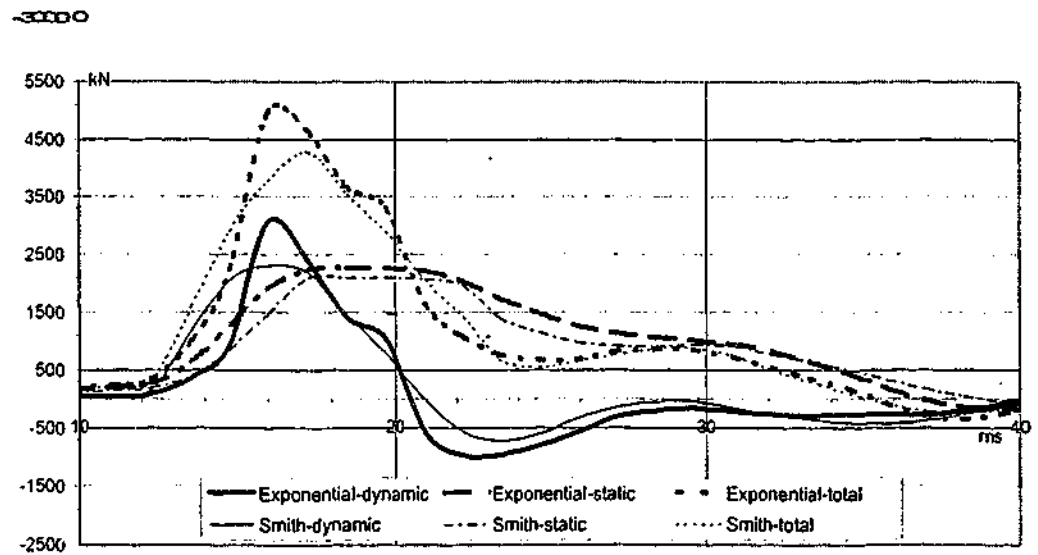
(A) Soil Data
Depth (m) Soil description
0.0 Sandy LOAM or clayey fine SAND (FILL)
3 Silt, fissured and stratified Boom CLAY



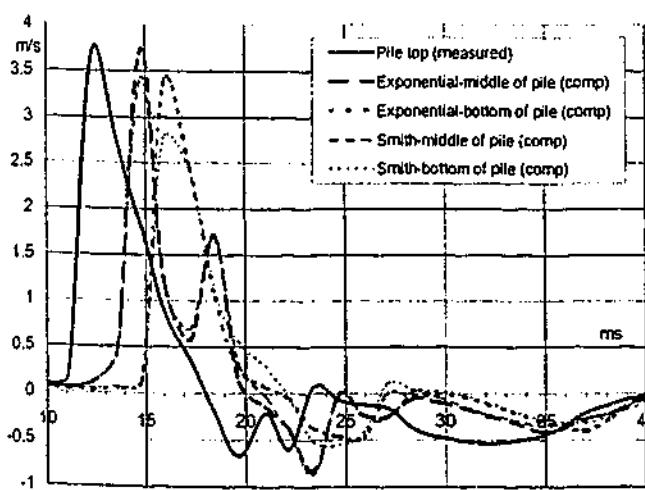
(B) Measured Force & Velocity at Pile Top



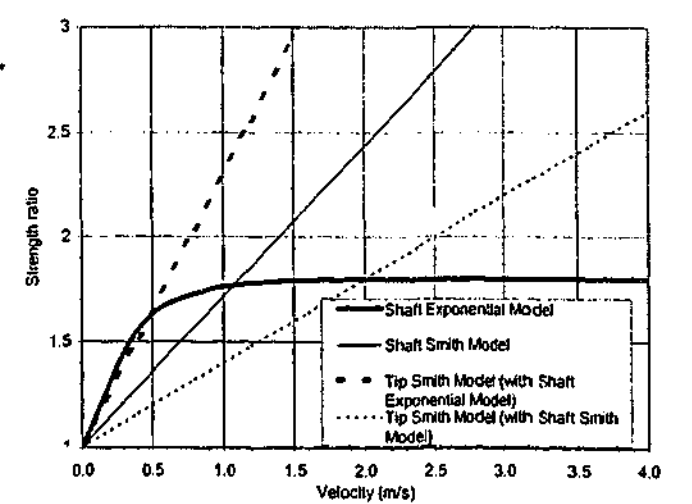
(C) Computed Resistances



(D) Velocities at Top, Middle & Bottom of Pile



(E) Strength Ratio-Velocity Models for Shaft & Tip



ID12
R119/13D 356mm H 317286-334X;CL;CL

Filename Id12 def
Smith Linear Viscous Damping using Rull for Shaft

Filename Id12 rinst
Exponential Viscous Damping using Rinst for shaft

(A) Pile Model

Depth	Area	E-Mod	Spec Wei	Circum	Impedance
m	cm ²	MPa	kN/m ³	m	1090.72kN/m/s
0	270.32	206578.9	77.287	1.422	Added Impedance 2918.96kN/m/s
16	270.32	206578.9	77.287	1.422	Wave Speed 5119.8 m/s

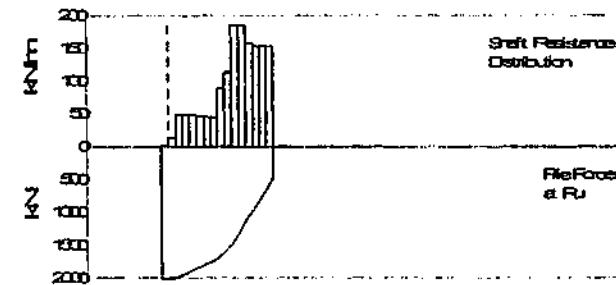
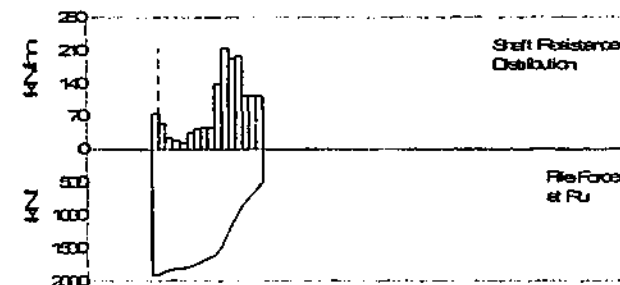
(A) Pile Model
As per Smith Linear Viscous Damping

(B) Resistance Distribution

Depth	Ru	Unit	Total capacity
Below	Ru		Shaft capacity
Grade	(Area)		Toe capacity
m	kN	kPa	kN
-0.7	75.8	53.27	1954
0.3	54.8	38.52	1480.4
1.3	25	17.55	493.6
2.3	19.2	13.48	
3.3	14.8	10.42	
4.3	35.8	25.17	
5.3	44.3	31.16	
6.3	47.2	33.21	
7.3	47.9	33.7	
8.3	139.9	98.36	
9.3	218.9	152.55	
10.3	183.9	136.33	
11.3	200	140.66	
12.3	114.9	80.82	
13.3	114.9	80.82	
14.3	114.9	80.82	
Avg Skin	91.3	64.18	
Toe	493.6	3904.18	

(B) Resistance Distribution

Depth	Ru	Unit	Total capacity
Below	Ru		Shaft capacity
Grade	(Area)		Toe capacity
m	kN	kPa	kN
-0.7	3.6	2.52	1988.7
0.3	13.8	9.72	1506.7
1.3	49.4	34.75	482.2
2.3	49.4	34.75	
3.3	48.3	33.98	
4.3	47.0	33.49	
5.3	45.6	32.09	
6.3	45.6	32.09	
7.3	90.5	63.63	
8.3	114.5	80.48	
9.3	187.2	131.66	
10.3	186.8	131.38	
11.3	159	111.8	
12.3	155.6	109.42	
13.3	154.6	108.86	
14.3	154.6	108.86	
Avg Skin	94.2	66.22	
Toe	482	3811.77	



(C) CAPWAP Parameters

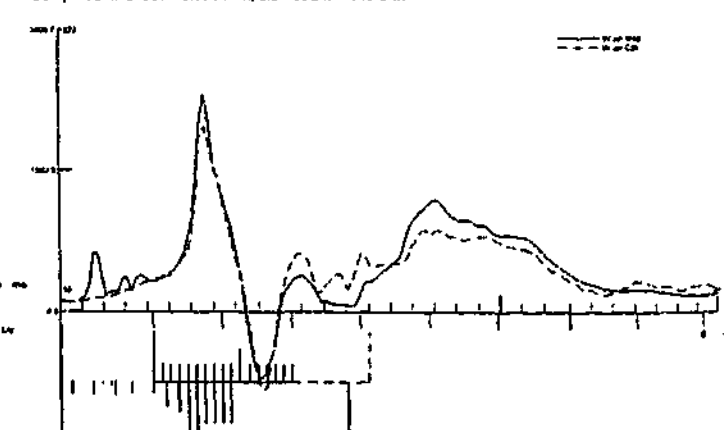
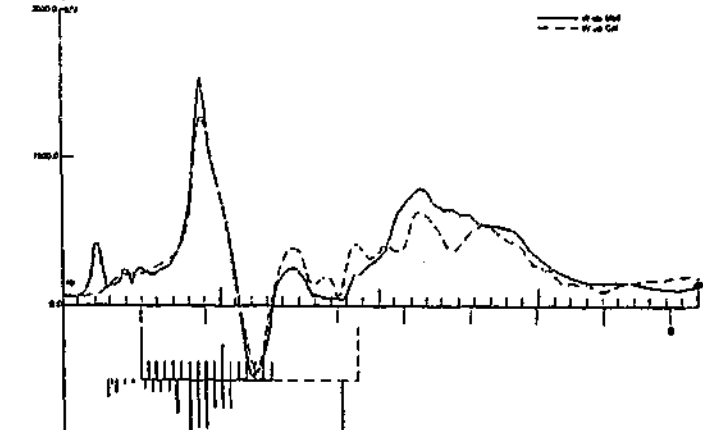
JS	SS	QS	UN	CS	LS	PI	OP
0.552	0.41	0.97	0	1	0	0.01	0
JT	ST	QT	TG	CT	LT	PL	
0.191	0.419	11.24	0	1	0	2.45	

(C) CAPWAP Parameters

JS	SS	QS	UN	CS	LS	PI	OP
1.25	0.9	0.5	0	1	0	0.01	0
JT	ST	QT	TG	CT	LT	PL	
0.12	0.27	1	10	1.8	0	2	

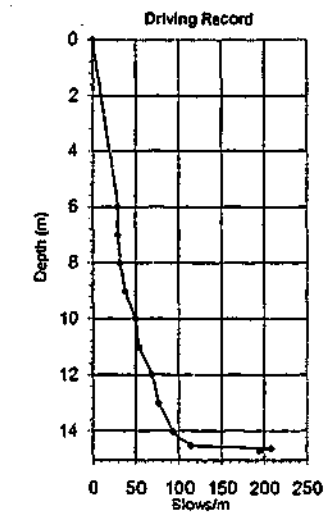
(D) Match
CAPWAP match quality: 4.60 (Wave Up Match)
Observed: final set = 5.080 mm; blow count = 197 b/m
Computed: final set = 5.978 mm; blow count = 167 b/m

(D) Match
CAPWAP match quality: 4.51 (Wave Up Match)
Observed: final set = 5.080 mm; blow count = 197 b/m
Computed: final set = 6.059 mm; blow count = 165 b/m

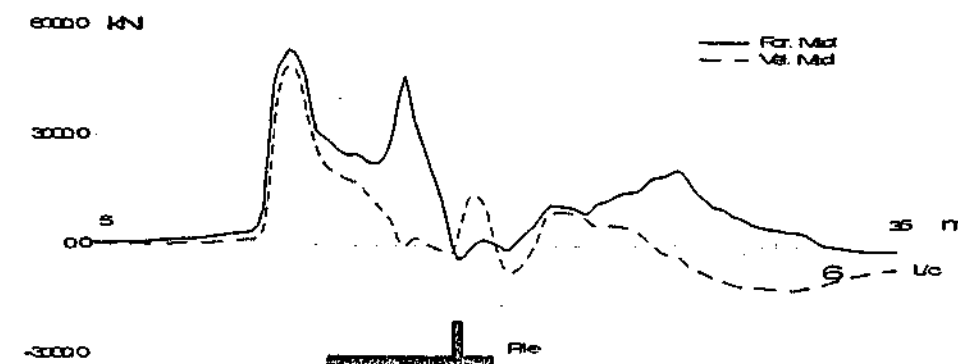


(A) Soil Data
Depth (m) Soil description
0.0 Sandy LOAM or clayey fine SAND (FILL)

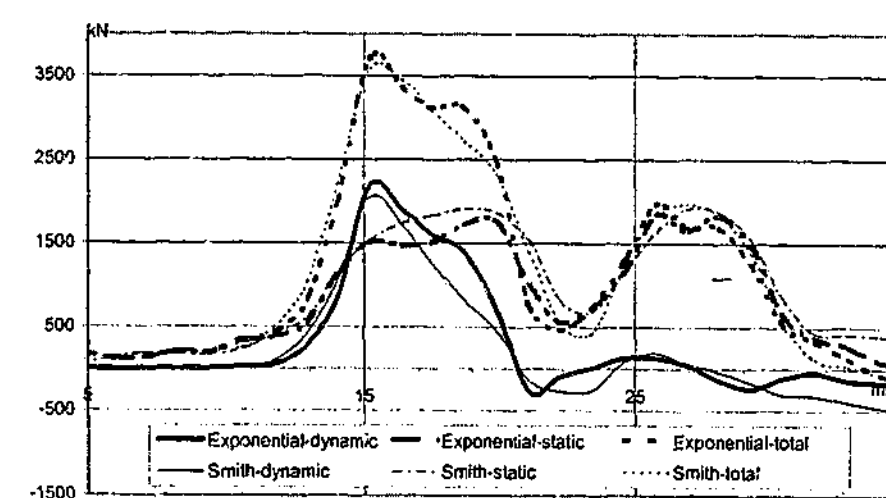
3.0 Stiff, fissured and stratified Boom CLAY



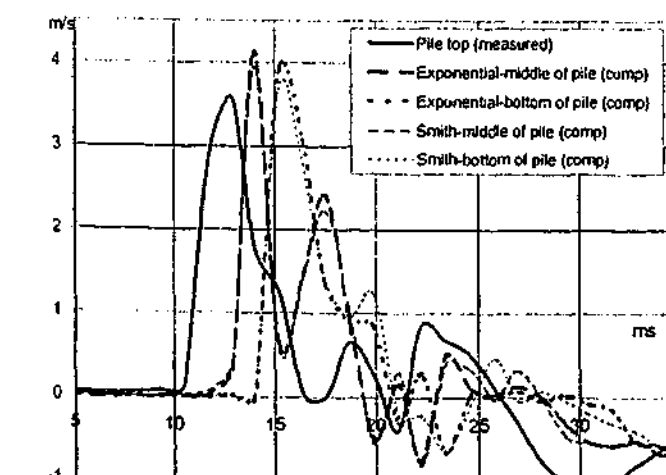
(B) Measured Force & Velocity at Pile Top



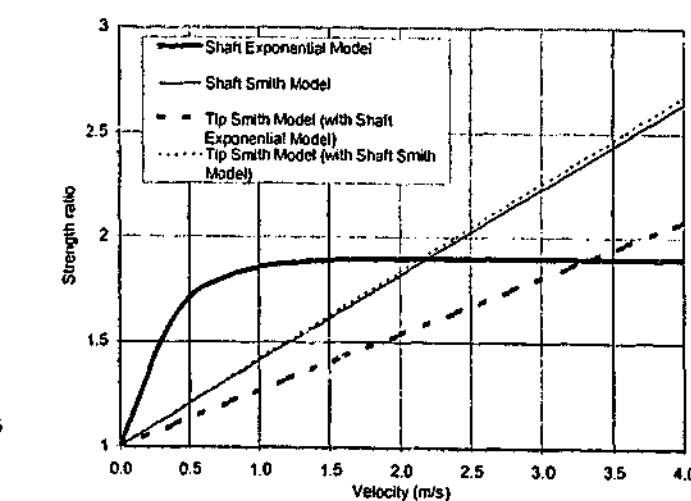
(C) Computed Resistances



(D) Velocities at Top, Middle & Bottom of Pile



(E) Strength Ratio-Velocity Models for Shaft & Tip



ID13
R126/1D OEP 4d609;CL;CL30; Blow: 538

Filename 13 def
Smith Linear Viscous Damping using Rinf for Shaft

(A) Pile Model

Depth (m)	Area (cm ²)	E-Mod (MPa)	Spec Wei (kN/m ³)	Circum (m)	Impedance (kN/m/s)
0	359.74	206579	77.287	2.871	1451.53
29.38	359.74	206579	77.287	2.871	None

Wave Speed 5119.8 m/s

(B) Resistance Distribution

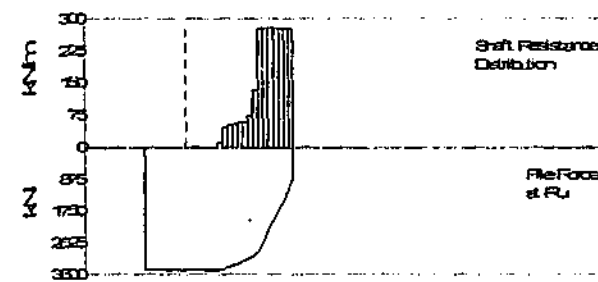
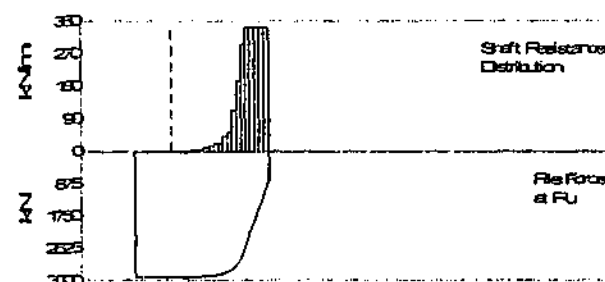
Depth (m)	Ru (kPa)	Unit	Total capacity (kN)
Below	Ru		3338
Grade	(Area)		2549.8
			788.8
1.4	0.9	0.31	
2.5	0.9	0.31	
3.5	1.9	0.64	
4.5	2.4	0.81	
5.5	4.3	1.49	
6.5	7	2.41	
7.5	13.1	4.51	
8.5	17.7	6.07	
9.6	23.6	8.11	
10.6	23.2	7.97	
11.6	43.9	15.1	
12.6	54.6	18.76	
13.6	115.9	39.86	
14.6	192.7	68.32	
15.6	299.0	103.09	
16.6	348.3	119.74	
17.7	348.3	119.74	
18.7	348.3	119.74	
19.7	348.3	119.74	
20.7	348.3	119.74	
Avg Skin	127.5	43.82	
Toe	788.4	1210.63	

Filename 13 rinf nm
Exponential Viscous Damping using Rinf for shaft

(A) Pile Model
As per Smith Linear Viscous Damping

(B) Resistance Distribution

Depth (m)	Ru (kPa)	Unit	Total capacity (kN)
Below	Ru		3304.6
Grade	(Area)		2490.6
			814.0
1.4	0.8	0.27	
2.5	0.8	0.27	
3.5	0.8	0.27	
4.5	0.8	0.27	
5.5	0.8	0.27	
6.5	11.9	4.1	
7.5	48.1	16.55	
8.5	52.8	18.15	
9.6	56.4	19.4	
10.6	61.1	20.99	
11.6	61.1	20.99	
12.6	70.1	24.15	
13.6	138.1	46.77	
14.6	284.1	97.65	
15.6	283.2	97.34	
16.6	283.2	97.34	
17.7	283.2	97.34	
18.7	283.2	97.34	
19.7	283.2	97.34	
20.7	283.2	97.34	
Avg Skin	124.5	42.81	
Toe	814.1	1250.01	



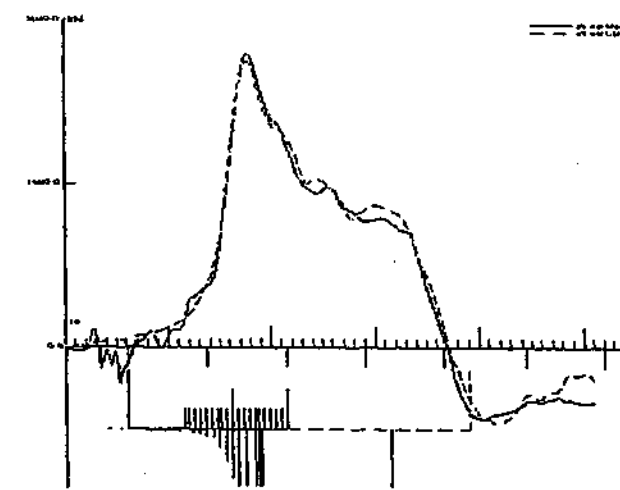
(C) CAPWAP Parameters

JS	SS	QS	UN	CS	LS	PI	OP
3.027	1.7	0.5	1	0.07	0	0.01	0
JT	ST	QT	TG	CT	LT	PL	
0.429	0.7B	4	0	1	0	0	

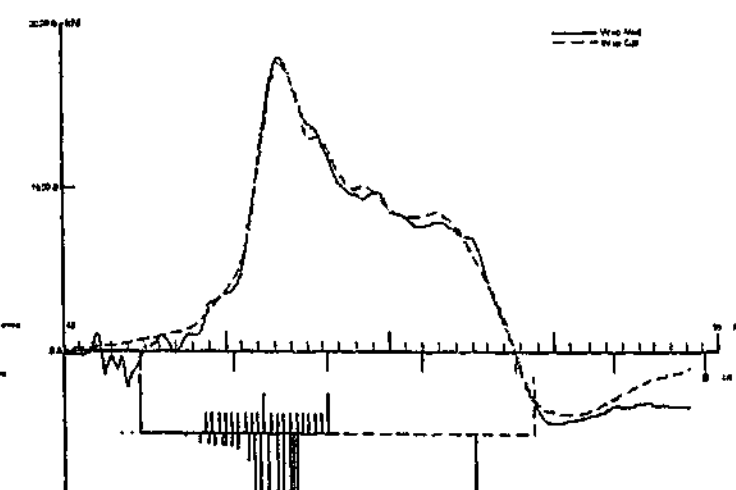
(C) CAPWAP Parameters

JS	SS	QS	UN	CS	LS	PI	OP
3.87	2.225	0.5	0.65	0.5	0	0.01	0
JT	ST	QT	TG	CT	LT	PL	
0.114	0.2	4.2	0	1	0	3	

(D) Match
CAPWAP match quality: 3.81 (Wave Up Match)
Observed: final set = 2.796 mm; blow count = 358 b/m
Computed: final set = 4.803 mm; blow count = 208 b/m



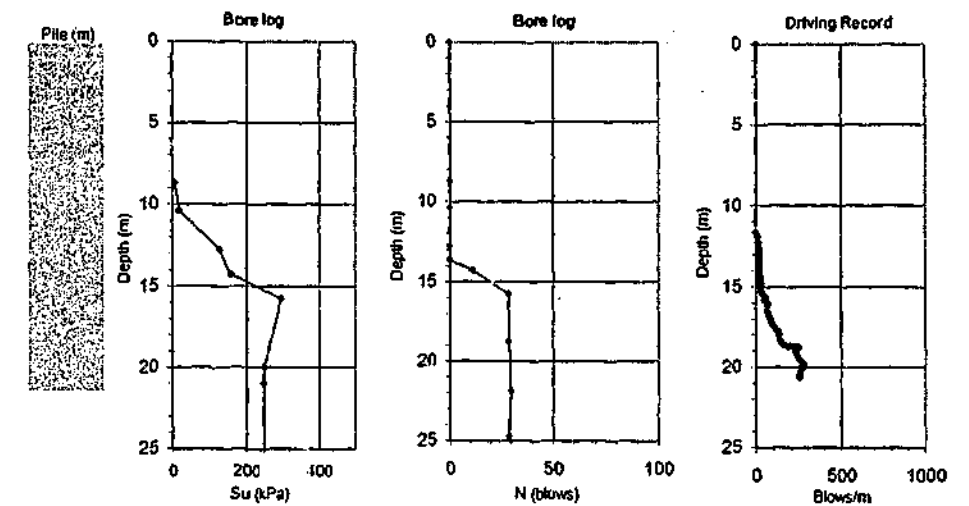
(D) Match
CAPWAP match quality: 3.55 (Wave Up Match)
Observed: final set = 2.796 mm; blow count = 358 b/m
Computed: final set = 4.513 mm; blow count = 222 b/m



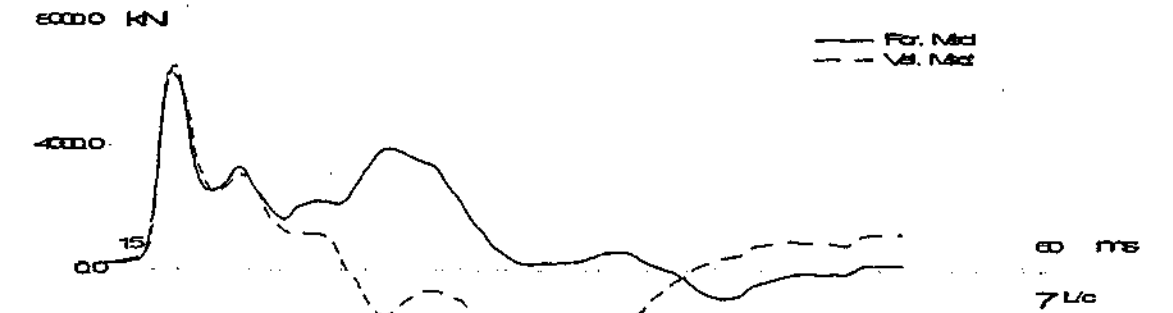
(A) Soil Data
Depth (m) Soil description
0.0 Very soft to soft CLAY (mc=40-85)

13.6 Very stiff to hard CLAY (mc=20-25)

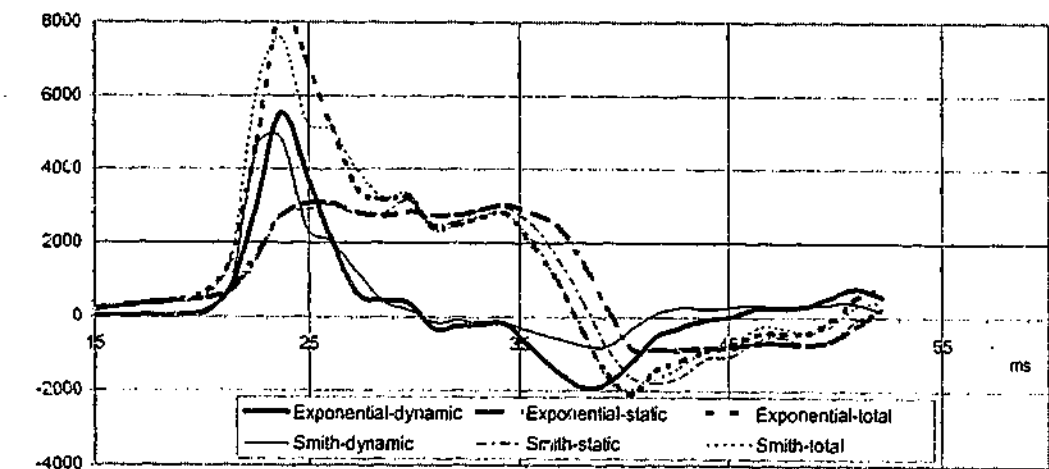
RIVER LEVEL: 2.00 ft



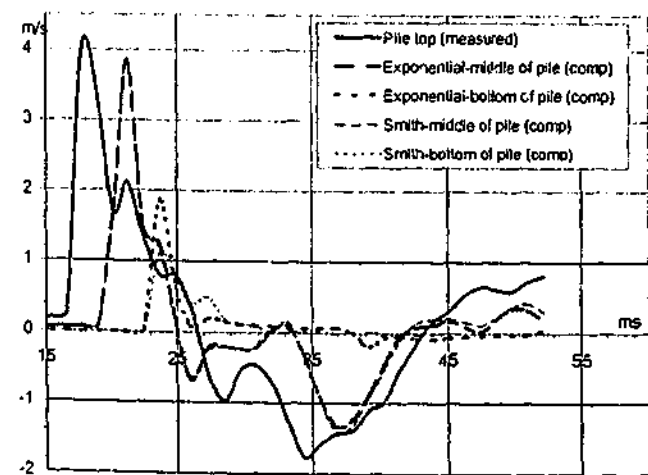
(B) Measured Force & Velocity at Pile Top



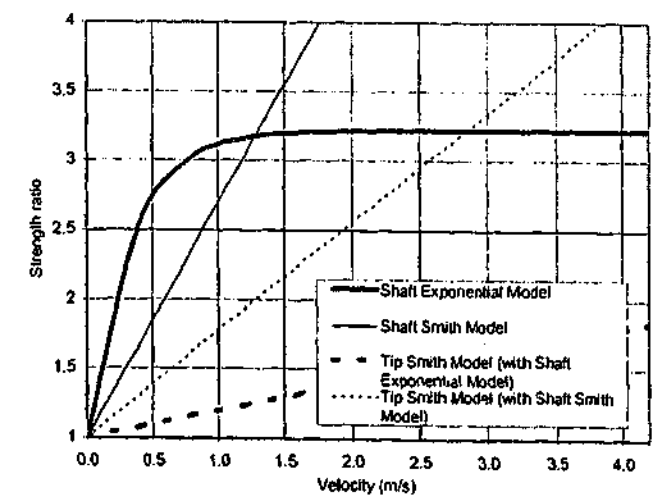
(C) Computed Resistances



(D) Velocities at Top, Middle & Bottom of Pile



(E) Strength Ratio-Velocity Models for Shaft & Tip



ID14
R129/1D TIMB 1d169;CL;CL-TILL N=19;

Filename 14 def
Smith Linear Viscous Damping using Rult for Shaft

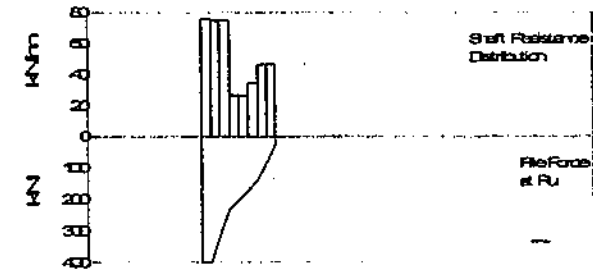
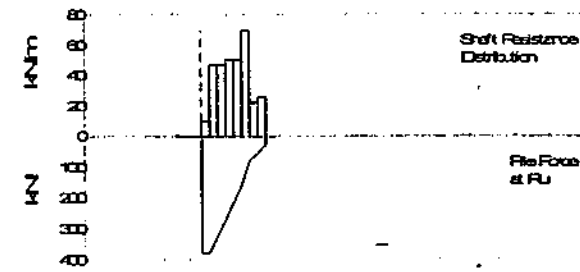
Filename 14 nm rinst
Exponential Viscous Damping using Rinst for shaft

(A) Pile Model
Depth m Area cm² E-Mod MPa Spec Wei kN/m³ Circum m
0 856.77 8957.4 7.54 1.036
8.84 322.58 8957.4 7.54 0.84
Impedance decreases from 216.08kN/m/s at depth of 1.10m to 83.42kN/m/s at depth of 8.84m
Wave Speed 3413.2 m/s

(A) Pile Model
As per Smith Linear Viscous Damping

Depth	Ru	Unit	Total capacity	386.5	kN
Below	Ru		Shaft capacity	360.9	kN
Grade	(Area)		Toe capacity	25.6	kN
m	kN	kPa			
1.1	11.3	10.13			
2.2	52.6	49.48			
3.3	52.6	52.17			
4.4	56.5	59.26			
5.5	56.5	62.86			
6.6	77.3	91.62			
7.7	24.8	31.47			
8.8	29.2	39.82			
Avg Skin	45.1	48.72			
Toe	25.6	788.51			

Depth	Ru	Unit	Total capacity	481.6	kN
Below	Ru		Shaft capacity	453.3	kN
Grade	(Area)		Toe capacity	28.5	kN
m	kN	kPa			
1.1	84.5	75.63			
2.2	83	78.11			
3.3	83	82.35			
4.4	29.9	31.4			
5.5	29.9	33.32			
6.6	38.9	46.15			
7.7	52	65.85			
8.8	52	70.75			
Avg Skin	56.7	61.19			
Toe	28.3	871.41			



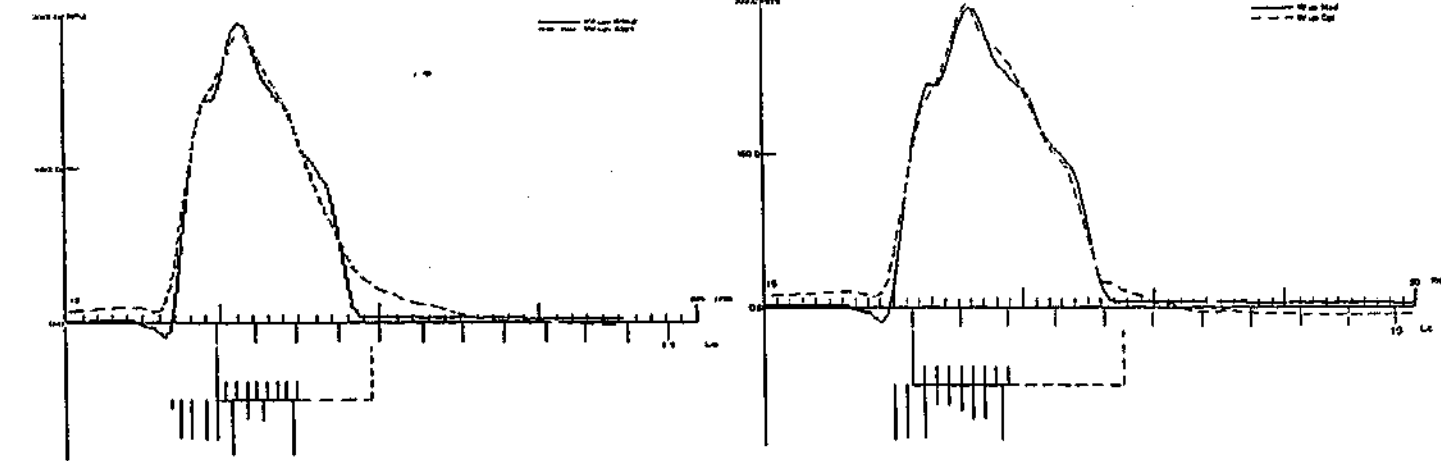
(C) CAPWAP Parameters

JS	SS	QS	UN	CS	LS	PI	OP
2.244	1.4	1	0.01	1	0	0.02	0
JT	ST	QT	TG	CT	LT	PL	
0.034	0.3	1	2	0.01	0	1.5	

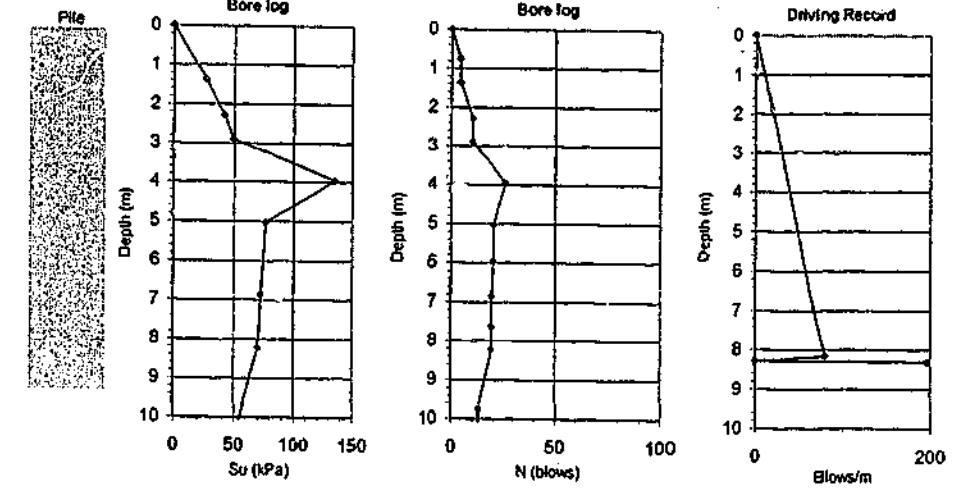
(C) CAPWAP Parameters

JS	SS	QS	UN	CS	LS	PI	OP
2.014	1	2	1	0.5	0	0.02	0
JT	ST	QT	TG	CT	LT	PL	
0.025	0.2	3	0	1	0	0.15	

(D) Match
CAPWAP match quality: 2.82 (Wave Up Match)
Observed: final set = 5.080 mm; blow count = 197 b/m
Computed: final set = 4.741 mm; blow count = 211 b/m



(A) Soil Data
Depth (m) Soil description
0 Organic, Silt, Clay, Loam
0.762 Organic, Silt, Clay, Till (mc=30%)
1.3716 Silt, Clay, Loam, Till (mc=25%)
2.286 Silt, Clay, Loam, Till (mc=22%)
2.8956 Silt, Clay, Loam, Till (mc=20%)

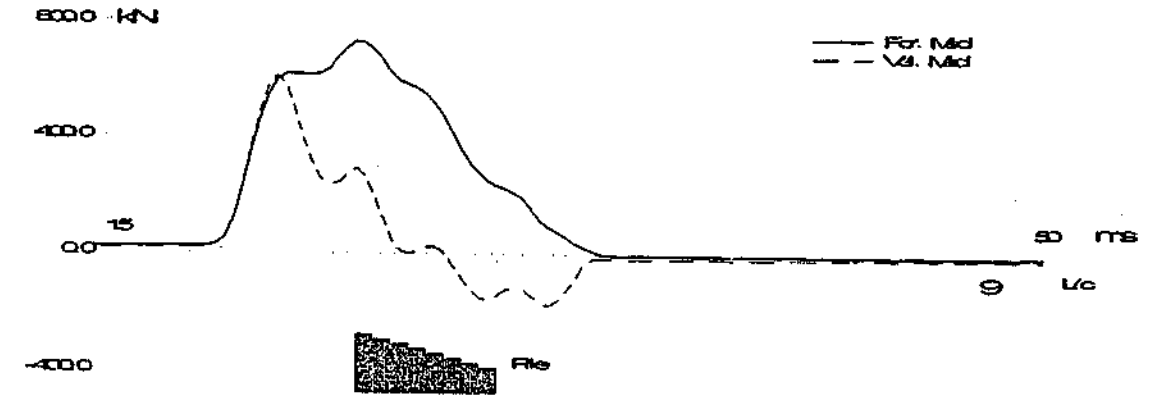


5.9436 Clay, Till (mc=17%)

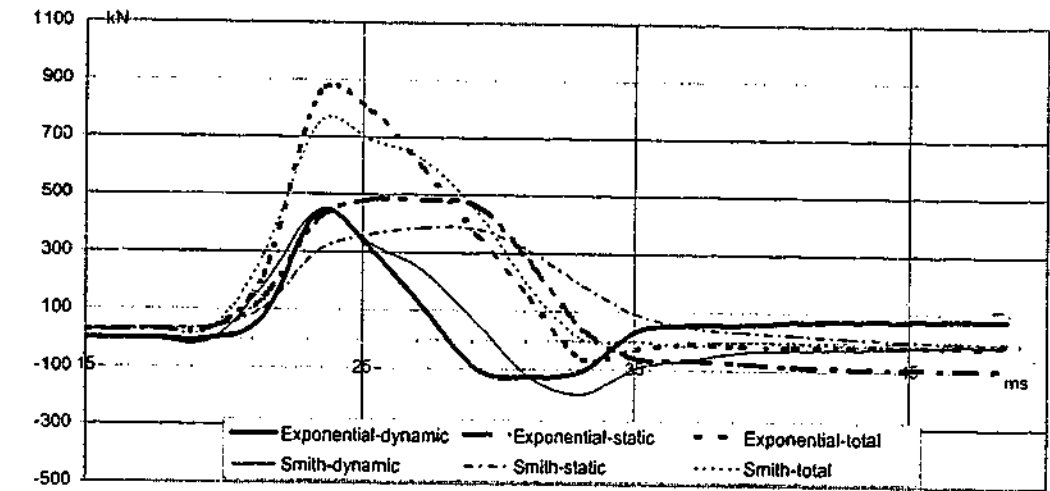
7.62 Clay, Till (mc=21%)

11.43 Clay, Loam, Till (mc=20%)
12.0396 Clay, Till

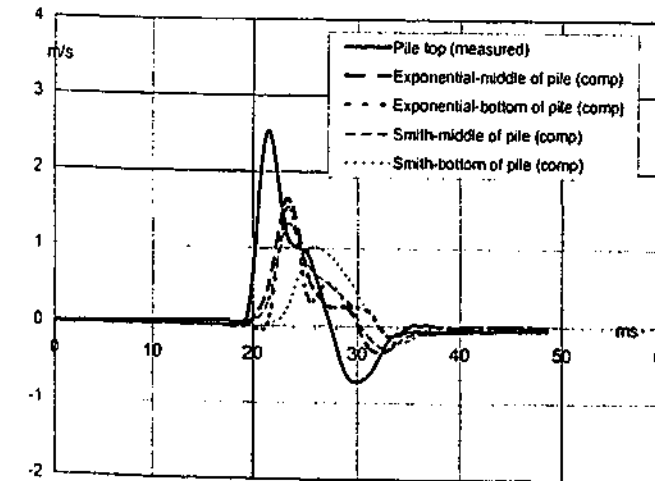
(B) Measured Force & Velocity at Pile Top



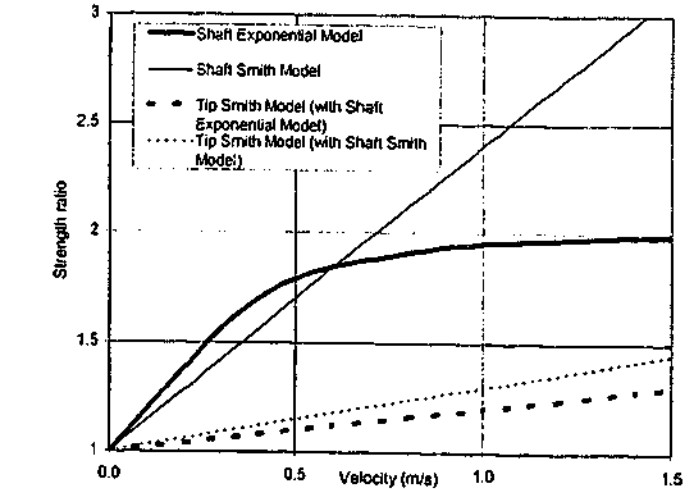
(C) Computed Resistances



(D) Velocities at Top, Middle & Bottom of Pile



(E) Strength Ratio-Velocity Models for Shaft & Tip

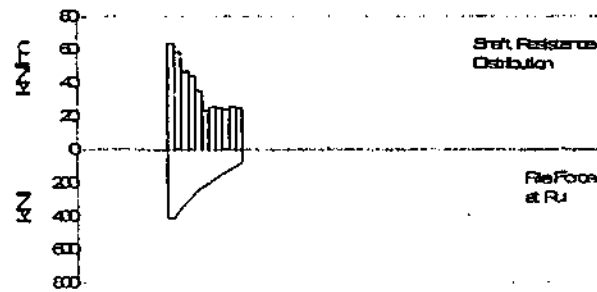


ID15
R1403D PSC >1708074X;SA;SA9

Filename 15def
Smith Linear Viscous Damping using Rult for Shaft

Depth (m)	Area (cm ²)	E-Mod (MPa)	Spec Wel (kN/m ³)	Circum (m)	Impedance (kN/m/s)
0	609.03	34686.4	23.563	1.016	555.84
10.9	609.03	34686.4	23.563	1.016	555.84

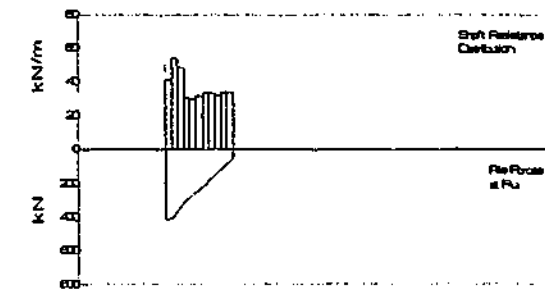
Depth (m)	Ru (kN/m)	Unit (kPa)	Total capacity (kN)
1	83.4	82.99	470.9
2	58.2	57.82	396.9
3	46.7	46.4	74
4	44	43.72	
5	35.4	35.17	
5.9	24	23.85	
6.9	25.6	25.44	
7.9	25.1	24.94	
8.9	24	23.85	
9.9	25.6	25.44	
10.9	24.9	24.74	
Avg Skin			36.1
Toe			74



Filename 15 rult nm
Exponential Viscous Damping using Rult for shaft

(A) Pile Model
As per Smith Linear Viscous Damping

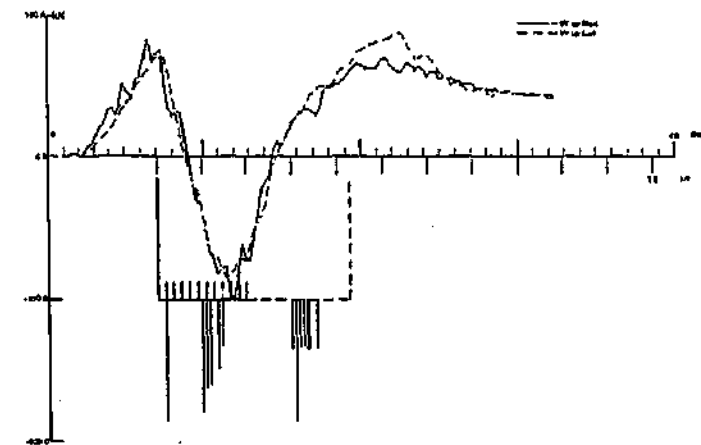
Depth (m)	Ru (kN/m)	Unit (kPa)	Total capacity (kN)
1	40.9	40.64	450.8
2	53.2	52.66	396.4
3	46	47.69	52.4
4	30.4	30.2	
5	29.9	29.71	
5.9	31.6	31.4	
6.9	33.3	33.09	
7.9	32.7	32.49	
8.9	31.6	31.4	
9.9	33.3	33.09	
10.9	33.5	33.28	
Avg Skin			36.2
Toe			52.4



(C) CAPWAP Parameters

JS	SS	QS	UN	CS	LS	PI	OP
0.473	0.662	6.4	1	0.5	0	0.02	2
JT	ST	QT	TG	CT	LT	PL	
0.133	1	14	0	1	0	0.89	

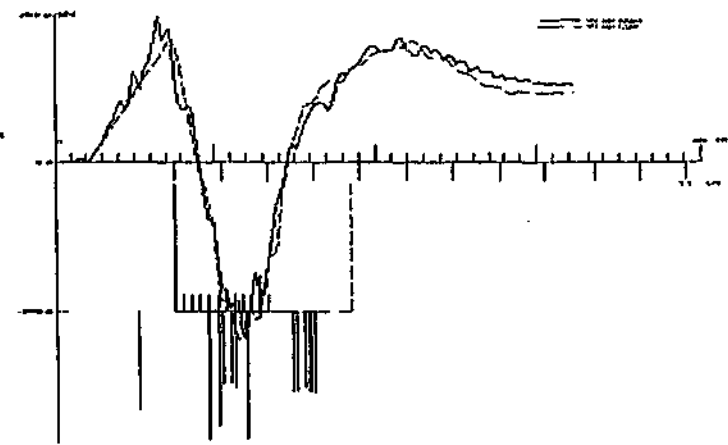
(D) Match
CAPWAP match quality: 3.25 (Wave Up Match)
Observed: final set = 10.510 mm; blow count = 95 b/m
Computed: final set = 11.564 mm; blow count = 86 b/m



(C) CAPWAP Parameters

JS	SS	QS	UN	CS	LS	PI	OP
0.659	0.92	2.54	0	1	0	0.02	0
JT	ST	QT	TG	CT	LT	PL	
0.073	0.78	7	0	1	0	0.6	

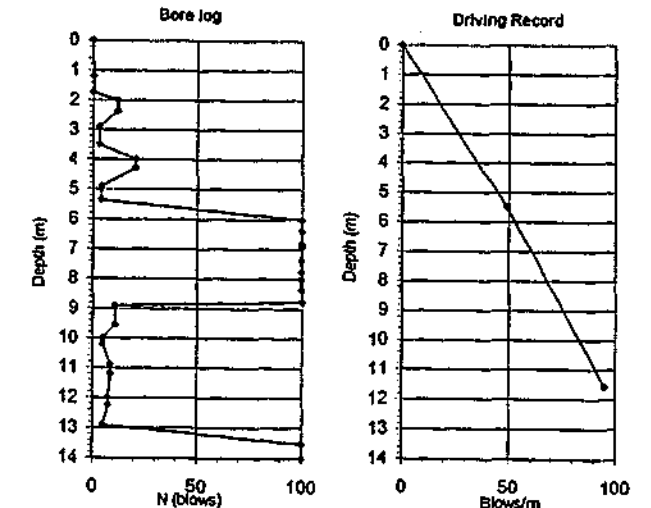
(D) Match
CAPWAP match quality: 3.91 (Wave Up Match)
Observed: final set = 10.510 mm; blow count = 95 b/m
Computed: final set = 12.388 mm; blow count = 81 b/m



(A) Soil Data

Depth (m)	Soil description
1.2	Lean CLAY
1.7	Sandy CLAY
2.4	Clayey SAND
3.5	Silty SAND
5.0	Sandy CLAY
5.4	PEAT
6.4	Fat CLAY
8.4	Lean CLAY
8.6	Poorly graded SAND w/clay
9.5	Poorly graded SAND
13.5	Lean CLAY

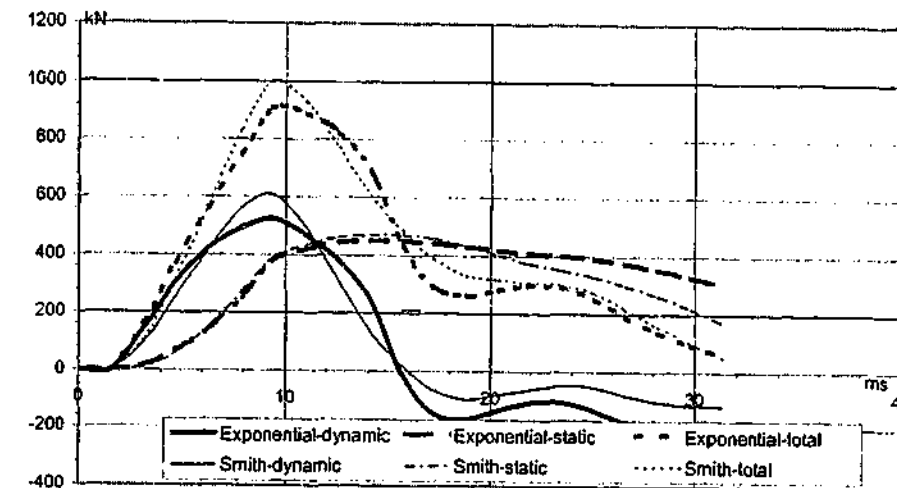
WATER TABLE elevation: unknown



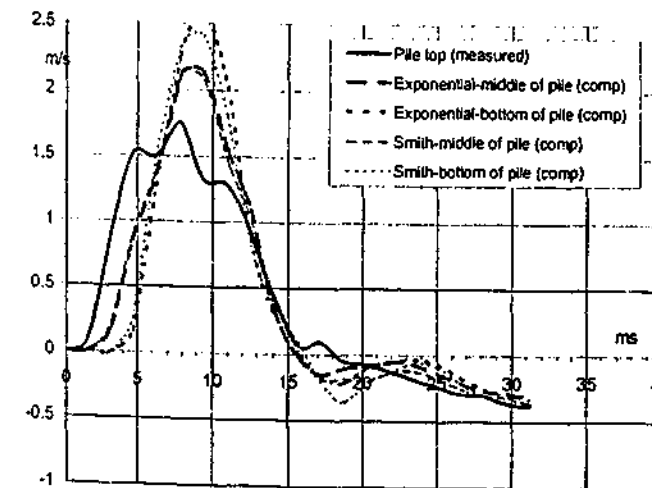
(B) Measured Force & Velocity at Pile Top



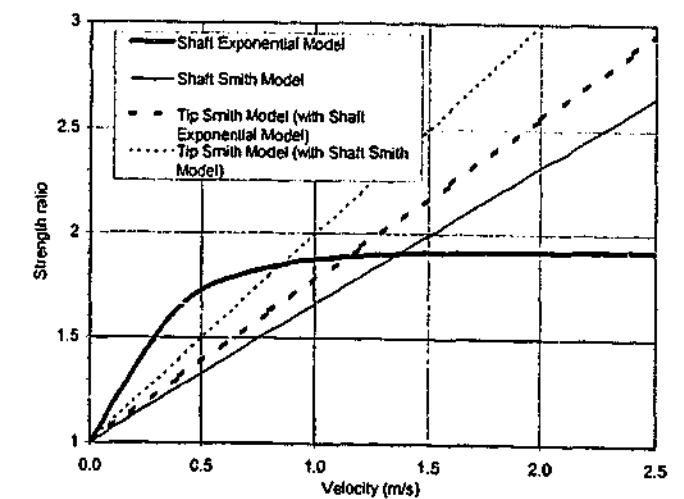
(C) Computed Resistances



(D) Velocities at Top, Middle & Bottom of Pile



(E) Strength Ratio-Velocity Models for Shaft & Tip



ID16
R1433D PSC >17d240264X; SA:SA8; Blow: 538 CAPWAP Ver. 2003-1

Filename 16 def
Smith Linear Viscous Damping using Ruit for Shaft

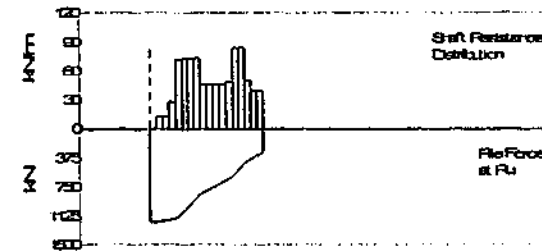
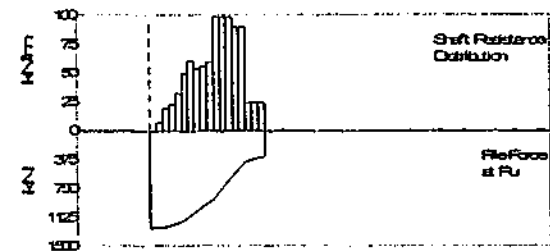
Depth (m)	Area (cm ²)	E-Mod (MPa)	Spec Wei (kN/m ³)	Circum (m)	Impedance (kN/m/s)
0	809.03	34656.4	23.563	1.016	555.84
18.29	809.03	34656.4	23.563	1.016	None

Depth (m)	Ru (kN)	Unit (kPa)	Total capacity (kN)
Below Grade			1257.9
0	0	0	928.1
1	7.6	7.36	329.1
2	19.8	19.17	
3	23.4	22.60	
4.1	33	31.95	
5.1	51.1	49.48	
6.1	61.9	59.94	
7.1	55.8	54.03	
8.1	57	55.19	
9.1	60.7	58.78	
10.2	100.3	97.12	
11.2	100.4	97.22	
12.2	100.4	97.22	
13.2	91.8	88.89	
14.2	91.8	88.89	
15.2	24.3	23.53	
16.3	24.5	23.72	
17.3	24.7	23.92	
18.3	51.6	49.95	
Avg skin	329.8	5420.44	
Toe			

Filename 16 nm rinst
Exponential Viscous Damping using Rinst for shaft

Depth (m)	Ru (kN)	Unit (kPa)	Total capacity (kN)
Below Grade			1199
0	0	0	900.8
1	13.2	12.78	298.4
2	13.4	12.97	
3	29	28.08	
4.1	73.6	71.26	
5.1	75.5	73.1	
6.1	75.5	73.1	
7.1	75.3	72.91	
8.1	47.2	45.7	
9.1	47.2	45.7	
10.2	47.2	45.7	
11.2	47.6	46.09	
12.2	49.9	48.32	
13.2	86.6	83.85	
14.2	86.6	83.85	
15.2	51.8	50.16	
16.3	40.7	39.41	
17.3	41	39.7	
18.3	50	48.48	
Avg skin	298.2	4899.63	
Toe			

Depth (m)	Ru (kN)	Unit (kPa)	Total capacity (kN)
Below Grade			1199
0	0	0	900.8
1	13.2	12.78	298.4
2	13.4	12.97	
3	29	28.08	
4.1	73.6	71.26	
5.1	75.5	73.1	
6.1	75.5	73.1	
7.1	75.3	72.91	
8.1	47.2	45.7	
9.1	47.2	45.7	
10.2	47.2	45.7	
11.2	47.6	46.09	
12.2	49.9	48.32	
13.2	86.6	83.85	
14.2	86.6	83.85	
15.2	51.8	50.16	
16.3	40.7	39.41	
17.3	41	39.7	
18.3	50	48.48	
Avg skin	298.2	4899.63	
Toe			



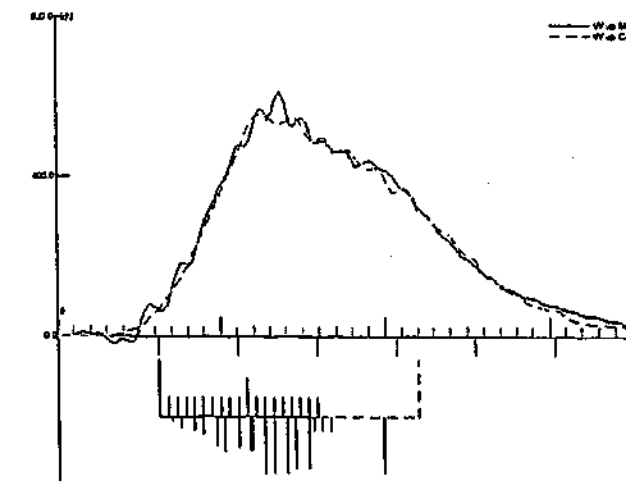
(C) CAPWAP Parameters

JS	SS	QS	UN	CS	LS	PI	OP
0.636	0.501	4.7	0	1	0	0.02	0
JT	ST	QT	TG	CT	LT	PL	
0.459	0.772	6.2	0	1	0	4.9	

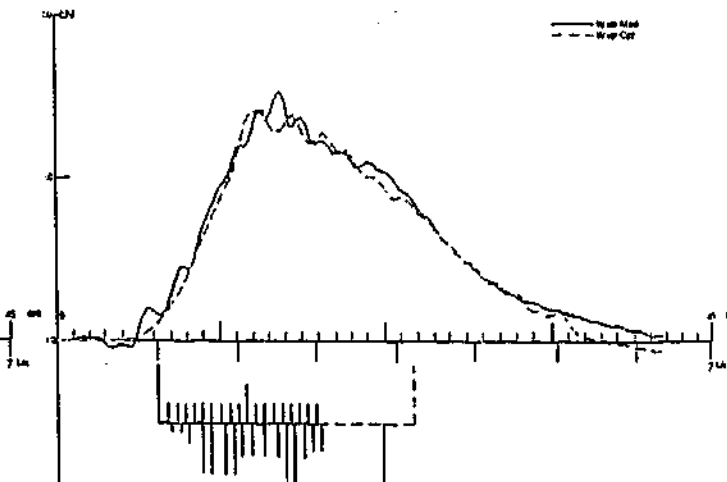
(C) CAPWAP Parameters

JS	SS	QS	UN	CS	LS	PI	OP
1.019	0.628	4.7	0.15	0.8	0	0.02	0
JT	ST	QT	TG	CT	LT	PL	
0.596	1.11	4.9	1.5	1.306	0	3.5	

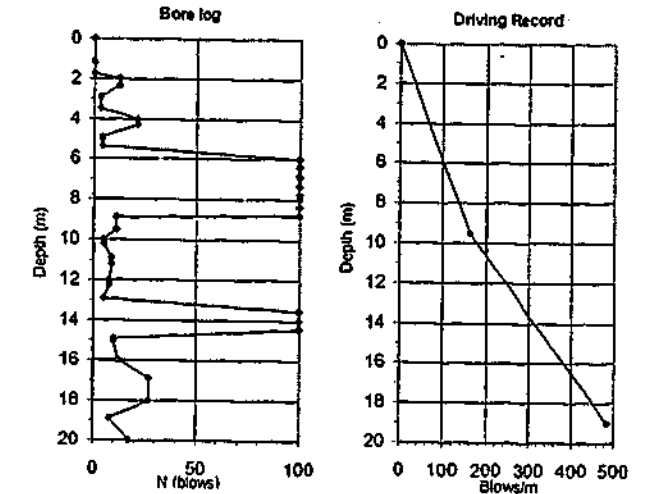
(D) Match
CAPWAP match quality: 3.50 (Wave Up Match)
Observed: final set = 2.058 mm; blow count = 486 b/m
Computed: final set = 0.365 mm; blow count = 2738 b/m



(D) Match
CAPWAP match quality: 4.05 (Wave Up Match)
Observed: final set = 2.058 mm; blow count = 486 b/m
Computed: final set = 1.069 mm; blow count = 935 b/m

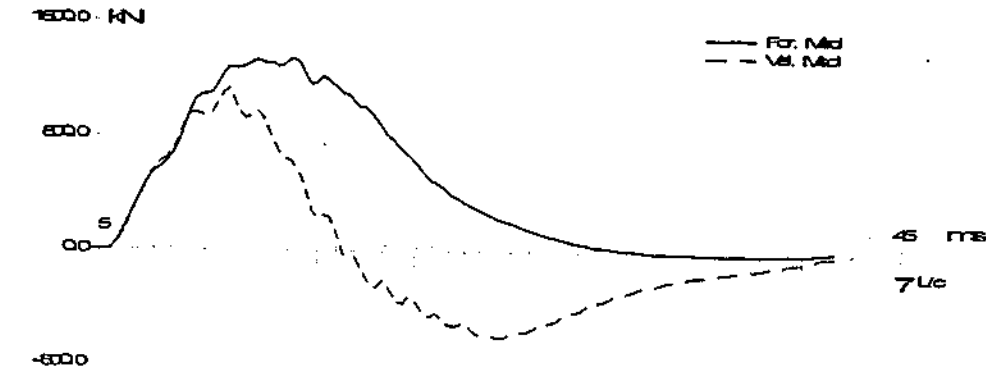


- (A) Soil Data
- 1.2 Lean CLAY (mc=48%;LL=44%;PI=20)
 - 1.7 Sandy CLAY (mc=51%)
 - 2.4 Clayey SAND (mc=37%)
 - 3.5 Silty SAND (mc=40%)
 - 5.0 Sandy CLAY (mc=81%)
 - 5.4 PEAT (mc=27.1)
 - 6.4 Fat CLAY (mc=103%;LL=115%;PI=70%)
 - 8.4 Lean CLAY (mc=73%)
 - 8.8 Poorly graded SAND w/clay (mc=45%)
 - 9.5 Poorly graded SAND (mc=35%)
 - 13.5 Lean CLAY (mc=46%)
 - 14.9 Clayey PEAT (mc=156%)
 - 15.0 Lean CLAY (mc=38%)

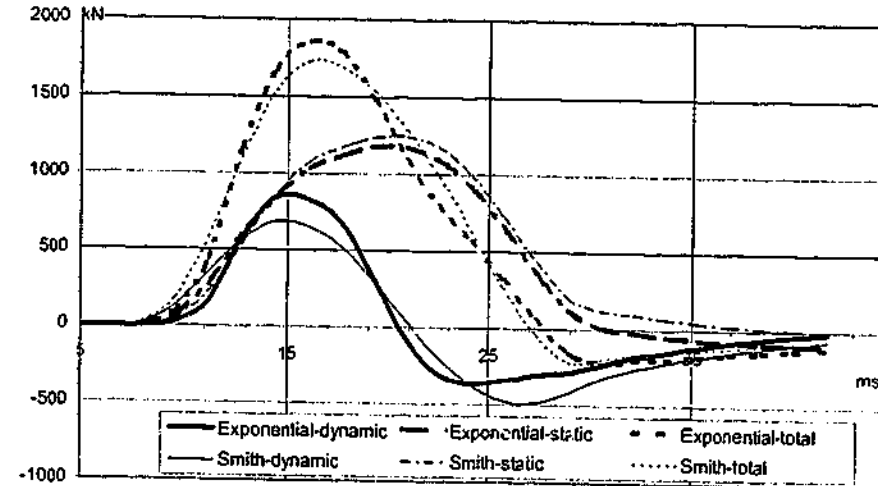


WATER TABLE elevation: unknown

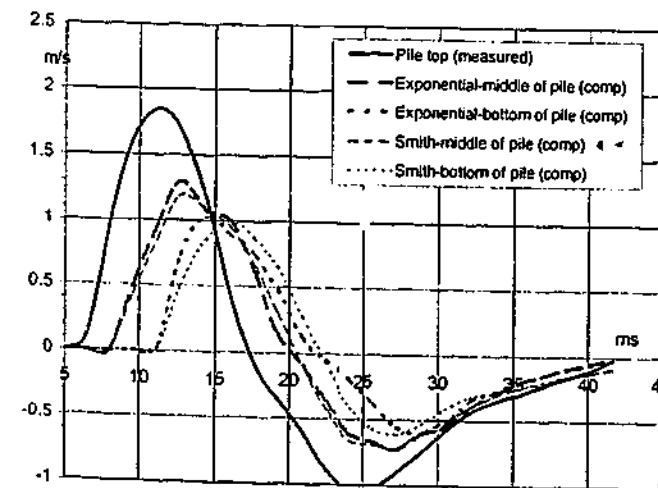
(B) Measured Force & Velocity at Pile Top



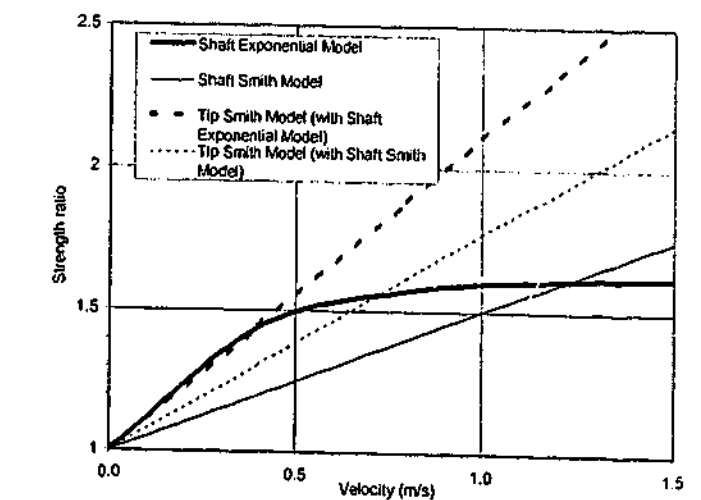
(C) Computed Resistances



(D) Velocities at Top, Middle & Bottom of Pile



(E) Strength Ratio-Velocity Models for Shaft & Tip



ID17

R145/11D CEP 18d200/220X;SA;GRZ7; Blow: 538

Filename 17 def
Smith Linear Viscous Damping using Rult for Shaft

(A) Pile Model

Depth	Area	E-Mod	Spec Wei	Circum	Impedance
m	cm ²	MPa	kN/m ³	m	kN/m/s
0	63.35	206824.9	77.287	1.017	255.76
32	63.35	206824.9	77.287	1.017	None

Added impedance None
Wave Speed 5122.8 m/s

(B) Resistance Distribution

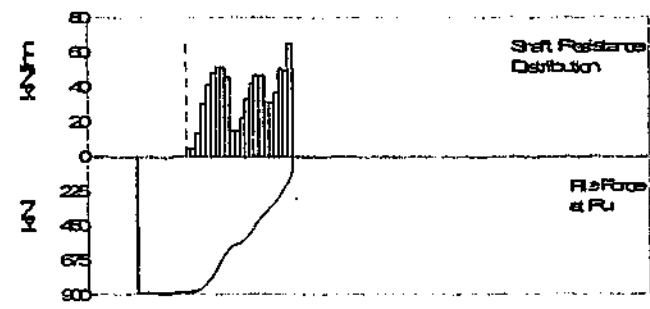
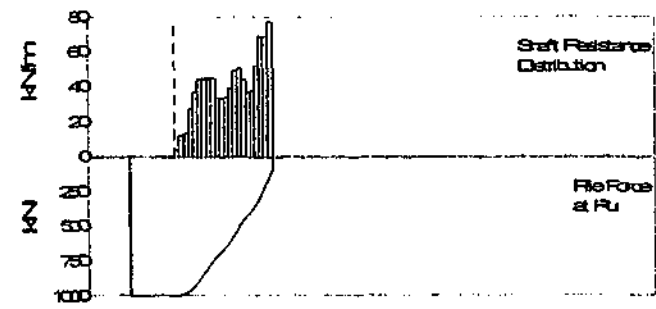
Depth	Ru	Unit	Total capacity	Shaft capacity	Toe capacity
m	kN	kPa	kN	kN	kN
0.3	4.5	4.42	999.1	902.8	96.5
1.3	12.5	12.29			
2.3	13.5	13.27			
3.3	27.5	27.04			
4.3	37.1	36.47			
5.3	44.5	43.75			
6.3	44.9	44.14			
7.3	44.9	44.14			
8.3	45.1	44.34			
9.3	33.8	33.23			
10.3	33.8	33.23			
11.3	34.2	33.62			
12.3	39.7	39.03			
13.3	49.3	48.47			
14.3	50.7	49.85			
15.3	44.5	43.75			
16.3	37.1	36.47			
17.3	37.9	37.26			
18.3	52.1	51.22			
19.3	68.9	67.74			
20.3	68.9	67.74			
21.3	77.4	76.1			
Avg Skin	41	40.34			
Toe	96.3	1169.13			

Filename 17 rinst nm
Exponential Viscous Damping using Rinst for shaft

(A) Pile Model
As per Smith Linear Viscous Damping

(B) Resistance Distribution

Depth	Ru	Unit	Total capacity	Shaft capacity	Toe capacity
m	kN	kPa	kN	kN	kN
0.3	4.4	4.33	880.4	779.5	100.11
1.3	4.4	4.33			
2.3	13.9	13.87			
3.3	30.8	30.28			
4.3	41.6	40.8			
5.3	48.4	47.58			
6.3	51.5	50.63			
7.3	51.5	50.63			
8.3	45.9	45.13			
9.3	15.1	14.85			
10.3	15.1	14.85			
11.3	22.2	21.83			
12.3	33.1	32.54			
13.3	42.1	41.39			
14.3	47	46.21			
15.3	47	46.21			
16.3	31.8	31.07			
17.3	31.5	30.97			
18.3	36.8	36.18			
19.3	50.8	49.75			
20.3	49.5	48.67			
21.3	65.5	64.4			
Avg Skin	35.4	34.83			
Toe	100.9	1224.98			



(C) CAPWAP Parameters

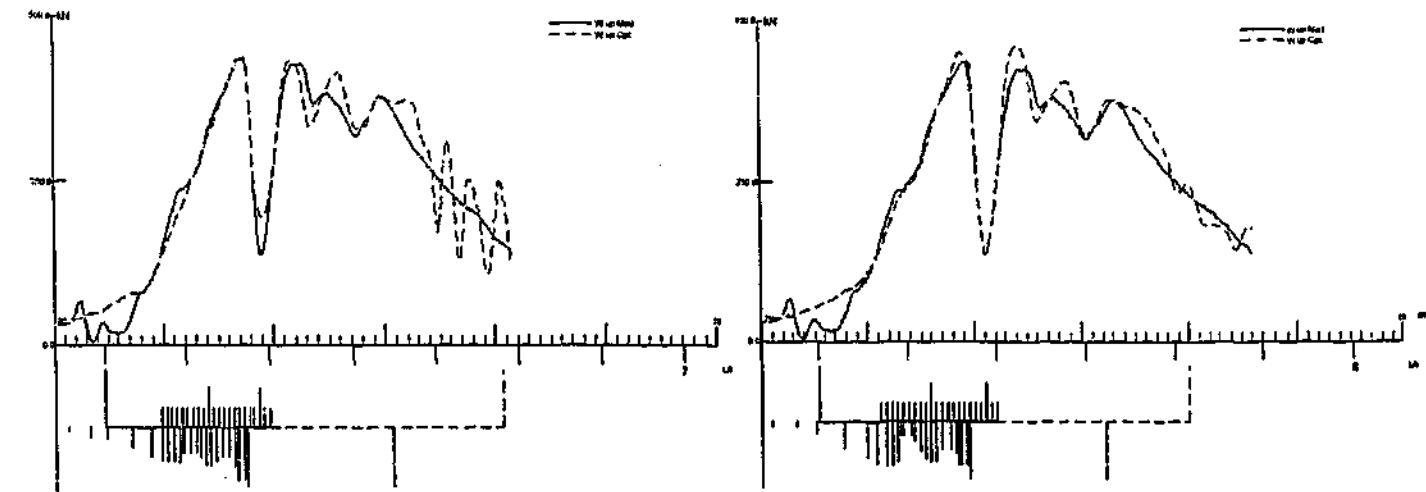
JS	SS	QS	UN	CS	LS	PI	OP
0.534	0.151	0.3	0.01	1	0	0.01	1
JT	ST	QT	TG	CT	LT	PL	
0.09	0.239	7	8	1	0	0	

(C) CAPWAP Parameters

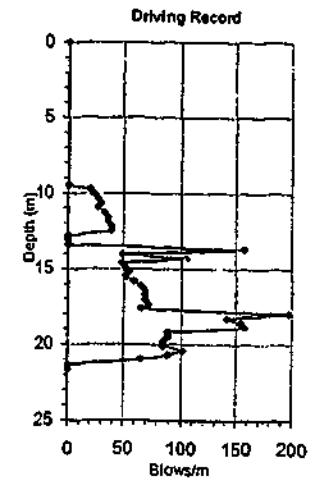
JS	SS	QS	UN	CS	LS	PI	OP
1.22	0.4	0.3	0	1	0	0.01	0
JT	ST	QT	TG	CT	LT	PL	
0.039	0.1	3	11	1	0	0	

(D) Match
CAPWAP match quality: 5.75 (Wave Up Match)
Observed: final set = 15.240 mm; blow count = 66 bl/m
Computed: final set = 17.502 mm; blow count = 57 bl/m

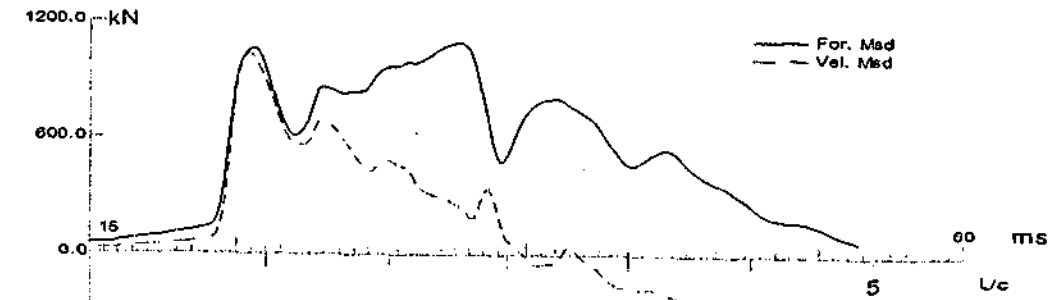
(D) Match
CAPWAP match quality: 4.48 (Wave Up Match)
Observed: final set = 15.240 mm; blow count = 66 bl/m
Computed: final set = 17.225 mm; blow count = 58 bl/m



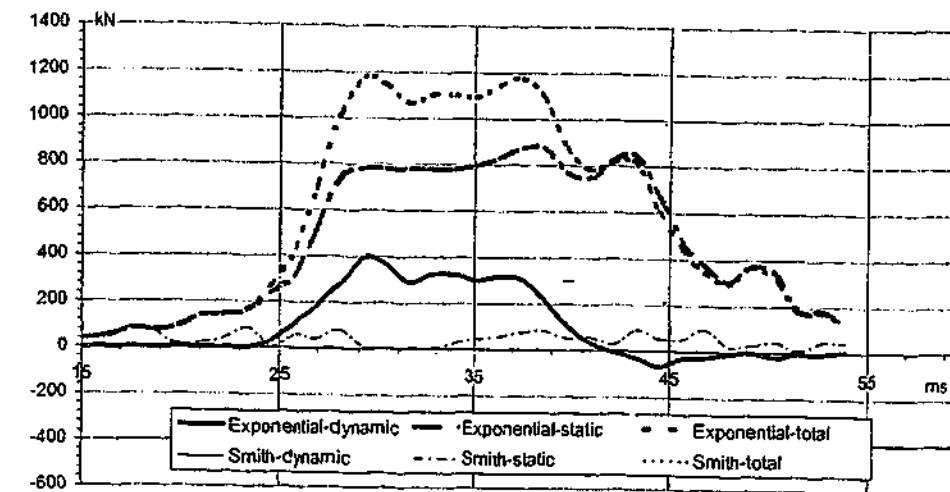
(A) Soil Data
Depth (m) Soil description



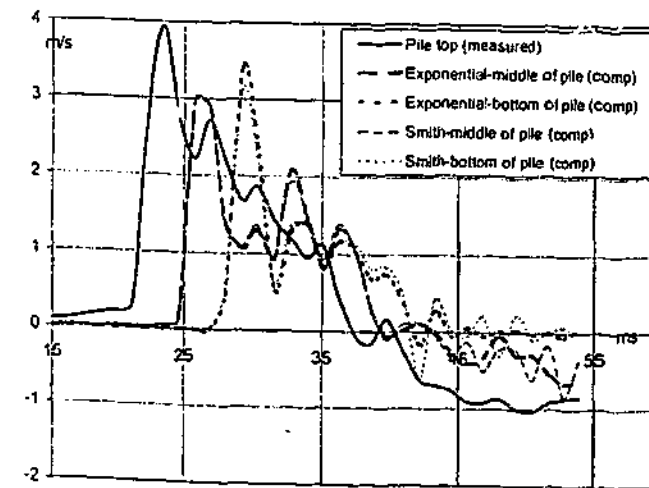
(B) Measured Force & Velocity at Pile Top



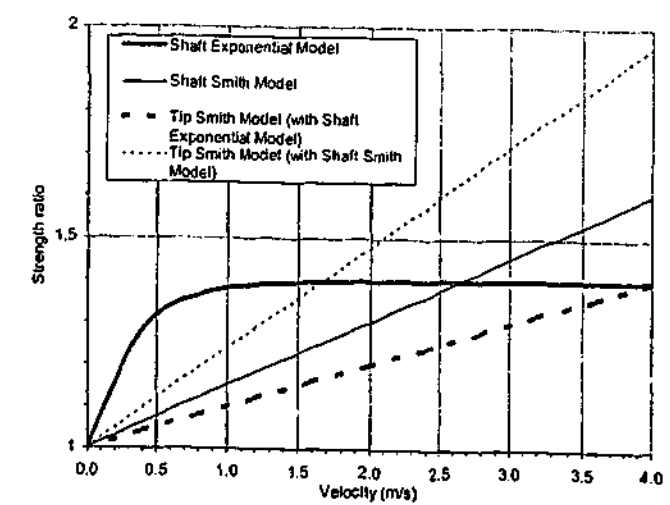
(C) Computed Resistances



(D) Velocities at Top, Middle & Bottom of Pile



(E) Strength Ratio-Velocity Models for Shaft & Tip



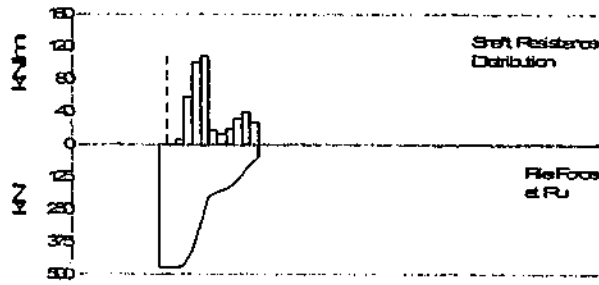
ID18

R148.75D PSC 6d180/200X;CLSL;CLSL18

Filename 18 del
Smith Linear Viscous Damping using Rult for Shaft

Depth	Area	E-Mod	Spec We	Circum	Impedance
m	cm ²	MPa	kN/m ³	m	814.26 kN/m/s
0	929.03	31972.9	23.583	1.219	Added Impedance None
12.04	929.03	31972.9	23.583	1.219	Wave Speed 3200.0 m/s

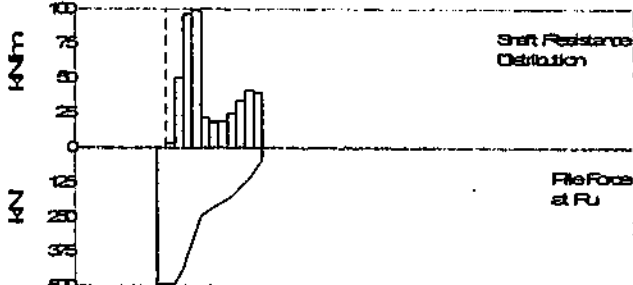
(B) Resistance Distribution		Total capacity	479.7	kN
Depth	Ru	Unit	Shaft capacity	430
Below	Ru	Unit	Toe capacity	49.9
Grade	(Area)			
m	kN	kPa		
1	0	0		
2	6.1	5.01		
3	59.3	48.49		
4	101.8	83.03		
5	109.6	89.63		
6	17.8	14.52		
7	13.4	10.83		
8	20.1	16.44		
9	33	26.95		
10	41	33.55		
11	28.2	23.03		
Avg Skin	39.1	31.95		
Toe	49.7	535.04		



Filename 18 nm rinst
Exponential Viscous Damping using Rinst for shaft

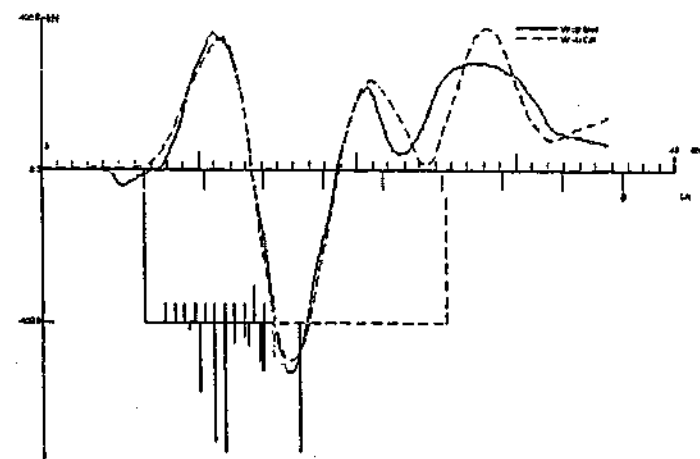
(A) Pile Model		Total capacity	499.7	kN
Depth	Ru	Unit	Shaft capacity	454.9
Below	Ru	Unit	Toe capacity	44.8
Grade	(Area)			
m	kN	kPa		
1	3.8	3.92		
2	51.1	41.77		
3	97.1	79.38		
4	99.9	81.72		
5	22.3	18.28		
6	19.2	15.68		
7	19.8	16.18		
8	25.4	20.78		
9	34.5	28.18		
10	41.7	34.1		
11	40.4	33.02		
Avg Skin	41.4	33.82		
Toe	44.8	481.9		

(B) Resistance Distribution		Total capacity	499.7	kN
Depth	Ru	Unit	Shaft capacity	454.9
Below	Ru	Unit	Toe capacity	44.8
Grade	(Area)			
m	kN	kPa		
1	3.8	3.92		
2	51.1	41.77		
3	97.1	79.38		
4	99.9	81.72		
5	22.3	18.28		
6	19.2	15.68		
7	19.8	16.18		
8	25.4	20.78		
9	34.5	28.18		
10	41.7	34.1		
11	40.4	33.02		
Avg Skin	41.4	33.82		
Toe	44.8	481.9		



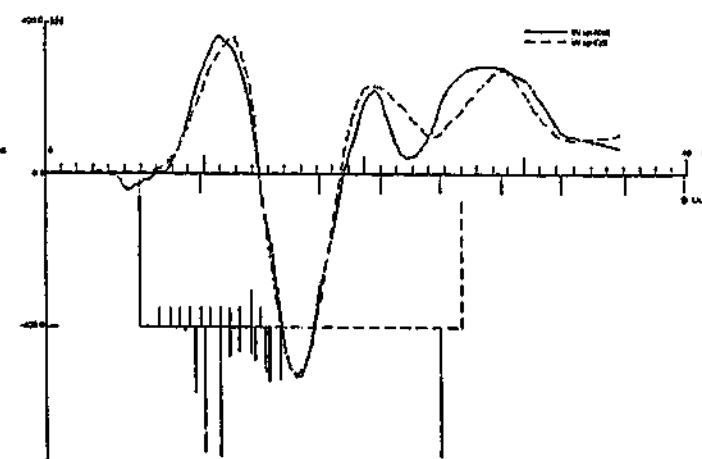
(C) CAPWAP Parameters							
JS	SS	QS	UN	CS	LS	PI	OP
0.436	0.843	3.8	0.415	1	0	0.02	0
JT	ST	QT	TG	CT	LT	PL	
0.067	1.117	5.08	3	1	0	3.2	

(D) Match
CAPWAP match quality: 4.68 (Wave Up Match)
Observed: final set = 11.723 mm; blow count = 85 b/m
Computed: final set = 11.209 mm; blow count = 89 b/m



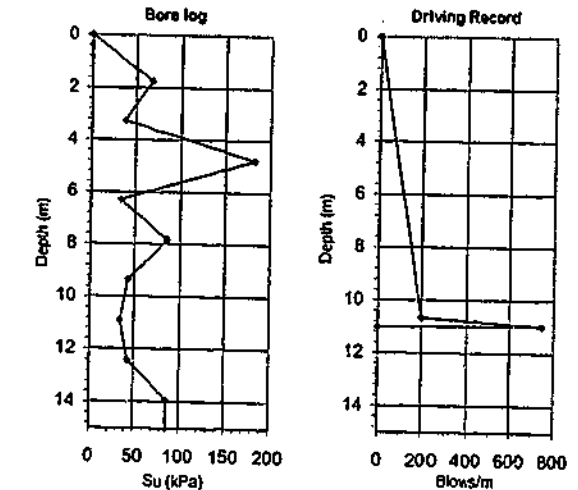
(C) CAPWAP Parameters							
JS	SS	QS	UN	CS	LS	PI	OP
0.704	1.284	4.1	0	1	0	0.02	0
JT	ST	QT	TG	CT	LT	PL	
0.029	0.543	9.8	3.3	0.9	0	4.35	

(D) Match
CAPWAP match quality: 4.25 (Wave Up Match)
Observed: final set = 11.723 mm; blow count = 85 b/m
Computed: final set = 11.356 mm; blow count = 88 b/m

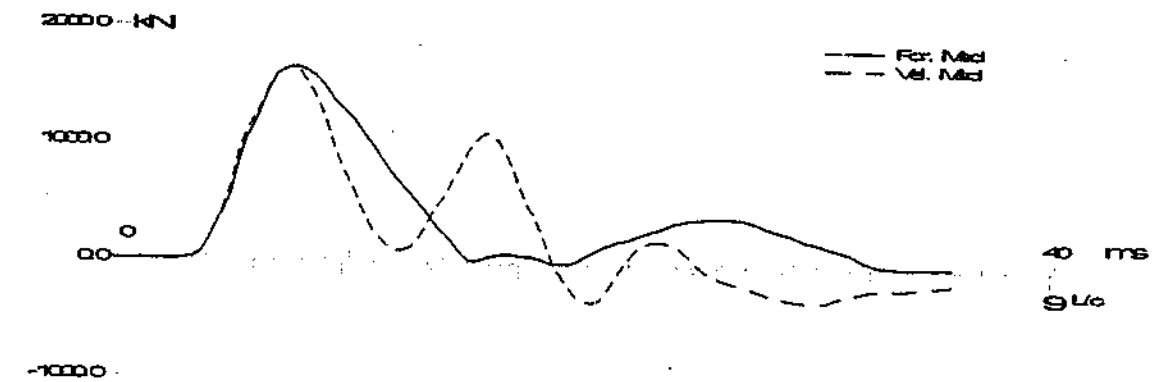


(A) Soil Data
Depth (m) Soil description
0 Stiff, brown CLAY, dry to damp

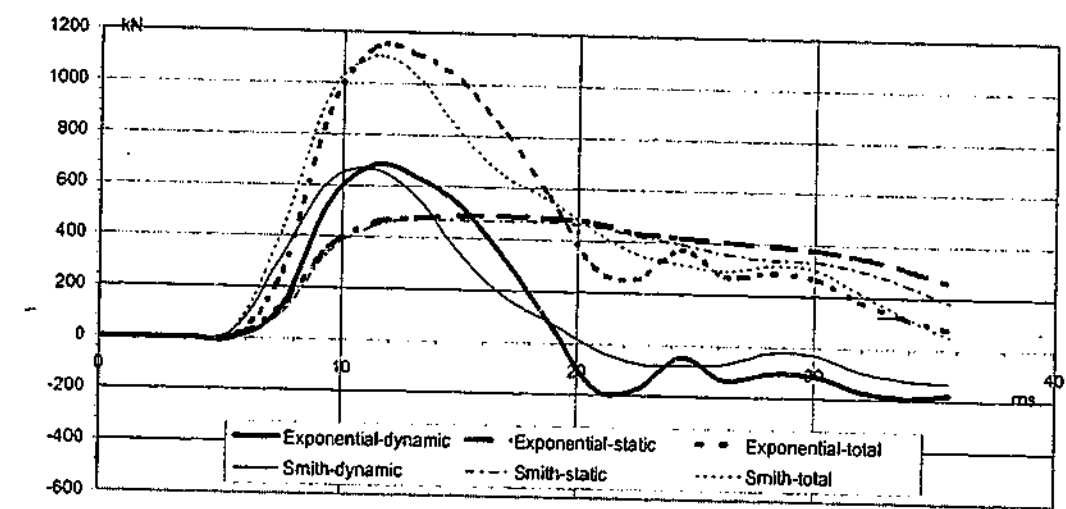
- 2.65176 Soft, gray brown with limonite staining, damp silty CLAY, occasional gravel
- 4.79536 Dense, brown, fine to coarse grained gravelly silty SAND, damp
- 6.30836 Soft, gray brown silty CLAY, moist, some limonite staining
- 7.83336 Slightly compact, gray brown, very fine-to-fine-grained silty clayey SAND, moist
- 8.74776 Soft, dark gray CLAY with limonite staining, moist
- 10.27176 Soft, gray with limonite mottling silty CLAY, moist
- 13.92936 Compact, gray, very fine-to-fine-grained clayey SAND, wet w/limonite staining
- 14.84376 Stiff, gray, interbedded silty CLAY & clayey SILT, w/ limonite staining
- 16.50136 Dense, brown, fine-to-coarse-grained silty sandy GRAVEL, wet
- 20.02536 Gravel common to plus 1.4", mostly 0.25" to 0.5"



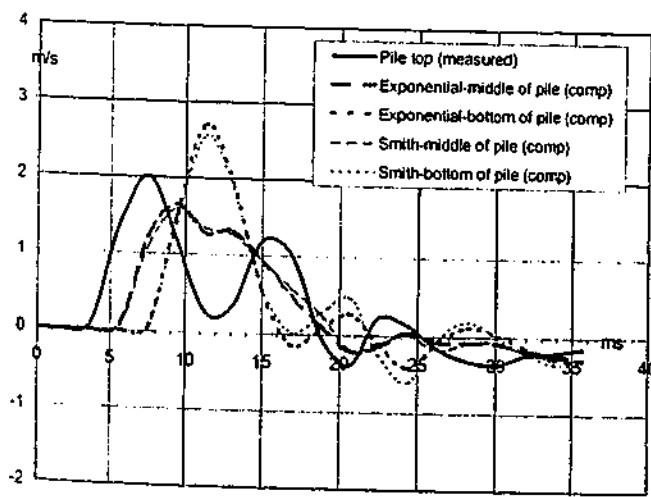
(B) Measured Force & Velocity at Pile Top



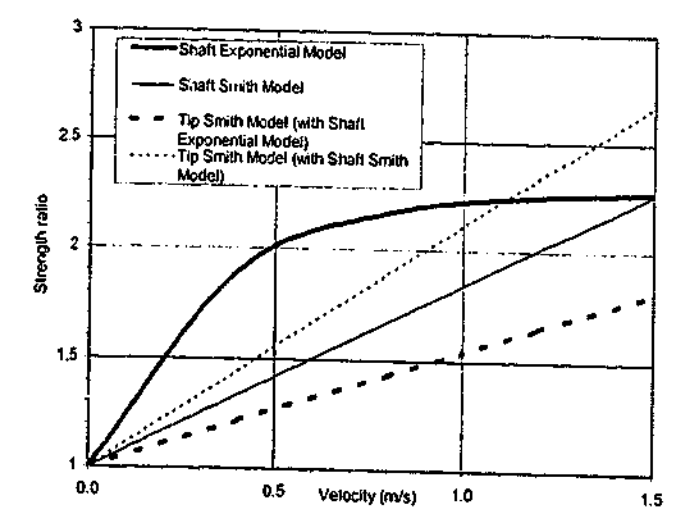
(C) Computed Resistances



(D) Velocities at Top, Middle & Bottom of Pile



(E) Strength Ratio-Velocity Models for Shaft & Tip



ID19

Filename 19 def
Smith Linear Viscous Damping using Rult for Shaft

(A) Pile Model

Depth	Area	E-Mod	Spec Wei	Circum	Impedance
m	cm ²	MPa	kN/m ³	m	1348.97 kN/m/s
0	1264.51	47384.5	23.563	1.422	Added Impedance None
42.06	1264.51	47384.5	23.563	1.422	Wave Speed 3911.0 m/s

(B) Resistance Distribution

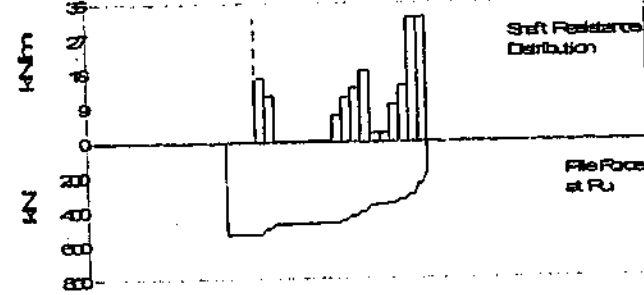
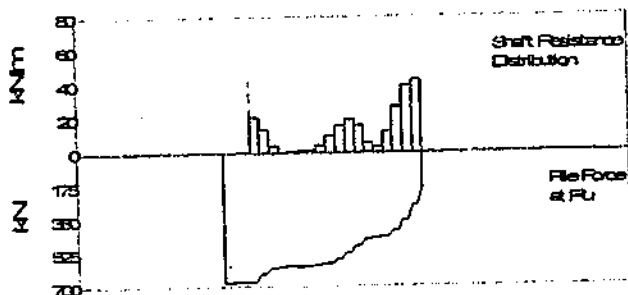
Depth	Ru	Unit	Total capacity
Below	Ru	(Area)	Shaft capacity
Grade	m	kPa	Toe capacity
1.9	42.6	15.03	669.9 kN
3.9	28.1	9.87	484.9 kN
5.9	8.5	2.98	185.2 kN
7.9	0.3	0.11	
9.9	1.2	0.42	
11.9	2.7	0.85	
13.9	3.8	1.33	
15.9	8.5	2.98	
17.9	20.5	7.2	
19.9	32.4	11.38	
21.9	39.5	13.87	
23.9	32.4	11.38	
26	11.4	4	
28	7.4	2.8	
30	25.8	9.06	
32	53.9	18.92	
34	79.5	27.91	
36	86.2	30.28	
Avg Skin	26.9	9.46	
Toe	185	1463.01	

Filename 19 nm rult
Exponential Viscous Damping using Rult for shaft

(A) Pile Model
As per Smith Linear Viscous Damping

(B) Resistance Distribution

Depth	Ru	Unit	Total capacity
Below	Ru	(Area)	Shaft capacity
Grade	m	kPa	Toe capacity
1.9	33.7	11.83	529.8 kN
3.9	24.3	8.53	353 kN
5.9	0.8	0.28	176.1 kN
7.9	0.8	0.28	
9.9	0.8	0.28	
11.9	0.8	0.28	
13.9	0.8	0.28	
15.9	0.8	0.28	
17.9	13.9	4.88	
19.9	23.4	8.22	
21.9	28.1	9.87	
23.9	37.1	13.03	
26	4.7	1.65	
28	4.8	1.62	
30	19.4	6.81	
32	29.2	10.25	
34	64.9	22.79	
36	64.9	22.79	
Avg Skin	19.8	6.89	
Toe	176.8	1398.17	



(C) CAPWAP Parameters

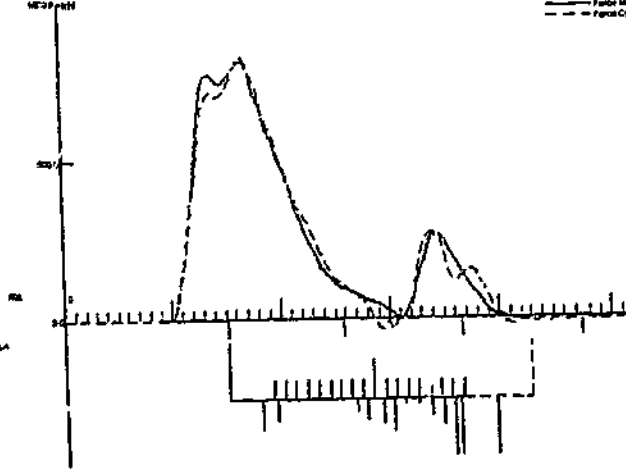
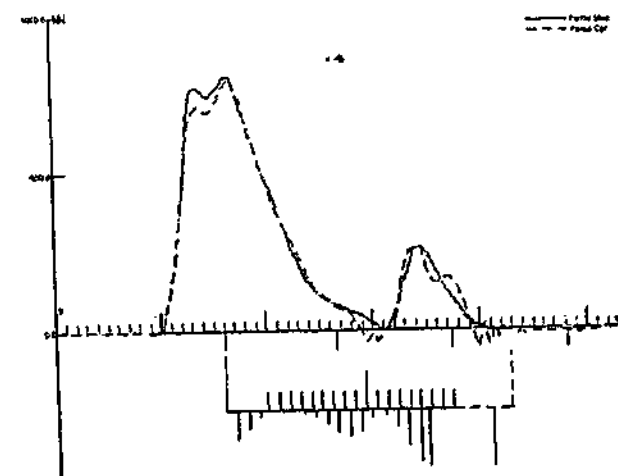
JS	SS	QS	UN	CS	LS	PI	OP
0.611	1.7	0.5	0.7	1	1	0.02	0
JT	ST	QT	TG	CT	LT	PL	
0.192	1.4	2	0.5	1	1	9	

(C) CAPWAP Parameters

JS	SS	QS	UN	CS	LS	PI	OP
0.615	2.35	1	1	1	1	0.02	0
JT	ST	QT	TG	CT	LT	PL	
0.19	1.45	1.1	1	1	1	6.5	

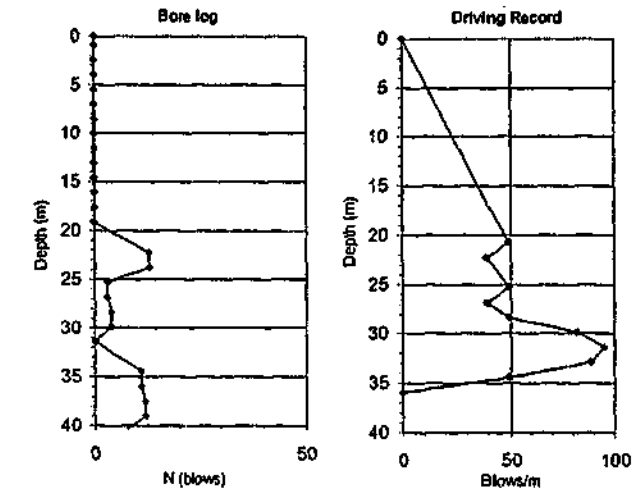
(D) Match
CAPWAP match quality: 2.64 (Force Match)
Observed: final set = 2.400 mm; blow count = 417 b/m
Computed: final set = 1.916 mm; blow count = 522 b/m

(D) Match
CAPWAP match quality: 2.98 (Force Match)
Observed: final set = 2.400 mm; blow count = 417 b/m
Computed: final set = 1.590 mm; blow count = 629 b/m

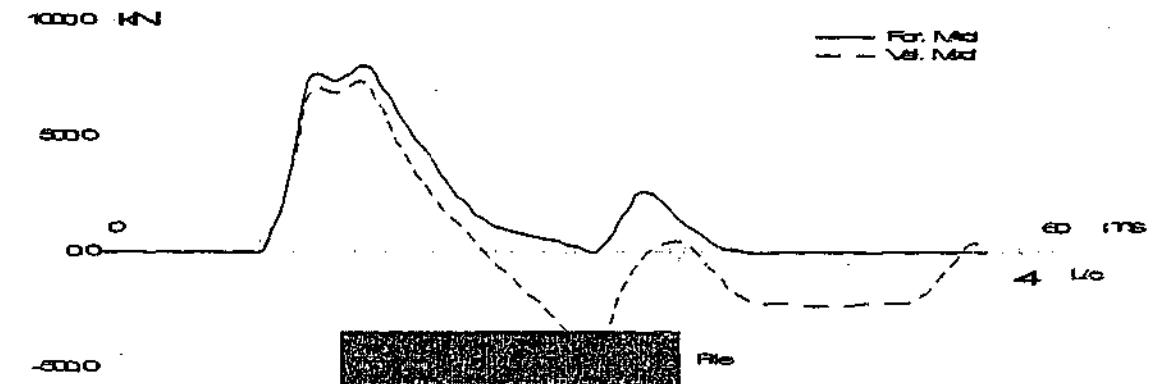


(A) Soil Data
Depth Soil description

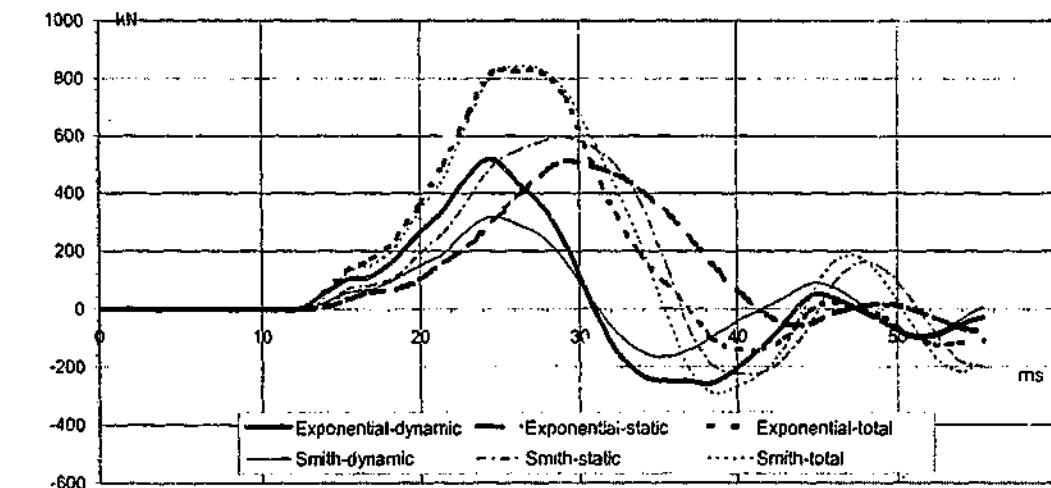
Depth	Soil description
0	Gray SILT, some clay, and organic matter-very soft
19.2024	Gray SILT + CLAY with some gravel and sand-firm
25.2984	Gray SILT and CLAY soft-very soft
40.5384	Gray SILT and CLAY, firm-hard



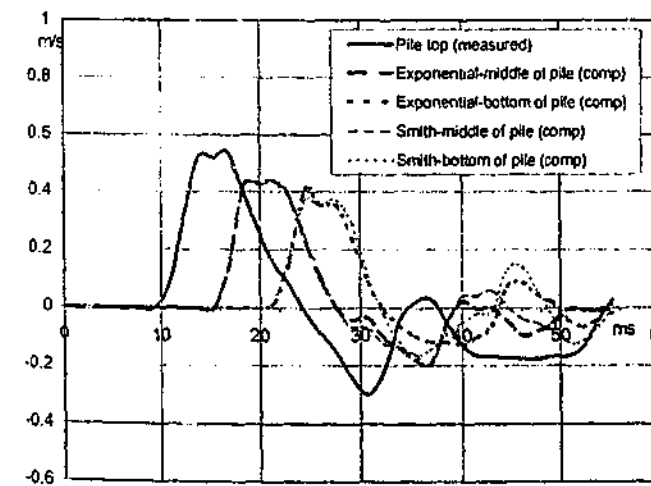
(B) Measured Force & Velocity at Pile Top



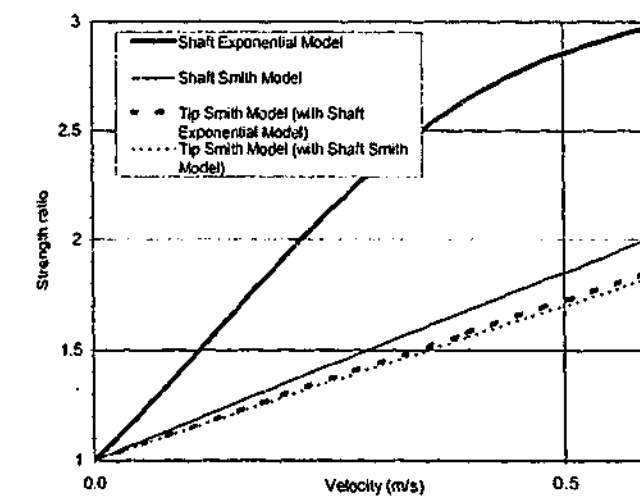
(C) Computed Resistances



(D) Velocities at Top, Middle & Bottom of Pile



(E) Strength Ratio-Velocity Models for Shaft & Tip



ID20 (end of ID1)
S1712D L310K/300-320:CL11;CL-TLL; H pile

Filename 20 d61
Smith Linear Viscous Damping using Rult for Shaft

(A) Pile Model

Depth (m)	Area (cm ²)	E-Mod (MPa)	Spec Weir (kN/m ³)	Circum (m)	Impedance (kN/m/s)
0	80	206579	77.287	1.016	322.90
21.95	80	206579	77.287	1.016	None

Added Impedance None
Wave Speed 5123.9 m/s

(B) Resistance Distribution

Depth (m)	Ru (kPa)	Unit (Area)	Total capacity (kN)	Shaft capacity (kN)	Toe capacity (kN)
1.2	49.3	23.35	1092.2	998.7	93.5
3.2	37.6	17.83			
5.3	31.6	14.95			
7.4	48.5	23.45			
9.5	92.9	44.02			
11.6	146.6	69.44			
13.6	189.4	89.73			
15.7	134.7	62.23			
17.8	142.2	67.37			
19.9	59.6	28.21			
21.9	5.2	2.45			
Avg Skin	90.8	43			
Toe	93.5	1450.56			

Filename 20 nm riant
Exponential Viscous Damping using Rinet for shaft

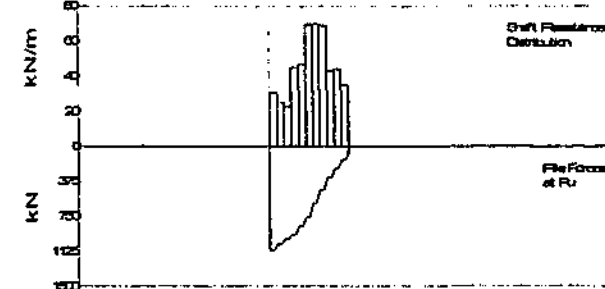
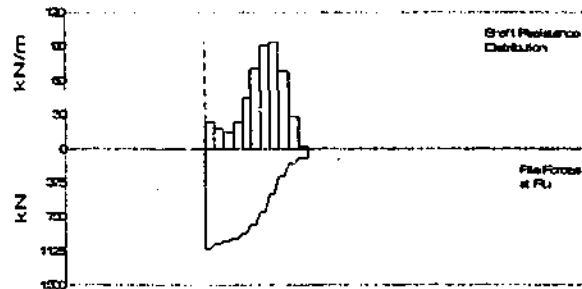
(A) Pile Model

Depth (m)	Area (cm ²)	E-Mod (MPa)	Spec Weir (kN/m ³)	Circum (m)	Impedance (kN/m/s)
0	80	206579	77.287	1.016	322.90
21.95	80	206579	77.287	1.016	None

Added Impedance None
Wave Speed 5123.9 m/s

(B) Resistance Distribution

Depth (m)	Ru (kPa)	Unit (Area)	Total capacity (kN)	Shaft capacity (kN)	Toe capacity (kN)
1.2	83.3	30.01	1108.9	1038.9	70
3.2	52.2	24.72			
5.3	47.1	22.32			
7.4	92.9	44.02			
9.5	97	45.95			
11.6	144.7	68.55			
13.6	144.7	68.55			
15.7	143.2	67.84			
17.8	89.7	42.51			
19.9	91.3	43.28			
21.9	72.5	34.35			
Avg Skin	94.4	44.73			
Toe	70	1088.06			



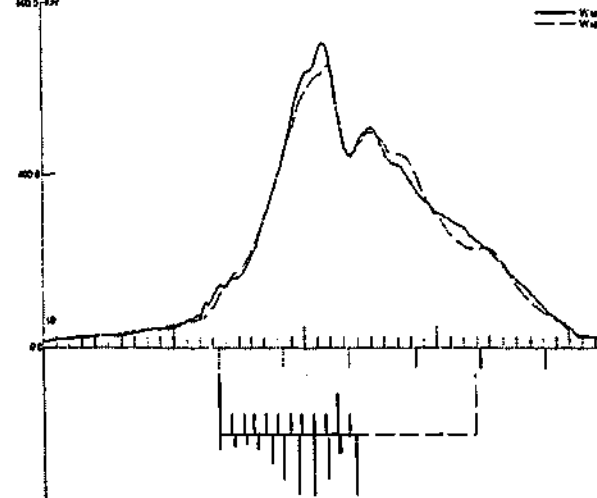
(C) CAPWAP Parameters

JS	SS	QS	UN	CS	LS	PI	OP
1.139	0.367	3	0.048	1	1	0.01	0
JT	ST	QT	TG	CT	LT	PL	
0.25	0.86	4.11	0	1	1	1.159	

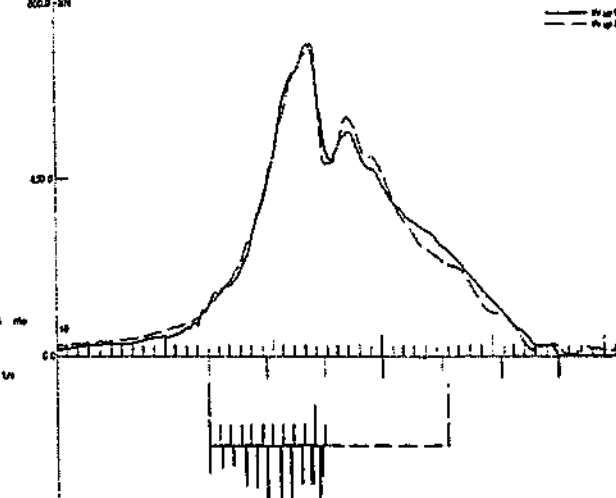
(C) CAPWAP Parameters

JS	SS	QS	UN	CS	LS	PI	OP
1.799	0.557	1.5	0	1	1	0.01	0
JT	ST	QT	TG	CT	LT	PL	
0.065	0.3	1	0	1	1	0.8	

(D) Match
CAPWAP match quality: 2.05 (Wave Up Match)
Observed: final set = 8.965 mm; blow count = 112 b/m
Computed: final set = 9.508 mm; blow count = 105 b/m



(D) Match
CAPWAP match quality: 2.26 (Wave Up Match)
Observed: final set = 8.965 mm; blow count = 112 b/m
Computed: final set = 8.129 mm; blow count = 110 b/m



(A) Soil Data
Depth (m) Soil description
0.0 Tan silty CLAY
Silt: 75%; Clay: 24%; LL=34%; PI=13%

7.6 Silt: 73%; % Clay: 25%; LL=36%; PI=17%

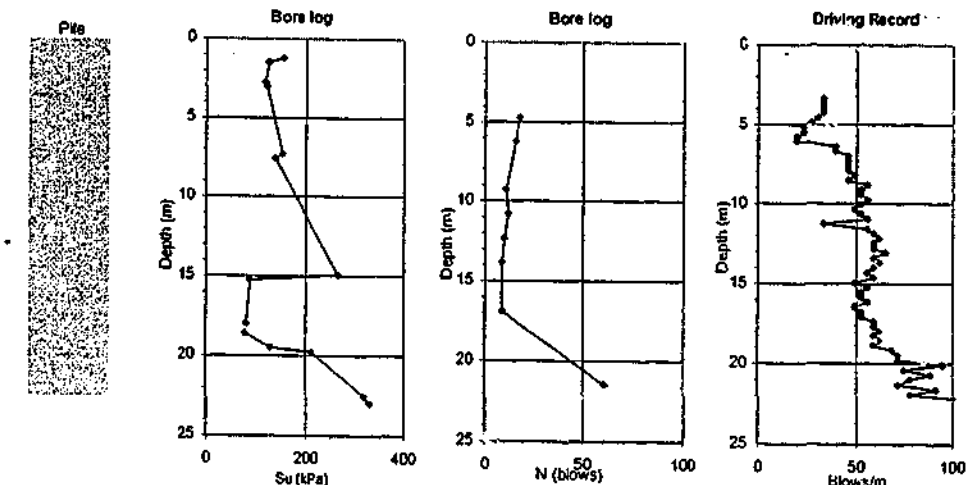
12.3 Grey tan silty CLAY

18.0 Sil: 47%; Clay: 25%; LL=32%; PI=18%

18.6 GLACIAL TILL: CLAY, silt, contains sand/gravel grains, pebbles/stones

21.5 Hard Layer

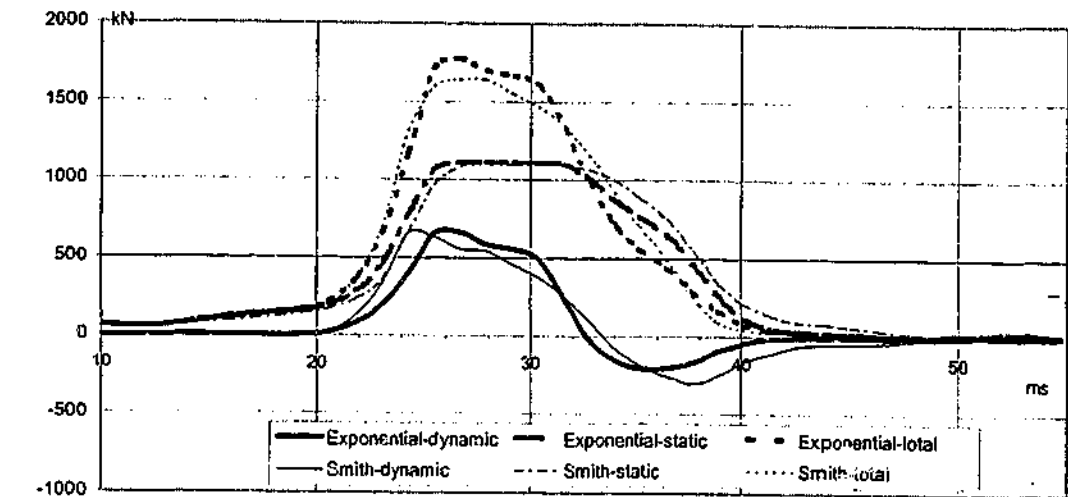
22.6 Silt: 45%; Clay: 31%; LL=38%; PI=22%



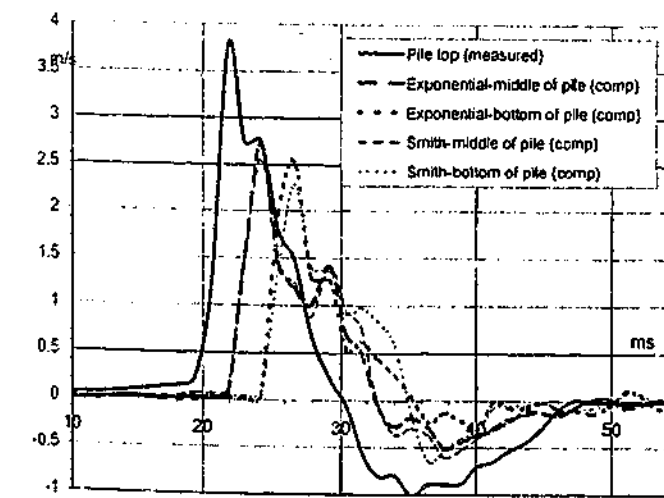
(B) Measured Force & Velocity at Pile Top



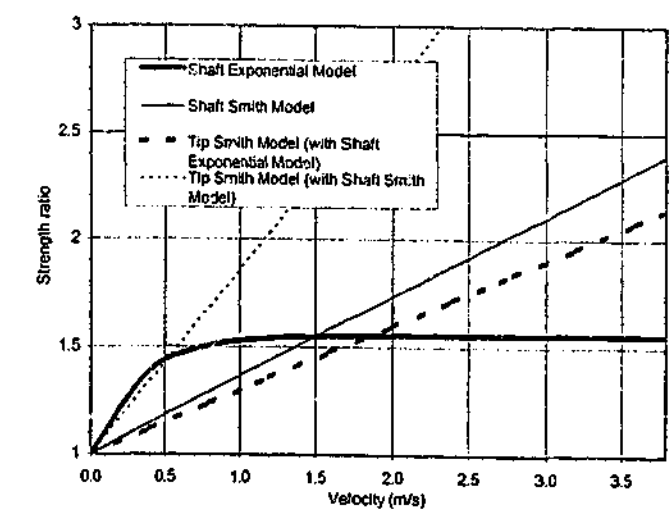
(C) Computed Resistances



(D) Velocities at Top, Middle & Bottom of Pile



(E) Strength Ratio-Velocity Models for Shaft & Tip

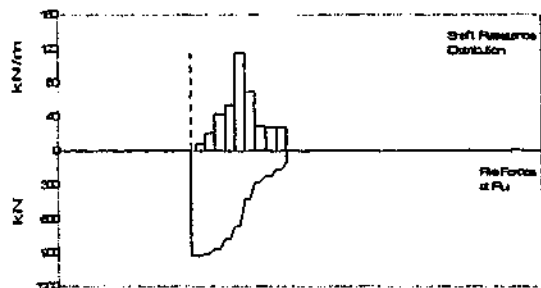


ID21 (end of ID2)
 S18100 L360K350-360; sICL10; CL-TILL; 305mm PSC

Filename 21.dcf
 Smith Linear Viscous Damping using Rult for Shaft

Depth (m)	Area (cm ²)	E-Mod (MPa)	Spec Wei (kN/m ³)	Circum (m)	Impedance (682.77 kN/m/s)
0	929.03	37590.2	23.563	1.219	Added Impedance None
18.9	929.03	37590.2	23.563	1.219	Wave Speed 3856.0 m/s

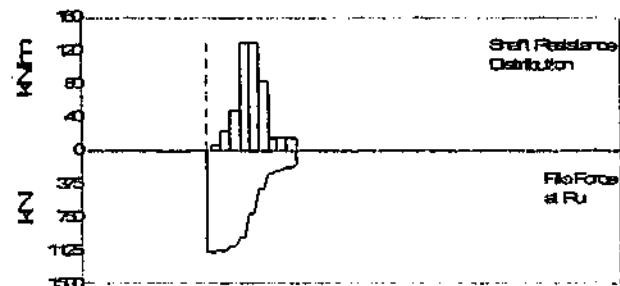
Depth (m)	Ru (kN)	Unit (kPa)	Total capacity (kN)	929.2 (kN)
Below Grade			Shaft capacity	823.7 (kN)
			Toe capacity	105.4 (kN)
2.2	17.1	6.73		
4.3	43.7	17.19		
6.4	89.6	35.25		
8.5	112.9	44.4		
10.6	240.2	94.46		
12.6	144.5	56.83		
14.7	58.7	23.49		
16.8	58	22.81		
18.9	58	22.81		
Avg Skin	91.5	36		
Toe	105.4	1134.68		



Filename 21 nm rult
 Exponential Viscous Damping using Rinst for shaft

(A) Pile Model
 As per Smith Linear Viscous Damping

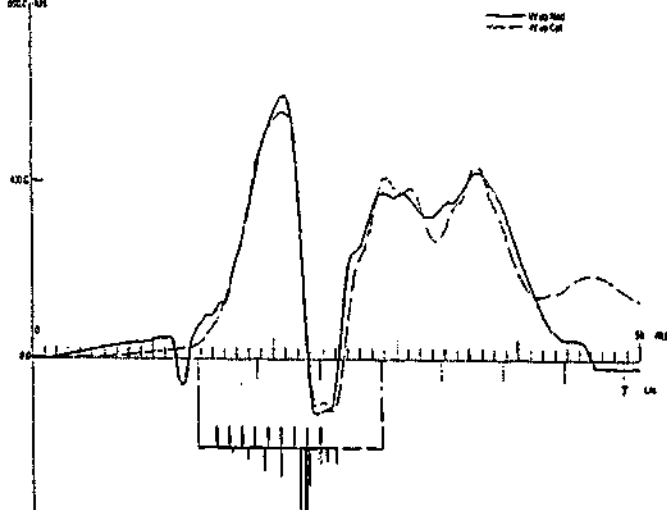
Depth (m)	Ru (kN)	Unit (kPa)	Total capacity (kN)	1138.5 (kN)
Below Grade			Shaft capacity	978.8 (kN)
			Toe capacity	157.9 (kN)
2.2	14.3	5.62		
4.3	49.2	19.34		
6.4	101.3	39.83		
8.5	270.7	106.48		
10.6	270.7	106.48		
12.6	178.3	69.34		
14.7	32.1	12.62		
16.8	32.1	12.62		
18.9	32.1	12.62		
Avg Skin	108.8	42.77		
Toe	157.7	1697.44		



(C) CAPWAP Parameters

JS	SS	QS	UN	CS	LS	PI	OP
0.746	0.805	6.5	0	1	1	0.02	0
JT	ST	QT	TG	CT	LT	PL	
0.1	0.64	1.5	0	1	1	0	

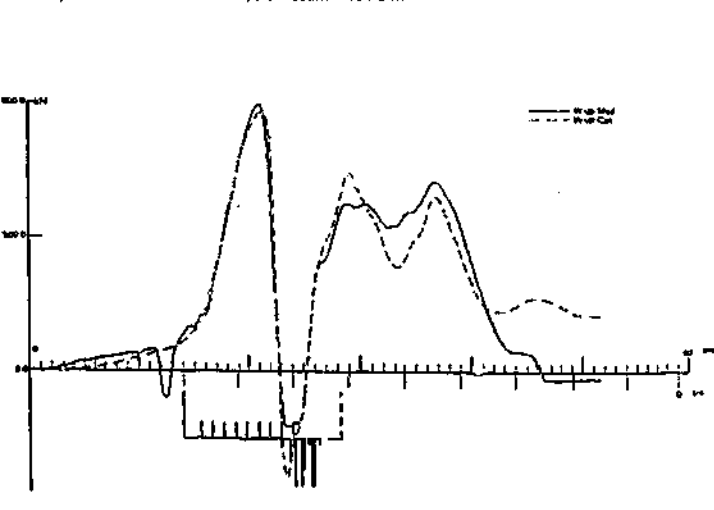
(D) Match
 CAPWAP match quality: 4.95 (Wave Up Match)
 Observed: final set = 5.080 mm; blow count = 197 b/m
 Computed: final set = 5.409 mm; blow count = 185 b/m



(C) CAPWAP Parameters

JS	SS	QS	UN	CS	LS	PI	OP
0.904	0.82	9.5	1	1	1	0.02	0
JT	ST	QT	TG	CT	LT	PL	
0.163	0.92	4	5	1	1	0	

(D) Match
 CAPWAP match quality: 5.16 (Wave Up Match)
 Observed: final set = 5.080 mm; blow count = 197 b/m
 Computed: final set = 5.526 mm; blow count = 191 b/m



(A) Soil Data
 Depth (m) Soil description
 0.0 Tan silty CLAY
 Silt: 75%; Clay: 24%; LL=34%; PI=13%

7.6 SR: 73%; % Clay: 25%; LL=36%; PI=17%

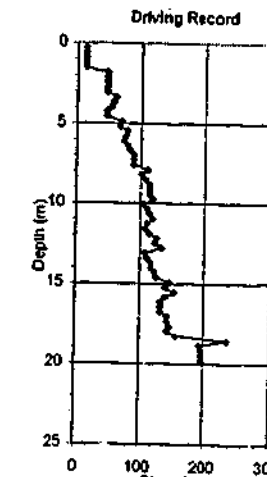
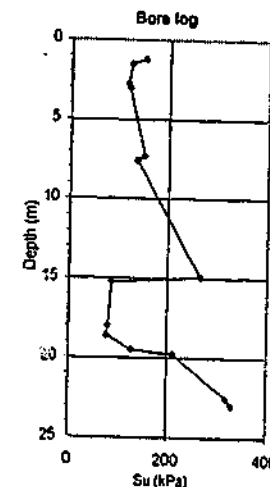
12.3 Grey tan silty CLAY

18.0 Silt: 47%; Clay: 25%; LL=32%; PI=16%

18.6 GLACIAL TILL: CLAY, silt, contains sand/gravel grains, pebbles/stones

21.5 Hard Layer

22.6 Silt: 45%; Clay: 31%; LL=36%; PI=22%



(B) Measured Force & Velocity at Pile Top

30000 kN

15000

-15000

-2000

-1000

-500

0

500

1000

1500

2000

2500 kN

10

20

30

40

50

ms

7 L/c

50 ms

7 L/c

50 ms

7 L/c

50 ms

7 L/c

50 ms

7 L/c

50 ms

7 L/c

50 ms

7 L/c

50 ms

7 L/c

50 ms

7 L/c

50 ms

7 L/c

50 ms

7 L/c

50 ms

7 L/c

50 ms

7 L/c

50 ms

7 L/c

50 ms

7 L/c

50 ms

7 L/c

50 ms

7 L/c

50 ms

7 L/c

50 ms

7 L/c

50 ms

7 L/c

50 ms

7 L/c

50 ms

7 L/c

50 ms

7 L/c

50 ms

7 L/c

50 ms

7 L/c

50 ms

7 L/c

50 ms

7 L/c

50 ms

7 L/c

50 ms

7 L/c

50 ms

7 L/c

50 ms

7 L/c

50 ms

7 L/c

50 ms

7 L/c

50 ms

7 L/c

50 ms

7 L/c

50 ms

7 L/c

50 ms

7 L/c

50 ms

7 L/c

50 ms

7 L/c

50 ms

7 L/c

50 ms

7 L/c

50 ms

7 L/c

50 ms

7 L/c

50 ms

7 L/c

50 ms

7 L/c

50 ms

7 L/c

50 ms

7 L/c

50 ms

7 L/c

50 ms

7 L/c

50 ms

7 L/c

50 ms

7 L/c

50 ms

7 L/c

50 ms

7 L/c

50 ms

7 L/c

50 ms

7 L/c

50 ms

7 L/c

50 ms

7 L/c

50 ms

7 L/c

50 ms

7 L/c

50 ms

7 L/c

50 ms

7 L/c

50 ms

7 L/c

50 ms

7 L/c

50 ms

7 L/c

50 ms

7 L/c

50 ms

7 L/c

50 ms

7 L/c

50 ms

7 L/c

50 ms

7 L/c

50 ms

7 L/c

50 ms

7 L/c

50 ms

7 L/c

50 ms

7 L/c

50 ms

7 L/c

50 ms

7 L/c

50 ms

7 L/c

50 ms

7 L/c

50 ms

7 L/c

50 ms

7 L/c

50 ms

7 L/c

50 ms

7 L/c

50 ms

7 L/c

50 ms

7 L/c

50 ms

7 L/c

50 ms

7 L/c

50 ms

7 L/c

50 ms

7 L/c

50 ms

7 L/c

50 ms

7 L/c

50 ms

7 L/c

50 ms

7 L/c

50 ms

7 L/c

50 ms

7 L/c

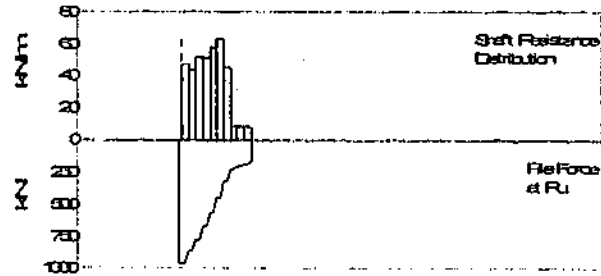
ID22 (eod ID3)

S1712D L310K/300-320;SICL11;CL-TILL; H pile

Filename 22 def
Smith Linear Viscous Damping using Rult for Shaft

Depth	Area	E-Mod	Spec Wel	Circum	Impedance
m	cm ²	MPa	kN/m ³	m	500.04 kN/m/s
0	123.87	206579.3	77.287	1.018	Added Impedance None
23.12	123.87	206579.3	77.287	1.018	Wave Speed 5123.9 m/s

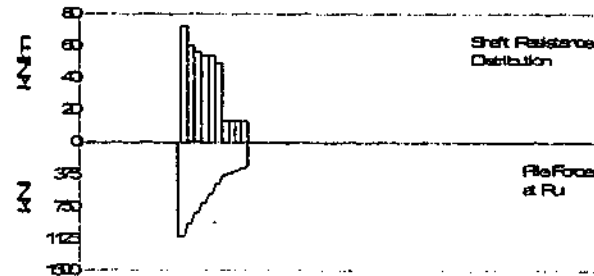
(B) Resistance Distribution		Total capacity	958.5	kN
Depth	Ru	Unit	Shaft capacity	791.9
Below	Ru	Unit	Toe capacity	168.8
Grade	(Area)			
m	kN	kPa		
1.8	98.9	46.82		
3.8	89	43.03		
5.8	105.9	51.2		
7.8	105.9	51.2		
10	118.7	57.37		
12	126.5	62.62		
14	92.5	44.73		
16.1	18.3	8.85		
18.1	17.6	8.51		
20.1	17.8	8.51		
Avg Skin	79.2	38.28		
Toe	168.8	2014.36		



Filename 22 nm rult
Exponential Viscous Damping using Rult for shaft

(A) Pile Model
As per Smith Linear Viscous Damping

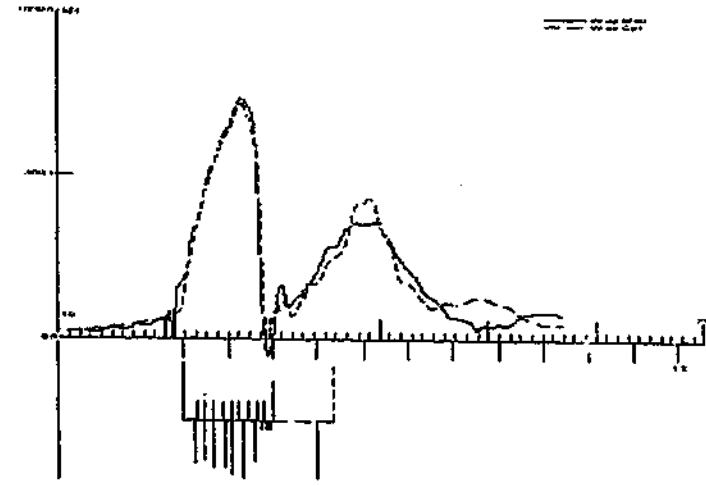
(B) Resistance Distribution		Total capacity	1089.8	kN
Depth	Ru	Unit	Shaft capacity	819.8
Below	Ru	Unit	Toe capacity	270.2
Grade	(Area)			
m	kN	kPa		
1.8	147.7	71.42		
3.8	123.4	59.66		
5.8	114.9	55.53		
7.8	111.6	53.93		
10	111.6	53.93		
12	101.2	48.93		
14	27.2	13.17		
16.1	27.3	13.22		
18.1	27.3	13.22		
20.1	27.3	13.22		
Avg skin	82	39.62		
Toe	270	3264.99		



(C) CAPWAP Parameters

JS	SS	QS	UN	CS	LS	PI	OP
1.165	0.74	4	0.242	0.971	1	0.01	0
JT	ST	QT	TG	CT	LT	PL	
0.01	0.03	12.5	0	0.971	1	0	

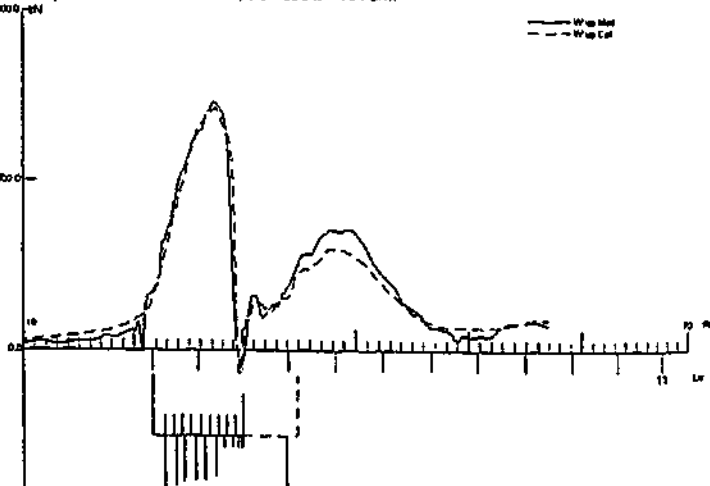
(D) Match
CAPWAP match quality: 3.53 (Wave Up Match)
Observed: final set = 10.160 mm; blow count = 98 b/m
Computed: final set = 9.353 mm; blow count = 107 b/m



(C) CAPWAP Parameters

JS	SS	QS	UN	CS	LS	PI	OP
1.783	1.093	4	1	1	1	0.01	0
JT	ST	QT	TG	CT	LT	PL	
0.173	0.322	3.5	8	1	1	0	

(D) Match
CAPWAP match quality: 3.06 (Wave Up Match)
Observed: final set = 10.160 mm; blow count = 98 b/m
Computed: final set = 9.577 mm; blow count = 104 b/m



(A) Soil Data
Depth (m) Soil description
0.0 Tan silty CLAY
SM: 75%; Clay: 24%; LL=34%; PI=13%

7.6 Silt: 73%; % Clay: 25%; LL=38%; PI=17%

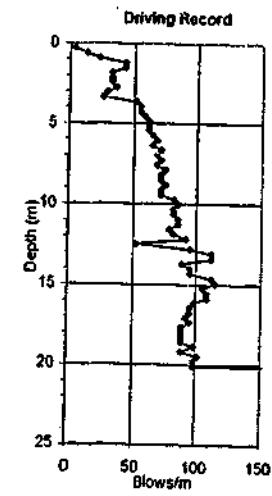
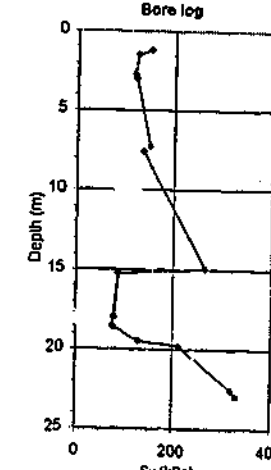
12.3 Grey tan silty CLAY

18.0 Silt: 47%; Clay: 25%; LL=32%; PI=18%

18.6 GLACIAL TILL: CLAY, stiff, contains sand/gravel grains, pebbles/stones

21.5 Hard Layer

22.8 Silt: 45%; Clay: 31%; LL=38%; PI=22%



(B) Measured Force & Velocity at Pile Top

30000 kN

15000

10

-15000

File

For. Mod
Vel. Mod

60 ms

g/c

(C) Computed Resistances

2500 kN

2000

1500

1000

500

0

-500

-1000

Exponential-dynamic Exponential-static Exponential-total
Smith-dynamic Smith-static Smith-total

ms 60

(D) Velocities at Top, Middle & Bottom of Pile

4 m/s

3.5

3

2.5

2

1.5

1

0.5

-0.5

-1

Pile top (measured)
Exponential-middle of pile (comp)
Exponential-bottom of pile (comp)
Smith-middle of pile (comp)
Smith-bottom of pile (comp)

(E) Strength Ratio-Velocity Models for Shaft & Tip

4

3.5

3

2.5

2

1.5

1

4

3.5

3

2.5

2

1.5

1

0.5

0

-0.5

-1

Shaft Exponential Model
Shaft Smith Model
Tip Smith Model (with Shaft Exponential Model)
Tip Smith Model (with Shaft Smith Model)

Velocity (m/s)

0.0

0.5

1.0

1.5

2.0

2.5

3.0

3.5

4.0

ID23 (eod ID4)

Filename 23 def
Smith Linear Viscous Damping using Roll for Shaft

(A) Pile Model

Depth	Area	E-Mod	Spec Wel	Circum	Impedance
m	cm ²	MPa	kN/m ³	m	2973.37kN/m/s
0	2987.09	41251.3	23.563	2.433	Added Impedance None
31.39	2987.09	41251.3	23.563	2.438	Wave Speed 4144.2 m/s

(B) Resistance Distribution

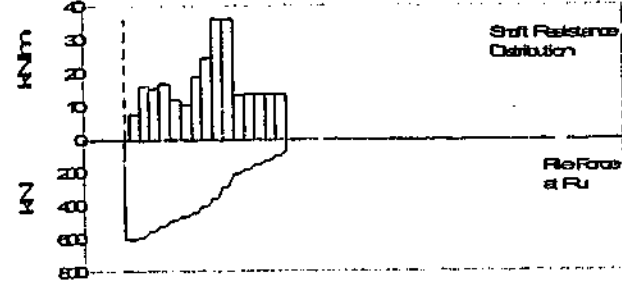
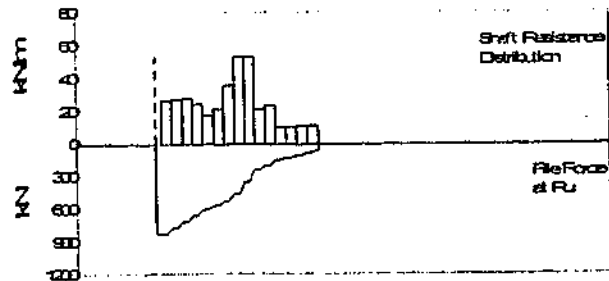
Depth	Ru	Unit	Total capacity	827.8	kN
Below	Ru	(Area)	Shaft capacity	766.9	kN
Grade	(Area)		Toe capacity	60.1	kN
m	kN	kPa			
2.1	54.4	11.01			
4.1	56.1	11.36			
6.2	57	11.54			
8.2	50.1	10.15			
10.2	35.8	7.25			
12.3	43.6	8.82			
14.3	72.9	14.77			
16.3	108	21.88			
18.5	107.8	21.84			
20.4	43.6	8.82			
22.4	48.9	9.91			
24.4	20.7	4.19			
26.4	21.7	4.36			
28.5	23.1	4.68			
30.5	23.1	4.66			
Avg Skin	51.1	10.35			
Toe	60.8	163.7			

Filename 23 nm rlnet
Exponential Viscous Damping using Flist for shaft

(A) Pile Model
As per Smith Linear Viscous Damping

(B) Resistance Distribution

Depth	Ru	Unit	Total capacity	607.4	kN
Below	Ru	(Area)	Shaft capacity	535.4	kN
Grade	(Area)		Toe capacity	72.2	kN
m	kN	kPa			
2.1	15.9	3.22			
4.1	32.9	6.66			
6.2	31.5	6.37			
8.2	34.4	6.97			
10.2	24.8	5.02			
12.3	21.5	4.34			
14.3	38.9	7.87			
16.3	49.8	10.04			
18.3	73.8	14.9			
20.4	73.6	14.9			
22.4	27.5	5.57			
24.4	27.8	5.64			
26.4	27.8	5.64			
28.5	27.8	5.64			
30.5	27.8	5.64			
Avg Skin	35.7	7.23			
Toe	72	193.64			



(C) CAPWAP Parameters

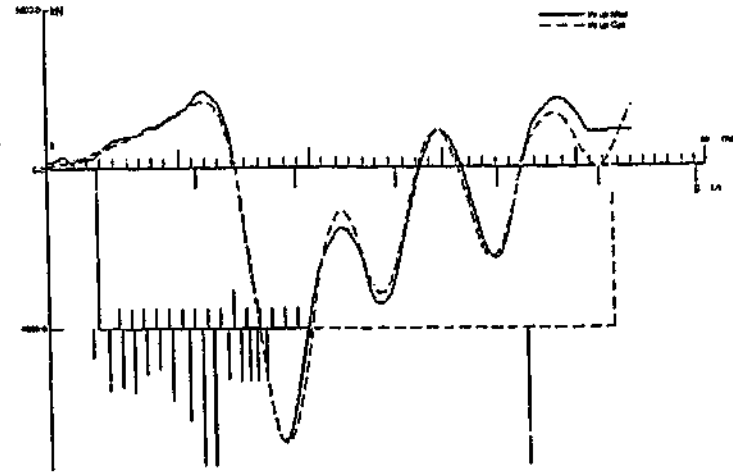
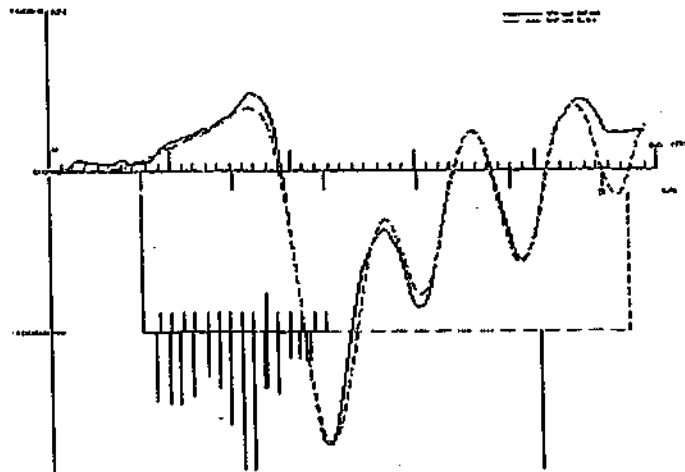
JS	SS	QS	UN	CS	LS	PI	OP
0.123	0.483	2.5	1	0.2	1	0.02	0
JT	ST	QT	TG	CT	LT	PL	
0.027	1.312	16	0	1	1	4.9	

(C) CAPWAP Parameters

JS	SS	QS	UN	CS	LS	PI	OP
0.234	1.318	2.1	1	1	1	0.02	1
JT	ST	QT	TG	CT	LT	PL	
0.003	0.134	4	12	1	1	2.8	

(D) Match
CAPWAP match quality: 7.82 (Wave Up Match)
Observed: final set = 15.223 mm; blow count = 66 b/m
Computed: final set = 15.252 mm; blow count = 66 b/m

(D) Match
CAPWAP match quality: 7.78 (Wave Up Match)
Observed: final set = 15.223 mm; blow count = 66 b/m
Computed: final set = 14.804 mm; blow count = 68 b/m



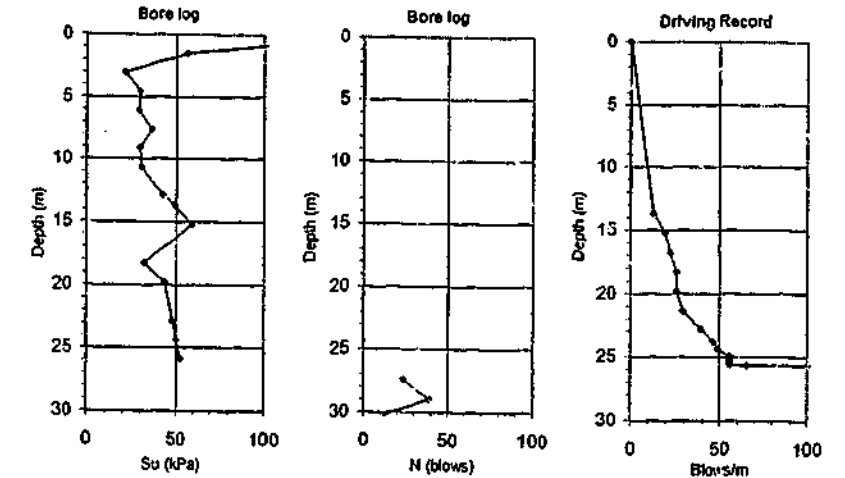
(A) Soil Data

0.762 Brown silty CLAY w/ trace gravel (mc=25%)
1.524 Gray silty CLAY w/ lenses silt
3.048 Organic silty clay w/ trace rotting wood (mc=35%)
4.572 Gray silty CLAY w/ trace rotting wood, organic (mc=49%)
6.096 Gray CLAY w/ trace rotting wood, organic (ms=56%)

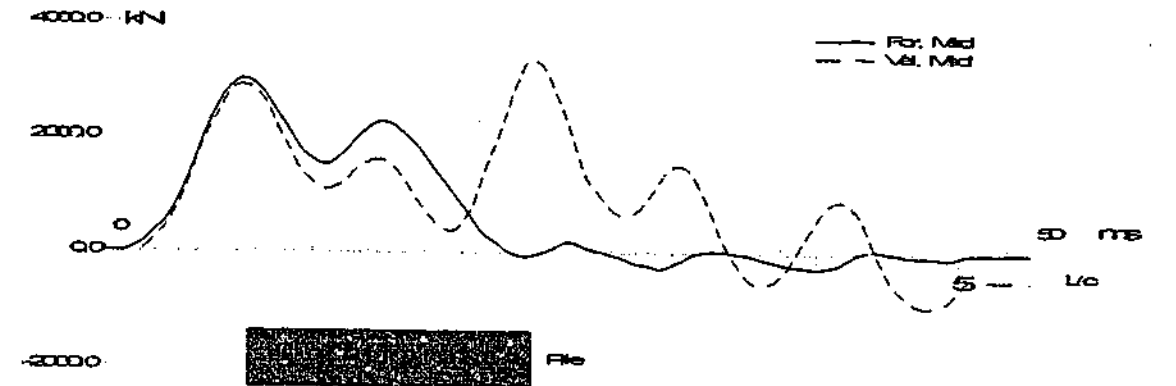
12.192 Gray clay with rotting wood (ms=86%)
12.954 Gray clay (mc=40%)
13.716 Gray silty clay w/ trace rotting wood (mc=37%)
15.24 Gray clay w/ trace rotting wood (mc=48%)
18.288 Gray CLAY w/ trace shell (mc=49%)
18.812 Gray CLAY (mc=54%)

22.86 Gray CLAY w/ trace shell (mc=42%)

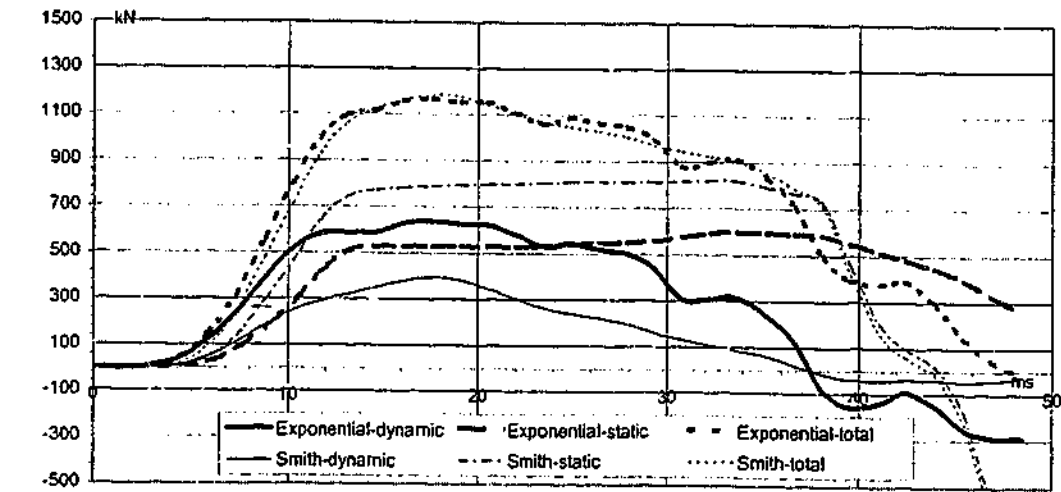
25.908 Gray silty CLAY w/ trace organics (mc=25%)
27.432 Gray fine silty SAND
28.956 Gray fine SAND



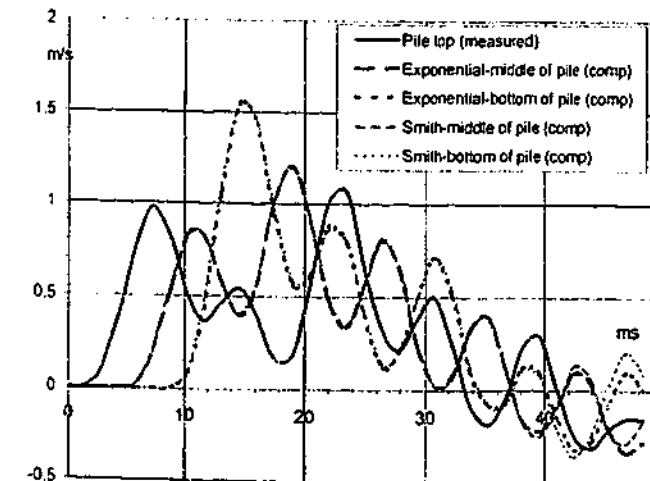
(B) Measured Force & Velocity at Pile Top



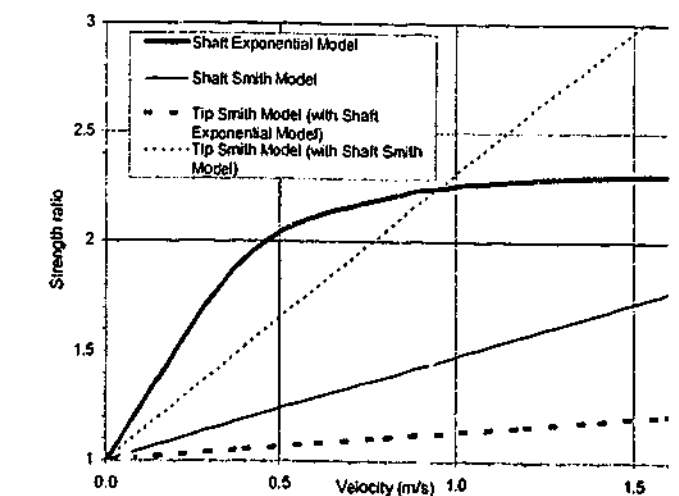
(C) Computed Resistances



(D) Velocities at Top, Middle & Bottom of Pile



(E) Strength Ratio-Velocity Models for Shaft & Tip



ID24 (cod ID6)
 S89/150 16PSC 13dL596;ISA;ICL;ICL;

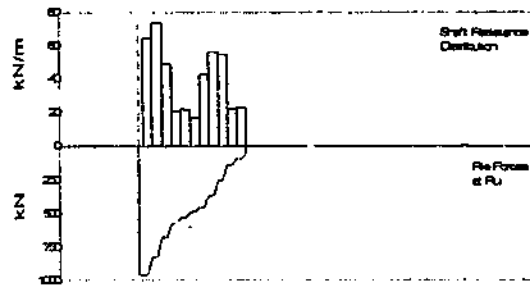
Filename 24 del
 Smith Linear Viscous Damping using Rull for Shaft

(A) Pile Model

Depth	Area	E-Mod	Spec Wei	Circum	Impedance
m	cm ²	MPa	kN/m ³	m	1541.55kN/m/s
0	1574.19	30143.6	24.034	1.587	Added Impedance None
23.01	1574.19	30143.6	24.034	1.587	Wave Speed 3987.1 m/s

(B) Resistance Distribution

Depth	Ru	Unit	Total capacity	939.8	kN
Below	Ru	Unit	Shaft capacity	692.9	kN
Grade	(Area)		Toe capacity	46.7	kN
m	kPa				
3	128.9	40.59			
5	147.8	46.55			
7	58.6	31.03			
9	41.6	13.1			
11	43.6	13.72			
13	33.9	10.67			
15	85.3	26.87			
17	112.7	35.5			
19	110.2	34.89			
21	44.5	14.03			
23	45.7	14.4			
Avg Skin	81.2	25.56			
Toe	46.7	296.83			



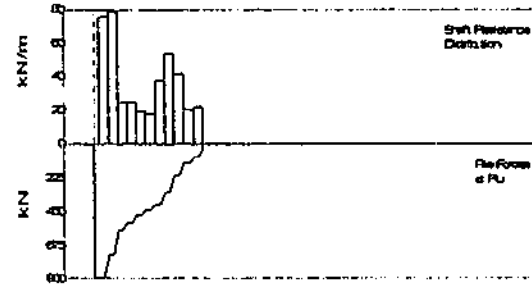
Filename 24 mm rinst
 Exponential Viscous Damping using Rull for shaft

(A) Pile Model

Depth	Area	E-Mod	Spec Wei	Circum	Impedance
m	cm ²	MPa	kN/m ³	m	1541.55kN/m/s
0	1574.19	30143.6	24.034	1.587	Added Impedance None
23.01	1574.19	30143.6	24.034	1.587	Wave Speed 3987.1 m/s

(B) Resistance Distribution

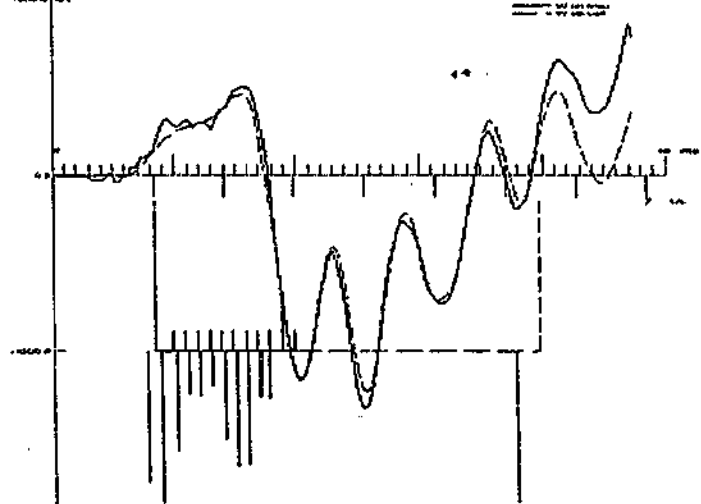
Depth	Ru	Unit	Total capacity	874.2	kN
Below	Ru	Unit	Shaft capacity	834.8	kN
Grade	(Area)		Toe capacity	39.4	kN
m	kPa				
3	151.2	47.61			
5	157.5	49.6			
7	48.2	15.5			
9	49.2	15.5			
11	39.4	12.4			
13	35.9	11.31			
15	75.7	23.84			
17	108.3	34.1			
19	83.2	28.19			
21	41.1	12.93			
23	44.1	13.89			
Avg Skin	75.9	23.9			
Toe	39.4	250.22			



(C) CAPWAP Parameters

JS	SS	QS	UN	CS	LS	PI	OP
0.144	0.245	1	0	1	1	0.02	0
JT	ST	QT	TG	CT	LT	PL	
0.006	0.201	20	10	1	1	4.5	

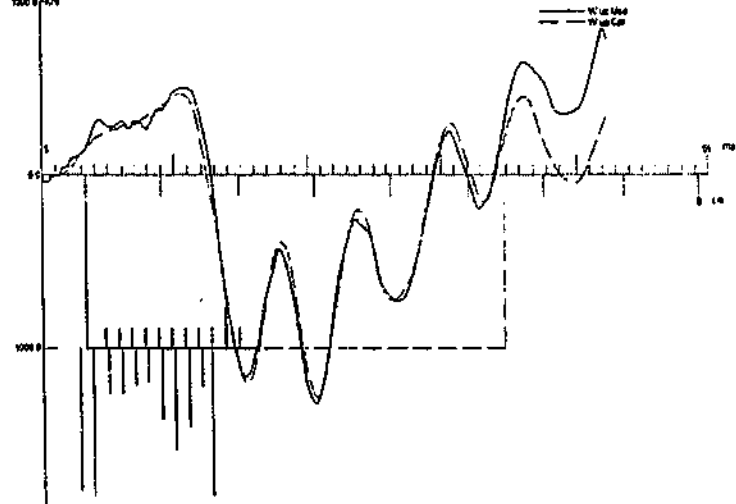
(D) Match
 CAPWAP match quality: 8.15 (Wave Up Match)
 Observed: final set = 21.771 mm, blow count = 46 b/m
 Computed: final set = 26.815 mm, blow count = 38 b/m



(C) CAPWAP Parameters

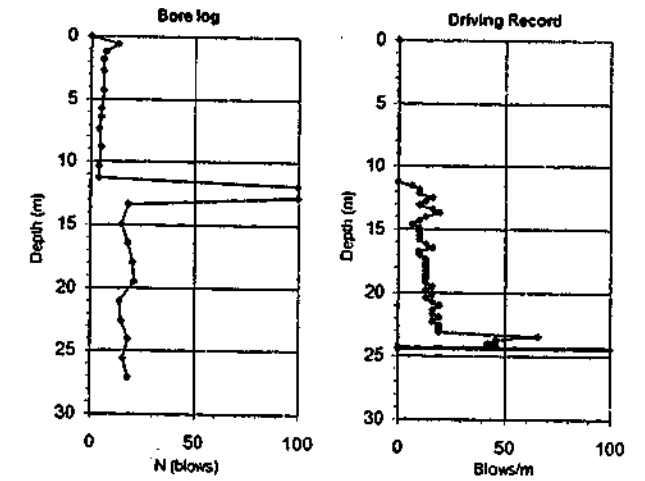
JS	SS	QS	UN	CS	LS	PI	OP
0.217	0.395	1	0	1	1	0.02	0
JT	ST	QT	TG	CT	LT	PL	
0.005	0.2	1	0	1	1	4.5	

(D) Match
 CAPWAP match quality: 8.39 (Wave Up Match)
 Observed: final set = 21.771 mm, blow count = 46 b/m
 Computed: final set = 26.761 mm, blow count = 37 b/m

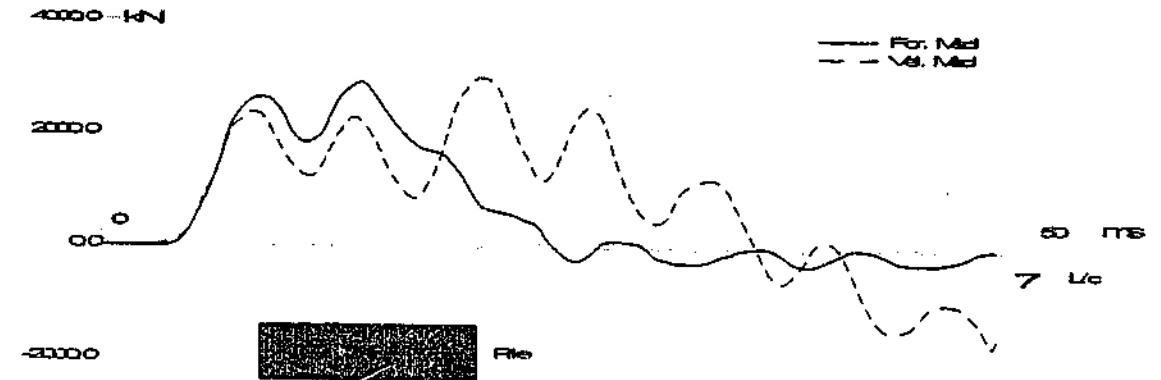


(A) Soil Data

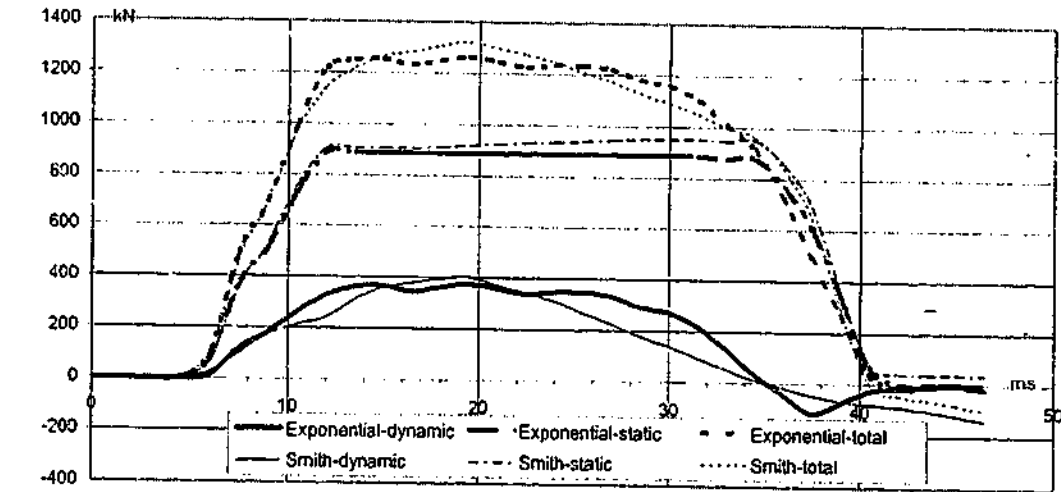
Depth	Soil description
0.0	FILL: medium dense-loose tan grey slightly silty fine SAND
6.4	Soft to firm dark black grey organic silty CLAY w/marsh roots
11.3	Very dense dark grey medium to coarse SAND
12.8	Very stiff to stiff olive green silty CLAY (Marl)



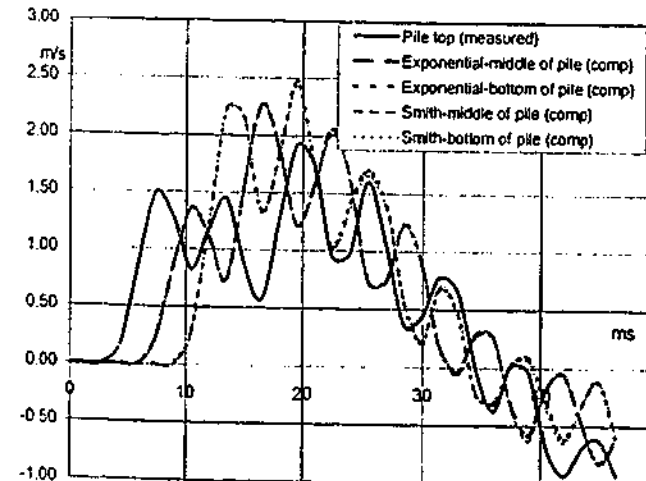
(B) Measured Force & Velocity at Pile Top



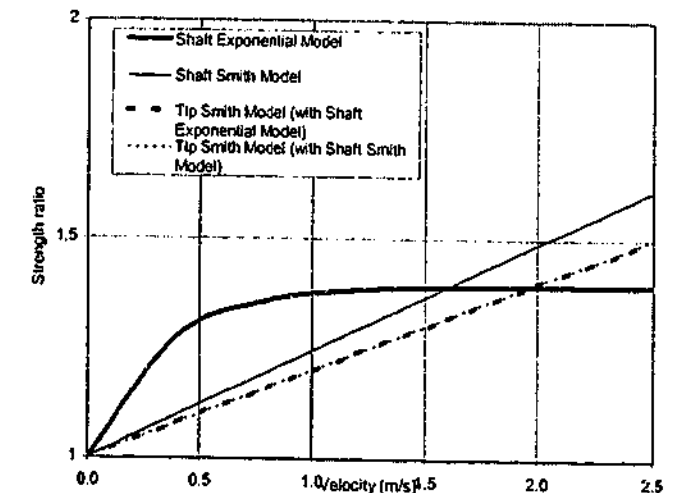
(C) Computed Resistances



(D) Velocities at Top, Middle & Bottom of Pile



(E) Strength Ratio-Velocity Models for Shaft & Tip



ID25 (end of ID9)
R1025H H 3d7390K;S1+SA1;SAsh125

Filename 25 del
Smith Linear Viscous Damping using Ruit for Shaft

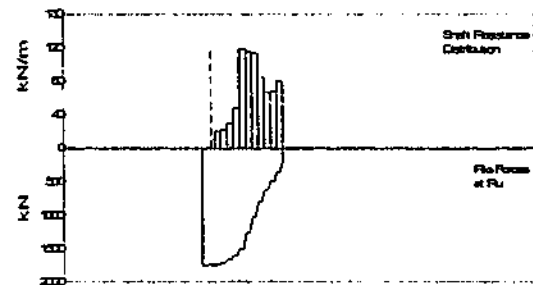
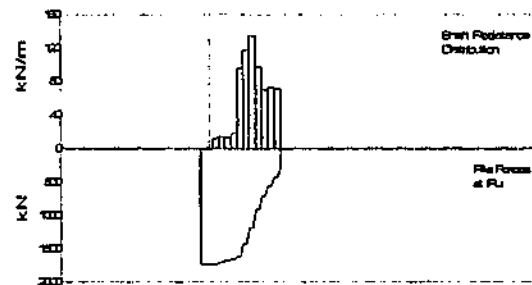
Depth (m)	Area (cm ²)	E-Mod (MPa)	Spec Wei (kN/m ³)	Circum (m)	Impedance (kN/m/s)
0	100	206579	77.287	1.219	403.42
23.16	100	206579	77.287	1.219	None

Depth (m)	Ru (kN/m ²)	Unit	Total capacity (kN)
Below Grade	Ru (Area)		1734.8
2.8	25.3	10.21	
4.9	28.4	11.47	
6.9	28	11.3	
8.9	37.6	15.18	
11	194.8	78.61	
13	240.3	96.96	
15	275.1	111.03	
17.1	198.5	80.1	
19.1	143.1	57.78	
21.1	147.4	59.51	
23.2	145.6	58.79	
Avg skin	133.1	53.72	
Toe	270.7	2913.54	

Filename 25 nm rinst
Exponential Viscous Damping using Ruit for shaft

(A) Pile Model
As per Smith Linear Viscous Damping

Depth (m)	Ru (kN/m ²)	Unit	Total capacity (kN)
Below Grade	Ru (Area)		1745.3
2.8	40.6	16.39	
4.9	48.0	18.69	
6.9	61.5	24.83	
8.9	98.2	39.65	
11	241.9	97.5	
13	234.7	94.72	
15	230.9	93.18	
17.1	170.8	69.96	
19.1	135.2	54.59	
21.1	139	55.72	
23.2	163.5	66.01	
Avg skin	141.9	57.3	
Toe	183.9	1078.97	



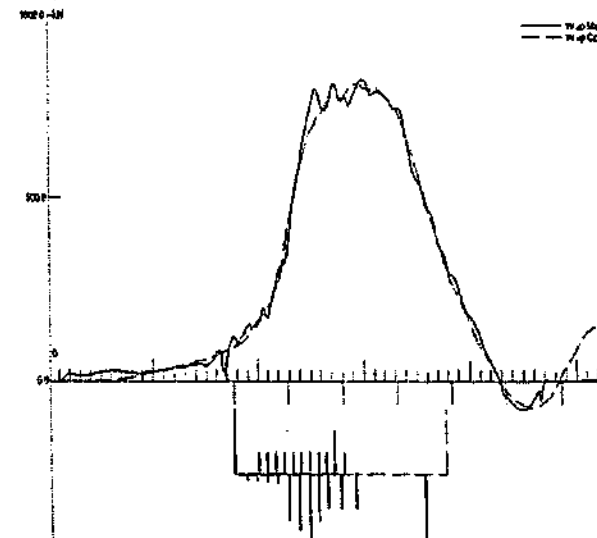
(C) CAPWAP Parameters

JS	SS	QS	UN	CS	LS	PI	OP
1.502	0.414	1.8	0.37	1	1	0.01	0
JT	ST	QT	TG	CT	LT	PL	
0.872	1.3	3	0	1	1	0.448	

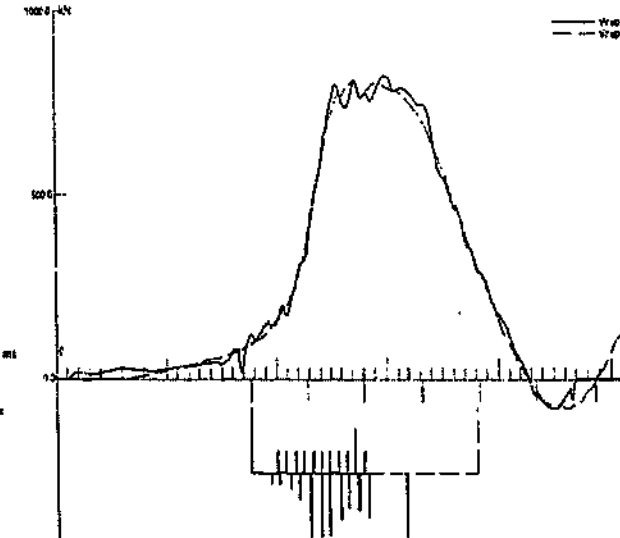
(C) CAPWAP Parameters

JS	SS	QS	UN	CS	LS	PI	OP
1.528	0.395	2.5	0.27	1	1	0.01	0
JT	ST	QT	TG	CT	LT	PL	
0.592	1.3	3.13	0	0.35	1	0.5	

(D) Match
CAPWAP match quality: 2.57 (Wave Up Match)
Observed: final set = 3.387 mm; blow count = 295 b/m
Computed: final set = 2.482 mm; blow count = 401 b/m



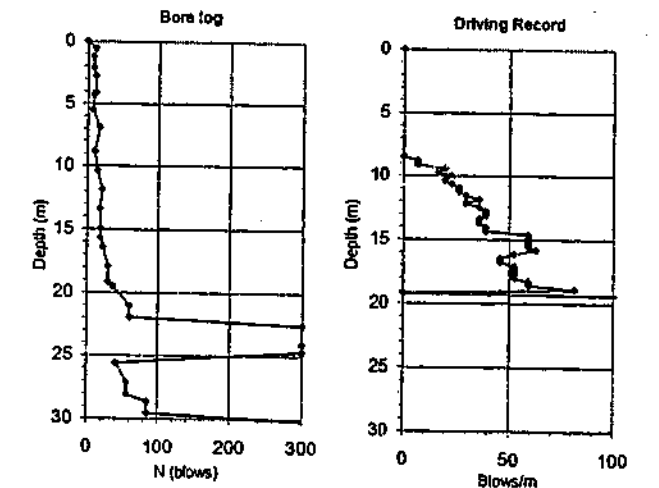
(D) Match
CAPWAP match quality: 3.60 (Wave Up Match)
Observed: final set = 3.387 mm; blow count = 295 b/m
Computed: final set = 2.239 mm; blow count = 447 b/m



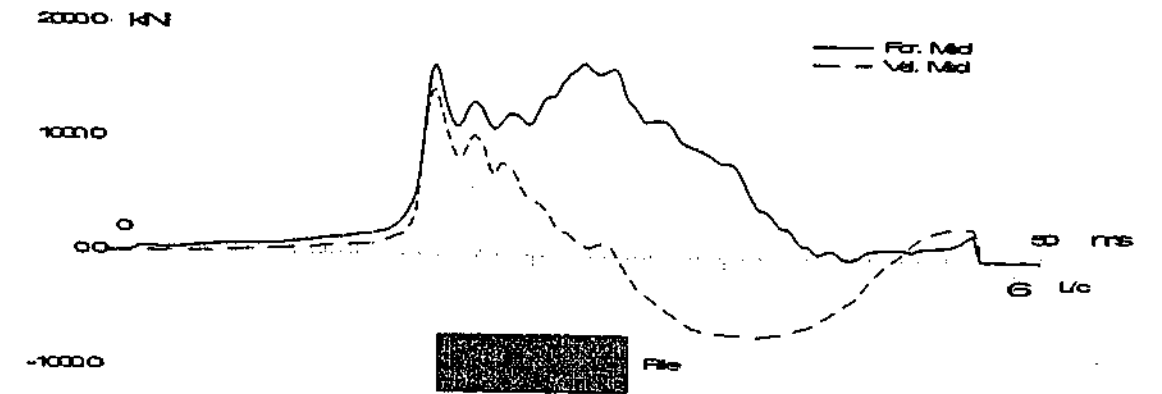
(A) Soil Data

Depth (m) Soil description
0.0 Asphalt and aggregate base course STONE
0.6 Stiff brown and black micaceous medium to fine sandy SILT
4.1 Loose gray-brown and tan micaceous silty fine SAND
6.9 Very stiff and stiff brown, gray, black micaceous fine sandy SILT

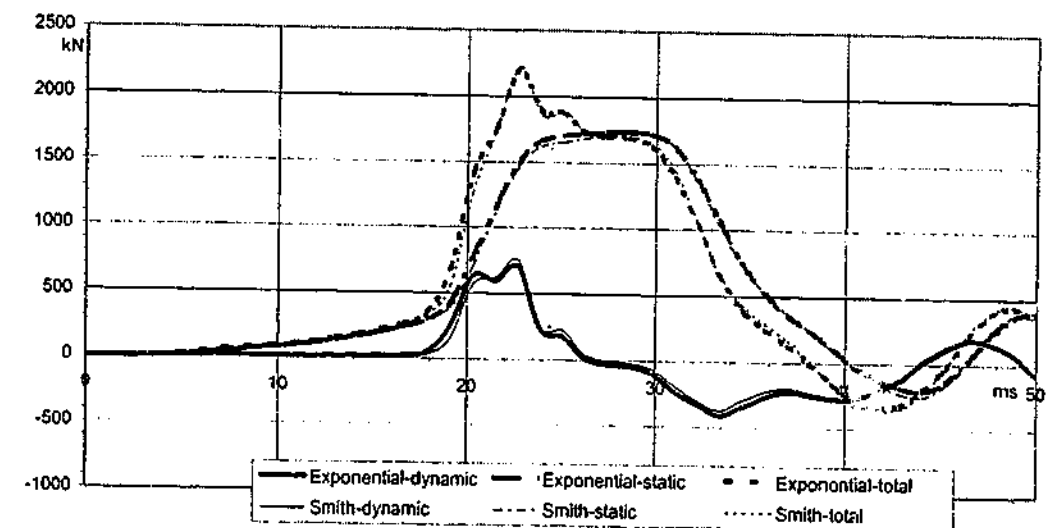
15.7 Very firm gray, brown and black micaceous silty fine SAND
19.2 Dense to very dense gray and brown micaceous silty medium to fine SAND
21.9 Partially weathered rock when sampled becomes very dense gray, brown and tan micaceous silty medium to fine SAND
24.7 Dense to very dense brown and black micaceous silty medium to fine SAND
28.0 Very dense brown and black micaceous silty medium to fine SAND
30.2 Partially weathered rock when sampled becomes very dense gray, WATER TABLE elevation: 922.00 ft



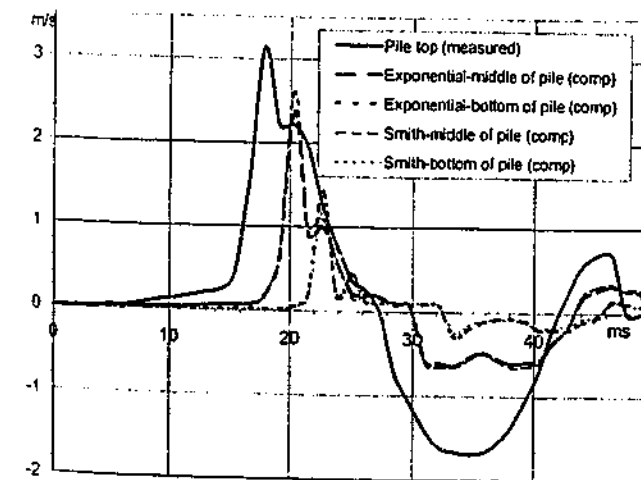
(B) Measured Force & Velocity at Pile Top



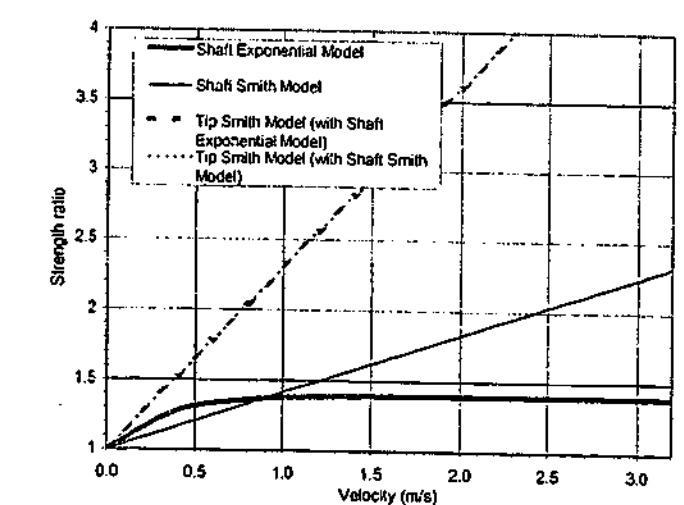
(C) Computed Resistances



(D) Velocities at Top, Middle & Bottom of Pile



(E) Strength Ratio-Velocity Models for Shaft & Tip



ID26 (end of ID11)
R118/13D H 7497/482-502X;CL:CL;Blow: 538

Filename 28 def
Smith Linear Viscous Damping using Rult for Shaft

Filename 28 nm rlnst
Exponential Viscous Damping using Rlnst for shaft

(A) Pile Model

Depth	Area	E-Mod	Spec Wei	Circum	Impedance
m	cm ²	MPa	kN/m ³	m	kN/m/s
18.99	270.32	206579	77.267	1.422	1099.2
18.98	270.32	206579	77.267	1.422	1300

Added impedance 1300kN/m/s bet 16m and 17m, and 1700kN/m/s bet 17m and 19m
Wave Speed 5119.8 m/s

(A) Pile Model

Depth	Area	E-Mod	Spec Wei	Circum	Impedance
m	cm ²	MPa	kN/m ³	m	kN/m/s
18.99	270.32	206579	77.267	1.422	1099.2
18.98	270.32	206579	77.267	1.422	1300

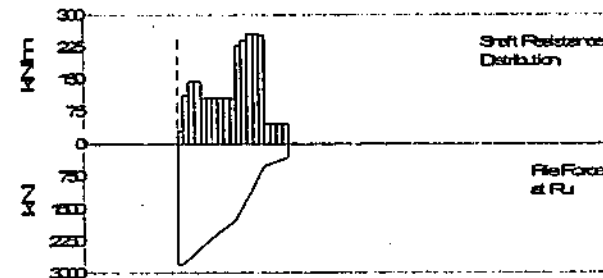
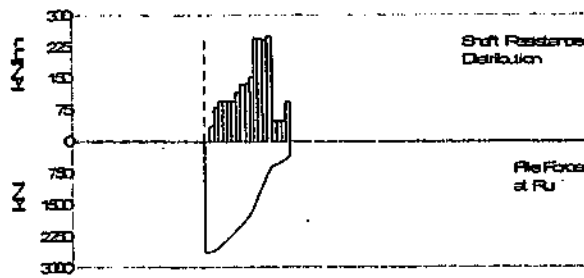
As per Smith Linear Viscous Damping
Added impedance 1600kN/m/s bet 17m and 19m

(B) Resistance Distribution

Depth	Ru	Unit	Total capacity
m	kN	kPa	kN
1	0	0	2612.2
2	37.7	26.48	2277.4
3	81	56.9	334.1
4	98	67.44	
5	97.2	68.28	
6	96.1	67.51	
7	95.7	67.23	
8	117.4	82.47	
9	135.6	95.4	
10	138.7	97.44	
11	153.6	107.9	
12	246	174.22	
13	246.3	173.02	
14	241.7	169.78	
15	251.2	176.47	
16	49.2	34.56	
17	49.2	34.56	
18	49.2	34.56	
19	93.4	65.61	
Avg Skin	119.9	84.2	
Toe	334.8	0	

(B) Resistance Distribution

Depth	Ru	Unit	Total capacity
m	kN	kPa	kN
1	30.4	21.38	2810.3
2	113.4	79.68	2505.6
3	144.4	101.44	304.9
4	144.5	101.51	
5	106.3	74.68	
6	107	75.17	
7	107	75.17	
8	107	75.17	
9	107	75.17	
10	106.7	74.96	
11	230.7	162.07	
12	241.6	169.72	
13	257	180.54	
14	258.9	180.47	
15	254.5	178.79	
16	47.8	33.58	
17	47.8	33.58	
18	47.8	33.58	
19	47.8	33.58	
Avg Skin	131.9	92.64	
Toe	304.7	0	



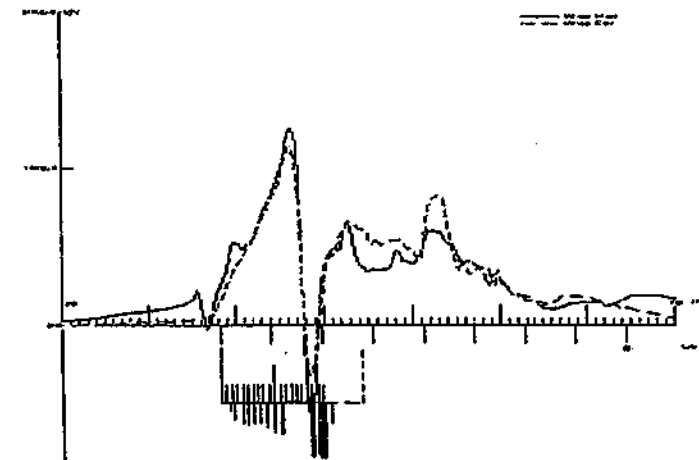
(C) CAPWAP Parameters

JS	SS	QS	UN	CS	LS	PI	OP
1.006	0.485	6	0	1	1	0.01	1
JT	ST	QT	TG	CT	LT	PL	
0.24	0.787	1	6	0.01	1	0	

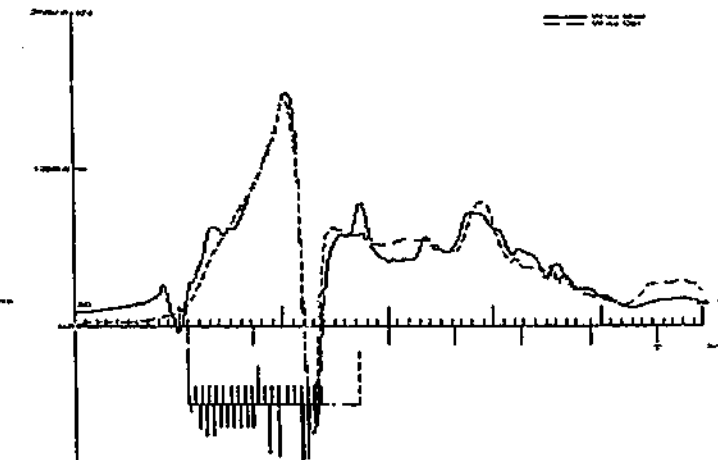
(C) CAPWAP Parameters

JS	SS	QS	UN	CS	LS	PI	OP
2.052	0.9	4	0	1	1	0.01	1
JT	ST	QT	TG	CT	LT	PL	
0.059	0.212	1	0	0.01	1	0.55	

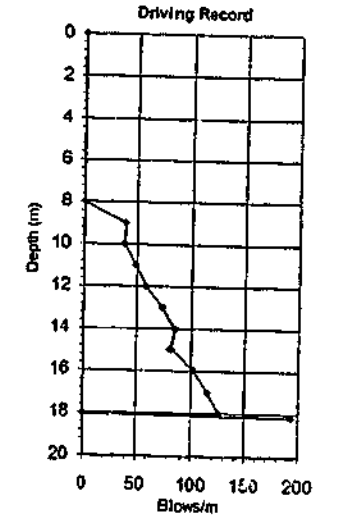
(D) Match
CAPWAP match quality: 6.08 (Wave Up Match)
Observed: final set = 8.021 mm; blow count = 125 b/m
Computed: final set = 2.779 mm; blow count = 380 b/m



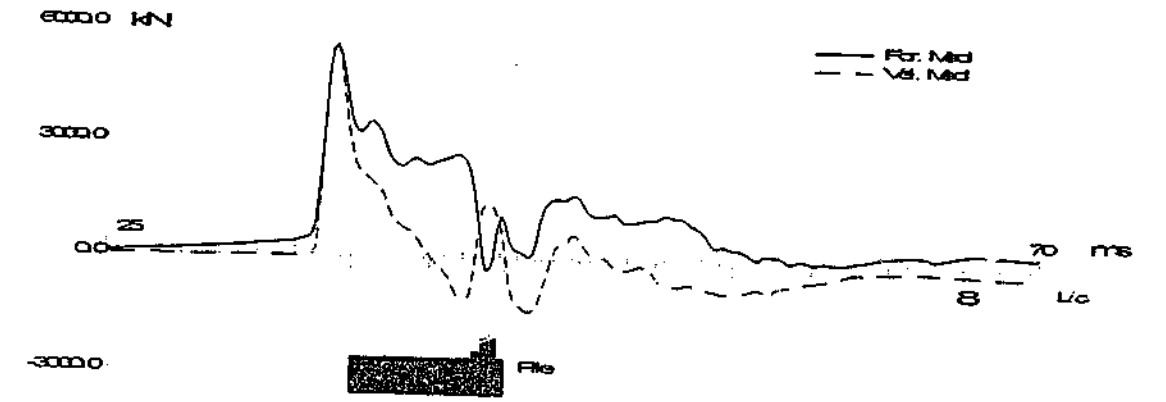
(D) Match
CAPWAP match quality: 5.51 (Wave Up Match)
Observed: final set = 8.021 mm; blow count = 125 b/m
Computed: final set = 3.341 mm; blow count = 299 b/m



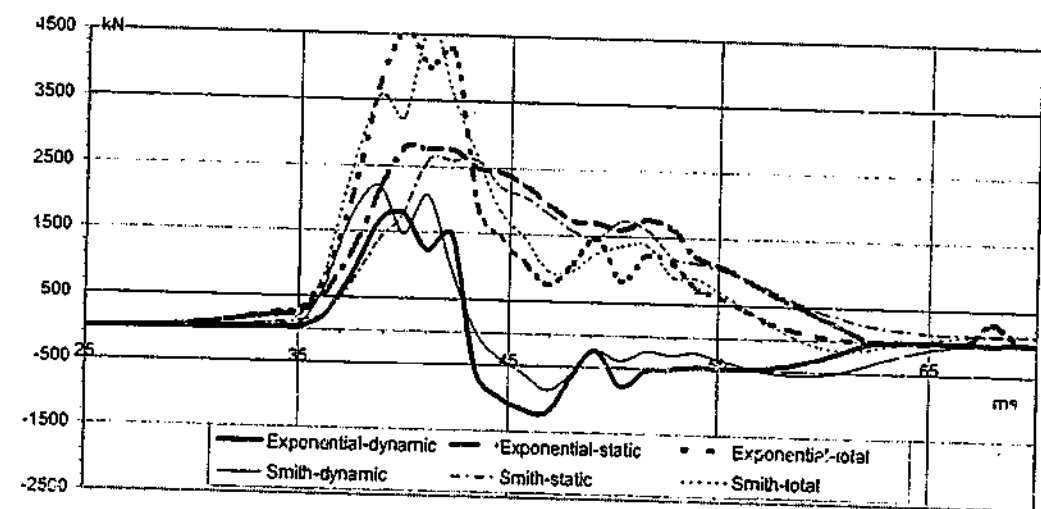
(A) Soil Data
Depth (m) Soil description
0.0 Sandy LOAM or clayey fine SAND (FILL)
3 Soft, fissured and stratified Boom CLAY



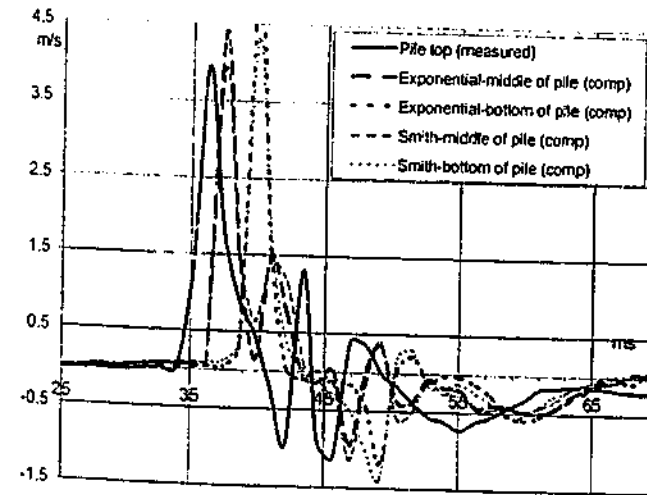
(B) Measured Force & Velocity at Pile Top



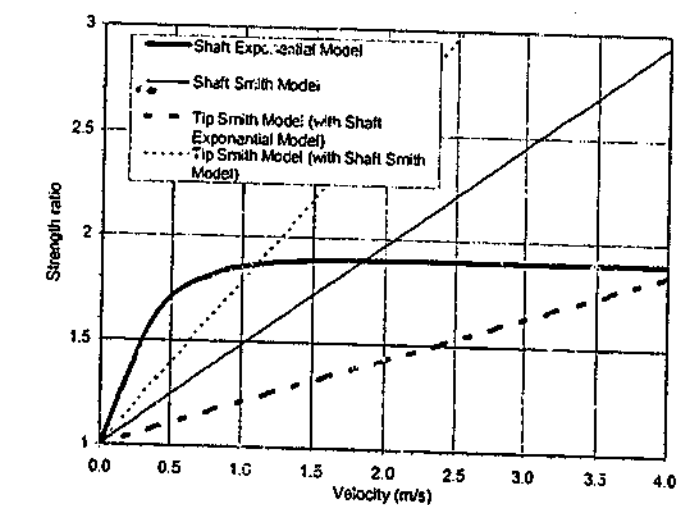
(C) Computed Resistances



(D) Velocities at Top, Middle & Bottom of Pile



(E) Strength Ratio-Velocity Models for Shaft & Tip



ID27
 EX1; SENT 17-2; Pile: EX-1 D38-23; silt; 16" PSC; Blow: 1171

Filename 27 def
 Smith Linear Viscous Damping using Rult for Shaft

(A) Pile Model

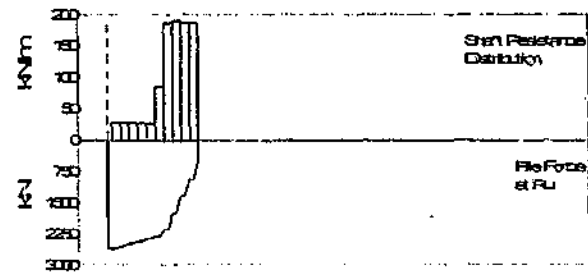
Depth (m)	Area (cm ²)	E-Mod (MPa)	Spec Wei (kN/m ³)	Circum (m)	Impedance (kN/m/s)
0	1651.8	57725	23.563	1.6	1572.44
21.95	1651.8	37725	23.563	1.6	None

Wave Speed 3962.4 m/s

(B) Resistance Distribution

Depth (m)	Ru (kN)	Unit (kPa)	Total capacity (kN)
3.1	61.7	18.45	2593.3
5.2	59.1	17.67	2057.5
7.3	56.8	17.58	535.8
9.4	56.6	17.52	
11.5	58.4	17.46	
13.6	180.7	54.03	
15.7	393.5	117.67	
17.8	400.5	118.78	
19.9	393.4	117.64	
21.9	392.8	117.48	

Avg Skin 205.8 61.53
 Toe 535.8 3245.31



EOD 406mm PSC

Filename 27 rult nm
 Exponential Viscous Damping using Rult for shaft

(A) Pile Model

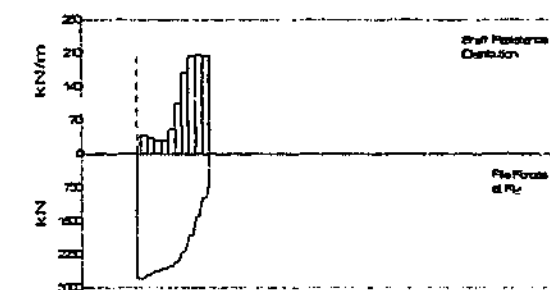
Depth (m)	Area (cm ²)	E-Mod (MPa)	Spec Wei (kN/m ³)	Circum (m)	Impedance (kN/m/s)
0	1651.8	57725	23.563	1.6	1572.44
21.95	1651.8	37725	23.563	1.6	None

Wave Speed 3962.4 m/s

(B) Resistance Distribution

Depth (m)	Ru (kN)	Unit (kPa)	Total capacity (kN)
3.1	83.3	24.91	2777
5.2	68.4	20.78	2239
7.3	57.7	17.27	538
9.4	56.8	17.83	
11.5	107.6	32.17	
13.6	221.8	66.32	
15.7	352.8	105.45	
17.8	426.8	127.81	
19.9	430.5	128.72	
21.9	429.7	128.48	

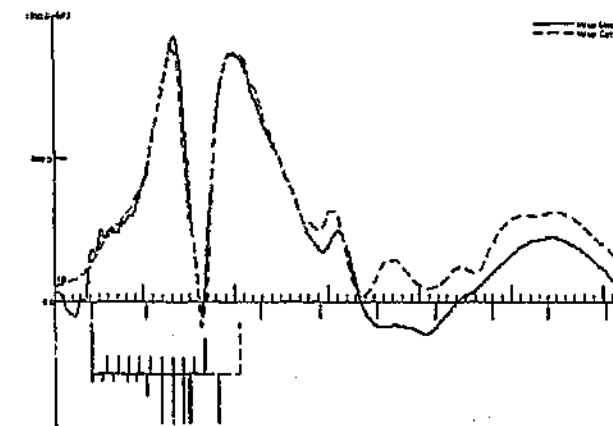
Avg Skin 223.9 66.85
 Toe 538 3258.89



(C) CAPWAP Parameters

JS	SS	QS	UN	CS	LS	PI	OP
0.707	0.54	1.8	0	1	1	0.01	1
JT	ST	QT	TG	CT	LT	PL	
0.17	0.5	1.8	5	1	1	0	

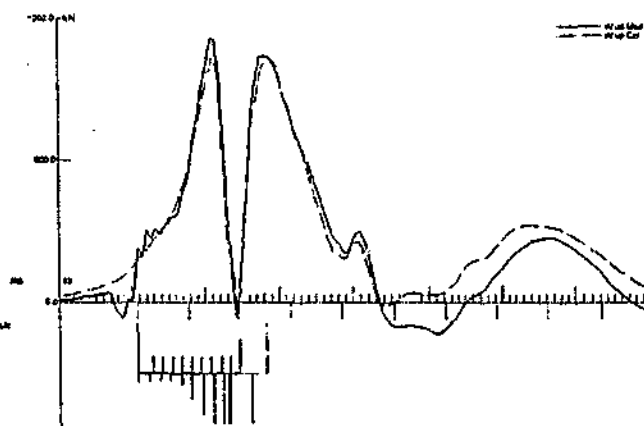
(D) Match
 CAPWAP match quality: 6.11 (Wave Up Match)
 Observed: final set = 9.100 mm, blow count = 110 b/m
 Computed: final set = 5.523 mm, blow count = 181 b/m



(C) CAPWAP Parameters

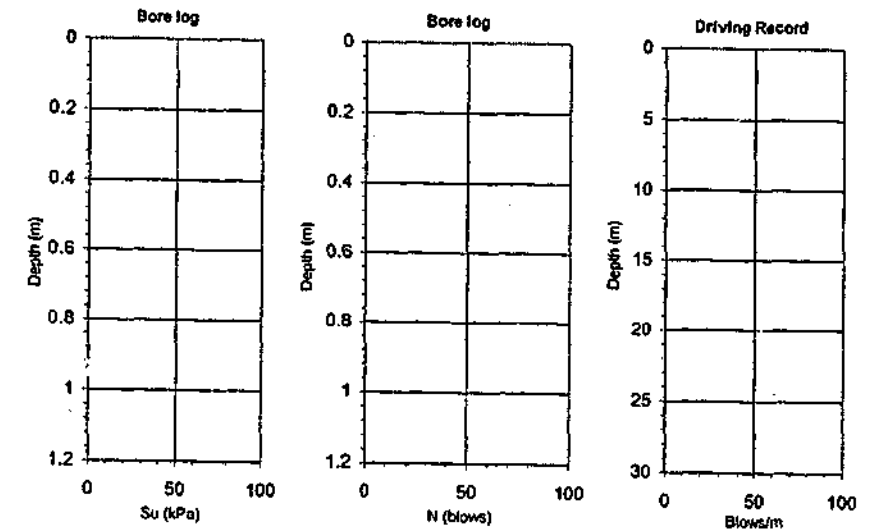
JS	SS	QS	UN	CS	LS	PI	OP
0.708	0.497	1.94	1	1	1	0.02	1
JT	ST	QT	TG	CT	LT	PL	
0.645	0.132	6.89	0	1	1	0.5	

(D) Match
 CAPWAP match quality: 4.65 (Wave Up Match)
 Observed: final set = 9.100 mm, blow count = 110 b/m
 Computed: final set = 6.432 mm, blow count = 155 b/m

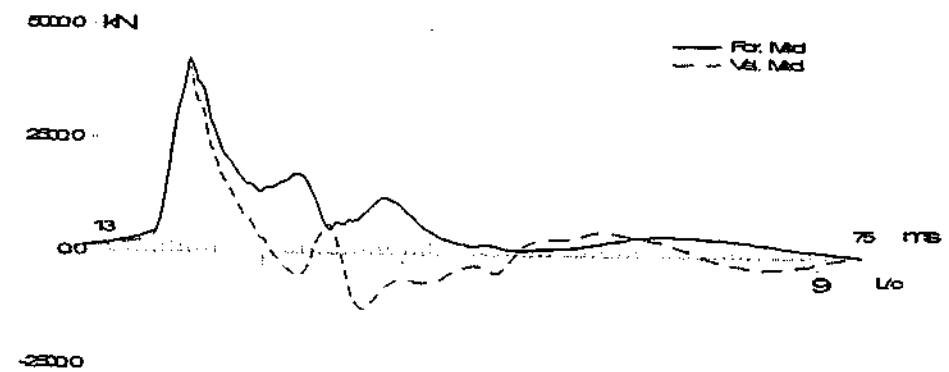


(A) Soil Data (general)
 Depth (m) Soil description

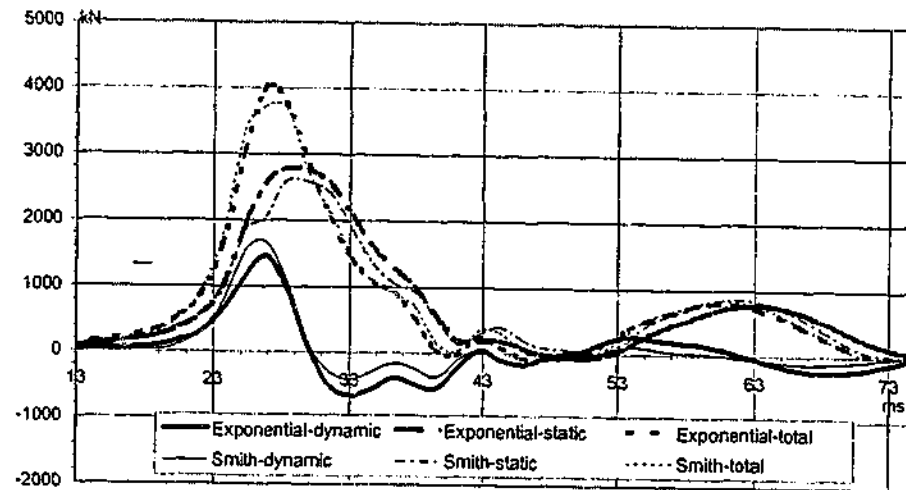
Soil with silt
 Bore log & driving record NA



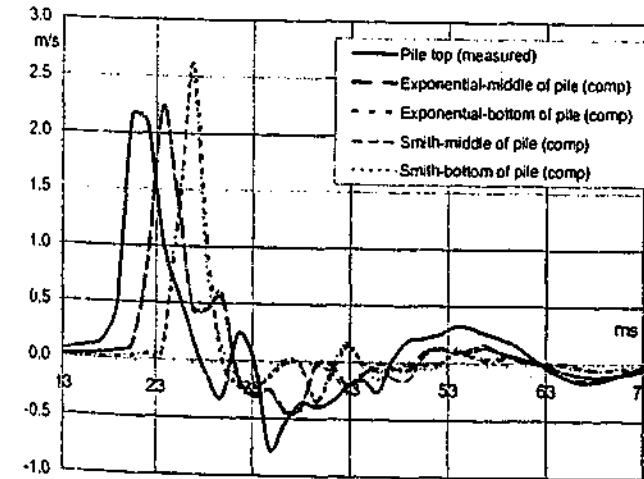
(B) Measured Force & Velocity at Pile Top



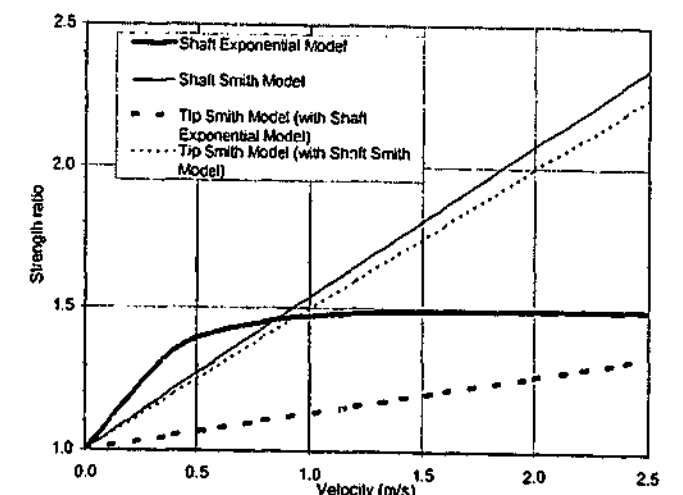
(C) Computed Resistances



(D) Velocities at Top, Middle & Bottom of Pile



(E) Strength Ratio-Velocity Models for Shaft & Tip



ID28
 EX3, JAMESVILLE 10.75"; Pile: EX-3 VUL014, COMPOSITE; Blow: 20

Filename 28 def
 Smith Linear Viscous Damping using Rult for Shaft

(A) Pile Model

Depth (m)	Area (cm ²)	E-Mod (MPa)	Spec Wel (kN/m ³)	Circum (m)	Impedance (kN/m/s)
0	585.55	45728	30.632	0.968	899.81
23.53	585.55	45728	30.632	0.968	None

Wave Speed 3826.2 m/s

(B) Resistance Distribution

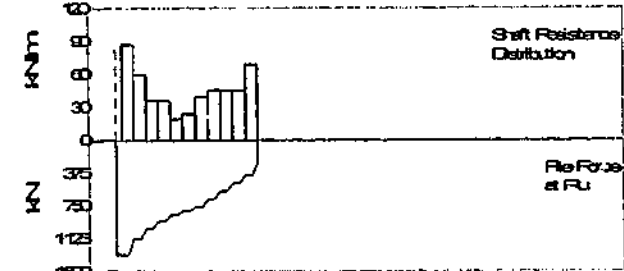
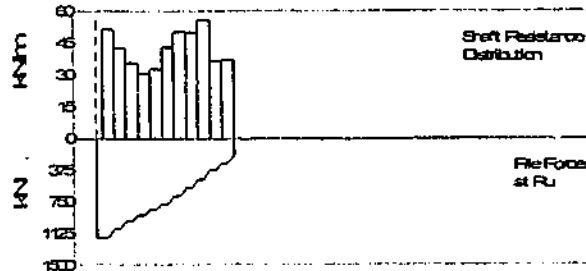
Depth (m)	Ru (kN)	Unit (kPa)	Total capacity (kN)
2.5	105.8	53.32	1169.8
4.6	89.4	44.63	958.7
6.6	73.3	37.01	211.3
8.7	62.9	31.76	
10.7	67.5	34.09	
12.8	88.6	44.73	
14.8	103.4	52.21	
16.9	102.9	51.96	
18.9	115	58.06	
21	74.7	37.72	
23	76.4	38.58	
Avg Skin	87.2	44.01	
Toe	211.1	3805.16	

Filename 28 rult
 Exponential Viscous Damping using Rult for shaft

(A) Pile Model
 As per Smith Linear Viscous Damping

(B) Resistance Distribution

Depth (m)	Ru (kN)	Unit (kPa)	Total capacity (kN)
2.5	179.5	90.63	1300.2
4.6	123.3	62.26	1048.2
6.6	75.5	38.12	252
8.7	75.5	38.12	
10.7	40.8	20.5	
12.8	49.7	25.09	
14.8	81.9	41.35	
16.9	83.7	42.31	
18.9	94	47.48	
21	92.4	46.85	
23	142.1	71.75	
Avg Skin	85.3	48.11	
Toe	252	4303.65	



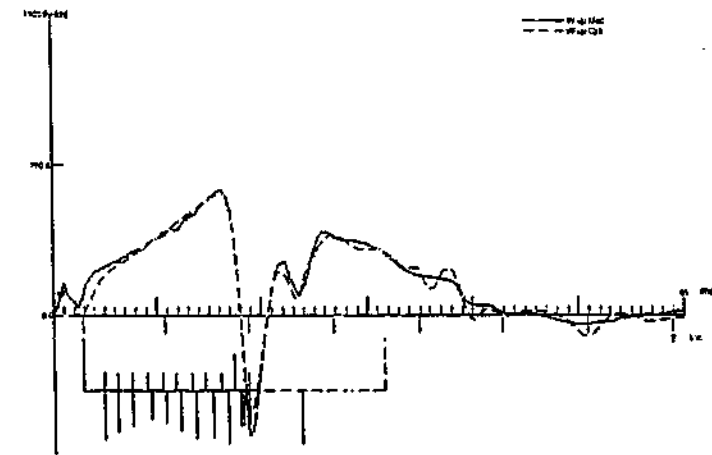
(C) CAPWAP Parameters

JS	SS	QS	UN	CS	LS	PI	OP
0.712	0.52	4	0.16	0.8	1	0.02	2
JT	ST	QT	TG	CT	LT	PL	
0.113	0.376	1	11.5	1	1	1.1	

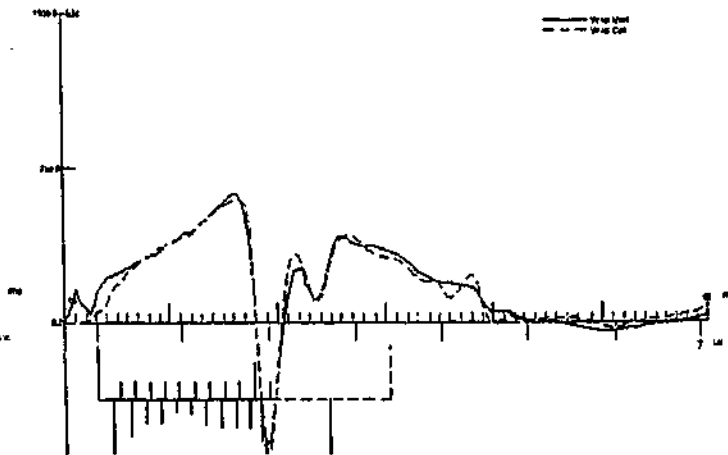
(C) CAPWAP Parameters

JS	SS	QS	UN	CS	LS	PI	OP
0.839	0.59	3.3	0	1	1	0.02	0
JT	ST	QT	TG	CT	LT	PL	
0.072	0.2	2.5	11.8	1	1	1.1	

(D) Match
 CAPWAP match quality: 2.17 (Wave Up Match)
 Observed: final set = 11,800 mm; blow count = 85 b/m
 Computed: final set = 12,683 mm; blow count = 79 b/m

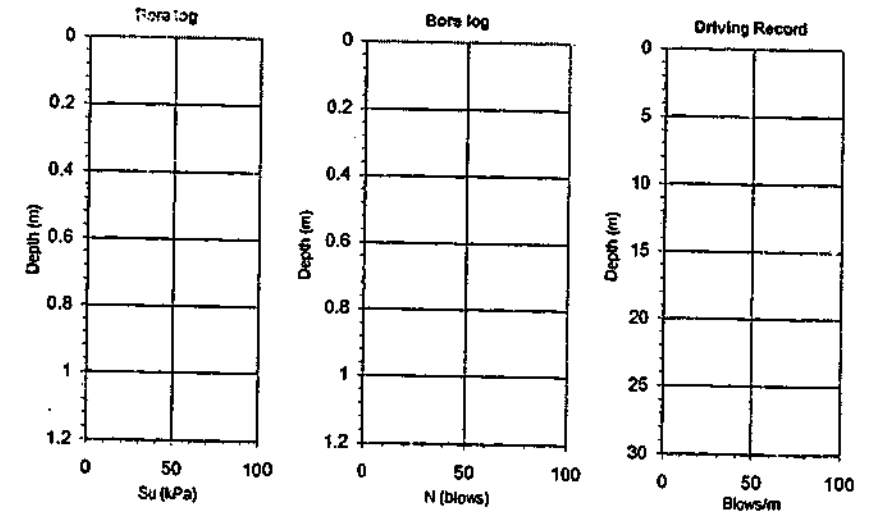


(D) Match
 CAPWAP match quality: 2.35 (Wave Up Match)
 Observed: final set = 11,890 mm; blow count = 85 b/m
 Computed: final set = 12,160 mm; blow count = 82 b/m

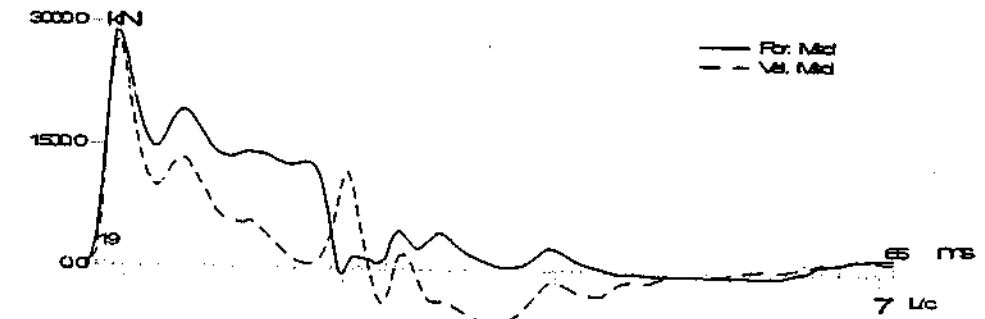


(A) Soil Data (general)
 Depth (m) Soil description

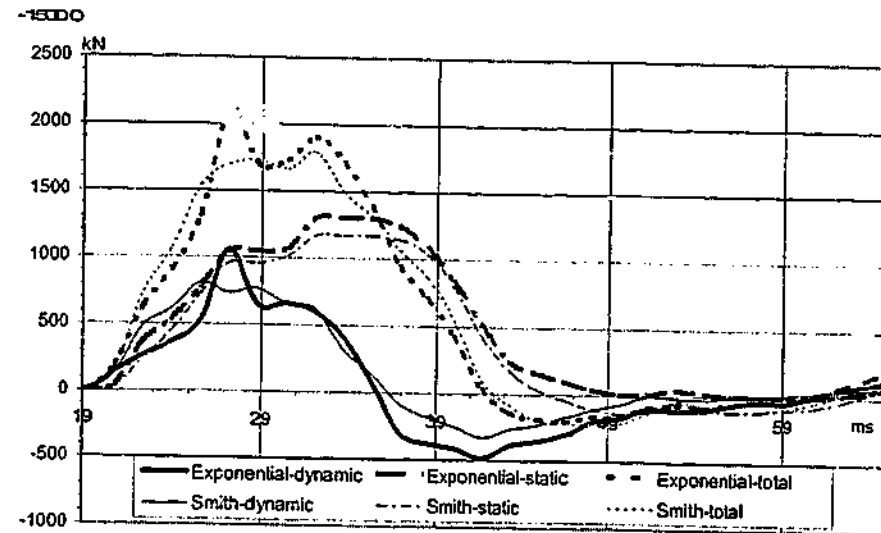
Fine grained soil
 Bore log and driving record NA



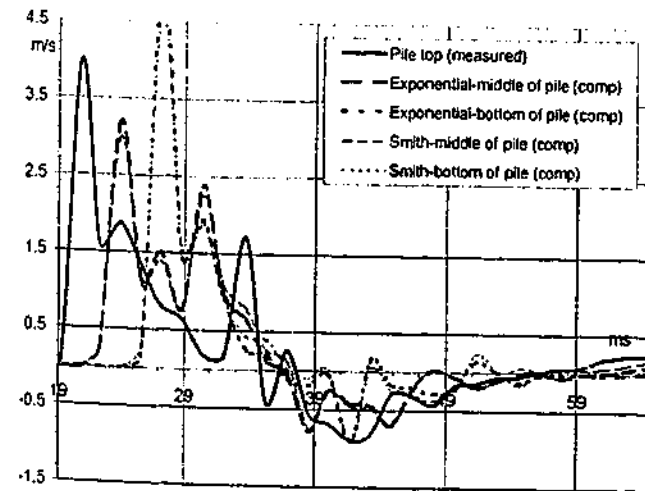
(B) Measured Force & Velocity at Pile Top



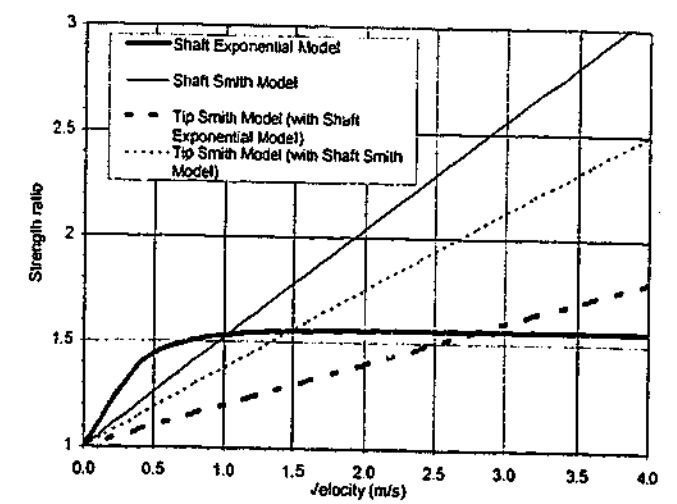
(C) Computed Resistances



(D) Velocities at Top, Middle & Bottom of Pile



(E) Strength Ratio-Velocity Models for Shaft & Tip



ID29
 EX5; RTA517; SOFT->TILL; Pile: EX-5 Vulcan 508; 14X.312 CEP; Blow: 584

Filename 29 ok
 Smith Linear Viscous Damping using Rult for Shaft

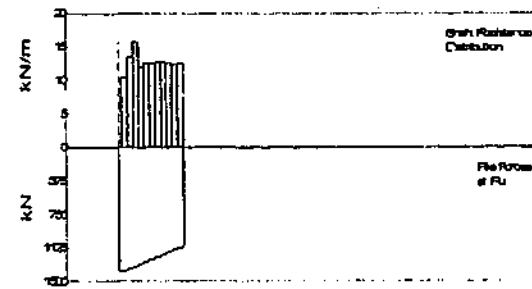
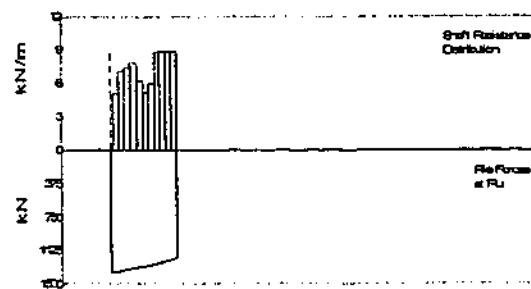
Depth	Area	E-Mod	Spec We	Circum	Impedance
m	cm ²	MPa	kN/m ³	m	349.53 kN/m/s
0	86.56	206900	77.287	1.117	Added impedance None
23.47	86.56	206900	77.287	1.117	Wave Speed 5123.7 m/s

(B) Resistance Distribution					
Depth	Ru	Unit	Total capacity	Shaft capacity	Toe capacity
Below	Ru		kN	kN	kN
Grade	(Area)				
m	kN	kPa			
3.1	10.4	4.56	1367.4	183.1	1204.3
5.1	14.4	6.32			
7.1	15	6.58			
9.2	15.9	6.97			
11.2	12.6	5.81			
13.3	10.5	4.81			
15.3	12.2	5.35			
17.3	17.6	7.85			
19.4	18	7.9			
21.4	18	7.9			
23.5	18	7.9			
Avg skin	14.8	6.5			
Toe	1204.3	0			

Filename 29 nm rinst
 Exponential Viscous Damping using Rinst for shaft

(A) Pile Model
 As per Smith Linear Viscous Damping

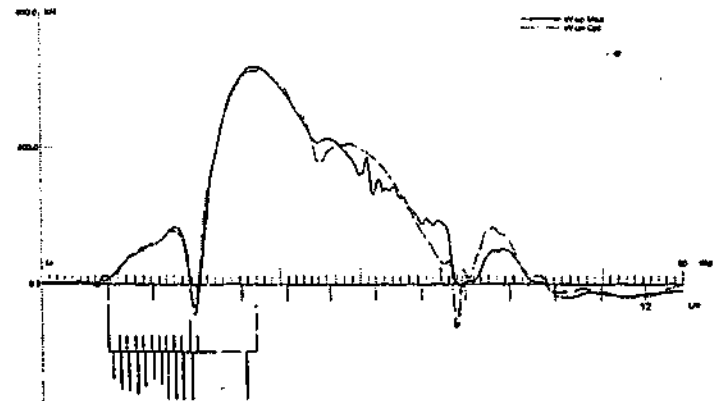
(B) Resistance Distribution					
Depth	Ru	Unit	Total capacity	Shaft capacity	Toe capacity
Below	Ru		kN	kN	kN
Grade	(Area)				
m	kN	kPa			
3.1	21.3	8.34	1384.2	284	1100.2
5.1	27.4	12.02			
7.1	32	14.04			
9.2	24.4	10.7			
11.2	25.5	11.11			
13.3	25.5	11.19			
15.3	25.8	11.32			
17.3	25.8	11.32			
19.4	25.7	11.27			
21.4	25	10.97			
23.5	25.6	11.23			
Avg skin	25.8	11.33			
Toe	1100.2	0			



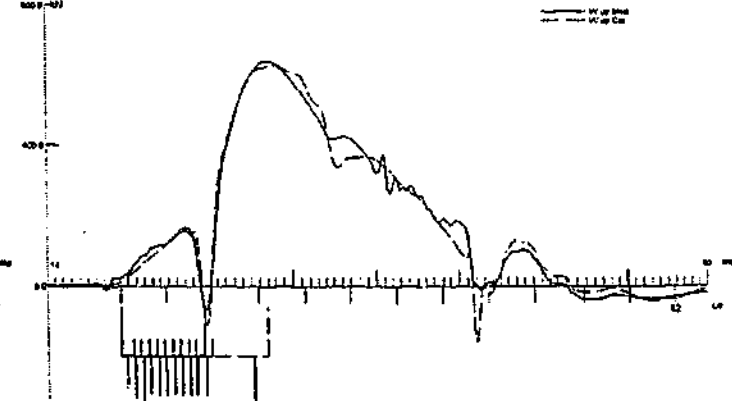
(C) CAPWAP Parameters								
JS	GS	QS	UN	CS	LS	PI	OP	
0.268	0.574	1.96	0.628	1	1	0.01	0	
JT	ST	QT	TG	CT	LT	PL		
0.425	0.123	13.01	0	0.8	1	0.33		

(C) CAPWAP Parameters								
JS	SS	QS	UN	CS	LS	PI	OP	
0.326	0.401	3.5	0.75	1	1	0.01	0	
JT	ST	QT	TG	CT	LT	PL		
0.456	0.145	13.8	0	1	1	0.5		

(D) Match
 CAPWAP match quality: 2.34 (Wave Up Match)
 Observed: final set = 2.540 mm; blow count = 394 b/m
 Computed: final set = 1.791 mm; blow count = 558 b/m

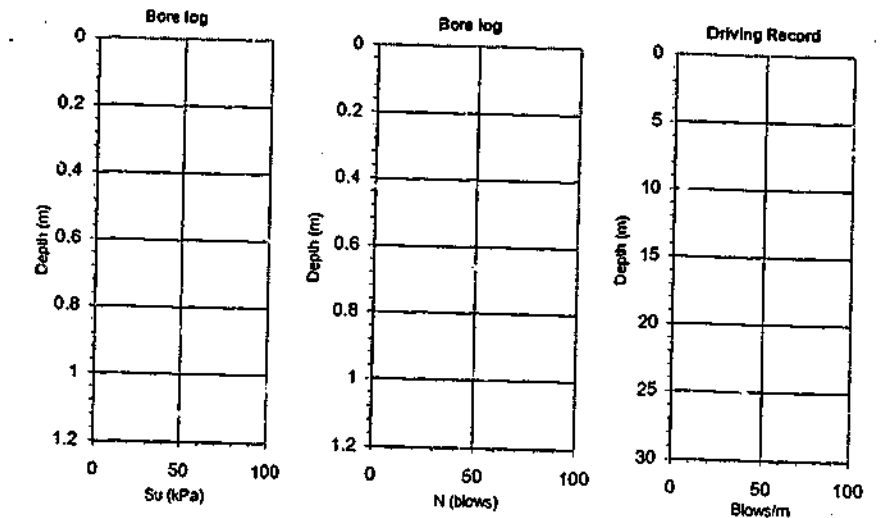


(D) Match
 CAPWAP match quality: 2.86 (Wave Up Match)
 Observed: final set = 2.540 mm; blow count = 394 b/m
 Computed: final set = 2.421 mm; blow count = 413 b/m

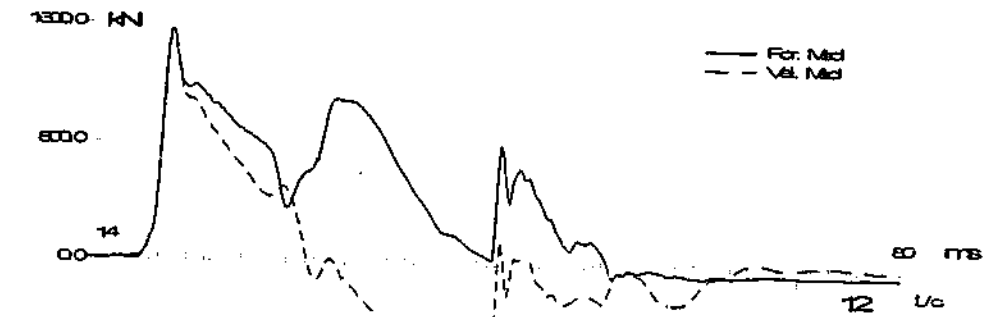


(A) Soil Data (general)
 Depth (m) Soil description

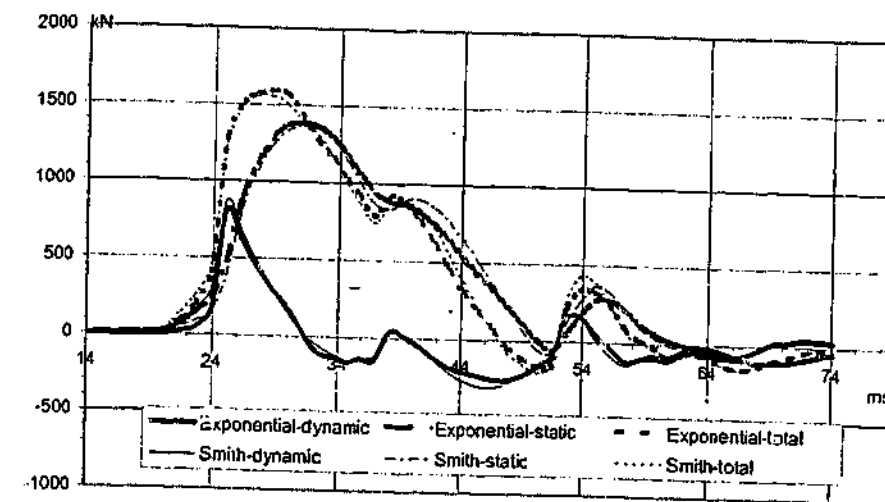
Clay and till
 Bore log and driving record NA



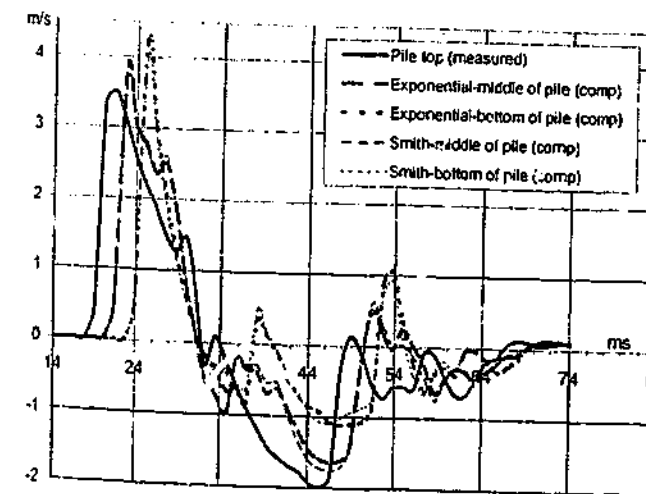
(B) Measured Force & Velocity at Pile Top



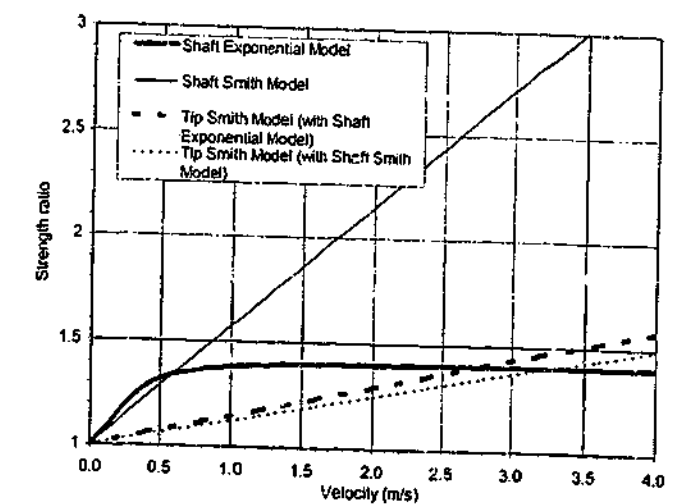
(C) Computed Resistances



(D) Velocities at Top, Middle & Bottom of Pile



(E) Strength Ratio-Velocity Models for Shaft & Tip



ID30

EX20: TOP YIELD NONUNIF; Pile: EX-20 D12-32 12.75x.25" CLAY; Blow: 10

Filename 30 def
Smith Linear Viscous Damping using Rinst for Shaft

Filename 30 nm rinst
Exponential Viscous Damping using Rinst for shaft

(A) Pile Model

Depth	Area	E-Mod	Spec Wel	Circum	Impedance
m	cm ²	MPa	kN/m ³	m	kN/m/s
0	63.34	208895.6	77.287	1.017	255.77
17.68	63.34	208895.6	77.287	1.017	None

Wave Speed 5123.7 m/s

(A) Pile Model
As per Smith Linear Viscous Damping

(B) Resistance Distribution

Depth	Ru	Unit	Total capacity
Below	Ru		Shaft capacity
Grade	(Area)		Toe capacity
m	kN	kPa	kN
1.5	48.6	45.94	1485.4
2.5	31	29.3	1135.3
3.6	5.2	4.92	350.1
4.8	0	0	
5.8	0	0	
6.7	10.7	10.11	
7.7	52.9	50.01	
8.7	97.9	92.54	
9.8	117.9	111.45	
10.8	110.2	104.17	
11.9	99.1	93.68	
12.9	104.1	98.4	
13.9	112.9	106.72	
15	111.1	105.02	
16	112.1	105.97	
17.1	122	115.32	

Depth	Ru	Unit	Total capacity
Below	Ru		Shaft capacity
Grade	(Area)		Toe capacity
m	kN	kPa	kN
1.5	19.4	18.34	1405.8
2.5	19	17.96	1003.1
3.6	18.8	17.77	402.8
4.6	18.7	17.69	
5.6	18.6	17.59	
6.7	28.6	27.03	
7.7	86.3	81.58	
8.7	155.9	150.1	
9.8	121.5	114.85	
10.8	123.1	116.36	
11.9	73.5	69.46	
12.9	73.7	69.87	
13.9	73.9	69.85	
15	73.8	69.76	
16	73.7	69.67	
17.1	74.9	70.8	

(B) Resistance Distribution

Depth	Ru	Unit	Total capacity
Below	Ru		Shaft capacity
Grade	(Area)		Toe capacity
m	kN	kPa	kN
1.5	48.6	45.94	1485.4
2.5	31	29.3	1135.3
3.6	5.2	4.92	350.1
4.8	0	0	
5.8	0	0	
6.7	10.7	10.11	
7.7	52.9	50.01	
8.7	97.9	92.54	
9.8	117.9	111.45	
10.8	110.2	104.17	
11.9	99.1	93.68	
12.9	104.1	98.4	
13.9	112.9	106.72	
15	111.1	105.02	
16	112.1	105.97	
17.1	122	115.32	

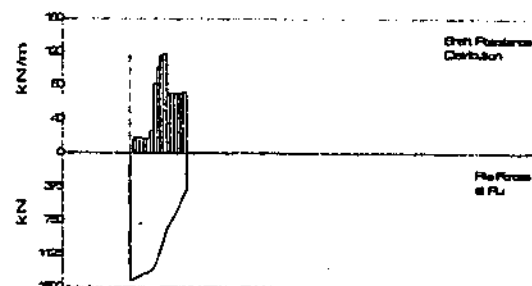
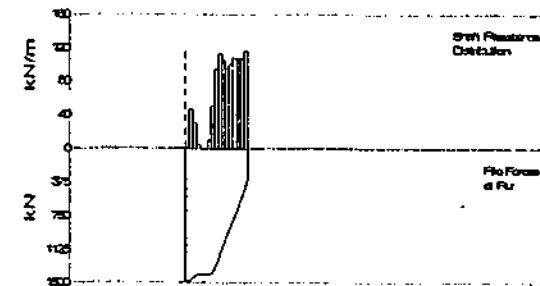
Depth	Ru	Unit	Total capacity
Below	Ru		Shaft capacity
Grade	(Area)		Toe capacity
m	kN	kPa	kN
1.5	19.4	18.34	1405.8
2.5	19	17.96	1003.1
3.6	18.8	17.77	402.8
4.6	18.7	17.69	
5.6	18.6	17.59	
6.7	28.6	27.03	
7.7	86.3	81.58	
8.7	155.9	150.1	
9.8	121.5	114.85	
10.8	123.1	116.36	
11.9	73.5	69.46	
12.9	73.7	69.87	
13.9	73.9	69.85	
15	73.8	69.76	
16	73.7	69.67	
17.1	74.9	70.8	

Avg Skin 71 67.1

Toe 350.1 4250.12

Avg Skin 62.7 59.28

Toe 402.8 4869.62



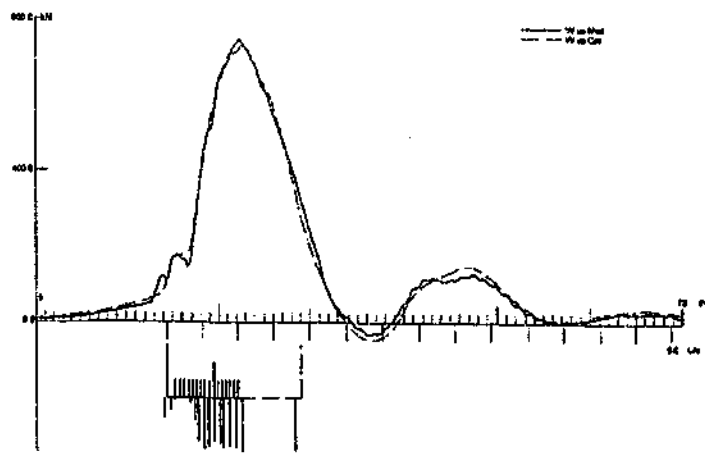
(C) CAPWAP Parameters

JS	SS	QS	UN	CS	LS	PI	OP
2.156	0.486	1.01	0.498	1	1	0.01	0
JT	ST	QT	TG	CT	LT	PL	
1.158	0.846	3.06	0	1	1	0.237	

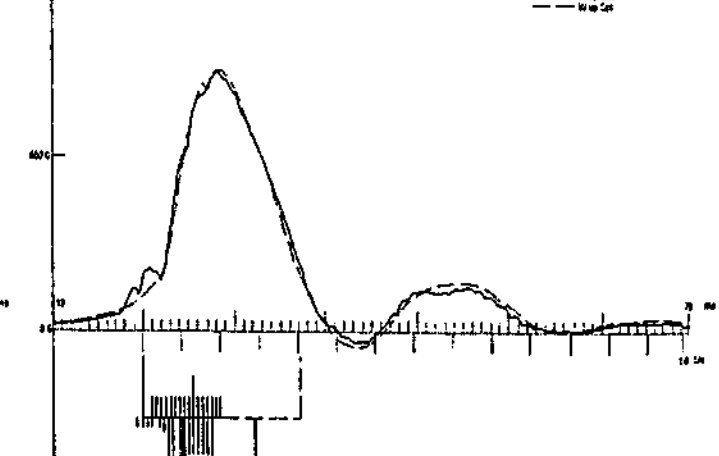
(C) CAPWAP Parameters

JS	SS	QS	UN	CS	LS	PI	OP
2.856	0.728	1.01	0.342	1	1	0.01	0
JT	ST	QT	TG	CT	LT	PL	
0.394	0.25	3.48	0	1	1	0	

(D) Match
CAPWAP match quality: 2.04 (Wave Up Match)
Observed: final set = 4.064 mm; blow count = 246 b/m
Computed: final set = 3.129 mm; blow count = 320 b/m



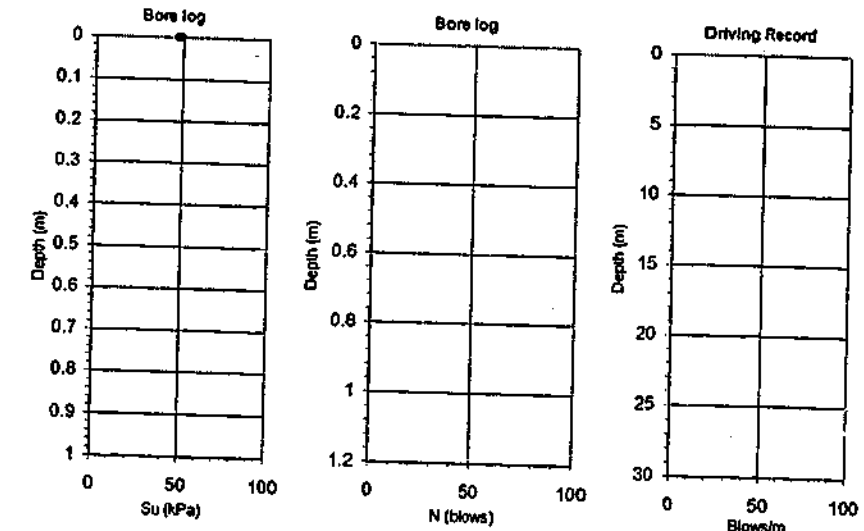
(D) Match
CAPWAP match quality: 2.33 (Wave Up Match)
Observed: final set = 4.064 mm; blow count = 246 b/m
Computed: final set = 3.322 mm; blow count = 301 b/m



(A) Soil Data (general)
Depth (m) Soil description

Clays

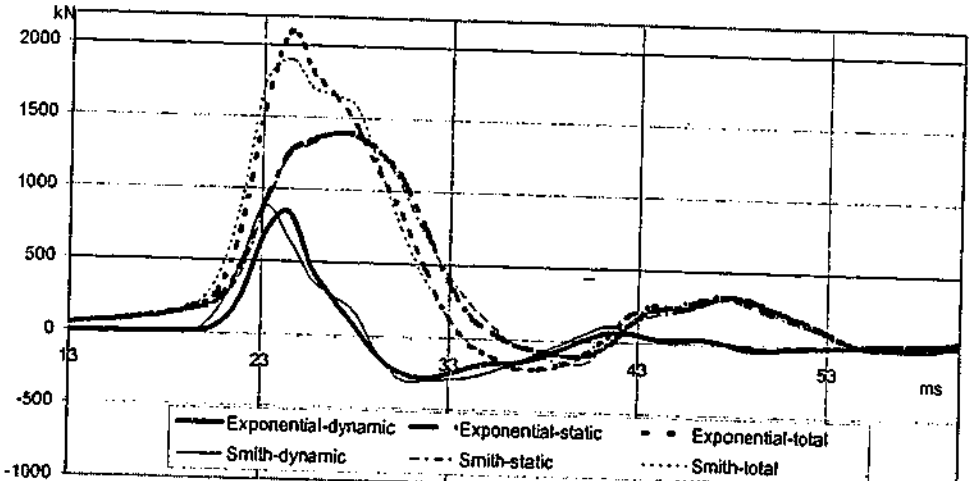
Bore log and driving record NA



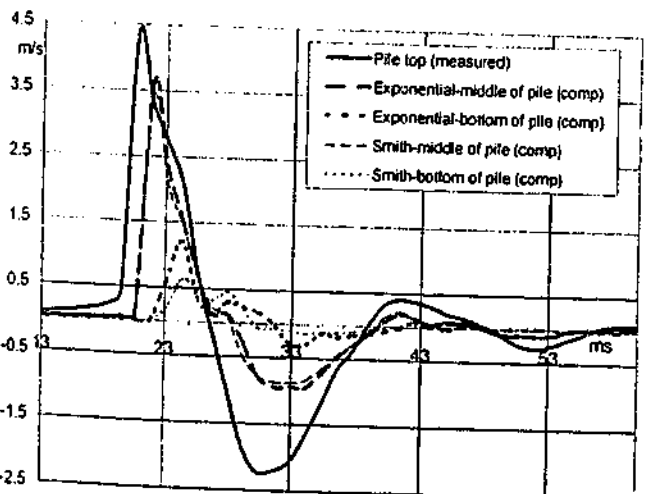
(B) Measured Force & Velocity at Pile Top



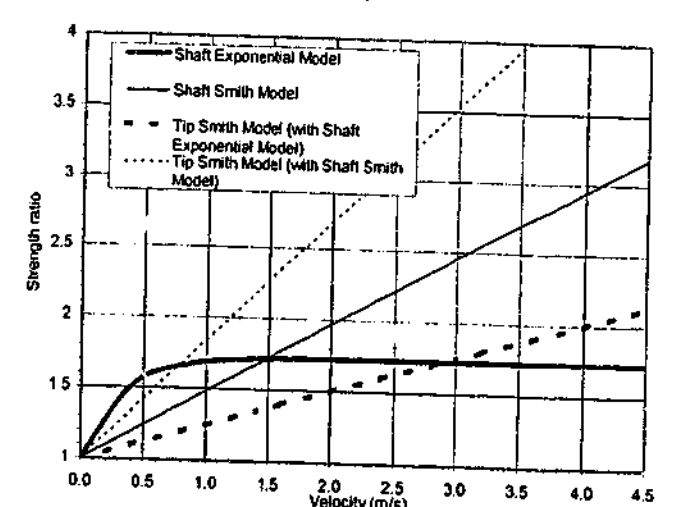
(C) Computed Resistances



(D) Velocities at Top, Middle & Bottom of Pile



(E) Strength Ratio-Velocity Models for Shaft & Tip



ID31
EX21; RESTRIKE 1 DAY; Pile: EX-21B K35; CL-SA SOIL; Blow: 2

Filename 31 def
Smith Linear Viscous Damping using Rult for Shaft

(A) Pile Model

Depth	Area	E-Mod	Spec Wei	Circum	Impedance
m	cm ²	MPa	kN/m ³	m	1808.43 kN/m/s
0	2090.32	31081.8	23.563	1.829	Added Impedance None
30.78	2090.32	31081.8	23.563	1.829	Wave Speed 3596.8 m/s

(B) Resistance Distribution

Depth	Ru	Unit	Total capacity	1816	kN
Below	Ru		Shaft capacity	1454.6	kN
Grade	(Area)		Toe capacity	161.4	kN
m	kN	kPa			
1.7	10.3	2.74			
3.8	7.7	2.05			
5.9	7.5	2			
7.9	10.9	2.9			
10	16	4.26			
12	25.2	6.71			
14.1	56.8	15.13			
16.1	173.9	46.33			
18.2	183.5	48.89			
20.2	186.3	50.17			
22.3	198.6	53.23			
24.3	199.1	53.05			
26.4	113.3	30.19			
28.4	158.4	42.2			
30.5	103.9	27.88			
Avg Skin	97	25.84			
Toe	161.4	772.13			

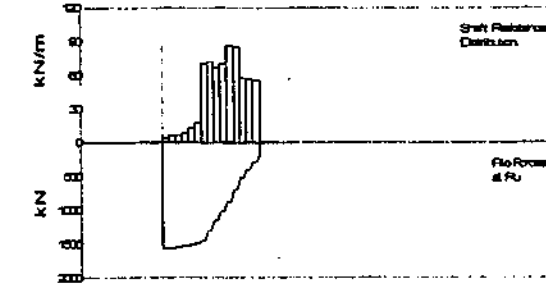
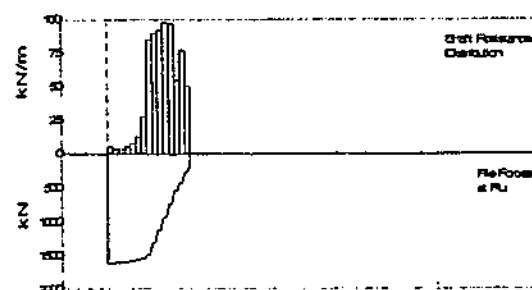
Filename 31 rinst nm
Exponential Viscous Damping using Rinst for shaft

(A) Pile Model

Depth	Area	E-Mod	Spec Wei	Circum	Impedance
m	cm ²	MPa	kN/m ³	m	1808.43 kN/m/s
0	2090.32	31081.8	23.563	1.829	Added Impedance None
30.78	2090.32	31081.8	23.563	1.829	Wave Speed 3596.8 m/s

(B) Resistance Distribution

Depth	Ru	Unit	Total capacity	1581.2	kN
Below	Ru		Shaft capacity	1309.2	kN
Grade	(Area)		Toe capacity	162	kN
m	kN	kPa			
1.7	9.1	2.42			
3.8	13.5	3.6			
5.9	13.5	3.6			
7.9	18.5	4.93			
10	27.7	7.38			
12	37	9.86			
14.1	145.5	38.77			
16.1	148.3	39.51			
18.2	137.5	36.63			
20.2	144.7	38.55			
22.3	177.6	47.32			
24.3	175.9	46.87			
26.4	118.5	31.57			
28.4	116.7	31.09			
30.5	115.2	30.89			
Avg Skin	93.3	24.85			
Toe	162	775			



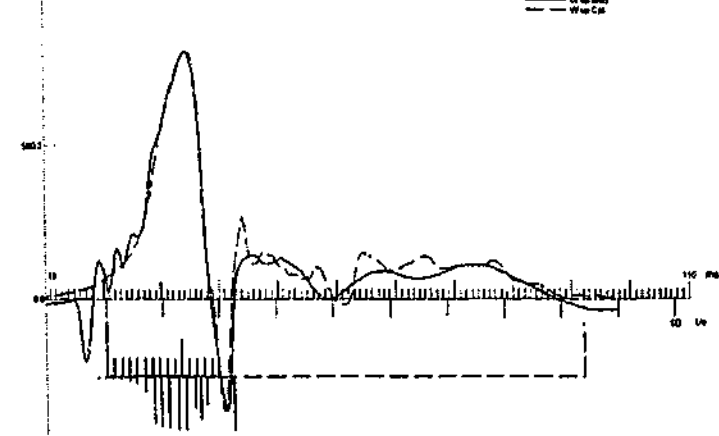
(C) CAPWAP Parameters

JS	SS	QS	UN	CS	LS	PI	OP
0.576	0.715	1.7	0	0.01	-1	0.02	0
JT	ST	QT	TG	CT	LT	PL	
0.063	0.703	7.3	0	0.1	-1	8.5	

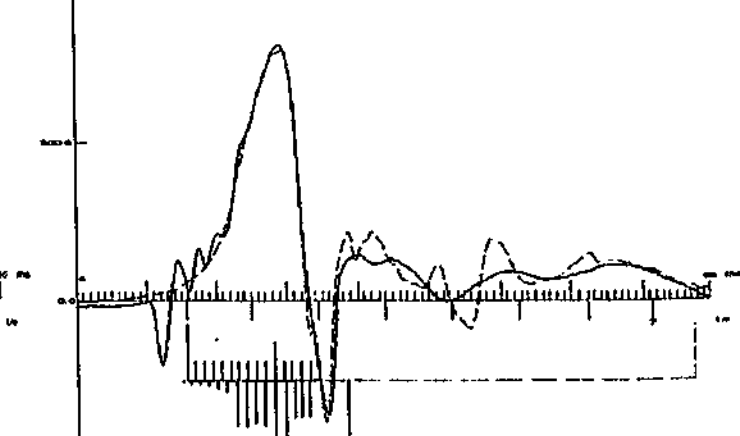
(C) CAPWAP Parameters

JS	SS	QS	UN	CS	LS	PI	OP
0.775	1	2.7	0	0.005	-1	0.02	0
JT	ST	QT	TG	CT	LT	PL	
0.022	0.25	8.5	0	0.15	-1	11	

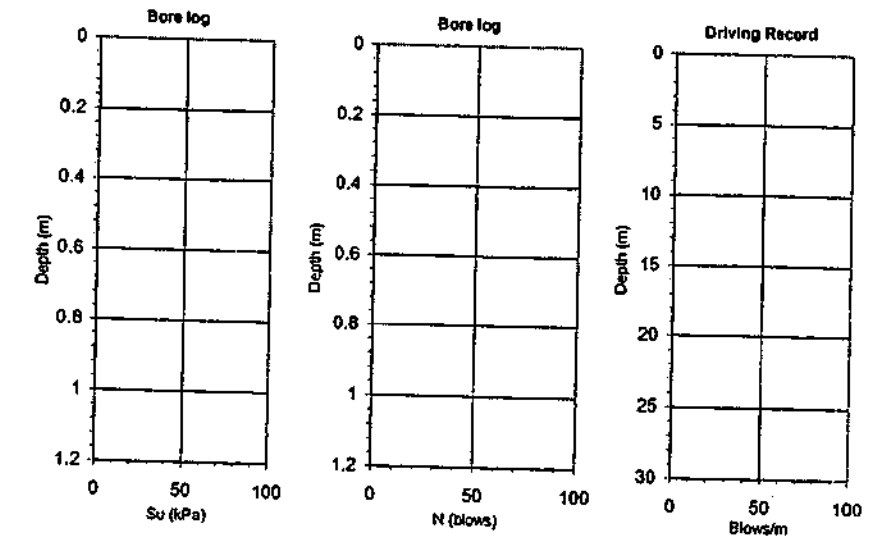
(D) Match
CAPWAP match quality: 2.55 (Wave Up Match)
Observed: final set = 10.160 mm; blow count = 98 b/m
Computed: final set = 9.116 mm; blow count = 110 b/m



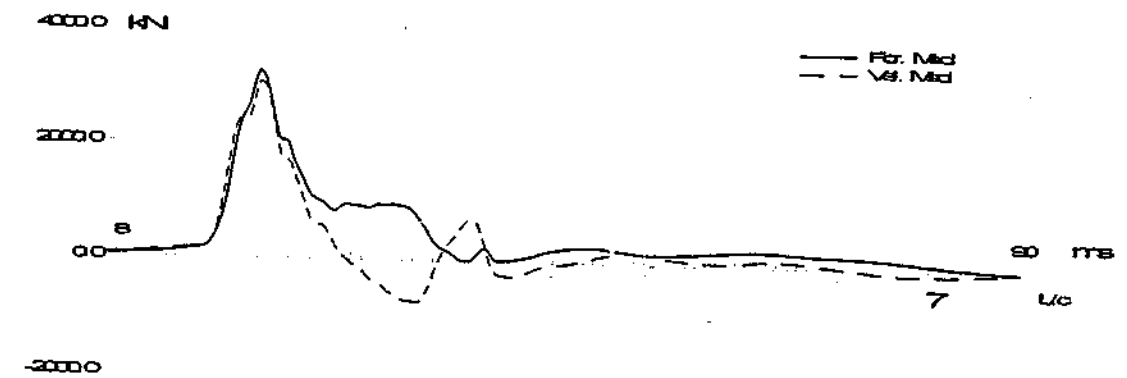
(D) Match
CAPWAP match quality: 2.91 (Wave Up Match)
Observed: final set = 10.160 mm; blow count = 98 b/m
Computed: final set = 9.164 mm; blow count = 109 b/m



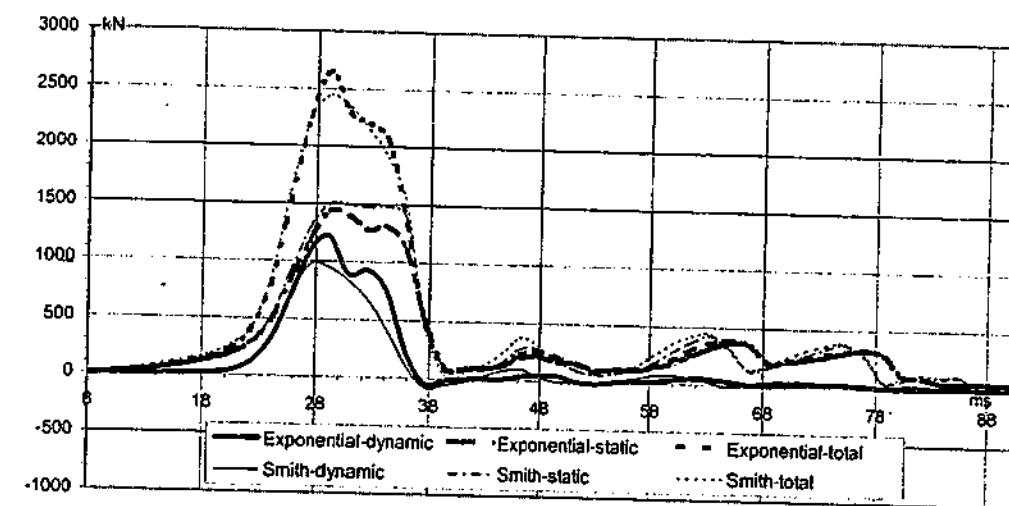
(A) Soil Data
Depth (m) Soil description



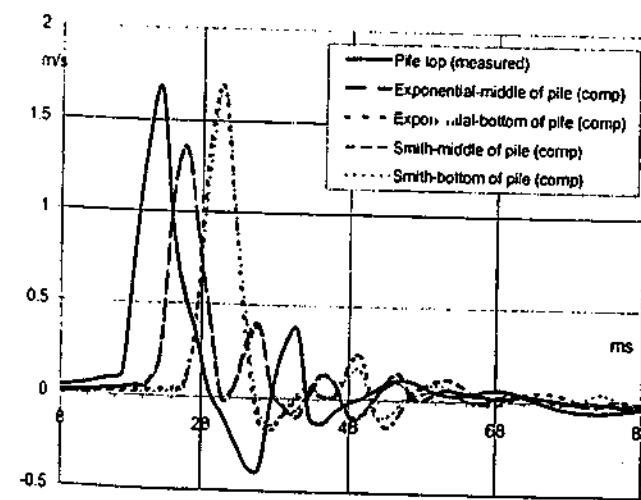
(B) Measured Force & Velocity at Pile Top



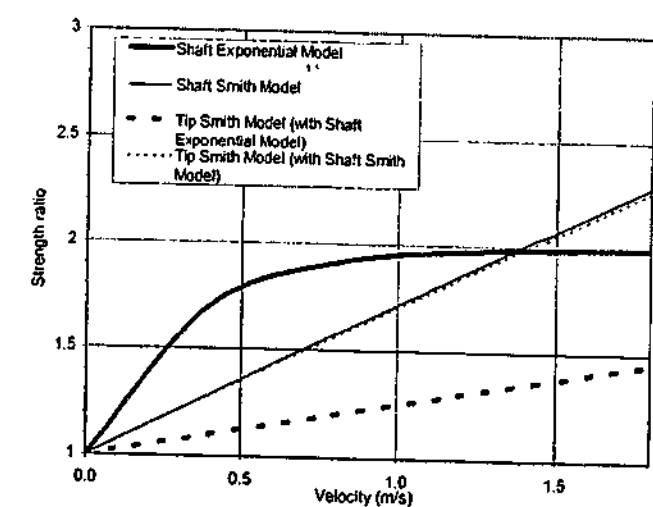
(C) Computed Resistances



(D) Velocities at Top, Middle & Bottom of Pile



(E) Strength Ratio-Velocity Models for Shaft & Tip



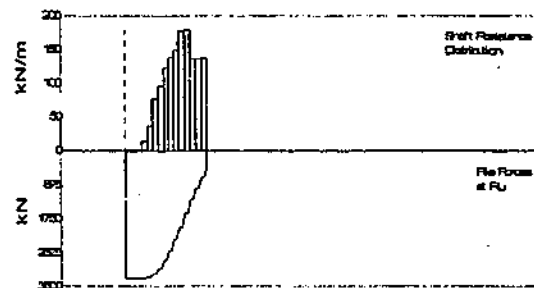
EX21; RESTRIKE 75 DAY; Pile: EX-21C K35; CL-SA SOIL; Blow: 12 ID32

Filename 32 def
Smith Linear Viscous Damping using Rint for Shaft

Depth	Area	E-Mod	Spec Wei	Circum	Impedance
m	cm ²	MPa	kN/m ³	m	1898.28 kN/m/s
0	2090.3	34323	23.563	1.829	Added Impedance None
30.79	2090.3	34323	23.563	1.829	Wave Speed 3600.0 m/s

(B) Resistance Distribution

Depth	Ru	Unit	Total capacity	3280.8 kN
Below	Ru		Shaft capacity	2880.5 kN
Grade	(Area)		Toe capacity	400.3 kN
m	kN	kPa		
2.1	0	0		
4.1	0	0		
6.2	4.9	1.31		
8.2	30.7	8.18		
10.3	73.8	19.65		
12.3	156.7	41.75		
14.4	197.9	52.73		
16.4	253.6	67.55		
18.5	283.2	75.45		
20.5	304.9	81.23		
22.6	363.6	96.85		
24.6	367.8	97.97		
26.7	280.5	74.73		
28.7	280.5	74.73		
30.8	282.5	75.26		
Avg Skin	192	51.16		
Toe	400.3	1914.85		

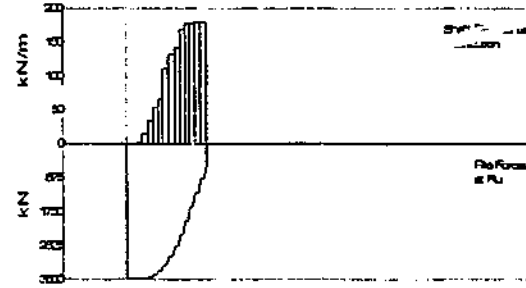


Filename 32mm rinst
Exponential Viscous Damping using Rint for shaft

(A) Pile Model
As per Smith Linear Viscous Damping

(B) Resistance Distribution

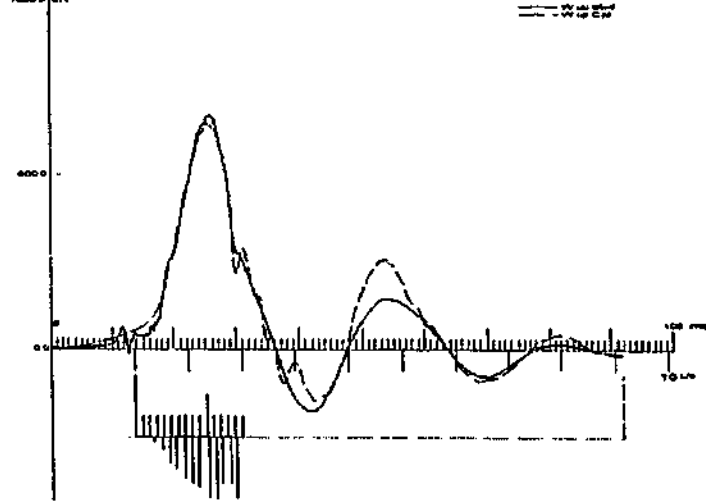
Depth	Ru	Unit	Total capacity	3470.7 kN
Below	Ru		Shaft capacity	2955.3 kN
Grade	(Area)		Toe capacity	515.4 kN
m	kN	kPa		
2.1	0	0		
4.1	0	0		
6.2	4.8	1.23		
8.2	29.3	7.61		
10.3	70.5	18.79		
12.3	108.4	28.67		
14.4	134.6	35.66		
16.4	228.7	60.91		
18.5	270.9	72.16		
20.5	291.8	77.73		
22.6	347.9	92.69		
24.6	385.6	97.41		
26.7	355.6	97.41		
28.7	388.6	98.21		
30.8	388.6	98.21		
Avg Skin	197	52.49		
Toe	515.4	2465.89		



(C) CAPWAP Parameters

JS	SS	QS	UN	CS	LS	PI	OP
0.98	0.646	1	0.4	0.5	-1	0.02	0
JT	ST	QT	TG	CT	LT	PL	
0.274	1.3	1	0	0.01	-1	3	

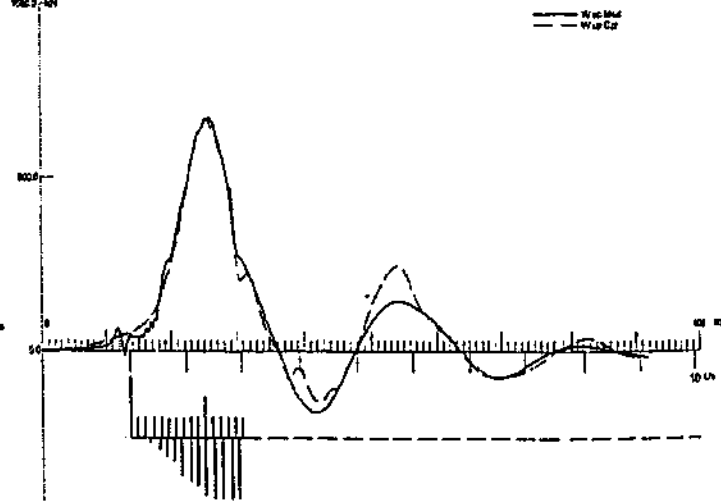
(D) Match
CAPWAP match quality: 2.81 (Wave Up Match)
Observed: final set = 3.850 mm; blow count = 260 b/m
Computed: final set = 2.718 mm; blow count = 368 b/m



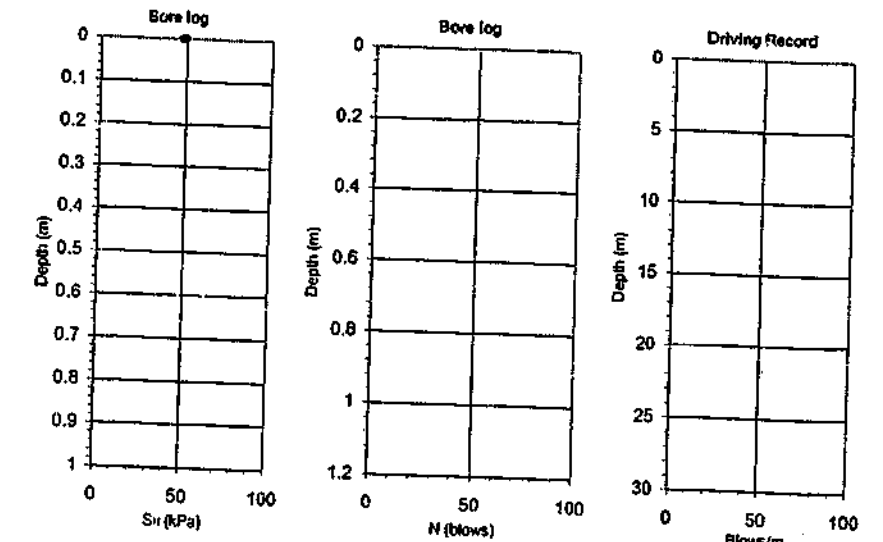
(C) CAPWAP Parameters

JS	SS	QS	UN	CS	LS	PI	OP
1.556	1	1	0.7	0.3	-1	0.02	0
JT	ST	QT	TG	CT	LT	PL	
0.271	0.998	1	0	0.1	-1	9	

(D) Match
CAPWAP match quality: 2.27 (Wave Up Match)
Observed: final set = 3.850 mm; blow count = 260 b/m
Computed: final set = 2.958 mm; blow count = 338 b/m



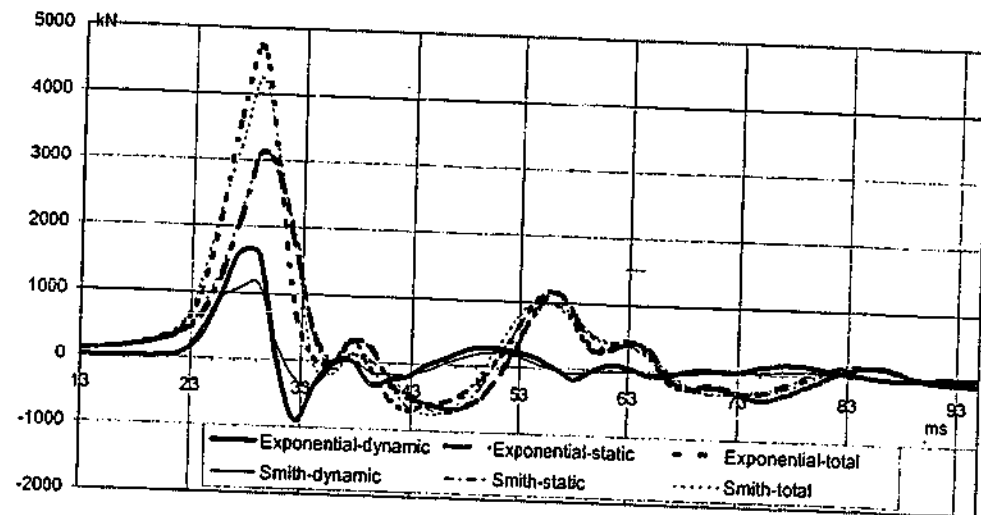
(A) Soil Data
Soil description
Clayey sand



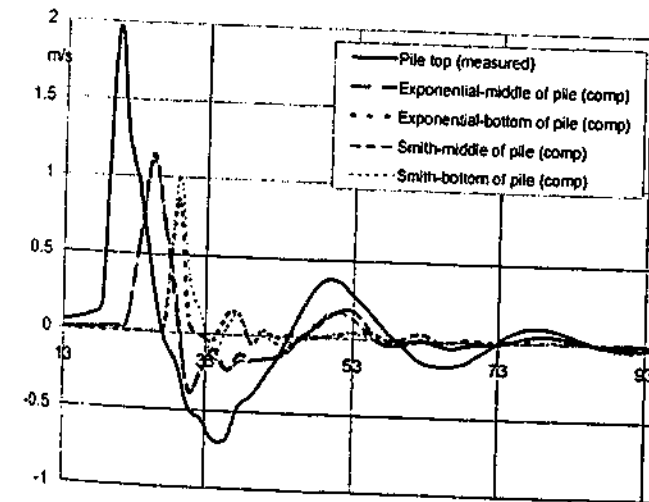
(B) Measured Force & Velocity at Pile Top



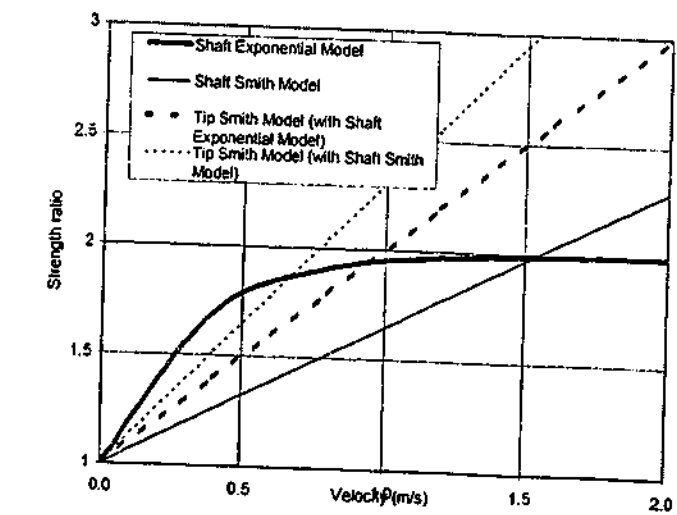
(C) Computed Resistances



(D) Velocities at Top, Middle & Bottom of Pile



(E) Strength Ratio-Velocity Models for Shaft & Tip



ID33 (eod of ID34,35,36)
 EOD LP37 37BPF SICLAY; Pile: EX-26A BERMS505; FC4 FP.86 12"; Blow: 2035

Filename 33 Ex26A def
 Smith Linear Viscous Damping using Rult for Shaft

(A) Pile Model

Depth	Area	E-Mod	Spec Wel	Circum	Impedance
m	cm ²	MPa	kN/m ³	m	2104.92 kN/m/s
0	2090.3	42203	23.563	1.829	Added impedance None
28.66	2090.3	42203	23.563	1.829	Wave Speed 4191.0 m/s

(B) Resistance Distribution

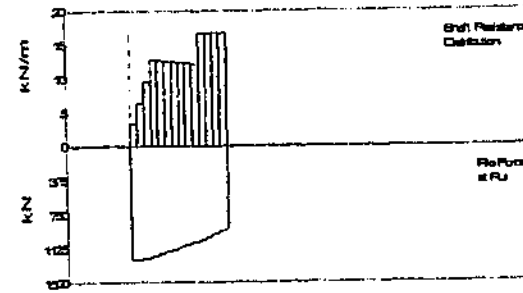
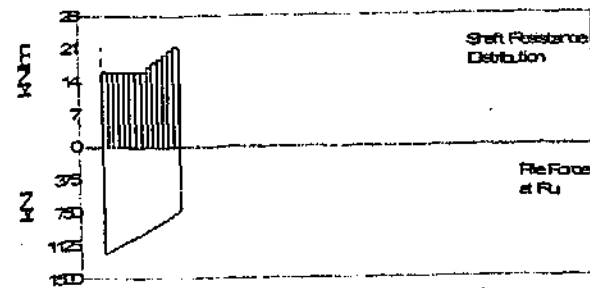
Depth	Ru	Unit	Total capacity
m	kN	MPa	kN
2.1	33.4	8.83	1206.7
4.1	33.4	8.83	507.6
6.2	33.4	8.83	699.3
8.3	33.4	8.83	
10.3	33.4	8.83	
12.4	33.4	8.83	
14.5	33.4	8.83	
16.5	33.4	8.83	
18.6	35.5	9.39	
20.7	37.4	9.89	
22.8	39.2	10.36	
24.8	41	10.84	
26.9	42.8	11.32	
29	44.5	11.76	
Avg Skin	36.3	9.59	
Toe	699.1	3344.5	

Filename 33 Ex26 rult
 Exponential Viscous Damping using Rult for shaft

(A) Pile Model
 As per Smith Linear Viscous Damping

(B) Resistance Distribution

Depth	Ru	Unit	Total capacity
Below Grade	Ru (Area)	kPa	kN
2.1	7.1	1.88	1248.6
4.1	13.2	3.48	359
6.2	19.9	5.26	889.6
8.3	26.4	6.98	
10.3	26.2	6.93	
12.4	25.9	6.85	
14.5	25.9	6.85	
16.5	25.6	6.77	
18.6	25.4	6.72	
20.7	25	6.61	
22.8	34.6	9.15	
24.8	34.6	9.15	
26.9	34.6	9.15	
29	34.6	9.15	
Avg Skin	25.6	6.78	
Toe	889.6	4255.85	



(C) CAPWAP Parameters

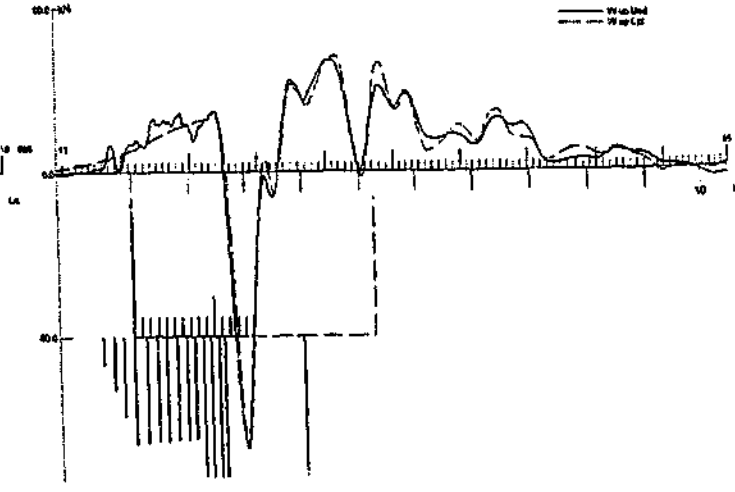
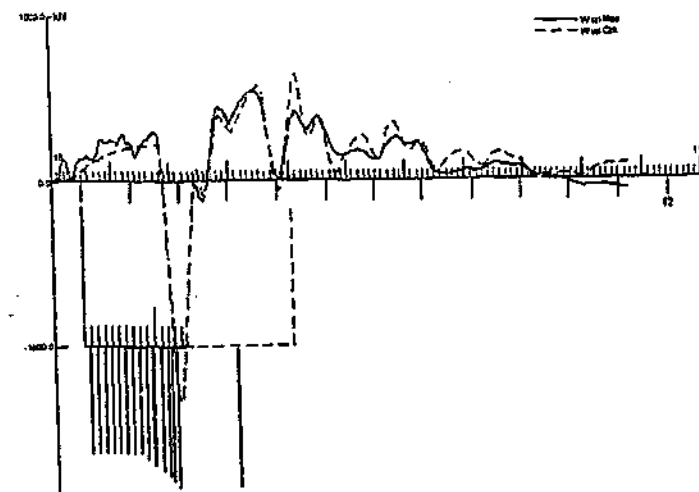
JS	SS	QS	UN	CS	LS	PI	OP
0.293	1.216	3	0.01	0.1	1	0.02	1
JT	ST	QT	TG	CT	LT	PL	
0.196	0.59	9.5	1	0.2	-1	0	

(C) CAPWAP Parameters

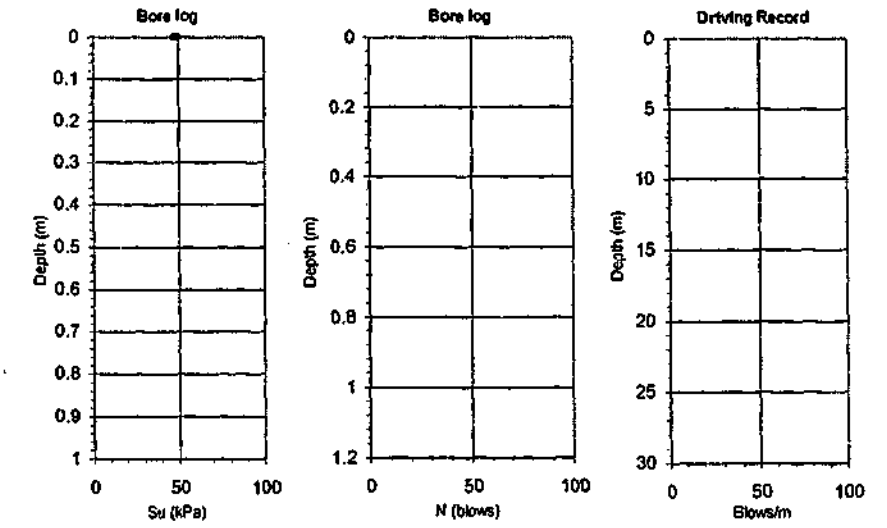
JS	SS	QS	UN	CS	LS	PI	OP
0.205	1.2	0.6	0	0.1	-1	0.02	0
JT	ST	QT	TG	CT	LT	PL	
0.182	0.43	6	1.5	0.2	-1	0	

(D) Match
 CAPWAP match quality: 3.23 (Wave Up Match)
 Observed: final set = 9.500 mm; blow count = 105 b/m
 Computed: final set = 8.793 mm; blow count = 114 b/m

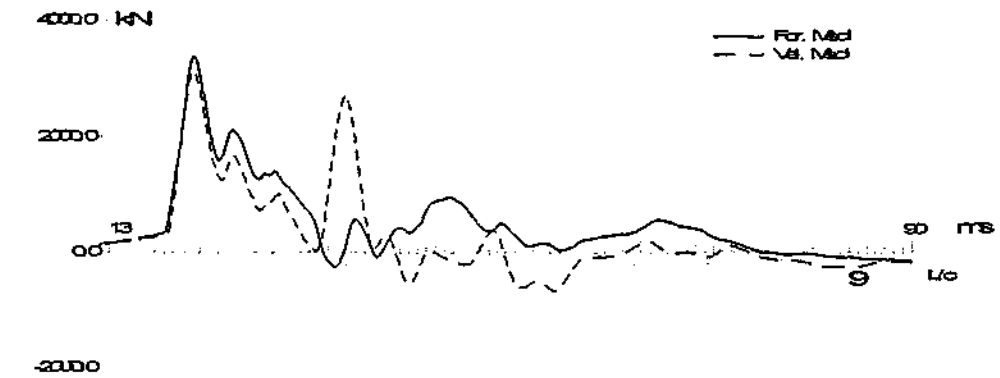
(D) Match
 CAPWAP match quality: 3.01 (Wave Up Match)
 Observed: final set = 9.500 mm; blow count = 105 b/m
 Computed: final set = 9.123 mm; blow count = 110 b/m



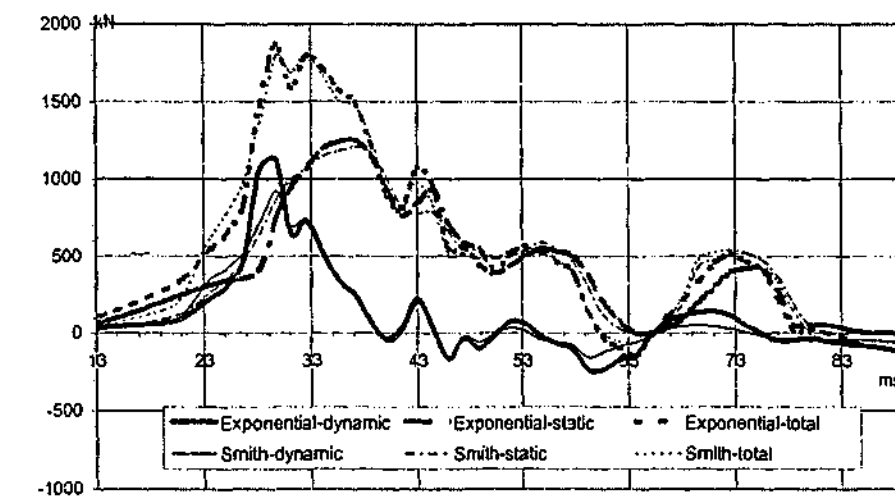
(A) Soil Data



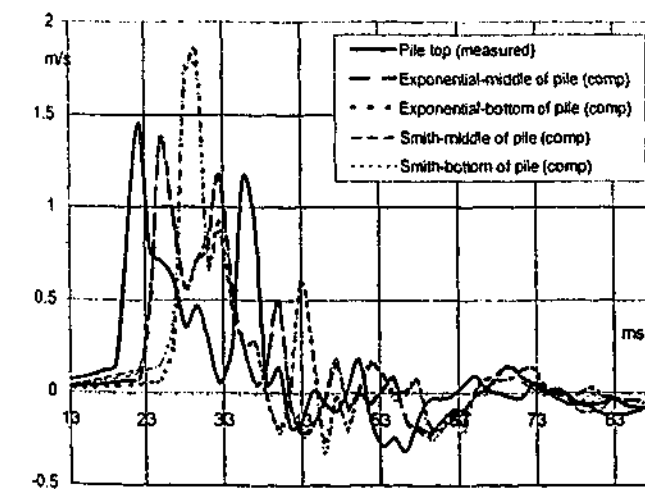
(B) Measured Force & Velocity at Pile Top



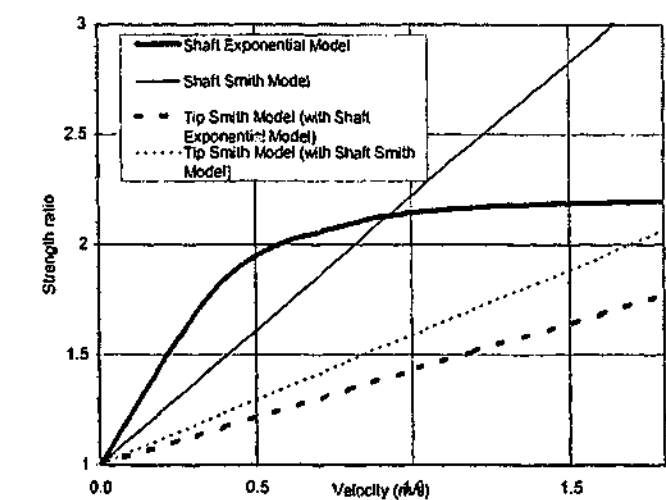
(C) Computed Resistances



(D) Velocities at Top, Middle & Bottom of Pile



(E) Strength Ratio-Velocity Models for Shaft & Tip



ID34
EX26; BCR2DAY 24BP; Pile: EX-26B B5505 WR9K ER106KF 12"PI; Blow: 1

Filename 34 def
Smith Linear Viscous Damping using Ruit for Shaft

(A) Pile Model

Depth	Area	E-Mod	Spec Wel	Circum	Impedance
m	cm ²	MPa	kg/m ³	m	2097.27 kN/m/s
0	2090.3	41897	23.563	1.829	Added Impedance None
26.96	2090.3	41897	23.563	1.829	Wave Speed 4175.6 m/s

(B) Resistance Distribution

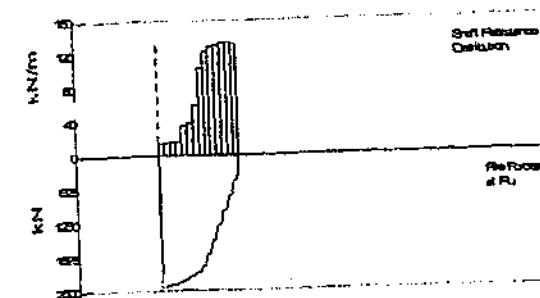
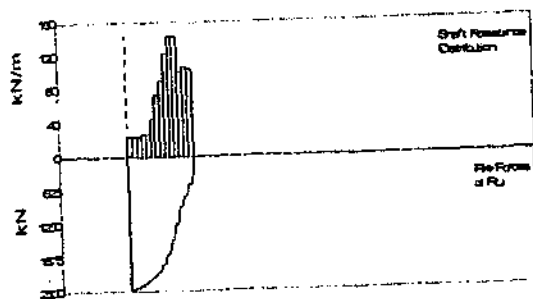
Depth	Ru	Unit	Total capacity	2465.2	kN
Below	Ru	(Area)	Shaft capacity	2190.7	kN
Grade	(Area)		Toe capacity	274.5	kN
m	kN	kPa			
2.1	49.1	12.97			
4.1	49.3	13.03			
6.2	49.2	13			
8.3	56.4	14.9			
10.3	55.6	14.69			
12.4	93.6	24.73			
14.5	151.6	40.08			
16.5	167.9	48.88			
18.6	254.8	67.37			
20.7	297.3	78.61			
22.8	296.8	78.47			
24.8	208.9	55.22			
26.9	222.3	58.78			
29	218	57.64			
Avg Skin	156.5	41.37			
Toe	274.5	1313.15			

Filename 34 rinst nm
Exponential Viscous Damping using Rinst for shaft

(A) Pile Model
As per Smith Linear Viscous Damping

(B) Resistance Distribution

Depth	Ru	Unit	Total capacity	2410.1	kN
Below	Ru	(Area)	Shaft capacity	2237.1	kN
Grade	(Area)		Toe capacity	162	kN
m	kN	kPa			
2.1	29	7.07			
4.1	30.6	6.09			
6.2	32.2	8.52			
8.3	33.9	8.97			
10.3	70.6	18.67			
12.4	78.1	20.65			
14.5	126.5	33.17			
16.5	215.9	57.09			
18.6	255	67.42			
20.7	267.2	70.64			
22.8	270.3	71.46			
24.8	276.0	73.12			
26.9	277.5	73.36			
29	274.7	72.62			
Avg Skin	159.6	42.25			
Toe	162	670.78			



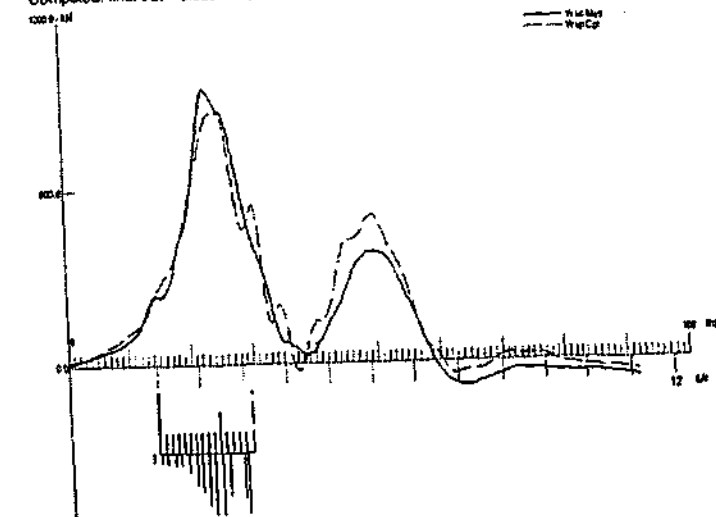
(C) CAPWAP Parameters

JS	SS	OS	UN	CS	LS	PI	OP
1.257	1.2	1	0.3	1	1	0.02	0
0.131	1	1	0	1	1	15	

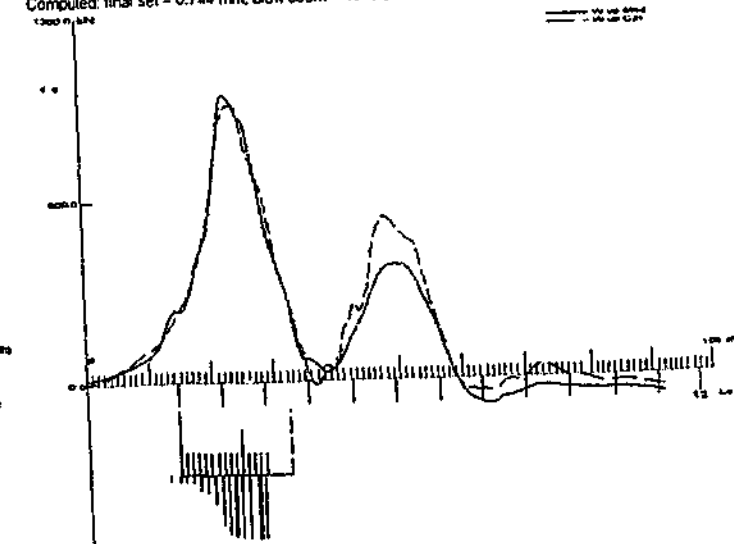
(C) CAPWAP Parameters

JS	SS	OS	UN	CS	LS	PI	OP
1.339	1.252	0.9	0.5	1	1	0.02	0
0.091	1.041	0.6	0	0.1	1	0	

(D) Match
CAPWAP match quality: 5.20 (Wave Up Match)
Observed: final set = 2.000 mm; blow count = 500 b/m
Computed: final set = 0.825 mm; blow count = 1212 b/m

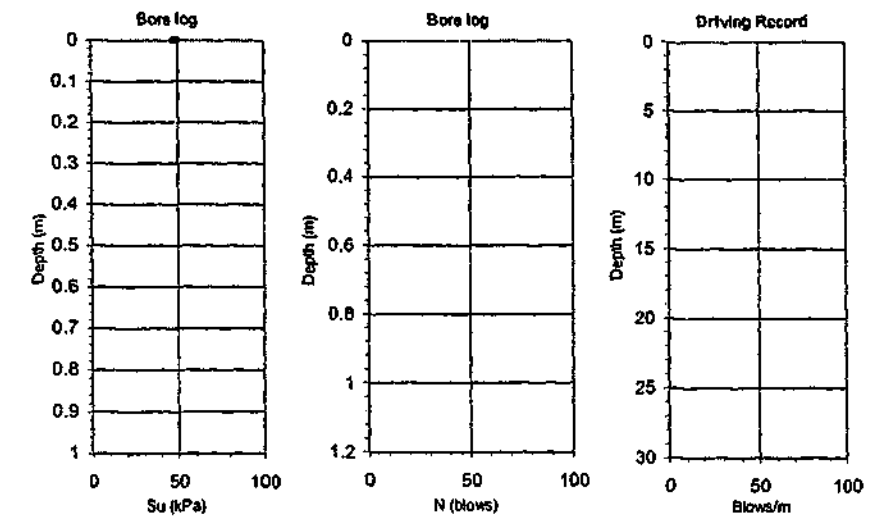


(D) Match
CAPWAP match quality: 3.10 (Wave Up Match)
Observed: final set = 2.000 mm; blow count = 500 b/m
Computed: final set = 0.744 mm; blow count = 1345 b/m

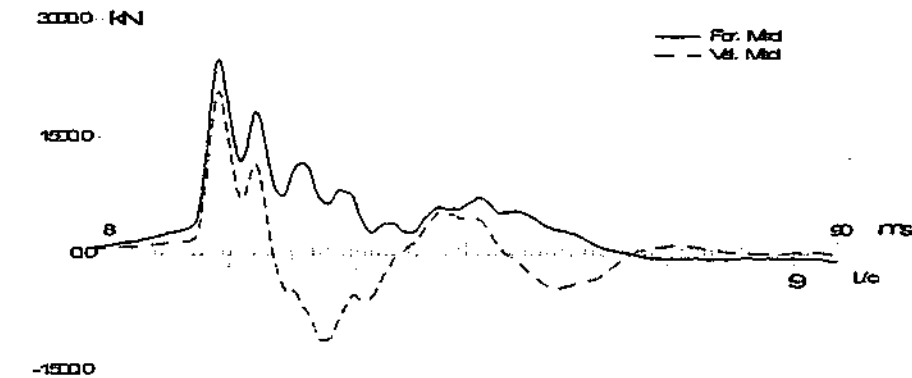


(A) Soil Data (general)
Depth (m) Soil description

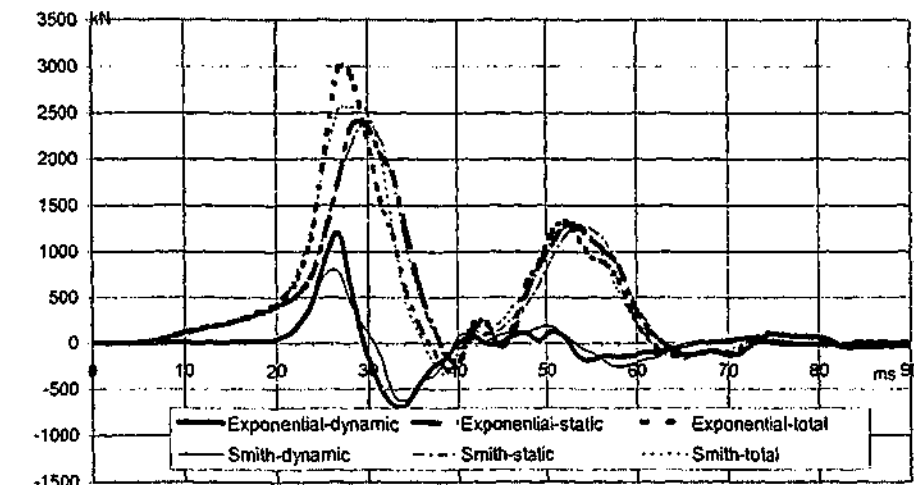
Silty clay
Bore log and driving record NA



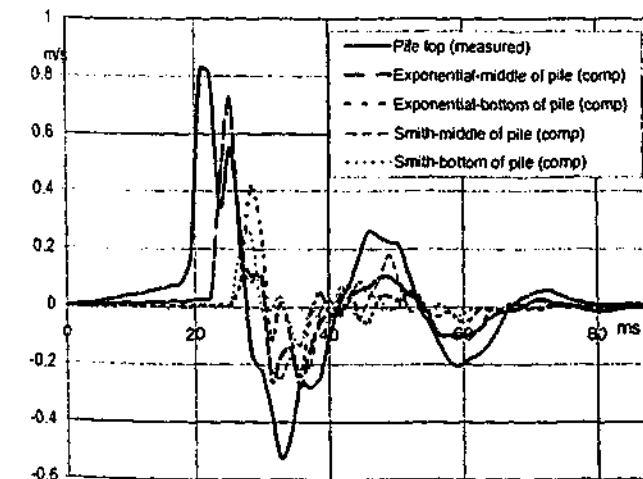
(B) Measured Force & Velocity at Pile Top



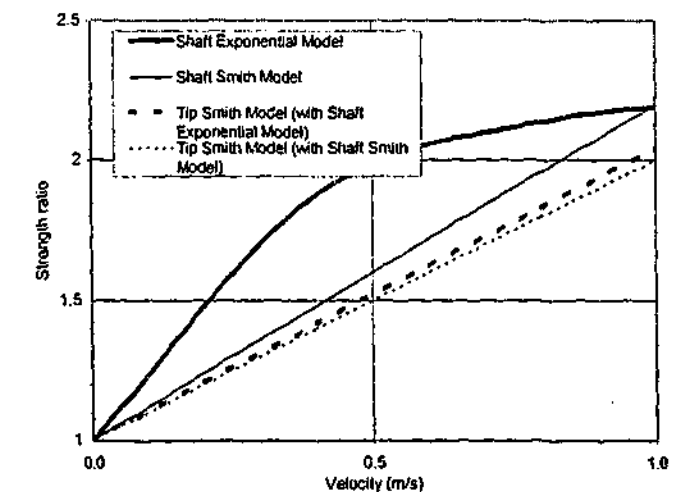
(C) Computed Resistances



(D) Velocities at Top, Middle & Bottom of Pile



(E) Strength Ratio-Velocity Models for Shaft & Tip



ID35

EX26; BOR6DAY 47BPI; Pile: EX-28C B5505 RUS60K >REDUCE LP; Blow: 1

Filename 35 def
Smith Linear Viscous Damping using Rutt for Shaft

Filename 35 nm first
Exponential Viscous Damping using Rinst for shaft

(A) Pile Model

Depth	Area	E-Mod	Spec Wei	Circum	Impedance
m	cm ²	MPa	kN/m ³	m	2097.3kN/m/s
0	2090.3	41897	23.563	1.829	Added impedance 2500kN/m/s at between 20.7m and 23.6
28.96	2090.3	41897	23.563	1.829	Wave Speed 4175.8 m/s

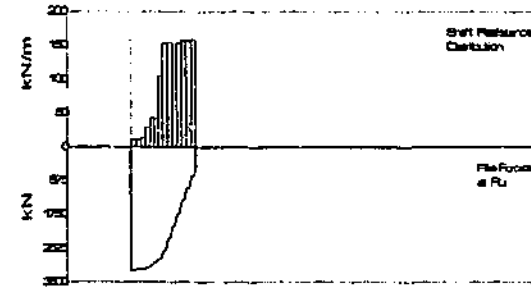
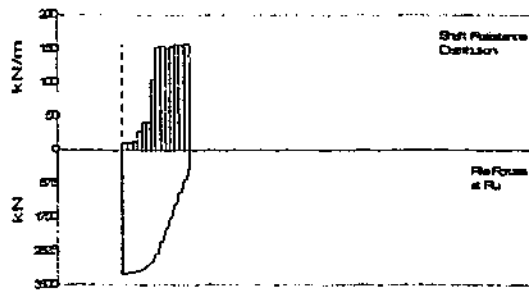
(A) Pile Model
As per Smith Linear Viscous Damping

(B) Resistance Distribution

Depth	Ru	Unit	Total capacity
Below	Ru		3200.1 kN
Grade	(Area)		Shaft capacity 2769.6 kN
			Toe capacity 430.5 kN
m	kN	kPa	
2.1	22.6	5.97	
4.1	22.8	6.03	
6.2	27.6	7.3	
8.3	60.8	16.07	
10.3	89.1	23.56	
12.4	87.5	23.13	
14.5	217.1	57.4	
16.5	315.9	83.52	
18.6	319.6	84.49	
20.7	313	82.75	
22.8	318.1	84.1	
24.8	324.1	85.68	
26.9	323.3	85.47	
29	328.1	86.74	
Avg Skin	197.8	52.3	
Toe	430.5	2059.51	

(B) Resistance Distribution

Depth	Ru	Unit	Total capacity
Below	Ru		3200.1 kN
Grade	(Area)		Shaft capacity 2769.6 kN
			Toe capacity 430.5 kN
m	kN	kPa	
2.1	22.6	5.97	
4.1	22.8	6.03	
6.2	27.6	7.3	
8.3	60.8	16.07	
10.3	89.1	23.56	
12.4	87.5	23.13	
14.5	217.1	57.4	
16.5	315.9	83.52	
18.6	319.6	84.49	
20.7	313	82.75	
22.8	318.1	84.1	
24.8	324.1	85.68	
26.9	323.3	85.47	
29	328.1	86.74	
Avg Skin	197.8	52.3	
Toe	430.5	2059.51	



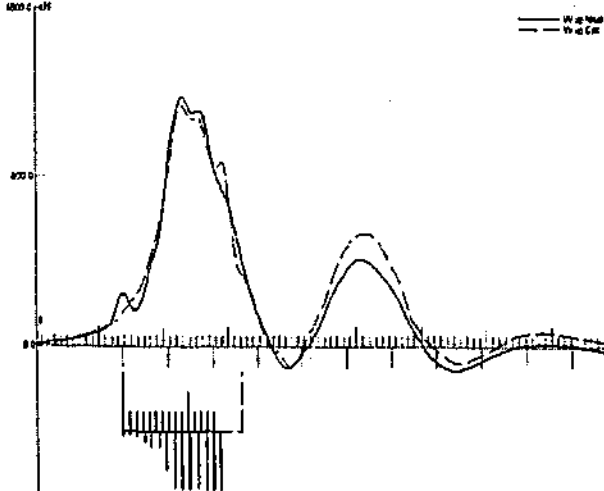
(C) CAPWAP Parameters

JS	SS	QS	UN	CS	LS	PI	OP
1.555	1.2	1.5	1	1	-1	0.02	0
JT	ST	QT	TG	CT	LT	PL	
0.212	1.031	1	0	0.1	-1	1	

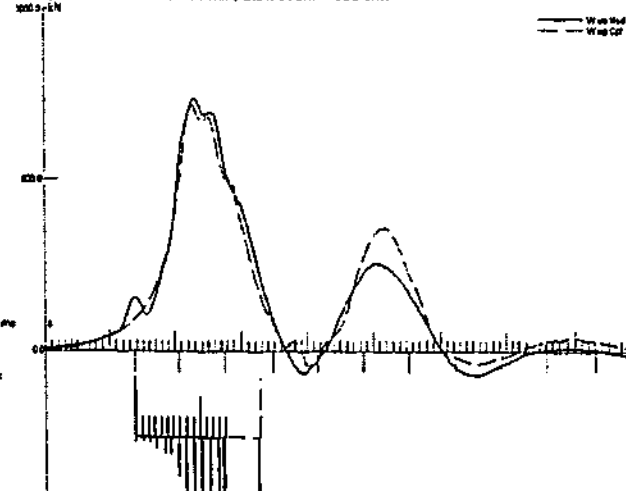
(C) CAPWAP Parameters

JS	SS	QS	UN	CS	LS	PI	OP
1.609	1.219	1.7	1	0.8	-1	0.02	0
JT	ST	QT	TG	CT	LT	PL	
0.212	1.631	1	0	0.1	-1	1	

(D) Match
CAPWAP match quality: 3.37 (Wave Up Match)
Observed: final set = 2.500 mm; blow count = 400 b/m
Computed: final set = 1.024 mm; blow count = 976 b/m



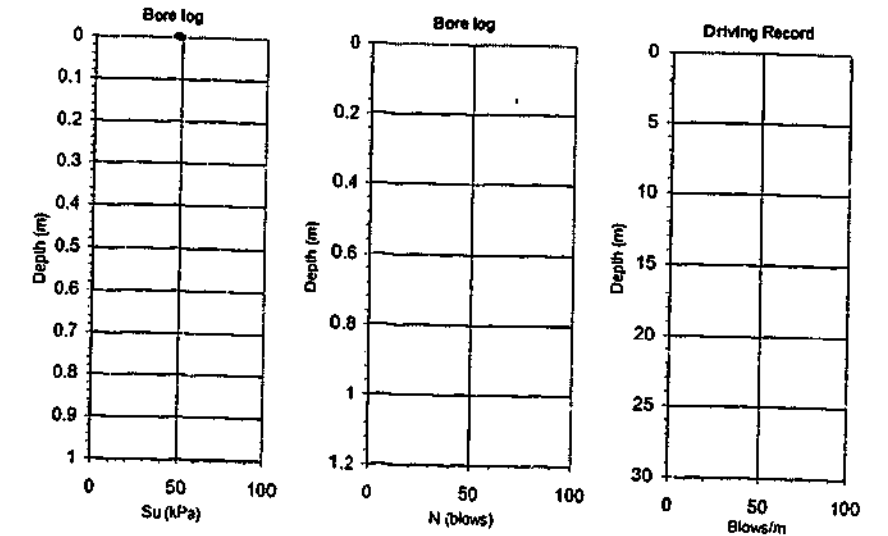
(D) Match
CAPWAP match quality: 2.80 (Wave Up Match)
Observed: final set = 2.500 mm; blow count = 400 b/m
Computed: final set = 1.531 mm; blow count = 653 b/m



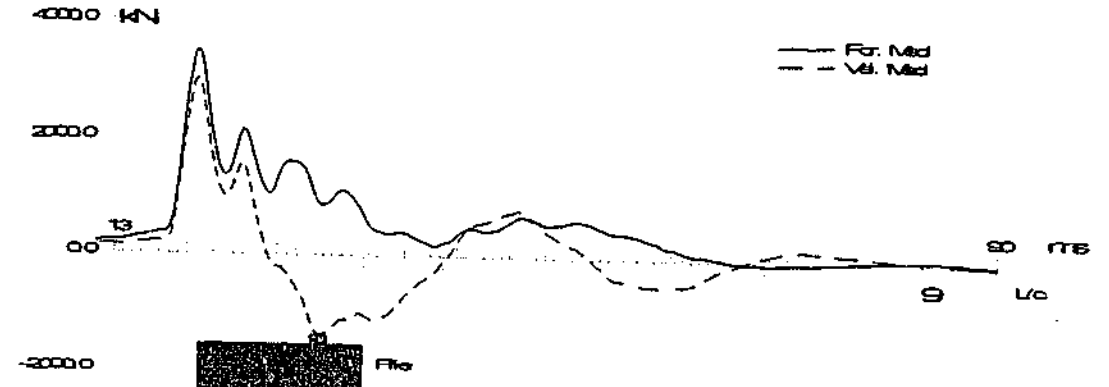
(A) Soil Data

Silty clay

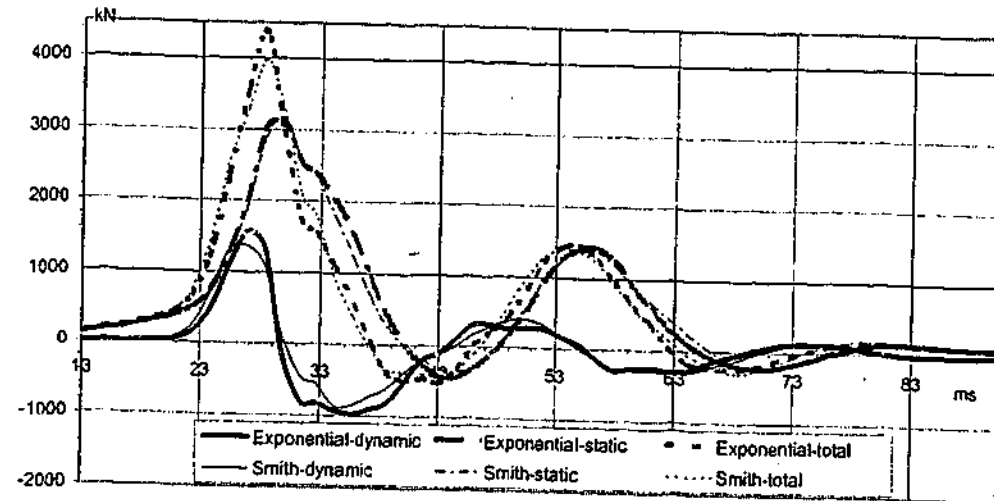
Driving record and bore log NA



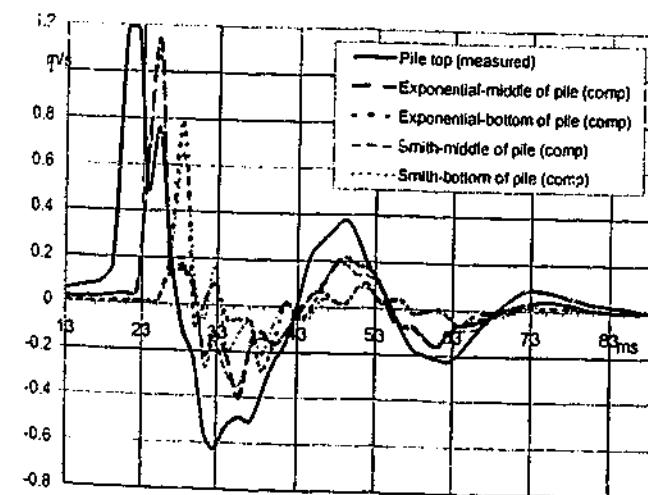
(B) Measured Force & Velocity at Pile Top



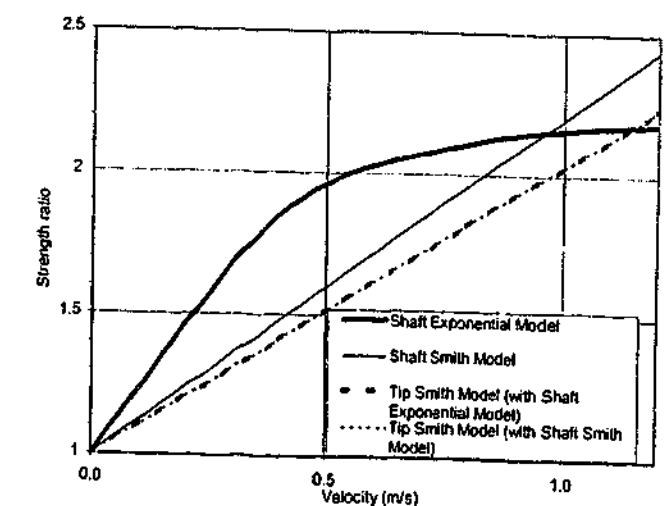
(C) Computed Resistances



(D) Velocities at Top, Middle & Bottom of Pile



(E) Strength Ratio-Velocity Models for Shaft & Tip



ID36

EX26; BORSDAY 47BP; Pile: EX-26C B5505 RU580K >REDUCE LP; Blow: 17

Filename 36 def
Smith Linear Viscous Damping using Rult for Shaft

(A) Pile Model

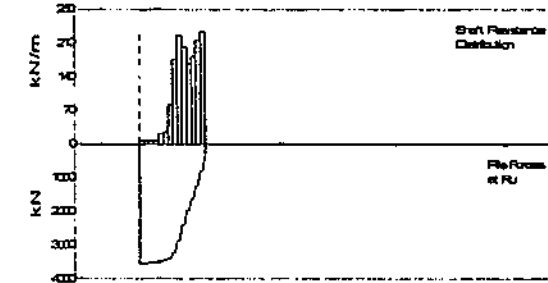
Depth (m)	Area (cm ²)	E-Mod (MPa)	Spec Wei (kN/m ³)	Circum (m)	Impedance (kN/m/s)
0	2090.3	41897	23.563	1.829	2097.30
28.96	2090.3	41897	23.563	1.829	2097.30

Added Impedance None
Wave Speed 4175.8 m/s

(B) Resistance Distribution

Depth (m)	Ru (kN)	Unit (kPa)	Total capacity (kN)
2.1	15.8	4.18	3555.6
4.1	16.5	4.36	3237.8
6.2	15.8	4.18	317.8
8.3	15.8	4.18	
10.3	46.1	12.18	
12.4	53	14.01	
14.5	189.5	48.82	
16.5	364.3	98.3	
18.6	486.2	123.79	
20.7	417.1	110.28	
22.8	346.6	91.63	
24.8	377.6	99.82	
26.9	448.3	118.53	
29	483.2	127.75	

Avg Skin 231.3 61.14
Toe 317.8 1520.29



Filename 36 nm rinst
Exponential Viscous Damping using Rinst for shaft

(A) Pile Model

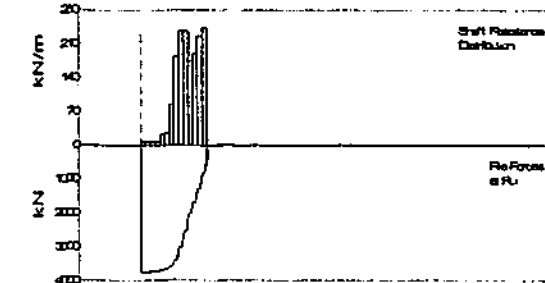
As per Smith Linear Viscous Damping

Impedance 2097.30 kN/m/s
Added Impedance 2500kN/m/s at bet 19.65m and 22.75m

(B) Resistance Distribution

Depth (m)	Ru (kN)	Unit (kPa)	Total capacity (kN)
2.1	16.5	4.36	3755.8
4.1	17.2	4.55	3425
6.2	16.5	4.36	330.8
8.3	16.5	4.36	
10.3	49	12.69	
12.4	55.1	14.56	
14.5	176.4	48.85	
16.5	379.2	100.24	
18.6	487.4	128.87	
20.7	488.9	129.26	
22.8	350.7	95.35	
24.8	393	103.89	
26.9	466.7	123.4	
29	502.9	132.96	

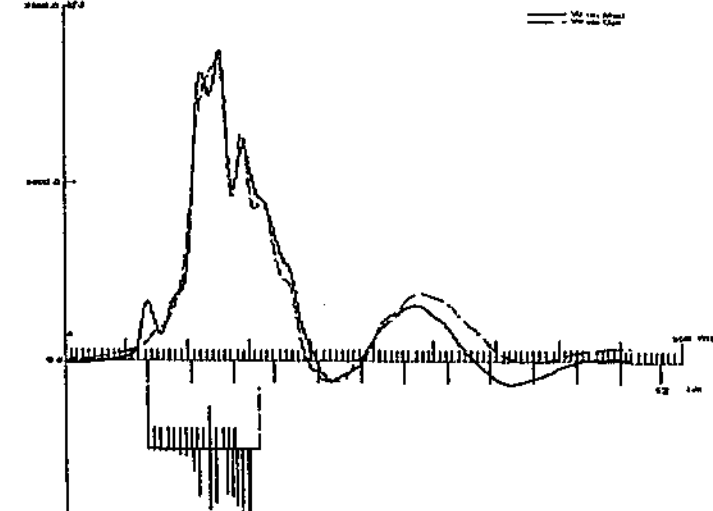
Avg Skin 244.6 64.68
Toe 330.8 1562.49



(C) CAPWAP Parameters

JS	SS	QS	UN	CS	LS	PI	OP
1.544	1	4	1	0.8	-1	0.02	0
JT	ST	QT	TG	CT	LT	PL	
0.167	1.1	4.3	0	0.8	-1	0	

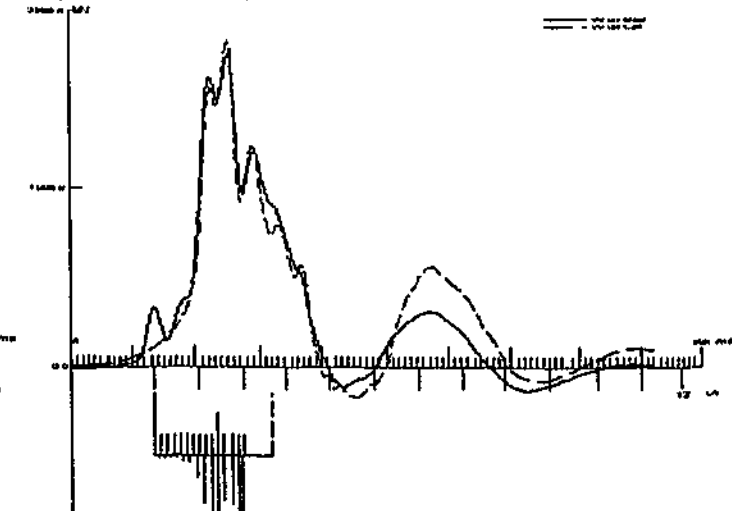
(D) Match
CAPWAP match quality: 2.64 (Wave Up Match)
Observed: final set = 5.000 mm; blow count = 200 b/m
Computed: final set = 3.393 mm; blow count = 295 b/m



(C) CAPWAP Parameters

JS	SS	QS	UN	CS	LS	PI	OP
1.72	1.053	3	0.4	0.9	-1	0.02	0
JT	ST	QT	TG	CT	LT	PL	
0.15	0.948	2	0	0.9	-1	0	

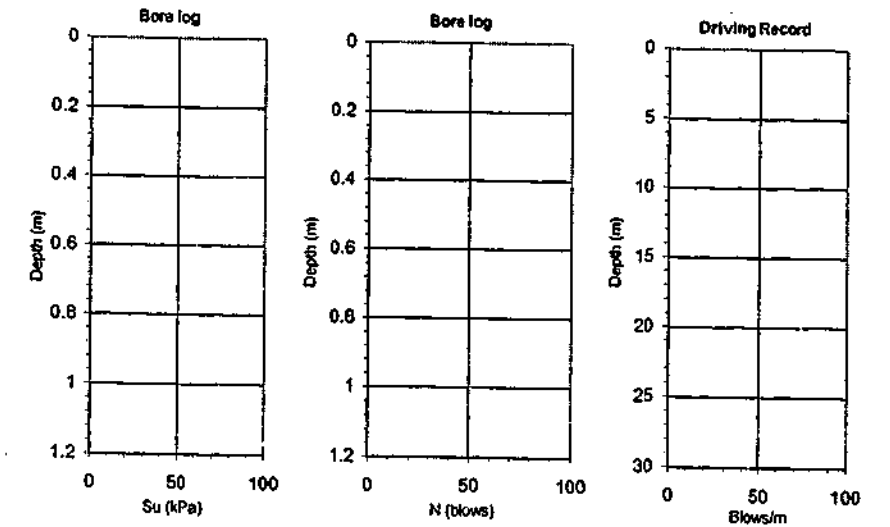
(D) Match
CAPWAP match quality: 2.62 (Wave Up Match)
Observed: final set = 5.000 mm; blow count = 200 b/m
Computed: final set = 3.430 mm; blow count = 292 b/m



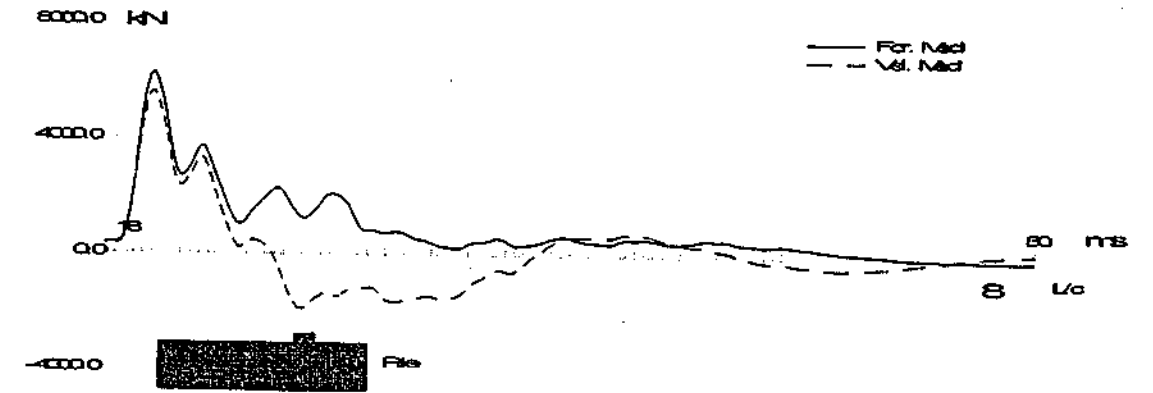
(A) Soil Data

Silty clay

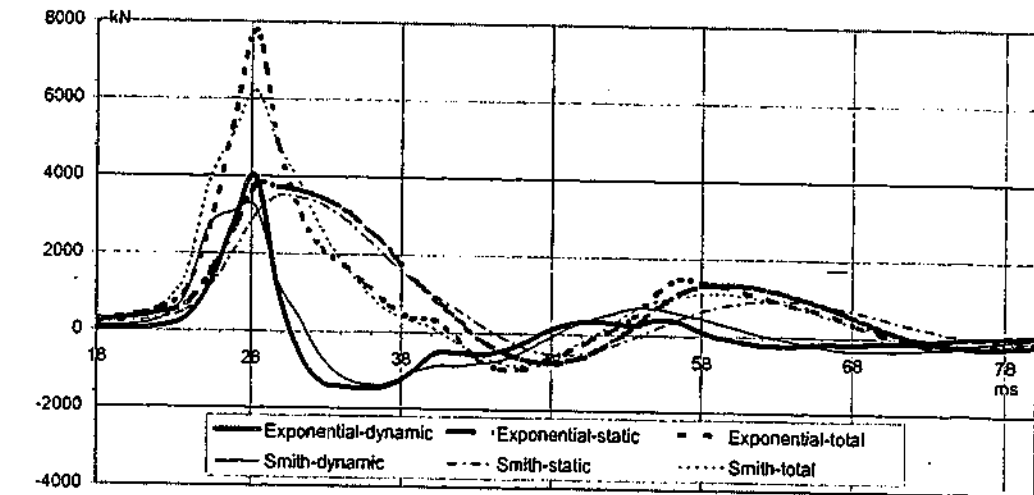
Driving record and bore log NA



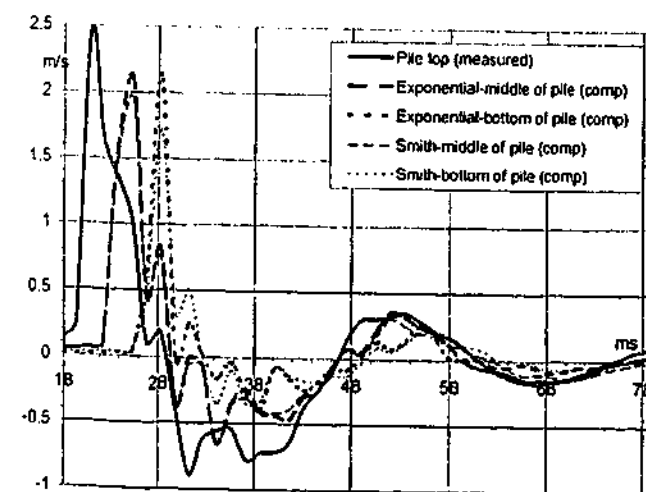
(B) Measured Force & Velocity at Pile Top



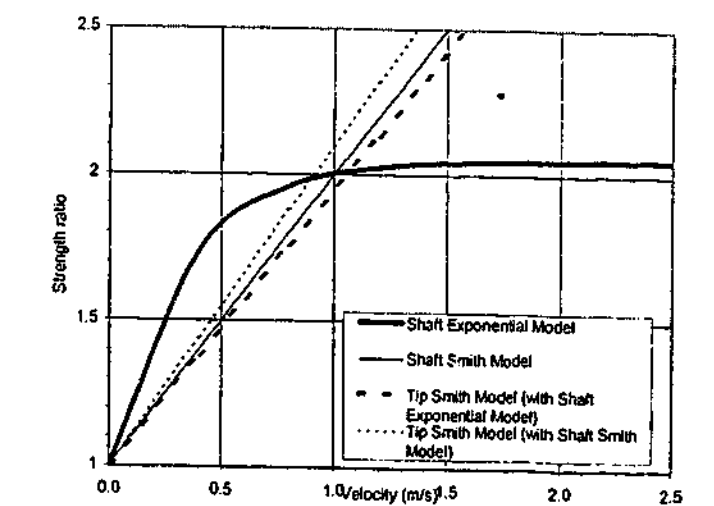
(C) Computed Resistances



(D) Velocities at Top, Middle & Bottom of Pile



(E) Strength Ratio-Velocity Models for Shaft & Tip



ID37 (end of ID38)
EX28 RELAX EOD 218PI; Pile: EX-28A MKT DA35C 12x74 CLSTONE; Blow: 778

Filename: 37 def
Smith Linear Viscous Damping using Rult for Shaft

(A) Pile Model

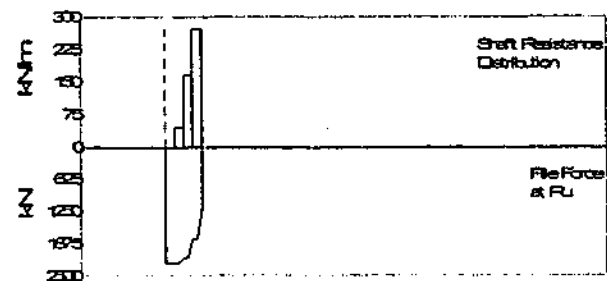
Depth (m)	Area (cm ²)	E-Mod (MPa)	Spec Wei (kN/m ³)	Circum (m)	Impedance (kN/m/s)
0	1385.44	206900	77.287	1.319	567.91
8.38	1385.44	206900	77.287	1.319	None

Wave Speed: 5123.7 m/s

(B) Resistance Distribution

Depth (m)	Ru (kN)	Unit (kPa)	Total capacity (kN)
2.1	0	0	2230.5
4.2	97.6	73.99545	1022.1
8.3	351.6	265.5656	1208.6
8.4	572.9	434.3442	

Avg Skin: 255.5
Toe: 1208.4



Filename: 37 nm rinst
Exponential Viscous Damping using Rinst for shaft

(A) Pile Model

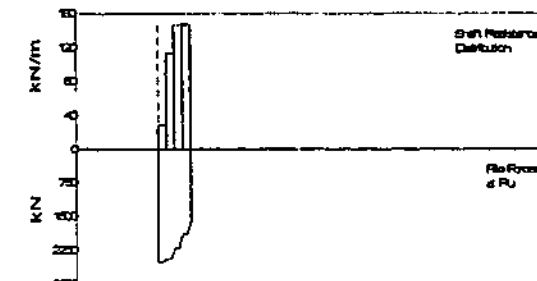
Depth (m)	Area (cm ²)	E-Mod (MPa)	Spec Wei (kN/m ³)	Circum (m)	Impedance (kN/m/s)
0	1385.44	206900	77.287	1.319	567.91
8.38	1385.44	206900	77.287	1.319	None

Wave Speed: 5123.7 m/s

(B) Resistance Distribution

Depth (m)	Ru (kN)	Unit (kPa)	Total capacity (kN)
2.1	0	0	2500
4.2	97.6	73.99545	914.2
8.3	351.6	265.5656	1585.8
8.4	572.9	434.3442	

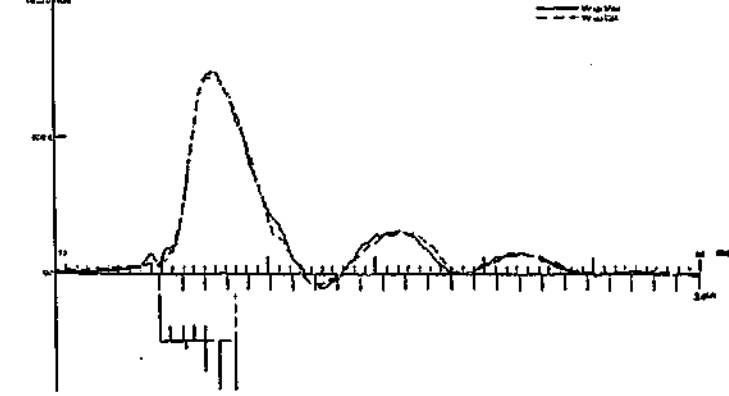
Avg Skin: 226.6
Toe: 1585.8



(C) CAPWAP Parameters

JS	SS	QS	UN	CS	LS	PI	OP
1.53	0.85	3.12	1	0.783	-1	0.01	0
JT	ST	QT	TG	CT	LT	PL	
1.167	0.558	2.14	0	0.199	-1	0	

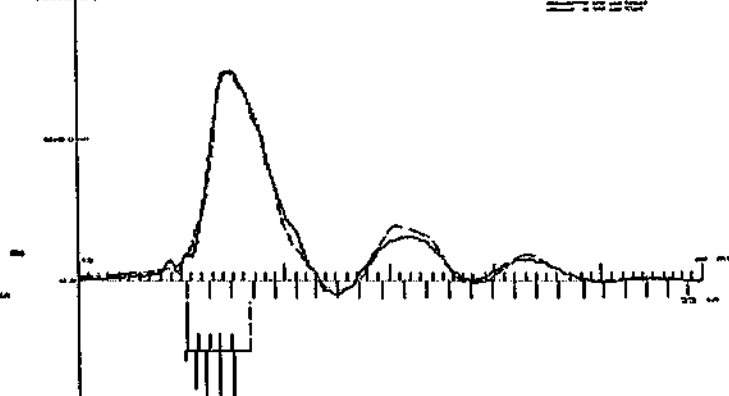
(D) Match
CAPWAP match quality: 2.01 (Wave Up Match)
Observed: final set = 2,000 mm; blow count = 500 b/m
Computed: final set = 1,310 mm; blow count = 763 b/m



(C) CAPWAP Parameters

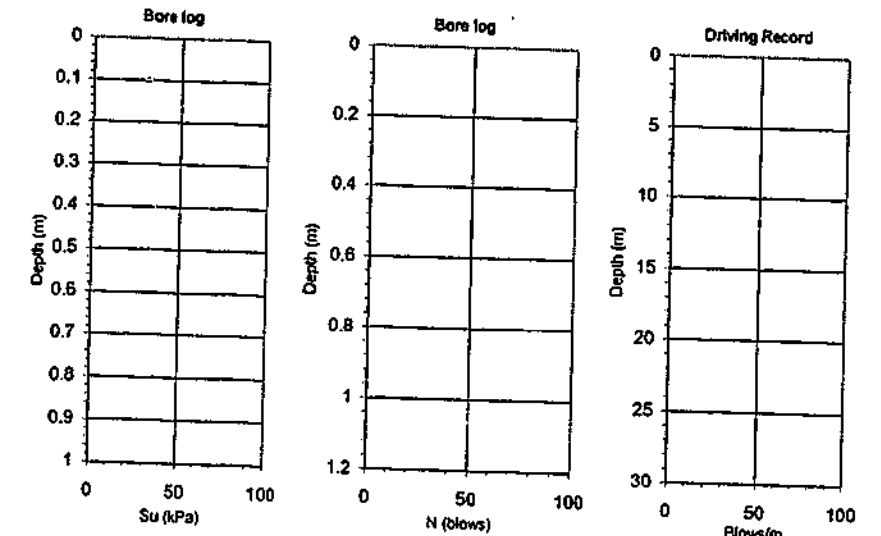
JS	SS	QS	UN	CS	LS	PI	OP
1.038	0.645	1	0.75	1	-1	0.01	0
JT	ST	QT	TG	CT	LT	PL	
1.069	0.39	2.1	0	1	-1	0	

(D) Match
CAPWAP match quality: 2.73 (Wave Up Match)
Observed: final set = 2,000 mm; blow count = 500 b/m
Computed: final set = 1,261 mm; blow count = 793 b/m



(A) Soil Data

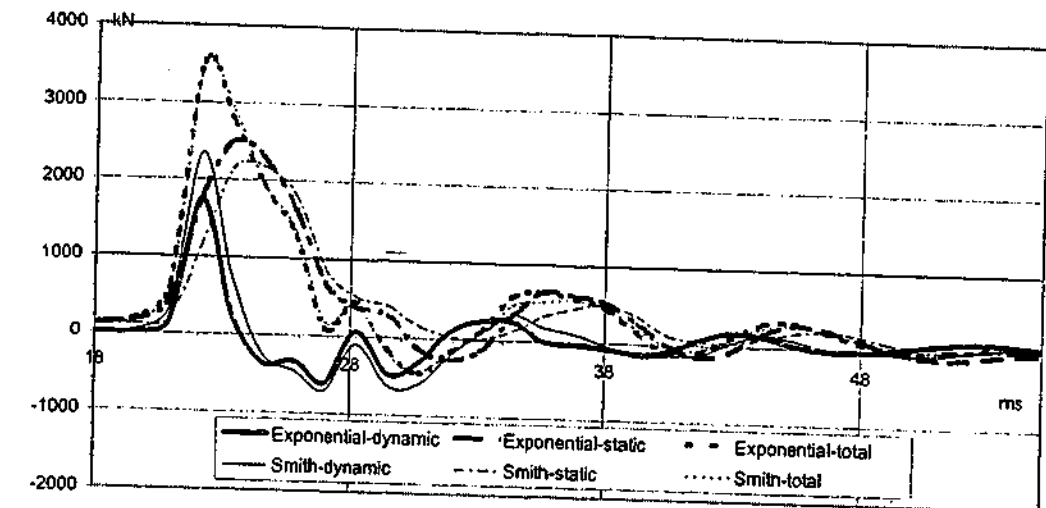
Clayey silt over weathered shale
Driving record and bore log NA



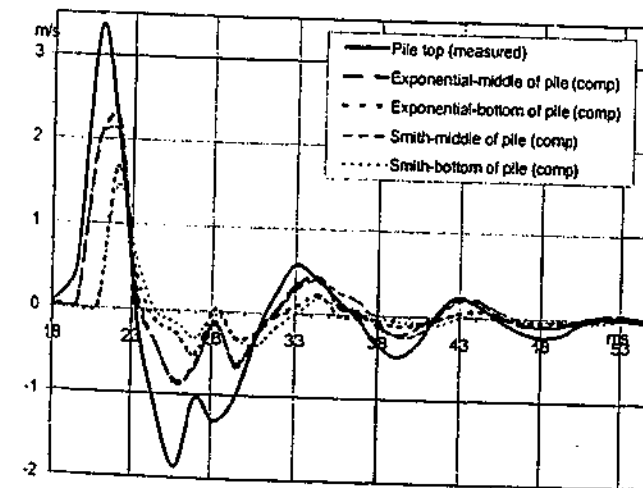
(B) Measured Force & Velocity at Pile Top



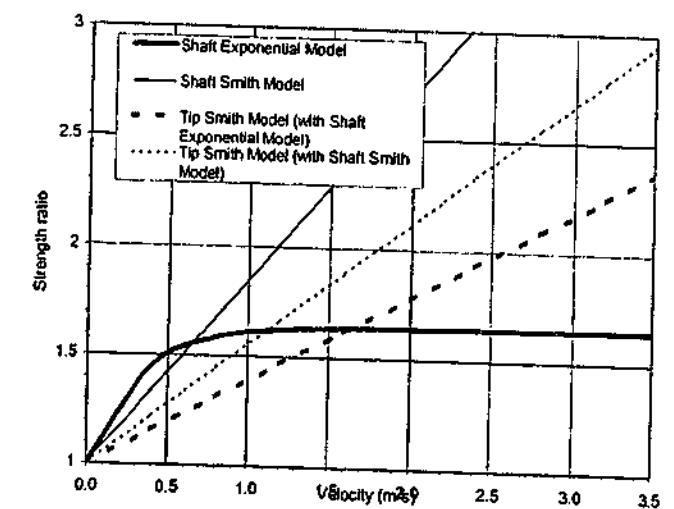
(C) Computed Resistances



(D) Velocities at Top, Middle & Bottom of Pile



(E) Strength Ratio-Velocity Models for Shaft & Tip



ID38
EX28 RELAX BOR 10>21BPI; Pile: EX-28B CLSIWEATH.CLSTN SHALE; Blow: 204

Filename 38 def
Smith Linear Viscous Damping using Rult for Shaft

(A) Pile Model

Depth	Area	E-Mod	Spec Wei	Circum	Impedance
m	cm ²	MPa	kN/m ³	m	kN/m/s
0	140.64	206900	77.287	0.474	None
7.77	140.64	206900	77.287	0.474	5123.7 m/s

(B) Resistance Distribution

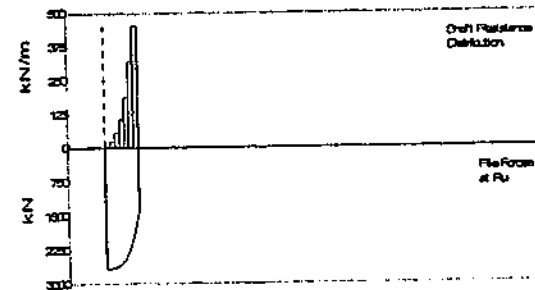
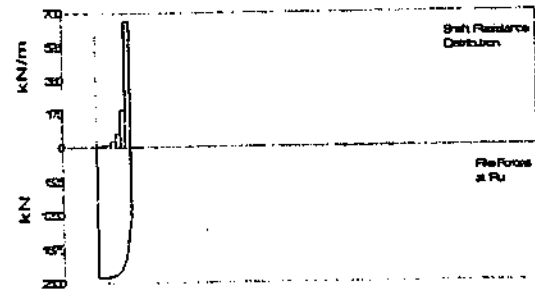
Depth	Ru	Unit	Total capacity
m	kN	kPa	kN
1.1	5	9.5	2395.7
2.2	10	18.99	1094.8
3.3	15	28.49	1300.9
4.4	35.8	68	
5.6	79.7	151.39	
6.7	217.3	412.95	
7.8	732	1390.81	
Avg Skin	158.4	297.16	
Toe	1300.9	0	

Filename 38 rult nm
Exponential Viscous Damping using Rult for shaft

(A) Pile Model
As per Smith Linear Viscous Damping

(B) Resistance Distribution

Depth	Ru	Unit	Total capacity
m	kN	kPa	kN
1.1	5.9	11.21	2653.9
2.2	26.2	49.77	1284.1
3.3	63.3	120.24	1369.8
4.4	118.4	224.91	
5.6	208.3	395.87	
6.7	358.1	680.42	
7.8	503.9	957.37	
Avg Skin	183.4	348.54	
Toe	1369.8	0	



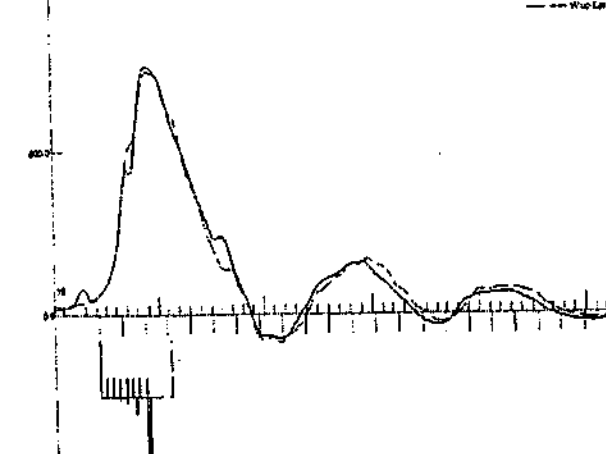
(C) CAPWAP Parameters

JS	SS	QS	UN	CS	LS	PI	OP
1.201	0.823	2.62	1	0.2	-0.8	0.01	0
JT	ST	QT	TG	CT	LT	PL	
0.355	0.165	3.32	0	1	-1	0.458	

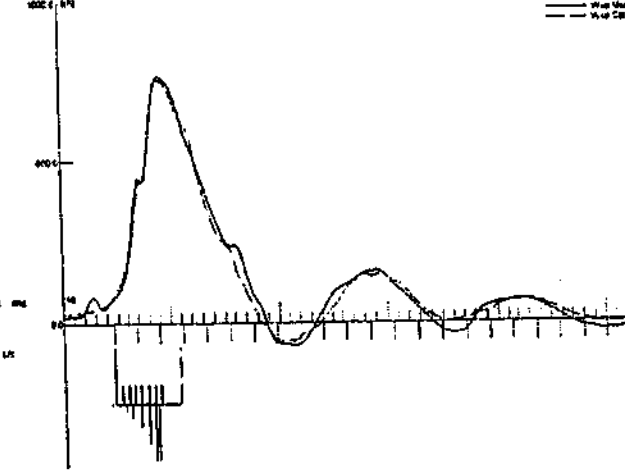
(C) CAPWAP Parameters

JS	SS	QS	UN	CS	LS	PI	OP
1.221	0.54	3	1	0.4	-1	0.01	0
JT	ST	QT	TG	CT	LT	PL	
0.436	0.181	3	0.5	0.9	-1	0.5	

(D) Match
CAPWAP match quality: 2.53 (Wave Up Match)
Observed: final set = 4.500 mm; blow count = 222 b/m
Computed: final set = 3.220 mm; blow count = 311 b/m

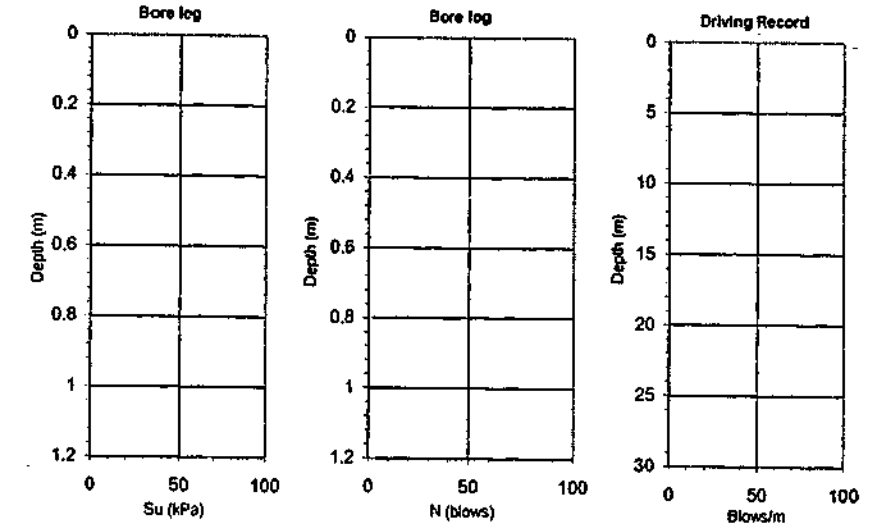


(D) Match
CAPWAP match quality: 2.40 (Wave Up Match)
Observed: final set = 4.500 mm; blow count = 222 b/m
Computed: final set = 3.426 mm; blow count = 292 b/m



(A) Soil Data
Depth (m) Soil description

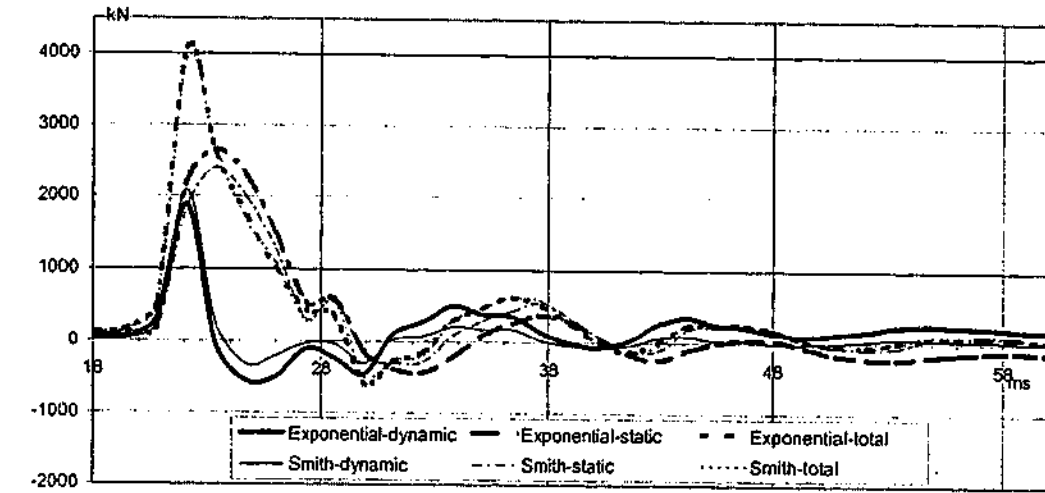
Clayey silt over weathered shale
Bore log and driving record NA



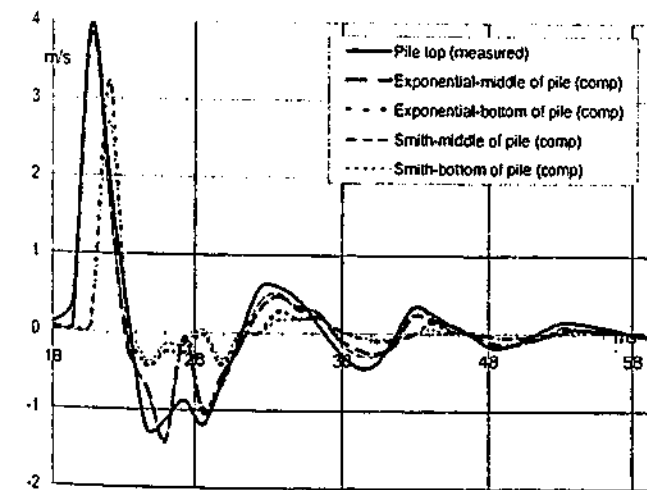
(B) Measured Force & Velocity at Pile Top



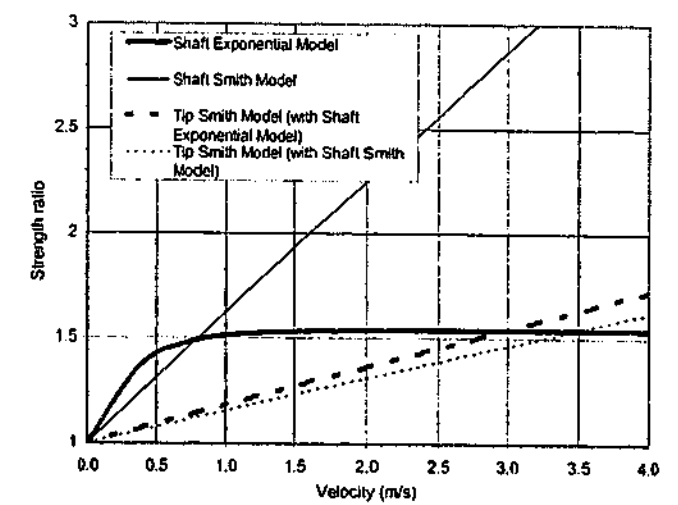
(C) Computed Resistances



(D) Velocities at Top, Middle & Bottom of Pile



(E) Strength Ratio-Velocity Models for Shaft & Tip



ID39
MELBOURNE GRAMMAR SPORTS FIELDS, BANUT 5 6-TONNE HAMMER

Filename 39 del
Smith Linear Viscous Damping using Rult for Shaft

Filename 39 rinst nm
Exponential Viscous Damping using Rinst for shaft

(A) Pile Model

Depth (m)	Area (cm ²)	E-Mod (MPa)	Spec Wei (kN/m ³)	Circum (m)	Impedance (kN/m/s)
0	756.25	39253.4	24.035	1.1	741.8
34.4	756.25	39253.4	24.035	1.1	3690.0

Reduced impedance at between 11 and 12m below grade

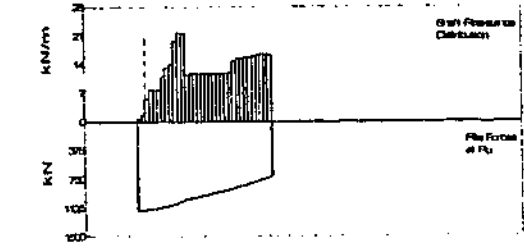
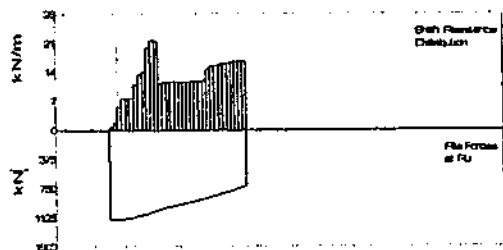
(A) Pile Model
As per Smith Linear Viscous Damping

(B) Resistance Distribution

Depth (m)	Ru (kN)	Unit (kPa)	Total capacity (kN)	Shaft capacity (kN)	Toe capacity (kN)
-1.9	0.7	0.63	1149.9	434.3	715.6
-0.9	1.7	1.53			
0.1	5.7	5.12			
1.1	7.8	7.01			
2.2	7.8	7.01			
3.2	7.8	7.01			
4.2	11.1	9.97			
5.2	13.3	11.95			
6.2	14	12.58			
7.2	20	17.97			
8.2	21.9	19.67			
9.2	21.9	19.67			
10.3	11.4	10.24			
11.3	11.7	10.51			
12.3	11.7	10.51			
13.3	11.7	10.51			
14.3	11.7	10.51			
15.3	11.7	10.51			
16.3	11.7	10.51			
17.3	11.7	10.51			
18.3	11.7	10.51			
19.4	11.7	10.51			
20.4	11.8	10.6			
21.4	12	10.78			
22.4	14.9	13.39			
23.4	15.5	13.92			
24.4	15.5	13.92			
25.4	15.8	14.19			
26.4	16	14.37			
27.5	16.2	14.55			
28.5	16.5	14.82			
29.5	16.6	14.91			
30.5	16.6	14.91			
31.5	16.6	14.91			
Avg Skin	12.8	11.48			
Toe	715.6	9461.94			

(B) Resistance Distribution

Depth (m)	Ru (kN)	Unit (kPa)	Total capacity (kN)	Shaft capacity (kN)	Toe capacity (kN)
-1.9	0.7	0.63	1149.9	434.3	715.6
-0.9	1.7	1.53			
0.1	5.7	5.12			
1.1	7.8	7.01			
2.2	7.8	7.01			
3.2	7.8	7.01			
4.2	11.1	9.97			
5.2	13.3	11.95			
6.2	14	12.58			
7.2	20	17.97			
8.2	21.9	19.67			
9.2	21.9	19.67			
10.3	11.4	10.24			
11.3	11.7	10.51			
12.3	11.7	10.51			
13.3	11.7	10.51			
14.3	11.7	10.51			
15.3	11.7	10.51			
16.3	11.7	10.51			
17.3	11.7	10.51			
18.3	11.7	10.51			
19.4	11.8	10.6			
20.4	12	10.78			
21.4	14.9	13.39			
22.4	15.5	13.92			
23.4	15.5	13.92			
24.4	15.8	14.19			
25.4	16	14.37			
26.4	16.2	14.55			
27.5	16.5	14.82			
28.5	16.6	14.91			
29.5	16.6	14.91			
30.5	16.6	14.91			
31.5	16.6	14.91			
Avg Skin	12.8	11.48			
Toe	715.6	9461.94			



(C) CAPWAP Parameters

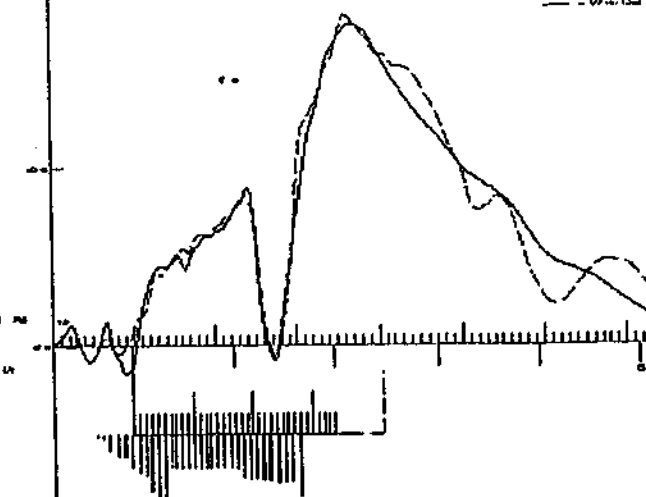
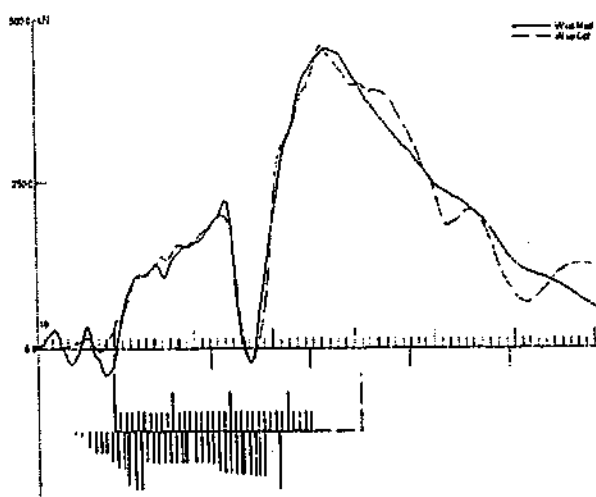
JS	SS	QS	UN	CS	LS	PI	OP
0.117	0.2	3.5	0.4	0.45	1	0.02	0
JT	ST	QT	TG	CT	LT	PL	
0.328	0.34	5.5	0	1	1	G	

(C) CAPWAP Parameters

JS	SS	QS	UN	CS	LS	PI	OP
0.164	0.28	3.99	0.4	0.45	1	0.02	0
JT	ST	QT	TG	CT	LT	PL	
0.339	0.351	5.3	0	1	1	0	

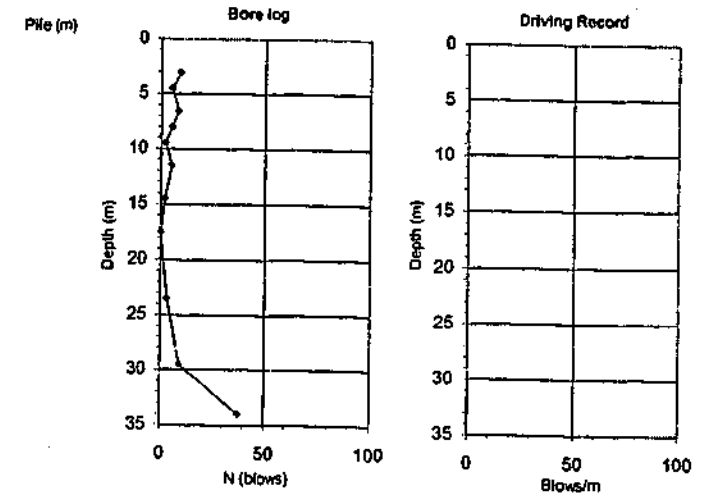
(D) Match
CAPWAP match quality: 2.67 (Wave Up Match)
Observed: final set = 5.000 mm; blow count = 200 b/m
Computed: final set = 4.533 mm; blow count = 221 b/m

(D) Match
CAPWAP match quality: 2.68 (Wave Up Match)
Observed: final set = 5.000 mm; blow count = 200 b/m
Computed: final set = 4.589 mm; blow count = 218 b/m

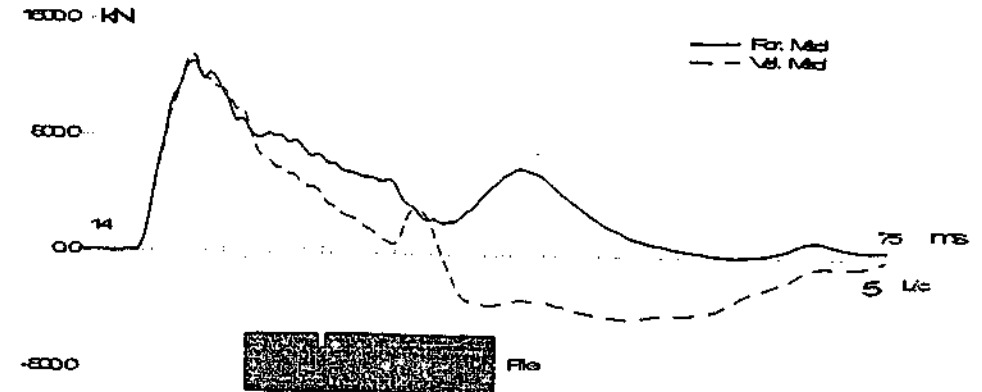


(A) Soil Data

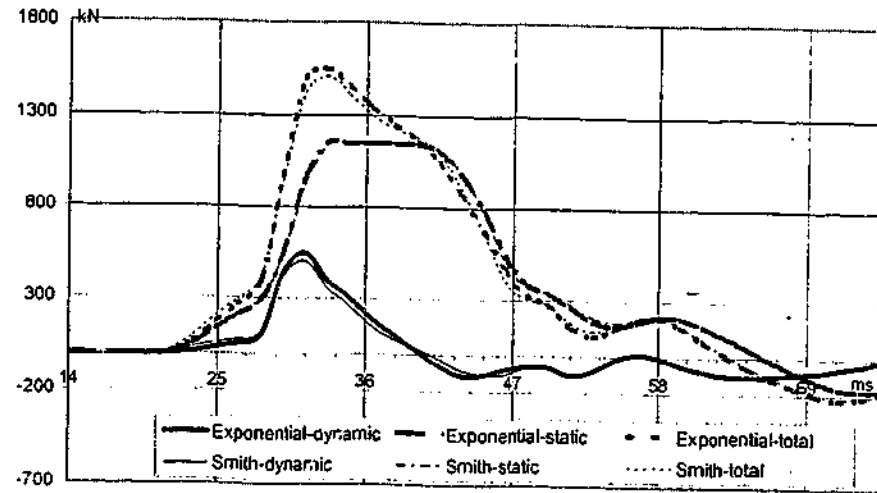
Depth (m)	Soil description
0	fill: fine to coarse silty SAND
0.3	fill: silty SAND and REFUSE
3.4	fill: sandy GRAVEL and REFUSE
7.5	fill: high plasticity sandy CLAY, trace fine to medium gravel, trace shell fragments
9	fill: low plasticity, clayey SILT, trace fine gravel
10.6	fill: fine to medium silty SAND, trace shell
13.2	fill: high plasticity silty CLAY
29.5	low to medium plasticity silty CLAY
31.2	sandy GRAVEL, fine to medium, sand fine to coarse
34.1	fine to coarse silty SAND



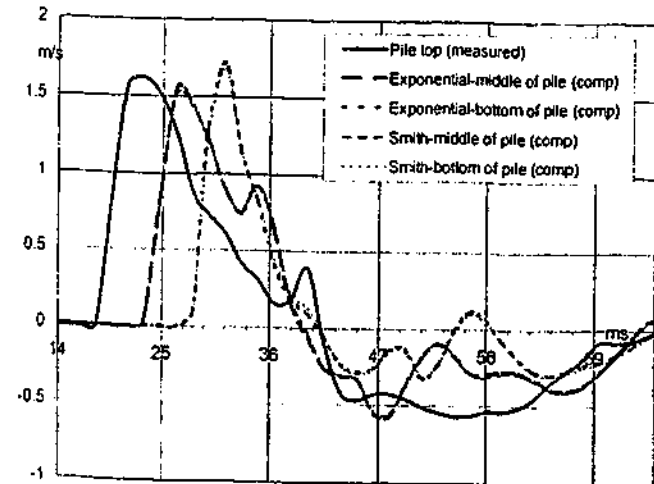
(B) Measured Force & Velocity at Pile Top



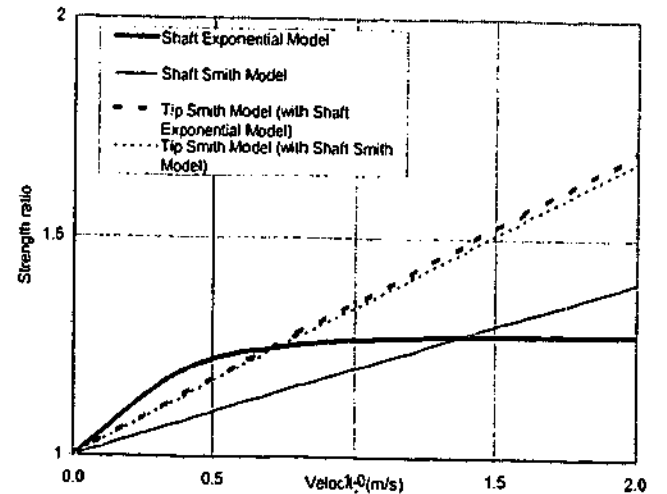
(C) Computed Resistances



(D) Velocities at Top, Middle & Bottom of Pile



(E) Strength Ratio-Velocity Models for Shaft & Tip



ID40
 JONES BAY WHARF; Pile: TP1_RS3 5T DROP HAMMER; Blow: 8

Filename TP1_RS3_8 def v2 lower
 Smith Linear Viscous Damping using Rult for Shaft

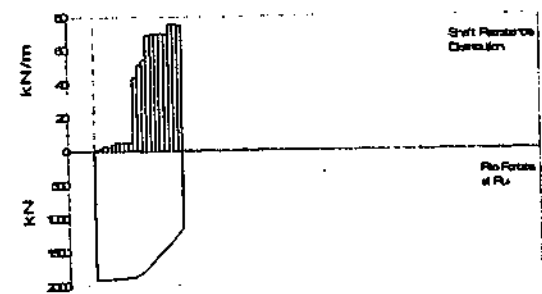
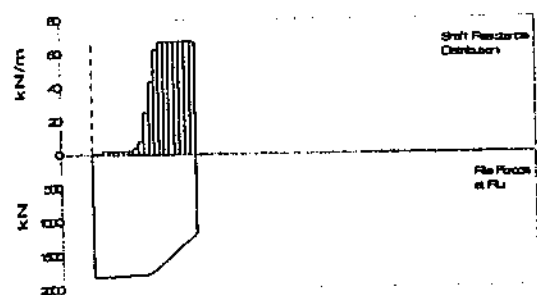
Depth (m)	Area (cm ²)	E-Mod (MPa)	Spec Wel (kN/m ³)	Circum (m)	Impedance (1201.1kNm/s)	Added Impedance (None)	Wave Speed (5123.1 m/s)
0	298.6	206080	77	1.889			
20	298.6	206080	77	1.889			

Depth (m)	Resistance Distribution		Total capacity (kN)	Shaft capacity (kN)	Toe capacity (kN)
	Ru (kN)	Unit (kPa)			
1	0.7	0.37	1799.7	629.1	1170.7
2	1	0.53			
3	2.4	1.28			
4	2	1.07			
5	2	1.07			
6	2.3	1.23			
7	2.3	1.23			
8	2.3	1.23			
9	3.9	2.09			
10	7.8	4.17			
11	25.1	13.43			
12	43.8	23.43			
13	62.5	33.43			
14	67.3	36			
15	67.3	36			
16	67.3	36			
17	67.3	36			
18	67.3	36			
19	67.3	36			
20	67.3	36			
Avg Skin			31.5	16.83	
Toe			1170.7	4211.01	

Filename TP1_RS3_8 nm rinst Improve
 Exponential Viscous Damping using Rinst for shaft

(A) Pile Model
 As per Smith Linear Viscous Damping

Depth (m)	Resistance Distribution		Total capacity (kN)	Shaft capacity (kN)	Toe capacity (kN)
	Ru (kN)	Unit (kPa)			
1	1.2	0.84	1900	755.6	1144.5
2	1.9	1.02			
3	3.1	1.66			
4	2.0	1.39			
5	4.1	2.19			
6	5.1	2.73			
7	5.1	2.73			
8	5.1	2.73			
9	5.1	2.73			
10	43.5	23.27			
11	51.3	27.44			
12	54.4	29.1			
13	69	36.91			
14	69.7	37.29			
15	69.7	37.29			
16	69.9	37.39			
17	69.7	37.29			
18	75.2	40.23			
19	75.2	40.23			
20	74.8	40.01			
Avg Skin			37.8	20.21	
Toe			1144.5	4116.83	



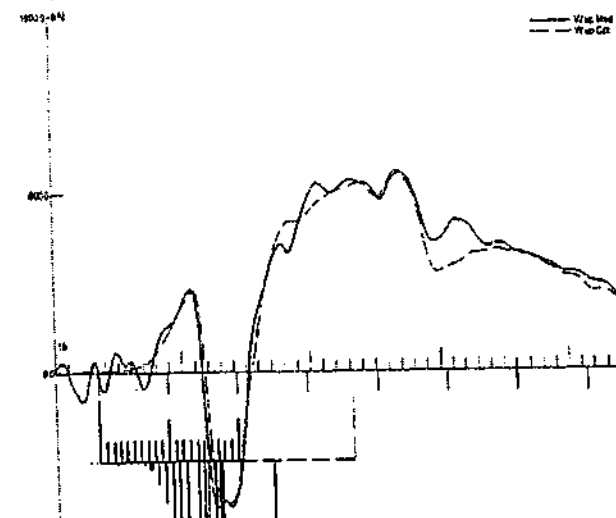
(C) CAPWAP Parameters

JS	SS	QS	UN	CS	LS	PI	OP
0.146	0.278	2.5	0	1	1	0.01	0
JT	ST	QT	YG	CT	LT	PL	
0.502	0.515	5.5	6	1.8	1	0	

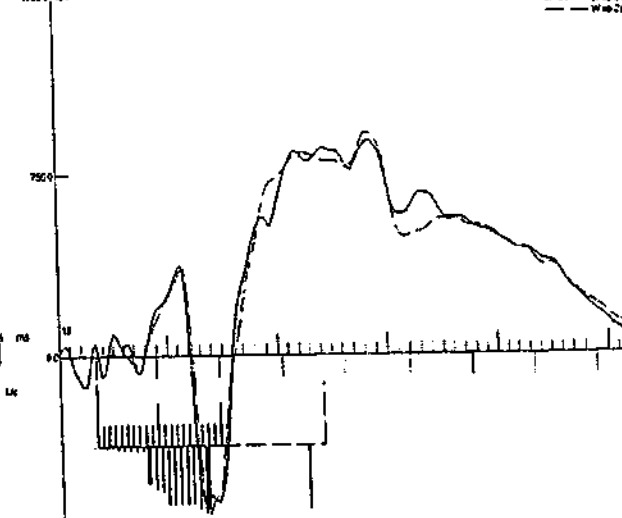
(C) CAPWAP Parameters

JS	SS	QS	UN	CS	LS	PI	OP
0.34	0.54	3	0.1	1	1	0.01	0
JT	ST	QT	TG	CT	LT	PL	
0.476	0.5	8.8	5.7	1.2	1	0	

(D) Match
 CAPWAP match quality: 2.50 (Wave Up Match)
 Observed: final set = 2.803 mm; blow count = 357 b/m
 Computed: final set = 2.795 mm; blow count = 358 b/m



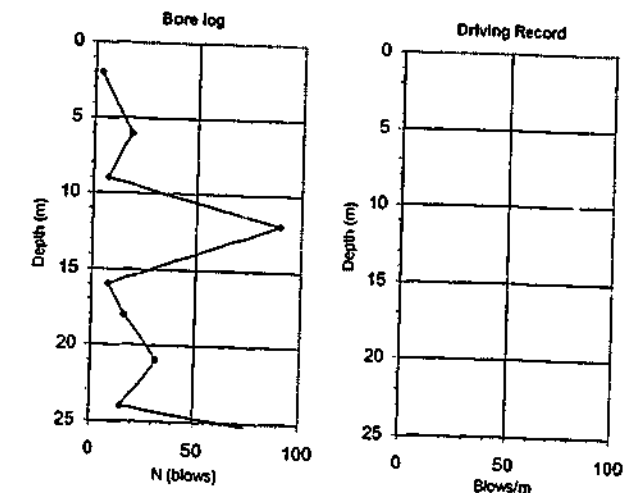
(D) Match
 CAPWAP match quality: 2.34 (Wave Up Match)
 Observed: final set = 2.800 mm; blow count = 357 b/m
 Computed: final set = 3.013 mm; blow count = 332 b/m



(A) Soil Data
 Depth (m) Soil description
 0.35 FW, gravelly sand, fine to coarse

Driving record NA

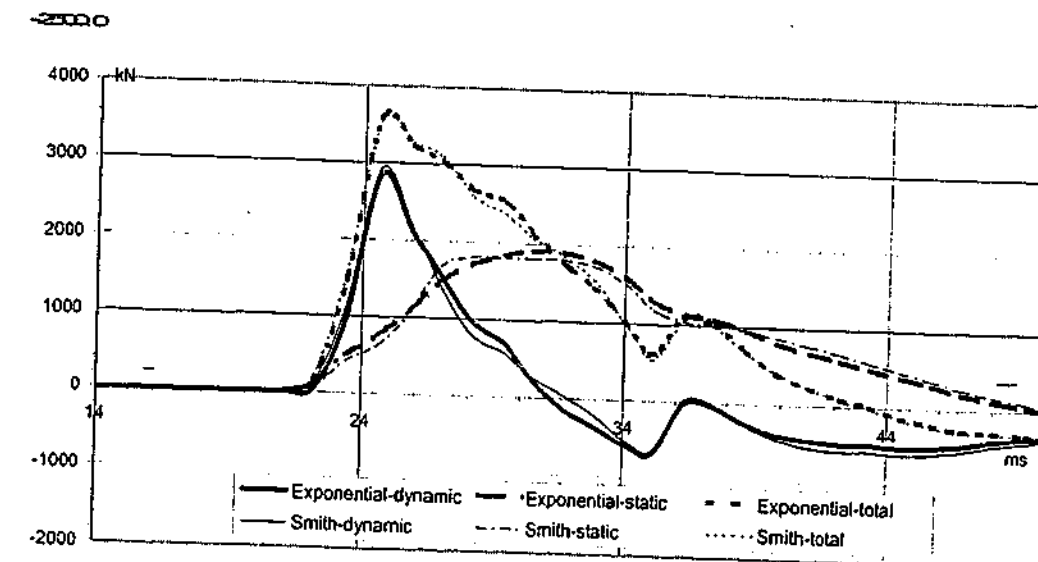
14 soft to firm low plasticity clay
 17 stiff clayey sand, poorly graded
 20 stiff slightly sandy low plasticity clay
 21.2 medium dense to dense clayey sand, poorly graded



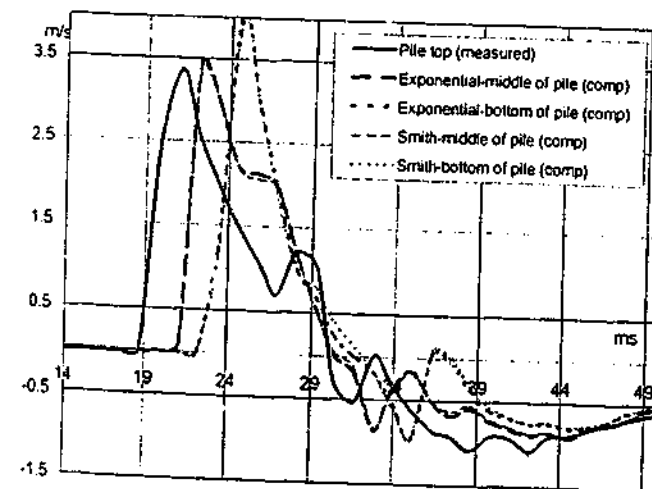
(B) Measured Force & Velocity at Pile Top



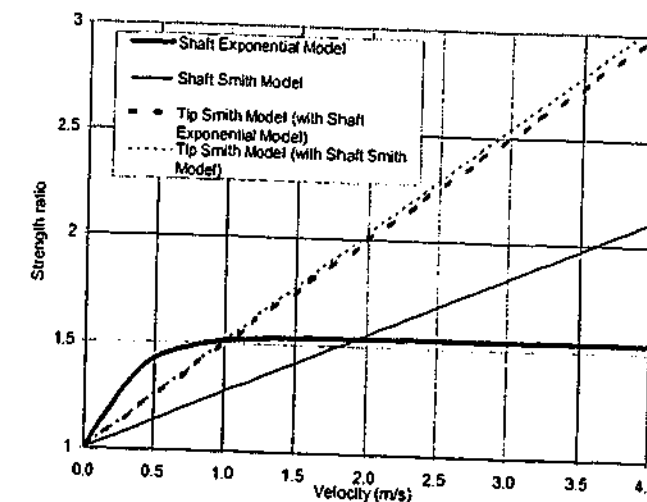
(C) Computed Resistances



(D) Velocities at Top, Middle & Bottom of Pile



(E) Strength Ratio-Velocity Models for Shaft & Tip



ID41

MILWAUKEE MUSEUM: Pile: TP-3BOR

VUL 010, 273mm CEP; Blow: 3

Filename 42 def
Smith Linear Viscous Damping using Rul for Shaft

(A) Pile Model

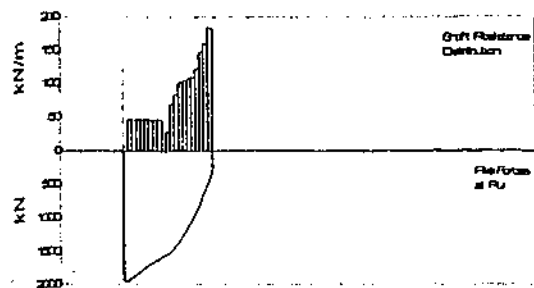
Depth (m)	Area (cm ²)	E-Mod (MPa)	Spec Weir (kN/m ³)	Circum (m)	Impedance (kN/m/s)
0	585.55	45521.4	28.433	0.968	672.70
21.18	585.55	45521.4	28.433	0.968	672.70

Added Impedance None
Wave Speed 3982.4 m/s

(B) Resistance Distribution

Depth (m)	Ru (kN)	Unit (kPa)	Total capacity (kN)	Shaft capacity (kN)	Toe capacity (kN)
1.9	48.4	47.53	1940.5	1624.3	316.2
2.9	46.4	47.53			
3.9	46.4	47.53			
4.9	46.4	47.53			
5.9	46.4	47.53			
6.9	46.4	47.53			
7.9	46.4	47.53			
8.9	46.4	47.53			
9.9	28.5	28.19			
10.9	28.5	28.19			
12	70.2	71.91			
13	83.5	85.53			
14	101.2	103.86			
15	104.9	107.45			
16	107.8	110.42			
17	110.6	113.29			
18	124	127.01			
19	148	151.6			
20	180.8	184.5			
21	185	189.5			

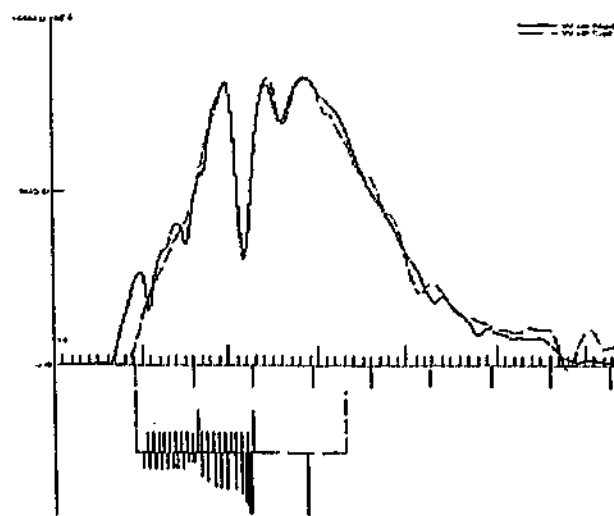
Avg Skin 81.2 63.17
Toe 316.2 17714.81



(C) CAPWAP Parameters

JS	SS	QS	UN	CS	LS	PI	OP
1.086	0.45	3.5	0	1	1	0.01	1
JT	ST	QT	TG	CT	LT	PL	
0.114	0.243	2.54	6	1	1	0	

(D) Match
CAPWAP match quality: 2.02 (Wave Up Match)
Observed: final set = 5.600 mm; blow count = 179 b/m
Computed: final set = 5.246 mm; blow count = 191 b/m



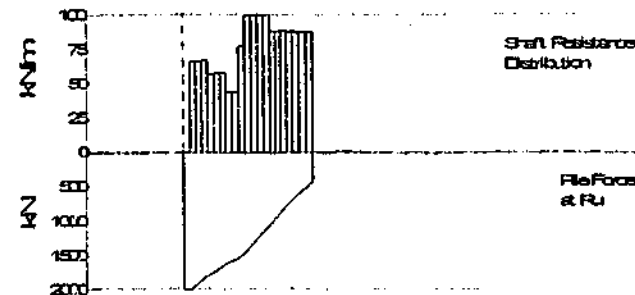
Filename 42 rultm nm
Exponential Viscous Damping using for shaft

(A) Pile Model
As per Smith Linear Viscous Damping

(B) Resistance Distribution

Depth (m)	Ru (kN)	Unit (kPa)	Total capacity (kN)	Shaft capacity (kN)	Toe capacity (kN)
1.9	67	68.61	1889.6	1572.1	417.7
2.8	67.1	68.72			
3.9	68	69.84			
4.9	57.5	58.88			
5.9	58.3	59.7			
6.9	59.2	60.63			
7.9	44.7	45.78			
8.9	44.7	45.78			
9.9	78.3	80.19			
10.9	100.7	103.13			
12	100.7	103.13			
13	100.7	103.13			
14	100.7	103.13			
15	89.5	91.66			
16	89.5	91.66			
17	89.5	91.66			
18	89	91.14			
19	89	91.14			
20	89	91.14			
21	89	91.14			

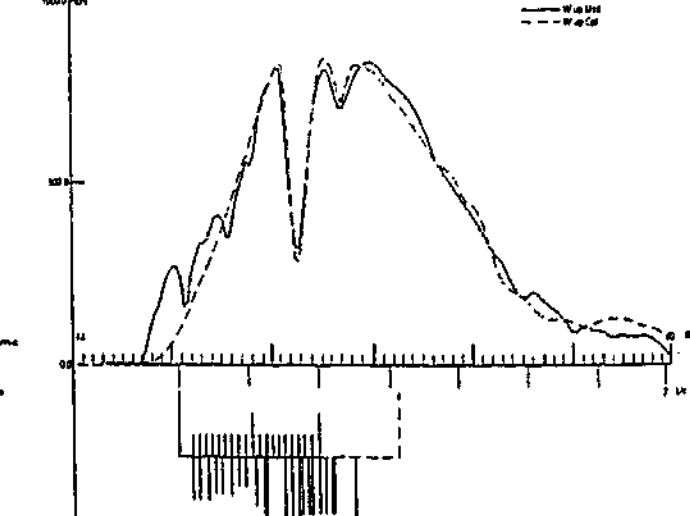
Avg Skin 78.6 80.5
Toe 417.5 0



(C) CAPWAP Parameters

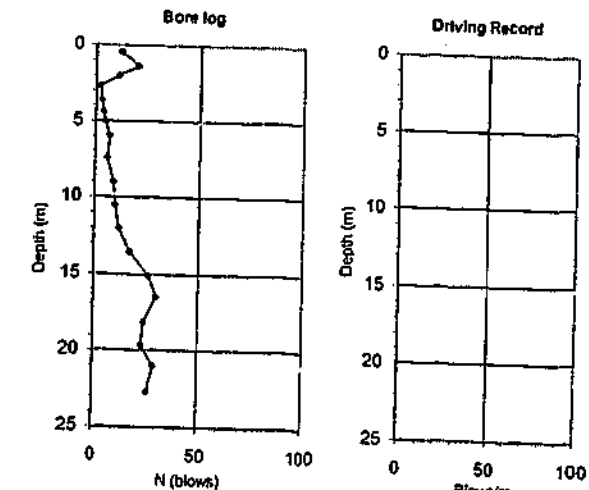
JS	SS	QS	UN	CS	LS	PI	OP
1.077	0.461	7.2	0.1	1	1	0.01	0
JT	ST	QT	TG	CT	LT	PL	
0.41	0.66	1	63	3	1	0	

(D) Match
CAPWAP match quality: 2.87 (Wave Up Match)
Observed: final set = 5.600 mm; blow count = 179 b/m
Computed: final set = 4.748 mm; blow count = 211 b/m



(A) Soil Data

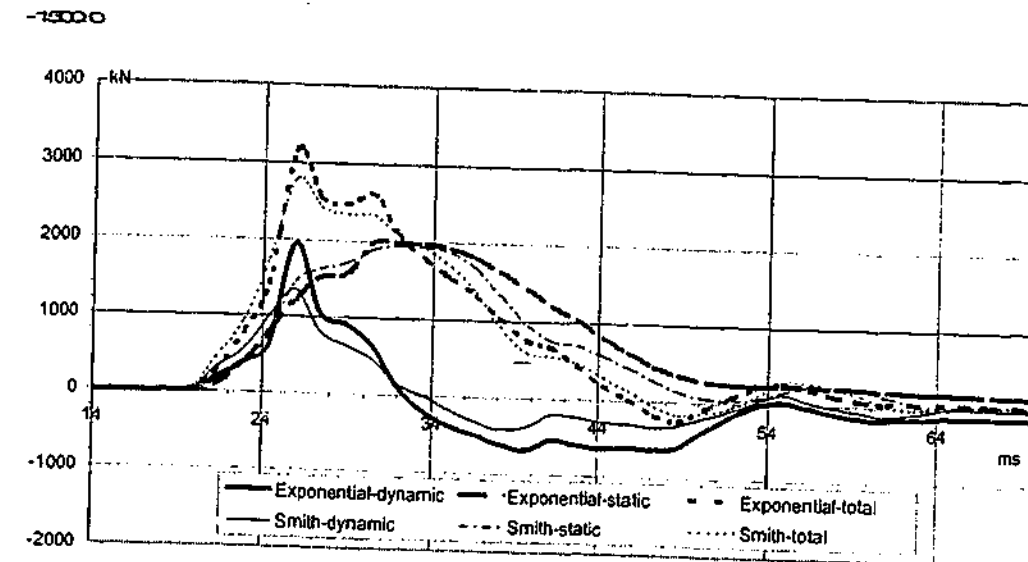
Depth (m) Soil description
0.2 Dense silty, clayey SAND, silty, sandy CLAY
2.1 Very loose silty, clayey SAND, sandy CLAY
3.2 Very loose sandy SILT to silty fine to coarse SAND
4.3 Medium stiff silty CLAY
6.7 Medium stiff to stiff silty CLAY
12.8 Very stiff sandy silty CLAY
14.3 Very stiff silty CLAY
15.5 Medium dense silty fine SAND
18.9 Medium dense fine to medium SAND
20.4 Very stiff fine sandy silty CLAY
21.6 Medium dense silty fine to coarse SAND



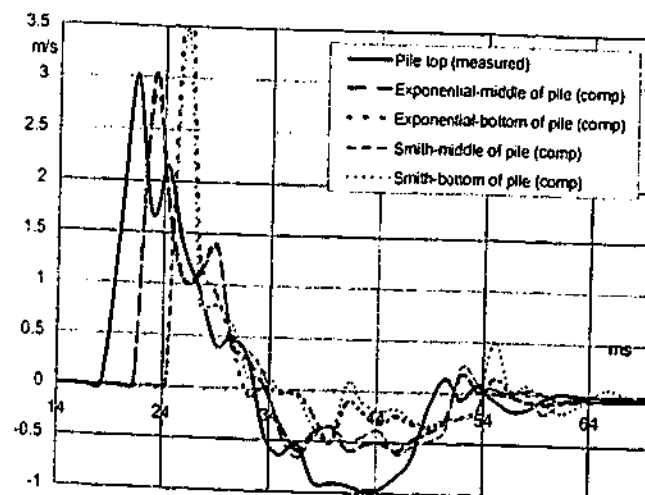
(B) Measured Force & Velocity at Pile Top



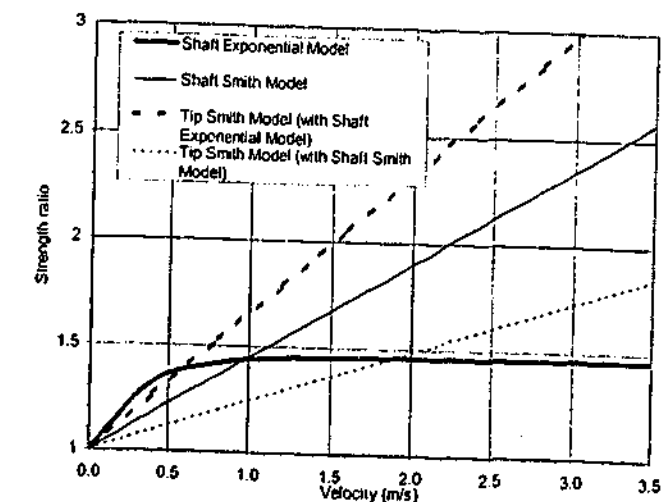
(C) Computed Resistances



(D) Velocities at Top, Middle & Bottom of Pile



(E) Strength Ratio-Velocity Models for Shaft & Tip



ID42
CASINO TOWER NO.2; Pile: C15_RST PSH3 6-TONNE; Blow: 6

Filename 42 del w
Smith Linear Viscous Damping using Rult for Shaft

Filename 42 rinst nm
Exponential Viscous Damping using Rinst for shaft

(A) Pile Model

Depth (m)	Area (cm ²)	E-Mod (MPa)	Spec Wei (kN/m ³)	Circum (m)	Tension stack 100kN top 8m
0-3.8	1225	39214.2	24.035	1.4	Impedance changes along shaft
3.8-26	1600	39214.2	24.035	1.6	Added impedance None
26-35.1	1225	39214.2	24.035	1.4	Wave Speed 3620.0 m/s

(A) Pile Model
As per Smith Linear Viscous Damping

(B) Resistance Distribution

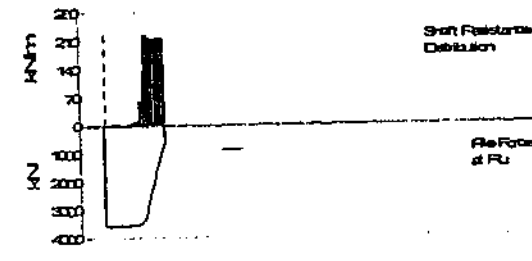
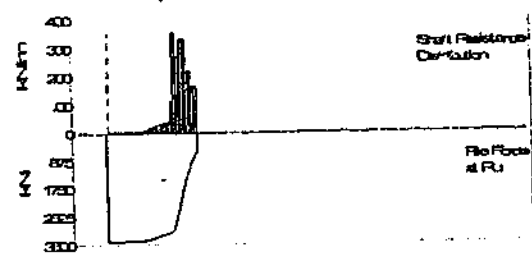
Depth (m)	Ru (kPa)	Unit	Total capacity (kN)
0.7	1.8	1.28	3560.1
1.7	1.8	1.28	2970.3
2.7	1.8	1.24	589.8
3.7	1.8	1.12	
4.7	1.8	1.12	
5.7	1.8	1.12	
6.7	1.8	1.12	
7.7	1.8	1.12	
8.7	1.8	1.12	
9.7	1.8	1.12	
10.7	1.8	1.12	
11.7	1.8	1.12	
12.7	1.8	1.12	
13.7	4.3	2.68	
14.7	5.7	3.55	
15.7	7	4.36	
16.8	8.4	5.24	
17.8	9.8	6.11	
18.8	11.3	7.04	
19.8	63	39.26	
20.8	60.6	37.89	
21.8	139.5	86.94	
22.8	229	142.09	
23.8	227.9	142.03	
24.8	223.5	140.59	
25.2	219.6	138.41	
26.8	216.4	134.13	
27.8	216.8	134.42	
28.8	216.8	134.42	
29.8	216.8	134.42	
30.8	216.8	134.42	
31.8	216.5	133.63	
32.8	216	133.27	
33.8	218	135.27	
Avg Skin	67.4	56.93	
Toe	589.8	4814.66	

(B) Resistance Distribution

Depth (m)	Ru (kPa)	Unit	Total capacity (kN)
0.7	3.3	2.35	3380
1.7	3.3	2.35	2780
2.7	3.3	2.28	600.2
3.7	3.3	2.08	
4.7	3.3	2.06	
5.7	3.3	2.06	
6.7	3.3	2.06	
7.7	3.3	2.06	
8.7	3.3	2.06	
9.7	3.3	2.06	
10.7	3.3	2.06	
11.7	3.3	2.06	
12.7	3.3	2.06	
13.7	8.9	5.55	
14.7	12	7.48	
15.7	15.2	9.47	
16.8	18	11.22	
17.8	21.1	13.15	
18.8	24.3	15.14	
19.8	27.3	17.01	
20.8	30.4	18.96	
21.8	33.4	20.82	
22.8	36.6	22.81	
23.8	39.5	24.62	
24.8	116.2	73.09	
25.8	356.9	254.2	
26.8	274.1	195.23	
27.8	274.1	195.23	
28.8	335.2	238.75	
29.8	335.2	238.75	
30.8	219.7	156.48	
31.8	223.6	159.28	
32.8	167.7	119.44	
33.8	167.7	119.44	
Avg Skin	81.8	53.28	
Toe	600	4897.96	

(B) Resistance Distribution

Depth (m)	Ru (kPa)	Unit	Total capacity (kN)
0.7	1.8	1.28	3560.1
1.7	1.8	1.28	2970.3
2.7	1.8	1.24	589.8
3.7	1.8	1.12	
4.7	1.8	1.12	
5.7	1.8	1.12	
6.7	1.8	1.12	
7.7	1.8	1.12	
8.7	1.8	1.12	
9.7	1.8	1.12	
10.7	1.8	1.12	
11.7	1.8	1.12	
12.7	1.8	1.12	
13.7	4.3	2.68	
14.7	5.7	3.55	
15.7	7	4.36	
16.8	8.4	5.24	
17.8	9.8	6.11	
18.8	11.3	7.04	
19.8	63	39.26	
20.8	60.6	37.89	
21.8	139.5	86.94	
22.8	229	142.09	
23.8	227.9	142.03	
24.8	223.5	140.59	
25.2	219.6	138.41	
26.8	216.4	134.13	
27.8	216.8	134.42	
28.8	216.8	134.42	
29.8	216.8	134.42	
30.8	216.8	134.42	
31.8	216.5	133.63	
32.8	216	133.27	
33.8	218	135.27	
Avg Skin	67.4	56.93	
Toe	589.8	4814.66	



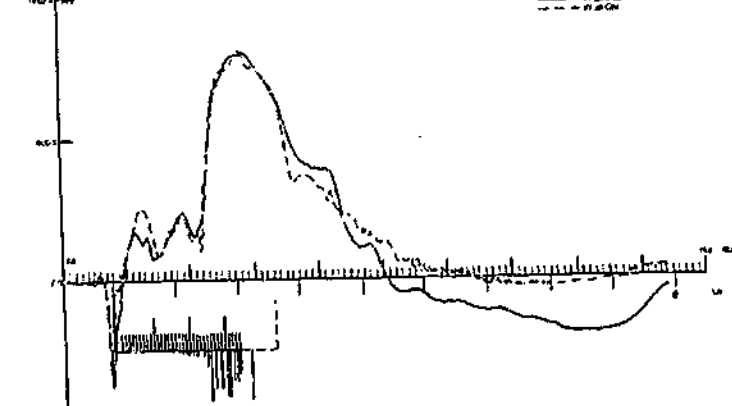
(C) CAPWAP Parameters

JS	SS	QS	UN	CS	LS	PI	OP
1.338	0.578	2.3	0.65	1	1	0.02	0
JT	ST	QT	TG	CT	LT	PL	
0.21	0.42	2.9	0	1	1	0	

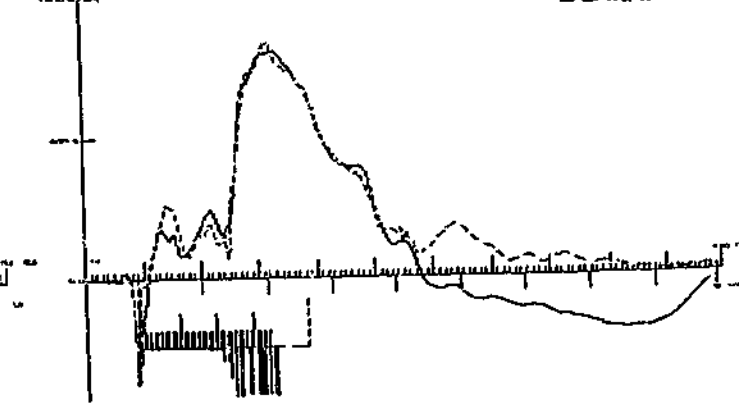
(C) CAPWAP Parameters

JS	SS	QS	UN	CS	LS	PI	OP
1.657	0.67	4.5	0	1	1	0.02	0
JT	ST	QT	TG	CT	LT	PL	
0.314	0.64	3.9	0	1	1	0	

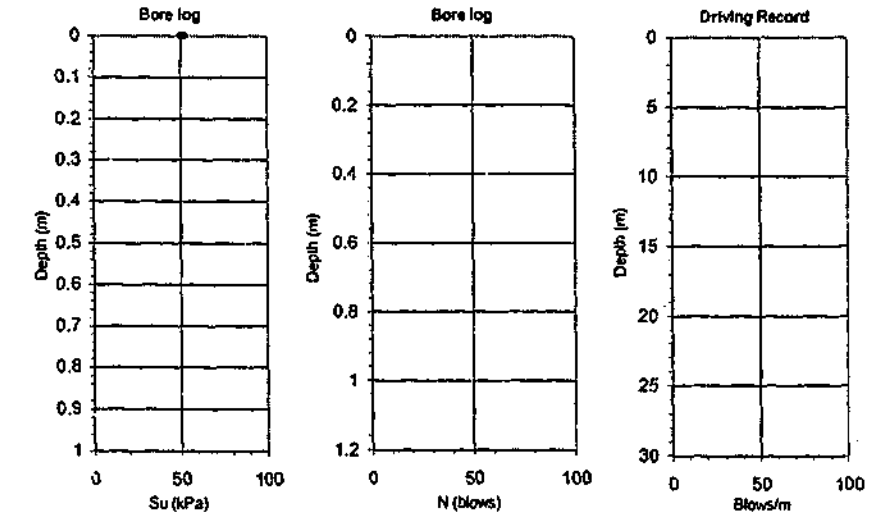
(D) Match
CAPWAP match quality: 4.37 (Wave Up Match)
Observed: final set = 0.100 mm; blow count = 10000 b/m
Computed: final set = 0.100 mm; blow count = 9999 b/m



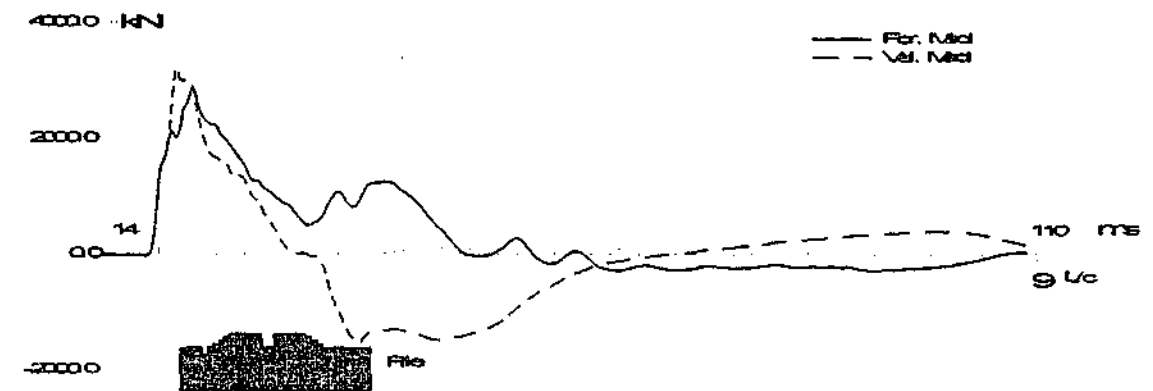
(D) Match
CAPWAP match quality: 3.41 (Wave Up Match)
Observed: final set = 0.100 mm; blow count = 10000 b/m
Computed: final set = 0.100 mm; blow count = 9999 b/m



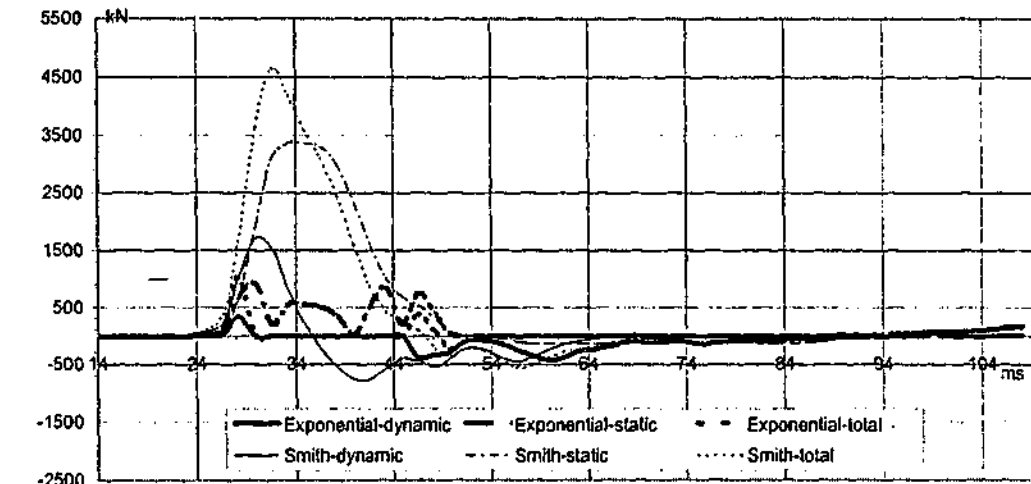
(A) Soil Data



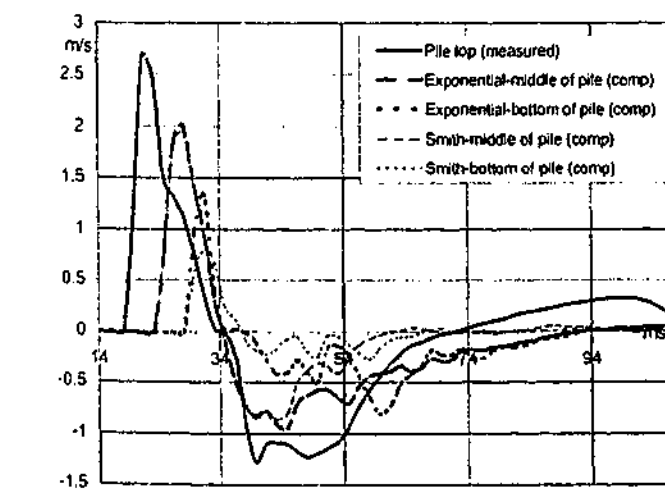
(B) Measured Force & Velocity at Pile Top



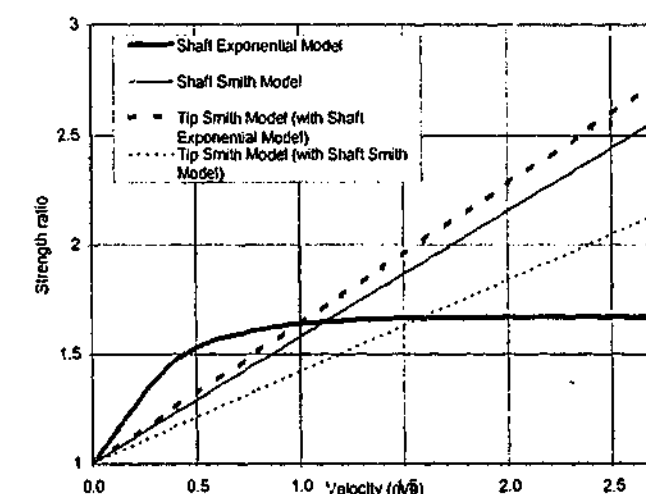
(C) Computed Resistances



(D) Velocities at Top, Middle & Bottom of Pile



(E) Strength Ratio-Velocity Models for Shaft & Tip



ID43
CASINO TOWER NO.2; Pile: C71TP1_R PSH3 6-TGNNE; Blow: 7

Filename 43 det
Smith Linear Viscous Damping using Ruit for Shaft

(A) Pile Model

Depth (m)	Area (cm ²)	E-Mod (MPa)	Spec We (kN/m ³)	Circum (m)	Added Impedance
0	1600	43234	24.035	1.6	1200kN/m/s at bet 11 & 12m; 1000kN/m/s at bet 22 and 23m
35.3	1600	43234	24.035	1.6	Added Impedance None

(B) Resistance Distribution

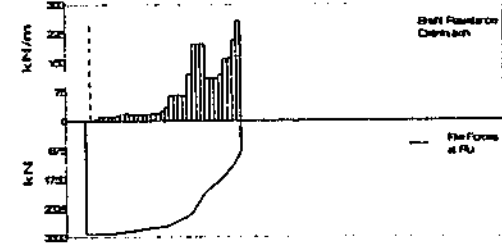
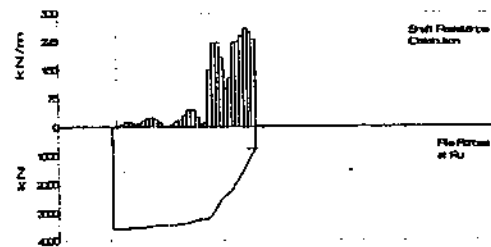
Depth (m)	Ru (kN/m)	Unit (kPa)	Total capacity (kN)	Shaft capacity (kN)	Toe capacity (kN)
0.5	0.7	0.43	3562	2783.5	778.5
1.5	5.7	3.53			
2.5	10.5	6.5			
3.5	10.3	6.36			
4.6	7.4	4.58			
5.6	9.1	5.64			
6.8	15.5	9.6			
7.6	21.8	13.51			
8.6	23.2	14.37			
9.8	19.7	12.2			
10.6	10.4	6.44			
11.6	1.7	1.05			
12.6	0.6	0.37			
13.6	6.6	4.09			
14.6	13.8	8.55			
15.6	19.5	12.08			
16.7	29.2	18.09			
17.7	43.4	26.69			
18.7	45.2	28			
19.7	26.4	16.36			
20.7	8	4.98			
21.7	9.6	5.95			
22.7	150.1	92.99			
23.7	222.2	137.72			
24.7	223.4	138.46			
25.7	183.6	113.8			
26.7	100.3	62.14			
27.7	128.3	79.48			
28.8	223.7	138.65			
29.8	225.9	140.01			
30.8	241.3	149.59			
31.8	261.7	162.19			
32.8	251.3	155.75			
33.8	233.3	144.59			
Avg Skin	81.9	50.73			
Toe	778.5	0.49			

Filename 43 nm rinst wo
Exponential Viscous Damping using Rinst for shaft

(A) Pile Model
As per Smith Linear Viscous Damping

(B) Resistance Distribution

Depth (m)	Ru (kN/m)	Unit (kPa)	Total capacity (kN)	Shaft capacity (kN)	Toe capacity (kN)
0.5	0.7	0.43	3385.1	2501.8	883.3
1.5	5.1	3.16			
2.5	11	6.81			
3.5	11	6.81			
4.6	11	6.81			
5.6	11	6.81			
6.8	13.4	8.3			
7.6	18.3	11.34			
8.6	19.6	12.14			
9.8	17	10.53			
10.6	17.1	10.59			
11.6	17.1	10.59			
12.6	17.1	10.59			
13.6	17.1	10.59			
14.6	17.1	10.59			
15.6	17	10.53			
16.7	24.8	15.36			
17.7	35.8	22.18			
18.7	66.4	41.14			
19.7	66.4	41.14			
20.7	65.4	40.52			
21.7	64.5	39.06			
22.7	120.7	74.77			
23.7	199.1	123.41			
24.7	199.1	123.41			
25.7	199.1	123.41			
26.7	110	68.15			
27.7	110	68.15			
28.8	110	68.15			
29.8	119.5	74.03			
30.8	158.8	98.38			
31.8	162	100.36			
32.8	209.9	130.1			
33.8	259.9	161.07			
Avg Skin	73.6	45.6			
Toe	883.3	5521			



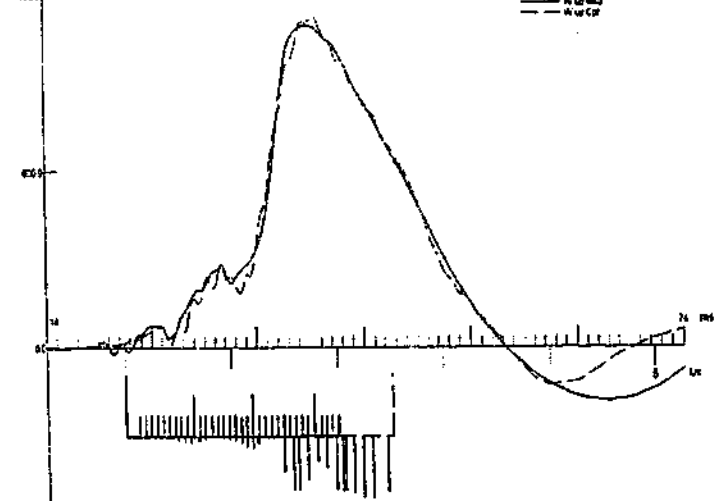
(C) CAPWAP Parameters

JS	SS	QS	UN	CS	LS	PI	OP
1.99	1.177	3.3	0	1	1	0.02	0
JT	ST	QT	TG	CT	LT	PL	
0.349	0.738	3	0	1	1	0	

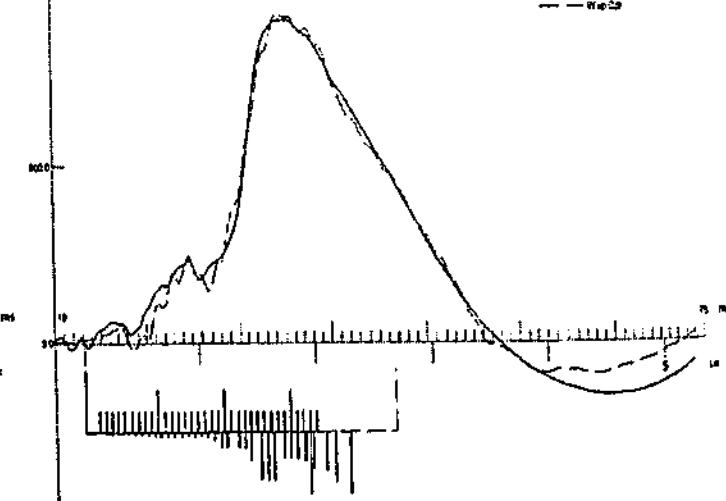
(C) CAPWAP Parameters

JS	SS	QS	UN	CS	LS	PI	OP
2.322	1.529	3	0.15	1	1	0.02	0
JT	ST	QT	TG	CT	LT	PL	
0.432	0.605	1	0	0.8	1	0	

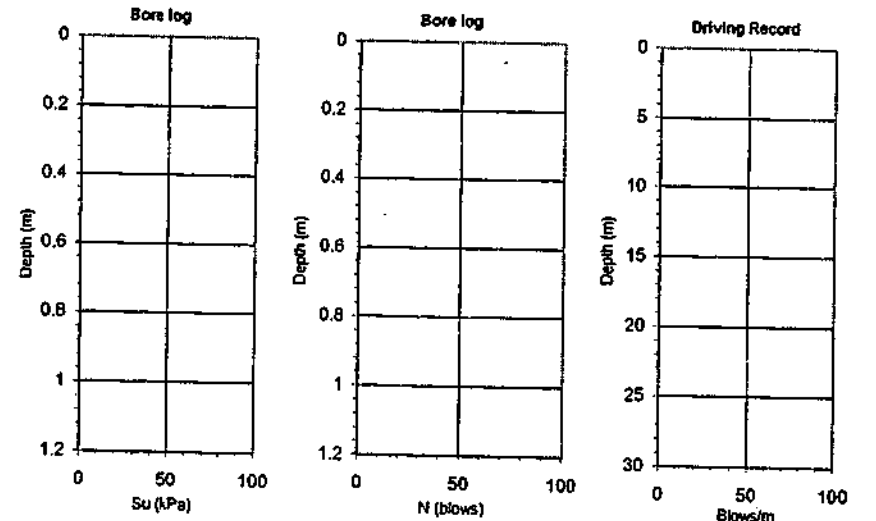
(D) Match
CAPWAP match quality: 1.32 (Wave Up Match)
Observed: final set = 0.100 mm, blow count = 10000 b/m
Computed: final set = 0.100 mm, blow count = 9999 b/m



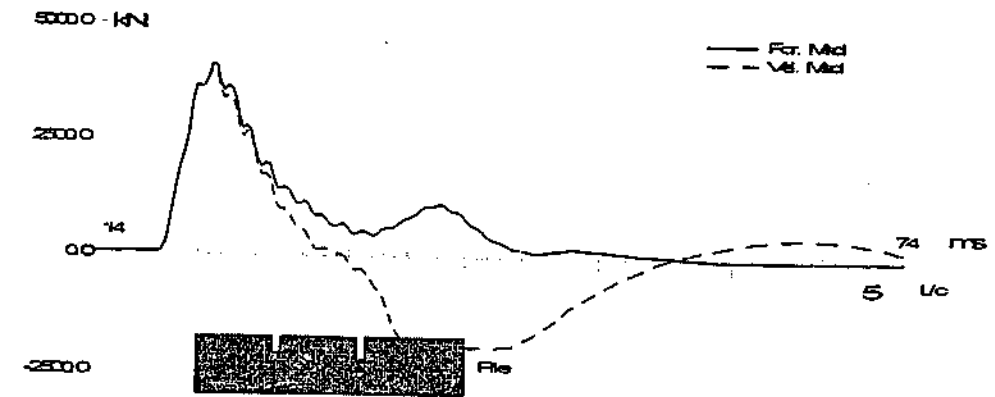
(D) Match
CAPWAP match quality: 1.63 (Wave Up Match)
Observed: final set = 0.100 mm, blow count = 10000 b/m
Computed: final set = 0.100 mm, blow count = 9999 b/m



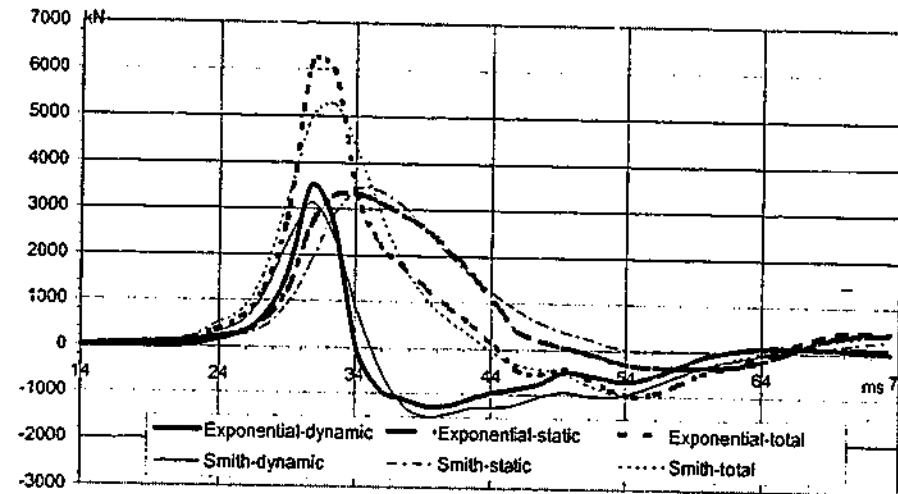
(A) Soil Data



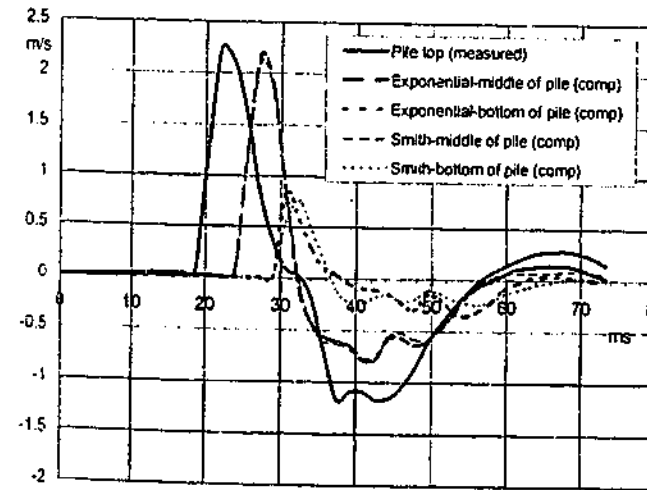
(B) Measured Force & Velocity at Pile Top



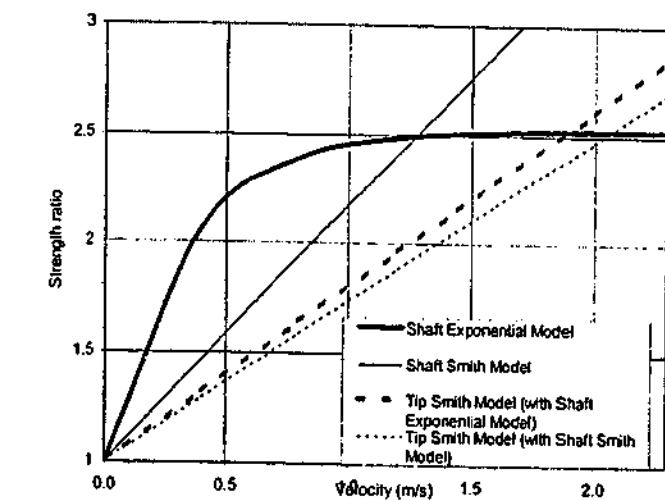
(C) Computed Resistances



(D) Velocities at Top, Middle & Bottom of Pile



(E) Strength Ratio-Velocity Models for Shaft & Tip



IC44
Route 202; Blow: 15; 609mm PSC

Filename 44 def
Smith Linear Viscous Damping using Ruit for Shaft

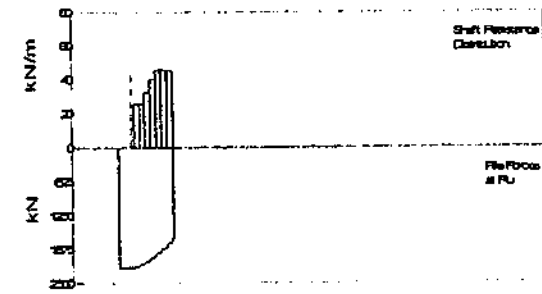
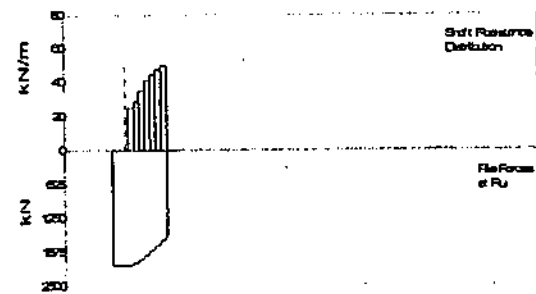
(A) Pile Model					
Depth	Area	E-Mod	Spec Wel	Circum	Impedance
m	cm ²	MPa	kN/m ³	m	3575.83 kN/m ³
0	3716	36401	23.6	2.44	Added Impedance None
20.8	3716	38491	23.6	2.44	Wave Speed 4000.0 m/s

(B) Resistance Distribution					
Depth	Ru	Unit	Total capacity		
Below	Ru		Shaft capacity		
Grade	(Area)		Toe capacity		
m	kN	kPa	kN		
2.7	51.5	10.15	2113.8	kN	
4.8	59.7	11.76	565.7	kN	
6.9	73.8	14.54	1548.1	kN	
9	85.8	16.81			
11	92.6	18.25			
13.1	98.6	19.43			
15.2	103.7	20.43			
Avg Skin	80.8	15.92			
Toe	1548.1	4161.56			

Filename 44 rinst nm
Exponential Viscous Damping using Rinst for shaft

(A) Pile Model
As per Smith Linear Viscous Damping

(B) Resistance Distribution					
Depth	Ru	Unit	Total capacity		
Below	Ru		Shaft capacity		
Grade	(Area)		Toe capacity		
m	kN	kPa	kN		
2.7	53.4	10.52	2200.2	kN	
4.8	53.4	10.52	543.2	kN	
6.9	67.2	13.24	1657	kN	
9	83.6	16.47			
11	95.2	18.76			
13.1	95.2	18.76			
15.2	95.2	18.76			
Avg Skin	77.6	15.29			
Toe	1657	4454.3			



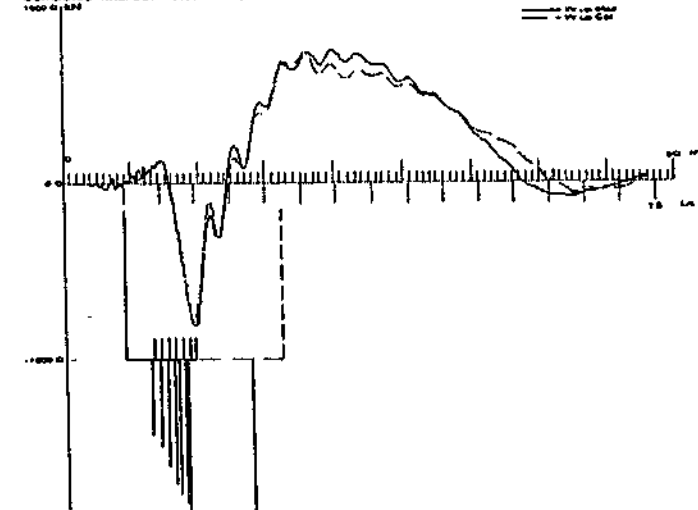
(C) CAPWAP Parameters

JS	SS	QS	UN	CS	LS	PI	OP
0.153	1.032	1.58	0.2	1	1	0.03	1
JT	ST	QT	TG	CT	LT	PL	
0.35	0.808	10.17	0	1	1	0.2	

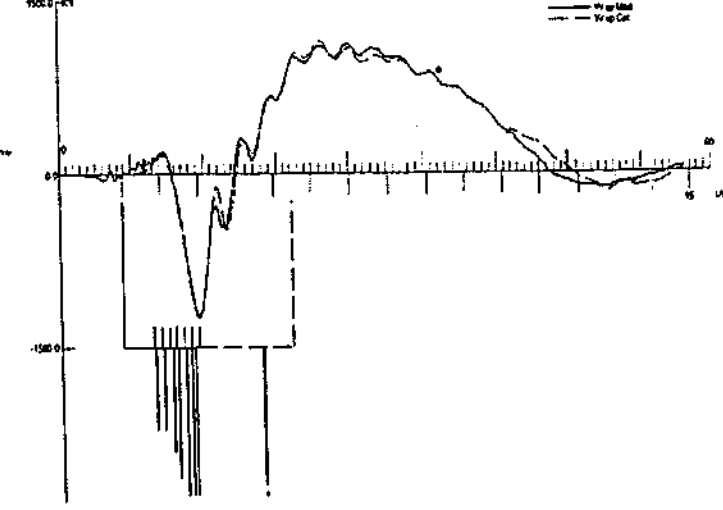
(C) CAPWAP Parameters

JS	SS	QS	UN	CS	LS	PI	OP
0.18	1.187	2.03	0.36	0.7	1	0.03	1
JT	ST	QT	TG	CT	LT	PL	
0.309	0.667	10.41	0	1	1	4	

(D) Match
CAPWAP match quality: 2.53 (Wave Up Match)
Observed: final set = 0.370 mm, blow count = 2700 b/m
Computed: final set = 0.374 mm, blow count = 2673 b/m

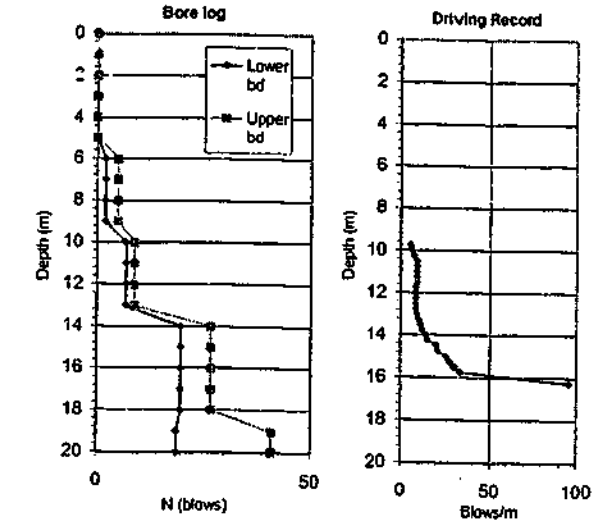


(D) Match
CAPWAP match quality: 2.01 (Wave Up Match)
Observed: final set = 0.370 mm, blow count = 2700 b/m
Computed: final set = 0.360 mm, blow count = 2775 b/m

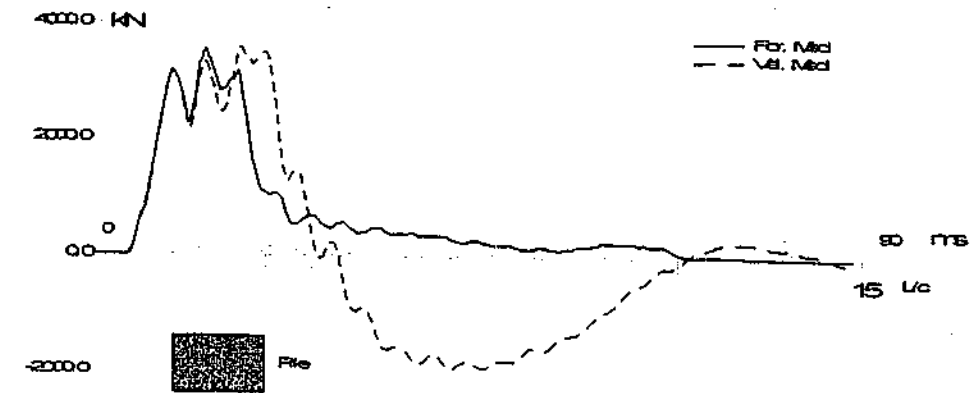


(A) Soil Data (general only)

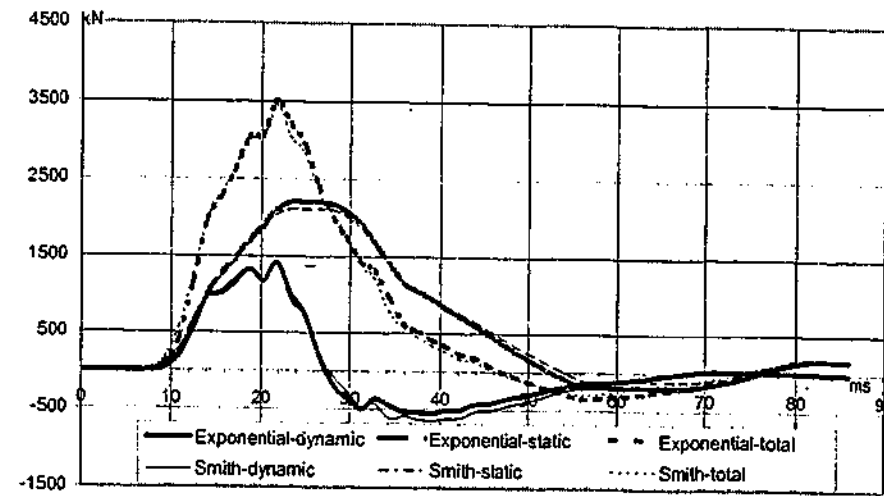
Depth (m)	Soil description
0.0	SILT, trace organic
6.0	SAND, trace silt
14.0	Clayey SILT, with shells
18.5	SILT, with shells



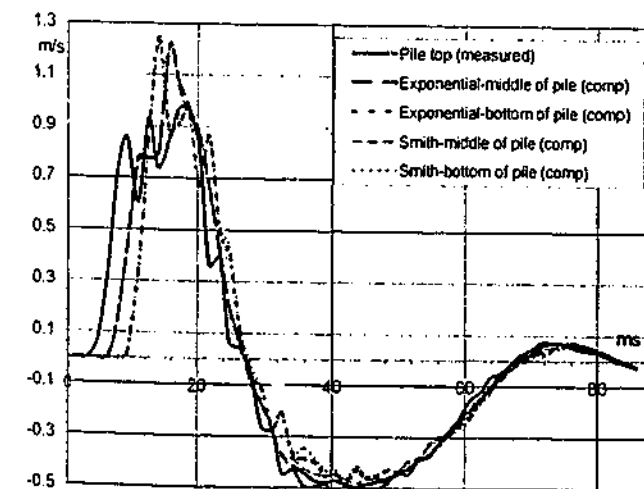
(B) Measured Force & Velocity at Pile Top



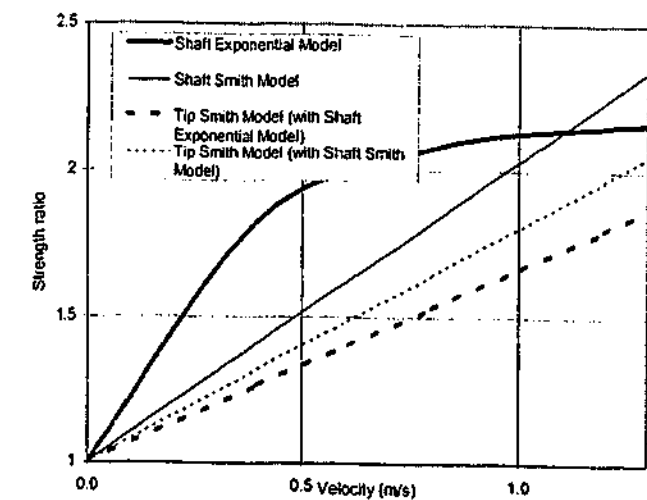
(C) Computed Resistances



(D) Velocities at Top, Middle & Bottom of Pile



(E) Strength Ratio-Velocity Models for Shaft & Tip



Appendix D

D. Estimation of Shaft & Toe Capacities Based on Static Analyses

D.1 Shaft Capacity

The shaft friction values for all the piles, which were installed in clay, were calculated from:

$$\alpha c_s$$

where

c_s = undrained cohesion determined from in-situ or laboratory tests

α = adhesion factor obtained from AS2159 (1978) (Standards Australia, 1978)

For brevity, the computed values have not been presented numerically but have been presented graphically in Section 9.4.

D.2 Toe capacity

The toe capacities for piles (with their tips) founded on clay was calculated from:

$$c_b N_c$$

where

c_b = undrained cohesion determined from in-situ or laboratory tests

N_c = bearing capacity factor

ID	Soil strength	N_c (lower)	N_c (upper)	S_u (kPa)	SPT*	c_b (kPa)	$N_c c_b$ (lower) (kPa)	$N_c c_b$ (upper) (kPa)
1	Stiff	9	15	300	NA	300	2700	4500
2	Stiff	9	15	150	NA	150	1350	2250
3	Stiff	9	15	200	40	200	1800	3000
5	Soft	9	9	NA	8	72	648	648
6	Stiff	9	15	NA	20	180	1620	2700
7	Stiff	9	15	NA	70	630	5670	9450
8	Stiff	9	15	NA	65	585	5265	8775
13	Stiff	9	15	240	NA	240	2160	3600
14	Stiff	9	15	70	NA	70	630	1050
16	Stiff	9	15	NA	25	225	2025	3375
18	Soft	9	9	50	NA	50	450	450
19	Soft	9	9	NA	12	108	972	972

*NA = Not Available

The toe capacities for piles (with their tips) founded on sand was calculated from:

$$P'_{ob} N_q$$

where

N_q (lower) = lower bound value of bearing capacity factor

N_q (upper) = upper bound value bearing capacity factor

P'_{ob} = effective overburden pressure based on the limited depth method detailed in AS2159 (1978) (Standards Australia, 1978) based on Vesic (1967))

ID	SPT	σ' (kPa)	SPT'	ϕ (°)	ϕ' (°)	N_q	ϕ'' (°)	z_c/d	d (m)	z_c (m)	P'_{ob} (m)	$P'_{ob} N_q$ (kPa)
9	40	168	52	41	40.5	200	40.75	17	0.305	5.2	41.5	8300
15	10	88	22	33	36.5	80	34.75	6.5	0.247	1.6	12.8	1030
17	25	168	168	37	38.5	160	37.75	10	0.286	2.9	22.9	3660
4	10	208	208	30	35	70	32.5	7	0.610	4.3	34.2	2390

SPT' = SPT number corrected according to Gibbs and Holtz (1957)

ϕ' = ϕ corrected for determination of N_q

ϕ'' = ϕ corrected for determination of z_c

d = diameter

z_c = critical depth

P'_{ob} = effective overburden based on limited depth theory

REFERENCES

- Abou-matar, H., Rausche, F., Thendean, G., Likins, G. and Goble, G. (1996). *Wave equation soil constants from dynamic measurements on SPT*. Proceedings of the 5th International Conference on the Application of Stress-Wave Theory to Piles, Orlando, Florida, USA, Balkema, Vol., 163-175.
- Abrantes, A. E. and Yamamuro, J. A. (2002a). *Experimental and data analysis techniques used for high strain rate tests on cohesionless soil*. Geotechnical Testing Journal, GTJODJ, 25(2), 128-141.
- Abrantes, A. E. and Yamamuro, J. A. (2002b). *Effect of strain rate in cohesionless soil*. Proceedings of the 15th ASCE Engineering Mechanics Conference, New York, NY, Vol., 1-8.
- Acar, Y. B., Durgunoglu, H. T. and Tumay, M. T. (1982). *Interface properties of sand*. Journal of Geotechnical Division, ASCE, 108(GT4), 648-654.
- Al-Douri, R. H. and Poulos, H. G. (1992). *Static and cyclic direct shear tests on carbonate sands*. Geotechnical Testing Journal, 15(2), 138-157.
- Andresen, A., Berne, T., Kleven, A. and Lunne, T. (1979). *Procedures used to obtain soil parameters for foundation engineering in the North Sea*. Marine Geotechnology, 3, 201-266.
- Benamar, A. (1996). *Dynamic soil resistance from pile driving analysis*. Structural Dynamics - EURO DYN'96, Rotterdam, Balkema, Vol., 1039-1043.
- Benamar, A. (1999). *Pile behaviour during driving*. 8th Australia New Zealand Conference on Geomechanics, Hobart, Tasmania, Australia, Australian Geomechanics Society, Vol. 1, 363-366.
- Benamar, A. (2000). *The shaft dynamic response of a pile in clay: induced pore pressure*. Proceedings of the 6th International Conference on the Application of Stress-Wave Theory to Piles, Sao Paulo, Brazil, Balkema, Vol., 255-259.
- Benamar, A., Lepert, P., Levacher, D. and Boisard, P. (1991). *Shaft resistance during driving in clay from laboratory tests*. Proceedings of the 2nd International

- Conference on Recent Advances in Geotechnical Earthquake Engineering and Soil Dynamics, St. Louis, Missouri, Vol., 291-297.
- Benamar, A., Levacher, D. and Lepert, P. (1992). *Physical and numerical simulation of lateral shaft friction along driven piles*. Proceedings of the 4th International Conference on the Application of Stress-wave Theory to Piles, The Hague, The Netherlands, Balkema, Vol., 37-42.
- Bishop, A. W., Green, G. E., Garga, V. K., Andresen, A. and Brown, J. D. (1971). *A new ring shear apparatus and its application to the measurement of residual strength*. Geotechnique, 21(4), 273-328.
- Bjerrum, L., Simons, N. and Torblaa, I. (1958). *The effect of time on the shear strength of a soft marine clay*. Proceedings of the Brussels Conference on Earth Pressure Problems, Vol. I, 148-158.
- Bond, A. J. and Jardine, R. J. (1991). *Effects of installing displacement piles on a high OCR clay*. Geotechnique, 41(3), 341-363.
- Briaud, J. and Garland, E. (1985). *Loading rate method for pile response in clay*. Journal of Geotechnical Engineering, ASCE, 111(1), 319-335.
- Butterfield, R. and Ghosh, N. (1978). *Response of single piles in clay to axial load*. Bell Laboratories Record, 1, 451-457.
- Casagrande, A. and Wilson, S. D. (1951). *Effect of rate of loading on the strength of clays and shales at constant water content*. Geotechnique, 2(3), 251-263.
- Clark, J. I. and Meyerhof, G. G. (1972). *The behaviour of piles driven in clay. I. An investigation of soil stress and pore water pressure as related to soil properties*. Canadian Geotechnical Journal, 9(351), 351-373.
- Coop, M. R. and Wroth, C. P. (1989). *Field studies of an instrumented model pile in clay*. Geotechnique, 39(4), 679-696.
- Coyle, H. M., Bartoskewitz, R. E. and W., K. K. (1972). *Soil resistance parameters for wave equation analysis*. Journal of Materials, 7(4), 486-495.
- Coyle, H. M. and Gibson, G. C. (1970). *Empirical damping constants for sands and clays*. Journal of the Soil Mechanics and Foundation Division, ASCE, 96(SM 3), 949-965.
- Crawford, C. B. (1959). *The influence of rate of strain on effective stresses in sensitive clay*. American Society for Testing and Materials, Special Technical Publication, 254, 36-61.
- Crawford, C. B. (1965). *The resistance of soil structure to consolidation*. Canadian Geotechnical Journal, 2(2), 90-97.

- Danziger, B. R., Costa, A. M., Lopes, F. R. and Pacheco, M. P. (1999). *Back analysis of offshore pile driving with an improved soil model*. Geotechnique, 49(6), 777-799.
- Dayal, U. (1974). *Instrumented impact cone penetrometer*. Faculty of Engineering and Applied Science, Newfoundland, Memorial University of Newfoundland.
- Dayal, U. and Allen, J. H. (1973). *Instrumented impact cone penetrometer*. Canadian Geotechnical Journal, 10, 397-409.
- Dayal, U. and Allen, J. H. (1975). *The effect of penetration rate on the strength of remolded clay and sand samples*. Canadian Geotechnical Journal, 12, 336-348.
- Desai, C. S., Drumm, E. C. and Zaman, M. M. (1985). *Cyclic testing and modeling of interfaces*. Journal of Geotechnical Engineering, ASCE, 111(6), 793-815.
- Evgin, E. and Fakharian, K. (1996). *Effect of stress paths on the behaviour of sand-steel interfaces*. Canadian Geotechnical Journal, 33, 853-865.
- Fakharian, K. and Evgin, E. (1997). *Cyclic simple shear behaviour of sand-steel interfaces under constant normal stiffness condition*. Journal of Geotechnical and Geoenvironmental Engineering, 123(12), 1096-1105.
- Feda, J. (1976). *Skin friction of piles*. Sixth European Conference on Soil Mechanics and Foundation Engineering, Vienna, Vol. 1.2, 423-428.
- Fellenius, B. H. (1988). *Variation of CAPWAP results as a function of the operator*. Proceedings of the 3rd International Conference on the Application of Stress-Wave Theory to Piles, Ottawa, Canada, Balkema, Vol., 814-825.
- Fleming, W. G. K., Weltman, A. J., Randolph, M. F. and Elson, W. K. (1992). *Piling Engineering*. 2nd edition. Glasgow, Blackie A & P.
- Gazetas, G. and Dobry, R. (1984). *Simple radiation damping model for piles and footings*. Journal of Engineering Mechanics, 110(6), 937-956.
- Gibbs, H. J. and Holtz, W. G. (1957). *Research on determining the density of sands by spoon penetration testing*. Proceedings of the 4th International Conference on Soil Mechanics & Foundation Engineering, Vol. 1, 35-39.
- Goble, G. G., Likins, G. J. and Rausche, F. (1975). *Bearing capacity of piles from dynamic measurements*. OHIO-DOT-05-75, Department of Civil Engineering, Case Western Reserve University, Cleveland, Ohio.
- Goble, G. G. and Rausche, F. (1980). *Pile drivability predictions by CAPWAP*. Numerical Methods in Offshore Piling, ICE, London, 29-36.
- Graham, J., Crooks, J. H. A. and Bell, A. L. (1983). *Time effects on the stress-strain behaviour of natural soft clays*. Geotechnique, 33(3), 327-340.

- Head, K. H. (1994). *Manual of soil laboratory testing - Volume 2: Permeability, shear strength and compressibility tests*. New York, John Wiley & Sons, Inc.
- Heerema, E. P. (1979). *Relationships between wall friction, displacement velocity and horizontal stress in clay and in sand for pile driveability analysis*. *Ground Engineering*, 12(1), 55-65.
- Heerema, E. P. (1981). *Dynamic point resistance in sand and in clay, for pile driveability analysis*. *Ground Engineering*, 14(6), 30-35, 46.
- Holtz, R. D. and Kovacs, W. D. (1981). *An introduction to geotechnical engineering*. Englewood Cliffs, New Jersey, Prentice-Hall.
- Hungr, O. and Morgenstern, N. R. (1984a). *Experiments on the flow behaviour of granular materials at high velocity in an open channel*. *Geotechnique*, 34(3), 405-413.
- Hungr, O. and Morgenstern, N. R. (1984b). *High velocity ring shear tests on sand*. *Geotechnique*, 34(3), 415-421.
- Hunt, C. E., Pestana, J. M., Bray, J. D. and Riemer, M. (2002). *Effect of pile driving on static and dynamic properties of soft clay*. *Journal of Geotechnical and Geoenvironmental Engineering*, 128(1), 13-24.
- IST (1998). *Instron Schenck testing systems labtronic 8800 structural test control system - Reference manual*. Buckingham, Instron Schenck Testing Ltd.
- Jardine, R. J. (1985). *Investigations of pile-soil behaviour, with special reference to the foundations of offshore structures*. Department of Civil and Environmental Engineering. London, Imperial College.
- Jardine, R. J. and Bond, A. J. (1989). *Behaviour of displacement piles in a heavily over-consolidated clay*. *Proceedings of the 12th International Conference on Soil Mechanics and Foundation Engineering*, Rio de Janeiro, Vol. 2, 1147-1151.
- Jardine, R. J. and Chow, F. C. (1996). *New design methods for offshore piles*. London, Marine Technology Directorate Ltd.
- Kanji, M. A. (1974). *Unconventional laboratory tests for the determination of the shear strength of soil-rock contacts*. *Proceedings of the 3rd Congress of the International Conference on Rock Mechanics*, Denver, Vol. 2A, 241-247.
- Kraft, L. M. J., Cos, W. R. and Verner, E. A. (1981). *Pile load tests: cyclic loads and varying load rates*. *Journal of the Geotechnical Engineering Division, ASCE*, 107(GT1), 1-19.
- Kulhawy, F. H. and Mayne, P. W. (1990). *Manual on estimating soil properties for foundation design*. EL-6800, Research Project 1493-6, Cornell University, Ithaca, New York.

- Kulhawy, H. K. and Peterson, M. S. (1979). *Behaviour of sand-concrete interfaces*. *Proceedings 6th Pan-American Conference on Soil Mechanics and Foundation Engineering*, Vol. 2, 225-236.
- Ladd, C. C. and Edgers, L. (1972). *Consolidated-undrained direct-simple shear tests on saturated clays*. MIT Research Report R72-82, Massachusetts Institute of Technology, Cambridge.
- Ladd, C. C., Foott, R., Ishihara, K., Schlosser, F. and Poulos, H. G. (1977). *Stress-deformation and strength characteristics: state of the art report*. *Proceedings of the 9th International Conference on Soil Mechanics*, Tokyo, Vol. 2, 421-494.
- Lade, P. V. (2002). *Instability, shear banding, and failure in granular materials*. *International Journal of Solids and Structures*, 39(13), 3337-3357.
- Lai, P. W., Kuo, C. L. and Puckett, T. (1996). *Dynamic soil responses of impact pile driving - a case history study*. *Proceedings of the 5th International Conference on the Application of Stress-Wave Theory to Piles*, Orlando, Florida, Balkema, Vol., 300-312.
- Lee, K. L., Seed, H. B. and Dunlop, P. (1969). *Effect of transient loading on the strength of sand*. *Proceedings of the 7th International Conference on Soil Mechanics and Foundation Engineering*, Mexico, Vol., 239-247.
- Lee, S. L., Chow, Y. K., Karunaratne, G. P. and Wong, K. Y. (1988). *Rational wave equation model for pile-driving analysis*. *Journal of Geotechnical Engineering, ASCE*, 114(3), 306-325.
- Lefebvre, G. and LeBoeuf, D. (1987). *Rate effects and cyclic loading of sensitive clays*. *Journal of Geotechnical Engineering, ASCE*, 113(5), 476-489.
- Lehane, B. M., Jardine, R. J., Bond, A. J. and Frank, R. (1993). *Mechanisms of shaft friction in sand from instrumented pile tests*. *Journal of Geotechnical Engineering, ASCE*, 119(1), 19-35.
- Lemos, L. J. L. (1986). *The effect of rate on the residual strength of soil*. Department of Civil and Environmental Engineering. London, Imperial College.
- Lemos, L. J. L. and Vaughan, P. R. (2000). *Clay-interface shear resistance*. *Geotechnique*, 50(1), 55-64.
- Lepert, P., Corte, J. and Goulois, A. (1988b). *An experimental set-up for investigation of shaft resistance during driving*. *Proceedings of the 3rd International Conference on the Application of Stress-Wave Theory to Piles*, Ottawa, Canada, Balkema, Vol., 422-430.
- Lepert, P., Corte, J., Goulois, A. and Meunier, J. (1988a). *Shaft resistance during driving in sand from laboratory tests*. *Proceedings of the 3rd International Conference on the Application of Stress-Wave Theory to Piles*, Ottawa, Canada, Balkema, Vol., 431-440.

- Leroueil, S., Tavenas, F., Samson, L. and Morin, P. (1983). *Preconsolidation pressure of Champlain clays. Part II. Laboratory determination*. Canadian Geotechnical Journal, 20, 803-816.
- Levacher, D. R. and Sieffert, J.-G. (1984). *Tests on model tension piles*. Journal of Geotechnical Engineering, ASCE, 110(12), 1735-1748.
- Liang, R. Y. and Zhou, J. (1996). *Pile capacity estimation using new HST interpretation method*. Proceedings of the 5th International Conference on the Application of Stress-Wave Theory to Piles, Orlando, Florida, USA, Balkema, Vol., 367-381.
- Liang, R. Y. and Zhou, J. (1997). *Probability method applied to dynamic pile-driving control*. Journal of Geotechnical and Geoenvironmental Engineering, 123(2), 137-144.
- Likins, G. E., Rausche, F., Thendean, G. and Svinkin, M. (1996). *CAPWAP correlation studies*. Proceedings of the 5th International Conference on the Application of Stress-Wave Theory to Piles, Orlando, Florida, USA, Balkema, Vol.,
- Litkouhi, S. and Poskitt, T. J. (1980). *Damping constants for pile driveability calculations*. Geotechnique, 30(1), 77-86.
- Littleton, I. (1976). *An experimental study of the adhesion between clay and steel*. Journal of Terramechanics, 13(3), 141-152.
- Lupini, J. F., Skinner, A. E. and Vaughan, P. R. (1981). *The drained residual strength of cohesive soils*. Geotechnique, 31(2), 181-213.
- Martins, J. P. (1983). *Shaft resistance of axially loaded piles in clay*. Department of Civil and Environmental Engineering. London, Imperial College.
- Meyerhof, G. G. and Murdock, L. J. (1953). *An investigation of the bearing capacity of some bored and driven piles in London clay*. Geotechnique, 3(7), 267-282.
- Michaelides, O., Gazetas, G., Bouckovalas, G. and Chryssikou, E. (1997). *Approximate non-linear dynamic axial response of piles*. Geotechnique, 48(1), 33-53.
- Middendorp, P. and van Weele, A. F. (1986). *Application of characteristic stress wave method, in offshore practice*. Proceedings of the 3rd International Conference on Numerical Methods in Offshore Piling, Nantes, France, Vol., 6-18.
- Mitchell, J. K. (1964). *Shearing resistance of soils as a rate process*. Journal of the Soil Mechanics and Foundations Division, ASCE, 90(SM1), 29-61.
- Mitchell, J. K. (1993). *Fundamentals of soil behavior*. 2nd Edition. New York, John Wiley & Sons, Inc.

- Mitchell, J. K. (2002). *Mechanism of strength increase in sand*. Personal Communication.
- MSI (2000). *Pressure sensors, accelerometers, and custom microstructures - IC sensors products databook 2000*. Milpitas, California, USA, Measurement Specialties, Inc.
- Novak, M., Nogami, T. and Aboul-Ella, F. (1978). *Dynamic soil reactions for plane strain case*. Journal of Engineering Mechanics Division, ASCE, 104(EM4), 953-959.
- Novosad, J. (1964). *Studies on granular materials II*. Collection of Czechoslovak Chemical Communications, 29, 2697.
- O'Rourke, T. D., Druschel, S. J. and Netravali, A. N. (1990). *Shear strength characteristics of sand-polymer interfaces*. Journal of Geotechnical Engineering, ASCE, 116(3), 451-469.
- Paikowsky, S. G., Player, C. M. and Connors, P. J. (1995). *A dual interface apparatus for testing unrestricted friction of soil along solid surfaces*. Geotechnical Testing Journal, 18(2), 168-193.
- PDI (1994). *CAPWAP for Windows Manual - CAsE Pile Wave Analysis Program*. 1.994. Cleveland, Ohio, USA, Pile Dynamics, Inc.
- PDI (1998). *GRLWEAP Manual*. Cleveland, Ohio, USA, Pile Dynamics, Inc.
- PDI (2000). *CAPWAP for Windows Manual - CAsE Pile Wave Analysis Program*. 2000-1. Cleveland, Ohio, USA, Pile Dynamics, Inc.
- PDI and GRL (2003). *The PDA unit photograph from www.pile.com website*.
- Pestana, J. M., Hunt, C. E. and Bray, J. D. (2002). *Soil deformation and excess pore pressure field around a closed-ended pile*. Journal of Geotechnical and Geoenvironmental Engineering, 128(1), 1-12.
- Poskitt, T. J. (1991b). *Energy losses in pile-driving due to soil rate effects and hammer misalignment*. Proceedings of the Institution of Civil Engineers, Part 2: Research and Theory, 91, 823-851.
- Poskitt, T. J. and Leonard, C. (1982). *Effect of velocity on penetrometer resistance*. Proceedings of the 2nd European Symposium on Penetration Testing, Amsterdam, Vol., 331-336.
- Potyondy, J. G. (1961). *Skin friction between various soils and construction materials*. Geotechnique, 11(4), 339-353.
- Poulos, H. G. (1998). *Pile testing - from the designer's viewpoint*. Proceedings of the 2nd International Static Seminar, Tokyo, Japan, Vol., 3-21.

- Randolph, M. F. (1990). *Chapter 6: Analysis of the dynamics of pile driving*. Developments in soil mechanics IV: Advanced geotechnical analyses. Banerjee, P. K. and Butterfield, R., Eds., Elsevier Applied Science Publishers Ltd.
- Randolph, M. F. (1991). *The effect of residual stresses in interpreting stress wave data*. Computer Methods and Advances in Geomechanics, Balkema, Rotterdam, Vol., 777-782.
- Randolph, M. F. (1992). *IMPACT Program manual - Dynamic analysis of pile driving Part I - Theory & Background*. Perth, Western Australia, Department of Civil & Environmental Engineering, The University of Western Australia.
- Randolph, M. F. (2000). *Pile-soil interaction for dynamic and static loading*. Proceedings of the 6th International Conference on the Application of Stress-Wave Theory to Piles, Sao Paulo, Brazil, Balkema, Vol., Appendix 3-11.
- Randolph, M. F. (2003). *Source of rate-dependence of pile-sand interface strength*. Personal Communication.
- Randolph, M. F. and Deeks, A. J. (1992). *Keynote lecture: Dynamic and static soil models for axial pile response*. Proceedings of the 4th International Conference on the Application of Stress-wave Theory to Piles, The Hague, The Netherlands, Balkema, Rotterdam, Vol., 3-14.
- Randolph, M. F. and Simons, H. A. (1986). *An improved soil model for one-dimensional pile driving analysis*. Proceedings of the 3rd International Conference in Numerical Methods in Offshore Piling, Nantes, Vol., 3-17.
- Randolph, M. F. and Wroth, C. P. (1981). *Application of the failure state in undrained simple shear to the shaft capacity of driven piles*. Geotechnique, 31(1), 143-157.
- Rausche, F., Goble, G. G. and Likins, G. E. J. (1985). *Dynamic determination of pile capacity*. Journal of Geotechnical Engineering, ASCE, 11(3), 367-383.
- Rausche, F., Moses, F. and Goble, G. (1972). *Soil resistance predictions from pile dynamics*. Journal of Soil Mechanics and Foundations Division, ASCE, 98(SM9), 917-937.
- Rausche, F., Thendean, G., Abou-matar, H., Likins, G. L. and Goble, G. (1996). *Determination of pile driveability and capacity from penetration tests (Volume I: final report)*. FHWA contract no. DTFH61-91-00047, Goble Rausche Likins and Associates, Inc., Cleveland, Ohio.
- Richardson, A. M. J. and Whitman, R. V. (1962). *Effect of strain-rate upon undrained shear resistance of a saturated remoulded fat clay*. Geotechnique, 12, 310-324.
- Roy, M., Blanchet, R., Tavenas, F. and La Rochelle, P. (1981). *Behaviour of a sensitive clay during pile driving*. Canadian Geotechnical Journal, 18, 67-85.

- Sassa, K. (1984). *The mechanism starting landslides and debris flows*. Proceedings of the 4th Symposium on Landslides, Toronto, Vol. 2, 349-354.
- Sassa, K. (1985). *The mechanism of debris flow*. Proceedings of the 11th International Conference on Soil Mechanics, San Francisco, Vol. 3, 1173-1176.
- Savage, S. B. (1982). *Granular flows at high shear rates*. Theory of dispersed multiphase flow. Meyer, R. R., Ed., Mathematical Research Center, University of Wisconsin, 339-358.
- Scarlett, B. and Todd, A. C. (1969). *The critical porosity of free-flowing solids*. Journal of Engineering for Industry(A91 Part 1), 478-488.
- Schimming, B. B., Haas, H. J. and Saxe, H. C. (1966). *Study of dynamic and static failure envelopes*. Journal of Soil Mechanics and Foundations Division, ASCE, 92(SM1), 105-124.
- Seed, H. B. and Lundgren, R. (1954). *Investigation of the effect of transient loading on the strength and deformation characteristics of saturated sands*. Proceedings of the American Society for Testing and Materials, Vol. 54, 1288-1306.
- Seidel, J. P. (1993). *The analysis and design of pile shafts in weak rock*. Department of Civil Engineering, Melbourne, Australia, Monash University.
- Seidel, J. P. (1998). *The response of pile-soil interfaces during pile driving and dynamic testing events*. Research Grants and Ethics Branch - Australian Research Council (ARC) Large Grant application proposal.
- Seidel, J. P., GRL and PDI (1997). *CAPWAP Powerpoint Presentation*.
- Seidel, J. P., Klingberg, D. J. and Canno, J. G. (1996). *Dynamic testing of barrettes for a cement-silo project*. Proceedings of the 5th International Conference on the Application of Stress-Wave Theory to Piles, Orlando, Florida, USA, Balkema, Vol., 748-758.
- Seidel, J. P. and Rausche, F. (1984). *Correlation of static and dynamic pile tests on large diameter drilled shafts*. Proceedings of the 2nd International Conference on the Application of Stress-Wave Theory to Piles, Stockholm, Sweden, Balkema, Vol., 313-318.
- Sheahan, T. C., Ladd, C. C. and Germaine, J. T. (1996). *Rate-dependent undrained shear behaviour of saturated clay*. Journal of Geotechnical Engineering, ASCE, 122(2), 99-108.
- Simons, H. A. and Randolph, M. F. (1985). *A new approach to one dimensional pile driving analysis*. Proceedings of the 5th International Conference on Numerical Methods in Geomechanics, Nagoya, Japan, Vol., 1457-1464.

- Skempton, A. W. (1951). *The bearing capacity of clays*. Building Research Congress, London, Vol. 1, 180-189.
- Smith, E. A. L. (1960). *Pile-driving analysis by the wave equation*. American Society of Civil Engineers Transactions, 127(Part 1), 1145-1193.
- Smith, I. M., To, P. and Wilson, S. M. (1986). *Plugging of pipe piles*. Proceedings of the 3rd International Conference on Numerical Methods in Offshore Piling, Nantes, Vol., 53-73.
- Standards Australia (1978). *Australian Piling Code*. Homebush, New South Wales.
- Standards Australia (1998). *Australian Standard for Civil Engineering Students Part 1: Materials and testing SAA HB.21. - 1998*. Second Edition. Homebush, New South Wales.
- Steele, R. B., Seidel, J. P. and Klingberg, D. (1990). *Test piling program for bridges on the Sunshine Motorway in Queensland*. 15th ARRB Conference, Darwin, Vol. Part 3, 139-153.
- Subba Rao, K. S., Allam, M. M. and Robinson, R. G. (1998). *Interfacial friction between sands and solid surfaces*. Proceedings of the Institution of Civil Engineers, Geotechnical Engineering, 131, 75-82.
- Subba Rao, K. S., Allam, M. M. and Robinson, R. G. (2000). *Drained shear strength of fine-grained soil-solid surface interfaces*. Proceedings of the Institution of Civil Engineers, Geotechnical Engineering, 143, 75-81.
- Svinkin, M. R. and Teferra, W. (1994). *Some aspects of determination of pile capacity by the wave equations*. Proceedings of the Structures Congress '94, Atlanta, GA, USA, ASCE, Vol., 946-951.
- Terzaghi, K. and Peck, R. B. (1967). *Soil mechanics in engineering practice*. 2nd. New York, John Wiley and Sons.
- Terzaghi, K., Peck, R. B. and Mesri, G. (1996). *Soil mechanics in engineering practice*. Third edition. New York, John Wiley & Sons, Inc.
- Thendean, G., Rausche, F., Svinkin, M. R. and Likins, G. E. (1996). *Wave equation correlation studies*. Proceedings of the 5th International Conference on the Application of Stress-Wave Theory to Piles, Orlando, Florida, USA, Vol., 144-162.
- Tika, T. E., Vaughan, P. R. and Lemos, L. J. L. (1996). *Fast shearing of pre-existing shear zones in soil*. Geotechnique, 46(2), 197-233.
- Tika-Vassilikos, T. (1991). *Clay-on-steel ring shear tests and their implications for displacement piles*. Geotechnical Testing Journal, 14(4), 457-463.
- Tika-Vassilikos, T. E., Bond, A. J. and Jardine, R. J. (1992). *Correlation of the results from field experiments with instrumented model piles in London clay and*

- laboratory ring shear interface tests*. Proceedings of the 6th International Conference on Behaviour of Offshore Structures, London, Vol., 661-672.
- Tsubakihara, Y. and Kishida, H. (1993). *Frictional behaviour between normally consolidated clay and steel by two direct shear type apparatuses*. Soils and Foundations, 33(2), 1-13.
- Tsubakihara, Y., Kishida, H. and Nishiyama, T. (1993). *Friction between cohesive soils and steel*. Soils and Foundations, 33(2), 145-156.
- Turner, J. P. and Kulhawy, F. H. (1990). *Drained uplift capacity of drilled shafts under repeated axial loading*. Journal of Geotechnical Engineering, ASCE, 116(3), 470-491.
- Uesugi, M. and Kishida, H. (1986a). *Influential factors of friction between steel and dry sands*. Soils and Foundations, 26(2), 33-46.
- Uesugi, M. and Kishida, H. (1986b). *Frictional resistance at yield between dry sand and mild steel*. Soils & Foundations, 26(4), 139-149.
- Uesugi, M., Kishida, H. and Uchikawa, Y. (1990). *Friction between dry sand and concrete under monotonic and repeated loading*. Soils & Foundations, 30(1), 115-128.
- USACE (1996). *Engineering and design - soil sampling*. U.S. Army Corps of Engineers. CECW-EG, EM No. 1101-1-1906. Washington, DC.
- Vesic, A. S. (1967). *A study of bearing capacity of deep foundations*. Final Rep., Proj. B-189, School of Civil Engineering, Georgia Institution of Technology, Atlanta, Georgia.
- Wang, Q. and Lade, P. V. (2001). *Shear banding in true triaxial tests and its effect on failure in sand*. Journal of Engineering Mechanics, ASCE, 127(8), 754-761.
- Whitman, R. V. and Healy, K. A. (1962). *Shear strength of sands during rapid loadings*. Journal of the Soil Mechanics and Foundations Division, ASCE, 88(2), 99-132.
- Wroth, C. P. (1979). *Correlations of some engineering properties of soils*. Proceedings of the 2nd International Conference on Behaviour of Offshore Structures, London, England, Vol., 121-132.
- Wroth, C. P. (1984). *The interpretation of in situ soil tests*. Geotechnique, 34(4), 449-489.
- Wroth, C. P., Carter, J. P. and Randolph, M. F. (1979). *Stress changes around a pile driven into cohesive soil*. Recent developments in the design and construction of piles, London, ICE, Vol.,

-
- Wroth, C. P. and Houlsby, G. T. (1985). *Soil mechanics - property characterization and analysis procedures*. Proceedings of the 11th International Conference on Soil Mechanics, San Francisco, USA, Balkema, Vol. 1, 1-55.
- Yamamuro, J. A. (2002). *Mechanism of strength increase in sand*. Personal Communication.
- Yamamuro, J. A. and Abrantes, A. E. (2003). *Effect of strain rate on the stress-strain behavior of granular materials*. Journal of Geotechnical and Geoenvironmental Engineering, ASCE, Submitted for publication.
- Yamamuro, J. A. and Lade, P. V. (1993). *Effects of strain rate on instability of granular soils*. Geotechnical Testing Journal, GTJODJ, 16(3), 304-313.
- Yin, Z.-Z., Zhu, H. and Xu, G.-H. (1995). *A study of deformation in the interface between soil and concrete*. Computers and Geotechnics, 17(1), 75-92.
- Yoshimi, Y. and Kishida, T. (1981). *Friction between sand and metal surface*. Proceedings of the 10th International Conference on Soil Mechanics and Foundation Engineering, Stockholm, Balkema, Vol., 831-834.
- Yoshimi, Y. and Kishida, T. (1982). *A ring torsion apparatus for evaluating friction between soil and metal surfaces*. Geotechnical testing Journal, 4(4), 145-152.
- Zhang, L., McVay, M. C. and Ng, C. W. W. (2001). *A possible physical meaning of Case damping in pile dynamics*. Canadian Geotechnical Journal, 38, 83-94.